New−Generation Electron Propagators for Molecules, Ions, and Clusters

by

Ernest Opoku

A dissertation submitted to the Graduate Faculty of
Auburn University
in partial fulfillment of the
requirements for the Degree of
Doctor of Philosophy

Auburn, Alabama
August 9, 2025

Keywords: Quantum Chemistry, Green's Functions; Electron Propagators; Ionization Energies; Electron Affinities; Dyson orbitals

Copyright © 2025 by Ernest Opoku

Approved by

J. V. Ortiz, Chair, Ruth W. Molette Professor Emeritus of Chemistry and Biochemistry
Filip Pawłowski, Assistant Research Professor of Chemistry and Biochemistry
Evangelos Miliordos, James E. Land Associate Professor of Chemistry and Biochemistry
German Mills, Professor Emeritus of Chemistry and Biochemistry
Hans Werner Van Wyk, Associate Professor of Mathematics and Statistics

Abstract

New *ab initio* electron propagator self−energies (one−particle Green's function methods) for calculating electron binding energies and Dyson orbitals have been derived from an intermediately normalized, Hermitized superoperator metric. No adjustable or empirical parameters are tolerated in the derivation of the new self−energies or their reference Hartree−Fock orbital bases. The cubically scaling diagonal second order method (D2) has been demonstrated to systematically underestimate (overestimate) ionization energies (electron affinities). To ameliorate this deficiency, same−spin correlation is neglected in the opposite−spin second order method (os−D2) that significantly improves accuracy and efficiency.

Renormalizations of the ring and ladder terms in the diagonal *2ph*−TDA self−energy lead to the diagonal ring (DR) and diagonal ladder (DL) methodologies that have achieved improved efficiency and accuracy. Modification of the Outer Valence Green's Function (OVGF) method because of the new choice of intermediately normalized, Hermitized superoperator metric leads to the derivation of the approximately renormalized linear third order (L3+). Simplification of the L3+ method leads to the approximately renormalized quasiparticle third order (Q3+) and the approximately renormalized partial third order method (P3+). When the approximate estimation of post−third−order terms is replaced by the explicit evaluation of all contributions from the expansion of inverted matrices, the resulting explicitly renormalized variants of L3+, Q3+, and P3+ are obtained, referred to as RL3, RQ3, and RP3, respectively. Restoration of off−diagonal matric elements leads to the NRL3, NRQ3 and NRP3 self−energies.

In addition, non−Dyson (nD) versions of D2, os−D2, OVGF, L3+ and RL3 self−energies are obtained by deactivating energy dependence in $2ph$ denominators for electron detachment

energies calculations and in $2hp$ denominators for electron attachment energies calculations. This deactivation is achieved by setting the $E = \varepsilon_p$ in the $\Sigma_{pq}(E)$ self−energy terms with these denominators. The non−Dyson version has improved efficiency in electron detachment energies calculations as the arithmetic bottlenecks are no longer iterative. This advantage does not necessarily occur for electron attachment energies calculations.

Performance of the new methods has been evaluated using extensive experimental and computational benchmark databases for vertical ionization energies (VIEs), vertical electron affinities (VEAs), and vertical electron detachment energies (VEDEs) of anions. For VIEs and VEDEs, the best compromises of accuracy and cost, expressed in terms of mean absolute errors (MAEs) in eV, and arithmetic efficiency, expressed in terms of powers of occupied (O) and virtual (V) orbital dimensions in bottleneck operations, are os−nD−D2, Q3+, nD−L3+, and nD−RL3 diagonal self−energies. The corresponding MAEs and arithmetic scaling factors respectively are: (∼0.18, OV^2), (∼0.15, O^2V^3), (∼0.08, OV^4), and (∼0.07, OV^4). NRL3 is the best non−diagonal method with an MAE of ∼0.06 eV and a non−iterative O^2V^4 scaling. For VEAs, the best compromises of accuracy and cost are D2, nD−L3+, and nD−RL3 diagonal self−energies. Their corresponding MAEs and arithmetic scaling factors respectively are: (∼0.18, OV^2), (∼0.08, OV^4), and (∼0.07, OV^4). NRL3 is the best non−diagonal method with an MAE of ∼0.06. Tests on open−shell atoms, molecules, and ions show similar trends except that MAEs generally increase by ∼0.05 eV due to spin contamination.

For molecules with nuclei of the fourth or higher periods, RL3 and nD−RL3 are the best methods with MAEs of ∼0.14 eV. For core $1s$ ionizations, the Brueckner doubles with triple field operators (BD−T1) method exhibits the highest accuracy with a MAE of ∼0.39 eV. It shows excellent agreement with experimental data and minimal systematic bias.

Composite schemes that incorporate the new methods for estimating basis−set effects have enabled highly accurate calculations of VIEs and VEDEs for organic photovoltaic

molecules, which are important for optimizing solar energy devices, achieving MAEs that approach chemical accuracy (average errors of 0.04 eV). The new methods and their composite schemes also produce excellent predictions and clear interpretations based on Dyson orbitals for the photoelectron spectra of DNA nucleotide anions and green fluorescent protein (GFP) chromophore anions.

Because the new methods developed in this dissertation require no adjustable or empirical parameters and the accuracy of several of them approaches chemical accuracy, they are reliable for predictions on novel molecules, ions, and clusters. Therefore, the existence, stability and VEDEs of $O_nH_{2n+1}^-$ and $NH_4^-(H_2O)_n$ double Rydberg anions have been predicted. These clusters are predicted to have well separated VEDEs and experimentally accessible total energies and therefore are expected to appear in mass−selected, anion photoelectron spectra that typically detect low−lying isomers.

Dedication

To Professor Richard Tia *of blessed memory*

Kwame Nkrumah University of Science and Technology, Kumasi, Ghana

(Deceased: November 30, 2022)

In honor of your enduring inspiration, mentorship, and the foundational role you played in shaping my academic path. Your legacy continues to guide and motivate me.

Acknowledgments

I am very grateful to my PhD advisor, Professor J. V. Ortiz, not only for his distinctive mentorship, strong intellectual rigor, and dedication to scientific excellence but for the numerous excellent examples he has set for me.

My sincere thanks to my advisory committee members for their steadfast dedication and service to my education. I thank Professor Filip Pawłowski for his consistent encouragement and valuable support throughout my graduate studies. His guidance and collaborations greatly enhanced my research experience. Special gratitude goes to Professor Evangelos Miliordos, whose early support made my admission to Auburn University possible. His prompt and gracious response to my emails was decisive in my choosing Auburn, and his ongoing provision of resources and mentorship has been invaluable to my success.

I acknowledge the insightful discussions with former members of the Ortiz quantum chemistry group, as well as the graduate assistantship from the Department of Chemistry & Biochemistry, Auburn University.

To my beloved wife, Dr. Benedicta Donkor, thank you for your love, patience, and unwavering support. To our son, Jeremiah, thank you for bringing joy and a profound sense of purpose into my life. Special gratitude goes to my mother, Mrs. Ruth Agyekum, whose steadfast dedication to my education has been a source of continuous inspiration. I am also thankful to my father, Mr. Emmanuel Kwadwo Opoku, for his wisdom, support, and compassionate guidance.

Special thanks to Ms. Abigail O. Gyamfi and Mr. George B. Pipim for indispensable academic conversations. I also acknowledge the support and effort of all my teachers, advisors, collaborators, family, friends, and colleagues at various stages of my education.

Most importantly, I thank my Creator for the gift of life and many blessings.

Table of Contents

Abstract ii

Dedication v

Acknowledgments vi

List of Tables xi

List of Figures xii

1 **Introduction** 1

1.1 The Schrödinger Equation 1

1.2 The Born−Oppenheimer Approximation and the Electronic Hamiltonian . . 1

1.3 Approximating the Wavefunction: The Hartree−Fock Method 2

1.4 Koopmans's Theorem 3

1.5 Methodologies for Calculating Electron Binding Energies 4

1.6 Account of Evolutionary Stages of Electron Propagator Theory 6

1.7 Brief Survey of Applications 8

1.8 New−Generation *Ab Initio* Electron Propagators 8

1.9 Outline of the Dissertation 9

2 **Green's Functions and Dyson's Equation** 11

2.1 Creation and Annihilation Operators 11

2.2 The Electron Propagator (One−Body Green's Function) 12

2.3 Superoperator Theory 15

2.4 Dyson's Equation and Hartree−Fock Theory 17

2.5 Quasiparticle Theory 19

3 **Approximate Electron−Propagator Self−Energies** 21

3.1 Diagonal Second−Order Methods 24

3.2 Simplified Renormalized Diagonal Ring and Ladder Approximations 26
3.3 Diagonal Full Third Order Approximation 28
3.4 Outer−Valence Green's Function (OVGF) Method 30
3.5 Diagonal Linear Third Order Methods 31
3.6 Diagonal Quasiparticle Third Order Methods 34
3.7 Diagonal Partial Third Order Methods 36
3.8 Non−diagonal and Renormalized Electron Propagator Methods 37
4 **Numerical Results: Performance of the New and Old Generation Electron−Propagtor Methods** 40
4.1 Vertical Ionization Energies of Molecules 40
4.2 Vertical Electron Detachment Energies of Molecular Anions 44
4.3 Vertical Electron Affinities of Molecules 45
4.4 Vertical Electron Binding Energies of Open−Shell Atoms and Molecules . . . 46
4.4.1 Open−Shell Atomic Electron Binding Energies 47
4.4.2 Open−Shell Molecular Ionization Energies 47
4.4.3 Open−Shell Molecular Electron Affinities 48
4.4.4 Performance Across Various Classes of Vertical Transitions 48
4.5 Vertical Ionization Energies of Heavy−Element−Containing (HEC) Molecules 49
4.5.1 Introduction to VIEs of HEC Molecules 49
4.5.2 Results and Discussion: Experimental Reference Ionization Energies of HEC Molecules Versus Electron Propagator Methods 50
4.5.3 Results and Discussion: ΔCCSD(T) Reference Vertical Ionization Energies of HEC Molecules Versus Electron Propagator Methods 52
4.6 K−Shell Core Ionization Energies 55
5 **Applications of New−Generation Electron−Propagator Methods** . . . 61
5.1 Vertical Electron Detachment Energies of DNA Nucleotide Anions 61
5.2 Vertical Electron Detachment Energies of GFP Chromophore Anions 65

6 **Prediction of New Molecules and Anions: Double Rydberg Anions and Rydberg Molecules** . . . 68
6.1 Electron Binding Energies and Dyson Orbitals of $O_nH_{2n+1}^{+,0,-}$ Clusters . . . 68
6.2 $O_nH_{2n+1}^{-}$ Double Rydberg Anions . . . 69
6.3 Concluding Remarks on $O_nH_{2n+1}^{-}$ Double Rydberg Anions . . . 82
7 **Prediction of New Molecules and Anions: Double Rydberg Anions, Rydberg Radicals and Micro−solvated Cations with Ammonium−Water Kernels** . . . 84
7.1 Electron Binding Energies and Dyson Orbitals of $NH_4^-(H_2O)_n$ Clusters . . . 84
7.2 Vertical Electron Detachment Energies and Dyson Orbitals of $NH_4^-(H_2O)_n$ Double Rydberg Anions . . . 88
7.3 Concluding Remarks on $NH_4^-(H_2O)_n$ Double Rydberg Anions . . . 97
8 **General Conclusions and Outlook** . . . 99
Bibliography . . . 117
Appendices . . . 118
A **E. Opoku**, F. Pawłowski and J. V. Ortiz, "New−Generation Electron−Propagator Methods for Molecular Electron−Binding Energies", *J. Phys. Chem. A*, **128**, 1399–1416 (2024) . . . 119
B **E. Opoku**, F. Pawłowski and J. V. Ortiz, "A New Generation of Diagonal Self−Energies for the Calculation of Electron Removal Energies", *J. Chem. Phys.*, **155**, 204107 (2021) . . . 138
C **E. Opoku**, F. Pawłowski and J. V. Ortiz, "A New Generation of Non−diagonal, Renormalized Self−Energies for Calculation of Electron Removal Energies", *J. Chem. Phys.*, **159**, 124109 (2023) . . . 156
D **E. Opoku**, F. Pawłowski and J. V. Ortiz, "Electron−Propagator Self−Energies Versus Improved GW100 Vertical Ionization Energies", *J. Chem. Theory Comp.*, **18**, 4927–44 (2022) . . . 183

E **E. Opoku**, F. Pawłowski and J. V. Ortiz, "Electron−Propagator Methods Versus Experimental Ionization Energies", *J. Chem. Phys.*, **162**, 064102 (2025) 202

F **E. Opoku**, F. Pawłowski and J. V. Ortiz, "Simplified Ring and Ladder Renormalizations in Electron−Propagator Calculations of Molecular Ionization Energies", *J. Phys. Chem. A*, **129**, 3597–3612 (2025) 218

G **E. Opoku**, F. Pawłowski and J. V. Ortiz, "New−Generation Electron−Propagator Methods for Calculations of Electron Affinities and Ionization Energies: Tests on Organic Photovoltaic Molecules", *J. Chem. Theory Comp.*, **20**, 290–306 (2024) . 235

H **E. Opoku**, F. Pawłowski and J. V. Ortiz, "Electron Propagator Theory of Vertical Electron Detachment Energies of Anions: Benchmarks and Applications to Nucleotides", *J. Phys. Chem. A*, **127**, 1085–101 (2023) 253

I **E. Opoku**, F. Pawłowski and J. V. Ortiz, "New−Generation Electron−Propagator Methods for Vertical Electron Detachment Energies of Molecular Anions: Benchmarks and Applications to Model Green−Fluorescent−Protein Chromophores", *Phys. Chem. Chem. Phys.* **26**, 9915–9930 (2024) 271

J **E. Opoku**, F. Pawłowski and J. V. Ortiz, "*Ab Initio* Electron Propagators with an Hermitian, Intermediately Normalized Superoperator Metric Applied to Vertical Electron Affinities", *J. Phys. Chem. A*, **128**, 4730–4749 (2024) 288

K **E. Opoku**, F. Pawłowski and J. V. Ortiz, "Electron Binding Energies of Open−Shell Species from Diagonal Electron−Propagator Self−Energies with Unrestricted Hartree−Fock Spin−Orbitals", *J. Phys. Chem. A*, **128**, 7311–7330 (2024) 309

L **E. Opoku**, F. Pawłowski and J. V. Ortiz, "Electron Binding Energies and Dyson Orbitals of $O_nH_{2n+1}^{+,0,-}$ Clusters: Double Rydberg Anions, Rydberg Radicals and Micro−Solvated Hydronium Cations", *J. Chem. Phys.*, **154**, 234304 (2021) 330

M **E. Opoku**, F. Pawłowski and J. V. Ortiz, "Double Rydberg Anions, Rydberg Radicals and Micro−solvated Cations with Ammonium−Water Kernels", *Phys. Chem. Chem. Phys.*, **24**, 18347-60 (2022). 349

List of Tables

3.1 Acronyms and names of electron−propagator methods 22

3.2 Arithmetic scaling and transformed integral requirements of electron−propagator methods.[a] 23

3.3 Orders retained in superoperator Hamiltonian matrices ($\hat{\mathbf{H}}$) of NRP3, NRQ3 and NRL3 self−energies for hole (h), particle (p), two−hole−one−particle ($2hp$), and two−particle−one−hole ($2ph$) operators.[a,b,c,d,e,f] 38

4.1 MAEs (eV) of diagonal second−order electron−propagator methods versus VIE, VEDE and VEA standards. 40

4.2 MAEs (eV) of diagonal third order and approximately renormalized electron−propagator methods versus VIE, VEDE and VEA standards. 42

4.3 MAEs (eV) of diagonal post second order and explicitly renormalized electron−propagator methods versus VIE, VEDE and VEA standards. 43

4.4 MAEs (eV) of non−diagonal and renormalized electron−propagator methods versus VIE, VEDE and VEA standards. 44

4.5 HEC Molecules, Point Groups, Hole States, Experimental and ΔCCSD(T) Ionizations Energies Standards. All ΔCCSD(T) calculations were executed with the def2TZVPP basis set. 56

4.6 Electron propagator methods versus core $1s$ experimental electron binding energies.[a] 60

5.1 Vertical electron detachment energies (eV) of deoxyribonucleotide anions.[64] . . 63

5.2 Vertical electron detachment energies of GFP model anions.[63] 66

6.1 Comparison of VEDEs (eV) of the OH_3^- DRA calculated at different levels of theory. Pole strengths are in parentheses. 70

6.2 $O_nH_{2n+1}^-$ isomerization and vertical electron detachment energies (VEDEs). Pole strengths are in parentheses. All energies are in eV. Calculations were executed with the d−aug−cc−pVTZ basis set. [88] 72

7.1 $NH_4^-(H_2O)_n$ isomers and their vertical electron detachment energies (VEDEs). Pole strengths are in parentheses. All energies are in eV. [a] 88

List of Figures

4.1 Histograms of error distributions (eV) versus experimental VIEs of 81 heavy−element−containing molecules[121]: diagonal EP methods. All calculations were executed with the def2TZVPP basis set. 51

4.2 Histograms of error distributions (eV) versus experimental VIEs of 81 heavy−element−containing molecules[121]: non−diagonal EP methods. All calculations were executed with the def2TZVPP basis set. 53

4.3 Histograms of error distributions (eV) versus ΔCCSD(T) VIEs of 81 HEC molecules: Diagonal EP methods. All calculations were executed with the def2TZVPP basis set. 58

4.4 Histograms of error distributions (eV) versus ΔCCSD(T) VIEs of 81 HEC molecules: Non−diagonal EP methods. All calculations were executed with the def2TZVPP basis set. 59

5.1 Dyson orbitals of vertical electron detachment of deoxyribonucleotide anions[64] 64

5.2 Structures and Dyson orbitals for vertical electron detachment energies of model GFP anions.[63] 67

6.1 $n = 1$: Optimized geometries and Dyson orbitals of electron detachment from anions 73

6.2 $n = 2$: Optimized geometries and Dyson orbitals of electron detachment from anions. 74

6.3 $n = 3$: Optimized geometries and Dyson orbitals of electron detachment from anions. 76

6.4 $n = 4$: Optimized geometries and Dyson orbitals of electron detachment from $O_4H_9^-$ anions. 78

6.5 $n = 5$: Optimized geometries and Dyson orbitals of electron detachment from $O_5H_{11}^-$ anions. 80

6.6 n = 6: Optimized geometries and Dyson orbitals of electron detachment from $O_6H_{13}^-$ anions. 82

7.1 $n = 1$ Optimized geometries and Dyson orbitals of electron detachment from $NH_4^-(H_2O)$ isomers. 91

7.2 $n = 2$ Optimized geometries and Dyson orbitals of electron detachment from $NH_4^-(H_2O)_2$ isomers. 93

7.3 $n = 3$ Optimized geometries and Dyson orbitals of electron detachment from $NH_4^-(H_2O)_3$ isomers. 95

7.4 $n = 4$ Optimized geometries and Dyson orbitals of electron detachment from $NH_4^-(H_2O)_4$ isomers. 97

Chapter 1

Introduction

1.1 The Schrödinger Equation

A key turning point in modern chemistry came with the formulation of the Schrödinger equation.[1] It mathematically described the behavior of quantum particles, such as electrons, and laid the foundation for quantum chemistry. For a molecular system containing N electrons and M nuclei, the time−independent non−relativistic Schrödinger equation is given by

$$\hat{\mathrm{H}}|\Psi\rangle = E|\Psi\rangle \tag{1.1.1}$$

Here, $\hat{H}$ is the full molecular Hamiltonian, Ψ is the total wavefunction, and E is the total energy. The full Hamiltonian is expressed as

$$\begin{aligned}\hat{H} = &-\sum_{i=1}^{N}\frac{\hbar^2}{2m_e}\nabla_i^2 - \sum_{A=1}^{M}\frac{\hbar^2}{2M_A}\nabla_A^2 \\ &-\sum_{i=1}^{N}\sum_{A=1}^{M}\frac{Z_A e^2}{|\mathbf{r}_i - \mathbf{R}_A|} + \sum_{i<j}^{N}\frac{e^2}{|\mathbf{r}_i - \mathbf{r}_j|} + \sum_{A<B}^{M}\frac{Z_A Z_B e^2}{|\mathbf{R}_A - \mathbf{R}_B|}.\end{aligned} \tag{1.1.2}$$

The full Hamiltonian in equation 1.1.2 incorporates kinetic energy of electrons and nuclei, electron−nuclear attraction, electron−electron repulsion, and nuclear−nuclear repulsion.

1.2 The Born−Oppenheimer Approximation and the Electronic Hamiltonian

The Born−Oppenheimer approximation[2] exploits the fact that nuclei are much heavier and slower than electrons. This assumption allows the separation of electronic and nuclear motion by treating nuclear positions as fixed parameters. The resulting electronic

Schrödinger equation becomes

$$\hat{H}_{\text{el}}\Psi_{\text{el}}(\{\mathbf{r}_i\};\{\mathbf{R}_A\}) = E_{\text{el}}\Psi_{\text{el}}(\{\mathbf{r}_i\};\{\mathbf{R}_A\}), \tag{1.2.1}$$

where the electronic Hamiltonian can be expressed as

$$\hat{H}_{\text{el}} = -\sum_{i=1}^{N}\frac{\hbar^2}{2m_e}\nabla_i^2 - \sum_{i=1}^{N}\sum_{A=1}^{M}\frac{Z_A e^2}{|\mathbf{r}_i - \mathbf{R}_A|} + \sum_{i<j}^{N}\frac{e^2}{|\mathbf{r}_i - \mathbf{r}_j|}. \tag{1.2.2}$$

To further simplify the electronic Hamiltonian, atomic units (a.u.) are adopted by setting $\hbar = m_e = e = 4\pi\varepsilon_0 = 1$.[3] This simplification leads to the electronic Hamiltonian in atomic units expressed as

$$\hat{H}_{\text{el}} = -\sum_{i=1}^{N}\frac{1}{2}\nabla_i^2 - \sum_{i=1}^{N}\sum_{A=1}^{M}\frac{Z_A}{|\mathbf{r}_i - \mathbf{R}_A|} + \sum_{i<j}^{N}\frac{1}{|\mathbf{r}_i - \mathbf{r}_j|}. \tag{1.2.3}$$

This is the fundamental starting point for almost every *ab initio* electronic structure theory development.

1.3 Approximating the Wavefunction: The Hartree−Fock Method

Having seen how the Hamiltonian is simplified to the electronic Hamiltonian in atomic units, we need to equally find some conceptually equivalent approximate treatment for the wavefunction.[3] The exact solution of the many−electron Schrödinger equation is computationally unfeasible for systems larger than hydrogen. The Hartree−Fock (HF) method approximates the full electronic wavefunction as a single Slater determinant[4] of spin−orbitals

$$\Psi^{\text{HF}}(\mathbf{x}_1,\ldots,\mathbf{x}_N) = \frac{1}{\sqrt{N!}}\begin{vmatrix} \phi_1(\mathbf{x}_1) & \phi_2(\mathbf{x}_1) & \cdots & \phi_N(\mathbf{x}_1) \\ \phi_1(\mathbf{x}_2) & \phi_2(\mathbf{x}_2) & \cdots & \phi_N(\mathbf{x}_2) \\ \vdots & \vdots & \ddots & \vdots \\ \phi_1(\mathbf{x}_N) & \phi_2(\mathbf{x}_N) & \cdots & \phi_N(\mathbf{x}_N) \end{vmatrix}. \tag{1.3.1}$$

Each spin−orbital $\phi_i(\mathbf{x})$ is a function of spatial and spin coordinates. The Slater determinant ensures antisymmetry under particle exchange, satisfying the Pauli exclusion principle. Based on the variational principle, the Hartree–Fock method minimizes the total electronic energy with respect to the molecular orbitals, subject to the constraint that these orbitals remain orthonormal. This constrained minimization leads to the self−consistent field (SCF) equations also known as the Hartree–Fock equations

$$\hat{f}\phi_i = \varepsilon_i \phi_i, \tag{1.3.2}$$

where the Fock operator $\hat{f}$ is given by

$$\hat{f} = \hat{h} + \sum_{j=1}^{N} \left(\hat{J}_j - \hat{K}_j \right). \tag{1.3.3}$$

In this notation, $\hat{h}$ denotes the customary one−electron operator (kinetic energy + nuclear attraction), $\hat{J}_j$ for Coulomb operator, and $\hat{K}_j$ representing the exchange operator. The HF equations are solved iteratively using a self−consistent field (SCF) procedure. The key deficiency of the HF method is the lack of *explicit* treatment of electron correlation for which nearly all post−HF methods attempt to address. Only the the Fermi or exchange correlation occurs at the HF level. Fermi correlation occurs due to the antisymmetry of the wavefunction (Pauli exclusion principle). Thus, same−spin electrons cannot occupy the same spatial region, which naturally leads to a kind of correlation between their positions. HF does account for this via the exchange term.

1.4 Koopmans's Theorem

Koopmans' theorem (KT)[5] provides an important interpretation of Hartree−Fock orbital energies. The ionization energy required to remove an electron from a closed−shell system is approximately equal to the negative of the Hartree−Fock orbital energy of that

electron.

$$I \approx -\varepsilon_i \tag{1.4.1}$$

KT is derived by assuming frozen orbitals (i.e., orbitals do not relax upon ionization). Thus, the KT is an excellent approximation to vertical ionization energy which can be considered as an instantaneous response to a molecule upon photoionization prior to relaxation. The energy difference between the neutral and ionized systems simplifies to the orbital energy of the removed electron,

$$I = E^{N-1} - E^N \approx -\varepsilon_i. \tag{1.4.2}$$

Although KT neglects relaxation and correlation effects, it serves as good starting point for estimating vertical electron binding energies to facilitate interpretation of photoelectron spectroscopy and scattering experiments.

There are four broad categories of *ab initio* techniques widely known to systematically address the electron correlation deficiency in HF theory. These comprise configuration−interaction methods, coupled−cluster methods, many−body perturbation theories, one−particle many−body Green's functions (MBGF) also known as electron propagators. The electron propagator theory (EPT) particularly differs from the others as its Feynman–Dyson perturbation series converges at the exact basis−set solutions of a many−electron Schrödinger equation within the framework of a one−particle theory.[6]

1.5 Methodologies for Calculating Electron Binding Energies

Electron binding energies (EBEs) are essential properties crucial to understanding molecular electronic structure, ionization processes, and electron affinities.[7] These energies, which represent the cost or gain associated with removing or adding an electron to a molecule, ion or atom, play a critical role in a variety of fields, from spectroscopy and chemical reactivity to material science and catalysis. The accurate and efficient calculation of EBEs has long been a significant challenge in theoretical and computational chemistry, primarily due to the

necessity of incorporating electron correlation effects, which are intrinsically many−body in nature.

Among the many methodologies developed to tackle this challenge, electron propagator theory (EPT) stands out as a powerful and versatile approach.[8–10] Grounded in the framework of Green's functions, EPT directly relates the electronic structure of a system to experimental observables such as ionization potentials (also known as ionization energies) and electron affinities.[11] Many traditional wavefunction−based methods for calculating EBEs often require separate optimizations for ground and final state wavefunctions. EPT departs from this convention by formulating the problem in terms of the ground state's response to the addition or removal of an electron. This makes it particularly well−suited for calculating spectral properties and interpreting data from spectroscopic and scattering experiments.

EPT provides a systematic framework for calculating electron−binding energies by leveraging the properties of the one−electron Green's function and the Dyson equation.[12, 13] The advantage of using this approach lies in its *accuracy*, *efficiency*, and *interpretability*. EPT rigorously builds on the familiar one−electron molecular orbital theory.[14] The canonical molecular orbital energies from Koopmans's theorem[5] (KT) define the zeroth order theory. The energy dependent self−energy operator of EPT includes corrections to KT from orbital relaxation effects and electron correlation.

By defining electron detachment and attachment energies as poles of the electron propagator, we can extract meaningful and accurate predictions for both valence and inner−shell electron−binding energies. These calculations, which serve as a bridge between experimental and theoretical chemistry, help validate and interpret experimental measurements, such as photoelectron spectroscopy, electron scattering and Penning ionization experiments.[15–18]

1.6 Account of Evolutionary Stages of Electron Propagator Theory

The field of electron propagator theory has seen several evolutionary stages, with each improving accuracy and computational efficiency. The first generation of methods focused primarily on accuracy, aiming to make electron−binding energy predictions that closely match experimental results. Many of these methods focused on deriving and implementing perturbative expansions that improve on Koopmans's theorem.[5] Many of these early methods are efficient while others often involved high computational costs due to the complexity of handling higher order many body effects. The development of second order[19] and third order[20] self−energies marked significant progress, as they introduced the diagonal approximation that enhanced both computational speed and accuracy. To account for primary and correlation states, the two-particle−one−hole−Tamm−Dancoff approximation (*2ph*−TDA)[21] was developed. The pursuit of higher accuracy led to the derivation of the third order algebraic diagrammatic construction, or ADC(3)[22], and alternatives in which the third order energy independent term is replaced with its fourth−order counterpart or renormalization schemes.[23] The fourth order extension, ADC(4), has been evaluated more recently for electron attachments and detachments.[24] These computationally demanding efforts did realize improvements over KT. The ADC(3) method has been coupled with a complex absorbing potential to efficiently compute metastable electronic states in electron–molecule scattering and ionization processes.[25] ADC methods utilizing multireference wavefunctions have been discussed elsewhere.[26, 27]

The *GW* family of methods[28] [Green's function (G) and the screened Coulomb interaction (W)] includes variants with renormalized self−energies, which can be based on either diagonal−approximation or non−diagonal self−energy schemes. In all cases, ring diagrams for all orders are incorporated into the *GW* self−energy.[29] In most cases, the orbital basis is obtained from Kohn−Sham density functional theory (DFT) calculations, although there is no impediment to using HF reference states. This approximation is characteristic of the

G_0W_0 approach. While GW self−energies are exact up to second order in the fluctuation potential, they neglect several significant third−order contributions.

Subsequent developments such as the outer valence Green's function (OVGF)[30] method, the partial third−order (P3)[31] self−energy and its approximately renormalized extension (P3+)[32] focused on estimating higher order effects to achieve improved accuracy and efficiency. Extension of the diagonal approximation to partial fourth order (P4+)[33] and its non−diagonal version[34] were also considered. The nondiagonal renormalized second order (NR2)[35] has been highly successful with its favorable arithmetic scaling requirements. Methods that use approximate Brueckner reference orbitals instead of the customary Hartree−Fock (HF) reference state have proven highly accurate especially on molecules with relatively strong correlation.[36–38] Multireference electron propagator (EP) methods utilizing multireference spin−tensors have also been reported.[39] Another alternative may be based on transition operator reference states.[40] Improved algorithms that take advantage of Abelian point group symmetry for efficient computation of electron repulsion integrals (ERIs) were also developed.[41] Techniques of resolution of the identity were also invoked for electron propagator calculations.[42] Truncation of virtual orbital dimensions were also employed to facilitate studies of large molecules.[43, 44] In a quest for efficiency, Danovich and co-workers developed semi−empirical versions of the OVGF method.[45] Algebraic diagrammatic construction methods utilizing non−Dyson procedures (*vide infra*) were also developed to improve computational efficiency.[46–50]

Later efforts focused on development of relativistic[51] versions of quasiparticle EP methods as well as composite schemes[52] that exploit basis set additivity schemes to study large molecules. Cholesky decomposition has been applied to electron propagator methods to efficiently handle large systems.[53] Monte Carlo versions of second and third order EP methods have also appeared and have been applied to extended systems.[54–56]

1.7 Brief Survey of Applications

Rapidly evolving methodological advances continue to expand the capabilities of EP methods. The performance of several of these methods has been evaluated against benchmark standards of ionization energies, [26, 27, 49, 52, 57–61] electron detachment energies of anions,[62–64] and electron affinities.[59, 65, 66] This has allowed the spectral assignment and interpretation of a wide range of molecules and anions including fullerenes,[52, 53, 65, 67, 68] nucleic acid fragments,[69–71] borane and carborane anions,[72–74] superhalogens and superacids,[75–77] metalloporphyrins,[78, 79] polypeptides,[80–82] organometallic complexes,[83, 84] and molecular wires,[85, 86] among others. Prediction, assignment and interpretation of novel electronic structures in double Rydberg anions[87–89] have also been executed as well as in the closely related solvated electron precursors.[90]

1.8 New−Generation *Ab Initio* Electron Propagators

During my PhD research, I have focused on the development and applications of new−generation methods[91, 92] that represent a major advancement in the field, as they offer improved *accuracy*, *efficiency*, and *interpretability*.[93] In analogy to several of their antecedents, adjustable parameters are *not* tolerated in the design of the new self−energies or their reference orbital bases. These methods include simplified and optimal second order methods, simplified ring and ladder renormalized methods, explicitly and approximately renormalized class of methods, such as the quasiparticle third order (Q3) and the linear third order (L3) methods. These methods have favorable cubic and quintic scaling in computational costs, respectively. The new methods also show unprecedented accuracy when compared with experimental and computational standards of EBEs, with several achieving mean absolute errors below 0.1 eV for electron detachment[63, 64, 94–96] and attachment energies[66, 95] with respect to high quality computational standards as well as experimental reference ionization energies.[97] Several of the new methods have been extended to open−shell molecules and atoms and

demonstrate exceptional performance with error margins generally increasing by only 0.05 eV as a result of spin contamination.[98]

1.9 Outline of the Dissertation

Chapter 2 presents the theoretical foundation of the one−electron Green's function (the electron propagator) and its rigorous connection to the Dyson equation. Procedures for obtaining the poles and Dyson orbitals are discussed. It is followed by discussion on super-operator theory and how it is pertinent to developing approximate self−energies. The latter part pertains to discussion on the equivalency of the Dyson equation and Hartree−Fock theory as well as the eventual evolution of the quasiparticle theory. This chapter is a partial summary of Appendix A—Appendix C. Chapter 3 introduces the derivations of the new−generation electron propagator methods developed in this dissertation research and their rigorous relationships to older electron propagator methods where applicable. This chapter is a partial summary of Appendix A—Appendix C.

Chapter 4 is devoted to numerical results calibrating the new−generation electron propagator methods versus their antecedents and related many−body methods (where applicable). Thus, the performance of the new methods on vertical ionization energies, vertical electron affinities, and vertical electron detachment energies of closed−shell and open−shell molecules and molecular ions are discussed. Their performance on VIEs of heavy−element−containing molecules as well as K−shell ionization energies is also presented. Most sections of this chapter are summaries of Appendix A—Appendix K.

Chapter 5 focuses on applications of the new−generation electron propagator methods to the assignment and interpretation of the photoelectron spectra of DNA nucleotide anions and green florescent proteins (GFP) chromophore anions. This chapter is a summary of Appendix H and Appendix I.

Chapter 6 is a summary of my research on the prediction of stability, VEDEs and Dyson orbitals of new double Rydberg anions and Rydberg molecules based on $O_nH_{2n+1}{}^{+,0,-}$

clusters. This chapter is a summary of Appendix L. Chapter 7 also presents my work on the prediction of stability, VEDEs and Dyson orbitals of new double Rydberg anions and Rydberg molecules based on $NH_4^-(H_2O)_n$ clusters with ammonium−water kernels. This chapter is a summary of Appendix M.

Chapter 8 presents general conclusions and an outlook for the entire dissertation.

This dissertation is primarily based on the content of my 13 peer-reviewed articles published during the course of my PhD research. Reprints of these articles are included in the appendices, with permissions obtained from the respective publishers. In addition, parts of this dissertation, specifically selected sections of Chapter 1 through Chapter 5 and Chapter 8, are adapted from the following article I authored, which is currently in press:

E. Opoku, F. Pawłowski and J. V. Ortiz, "*Green's Function Methods: Theory and Applications for Ionization Potentials and Electron Affinities", In Handbook of Electronic Structure Theory: Methods and Applications* (Editors: V. Barone and M. Hochlaf), Elsevier, Amsterdam, **2026**. *In Press*

Sections 4.5 and 4.6 are based on two ongoing research projects, the results of which are intended for publication at a later stage. Additionally, the following article was published during the course of my PhD studies; however, its contents are not included or discussed within this dissertation:

J. C. Cruz, **E. Opoku**, S. Śmiga, I. Grabowski, J. V. Ortiz and S. Hirata, "*Performance of the Spin-Component-Scaled Methods for Energy Bands*", *Mol. Phys.*, 123, e2504545 **(2025)**.

Chapter 2

Green's Functions and Dyson's Equation

2.1 Creation and Annihilation Operators

Throughout the entire text, occupied and virtual spin−orbitals are designated respectively as *i,j,k,l* and *a,b,c,d,* while generic spin−orbitals are denoted as *p, q, r, s.*

In second quantization, the state of a many−electron system is described in terms of occupation numbers relative to a chosen one−electron basis, typically a set of orthonormal molecular spin−orbitals. Within this formalism, *creation* and *annihilation* operators provide a rigorous algebraic framework for constructing and manipulating fermionic many−body wavefunctions. Let $\{\phi_p\}$ denote a complete orthonormal set of spin−orbitals. For each spin−orbital ϕ_p, we define the *creation operator* $\hat{a}_p^\dagger$ and the *annihilation operator* $\hat{a}_p$ as follows

- The **creation operator** $\hat{a}_p^\dagger$ adds an electron to spin−orbital ϕ_p.
- The **annihilation operator** $\hat{a}_p$ removes an electron from spin−orbital ϕ_p.

These operators act on *Fock space*, which is the direct sum of all $N-$electron Hilbert spaces for $N = 0, 1, 2, \ldots$, and they obey the fermionic anti−commutation relations:

$$\{\hat{a}_p, \hat{a}_q\} = 0 \tag{2.1.1}$$

$$\{\hat{a}_p^\dagger, \hat{a}_q^\dagger\} = 0 \tag{2.1.2}$$

$$\{\hat{a}_p, \hat{a}_q^\dagger\} = \delta_{pq} \tag{2.1.3}$$

where $\{A, B\} = AB + BA$ denotes the anti−commutator, and δ_{pq} is the Kronecker delta.

When acting on a Slater determinant $|\Phi\rangle$, which is a normalized antisymmetrized product of occupied spin−orbitals, the operators yield

$$\hat{a}_p |\Phi\rangle = \begin{cases} (-1)^{n_p} |\Phi'\rangle & \text{if } \phi_p \text{ is occupied in } |\Phi\rangle \\ 0 & \text{otherwise} \end{cases} \tag{2.1.4}$$

$$\hat{a}_p^\dagger |\Phi\rangle = \begin{cases} 0 & \text{if } \phi_p \text{ is already occupied in } |\Phi\rangle \\ (-1)^{n_p} |\Phi''\rangle & \text{otherwise} \end{cases} \tag{2.1.5}$$

Here, $|\Phi'\rangle$ and $|\Phi''\rangle$ are determinants resulting from the removal or addition of spin−orbital ϕ_p, respectively, and n_p is the number of occupied orbitals preceding ϕ_p in a chosen ordering. The sign $(-1)^{n_p}$ accounts for the fermionic antisymmetry.

Creation and annihilation operators also provide a compact representation of the electronic Hamiltonian. The second−quantized form of the non−relativistic electronic Hamiltonian is

$$\hat{H} = \sum_{pq} h_{pq}\, \hat{a}_p^\dagger \hat{a}_q + \frac{1}{4} \sum_{pqrs} \langle pq||rs\rangle\, \hat{a}_p^\dagger \hat{a}_q^\dagger \hat{a}_s \hat{a}_r \tag{2.1.6}$$

where h_{pq} are the one−electron integrals and $\langle pq||rs\rangle$ are the antisymmetrized two−electron integrals. This operator formalism is foundational in electronic structure theory and underlies the formulation of methods discussed in this dissertation.

2.2 The Electron Propagator (One−Body Green's Function)

In an orthonormal spin−orbital basis, u, the elements of the Fourier transform of the one−body Green's function (electron propagator) matrix expressed in the energy domain

(spectral form) are given by

$$G_{pq}(\omega) = \lim_{\eta \to 0^+} \left[\sum_A \frac{\langle \Psi_0^N | a_p | \Psi_A^{N+1} \rangle \langle \Psi_A^{N+1} | a_q^\dagger | \Psi_0^N \rangle}{\omega + E_0^N - E_A^{N+1} + i\eta} + \sum_D \frac{\langle \Psi_0^N | a_q^\dagger | \Psi_D^{N-1} \rangle \langle \Psi_D^{N-1} | a_p | \Psi_0^N \rangle}{\omega - E_0^N + E_D^{N-1} - i\eta} \right] \tag{2.2.1}$$

Equation 2.2.1 involves two summations describing electron attachment and detachment processes, respectively. Thus, calculating electron attachment energies (electron affinities) and detachment energies (ionization energies) is equivalent to finding the poles (see denominators) of equation 2.2.1 where singularities occur. Methods and techniques for searching the electron propagator (EP) poles are discussed extensively elsewhere.[99, 100] The residues (numerators) of the poles are expressed in terms of Feynman−Dyson amplitudes,

$$f_p^A = \langle \Psi_0^N | a_p | \Psi_A^{N+1} \rangle \tag{2.2.2}$$

$$g_p^D = \langle \Psi_D^{N-1} | a_p | \Psi_0^N \rangle \tag{2.2.3}$$

for electron attachments and detachments, respectively. The integrations that define Dyson spin−orbitals for attachment and ionization processes are related to these amplitudes according to

$$\begin{aligned} \varphi_A^{\text{Dyson}}(x_1) &= \sqrt{N+1} \int \Psi_0^{N^*}(x_2, x_3, x_4, \ldots, x_{N+1})\, \Psi_A(x_1, x_2, x_3, \ldots, x_{N+1})\, dx_2\, dx_3\, dx_4 \ldots dx_{N+1} \\ &= \sum_n f_p^A u_p(x_1) \end{aligned} \tag{2.2.4}$$

$$\varphi_D^{Dyson}(x_1) = \sqrt{N} \int \Psi_D^*(x_2, x_3, x_4, \ldots, x_N) \Psi_0^N(x_1, x_2, x_3, \ldots, x_N) dx_2 dx_3 dx_4 \ldots dx_N = \sum_S g_p^D u_p(x_1) \tag{2.2.5}$$

Dyson orbitals play a crucial role in describing electronic structure and the transitions associated with electron attachment and removal processes. Unlike canonical Hartree−Fock orbitals, Dyson orbitals are not eigenfunctions of the Fock operator but instead reflect the correlated nature of the system after an electron has been attached or detached. These

orbitals are critical in interpreting experimental observables such as photoelectron spectra, where the spectral shapes and probabilities of different ionization events can be directly linked to Dyson orbitals.[101, 102]

The perturbation series for the Green's function, while useful for capturing electron correlation and orbital relaxation effects, does not present a straightforward form for directly evaluating its poles. Instead, the Dyson equation, expressed in the $\omega-$representation, offers a more practical framework for identifying these poles. In this formulation, the Green's function $\mathbf{G}(E)$ is related to its non$-$interacting counterpart $\mathbf{G}_0(E)$ through the self$-$energy $\mathbf{\Sigma}(E)$, and the poles of the system are determined by solving the Dyson equation.

$$\mathbf{G}(E) = \mathbf{G}_0(E) - \mathbf{G}_0\mathbf{\Sigma}(E)\mathbf{G}(E) \tag{2.2.6}$$

The EBEs, however, are more conveniently obtained by seeking zero eigenvalues of the inverse electron propagator matrix

$$\mathbf{G}^{-1}(E) = \mathbf{G}_0^{-1}(E) - \mathbf{\Sigma}(E) \tag{2.2.7}$$

and the Dyson orbitals are then determined by the eigenvectors corresponding to the zero eigenvalues. This approach not only facilitates the identification of EBEs but also allows for the incorporation of many$-$body effects through the self$-$energy operator, which captures the influence of electron correlation and orbital relaxation effects.

In terms of perturbation series, the Dyson equation can be expanded iteratively. Assuming the self$-$energy $\mathbf{\Sigma}(E)$ is introduced as a perturbation to the non$-$interacting Green's function $\mathbf{G}_0(E)$, the series representation for $\mathbf{G}(E)$ can be expressed as

$$\mathbf{G}(E) = \mathbf{G}_0(E) + \mathbf{G}_0(E)\Sigma(E)\mathbf{G}_0(E) + \mathbf{G}_0(E)\Sigma(E)\mathbf{G}_0(E)\Sigma(E)\mathbf{G}_0(E) + \cdots \tag{2.2.8}$$

Thus, each successive term in the perturbation series includes an additional interaction mediated by $\mathbf{\Sigma}(E)$, capturing progressively higher$-$order many$-$body effects.

In principle, the propagator matrix $\mathbf{G}_0(E)$ can be solved to the exact limit corresponding to a one−electron basis. However, some form of truncation within the self−energy part is desired to obtain practical approximate methods.

2.3 Superoperator Theory

Superoperator theory provides a convenient framework for developing approximations to the self−energy part of the Dyson equation.[103] In this formalism, the attachment and detachment summations of equation 2.2.1 are joined by a superoperator metric, which is represented by the expression

$$[A|B] = \langle \Psi_0^N | A^\dagger B + B A^\dagger | \Psi_0^N \rangle \tag{2.3.1}$$

wherein A and B are part of a set of number−non−conserving second−quantized field operator products, where the number of creation operators exceeds the number of annihilation operators by one. Examples include single−particle operators $a_p^\dagger$ (h and p), two−particle operators $a_p^\dagger a_q^\dagger a_r$ ($2hp$ and $2ph$), and higher−order terms such as three−particle operators $a_p^\dagger a_q^\dagger a_r^\dagger a_s a_t$ ($3h2p$ and $3p2h$).

Three superoperators (identity, Hamiltonian, and resolvent) are needed to derive approximate self−energies. Identity, Hamiltonian and resolvent superoperators can be defined, respectively, as

$$\hat{I} A = A \tag{2.3.2}$$

$$\hat{H} A = HA - AH \tag{2.3.3}$$

$$G(E) = (E - \hat{H})^{-1}. \tag{2.3.4}$$

The resolvent superoperator [104, 105] is used in EPT to obtain the inverse of an operator. Thus, the resolvent superoperator allows expressing the electron−propagator matrix

elements in the following form

$$G_{pq}(E) = [a_p^\dagger|(E\hat{I} - \hat{H})^{-1}a_q^\dagger]. \tag{2.3.5}$$

The resolvent superoperator is expressed in the electron propagator matrix notation as

$$\mathbf{G}(E) = [\mathbf{a}^\dagger|(E\hat{I} - \hat{H})^{-1}\mathbf{a}^\dagger]. \tag{2.3.6}$$

The inverse operator of equation 2.3.6 may be circumvented by making use of inner projection superoperator techniques introduced by Löwdin [106–109] where w operators are introduced according to

$$\mathbf{G}(E) = [\mathbf{a}^\dagger|\mathrm{w}][\mathrm{w}|(E\hat{I} - \hat{H})\mathrm{w}]^{-1}[\mathrm{w}|\mathbf{a}^\dagger]. \tag{2.3.7}$$

It is now convenient to partition the w operator manifold into sets of simple ($\mathbf{a}$), and secondary ($\mathbf{t}$) normalized field operators such that $[\mathbf{a}^\dagger|\mathbf{t}] = \mathbf{0}$, thus producing an orthogonalized complement. The inverse form of the Dyson equation can now be recast as

$$\mathbf{G}^{-1}(E) = [\mathbf{a}^\dagger|(E\hat{I} - \hat{H})\mathbf{a}^\dagger] - [\mathbf{a}^\dagger|\hat{H}\mathbf{t}][\mathbf{t}|(E\hat{I} - \hat{H})\mathbf{t}]^{-1}[\mathbf{t}|\hat{H}\mathbf{a}^\dagger]. \tag{2.3.8}$$

In this formalism, $\mathbf{a}$ denotes simple second quantized field operators $a_p^\dagger$ (h and p), $\boldsymbol{t}_3$ includes triple field operators ($2hp$ and $2ph$) and $\boldsymbol{t}_5$ includes quintuple field operators ($3h2p$ and $3p2h$). Thus, if one considers only primary and triple field operators, the partitioned propagator matrix can now be expressed as

$$\mathbf{G}(E) = \begin{bmatrix} 1 & 0 \end{bmatrix} \begin{bmatrix} E\mathbf{1} - (\mathbf{a} \mid \hat{H}\mathbf{a}) & -(\mathbf{a} \mid H\mathbf{t}_3) \\ -(\mathbf{t}_3 \mid \hat{H}\mathbf{a}) & E\mathbf{1} - (\mathbf{t}_3 \mid H\mathbf{t}_3) \end{bmatrix}^{-1} \begin{bmatrix} \mathbf{1} \\ \mathbf{0} \end{bmatrix}. \tag{2.3.9}$$

With the partitioned spaces, poles of the EP are obtained when values of E are equal to the eigenvalues, ω, of an Hamiltonian superoperator matrix [16, 110] for which the eigenvalue problem is formulated as,

$$\hat{\mathbf{H}}\mathbf{U} = \omega\mathbf{U} \tag{2.3.10}$$

and explicitly rendered as,

$$\begin{bmatrix} \left(\mathbf{a} \mid \hat{H}\mathbf{a}\right) & \left(\mathbf{a} \mid \hat{H}\mathbf{t}_3\right) \\ \left(\mathbf{t}_3 \mid \hat{H}\mathbf{a}\right) & (\mathbf{t}_3 \mid \hat{H}\mathbf{t}_3) \end{bmatrix} \begin{bmatrix} U_a \\ U_t \end{bmatrix} = \omega_n \begin{bmatrix} U_a \\ U_t \end{bmatrix}. \tag{2.3.11}$$

2.4 Dyson's Equation and Hartree−Fock Theory

The relationship between HF theory and the Dyson equation may be obtained by recognizing that

$$[a_p^\dagger|\hat{H}a_q^\dagger] = h_{pq}^{(1)} + \sum_{rs} \langle pr||qs\rangle \rho_{rs} = F_{pq}^{HF} \tag{2.4.1}$$

where $\mathbf{F}^{\mathrm{HF}}$ is a generalized Fock matrix with the usual one−electron ($h^{(1)}$) and anti−symmetrized, two−electron matrix elements, and ρ is the one−electron reduced−density matrix of the reference state. In a spin−orbital basis that diagonalizes a one−electron operator $h^{(1)} + v$ with eigenvalues e^v, the inverse electron propagator matrix can be defined in a reference form that is strictly diagonal,

$$\mathbf{G}_0^{-1}(E) = E\mathbf{1} - \mathbf{e}^v. \tag{2.4.2}$$

This choice leads to an inverse Dyson equation of the form

$$\mathbf{G}^{-1}(E) = \mathbf{G}_0^{-1}(E) - \mathbf{\Sigma}(E) \tag{2.4.3}$$

where the self−energy matrix, $\mathbf{\Sigma}(E)$, consists of both energy−independent (constant) and energy−dependent components according to

$$\mathbf{\Sigma}(E) = \mathbf{F} - \mathbf{h^{(1)}} - \mathbf{v} + [\mathbf{a}^\dagger|\hat{H}\mathbf{t}][\mathbf{t}|(E\hat{I} - \hat{H})\mathbf{t}]^{-1}[\mathbf{t}|\hat{H}\mathbf{a}^\dagger]. \tag{2.4.4}$$

When v corresponds to the usual Coulomb−exchange potential of a HF reference state, the self−energy operator can take the following form

$$\mathbf{\Sigma}(E) = \mathbf{\Sigma}(\infty) + [\mathbf{a}^\dagger|\hat{H}\mathbf{t}][\mathbf{t}|(E\hat{I} - \hat{H})\mathbf{t}]^{-1}[\mathbf{t}|\hat{H}\mathbf{a}^\dagger] \tag{2.4.5}$$

where elements of the energy−independent part of the self−energy matrix,

$$\Sigma_{pq}(\infty) = \sum_{rs} \langle pr||qs\rangle(\rho_{rs} - \rho_{rs}^{HF}) \tag{2.4.6}$$

depend only on the correlation contributions to the one−electron density matrix. This uncorrelated choice of v facilitates the analysis of results in terms of final−state orbital relaxation and differential correlation effects, both of which are explicitly confined to the self−energy matrix.

Note that the sum of the first three terms in Equation 2.4.4 vanishes through second order in the fluctuation potential and, at higher orders, corresponds to the energy−independent contributions in Equation 2.4.6. In contrast, eigenfunctions derived from alternative potentials designed to incorporate exchange or correlation effects in ground−state calculations generally lead to non−diagonal, energy−independent first−order terms in the self−energy. These terms explicitly involve the non−local HF exchange operator, as described in Equation 2.4.5.

For all choices of orbital bases, poles of $\mathbf{G}(E)$, or zeroes of $\mathbf{G}^{-1}(E)$, occur at energies (E_X) where the quasiparticle eigenvalue equation is satisfied:

$$\mathbf{F} + \mathbf{\Sigma}(E_X)]\mathbf{C}(E_X) = E_X\mathbf{C}(E_X). \tag{2.4.7}$$

The pole strength (probability factor), Π, equals the norm of the Dyson spin−orbital and may be determined with

$$\Pi_X = \int |\varphi^{Dyson}(x)|^2 dx = (1 - \mathbf{C}^{\dagger}(E_X)[\frac{d\mathbf{\Sigma}(E)}{dE}]_{E=E_X}\mathbf{C}(E_X))^{-1}. \tag{2.4.8}$$

Elements of the eigenvectors are related to Feynman−Dyson amplitudes and Dyson spin−orbitals via

$$\varphi_X^{Dyson}(x) = \Pi_X^{0.5}\sum_p C_p(E_X)u_p(x) \tag{2.4.9}$$

2.5 Quasiparticle Theory

The quasiparticle theory considers each electron as if it were an independent particle with renormalized properties, making it possible to describe highly correlated systems by only solving single−particle−like equations. Several old and recent electron−propagator methods use canonical HF spin−orbitals as their zeroth order and neglect off−diagonal couplings in the self−energy matrix elements. In these methods, each canonical spin−orbital independently produces a unique set of electron binding energies, determined iteratively via the diagonal quasiparticle equation

$$e_p^{HF} + \Sigma_{pp}(E_{Xp}) = E_{Xp}. \tag{2.5.1}$$

Thus, canonical HF orbital energies (e_p^{HF}) are refined by the diagonal elements of the self−energy matrix. Probability factors are given by

$$\Pi_{Xp} = [1 - \frac{d\Sigma_{pp}(E)}{dE}|_{E=E_{Xp}}]^{-1} \tag{2.5.2}$$

and the Dyson spin−orbitals are proportionally related to the canonical HF spin−orbitals

$$\varphi_{Xp}^{Dyson}(x) = \Pi_{Xp}^{0.5} u_p^{HF}(x). \tag{2.5.3}$$

In principle, multiple roots (E_{Xp}) may be obtained for a given p, but only those with probability factors ≥ 0.85 are acceptable within the quasiparticle framework. The remaining electron binding energies may have some qualitative meaning, but are likely to require improvements from renormalized, non−diagonal self−energy approximations that have the appropriate treatment of shakeup characters for correlation states.

Chapter 3

Approximate Electron−Propagator Self−Energies

Throughout this chapter, electron repulsion integrals (ERIs) are expressed as

$$\langle \mu\nu|\hat{g}|\lambda\sigma\rangle = \iint \phi_\mu^*(\mathbf{r}_1)\phi_\nu(\mathbf{r}_2)\frac{1}{|\mathbf{r}_1-\mathbf{r}_2|}\phi_\lambda^*(\mathbf{r}_1)\phi_\sigma(\mathbf{r}_2)\,d\mathbf{r}_1\,d\mathbf{r}_2, \tag{3.0.1}$$

where $\{\phi_\mu\}$ denote the one−electron basis functions, and the operator $\hat{g}$ corresponds to the Coulomb interaction

$$\hat{g} = \frac{1}{r_{12}} = \frac{1}{|\mathbf{r}_1-\mathbf{r}_2|}. \tag{3.0.2}$$

For brevity, the shorthand notation $(\mu\nu|\lambda\sigma)$ is used interchangeably with the notation $\langle \mu\nu|\hat{g}|\lambda\sigma\rangle$ throughout the text. Thus, an antisymmetrized electron repulsion integral is defined as

$$\langle \mu\nu||\lambda\sigma\rangle = \langle \mu\nu|\hat{g}|\lambda\sigma\rangle - \langle \mu\nu|\hat{g}|\sigma\lambda\rangle \tag{3.0.3}$$

which is equivalent to

$$\langle \mu\nu||\lambda\sigma\rangle = \langle \mu\nu|\lambda\sigma\rangle - \langle \mu\nu|\sigma\lambda\rangle. \tag{3.0.4}$$

Table 3.1 displays the acronyms and full names of electron propagator methods whose self−energy expressions are derived and discussed forthwith. For each approximation, arithmetic bottlenecks are given in terms of the dimensions of the occupied (O) and virtual (V) orbital spaces in Table 3.2. Most of the self−energies have identical formulas for calculations of VIEs and VEAs. For these cases, self−energy formulae remain the same for all values of p in Equation 2.4.7. Different formulas for VIEs and VEAs apply to the P3, P3+, Q3, Q3+, RP3, RQ3, NRP3 and NRQ3 self−energies. In addition, the non−Dyson (nD) versions of D2, os−D2, OVGF, L3, L3+ and RL3 self−energies deactivate energy dependence

in *2ph* denominators for VIE calculations and in *2hp* denominators for VEA calculations. This deactivation is achieved by setting the $E = \varepsilon_p$ in the self−energy terms with these denominators.

Table 3.1: Acronyms and names of electron−propagator methods

Acronyms[a]	**Full name**
Diagonal Second Order Self−Energies	
D2	Diagonal second order
os−D2	Opposite−spin D2
nD−D2	non−Dyson D2
os−nD−D2	Opposite−spin non−Dyson D2
Diagonal Post Second Order Self−Energies	
D3	Diagonal third order
nD−D3	non−Dyson D3
OVGF	Outer−Valence Green's Function (Versions A, B and C)
nD−OVGF	non−Dyson OVGF (Versions A, B and C)
P3	Partial third order
P3+	Approximately renormalized partial third order
Q3	Quasiparticle third order
Q3+	Approximately renormalized quasiparticle third order
L3	Linear third order
nD−L3	non−Dyson L3
L3+	Approximately renormalized linear third order (Versions A, B and C)
nD−L3+	non−Dyson L3+ (Versions A, B and C)
RP3	Explicitly renormalized partial third order
RQ3	Explicitly renormalized quasiparticle third order
RL3	Explicitly renormalized linear third order
nD−RL3	non−Dyson RL3
DR	Diagonal (renormalized) ring approximation (HF−TDA−G_0W_0)
Non−diagonal Second and Post Second Order Self−energies	
ND2	Non−diagonal, second order
2*ph*−TDA	Two−particle−one−hole Tamm−Dancoff approximation
3+	Non−diagonal third order
ADC(3)	Third order algebraic diagrammatic construction
NR2	Non−diagonal, renormalized, second order
BD−T1	Brueckner doubles with triple field operators
NRP3	Non−diagonal extension of RP3
NRQ3	Non−diagonal extension of RQ3
NRL3	Non−diagonal extension of RL3

[a]For new−generation methods in **bold type**: N = non−diagonal; nD = non−Dyson; R = explicitly renormalized; + = approximately renormalized

Table 3.2: Arithmetic scaling and transformed integral requirements of electron−propagator methods.[a]

Methods[b]	Arithmetics	Steps	ERI[c]
Diagonal Second Order Self−Energies			
D2, **os−D2**	OV^2	N_E	O^2V^2
RSPT2, nD−D2, **os−nD−D2**	OV^2	Non−iterative	O^2V^2
Diagonal Post Second Order Self−Energies			
RSPT3	OV^4	Non−iterative	V^4
D3, OVGF	OV^4	N_E[d]	V^4
IP: P3, P3+, **Q3**, **Q3+**	O^2V^3	Non−iterative	OV^3
EA: P3, P3+, **Q3**, **Q3+**	OV^4	N_E	V^4
L3, **L3+**	OV^4	N_E[d]	V^4
IP: **RP3**, **RQ3**	O^2V^3	Non−iterative	OV^3
EA: **RP3**, **RQ3**	OV^4	N_IN_E	V^4
RL3	OV^4	N_IN_E[d]	V^4
DL	OV^4	N_IN_E[d]	V^4
IP: DR	O^2V^3	N_IN_E	O^2V^2
EA: DR	O^2V^3	N_IN_E	OV^3
Non−diagonal Second and Post Second Order Self−energies			
ND2	OV^3	N_I	OV^3
2ph−TDA	OV^4	N_I	V^4
3+	O^2V^4	Non−iterative	V^4
ADC(3)	O^2V^4	N_I	V^4
IP: NR2	O^3V^3	Non−iterative[f]	OV^3
EA: NR2	O^2V^4	Non−iterative[f]	V^4
BD−T1	O^2V^4	BD[e]	V^4
NRP3	O^2V^4	Non−iterative[f]	V^4
NRQ3	O^2V^4	Non−iterative[f]	V^4
NRL3	O^2V^4	Non−iterative[f]	V^4

[a]O = # occupied orbital, V = # virtual orbitals, N_E = energy iterations, N_I = inverse−expansion or linear−equation iterations for diagonal methods and Hamiltonian−vector multiplications for non−diagonal methods. [b]New methods in **bold type**. IE = ionization energy (electron detachment). EA = electron affinity (electron attachment). [c]ERI = largest electron repulsion integral set. [d]Reduction by a factor of N_E occurs in non−Dyson (nD) versions for electron detachments. [e]The O^2V^4 arithmetic bottleneck occurs in the Brueckner Doubles, coupled−cluster, reference−state calculation; the subsequent electron−propagator bottleneck is OV^4. [f] N_I OV^4 iterative steps for 3+, ADC(3) and NRL3; N_I O^3V^2 iterative steps for NR2, NRP3 and NRQ3 IEs; N_I OV^4 iterative steps for NR2, NRP3 and NRQ3 EAs.

3.1 Diagonal Second−Order Methods

Koopmans's results (canonical HF orbital energies) are employed as the zeroth order self−energy for all the diagonal methods discussed in this work. The first order energy dependent self−energy correction for the Møller−Plesset fluctuation potential vanishes. Energy independent correction terms, $\mathbf{\Sigma}(\infty)$, vanish through second order. The simplest correction to the KT result occurs in the so−called diagonal second order (D2) self−energy for which off diagonal matrix elements are completely neglected. The D2 self−energy matrix elements have two ($2hp$ and $2ph$) summations over canonical HF spin−orbitals.

$$\Sigma_{pp}^{D2}(E) = \frac{1}{2}\sum_{a}^{vir}\sum_{ij}^{occ}\frac{|\langle pa||ij\rangle|^2}{E + e_a - e_i - e_j} + \frac{1}{2}\sum_{i}^{occ}\sum_{ab}^{vir}\frac{|\langle pi||ab\rangle|^2}{E + e_i - e_a - e_b} = S_{2hp} + S_{2ph}. \quad (3.1.1)$$

Energy dependence is omitted in the S_{2hp} and S_{2ph} notations that represent the summations associated with two−hole−one−particle ($2hp$) and two−particle−one−hole ($2ph$) operators. When both the first and second terms of equation 3.1.1 are evaluated at $E = \varepsilon_p$, the resulting expression equals the second−order, Rayleigh−Schrödinger perturbation theory (RSPT2) value.[6, 111, 112] The D2 method has an iterative OV^2 (O and V denote occupied and virtual orbital dimensions) arithmetic bottleneck. Numerous benchmarks studies (*vide infra*) provide evidence that this method typically underestimates detachment energies while overestimating VEAs.

In several modified self−energy formulations that preserve the cubic arithmetic scaling of the D2 method, empirically adjusted weights have been assigned to the same−spin and opposite−spin terms in both summations.[113–116] To ameliorate the deficiency of D2 without introducing adjustable or empirical parameters, modification can be made to the D2 self−energy by separating the matrix components into same−spin (ss) and opposite−spin (os) contributions

$$\Sigma_{pp}^{D2}(E) = \Sigma_{pp}^{ss(2)}(E) + \Sigma_{pp}^{os(2)}(E). \quad (3.1.2)$$

The D2 self−energy can then be expressed in an extended notation in which capital letters denote spin−orbitals with spin opposite to that of p whereas small letters denote same−spin orbitals,

$$\begin{aligned}\Sigma_{pp}^{D2}(E) = &\frac{1}{2}\sum_{a}^{vir}\sum_{ij}^{occ}\frac{|\langle pa||ij\rangle|^2}{E+\epsilon_a-\epsilon_i-\epsilon_j} \\ &+\frac{1}{2}\sum_{i}^{occ}\sum_{ab}^{vir}\frac{|\langle pi||ab\rangle|^2}{E+\epsilon_i-\epsilon_a-\epsilon_b} \\ &+\sum_{A}^{vir}\sum_{iJ}^{occ}\frac{|\langle pA|iJ\rangle|^2}{E+\epsilon_A-\epsilon_i-\epsilon_J} \\ &+\sum_{I}^{occ}\sum_{aB}^{vir}\frac{|\langle pI|aB\rangle|^2}{E+\epsilon_I-\epsilon_a-\epsilon_B}.\end{aligned} \tag{3.1.3}$$

Thus, the first two terms correspond to same−spin contributions and the last two terms pertain to opposite−spin terms. A cleaner modification to the D2 self−energy leverages Fermi correlation treated at the HF level through the antisymmetric reference determinant and only adds the opposite−spin self−energy to provide a balanced treatment of exchange and correlation.[91] The resulting opposite−spin, second−order self−energy is labeled as os−D2.

$$\Sigma_{pp}^{os-D2}(E) = \sum_{A}^{vir}\sum_{iJ}^{occ}\frac{|\langle pA|iJ\rangle|^2}{E+\epsilon_A-\epsilon_i-\epsilon_J} + \sum_{I}^{occ}\sum_{aB}^{vir}\frac{|\langle pI|aB\rangle|^2}{E+\epsilon_I-\epsilon_a-\epsilon_B}. \tag{3.1.4}$$

Other modifications to D2 and os−D2 require that the S_{2hp} and S_{2ph} summations be analytically decoupled to obtain non−Dyson (nD) variants. The resulting nD−D2 method is equivalent to D2, except that the second (S_{2ph}) term is energy−independent, using $E = \varepsilon_p$ for electron detachments. An analogous modification that is applicable to os−D2 produce the os−nD−D2 self−energy. These modifications bestow on the nD−D2 and os−nD−D2 methods a minor computational advantage in detachment energy calculations as the OV^2 arithmetic bottleneck is no longer energy−dependent, thus eliminating iterative requirements.

The roles of the S_{2hp} and S_{2ph} summations reverse in VEA calculations. For VEA calculations, the O^2V ($2hp$) term similarly bypasses iteration, though the computational gain is minimal. Practically, the primary bottleneck lies in the ERI transformation to the canonical HF basis, where the computational scaling can be reduced from fifth to fourth power for a given orbital index p.

3.2 Simplified Renormalized Diagonal Ring and Ladder Approximations

Several members of the GW family of self−energy methods incorporate infinite−order summation of rings while neglecting exchange terms.[28] Another alternative, commonly referred to as the T−matrix method, retains ladders and neglects ring and ring−exchange terms. Although most of the GW methods use Kohn−Sham reference orbitals, there are a few instances where HF orbitals are used instead. There is a recent derivation of GW approximations that considers ring and ladder renormalizations using HF orbitals within the framework of the random−phase approximation.[117]

Here I present two straightforward simplifications to the *2ph*−TDA [21] self−energy. Take note that the first−order couplings between $\mathbf{t_3}$ operators in the *2ph*−TDA self−energy,

$$\mathbf{\Sigma}^{2ph-TDA}(E) = [\mathbf{a}^\dagger|\hat{H}\mathbf{t}_3]_1[\mathbf{t}_3|(E\hat{I} - \hat{H})\mathbf{t}_3]_1^{-1}[\mathbf{t}_3|\hat{H}\mathbf{a}^\dagger]_1, \tag{3.2.1}$$

generate ring and ladder terms of all orders with anti−symmetrized vertices. These vertices are defined through ERIs as (see equations 3.0.1 – 3.0.4 for definition of ERIs)

$$\langle pq||rs\rangle = \langle pq|rs\rangle - \langle pq|sr\rangle. \tag{3.2.2}$$

A simplified self−energy called **diagonal (renormalized) ring (DR)** [96] can be obtained by the following considerations to equation 3.2.1 (*2ph*−TDA self−energy)

- neglecting off−diagonal elements of the *2ph*−TDA self−energy

- omitting ladder and ring−exchange terms in the $[\mathbf{t}_3|(E\hat{I}-\hat{H})\mathbf{t}_3]_1$ matrix
- discarding the exchange terms in the $[\mathbf{a}^\dagger|\hat{H}\mathbf{t}_3]_1$ and $[\mathbf{t}_3|\hat{H}\mathbf{a}^\dagger]_1$ matrices.

The resulting DR self−energy retains a subset of the terms appearing in Equation 3.2.1. Thus, only terms appearing in bold orbital indices (of the *2ph*−TDA self−energy) in equations 3.2.3–3.2.8 are retained.

$$[a_p^\dagger|\hat{H}a_a a_i^\dagger a_j^\dagger]_1 = \langle \mathbf{pa}|\mathbf{ij}\rangle - \langle pa|ji\rangle \tag{3.2.3}$$

$$[a_p^\dagger|\hat{H}a_i a_a^\dagger a_b^\dagger]_1 = \langle \mathbf{pi}|\mathbf{ab}\rangle - \langle pi|ba\rangle \tag{3.2.4}$$

$$[a_a a_i^\dagger a_j^\dagger|\hat{H}_0 a_b a_k^\dagger a_l^\dagger]_0 = \boldsymbol{\delta}_{\mathbf{ab}}\boldsymbol{\delta}_{\mathbf{ik}}\boldsymbol{\delta}_{\mathbf{jl}}(\boldsymbol{\epsilon}_{\mathbf{i}} + \boldsymbol{\epsilon}_{\mathbf{j}} - \boldsymbol{\epsilon}_{\mathbf{a}}) \tag{3.2.5}$$

$$[a_i a_a^\dagger a_b^\dagger|\hat{H}_0 a_j a_c^\dagger a_d^\dagger]_0 = \boldsymbol{\delta}_{\mathbf{ij}}\boldsymbol{\delta}_{\mathbf{ac}}\boldsymbol{\delta}_{\mathbf{bd}}(\boldsymbol{\epsilon}_{\mathbf{a}} + \boldsymbol{\epsilon}_{\mathbf{b}} - \boldsymbol{\epsilon}_{\mathbf{i}}) \tag{3.2.6}$$

$$[a_a a_i^\dagger a_j^\dagger|\hat{V}a_b a_k^\dagger a_l^\dagger]_1 = (1-P_{ij})(1-P_{kl})\delta_{ik}[\langle bj|al\rangle - \langle \mathbf{bj}|\mathbf{la}\rangle] - \delta_{ab}\langle ij||kl\rangle \tag{3.2.7}$$

$$[a_i a_a^\dagger a_b^\dagger|\hat{V}a_j a_c^\dagger a_d^\dagger]_1 = -(1-P_{ab})(1-P_{cd})\delta_{ac}[\langle jb|id\rangle - \langle \mathbf{jb}|\mathbf{di}\rangle] + \delta_{ij}\langle ab||cd\rangle \tag{3.2.8}$$

An alternative method called **diagonal (renormalized) ladders (DL)** [96] also neglects off−diagonal matrix elements, retains ladders, neglects ring and ring−exchange terms in the $[\mathbf{t}_3|(E\hat{I}-\hat{H})\mathbf{t}_3]_1$ matrix while keeping the exchange terms in the $[\mathbf{a}^\dagger|\hat{H}\mathbf{t}_3]_1$ and $[\mathbf{t}_3|\hat{H}\mathbf{a}^\dagger]_1$ matrices. Thus, terms appearing in bold indices in equations 3.2.9 – 3.2.14 are retained in the DL approximation.

$$[a_p^\dagger|\hat{H}a_a a_i^\dagger a_j^\dagger]_1 = \langle \mathbf{pa}|\mathbf{ij}\rangle - \langle \mathbf{pa}|\mathbf{ji}\rangle \tag{3.2.9}$$

$$[a_p^\dagger|\hat{H}a_i a_a^\dagger a_b^\dagger]_1 = \langle \mathbf{pi}|\mathbf{ab}\rangle - \langle \mathbf{pi}|\mathbf{ba}\rangle \tag{3.2.10}$$

$$[a_a a_i^\dagger a_j^\dagger|\hat{H}_0 a_b a_k^\dagger a_l^\dagger]_0 = \boldsymbol{\delta}_{\mathbf{ab}}\boldsymbol{\delta}_{\mathbf{ik}}\boldsymbol{\delta}_{\mathbf{jl}}(\boldsymbol{\epsilon}_{\mathbf{i}} + \boldsymbol{\epsilon}_{\mathbf{j}} - \boldsymbol{\epsilon}_{\mathbf{a}}) \tag{3.2.11}$$

$$[a_i a_a^\dagger a_b^\dagger|\hat{H}_0 a_j a_c^\dagger a_d^\dagger]_0 = \boldsymbol{\delta}_{\mathbf{ij}}\boldsymbol{\delta}_{\mathbf{ac}}\boldsymbol{\delta}_{\mathbf{bd}}(\boldsymbol{\epsilon}_{\mathbf{a}} + \boldsymbol{\epsilon}_{\mathbf{b}} - \boldsymbol{\epsilon}_{\mathbf{i}}) \tag{3.2.12}$$

$$[a_a a_i^\dagger a_j^\dagger|\hat{V}a_b a_k^\dagger a_l^\dagger]_1 = (1-P_{ij})(1-P_{kl})\delta_{ik}[\langle bj|al\rangle - \langle bj|la\rangle] - \boldsymbol{\delta}_{\boldsymbol{ab}}\langle \mathbf{ij}||\mathbf{kl}\rangle \tag{3.2.13}$$

$$[a_i a_a^\dagger a_b^\dagger | \hat{V} a_j a_c^\dagger a_d^\dagger]_1 = -(1-P_{ab})(1-P_{cd})\delta_{ac}[\langle jb|id\rangle - \langle jb|di\rangle] + \boldsymbol{\delta_{ij}}\langle \mathbf{ab}||\mathbf{cd}\rangle \quad (3.2.14)$$

Note that in both DR and DL methods, the Hamiltonian superoperator consists of the sum of the $\hat{H}_0$ and $\hat{V}$ superoperators. Equations 3.2.5, 3.2.6, 3.2.11 and 3.2.12 assume that i<j and k<l. This convention avoids the need to substitute $\delta_{ik}\ \delta_{jl} - \delta_{il}\ \delta_{jk}$ for $\delta_{ik}\ \delta_{jl}$ in these equations.

3.3 Diagonal Full Third Order Approximation

There are eight terms that appear in the diagonal third order (D3) self−energy.[20] Adopting a previous [91] notation, self−energy matrix elements can be expressed as

$$D3 = S_{2hp} + S_{2ph} + C_D + C_S + R_{2hp} + R_{2ph} + P_{2hp} + P_{2ph}. \quad (3.3.1)$$

The D3 self−energy retains all diagonal matrix elements up to third order. The first two terms (S_{2hp}+S_{2ph}) of equation 3.3.1 pertain to D2 matrix elements as shown in equation 3.1.1. The contributions are constant terms arising from first−order double and second−order single substitutions in the reference canonical HF state. The next two terms $R_{2hp} + R_{2ph}$ are the ring and ladder contributions. The last two terms $P_{2hp} + P_{2ph}$ arise from perturbative first−order replacements. The R and P contributions have energy dependence that is suppressed in this notation. The $R_{2hp} + R_{2ph}$ terms have two energy dependent denominators whereas $P_{2hp} + P_{2ph}$ contain terms that are Hermitian conjugates.

A non−Dyson D3 (nD−D3) approach establishes that the energy−dependent two−particle hole ($2ph$) terms in the D3 self−energy are assigned to $E = \varepsilon_p$, which represents the unperturbed HF orbital energy for electron removals. For electron attachment, $E = \varepsilon_p$ applies to the two−hole particle ($2hp$) terms. Thus, the energy dependent $2ph$ and $2hp$ terms of the self−energy are analytically decoupled in nD−Dyson methods. In the third−order Rayleigh−Schrödinger perturbation theory (RSPT3), the energy dependent terms in both

the $2ph$ and $2hp$ summations are kept at $E = \varepsilon_p$.[6, 111, 112] Thus, the attachment and detachment parts of the self−energy are still present but there are no energy iterations.

All eight terms appearing in the D3 self−energy have the following explicit matrix elements in a real spin−orbitals basis.

$$S_{2hp} = \frac{1}{2}\sum_{a}^{vir}\sum_{ij}^{occ}\frac{|\langle pa||ij\rangle|^2}{E + e_a - e_i - e_j} \tag{3.3.2}$$

$$S_{2ph} = \frac{1}{2}\sum_{i}^{occ}\sum_{ab}^{vir}\frac{|\langle pi||ab\rangle|^2}{E + e_i - e_a - e_b} \tag{3.3.3}$$

$$C_D = \frac{1}{2}\sum_{ab}\langle ap||bp\rangle\sum_{ijc} t_{ij}^{ac(1)} t_{ij}^{bc(1)} - \frac{1}{2}\sum_{ij}\langle ip||jp\rangle\sum_{abk} t_{ik}^{ab(1)} t_{jk}^{ab(1)} \tag{3.3.4}$$

$$C_S = 2\sum_{ia}\langle ip||ap\rangle t_i^{a(2)} \tag{3.3.5}$$

$$R_{2hp} = \sum_{ai<j}\frac{U_{paij}(E)\langle ij||pa\rangle}{E + \epsilon_a - \epsilon_i - \epsilon_j} \tag{3.3.6}$$

where

$$U_{paij}(E) = -\sum_{k<l}\frac{\langle pa||kl\rangle\langle kl||ij\rangle}{E + \epsilon_a - \epsilon_k - \epsilon_l} - (1 - P_{ij})\sum_{kb}\frac{\langle pb||jk\rangle\langle ak||bi\rangle}{E + \epsilon_b - \epsilon_j - \epsilon_k}. \tag{3.3.7}$$

$$R_{2ph} = \sum_{ia<b}\frac{U_{piab}(E)\langle ab||pi\rangle}{E + \epsilon_i - \epsilon_a - \epsilon_b}, \tag{3.3.8}$$

where

$$U_{piab}(E) = \sum_{c<d}\frac{\langle pi||cd\rangle\langle cd||ab\rangle}{E + \epsilon_i - \epsilon_c - \epsilon_d} + (1 - P_{ab})\sum_{jc}\frac{\langle pj||bc\rangle\langle ic||ja\rangle}{E + \epsilon_j - \epsilon_b - \epsilon_c}. \tag{3.3.9}$$

$$P_{2hp} = 2\sum_{ai<j}\frac{\langle pa||ij\rangle W_{paij}}{E + \epsilon_a - \epsilon_i - \epsilon_j}, \tag{3.3.10}$$

where

$$W_{paij} = \sum_{b<c} t_{ij}^{bc(1)}\langle bc||pa\rangle + (1 - P_{ij})\sum_{kb} t_{jk}^{ba(1)}\langle bi||pk\rangle \tag{3.3.11}$$

$$P_{2ph} = 2\sum_{ia<b} \frac{\langle pi||ab\rangle W_{piab}}{E + \epsilon_i - \epsilon_a - \epsilon_b}, \tag{3.3.12}$$

where

$$W_{piab} = -\sum_{j<k} t_{jk}^{ab(1)} \langle jk||pi\rangle - (1 - P_{ab}) \sum_{jc} t_{ji}^{bc(1)} \langle ja||pc\rangle. \tag{3.3.13}$$

3.4 Outer−Valence Green's Function (OVGF) Method

The extension of the self−energy component to third order in perturbation theory (D3) was immediately assessed numerically in several studies. Unfortunately, it did not yield satisfactory numerical results and improved self−energies were sought after. In 1975, Cederbaum used diagrammatic arguments to introduce renormalized interaction terms that estimate higher many−body effects in the self−energy.[118] The renormalization interaction is based on computationally trivial estimates of higher−order effects that are based on the second and third order terms. Three versions (A, B, C) of the renormalizations were proposed for the outer valence Green's function (OVGF).[30]

The formula for each of the three OVGF self−energies can be given in a similar manner to the D3 notation. The A version reads,

$$\Sigma^{OVGF-A} = S_{2hp} + S_{2ph} + \frac{S_{2hp} + S_{2ph}}{S_{2hp} + S_{2ph} - P_{2hp} - P_{2ph}} (C_D + C_S + R_{2hp} + R_{2ph} + P_{2hp} + P_{2ph}). \tag{3.4.1}$$

Notice that the renormalization treatment is carried out over all constant, ring, ladder and perturbative terms. The B version adopts a more uniform approach in the renormalization. Energy independent terms are excluded while separating the R and P terms into their respective $2hp$ and $2ph$ components,

$$\Sigma^{OVGF-B} = S_{2hp} + S_{2ph} + C_D + C_S + \frac{S_{2hp}}{S_{2hp} - P_{2hp}} (R_{2hp} + P_{2hp}) + \frac{S_{2ph}}{S_{2ph} - P_{2ph}} (R_{2ph} + P_{2ph}). \tag{3.4.2}$$

In analogy to version A, the C version also performs renormalizations over all post second−order terms. However, the nature of the renormalization terms differs from version A.

$$\begin{aligned}\Sigma^{\text{OVGF-C}} = S_{2hp} + S_{2ph} \\ + \frac{R_{2hp} + R_{2ph} + P_{2hp} + P_{2ph}}{\frac{S_{2hp} - P_{2hp}}{S_{2hp}}(R_{2hp} + P_{2hp}) + \frac{S_{2ph} - P_{2ph}}{S_{2ph}}(R_{2ph} + P_{2ph})} \\ \times (C_D + C_S + R_{2hp} + R_{2ph} + P_{2hp} + P_{2ph})\end{aligned} \tag{3.4.3}$$

The OVGF method has the same OV^4 arithmetic scaling as D3. At the end of D3 calculation, pole contributions from second and third order terms are used to perform the computationally trivial estimates of higher order terms. Similar arguments for nD−D3 suffice to derive nD−OVGF for electron attachments and detachments.

3.5 Diagonal Linear Third Order Methods

My contributions to developments[91, 92] have focused on deriving new electron−propagator methods that retain the conceptual clarity discussed so far while achieving increased accuracy and efficiency. Thus, no adjustable or empirical parameters are tolerated in deriving the new self−energies. Therefore, the new class of methods has been derived using the superoperator metric below that enforces Hermiticity and intermediate normalization,

$$[A|B] = \frac{1}{2}(\langle HF|(A^\dagger B + BA^\dagger)(1 + T_2^{(1)} + T_1^{(2)})|HF\rangle + \langle HF|(1 + T_2^{(1)} + T_1^{(2)})^\dagger (A^\dagger B + BA^\dagger)|HF\rangle). \tag{3.5.1}$$

This choice of superoperator metric starts with a HF wavefunction and adds perturbative corrections. Examples of A and B in the square brackets include simple and triple second−quantized field operators, h, p, $2hp$ or $2ph$. The $T_2{}^{(1)}$ and $T_1{}^{(2)}$ terms incorporate

first−order, double and second−order, single replacements, respectively, with the following explicit formulae

$$T_2^{(1)} = \frac{1}{4}\sum_{ij}^{occ}\sum_{ab}^{vir}\frac{\langle ij||ab\rangle}{e_i+e_j-e_a-e_b}a_a^\dagger a_b^\dagger a_i a_j = \frac{1}{4}\sum_{ij}^{occ}\sum_{ab}^{vir} t_{ij}^{ab(1)} a_a^\dagger a_b^\dagger a_i a_j \tag{3.5.2}$$

$$T_1^{(2)} = \sum_{i}^{occ}\sum_{a}^{vir}\frac{1}{2(e_i-e_a)}(\sum_{jk}^{occ}\sum_{b}^{vir} t_{jk}^{ab(1)}\langle bi||jk\rangle + \sum_{j}^{occ}\sum_{bc}^{vir} t_{ij}^{bc(1)}\langle bc||aj\rangle)a_a^\dagger a_i = \sum_{i}^{occ}\sum_{a}^{vir} t_i^{a(2)} a_a^\dagger a_i. \tag{3.5.3}$$

This choice of superoperator metric suffices to generate all third−order matrix elements that occur linearly in the reference state substitutions as well as ring and ladder renormalizations. Note that the perturbation terms in the superoperator metric are denoted as $T_n^{(m)}$ where n indicates the level of excitation and m represents the order of the excitation. In principle, $T_n^{(m)}$ can be expanded to include several excitations and orders in the following fashion,

$$T = T_2^{(1)} + T_1^{(2)} + T_2^{(2)} + T_3^{(2)} + T_4^{(2)} + \cdots . \tag{3.5.4}$$

However, only the lowest−order linear parametrization of the HF wavefunction is preserved for single and double substitutions. Double substitutions contribute at first order, while single substitutions appear at second order, as their first−order terms vanish.

In the **diagonal explicitly renormalized linear third order (RL3)[91, 92] method**, all linear third order, ring−ladder terms, and higher order terms obtained upon expansion of the inverted matrices are retained,

$$\begin{aligned}\mathbf{\Sigma}^{\mathrm{RL3}}(E) = \frac{1}{2}\Big(&\mathbf{C}_S + [\mathbf{a}^\dagger|\hat{H}\mathbf{t}_{2ph}]_2\left[\mathbf{t}_{2ph}|(E\hat{I}-\hat{H})\mathbf{t}_{2ph}\right]_1^{-1}[\mathbf{t}_{2ph}|\hat{H}\mathbf{a}^\dagger]_1 \\ &+ [\mathbf{a}^\dagger|\hat{H}\mathbf{t}_{2ph}]_1\left[\mathbf{t}_{2ph}|(E\hat{I}-\hat{H})\mathbf{t}_{2ph}\right]_1^{-1}[\mathbf{t}_{2ph}|\hat{H}\mathbf{a}^\dagger]_2 \\ &+ [\mathbf{a}^\dagger|\hat{H}\mathbf{t}_{2hp}]_1\left[\mathbf{t}_{2hp}|(E\hat{I}-\hat{H})\mathbf{t}_{2hp}\right]_1^{-1}[\mathbf{t}_{2hp}|\hat{H}\mathbf{a}^\dagger]_2 \\ &+ [\mathbf{a}^\dagger|\hat{H}\mathbf{t}_{2hp}]_2\left[\mathbf{t}_{2hp}|(E\hat{I}-\hat{H})\mathbf{t}_{2hp}\right]_1^{-1}[\mathbf{t}_{2hp}|\hat{H}\mathbf{a}^\dagger]_1\Big),\end{aligned} \tag{3.5.5}$$

where $\mathbf{C}_{\mathrm{S}}$ represents the non−diagonal matrix generalization of C_{S} contributions. The C_{S} is responsible for energy−independent third−order correlation contributions to the ground state. The C_{D} term which depends on first−order double replacements is excluded because of its quadratic dependence. The ring and ladder terms are independent of reference state amplitudes and are the same as those found in the *2ph*−TDA, 3+, and ADC(3) methods. However, terms that have linear dependence on the reference−state correlation amplitudes are now scaled by a factor of one−half because of the choice of superoperator metric.

Expansion of the inverted matrices in the **RL3** formula will lead to the identification of many fourth and higher order terms. When one neglects these higher order terms and restricts the inverted matrix elements to only third order, the resulting **diagonal linear third order (L3)** [91, 92] self−energy has the following formula,

$$\Sigma^{L3} = S_{2hp} + S_{2ph} + \frac{1}{2}(C_S + P_{2hp} + P_{2ph}) + R_{2hp} + R_{2ph}. \tag{3.5.6}$$

The L3 method differs from D3 in two respects. First, because the C_{D} term in D3 has a quadratic dependence on reference−state amplitudes, L3, with restrictions imposed by the new superoperator metric, completely neglects it. Also, the constant and perturbative first−order terms have factors of one−half which are absent in the D3 formula. As L3 treats $2ph$ and $2hp$ terms on the same footing, a non−Dyson version also exists based on similar arguments discussed earlier in favor of OVGF.

The **L3** method treats $2ph$ and $2hp$ terms on equal footing. Therefore, approximate renormalization of third−order terms can be carried out in analogy to OVGF. The resulting self−energy expression is called the **approximately renormalized linear third order (L3+)** [91, 92] method with versions A, B and C alternatives for calculating detachment and attachment energies defined as,

$$\Sigma^{L3+A} = S_{2hp} + S_{2ph} + \frac{S_{2hp} + S_{2ph}}{S_{2hp} + S_{2ph} - \frac{1}{2}(P_{2hp} + P_{2ph})}[\frac{1}{2}C_S + R_{2hp} + R_{2ph} + \frac{1}{2}(P_{2hp} + P_{2ph})] \tag{3.5.7}$$

$$\Sigma^{L3+B} = S_{2hp} + S_{2ph} + \frac{1}{2}C_S + \frac{S_{2hp}}{S_{2hp} - \frac{1}{2}P_{2hp}}(R_{2hp} + \frac{1}{2}P_{2hp}) + \frac{S_{2ph}}{S_{2ph} - \frac{1}{2}P_{2ph}}(R_{2ph} + \frac{1}{2}P_{2ph}) \tag{3.5.8}$$

$$\begin{aligned}\Sigma^{L3+C} = S_{2hp} + S_{2ph} + \left[\frac{1}{2}C_S + R_{2hp} + R_{2ph} + \frac{1}{2}(P_{2hp} + P_{2ph})\right] \\ \times \frac{R_{2hp} + R_{2ph} + \frac{1}{2}(P_{2hp} + P_{2ph})}{\frac{S_{2hp} - \frac{1}{2}P_{2hp}}{S_{2hp}}(R_{2hp} + \frac{1}{2}P_{2hp}) + \frac{S_{2ph} - \frac{1}{2}P_{2ph}}{S_{2ph}}(R_{2ph} + \frac{1}{2}P_{2ph})}.\end{aligned} \tag{3.5.9}$$

Here again, only two minor differences exist between OVGF formulas and the L3+ alternatives. The C_{D} term is absent and the C_{S}, P_{2hp} and P_{2ph} terms have a factor of one−half. Hence, only trivial modifications are required in codes that perform OVGF calculations to incorporate the L3+ method. The non−Dyson version of L3+ (nD−L3+) is easily derived with the same approach as nD−OVGF.

3.6 Diagonal Quasiparticle Third Order Methods

The most computationally intensive arithmetic operations in the RL3 method are the couplings between $2ph$ operators at third order and beyond, as they have ERIs with four virtual orbital indices. It has been established that these terms generally have a minimal impact on detachment energies. By omitting these terms, an **explicitly renormalized quasiparticle self−energy (RQ3)**[91, 92] is defined for detachment energy calculations,

$$\begin{aligned}\boldsymbol{\Sigma}^{\text{IP-RQ3}}(E) = \frac{1}{2}\mathbf{C}_S + \left[\mathbf{a}^\dagger\middle|\hat{H}\mathbf{t}_{2ph}\right]_1\left[\mathbf{t}_{2ph}\middle|(E\hat{I} - \hat{H})\mathbf{t}_{2ph}\right]_0^{-1}\left[\mathbf{t}_{2ph}\middle|\hat{H}\mathbf{a}^\dagger\right]_1 \\ + \frac{1}{2}\left[\mathbf{a}^\dagger\middle|\hat{H}\mathbf{t}_{2hp}\right]_2\left[\mathbf{t}_{2hp}\middle|(E\hat{I} - \hat{H})\mathbf{t}_{2hp}\right]_1^{-1}\left[\mathbf{t}_{2hp}\middle|\hat{H}\mathbf{a}^\dagger\right]_1 \\ + \frac{1}{2}\left[\mathbf{a}^\dagger\middle|\hat{H}\mathbf{t}_{2hp}\right]_1\left[\mathbf{t}_{2hp}\middle|(E\hat{I} - \hat{H})\mathbf{t}_{2hp}\right]_1^{-1}\left[\mathbf{t}_{2hp}\middle|\hat{H}\mathbf{a}^\dagger\right]_2\end{aligned} \tag{3.6.1}$$

This self−energy is denoted as IP−RQ3 to indicate the ionization potential version of RQ3. For electron attachment energies, the roles of the $2ph$ and $2hp$ terms are reversed.

Hence, an electron affinity (EA−RQ3) version of RQ3 may be defined as,

$$\begin{aligned}\boldsymbol{\Sigma}^{EA\text{-}RQ3}(E) = \frac{1}{2}\mathbf{C}_S + [\mathbf{a}^\dagger|\hat{H}\mathbf{t}_{2hp}]_1 \left[\mathbf{t}_{2hp}\middle|(E\hat{I}-\hat{H})\mathbf{t}_{2hp}\right]_0^{-1} [\mathbf{t}_{2hp}|\hat{H}\mathbf{a}^\dagger]_1 \\ + \frac{1}{2}[\mathbf{a}^\dagger|\hat{H}\mathbf{t}_{2ph}]_2 \left[\mathbf{t}_{2ph}\middle|(E\hat{I}-\hat{H})\mathbf{t}_{2ph}\right]_1^{-1} [\mathbf{t}_{2ph}|\hat{H}\mathbf{a}^\dagger]_1 \\ + \frac{1}{2}[\mathbf{a}^\dagger|\hat{H}\mathbf{t}_{2ph}]_1 \left[\mathbf{t}_{2ph}\middle|(E\hat{I}-\hat{H})\mathbf{t}_{2ph}\right]_1^{-1} [\mathbf{t}_{2ph}|\hat{H}\mathbf{a}^\dagger]_2. \end{aligned} \tag{3.6.2}$$

By neglecting terms beyond third order that emerge in the expansion of the inverted matrix of RQ3, a **quasiparticle third order (Q3)** [91, 92] method is obtained for calculating detachment energies (ionization energies) and electron attachment energies (electron affinities),

$$\Sigma^{IP-Q3} = S_{2hp} + S_{2ph} + \frac{1}{2}(C_S + P_{2hp}) + R_{2hp} \tag{3.6.3}$$

$$\Sigma^{EA-Q3} = S_{2hp} + S_{2ph} + \frac{1}{2}(C_S + P_{2ph}) + R_{2ph}. \tag{3.6.4}$$

An approximately renormalized Q3 method can also be derived that resembles the L3 and D3 methods. On examining the renormalization approaches in L3+ and OVGF, we find that only the B variant treats renormalization separately for the energy−dependent $2ph$ and $2hp$ third−order terms, as well as for the ring−ladder terms. Since we focus exclusively on the $2hp$ third−order terms in Q3 for calculating VIEs and the $2ph$ third−order terms for VEAs, the B variant of the approximate renormalization is the most suitable choice. Therefore, **approximately renormalized quasiparticle third order (Q3+)**[91, 92] expressions for VIEs and VEAs are defined as,

$$\Sigma^{IP-Q3+} = S_{2hp} + S_{2ph} + \frac{1}{2}C_S + \frac{S_{2ph}}{S_{2ph} - \frac{1}{2}P_{2hp}}(R_{2hp} + \frac{1}{2}P_{2hp}) \tag{3.6.5}$$

$$\Sigma^{EA-Q3+} = S_{2hp} + S_{2ph} + \frac{1}{2}C_S + \frac{S_{2ph}}{S_{2ph} - \frac{1}{2}P_{2ph}}(R_{2ph} + \frac{1}{2}P_{2ph}) \tag{3.6.6}$$

3.7 Diagonal Partial Third Order Methods

The **explicitly renormalized partial third order (RP3)** [91, 92] method is derived by omitting the third−order constant term, denoted as C_{S}, in the RQ3 formulation. The C_{S} term originates from second−order single replacements in the reference state and contributes primarily to ground−state correlation amplitudes. However, this term is often less critical, particularly in calculations involving electron attachments, where the correlation treatment of the final state typically has a greater impact than that of the ground state. Therefore, the resulting self−energy has the following expressions for VIEs,

$$\begin{aligned}\mathbf{\Sigma}^{IP\text{-}RP3}(E) = [\mathbf{a}^\dagger|\hat{H}\mathbf{t}_{2ph}]_1 \left[\mathbf{t}_{2ph}\middle|(E\hat{I}-\hat{H})\mathbf{t}_{2ph}\right]_0^{-1} [\mathbf{t}_{2ph}|\hat{H}\mathbf{a}^\dagger]_1 \\ + \frac{1}{2}[\mathbf{a}^\dagger|\hat{H}\mathbf{t}_{2hp}]_2 \left[\mathbf{t}_{2hp}\middle|(E\hat{I}-\hat{H})\mathbf{t}_{2hp}\right]_1^{-1} [\mathbf{t}_{2hp}|\hat{H}\mathbf{a}^\dagger]_1 \\ + \frac{1}{2}[\mathbf{a}^\dagger|\hat{H}\mathbf{t}_{2hp}]_1 \left[\mathbf{t}_{2hp}\middle|(E\hat{I}-\hat{H})\mathbf{t}_{2hp}\right]_1^{-1} [\mathbf{t}_{2hp}|\hat{H}\mathbf{a}^\dagger]_2. \end{aligned} \tag{3.7.1}$$

The VEA counterpart also has the following formula,

$$\begin{aligned}\mathbf{\Sigma}^{EA\text{-}RP3}(E) = [\mathbf{a}^\dagger|\hat{H}\mathbf{t}_{2hp}]_1 \left[\mathbf{t}_{2hp}\middle|(E\hat{I}-\hat{H})\mathbf{t}_{2hp}\right]_0^{-1} [\mathbf{t}_{2hp}|\hat{H}\mathbf{a}^\dagger]_1 \\ + \frac{1}{2}[\mathbf{a}^\dagger|\hat{H}\mathbf{t}_{2ph}]_2 \left[\mathbf{t}_{2ph}\middle|(E\hat{I}-\hat{H})\mathbf{t}_{2ph}\right]_1^{-1} [\mathbf{t}_{2ph}|\hat{H}\mathbf{a}^\dagger]_1 \\ + \frac{1}{2}[\mathbf{a}^\dagger|\hat{H}\mathbf{t}_{2ph}]_1 \left[\mathbf{t}_{2ph}\middle|(E\hat{I}-\hat{H})\mathbf{t}_{2ph}\right]_1^{-1} [\mathbf{t}_{2ph}|\hat{H}\mathbf{a}^\dagger]_2. \end{aligned} \tag{3.7.2}$$

A **partial third order (P3)** [91, 92] method is obtained when fourth and higher order terms that are recoverable from the inverted matrices of RP3 are neglected. The P3 also has different formulae for VIEs and VEAs,

$$\Sigma^{IP-P3} = S_{2hp} + S_{2ph} + \frac{1}{2}P_{2hp} + R_{2hp} \tag{3.7.3}$$

$$\Sigma^{EA-P3} = S_{2hp} + S_{2ph} + \frac{1}{2}P_{2ph} + R_{2ph}. \tag{3.7.4}$$

The P3 method was first derived and implemented in 1996 using an asymmetric superoperator metric with distinct definitions for VIE[31] and VEA.[119]

Here also, an **approximately renormalized partial third order (P3+)** [91, 92] self−energy can be defined by performing computationally simple estimates of higher−order terms, in analogy to the B versions of OVGF, L3+, as well as Q3+. There are separate formulas for VIEs and VEAs,

$$\Sigma^{IP-P3+} = S_{2hp} + S_{2ph} + \frac{S_{2ph}}{S_{2ph} - \frac{1}{2}P_{2hp}}(R_{2hp} + \frac{1}{2}P_{2hp}) \tag{3.7.5}$$

$$\Sigma^{EA-P3+} = S_{2hp} + S_{2ph} + \frac{S_{2ph}}{S_{2ph} - \frac{1}{2}P_{2ph}}(R_{2ph} + \frac{1}{2}P_{2ph}). \tag{3.7.6}$$

P3+ was first introduced in 2005[32] as an extension of P3 and has been highly successful in numerous applications.

3.8 Non−diagonal and Renormalized Electron Propagator Methods

Aside developments of new quasiparticle (diagonal) electron−propagator methods, I have also made contributions to generalized self−energies where all matrix elements (diagonal and off−diagonal) are explicitly evaluated. Dyson orbitals also appear as linear combination of reference state orbitals, and therefore suffice to produce reliable qualitative descriptions of transition processes when the quasiparticle picture is no longer valid. Methods of this class are named non−diagonal electron−propagator methods.[92]

The newly introduced non−diagonal renormalized methods (NRP3, NRQ3, and NRL3) [92] are formulated in terms of superoperator Hamiltonian couplings that recover all self−energy terms present in their diagonal, explicitly renormalized counterparts (RP3, RQ3, and RL3). A summary of the order of terms contributing to each block of the Hamiltonian $\hat{\mathrm{H}}$ is provided in Table 3.3. These approximations are also based on the Hermitized, intermediately normalized metric defined in Equation 3.6.1.

Table 3.3: Orders retained in superoperator Hamiltonian matrices ($\hat{\mathbf{H}}$) of NRP3, NRQ3 and NRL3 self−energies for hole (h), particle (p), two−hole−one−particle ($2hp$), and two−particle−one−hole ($2ph$) operators.[a,b,c,d,e,f]

$\hat{\mathbf{H}}$	h	p	$2hp$	$2ph$
h	**NRP3** 0[e] **NRQ3** 3 **NRL3** 3 ND2 0[e] 3+ 3[c]	**NRP3** 0[e] **NRQ3** 3 **NRL3** 3 ND2 0[e] 3+ 3[c]	**NRP3** 2 **NRQ3** 2 **NRL3** 2 ND2 1 3+ 2	**NRP3** 1 **NRQ3** 1 **NRL3** 2 ND2 1 3+ 2
p		**NRP3** 0[e] **NRQ3** 3 **NRL3** 3 ND2 0[e] 3+ 3[c]	**NRP3** 2[b] **NRQ3** 2 **NRL3** 2 ND2 1 3+ 2	**NRP3** 1 **NRQ3** 1 **NRL3** 2 ND2 1 3+ 2
2hp			**NRP3** 1 **NRQ3** 1 **NRL3** 1 ND2 0[d,e] 3+ 1	**NRP3** 0[e,f] **NRQ3** 0[e,f] **NRL3** 0[e,f] ND2 0[e,f] 3+ 0[f]
2ph				**NRP3** 0[e] **NRQ3** 0[e] **NRL3** 1 ND2 0[d,e] 3+ 1

[a]Evaluation of $\hat{\mathbf{H}}$ with Hermitized, intermediately normalized metric in **bold type**. [b] NR2 is the same as NRP3 except that $p-2hp$ couplings are evaluated in first instead of second order. [c]3+ is identical to strict ADC(3); other versions of ADC(3) differ in their treatment of $h-h$, $h-p$ and $p-p$ couplings. [d]*2ph*−TDA differs from ND2 by introducing first order terms in the $2hp-2hp$ and $2ph-2ph$ blocks. [e]First order terms and off−diagonal zeroth order terms vanish. CHF orbital energies of zeroth order occur in diagonal matrix elements. In the $h-h$, $p-p$ and $h-p$ blocks, second order terms also vanish. [f]The first non−vanishing $2hp-2ph$ couplings appear in second order and contribute to fourth−order and higher−order self−energies.

Older non−diagonal methods such as ND2, *2ph*−TDA, and 3+ evaluate all contributions up to a fixed order in the fluctuation potential and are often based on the unit−normalized, symmetric superoperator metric as I have discussed elsewhere.[92] Terms that are quadratic in ground−state correlation amplitudes emerge at third order in the couplings between primary creation and annihilation operators (h and p). For real orbitals, the difference between these older methods (e.g., 3+) and the newly developed approaches is limited to a factor of two in their second−order couplings between simple (h and p) operators. A similar distinction exists in their treatment of couplings between simple operators that incorporate second−order single replacement amplitudes.

The NR2 method has strong similarity to the NRP3 self−energy expression. Both methods have identical expressions in the zeroth−order and first−order terms. The only notable difference pertains to the first−order treatment of the $p-2hp$ block for which the NR2 method effectively obviates the need for ERIs involving four virtual indices.

All the methods shown in Table 3.3 use canonical HF reference states except the BD−T1 method that employs approximate Brueckner orbitals. The same set of primary and secondary field operators, h, p, $2hp$ and $2ph$, also appear in the superoperator Hamiltonian matrix. The couplings between $2ph$ and $2hp$ operators are neglected; however, the matrix elements within the $2ph-2ph$ and $2hp-2hp$ blocks remain linear in the double substitution amplitudes as well as the couplings between simple and triple operators. The pseudo−canonical Brueckner orbital energies are represented as diagonal elements in the $h-h$ and $p-p$ blocks of the generalized Fock matrix denoted as $\left[\mathbf{a}^\dagger \mid \hat{H}\mathbf{a}^\dagger\right]$. Non−vanishing couplings between h and p operators are present, as the Brillouin condition is not generally satisfied.

Chapter 4

Numerical Results: Performance of the New and Old Generation Electron−Propagtor Methods

4.1 Vertical Ionization Energies of Molecules

I have evaluated the performance of all the new and old electron−propagator methods for vertical ionization energies (VIEs) across four benchmark datasets: Cam−136−VIEs[96, 97], QTP−116−VIEs[91, 92], GW100−VIEs[94], and OPV−24−VIEs[95]. Mean absolute errors (MAEs) of KT and four second−order EP methods (D2, os−D2, nD−D2, os−nD−D2) are summarized in Table 4.1.

KT exhibited the largest errors across all datasets, with values ranging from 0.491 eV (OPV−24) to 1.445 eV (QTP−116). D2 and nD−D2 consistently underestimate VIEs in all cases. The os−D2 and os−nD−D2 methods have lower MAEs than D2 and nD−D2 and have nearly equal numbers of underestimates and overestimates. QTP−116−VIEs displayed the largest error range, with values spanning 0.235 eV (os−nD−D2) to 1.445 eV (KT). Cam−136−VIEs and GW100−VIEs exhibited a moderate error range, with values for os−D2, os−nD−D2 consistently below 0.247 eV. OPV−24−VIEs displayed the smallest

Table 4.1: MAEs (eV) of diagonal second−order electron−propagator methods versus VIE, VEDE and VEA standards.

Method[a]	**Cam-136-VIEs**[96, 97]	**QTP-116-VIEs**[91, 92]	**GW100-VIEs**[94]	**OPV-24-VIEs**[95]	**VEDEs-55**[63, 64]	**OPV-23-VEAs**[95]	**NIST-50-VEAs**[66]
KT	0.756	1.445	0.646	0.491	0.613	1.308	0.730
D2	0.380	0.594	0.511	0.425	0.482	0.387	0.179
os-D2	0.188	0.247	0.182	0.185	0.176	0.386	0.280
nD-D2	0.401	0.626	0.534	0.453	0.506	0.454	0.197
os-nD-D2	0.182	0.235	0.182	0.181	0.180	0.359	0.265

[a]New methods in **bold type.**

overall errors, with a range of 0.181 eV (os−nD−D2) to 0.491 eV (KT). The performance improvement achieved by the os−D2 and os−nD−D2 methods over their respective baselines (D2, nD−D2) is evident across all datasets. For instance, in the GW100−VIEs dataset, the error decreased from 0.51 eV (D2) to 0.18 eV (os−nD−D2), indicating a substantial enhancement in accuracy. The favorable non−iterative cubic scaling of os−nD−D2 and MAEs < 0.2 eV makes it very attractive for assigning photoelectron spectra of larger molecules.

Error measures of the diagonal third order and approximately renormalized third−order methods are displayed in Table 4.2. D3 and nD−D3 overestimate VIEs in all four benchmark sets: Cam−136−VIEs, QTP−116−VIEs, GW100−VIEs, and OPV−24−VIEs. D3 and OVGF have OV^4 arithmetic scaling but do not perform as well as the non−iterative cubically scaling os−nD−D2 method in Table 4.1. L3+, which also has the same OV^4 scaling suffices to produce MAEs below 0.1 eV in most cases. The nD−L3+ methods are as good as their L3+ counterparts with slight improvements in their accuracy and efficiency. Therefore nD−L3+ is the best method among the OV^4 scaling class of methods and can be used for definitive assignment of spectra with errors below 0.1 eV. With O^2V^3 scaling, P3+ procures MAEs near 0.15 eV in all VIEs standards. Q3+ also performs slightly better than P3+ at practically the same computational cost. Because Q3+ has better ground state correlation than P3+, it is favorably considered for routine assignment of photoelectron spectra when errors near 0.15 eV are acceptable. When considering organic systems with significant conjugation such as those in the OPV−24−VIEs set, Q3+ suffices to produce an MAE of 0.06 eV, approaching chemical accuracy.

Table 4.2: MAEs (eV) of diagonal third order and approximately renormalized electron−propagator methods versus VIE, VEDE and VEA standards.

Method[a]	**Cam-136-VIEs**[96, 97]	**QTP-116-VIEs**[91, 92]	**GW100-VIEs**[94]	**OPV-24-VIEs**[95]	**VEDEs-55**[63, 64]	**OPV-23-VEAs**[95]	**NIST-50-VEAs**[66]
D3	0.388	0.674	0.345	0.185	0.642	0.465	0.232
nD-D3	0.381	0.662	0.304	0.183	0.581	0.434	0.227
OVGF-A	0.122	0.214	0.167	0.233	0.136	0.168	0.165
OVGF-B	0.190	0.333	0.210	0.267	0.235	0.250	0.194
OVGF-C	0.197	0.345	0.167	0.127	0.249	0.254	0.183
nD-OVGF-A	0.121	0.203	0.161	0.242	0.135	0.130	0.151
nD-OVGF-B	0.184	0.319	0.191	0.277	0.212	0.211	0.183
nD-OVGF-C	0.186	0.327	0.145	0.132	0.224	0.215	0.170
P3	0.233	0.250	0.180	0.170	0.288	0.138	0.099
P3+	0.156	0.153	0.138	0.116	0.159	0.108	0.095
Q3	0.170	0.232	0.194	0.088	0.280	0.210	0.133
Q3+	0.116	0.138	0.154	0.063	0.158	0.145	0.111
L3	0.139	0.206	0.129	0.092	0.228	0.147	0.121
nD-L3	0.133	0.189	0.125	0.084	0.220	0.105	0.096
L3+A	0.100	0.124	0.152	0.189	0.125	0.071	0.107
L3+B	0.083	0.109	0.104	0.106	0.098	0.090	0.111
L3+C	0.086	0.109	0.102	0.093	0.101	0.086	0.109
nD-L3+A	0.110	0.115	0.160	0.206	0.124	0.053	0.091
nD-L3+B	0.079	0.103	0.107	0.118	0.086	0.061	0.097
nD-L3+C	0.080	0.104	0.102	0.102	0.089	0.061	0.108

[a]New methods in **bold type.**

Table 4.3: MAEs (eV) of diagonal post second order and explicitly renormalized electron−propagator methods versus VIE, VEDE and VEA standards.

Method[a]	**Cam-136-VIEs**[96, 97]	**QTP-116-VIEs**[91, 92]	**GW100-VIEs**[94]	**OPV-24-VIEs**[95]	**VEDEs-55**[63, 64]	**OPV-23-VEAs**[95]	**NIST-50-VEAs**[66]
DR	0.396	0.247	0.229	0.163	0.258	0.141	0.190
DL	0.116	0.161	0.157	0.158	0.125	0.122	0.15
nD-DL	0.110	0.151	0.159	0.168	0.125	0.131	0.15
RP3	0.130	0.122	0.158	0.112	0.129	0.098	0.118
RQ3	0.117	0.112	0.172	0.107	0.160	0.091	0.104
RL3	0.073	0.082	0.104	0.115	0.076	0.079	0.090
nD-RL3	0.075	0.081	0.111	0.127	0.081	0.057	0.093

[a]New methods in **bold type.**

Table 4.3 also displays MAEs for diagonal EP methods that involve explicit evaluation of matrix elements beyond third order in their self−energies. Of this set, DR requires the least computational effort, and it is also the least accurate in all cases. In terms of computational effort, RP3 and RQ3 have identical requirements but RQ3 performs slightly better than RP3 owing to the ground state correlation term in its self−energy formula [see equations 3.6.1 and 3.7.1]. DL and nD−DL have identical OV^4 scaling requirements as RL3 and nD−RL3, but the former does not compete favorably in terms of accuracy. Notably, RL3 and nD−RL3 systematically produce MAEs below 0.1 eV on the experimental ionization energy standard, Cam−136−VIEs, and the more challenging computational QTP−116−VIEs test set.

Error measures obtained from tests of non−diagonal EP methods are shown in Tables 4.4. Among the older methods, ND2, *2ph*−TDA, and 3+ have no practical advantage. They are relatively inaccurate and inefficient. With an iterative O2V4 scaling, ADC(3) obtains higher MAEs. NR2 and BD−T1 are older methods that produce acceptable MAEs. BD−T1 is more reliable in many unusual cases such as systems with considerable biradical character. With an MAE of 0.04 eV, BD−T1 reaches chemical accuracy on the OPV−24−VIEs and renders it very attractive on applications to organic conjugated molecules. Among the new generation methods, NRL3 notably obtains MAEs well below 0.1 eV in all cases. The

Table 4.4: MAEs (eV) of non−diagonal and renormalized electron−propagator methods versus VIE, VEDE and VEA standards.

Method[a]	**Cam-136-VIEs**[96, 97]	**QTP-116-VIEs**[91, 92]	**GW100-VIEs**[94]	**OPV-24-VIEs**[95]	**VEDEs-55**[63, 64]	**OPV-23-VEAs**[95]	**NIST-50-VEAs**[66]
ND2	0.422	0.646	0.452	0.456	0.508	0.415	0.234
2ph-TDA	0.527	0.610	0.510	0.563	0.521	0.433	0.271
3+	0.252	0.372	0.244	0.216	0.230	0.299	0.127
ADC(3)	0.211	0.343	0.161	0.115	0.201	0.096	0.104
NR2	0.123	0.097	0.157	0.119	0.123	0.095	0.153
BD-T1	0.091	0.104	0.063	0.043	0.066	0.182	0.167
NRP3	0.124	0.096	–	0.116	0.126	0.095	0.153
NRQ3	0.123	0.100	–	0.145	0.161	0.069	0.091
NRL3	0.078	0.065	–	0.142	0.079	0.063	0.059

[a]New methods in **bold type.**

consistency of its predictions makes it very attractive for generating and interpreting high quality data.

4.2 Vertical Electron Detachment Energies of Molecular Anions

Results for 55 vertical electron detachment energies (VEDE−55), obtained using quartic extrapolated complete basis set (CBS) limits from ΔCCSD(T) calculations with the aug−cc−pVTZ and aug−cc−pVQZ basis sets, are presented in Tables 4.1 — 4.4. All the calculations are based on anionic closed−shell reference HF orbitals from which electrons are detached. In Table 4.1, whereas KT mainly overestimates with an MAE of 0.6 eV, D2 produces underestimates with an MAE of 0.5 eV. Os−D2 and os−nD−D2 provide balanced predictions of underestimates and overestimates while obtaining MAEs of 0.18 eV.

The data in Table 4.2 show that D3 and OVGF are not competitive. Q3+ is slightly better than P3+ although both methods obtain MAEs near 0.15 eV. L3+ and nD−L3+ produce MAEs below 0.1 and demonstrate ideal success here as already observed on VIEs of neutral molecules. In Table 4.3, DR is the least accurate. DL and nD−DL produce MAEs near 0.12 eV with fifth−power scaling. RP3 and RQ3 obtain similar errors at a reduced cost.

Again, RL3 and nD−RL3 have MAEs well below 0.1 eV with the majority of its predicted VEDEs centered near zero.

Results in Table 4.4 clearly indicate that ND2, *2ph*−TDA and 3+ are not reliable due to their high MAEs. ADC(3) is also not competitive, especially given its demanding arithmetic operations. BD−T1 has an equal arithmetic bottleneck as ADC(3) but has a much better MAE of 0.07 eV and remains the best among the old methods. The costliest arithmetic operations of all the new non−diagonal methods involve non−iterative O^2V^4 scaling. Thus, ADC(3) with an MAE of 0.20 eV is more expensive than all the new methods. However, NRL3 outperforms ADC(3) with an MAE near 0.08 eV.

4.3 Vertical Electron Affinities of Molecules

There are two sets of standard reference values for vertical electron affinities (VEAs). The first one pertains to 23 large organic conjugated photovoltaic molecules generated with ΔCCSD(T)/aug−cc−pVDZ and denoted as OPV−23−VEAs. Secondly, I have created a dataset of 50 small, closed−shell molecules (NIST−50−VEAs) with bound final anionic states which I compiled from the NIST database. (NIST stands for the National Institute of Standards and Technology). The VEA standard reference values for these molecules have been determined using quartic extrapolated complete basis set (CBS) limits from ΔCCSD(T) calculations with the aug−cc−pVTZ and aug−cc−pVQZ basis sets.

Results from Table 4.1 show that D2 suffices to reduce KT errors severalfold. Unlike VIEs, the os−D2 and os−nD−D2 methods have no advantages for VEA calculations. Their MAEs are not better than D2. D3, OVGF, P3+, Q3+, L3+ and nD−L3+ results are shown in Table 4.2. Take note that P3+ and Q3+ have the same arithmetic scaling as D3, OVGF, and L3+ for VEA calculations. For the OPV−23−VEAs standards, only L3+ and nD−L3+ obtain MAEs below 0.1 eV. nD−L3+ A approaches chemical accuracy with an MAE of 0.05 eV. For the NIST−50−VEAs dataset, P3+ and the L3+ produce errors below 0.1 eV. Since

P3+ and L3+ have identical arithmetic bottlenecks for VEAs, there is no advantage to using P3+ instead of L3+ and its non−Dyson version.

In Table 4.3, DR is the least accurate of all in this category of methods. All the new methods obtain smaller MAEs for the OPV−23−VEAs dataset. RP3, RQ3, RL3 and nD−RL3 have identical arithmetic scaling when considering VEA calculations. Therefore, RL3 and nD−RL3 are the best methods since their errors are significantly lower. For the NIST−50−VEAs standard, only RL3 and nD−RL3 produce MAEs below 0.1 eV, vindicating its repeated success on VIEs and VEDEs.

Results on non−diagonal EP methods in Table 4.4 show that ND2, *2ph*−TDA and 3+ are obsolete as they offer no practical benefits in their usage. ADC(3) performs well on VEAs as it obtains MAEs near 0.1 eV at the cost of iterative sixth−power arithmetic contractions. BD−T1 does not produce excellent MAEs as it does for VIEs and VEDEs. Plots of histograms that have been published elsewhere[66, 95] show that BD−T1 produces very precise albeit less accurate predictions. The impressive success of NRL3 on VEAs as well as on VIEs and VEDEs suggests that the second−order couplings between $2ph$ and $2hp$ operators may be necessary in BD−T1 to obtain MAEs consistent with its performance on electron detachment energies calculations.

4.4 Vertical Electron Binding Energies of Open−Shell Atoms and Molecules

Here, I present the summary of my study[98] that evaluates the performance of various diagonal self−energy approximations within the framework of electron propagator theory for EBEs of open−shell species. Using unrestricted Hartree–Fock (UHF) spin–orbitals as the reference, the work systematically benchmarks EP methods against ΔCCSD(T) standards for atoms and molecules comprising the OM−40 dataset, with emphasis on both electron detachment and attachment energies.

4.4.1 Open−Shell Atomic Electron Binding Energies

For atomic species, detachment energies (EDEs) of 12 atoms and 7 atomic anions were compared across multiple methods. The ΔCCSD(T) benchmark yields chemical accuracy (mean absolute error, MAE ∼0.04 eV) when quintuple-ζ quality basis sets with diffuse functions are used. Koopmans's theorem (KT) gives a much larger MAE (∼0.4 eV), and although the D2 approximation improves this to ∼0.2 eV, os−nD−D2 offers no significant advantage. Among outer valence Green's function (OVGF) variants, version A performs best. Explicitly renormalized self−energies such as RL3 and nD−RL3 yield MAEs below 0.1 eV and are more competitive with ΔCCSD(T).[98]

4.4.2 Open−Shell Molecular Ionization Energies

Ionization energies (IEs) were assessed for several transition types using UHF−based ΔCCSD(T) data as a benchmark. For doublet−to−singlet transitions (i.e., ionization of doublet molecules to closed−shell cations), KT results are qualitatively incorrect in many cases, yielding a large MAE (∼1.2 eV). D2 reduces this to 0.19 eV, with OVGF and other fifth−order methods failing to surpass this improvement. Notably, methods such as L3+B and RL3 reach MAEs of 0.07—0.08 eV when closed−shell references are used, indicating that such references provide a distinct advantage over open−shell determinants.[98]

Doublet−to−triplet ionization transitions also reveal improved performance when D2 corrections are applied to KT, reducing the MAE from 0.75 eV to 0.48 eV. The os−nD−D2 method outperforms other fifth−order methods, producing an MAE of 0.18 eV. More advanced methods such as L3+B and nD−L3+B attain even lower MAEs (∼0.12–0.13 eV). Explicitly renormalized methods (RL3, nD−RL3) perform slightly worse, but still below 0.2 eV. IP−EOM−CCSD and ADC(3) show marginally better performance, although at greater computational cost.[98]

4.4.3 Open−Shell Molecular Electron Affinities

Electron affinities (EAs) were explored through transitions from doublet or triplet states to singlet or doublet anions. Direct calculation of EAs using UHF virtual β spin–orbitals is shown to be unreliable. For example, KT MAEs can exceed 2 eV. D2 and explicitly renormalized self−energies (RL3, nD−RL3) significantly lower these errors, but only the latter achieve acceptable MAEs near 0.5 eV. High−accuracy methods like IP−EOM−CCSD and ADC(3) confirm the need for non−diagonal self−energies to capture strong orbital relaxation effects in EAs.[98]

In contrast, computing electron detchament energies (EDEs) of anions yields far superior accuracy. The use of closed−shell anionic references leads to much smaller MAEs. For instance, Q3+ and L3+B achieve MAEs of 0.11 eV and 0.07 eV, respectively, while RL3 and nD−RL3 closely follow. These results even outperform UHF−based IP−EOM−CCSD and ADC(3) under equivalent conditions. This trend holds consistently across other transitions such as triplet−to−doublet or doublet−to−triplet electron detachment/attachment cases, where EDE−based approaches outshine EA−based computations.[98]

4.4.4 Performance Across Various Classes of Vertical Transitions

Aggregate error analysis across various transition classes−Singlet−Doublet IEs, Doublet EAs, Mixed−Spin IEs, and Mixed−Spin EAs−reveals that D2 and os−nD−D2 provide robust, cubically scaling approximations with MAEs typically near or below 0.2 eV. The higher−order L3+B and RL3 methods further improve accuracy at the cost of quintic computational scaling. Non−Dyson variants of these methods offer practical benefits by reducing the number of bottleneck contractions in detachment energy calculations, though they offer no advantage for attachments.[98]

The use of UHF−based diagonal self−energies generally performs well when Koopmans's identity is qualitatively valid, i.e., then the final state is dominated by a single Slater determinant and spin contamination is minimal. However, for many open−shell species with

strongly correlated initial or final states, especially those involving electron attachment to diffuse virtual orbitals, nondiagonal formulations or explicitly correlated methods are necessary to achieve chemical accuracy.[98]

4.5 Vertical Ionization Energies of Heavy−Element−Containing (HEC) Molecules

4.5.1 Introduction to VIEs of HEC Molecules

The accurate prediction of VIEs is a fundamental challenge in quantum chemistry, particularly for molecules containing heavy elements where both electron correlation, relaxation and relativistic effects become significant. Although both the new and old generation EP methods discussed so far in this work have proven effective for molecules composed of lighter elements, their applications to systems involving heavy atoms remain a virgin zone.

Relativistic effects, including scalar relativistic corrections and spin−orbit coupling (SOC), can dramatically influence the electronic structure of heavy−element−containing molecules. These effects not only alter orbital energies but also modify the character and ordering of ionized states, complicating both their computation and interpretation. There also comes the computational complexity of implementing EP methods when treating SOC explicitly which may pose substantial barriers for routine use in chemical applications.[120]

A viable compromise may involve the use of effective core potentials (pseudopotentials) in conjunction with diagonal electron propagator methods to offer a more computationally affordable alternative. Pseudopotential techniques replace the core electrons of an atom with a potential energy function. This simplifies calculations, particularly for heavier elements, by focusing on the valence electrons that are most involved in chemical reactions. Pseudopotentials can also be used to incorporate relativistic effects into the calculation.

In this project, I combine pseudopotentials with both new and established electron propagator methods. The goal is to examine their performance in capturing electron correlation and relativistic effects in heavy−element compounds, an area that has not yet been systematically assessed. This gap in the literature motivates the present study, which aims

to evaluate the reliability and accuracy of various electron propagator schemes for computing ionization energies of molecules with heavy atoms. By benchmarking against available experimental reference data[121], I assess the extent to which EPT can serve as a viable alternative for heavy−element quantum chemistry. The list of 81 heavy elements containing molecules studied here is published elsewhere.[121]

4.5.2 Results and Discussion: Experimental Reference Ionization Energies of HEC Molecules Versus Electron Propagator Methods

The data presented in Figure 4.1 show KT has the largest MAE at 0.59 eV, with D2 and os−D2 decreasing it to 0.29 eV and 0.28 eV, respectively. With favorable non−iterative cubic scaling and MAE of 0.24 eV, os−nD−D2 is a very attractive method for studying heavy−element−containing molecules. This error margin is almost identical to those obtained on the QTP VIEs standards of small and medium sized main group molecules. D3 is as bad as D2 and offers no advantage. DR's MAE is almost equal to os−nD−D2, but less efficient than the latter. All the OVGF variants and their non−Dyson versions obtain MAEs near 0.20 eV with their OV^4 scaling requirements. At the same cost, all L3+ and nD−L3+ variants procure MAEs near 0.17 eV. Q3+ and P3+ also obtain MAEs near 0.23 eV. They do not clearly surpass the non−iterative cubically scaling os−nD−D2 and therefore offer no practical advantages. The RL3 and nD−RL3 are the most accurate self−energies obtaining MAEs of 0.14 eV. A close look at the histograms reveals that RL3 and nD−RL3 have peaks largely centered near zero with maximum error at 0.60 eV. With these error margins, RL3 and nD−RL3 suffice for definitive assignment of ionization energy peaks in heavy−element−containing molecules.

The data in Figure 4.2 also show that many of the old non−diagonal EP methods (e.g., ND2, *2ph*−TDA) are not competitive as they obtain MAEs near 0.4 eV. Only BD−T1 obtains an acceptable MAE of 0.16 eV among the old non−diagonal EP methods. NRL3

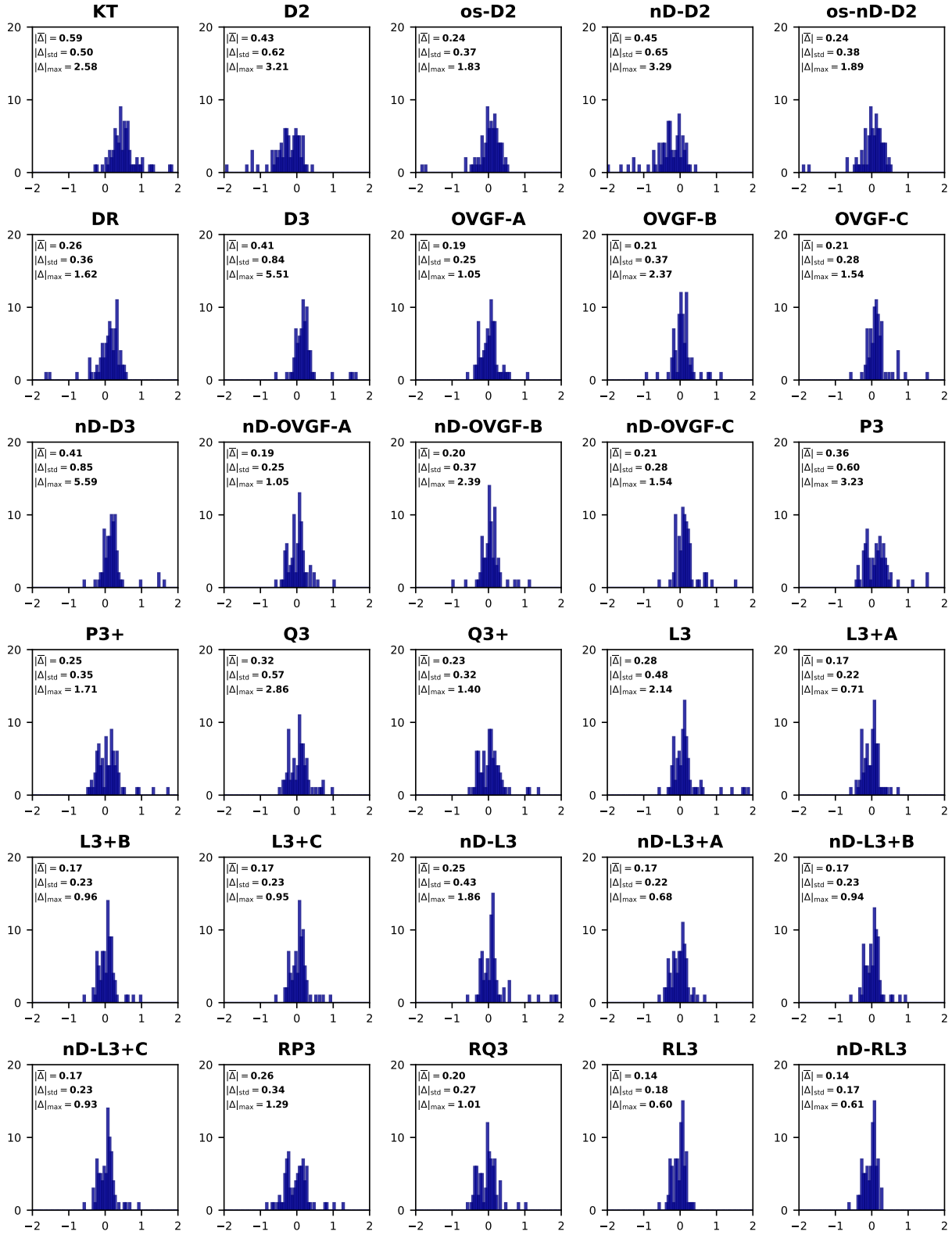


Figure 4.1: Histograms of error distributions (eV) versus experimental VIEs of 81 heavy−element−containing molecules[121]: diagonal EP methods. All calculations were executed with the def2TZVPP basis set.

is the best among the non−diagonal EP methods but its accuracy does not surpass the diagonal RL3 and nD−RL3 methods.

In summary, RL3 and nD−RL3 are the best methods when iterative OV^4 arithmetic requirements are met and MAE near 0.14 eV is desired. NRL3 is preferred when Dyson orbitals in their more generalized form are needed. nD−L3+B is the next ranking method with approximately renormalized OV^4 scaling which also produces a MAE near 0.17 eV. Q3+ follows with non−iterative O^2V^3 scaling and a MAE near 0.23 eV. The os−nD−D2 with non−iterative cubic scaling has a MAE of 0.24 eV and it is practically free following HF self−consistent−field calculations.

4.5.3 Results and Discussion: ΔCCSD(T) Reference Vertical Ionization Energies of HEC Molecules Versus Electron Propagator Methods

A close examination of the experimental reference VIEs from previous publications[120, 121] and presented in Table 4.5 indicates that each entry represents an average or estimate derived from multiple experimental measurements. As a result, these values carry inherent uncertainties that diminish their reliability as benchmarks for assessing the accuracy of emerging computational methods.

To address this limitation, I have generated a new benchmark dataset of VIEs for the HEC molecules using the ΔCCSD(T)/def2-TZVPP level of theory, also provided in Table 4.5. This method yields a mean absolute error (MAE) of 0.14 eV and a MSE of 0.03 eV relative to the available experimental standards. The strong agreement between the ΔCCSD(T)/def2-TZVPP results, and experimental data supports the use of these theoretical values as reliable reference standards for evaluating both novel and established electron propagator methods.

Figure 4.3 presents a comparison of various diagonal electron propagator methods against the ΔCCSD(T)/def2-TZVPP VIE benchmark standards. Among these methods, KT consistently overestimates ionization energies, whereas D2 tends to systematically underestimate them. The os−D2 and os−nD−D2 methods emerge as the most accurate among

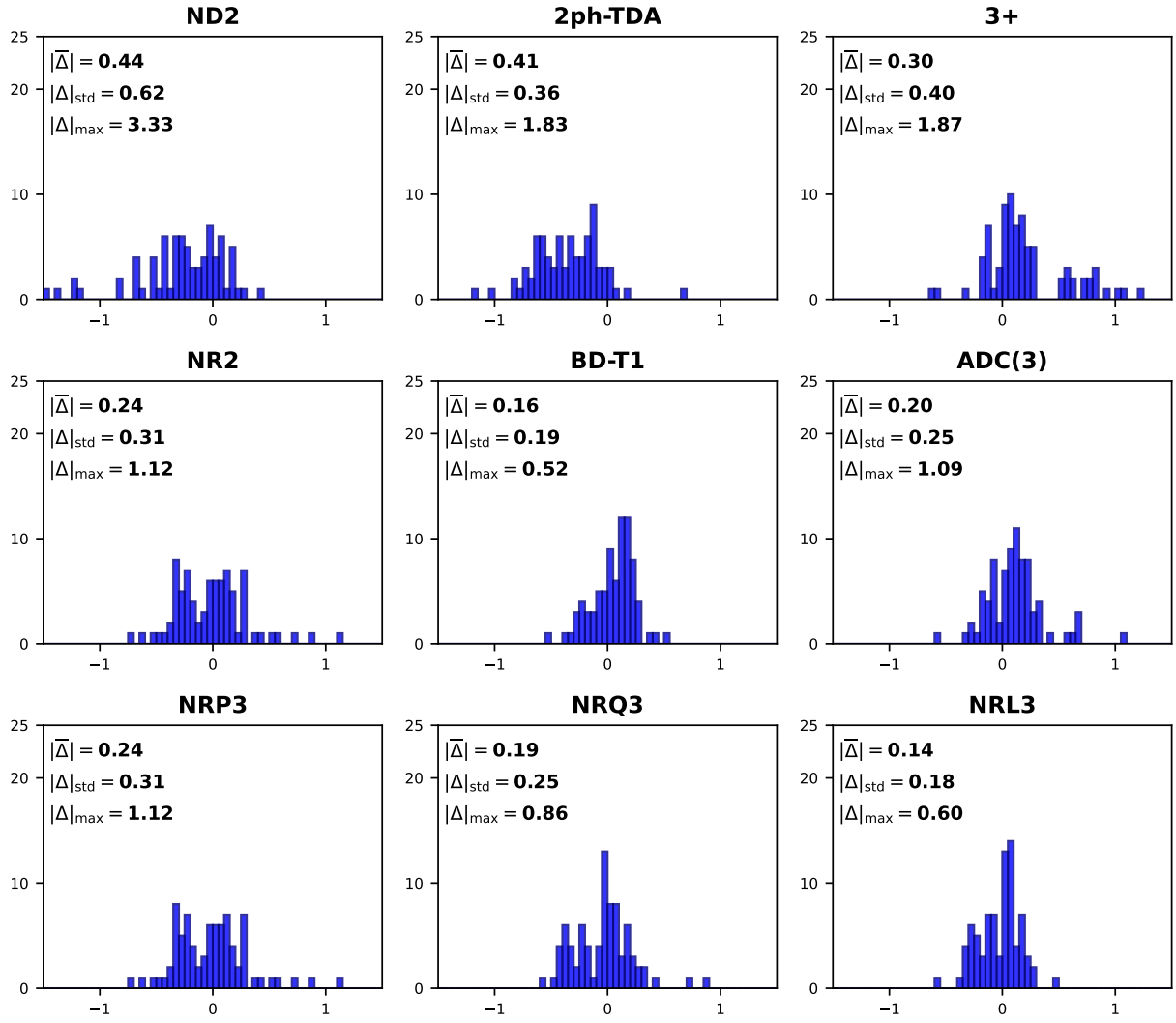


Figure 4.2: Histograms of error distributions (eV) versus experimental VIEs of 81 heavy−element−containing molecules[121]: non−diagonal EP methods. All calculations were executed with the def2TZVPP basis set.

the cubically scaling approaches, each achieving a MAE of 0.17 eV comparable to the accuracy typically observed in main group chemistry. The corresponding error histograms for these methods are centered near zero, with only a few outliers on the side of underestimation.

Within the more computationally intensive O^2V^3 scaling category, the Q3+ method demonstrates the best performance, with an MAE of 0.15 eV and an error distribution centered near zero, exhibiting minimal overestimation bias. The P3+ method, with an MAE of 0.18 eV and a similarly shaped histogram, represents a viable alternative. In contrast, the

DR method is less competitive, yielding a higher MAE of 0.21 eV. Nonetheless, the RQ3 and RP3 methods may serve as practical alternatives in applications where explicit evaluation of all higher-order terms in the inverted matrices is required.

Within the OV^4 category of methods, OVGF−A performs competitively, achieving an MAE of 0.11 eV. The nD−OVGF−A variant demonstrates equivalent accuracy, offering a comparably effective alternative. The L3+A method yields a slightly lower MAE of 0.10 eV, indicating a modest improvement over OVGF−A. All nD−L3+ variants exhibit identical MAEs, making them more computationally efficient alternatives for achieving similar levels of accuracy.

The RL3 and nD−RL3 methods emerge as the most accurate among all diagonal electron propagator methods, each producing an MAE of 0.07 eV. Their error distributions are sharply centered at zero, with an MSE of 0.00 eV. These results suggest that the use of a triple-zeta quality basis set is sufficient to attain accuracy approaching the chemical accuracy threshold.

The data presented in Figure 4.4 indicate that many of the older non-diagonal electron propagator methods are not sufficiently reliable for the systems considered in this study. For example, the ND2, 2ph−TDA, and 3+ methods exhibit MAEs in the range of 0.3 to 0.4 eV, which limits their utility in high-accuracy applications. In contrast, the NR2, ADC(3), and NRP3 methods demonstrate more competitive accuracy, with NR2 offering greater computational efficiency relative to the other two. The NRQ3 method provides a slight improvement in accuracy over NRP3 while maintaining a comparable computational cost.

Among the older non−diagonal approaches, only BD−T1 achieves an MAE below 0.1 eV. Overall, the NRL3 method emerges as the most accurate within this category, yielding an MAE of 0.08 eV. Its error distribution is sharply peaked and centered at zero, and it exhibits a mean signed error of exactly zero, indicating excellent agreement with benchmark values.

The influence of spin−orbit coupling and relativistic effects on these results remains an active area of investigation and will be published at a later time.

4.6 K−Shell Core Ionization Energies

Table 4.6 presents a comparative analysis of computed core−level electron binding energies for a set of small molecules consisting of methane (CH_4), water (H_2O), ammonia (NH_3), hydrogen fluoride (HF), and neon (Ne) using various EP methods against experimental reference values.[122] The evaluation includes the methods KT, D2, ND2, NRL3, ADC(3), and BD−T1. The accuracy of each method is quantitatively assessed using mean signed error (MSE), mean absolute error (MAE), and maximum error (Max. Error) criteria.

Among the methods evaluated, BD−T1 exhibits the highest accuracy, with the lowest MAE (0.39 eV), MSE (0.06 eV), and maximum deviation (0.57 eV). This indicates excellent agreement with experimental data and minimal systematic bias. Although NRL3 involves all important linear triple operator couplings, it obtains a MAE of 1.09 which is inferior to BD−T1. This preliminary observation suggests that BD reference orbitals procure some advantages over HF reference during core ionizations where there are strong relaxation effects.

ADC(3) performs poorly as it achieves a low MAE of 3.59 eV and a maximum error of 4.75 eV, while its MSE suggests a tendency to overestimate the core−level energies. KT shows significantly larger deviations, with a MAE value of 17.05 eV and maximum error approaching 20 eV, indicating a systematic overestimation (as reflected by the MSE of 17.05 eV). These observations demonstrate that the KT method is less reliable for quantitative predictions of core ionization energies in the studied systems. Its pathologies likely extend to all electron propagator (EP) methods based on the Hartree–Fock (HF) reference, which is equivalent to KT.

The NRL3 method shows intermediate performance, with an MAE and MSE of 1.09 eV and a maximum error of 1.49 eV. While more accurate than KT, D2, and ND2, it does not reach the precision of BD−T1. Overall, BD−T1 emerges as the most robust

Table 4.5: HEC Molecules, Point Groups, Hole States, Experimental and ΔCCSD(T) Ionizations Energies Standards. All ΔCCSD(T) calculations were executed with the def2TZVPP basis set.

Molecules	**Point group**	**Hole**	**Experimental VIEs**	**ΔCCSD(T) VIEs**
AgBr	$C_{\infty v}$	π	9.59	9.42
AgCl	$C_{\infty v}$	π	10.08	9.83
AgI	$C_{\infty v}$	π	8.80	8.81
Al_2Br_6	D_{2h}	b_{2u}	10.97	10.84
$AlBr_3$	D_{3h}	a_2'	10.91	10.94
AlI_3	D_{3h}	a_2'	9.66	9.71
$AsBr_3$	C_{3v}	a_1	10.21	10.02
$AsCl_3$	C_{3v}	a_1	10.90	10.63
AsF_3	C_{3v}	a_1	13.00	12.62
AsF_5	D_{3h}	e''	15.53	15.57
AsH_3	C_{3v}	a	10.58	10.40
AsI_3	C_{3v}	e	9.00	9.22
Br_2	$D_{\infty h}$	π_g	10.54	10.56
BrCl	$C_{\infty v}$	π	11.01	10.94
$C_{10}H_{10}Ru$	D_{5h}	e_2'	7.45	7.38
C_2H_2Se	C_{2v}	b_1	8.71	8.62
C_2H_6Cd	D_{3h}	a_2''	8.80	8.91
C_2H_6Hg	D_{3h}	a_2''	9.32	9.08
C_2H_6Se	C_{2v}	b_1	8.40	8.32
C_2H_6Zn	S_6	a_u	9.40	9.53
C_2HBrO	C_s	a''	9.10	9.17
C_4H_4Se	C_{2v}	a_2	8.86	8.96
$CaBr_2$	$D_{\infty h}$	π_u	10.35	10.29
CaI_2	$D_{\infty h}$	π_u	9.39	9.46
$CdBr_2$	$D_{\infty h}$	π_g	10.58	10.66
$CdCl_2$	$D_{\infty h}$	π_g	11.44	11.31
CdI_2	$D_{\infty h}$	π_g	9.57	9.73
CF_3I	C_{3v}	e	10.45	10.73
CH_3HgBr	$C_{3\mathbf{v}}$	e	10.16	10.10
CH_3HgCl	C_{3v}	a_1	10.84	10.65
CH_3HgI	C_{3v}	e	9.25	9.33
CH_3I	C_{3v}	e	9.52	9.68
CI_4	T_d	t_1	9.10	9.19
CsCl	$C_{\infty v}$	π	8.69	8.38
CsF	$C_{\infty v}$	σ	9.68	9.34
CsI	$C_{\infty v}$	π	7.46	7.34
CuF	$C_{\infty v}$	σ	10.90	10.79
$HgCl_2$	$D_{\infty h}$	π_g	11.37	11.27
I_2	$D_{\infty h}$	π_g	9.35	9.48
IBr	$C_{\infty v}$	π	9.85	9.94
ICl	$C_{\infty v}$	π	10.10	10.18

Table 4.5 Continued

Molecules	**Point group**	**Hole**	**Experimental VIEs**	**ΔCCSD(T) VIEs**
IF	$C_{\infty v}$	π	10.62	10.68
KBr	$C_{\infty v}$	π	8.10	8.14
KI	$C_{\infty v}$	π	7.40	7.64
Kr_2	$D_{\infty h}$	σ_u	13.77	13.67
KrF_2	$D_{\infty h}$	σ_g	13.34	13.30
$LaBr_3$	C_{3v}	a_2	10.68	10.62
$LaCl_3$	C_3	e	11.29	11.17
LiBr	$C_{\infty v}$	π	9.44	9.29
LiI	$C_{\infty v}$	π	8.44	8.55
$MgBr_2$	$D_{\infty h}$	π_g	10.85	10.94
MgI_2	$D_{\infty h}$	π_g	10.50	9.93
MoC_6O_6	O_h	t_{2g}	8.50	8.40
NaBr	$C_{\infty v}$	π	8.70	8.62
NaI	$C_{\infty v}$	π	8.00	8.03
OsO_4	T_d	t_1	12.35	12.46
PBr_3	C_{3v}	a_1	10.00	9.83
$POBr_3$	C_{3v}	a_2	11.03	11.12
RbBr	$C_{\infty v}$	π	8.00	8.16
RbCl	$C_{\infty v}$	π	8.70	8.45
RbI	$C_{\infty v}$	π	7.30	7.44
RuO_4	T_d	t_1	12.15	12.18
$SeCl_2$	C_{2v}	b_1	9.50	9.28
SeO_2	C_{2v}	a_1	11.76	11.66
$SiBrF_3$	C_3	e	12.46	12.05
SiH_3I	C_{3v}	e	9.82	10.08
$SOBr_2$	C_s	a′	10.59	10.57
$SPBr_3$	C_{3v}	e	9.89	9.69
$SrBr_2$	$D_{\infty h}$	π_u	9.82	9.98
$SrCl_2$	C_{2v}	b_2	10.20	10.49
SrI_2	$D_{\infty h}$	π_u	9.01	9.19
SrO	$C_{\infty v}$	σ	6.91	6.26
$TiBr_4$	T_d	t_1	10.57	10.65
TiI_4	T_d	t_1	9.27	9.37
$ZnBr_2$	$D_{\infty h}$	π_g	10.89	10.95
$ZnCl_2$	$D_{\infty h}$	π_g	11.80	11.71
ZnF_2	$D_{\infty h}$	π_g	13.91	13.83
ZnI_2	$D_{\infty h}$	π_g	9.73	9.93
$ZrBr_4$	T_d	t_1	10.86	10.92
$ZrCl_4$	T_d	t_1	11.94	11.93
ZrI_4	T_d	t_1	9.55	9.61

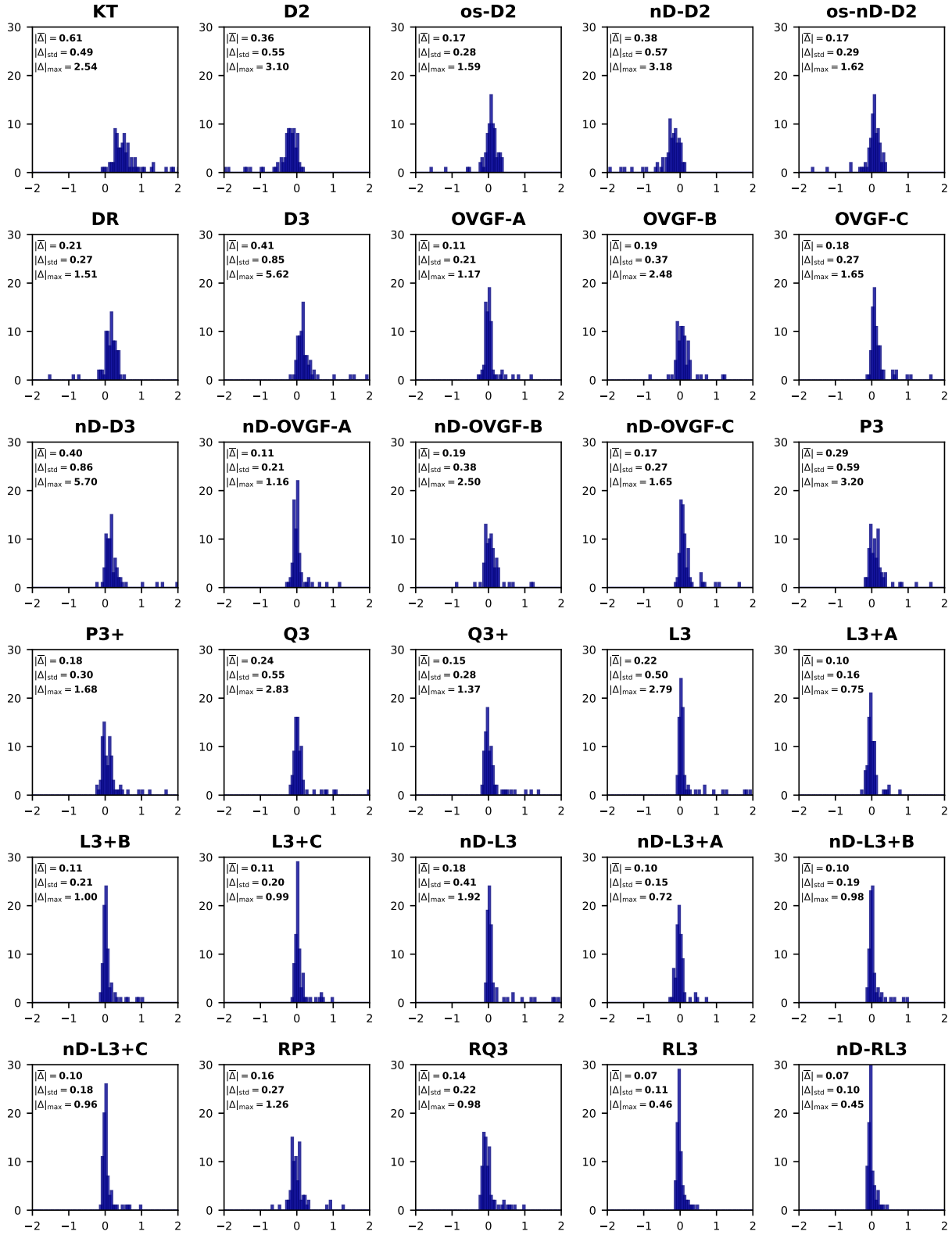


Figure 4.3: Histograms of error distributions (eV) versus ΔCCSD(T) VIEs of 81 HEC molecules: Diagonal EP methods. All calculations were executed with the def2TZVPP basis set.

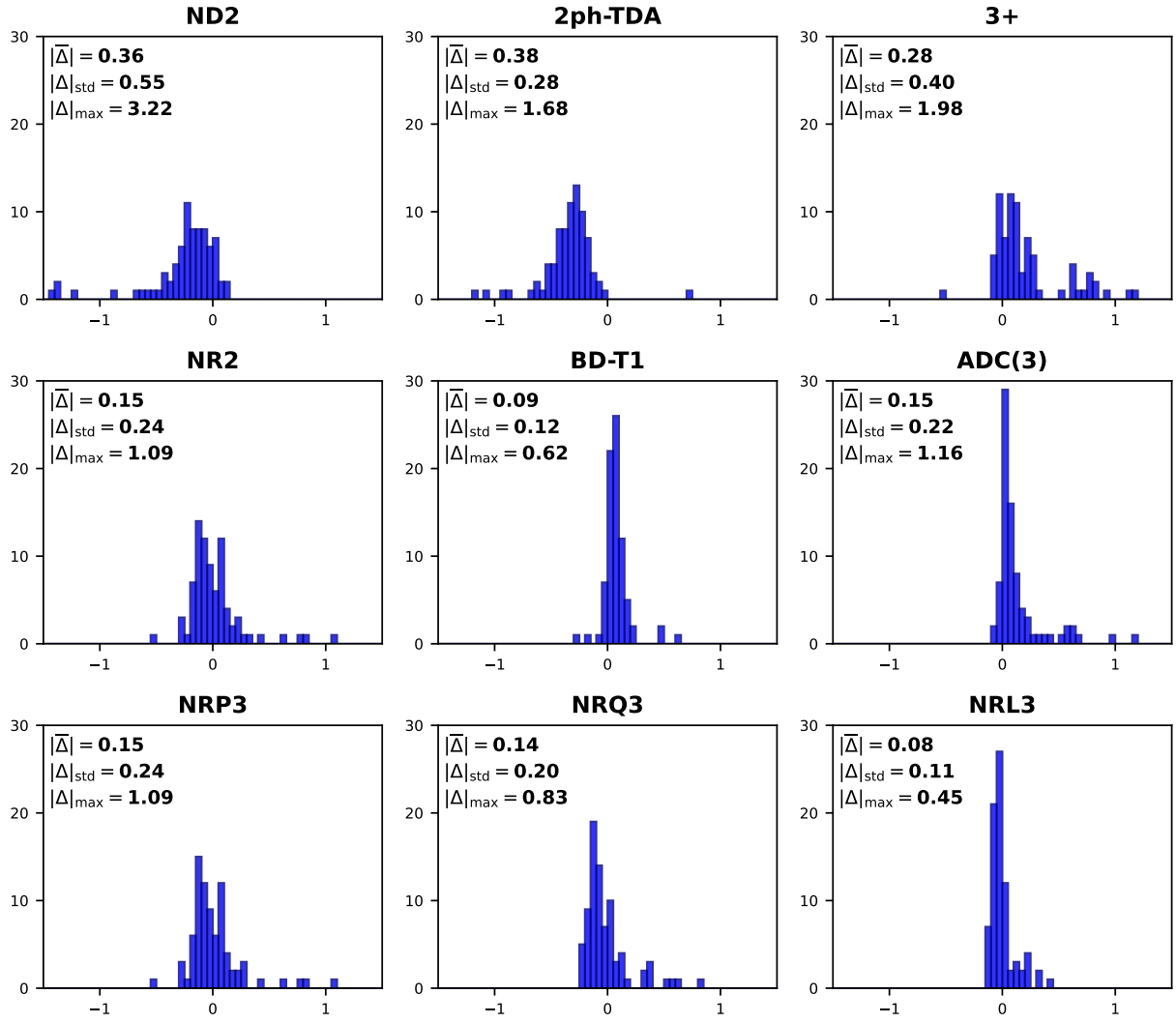


Figure 4.4: Histograms of error distributions (eV) versus ΔCCSD(T) VIEs of 81 HEC molecules: Non−diagonal EP methods. All calculations were executed with the def2TZVPP basis set.

method for reproducing experimental core−level electron−binding energies in this benchmark. KT and ADC(3) demonstrate substantial errors that may limit their predictive utility in high−accuracy applications. D2 and ND2 predictions with MAEs near 1.0 eV are very promising in view of their lower cubic arithmetic scaling. When a shifting near 1.0 eV is applied to D2 or ND2 (to estimate relativistic effects), their MAEs are likely to go below 0.1 eV.

Table 4.6: Electron propagator methods versus core $1s$ experimental electron binding energies.[a]

Species	**Core**	**Exp**[122]	**KT**	**D2**	**ND2**	**NRL3**	**ADC(3)**	**BD-T1**
CH_4	C1s	290.84	305.04	291.68	291.68	291.51	293.18	290.95
H_2O	O1s	539.70	559.38	537.87	537.88	541.20	544.45	540.27
NH_3	N1s	405.52	422.79	405.08	405.09	406.64	409.19	405.01
HF	F1s	694.22	715.29	690.96	690.97	695.66	699.13	694.80
Ne	Ne1s	870.31	891.69	866.05	866.06	871.16	874.41	870.53
		MSE	17.05	-0.47	-0.47	1.09	3.59	0.060
		MAE	17.05	1.03	1.03	1.09	3.59	0.39
		Max. Error	19.68	1.83	1.81	1.50	4.75	0.57

[a]All calculations were executed with the cc−pVTZ basis set using experimental reference geometries. All energies are in eV. Exp denote experimental reference values.[122]

Chapter 5

Applications of New−Generation Electron−Propagator Methods

5.1 Vertical Electron Detachment Energies of DNA Nucleotide Anions

DNA, a multiply charged anion, consists of two helical polymers held together by hydrogen bonds between purine−pyrimidine base pairs. Each polymer is composed of nucleotide monomers, which consist of a phosphate group covalently bound to a nucleoside (sugar and base). The localization of holes generated by photoionization on the base, sugar, or phosphate components significantly influences subsequent chemical reactivity and radiation−induced damage.[123, 124] The new−generation EP methods have been used to calculate the VEDEs and analyze hole localization in the nucleotide anions.[64]

Dyson orbital analysis (since spatial symmetry is absent) was used to ascertain whether electron density is primarily removed from the phosphate anion, sugar, or base (see Figure 5.1). For bases, holes may occupy delocalized π orbitals or more localized σ lone−pair orbitals. Calculations were conducted using a composite model (See CM1 below) comprising five terms, incorporating results from os−D2, os−nD−D2, Q3+, and nD−L3+B methods with aug−cc−pVDZ, aug−cc−pVTZ, and aug−cc−pVQZ basis sets. Basis−set effects were approximated using cubic extrapolation to achieve a complete basis set (CBS) limit.

$$E^{CM1} = E^{Q3+}_{aTZ} + E^{nD-L3+B}_{aDZ} - E^{Q3+}_{aDZ} + E^{os-nD-D2}_{CBS} - E^{os-nD-D2}_{aTZ} \tag{5.1.1}$$

The results in Table 5.1 demonstrate that the composite electron−propagator model consistently refines and corrects qualitative deficiencies in KT assignments. For guanosine monophosphate ($dGMP^-$), the lowest VEDE (5.01 eV) is assigned to a base π orbital, in agreement with experimental photoelectron spectroscopy (5.05 ± 0.10 eV). Phosphate−centered

transitions follow at higher energies. In contrast, KT defects occur for several states, notably the fourth VEDE at 8.09 eV. Predicted states based on CM1 align well with experimental broad features, showing discrepancies of ≤ 0.2 eV compared to prior calculations employing the older P3 method in a small basis set.

For adenosine monophosphate ($dAMP^-$), the composite model identifies a nearly degenerate lowest VEDE for a base π orbital (6.14 eV) and a phosphate orbital (6.20 eV), consistent with experimental estimates (6.05 ± 0.50 eV). KT incorrectly predicts a 1.7 eV gap, with the base π orbital appearing lower. Subsequent transitions align with spectral features, with σ-hole states matching a peak near 7.1 eV. Prior calculations again show minor discrepancies in state ordering.

In thymidine monophosphate ($dTMP^-$), the composite model places the lowest VEDE at 6.14 eV (base π orbital), closely matching the experimental estimate (5.85 ± 0.50 eV). KT predicts a 1.4 eV separation between base and phosphate states, whereas the composite model suggests only a 0.2 eV difference. Higher transitions, including phosphate and delocalized orbitals, agree with experimental spectral features.

For cytidine monophosphate ($dCMP^-$), the lowest VEDE (6.17 eV) is assigned to a phosphate orbital, contrasting with KT's prediction of a base π orbital. Experimental estimates (5.80 ± 0.50 eV) support the composite model. Higher transitions align well with broad spectral features, with discrepancies from prior calculations under 0.2 eV.

Thus, the composite model predicts that the lowest VEDE corresponds to a base π Dyson orbital in three of four nucleotides, with cytidine being the exception (phosphate orbital). Guanosine exhibits a clear separation between the lowest VEDE and subsequent transitions, while other nucleotides show neardegeneracy between base π and phosphate orbitals. Agreement with experimental spectra underscores the composite model's reliability for characterizing electron detachment in nucleotides.

Table 5.1: Vertical electron detachment energies (eV) of deoxyribonucleotide anions.[64]

Anion	**Experiment**	**KT**	**CM1**	**Dyson Orbital**
dAMP$^-$	6.05 ±0.50	6.092	6.138	Aπ
	6.05 ±0.50	7.797	6.204	PO_4^-
	∼6.4	8.128	6.502	PO_4^-, S
	∼6.7	8.301	6.727	PO_4^-, S
	∼6.7	7.696	6.728	PO_4^-, S
	∼6.9	8.352	6.958	Aπ_2
	∼7.1	8.860	7.202	n_1 A
	∼7.1	8.971	7.296	n_2 A
dGMP$^-$	5.05 ±0.10	5.202	5.008	Gπ_1
	∼6.1	7.908	6.393	PO_4^-
	∼6.4	8.248	6.709	PO_4^-
	∼6.8	8.091	6.782	n, G, S, PO_4^-
	∼6.9	8.481	6.823	G, S, PO_4^-
	∼7.0	8.597	6.939	π_2, G, S
dTMP$^-$	5.85 ±0.50	6.667	6.137	Tπ_1
	∼6.2	8.035	6.338	PO_4^-
	∼6.6	8.333	6.677	PO_4^-, S
	∼6.8	8.544	6.902	PO_4^-, S
	∼6.8	8.490	6.904	PO_4^-, S
	∼7.4	9.114	7.435	PO_4^-, S
	∼7.5	9.300	7.800	T, S, PO_4^-
	∼7.5	9.350	7.815	n T, PO_4^-
dCMP$^-$	5.80 ±0.50	7.674	6.170	PO_4^-
	∼6.4-6.5	7.061	6.464	Cπ_1
	∼6.4-6.5	8.026	6.580	PO_4^-
	∼6.7	8.356	6.847	C, S, PO_4^-
	∼6.9	8.472	7.044	C, S, PO_4^-
	∼7.1	8.991	7.368	C, S, PO_4^-
	∼7.3	8.613	7.477	PO_4^-, S

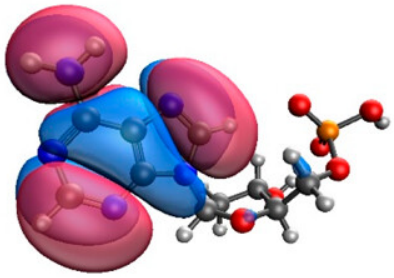
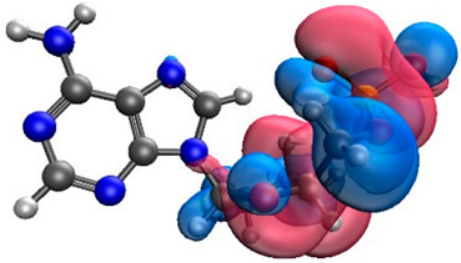
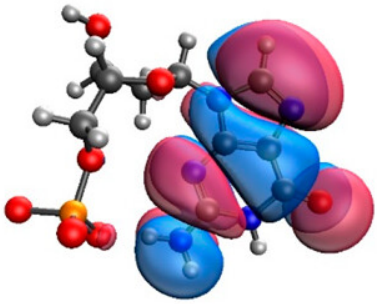
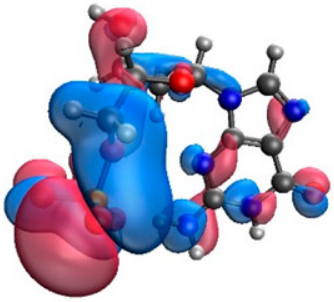
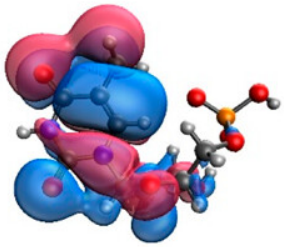
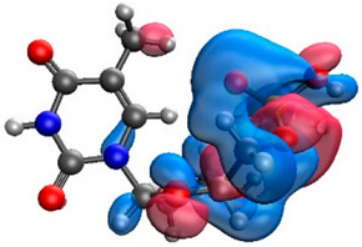
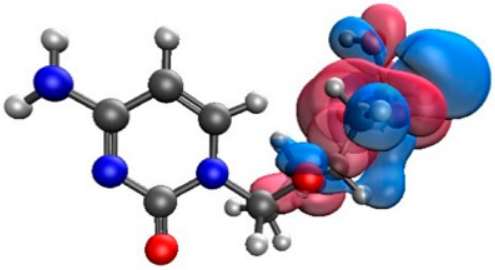
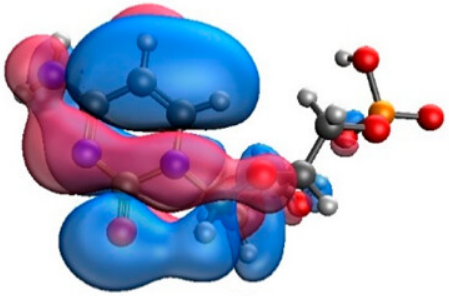
Anion	First Dyson Orbital	Second Dyson Orbital
$dAMP^-$	 A π_1	 PO_4^-
$dGMP^-$	 G π_1	 PO_4^-
$dTMP^-$	 T π_1	 PO_4^-
$dCMP^-$	 PO_4^-	 C π_1

Figure 5.1: Dyson orbitals of vertical electron detachment of deoxyribonucleotide anions[64]

5.2 Vertical Electron Detachment Energies of GFP Chromophore Anions

The lowest VEDEs of three green fluorescent protein (GFP) model anions [125, 126] were evaluated using composite models with explicitly renormalized diagonal (CM2) and nondiagonal (CM3) selfenergy components (Table 5.2). Both models show excellent agreement with experimental values, with CM3 predictions falling within experimental error for *p*-hydroxybenzylidene-2,3-dimethylimidazoline anion (*p*-HBDI$^-$). Discrepancies between CM2 and CM3 are negligible, as both accurately account for basisset effects beyond the augc-cpVTZ level.

$$E^{CM2} = E^{nD-RL3}_{aug-cc-pVDZ} + E^{os-nD-D2}_{CBS(DT)} - E^{os-nD-D2}_{aug-cc-pVDZ} \tag{5.2.1}$$

$$E^{CM3} = E^{NRL3}_{aug-cc-pVDZ} + E^{os-nD-D2}_{CBS(DT)} - E^{os-nD-D2}_{aug-cc-pVDZ}. \tag{5.2.2}$$

Prior studies [127] noted that VEDEs calculated with the aug−cc−pVDZ basis set are ∼0.2 eV lower than those obtained with aug−cc−pVTZ, and basis sets of quadruple-ζ or higher quality increase VEDEs by at least 0.1 eV. These trends were confirmed at the os−D2/aug−cc−pVQZ level. However, previous calculations lacked estimates for the effects of larger basis sets. Methods such as EOM−CCSD and ΔCCSD(T) involve iterative procedures with O^2V^4 arithmetic scaling and, for ΔCCSD(T), a non−iterative seventh−power step. By contrast, the renormalized terms in CM2 and CM3, which require lower arithmetic scaling, can be computed at the aug−cc−pVDZ level without significant loss of accuracy.

The lowest VEDEs for all three anions correspond to delocalized π Dyson orbitals of b_1 or a" −type symmetry (see Figure 5.2).[125, 126] Antibonding interactions between oxygen and adjacent carbon atoms in the chromophore ring are observed, with significant contributions from basis functions on fluoride and methoxy oxygen nuclei in substituted anions. These features emphasize the necessity of explicitly renormalized self−energies, which improve accuracy by reducing VEDEs by ∼0.05 eV (nD−RL3 vs. nD−L3+B). Such corrections are crucial for the high precision achieved by the CM5 and CM8 models.

Table 5.2: Vertical electron detachment energies of GFP model anions.[63]

GFP Anions	**Experiment**	**CM2**	**CM3**
***p*−HBDI$^-$**	2.74 ± 0.04	2.80	2.78
DF−HBDI$^-$	2.98 ± 0.04	3.05	3.04
***Syn*−DM−HBDI$^-$**	2.7 ± 0.04	2.82	2.81

Probability factors offer further insight into the influence of relaxation and correlation effects. For the three phenolate anions (see Appendix I or reference [63]), nD−L3+B, nD−RL3, and NRL3 calculations using the aug−cc−pVDZ basis yield probability factors of 0.92, 0.90, and 0.86, respectively. (See equations 2.4.8 and 2.5.2 for definition of probability factors). In the NRL3 case, the canonical Hartree−Fock orbital contributes a coefficient of 0.99 to the normalized Dyson orbitals, validating the diagonal self−energy approximation. Relaxation and correlation effects are slightly stronger for the three HBDI$^-$ anions, with corresponding probability factors of 0.90, 0.87, and 0.83, respectively.

These findings affirm the qualitative reliability of the diagonal self−energy approximation while highlighting the importance of off−diagonal couplings for capturing relaxation and correlation effects in GFP model anions. CM2 and CM3 models provide a robust framework for studying VEDEs with excellent experimental agreement and computational efficiency.

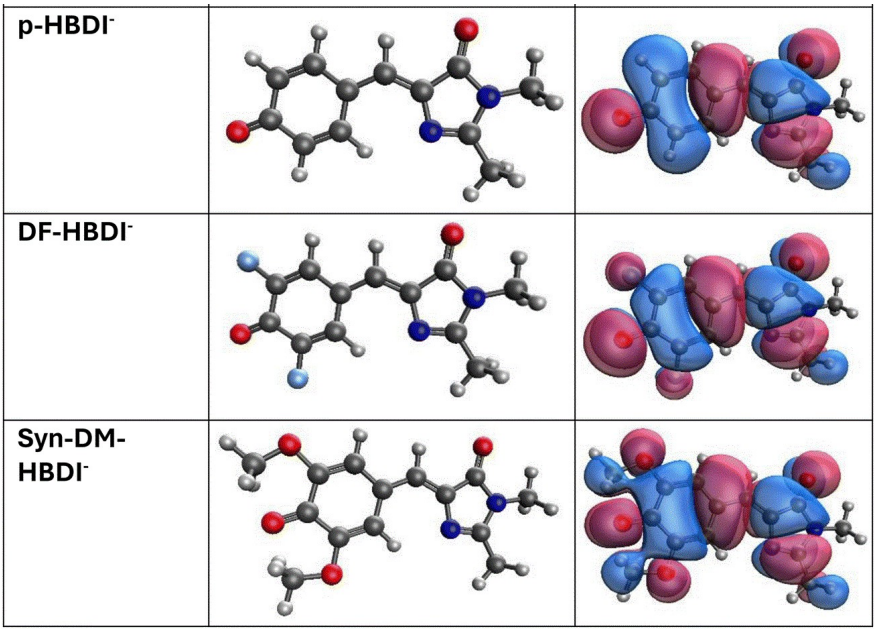


Figure 5.2: Structures and Dyson orbitals for vertical electron detachment energies of model GFP anions.[63]

Chapter 6

Prediction of New Molecules and Anions: Double Rydberg Anions and Rydberg Molecules

In this chapter, I present the major findings from my work on $O_nH_{2n+1}{}^{+,0,-}$ double Rydberg anions (DRAs) published elsewhere.[88]

6.1 Electron Binding Energies and Dyson Orbitals of $O_nH_{2n+1}{}^{+,0,-}$ Clusters

Rydberg neutrals and DRAs arising from $OH_3{}^+$ have been studied since 1990.[128, 129] Ortiz[130] previously presented structural and spectral predictions of the $OH_3{}^-$ DRA. Electron propagator calculations combined with larger diffuse basis sets were used to obtain vertical electron binding energies for the $OH_3{}^-$ DRA at the geometry of the anionic minimum. A later study[131] provided predictions of structures, vibrational frequencies, relative total energies, and electron binding energies on isomers of $OH_3{}^-$ and $O_2H_5{}^-$ DRAs in comparison to $NH_4{}^-$ and $N_2H_7{}^-$. No studies on $H^-(H_2O)_n$ ($n \geq 3$) isomers have been performed. A careful search of the literature reveals no experimental evidence of the $OH_3{}^-$ DRA or any of its higher clusters.

However, the $H^-(H_2O)$ isomer of the $OH_3{}^-$ DRA has been observed experimentally with a VEDE of 1.53 eV.[132] The $H^-(H_2O)$ isomer can be considered to be an H^- anion solvated by one water molecule. Considerable experimental efforts have been made to produce the $OH_3{}^-$ DRA with no success, perhaps because this species is much higher in energy than the $H^-(H_2O)$ isomer.

At the same time, the metastable Rydberg radicals, OH_3 and OD_3, have been identified using neutralized ion beam spectroscopy experiments. Despite all this progress, a thorough

search of the chemical literature reveals no studies on the O_2H_5 Rydberg radical and corresponding higher $H(H_2O)_n$ clusters. In the case of DRAs, I found studies only on the OH_3^- and $O_2H_5^-$ species, prompting the need for theoretical studies on larger clusters to offer correlative guidance for future experiments. Techniques of EPT provide reliable predictions for the discovery and identification of novel DRAs, and related solvated−electron precursors. To extend the scope of double Rydberg concepts to oxygen−based systems, stabilization of the pyramidal H_3O^- DRA by hydrogen bonding and electrostatic interactions ought to be considered.

I employed high−accuracy, *ab initio* EPT and CC methods with large, diffuse basis sets to study the hydronium O_nH_{2n+1} Rydberg molecules, $O_nH_{2n+1}^-$ DRAs and related solvated species. In completing the first solvation shell, both the Eigen−like $H_3O^{\pm}(H_2O)_n$ structures and Zundel's $H_5O_2^{\pm}(H_2O)_{n\text{-}1}$ models are considered. Predictions of structures, vibrational frequencies, relative total energies, vertical electron binding energies and Dyson orbitals associated with Rydberg neutrals and DRAs are investigated. Isomers that arise from electrostatic intermolecular interactions and hydrogen bonding to form hydride− and DRA−molecule complexes are all considered. Calculations on isomers of $O_nH_{2n+1}^{\pm}$ complexes with only their first solvation shells provide Aufbau rules for electrons that occupy the periphery of these complexes.

6.2 $O_nH_{2n+1}^-$ Double Rydberg Anions

Geometry optimizations performed at the CCSD(T)/aug−cc−pVTZ level (for n = 1, 2) and MP2/aug−cc−pVTZ level (for n = 3–6), using default convergence criteria, led to minima for all isomers. A change in convergence criteria to 300 maximum cycles was necessary for the *trans*−H_2O−$O_2H_5^-(H_2O)$ and for the Z1 $O_6H_{13}^-$ isomer.

To judge the reliability of EPT methods for calculating VEDEs, a preliminary comparison with ΔCCSD(T) results was conducted for the OH_3^- DRA. The results shown in Table 6.1 were obtained with various basis sets to evaluate the effectiveness of each method

Table 6.1: Comparison of VEDEs (eV) of the OH_3^- DRA calculated at different levels of theory. Pole strengths are in parentheses.

OH_3^-	**VEDE**
KT[a]	0.362
D2[a]	0.633 (0.830)
D3[a]	0.620 (0.874)
P3+[a]	0.622 (0.870)
OVGF[a]	0.481 (0.772)
BD-T1[a]	0.539 (0.862)
ΔCCSD(T)/aug−cc−pVTZ	0.536
BD−T1/aug−cc−pVTZ	0.431 (0.894)
BD−T1/d−aug−cc−pVTZ	0.537 (0.864)
BD−T1/t−aug−cc−pVTZ	0.539 (0.862)
BD−T1/q−aug−cc−pVTZ	0.539 (0.862)
BD−T1/aug−cc−pVQZ	0.458 (0.889)
BD−T1/aug−cc−pV5Z	0.486 (0.884)

[a]Calculation performed with the aug−cc−pVTZ basis augmented with an additional set of diffuse functions: 4s4p4d on all H atoms and 4s4p4d4f on all O atoms.

in describing electron correlation and orbital relaxation corrections to the KT results. Only the lowest VEDE was considered.

Compared to ΔCCSD(T), KT results are too small, whereas D2, D3, P3+, and OVGF self−energy approximations are too large. D2 and OVGF have lower pole strengths. The BD−T1 result is the closest to ΔCCSD(T). A comparison of BD−T1 results obtained with various basis sets shows that BD−T1/d−aug−cc−pVTZ is the optimal level in terms of computational accuracy and cost.

Data from Table 6.1 suggest that for DRAs, BD−T1 is the best EPT method. Of the remaining EPT methods, P3+ generally performs better than OVGF with respect to VEDEs and pole strengths. The data also indicate that improvements corresponding to the t−aug−cc−pVTZ, q−aug−cc−pVTZ, aug−cc−pVQZ, and aug−cc−pV5Z basis sets are not needed. Hence, unless stated otherwise, BD−T1/d−aug−cc−pVTZ results are discussed throughout the text.

OH_3^- isomers: Figure 6.1 displays the optimized geometries and Dyson orbitals for the lowest vertical electron detachment energies (VEDEs) for the hydride−water complex

$H^-(OH_2)$ and the $OH_3{}^-$ DRA. Numerical results for relative energies and electron binding energies are shown in Table 6.2. The hydride−molecule complex is more stable than the $OH_3{}^-$ DRA. In the former anion, the VEDE of the free hydride (0.75 eV) increases by 0.9 due chiefly to electrostatic interactions with the water molecule. The H_2O molecule approaches the free hydride with one of its protons in a C_s geometry. There is a minor increase in the length of the O−H bond that approaches H^-. A structure in which the hydride anion forms a symmetric bonding arrangement with the molecule's protons is a transition state. The Dyson orbital is composed chiefly of diffuse s functions which display no bonding relationship with valence functions on the closest O−H bonds. A totally symmetric Dyson orbital whose amplitudes are beyond the hydrogen nuclei is observed for the lowest VEDE of the $OH_3{}^-$ DRA. This Dyson orbital correlates smoothly to the $3s$ orbital of Na^- in the united atom limit, for it has two radial nodes. The lowest VEDE of 0.537 eV nearly equals that of Na^- (0.55 eV). The Dyson orbital for the lowest VEDE closely resembles that of the first electron attachment energy of the cationic core $OH_3{}^+$, for both electron binding energies correspond to the same final uncharged doublet OH_3 state. The O−H bond lengths are almost the same in the cation, neutral and anion, and imply the insignificance of the antibonding features in the Dyson orbital. The present results can be considered as an upper bound to previous calculations.

Table 6.2: $O_nH_{2n+1}^-$ isomerization and vertical electron detachment energies (VEDEs). Pole strengths are in parentheses. All energies are in eV. Calculations were executed with the d−aug−cc−pVTZ basis set. [88]

n	**Isomer**		**KT**	**D2**	**D3**	**OVGF**	**P3**	**P3+**	**BD−T1**
1	$H^-(OH_2)$	0.000	2.009	1.522 (0.881)	1.695 (0.901)	1.732 (0.899)	1.505 (0.906)	1.506 (0.904)	1.659 (0.864)
	OH_3^-	1.540	0.338	0.658(0.867)	0.494 (0.833)	0.409 (0.750)	0.585 (0.831)	0.591 (0.834)	0.537 (0.864)
2	$H^-(H_2O)_2$	0.000	8.159	5.446 (0.858)	7.501 (0.923)	6.925 (0.900)	6.656 (0.901)	2.401 (0.911)	2.570 (0.819)
	$OH_3^-(H_2O)$	2.238	0.500	0.873 (0.863)	0.726 (0.851)	0.700 (0.844)	0.837 (0.847)	0.840 (0.849)	0.803 (0.881)
	$O_2H_5^-$	1.323	0.244	0.603 (0.865)	0.435 (0.825)	0.336 (0.696)	0.529 (0.822)	0.536 (0.826)	0.519 (0.860)
3	$H^-(OH_2)_3$	0.000	3.715	3.131 (0.908)	3.392 (0.912)	3.394 (0.909)	3.159 (0.911)	3.156 (0.911)	3.352 (0.899)
	$OH_3^-[OH_2]_2$	2.454	0.685	1.105 (0.871)	0.974 (0.866)	0.961 (0.867)	1.089 (0.864)	1.090 (0.865)	1.066 (0.924)
	$O_2H_5^-(H_2O)$	2.607	0.371	0.781 (0.851)	0.607 (0.833)	0.572 (0.818)	0.736 (0.826)	0.740 (0.828)	0.731 (0.879)
	$O_3H_7^-$	2.491	0.209	0.609 (0.863)	0.432 (0.823)	0.341 (0.700)	0.540 (0.817)	0.547 (0.821)	0.537 (0.865)
4	$H^-(H_2O)_4$	0.000	4.303	3.669 (0.909)	3.947 (0.911)	3.936 (0.910)	3.711 (0.911)	3.707 (0.911)	3.899 (0.900)
	$[OH_2]_2OH_3^-H_2O$	2.704	0.198	0.597 (0.844)	0.407 (0.809)	0.327 (0.706)	0.528 (0.798)	0.535 (0.803)	0.535 (0.867)
	Eigen $O_4H_9^-$	2.629	0.200	0.605 (0.857)	0.430 (0.820)	0.360 (0.736)	0.540 (0.812)	0.549 (0.817)	0.574 (0.874)
	Ring $O_4H_9^-$	2.780	0.157	0.610 (0.871)	0.437 (0.830)	0.342 (0.684)	0.551 (0.822)	0.557 (0.828)	0.521 (0.882)
	Cis $(H_2O)O_2H_5^-(H_2O)$	2.789	0.151	0.541 (0.856)	0.364 (0.809)	0.244 (0.491)	0.465 (0.800)	0.472 (0.806)	0.450 (0.840)
	Trans $(H_2O)O_2H_5^-(H_2O)$	2.638	0.151	0.541 (0.856)	0.364 (0.809)	0.244 (0.491)	0.465 (0.800)	0.599 (0.809)	0.596 (0.879)
5	$H^-(H_2O)_5$	0.000	4.655	3.984 (0.910)	4.270 (0.912)	4.250 (0.912)	4.042 (0.912)	4.036 (0.910)	4.218 (0.901)
	B1 $O_5H_{11}^-$	2.802	0.194	0.574 (0.833)	0.389 (0.801)	0.314 (0.708)	0.506 (0.788)	0.513 (0.793)	0.527 (0.905)
	B2 $O_5H_{11}^-$	2.745	0.179	0.544 (0.835)	0.358 (0.802)	0.281 (0.698)	0.475 (0.788)	0.482 (0.794)	0.484 (0.905)
	C $O_5H_{11}^-$	2.860	0.160	0.502 (0.823)	0.308 (0.788)	0.208 (0.599)	0.424 (0.773)	0.432 (0.779)	0.424 (0.848)
	PR $O_5H_{11}^-$	2.946	0.165	0.595 (0.838)	0.383 (0.793)	0.269 (0.521)	0.515 (0.777)	0.523 (0.785)	0.499 (0.845)
	R $O_5H_{11}^-$	2.884	0.146	0.576 (0.854)	0.397 (0.810)	0.296 (0.617)	0.508 (0.800)	0.515 (0.806)	0.506 (0.853)
6	$H^-(H_2O)_6$	0.000	5.233	4.514 (0.910)	4.774 (0.909)	4.755 (0.908)	4.558 (0.908)	4.553 (0.908)	
	C1 $O_6H_{13}^-$	3.025	0.101	0.522 (0.868)	0.379 (0.816)	0.275 (0.566)	0.379 (0.816)	0.469 (0.818)	
	E1 $O_6H_{13}^-$	2.878	0.154	0.490 (0.15)	0.292 (0.782)	0.208 (0.639)	0.414 (0.764)	0.422 (0.770)	
	E2 $O_6H_{13}^-$	2.868	0.160	0.548 (0.833)	0.361 (0.795)	0.267 (0.623)	0.477 (0.780)	0.484 (0.780)	
	P1 $O_6H_{13}^-$	2.906	0.154	0.549 (0.821)	0.339 (0.77)	0.225 (0.430)	0.464 (0.759)	0.472 (0.765)	
	T1 $O_6H_{13}^-$	3.174	0.161	0.567 (0.814)	0.337 (0.765)	0.224 (0.311)	0.473 (0.744)	0.482 (0.751)	
	T2 $O_6H_{13}^-$	3.026	0.165	0.620 (0.848)	0.445 (0.814)	0.376 (0.734)	0.565 (0.801)	0.570 (0.807)	
	T3 $O_6H_{13}^-$	2.997	0.118	0.490 (0.842)	0.322 (0.799)	0.210 (0.493)	0.421 (0.785)	0.428 (0.792)	
	T4 $O_6H_{13}^-$	2.898	0.159	0.573 (0.845)	0.397 (0.810)	0.313 (0.685)	0.512 (0.796)	0.518 (0.802)	
	Z1 $O_6H_{13}^-$	3.028	0.123	0.500 (0.826)	0.295 (0.776)	0.181 (0.284)	0.411 (0.759)	0.421 (0.767)	

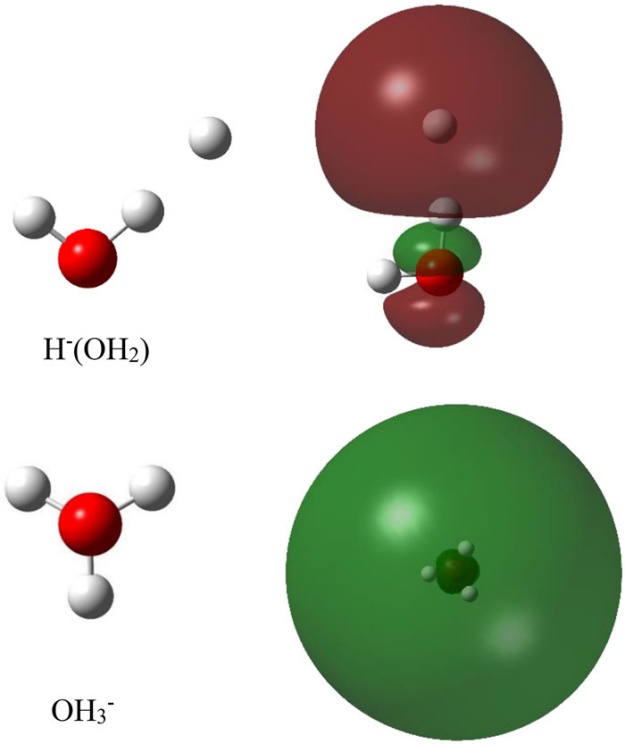


Figure 6.1: $n = 1$: Optimized geometries and Dyson orbitals of electron detachment from anions

$O_2H_5^-$ isomers: There are three $O_2H_5^-$ isomers and their optimized structures and Dyson orbitals are illustrated in Figure 6.2. The most stable isomer is the hydride anion complex which has two water molecules that weakly coordinate to the H^- via attractions to their protons. A peak around 2.5 eV is expected to dominate the photoelectron spectrum of $O_2H_5^-$ considering its high stability. The new water molecule increases the VEDE of the $H^-(OH_2)$ by 0.911 eV and the Dyson orbital is localized on the hydride's nucleus.

The asymmetric hydrogen−bridged isomer has discernible OH_3^- and H_2O molecular fragments. The binding of the same two fragments by electrostatic interactions results in the least stable isomer. In the latter isomer, the Dyson orbital's amplitudes are largest outside the three H nuclei of the OH_3^- fragment. Minor delocalization onto the coordinated water molecule can be seen. The VEDE of the asymmetric hydrogen−bridged isomer of $O_2H_5^-$ differs by approximately 0.3 eV from $OH_3^-(H_2O)$. The Dyson orbital is a nearly symmetric s function with its largest lobes occurring on the protons. Plots of lower iso−values

give credence to a Dyson orbital which accumulates predominantly on the OH_3^- fragment with minor delocalization to regions near the water molecule's H nuclei as observed in a preceding study and in isomers of the $N_2H_7^-$ DRAs.

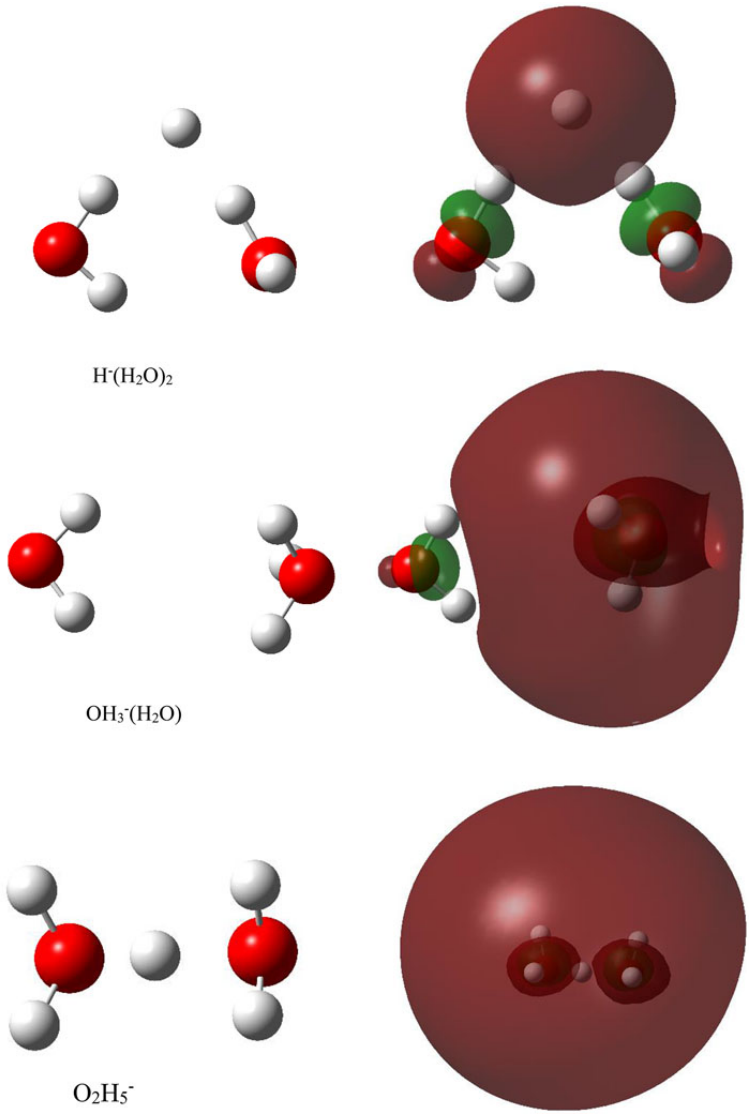


Figure 6.2: $n = 2$: Optimized geometries and Dyson orbitals of electron detachment from anions.

$O_3H_7^-$ isomers: Interaction of a water molecule with the $O_2H_5^-$ isomers gives rise to four different anionic $O_3H_7^-$ clusters. The optimized structures and associated Dyson orbitals are displayed in Figure 6.3. The hydride−molecule complex is the most energetically stable. This complex has a C_3 axis and a perpendicular plane through the hydride's nucleus.

Two water molecules coordinate to $H^-(OH_2)$ with their protons. The coordination of an H_2O molecule increases the VEDE by 0.782 eV compared to $H^-(H_2O)_2$. The Dyson orbital is dominated by delocalized s functions on the hydride, whereas an antibonding relationship with the neighboring O−H bonds is seen. Given the high stability of this isomer, a peak near 3.4 eV is expected to dominate the photoelectron spectrum of $O_3H_7^-$. Other isomers containing the OH_3^- and the $O_2H_5^-$ DRA are energetically unstable and have VEDEs that are higher than the $O_3H_7^-$ DRA. The $OH_3^-[OH_2]_2$ isomer arises from addition of a water molecule to $OH_3^-(H_2O)$. The new water molecule forms a hydrogen−bonded water dimer, denoted as $[OH_2]_2$ with the H_2O fragment in $OH_3^-(H_2O)$. The newly coordinated water increases the VEDE by 0.263 eV compared with $OH_3^-(H_2O)$. The Dyson orbital is retained on the OH_3^- kernel with negligible red contours on the surrounding water dimer.

Addition of a water molecule to the $O_2H_5^-$ DRA through weak electrostatic interactions leads to the $O_2H_5^-(H_2O)$ isomer. The water molecule interacts with the hydrogen nuclei. The Dyson orbital closely resembles that of $O_2H_5^-$, with its largest amplitudes at the peripherical hydrogens on the $O_2H_5^-$ fragment. Negligible antibonding relationships between the Dyson orbitals and valence functions on the water molecule are seen. This isomer is the least energetically stable among all the $O_3H_7^-$ isomers. The VEDE of $O_2H_5^-(H_2O)$ is 0.212 eV above that of $O_2H_5^-$. In the $O_3H_7^-$ DRA, two water molecules interact with two of the OH_3^- protons through hydrogen bonding. This structure can be considered as an $O_2H_5^-$ DRA in which one of the non−bonding hydrogens in OH_3^- forms a hydrogen bond with the water molecule. The VEDE of the $O_3H_7^-$ isomer is 0.018 eV larger than that of the $O_2H_5^-$ DRA. The Dyson orbital accumulates on the peripheral non−bonding hydrogens, with its largest amplitudes on the non−bonding H's in the OH_3^- core and water fragments. The $O_3H_7^-$ DRA has almost the same VEDE as OH_3^-.

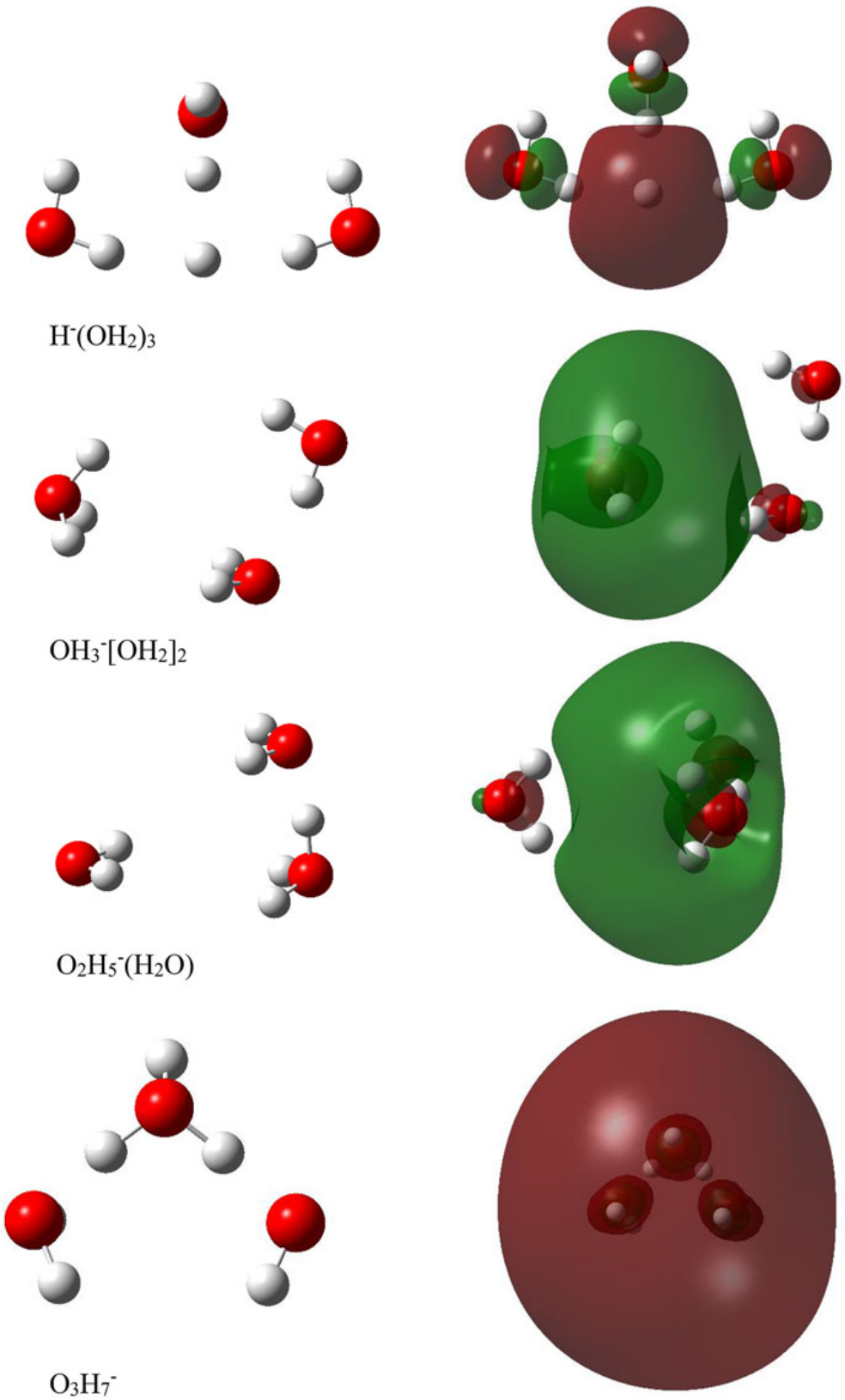


Figure 6.3: $n = 3$: Optimized geometries and Dyson orbitals of electron detachment from anions.

$O_4H_9^-$ isomers: For n=4, six isomers were found on the PES. The graphical results are displayed in Figure 6.4. The hydride−molecule complex is the global minimum. In this $H^-(H_2O)_4$ structure, each of the three coordinating water molecules interacts through one of its H nuclei with the hydride anion in $H^-(H_2O)_3$, increasing the VEDE of the latter anion−complex by 0.547 eV. Delocalization of s functions on H^- is the most important feature of the Dyson orbital, with minor green and red contours on three of the neighboring water molecules. Addition of a water molecule to the $O_3H_7^-$ DRA leads to the $[OH_2]_2OH_3^-(H_2O)$ isomer. The new water molecule forms a hydrogen bonded water dimer with one of the H_2O molecules in $O_3H_7^-$. This isomer is relatively unstable energetically and has a VEDE of 0.535 eV.

In the Eigen $O_4H_9^-$ isomer, three water molecules are hydrogen bonded with the OH_3^- protons. It is the most energetically stable isomer after the hydride ion complex. The OH_3^- fragment imposes a rigid three−fold geometry on this cluster. The relative stability of this isomer suggests that a micro−solvated OH_3^- cluster with a complete solvation shell is more stable than other isomers. The Dyson orbital is a localized function represented by red contours that spread over all the exterior non−bonding H nuclei in the water network. The next isomer is the Ring form of $O_4H_9^-$, in which the $O_3H_7^-$ kernel is connected to a bridging water molecule that forms a four−member ring. The dominance of green contours on the acceptor water molecule is the characteristic feature of the Dyson orbital. Delocalization of the Dyson orbital over the remaining unshared H's can also be seen.

The last two structural isomers originate from the typical Zundel cationic structures where the proton is shared by two water molecules. For these isomers, each of the water molecules in the $O_2H_5^-$ fragment forms a hydrogen bond with one water molecule in the *cis* and *trans* orientations. In the *cis* isomer, the new water molecule forms a water dimer. At the initial cationic geometry, the *trans* anionic isomer converges to a structure that closely resembles the *cis* isomer except for the orientation of H nuclei in the periphery. The structural distortion arises from the rotation of one $[H_2O]_2$ about the bridging H nuclei. The

trans isomer is more energetically stable than the *cis* by 0.151 eV. Also, the VEDE of the *trans* isomer is more than that of the *cis* isomer by 0.146 eV. The Dyson orbitals of both anions correspond to diffuse, red contours whose largest amplitudes occur on the exterior H nuclei. Minor antibonding relationships with the neighboring valence functions can also be seen.

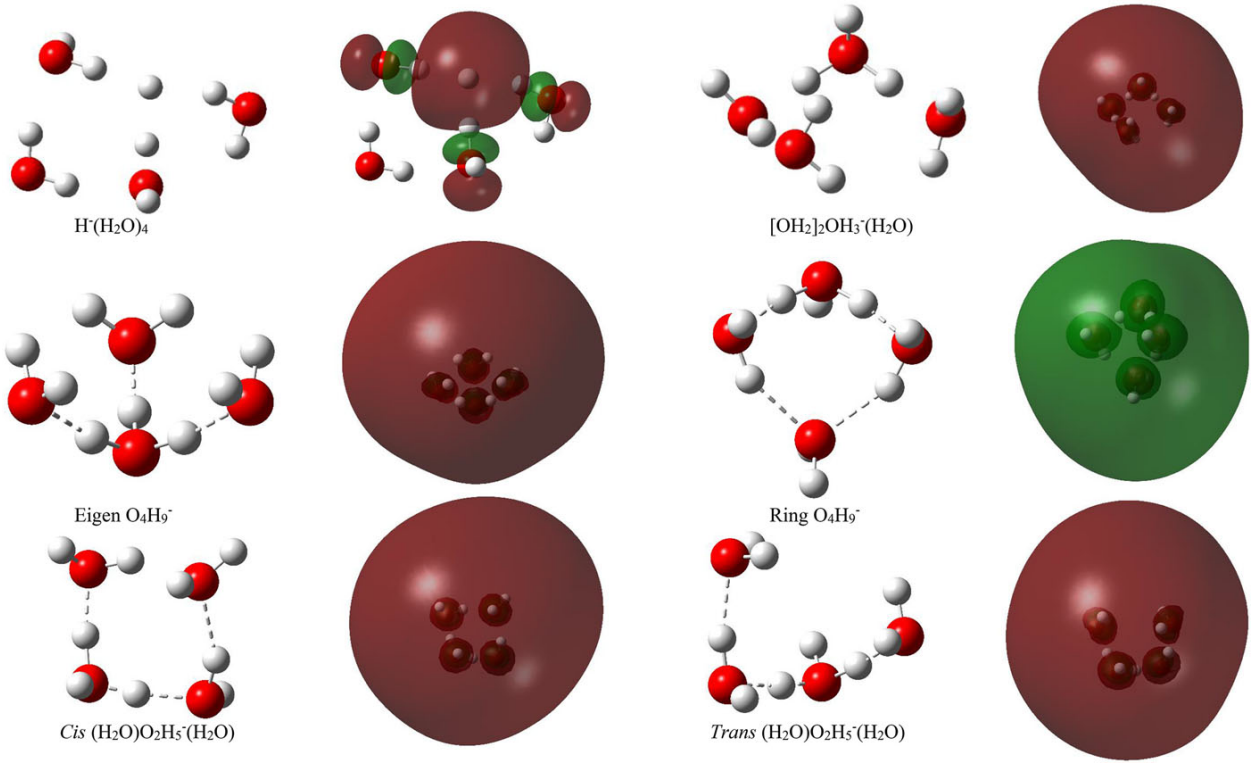


Figure 6.4: $n = 4$: Optimized geometries and Dyson orbitals of electron detachment from $O_4H_9^-$ anions.

$O_5H_{11}^-$ isomers: The coordination of a water molecule to the $O_4H_9^-$ isomers through hydrogen bonding or electrostatic interactions leads to six $O_5H_{11}^-$ isomers. Graphical results for the $O_5H_{11}^-$ isomers are displayed in Figure 6.5. The $H^-(H_2O)_5$ is at least 2.7 eV more energetically stable than the DRAs. The VEDE of $H^-(H_2O)_4$ increases by 0.329 eV upon the addition of an H_2O through electrostatic interactions. The Dyson orbital remains localized on the hydride's nucleus with slight delocalization onto the water H's. Addition of a hydrogen−bonded water dimer denoted by $[H_2O]_2$ to the $O_3H_7^-$ DRA results in B1 $O_5H_{11}^-$ isomer whose VEDE has decreased by 0.01 eV. In other words, the B1

$O_5H_{11}^-$ isomer is an Eigen $O_4H_9^-$ ion in which one of the H's in the OH_3^- fragment engages in further hydrogen bonding. The Dyson orbital accumulates on the external hydrogens. The B2 $O_5H_{11}^-$ structure consists of an Eigen−like anionic fragment in which two of the H's in the OH_3^- fragment engage in further hydrogen bonding with a water molecule. The three water molecules that form hydrogen bonds with the H nuclei of OH_3^- DRA do so at 1.55 Å, suggesting typical hydrogen bonds. The water in the second solvation shell forms a hydrogen bond at 1.84 Å, suggesting a relatively weak hydrogen bond compared with those in the first solvation shell. There is a decrease in the VEDE by 0.09 eV compared to the Eigen $O_4H_9^-$ DRA.

The C $O_5H_{11}^-$ isomer has the smallest VEDE among the $O_5H_{11}^-$ structures. The parent cationic core forms a linear chain of water molecules with two H nuclei in the OH_3^+ unit. After optimization, the cationic Chain $O_5H_{11}^+$ rearranges to form a book−like anionic isomer. Three water molecules form hydrogen bonds with the OH_3^- framework to complete the primary solvation shell while the remaining water enters the secondary solvation shell. The Dyson orbital is diffused over the non−bonding H nuclei with its largest amplitudes on the exterior water H nuclei. The PR $O_5H_{11}^-$ isomer also undergoes structural rearrangement upon optimization at the cationic geometry to form another book−like isomer. In this isomer, an $O_3H_7^-$ DRA fragment can be seen. Each of the two water molecules forms hydrogen bonds with the H_2O molecules originally bonded to H nuclei in the OH_3^- fragment. This isomer has the lowest VEDE of 0.499 eV. The positive red contour of the Dyson orbital densely populates the regions between the non−bonded H nuclei in the OH_3^- fragment and those from the two acceptor water molecules. Small, delocalized, green contours are seen on the remaining non−bonding H nuclei. In the remaining Ring $O_5H_{11}^-$ isomer, the parent cationic core forms a tetramer ring through hydrogen bonding with one acceptor H_2O. The optimized anionic geometry looks structurally like the parent cationic core. It has the lowest VEDE of 0.506 eV. The Dyson orbital spreads over the H nuclei of the acceptor water molecule with some negligible delocalization on neighboring non−bonding protons.

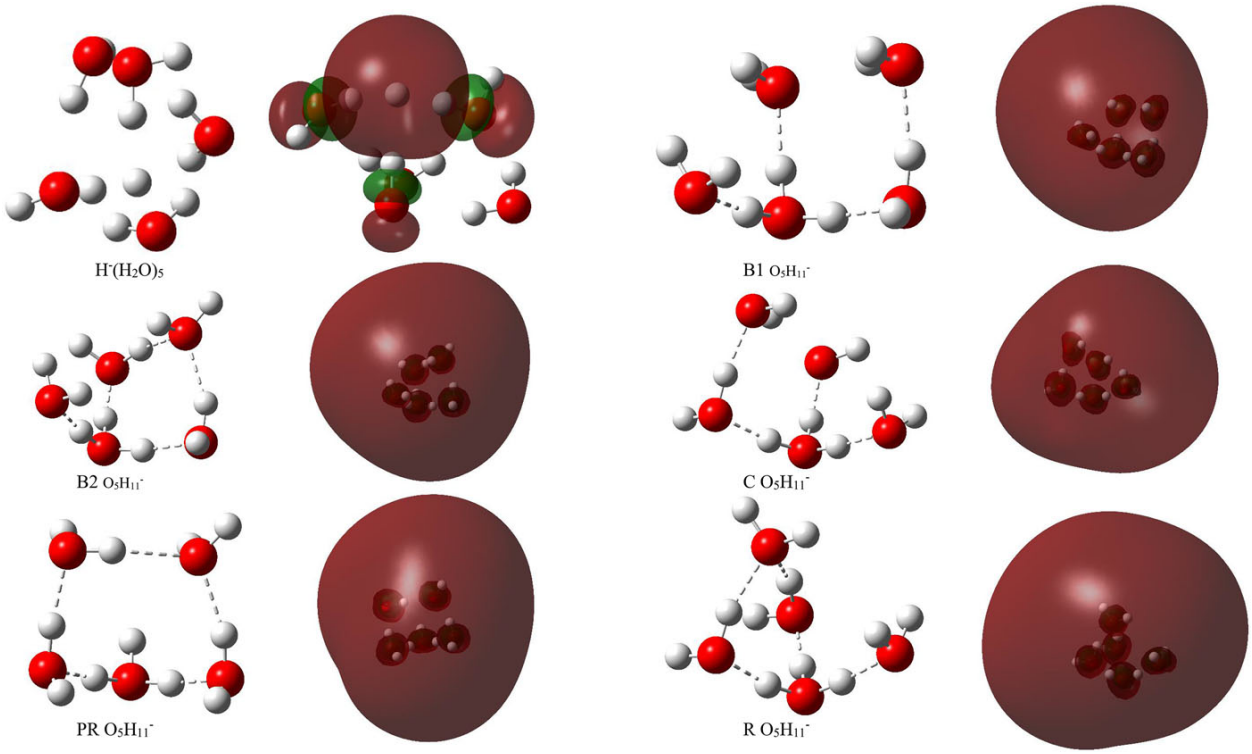


Figure 6.5: $n = 5$: Optimized geometries and Dyson orbitals of electron detachment from $O_5H_{11}^-$ anions.

$O_6H_{13}^-$ isomers: There are ten geometric isomers of the anionic hydronium water hexamer clusters. The optimized geometries and Dyson orbitals of the lowest VEDE are illustrated in Figure 6.6. Only P3+ electron propagator calculations were carried out for these isomers, for data in Table 6.2 show that P3+ generally gives good VEDEs compared to BD−T1, albeit with lower pole strengths. Hereafter, only P3+ results are discussed.

The hydride anion−molecule complex is the most energetically stable with the lowest VEDE of 4.553 eV. All the water molecules have their protons oriented towards the H^- anion. The Dyson orbital accumulates on the hydride anion and has antibonding relationships with valence functions on the neighboring O−H bonds. The remaining nine $O_6H_{13}^-$ isomers were obtained from their corresponding parent cationic cores. The cage C1 $O_6H_{13}^-$ isomer strongly retains its cationic geometry orientation with a VEDE of 0.469 eV. The diffuse Dyson orbital is spread chiefly over the H's in the water network. Two structures pertain to the Eigen−like configurations E1 $O_6H_{13}^-$and E2 $O_6H_{13}^-$, for their corresponding cationic

cores contain the $O_4H_9^+$ Eigen fragment. The two new water molecules enter the second solvation shell through hydrogen bonding. The optimized anionic structures are distorted when compared with their cationic counterparts, for the two water molecules originally in the second solvation shell of the cationic core form a water dimer acceptor molecule in the molecular anion. The E1 $O_6H_{13}^-$ isomer has a smaller VEDE than the E2 $O_6H_{13}^-$. In both E1 $O_6H_{13}^-$ and E2 $O_6H_{13}^-$, the nearly symmetric diffuse Dyson orbitals are localized on the H's of the water network.

The P1 $O_6H_{13}^-$ isomer arises from the parent cationic core in which the new water molecule enters the secondary solvation shell from the Ring $O_5H_{11}^+$ isomer. A water dimer is formed in the second coordination shell of the anionic P1 $O_6H_{13}^-$ isomer. A near symmetric $s-$like Dyson orbital whose largest amplitudes occur over the peripheral water network can be seen. Four isomers arise from parent cationic cores that contain water tetramer rings. In the T1 $O_6H_{13}^-$ isomer, an Eigen$-$like $O_4H_9^-$ can been seen with a water molecule forming a bridging hydrogen bond with two of the water molecules in $O_4H_9^-$. The bridging water molecule forms an additional hydrogen bond with one of its protons to form a water dimer. A diffuse Dyson orbital spreads over the H nuclei of the water network. In the T2 $O_6H_{13}^-$ isomer, the bridging water molecule does not interact with the water in the second solvation shell as it forms a hydrogen bond with one of the water molecules directly bonded to the OH_3^- fragment. The Dyson orbital is diffused over the peripheral hydrogens with its largest amplitudes on the bridging water molecule and the one in the secondary shell. There are low amplitudes near the lone pairs on the oxygens.

The T3 and T4 $O_6H_{13}^-$ isomers have book$-$like structures. The Dyson orbital in both instances spreads over the regions of the water network with its highest amplitudes on the acceptor water molecules. The last isomer is the Z1 $O_6H_{13}^-$ isomer, which arises from the Zundel$-$like solvated cationic core. The anionic geometry contains the $O_2H_5^-$ fragment with a non$-$symmetric proton. Each of the exterior hydrogens in the $O_2H_5^-$ fragment was anticipated to form a hydrogen bond with a water molecule to complete the first solvation

shell of the Zundel−like anionic isomer. However, the optimized geometry shows that one of the water molecules leaves the second solvation shell to form a water dimer with one of the exterior water molecules. This observation indicates that anionic hydronium water clusters prefer the Eigen $O_4H_9^-$ geometry over the Zundel $O_6H_{13}^-$structure. Sobolewski and Domcke[133] observed the same trend in $H_3O(H_2O)_n$ clusters composed of a hydronium radical and water molecules. The Dyson orbital of electron attachment is diffused over the $O_6H_{13}^+$ core.

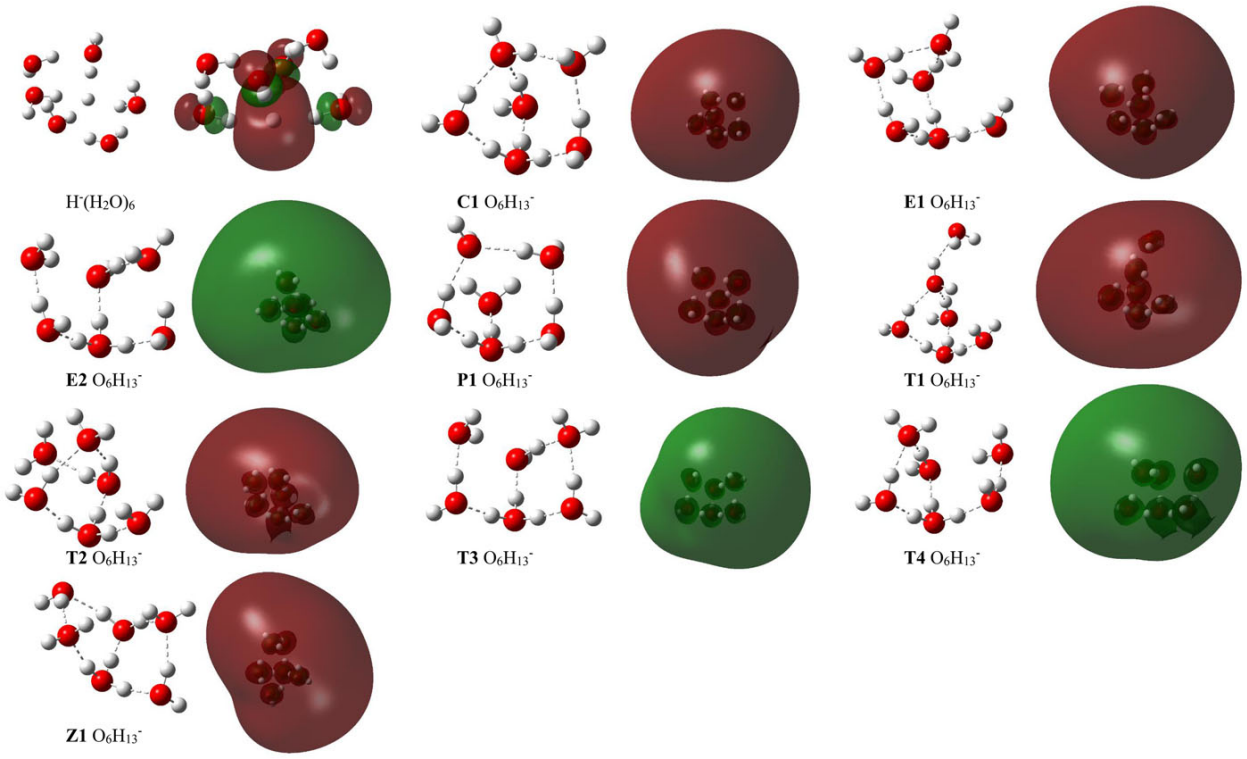


Figure 6.6: n = 6: Optimized geometries and Dyson orbitals of electron detachment from $O_6H_{13}^-$ anions.

6.3 Concluding Remarks on $O_nH_{2n+1}^-$ Double Rydberg Anions

Micro−solvated H_3O^+ can exist in both Eigen−like $H_9O_4^+(H_2O)_n$ and Zundel−like $H_5O_2^+(H_2O)_n$ structures. The VEAEs of these cations decrease with increasing cluster size. The corresponding Dyson orbitals show that with increasing cluster size, the diffuse electron migrates from the closed shell H_3O^+ core to form a cloud in the network of water molecules.

Solvation of the OH_3^- and $O_2H_5^-$ DRAs through electrostatic interactions or hydrogen bonding with their solvation shells results in remarkable changes in geometry with respect to cationic antecedents. Interaction of water molecules with the OH_3^- DRA leads to several cluster isomers in which the Dyson orbital is held at the periphery of the hydrogens in the water network. It is seen that the stable H_3O^- unit imposes a rigid structure on these complexes, especially for isomers with closed solvation shells such as the Eigen $H_3O^-(H_2O)_3$ structure. The $O_2H_5^-$ fragment ion also imposes a rigid geometry on the Zundel $O_2H_5^-(H_2O)_4$ isomer. For all these clusters, the Rydberg electrons are held by the exterior protons from the water network.

Several isomers of oxygen−based OH_3^-DRAs may occur through hydrogen bonding, as $OH_3^-(H_2O)_n$ structures or as electrostatic $H^-(H_2O)_n$ complexes. For all values of n, the anion−water complex $H^-(H_2O)_n$ is always the most stable, with large VEDEs which increase with cluster size. Generally, the $OH_3^-(H_2O)_n$DRA isomers have well separated VEDEs and therefore should be visible in anion photoelectron spectra.

Chapter 7

Prediction of New Molecules and Anions: Double Rydberg Anions, Rydberg Radicals and Micro−solvated Cations with Ammonium−Water Kernels

In this chapter, I present the major findings from my work on $NH_4^-(H_2O)_n$ double Rydberg anions published elsewhere.[89]

7.1 Electron Binding Energies and Dyson Orbitals of $NH_4^-(H_2O)_n$ Clusters

In double Rydberg anions (DRAs), a closed−shell, cationic core binds a pair of electrons held in diffuse orbitals. For example, in the NH_4^- or OH_3^- DRAs, an ammonium or hydronium cation is surrounded by a pair of peripheral electrons. The first DRA, tetrahedral NH_4^-, was discovered during a pioneering photoelectron spectroscopic study on an anion−molecule complex, $H^-(NH_3)$.[134] Since NH_4^- and $H^-(NH_3)$ have identical mass, their electron detachment energies appeared as separate peaks in the same spectrum. The persistence of the spectral peak at a low vertical electron detachment energy (VEDE) under a variety of ion−source conditions, the absence of an energetic shift after full deuterium substitution for the hydrogens, and previous investigations on the NH_4 radical led to the identification of tetrahedral NH_4^- as a DRA. The measured VEDE of NH_4^- was 0.472 eV, an amount resembling that of the sodium atomic anion (0.548 eV).

High−level theoretical calculations have provided strong complementary support for the identification of DRAs. Prior to the discovery of the NH_4^- DRA, some theoretical studies had considered the existence of a tetrahedral isomer of NH_4^-. Ortiz[135] applied techniques of *ab initio* electron propagator theory (EPT) to study the geometric isomers and vertical ionization energies of NH_4^- and proposed the tetrahedral structure to be a viable DRA. The two stable isomers were assigned to a hydride–molecule complex $H^-(NH_3)$ and a tetrahedral

counterpart, NH_4^-, with VEDEs of 1.20 eV and 0.42 eV, respectively, in precise agreement with the experimental results. Evidence of the diffuse, Rydberg−state distribution of the two diffuse electrons which surround the NH_4^+ cationic core was provided. Subsequent theoretical studies on the NH_4^- DRA also reported the VEDE to be near 0.45 eV.

Photoelectron spectroscopy has enabled the identification of several DRA clusters among the $N_nH_{3n+1}^-$ (n = 1–5) isomers. Isomers of DRAs belong to three categories: (1) hydrides coordinated to n solvent molecules, (2) electrostatically bound intermolecular complexes with solvent molecules, and (3) hydrogen−bonded DRA−molecule complexes. *Ab initio* EPT studies[15,16] have revealed identical isomeric patterns and electron binding energies in close agreement with experimental data. More recent EPT investigations have found three new classes of DRAs: methylated, annulated, and paramagnetic. Prior to this investigation, the existence of NH_3R^- and OH_2R^- (R = F, OH, NH_2, and CH_3) sets of DRAs that are stable minima in their potential energy surfaces and have positive VEDEs had been reported. A tetrahedral PH_4^- DRA has been identified in a study that also predicted a C_{2v} isomer with a lone pair of electrons occupying an equatorial position in a trigonal bipyramidal arrangement.

Ortiz performed computational studies on OH_3^- isomers and identified a pyramidal, C_{3v} DRA with a VEDE of 0.43 eV. However, several experimental efforts to characterize the OH_3^- DRA have not been successful. Melin and Ortiz therefore conducted *ab initio* EPT studies on the reaction barrier between the OH_3^- DRA and a hydride–water complex. The barrier between the NH_4^- DRA and a hydride–ammonia complex also was examined. The low reaction barrier between the OH_3^- DRA and the hydride–water complex indicates that the former species may be difficult to isolate. Evidence of the existence of $O_2H_5^-$ DRAs in analogy with $N_2H_7^-$ was also reported. Several DRAs based on elements other than N are also known from computational studies.

DRAs, Rydberg radicals, their electronic structure and reactivity have been reviewed elsewhere. The lowest diffuse orbitals in DRAs and Rydberg radicals are spheroidal and

mimic valence s orbitals of alkali atoms. In their excited states, orbitals with major contributions from diffuse s−, p−, d−, f−, or g−functions may be occupied. Large molecular systems (such as clusters) may feature different types of Rydberg states and orbitals. Previous and recent studies have established that these unique molecular systems also participate in Rydberg–type chemical bonding in analogy with alkali–metal diatomic molecules and larger clusters. Rydberg patterns of chemical bonding also manifest in protein fragments.

Discovery and identification of novel DRAs and solvated–electron precursors (which include metal–ammonia complexes with diffuse electrons) have relied heavily on techniques of *ab initio* EPT. In a recent publication on this subject, we extended the scope of the DRA concept to oxygen−based systems with the general formula $O_nH_{2n+1}{}^-$. Isomers that feature hydride–water interactions were compared with species in which the pyramidal H_3O^- DRA is stabilized by ion–dipole or hydrogen–bonding interactions with water molecules. For all values of n studied, the anion–water complex $H^-(H_2O)_{n+1}$ is always the most stable and has relatively large VEDEs. DRA–molecule complexes (i.e., $OH_3{}^-(H_2O)_n$ isomers) have much lower VEDEs and may be detectable in anion photoelectron spectra. For all $O_nH_{2n+1}{}^-$ DRAs, Dyson orbitals occupy regions beyond the peripheral O–H bonds. We also calculated the vertical electron attachment energies (VEAEs) of $OH_3{}^+(H_2O)_n$ clusters and excitation energies of the $OH_3{}^+(H_2O)_n$ Rydberg radicals. The VEAEs decrease with increasing n and the corresponding Dyson orbitals are diffused over exterior, non-hydrogen bonded protons.

Can the concepts of DRAs and their ion-molecule clusters be extended to systems in which the cationic kernel is not a protonated micro-solvent molecule? Are the same extensions applicable to Rydberg radicals and their micro-solvated clusters? These questions prompted a thorough search of the chemical literature and evidence of ammonium–water cationic clusters $NH_4{}^+(H_2O)_n$ was found. Structural and energetic properties of $NH_4{}^+(H_2O)_n$ clusters were probed by free jet expansion experiments and *ab initio* calculations decades ago. Later computational studies also found several other low–lying isomers. At the MP2 level of theory, in conjunction with correlated basis sets, the $NH_4{}^+(H_2O)_n$ (n =1–10) isomers

have been studied with a view to their atmospheric abundance as a function of temperature. An extensive study on $NH_4^+(H_2O)_n$ (n =1–10) isomers and the effects of temperature and humidity on cluster growth patterns has also appeared in the literature.

$NH_4^+(H_2O)_n$ clusters are reportedly abundant in the biosphere and an understanding of them is essential for modeling atmospheric and interstellar processes. Studies on electronic structure and properties of molecular ions in aqueous media provide theoretical guidance in many chemical and biological processes. Concepts of acid-base chemistry, redox reactions, electrochemistry, and a multitude of organic and inorganic reactions are often defined in terms of proton and electron transfer. Understanding the behavior of protons and electrons in aqueous media is a perennial concern in physical chemistry.

Structure and bonding in micro-solvated $NH_4^{+,0,-}(H_2O)_n$ (n = 1–4) clusters therefore deserve further study. All cationic $NH_4^+(H_2O)_n$ isomers reported in the literature so far are reconsidered. Addition of an electron produces uncharged clusters in which an NH_4 Rydberg radical is coordinated to water molecules. Excitation energies of several low-lying states of $NH_4(H_2O)_n$ Rydberg radicals are also calculated. Three kinds of anionic structures emerge from geometry optimizations. Micro-solvated hydride anions are denoted henceforth by $H^-(NH_3)(H_2O)_n$. The NH_4^- DRA with coordinated water molecules is represented by $[NH_4^-](H_2O)_n$. The formula $NH_4^-(H_2O)_n$ stands for structures with two diffuse electrons and a cationic kernel in which ammonium forms hydrogen bonds with water molecules.

I have employed correlated *ab initio* electron-propagator and coupled-cluster methods with large, diffuse basis sets to study $NH_4^+(H_2O)_n$ clusters, $NH_4(H_2O)_n$ Rydberg molecules, $H^-(NH_3)(H_2O)_n$, $[NH_4^-](H_2O)_n$, $NH_4^-(H_2O)_n$ DRAs, and related micro-solvated species. The primary focus of this work is prediction of structures, relative total energies, vertical electron binding energies, and Dyson orbitals of $NH_4^{+,0,-}(H_2O)_n$ (n = 1–4) clusters. Calculations on micro-solvated $NH_4^{+,0,-}(H_2O)_n$ (n = 1–4) clusters provide Aufbau rules for electrons that occupy the periphery of these complexes.

Table 7.1: $NH_4^-(H_2O)_n$ isomers and their vertical electron detachment energies (VEDEs). Pole strengths are in parentheses. All energies are in eV. [a]

n	Isomer		KT	D2	P3+	BD−T1	ΔCCSD(T)
1	$H^-(NH_3)H_2O$	0.000	2.512	1.969 (0.893)	1.985 (0.908)	2.172 (0.882)	2.085
	$[NH_4^-]H_2O$	1.148	0.368	0.770 (0.877)	0.723 (0.854)	0.684 (0.881)	0.675
	1a $NH_4^-(H_2O)$	1.194	0.211	0.575 (0.872)	0.517 (0.835)	0.495 (0.862)	0.491
2	$H^-(NH_3)(H_2O)_2$	0.000	3.135	2.574 (0.903)	2.576 (0.908)	2.771 (0.831)	2.693
	$[NH_4^-](H_2O)_2$	1.667	0.490	0.954 (0.881)	0.920 (0.866)	0.886 (0.894)	0.886
	2a $NH_4^-(H_2O)_2$	1.641	0.186	0.607 (0.873)	0.558 (0.835)	0.539 (0.870)	0.553
	2b $NH_4^-(H_2O)_2$	1.557	0.238	0.621 (0.862)	0.568 (0.829)	0.552 (0.864)	0.556
3	$H^-(NH_3)(H_2O)_3$	0.000	3.980	3.352 (0.908)	3.364 (0.908)	3.567 (0.900)	3.470
	$[NH_4^-](H_2O)_3$	1.923	0.632	1.138 (0.886)	1.112 (0.874)	1.075 (0.899)	1.081
	3a $NH_4^-(H_2O)_3$	1.925	0.143	0.534 (0.860)	0.471 (0.812)	0.459 (0.856)	0.481
	3b $NH_4^-(H_2O)_3$	1.971	0.169	0.575 (0.857)	0.513 (0.809)	0.498 (0.856)	0.517
	3c $NH_4^-(H_2O)_3$	1.809	0.186	0.574 (0.863)	0.525 (0.827)	0.537 (0.868)	0.551
4	$H^-(NH_3)(H_2O)_4$	0.000	4.192	3.543 (0.908)	3.551 (0.903)	3.756 (0.896)	3.659
	$[NH_4^-](H_2O)_4$	2.061	0.730	1.240 (0.889)	1.213 (0.877)	1.177 (0.900)	1.183
	4a $NH_4^-(H_2O)_4$	2.126	0.141	0.523 (0.861)	0.470 (0.817)	0.473 (0.860)	0.481
	4b $NH_4^-(H_2O)_4$	2.195	0.148	0.522 (0.838)	0.452 (0.785)	0.432 (0.853)	0.439
	4c $NH_4^-(H_2O)_4$	2.178	0.162	0.521 (0.840)	0.457 (0.795)	0.455 (0.858)	0.474
	4d $NH_4^-(H_2O)_4$	2.264	0.173	0.586 (0.848)	0.529 (0.803)	0.515 (0.859)	0.530
	4e $NH_4^-(H_2O)_4$	2.318	0.183	0.566 (0.839)	0.509 (0.799)	0.534 (0.863)	0.564

[a]Isomerization energies in third column are obtained at the CCSD(T) with MP2 zero-point energy corrections.

7.2 Vertical Electron Detachment Energies and Dyson Orbitals of $NH_4^-(H_2O)_n$ Double Rydberg Anions

Table 7.1 presents various isomers and their relative energies that pertain to $NH_4^-(H_2O)_n$ (n=1–4) DRAs. It is evident that for all values of n, the hydride–molecule complex is the most stable isomer. Similar conclusions were reached for DRAs based on nitrogen [87] and oxygen.[88] Isomerization energies obtained with lower levels of theory do not differ significantly from those obtained at the CCSD(T) plus MP2 zero−point corrections shown in Table IV. Only results from the latter method are discussed in the text.

Results for the lowest VEDEs obtained at the uncorrelated (KT) level and with various diagonal self−energy approximations (D2, D3, OVGF, P3, and P3+) are reported in the published article[89] and Appendix L. In most cases, VEDEs calculated with EPT methods

that retain only the diagonal self−energy matrix elements have pole strengths below 0.85. OVGF results are unencouraging and therefore not recommended for studies on DRAs, as earlier noted in studies on $O_nH_{2n+1}^-$ DRAs.[88] When pole strengths are below 0.85, electron binding energies and associated Dyson orbitals of diagonal self−energy approximations should be treated with caution. Thus, approximations that retain the full self−energy matrix are convenient for such instances.

To facilitate reliable prediction of VEDEs, pole strengths and corresponding Dyson orbitals, we made use of the non−diagonal BD−T1 approximation, and the resulting data are included in Table 7.1. In BD−T1, all matrix blocks of the superoperator Hamiltonian that occur in the hole (h), particle (p), two−hole−one−particle ($2hp$) and two−particle−one−hole ($2ph$) operator manifolds are explicitly evaluated except the second−order couplings between $2ph$ and $2hp$ operators. The BD−T1 approximation employs the Brueckner doubles (BD) reference determinant and its doubly excited amplitudes instead of the Hartree−Fock reference state. In addition to predicting high−accuracy VEDEs, Dyson orbitals from BD−T1 have better qualitative features than canonical molecular orbitals. Hence, only VEDEs obtained with the BD−T1 method are discussed in the text.

To judge the reliability of the VEDEs predicted with EPT methods, we performed ΔCCSD(T) estimations of VEDEs with the d−aug−cc−pVTZ basis set, and the results are also presented in Table 7.1. Optimized geometries and Dyson orbitals of the DRAs are displayed in Figures 7.1–7.4. Note that all the reported Dyson orbitals are based on the highly accurate BD−T1 approximation. VEDEs obtained at the BD−T1 level agree closely with those from indirect ΔCCSD(T) calculations. Note that throughout this section on anions, $H^-(NH_3)_n$ denotes hydride-molecule complexes, $[NH_4^-](H_2O)_n$ designates NH_4^- DRA−water complexes without NH−O bridges, and $NH_4^-(H_2O)_n$ corresponds to micro-solvated DRAs that form H bridges with water molecules.

$NH_4^-(H_2O)$ isomers: For $n = 1$, three isomers are obtained as displayed in Figure 7.1. In the $H^-(NH_3)H_2O$ complex, the hydride anion is weakly coordinated by the ammonia

and water molecules, but this structure is the most stable. The predicted VEDE is near 2 eV. Given the high stability of this complex, a dominant peak near this range is anticipated in anion photoelectron spectra. The Dyson orbital of this complex is chiefly a totally symmetric s-function on the hydride's nucleus that displays anti−bonding relationships with N–H and O–H bond functions. The optimized geometry suggests that H^- has a stronger attraction towards the water molecule than the ammonia molecule. Thus, the VEDE of the free H^- (0.75 eV) has been increased by electrostatic and other interactions with the solvent molecules.

In the next most stable isomer, an NH_4^- DRA−molecule complex is formed and denoted by $[NH_4^-]H_2O$. This complex has C_{2v} symmetry with a VEDE of 0.684 eV. The diffuse Dyson orbital is held at the periphery of the NH_4^- DRA with minor delocalization. The two radial nodes anticipate the $3s$ united-atom limit for the Dyson orbital. Alternative DRA-molecule structures composed of OH_3^- and NH_3 fragments rearrange without a barrier under optimization to the $[NH_4^-]H_2O$ minimum.

In the least stable **1a** $NH_4^-(H_2O)$ isomer, a C_s cluster complex is obtained. The existing hydrogen bond between the N and O nuclei occurs at 1.8371 Å. The predicted VEDE of 0.495 eV is slightly above that of NH_4^- and $N_2H_7^-$ as well as slightly below those of OH_3^- and $O_2H_5^-$ DRAs. The Dyson orbital is an approximately spherical function whose highest amplitudes occur beyond the non-bridging protons.

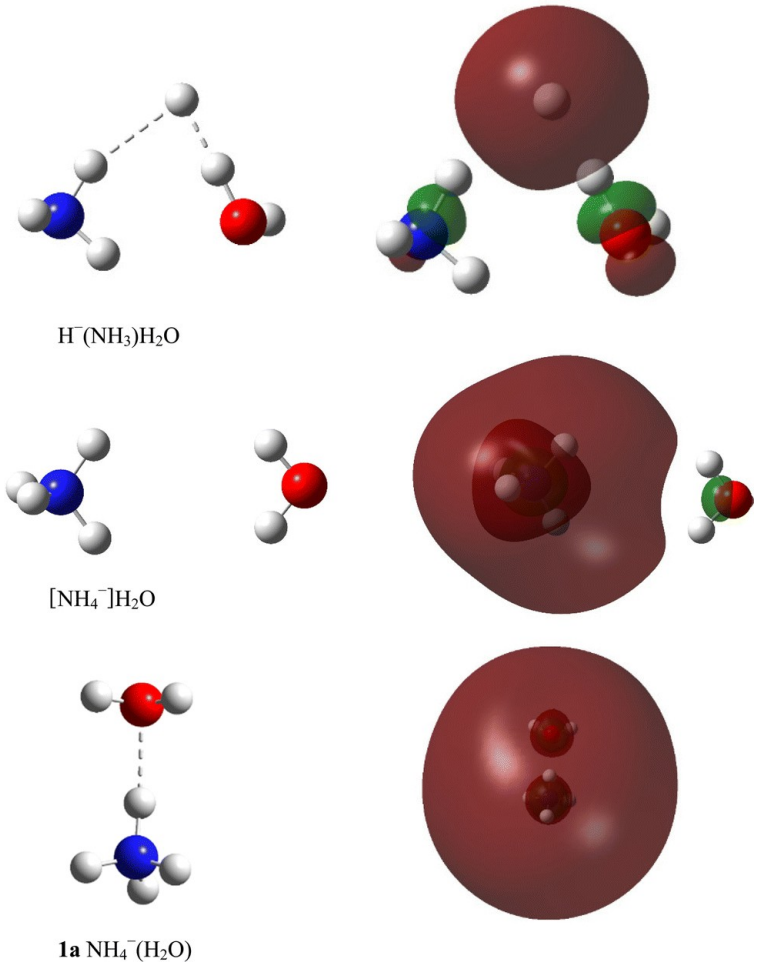


Figure 7.1: $n = 1$ Optimized geometries and Dyson orbitals of electron detachment from $NH_4^-(H_2O)$ isomers.

$NH_4^-(H_2O)_2$ isomers:

The hydride–molecule complex retains its high stability upon addition of H_2O to form $H^-(NH_3)(H_2O)_2$. The VEDE increases by 0.599 eV from the $H^-(NH_3)H_2O$ complex. Thus, addition of a water molecule increases the VEDE. This may be attributed to the stronger attraction of the H^- towards the water molecules than the ammonia. The totally symmetric diffuse Dyson orbital localizes near the $H^-$with slight anti-bonding relationships involving nearby solvent molecules.

In the $[NH_4^-](H_2O)_2$ DRA-molecule complex from Figure 7.2, the NH_4^- DRA weakly interacts with the protons of the water molecules through electrostatic interactions in a C_{2v}

arrangement. The VEDE is 0.886 eV. The Dyson orbital is a diffuse *s*-like function with two radial nodes and minor delocalization to neighboring solvent molecules.

The remaining two isomers, **2a** $NH_4^-(H_2O)_2$ and **2b** $NH_4^-(H_2O)_2$, are hydrogen-bonded DRA clusters. **2b** $NH_4^-(H_2O)_2$ is more stable than **2a** $NH_4^-(H_2O)_2$. In **2a** $NH_4^-(H_2O)_2$, two of the protons of NH_4^- engage in hydrogen bonding with water molecules in a C_{2v} arrangement. **2b** $NH_4^-(H_2O)_2$ has a discernable $NH_4^-(H_2O)$ fragment interacting with an additional water molecule engaging in hydrogen bonding to form a water dimer. VEDEs of 0.539 and 0.552 eV, respectively, are obtained for the **2a** and **2b** isomers. Both isomers have Dyson orbitals whose maximum amplitudes lie beyond the non-bridging protons on the periphery of the complex, especially those associated with the NH_4^- fragment.

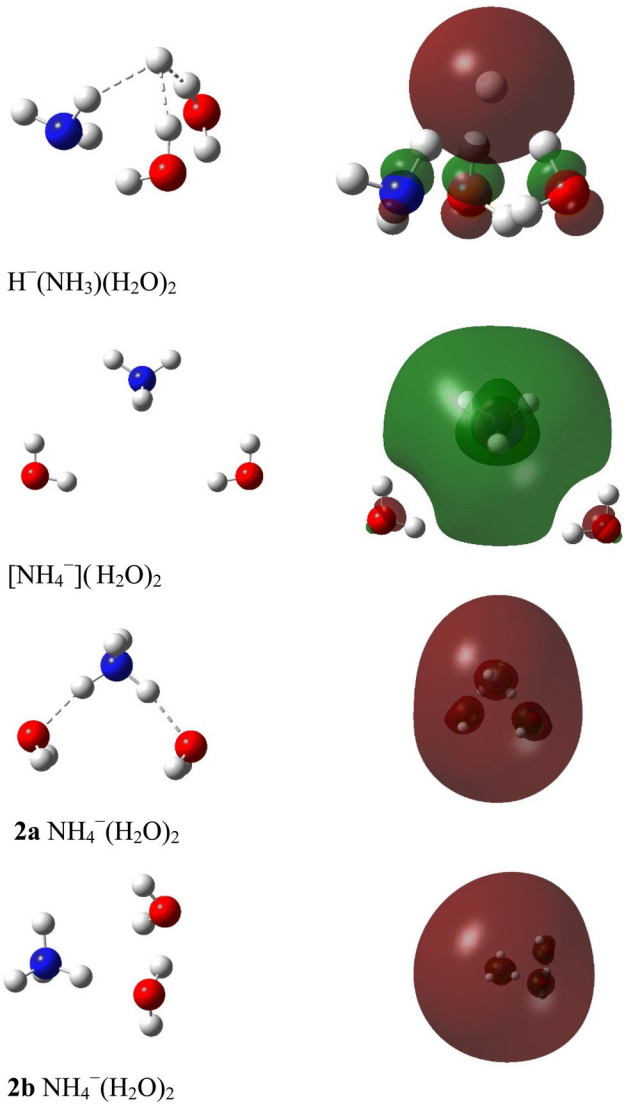


Figure 7.2: $n = 2$ Optimized geometries and Dyson orbitals of electron detachment from $NH_4^-(H_2O)_2$ isomers.

$NH_4^-(H_2O)_3$ isomers:

For $n = 3$, five isomers are obtained: a hydride-molecule complex, a DRA-molecule complex, and three hydrogen-bonded DRA clusters as displayed in Figure 7.3. The hydride-molecule complex $H^-(NH_3)(H_2O)_3$, emerges as the most stable isomer with a VEDE of 3.567 eV. Again, the new water molecule contributes to an increase in the VEDE. The Dyson orbital is a totally symmetric function centered chiefly on the hydride's nucleus that forms anti-bonding relationships with neighboring N-H and O-H bond functions.

In the next isomer, the NH_4^- DRA weakly interacts with the protons of the three water molecules to form the DRA-molecule $[NH_4^-](H_2O)_3$ complex in which two H_2O molecules form a dimer. The VEDE is 1.075 eV, which is 0.189 eV higher than that of the $[NH_4^-](H_2O)_2$ DRA-molecule complex. The Dyson orbital is a symmetric *s*-like function spread over the NH_4^- kernel with minimal delocalization.

The remaining three isomers are micro-solvated DRA clusters: **3a** $NH_4^-(H_2O)_3$, **3b** $NH_4^-(H_2O)_3$, and **3c** $NH_4^-(H_2O)_3$. Of this set, **3c** is the most stable. **3a** and **3c** are ring structures that differ in relative orientations of their protons. **3b** retains its C_3 symmetry upon addition of two electrons to the **3b** $NH_4^+(H_2O)_3$ cation. VEDEs near 0.5 eV are obtained for the three micro-solvated DRAs. The Dyson orbitals of **3a** and **3c** are diffused over the non-bridging protons. For **3b**, the pyramidal C_3 symmetry of its cation and anion yields a symmetric diffuse Dyson orbital that extends beyond the outer protons.

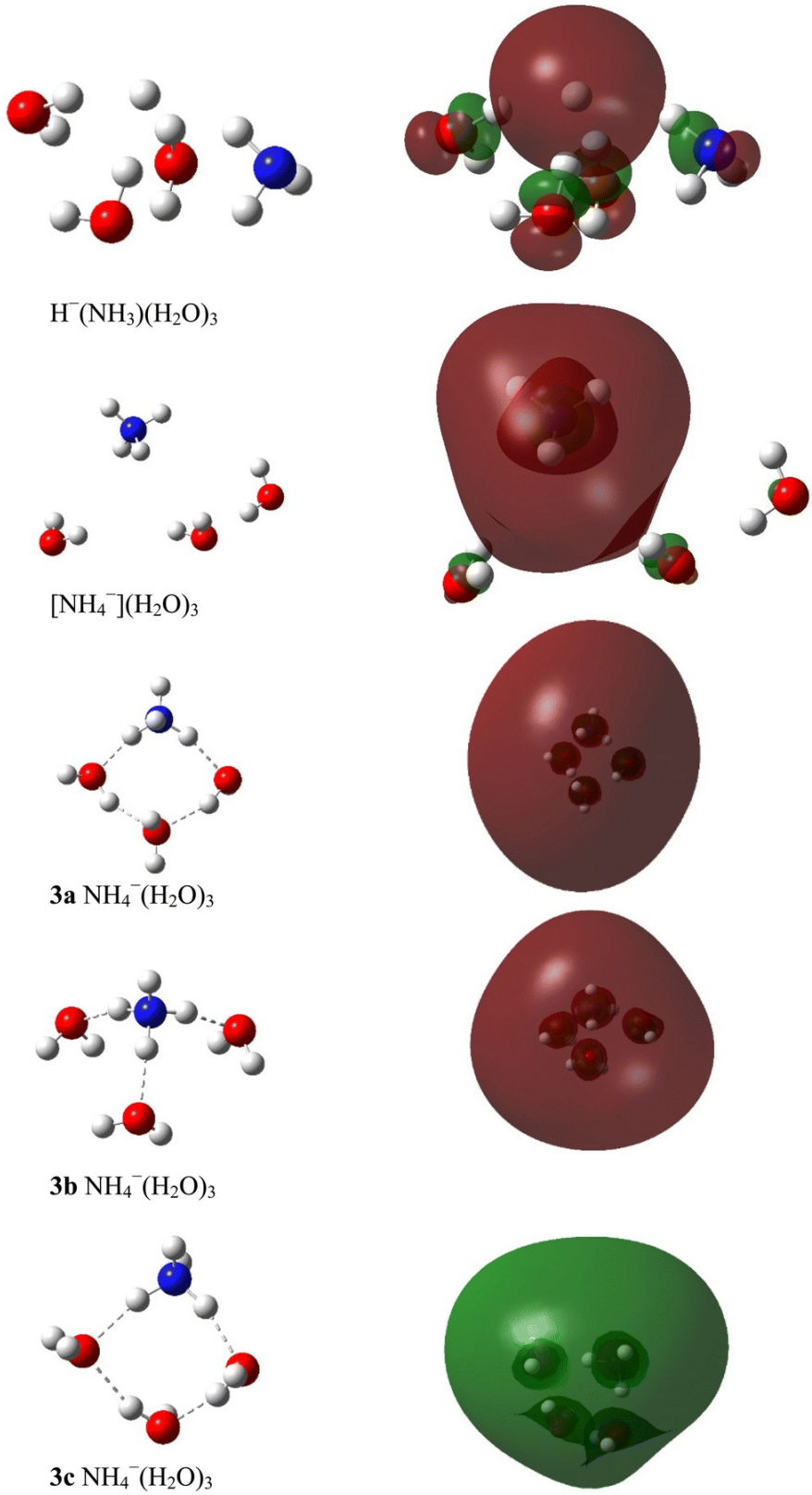


Figure 7.3: $n = 3$ Optimized geometries and Dyson orbitals of electron detachment from $NH_4^-(H_2O)_3$ isomers.

$NH_4^-(H_2O)_4$ isomers:

Coordination of a water molecule through hydrogen bonding or electrostatic interactions to the five latter structures accounts for all seven isomers in Figure 7.4 when $n = 4$. The hydride cluster, $H^-(NH_3)(H_2O)_4$, is the most stable with a large VEDE of 3.756 eV. The spherical Dyson orbital occupying the H^- ion also has some antibonding relationships with nearby N-H and O-H bond functions. The H^- ion is closer to the water molecules than to the ammonia molecule.

In the DRA-molecule complex, $[NH_4^-](H_2O)_4$, the NH_4^- DRA is stabilized by a linear chain of four water molecules. With a VEDE of 1.177 eV, its Dyson orbital spreads over the NH_4^- fragment. Minor delocalization from the nearest H_2O is discernable, and the green contours arise from orthogonalization to the valence nitrogen functions with three radial nodes. The data of Table IV indicate that the DRA-molecule complex, $[NH_4^-](H_2O)_4$, is the second most stable isomer.

The five remaining isomers, **4a-4e** $NH_4^-(H_2O)_4$, are micro-solvated DRAs arising from the reduction of their respective cationic congeners. **4a** has a three-dimensional cage structure with C_s symmetry. **4e** has a tetracoordinate NH_4^- fragment joined to a water molecule that forms hydrogen bonds with another water molecule and the anionic center. Note that a tetracoordinate NH_4^- was identified in $N_nH_{3n+1}^-$ DRAs with similar geometric features.[87] All the micro-solvated DRAs have VEDEs near 0.5 eV. The diffuse *s*-like Dyson orbitals spread over the exterior nonbonding protons with orthogonalizations to the valence functions on the nitrogen and the oxygen nuclei. For **4e**, a symmetric Dyson orbital whose amplitudes in green surround the peripheral protons displays nodes that result in red *s*-like contours on the N and O centers.[87]

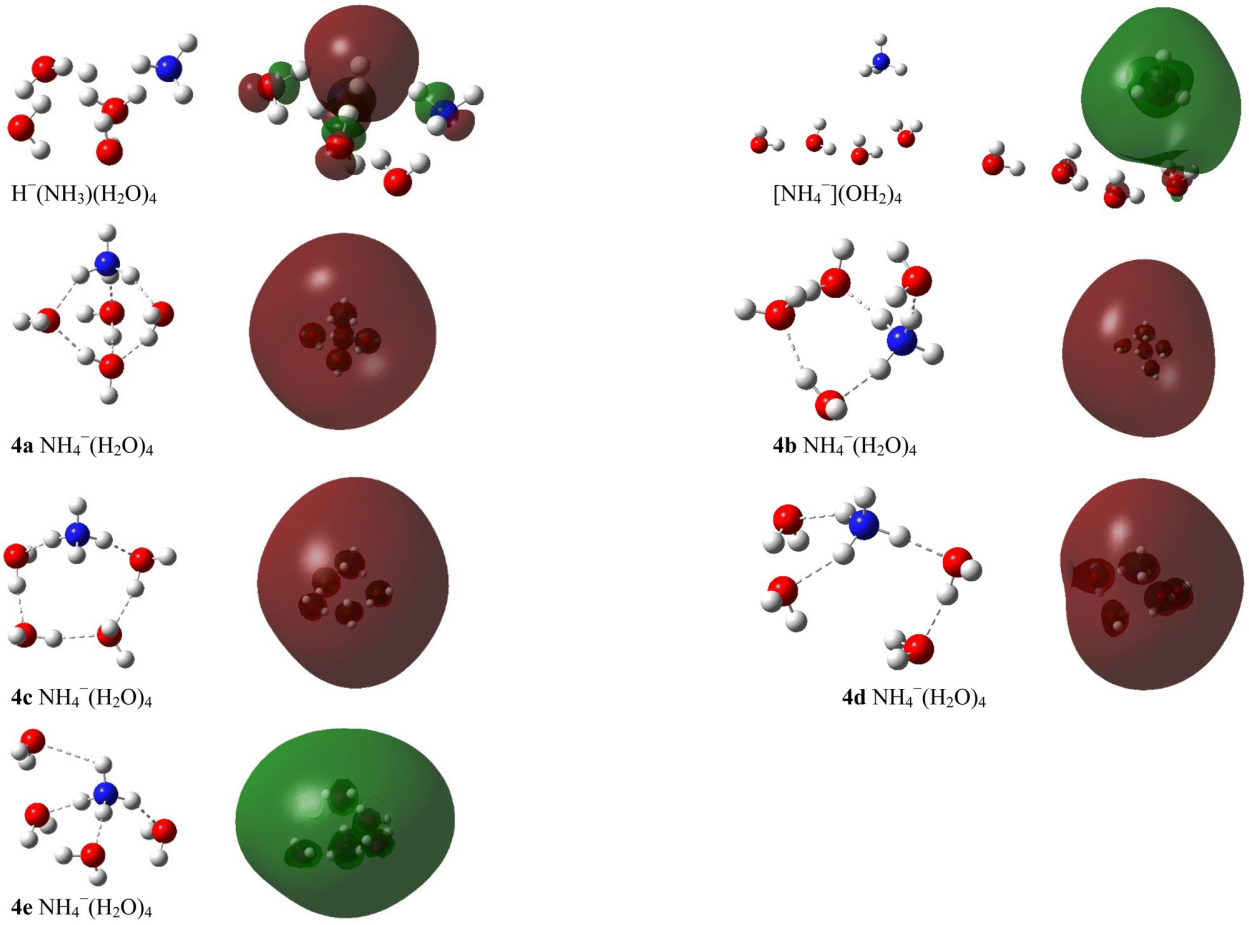


Figure 7.4: $n = 4$ Optimized geometries and Dyson orbitals of electron detachment from $NH_4^-(H_2O)_4$ isomers.

7.3 Concluding Remarks on $NH_4^-(H_2O)_n$ Double Rydberg Anions

A new family of DRAs that is based on micro-solvation of tetrahedral NH_4^- by one to four water molecules has been identified and its VEDEs and corresponding Dyson orbitals have been predicted. *Ab initio* electron-propagator (i.e., direct) and coupled-cluster (i.e., indirect) methods have been employed to predict electron binding energies of cationic, radical and anionic species. Several approximate electron propagator methods predict VEDEs that are in close agreement with those obtained with ΔCCSD(T). The BD-T1 method predicts the most reliable VEDEs. Vertical electron attachment energies (VEAEs) of $NH_4^+(H_2O)_n$ (n =1–4) cationic clusters were calculated with the direct and indirect methods. The VEAEs

decrease with increasing n and the corresponding Dyson orbitals are diffused over peripheral, non-hydrogen bonded protons.

Clusters formed from NH_4^- DRAs and stabilized by hydrogen bonding or electrostatic interactions are less stable than $H^-(NH_3)(H_2O)_n$ isomers. For all values of n, the hydride-molecule complex $H^-(NH_3)(H_2O)_n$ is always the most stable and has the largest VEDEs. DRAs formed from electrostatic interactions between NH_4^- and water molecules, denoted by $[NH_4^-](H_2O)_n$, are more stable than the $NH_4^-(H_2O)_n$ DRAs that exhibit NH-O hydrogen bridges. The latter species have VEDEs near 0.5 eV and therefore resemble the original DRAs. Variations in these VEDEs are consequences of distinct coordination environments that include proton donations by the tetrahedral anion to water molecules. Whereas total energies of $N_nH_{3n+1}^-$ [87] and $O_nH_{2n+1}^-$[88] DRAs favor formation of H bonds, the opposite trend emerges for the present systems. An increasing sequence of larger, well-separated VEDEs for the $[NH_4^-](H_2O)_n$ DRAs, wherein the tetrahedral NH_4^- fragment interacts with water molecules without formation of H bridges, has been established. Dyson orbitals of electron attachment to $NH_4^+(H_2O)_n$ cations and of detachment from $NH_4^-(H_2O)_n$ DRAs occupy regions beyond the exterior non-bridging O−H and N−H bonds. Thus, the Rydberg electrons in the uncharged Rydberg radicals and DRAs are held near the outer protons of the water and ammonia molecules. The low-lying excited states of the doublet Rydberg radicals have a single electron occupying extended $s-$like, $p-$like, $d-$like, or $f-$like Dyson orbitals with the following Aufbau principle: 1s, 1p, 1d, 2s, 2p, 1f. As $NH_4^-(H_2O)_n$ DRAs isomers have well separated VEDEs and experimentally accessible total energies, they are expected to appear in mass-selected, anion photoelectron spectra that typically detect low-lying isomers.

Chapter 8

General Conclusions and Outlook

The theoretical foundations underlying new-generation one-particle Green's function (electron propagator) methods for calculating electron detachment and attachment energies and their associated Dyson orbitals have been presented. The theoretical connections between new-generation and older methods have been established. The cubically scaling diagonal second order method (D2) has been demonstrated to systematically underestimate ionization energies. To ameliorate this deficiency, same-spin correlation is neglected in the os-D2 and os-nD-D2 self-energies that significantly improve accuracy and efficiency. Optimal ring and ladder renormalizations in the diagonal *2ph*-TDA self-energy led to the DR and DL methodologies that have shown improved efficiency and accuracy. Modification of the OVGF method because of the new choice of superoperator metric leads to the derivation of L3+ and its simplification to Q3+ and P3+. When approximate estimation of post third order terms is abandoned in favor of explicit evaluation of all terms arising from the expansion of inverted matrices, the RL3, RQ3 and RP3 self-energies are obtained. Restoration of off-diagonal metric elements leads to the NRL3, NRQ3 and NRP3 methods.

New and old self-energy approximations have been systematically evaluated for VIEs, VEDEs, and VEAs. The benchmark studies highlight the performance of both diagonal and non-diagonal methods, providing key insights into their accuracy, efficiency and applicability. For VIEs[91–97] and VEDEs[63, 64], the non-diagonal NRL3 method demonstrated the highest accuracy, achieving an MAE of ∼0.06 eV or below, making it the most reliable method. Other promising non-diagonal alternatives include NR2, NRQ3, NRP3, and BD-T1, whereas ND2, *2ph*-TDA, 3+, and ADC(3) were found to be obsolete on grounds of efficiency and accuracy. Among the diagonal approaches, nD-RL3 and nD-L3+ emerged

as the most accurate with an MAE mostly ∼0.07 eV, while Q3+ also exhibited strong performance with an MAE of near 0.15 eV. The os-nD-D2 method remains useful for larger molecules but is less suitable for VEAs. The accuracy of OVGF and D3 is outperformed by their new-generation L3+, nD-L3+ and L3 competitors.

For VEAs[66, 95], NRL3 was the most accurate non-diagonal approach, yielding an MAE of ∼0.06 eV or below. Among diagonal methods, nD-L3+ provided high accuracy with an MAE mostly below 0.1 eV, whereas D2, with an MAE of $\geq$ 0.18 eV remains a viable option. Also, for open-shell molecules and atoms, a systematic increase in MAE by ∼0.05 eV was observed compared to closed-shell species due to spin contaminations.[98]

For heavy-element-containing molecules, RL3 and nD-RL3 are the best methods with an MAE of 0.14 eV. NRL3 has identical accuracy as RL3 but is preferred when Dyson orbitals in their more generalized form are needed. nD-L3+B is the next ranking method which also produces MAE ∼0.17 eV. Q3+ follows with non-iterative O^2V^3 scaling and an MAE ∼0.23 eV. The os-nD-D2 with non-iterative cubic scaling has an MAE of 0.24 eV and it is practically free following HF self-consistent-field calculations.

For core 1s ionization, BD-T1 exhibits the highest accuracy with an MAE of 0.39 eV. It shows excellent agreement with experimental data and minimal systematic bias. D2 and ND2 predictions with MAEs near 1.0 eV are very promising, giving their lower cubic arithmetic scaling. When a shifting near 1.0 eV is applied to D2 or ND2, their MAEs are likely to go below 0.1 eV.

Composite procedures for estimating basis-set effects produce excellent predictions and clear interpretations of the photoelectron spectra of several important biological anions and photovoltaic molecules.

A composite model predicts that the lowest VEDE corresponds to a base π Dyson orbital in three of four nucleotides, with cytidine being the exception (phosphate orbital). Guanosine exhibits a clear separation between the lowest VEDE and subsequent transitions, while other nucleotides show near-degeneracy between base π and phosphate orbitals. Agreement with

experimental spectra underscores the composite model's reliability for characterizing electron detachment in nucleotides.[64]

Composite schemes have also allowed calculations on VEAs and VIEs of organic photovoltaic molecules relevant for the optimization of solar energy devices with exceptional accuracy and efficiency. MAEs versus standards VEAs and VIEs are ∼0.05 eV or below.[95]

Composite schemes based on the new EP methods produce accurate predictions and clear interpretations based on DOs for the photoelectron spectra of green fluorescent protein (GFP) model chromophore anions.[63]

The new-generation EP methods developed in this dissertation require no adjustable or empirical parameters and achieve accuracy close to chemical precision. As a result, they are suitable for reliably predicting novel molecules, ions, and clusters. Based on these methods, the existence, stability, and VEDEs of new types of DRAs have been predicted.

Solvation of the OH_3^- and $O_2H_5^-$ DRAs through electrostatic interactions or hydrogen bonding with their solvation shells results in remarkable changes in geometry with respect to cationic antecedents. Interaction of water molecules with the OH_3^- DRA leads to several cluster isomers in which the Dyson orbital is held at the periphery of the hydrogens in the water network. It is seen that the stable H_3O^- unit imposes a rigid structure on these complexes, especially for isomers with closed solvation shells such as the Eigen $H_3O^-(H_2O)_3$ structure. The $O_2H_5^-$ fragment ion also imposes a rigid geometry on the Zundel $O_2H_5^-(H_2O)_4$ isomer. For all these clusters, the Rydberg electrons are held by the exterior protons from the water network. Several isomers of oxygen-based OH_3^- DRAs may occur through hydrogen bonding, as $OH_3^-(H_2O)_n$ structures or as electrostatic $H^-(H_2O)_n$ complexes. For all values of n, the anion-water complex $H^-(H_2O)_n$ is always the most stable, with large VEDEs which increase with cluster size. Generally, the $OH_3^-(H_2O)_n$ DRA isomers have well separated VEDEs and therefore should be visible in anion photoelectron spectra.

I have also predicted the existence, stability and VEDEs of $NH_4^-(H_2O)_n$ DRAs.[89] Clusters formed from NH_4^- DRAs and stabilized by hydrogen bonding or electrostatic interactions are predicted to be less stable than $H^-(NH_3)(H_2O)_n$ isomers. For all values of n, the hydride-molecule complex $H^-(NH_3)(H_2O)_n$ is always the most stable and has the largest VEDEs. DRAs formed from electrostatic interactions between NH_4^- and water molecules, denoted by $[NH_4^-](H_2O)_n$, are more stable than the $NH_4^-(H_2O)_n$ DRAs that exhibit NH−O hydrogen bridges. The latter species have VEDEs near 0.5 eV and therefore resemble the original DRAs. Variations in these VEDEs are consequences of distinct coordination environments that include proton donations by the tetrahedral anion to water molecules. Whereas total energies of $N_nH_{3n+1}^-$ [87] and $O_nH_{2n+1}^-$ [88] DRAs favor formation of H bonds, the opposite trend emerges for the present systems. An increasing sequence of larger, well-separated VEDEs for the $[NH_4^-](H_2O)_n$ DRAs, wherein the tetrahedral NH_4^- fragment interacts with water molecules without formation of H bridges, has been established. Dyson orbitals of electron attachment to $NH_4^+(H_2O)_n$ cations and of detachment from $NH_4^-(H_2O)_n$ DRAs occupy regions beyond the exterior non-bridging O−H and N−H bonds. Thus, the Rydberg electrons in the uncharged Rydberg radicals and DRAs are held near the outer protons of the water and ammonia molecules. The low-lying excited states of the doublet Rydberg radicals have a single electron occupying extended $s-$like, $p-$like, $d-$like, or $f-$like Dyson orbitals with the following Aufbau principle: 1s, 1p, 1d, 2s, 2p, 1f. As $NH_4^-(H_2O)_n$ DRAs isomers have well separated VEDEs and experimentally accessible total energies, they are expected to appear in mass−selected, anion photoelectron spectra that typically detect low−lying isomers.

Looking into the future, the new generation of EP methods will benefit significantly from computational techniques that enhance efficiency, such as Monte Carlo implementations. Furthermore, density fitting algorithms and Cholesky decomposition present promising strategies to further optimize the performance. Given the accuracy of the new non−diagonal methods (especially NRL3), it is imperative to implement gradients of ground and excited

state potential energy surfaces as has been done previously for the NR2 method[136] and second−order self−energies.[137] Such an implementation will facilitate the use of the new methods to calculate adiabatic ionization energies and electron affinities. Future research would also prioritize extending the capabilities of the new highly accurate and efficient electron propagator methods to the condensed−phase and explore their utility on quantum computers.

To this end, the findings from a collaborative project pave the way for further explorations.[138] The study demonstrates that the non−diagonal second−order self−energy achieves remarkably accurate valence energy band predictions for experimentally well−characterized polymers such as polyethylene, polytetrafluoroethylene, and polyacetylene. The spin−component−scaled variant also emerges as a promising alternative due to its compatibility with a quartic−scaling algorithm, offering substantial computational efficiency without significant loss of accuracy. This method holds promise for solid−state applications, aligning well with the success of methods such as G_0W_0 that similarly emphasize the opposite−spin correlation contribution. These findings suggest that cost−effective, scalable methods can support reliable band structure calculations in extended systems. This study also demonstrates that spin−component scaling, while mostly beneficial for molecules, does not universally translate to solids.

Bibliography

[1]E. Schrödinger, "An undulatory theory of the mechanics of atoms and molecules", *Phys. Rev.* **28**, 1049 (1926).

[2]M. Born and R. Oppenheimer, "Zur Quantentheorie der Molekeln", *Ann. Phys.* **389**, 457–484 (1927).

[3]A. Szabo and N. S. Ostlund, *Modern quantum chemistry: introduction to advanced electronic structure theory* (Courier Corporation, 1996).

[4]J. C. Slater, "The Self Consistent Field and the Structure of Atoms", *Phys. Rev.* **32**, 339 (1928).

[5]T. Koopmans, "Über die Zuordnung von Wellenfunktionen und Eigenwerten zu den Einzelnen Elektronen Eines Atoms", *Physica* **1**, 104–113 (1934).

[6]S. Hirata, A. E. Doran, P. J. Knowles, and J. V. Ortiz, "One-particle many-body Green's function theory: Algebraic recursive definitions, linked-diagram theorem, irreducible-diagram theorem, and general-order algorithms", *J. Chem. Phys.* **147** (2017).

[7]Y. Öhrn and G. Born, "Molecular Electron Propagator Theory and Calculations", *Adv. Quantum Chem.* **13**, 1–88 (1981).

[8]L. Hedin, "New method for calculating the one-particle Green's function with application to the electron-gas problem", *Phys. Rev.* **139** (1965).

[9]J. Linderberg and Y. Öhrn, *Propagators in Quantum Chemistry* (Wiley-InterScience, 2004).

[10]J. Schirmer, *Many-Body Methods for Atoms, Molecules and Clusters*, Vol. 94, Lecture Notes in Chemistry (Springer International Publishing, 2018).

[11]M. D. Prasad, S. Pal, and D. Mukherjee, "Some aspects of self-consistent propagator theories", *Phys. Rev.* A. **31**, 1287 (1985).

[12]J. V. Ortiz, "Interpreting Bonding and Spectra With Correlated, One-Electron Concepts From Electron Propagator Theory", *Ann. Rep. Comput. Chem.* **13**, 139–182 (2017).

[13]J. V. Ortiz, "Electron propagator theory: an approach to prediction and interpretation in quantum chemistry", *Wiley Interdiscip. Rev. Comput. Mol. Sci.* **3**, 123–142 (2013).

[14]J. V. Ortiz, "Toward an Exact One–Electron Picture of Chemical Bonding", *Adv. Quantum Chem.* **35**, 33–52 (1999).

[15]L. S. Cederbaum, G. Hohlneicher, and S. Peyerimhoff, "Calculation of the vertical ionization potentials of formaldehyde by means of perturbation theory", *Chem. Phys. Lett.* **11**, 421–424 (1971).

[16]G. D. Purvis and Y. Öhrn, "Atomic and molecular electronic spectra and properties from the electron propagator", *J. Chem. Phys.* **60**, 4063–9 (1974).

[17]J. Simons and W. D. Smith, "Theory of electron affinities of small molecules", *J. Chem. Phys.* **58**, 4899–907 (1973).

[18]N. Kishimoto, M. Kimura, and K. Ohno, "Two-dimensional penning ionization electron spectroscopy of open-shell metallocenes: Outer valence ionic states of vanadocene and nickelocene", *J. Phys. Chem. A* **117**, 3025–3033 (2013).

[19]D. J. Thouless, *Quantum mechanics of many-body systems* (Academic Press, Inc., 1964).

[20]L. S. Cederbaum, "Direct calculation of ionization potentials of closed-shell atoms and molecules", *Theor. Chim. Acta.* **31**, 239–260 (1973).

[21]V. Salnikov, D. Cassese, R. Lambiotte, R. Chen, R. Poon, R. P. Sahu, J. Schirmer, and L. S. Cederbaum, "The two-particle-hole Tamm-Dancoff approximation (*2ph*-TDA) equations for closed-shell atoms and molecules", *J. Phys. B: At. Mol. Opt.* **11**, 1889 (1978).

[22]J. Schirmer, L. S. Cederbaum, and O. Walter, "New approach to the one-particle Green's function for finite Fermi systems", *Phys. Rev.* A. **28**, 1237 (1983).

[23]J. Schirmer and G. Angonoa, "On Green's function calculations of the static self-energy part, the ground state energy and expectation values", *J. Chem. Phys.* **91**, 1754–1761 (1989).

[24]J. Leitner, A. L. Dempwolff, and A. Dreuw, "Fourth-Order Algebraic Diagrammatic Construction for Electron Detachment and Attachment: The IP- and EA-ADC(4) Methods", *J. Phys. Chem. A* **128**, 53 (2024).

[25]R. Santra and L. S. Cederbaum, "Complex absorbing potentials in the framework of electron propagator theory. i. general formalism", *J. Chem. Phys.* **117**, 5511–5521 (2002).

[26]K. Chatterjee and A. Y. Sokolov, "Extended Second-Order Multireference Algebraic Diagrammatic Construction Theory for Charged Excitations", *J. Chem. Theory Comput.* **16**, 6343–6357 (2020).

[27]K. Chatterjee and A. Y. Sokolov, "Second-Order Multireference Algebraic Diagrammatic Construction Theory for Photoelectron Spectra of Strongly Correlated Systems", *J. Chem. Theory Comput.* **15**, 5908–5924 (2019).

[28]L. Reining, "The GW approximation: content, successes and limitations", *Wiley Interdiscip. Rev. Comput. Mol. Sci.* **8**, e1344 (2018).

[29]S. J. Bintrim and T. C. Berkelbach, "Full-frequency GW without frequency", *J. Chem. Phys.* **154**, 041101 (2021).

[30]W. von Niessen, J. Schirmer, and L. S. Cederbaum, "Computational methods for the one-particle green's function", *Comput. Phys. Rep.* **1**, 57–125 (1984).

[31]J. V. Ortiz, "Partial third-order quasiparticle theory: Comparisons for closed-shell ionization energies and an application to the Borazine photoelectron spectrum", *J. Chem. Phys.* **104**, 7599–7605 (1996).

[32]J. V. Ortiz, "An efficient, renormalized self-energy for calculating the electron binding energies of closed-shell molecules and anions", *Int. J. Quantum Chem.* **105**, 803–808 (2005).

[33]J. V. Ortiz, "Partial fourth order electron propagator theory", *Int. J. Quantum Chem.* **34**, 431–436 (1988).

[34]J. V. Ortiz, "Electron propagator calculations with nondiagonal partial fourth-order self-energies and unrestricted hartree-fock reference states", *Int. J. Quantum Chem.* **36**, 321–332 (1989).

[35]J. V. Ortiz, "A nondiagonal, renormalized extension of partial third-order quasiparticle theory: Comparisons for closed-shell ionization energies", *J. Chem. Phys.* **108**, 1008–1014 (1998).

[36]J. Ortiz, "Approximate Brueckner Orbitals in Electron Propagator Calculations", *Int. J. Quantum Chem.* **75**, 615621 (1999).

[37]J. V. Ortiz, "Approximate Brueckner Orbitals and Shakeup Operators in Electron Propagator Calculations: Applications to F^- and OH^-", *Int. J. Quantum Chem.* **70**, 651658 (1998).

[38]J. V. Ortiz, "Orbital and shakeup operator renormalizations in electron propagator theory", *J. Chem. Phys.* **109**, 5741–5746 (1998).

[39]D. L. Yeager, "The Multiconfigurational Spin-Tensor Electron Propagator Method (MCSTEP)", *Adv. Quantum Chem.* **50**, 289–313 (2005).

[40]R. Flores-Moreno, V. G. Zakrzewski, and J. V. Ortiz, "Assessment of transition operator reference states in electron propagator calculations", *J. Chem. Phys.* **127**, 134106 (2007).

[41]V. G. Zakrzewski and J. V. Ortiz, "Semidirect algorithms in electron propagator calculations", *Int. J. Quantum Chem.* **52**, 23–27 (1994).

[42]R. Flores-Moreno and J. V. Ortiz, "Integral approximations in *ab Initio*, electron propagator calculations", *J. Chem. Phys.* **131**, 124110 (2009).

[43]J. V. Ortiz and V. G. Zakrzewski, "A test of partial third order electron propagator theory: Vertical ionization energies of azabenzenes", *J. Chem. Phys.* **105**, 2762–2769 (1996).

[44]R. Flores-Moreno and J. V. Ortiz, "Quasiparticle virtual orbitals in electron propagator calculations", *J. Chem. Phys.* **128**, 164105 (2008).

[45]D. Danovich, "Green's function methods for calculating ionization potentials, electron affinities, and excitation energies", *Wiley Interdiscip. Rev. Comput. Mol. Sci.* **1**, 377–387 (2011).

[46]J. Schirmer, A. B. Trofimov, and G. Stelter, "A non-Dyson third-order approximation scheme for the electron propagator", *J. Chem. Phys.* **109**, 4734–4744 (1998).

[47]J. Schirmer, "Direct ADC Procedure for the Electron Propagator", in *Many-body methods for atoms, molecules and clusters* (Springer, Cham, 2018), pp. 147–159.

[48]A. B. Trofimov and J. Schirmer, "Molecular ionization energies and ground- and ionic-state properties using a non-Dyson electron propagator approach", *J. Chem. Phys.* **123**, 144115 (2005).

[49]S. Banerjee and A. Y. Sokolov, "Non-Dyson Algebraic Diagrammatic Construction Theory for Charged Excitations in Solids", *J. Chem. Theory Comput.* **18**, 5337–5348 (2022).

[50]L. Storchi, G. Vitillaro, and F. Tarantelli, "Implementation and use of a direct, partially integral-driven non-Dyson propagator method for molecular ionization", *J. Comput. Chem.* **30**, 818–825 (2009).

[51]F. Pawłowski and J. V. Ortiz, "Relativistic electron detachment energies and spin–orbit splittings from quasiparticle electron propagator calculations", *Mol. Phys.* **118** (2020).

[52]M. Díaz-Tinoco, O. Dolgounitcheva, V. G. Zakrzewski, and J. V. Ortiz, "Composite electron propagator methods for calculating ionization energies", *J. Chem. Phys.* **144**, 224110 (2016).

[53]V. P. Vysotskiy and L. S. Cederbaum, "On the Cholesky decomposition for electron propagator methods: General aspects and application on C60", *J. Chem. Phys.* **132**, 0 (2010).

[54]A. E. Doran and S. Hirata, "Monte Carlo Second- And Third-Order Many-Body Green's Function Methods with Frequency-Dependent, Nondiagonal Self-Energy", *J. Chem. Theory Comp.* **15**, 6097–6110 (2019).

[55]C. M. Johnson, A. E. Doran, S. L. Ten-No, and S. Hirata, "Monte Carlo explicitly correlated many-body Green's function theory", *J. Chem. Phys.* **149**, 174112 (2018).

[56]S. Y. Willow, K. S. Kim, and S. Hirata, "Stochastic evaluation of second-order Dyson self-energies", *J. Chem. Phys.* **138**, 164111 (2013).

[57]H. H. Corzo, A. Galano, O. Dolgounitcheva, V. G. Zakrzewski, and J. V. Ortiz, "NR2 and P3+: Accurate, Efficient Electron-Propagator Methods for Calculating Valence, Vertical Ionization Energies of Closed-Shell Molecules", *J. Phys. Chem. A.* **119**, 8813–8821 (2015).

[58]J. W. Knight, X. Wang, L. Gallandi, O. Dolgounitcheva, X. Ren, J. V. Ortiz, P. Rinke, T. Körzdörfer, and N. Marom, "Accurate Ionization Potentials and Electron Affinities of Acceptor Molecules III: A Benchmark of GW Methods", *J. Chem. Theory Comput.* **12**, 615–626 (2016).

[59]O. Dolgounitcheva, M. Díaz-Tinoco, V. G. Zakrzewski, R. M. Richard, N. Marom, C. D. Sherrill, and J. V. Ortiz, "Accurate Ionization Potentials and Electron Affinities of Acceptor Molecules IV: Electron-Propagator Methods", *J. Chem. Theory Comput.* **12**, 627–637 (2016).

[60]A. L. Dempwolff, M. Schneider, M. Hodecker, and A. Dreuw, "Efficient implementation of the non-Dyson third-order algebraic diagrammatic construction approximation for the electron propagator for closed- and open-shell molecules", *J. Chem. Phys.* **150**, 64108 (2019).

[61]A. L. Dempwolff, A. C. Paul, A. M. Belogolova, A. B. Trofimov, and A. Dreuw, "Intermediate state representation approach to physical properties of molecular electron-detached states. II. Benchmarking", *J. Chem. Phys.* **152**, 24125 (2020).

[62]M. Díaz-Tinoco, H. H. Corzo, and J. V. Ortiz, "Electron Propagator Methods for Vertical Electron Detachment Energies of Anions: Benchmarks and Case Studies", *J. Chem. Theory Comput.* **14**, 5881–5895 (2018).

[63]E. Opoku, F. Pawłowski, and J. V. Ortiz, "New-generation electron-propagator methods for vertical electron detachment energies of molecular anions: benchmarks and applications to model green-fluorescent-protein chromophores", *Phys. Chem. Chem. Phys.* **26**, 9915–9930 (2024).

[64]E. Opoku, F. Pawłowski, and J. V. Ortiz, "Electron Propagator Theory of Vertical Electron Detachment Energies of Anions: Benchmarks and Applications to Nucleotides", *J. Phys. Chem. A* **127**, 1085–1101 (2023).

[65]V. G. Zakrzewski, O. Dolgounitcheva, and J. V. Ortiz, "Electron propagator calculations on the ground and excited states of C_{60}^-", *J. Phys. Chem. A.* **118**, 7424–7429 (2014).

[66]E. Opoku, F. Pawłowski, and J. V. Ortiz, "*Ab initio* electron propagators with an hermitian, intermediately normalized superoperator metric applied to vertical electron affinities", *J. Phys. Chem. A* **128**, 4730–4749 (2024).

[67]V. G. Zakrzewski, O. Dolgounitcheva, and J. V. Ortiz, "Electron propagator calculations on C_{60} and C_{70} photoelectron spectra", *J. Chem. Phys.* **129**, 104306 (2008).

[68]V. G. Zakrzewski, O. Dolgounitcheva, A. V. Zakjevskii, and J. V. Ortiz, "*Ab initio* electron propagator calculations on electron detachment energies of fullerenes, macrocyclic molecules, and nucleotide fragments", *Adv. Quantum Chem.* **62**, 105–136 (2011).

[69]V. G. Zakrzewski, O. Dolgounitcheva, A. V. Zakjevskii, and J. V. Ortiz, "*Ab initio* electron propagator methods: applications to nucleic acids fragments and metallophthalocyanines", *Int. J. Quantum Chem.* **110**, 2918–2930 (2010).

[70]V. G. Zakrzewski, O. Dolgounitcheva, A. V. Zakjevskii, and J. V. Ortiz, "*Ab initio* electron propagator methods. applications to fullerenes and nucleic acid fragments", in *Ann. Rep. Comput. Chem.* Vol. 6, C (2010), pp. 79–94.

[71]O. Dolgounitcheva, V. G. Zakrzewski, and J. V. Ortiz, "Electron Propagator Calculations on Uracil and Adenine Ionization Energies", *Int. J. Quantum Chem.* **80**, 831–835 (2000).

[72]M. Díaz-Tinoco and J. V. Ortiz, "Carborane superhalide bases and their conjugate Brønsted-Lowry Superacids: Electron binding energies and Dyson orbitals", *Chem. Phys.* **521**, 77–84 (2019).

[73]J. Brzeski, M. Czapla, and P. Skurski, "Icosahedral Carborane Superacids and their Conjugate Bases Comprising H, F, Cl, and CN Substituents: A Theoretical Investigation of Monomeric and Dimeric Cages", *ChemPlusChem* **85**, 312–318 (2020).

[74]S. X. Tian, "*Ab initio* and electron propagator theory study of boron hydrides", *J. Phys. Chem. A.* **109**, 5471–5480 (2005).

[75]M. Enlow and J. V. Ortiz, "Aromatic carboxylate superhalogens and multiply charged anions", *J. Phys. Chem. A.* **106**, 5373–5379 (2002).

[76]X. B. Wang, C. F. Ding, L. S. Wang, A. I. Boldyrev, and J. Simons, "First experimental photoelectron spectra of superhalogens and their theoretical interpretations", *J. Chem. Phys.* **110**, 4763–4771 (1999).

[77]A. Srivastava, "Recent progress on the design and applications of superhalogens", *Chem. Commun.* **59**, 5943–5960 (2023).

[78]O. Dolgounitcheva, V. G. Zakrzewski, and J. V. Ortiz, "Electron propagator calculations show that alkyl substituents alter porphyrin ionization energies", *J. Am. Chem. Soc.* **127**, 8240–8241 (2005).

[79]O. Dolgounitcheva, V. G. Zakrzewski, and J. V. Ortiz, "*Ab initio* electron propagator calculations on the ionization energies of free base porphine, magnesium porphyrin, and zinc porphyrin", *J. Phys. Chem. A.* **109**, 11596–11601 (2005).

[80]D. Barreiro-Lage, J. Chiarinelli, P. Bolognesi, R. Richter, H. Zettergren, M. H. Stockett, S. Díaz-Tendero, and L. Avaldi, "Photofragmentation specificity of photoionized cyclic amino acids (diketopiperazines) as precursors of peptide building blocks", *Phys. Chem. Chem. Phys.* **25**, 15635–15646 (2023).

[81]O. Dolgounitcheva, V. G. Zakrzewski, and J. V. Ortiz, "Electron binding energies of nucleobases and nucleotides", *Int. J. Quantum Chem.* **90**, 1547–1554 (2002).

[82]D. M. Close, "Calculated vertical ionization energies of the common α-amino acids in the gas phase and in solution", *J. Phys. Chem. A.* **115**, 2900–2912 (2011).

[83]V. G. Zakrzewski and J. V. Ortiz, "Electron Propagator Theory of ZnCsHs, $Zn(CsHs)_2$, and Related Ions", *J. Phys. Chem.* **98**, 13198–13202 (1994).

[84]S. Kambalapalli and J. V. Ortiz, "Electronic Structure of $ScC_6H_6^-$ and ScC_6H_6: Geometries, Electron Binding Energies, and Dyson Orbitals", *J. Phys. Chem. A.* **108**, 2988–2992 (2004).

[85]Y. Dahnovsky, V. G. Zakrzewski, A. Kletsov, and J. V. Ortiz, "*Ab initio* electron propagator theory of molecular wires: i. formalism", *J. Chem. Phys.* **123**, 184711 (2005).

[86]Y. Dahnovsky and J. V. Ortiz, "*Ab initio* electron propagator theory of molecular wires. ii. multiorbital terminal description", *J. Chem. Phys.* **124**, 144114 (2006).

[87]M. Díaz-Tinoco and J. V. Ortiz, "Double Rydberg anions with solvated ammonium kernels: electron binding energies and Dyson orbitals", *J. Chem. Phys.* **151** (2019).

[88]E. Opoku, F. Pawłowski, and J. V. Ortiz, "Electron binding energies and Dyson orbitals of $O_nH_{2n+1}^-$ clusters: Double Rydberg anions, Rydberg radicals, and micro-solvated hydronium cations", *J. Chem. Phys.* **154**, 234304 (2021).

[89]E. Opoku, F. Pawłowski, and J. V. Ortiz, "Double Rydberg anions, Rydberg radicals and micro-solvated cations with ammonium-water kernels", *Phys. Chem. Chem. Phys.* **24**, 18347–18360 (2022).

[90]I. R. Ariyarathna, S. N. Khan, F. Pawłowski, J. V. Ortiz, and E. Miliordos, "Aufbau Rules for Solvated Electron Precursors: $Be(NH_3)_40^{\pm}$ Complexes and beyond", *J. Phys. Chem. Lett.* **9**, 84–88 (2018).

[91]E. Opoku, F. Pawłowski, and J. V. Ortiz, "A new generation of diagonal self-energies for the calculation of electron removal energies", *J. Chem. Phys.* **155**, 204107 (2021).

[92]E. Opoku, F. Pawłowski, and J. V. Ortiz, "A new generation of non-diagonal, renormalized self-energies for calculation of electron removal energies", *J. Chem. Phys.* **159**, 124109 (2023).

[93]E. Opoku, F. Pawłowski, and J. V. Ortiz, "New-Generation Electron-Propagator Methods for Molecular Electron-Binding Energies", *J. Phys. Chem. A* **128**, 1399–1416 (2024).

[94]E. Opoku, F. Pawłowski, and J. V. Ortiz, "Electron Propagator Self-Energies versus Improved GW100 Vertical Ionization Energies", *J. Chem. Theory Comp.* **18**, 4927–4944 (2022).

[95]E. Opoku, F. Pawłowski, and J. V. Ortiz, "New-Generation Electron-Propagator Methods for Calculations of Electron Affinities and Ionization Energies: Tests on Organic Photovoltaic Molecules", *J. Chem. Theory Comp.* **20**, 290–306 (2024).

[96]E. Opoku, F. Pawłowski, and J. V. Ortiz, "Simplified Ring and Ladder Renormalizations in Electron-Propagator Calculations of Molecular Ionization Energies", *J. Phys. Chem. A* **129**, 26 (2025).

[97]E. Opoku, F. Pawłowski, and J. V. Ortiz, "Electron-propagator methods versus experimental ionization energies", *J. Chem. Phys.* **162**, 64102 (2025).

[98]E. Opoku, F. Pawłowski, and J. V. Ortiz, "Electron Binding Energies of Open-Shell Species from Diagonal Electron-Propagator Self-Energies with Unrestricted Hartree-Fock Spin-Orbitals", *J. Phys. Chem. A* **128**, 7311–7330 (2024).

[99]J. V. Ortiz, "Contour integrals in electron propagator theory", *Int. J. Quantum Chem.* **56**, 331–337 (1995).

[100]J. V. Ortiz, "Improved electron propagator methods: an investigation of C_4, C_4^-, and C_4^+", *J. Chem. Phys.* **99**, 6716–6726 (1993).

[101]A. I. Krylov, "From orbitals to observables and back", *J. Chem. Phys.* **153**, 80901 (2020).

[102]J. V. Ortiz, "Dyson-orbital concepts for description of electrons in molecules", *J. Chem. Phys.* **153**, 70902 (2020).

[103]L. Redmon, G. Purvis, and Y. Öhrn, "Higher-order decoupling of the electron propagator", *J. Chem. Phys.* **63**, 5011–5017 (1975).

[104]O. Goscinski and B. Lukman, "Moment-conserving decoupling of green functions via pade approximants", *Chem. Phys. Lett.* **7**, 573–576 (1970).

[105]J. Simons, "The electron propagator and superoperator resolvent", *J. Chem. Phys.* **64**, 4541–4543 (1976).

[106]P.-O. Löwdin and O. Goscinski, "Studies in perturbation theory. XIV. Treatment of constants of motion, degeneracies and symmetry properties by means of multidimensional partitioning", *Int. J. Quantum Chem.* **5**, 685–705 (1971).

[107]R. G. Wilson and C. S. Sharma, "Studies in löwdin's partitioning technique in quantum theory. I. Invertibility of the operator K", *Int. J. Quantum Chem.* **20**, 927–932 (1981).

[108]P.-O. Löwdin, "Partitioning technique, perturbation theory, and rational approximations", *Int. J. Quantum Chem.* **21**, 69–92 (1982).

[109]P. O. Löwdin, "Studies in perturbation theory. IX. Connection between various approaches in the recent development - Evaluation of upper bounds to energy eigenvalues in Schrödinger's perturbation theory", *J. Math. Phys.* **6**, 1341–1353 (1965).

[110]R. Longo, B. Champagne, and Y. Öhrn, "Electron propagator theory and application", *Theor. Chim. Acta.* **90**, 397–419 (1995).

[111]G. Born, H. A. Kurtz, and Y. Öhrn, "Elementary finite order perturbation theory for vertical ionization energies", *J. Chem. Phys.* **68**, 74–85 (1978).

[112]S. Hirata, M. R. Hermes, J. Simons, and J. V. Ortiz, "General-order many-body greens function method", *J. Chem. Theory Comput.* **11**, 1595–1606 (2015).

[113]C. H. Hu, D. P. Chong, and M. E. Casida, "The parametrized second-order Green function times screened interaction (pGW2) approximation for calculation of outer valence ionization potentials", *J. Electron Spectros. Relat. Phenomena.* **85**, 39–46 (1997).

[114]J. Romero, J. A. Charry, H. Nakai, and A. Reyes, "Improving quasiparticle second order electron propagator calculations with the spin-component-scaled technique", *Chem. Phys. Lett.* **591**, 82–87 (2014).

[115]F. H. Lim, M. Nishida, Y. Hori, T. Ida, and M. Mizuno, "Optimization of the spin-component-scaled factor for electron propagator method", *Chem. Phys. Lett.* **678**, 159–166 (2017).

[116]S. Śmiga and I. Grabowski, "Spin-Component-Scaled ΔMP2 parametrization: Toward a Simple and Reliable Method for Ionization Energies", *J. Chem. Theory Comput.* **14**, 4780–4790 (2018).

[117]R. Orlando, P. Romaniello, and P. F. Loos, "The three channels of many-body perturbation theory: GW, particle-particle, and electron-hole T-matrix self-energies", *J. Chem. Phys.* **159** (2023).

[118]L. S. Cederbaum, "One-body Green's function for atoms and molecules: Theory and application", *J. Phys. B: At. Mol. Opt.* **8**, 290–303 (1975).

[119]H. H. Corzo and J. V. Ortiz, "Electron Propagator Theory: Foundations and Predictions", *Adv. Quantum Chem.* **74**, 267–298 (2017).

[120]V. Abraham, G. Harsha, and D. Zgid, "Relativistic Fully Self-Consistent GW for Molecules: Total Energies and Ionization Potentials", *J. Chem. Theory Comp.* **20**, 4579–4590 (2024).

[121]P. Scherpelz, M. Govoni, I. Hamada, and G. Galli, "Implementation and Validation of Fully Relativistic GW Calculations: Spin-Orbit Coupling in Molecules, Nanocrystals, and Solids", *J. Chem. Theory Comp.* **12**, 3523–3544 (2016).

[122]D. Golze, L. Keller, and P. Rinke, "Accurate Absolute and Relative Core-Level Binding Energies from GW", *J. Phys. Chem. Lett.* **11**, 1840–1847 (2020).

[123]B. Boudaïffa, P. Cloutier, D. Hunting, M. A. Huels, and L. Sanche, "Resonant formation of DNA strand breaks by low-energy (3 to 20 eV) electrons", *Science* **287**, 1658–1660 (2000).

[124]E. Alizadeh, T. M. Orlando, and L. Sanche, "Biomolecular damage induced by ionizing radiation: The direct and indirect effects of low-energy electrons on DNA", *Annu. Rev. Phys. Chem.* **66**, 379–398 (2015).

[125]A. V. Bochenkova, C. R. Mooney, M. A. Parkes, J. L. Woodhouse, L. Zhang, R. Lewin, J. M. Ward, H. C. Hailes, L. H. Andersen, and H. H. Fielding, "Mechanism of resonant electron emission from the deprotonated GFP chromophore and its biomimetics", *Chem. Sci.* **8**, 3154–3163 (2017).

[126]J. L. Woodhouse, A. Henley, R. Lewin, J. M. Ward, H. C. Hailes, A. V. Bochenkova, and H. H. Fielding, "A photoelectron imaging study of the deprotonated GFP chromophore anion and RNA fluorescent tags", *Phys. Chem. Chem. Phys.* **23**, 19911–19922 (2021).

[127]K. B. Bravaya and A. I. Krylov, "On the photodetachment from the green fluorescent protein chromophore", *J. Phys. Chem. A.* **117**, 11815–11822 (2013).

[128]M. Gutowski and J. Simons, "Double-Rydberg anions: ground-state electronic and geometric stabilities", *J. Chem. Phys.* **93**, 3874–3880 (1990).

[129]J. V. Ortiz, "Structures and properties of double-Rydberg anions", *J. Phys. Chem.* **94**, 4762–4763 (1990).

[130]J. V. Ortiz, "Ionization energies of OH_3^- isomers", *J. Chem. Phys.* **91**, 7024–7029 (1989).

[131]J. Melin and J. V. Ortiz, "OH_3^- and $O_2H_5^-$ double Rydberg anions: predictions and comparisons with NH_4^- and $N_2H_7^-$", *J. Phys. Chem.* **127** (2007).

[132]R. F. Gunion and W. C. Lineberger, "Transition state spectroscopy of the OH–H_20 of H_3O^- and D_30", *J. Chem. Phys.* **99**, 13627–13636 (1995).

[133]A. L. Sobolewski and W. Domcke, "*Ab initio* investigation of the structure and spectroscopy of hydronium- water clusters", *J. Phys. Chem. A* **106**, 4158–4167 (2002).

[134]J. V. Coe, J. T. Snodgrass, C. B. Freidhoff, K. M. McHugh, and K. H. Bowen, "Negative ion photoelectron spectroscopy of the negative cluster ion $H^-(NH_3)_1$", *J. Chem. Phys.* **83**, 3169–3170 (1985).

[135]J. Ortiz, "Vertical and adiabatic ionization energies of NH_4^- isomers via electron propagator theory and many body perturbation theory calculations with large basis sets", *J. Chem. Phys.* **87**, 3557–3562 (1987).

[136]J. V. Ortiz, "Energy gradients and effective density differences in electron propagator theory", *J. Chem. Phys.* **112**, 56–68 (2000).

[137]J. Cioslowski and J. V. Ortiz, "One-electron density matrices and energy gradients in second-order electron propagator theory", *J. Chem. Phys.* **96**, 8379–8389 (1992).

[138]J. C. Cruz, E. Opoku, S. Śmiga, I. Grabowski, J. V. Ortiz, and S. Hirata, "Performance of the spin-component-scaled methods for energy bands", *Mol. Phys.* **e2504545** (2025).

Appendices

All reprints of articles were made with permissions from the publishers.

Appendix A

E. Opoku, F. Pawłowski and J. V. Ortiz, "New−Generation Electron−Propagator Methods for Molecular Electron−Binding Energies", *J. Phys. Chem. A*, 128, 1399–1416 (2024)

THE JOURNAL OF PHYSICAL CHEMISTRY A
A JOURNAL OF THE AMERICAN CHEMICAL SOCIETY

pubs.acs.org/JPCA

Featured Article

New-Generation Electron-Propagator Methods for Molecular Electron-Binding Energies

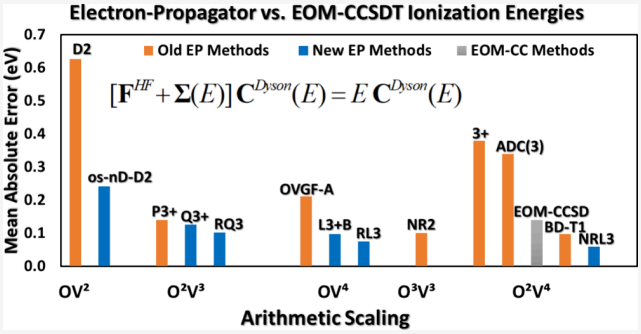
Ernest Opoku, Filip Pawłowski, and J. V. Ortiz*

Cite This: *J. Phys. Chem. A* 2024, 128, 1399−1416

Read Online

ACCESS | Metrics & More | Article Recommendations | Supporting Information

ABSTRACT: A new generation of electron-propagator methods for the calculation of electron binding energies has surpassed its antecedents with respect to accuracy, efficiency, and interpretability. No adjustable parameters are introduced in these fully *ab initio* procedures. Numerical tests versus several databases of valence, vertical electron binding energies of closed-shell molecules and atoms have been performed. Easily interpreted self-energy approximations with cubic arithmetic scaling produce mean absolute errors (MAEs) of 0.2 and 0.3 eV for electron detachments and attachments, respectively. The most accurate explicitly renormalized methods with fifth-power arithmetic scaling yield MAEs below 0.1 eV for detachments and attachments. Approximate renormalization leads to more efficient fifth-power alternatives for electron detachments that achieve similar accuracy with fewer bottleneck operations. Composite protocols generate excellent predictions versus highly accurate basis-extrapolated standards and experiments. The validity of the diagonal self-energy approximation and the accuracy of the approximate renormalizations are confirmed. The success of these perturbative methods based on canonical Hartree−Fock orbitals rests on a Hermitized, intermediately normalized superoperator metric. The results of all of the new-generation calculations may be analyzed in terms of final-state orbital relaxation and differential correlation effects.



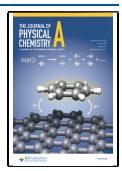
INTRODUCTION

Electron propagator theory[1−8] is the ideal theoretical and computational companion to experimental characterizations of molecules that measure electron binding energies. It provides an exact computational framework for predicting spectra and rigorous concepts for understanding chemical bonding. The Fourier transform of the time-dependent electron propagator is a function of only three variables: an energy parameter and two space-spin coordinates. Information in this function suffices to determine energies of electron detachment and attachment. It also contains amplitudes of Dyson orbitals,[9,10] which are proportional to overlaps between initial-state, N-electron wave functions, and wave functions of final states with $N \pm 1$ electrons. Whereas measurements of electron binding energies have a long, varied history, only in recent years have measurements of Dyson orbitals become feasible.[9] Electron propagator theory's ability to generalize molecular orbital concepts to the exact limit portends a promising future for its partnership with advancing experimental techniques.

That partnership has motivated developments in *ab initio* electron propagator methodology since their appearance in the early 1970s.[11−13] The chief goal, now and then, has been to participate in a dialogue with experimentalists who measure electron binding energies. To enter this conversation, the price of admission is reliable data. Early developers concentrated on the biggest prize: timely production of accurate electron binding energies by *ab initio* means. At that time, it was generally assumed that such information would be intelligible, i.e., capable of being analyzed in depth to discover deeper relationships.

Self-energy corrections to the Coulomb-exchange potential of Koopmans's identity[14] were implemented in codes that conformed to contemporary standards of efficiency. Perturbative self-energy approximations through third order in the Møller-Plesset fluctuation potential[15] were programmed. Dyson orbitals were restricted to being proportional to canonical Hartree−Fock orbitals by annulling off-diagonal elements of the self-energy operator. These diagonal self-energy methods improved canonical Hartree−Fock orbital energies, but they did not suffice to make definitive assignments of molecular photoelectron spectra. An important advance was based on the observation that diagonal second-order (D2) and diagonal third-order (D3) results tended to have errors of opposite sign. (See Table 1 for a complete set of

Received: December 28, 2023
Revised: January 25, 2024
Accepted: January 29, 2024
Published: February 20, 2024



ACS Publications
© 2024 American Chemical Society

https://doi.org/10.1021/acs.jpca.3c08455
J. Phys. Chem. A 2024, 128, 1399−1416

Table 1. Acronyms for Electron-Propagator Self-Energies

Acronym[a]	Full name
Diagonal Self-energies	
D2	Diagonal second order
os-D2	Opposite-spin D2
nD-D2	non-Dyson D2
os-nD-D2	Opposite-spin non-Dyson D2
D3	Diagonal third order
nD-D3	non-Dyson D3
OVGF	Outer-Valence Green's Function (Versions A, B and C)
nD-OVGF	non-Dyson OVGF (Versions A, B and C)
P3	Partial third order
P3+	Approximately renormalized partial third order
Q3	Quasiparticle third order
Q3+	Approximately renormalized quasiparticle third order
L3	Linear third order
nD-L3	non-Dyson L3
L3+	Approximately renormalized linear third order (Versions A, B and C)
nD-L3+	non-Dyson L3+ (Versions A, B and C)
RP3	Explicitly renormalized partial third order
RQ3	Explicitly renormalized quasiparticle third order
RL3	Explicitly renormalized linear third order
nD-RL3	non-Dyson RL3
DR	Diagonal (renormalized) ring approximation (HF-TDA-G_0W_0)
Nondiagonal Self-energies	
ND2	Nondiagonal, second order
2ph-TDA	Two-particle-one-hole Tamm-Dancoff approximation
3+	Nondiagonal third order
ADC(3)	Third order algebraic diagrammatic construction
NR2	Nondiagonal, renormalized, second order
BD-T1	Brueckner Doubles with triple field operators
NRP3	Nondiagonal extension of RP3
NRQ3	Nondiagonal extension of RQ3
NRL3	Nondiagonal extension of RL3

[a]For new-generation methods in **bold type:** *N* = nondiagonal; nD = non-Dyson; R = renormalized; + = approximately renormalized.

acronyms.) Approximate schemes for estimating higher-order terms with diagrammatic arguments interpolated between the two finite-order values and produced useful data. Examples included the three outer valence Green function (OVGF) formulas[4,16] and the approximately renormalized partial third order (P3+) method.[17−20] (Partial summations of certain classes of self-energy corrections in all orders of the fluctuation potential are called renormalizations.) With triple-ζ-plus-polarization basis sets, the inherent limitations of these self-energy approximations and the effects of additional basis functions often canceled each other.

With these efficient and flexible tools, valence photoelectron spectra of many molecules and molecular ions were assigned.[4,21,22] Discoveries of novel chemical bonding in molecular anions were facilitated by convincing assignments of their photodetachment spectra.[23] Agreement between electron propagator calculations and experiment enabled deeper understanding of Penning ionization[24] spectra.

Consideration of higher electron binding energies and the pursuit of greater accuracy motivated the development of nondiagonal, renormalized self-energies. Efforts to replace approximate renormalization schemes took the form of explicit evaluation of ring, ladder, and mixed ring-ladder self-energy terms in all orders. The diagonal self-energy matrix approximation was also abandoned. These extensions were realized with a variety of algorithms for diagonalization of large, symmetric matrices.[25] Early examples of this trend included the two-particle-one-hole Tamm-Dancoff approximation[26] (2ph-TDA) and the first versions of the third-order algebraic diagrammatic construction, or ADC(3).[27] These approaches sufficed to demonstrate the collapse of quasiparticle pictures in the inner-valence region of molecular photoelectron spectra.[28] (The inner-valence region of photoelectron spectra displays relatively broad features and is observed with higher-energy photon sources, e.g., He II, 40.8 eV radiation.) Improved accuracy, accompanied by greater computational demands, was attained with ADC(4).[29] Other nondiagonal, renormalized self-energies aimed more at improved accuracy for outer valence electron binding energies. The nondiagonal, renormalized second order[19,30] (NR2) method for electron detachment energies obtained higher accuracy than ADC(3) with markedly lower computational effort. A self-energy based on the orbitals of the Brueckner Doubles coupled-cluster wave function[31−35] (BD-T1) has proven to be an excellent standard for electron detachment energies.[23,36−38] It also has been a useful improvement on its perturbative antecedents in the presence of strong initial-state correlation.

The family of GW methods[39] also has members with renormalized self-energies that can be diagonal or nondiagonal. Ring diagrams in all orders are always included in the GW self-energies. In most applications, the orbital basis is supplied by Kohn−Sham density functional calculations, and the diagonal approximation is made. The latter approximation is implied by the G_0W_0 appellation.[40] Whereas GW self-energies are complete through second order in the fluctuation potential, they omit many important third-order terms in the self-energy. Despite this limitation, G_0W_0 self-energies may be classified as diagonal and renormalized. In this sense, they occupy an intermediate position between the diagonal, approximately renormalized methods and the nondiagonal, renormalized methods discussed above.

In the last three years, a new generation of electron-propagator approximations has emerged with representatives in all three categories of self-energies.[23,36−38,41,42] These classifications include diagonal approximately renormalized (+), diagonal explicitly renormalized (R), and nondiagonal renormalized (NR) methods. Slightly modified, easily interpretable modifications of the second-order self-energy have also emerged recently. Extensive numerical tests on valence electron binding energies of closed-shell molecules have established the new methods' superior accuracy and computational efficiency versus older approximations. They also have retained the interpretive lucidity of *ab initio* electron-propagator theory. No adjustable parameters have been tolerated in the preparation of orbitals or in the self-energy formulas. The physical meaning of the self-energy terms is emphasized at each level of theory in the discussion below. Algorithmic implications and predictive advantages of successive improvements to the theory are also presented. Table 2 and Figure 1 guide the reader to the recommended new-generation methods.

METHODS

Before undertaking a procession through acronyms and numerical data, a summary of basic concepts is presented in this section. Let *p* and *q* be general indices for an orthonormal

https://doi.org/10.1021/acs.jpca.3c08455
J. Phys. Chem. A 2024, 128, 1399−1416

Table 2. Acronyms of Recommended New-Generation Electron-Propagator Self-Energy Approximations, Arithmetic Scaling of Bottleneck Matrix Multiplications, and Mean Absolute Errors (eV) for the QTP96 Data Set of Molecular Ionization Energies[a]

Fifth-power methods	Retention of terms that are *linear* in reference-state correlation amplitudes (L)	Neglect of postsecond-order 2ph terms for e^- detachments (Q)
Nondiagonal, renormalized (NR)	NRL3 O^2V^4 0.06	NRQ3 O^2V^4 0.10
Diagonal, explicitly renormalized (R)	nD-RL3 OV^4 0.08	RQ3 O^2V^3 0.10
Diagonal, approximately renormalized (+)	nD-L3+B OV^4 0.09	Q3+ O^2V^3 0.13
Third Order	L3 OV^4 0.20	Q3 O^2V^3 0.22
Third-power methods	Neglect of opposite-spin relaxation and differential correlation	
Second Order	os-nD-D2 OV^2 0.18	

[a]Transitions with probability factors >0.85.

spin−orbital basis, u. The p-q element of the electron propagator matrix

$$\langle\langle a_p(t);\, a_q^\dagger(t')\rangle\rangle = -i\Theta(t-t')\langle\Psi_0^N|a_p(t)a_q^\dagger(t')|\Psi_0^N\rangle + i\Theta(t'-t)\langle\Psi_0^N|a_q^\dagger(t')a_p(t)|\Psi_0^N\rangle \quad (1)$$

is defined in terms of the Heaviside step function (θ), an N-electron reference eigenstate, Ψ_0^N, the time-dependent creation operator $a_q^\dagger$, and the time-dependent annihilation operator a_p. The spectral form of the Fourier transform

$$\langle\langle a_p;\, a_q^\dagger\rangle\rangle_E = \lim_{\eta\to 0^+}\left[\sum_R \frac{\langle\Psi_0^N|a_p|R\rangle\langle R|a_q^\dagger|\Psi_0^N\rangle}{E + E_0(N) - E_R(N+1) + i\eta} + \sum_S \frac{\langle\Psi_0^N|a_q^\dagger|S\rangle\langle S|a_p|\Psi_0^N\rangle}{E - E_0(N) + E_S(N-1) - i\eta}\right] = G_{pq}(E) \quad (2)$$

displays summations over final eigenstates with $N+1$ or $N-1$ electrons. Energies of electron attachment and detachment correspond, respectively, to poles in the R and S summations. Residues (numerators associated with poles) are expressed in terms of products of Feynman-Dyson amplitudes, where

$$f_p^R = \langle\Psi_0^N|a_p|R\rangle \quad (3)$$

$$g_p^S = \langle S|a_p|\Psi_0^N\rangle \quad (4)$$

These amplitudes suffice to construct Dyson spin−orbitals of attachment and detachment according to

$$\varphi_R^{\text{Dyson}}(x_1) = \sqrt{N+1}\int \Psi_0^{N*}(x_2, x_3, x_4, ..., x_{N+1}) \times \Psi_R(x_1, x_2, x_3, ..., x_{N+1})\, dx_2\, dx_3\, dx_4 \ldots dx_{N+1} = \sum_R f_p^R u_p(x_1) \quad (5)$$

$$\varphi_S^{\text{Dyson}}(x_1) = \sqrt{N}\int \Psi_S^*(x_2, x_3, x_4, ..., x_N) \times \Psi_0^N(x_1, x_2, x_3, ..., x_N)\, dx_2\, dx_3\, dx_4 \ldots dx_N = \sum_S g_p^S u_p(x_1) \quad (6)$$

Poles of $\mathbf{G}(E)$ occur at energies (E_X) where the quasiparticle eigenvalue equation

$$[\mathbf{F}^{\text{HF}} + \mathbf{\Sigma}(E_X)]\mathbf{C}(E_X) = E_X\mathbf{C}(E_X) \quad (7)$$

is satisfied. $\boldsymbol{F}^{\text{HF}}$ is the Fock matrix of Hartree−Fock theory. All effects of orbital relaxation in final states and differential correlation between initial and final states reside in the energy-dependent self-energy matrix, $\mathbf{\Sigma}(E)$. For each electron binding energy, there is a probability factor (or pole strength), Π, that equals the norm of the Dyson spin−orbital. Transition probabilities are proportional to these factors in the sudden approximation.[43] They may be determined with eq 8.

$$\Pi_X = \int |\varphi^{\text{Dyson}}(x)|^2\, dx = \left(1 - \mathbf{C}^\dagger(E_X)\left[\frac{d\mathbf{\Sigma}(E)}{dE}\right]_{E=E_X}\mathbf{C}(E_X)\right)^{-1} \quad (8)$$

The eigenvectors provide the Feynman-Dyson amplitudes and Dyson spin−orbitals according to eq 9.

$$\varphi_X^{\text{Dyson}}(x) = \Pi_X^{0.5}\sum_p C_p(E_X)u_p(x) \quad (9)$$

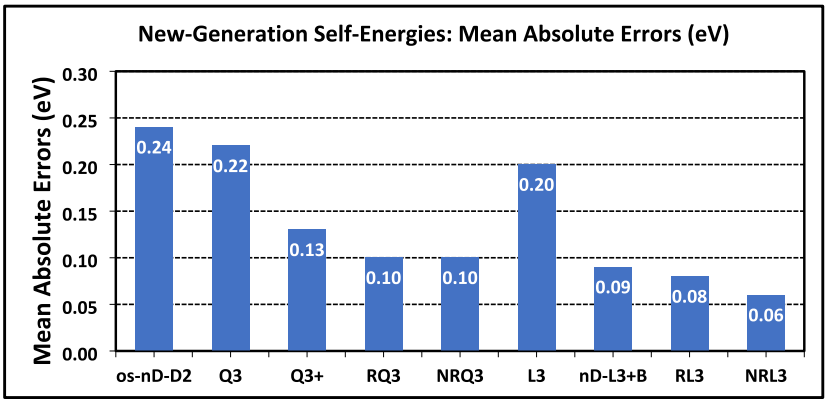


Figure 1. Mean absolute errors (eV) vs QTP96 ionization energies for new-generation self-energies.

https://doi.org/10.1021/acs.jpca.3c08455
J. Phys. Chem. A 2024, 128, 1399−1416

Many of the methods examined below are based on the diagonal self-energy approximation in the canonical, Hartree–Fock basis. When off-diagonal elements of $\mathbf{\Sigma}(E)$ are ignored, each spin–orbital possesses a set of electron binding energies that are solutions to the *diagonal quasiparticle equation*.

$$e_p^{HF} + \Sigma_{pp}(E_{Xp}) = E_{Xp} \tag{10}$$

Koopmans results (e_p^{HF}) are corrected only by diagonal elements of the self-energy matrix. Probability factors have a simple form (eq 11).

$$\Pi_{Xp} = \left[1 - \left.\frac{\mathrm{d}\Sigma_{pp}(E)}{\mathrm{d}E}\right|_{E=E_{Xp}}\right]^{-1} \tag{11}$$

In this simplified approach, Dyson spin–orbitals are proportional to canonical Hartree–Fock spin–orbitals (eq 12).

$$\varphi_{Xp}^{\mathrm{Dyson}}(x) = \Pi_{Xp}^{0.5} u_p^{\mathrm{HF}}(x) \tag{12}$$

RESULTS AND DISCUSSION

Second-Order Theory and Pair-Energy Interpretations. The *p*-*q* element of the nondiagonal second-order (ND2) self-energy[44] matrix comprises two summations (eq 13).

$$\Sigma_{pq}^{\mathrm{ND2}}(E) = \frac{1}{2}\left[\frac{\langle pa\|ij\rangle\langle ij\|qa\rangle}{E + \epsilon_a - \epsilon_i - \epsilon_j} + \frac{\langle pi\|ab\rangle\langle ab\|qi\rangle}{E + \epsilon_i - \epsilon_a - \epsilon_b}\right] \tag{13}$$

Occupied (i,j,k,...) and virtual (a,b,c,...) canonical Hartree–Fock spin–orbital indices, antisymmetrized electron repulsion integrals in Dirac notation, and Einstein summation notation are employed in eq 13. In the diagonal second order (D2) approximation, the *p*-*p* element evaluated at $E = \varepsilon_p$ is related to second-order Møller-Plesset[15] (MP2) pair correlation energies and orbital relaxation. These pair correlation energies read

$$e_{kl}^{\mathrm{MP2}} = \frac{1}{2}\frac{\langle kl\|cd\rangle\langle cd\|kl\rangle}{\epsilon_k + \epsilon_l - \epsilon_c - \epsilon_d} = \frac{1}{2}\langle kl\|cd\rangle t_{kl}^{cd(1)} \tag{14}$$

where the last expression includes first-order double replacement amplitudes. The non-Dyson, second-order, diagonal self-energy (nD-D2) fixes one summation at $E = \varepsilon_p$, whereas the remaining summation retains its dependence on E. For electron detachment and attachment energies, dependence on E appears in the 2hp (first) term and 2ph (second) terms, respectively.

Electron detachment energies in the diagonal self-energy approximation are calculated when p is occupied. Orbital relaxation and correlation components of the self-energy may be mapped to differences of pair correlation energies when E is set to ε_p.[45] Iterations with respect to E after this initial guess generate higher-order relaxation and correlation contributions to electron binding energies.[46,47] For electron detachment, the 2ph summation corresponds to pair correlation energies in the initial state with no counterparts (i.e., no canceling values) in the frozen-orbital final state. This initial-state differential correlation term *increases* electron detachment energies and converges slowly as basis sets become larger and more flexible. Terms in the 2hp summation of eq 13 where i or j equals p arise because of orbital relaxation in final states. The remaining terms in the 2hp summation, when neither i nor j equal p, are augmentations to final-state pair-correlation energies associated with the vacated p spin–orbital. Final-state, differential correlation is described by these terms. Convergence with respect to basis sets occurs more rapidly in the 2hp summation, which typically *decreases* outer-valence electron detachment energies. The predictions of Koopmans's identity often benefit from approximate cancellations of the two summations. Overcorrections from the 2hp term usually result in electron detachment energies that are too small. These errors are incompletely offset by 2ph terms that grow with larger basis sets. Final predictions with saturated basis sets tend to underestimate the electron detachment energies.

The roles of the 2hp and 2ph summations are reversed in diagonal self-energy calculations of electron affinities, i.e., when p is virtual. Contributions to initial-state pair correlation energies associated with spin–orbital p have no canceling counterparts in the frozen-orbital final state wherein p is no longer unoccupied. Negatives of these contributions occur in the first summation, which diminishes the electron attachment energies. Orbital relaxation is associated with terms in the second summation where p equals a or b. Pair correlation energies in final states associated with the newly occupied p spin–orbital account for the remaining 2ph terms, where $a, b \neq p$. In calculations of a molecule's largest electron affinities, the 2ph term typically has a negative sign and therefore increases electron attachment energies. Basis-set convergence is slower in the 2ph summation, because each term depends on three instead of two virtual indices. Koopmans predictions again benefit from the differing signs of the two summations, but the second term's magnitude is typically larger. Overestimates of electron attachment energies grow as basis sets are improved.

Opposite-Spin, Second-Order Methods. Canonical Hartree–Fock orbital energies and D2 poles often have errors of opposite sign, with respect to exact values. For electron detachment energies, these two approximations usually lead to overestimates and underestimates, respectively. The signs of the two errors are reversed for the electron attachment energies. In both cases, the D2 self-energy tends to exaggerate the size of the exact relaxation-correlation correction to the Koopmans results. An unbiased approach to obtaining better estimates with equal or decreased arithmetic effort recognizes that the self-energy summations contain same-spin and opposite-spin terms. In terms of α (lower case) and β (upper case) spin–orbitals, we have the following (eq 15).

$$\begin{aligned}\Sigma_{pp}^{\mathrm{D2}}(E) = {} & \frac{1}{2}\frac{\langle pa\|ij\rangle\langle ij\|pa\rangle}{E + \epsilon_a - \epsilon_i - \epsilon_j} + \frac{\langle pA|iJ\rangle\langle iJ|pA\rangle}{E + \epsilon_A - \epsilon_i - \epsilon_J} \\ & + \frac{1}{2}\frac{\langle pi\|ab\rangle\langle ab\|pi\rangle}{E + \epsilon_i - \epsilon_a - \epsilon_b} + \frac{\langle pI|aB\rangle\langle aB|pI\rangle}{E + \epsilon_I - \epsilon_a - \epsilon_B}\end{aligned} \tag{15}$$

For the *P*–*P* element of the self-energy matrix, the roles of lower-case and upper-case indices are reversed. Orbital relaxation and differential correlation effects that involve same-spin electron repulsion and exchange occur in the first and third terms with antisymmetrized electron repulsion integrals. Opposite-spin (os) electron repulsion without exchange is represented in the second and fourth terms with simple electron repulsion integrals in the Dirac notation. Neglect of the same-spin terms in the D2 and nD-D2 self-energies defines the os-D2 and os-nD-D2 self-energy

https://doi.org/10.1021/acs.jpca.3c08455
J. Phys. Chem. A 2024, 128, 1399–1416

Table 3. Mean Absolute Errors (eV) of Diagonal, Second-Order Self-Energies Versus VIE and VEA Standards

	QTP160[38]	QTP96[38]	GW100[37]	VEDE55[38]	OPV20 VIE[59]	OPV19 VEA[59]
Koopmans	1.82	1.50	0.65	0.60	0.49	1.43
D2	0.59	0.63	0.51	0.48	0.32	0.49
nD-D2	0.62	0.66	0.53	0.51	0.34	0.56
os-D2	0.36	0.25	0.18	0.17	0.19	0.34
os-nD-D2	0.34	0.24	0.18	0.18	0.18	0.31

approximations.[36] No fitting parameters have been introduced for any of the four terms.[48−51]

Several numerical tests on the D2, nD-D2, os-D2, and os-nD-D2 methods for vertical electron detachment energies have been conducted. Initial tests employed IP-EOM-CCSDT/cc-pVTZ data as a standard of comparison. (Standard ionization potentials were calculated with equation-of-motion, coupled-cluster[52,53] singles, doubles, and triples wave functions, and the cc-pVTZ basis set.[54]) This data set had been used previously in developing the Quantum Theory Project (QTP) density functionals.[55] In a subset of these data, the mean absolute error (MAE) with respect to IP-EOM-CCSDTQ (i.e., with added quadruples) data was only 0.03 eV. Closed-shell molecules with nuclei of the first nine elements were considered. MAEs with respect to the consequent set of 160 electron detachment energies are in the QTP160 column of Table 3.[38]

For most of the QTP160 molecules, several electron detachment energies were considered, including cases of excited final states where the probability factors were below 0.85. Such transitions are likely to be inappropriate for diagonal self-energy methods, which assume that the Koopmans description of final states is qualitatively correct. Correlation-state (shakeup or 2hp) character is not negligible when probability factors are low. These transitions are best treated with nondiagonal, renormalized self-energies.

Elimination of energy-dependence in the 2ph term in the non-Dyson variant of D2 is of little numerical consequence. The MAE for nD-D2 is only slightly worse. D2 and nD-D2 have a pronounced tendency to underestimate electron detachment energies.

MAEs are reduced to a useful level in the os versions, which tend to overestimate electron detachment energies. When states with low probability factors are excluded from consideration, a smaller data set with 96 electron detachment energies is produced. Error measures for this less challenging but more realistic standard (see QTP96 column in Table 3) for outer-valence ionization energies are markedly smaller.

When cubically scaling os self-energies are used as intended (i.e., when $\Pi_X \geq 0.85$), they produce average errors near a quarter of an eV. For electron detachment energies, they are competitive with *ab initio* techniques of greater cost and other approaches that introduce adjustable parameters.

Confirmation of the advantages of os-D2 and os-nD-D2 for a more chemically diverse set of systems was provided by a study of the GW100 atoms and molecules.[37] These data pertain to the lowest vertical ionization energies of 100, closed-shell, main-group species. Standard values were recalculated at the ΔCCSD(T)/def2-TZVPP level. (Differences between coupled-cluster singles and doubles plus perturbative triples total energies[56] were calculated with the def2-TZVPP[57] basis set.) Point-group symmetry was imposed on reoptimized structures, and the correct choices for cationic states were identified.[37]

Because the GW100 data set includes only the lowest vertical ionization energy of each atom or molecule, it provides an easier test of predictive quality in comparison to the QTP standards. Error measures for all five approximations in Table 3 are lower. MAEs for the two os methods are below 0.2 eV. D2 and nD-D2 underestimate vertical ionization energies in more than 90% of the cases. Most of the os-D2 and os-nD-D2 errors are overestimates. The MAEs of D2 and nD-D2 are reduced by about a factor of 3 in the os calculations.

Similar conclusions were reached in a study of 55 vertical electron detachment energies of 36 closed-shell anions.[23] The VEDE55 column in Table 3 displays MAEs relative to ΔCCSD(T)/CBS (complete basis set extrapolation) standards obtained with augmented, correlation-consistent basis sets.[58] Inverse cubic extrapolations with triple-quadruple ζ data were performed.

The most recent test considered vertical ionization energies of 20 organic acceptors of interest in the field of organic photovoltaics (OPVs).[59] These molecules are considerably larger than those considered in previous tests. Errors versus ΔCCSD(T)/aug-cc-pVTZ[58] data produced with the same basis are analyzed in the OPV20 VIE (vertical ionization energy) column of Table 3.

In all cases, the D2 and nD-D2 results were underestimates. Approximately equal numbers of overestimates and underestimates occurred for the two os alternatives.

The MAE data in Table 3 provide convincing and remarkably consistent evidence for the utility of the os-D2 and os-nD-D2 self-energies. A similar level of accuracy is realized in calculations of the lowest vertical ionization energies of molecules and vertical electron detachment energies of molecular anions. In addition to their useful MAEs below 0.2 eV, these cubically scaling methods are practically free after a partial transformation of electron repulsion integrals. When only one electron detachment energy is sought, the latter step may be completed with a quartically scaling algorithm.

An equally important dimension of the usefulness of the two os methods is interpretability. No adjustable parameters have been introduced in the generation of orbitals or in the mathematical form of the self-energy matrix elements. Interactions between electrons of the same spin are treated at the Hartree−Fock level with a Coulomb-exchange effective potential. Opposite-spin repulsions are described with an energy-dependent, second-order self-energy that generalizes the easily interpretable pair-correlation terms of Rayleigh−Schrödinger perturbation theory.

The computational demands of the two os methods are low compared to their predictive power and conceptual lucidity. They can be useful in generating large data sets based on diverse varieties of molecules and molecular anions. Integral approximation techniques (e.g., density fitting,[60,61] Cholesky decomposition[62]) are likely to reduce arithmetic bottlenecks in future os-D2 and os-nD-D2 implementations.

https://doi.org/10.1021/acs.jpca.3c08455
J. Phys. Chem. A 2024, 128, 1399−1416

Table 4. Scaling of Arithmetic Operations Per Final State and Memory Requirements of Electron-Propagator Self-Energy Approximations[a]

Category	Self-Energy[b]	Scaling of Arithmetic Bottleneck	Number of Bottleneck Steps	Size of Largest ERI[c] Subset
Diagonal 2nd order	D2, **os-D2**	OV^2	N_E	(O^2V^2,OV^3)
	RSPT2, nD-D2, **os-nD-D2**	OV^2	$(1,N_E)$	(O^2V^2,OV^3)
Diagonal Post 2nd order	RSPT3	OV^4	1	V^4
	D3, OVGF	OV^4	N_E[d]	V^4
	P3, P3+, **Q3**, **Q3+**	(O^2V^3,OV^4)	$(1, N_E)$	(OV^3,V^4)
	L3, **L3+**	OV^4	N_E[d]	V^4
	RP3, **RQ3**	(O^2V^3,OV^4)	$(1,N_IN_E)$	(OV^3,V^4)
	RL3	OV^4	N_IN_E[d]	V^4
	DR	O^2V^3	N_IN_E	(O^2V^2,OV^3)
Nondiagonal 2nd order	ND2	OV^3	N_I	OV^3
Nondiagonal and	2ph-TDA	OV^4	N_I	V^4
Renormalized	3+	O^2V^4	1[f]	V^4
	ADC(3)	O^2V^4	N_I[f]	V^4
	NR2	(O^3V^3,O^2V^4)	$(1, 1)$[f]	(OV^3,V^4)
	BD-T1	O^2V^4	BD[e]	V^4
	NRP3, **NRQ3**	O^2V^4	$(1,1)$[f]	V^4
	NRL3	O^2V^4	1	V^4

[a]Ordered pairs refer to electron detachment and attachment versions, respectively. O = # occupied orbital, V = # virtual orbitals, N_E = energy iterations, N_I = inverse-expansion or linear-equation iterations for diagonal methods and Hamiltonian-vector multiplications for nondiagonal methods. O^2V^4 bottleneck steps for renormalized methods produce intermediates that may be stored and reused for more than one final state. [b]New-generation methods in **bold type**. [c]ERI = electron repulsion integral. [d]Reduction by a factor of N_E occurs in non-Dyson (nD) versions for electron detachment energies. [e]The O^2V^4 arithmetic bottleneck occurs in the Brueckner Doubles, coupled-cluster, reference-state calculation; the subsequent electron-propagator bottleneck is OV^4. [f]N_I OV^4 iterative steps for 3+, ADC(3), and NRL3; N_I O^3V^2 iterative steps for NR2, NRP3, and NRQ3 electron detachment energies.

Methods with MAEs ≤ 0.2 eV are useful in the assignment of photoelectron spectra, but some cases require higher accuracy. The deficiencies of D2 arise chiefly from the exaggeration of relaxation and final-state correlation effects relative to initial-state correlation. Ample computational experience gained over decades has shown which third-order self-energy summations, or diagrams (see Chapter 9 and Appendix D in ref 1), are largest. These terms have one energy-dependent denominator and a linear dependence on first-order, double replacement, or $T_2^{(1)}$, amplitudes. (See the next section for typical numerical evidence.) Thus, the bare $\langle pallij\rangle$ vertices in the 2hp summation of eq 13 are diminished with ground-state correlation amplitudes. Less important but physically meaningful contributions are made by third-order ring and ladder diagrams, which also generate effective interactions. The remaining class of third-order terms is energy-independent and arises from correlation contributions that alter the initial state's Coulomb-exchange potential. These constant terms arise from orbital relaxation in pair-correlation energies of the final state.

Evaluation of crucial, higher-order terms in the self-energy necessitates summations with quintic arithmetic scaling. (See Table 4 for scaling factors per final state and memory requirements.) In many cases, the costliest steps may be avoided without a significant loss of predictive accuracy.

In the OPV test, the D2, nD-D2, os-D2, and os-nD-D2 self-energies were tested also on 19 vertical electron affinities.[59] (One molecule lacks a bound anion.) This preliminary test produced the data in the OPV19 VEA column of Table 3.

The somewhat larger MAE of nD-D2 versus D2 indicates the greater energy dependence of the 2hp term in electron affinity calculations. This result differs from the small energy dependence in the 2ph term seen for ionization energies of molecules and electron detachment energies of anions. Whereas all D2 and nD-D2 predictions were overestimates of vertical electron affinities, os-D2 and os-nD-D2 invariably produced underestimates. The two os self-energies produce smaller error measures, but they are larger than their counterparts for vertical ionization energies in Table 3. MAEs of 0.3 eV and the smaller magnitudes of electron affinities versus ionization energies indicate that better methods are needed for electron attachments.

To ameliorate D2's exaggeration of final-state orbital relaxation and differential correlation effects, same-spin correlation is neglected in the two os methods. This choice produces useful numerical results for the outer valence electron binding energies of closed-shell species at almost no cost after the electron integral transformation. The effective nonlocal potential is easy to interpret in terms of exchange and opposite-spin pair correlation energies.

Third-Order Methods. Systematic approaches to superseding second-order methodology may be based on superoperator expressions.[63] Superoperators (denoted with circumflex accents) act on second-quantized operators according to

$$\hat{I}z = z \tag{16}$$

$$\hat{H}z = Hz - zH \tag{17}$$

where H is the second-quantized Hamiltonian and z in general is a linear combination of products of n creators and $n - 1$ annihilators. The superoperator metric reads

$$[z_1|z_2] = \langle N|(z_1^\dagger z_2 + z_2 z_1^\dagger)|N\rangle \tag{18}$$

where $|N\rangle$ is the N-electron reference state. The plus sign between the two operator products is a consequence of the plus sign between the detachment and attachment terms in eq 2. The z operators are partitioned into a primary space of simple creators and an orthogonalized secondary space, $\mathbf{f}$, such that $[\mathbf{a}^\dagger|\mathbf{f}]$ and $[\mathbf{f}|\mathbf{a}^\dagger]$ elements vanish. Orthonormalization also implies that $[\mathbf{a}^\dagger|\mathbf{a}^\dagger]$ and $[\mathbf{f}|\mathbf{f}]$ are unit matrices.

https://doi.org/10.1021/acs.jpca.3c08455
J. Phys. Chem. A 2024, 128, 1399−1416

With these foundations, the generalized Fock matrix, $\mathbf{F}^{G}$, and the energy-dependent part of the self-energy matrix, $\mathbf{\Sigma}^{ED}(E)$, are given by eqs 19 and 20.

$$F_{pq}^{G} = [a_p^{\dagger}|\hat{H}a_q^{\dagger}] \tag{19}$$

$$\Sigma_{pq}^{ED}(E) = [a_p^{\dagger}|\hat{H}\mathbf{f}][\mathbf{f}|(E\hat{I} - \hat{H})\mathbf{f}]^{-1}[\mathbf{f}|\hat{H}a_q^{\dagger}] \tag{20}$$

Corrections to $\mathbf{F}^{G}$ that arise from correlation in the N-electron reference state are usually known as energy-independent (or constant) self-energy terms. In the canonical Hartree−Fock basis, we have eq 21.

$$F_{pq}^{G} = \delta_{pq}\epsilon_p + \Sigma_{pq}(\infty) \tag{21}$$

The self-energy matrix elements therefore are defined by eq 22.

$$\Sigma_{pq}(E) = \Sigma_{pq}^{ED}(E) + \Sigma_{pq}(\infty) \tag{22}$$

As the absolute value of E increases without bound, the self-energy matrix approaches its constant component. Constant self-energy terms vanish in first order and second order with Hartree−Fock orbitals.

The ND2 self-energy of eq 13 also may be expressed as

$$\Sigma_{pq}^{ND2}(E) = [a_p^{\dagger}|\hat{H}\mathbf{f}_3]_1[\mathbf{f}_3|(E\hat{I} - \hat{H})\mathbf{f}_3]_0^{-1}[\mathbf{f}_3|\hat{H}a_q^{\dagger}]_1 \tag{23}$$

Integers in the subscripts designate the order of the matrix element in the Møller-Plesset fluctuation potential. The triple field operator subset, $\boldsymbol{f}_3$, comprises 2hp and 2ph products of two creators and one annihilator (e.g., $a_i^{\dagger}a_j^{\dagger}a_a$ and $a_a^{\dagger}a_b^{\dagger}a_i$). In order zero, the inverted matrix is diagonal in the canonical Hartree−Fock basis. (The *ija* and *abi* diagonal elements occur in the denominators of eq 13.) Only the Hartree−Fock contribution to $|N\rangle$ need be invoked to derive the ND2 self-energy from the general expression for $\mathbf{\Sigma}(E)$.

Before deriving third-order terms, the following approximation for the superoperator metric is made:[36]

$$[z_1|z_2] = \frac{1}{2}[\langle HF|(z_1^{\dagger}z_2 + z_2z_1^{\dagger})(1 + T_2^{(1)} + T_1^{(2)})|HF\rangle + \langle HF|(1 + T_2^{(1)} + T_1^{(2)})^{\dagger}(z_1^{\dagger}z_2 + z_2z_1^{\dagger})|HF\rangle] \tag{24}$$

Equation 24 imposes Hermiticity on the superoperator Hamiltonian matrix. (This condition is also met when $|N\rangle$ and $\langle N|$ in eq 18 are exact.) Its intermediate normalization also retains size-extensivity in the total energies of the reference state. These energies may be evaluated with contour integrals that enclose all electron detachment poles in the complex plane.[1,9] First-order double substitutions and second-order single substitutions suffice to produce third-order constant and energy-dependent self-energy terms that are linear in T amplitudes.

Hermiticity in equation-of-motion theory[64] is imposed by other means. The superoperator Hamiltonian matrix with elements $[z_1|\hat{H}z_2]$ is defined by eqs 17 and 18 and various choices of $|N\rangle$ and $\langle N|$. Eigenvalues of the mean of this matrix and its adjoint are calculated. For some choices of $|N\rangle$ or $\langle N|$, unphysical terms may be included in the Hermitization.

Another strategy was adopted in previous perturbative approaches to higher-order electron-propagator methods. Order-by-order improvements in $|N\rangle$ and $\langle N|$ were employed to systematically eliminate non-Hermitian terms in superoperator Hamiltonian matrices.[6,65] Terms that are bilinear (i.e., quadratic with real arithmetic) in T amplitudes therefore appear in third order. This approach yields poor total energies and one-electron properties of the reference state calculated by contour integrations.[66]

No reference-state substitutions are needed to produce the first-order couplings between $\boldsymbol{f}_3$ operators that occur in the inverted matrix of eq 20. Expansion of this inverse about its zeroth order, diagonal part produces ring and ladder self-energy terms in all orders, i.e., a renormalization. The $T_1^{(2)}$ operator is needed for third-order corrections to the constant self-energy matrix. Numerical evidence indicates that the most important terms (see below) require second-order couplings between $\boldsymbol{a}^{\dagger}$ and $\boldsymbol{f}_3$ operators that are linear in $T_2^{(1)}$ amplitudes.

The sum of these improvements produces the linear, third-order[23,36−38] (L3) self-energy:

$$\begin{aligned}\Sigma_{pq}^{L3}(E) = \Sigma_{pq}^{ND2}(E) &+ [a_p^{\dagger}|\hat{H}\mathbf{f}_3]_2[\mathbf{f}_3|(E\hat{I} - \hat{H})\mathbf{f}_3]_0^{-1}[\mathbf{f}_3|\hat{H}a_q^{\dagger}]_1 \\ &+ [a_p^{\dagger}|\hat{H}\mathbf{f}_3]_1[\mathbf{f}_3|(E\hat{I} - \hat{H})\mathbf{f}_3]_0^{-1}[\mathbf{f}_3|\hat{H}a_q^{\dagger}]_2 \\ &+ [a_p^{\dagger}|\hat{H}\mathbf{f}_3]_1[\mathbf{f}_3|(E\hat{I} - \hat{H})\mathbf{f}_3]_0^{-1}[\mathbf{f}_3|\hat{V}\mathbf{f}_3]_1 \\ &[\mathbf{f}_3|(E\hat{I} - \hat{H})\mathbf{f}_3]_0^{-1}[\mathbf{f}_3|\hat{H}a_q^{\dagger}]_1 + \Sigma_{pq3}(\infty)\end{aligned} \tag{25}$$

Terms two and three are Hermitian conjugates of each other and depend linearly on perturbative $T_2^{(1)}$ amplitudes. Third-order ring and ladder diagrams are represented by the fourth term. (See eqs A6−A9 in Appendix 1.) Each of the E-dependent terms comprises 2hp and 2ph summations. For diagonal self-energy calculations of electron detachment energies, contributions from the 2ph summations in the second, third, and fourth terms often have little numerical importance.[17] In this portion of such calculations, the OV^4 arithmetic bottleneck of the fourth term occurs. (O and V are the numbers of occupied and virtual orbitals, respectively.) An advantageous compromise between accuracy and efficiency can be realized by neglecting the 2ph portion of the third-order terms. The resulting quasiparticle, third-order (Q3) self-energy for electron detachment energies has the following form:

$$\begin{aligned}\Sigma_{pq}^{Q3}(E) = \Sigma_{pq}^{ND2}(E) &+ [a_p^{\dagger}|\hat{H}\mathbf{f}_{2hp}]_2[\mathbf{f}_{2hp}|(E\hat{I} - \hat{H})\mathbf{f}_{2hp}]_0^{-1} \\ &[\mathbf{f}_{2hp}|\hat{H}a_q^{\dagger}]_1 \\ &+ [a_p^{\dagger}|\hat{H}\mathbf{f}_{2hp}]_1[\mathbf{f}_{2hp}|(E\hat{I} - \hat{H})\mathbf{f}_{2hp}]_0^{-1}[\mathbf{f}_{2hp}|\hat{H}a_q^{\dagger}]_2 + [a_p^{\dagger}|\hat{H}\mathbf{f}_{2hp}]_1 \\ &[\mathbf{f}_{2hp}|(E\hat{I} - \hat{H})\mathbf{f}_{2hp}]_0^{-1}[\mathbf{f}_{2hp}|\hat{V}\mathbf{f}_{2hp}]_1[\mathbf{f}_{2hp}|(E\hat{I} - \hat{H})\mathbf{f}_{2hp}]_0^{-1} \\ &[\mathbf{f}_{2hp}|\hat{H}a_q^{\dagger}]_1 + \Sigma_{pq3}(\infty)\end{aligned} \tag{26}$$

Terms that pertain to 2ph operators are confined to the ND2 self-energy. Diagonal Q3 calculations have an O^2V^3 arithmetic bottleneck. The Q3 self-energy for electron attachments wherein 2hp terms in third order are neglected has no arithmetic scaling advantage over L3 when V > O. The widely used P3 self-energy is identical to Q3 but for the absence of $\Sigma_{pq3}(\infty)$, which involves single replacements in the reference state. Formulas for the diagonal elements of the L3, Q3, and P3 self-energies for real spin−orbitals are given in Appendix 1.

L3 differs from D3, the diagonal version of the third-order many-body Green's function,[46,47] in two respects.[23,36−38] First, L3 has no terms with a quadratic dependence on reference-state correlation amplitudes. Such terms occur in the constant portion of the D3 self-energy. Second, all terms with a linear dependence on reference-state correlation amplitudes are accompanied by a factor of one half in L3. The corresponding

https://doi.org/10.1021/acs.jpca.3c08455
J. Phys. Chem. A 2024, 128, 1399−1416

Table 5. Mean Absolute Errors (eV) of D3, P3, Q3, and L3 Diagonal Self-Energies Versus VIE and VEA Standards

	QTP160[38]	QTP96[38]	GW100[37]	VEDE55[23]	OPV20 VIE[59]	OPV19 VEA[59]
D2	0.59	0.63	0.51	0.48	0.32	0.49
D3	0.83	0.69	0.34	0.64	0.22	0.54
P3	0.35	0.24	0.18	0.29	0.30	0.11
Q3	0.30	0.22	0.19	0.28	0.12	0.22
L3	0.28	0.20	0.13	0.23	0.10	0.15

Table 6. Average Values and Average Absolute Values (eV) for Second-Order and Third-Order Self-Energy Terms (See Abbreviations in Appendix 1) in aug-cc-pVTZ/L3 Calculations on OPV Molecules

	S_{2hp}	V_{2hp}	$\lvert R_{2hp}\rvert$	S_{2ph}	$\lvert V_{2ph}\rvert$	R_{2ph}	K_S
24 VIEs	3.40[a]	−0.66[a]	0.07[b]	2.72[a]	0.02[b]	0.13[a]	0.40[a]
23 VEAs	1.77[a]	−0.07[a]	0.02[b]	−3.79[a]	0.50[a]	0.15[a]	0.34[a]

[a]All results have the same sign. [b]Positive and negative values of R_{2hp} or V_{2ph} are obtained.

factor in D3 is unity. Second-order and third-order ring and ladder terms are identical in L3 and D3.

In the six numerical tests listed in Table 5, the new-generation methods, Q3 and L3, provide superior accuracy versus D3 and D2. Q3 also possesses a substantial computational advantage over D3 (O^2V^3 versus OV^4 arithmetic scaling) for electron detachment energies. In addition to Q3's lower arithmetic scaling, it also has no need for electron repulsion integrals with four virtual indices. These integrals are needed in all four post-second-order options of Table 5 for electron attachment energies. The OV^4 bottleneck also remains in effect for the OPV19 VEA tests.

L3 is especially effective in avoiding the large underestimates of D2 and overestimates of D3 for electron detachment energies. The former defect originates in D2's exaggerated treatment of final-state orbital relaxation and differential correlation effects. The chief difference between L3 and D3 stems from the factor of one half that is missing from D3's 2hp terms that are linear in $T_2^{(1)}$ amplitudes. L3 thereby avoids exaggeration of the importance of these 2hp corrections.

Q3's MAEs for electron detachment energies mostly lie between those of P3 and L3. Inclusion of the constant self-energy terms that arise from $T_1^{(2)}$ amplitudes produces better results except in the GW100 case, where the MAEs are almost equal.

For electron attachments, L3's arithmetic bottleneck has the same scaling factor as P3 and Q3. All three new-generation methods produce MAEs that are markedly lower than those of D2 and D3. OPV19 results suggest that constant terms included in Q3 and L3 and third-order 2ph terms included in L3 offset each other. As for detachment energies, improvements realized by P3, Q3, and L3 originate chiefly in their treatment of final-state orbital relaxation and differential correlation effects.

L3 calculations on the OPV molecules with the aug-cc-pVTZ basis yield the data of Table 6, which displays averages for each of the self-energy terms. (See abbreviations in Appendix 1.) All 24 VIEs and 23 VEAs are considered, since there is no need for reference ΔCCSD(T) data. In most cases, the sign of the term does not vary from one molecule to another. Positive and negative values are present in this set of molecules for the R_{2hp} terms and for the V_{2ph} terms in electron-affinity calculations. The second-order (S_{2hp} and S_{2ph}) terms have opposite signs and the largest absolute values. The next most important terms (V_{2hp} and V_{2ph} for VIEs and VEAs, respectively) are linear in reference-state $T_2^{(1)}$ amplitudes. They invariably counter the exaggerated final-state relaxation and correlation effects produced by the second-order terms. Third-order constant (K_S) terms that are linear in $T_1^{(2)}$ amplitudes diminish the vertical ionization energies and electron affinities. The smallest absolute values belong to the ring-ladder (R_{2hp} and R_{2ph}) terms; ring and ladder contributions often approximately cancel in third order. Absolute values of R_{2hp} terms exceed 0.07 eV in only two VIE cases (see Supporting Information), but the V_{2hp} terms are about three times larger. In no case does the absolute value of R_{2hp} surpass 0.06 eV in VEA calculations. R_{2ph} terms have a relatively minor role in reducing the predictions of vertical ionization energies and electron affinities.

Whereas the os second-order approximations overcome exaggerated final-state effects through omission, the new-generation, third-order methods explicitly ameliorate these errors with additional self-energy terms. Fifth-power algorithms are the price of these improvements. In L3 calculations, an iterative step with OV^4 scaling becomes the arithmetic bottleneck. For electron detachment energies, Q3 provides an alternative with O^2V^3 scaling, no electron repulsion integrals with four virtual indices, and only slightly lower accuracy.

Approximate Renormalizations. Greater accuracy with almost no additional computational effort has been extracted from D3 calculations by estimating higher-order terms. In the three outer valence Green function (OVGF) formulas, ratios of second-order and third-order diagrams have produced improved estimates for electron binding energies.[4,67] These results typically have lain between the underestimates of D2 and the overestimates of D3. A selection procedure with several parameters has been employed to choose one of the three (A, B, C) options.[68,69]

The same techniques have been applied to P3 to give the parameter-free P3+ self-energy[70] and may also be applied to Q3 and L3. P3+ and Q3+ are based on the OVGF-B option, for the latter choice performs separate extrapolations on 2hp and 2ph terms.[23,36−38] This option is preferable because it does not obliterate the distinction between initial-state and final-state terms in the self-energy. (See formulas for diagonal, approximately renormalized self-energies in Appendix 1.) Interpretations in terms of relaxation and differential correlation therefore remain possible. In the A and C versions, third-order terms are collectively multiplied by factors that involve summations of 2hp and 2ph diagrams. Interpolations between D2 and D3 results are made, but analysis is problematic.

https://doi.org/10.1021/acs.jpca.3c08455
J. Phys. Chem. A 2024, 128, 1399−1416

Table 7. Mean Absolute Errors (eV) of Approximately Renormalized Diagonal Self-Energies Versus VIE and VEA Standards

	QTP160[38]	QTP96[38]	GW100[37]	VEDE55[23]	OPV20 VIE[59]	OPV19 VEA[59]
OVGF-A	0.29	0.21	0.17	0.14	0.18	0.23
OVGF-B	0.39	0.34	0.21	0.23	0.31	0.34
OVGF-C	0.43	0.35	0.17	0.24	0.13	0.30
P3+	0.22	0.14	0.14	0.17	0.20	0.09
Q3+	0.17	0.13	0.15	0.16	0.05	0.16
L3+A	0.14	0.10	0.15	0.13	0.15	0.07
L3+B	0.15	0.10	0.10	0.10	0.09	0.09
L3+C	0.16	0.10	0.10	0.10	0.08	0.08

Table 8. Mean Absolute Errors (eV) of Non-Dyson Approximately Renormalized Diagonal Self-Energies Versus VIE and VEA Standards

	QTP160[38]	QTP96[38]	GW100[37]	VEDE55[23]	OPV20 VIE[59]	OPV19 VEA[59]
nD-L3	0.26	0.18	0.12	0.22	0.08	0.10
nD-L3+A	0.14	0.10	0.16	0.13	0.16	0.06
nD-L3+B	0.15	0.09	0.11	0.09	0.09	0.06
nD-L3+C	0.16	0.09	0.10	0.09	0.07	0.06

Only the L3 method is amenable to the extrapolation estimates of all three OVGF versions. Thus, L3+A, L3+B, and L3+C have been examined numerically in addition to P3+ and Q3+. Data for approximately renormalized self-energies are shown in Table 7.

With fewer arithmetic operations for electron detachment energies, Q3+ outperforms the OVGF options, except in the VEDE55 case, where OVGF-A is slightly better. An exceptionally good outcome is obtained for the OPV20 VIE set. Even when the arithmetic advantage over OVGF is diminished in electron attachment (OPV19 VEA) calculations, Q3+'s MAE is lower. L3+B and L3+C give the best data for electron detachments. The quality of the three L3+ options is approximately equal for the electron attachment set and is better than that of Q3+. L3+B employs the same 2hp or 2ph approximate renormalization procedure as P3+ and Q3+ for electron detachment or attachment, respectively. It therefore may be considered an extension of the two latter options. The foundation of the superior performance of the approximately renormalized, new-generation self-energies is the set of third-order reference results produced by P3, Q3, and L3. L3+B may serve as a standard for the set of methods that require evaluation of second- and third-order self-energy diagrams only. Q3+ is a more efficient option for electron detachment energies that usually delivers somewhat lower accuracy.

Once P3, Q3, or L3 calculations are complete, their + versions provide additional improvements at practically no cost. Approximate renormalization formulas (see Appendix 1) multiply third-order terms by factors that reduce their magnitudes. These final refinements to finite-order calculations tend to diminish the third-order corrections to second-order results.

Improved Efficiency with Non-Dyson Methods. The OV^4 arithmetic bottleneck of L3+ calculations of electron detachment energies may be mitigated by employing nD versions. In nD-L3+ self-energies, the energy dependence of the 2ph terms in $\Sigma_{ii}(E)$ is eliminated by performing a calculation with E set equal to ε_i. The number of OV^4 summations is thereby reduced to one. Table 8 shows the MAEs for the nD versions of L3 and the three L3+ variants. For every data set, the nD-L3 MAE is lower than its L3 counterpart in Table 5. Small improvements accompany substitution of nD-L3+ for L3+ in their A, B, and C versions.

The nD versions of the L3 and L3+ self-energies for electron affinities eliminate the energy dependence of the 2hp terms. This variation has no effect on the bottleneck contractions but does reduce MAEs. This trend is especially large in the L3 case, where the MAE declines from 0.15 to 0.10 eV when the nD version is employed for the OPV19 VEA set.

Composite Models. MAEs in Tables 3, 5, 7, and 8 refer to standards generated with high-level methods such as IP-EOM-CCSDT or ΔCCSD(T). The basis sets suffice to inspire confidence in the transferability of the conclusions regarding the predictive capabilities of various self-energy approximations. For vertical electron detachment energies of anions, L3+B calculations with the aug-cc-pVQZ basis sets are likely to provide accurate predictions. A composite model[71] for vertical electron detachment energies[23] (C-VEDE) that avoids most of the computational cost of such calculations employs five more easily executed components.

$$E_{\text{C-VEDE}} = E_{\text{adz}}^{\text{nD-L3+B}} + E_{\text{atz}}^{\text{Q3+}} - E_{\text{adz}}^{\text{Q3+}} + E_{\text{cbs}}^{\text{os-nD-D2}} - E_{\text{atz}}^{\text{os-nD-D2}} \quad (27)$$

In C-VEDE calculations, Q3+ values are generated with aug-cc-pVDZ (adz) and aug-cc-pVTZ (atz) basis sets. Higher basis effects are represented in the last two terms. The complete basis set (cbs) estimate for os-nD-D2 is obtained with a cubic extrapolation of the atz and aug-cc-pVQZ results. The efficiency of this model enabled a study of the four nucleotide anions of DNA.[23] Many spectral features have been accurately assigned to Dyson orbitals localized on base, phosphate, or sugar fragments of the nucleotides. Only one peak, pertaining to the lowest vertical electron detachment energy of guanidine, has an error bar below 0.5 eV. The C-VEDE prediction of 5.01 eV is in excellent agreement with the experimental value of 5.05 ± 0.10 eV.[72]

Additional convincing evidence of the predictive power of composite models was provided by comparisons with standard data for the 24 OPV molecules.[59] Basis-set extrapolated total energies based on ΔCCSD(T) and MP2 calculations provide reference data with error bars estimated at 0.03 eV.[73] A series

https://doi.org/10.1021/acs.jpca.3c08455
J. Phys. Chem. A 2024, 128, 1399−1416

of composite models has been defined according to the following equations:

$$E^{\mathrm{CM1}} = E_{\mathrm{adz}}^{\mathrm{nD\text{-}L3+B}} + E_{\mathrm{CBS(DT)}}^{\mathrm{os\text{-}nD\text{-}D2}} - E_{\mathrm{adz}}^{\mathrm{os\text{-}nD\text{-}D2}} \quad (28)$$

$$E^{\mathrm{CM2}} = E_{\mathrm{adz}}^{\mathrm{Q3+}} + E_{\mathrm{CBS(DT)}}^{\mathrm{os\text{-}nD\text{-}D2}} - E_{\mathrm{adz}}^{\mathrm{os\text{-}nD\text{-}D2}} \quad (29)$$

$$E^{\mathrm{CM3}} = E_{\mathrm{atz}}^{\mathrm{nD\text{-}L3+B}} + E_{\mathrm{CBS(TQ)}}^{\mathrm{os\text{-}nD\text{-}D2}} - E_{\mathrm{atz}}^{\mathrm{os\text{-}nD\text{-}D2}} \quad (30)$$

$$E^{\mathrm{CM4}} = E_{\mathrm{atz}}^{\mathrm{Q3+}} + E_{\mathrm{CBS(TQ)}}^{\mathrm{os\text{-}nD\text{-}D2}} - E_{\mathrm{atz}}^{\mathrm{os\text{-}nD\text{-}D2}} \quad (31)$$

For each model, a Q3+ or an nD-L3+B calculation is performed with adz or atz basis sets. Higher basis set effects are estimated with a quartic extrapolation, i.e., fitted to $(l + 0.5)^{-4}$, of os-nD-D2 data. Table 9 shows results for the 24 VIEs of the OPV set. Comparison of CM1 and CM2 results indicates that little accuracy is lost for vertical ionization energies when Q3+ is substituted for nD-L3+B. Dependence on triple-quadruple extrapolation in CM3 and CM4 instead of double-triple extrapolation in CM1 and CM2 also is of only minor consequence. CM2 is the most promising technique for the vertical ionization energies of OPV candidates. CM1 has comparable accuracy but is more difficult to execute.

Table 9. Mean Absolute Errors (eV) of Composite Models for the OPV24 VIE and OPV23 VEA Standards

	OPV24 VIE[59]	OPV23 VEA[59]
CM1	0.07	0.05
CM2	0.05	0.13
CM3	0.06	0.06
CM4	0.06	0.15

Data on electron attachment energies are displayed in the OPV23 VEA column of Table 9. Based on the behavior of Q3+ seen in previous tables and on its lack of an arithmetic advantage over nD-L3+B, one expects CM1 and CM3 to be more useful than CM2 and CM4. The former pair of models is equally successful as its counterpart for vertical ionization energies. The MAEs of CM1 and CM3 are very close to each other. CM1 is the optimal choice for the electron affinities of potential OPV molecules.

Explicit Versus Approximate Renormalizations. The numerical, computational, and interpretive success of the os-nD-D2, Q3+, nD-L3+B, and other new-generation self-energies rests partly on two testable assumptions. In the first test, diagonal methods that explicitly evaluate higher-order terms instead of approximating them are considered. Non-diagonal, renormalized self-energies that contain all terms included in the first test are examined in the second.

Instead of the expansion of $[\mathbf{f}_3|(E\hat{I}\text{-}\hat{H})\mathbf{f}_3]_{0+1}^{-1}$ to first order executed in Q3+ and L3+ calculations, where

$$[\mathbf{f}_3|(E\hat{I} - \hat{H})\mathbf{f}_3]_{0+1}^{-1} \approx [\mathbf{f}_3|(E\hat{I} - \hat{H})\mathbf{f}_3]_0^{-1} + [\mathbf{f}_3|(E\hat{I} - \hat{H})\mathbf{f}_3]_0^{-1}[\mathbf{f}_3|\hat{V}\mathbf{f}_3]_1 [\mathbf{f}_3|(E\hat{I} - \hat{H})\mathbf{f}_3]_0^{-1} \quad (32)$$

one can sum higher orders until numerical convergence is achieved. (The 0 + 1 subscript on the left side of eq 32 indicates the sum of the zeroth-order and first-order terms.) Initial studies of the resulting explicitly renormalized, diagonal self-energies performed these summations but encountered convergence difficulties for many excited final states.[36]

A more dependable and efficient approach[38] solves linear equations for $[\mathbf{f}_3|(E\hat{I}\text{-}\hat{H})\mathbf{f}_3]_{0+1}{}^{-1}[\mathbf{f}_3|\hat{H}\mathbf{a}^\dagger]$. This algorithm has not failed to converge in the numerical tests reviewed in this work. It also decreases the number of contractions associated with multiplication by the first-order matrix of the fluctuation-potential superoperator. In L3+ calculations, the number of bottleneck steps with OV^4 arithmetic scaling is reduced when this algorithm is used.

The $[\mathbf{f}_3|(E\hat{I}\text{-}\hat{H})\mathbf{f}_3]_{0+1}{}^{-1}[\mathbf{f}_3|\hat{H}\mathbf{a}^\dagger]$ intermediate appears in the last term of the diagonal, renormalized, linear third order (RL3) self-energy,[23,36−38] where

$$\Sigma_{pp}^{\mathrm{RL3}}(E) = [a_p^\dagger|\hat{H}\mathbf{f}_3]_2[\mathbf{f}_3|(E\hat{I} - \hat{H})\mathbf{f}_3]_0^{-1}[\mathbf{f}_3|\hat{H}a_p^\dagger]_1 + [a_p^\dagger|\hat{H}\mathbf{f}_3]_1[\mathbf{f}_3|(E\hat{I} - \hat{H})\mathbf{f}_3]_0^{-1}[\mathbf{f}_3|\hat{H}a_p^\dagger]_2 + [a_p^\dagger|\hat{H}\mathbf{f}_3]_1[\mathbf{f}_3|(E\hat{I} - \hat{H})\mathbf{f}_3]_{0+1}^{-1}[\mathbf{f}_3|\hat{H}a_p^\dagger]_1 + \Sigma_{pq3}(\infty) \quad (33)$$

$\boldsymbol{\Sigma}^{\mathrm{ND2}}(E)$ is now contained in the third term. Ring, ladder, and mixed ring-ladder diagrams in all orders of the Møller-Plesset fluctuation potential are included in the diagonal self-energy matrix elements. For RQ3 electron detachment energies, it is necessary to substitute the renormalized matrix for the finite expansion only in the 2hp terms (R designates a diagonal, renormalized self-energy.) The RQ3 self-energy for electron detachment energies reads

Table 10. Mean Absolute Errors (eV) of Explicitly and Approximately Renormalized Diagonal Self-Energies Versus VIE and VEA Standards

	QTP160[38]	QTP96[38]	GW100[37]	VEDE55[23]	OPV20 VIE[59]	OPV23 VEA[59a]
P3+	0.22	0.14	0.14	0.17	0.20	0.11
RP3	0.16	0.12	0.16	0.13	0.14	0.10
Q3+	0.17	0.13	0.15	0.16	0.05	0.14
RQ3	0.14	0.10	0.17	0.16	0.06	0.09
L3+B	0.15	0.10	0.10	0.10	0.09	0.09
RL3	0.12	0.08	0.10	0.08	0.09	0.08
nD-RL3	0.11	0.08	0.11	0.08	0.10	0.06
DR	0.34	0.25	0.23	0.26	0.37	0.14

[a]OPV23 EA tests employed the aug-cc-pVDZ basis.

https://doi.org/10.1021/acs.jpca.3c08455
J. Phys. Chem. A 2024, 128, 1399−1416

$$\Sigma_{pp}^{RQ3}(E) = \Sigma_{pp}^{ND2\text{-}2ph}(E) + [a_p^\dagger|\hat{H}\mathbf{f}_{2hp}]_2[\mathbf{f}_{2hp}|(E\hat{I} - \hat{H})\mathbf{f}_{2hp}]_0^{-1}[\mathbf{f}_{2hp}|\hat{H}a_p^\dagger]_1 + [a_p^\dagger|\hat{H}\mathbf{f}_{2hp}]_1[\mathbf{f}_{2hp}|(E\hat{I} - \hat{H})\mathbf{f}_{2hp}]_0^{-1}[\mathbf{f}_{2hp}|\hat{H}a_p^\dagger]_2 + [a_p^\dagger|\hat{H}\mathbf{f}_{2hp}]_1[\mathbf{f}_{2hp}|(E\hat{I} - \hat{H})\mathbf{f}_{2hp}]_{0+1}^{-1}[\mathbf{f}_{2hp}|\hat{H}a_p^\dagger]_1 + \Sigma_{pp3}(\infty) \quad (34)$$

The 2hp part of $\mathbf{\Sigma}^{ND2}(E)$ (see eq 13) lies within the fourth term; the 2ph part of $\mathbf{\Sigma}^{ND2}(E)$ equals the first term. By permuting 2ph and 2hp in the latter formula, the RQ3 self-energy for electron attachment energies is defined. In practical calculations, it cannot be expected to have any important advantage over its RL3 counterpart with respect to arithmetic bottlenecks. When the constant term is removed, the RP3 self-energies for electron attachment and detachment energies are also defined. The RL3, RQ3, and RP3 self-energies comprise, respectively, all terms present in their L3, Q3, and P3 antecedents. A similar generalization is in effect for the nD version of RL3 with respect to nD-L3. The solution of linear equations requires more bottleneck (OV^4) steps for RL3 than for L3+ methods. A similar repetition of rate-limiting O^2V^3 steps occurs for RQ3 calculations of electron detachment energies.

Table 10 displays the results of numerical tests of diagonal, explicitly renormalized self-energies and facilitates comparisons with their approximately renormalized counterparts. For electron detachment energies, RQ3 and RL3 realize their greatest improvements of 0.02−0.03 eV for the two (QTP) sets, which include excited final states. For the GW100 case, Q3+ performs slightly better than RQ3. As the probability factors approach the 0.85 criterion for the validity of diagonal self-energy approximations, the RL3 and RQ3 options become more useful. Whereas they are slower than L3+B and Q3+, respectively, they also are likely to be more accurate. The computational disadvantages of RL3 may be mitigated with nD-RL3 calculations, for the latter variant's MAEs are not demonstrably worse.

A smaller basis was employed for 23 OPV electron affinities. The RL3 self-energy yields a negligible improvement over L3+B. Slightly better performance is obtained from the nD-RL3 calculations.

The self-energies of the G_0W_0 family[39] are also diagonal and renormalized. A fully *ab initio* version may be defined by employing canonical Hartree−Fock orbitals and the excitation operators and energies of the Tamm-Dancoff approximation.[23,36−38,74] (Most G_0W_0 calculations are based on Kohn−Sham orbitals and random-phase-approximation excitations.) Instead of the full expression of the $[\mathbf{f}_3|(E\hat{I}\text{-}\hat{H})\mathbf{f}_3]_{0+1}^{-1}$ matrix found in the RL3 self-energy, only terms that generate exchange-less ring diagrams are retained. Exchange terms in the $[\mathbf{f}_3|\hat{H}\mathbf{a}^\dagger]$ matrix and its Hermitian conjugate also are neglected. Only terms in boldface in the following equations are retained.

$$[a_p^\dagger|\hat{H}a_a a_i^\dagger a_j^\dagger]_1 = \langle \mathbf{pa}|\mathbf{ij}\rangle - \langle pa|ji\rangle \quad (35)$$

$$[a_p^\dagger|\hat{H}a_i a_a^\dagger a_b^\dagger]_1 = \langle \mathbf{pi}|\mathbf{ab}\rangle - \langle pi|ba\rangle \quad (36)$$

$$[a_a a_i^\dagger a_j^\dagger|\hat{V}a_b a_k^\dagger a_l^\dagger]_1 = (1 - P_{ij})(1 - P_{kl})\delta_{ik}[\langle bj|al\rangle - \langle \mathbf{bj}|\mathbf{la}\rangle] - \delta_{ab}\langle ij||kl\rangle \quad (37)$$

$$[a_i a_a^\dagger a_b^\dagger|\hat{V}a_j a_c^\dagger a_d^\dagger]_1 = -(1 - P_{ab})(1 - P_{cd})\delta_{ac}[\langle jb|id\rangle - \langle \mathbf{jb}|\mathbf{di}\rangle] + \delta_{ij}\langle ab||cd\rangle \quad (38)$$

Second-order extensions in the primary-secondary block of $\hat{\boldsymbol{H}}$ also are absent. The resulting HF-TDA-G_0W_0 or diagonal ring (DR) self-energy may be used for electron attachments or detachments. DR bottleneck contractions scale as O^2V^3. This approximation has no need for electron repulsion integrals with four virtual indices. For electron detachment energies, integrals with three virtual indices are not required either. So-called one-shot G_0W_0 calculations evaluate $\Sigma_{pp}(E)$ and $d\Sigma_{pp}(E)/dE$ at only one value of E and use Newton's method to produce a final estimate of the solution to eq 10. The present DR calculations iteratively search for poles until convergence to within 0.01 eV is reached. Data are shown at the bottom of Table 10. The DR approximation is competitive with os-nD-D2 only for electron affinities, where it enjoys an advantage of accuracy but not of arithmetic efficiency.

For electron detachment energies, the explicitly renormalized (R) extensions of P3, Q3, and L3 display minor improvements in MAEs versus their approximately (+) renormalized counterparts. This advantage is realized at the cost of an increased number of bottleneck steps. These extensions are likely to be more accurate when excited final states are considered. Similar trends emerge from preliminary tests on electron attachment energies, where RP3, RQ3, and RL3 have the same (OV^4) arithmetic bottleneck. For both types of electron binding energies, RL3 is the most accurate alternative. The more efficient nD version for electron detachment energies has almost identical MAEs. These methods provide a more exact way of correcting the principal deficiency of D2, i.e., its treatment of orbital relaxation and final-state differential electron correlation.

The DR approximation, a fully *ab initio* member of the G_0W_0 family, also has a explicitly renormalized, diagonal self-energy. For electron detachment energies, it has an advantage over other diagonal, renormalized methods, for it does not require electron repulsion integrals with three virtual indices. Its mean absolute errors are no better than those of the cubically scaling os-D2 and os-nD-D2 self-energies (see Tables 2 and 8). Preliminary tests indicate greater success for electron attachment energies, but the need for electron repulsion integrals with three virtual indices reappears. Other diagonal, renormalized alternatives with similar computational requirements produce lower MAEs.

Nondiagonal Versus Diagonal Self-Energies. The second test mentioned above considers the validity of the diagonal self-energy approximation with the canonical Hartree−Fock basis. This approximation requires that Dyson orbitals be proportional to canonical Hartree−Fock orbitals. An alternative route to electron binding energies and Dyson orbitals without this restriction is provided by diagonalizations of the superoperator Hamiltonian matrix, $\hat{\boldsymbol{H}}$. In this approach, electron binding energies are equal to eigenvalues. Dyson orbitals are equal to the linear combination of orbitals defined by the primary-operator (i.e., $\boldsymbol{a}^\dagger$) elements of the eigenvectors.

Nondiagonal, renormalized self-energies are often defined in terms of the secondary operator manifold, $\boldsymbol{f}$, and the approximations made in each block of $\hat{\boldsymbol{H}}$.[38] (See Table 11.) For example, the 2ph-TDA self-energy has a zeroth-order primary−primary block and first-order primary-secondary and secondary-secondary blocks. The secondary operator manifold

https://doi.org/10.1021/acs.jpca.3c08455
J. Phys. Chem. A 2024, 128, 1399−1416

Table 11. Orders Retained in Super-Operator Hamiltonian Matrices ($\hat{H}$) of NRP3, NRQ3, and NRL3 Self-Energies for Hole (h), Particle (p), Two-Hole-One-Particle (2hp), and Two-Particle-One-Hole (2ph) Operators[a,b,c,d,e,f,g]

$\hat{\mathbf{H}}$	h	p	2hp	2ph
h	**NRP3** 0[e]	**NRP3** 0[e]	**NRP3** (2,1)	**NRP3** (1,2)
	NRQ3 3	**NRQ3** 3	**NRQ3** (2,1)	**NRQ3** (1,2)
	NRL3 3	**NRL3** 3	**NRL3** 2	**NRL3** 2
	ND2 0[e]	ND2 0[e]	ND2 1	ND2 1
	3+ 3[c]	3+ 3[c]	3+ 2	3+ 2
p		**NRP3** 0[e]	**NRP3** (2,1)[b]	**NRP3** (1,2)
		NRQ3 3	**NRQ3** (2,1)	**NRQ3** (1,2)
		NRL3 3	**NRL3** 2	**NRL3** 2
		ND2 0[e]	ND2 1	ND2 1
		3+ 3[c]	3+ 2	3+ 2
2hp			**NRP3** (1,0)	**NRP3** 0[e,f]
			NRQ3 (1,0)	**NRQ3** 0[e,f]
			NRL3 1	**NRL3** 0[e,f]
			ND2 0[d,e]	ND2 0[e,f]
			3+ 1	3+ 0[f]
2ph				**NRP3** (0,1)[e]
				NRQ3 (0,1)[e]
				NRL3 1
				ND2 0[d,e]
				3+ 1

[a]Evaluation of $\hat{\mathbf{H}}$ with Hermitized, intermediately normalized metric in **bold type**. [b]NR2 is the same as NRP3 except that p-2hp (h-2ph) couplings are evaluated in first instead of second order for electron detachment (attachment) energies. [c]3+ is identical to strict ADC(3); other versions of ADC(3) differ in their treatment of h-h, h-p, and p-p couplings. [d]2ph-TDA differs from ND2 by introducing first-order terms in the 2hp-2hp and 2ph-2ph blocks. [e]First-order terms and off-diagonal zeroth-order terms vanish. CHF orbital energies of zeroth order occur in diagonal matrix elements. In the h-h, p-p, and h-p blocks, second-order terms also vanish. [f]The first nonvanishing 2hp-2ph couplings appear in second order and contribute to fourth-order and higher-order self-energies. [g]Ordered pairs indicate separate treatments of electron detachment and attachment energies, respectively.

is f_3. A diagonal self-energy version of 2ph-TDA has only one member in the set of primary operators.

Nondiagonal, renormalized generalizations of RP3, RQ3, and RL3 require that $\hat{\boldsymbol{H}}$ be constructed such that the self-energy retains all terms included in these three antecedents. A third-order primary−primary block recovers the constant self-energy term for the nondiagonal, renormalized generalizations of RQ3 and RL3. (Zeroth-order suffices to generalize RP3.) Second-order primary-2hp and first-order 2hp-2hp blocks are needed to generalize the energy-dependent parts of RQ3 for electron detachment energies. To generalize RL3, second-order primary-f_3 and first-order f_3-f_3 blocks are required. The resulting nondiagonal, renormalized self-energies are given in the following three equations:

$$\Sigma_{pq}^{\mathrm{NRL3}}(E) = [a_p^\dagger|\hat{H}\mathbf{f}_3]_{1+2}[\mathbf{f}_3|(E\hat{I} - \hat{H})\mathbf{f}_3]_{0+1}^{-1}[\mathbf{f}_3|\hat{H}a_q^\dagger]_{1+2} + \Sigma_{pq3}(\infty) \tag{39}$$

$$\Sigma_{pq}^{\mathrm{NRQ3}}(E) = \Sigma_{pq}^{\mathrm{ND2\text{-}2ph}}(E) + [a_p^\dagger|\hat{H}\mathbf{f}_{2hp}]_{1+2}[\mathbf{f}_{2hp}|(E\hat{I} - \hat{H})\mathbf{f}_{2hp}]_{0+1}^{-1}[\mathbf{f}_{2hp}|\hat{H}a_q^\dagger]_{1+2} + \Sigma_{pq3}(\infty) \tag{40}$$

$$\Sigma_{pq}^{\mathrm{NRP3}}(E) = \Sigma_{pq}^{\mathrm{ND2\text{-}2ph}}(E) + [a_p^\dagger|\hat{H}\mathbf{f}_{2hp}]_{1+2}[\mathbf{f}_{2hp}|(E\hat{I} - \hat{H})\mathbf{f}_{2hp}]_{0+1}^{-1}[\mathbf{f}_{2hp}|\hat{H}a_q^\dagger]_{1+2} \tag{41}$$

In eqs 39−41, 1 + 2 subscripts indicate the sum of the first-order and second-order terms. In the NRQ3 and NRP3 equations, the first term is confined to the 2ph summation of ND2. (See eq 13.) For NRQ3 and NRP3 electron attachment calculations, the roles of the 2ph and 2hp terms are reversed. Both types of terms are present in the NRL3 case, for the f_3 manifold comprises 2hp and 2ph secondary operators.

A recent computational study on electron detachment energies compared data from older nondiagonal self-energies with those of the new generation.[38] The former set included ND2, 2ph-TDA, and the strict and Schirmer-Angonoa versions of the third-order algebraic diagrammatic construction [denominated, respectively, as 3+ and ADC(3)]. In addition, the nondiagonal, renormalized second-order (NR2) method and the BD-T1 approximation were considered. The latter option employs Brueckner Doubles coupled-cluster orbitals and double replacement amplitudes. Table 12 shows the results of numerical tests of nondiagonal, renormalized self-energies and juxtaposes them with their diagonal antecedents.

Table 12. Mean Absolute Errors (eV) of Nondiagonal, Renormalized Self-Energies Versus VIE and VEA Standards

	QTP160[38]	QTP96[38]
RP3	0.16	0.12
NRP3	0.13	0.10
RQ3	0.14	0.10
NRQ3	0.13	0.10
RL3	0.12	0.08
NRL3	0.09	0.06
ND2	0.61	0.68
2ph-TDA	0.66	0.63
3+	0.41	0.38
ADC(3)	0.43	0.34
NR2	0.13	0.10
BD-T1	0.14	0.10
IP-EOM-CCSD	0.21	0.14

The first three pairs of lines indicate that small improvements are realized with the nondiagonal extensions. These gains in accuracy are greater for the more challenging QTP160 set than for the smaller QTP96 set, wherein all probability factors are above 0.85. NRL3 attains an MAE below 0.1 eV for QTP160 VIEs, a notable achievement for a set with many final states having significant shakeup character. Its MAE of 0.06 eV when probability factors exceed 0.85 approaches the errors inherent in the IP-EOM-CCSDT reference data.

Only a small subset of the older methods remains competitive. ND2 has fourth-power arithmetic scaling but also has lower accuracy than the cubically scaling os-D2 and os-nD-D2 alternatives. Inclusion in 2ph-TDA of first-order, secondary-secondary couplings is not rewarded with markedly lower MAEs for either data set. Large improvements of 0.2−

https://doi.org/10.1021/acs.jpca.3c08455
J. Phys. Chem. A 2024, 128, 1399−1416

0.3 eV accompany use of 3+ and ADC(3). These two options have OV^4 and O^2V^4 arithmetic bottlenecks, and they are not as accurate as any of the new-generation methods, diagonal or nondiagonal. The superoperator Hamiltonian matrix of NR2 strongly resembles that of NRP3 and has practically identical MAEs. NR2 has an O^3V^3 arithmetic bottleneck for electron detachment energies, because it omits second-order p-2hp couplings. BD-T1, like IP-EOM-CCSD,[75] has an O^2V^4 bottleneck that arises from its reference-state, total-energy calculation. The former alternative has lower MAEs, but they are somewhat larger than those of NRL3.

The results of this test on electron detachment energies establish the obsolescence of ND2, 2ph-TDA, 3+, and ADC(3). Like all nondiagonal methods, NRP3, NRQ3, and NRL3 obtain Dyson orbitals in their general form, a linear combination of basis orbitals. NRQ3 and NRL3 also produce lower MAEs at reduced cost in comparison with older nondiagonal self-energy approximations and IP-EOM-CCSD. Among older self-energies, only NR2 and BD-T1 remain competitive with respect to accuracy and computational effort.

Nondiagonal, renormalized extensions of the RP3, RQ3, and RL3 methods enable Dyson orbitals to become linear combinations of canonical Hartree−Fock orbitals. NRP3, NRQ3, and NRL3 attain a slightly higher level of accuracy for electron detachment energies, especially for excited final states. These calculations involve noniterative, sixth-power contractions that produce second-order $\hat{\boldsymbol{H}}$ couplings between $a^\dagger$ and $\boldsymbol{f}_3$ operators. NRL3 is the most accurate alternative in this group.

CONCLUSIONS

A new generation of electron-propagator methods for calculating valence electron binding energies of closed-shell molecules and molecular ions has been introduced. Every member of this set is based on canonical Hartree−Fock orbitals and is free of adjustable parameters. No active valence orbital spaces or self-consistency procedures that require repeated transformations of the electron repulsion integrals are introduced. Energy iterations in the diagonal-self-energy Dyson equation (i.e., eq 10) lead to numerically precise values of the poles of the electron propagator. Diagonalizations of the superoperator Hamiltonian matrix provide data of equal quality (i.e., solutions of eq 7) for nondiagonal self-energies.

The most accurate self-energy approximations for a given arithmetic scaling factor were identified through comparisons to several sets of high-quality data. Optimal compromises of accuracy and efficiency have been based on two criteria: arithmetic scaling of bottleneck steps and mean absolute errors versus standard data. Every approximation may be interpreted with the concepts of differential pair correlation and final-state orbital relaxation. Several new-generation cubic (OV^2) and fifth-power (O^2V^3 or OV^4) options generate lower mean absolute errors than their antecedents with the same or larger arithmetic scaling factors. (See Table 4.) These diagonal self-energy methods produce Dyson orbitals that equal a canonical Hartree−Fock orbital times the square root of the probability factor.

The best options with cubic arithmetic scaling are practically free of cost once a partial electron integral transformation has been performed. For a single electron binding energy, the latter step has quartic arithmetic scaling. Two opposite-spin approximations, os-D2 and os-nD-D2, attain mean absolute errors of 0.2 and 0.3 eV for electron detachment and attachment energies, respectively. Whereas correlation between same-spin electrons is inherent in the preceding self-consistent-field calculation, opposite-spin correlation is described by a second-order self-energy expression. The constituent terms are related to pair correlation energies obtained with second-order perturbation theory. To compensate for the exaggeration of final-state differential correlation and orbital relaxation effects in D2 and nD-D2, same-spin correlation is neglected in the two os self-energies. These approximations are most advantageous when large amounts of moderately accurate data are sought for closed-shell reference states. They are attractive alternatives when the usual post-self-consistent-field approaches based on the variational method or many-body theories are infeasible. Their interpretive advantages over parametrized models also invite diverse applications, especially when novel patterns of chemical bonding are studied.

The next escalation of arithmetic effort pertains to electron detachment energies only. At this level, the arithmetic bottleneck has fifth-power scaling, with quadratic and cubic dependences, respectively, on occupied and virtual orbital-space dimensions. Transformed electron repulsion integrals with four virtual indices are not needed. The chief defect of the D2 self-energy is moderated by inclusion of higher-order terms pertaining to final-state differential pair correlation and orbital relaxation. Mean absolute errors are lowered below ∼0.15 eV with the approximately renormalized Q3+ self-energy. Explicitly renormalized diagonal (RQ3) and sixth-power nondiagonal (NRQ3) extensions produce mean absolute errors near 0.1 eV. These methods offer efficient, accurate interpretations of photoelectron spectra and other experiments that measure electron detachment energies.

Improvements that exhibit approximately equal success for detachments and attachments are realized with self-energies that have a more demanding fifth-power bottleneck. The arithmetic scaling factor of L3+B depends linearly and quartically on the occupied and virtual orbital-space dimensions, respectively. Its mean absolute errors amount to 0.1 eV or less, depending on the data set. Explicitly renormalized (RL3) and sixth-power nondiagonal (NRL3) generalizations depress the error measures even further. The number of bottleneck contractions may be reduced by employing the nD variants of L3+B and RL3. These methods feature the moderating, higher-order effects of final-state differential electron correlation and orbital relaxation.

Composite approaches employ nD-L3+B (or Q3+ for detachment energies) with a relatively small basis set and os-nD-D2 with a relatively large basis set. Mean absolute errors versus a high-level standard are well-below 0.1 eV. (See Table 9.) Results obtained with augmented double and triple ζ basis sets undergo little improvement when augmented triple and quadruple ζ sets are employed. The former procedure that requires smaller basis sets is recommended therefore for general use.

To program opposite-spin cubically scaling, approximately renormalized, or nondiagonal renormalized self-energies, only trivial changes are needed in codes that execute OVGF or ADC(3) calculations. Explicitly renormalized, diagonal methods are best implemented with their recently developed algorithm for solving linear equations. A fully *ab initio* member of the G_0W_0 family, the diagonal ring (DR) approximation, may also employ this algorithm.

The DR approximation, which employs canonical Hartree−Fock orbitals and Tamm-Dancoff excitations, produces larger

https://doi.org/10.1021/acs.jpca.3c08455
J. Phys. Chem. A 2024, 128, 1399−1416

errors than the two opposite-spin second-order self-energies for electron detachments. In preliminary tests on electron attachments, DR yields lower errors than these cubically scaling alternatives. (Tests with larger basis sets are needed to verify this trend.) DR does not require electron repulsion integrals, with four virtual indices in electron affinity calculations. A lower mean absolute error was achieved by the L3+B method, which does require the latter block of integrals.

The chief computational advantage of approximately renormalized diagonal self-energies over their explicitly renormalized counterparts is a reduction in the number of fifth-power bottleneck steps. Explicitly renormalized diagonal self-energies usually realize small improvements in error measures. Generalizations to nondiagonal self-energies from their diagonal, explicitly renormalized versions yield additional small reductions in errors. NRL3, the most computationally demanding of the new-generation options, produces MAEs that approach the errors that are found in the IP-EOM-CCSDT reference data. The computational disadvantage of the nondiagonal, renormalized self-energies is their need for noniterative, sixth-power steps. Their primary conceptual advantage is the production of Dyson orbitals in their most general form, a linear combination of all basis functions.

The new generation of electron-propagator methods for calculating electron binding energies and Dyson orbitals spans several levels of accuracy, computational efficiency, and interpretive depth. Its most accurate members for a given level of computational effort have been identified. (Table 2 and Figure 1 summarize outcomes for the QTP96 set, where probability factors exceed 0.85.) Algorithms with cubic or fifth-power arithmetic scaling are accompanied by mean absolute errors that vary between 0.3 and 0.1 eV. Dyson orbitals may be expressed as a single canonical Hartree−Fock orbital times the square root of a probability factor or, more generally, as a linear combination of all canonical Hartree−Fock orbitals. Each option has a well-defined effective potential expressed in terms of a Fock operator and an energy-dependent, nonlocal self-energy operator. This hierarchy of approximations enables the interpretation of numerical results in terms of specific orbital relaxation and differential correlation effects.

Comparisons between previously developed and new-generation methods for the QTP96 set of vertical ionization energies are summarized in Figure 2. These data pertain to cases wherein diagonal self-energies in the canonical Hartree−Fock basis are used appropriately, i.e., when probability factors (Dyson orbital norms) exceed 0.85. In four of the five categories of arithmetic scaling, the new-generation alternatives surpass their best predecessors with respect to mean absolute errors. Only the previously developed NR2 method, which strongly resembles the new-generation NRP3 approximation, has no new-generation counterpart in Figure 2. The opposite-spin second-order self-energies provide excellent compromises of accuracy and efficiency for the generation of large data sets of electron detachment energies. Their cubic arithmetic scaling factors and competitive average errors near 0.2 eV can facilitate interpretations of experiments when more demanding approaches are infeasible. The O^2V^3 arithmetic bottleneck of P3+ has been equaled and its accuracy has been surpassed by the Q3+ and RQ3 approximations. Whereas Q3+ is an approximately renormalized option that requires only energy iterations, RQ3 is an explicitly renormalized upgrade that involves solutions of linear equations. All of these methods

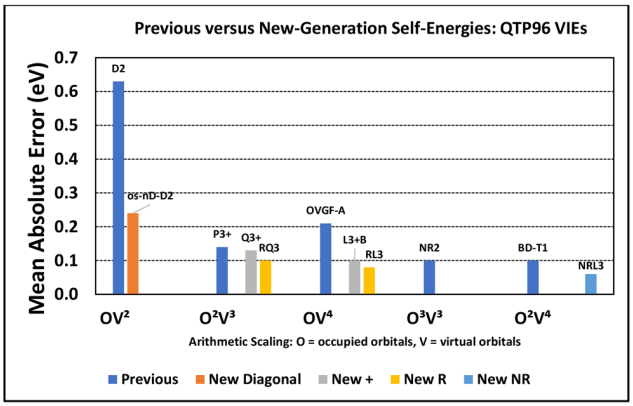


Figure 2. Arithmetic scaling factors and mean absolute errors (eV) for the QTP96 set of vertical ionization energies. Categories of self-energies: + = diagonal, approximately renormalized, R = diagonal, explicitly renormalized, NR = nondiagonal, renormalized. See Table 1 for self-energy acronyms. The QTP96 set includes 96 vertical ionization energies of closed-shell molecules where probability factors ≥0.85.

with O^2V^3 arithmetic scaling are more accurate (with average errors of 0.1 eV) than D3 and the three OVGF versions. The four latter precedents have two computational disadvantages versus Q3+ and RQ3: OV^4 bottlenecks and the use of transformed electron repulsion integrals with four virtual indices. New-generation self-energies with the same requirements produce lower errors than all other diagonal alternatives. In this group, the L3+B and RL3 approximations have average errors below 0.1 eV. Whereas the explicitly renormalized RL3 self-energy requires more bottleneck steps, it achieves a slightly lower mean absolute error. Several previously developed approaches have O^2V^4 bottlenecks, including the standard version of ADC(3), IP-EOM-CCSD, and BD-T1. The NRL3 self-energy produces lower errors than all of them. Its mean absolute error of 0.06 eV approaches that of the standard (IP-EOM-CCSDT) to which it is compared in this work. Whereas ADC(3), IP-EOM-CCSD and BD-T1 have reference-state optimizations that involve iterations with O^2V^4 scaling, NRL3's formal bottleneck is noniterative.

Preliminary studies of recently introduced, new-generation methods for electron affinities show similar promise. Numerical tests have been performed on a data set of electron-acceptor molecules with potential applications to organic photovoltaic materials. The opposite-spin, second-order self-energies produce smaller mean absolute errors of about 0.3 eV and retain the same efficiency as the D2 calculations. The L3+B approximation and its P3+ predecessor produce identical error measures (0.09 eV) that are smaller than those (0.2−0.3 eV) of the three OVGF procedures. These approximately renormalized approximations are slightly surpassed by the explicitly renormalized RL3 self-energy and its nD variant.

Further developments will consider electron affinities of molecules in greater depth and examine the performance of new-generation methods for open-shell initial states.

APPENDIX 1

Superoperator matrix elements obtained with the Hermitized, intermediately normalized metric read as follows for real spin−orbitals.

https://doi.org/10.1021/acs.jpca.3c08455
J. Phys. Chem. A 2024, 128, 1399−1416

$$\hat{H}^{(1)}_{p,aij} = \langle pa||ij\rangle \tag{A1}$$

$$\hat{H}^{(2)}_{p,aij} = \frac{1}{2}\left[\frac{1}{2}t^{bc(1)}_{ij}\langle bc||pa\rangle + (1 - P_{ij})t^{ba(1)}_{jk}\langle bi||pk\rangle\right] \tag{A2}$$

$$\hat{H}^{(1)}_{p,iab} = \langle pi||ab\rangle \tag{A3}$$

$$\hat{H}^{(2)}_{p,iab} = \frac{1}{2}\left[-\frac{1}{2}t^{ab(1)}_{jk}\langle jk||pi\rangle - (1 - P_{ab})t^{bc(1)}_{ji}\langle ja||pc\rangle\right] \tag{A4}$$

$$\Sigma^{(3)}_{pq}(\infty) = \langle ip||ap\rangle t^{a(2)}_{i} \tag{A5}$$

Superscripts in parentheses designate orders in the Møller-Plesset fluctuation potential. These formulas and those discussed in the context of the DR method suffice to implement the new generation self-energy methods.

Two additional intermediates are needed to compute ladder (first) and ring (second) terms, as follows.

$$U_{paij}(E) = -\frac{1}{2}\frac{\langle pa||kl\rangle\langle kl||ij\rangle}{E + \epsilon_a - \epsilon_k - \epsilon_l} - (1 - P_{ij})\frac{\langle pb||jk\rangle\langle ak||bi\rangle}{E + \epsilon_b - \epsilon_j - \epsilon_k} \tag{A6}$$

$$U_{piab}(E) = \frac{1}{2}\frac{\langle pi||cd\rangle\langle cd||ab\rangle}{E + \epsilon_i - \epsilon_c - \epsilon_d} + (1 - P_{ab})\frac{\langle pj||bc\rangle\langle ic||ja\rangle}{E + \epsilon_j - \epsilon_b - \epsilon_c} \tag{A7}$$

These intermediates may be used to express the L3 diagonal self-energy matrix elements.

$$\Sigma^{\mathrm{L3}}_{pp}(E) = \Sigma^{\mathrm{ND2\text{-}2hp}}_{pp}(E) + \Sigma^{\mathrm{ND2\text{-}2ph}}_{pp}(E) + 2\frac{\hat{H}^{(2)}_{p,aij}\hat{H}^{(1)}_{p,aij}}{(E + \epsilon_a - \epsilon_i - \epsilon_j)} + 2\frac{\hat{H}^{(2)}_{p,iab}\hat{H}^{(1)}_{p,iab}}{(E + \epsilon_i - \epsilon_a - \epsilon_b)} + \frac{U_{paij}(E)\hat{H}^{(1)}_{p,aij}}{(E + \epsilon_a - \epsilon_i - \epsilon_j)} + \frac{U_{piab}(E)\hat{H}^{(1)}_{p,iab}}{(E + \epsilon_i - \epsilon_a - \epsilon_b)} + \Sigma^{(3)}_{pp}(E) \tag{A8}$$

The seven terms are renamed as follows with suppression of their energy dependence and p indices.

$$\Sigma^{\mathrm{L3}}_{pp}(E) = S_{2hp} + S_{2ph} + V_{2hp} + V_{2ph} + R_{2hp} + R_{2ph} + K_S \tag{A9}$$

In this notation, the V_{2ph} and R_{2ph} (V_{2hp} and $\underline{R_{2hp}}$) terms are omitted in Q3 calculations of electron detachments (attachments). K_S terms are also omitted in P3 calculations.

Three approximate renormalizations based on L3 may be expressed as

$$\Sigma^{\mathrm{L3+A}}_{pp}(E) = \Sigma^{\mathrm{ND2}}_{pp}(E) + \frac{S_{2hp} + S_{2ph}}{S_{2hp} + S_{2ph} - (V_{2hp} + V_{2ph})}[K_S + R_{2hp} + R_{2ph} + V_{2hp} + V_{2ph}] \tag{A10}$$

$$\Sigma^{\mathrm{L3+B}}_{pp}(E) = \Sigma^{\mathrm{ND2}}_{pp}(E) + K_S + \frac{S_{2hp}}{S_{2hp} - V_{2hp}}(R_{2hp} + V_{2hp}) + \frac{S_{2ph}}{S_{2ph} - V_{2ph}}(R_{2ph} + V_{2ph}) \tag{A11}$$

$$\Sigma^{\mathrm{L3+C}}_{pp}(E) = \Sigma^{\mathrm{ND2}}_{pp}(E) + [K_S + R_{2hp} + R_{2ph} + V_{2hp} + V_{2ph}] \times \frac{R_{2hp} + R_{2ph} + V_{2hp} + V_{2ph}}{\frac{S_{2hp} - V_{2hp}}{S_{2hp}}(R_{2hp} + V_{2hp}) + \frac{S_{2ph} - V_{2ph}}{S_{2ph}}(R_{2ph} + V_{2ph})} \tag{A12}$$

In the Q3+ self-energy for electron detachments (attachments), the fourth (third) term in the L3+B equation is omitted. The second term is also omitted in P3+ calculations.

■ ASSOCIATED CONTENT

Supporting Information

The Supporting Information is available free of charge at https://pubs.acs.org/doi/10.1021/acs.jpca.3c08455.

OPV self-energy analysis (XLSX)

■ AUTHOR INFORMATION

Corresponding Author

J. V. Ortiz − *Department of Chemistry and Biochemistry, Auburn University, Auburn, Alabama 36849-5312, United States;* orcid.org/0000-0002-9277-0226; Email: ortiz@auburn.edu

Authors

Ernest Opoku − *Department of Chemistry and Biochemistry, Auburn University, Auburn, Alabama 36849-5312, United States;* orcid.org/0000-0002-4271-6838

Filip Pawłowski − *Department of Chemistry and Biochemistry, Auburn University, Auburn, Alabama 36849-5312, United States*

Complete contact information is available at: https://pubs.acs.org/10.1021/acs.jpca.3c08455

Notes

The authors declare no competing financial interest.

Biographies



Ernest Opoku received his B.Sc. (Honors) and M.Phil. degrees from the Kwame Nkrumah University of Science and Technology, Kumasi, Ghana under the supervision of Professor Richard Tia. Currently, he

https://doi.org/10.1021/acs.jpca.3c08455
J. Phys. Chem. A 2024, 128, 1399−1416

is a Ph.D. candidate in the quantum chemistry group of Professor J. V. Ortiz at Auburn University. His graduate research is focused on development and applications of new-generation electron and polarization propagator methods for electron binding and excitation energies. He established the Nesvard Institute of Molecular Sciences in Ghana with the aim of providing a platform for effective mentorship and collaborations to build the scientific capacity of diverse African talents.



Filip Pawłowski received his MSc in Chemistry from the Nicolas Copernicus University in Torun, Poland and his PhD in Theoretical Chemistry from Aarhus University, Denmark (under the supervision of Professor Poul Jørgensen). After working as a Postdoctoral Fellow with Professor Trygve Helgaker at the University of Oslo, Norway and, subsequently, holding several academic positions in Poland and Denmark, he joined Auburn University in 2017, where he was working in the group of Professor J.V. Ortiz as an Assistant Research Professor. In 2023, he transitioned to an independent Assistant Research Professor position at Auburn University. His main research interests include novel approaches to coupled cluster and perturbation theories (which resulted in a recent formulation of novel model–cluster perturbation theory), response function theory development (he developed and programmed CC3 response functions and recently provided a new formulation of response theory) and applications to nonlinear optics, development of electron propagator theory, and applications of accurate quantum chemistry to systems of experimental interest.



J. V. Ortiz attended public schools in Plainview, New York, received the B.S. and Ph.D. degrees from the University of Florida, was a postdoctoral fellow at Harvard University and Cornell University, advanced from Assistant Professor to Professor at the University of New Mexico, attained the rank of University Distinguished Professor at Kansas State University, became the first Ruth W. Molette Professor at Auburn University in 2006, and served until 2014 as Chairman of Chemistry and Biochemistry. In 2023, he became Molette Professor Emeritus and accepted the title of Courtesy Professor at his *alma mater*. Professor Ortiz continues to derive, program, and interpret *ab initio* propagator methods in quantum chemistry and to calculate electron binding energies and Dyson orbitals of double Rydberg anions, solvated electron precursors, diffusely bound negative ions, superhalogens, superalkalis, fullerenes, and nucleotides.

■ ACKNOWLEDGMENTS

The authors thank Dr. Manuel Díaz Tinoco for valuable discussions and the Alabama Supercomputer Center for computing resources.

■ REFERENCES

(1) Linderberg, J.; Öhrn, Y. *Propagators in Quantum Chemistry,* 2nd ed.; Wiley-Interscience: Hoboken NJ, 2004.
(2) Jørgensen, P.; Simons, J. *Second Quantization-Based Methods in Quantum Chemistry;* Academic Press: New York, 1981.
(3) Schirmer, J. *Many-Body Methods for Atoms, Molecules and Clusters;* Springer International Publishing AG, 2018.
(4) von Niessen, W.; Schirmer, J.; Cederbaum, L. S. Computational methods for the one-particle Green's function. *Comput. Phys. Rep.* **1984**, *1*, 57–125.
(5) Ortiz, J. V. Electron propagator theory: an approach to prediction and interpretation in quantum chemistry. *Wiley Interdisciplinary Reviews: Computational Molecular Science* **2013**, *3*, 123–142.
(6) Ortiz, J. V. Interpreting Bonding and Spectra With Correlated, One-Electron Concepts From Electron Propagator Theory. In *Annual Reports in Computational Chemistry*, Dixon, D. A., Ed.; Elsevier, 2017; Vol. *13*, pp 139–182. DOI: 10.1016/bs.arcc.2017.06.002
(7) Corzo, H. H.; Ortiz, J. V. Electron Propagator Theory: Foundations and Predictions. In *Advances in Quantum Chemistry;* Sabin, J. R., Brändas, E. J., Eds.; Academic Press, 2017; Vol. *74*, pp 267–298. DOI: 10.1016/bs.aiq.2016.05.001
(8) Ortiz, J. V. Recent progress in electron-propagator, extended-Koopmans-theorem and self-consistent-field approaches to the interpretation and prediction of electron binding energies. In *Advances in Quantum Chemistry;* Academic Press, 2022; Vol. *85*, pp 109–155. DOI: 10.1016/bs.aiq.2022.03.004
(9) Ortiz, J. V. Dyson-orbital concepts for description of electrons in molecules. *J. Chem. Phys.* **2020**, *153*, No. 070902.
(10) Díaz-Tinoco, M.; Pawłowski, F.; Ortiz, J. V. Dyson orbitals and chemical bonding. In *Chemical Reactivity;* Savas Kaya, L. v. S., Serdaroglu, G., Guo, L., Eds.; Elsevier: Amsterdam, Netherlands, 2023; Vol. *1*; p 606.
(11) Cederbaum, L. S.; Hohlneicher, G.; Peyerimhoff, S. Calculation of the vertical ionization potentials of formaldehyde by means of perturbation theory. *Chem. Phys. Lett.* **1971**, *11*, 421–424.
(12) Purvis, G. D.; Öhrn, Y. Atomic and molecular electronic spectra and properties from the electron propagator. *J. Chem. Phys.* **1974**, *60*, 4063–4069.
(13) Simons, J.; Smith, W. D. Theory of electron affinities of small molecules. *J. Chem. Phys.* **1973**, *58*, 4899–4907.
(14) Koopmans, T. Über die Zuordnung von Wellenfunktionen und Eigenwerten zu den Einzelnen Elektronen Eines Atoms. *Physica* **1934**, *1*, 104–113.
(15) Møller, C.; Plesset, M. S. Note on an Approximation Treatment for Many-Electron Systems. *Phys. Rev.* **1934**, *46*, 618–622.
(16) Ortiz, J. V. The electron propagator picture of molecular electronic structure. *Comput. Chem. (Singapore)* **1997**, *2*, 1–61.
(17) Ortiz, J. V. Partial third-order quasiparticle theory: Comparisons for closed-shell ionization energies and an application to the Borazine photoelectron spectrum. *J. Chem. Phys.* **1996**, *104*, 7599–7605.

https://doi.org/10.1021/acs.jpca.3c08455
J. Phys. Chem. A 2024, 128, 1399–1416

(18) Ortiz, J. V. An efficient, renormalized self-energy for calculating the electron binding energies of closed-shell molecules and anions. *Int. J. Quantum Chem.* **2005**, *105*, 803−808.
(19) Corzo, H. H.; Galano, A.; Dolgounitcheva, O.; Zakrzewski, V. G.; Ortiz, J. V. NR2 and P3+: Accurate, Efficient Electron-Propagator Methods for Calculating Valence, Vertical Ionization Energies of Closed-Shell Molecules. *J. Phys. Chem. A* **2015**, *119*, 8813−8821.
(20) Díaz-Tinoco, M.; Corzo, H. H.; Ortiz, J. V. Electron Propagator Methods for Vertical Electron Detachment Energies of Anions: Benchmarks and Case Studies. *J. Chem. Theory Comput.* **2018**, *14*, 5881−5895.
(21) Zakrzewski, V. G.; Dolgounitcheva, O.; Zakjevskii, A. V.; Ortiz, J. V. Ab initio electron propagator methods: applications to fullerenes and nucleic acid fragments. *Annu. Rep. Comput. Chem.* **2010**, *6*, 79−94.
(22) Zakrzewski, V. G.; Dolgounitcheva, O.; Zakjevskii, A. V.; Ortiz, J. V. Ab initio electron propagator calculations on electron detachment energies of fullerenes, macrocyclic molecules, and nucleotide fragments. *Adv. Quantum Chem.* **2011**, *62*, 105−136.
(23) Opoku, E.; Pawłowski, F.; Ortiz, J. V. Electron Propagator Theory of Vertical Electron Detachment Energies of Anions: Benchmarks and Applications to Nucleotides. *J. Phys. Chem. A* **2023**, *127*, 1085−1101.
(24) Kishimoto, N.; Kimura, M.; Ohno, K. Two-Dimensional Penning Ionization Electron Spectroscopy of Open-Shell Metallocenes: Outer Valence Ionic States of Vanadocene and Nickelocene. *J. Phys. Chem. A* **2013**, *117*, 3025−3033.
(25) Baker, J.; Pickup, B. T. A method for molecular ionization potentials. *Chem. Phys. Lett.* **1980**, *76*, 537−541.
(26) Schirmer, J.; Cederbaum, L. S. The two-particle-hole Tamm-Dancoff approximation (2ph-TDA) equations for closed-shell atoms and molecules. *J. Phys. B* **1978**, *11*, 1889−1900.
(27) Schirmer, J.; Cederbaum, L. S.; Walter, O. New approach to the one-particle Green's function for finite Fermi systems. *Phys. Rev. A* **1983**, *28*, 1237−1259.
(28) Cederbaum, L. S.; Domcke, W.; Schirmer, J.; Von Niessen, W. Correlation effects in the ionization of molecules: breakdown of the molecular orbital picture. *Adv. Chem. Phys.* **1986**, *65*, 115−159.
(29) Angonoa, G.; Walter, O.; Schirmer, J. Theoretical K-shell ionization spectra of N_2 and CO by a fourth-order Green's function method. *J. Chem. Phys.* **1987**, *87*, 6789−6801.
(30) Ortiz, J. V. A nondiagonal, renormalized extension of partial third-order quasiparticle theory: comparisons for closed-shell ionization energies. *J. Chem. Phys.* **1998**, *108*, 1008−1014.
(31) Ortiz, J. V. Orbital and shakeup operator renormalizations in electron propagator theory. *J. Chem. Phys.* **1998**, *109*, 5741−5746.
(32) Ortiz, J. V. Second-order shakeup terms in electron propagator calculations on F_2 and H_2O_2. *Int. J. Quantum Chem.* **1998**, *69*, 175−182.
(33) Ortiz, J. V. Electron detachment energies of closed-shell anions calculated with a renormalized electron propagator. *Chem. Phys. Lett.* **1998**, *296*, 494−498.
(34) Ortiz, J. V. Single-reference electron propagator calculations on vertical ionization energies of ozone. *Chem. Phys. Lett.* **1998**, *297*, 193−199.
(35) Ortiz, J. V. Approximate Brueckner orbitals and shakeup operators in electron propagator calculations: applications to F- and OH. *Int. J. Quantum Chem.* **1998**, *70*, 651−658.
(36) Opoku, E.; Pawłowski, F.; Ortiz, J. V. A new generation of diagonal self-energies for the calculation of electron removal energies. *J. Chem. Phys.* **2021**, *155*, 204107.
(37) Opoku, E.; Pawłowski, F.; Ortiz, J. V. Electron Propagator Self-Energies versus Improved GW100 Vertical Ionization Energies. *J. Chem. Theory Comput.* **2022**, *18*, 4927−4944.
(38) Opoku, E.; Pawłowski, F.; Ortiz, J. V. A new generation of non-diagonal, renormalized self-energies for calculation of electron removal energies. *J. Chem. Phys.* **2023**, *159*, 124109.
(39) Reining, L. The GW approximation: content, successes and limitations. *Wiley Interdiscip. Rev.: Comput. Mol. Sci.* **2018**, *8*, e1344.
(40) Knight, J. W.; Wang, X.; Gallandi, L.; Dolgounitcheva, O.; Ren, X.; Ortiz, J. V.; Rinke, P.; Körzdörfer, T.; Marom, N. Accurate Ionization Potentials and Electron Affinities of Acceptor Molecules III: A Benchmark of GW Methods. *J. Chem. Theory Comput.* **2016**, *12*, 615−626.
(41) Opoku, E.; Pawłowski, F.; Ortiz, J. V. Erratum: "A new generation of diagonal self-energies for the calculation of electron removal energies". *J. Chem. Phys.* **2023**, *159*, No. 069901.
(42) Opoku, E.; Pawłowski, F.; Ortiz, J. V. Correction to "Electron-Propagator Self-Energies versus Improved GW100 Vertical Ionization Energies". *J. Chem. Theory Comput.* **2023**, *19*, 5648−5648.
(43) Manne, R.; Åberg, T. Koopmans' theorem for inner-shell ionization. *Chem. Phys. Lett.* **1970**, *7*, 282−284.
(44) Thouless, D. J. *The Quantum Mechanics of Many-Body Systems;* Academic Press: New York, 1961.
(45) Pickup, B. T.; Goscinski, O. Direct calculation of ionization energies. I. Closed shells. *Mol. Phys.* **1973**, *26*, 1013−1035.
(46) Hirata, S.; Hermes, M. R.; Simons, J.; Ortiz, J. V. General-Order Many-Body Green's Function Method. *J. Chem. Theory Comput.* **2015**, *11*, 1595−1606.
(47) Hirata, S.; Doran, A. E.; Knowles, P. J.; Ortiz, J. V. One-particle many-body Green's function theory: Algebraic recursive definitions, linked-diagram theorem, irreducible-diagram theorem, and general-order algorithms. *J. Chem. Phys.* **2017**, *147*, No. 044108.
(48) Hu, C.-H.; Chong, D. P.; Casida, M. E. The parametrized second-order Green function times screened interaction (pGW2) approximation for calculation of outer valence ionization potentials. *J. Electron Spectrosc. Relat. Phenom.* **1997**, *85*, 39−46.
(49) Lim, F.-H.; Nishida, M.; Hori, Y.; Ida, T.; Mizuno, M. Optimization of the spin-component-scaled factor for electron propagator method. *Chem. Phys. Lett.* **2017**, *678*, 159−166.
(50) Romero, J.; Charry, J. A.; Nakai, H.; Reyes, A. Improving quasiparticle second order electron propagator calculations with the spin-component-scaled technique. *Chem. Phys. Lett.* **2014**, *591*, 82−87.
(51) Śmiga, S.; Grabowski, I. Spin-Component-Scaled ΔMP2 Parametrization: Toward a Simple and Reliable Method for Ionization Energies. *J. Chem. Theory Comput.* **2018**, *14*, 4780−4790.
(52) Stanton, J. F.; Bartlett, R. J. The equation of motion coupled-cluster method. A systematic biorthogonal approach to molecular excitation energies, transition probabilities, and excited state properties. *J. Chem. Phys.* **1993**, *98*, 7029−7039.
(53) Bartlett, R. J. Coupled-cluster theory and its equation-of-motion extensions. *WIREs Computational Molecular Science* **2012**, *2*, 126−138.
(54) Dunning, T. H. Gaussian basis sets for use in correlated molecular calculations. I. The atoms boron through neon and hydrogen. *J. Chem. Phys.* **1989**, *90*, 1007−1023.
(55) Ranasinghe, D. S.; Margraf, J. T.; Perera, A.; Bartlett, R. J. Vertical valence ionization potential benchmarks from equation-of-motion coupled cluster theory and QTP functionals. *J. Chem. Phys.* **2019**, *150*, No. 074108.
(56) Raghavachari, K.; Trucks, G. W.; Pople, J. A.; Head-Gordon, M. A fifth-order perturbation comparison of electron correlation theories. *Chem. Phys. Lett.* **1989**, *157*, 479−483.
(57) Weigend, F.; Ahlrichs, R. Balanced basis sets of split valence, triple zeta valence and quadruple zeta valence quality for H to Rn: Design and assessment of accuracy. *Phys. Chem. Chem. Phys.* **2005**, *7*, 3297−3305.
(58) Kendall, R. A.; Dunning, T. H.; Harrison, R. J. Electron affinities of the first-row atoms revisited. Systematic basis sets and wave functions. *J. Chem. Phys.* **1992**, *96*, 6796−6806.
(59) Opoku, E.; Pawłowski, F.; Ortiz, J. V. New-Generation Electron-Propagator Methods for Calculations of Electron Affinities and Ionization Energies: Tests on Organic Photovoltaic Molecules. *J. Chem. Theory Comput.* **2024**, *20*, 290−306.
(60) Flores-Moreno, R.; Ortiz, J. V. Integral approximations in ab initio, electron propagator calculations. *J. Chem. Phys.* **2009**, *131*, 124110.

https://doi.org/10.1021/acs.jpca.3c08455
J. Phys. Chem. A 2024, 128, 1399−1416

(61) Flores-Moreno, R.; Ortiz, J. V. Efficient and Accurate Electron Propagator Methods and Algorithms. In *Practical Aspects of Computational Chemistry: Methods, Concepts and Applications;* Leszczynski, J., Shukla, M. K., Eds.; Springer: Dordrecht, Netherlands, 2010; pp 1−17.
(62) Vysotskiy, V. P.; Cederbaum, L. S. On the Cholesky decomposition for electron propagator methods: General aspects and application on C60. *J. Chem. Phys.* **2010**, *132*, No. 044110.
(63) Goscinski, O.; Lukman, B. Moment-conserving decoupling of Green functions via Pade approximants. *Chem. Phys. Lett.* **1970**, *7*, 573−576.
(64) Rowe, D. J. Equations-of-Motion Method and the Extended Shell Model. *Rev. Mod. Phys.* **1968**, *40*, 153−166.
(65) Nehrkorn, C.; Purvis, G. D.; Öhrn, Y. Hermiticity of the superoperator Hamiltonian in propagator theory. *J. Chem. Phys.* **1976**, *64*, 1752−1756.
(66) Ortiz, J. V. Contour integrals in electron propagator theory. *Int. J. Quantum Chem.* **1995**, *56*, 331−337.
(67) Cederbaum, L. S. One-body Green's function for atoms and molecules. Theory and application. *J. Phys. B* **1975**, *8*, 290−303.
(68) Ortiz, J. V. The Electron Propagator Picture of Molecular Electronic Structure. In *Computational Chemistry: Reviews of Current Trends;* Leszczynski, J., Ed.; World Scientific: Singapore, 1997; Vol. 2, pp 1−61.
(69) Zakrzewski, V. G.; Ortiz, J. V.; Nichols, J. A.; Heryadi, D.; Yeager, D. L.; Golab, J. T. Comparison of perturbative and multiconfigurational electron propagator methods. *Int. J. Quantum Chem.* **1996**, *60*, 29−36.
(70) Ortiz, J. V. An efficient, renormalized self-energy for calculating the electron binding energies of closed-shell molecules and anions. *Int. J. Quantum Chem.* **2005**, *105*, 803−808.
(71) Díaz-Tinoco, M.; Dolgounitcheva, O.; Zakrzewski, V. G.; Ortiz, J. V. Composite electron propagator methods for calculating ionization energies. *J. Chem. Phys.* **2016**, *144*, 224110.
(72) Yang, X.; Wang, X.-B.; Vorpagel, E. R.; Wang, L.-S. Direct experimental observation of the low ionization potentials of guanine in free oligonucleotides by using photoelectron spectroscopy. *Proc. Natl. Acad. Sci. U. S. A.* **2004**, *101*, 17588−17592.
(73) Richard, R. M.; Marshall, M. S.; Dolgounitcheva, O.; Ortiz, J. V.; Brédas, J.-L.; Marom, N.; Sherrill, C. D. Accurate Ionization Potentials and Electron Affinities of Acceptor Molecules I. Reference Data at the CCSD(T) Complete Basis Set Limit. *J. Chem. Theory Comput.* **2016**, *12*, 595−604.
(74) Bintrim, S. J.; Berkelbach, T. C. Full-frequency GW without frequency. *J. Chem. Phys.* **2021**, *154*, No. 041101.
(75) Stanton, J. F.; Gauss, J. Analytic energy derivatives for ionized states described by the equation-of-motion coupled cluster method. *J. Chem. Phys.* **1994**, *101*, 8938−8944.

https://doi.org/10.1021/acs.jpca.3c08455
J. Phys. Chem. A 2024, 128, 1399−1416

Appendix B

E. Opoku, F. Pawłowski and J. V. Ortiz, "A New Generation of Diagonal Self−Energies for the Calculation of Electron Removal Energies", *J. Chem. Phys.*, 155, 204107 (2021)

The Journal of Chemical Physics ARTICLE scitation.org/journal/jcp

A new generation of diagonal self-energies for the calculation of electron removal energies

Cite as: J. Chem. Phys. 155, 204107 (2021); doi: 10.1063/5.0070849
Submitted: 9 September 2021 • Accepted: 7 November 2021 •
Published Online: 29 November 2021

View Online Export Citation CrossMark

Ernest Opoku, Filip Pawłowski, and J. V. Ortiz[a]

AFFILIATIONS

Department of Chemistry and Biochemistry, Auburn University, Auburn, Alabama 36849-5312, USA

[a]Author to whom correspondence should be addressed: ortiz@auburn.edu

ABSTRACT

A new generation of diagonal self-energy approximations in *ab initio* electron propagator theory for the calculation of electron removal energies of molecules and molecular ions has been derived from an intermediately normalized, Hermitized super-operator metric. These methods and widely used antecedents such as the outer valence Green's function and the approximately renormalized partial third order method are tested with respect to a dataset of vertical ionization energies generated with a valence, triple-ζ, correlation-consistent basis set and a converged series of many-body calculations whose accuracy approaches that of full configuration interaction. Several modifications of the diagonal second-order self-energy, a version of G_0W_0 theory based on Tamm–Dancoff excitations and several non-diagonal self-energies are also included in the tests. All new methods employ canonical Hartree–Fock orbitals. No adjustable or empirical parameters appear. A hierarchy of methods with optimal accuracy for a given level of computational efficiency is established. Several widely used diagonal self-energy methods are rendered obsolete by the new hierarchy whose members, in order of increasing accuracy, are (1) the opposite-spin non-Dyson diagonal second-order or os-nD-D2, (2) the approximately renormalized third-order quasiparticle or Q3+, (3) the renormalized third-order quasiparticle or RQ3, (4) the approximately renormalized linear third-order or L3+, and (5) the renormalized linear third-order or RL3 self-energies.

Published under an exclusive license by AIP Publishing. https://doi.org/10.1063/5.0070849

INTRODUCTION

Experiments that measure electron binding energies and associated transition probabilities often require interpretations based on *ab initio* electronic structure calculations. Confidence in these interpretations rises with the *accuracy* of the predicted data and with the *clarity* of the concepts that inform algorithms. *Ab initio* electron propagator[1–3] calculations that employ diagonal self-energies in a Hartree–Fock (HF) orbital basis certainly satisfy the latter criterion, for they produce Dyson orbitals[4] (DOs) that equal the product of the square root of a probability (i.e., intensity) factor times a canonical orbital.[5–8] In effect, the simplified DO is subjected to a relaxation–correlation potential embodied in the self-energy matrix that corrects the inaccuracy of the uncorrelated frozen-orbital approximation based on Koopmans's identity.[9] Neglect of the off-diagonal elements of the self-energy operator is usually an excellent approximation for outer-valence ionization energies (IEs) of closed-shell molecules and molecular ions and reduces arithmetic bottlenecks by at least a factor proportional to system size.[10] These conceptual and computational advantages are responsible for the widespread use of diagonal-self-energy methods of *ab initio* electron propagator theory (EPT) for the interpretation of photoelectron and electron-scattering spectra.[11–13] Diagonal self-energies are also assumed in G_0W_0 calculations that usually employ a Kohn–Sham (KS) orbital basis, although there is typically no computational impediment to choosing canonical HF orbitals instead.[14–16] Systematic comparisons of outer valence Green's function[12,13,17] (OVGF) and approximately renormalized partial third order[18–23] (P3+) EPT calculations with their G_0W_0 counterparts based on a variety of KS orbitals have found them to have similar accuracy and computational efficiency for IEs of organic acceptor molecules.[24]

Can a new generation of diagonal self-energy (or quasiparticle) approximations that retain the conceptual and computational advantages of their antecedents in EPT achieve a higher level of accuracy? All candidates considered presently require only diagonal elements of the self-energy matrix in a canonical HF basis. Arithmetic bottlenecks that exceed those of the four-index

electron-repulsion-integral transformation are avoided: the new methods' matrix multiplications have fifth or lower-power arithmetic scaling with respect to system size. No additional intermediate matrices with more than three orbital indices are generated. The new methods therefore remain as feasible as their OVGF or P3+ predecessors. Finally, no empirical or adjustable parameters are tolerated in the design of the self-energy operator or in the generation of molecular orbitals from basis functions. Methods with these characteristics are most likely to remain at least as useful as OVGF and P3+ in interpreting experiments on species with *unprecedented* patterns of chemical bonding and electronic structure. They may also be employed in the efficient generation of datasets, especially when experiments prove too expensive or technically difficult to perform.

One of the chief differences between quasiparticle EPT methods and those of the G_0W_0 family is the treatment of renormalization (infinite-order summations of selected classes of self-energy terms or diagrams). The former methods require the evaluation of diagrams of the second and third order only and perform computationally trivial estimates of higher-order effects by examining ratios of terms.[12,20] Thus, the typical underestimates of diagonal second-order (D2) and overestimates of diagonal third-order (D3) IEs that persist with basis-set saturation are systematically mitigated in an unbiased manner.[22–24] In the case of OVGF, three of these renormalization procedures have been defined, but P3+ has only a single version. An algorithm for choosing among the OVGF alternatives has been implemented and widely applied.[13,25,26] The latter procedure contains parameters and therefore is excluded from further consideration. All members of the G_0W_0 set of methods incorporate infinite-order summations of ring diagrams; in most cases, they neglect exchange in the two-electron vertices.[27] Renormalizations that include rings with exchange and ladder terms occur in the post-second-order non-diagonal self-energies of the 1970s and 1980s.[12,28] The new set of EPT methods spans both approaches. In some cases, only second-order and third-order diagrams are summed, whereas in others, explicit evaluation of higher-order terms is undertaken. The latter approach generally requires more matrix multiplications, but in no case is a fifth-power arithmetic bottleneck exceeded. Included in this set of explicitly renormalized self-energies is a version of G_0W_0 that employs HF orbitals and excitation energies and amplitudes at the Tamm–Dancoff[29,30] (single excitation) level. This member of the G_0W_0 family is a straightforward simplification of a well-known, non-diagonal EPT method, the two-particle-one-hole Tamm–Dancoff approximation (2ph-TDA),[31] that has recently been examined computationally[32] and will be denoted by HF-TDA G_0W_0.

Quasiparticle methods that involve no third-order or higher-order terms have cubic arithmetic scaling and therefore are practically free once an integral transformation has been performed. The usual D2 method, whose underestimates of vertical IEs (VIEs) are gradually reduced with improvements in basis sets, nonetheless converges to predictions that differ from experiment by 0.5 eV on the average.[22,23] A non-Dyson version[33] of this method that procures a small advantage by making its arithmetic bottleneck non-iterative instead of iterative is examined. The elimination of the same-spin terms in Dyson and non-Dyson second-order methods is also considered. (The D2 method has been modified with adjustable parameters in recent publications that follow the example of parameterized versions of second-order perturbation theory for total energies;[34–37] this kind of approach is avoided herein.)

Final states where the Koopmans description of an IE is qualitatively valid are the sole concern of this work. Searches for correlation (e.g., shake-up) states are not conducted. In fact, when probability factors (norms of DOs) are calculated to be lower than 0.85, quasiparticle calculations become suspect. More flexible methods with renormalized non-diagonal self-energies that treat simple and shake-up ionization operators on an equal basis are needed for such cases. In addition, DOs of correlation states may have large contributions from more than one canonical HF orbital. Fortunately, algorithms for finding the poles (electron binding energies) of the new approximate electron propagators require no diagonalizations and only a small number (usually three) of energy iterations (typically using Newton's method for finding the roots of a function of a single variable) to achieve convergence within 0.01 eV. In most G_0W_0 calculations, only one Newton iteration is performed at the value of the reference orbital energy. (Ring renormalizations still require iterations.) Most OVGF and P3+ calculations do the same at the value of a D3 or partial third-order (P3) pole.

To judge the quality of the new methods, standard values of VIEs are needed, but these data are notoriously hard to infer from experiments. Relaxation of nuclear positions from initial to final states and the spacing of vibrational levels complicate efforts to employ peaks or other features that occur in spectra. Relatively high-level *ab initio* results, such as those of coupled-cluster theory with single, double, and perturbative triple substitution operators, or CCSD(T),[38] may be pressed into service through a protocol of basis-set extrapolations and additivity schemes.[39] Error bars of 0.1 eV or greater are inevitably introduced with this choice of standard. A less ambiguous option is provided by full configuration interaction (FCI) calculations in a fixed basis. These results tend to be confined to just one state per irreducible representation for very small molecules. A better alternative is provided by calculations in a fixed basis in which a well-defined progression of approximate methods is demonstrably converged toward the FCI limit. Such a base of data was created recently wherein valence VIEs were calculated with a sequence of equation-of-motion coupled-cluster methods[40] for ionization potentials (IPs) such that the last two levels of theory, with full triple (IP-EOM-CCSDT) and full quadruple (IP-EOM-CCSDTQ) operators in the reference state, were in very close (mean absolute deviation = 0.03 eV) agreement.[41] These VIEs equal the difference between a coupled-cluster reference-state total energy and a total energy of a final state obtained by diagonalizing the non-Hermitian Jacobian with elements $\langle \mathrm{HF}|\tau_i^\dagger[e^{-T}He^T, \tau_j]|\mathrm{HF}\rangle$ in a space of operators, τ_i, of reduced rank compared to T. (For example, IP-EOM-CCSD VIEs[42] employ the space of h and 2hp ionization operators.) The latter methods, therefore, are acceptable substitutes for FCI in a cc-pVTZ[43] basis. The computational bottleneck occurs in the reference-state calculation of T.

The theory that underlies old and new diagonal self-energy formulas is presented in the sections entitled Electron Propagator Theory and Self-Energy Approximations, wherein a uniform notation for all these methods is introduced. A crucial improvement is realized through the choice of an intermediately normalized, Hermitian super-operator metric that leads to the identification of

Published under an exclusive license by AIP Publishing

third-order terms in the self-energy matrix. Numerical tests and a statistical analysis of results are followed by a discussion of the strengths and weaknesses of each method. Recommendations for routine use conclude this paper.

ELECTRON PROPAGATOR THEORY

In an orthonormal spin-orbital basis, u, with general indices p and q, the electron propagator matrix has the following elements:

$$\langle\langle a_p(t); a_q^\dagger(t')\rangle\rangle = -i\Theta(t-t')\langle\Psi_0^N|a_p(t)a_q^\dagger(t')|\Psi_0^N\rangle + i\Theta(t'-t)\langle\Psi_0^N|a_q^\dagger(t')a_p(t)|\Psi_0^N\rangle, \quad (1)$$

defined in terms of the Heaviside step function (Θ) and the N-electron reference eigenstate, $\Psi_0{}^N$. This element's Fourier transform in its spectral form,

$$\langle\langle a_p; a_q^\dagger\rangle\rangle_E = \lim_{\eta\to 0^+}\left[\sum_R \frac{\langle\Psi_0^N|a_p|R\rangle\langle R|a_q^\dagger|\Psi_0^N\rangle}{E+E_0(N)-E_R(N+1)+i\eta} + \sum_S \frac{\langle\Psi_0^N|a_q^\dagger|S\rangle\langle S|a_p|\Psi_0^N\rangle}{E-E_0(N)+E_S(N-1)-i\eta}\right], \quad (2)$$

involves summations over final eigenstates with N + 1 or N − 1 electrons. Poles in the R and S summations correspond, respectively, to energies of electron attachment and detachment. Residues (numerators) are expressed in terms of Feynman–Dyson amplitudes,

$$f_p^R = \langle\Psi_0^N|a_p|R\rangle, \quad (3)$$

$$g_p^S = \langle S|a_p|\Psi_0^N\rangle, \quad (4)$$

which suffice to construct Dyson spin-orbitals of attachment and detachment according to

$$\varphi_R^{Dyson}(x_1) = \sqrt{N+1}\int \Psi_0^{N^*}(x_2,x_3,x_4,\ldots,x_{N+1}) \times \Psi_R(x_1,x_2,x_3,\ldots,x_{N+1})dx_2dx_3dx_4\cdots dx_{N+1} = \sum_R f_p^R u_p(x_1), \quad (5)$$

$$\varphi_S^{Dyson}(x_1) = \sqrt{N}\int \Psi_S^*(x_2,x_3,x_4,\ldots,x_N) \times \Psi_0^N(x_1,x_2,x_3,\ldots,x_N)dx_2dx_3dx_4\cdots dx_N = \sum_S g_p^S u_p(x_1). \quad (6)$$

The plus sign between the attachment and detachment summations is reflected in the definition of a super-operator metric,

$$[X|Y] = \langle\Psi_0^N|X^\dagger Y + YX^\dagger|\Psi_0^N\rangle, \quad (7)$$

wherein X and Y are members of a set of second-quantized-operator products (w) in which the number of creators exceeds the number of annihilators by one, e.g., $a_p{}^\dagger$ (h and p), $a_p{}^\dagger a_q{}^\dagger a_r$ (2hp and 2ph), and $a_p{}^\dagger a_q{}^\dagger a_r{}^\dagger a_s a_t$ (3h2p and 3p2h).[44] Definitions of identity and Hamiltonian super-operators,

$$\hat{I}X = X, \quad (8)$$

$$\hat{H}X = HX - XH, \quad (9)$$

precede the expression of electron-propagator matrix elements as

$$\langle\langle a_p; a_q^\dagger\rangle\rangle_E = G_{pq}(E) = \left[a_p^\dagger\middle|\left(E\hat{I}-\hat{H}\right)^{-1}a_q^\dagger\right]. \quad (10)$$

The resolvent super-operator in the electron propagator matrix,

$$\mathbf{G}(E) = \left[\mathbf{a}^\dagger\middle|\left(E\hat{I}-\hat{H}\right)^{-1}\mathbf{a}^\dagger\right], \quad (11)$$

may be circumvented by introducing an inner projection[45] with w operators according to

$$\mathbf{G}(E) = \left[\mathbf{a}^\dagger\middle|\mathbf{w}\right]\left[\mathbf{w}\middle|\left(E\hat{I}-\hat{H}\right)\mathbf{w}\right]^{-1}\left[\mathbf{w}\middle|\mathbf{a}^\dagger\right]. \quad (12)$$

By partitioning the w manifold into a set of simple normalized field operators and an orthogonalized complement, $\boldsymbol{f}$, such that $[\boldsymbol{a}^\dagger|\boldsymbol{f}] = \mathbf{0}$, one may obtain the inverse form of the Dyson equation where

$$\mathbf{G}^{-1}(E) = \left[\mathbf{a}^\dagger\middle|\left(E\hat{I}-\hat{H}\right)\mathbf{a}^\dagger\right] - \left[\mathbf{a}^\dagger\middle|\hat{H}\mathbf{f}\right]\left[\mathbf{f}\middle|\left(E\hat{I}-\hat{H}\right)\mathbf{f}\right]^{-1}\left[\mathbf{f}\middle|\hat{H}\mathbf{a}^\dagger\right]. \quad (13)$$

A more familiar form of the inverse Dyson equation may be rederived by recognizing that

$$\left[a_p^\dagger\middle|\hat{H}a_q^\dagger\right] = h_{pq}^{(1)} + \sum_{rs}\langle pr\|qs\rangle\rho_{rs} = F_{pq}, \quad (14)$$

where ρ is the one-electron reduced-density matrix of the reference state and $\boldsymbol{F}$ is a generalized Fock matrix with the customary one-electron ($h^{(1)}$) and anti-symmetrized two-electron (Dirac notation) matrix elements. In a spin-orbital basis that diagonalizes a one-electron operator $h^{(1)}+v$ with eigenvalues e^v, one may define a reference inverse electron-propagator matrix according to

$$\mathbf{G}_0^{-1}(E) = E\mathbf{1} - \mathbf{e}^v, \quad (15)$$

which has vanishing off-diagonal elements. The inverse Dyson equation then reads

$$\mathbf{G}^{-1}(E) = \mathbf{G}_0^{-1}(E) - \boldsymbol{\Sigma}(E), \quad (16)$$

where the self-energy matrix, $\Sigma(E)$, contains constant (i.e., energy-independent) and energy-dependent terms according to

$$\boldsymbol{\Sigma}(E) = \mathbf{F} - \mathbf{h}^{(1)} - \mathbf{v} + \left[\mathbf{a}^\dagger|\hat{H}\mathbf{f}\right]\left[\mathbf{f}|\left(E\hat{I}-\hat{H}\right)\mathbf{f}\right]^{-1}\left[\mathbf{f}|\hat{H}\mathbf{a}^\dagger\right]. \quad (17)$$

When v is the Coulomb-exchange potential of a HF self-consistent field,

$$\boldsymbol{\Sigma}(E) = \boldsymbol{\Sigma}(\infty) + \left[\mathbf{a}^\dagger|\hat{H}\mathbf{f}\right]\left[\mathbf{f}|\left(E\hat{I}-\hat{H}\right)\mathbf{f}\right]^{-1}\left[\mathbf{f}|\hat{H}\mathbf{a}^\dagger\right], \quad (18)$$

where elements of the constant part of the self-energy matrix,

Published under an exclusive license by AIP Publishing

$$\Sigma_{pq}(\infty) = \sum_{rs}\langle pr\|qs\rangle\left(\rho_{rs} - \rho_{rs}^{HF}\right), \tag{19}$$

depend only on the correlation contributions to the one-electron density matrix. This uncorrelated choice of v propitiates analysis of results in terms of final-state-orbital relaxation and differential correlation effects that are confined to the self-energy matrix. In addition, the sum of the first three terms in Eq. (17) vanishes through the second order in the fluctuation potential and corresponds to the energy-independent terms of Eq. (19) in higher orders. Eigenfunctions obtained with alternative potentials that aim to capture exchange or correlation effects in ground-state calculations typically produce non-diagonal energy-independent first-order terms that involve the non-local HF exchange operator in Eq. (18).

For all choices of orbital bases, poles of $\boldsymbol{G}(E)$, or zeroes of $\boldsymbol{G}^{-1}(E)$, occur at energies (E_X) where the quasiparticle eigenvalue equation is satisfied,

$$[\mathbf{F} + \boldsymbol{\Sigma}(E_X)]\mathbf{C}(E_X) = E_X\mathbf{C}(E_X). \tag{20}$$

The probability factor (or pole strength), Π, equals the norm of the Dyson spin-orbital[4] and may be determined with

$$\Pi_X = \int |\varphi^{Dyson}(x)|^2 dx = \left(1 - \mathbf{C}^{\dagger}(E_X)\left[\frac{d\boldsymbol{\Sigma}(E)}{dE}\right]_{E=E_X}\mathbf{C}(E_X)\right)^{-1}. \tag{21}$$

Elements of the eigenvectors are related to Feynman–Dyson amplitudes and Dyson spin-orbitals via

$$\varphi_X^{Dyson}(x) = \Pi_X^{0.5}\sum_p C_p(E_X)u_p(x). \tag{22}$$

This work is chiefly concerned with methods that employ canonical HF spin-orbitals and that ignore off-diagonal elements of the self-energy matrix. For these methods, each canonical spin-orbital generates its own independent set of electron binding energies obtained iteratively with the *diagonal quasiparticle equation*,

$$e_p^{HF} + \Sigma_{pp}(E_{Xp}) = E_{Xp}, \tag{23}$$

where Koopmans results (e_p^{HF}) are corrected by diagonal elements of the self-energy matrix. Probability factors are given by

$$\Pi_{Xp} = \left[1 - \frac{d\Sigma_{pp}(E)}{dE}\bigg|_{E=E_{Xp}}\right]^{-1}, \tag{24}$$

and Dyson spin-orbitals are proportional to canonical Hartree–Fock spin-orbitals,

$$\varphi_{Xp}^{Dyson}(x) = \Pi_{Xp}^{0.5}u_p^{HF}(x). \tag{25}$$

For a given p, many values of E_{Xp} may be found in principle, but usually only those poles whose probability factors exceed 0.85 are of interest. The remaining electron binding energies may have some qualitative meaning but are likely to require improvements from renormalized non-diagonal self-energy approximations that are appropriate for correlation states.

SELF-ENERGY APPROXIMATIONS

The simplest self-energy corrections to canonical Hartree–Fock orbital energies occur in the second order in the Møller–Plesset fluctuation potential.[46] Choosing $|\Psi_0^N\rangle$ to be a HF wavefunction, restricting $\boldsymbol{f}$ to triple-field (2hp and 2ph) operator products and neglecting first-order couplings between the latter operators yield the non-diagonal second-order (ND2) self-energy,

$$\boldsymbol{\Sigma}^{(2)}(E) = \left[\mathbf{a}^{\dagger}|\hat{H}\mathbf{f}_3\right]_1\left[\mathbf{f}_3|\left(E\hat{I} - \hat{H}\right)\mathbf{f}_3\right]_0^{-1}\left[\mathbf{f}_3|\hat{H}\mathbf{a}^{\dagger}\right]_1. \tag{26}$$

The subscripts to the right of the brackets denote the highest order of the fluctuation potential that is retained in the corresponding matrix's elements. (Zeroth-order couplings between $\mathbf{f}_3$ and simple field operators vanish.) Diagonal second-order (D2) self-energy matrix elements read

$$\Sigma_{pp}^{D2}(E) = \frac{1}{2}\sum_a^{vir}\sum_{ij}^{occ}\frac{|\langle pa\|ij\rangle|^2}{E + e_a - e_i - e_j} + \frac{1}{2}\sum_i^{occ}\sum_{ab}^{vir}\frac{|\langle pi\|ab\rangle|^2}{E + e_i - e_a - e_b}. \tag{27}$$

Evaluation of the D2 self-energy at $E = \varepsilon_p$ produces the second-order Rayleigh–Schrödinger perturbation theory (RSPT2) result.[47–49] The same-spin and opposite-spin terms in both summations have been assigned empirically adjusted weights in several modified self-energies that retain the cubic arithmetic scaling of the D2 method.[34–37] To avoid the introduction of parameters adjusted with respect to a set of data, a simpler and interpretable alternative is considered presently: neglect of the same-spin terms. This opposite-spin second-order method is denoted by os-D2. The non-Dyson (nD) approach neglects the electron affinity (EA) term in the electron-propagator matrix [see Eq. (2)], has only one term in its super-operator metric [compared with Eq. (7)], and yields a diagonal second-order self-energy that is identical to D2 except that the second (2ph) term is energy-independent, with E set equal to ε_p for electron detachments.[33] (The roles of the 2hp and 2ph terms are reversed in EA calculations.) The nD-D2 and os-nD-D2 methods are based on these modifications. The non-Dyson methods procure a minor advantage: the usual OV^2 bottleneck (where O and V are dimensions of the occupied and virtual orbital spaces) is no longer energy-dependent and therefore requires no iterations. The real bottleneck, in practice, is the transformation of the electron repulsion integrals to the HF basis, which may be reduced from fifth to fourth power dependence for a given p in D2 calculations.

Restoration of the first-order couplings between the triple field-operators yields the 2ph-TDA[31] self-energy,

$$\boldsymbol{\Sigma}^{2ph-TDA}(E) = \left[\mathbf{a}^{\dagger}|\hat{H}\mathbf{f}_3\right]_1\left[\mathbf{f}_3|\left(E\hat{I} - \hat{H}\right)\mathbf{f}_3\right]_1^{-1}\left[\mathbf{f}_3|\hat{H}\mathbf{a}^{\dagger}\right]_1. \tag{28}$$

In the present case, no correlation corrections to the HF reference state are included. The inverted matrix suffices to generate ring and ladder terms of all orders with anti-symmetrized vertices.

Published under an exclusive license by AIP Publishing

This method provides a qualitatively correct account of primary and correlation states but has not been employed in the diagonal quasiparticle equation (23).

A member of the G_0W_0 family of methods that lies within the scope of the present study (see the second paragraph of the Introduction) may be defined by neglecting off-diagonal elements of the self-energy matrix, ladder and ring-exchange terms in the $[\boldsymbol{f}_3|(E\hat{I} - \hat{H})\boldsymbol{f}_3]_1$ matrix and exchange terms in the $[\boldsymbol{a}^\dagger|\hat{H}\boldsymbol{f}_3]_1$ and $[\boldsymbol{f}_3|\hat{H}\boldsymbol{a}^\dagger]_1$ matrices. Only electron repulsion integrals of the (single-bar) $\langle ab|ij\rangle$ type are needed in the couplings between $\mathbf{f}_3$ operators. Instead of the usual random-phase-approximation excitation energies and transition amplitudes of G_0W_0 practice, their Tamm–Dancoff-approximation (TDA) counterparts are inherent in this level of theory. The resulting HF-TDA G_0W_0 self-energy contains a subset of terms that occur in the 2ph-TDA self-energy.

All third-order contributions to the self-energy are retained in the 3+ self-energy, where

$$\boldsymbol{\Sigma}^{3+}(E) = \boldsymbol{\Sigma}_3(\infty) + \left[\mathbf{a}^\dagger|\hat{H}\mathbf{f}_3\right]_2\left[\mathbf{f}_3|\left(E\hat{I} - \hat{H}\right)\mathbf{f}_3\right]_1^{-1}\left[\mathbf{f}_3|\hat{H}\mathbf{a}^\dagger\right]_2. \quad (29)$$

Higher orders indicated in the subscripts may involve the first-order double and second-order single replacements with respect to $|\mathrm{HF}\rangle$ and $\langle\mathrm{HF}|$ in Eq. (7). Terms beyond the third order are again generated by the inverted matrix. This approximation is a member of the family of ADC(3) (third-order algebraic diagrammatic construction) methods.[28] Other members replace $\Sigma_3(\infty)$ with its fourth-order counterpart or with renormalized schemes[50] in which the trace of ρ used to evaluate the energy-independent term is not necessarily equal to the number of electrons. [A non-Dyson variant of ADC(3)[51] has recently been implemented efficiently.[52–54]] As in the case of 2ph-TDA, the full (non-diagonal) 3+ self-energy has always been evaluated, in practice; there is no precedent of diagonal ADC(3) calculations of any kind.

Neglect of terms beyond the third order results in

$$\begin{aligned}\boldsymbol{\Sigma}^{(3)}(E) = \boldsymbol{\Sigma}^{(2)}(E) + \boldsymbol{\Sigma}_3(\infty) &+ \left[\mathbf{a}^\dagger|\hat{H}\mathbf{f}_3\right]_1\left[\mathbf{f}_3|\left(E\hat{I} - \hat{H}\right)\mathbf{f}_3\right]_0^{-1} \\ &\times \left[\mathbf{f}_3|\hat{V}\mathbf{f}_3\right]_1\left[\mathbf{f}_3|\left(E\hat{I} - \hat{H}\right)\mathbf{f}_3\right]_0^{-1}\left[\mathbf{f}_3|\hat{H}\mathbf{a}^\dagger\right]_1 \\ &+ \left[\mathbf{a}^\dagger|\hat{H}\mathbf{f}_3\right]_2\left[\mathbf{f}_3|\left(E\hat{I} - \hat{H}\right)\mathbf{f}_3\right]_0^{-1}\left[\mathbf{f}_3|\hat{H}\mathbf{a}^\dagger\right]_1 \\ &+ \left[\mathbf{a}^\dagger|\hat{H}\mathbf{f}_3\right]_1\left[\mathbf{f}_3|\left(E\hat{I} - \hat{H}\right)\mathbf{f}_3\right]_0^{-1}\left[\mathbf{f}_3|\hat{H}\mathbf{a}^\dagger\right]_2, \end{aligned} \quad (30)$$

where $\hat{V}$ is the fluctuation-potential super-operator. The diagonal third-order self-energy (D3) is obtained by retaining only diagonal elements in Eq. (30). The D3 self-energy at $E = e_p$ equals the third-order Rayleigh–Schrödinger perturbation theory (RSPT3) result.[47–49] Evaluations of the D3 self-energy precede estimates obtained with the three OVGFs known as the A, B, and C versions.[12] Diagonal elements of the D3 self-energy matrix may be represented as follows:

$$\Sigma^{(3)} = S_{2hp} + S_{2ph} + C_D + C_S + R_{2hp} + R_{2ph} + P_{2hp} + P_{2ph}, \quad (31)$$

where the two *second-order* contributions that occur in Eq. (27) are represented by the first two terms, the *constant* terms arising from the first-order double and second-order single replacements in the reference state are denoted by the third and fourth terms, the *ring and ladder* terms occur in the fifth and sixth positions, and the energy-dependent terms that involve *perturbative* first-order double replacements are in the seventh and eighth positions. Whereas R_{2hp} and R_{2ph} correspond to the term with two energy-dependent denominators [i.e., the third term of Eq. (30)] in $\Sigma^{(3)}(E)$, the P_{2hp} and P_{2ph} terms have contributions from the last two matrix products in $\Sigma^{(3)}(E)$, which are Hermitian conjugates of each other. (Energy dependence has been suppressed for the S, R, and P terms in this notation.) Formulas for each of these third-order summations have been published in several reviews.[12,13] In this notation, the OVGF self-energies read

$$\begin{aligned}\Sigma^{OVGF-A} = \Sigma^{(2)} &+ \frac{S_{2hp} + S_{2ph}}{S_{2hp} + S_{2ph} - P_{2hp} - P_{2ph}} \\ &\times \left(C_D + C_S + R_{2hp} + R_{2ph} + P_{2hp} + P_{2ph}\right), \end{aligned} \quad (32)$$

$$\begin{aligned}\Sigma^{OVGF-B} = \Sigma^{(2)} + C_D + C_S &+ \frac{S_{2hp}}{S_{2hp} - P_{2hp}}\left(R_{2hp} + P_{2hp}\right) \\ &+ \frac{S_{2ph}}{S_{2ph} - P_{2ph}}\left(R_{2ph} + P_{2ph}\right), \end{aligned} \quad (33)$$

$$\begin{aligned}\Sigma^{OVGF-C} = \Sigma^{(2)} &+ \left(C_D + C_S + R_{2hp} + R_{2ph} + P_{2hp} + P_{2ph}\right) \\ &\times \frac{R_{2hp} + R_{2ph} + P_{2hp} + P_{2ph}}{\frac{S_{2hp} - P_{2hp}}{S_{2hp}}\left(R_{2hp} + P_{2hp}\right) + \frac{S_{2ph} - P_{2ph}}{S_{2ph}}\left(R_{2ph} + P_{2ph}\right)}. \end{aligned} \quad (34)$$

Despite the approximate character of these simple formulas for estimating higher-order self-energy terms, the accuracy of the computationally less demanding OVGF methods is competitive with that of the family of ADC(3) methods for the lowest ionization energies of closed-shell molecules and anions.[22,23] The OVGF methods require only trivial computational work at the end of a D3 calculation.

Whereas the ADC and OVGF methods may be improved by adding replacements of higher orders to $|\Psi_0{}^{\mathrm{N}}\rangle$ and $\langle\Psi_0{}^{\mathrm{N}}|$ in Eq. (7) and by increasing operator manifolds beyond $\boldsymbol{f}_3$, an alternative approach explores the consequences of adopting intermediate normalization, which is responsible for size-extensive total energies in many-body theories, in the choice of the super-operator metric. In the P3 self-energy's derivation,[18] such a choice recovers MP2 total energies evaluated with the electron propagator at the cost of producing non-Hermitian super-operator matrices that are subsequently Hermitized in calculations. In addition, separate approximations are required for IE and EA calculations.[8] To improve on this precedent, intermediate normalization may be combined with Hermitization and retention of all resulting third-order terms.

The new class of approximate self-energies may be based on an intermediately normalized, Hermitized super-operator metric,

$$\begin{aligned}[X|Y] = \frac{1}{2}\Big(&\langle HF|\left(X^\dagger Y + YX^\dagger\right)\left(1 + T_2^{(1)} + T_1^{(2)}\right)|HF\rangle \\ &+ \langle HF|\left(1 + T_2^{(1)} + T_1^{(2)}\right)^\dagger\left(X^\dagger Y + YX^\dagger\right)|HF\rangle\Big), \end{aligned} \quad (35)$$

Published under an exclusive license by AIP Publishing

where X and Y may be h, p, 2hp, or 2ph operators, and first-order double and second-order single replacements appearing in

$$T_2^{(1)} = \frac{1}{4}\sum_{ij}^{occ}\sum_{ab}^{vir}\frac{\langle ij\|ab\rangle}{e_i + e_j - e_a - e_b}a_i^\dagger a_j^\dagger a_a a_b, \tag{36}$$

$$T_1^{(2)} = \sum_{i}^{occ}\sum_{a}^{vir}\frac{1}{2(e_i - e_a)}\left(\sum_{jk}^{occ}\sum_{b}^{vir}\frac{\langle jk\|ab\rangle\langle bi\|jk\rangle}{e_j + e_k - e_a - e_b} + \sum_{j}^{occ}\sum_{bc}^{vir}\frac{\langle ij\|bc\rangle\langle bc\|aj\rangle}{e_i + e_j - e_b - e_c}\right)a_i^\dagger a_a \tag{37}$$

linearly occur in the consequent elements of the Hermitian super-operator matrix. (The P3 and non-diagonal renormalized second-order or NR2[7,8,55] self-energies were derived from a non-symmetric choice that omitted single replacement operators; separate choices for IE and EA cases were required in these derivations.[8]) The metric of Eq. (35) generates a self-energy with an equivalent treatment of 2hp and 2ph terms (*vide infra*) that is characteristic of theories that conserve time-reversal symmetry. All *third-order* terms that can be generated with this *linear* choice of metric and *ring-ladder renormalizations* are retained in the RL3 self-energy, whose elements employed in this work's calculations read

$$\begin{aligned}\boldsymbol{\Sigma}^{RL3}(E) = \frac{1}{2}\Big(&\mathbf{C}_S + \left[\mathbf{a}^\dagger|\hat{H}\mathbf{f}_{2ph}\right]_2\left[\mathbf{f}_{2ph}|\left(E\hat{I} - \hat{H}\right)\mathbf{f}_{2ph}\right]_1^{-1}\left[\mathbf{f}_{2ph}|\hat{H}\mathbf{a}^\dagger\right]_1 \\ &+ \left[\mathbf{a}^\dagger|\hat{H}\mathbf{f}_{2ph}\right]_1\left[\mathbf{f}_{2ph}|\left(E\hat{I} - \hat{H}\right)\mathbf{f}_{2ph}\right]_1^{-1}\left[\mathbf{f}_{2ph}|\hat{H}\mathbf{a}^\dagger\right]_2 \\ &+ \left[\mathbf{a}^\dagger|\hat{H}\mathbf{f}_{2hp}\right]_1\left[\mathbf{f}_{2hp}|\left(E\hat{I} - \hat{H}\right)\mathbf{f}_{2hp}\right]_1^{-1}\left[\mathbf{f}_{2hp}|\hat{H}\mathbf{a}^\dagger\right]_2 \\ &+ \left[\mathbf{a}^\dagger|\hat{H}\mathbf{f}_{2hp}\right]_2\left[\mathbf{f}_{2hp}|\left(E\hat{I} - \hat{H}\right)\mathbf{f}_{2hp}\right]_1^{-1}\left[\mathbf{f}_{2hp}|\hat{H}\mathbf{a}^\dagger\right]_1\Big),\end{aligned} \tag{38}$$

where $\boldsymbol{C}_S$ is the non-diagonal matrix generalization of C_S. The $T_1{}^{(2)}$ operators in Eq. (35) are necessary for recovering the third-order C_S term in Eq. (38). The C_D term, which, in practice, is often a source of instability with respect to basis sets, is eliminated by the choice of Eq. (35), for it has a quadratic dependence on reference-state substitution amplitudes. Improved stability and accuracy may be procured by inclusion of the fourth-order energy-independent self-energy, which includes many computationally demanding terms (e.g., those that depend on $T_3{}^{(2)}$ and $T_2{}^{(1)}$ amplitudes) that are quadratic in reference-state substitution amplitudes. [See, for example, the proposed $\Sigma(4+)$ self-energy in nD-ADC(3) calculations.[56]] The cost of this alternative in terms of efficiency and interpretability is unlikely to be proportionate to its benefits with respect to accuracy. Omission of quadratic terms, therefore, affords an attractive compromise of efficiency, interpretability, and (*vide infra*) accuracy. The ring and ladder terms that are independent of reference-state substitution amplitudes are identical to their counterparts in 2ph-TDA, 3+, and ADC(3), but the terms that are linear in those amplitudes are now multiplied by a factor of one-half as a result of the metric choice of Eq. (35). The latter terms are usually the largest in the third-order self-energy, and their double-weighting is chiefly responsible for the overestimated IEs that typify D3 calculations. Simplifications of IP-EOM-CCSD equations that employ $T_2{}^{(1)}$ amplitudes instead of their CCSD T_2 counterparts arrive at the same coefficients for analogous terms,[57,58] as was demonstrated in the original derivation of the P3 method,[18] and produce no analogs of the C_D term. Another justification for the omission of quadratic terms emerges from an equivalent expression for super-operator Hamiltonian matrix elements in terms of a single-determinant reference state (e.g., HF) and the similarity-transformed Hamiltonian that occurs in unitary coupled-cluster theory.[59] The latter operator's Baker–Campbell–Hausdorff expansion in terms of commutators of the original Hamiltonian with the cluster (T) operator yields a series of Hermitian model Hamiltonians which may be truncated after the term that is linear in T.

Fourth-order and many higher-order terms in the RL3 self-energy may be identified by expansion of the inverted matrices. The most demanding arithmetic operations involve couplings between 2ph operators that occur in third and higher orders. There is considerable numerical evidence that these terms are of relatively little importance in calculations of electron removal energies for closed-shell molecules.[18] Their neglect defines a renormalized quasi-particle self-energy for the calculation of IEs, denoted as RQ3, that retains RL3's 2hp third-order terms,

$$\begin{aligned}\boldsymbol{\Sigma}^{RQ3}(E) = \frac{1}{2}\mathbf{C}_S &+ \left[\mathbf{a}^\dagger|\hat{H}\mathbf{f}_{2ph}\right]_1\left[\mathbf{f}_{2ph}|\left(E\hat{I} - \hat{H}\right)\mathbf{f}_{2ph}\right]_0^{-1}\left[\mathbf{f}_{2ph}|\hat{H}\mathbf{a}^\dagger\right]_1 \\ &+ \frac{1}{2}\left[\mathbf{a}^\dagger|\hat{H}\mathbf{f}_{2hp}\right]_2\left[\mathbf{f}_{2hp}|\left(E\hat{I} - \hat{H}\right)\mathbf{f}_{2hp}\right]_1^{-1}\left[\mathbf{f}_{2hp}|\hat{H}\mathbf{a}^\dagger\right]_1 \\ &+ \frac{1}{2}\left[\mathbf{a}^\dagger|\hat{H}\mathbf{f}_{2hp}\right]_1\left[\mathbf{f}_{2hp}|\left(E\hat{I} - \hat{H}\right)\mathbf{f}_{2hp}\right]_1^{-1}\left[\mathbf{f}_{2hp}|\hat{H}\mathbf{a}^\dagger\right]_2.\end{aligned} \tag{39}$$

The second term is just the 2ph term in the usual second-order self-energy [i.e., the second term in Eq. (27)]. Dropping the constant term arising from second-order single replacements in the reference state yields the RP3 self-energy,

$$\begin{aligned}\boldsymbol{\Sigma}^{RP3}(E) = &\left[\mathbf{a}^\dagger|\hat{H}\mathbf{f}_{2ph}\right]_1\left[\mathbf{f}_{2ph}|\left(E\hat{I} - \hat{H}\right)\mathbf{f}_{2ph}\right]_0^{-1}\left[\mathbf{f}_{2ph}|\hat{H}\mathbf{a}^\dagger\right]_1 \\ &+ \frac{1}{2}\left[\mathbf{a}^\dagger|\hat{H}\mathbf{f}_{2hp}\right]_2\left[\mathbf{f}_{2hp}|\left(E\hat{I} - \hat{H}\right)\mathbf{f}_{2hp}\right]_1^{-1}\left[\mathbf{f}_{2hp}|\hat{H}\mathbf{a}^\dagger\right]_1 \\ &+ \frac{1}{2}\left[\mathbf{a}^\dagger|\hat{H}\mathbf{f}_{2hp}\right]_1\left[\mathbf{f}_{2hp}|\left(E\hat{I} - \hat{H}\right)\mathbf{f}_{2hp}\right]_1^{-1}\left[\mathbf{f}_{2hp}|\hat{H}\mathbf{a}^\dagger\right]_2.\end{aligned} \tag{40}$$

The RP3 self-energy is closely related to the NR2 approximation for IEs; its diagonal third-order terms are identical to those of P3.

Neglect of fourth and higher order terms generated by expansion of the inverted matrices in RL3, RQ3, and RP3, respectively, defines the L3, Q3, and P3 self-energy matrices,

$$\Sigma^{L3} = S_{2hp} + S_{2ph} + \frac{1}{2}\left(C_S + P_{2hp} + P_{2ph}\right) + R_{2hp} + R_{2ph}, \tag{41}$$

$$\Sigma^{Q3} = S_{2hp} + S_{2ph} + \frac{1}{2}\left(C_S + P_{2hp}\right) + R_{2hp}, \tag{42}$$

$$\Sigma^{P3} = S_{2hp} + S_{2ph} + \frac{1}{2}P_{2hp} + R_{2hp}. \tag{43}$$

Factors of one-half appear because of the new choice of super-operator metric. Only P3 has been derived and implemented previously.[18] Its original definition employed a super-operator metric with first-order double but without second-order single replacements.

Published under an exclusive license by AIP Publishing

The approximately renormalized partial third order self-energy[20] (P3+) for IEs may be recovered in an expression analogous to that used in OVGF-B so that

$$\Sigma^{P3+} = \Sigma^{(2)} + \frac{S_{2hp}}{S_{2hp} - \frac{1}{2}P_{2hp}}\left(R_{2hp} + \frac{1}{2}P_{2hp}\right). \tag{44}$$

(Note that P3+ is called the *approximately* renormalized partial third order method in this work, whereas it was previously denoted simply by renormalized partial third order.) The present convention assigns the + sign to approximately renormalized methods and reserves R for methods in which higher-order terms are explicitly evaluated. With similar arguments, the Q3+ method may be obtained,

$$\Sigma^{Q3+} = \Sigma^{(2)} + \frac{1}{2}C_S + \frac{S_{2hp}}{S_{2hp} - \frac{1}{2}P_{2hp}}\left(R_{2hp} + \frac{1}{2}P_{2hp}\right). \tag{45}$$

Because RL3 treats 2hp and 2ph operators on an equal footing, A, B, and C versions of L3+ may be defined by analogy to the three OVGF alternatives,

$$\Sigma^{L3+A} = \Sigma^{(2)} + \frac{S_{2hp} + S_{2ph}}{S_{2hp} + S_{2ph} - \frac{1}{2}\left(P_{2hp} + P_{2ph}\right)} \times \left[C_S + R_{2hp} + R_{2ph} + \frac{1}{2}\left(P_{2hp} + P_{2ph}\right)\right], \tag{46}$$

$$\Sigma^{L3+B} = \Sigma^{(2)} + C_S + \frac{S_{2hp}}{S_{2hp} - \frac{1}{2}P_{2hp}}\left(R_{2hp} + \frac{1}{2}P_{2hp}\right) + \frac{S_{2ph}}{S_{2ph} - \frac{1}{2}P_{2ph}}\left(R_{2ph} + \frac{1}{2}P_{2ph}\right), \tag{47}$$

$$\Sigma^{L3+C} = \Sigma^{(2)} + \left[C_S + R_{2hp} + R_{2ph} + \frac{1}{2}\left(P_{2hp} + P_{2ph}\right)\right] \times \frac{R_{2hp} + R_{2ph} + \frac{1}{2}\left(P_{2hp} + P_{2ph}\right)}{\frac{S_{2hp} - \frac{1}{2}P_{2hp}}{S_{2hp}}\left(R_{2hp} + \frac{1}{2}P_{2hp}\right) + \frac{S_{2ph} - \frac{1}{2}P_{2ph}}{S_{2ph}}\left(R_{2ph} + \frac{1}{2}P_{2ph}\right)}. \tag{48}$$

Pole search algorithms typically employ HF orbital energies as initial guesses, evaluate derivatives of the diagonal self-energy matrix elements with respect to E (these data are also needed to determine probability factors), and employ Newton's method for finding the roots of a function of a single variable [see Eq. (23)]. Three iterations usually suffice for convergence to within 0.01 eV. Pole searches with the OVGF, P3+, Q3+, and L3+ self-energies are initiated, respectively, at the D3, P3, Q3, and L3 poles; agreement to within 0.01 eV is usually obtained after a single Newton iteration. Improvements based on the three + (i.e., approximately renormalized) methods require practically no additional work once P3, Q3, or L3 calculations are complete.

RESULTS AND DISCUSSION

All calculations have been executed with a new link in the development version of Gaussian.[60] At the conclusion of self-consistent field calculations, electron repulsion integrals needed for the calculation of self-energy matrix elements are transformed to the HF basis and stored on disk.

Table I displays arithmetic bottlenecks, the number of bottleneck steps, and the scaling of the largest subset of transformed electron repulsion integrals needed for the evaluation of an electron removal energy according to various self-energy approximations. To determine the arithmetic bottlenecks, the number of virtual orbitals (V) is assumed to be larger than the number of occupied orbitals (O). New methods are denoted by bold type. The D2 method, in principle, requires a partial integral transformation with quartic instead of the usual fifth-power scaling because all its integrals have a single fixed index, p. Second-order methods scale cubically and are juxtaposed in Table I. Whereas the D3, OVGF, L3, L3+, and RL3 methods have OV^4 steps involving integrals with four virtual indices that are comparable in difficulty to the full integral transformation involving N_B atom-centered basis functions (i.e., $N_B{}^5 > V^5 > OV^4$), the P3, P3+, Q3, Q3+, and G_0W_0 methods have relatively fast O^2V^3 arithmetic bottlenecks. Among the latter five methods, HF-TDA G_0W_0 is the only one that does not require integrals with three virtual indices. The number of bottleneck steps is proportional to N_E, the number of energy iterations, in several methods. Expansion of an energy-dependent inverse matrix is considered to require N_I steps in the RP3, RQ3, RL3, and HF-TDA G_0W_0 methods. N_I may strongly depend on E and on gaps between occupied and virtual orbital energies. For methods in which such iterations occur for every value of E, such as RL3 and HF-TDA G_0W_0, the number of bottleneck steps may be estimated to be N_IN_E. For P3, P3+, Q3, Q3+, RP3, and RQ3, bottleneck contractions occur once in the evaluation of an energy-independent intermediate, the matrix of second-order couplings between h and 2hp operators. Therefore, Q3+ bottleneck steps are less numerous than their counterparts in HF-TDA G_0W_0. Diagonal methods that include post-second-order terms are placed together in Table I.

Non-diagonal 3+, ADC(3) (with the Schirmer–Angonoa treatment of the constant self-energy terms[50]), and BD-T1[61–65] self-energy matrices have identical arithmetic scaling factors that coincide with those of IP-EOM-CCSD,[42] O^2V^4. NR2's sixth-power bottleneck is lower at O^3V^3 and arises from second-order couplings between h and 2hp operators that require no iterations. All sixth-power arithmetic bottlenecks stem from treatments of reference-state correlation. Iterative diagonalization algorithms enable ND2 and 2ph-TDA, respectively, to have fourth-power and fifth-power arithmetic scaling factors.[66,67] The iterative nature of the ADC(3) method's bottleneck is a consequence of its constant (energy-independent) self-energy terms.

The IP-EOM-CCSDT, cc-pVTZ set includes 33 closed-shell molecules with H, C, N, O, and F nuclei and 170 valence IEs; the IP-EOM-CCSDTQ subset has 11 molecules and 34 IEs.[41] The mean absolute error of IP-EOM-CCSDT with respect to IP-EOM-CCSDTQ in the latter set is 0.03 eV, the standard deviation of these errors is 0.02 eV, and the maximum error is 0.10 eV. When signed errors are considered, these three criteria, respectively, become 0.00, 0.04, and 0.10 eV. These data indicate that results obtained at

Published under an exclusive license by AIP Publishing

TABLE I. Arithmetic scaling of computational requirements for self-energy approximations.[a]

Method class	Methods[b]	Arithmetic bottleneck	Bottleneck steps	Largest ERI[c] subset
Diagonal second order	D2 and os-D2	OV^2	N_E	O^2V^2
	RSPT2, nD-D2, and **os-nD-D2**	OV^2	1	O^2V^2
Diagonal post-second order	RSPT3	OV^4	1	V^4
	D3 and OVGF	OV^4	N_E	V^4
	P3, P3+, **Q3,** and **Q3**+	O^2V^3	1	OV^3
	L3 and **L3**+	OV^4	N_E	V^4
	RP3 and **RQ3**	O^2V^3	1	OV^3
	RL3	OV^4	N_IN_E	V^4
	HF-TDA G_0W_0	O^2V^3	N_IN_E	O^2V^2
Non-diagonal	ND2	OV^3	N_I	OV^3
	2ph-TDA	OV^4	N_I	V^4
	3+	O^2V^4	1	V^4
	ADC(3)	O^2V^4	N_I	V^4
	NR2	O^3V^3	1	OV^3
	BD-T1	O^2V^4	BD[d]	V^4

[a]O = No. of occupied orbitals, V = No. of virtual orbitals, N_E = energy iterations, and N_I = inverse-expansion iterations.
[b]New methods are shown in bold type.
[c]ERI = electron repulsion integral.
[d]The O^2V^4 arithmetic bottleneck occurs in the BD, coupled-cluster reference calculation; the subsequent electron-propagator bottleneck is OV^4.

both levels of theory are excellent approximations to FCI results in the cc-pVTZ basis. Many final states in both sets of data correspond to inner-valence DOs with large 2s atomic contributions whose probability factors [Π; see Eq. (21)] are likely to approach the 0.85 criterion of applicability that customarily applies to diagonal self-energy methods. These standards therefore present a realistic and challenging test of predictive capabilities in the methods under examination.

Mean absolute errors (MAEs or $|\overline{\Delta}|$), their standard deviations ($|\Delta|_{std}$), and maximum absolute errors ($|\Delta|_{max}$) with respect to the IP-EOM-CCSDT standards have been calculated for the self-energy approximations that require evaluation of no terms above the third order in the fluctuation potential. When one of these diagonal methods has a probability factor below 0.85, the IE is excluded from the error calculations, which leads to a subset of 116 IEs. Table II lists the molecules and final states in the latter subset. Numerical results are shown in Table III. Bold type denotes new methods in the first column and the best combinations of accuracy and efficiency in the second column. (For the IP-EOM-CCSDTQ set, exclusion of states with low probability factors reduces the number of IEs below the threshold of 30 needed for reliable statistical inferences; error measures listed in the supplementary material for this smaller dataset provide confirmation of the conclusions reached below.)

Whereas the errors of Koopmans's theorem (KT) in this set are reduced by more than a factor of two at the D2 level, even greater rewards (approximately another factor of two) occur with os-D2 and os-nD-D2 without the introduction of adjustable parameters. The two latter methods are, in fact, less arithmetically demanding than D2. In most cases, D2 underestimates IEs despite the reduction in absolute errors as basis sets are improved,[21–23] but os-D2 and os-nD-D2, with mean signed errors that are positive instead of negative (see the supplementary material), presently have a greater tendency to overestimate IEs. The most efficient cubically scaling method, os-nD-D2, also has the lowest MAE (0.29 eV). Thus, the tendency of D2 to exaggerate the correction to Koopmans results is ameliorated by the simple expedient of neglecting same-spin terms in the self-energy. Additional gains in accuracy over the os-D2 and os-nD-D2 methods are achieved with P3+ (MAE = 0.17 eV) at the cost of a single non-iterative O^2V^3 step and the employment of transformed integrals with three virtual indices. (The need to store the latter subset of integrals could be overcome with a semi-direct algorithm.[68,69]) The Q3+ self-energy realizes another improvement (MAE = 0.15 eV) over P3+ with the introduction of more O^2V^3 contractions that do not increase the arithmetic scaling bottleneck. The additional terms in Q3+, which describe orbital relaxation in final states, arise from contributions to the energy-independent portion of the self-energy made by the $T_1^{(2)}$ amplitudes in the super-operator metric and tend to reduce overestimates of IEs produced by P3+. The Q3+ and P3+ self-energies are more efficient and accurate than D3 and the three OVGF variants. Their three L3+ counterparts have similar computational requirements as OVGF and clearly superior accuracy (MAE = 0.12–0.13 eV for all three variants). They produce slight improvements over Q3+ at the cost of higher arithmetic scaling and the need for integrals with four virtual indices. Additional 2ph terms in the L3+ methods provide more refined descriptions of initial-state correlation and further diminish overestimates of IEs. Note that the P3+, Q3+, and L3+ extensions lower errors by about 0.1 eV with respect to their P3, Q3, and L3 precursors with practically no additional effort. The miniscule differences in error

Published under an exclusive license by AIP Publishing

TABLE II. 116 IEs used for the statistics. Bold face denotes 36 non-converged renormalizations.

Species	Orbital	IP-EOM-CCSDT[41] (eV)
C_2F_4	$2b_{3u}$	10.37
	$4b_{3g}$	15.78
	$6a_g$	16.11
	$4b_{2u}$	**16.32**
	$1a_u$	16.48
	$1\ b_{1g}$	16.64
	$5b_{1u}$	17.32
	$1b_{2g}$	**18.02**
	$3b_{3g}$	19.41
	$3b_{2u}$	**20.76**
	$5a_g$	**21.03**
CF_4	$1t_1$	16.09
	$4t_2$	17.24
	1e	18.18
	$3t_2$	21.93
HCN	1π	13.72
	4σ	**20.43**
C_2H_2	$1\pi_u$	11.42
	$3\sigma_g$	17.12
HCCF	2π	11.34
	1π	**17.90**
	7σ	18.12
HCCCN	**2π**	**11.69**
NNO	2π	12.74
C_2N_2	**$1\pi_g$**	**13.48**
	$1\pi_u$	**15.70**
CO	5σ	13.90
	1π	16.95
FCN	2π	13.50
	7σ	14.31
	1π	**19.39**
	6σ	**22.79**
N_2	$3\sigma_g$	15.45
$C_2H_2F_2$	$2b_1$	10.54
	$5b_2$	14.96
	$8a_1$	15.52
	$4b_2$	15.85
	$1a_2$	16.02
	$7a_1$	18.27
	$1b_1$	**18.10**
	$3b_2$	**19.63**
	$6a_1$	**21.41**
cis-$C_2H_2F_2$	$2b_1$	10.39
	$7a_1$	13.88
	$6b_2$	14.80
	$1a_2$	**16.07**
	$5b_2$	16.85
HC_4H	$1\pi_g$	10.20
HF	1π	15.90
	3σ	19.83
F_2	$1\pi_g$	15.58
H_2CO	$2b_2$	10.75
	$1b_1$	14.50
	$5a_1$	15.96
	$1b_2$	**17.10**
	$4a_1$	**21.30**
H_2O	$1b_1$	12.45
	$3a_1$	14.69
	$1b_2$	18.84
C_2H_4	$1b_{3u}$	10.64
	$1b_{3g}$	13.08
	$3a_g$	14.79
	$1b_{2u}$	**16.14**
$HCONH_2$	$10a'_1$	10.17
	$2a''$	10.56
	$9a'_1$	**14.67**
	$8a'_1$	**16.55**
	$7a'_1$	**19.25**
	$6a'_1$	**20.90**
HCOOH	$10a'$	11.33
	$2a''$	12.47
	$9a'$	14.79
	$8a'$	**17.06**
	$7a'$	**17.81**
	$6a'$	**22.08**
CH_3CN	2e	12.45
	1e	**16.24**
	$6a_1$	**17.38**
CH_3NC	2e	12.55
	1e	16.59
	$6a_1$	**18.38**
CH_3F	2e	13.17
	$5a_1$	17.01
	1e	17.04
	$4a_1$	**23.51**
CH_2F_2	$2b_1$	13.29
	$4b_2$	14.92
	$6a_1$	15.20
	$1a_2$	15.59
	$3b_2$	18.75
	$5a_1$	18.97
	$1b_1$	19.15
CHF_3	$6a_1$	14.76
	$1a_2$	15.33

Published under an exclusive license by AIP Publishing

TABLE II. (*Continued.*)

Species	Orbital	IP-EOM-CCSDT[41] (eV)	Species	Orbital	IP-EOM-CCSDT[41] (eV)
	$1b_1$	16.97		5e	15.93
	$6a_1$	**18.50**		4e	16.99
	$5a_1$	**18.88**		3e	20.41
	$4b_2$	**19.60**		$5a_1$	20.93
NH_3	$3a_1$	10.74		**$4a_1$**	**24.43**
	1e	16.48		$1e_g$	12.68
CH_4	$1t_2$	14.35	C_2H_6	$3a_{1g}$	13.06
	2e	10.46		$1e_u$	15.38
CH_3CCH	**1e**	**15.17**	CO_2	$1\pi_g$	13.63
	$7a_1$	**15.22**		$3\sigma_u$	17.85
	$6a_1$	**17.65**	C_3O_2	$2\pi_u$	10.62

data among the three L3+ alternatives suggest a slight preference in the interest of consistency for the B version, which has the same approximate renormalization scheme as Q3+ and P3+. ND2 has no advantage vs os-D2 or os-nD-D2; it is, in fact, slightly worse than D2. The non-diagonal 2ph-TDA, 3+, and ADC(3) methods are less efficient and accurate than the approximately renormalized diagonal methods, P3+, Q3+, and the three L3+ versions. Among the non-diagonal methods, only NR2 and BD-T1 are competitive for

TABLE III. Errors (eV) with respect to cc-pVTZ/IP-EOM-CCSDT standards[41] for 116 IEs listed in Table II.

Method class	Method[a]	Mean absolute error[b]	Standard deviation	Maximum absolute error
Uncorrelated	KT	1.595	0.857	3.780
Diagonal second order	D2	0.601	0.349	1.389
	os-D2	0.301	0.223	1.838
	nD-D2	0.633	0.363	1.442
	os-nD-D2	**0.289**	0.220	1.817
Diagonal post-second order	D3	0.724	0.462	2.324
	OVGF-A	0.242	0.213	1.739
	OVGF-B	0.367	0.265	1.900
	OVGF-C	0.382	0.271	1.933
	P3	0.267	0.202	1.623
	P3+	0.166	0.160	1.479
	Q3	0.246	0.204	1.624
	Q3+	**0.147**	0.155	1.480
	L3	0.227	0.201	1.648
	L3+A	**0.122**	0.154	1.418
	L3+B	**0.125**	0.158	1.505
	L3+C	**0.126**	0.158	1.504
Non-diagonal	ND2	0.632	0.468	3.081
	2ph-TDA	0.634	0.198	1.384
	3+	0.398	0.285	1.776
	ADC(3)	0.370	0.257	1.712
	NR2	0.113	0.135	1.166
	BD-T1	0.140	0.178	1.554
	IP-EOM-CCSD	0.174	0.165	1.593

[a]New methods are shown in bold type.
[b]Optimal methods are shown in bold type.

Published under an exclusive license by AIP Publishing

this dataset, with accuracy surpassing that of IP-EOM-CCSD. The approximately renormalized diagonal methods, P3+, Q3+, and L3+, are also slightly better than IP-EOM-CCSD.

When probability factors are above 0.85*, the os-nD-D2, Q3+, and L3+ methods offer the highest accuracy for their respective levels of computational effort, OV^2, O^2V^3, and OV^4.* NR2, BD-T1, and IP-EOM-CCSD remain useful for obtaining more general DOs. Figure 1 juxtaposes the errors of low-order and approximately renormalized diagonal self-energies according to their bottleneck arithmetic scaling factors. The top performers recommended for routine applications (os-nD-D2, Q3+, and L3+B) are compared with older self-energies in wide use, such as the three OVGF versions, ADC(3), P3+, NR2, and BD-T1, and with IP-EOM-CCSD.

Alternatives to the approximately renormalized (+) methods are provided by the HF-TDA G_0W_0, RP3, RQ3, and RL3 self-energies in which explicit evaluation of higher-order terms is performed. The latter three methods are (ring-ladder) renormalized extensions of P3, Q3, and L3, respectively. In some cases, the expansion of the inverted matrices that occur in these four methods does not converge. Such cases are also excluded (see Table II), along with cases with probability factors less than 0.85 (as in Table III), from the error analysis of Table IV, which is thus based on 80 IEs.

In this more restricted dataset, the errors of most methods are lower. For os-nD-D2, the MAE is now 0.23 eV. HF-TDA G_0W_0 achieves slightly greater accuracy (MAE = 0.21 eV) at the cost of repeated O^2V^3 steps. [An MAE of 0.24 eV for just the lowest IEs of species taken from the GW100 dataset with respect to CCSD(T) data was reported recently.[32]] The MAEs of P3+, Q3+, and L3+B (0.13, 0.12, and 0.09 eV, respectively) are improved slightly by the iterative steps required in RP3, RQ3, and RL3 (0.12, 0.10, and 0.08 eV, respectively). Because RQ3 and RP3 have identical bottleneck arithmetic scaling factors, the former of these two alternatives is preferred. RQ3's bottleneck arithmetic scaling factor (O^2V^3) occurs but once, and its iterative evaluations of higher-order terms have an O^3V^2 arithmetic dependence. An improved accuracy of ~0.1 eV in Q3+ and RQ3 relative to HF-TDA G_0W_0 is purchased at the cost of an OV^3 integral storage requirement, but the number of bottleneck steps is reduced. (See Table I.) The most accurate diagonal methods are L3+B (or L3+C) and RL3, which have the same arithmetic bottleneck scaling as that of D3 and OVGF. The L3+ methods do not require as many bottleneck steps as RL3. L3+B and RL3 perform better than all the non-diagonal self-energy methods and have slightly lower MAEs than IP-EOM-CCSD, NR2, and BD-T1. Non-Dyson versions of RL3 and the L3+ methods may procure comparable accuracy at reduced cost. Such methods bear close resemblance to third-order formulas that can be derived from cluster perturbation theory of excitation energies.[70–74]

For the calculation of valence IEs, several non-diagonal methods, including ND2, 2ph-TDA, 3+, and ADC(3), have no

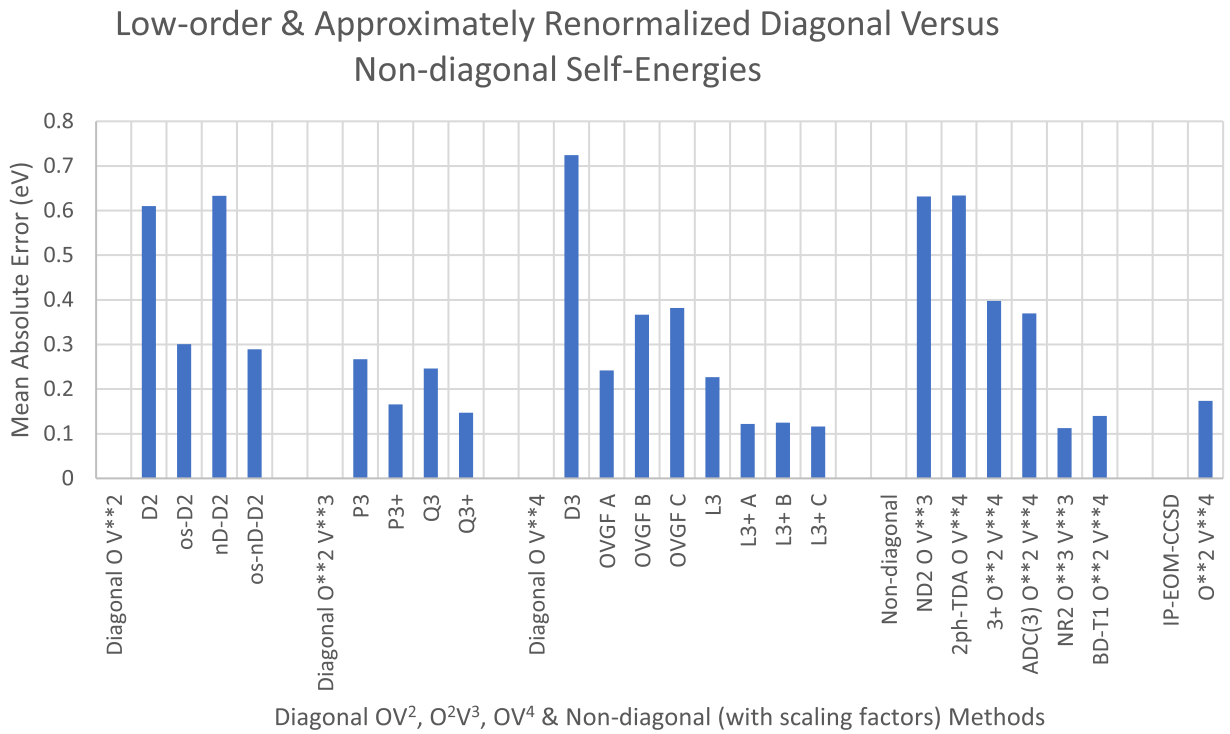


FIG. 1. Mean absolute errors (eV) of low-order and approximately renormalized diagonal vs non-diagonal self-energies for 116 IEs with $\Pi > 0.85$. Errors are calculated with respect to cc-pVTZ/IP-EOM-CCSDT results.[41]

Published under an exclusive license by AIP Publishing

TABLE IV. Errors (eV) with respect to cc-pVTZ/IP-EOM-CCSDT standards[41] for 80 IEs listed in Table II.

Method class	Method[a]	Mean absolute error[b]	Standard deviation	Maximum absolute error
Uncorrelated	KT	1.421	0.834	2.839
Diagonal second order	D2	0.628	0.349	1.389
	os-D2	0.237	0.151	0.643
	nD-D2	0.660	0.363	1.442
	os-nD-D2	**0.226**	0.148	0.634
Diagonal post-second order	HF-TDA G_0W_0	0.205	0.141	0.592
	D3	0.647	0.424	1.503
	OVGF-A	0.193	0.137	0.515
	OVGF-B	0.313	0.208	0.734
	OVGF-C	0.320	0.212	0.716
	P3	0.213	0.147	0.762
	P3+	0.134	0.087	0.425
	Q3	0.201	0.144	0.710
	Q3+	**0.117**	0.077	0.370
	L3	0.174	0.129	0.630
	L3+A	0.110	0.086	0.404
	L3+B	**0.090**	0.063	0.310
	L3+C	0.090	0.064	0.305
	RP3	0.119	0.090	0.368
	RQ3	**0.104**	0.078	0.306
	RL3	**0.077**	0.062	0.324
Non-diagonal	ND2	0.670	0.427	3.021
	2ph-TDA	0.626	0.203	1.384
	3+	0.360	0.236	0.792
	ADC(3)	0.323	0.205	0.761
	NR2	0.101	0.072	0.335
	BD-T1	0.092	0.063	0.243
	IP-EOM-CCSD	0.119	0.071	0.352

[a]New methods are shown in bold type.
[b]Optimal methods are shown in bold type.

apparent advantages with respect to accuracy or efficiency. (They may remain useful for the determination of DOs as linear combinations of HF orbitals.) Error measures for 3+ and ADC(3) are very close; there is no improvement to accompany the slower renormalized treatment[50] of energy-independent self-energy terms. Among these non-diagonal methods, only the NR2 and BD-T1 self-energies are competitive for valence IEs. Their sixth-power dependence is compensated by production of improved DOs.

Comparisons between mean signed and unsigned errors reveal that most of the methods in Table IV are more likely to overestimate than to underestimate IEs. (See the supplementary material for the full set of data.) Only D2, nD-D2, L3+A, RP3, RQ3, RL3, ND2, 2ph-TDA, and NR2 produce negative mean signed errors. These data are especially close to zero for RQ3, RL3, and NR2 (−0.04, −0.02, and −0.03 eV, respectively).

RP3 and NR2 results provide insights into the efficacy of the diagonal self-energy approximation, for the off-diagonal h–h elements of the RP3 self-energy suffice to recover their NR2 counterparts. For the present datasets, the two methods have almost identical predictive quality. It is likely that excursions into higher IEs may be facilitated by similar generalizations of RQ3 and RL3 to non-diagonal forms.

Figure 2 displays error data pertaining to five diagonal self-energy methods developed in this work (os-nD-D2, Q3+, L3+B, RQ3, and RL3), HF-TDA G_0W_0, two previously developed non-diagonal methods (NR2 and BD-T1), and IP-EOM-CCSD for the 80 IEs where probability factors are greater than or equal to 0.85 for all methods and where ring-ladder renormalizations are converged via an order-by-order expansion of an inverse matrix. *When the latter conditions are met, os-nD-D2, RQ3, and RL3 provide the highest accuracy for a given bottleneck scaling factor* (OV^2, O^2V^3, *and* OV^4, *respectively*), *but Q3+ and L3+B obtain similar accuracy in the last two classifications of arithmetic efficiency.* L3+B significantly reduces the number of OV^4 contractions in comparison with RL3. The + methods provide fast accurate estimates of ring-ladder renormalizations.

Published under an exclusive license by AIP Publishing

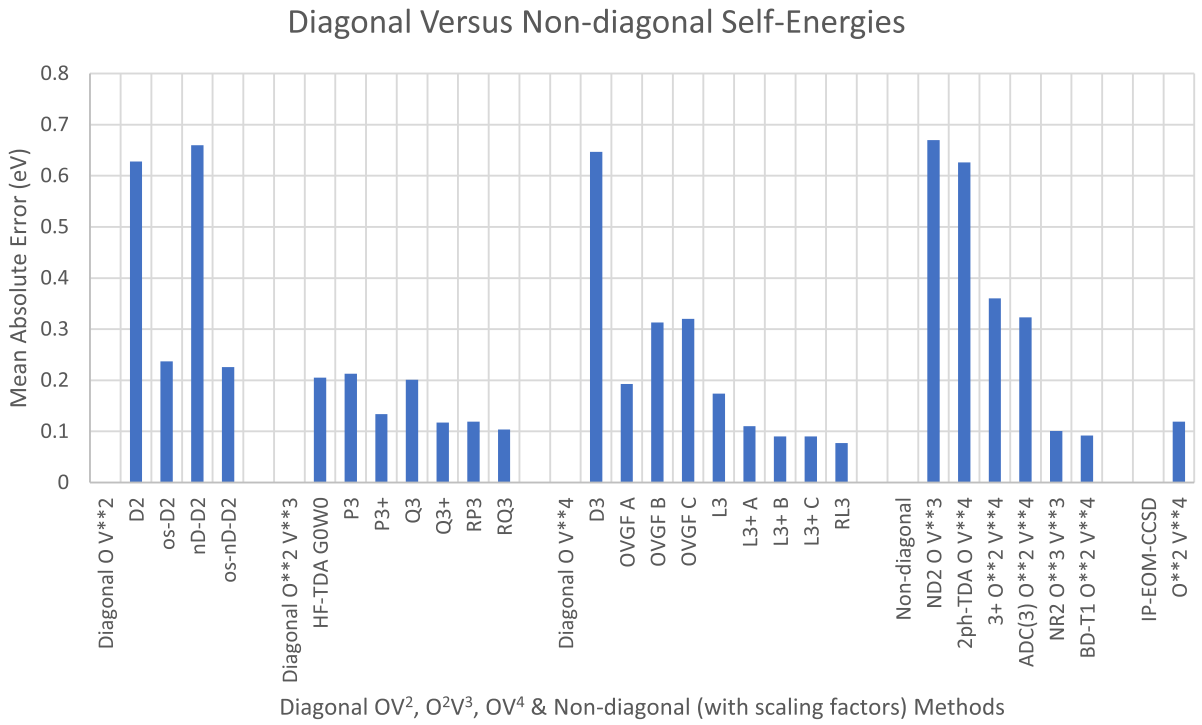


FIG. 2. Mean absolute errors (eV) of the diagonal vs non-diagonal self-energies for 80 IEs with $\Pi > 0.85$ and convergent renormalizations. Errors are calculated with respect to cc-pVTZ/IP-EOM-CCSDT results.[41]

The histograms of Fig. 3 display trends in the errors made by various methods for the dataset of 80 IEs. (MAEs, standard deviations, and maximum errors are also shown in the upper left corner of each graph.) To facilitate comparisons between the best methods, the abscissa varies between −1 and +1 eV in all cases. The first row begins with KT results, where many relatively large overestimates of VIEs that follow from an uncorrelated frozen-orbital theory lie outside the depicted range. The MAE and the standard deviation are large in comparison with other methods. D2 reduces both error criteria by more than a factor of two, but it also tends to underestimate VIEs. Restoration of off-diagonal elements of the self-energy matrix leads to a similar ND2 histogram with slightly worse error measures. The non-Dyson variant (nD-D2) also fails to improve on D2. The second-order self-energy clearly exaggerates the effects of orbital relaxation and electron correlation. Such overestimation of final-state relaxation and correlation is ameliorated in os-D2 and the slightly more efficient os-nD-D2 approximations. The lowered average absolute error and standard deviation indicate that, despite the presence of many overestimates between 0.3 and 0.6 eV, useful information on large sets of data may be obtained after a trivial increment of computational effort with respect to a partial integral transformation.

The next set of histograms (see the second and third rows of Fig. 3) pertains to D3, its OVGF extensions, P3, and P3+, i.e., the most widely employed diagonal self-energy methods. Whereas D3's deficiencies of accuracy and efficiency lead to no improvements over D2, it provides (despite its tendency to overestimate VIEs) useful information to the three OVGF versions. Overestimates outnumber underestimates in all three versions; OVGF-A has an average absolute error of only 0.2. The B and C versions are less reliable. Error data of similar quality as those of OVGF-A are produced more efficiently with the P3 method. A clearly improved profile is obtained after adding the computationally trivial approximate renormalization of the P3+ method: only five cases yield absolute errors between 0.3 and 0.4 eV. P3 and P3+ also produce more overestimates than underestimates of VIEs.

New methods based on diagrams of second and third orders and their approximately renormalized counterparts are compared in the fourth and fifth rows. Q3 and Q3+, respectively, display small improvements over P3 and P3+. With Q3+, only one absolute error exceeds 0.3 eV. These improved data are obtained with computational effort that is low in comparison with a transformation of electron repulsion integrals. When the latter step is feasible, Q3+ provides data of high quality with minimal extra arithmetic operations. The trend toward higher accuracy continues in the L3, L3+A, L3+B, and L3+C histograms. Additional computational effort that now is comparable to that of the integral transformation is rewarded with tighter error criteria. L3+B and L3+C, unlike L3+A, have a slight tendency to overestimate VIEs. In both cases, only three absolute errors exceed 0.2 eV.

Histograms of explicitly renormalized methods occur in the fifth and sixth rows. HF-TDA G_0W_0 generates a profile that is slightly better than that of os-nD-D2. These two methods produce more overestimates than underestimates. RP3 and P3+ also have

Published under an exclusive license by AIP Publishing

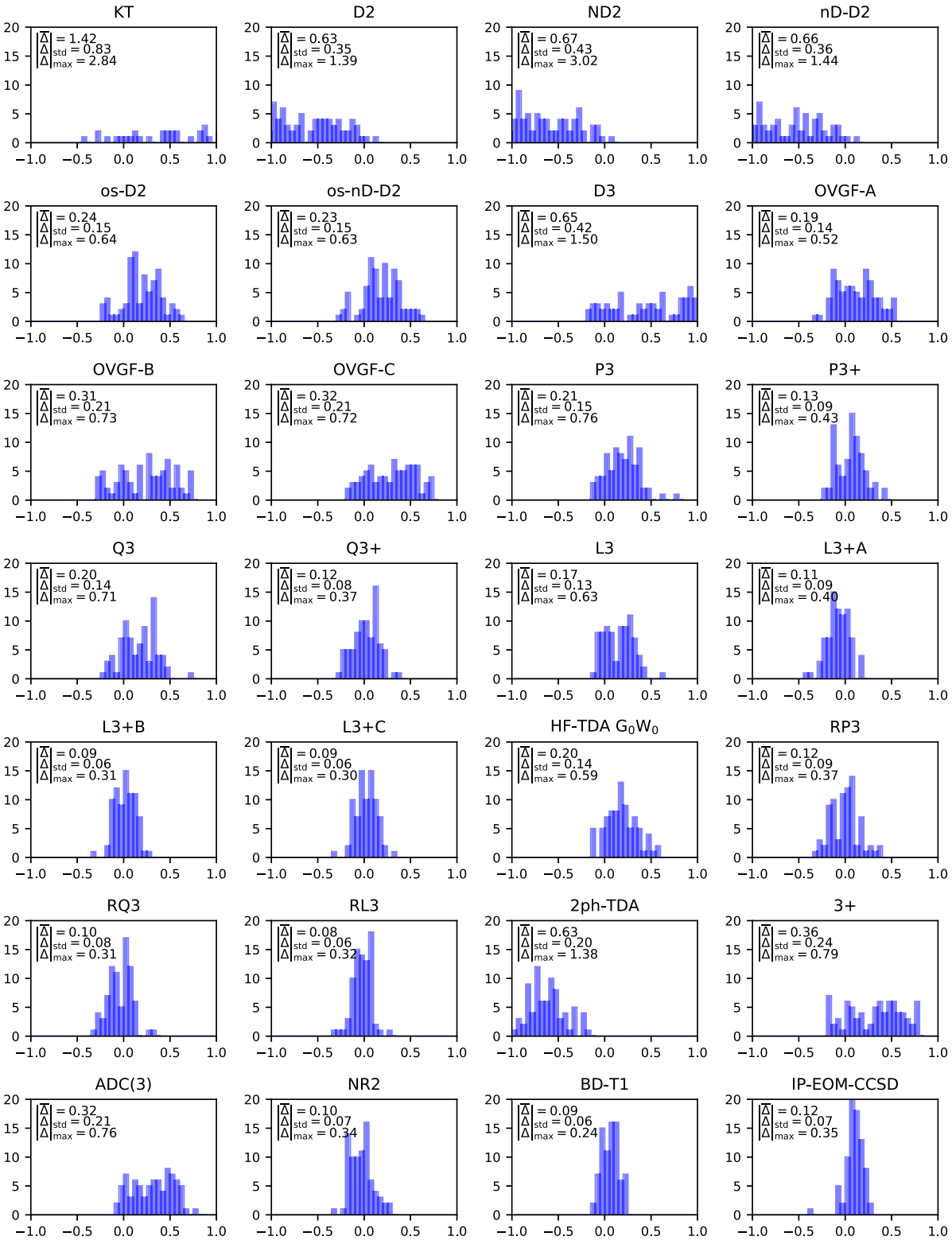


FIG. 3. Histograms of error (eV) distributions for 80 IEs.

Published under an exclusive license by AIP Publishing

similar profiles. RQ3, unlike Q3+, has a greater tendency to underestimate than to overestimate, but the two methods have similar error measures. A comparison of RL3 and L3+B (or L3+C) histograms leads to the same conclusions, with the former method's profile having a somewhat sharper appearance. The approximately renormalized methods are efficient and accurate alternatives to the three explicitly renormalized ones.

The results obtained with non-diagonal self-energies and IP-EOM-CCSD in the last two rows complete Fig. 3. The widely scattered results of 2ph-TDA are better than those of ND2, but they are hardly worth their additional computational effort. The broad profiles of 3+ and ADC(3) procure no advantage over OVGF-A but require considerably greater arithmetic work. An excellent compromise of accuracy and efficiency is realized in NR2 calculations at a cost that is often comparable to that of the preceding integral transformation (i.e., non-iterative O^3V^3 vs N_B^5). Even better data are obtained when BD-T1, the only present method that employs non-HF orbitals, is employed. The profile of BD-T1 resembles a tight Gaussian curve centered at 0.1 eV. The IP-EOM-CCSD histogram has error criteria that are close to those of NR2. NR2, BD-T1, and IP-EOM-CCSD have a greater tendency to overestimate than to underestimate VIEs, the ability to generate DOs that are not proportional to HF orbitals, and only slightly better error measures than those of the L3+B and L3+C diagonal self-energy methods.

The diagonal os-nD-D2 self-energy includes the largest terms for opposite-spin orbital relaxation and final-state correlation induced by the additional vacancy in the diagonal index's spin-orbital. It also includes an MP2 description of the opposite-spin pair correlation in the initial state that is absent in the final state. The P3, Q3, and L3 self-energies add terms of second and third orders. P3+ and RP3 provide renormalized descriptions of final-state relaxation and correlation by including 2hp ring-ladder terms with exchange. Q3+ and RQ3 further add response corrections to Koopmans results arising from occupied–virtual blocks of the density matrix. L3+ and RL3 include renormalized corrections for initial-state pair correlation energies beyond the MP2 level.

CONCLUSIONS

Tests of diagonal self-energy approximations in calculations of valence VIEs of closed-shell molecules have been performed. All self-energies except those of BD-T1 employ HF orbitals, and all are free of adjustable parameters. Among these methods are the well-known D2, D3, OVGF, P3, and P3+ approximations of electron propagator theory that require evaluation of second-order and third-order self-energy terms. A version of G_0W_0 based on HF orbitals and Tamm–Dancoff (single-replacement configuration interaction) excitations has also been examined. Two methods that again require only second-order and third-order self-energy terms, Q3 and L3, have been introduced. A computationally trivial pair of approximate renormalizations that build on these methods is present in the Q3+ and L3+ methods. In addition, the RP3, RQ3, and RL3 self-energies involve explicit evaluation of higher-order terms (as in the G_0W_0 family of methods), thereby extending P3, Q3, and L3 and competing, respectively, with P3+, Q3+, and L3+.

Statistical measures of errors with respect to the results of almost full-configuration-interaction quality in the cc-pVTZ basis have been assembled for VIEs of closed-shell molecules. These results, arithmetic scaling factors, and storage requirements are criteria of utility for the methods under study. From this evidence, the following conclusions follow:

- The os-D2 and os-nD-D2 methods drastically reduce the MAE of canonical HF orbital energies from over 1 to ~0.2–0.3 eV at essentially no cost after a partial transformation of electron repulsion integrals to the HF basis. There is no advantage in performing D2 or nD-D2 calculations, which usually exaggerate the correction to Koopmans results. The best of these cubically scaling methods is os-nD-D2, for it is the most accurate and efficient one.
- Two post-second-order alternatives offer distinct advantages. HF-TDA G_0W_0 and Q3+ have O^2V^3 arithmetic bottlenecks, but the former method performs many iterations of such fifth-power contractions. Whereas it is less accurate than Q3+ by ~0.1 eV, it does not require transformed electron repulsion integrals with three virtual indices. (The latter disadvantage of Q3+ could be overcome with a semi-direct algorithm for the lone matrix multiplication that involves transformed electron repulsion integrals with three virtual orbital indices.) The Q3+ MAE is ~0.12 eV.
- An additional advantage in accuracy over HF-TDA G_0W_0 (MAE = 0.20 eV) is also provided by RQ3 (MAE = 0.10 eV), which explicitly evaluates higher-order terms.
- RL3 is the most accurate of the diagonal self-energies, with its MAE below 0.1 eV. It is more efficient and accurate than several non-diagonal methods, including 3+ and ADC(3), and is a competitive alternative to non-diagonal self-energy methods, such as NR2 and BD-T1, and to IP-EOM-CCSD.
- All P3, Q3, and L3 calculations should be followed immediately by computationally trivial P3+, Q3+, and L3+ improvements, which provide fast and accurate approximations to RP3, RQ3, and RL3.
- The OVGF methods are slower and less accurate than Q3+ and P3+. Q3+ has a lower MAE than P3+, and its additional terms have the same arithmetic scaling as the bottleneck steps of P3+.
- For the calculation of valence IEs, the most competitive non-diagonal methods, which remain useful for determining DOs despite their sixth-power arithmetic scaling, are NR2 and BD-T1. Older non-diagonal methods, such as ND2, 2ph-TDA, 3+, and ADC(3), have exhibited no practical advantages of accuracy or efficiency in the present tests on VIEs.
- The following hierarchy of increasing accuracy (indicated by inequalities) accompanied by decreasing efficiency is indicated by the present results: os-nD-D2 < Q3+ < RQ3 < L3+ < RL3. These methods are the best compromises of accuracy, efficiency, and feasibility.

Data that underlie these conclusions are summarized in Figs. 1–3. The new approximations require only minor modifications to the existing programs that perform D2, OVGF, P3+, or ADC(3) calculations. To disclose whether the present trends persist for more

Published under an exclusive license by AIP Publishing

flexible basis sets, alternative sets of benchmark data, and larger molecules, additional calculations are in progress, as are straightforward extensions to electron attachment energies.

SUPPLEMENTARY MATERIAL

See the supplementary material for the results of calculations on IEs.

ACKNOWLEDGMENTS

This work was supported by Grant No. CHE-1565760 to Auburn University. The authors thank Manuel Díaz Tinoco and Héctor Hernández Corzo for valuable discussions and technical support and the Alabama Supercomputer Center for computing resources.

AUTHOR DECLARATIONS

Conflict of Interest

The authors have no conflicts to disclose.

DATA AVAILABILITY

The data that support the findings of this study are available within the article and its supplementary material.

REFERENCES

[1] J. Linderberg and Y. Öhrn, *Propagators in Quantum Chemistry*, 2nd ed. (Wiley-Interscience, Hoboken, NJ, 2004).
[2] P. Jørgensen and J. Simons, *Second Quantization-Based Methods in Quantum Chemistry* (Academic Press, New York, 1981).
[3] J. Schirmer, *Many-Body Methods for Atoms, Molecules and Clusters* (Springer International Publishing AG, 2018).
[4] J. V. Ortiz, "Dyson-orbital concepts for description of electrons in molecules," J. Chem. Phys. **153**(7), 070902 (2020).
[5] J. V. Ortiz, "Concepts of chemical bonding from electron propagator theory," AIP Conf. Proc. **1456**, 73–80 (2012).
[6] J. V. Ortiz, "Electron propagator theory: An approach to prediction and interpretation in quantum chemistry," Wiley Interdiscip. Rev.: Comput. Mol. Sci. **3**(2), 123–142 (2013).
[7] J. V. Ortiz, "Chapter four—Interpreting bonding and spectra with correlated, one-electron concepts from electron propagator theory," Annu. Rep. Comput. Chem. **13**, 139–182 (2017).
[8] H. H. Corzo and J. V. Ortiz, "Chapter thirteen—Electron propagator theory: Foundations and predictions," Adv. Quantum Chem. **74**, 267–298 (2017).
[9] T. Koopmans, "Über die zuordnung von wellenfunktionen und eigenwerten zu den einzelnen elektronen eines atoms," Physica **1**(1–6), 104–113 (1934).
[10] M. Díaz-Tinoco, H. H. Corzo, F. Pawłowski, and J. V. Ortiz, "Do Dyson orbitals resemble canonical Hartree–Fock orbitals?," Mol. Phys. **117**(17), 2275–2283 (2019).
[11] L. S. Cederbaum and W. Domcke, "Theoretical aspects of ionization potentials and photoelectron spectroscopy: A Green's function approach," Adv. Chem. Phys. **36**, 205–344 (1977).
[12] W. von Niessen, J. Schirmer, and L. S. Cederbaum, "Computational methods for the one-particle Green's function," Comput. Phys. Rep. **1**, 57–125 (1984).
[13] J. V. Ortiz, "The electron propagator picture of molecular electronic structure," Comput. Chem. **2**, 1–61 (1997).
[14] T. Körzdörfer and N. Marom, "Strategy for finding a reliable starting point for G_0W_0 demonstrated for molecules," Phys. Rev. B **86**(4), 041110 (2012).
[15] L. Gallandi, N. Marom, P. Rinke, and T. Körzdörfer, "Accurate ionization potentials and electron affinities of acceptor molecules II: Non-empirically tuned long-range corrected hybrid functionals," J. Chem. Theory Comput. **12**(2), 605–614 (2016).
[16] J. W. Knight, X. Wang, L. Gallandi, O. Dolgounitcheva, X. Ren, J. V. Ortiz, P. Rinke, T. Körzdörfer, and N. Marom, "Accurate ionization potentials and electron affinities of acceptor molecules III: A benchmark of GW methods," J. Chem. Theory Comput. **12**(2), 615–626 (2016).
[17] L. S. Cederbaum, "One-body Green's function for atoms and molecules. Theory and application," J. Phys. B: At. Mol. Phys. **8**, 290–303 (1975).
[18] J. V. Ortiz, "Partial third-order quasiparticle theory: Comparisons for closed-shell ionization energies and an application to the Borazine photoelectron spectrum," J. Chem. Phys. **104**(19), 7599–7605 (1996).
[19] A. M. Ferreira, G. Seabra, O. Dolgounitcheva, V. G. Zakrzewski, and J. V. Ortiz, "Application and testing of diagonal, partial third-order electron propagator approximations," in *Quantum-Mechanical Prediction of Thermochemical Data*, edited by J. Cioslowski (Springer Netherlands, Dordrecht, 2001), pp. 131–160.
[20] J. V. Ortiz, "An efficient, renormalized self-energy for calculating the electron binding energies of closed-shell molecules and anions," Int. J. Quantum Chem. **105**(6), 803–808 (2005).
[21] A. Pérez-González, A. Galano, and J. V. Ortiz, "Vertical ionization energies of free radicals and electron detachment energies of their anions: A comparison of direct and indirect methods versus experiment," J. Phys. Chem. A **118**(31), 6125–6131 (2014).
[22] H. H. Corzo, A. Galano, O. Dolgounitcheva, V. G. Zakrzewski, and J. V. Ortiz, "NR2 and P3+: Accurate, efficient electron-propagator methods for calculating valence, vertical ionization energies of closed-shell molecules," J. Phys. Chem. A **119**(33), 8813–8821 (2015).
[23] M. Díaz-Tinoco, H. H. Corzo, and J. V. Ortiz, "Electron propagator methods for vertical electron detachment energies of anions: Benchmarks and case studies," J. Chem. Theory Comput. **14**(11), 5881–5895 (2018).
[24] O. Dolgounitcheva, M. Díaz-Tinoco, V. G. Zakrzewski, R. M. Richard, N. Marom, C. D. Sherrill, and J. V. Ortiz, "Accurate ionization potentials and electron affinities of acceptor molecules IV: Electron-propagator methods," J. Chem. Theory Comput. **12**(2), 627–637 (2016).
[25] V. G. Zakrzewski, J. V. Ortiz, J. A. Nichols, D. Heryadi, D. L. Yeager, and J. T. Golab, "Comparison of perturbative and multiconfigurational electron propagator methods," Int. J. Quantum Chem. **60**(1), 29–36 (1996).
[26] J. V. Ortiz, V. G. Zakrzewski, and O. Dolgounitcheva, "One-electron pictures of electronic structure: Propagator calculations on photoelectron spectra of aromatic molecules," in Conceptual Perspectives in Quantum Chemistry, edited by J.-L. Calais and E. S. Kryachko (Kluwer, Dordrecht, 1997), Vol. 3, pp. 465–517.
[27] L. Reining, "The GW approximation: Content, successes and limitations," Wiley Interdiscip. Rev.: Comput. Mol. Sci. **8**(3), e1344 (2018).
[28] J. Schirmer, L. S. Cederbaum, and O. Walter, "New approach to the one-particle Green's function for finite Fermi systems," Phys. Rev. A **28**(3), 1237–1259 (1983).
[29] I. Tamm, "Relativistic interaction of elementary particles," J. Phys. USSR **9**, 449 (1945).
[30] S. M. Dancoff, "Non-adiabatic meson theory of nuclear forces," Phys. Rev. **78**(4), 382–385 (1950).
[31] J. Schirmer and L. S. Cederbaum, "The two-particle-hole Tamm-Dancoff approximation (2ph-TDA) equations for closed-shell atoms and molecules," J. Phys. B: At. Mol. Phys. **11**, 1889–1900 (1978).
[32] S. J. Bintrim and T. C. Berkelbach, "Full-frequency GW without frequency," J. Chem. Phys. **154**(4), 041101 (2021).
[33] J. Schirmer, A. B. Trofimov, and G. Stelter, "A non-Dyson third-order approximation scheme for the electron propagator," J. Chem. Phys. **109**(12), 4734–4744 (1998).
[34] C.-H. Hu, D. P. Chong, and M. E. Casida, "The parametrized second-order Green function times screened interaction (pGW2) approximation for calculation of outer valence ionization potentials," J. Electron Spectrosc. Relat. Phenom. **85**(1–2), 39–46 (1997).

Published under an exclusive license by AIP Publishing

[35]F.-H. Lim, M. Nishida, Y. Hori, T. Ida, and M. Mizuno, "Optimization of the spin-component-scaled factor for electron propagator method," Chem. Phys. Lett. **678**, 159–166 (2017).
[36]J. Romero, J. A. Charry, H. Nakai, and A. Reyes, "Improving quasiparticle second order electron propagator calculations with the spin-component-scaled technique," Chem. Phys. Lett. **591**, 82–87 (2014).
[37]S. Śmiga and I. Grabowski, "Spin-component-scaled ΔMP2 parametrization: Toward a simple and reliable method for ionization energies," J. Chem. Theory Comput. **14**(9), 4780–4790 (2018).
[38]K. Raghavachari, G. W. Trucks, J. A. Pople, and M. Head-Gordon, "A fifth-order perturbation comparison of electron correlation theories," Chem. Phys. Lett. **157**(6), 479–483 (1989).
[39]R. M. Richard, M. S. Marshall, O. Dolgounitcheva, J. V. Ortiz, J.-L. Brédas, N. Marom, and C. D. Sherrill, "Accurate ionization potentials and electron affinities of acceptor molecules I. Reference data at the CCSD(T) complete basis set limit," J. Chem. Theory Comput. **12**(2), 595–604 (2016).
[40]R. J. Bartlett, "Coupled-cluster theory and its equation-of-motion extensions," Wiley Interdiscip. Rev.: Comput. Mol. Sci. **2**(1), 126–138 (2012).
[41] D. S. Ranasinghe, J. T. Margraf, A. Perera, and R. J. Bartlett, "Vertical valence ionization potential benchmarks from equation-of-motion coupled cluster theory and QTP functionals," J. Chem. Phys. **150**(7), 074108 (2019).
[42]J. F. Stanton and J. Gauss, "Analytic energy derivatives for ionized states described by the equation-of-motion coupled cluster method," J. Chem. Phys. **101**(10), 8938–8944 (1994).
[43]T. H. Dunning, "Gaussian basis sets for use in correlated molecular calculations. I. The atoms boron through neon and hydrogen," J. Chem. Phys. **90**(2), 1007–1023 (1989).
[44]R. Manne, "A completeness theorem for operator spaces," Chem. Phys. Lett. **45**(3), 470–472 (1977).
[45]P. O. Löwdin, "Studies in perturbation theory. X. Lower bounds to energy eigenvalues in perturbation-theory ground state," Phys. Rev. **139**(2A), A357–A372 (1965).
[46]C. Møller and M. S. Plesset, "Note on an approximation treatment for many-electron systems," Phys. Rev. **46**(7), 618–622 (1934).
[47]S. Hirata, M. R. Hermes, J. Simons, and J. V. Ortiz, "General-order many-body Green's function method," J. Chem. Theory Comput. **11**(4), 1595–1606 (2015).
[48]S. Hirata, A. E. Doran, P. J. Knowles, and J. V. Ortiz, "One-particle many-body Green's function theory: Algebraic recursive definitions, linked-diagram theorem, irreducible-diagram theorem, and general-order algorithms," J. Chem. Phys. **147**(4), 044108 (2017).
[49]D. P. Chong, F. G. Herring, and D. McWilliams, "Perturbation corrections to Koopmans' theorem. I. Double-zeta Slater-type-orbital basis," J. Chem. Phys. **61**(1), 78–84 (1974).
[50]J. Schirmer and G. Angonoa, "On Green's function calculations of the static self-energy part, the ground state energy, and expectation values," J. Chem. Phys. **91**, 1754–1761 (1989).
[51] A. B. Trofimov and J. Schirmer, "Molecular ionization energies and ground- and ionic-state properties using a non-Dyson electron propagator approach," J. Chem. Phys. **123**(14), 144115 (2005).
[52]A. L. Dempwolff, M. Schneider, M. Hodecker, and A. Dreuw, "Efficient implementation of the non-Dyson third-order algebraic diagrammatic construction approximation for the electron propagator for closed- and open-shell molecules," J. Chem. Phys. **150**(6), 064108 (2019).
[53]S. Banerjee and A. Y. Sokolov, "Third-order algebraic diagrammatic construction theory for electron attachment and ionization energies: Conventional and Green's function implementation," J. Chem. Phys. **151**(22), 224112 (2019).
[54]S. Banerjee and A. Y. Sokolov, "Efficient implementation of the single-reference algebraic diagrammatic construction theory for charged excitations: Applications to the TEMPO radical and DNA base pairs," J. Chem. Phys. **154**(7), 074105 (2021).
[55]J. V. Ortiz, "A nondiagonal, renormalized extension of partial third-order quasiparticle theory: Comparisons for closed-shell ionization energies," J. Chem. Phys. **108**, 1008–1014 (1998).
[56]L. Storchi, G. Vitillaro, and F. Tarantelli, "Implementation and use of a direct, partially integral-driven non-Dyson propagator method for molecular ionization," J. Comput. Chem. **30**(5), 818–825 (2009).
[57]M. Nooijen and J. G. Snijders, "Second order many-body perturbation approximations to the coupled cluster Green's function," J. Chem. Phys. **102**(4), 1681–1688 (1995).
[58]J. F. Stanton and J. Gauss, "Perturbative treatment of the similarity transformed Hamiltonian in equation-of-motion coupled-cluster approximations," J. Chem. Phys. **103**(3), 1064–1076 (1995).
[59]M. D. Prasad, S. Pal, and D. Mukherjee, "Some aspects of self-consistent propagator theories," Phys. Rev. A **31**(3), 1287–1298 (1985).
[60]M. J. Frisch, G. W. Trucks, H. B. Schlegel, G. E. Scuseria, M. A. Robb, J. R. Cheeseman, G. Scalmani, V. Barone, G. A. Petersson, H. Nakatsuji, X. Li, M. Caricato, A. V. Marenich, J. Bloino, B. G. Janesko, R. Gomperts, B. Mennucci, H. P. Hratchian, J. V. Ortiz, A. F. Izmaylov, J. L. Sonnenberg, D. Williams-Young, F. Ding, F. Lipparini, F. Egidi, J. Goings, B. Peng, A. Petrone, T. Henderson, D. Ranasinghe, V. G. Zakrzewski, J. Gao, N. Rega, G. Zheng, W. Liang, M. Hada, M. Ehara, K. Toyota, R. Fukuda, J. Hasegawa, M. Ishida, T. Nakajima, Y. Honda, O. Kitao, H. Nakai, T. Vreven, K. Throssell, J. A. Montgomery, Jr., J. E. Peralta, F. Ogliaro, M. J. Bearpark, J. J. Heyd, E. N. Brothers, K. N. Kudin, V. N. Staroverov, T. A. Keith, R. Kobayashi, J. Normand, K. Raghavachari, A. P. Rendell, J. C. Burant, S. S. Iyengar, J. Tomasi, M. Cossi, J. M. Millam, M. Klene, C. Adamo, R. Cammi, J. W. Ochterski, R. L. Martin, K. Morokuma, O. Farkas, J. B. Foresman, and D. J. Fox, Gaussian Development Version, Revision I.14, Gaussian, Inc., Wallingford, CT, 2018.
[61] J. V. Ortiz, "Electron detachment energies of closed-shell anions calculated with a renormalized electron propagator," Chem. Phys. Lett. **296**(5), 494–498 (1998).
[62]J. V. Ortiz, "Single-reference electron propagator calculations on vertical ionization energies of ozone," Chem. Phys. Lett. **297**(3), 193–199 (1998).
[63]J. V. Ortiz, "Approximate Brueckner orbitals and shakeup operators in electron propagator calculations: Applications to F^- and OH^-," Int. J. Quantum Chem. **70**(4/5), 651–658 (1998).
[64]J. V. Ortiz, "Orbital and shakeup operator renormalizations in electron propagator theory," J. Chem. Phys. **109**, 5741–5746 (1998).
[65]J. V. Ortiz, "Approximate Brueckner orbitals in electron propagator calculations," Int. J. Quantum Chem. **75**(4–5), 615–621 (1999).
[66]J. Baker and B. T. Pickup, "A method for molecular ionization potentials," Chem. Phys. Lett. **76**, 537–541 (1980).
[67]J. Baker, "EOM/propagator ionization potentials: Prediction of complete valence-shell ionization spectra using direct diagonalization," Chem. Phys. Lett. **101**(2), 136–140 (1983).
[68]V. G. Zakrzewski and J. V. Ortiz, "Semidirect algorithms in electron propagator calculations," Int. J. Quantum Chem. **52**, 23–27 (1994), part of the Special Issue: Proceedings of the International Symposium on Atomic, Molecular, and Condensed Matter Theory and Computational Methods.
[69]V. G. Zakrzewski and J. V. Ortiz, "Semidirect algorithms for third-order electron propagator calculations," Int. J. Quantum Chem. **53**(6), 583–590 (1995).
[70]F. Pawłowski, J. Olsen, and P. Jørgensen, "Cluster perturbation theory. I. Theoretical foundation for a coupled cluster target state and ground-state energies," J. Chem. Phys. **150**(13), 134108 (2019).
[71] F. Pawłowski, J. Olsen, and P. Jørgensen, "Cluster perturbation theory. II. Excitation energies for a coupled cluster target state," J. Chem. Phys. **150**(13), 134109 (2019).
[72]P. Baudin, F. Pawłowski, D. Bykov, D. Liakh, K. Kristensen, J. Olsen, and P. Jørgensen, "Cluster perturbation theory. III. Perturbation series for coupled cluster singles and doubles excitation energies," J. Chem. Phys. **150**(13), 134110 (2019).
[73]F. Pawłowski, J. Olsen, and P. Jørgensen, "Cluster perturbation theory. IV. Convergence of cluster perturbation series for energies and molecular properties," J. Chem. Phys. **150**(13), 134111 (2019).
[74]F. Pawłowski, J. Olsen, and P. Jørgensen, "Cluster perturbation theory. V. Theoretical foundation for cluster linear target states," J. Chem. Phys. **150**(13), 134112 (2019).

Published under an exclusive license by AIP Publishing

Appendix C

E. Opoku, F. Pawłowski and J. V. Ortiz, "A New Generation of Non−diagonal, Renormalized Self−Energies for Calculation of Electron Removal Energies", *J. Chem. Phys.*, 159, 124109 (2023)

The Journal of Chemical Physics ARTICLE pubs.aip.org/aip/jcp

A new generation of non-diagonal, renormalized self-energies for calculation of electron removal energies

Cite as: J. Chem. Phys. **159**, 1241 09 (2023); doi: 1 0.1 063/5.01 68779
Submitted: 20 July 2023 • Accepted: 6 September 2023 •
Published Online: 26 September 2023

View Online Export Citation CrossMark

Ernest Opoku, Filip Pawłowski, and J. V. Ortiz[a)]

AFFILIATIONS

Department of Chemistry and Biochemistry, Auburn University, Auburn, Alabama 36849-5312, USA

[a)]Author to whom correspondence should be addressed: ortiz@auburn.edu

ABSTRACT

A new generation of diagonal self-energies for the calculation of electron removal energies of molecules and molecular ions that has superseded its predecessors with respect to accuracy, efficiency, and interpretability is extended to include non-diagonal self-energies that permit Dyson orbitals to be expressed as linear combinations of canonical Hartree–Fock orbitals. In addition, an improved algorithm for renormalized methods eliminates the convergence difficulties encountered in the first studies of the new, diagonal self-energies. A dataset of outer-valence, vertical ionization energies with almost full-configuration-interaction quality serves as a standard of comparison in numerical tests. The new non-diagonal, renormalized methods are slightly more accurate than their diagonal counterparts, with mean absolute errors between 0.10 and 0.06 eV for outer-valence final states. This advantage is procured at the cost of an increase in the scaling of arithmetic bottlenecks that accompany the inclusion of non-diagonal self-energy terms. The new, non-diagonal, renormalized self-energies are also more accurate and efficient than their non-diagonal predecessors.

Published under an exclusive license by AIP Publishing. https://doi.org/10.1063/5.0168779

14 April 2025 23:46:53

INTRODUCTION

Ionization energies (IEs) are among the most fundamental and widely sought-after properties of molecules. Practical theories of these and other kinds of electron binding energies may be judged according to their *predictive accuracy*, *computational efficiency*, and *interpretive clarity*. Canonical Hartree–Fock (HF) orbital energies and Koopmans's identity[1] provide a foundation for fulfillment of the second and third criteria, but satisfaction of the first criterion remains elusive for this level of theory. The appealing interpretive transparency of Koopmans's identity is accompanied by qualitative concepts that are inapplicable when orbitals are allowed to relax in final states[2] and electron correlation is *not* ignored.[3–6] Among these pitfalls are Dyson orbitals with:

- either unit or vanishing probability factors (i.e., norms of Dyson orbitals),
- vanishing occupation numbers in final states, and
- vanishing overlaps with their counterparts from different final states.

Quantitatively inaccurate predictions based on canonical Hartree–Fock (CHF) orbital energies may also yield qualitative defects in the ordering and, therefore, the spectral assignment of final states observed in photo-ionization and electron-detachment experiments. Such difficulties may manifest as incorrect sequences of final-state irreducible representations or, in the case of the simpler point groups, scrambling of Dyson orbitals with the same irreducible representation but chemically distinct amplitudes (e.g., localizations on different ligands in polynuclear coordination complexes,[7–9] base vs phosphate localizations in nucleotides[10,11]).

Remedies for the quantitative and qualitative deficiencies of predictions based on Koopmans's identity may be provided by indirect or direct procedures. The *indirect* approach requires the subtraction of the total energies of initial states with N electrons from their final-state counterparts with N − 1 electrons. Dyson orbitals are evaluated as scaled overlaps between initial-state and final-state wavefunctions. The *direct* calculation of electron binding energies and Dyson orbitals can be realized by diagonalizing an effective Hamiltonian matrix in a space of operators that change the

TABLE I. Acronyms for electron propagator self-energies.

Acronym[a]	Full name
	Diagonal self-energies
D2	Diagonal second order
os-D2	Opposite-spin D2
nD-D2	Non-Dyson D2
os-nD-D2	Opposite-spin non-Dyson D2
D3	Diagonal third order
nD-D3	Non-Dyson D3
OVGF	Outer-valence Green's function (versions A, B, and C)
nD-OVGF	Non-Dyson OVGF (versions A, B, and C)
P3	Partial third order
P3+	Approximately renormalized partial third order
Q3	Quasiparticle third order
Q3+	Approximately renormalized quasiparticle third order
L3	Linear third order
nD-L3	Non-Dyson L3
L3+	Approximately renormalized linear third order (versions A, B, and C)
nD-L3+	Non-Dyson L3+ (versions A, B, and C)
RP3	Explicitly renormalized partial third order
RQ3	Explicitly renormalized quasiparticle third order
RL3	Explicitly renormalized linear third order
nD-RL3	Non-Dyson RL3
DR	Diagonal (renormalized) ring approximation (HF-TDA-G_0W_0)
	Non-diagonal self-energies
ND2	Non-diagonal, second order
2ph-TDA	Two-particle-one-hole Tamm–Dancoff approximation
3+	Non-diagonal third order
ADC(3)	Third order algebraic diagrammatic construction
NR2	Non-diagonal, renormalized, second order
BD-T1	Brueckner doubles with triple field operators
NRP3	Non-diagonal extension of RP3
NRQ3	Non-diagonal extension of RQ3
NRL3	Non-diagonal extension of RL3

[a]For new-generation methods in **bold type:** N = non-diagonal; nD = non-Dyson; R = renormalized; and + = approximately renormalized.

number of electrons by one. The latter category includes wavefunction (Hilbert space) methods, such as equation-of-motion coupled-cluster (EOM-CC) theory[12] and non-Dyson (nD) propagators,[13] and Fock-space (i.e., graded Hilbert space) methods, such as the GW family of self-energies[14] and electron-propagator approaches.[3,15–20] The Fock-space alternatives bypass many-electron wavefunctions for final states and employ the Dyson equation, whose solutions pertain to energies of electron attachment in addition to energies of electron removal.

Practical procedures based on the Dyson equation for the calculation of vertical ionization energies (VIEs) of molecules (i.e., where final state nuclei do not relax from initial state positions) are the primary concern of this work. The historical progression of electron-propagator self-energy approximations is represented by the wealth of methods and acronyms presented in Table I. (Approaches that are based on multi-configurational, self-consistent-field wavefunctions are not considered.[21–23]) When the zeroth order electron propagator is defined with CHF orbitals and energies, the first order self-energy corrections vanish. The non-diagonal second order (ND2) self-energy[24] usually provides the largest corrections to Koopmans results. (Acronyms with N denote non-diagonal self-energies in the bottom sector of Table I.) For the lowest VIEs of closed-shell molecules, the diagonal second order (D2) simplification (i.e., where off-diagonal elements of the ND2 self-energy matrix in the CHF basis are ignored) introduces changes that are small in comparison with the quantitative errors inherent in ND2. (Several parameterized modifications of D2 have been introduced,[25–28] but they will not be considered in this work.) Much larger are the changes that follow from the inclusion of diagonal third order terms in the D3 approximation.[29] Whereas D2 tends to overestimate corrections to

Published under an exclusive license by AIP Publishing

CHF orbital energies (resulting in VIE predictions that are too low), D3 has the opposite tendency.[30] (Formulas for second and third order Rayleigh–Schrödinger perturbation theory, or RSPT2 and RSPT3,[31–33] may be recovered by inserting the Koopmans energy into the D2 and D3 self-energies.[34,35]) The renormalized estimates of the three outer-valence Green function methods (OVGF versions A, B, and C) typically fall between D2 and D3 results.[36] These approximate renormalization schemes depend on ratios of second order and third order self-energy terms and involve only trivial calculations. A selection scheme that relies on several numerical parameters has been employed to make an optimal choice among the three versions.[37] As in previous tests, we avoided procedures with adjustable parameters and examined separate data for the three versions of OVGF. The underestimating tendency of D2 and nD-D2 may be systematically reduced by including only opposite-spin (os) self-energy contributions in the os-D2 and os-nD-D2 methods.[11,38,39] Another diagonal option in wide use is the approximately renormalized, partial third order (P3+) self-energy, which enjoys the advantages of higher accuracy and lower arithmetic scaling with respect to D3 and the OVGF methods.[30,40–42] The G_0W_0 members of the GW family of methods (which all include infinite order summations of ring diagrams, usually without exchange terms) are defined by the diagonal self-energy approximation and the absence of self-consistency in the reference orbitals and the effective interactions.[14,43–46] These methods are most often implemented without energy iterations (i.e., variations with respect to E) in the Dyson equation. An *ab initio* variant that is based on CHF orbitals and Tamm–Dancoff[47,48] (configuration interaction with single replacements) excitations,[49] denoted by the long acronym HF-TDA-G_0W_0 in our previous studies,[11,38,39] is currently relabeled as the diagonal ring (DR) method. Unlike the majority of G_0W_0 methods in widespread use, DR avoids Kohn–Sham orbitals and performs self-consistent energy iterations in the Dyson quasiparticle equation. The diagonal self-energy matrix elements of DR are related to their counterparts in the two-particle-one-hole Tamm–Dancoff approximation (2ph-TDA)[50] by their neglect of ladder and ring-exchange terms.

The D2, D3, OVGF, P3+, and G_0W_0 methods make the diagonal approximation in the self-energy matrix, but the 2ph-TDA,[50] the third order algebraic diagrammatic construction, or ADC(3), family of methods,[51] the non-diagonal renormalized second order (NR2) approximation,[30,52] and the Brueckner Doubles[53–58] triple field operator (BD-T1) method[59–62] do not. The retention of the first order couplings between triple field operators in 2ph-TDA yields ring and ladder terms in all orders and retains all second order terms in the self-energy. After adding further perturbative corrections to couplings between simple and triple field operator products (now often known as vertex corrections) and third order constant (E-independent) terms, the 3+ method, which includes all terms present in 2ph-TDA, is defined. This method is also known as the strict version of ADC(3). (The second order version of ADC is equivalent to ND2.) The Schirmer–Angonoa renormalization of the constant terms (which are correct through the fourth order) is employed in the standard Dyson version of ADC(3).[63] The set of non-Dyson versions of ADC(3) includes the counterpart of 3+ (i.e., the strict version) and methods that retain all fourth order constant terms.[64,65] A fourth order ADC method that involves quintuple field operator products, ground-state wavefunction amplitudes up to third order, and seventh-power arithmetic scaling has also been implemented.[51,66] The non-diagonal renormalized second order (NR2) method improves on ND2 with infinite order 2hp ring and ladder terms and second order couplings between h and 2hp operators. All non-diagonal methods considered presently are based on CHF orbitals except the BD-T1 approximation, which includes couplings between operators through first order in the BD double replacement amplitudes except those between 2hp and 2ph operators.

The mean absolute errors (MAEs) of Koopmans's identity for valence VIEs of closed-shell molecules (1–2 eV) may be reduced by an order of magnitude with a new generation of diagonal approximations to the self-energy matrix of electron-propagator theory.[38,39] In so doing, these methods introduce no arithmetic bottlenecks that scale more sharply with the size of the system than those found in the quintically scaling, partial integral transformation of the usual algorithm of second order perturbation theory. Several of these methods are practically effortless once the transformation is complete. The foundation of this remarkable efficiency is the diagonal self-energy approximation, wherein off-diagonal elements of the self-energy matrix in the CHF orbital basis are set to zero. Another consequence of the diagonal approximation is the proportionality of Dyson orbitals to CHF orbitals, where the ratio equals the square-root of the probability factor (also known as the pole strength). The emergent picture of electron detachment is that of an unaltered CHF orbital subjected to the relaxation-correlation potential of a diagonal self-energy matrix element. Recent tests (see Table II) of diagonal self-energy methods vs a set of standard data whose quality approaches that of full configuration interaction (FCI) established the superiority of the newly introduced methods.[38] (MAEs with respect to these standard data are denoted by the Quantum Theory Project, or QTP, acronym in Table II because they were introduced during the production of the eponymous series of density functionals[67] with optimized Kohn–Sham orbital energies.) The opposite-spin, non-Dyson, second order (os-nD-D2) self-energy generated MAEs of ~0.2 eV with only cubic arithmetic scaling. The third order, approximately-renormalized, quasiparticle (Q3+) self-energy reduced the MAEs to ~0.15 eV with an O^2V^3 arithmetic bottleneck (where O and V are the dimensions of the occupied and virtual orbital spaces, see Table III) that remains far lower than that of the partial integral transformation that preceded it. (Similar performance was realized with the previously developed P3+ self-energy.) Even greater accuracy, where the MAE is ~0.1 eV, is attained by the approximately renormalized, linear, third order version B (L3+B) self-energy with an OV^4 bottleneck. The explicitly renormalized versions of the two latter methods, RQ3 and RL3, exhibit slight reductions in their error measures with respect to their approximately renormalized counterparts. Lower accuracy for a given level of arithmetic effort characterizes several antecedents, including D2 (OV^2 scaling, MAE = 0.6 eV), the A version of OVGF (OV^4 scaling, MAE = 0.2 eV), and DR (O^2V^3 scaling, MAE = 0.2 eV). Error measures for the new methods increase slightly when the more chemically diverse GW100 standard is employed.[39] This set of 100 VIEs is confined to the lowest VIEs of 100 species that include nuclei from the third and higher periods. Inherent errors in the GW100 benchmark's ΔCCSD(T) data probably exceed 0.14 eV.[68]

Whereas the foundation of the efficiency of the new methods is the diagonal approximation, an important pillar of their

Published under an exclusive license by AIP Publishing

TABLE II. Arithmetic scaling factors and mean absolute errors (eV) for diagonal self-energy methods.

Self-energy[a]	Scaling[b]	QTP[c] MAE (eV)	GW100[d] MAE (eV)
Koopmans		1.42	0.65
D2	OV^2	0.63	0.51
os-nD-D2	OV^2	0.23	0.18
P3+	O^2V^3	0.13	0.14
Q3+	O^2V^3	0.12	0.15
L3+B	OV^4	0.09	0.10
OVGF-A	OV^4	0.19	0.16
DR	O^2V^3	0.20	0.23
RP3	O^2V^3	0.12	0.16
RQ3	O^2V^3	0.10	0.17
RL3	OV^4	0.08	0.10

[a]**bold type** denotes new methods.
[b]O = number of valence occupied orbitals; V = number of valence virtual orbitals.
[c]80 VIEs.[38] MAE = mean absolute error.
[d]100 VIEs.[39] MAE = mean absolute error.

accuracy is renormalization. The inclusion of ring and ladder self-energy diagrams in all orders of the fluctuation potential may be accomplished approximately (through the evaluation of ratios of second order and third order terms) or explicitly. The former option requires practically no additional effort and produces MAEs that are only trivially worse than those produced by their explicitly renormalized counterparts. This conclusion was reached by comparing approximately and explicitly renormalized methods (e.g., L3+B vs RL3 in Table II) for those cases in which the infinite-order calculation converged.[38] Unfortunately, many cases in the original set of standard data had to be excluded because explicit, order-by-order summations failed to converge for some higher VIEs. To consolidate the characterization of the new methods, a more robust algorithm (*vide infra*) for diagonal, explicitly renormalized methods is desirable.

Non-diagonal self-energy approximations are needed to obtain Dyson orbitals in their general form, a linear combination of reference (e.g., HF) orbitals.[4] Because increased flexibility in the determination of Dyson orbitals does not necessarily entail more accurate VIEs, numerical tests of diagonal, renormalized self-energies, and closely related non-diagonal extensions will be conducted presently. To amplify the number of calculated VIEs that may be compared, a new algorithm has been developed for the evaluation of infinite-order summations required by diagonal, explicitly renormalized self-energies.

As in previous studies, no adjustable parameters are employed in the generation of molecular orbitals or in the derivation of self-energy formulas that pertain to any of the methods under consideration, for we regard the third criterion of this Introduction's first paragraph to be as important as the first two, especially when novel, unprecedented molecules or molecular ions are under consideration.

THEORY

Exact and approximate electron propagators

Consider a non-relativistic, electronic Hamiltonian in the Born–Oppenheimer approximation, its eigenvectors in Fock space for the reference, N-electron state, $|0\rangle$, electron-attached [$(N+1)$-electron] states, $|R\rangle$, and electron-detached [$(N-1)$-electron] states, $|S\rangle$, and corresponding eigenvalues, $E_0(N)$, $E_R(N+1)$, and $E_S(N-1)$. In the basis of these eigenfunctions, the spectral form of the electron propagator may be represented as a matrix whose pq element reads

$$\langle\langle a_p; a_q^\dagger\rangle\rangle_E = \lim_{\eta\to 0^+}\left[\sum_R \frac{\langle 0|a_p|R\rangle\langle R|a_q^\dagger|0\rangle}{E+E_0(N)-E_R(N+1)+i\eta} + \sum_S \frac{\langle 0|a_q^\dagger|S\rangle\langle S|a_p|0\rangle}{E-E_0(N)+E_S(N-1)-i\eta}\right], \quad (1)$$

where a_p and $a_q^\dagger$ are elementary field operators that annihilate an electron in a spin-orbital p and create an electron in a spin-orbital q, respectively.[15–17] The indices p, q, r, and s denote spin-orbitals of an unspecified occupancy. (The indices i, j, k, l and a, b, c, d will denote occupied and virtual spin-orbitals once reference determinants are introduced.) The infinitesimal $i\eta$ in Eq. (1) ensures proper behavior in the Fourier transformation between the spectral and time-dependent forms of the electron propagator matrix.

The physical content of Eq. (1) pertains to electron attachment and detachment energies (collectively referred to as electron binding energies) that occur at the poles, i.e., the values of the variable E that annihilate the denominators in the R and S summations, respectively. (Non-Dyson theories consider only the second term in calculations of VIEs.) Residues (numerators) at these poles may be written in terms of the Feynman–Dyson amplitudes,

$$f_p^R = \langle 0|a_p|R\rangle, \quad (2)$$

$$g_p^S = \langle S|a_p|0\rangle, \quad (3)$$

which, in turn, define (in an orthonormal spin-orbital basis, u) Dyson spin-orbitals,

$$\varphi_R^{Dyson}(x_1) = \sqrt{N+1}\int \Psi_0^*(x_2,x_3,x_4,\ldots,x_{N+1}) \times \Psi_R(x_1,x_2,x_3,\ldots,x_{N+1})dx_2dx_3dx_4\ldots dx_{N+1} = \sum_p f_p^R u_p(x_1), \quad (4)$$

$$\varphi_S^{Dyson}(x_1) = \sqrt{N}\int \Psi_S^*(x_2,x_3,x_4,\ldots,x_N) \times \Psi_0(x_1,x_2,x_3,\ldots,x_N)dx_2dx_3dx_4\ldots dx_N = \sum_p g_p^S u_p(x_1) \quad (5)$$

Published under an exclusive license by AIP Publishing

TABLE III. Arithmetic scaling requirements of electron-propagator methods.[a]

Method class	Methods[b]	Arithmetic bottleneck	Bottleneck steps	Largest ERI[c] subset
Diagonal second order	D2, os-D2	OV^2	N_E	O^2V^2
	RSPT2, nD-D2, **os-nD-D2**	OV^2	Non-iterative	O^2V^2
Diagonal post second order	RSPT3	OV^4	Non-iterative	V^4
	D3, OVGF	OV^4	N_E[d]	V^4
	P3, P3+, **Q3, Q3+**	O^2V^3	Non-iterative	OV^3
	L3, L3+	OV^4	N_E[d]	V^4
	RP3, RQ3	O^2V^3	Non-iterative	OV^3
	RL3	OV^4	N_IN_E[d]	V^4
	DR	O^2V^3	N_IN_E	O^2V^2
Non-diagonal	ND2	OV^3	N_I	OV^3
	2ph-TDA	OV^4	N_I	V^4
	3+	O^2V^4	Non-iterative[e]	V^4
	ADC(3)	O^2V^4	N_I[e]	V^4
	NR2	O^3V^3	Non-iterative[e]	OV^3
	BD-T1	O^2V^4	BD[f]	V^4
	NRP3, NRQ3, NRL3	O^2V^4	Non-iterative[e]	V^4

[a]O = No. occupied orbitals, V = No. virtual orbitals, N_E = energy iterations, N_I = inverse-expansion or linear-equation iterations for diagonal methods, and Hamiltonian-vector multiplications for non-diagonal methods.
[b]New methods in **bold type**.
[c]ERI = electron repulsion integral.
[d]Reduction by a factor of N_E occurs in non-Dyson (nD) versions.
[e]N_I OV^4 iterative steps for 3+, ADC(3), and NRL3; N_I O^3V^2 iterative steps for NR2, NRP3, and NRQ3.
[f]The O^2V^4 arithmetic bottleneck occurs in the Brueckner Doubles, coupled-cluster, reference-state calculation; the subsequent electron-propagator bottleneck is OV^4.

for electron attachment and detachment, respectively.[4]

The explicit summation over states in Eq. (1) is infeasible in practice but may be circumvented by expressing the electron propagator matrix element in the super-operator formalism[69,70] as

$$G_{pq}(E) \equiv \langle\langle a_p; a_q^\dagger \rangle\rangle_E = [a_p^\dagger \,|\, (E\hat{I} - \hat{H})^{-1} a_q^\dagger] \tag{6}$$

with the identity and Hamiltonian super-operators (denoted by circumflex accents) defined by

$$\hat{I}X = X, \tag{7}$$

$$\hat{H}X = HX - XH, \tag{8}$$

where H and X are standard Hamiltonian and generic operators. A specific definition of the metric $[X|Y]$ in Eq. (6) is one of the key choices (*vide infra*) in formulating electron propagator models.

The propagator matrix defined by the elements in Eq. (6),

$$\mathbf{G}(E) = [\mathbf{a}^\dagger \,|\, (E\hat{I} - \hat{H})^{-1} \mathbf{a}^\dagger], \tag{9}$$

contains an inverse (i.e., resolvent) super-operator. To avoid this inconvenience, a set of operators, w, may be used for an inner projection,[71] which permits the replacement of the super-operator inverse by a matrix inverse,

$$\mathbf{G}(E) = [\mathbf{a}^\dagger \,|\, \mathbf{w}][\mathbf{w}\,|\,(E\hat{I} - \hat{H})\mathbf{w}]^{-1}[\mathbf{w}\,|\,\mathbf{a}^\dagger]. \tag{10}$$

The set w comprises non-number-conserving operator strings, where the number of creators exceeds the number of annihilators by one: $a_p{}^\dagger$ (hole, h, and particle, p, operators), $a_p{}^\dagger a_q{}^\dagger a_r$ (2hp and 2ph), $a_p{}^\dagger a_q{}^\dagger a_r{}^\dagger a_s a_t$ (3h2p and 3p2h), and so on. If the complete set of operators, through Nh(N − 1)p and (N + 1)pNh,[72] is considered for an N-electron system in an infinite, one-electron basis, exact electron detachment and attachment energies are obtained from Eq. (10). In practice, a finite, one-electron basis is used, and the operator manifold, w, is truncated. The level of truncation constitutes another choice in defining electron-propagator models.

Even if the operator manifold is truncated, the explicit matrix inversion in the entire w space in Eq. (10) quickly becomes intractable in routine calculations. The operator manifold is, therefore, partitioned into a set of the simple, normalized field operators (h and p; *vide supra*) and an orthogonalized complement, $\boldsymbol{f}$ (composed of the remainder of the manifold w), such that $[\boldsymbol{a}^\dagger|\boldsymbol{f}] = 0$. Equation (10) may now be written in block form,

Published under an exclusive license by AIP Publishing

$$\mathbf{G}(E) = \begin{bmatrix} \mathbf{I} & \mathbf{0} \end{bmatrix} \begin{bmatrix} E\mathbf{I} - [\mathbf{a}^\dagger \,|\, \hat{H}\mathbf{a}^\dagger] & -[\mathbf{a}^\dagger \,|\, \hat{H}\mathbf{f}] \\ -[\mathbf{f}\,|\, \hat{H}\mathbf{a}^\dagger] & E\mathbf{I} - [\mathbf{f}\,|\, \hat{H}\mathbf{f}] \end{bmatrix}^{-1} \begin{bmatrix} \mathbf{I} \\ \mathbf{0} \end{bmatrix}, \tag{11}$$

where $\boldsymbol{I}$ is the unit matrix. If the lower, right block of the matrix in Eq. (11) and its Schur complement are invertible, one can invoke the identity,

$$\begin{bmatrix} \mathbf{A} & \mathbf{B} \\ \mathbf{C} & \mathbf{D} \end{bmatrix}^{-1} = \begin{bmatrix} \left(\mathbf{A} - \mathbf{B}\mathbf{D}^{-1}\mathbf{C}\right)^{-1} & -\left(\mathbf{A} - \mathbf{B}\mathbf{D}^{-1}\mathbf{C}\right)^{-1}\mathbf{B}\mathbf{D}^{-1} \\ -\mathbf{D}^{-1}\mathbf{C}\left(\mathbf{A} - \mathbf{B}\mathbf{D}^{-1}\mathbf{C}\right)^{-1} & \mathbf{D}^{-1} + \mathbf{D}^{-1}\mathbf{C}\left(\mathbf{A} - \mathbf{B}\mathbf{D}^{-1}\mathbf{C}\right)^{-1}\mathbf{B}\mathbf{D}^{-1} \end{bmatrix}, \tag{12}$$

which, together with the unit character of the row and column vectors in Eq. (11), leads to the following form of the electron-propagator matrix:

$$\mathbf{G}(E) = \left([\mathbf{a}^\dagger \,|\, (E\hat{I} - \hat{H})\mathbf{a}^\dagger] - [\mathbf{a}^\dagger \,|\, \hat{H}\mathbf{f}][\mathbf{f}\,|\, (E\hat{I} - \hat{H})\mathbf{f}]^{-1}[\mathbf{f}\,|\, \hat{H}\mathbf{a}^\dagger]\right)^{-1}. \tag{13}$$

Electron binding energies occur at the values of E equal to the poles of the matrix $\boldsymbol{G}(E)$ and may, therefore, be conveniently determined as zero eigenvalues of the inverse of $\boldsymbol{G}(E)$,

$$\mathbf{G}^{-1}(E) = [\mathbf{a}^\dagger \,|\, (E\hat{I} - \hat{H})\mathbf{a}^\dagger] - [\mathbf{a}^\dagger \,|\, \hat{H}\mathbf{f}][\mathbf{f}\,|\, (E\hat{I} - \hat{H})\mathbf{f}]^{-1}[\mathbf{f}\,|\, \hat{H}\mathbf{a}^\dagger]. \tag{14}$$

Equation (14), known as the inverse form of the Dyson equation, still contains the intractable inverse matrix in the (truncated) orthogonalized-complement space, $\boldsymbol{f}$. To pave the way for tackling this inverse matrix, the Hamiltonian, and hence its super-operator counterpart, are partitioned into zeroth- and first-order contributions. Typically, the Møller–Plesset partitioning[73] is employed,

$$\hat{H} = \hat{F} + \hat{V}, \tag{15}$$

where the super-operators $\hat{F}$ and $\hat{V}$ are defined as in Eq. (8) in terms of the usual Fock and fluctuation-potential operators, respectively. With the above partitioning, Eq. (14) may be written as

$$\mathbf{G}^{-1}(E) = \mathbf{G}_0^{-1}(E) - \mathbf{\Sigma}(E), \tag{16}$$

where the zeroth-order terms are contained in

$$\mathbf{G}_0^{-1}(E) = E\mathbf{I} - [\mathbf{a}\,|\, \hat{F}\mathbf{a}] \tag{17}$$

and all the higher-order terms constitute the self-energy matrix,

$$\mathbf{\Sigma}(E) = [\mathbf{a}^\dagger \,|\, \hat{V}\mathbf{a}^\dagger] + [\mathbf{a}^\dagger \,|\, \hat{H}\mathbf{f}][\mathbf{f}\,|\, (E\hat{I} - \hat{H})\mathbf{f}]^{-1}[\mathbf{f}\,|\, \hat{H}\mathbf{a}^\dagger]. \tag{18}$$

The first and second order contributions to the energy-independent (i.e., constant) term vanish for HF orbitals. Zeroth-order contributions to the $[\boldsymbol{a}^\dagger|\hat{H}\boldsymbol{f}]$ and $[\boldsymbol{f}|\hat{H}\boldsymbol{a}^\dagger]$ blocks also vanish. The presence of the inverse matrix in the self-energy generates terms of all orders, starting from the second order.

In the CHF basis, Eq. (17) takes on a particularly simple, diagonal form,

$$\mathbf{G}_0^{-1}(E) = E\mathbf{I} - \boldsymbol{\varepsilon}, \tag{19}$$

where $\boldsymbol{\varepsilon}$ is the diagonal matrix of canonical orbital energies. Substituting Eq. (19) into Eq. (16) and recalling that electron binding energies occur at zeros of the inverse electron-propagator matrix shows that the electron binding energies may be obtained as eigenvalues of $\boldsymbol{M}(E)$, where

$$\mathbf{M}(E) = \boldsymbol{\varepsilon} + \mathbf{\Sigma}(E). \tag{20}$$

The Dyson quasiparticle equation is therefore equivalent to the diagonalization of $\boldsymbol{M}(E)$. The main effort of calculating electron binding energies in this approach thus reduces to constructing the non-diagonal self-energy matrix at each energy (E) iteration. (Convergence is usually achieved within a few iterations for outer-valence VIEs.) The self-energy matrix, in turn, is built in terms of the blocks of the super-operator Hamiltonian matrix,

$$\widehat{\mathbf{H}} = \begin{bmatrix} [\mathbf{a}^\dagger \,|\, \hat{H}\mathbf{a}^\dagger] & [\mathbf{a}^\dagger \,|\, \hat{H}\mathbf{f}] \\ [\mathbf{f}\,|\, \hat{H}\mathbf{a}^\dagger] & [\mathbf{f}\,|\, \hat{H}\mathbf{f}] \end{bmatrix}. \tag{21}$$

The latter matrix appears in Eq. (11) and the poles of the electron-propagator matrix, $\boldsymbol{G}(E)$, therefore, occur at eigenvalues of $\widehat{\mathbf{H}}$,

$$\widehat{\mathbf{H}}\mathbf{C} = \mathbf{C}\boldsymbol{\omega}, \tag{22}$$

where elements of the eigenvector, $\boldsymbol{C}_n$, corresponding to a given eigenvalue, ω_n, appear in *normalized* Dyson spin-orbitals as

$$\phi_n^{Dyson}(x_1) = \left(\sqrt{\Pi_n}\right)^{-1} \sum_p C_{n,p} u_p(x_1). \tag{23}$$

The summation runs over the number of functions in the spin-orbital basis for coefficients of the simple operator space, $\boldsymbol{a}^\dagger$, suffice for fully determining Dyson spin-orbitals. The normalization factor is related to Π_n, also known as the probability factor or pole strength, which varies between 0 and 1 and is obtained from the norm of the Dyson spin-orbitals of Eqs. (4) and (5), where

$$\Pi_n = \int |\, \varphi^{Dyson}(x_1)\,|^2 dx_1 = \left(1 - \mathbf{C}_n^\dagger \left[\frac{d\mathbf{\Sigma}(E)}{dE}\right]_{E=\omega_n} \mathbf{C}_n\right)^{-1}. \tag{24}$$

[Note that two different symbols are used for the non-normalized and normalized Dyson spin-orbitals in Eqs. (4) and (5) and in Eq. (23), respectively.] The eigenvalue problem of the super-operator Hamiltonian thus offers a convenient, alternative way of obtaining the Feynman–Dyson amplitudes [cf. Eqs. (2) and (3)], in addition to electron binding energies.

The cost of constructing the self-energy matrix may be reduced by one order of magnitude if the off-diagonal elements of the matrix are neglected. In this approximation, the Dyson quasiparticle equation is reduced to its diagonal form,

$$E_n = \varepsilon_n + \Sigma_{nn}(E_n), \tag{25}$$

which must be evaluated iteratively. (Three iterations usually suffice to achieve convergence to within 0.01 eV for outer-valence VIEs.) As Eqs. (23) and (24) then become

$$\phi_n^{Dyson}(x_1) = \left(\sqrt{\Pi_n}\right)^{-1} u_n(x_1), \tag{26}$$

$$\Pi_n = \left(1 - \left[\frac{\Sigma_{nn}(E)}{dE}\right]_{E=\omega_n}\right)^{-1}, \tag{27}$$

Published under an exclusive license by AIP Publishing

the diagonal approximation is applicable only to those electron-attached or detached states whose Dyson spin-orbitals are properly described by the qualitative features of a single CHF orbital. (In other words, there are no contributions to the Dyson orbital from the other canonical spin-orbitals, and the premises of Koopmans's identity are qualitatively valid for such states.) A quantitative criterion of the diagonal approximation's applicability regime has, therefore, been defined in terms of the value of the probability factor, Π_n. If its value is not less than 0.85, the application of the diagonal approximation is justified. Ample numerical evidence has been generated showing that the diagonal approximation consistently yields accurate results for the first few states with VIEs lower than those in the inner-valence region.

We are now ready to return to the problem of calculating the inverse matrix $[\boldsymbol{f}|(E\hat{I}\text{-}\hat{H})\boldsymbol{f}]^{-1}$ efficiently. For both diagonal and non-diagonal methods, this is achieved by retaining the elements of the self-energy matrix in Eq. (18) only through a certain order in the fluctuation potential. For the non-diagonal methods, this is equivalent to keeping only those elements of the $\hat{\boldsymbol{H}}$ matrix in Eq. (21) that are necessary to obtain the self-energy matrix through that order. Furthermore, for both the diagonal and non-diagonal methods, by expanding the inverse $[\boldsymbol{f}|(E\hat{I}\text{-}\hat{H})\boldsymbol{f}]^{-1}$, one may choose to either truncate the expansion such that terms are kept strictly through a specific order (non-renormalized methods) or to keep the entire inverse, thus including additional contributions through infinite order (fully renormalized non-diagonal methods or explicitly renormalized diagonal methods). An economic alternative to the latter is offered by approximately renormalized methods, where the effect of the full inverse expansion is estimated by ratios of terms of different orders. Such estimates impose negligible costs after energy iterations of the underlying non-renormalized method have converged. The specific form of the self-energy matrix elements at each order depends on the choice of the metric $[X|Y]$ (*vide infra*).

A definition of a specific electron-propagator model may be summarized by the following choices:

- The form of the metric $[X|Y]$.
- Truncation level in the orthogonalized complement operator manifold, $\boldsymbol{f}$.
- Neglect or retention of non-diagonal elements in the self-energy matrix $\boldsymbol{\Sigma}(E)$ of Eq. (18).
- Neglect or retention of terms of a given order in the fluctuation potential.

The latter criterion determines whether the approximation is non-renormalized (i.e., strict retention of terms only through a selected order) or renormalized, with retention of certain classes of terms in all orders.

All the methods presently under consideration include only 2hp and 2ph operators in the manifold $\boldsymbol{f}$ and employ one of three metric choices in their derivations:

1. Unit-normalized, symmetric (S subscript) metric,

$$[X\,|\,Y]_S = \langle\,\mathrm{HF}\,|\left(1 + T_2^{(1)} + T_1^{(2)}\right)^{\dagger}\left(X^{\dagger}Y + YX^{\dagger}\right) \times \left(1 + T_2^{(1)} + T_1^{(2)}\right)|\,\mathrm{HF}\rangle\,. \tag{28}$$

2. Asymmetric metric, which requires separate definitions for electron attachment (A) and detachment (D),

$$[X\,|\,Y]_A = \langle \mathrm{HF}\,|\left(X^{\dagger}Y + YX^{\dagger}\right)\left(1 + T_2^{(1)}\right)|\,\mathrm{HF}\rangle, \tag{29}$$

$$[X\,|\,Y]_D = \langle \mathrm{HF}\,|\left(1 + T_2^{(1)}\right)^{\dagger}\left(X^{\dagger}Y + YX^{\dagger}\right)|\,\mathrm{HF}\rangle\,. \tag{30}$$

3. Intermediately normalized, Hermitized metric (denoted by the subscript H),

$$[X\,|\,Y]_H = \frac{1}{2}\Big(\langle \mathrm{HF}\,|\left(X^{\dagger}Y + YX^{\dagger}\right)\left(1 + T_2^{(1)} + T_1^{(2)}\right)|\,\mathrm{HF}\rangle + \langle \mathrm{HF}\,|\left(1 + T_2^{(1)} + T_1^{(2)}\right)^{\dagger}\left(X^{\dagger}Y + YX^{\dagger}\right)|\,\mathrm{HF}\rangle\Big). \tag{31}$$

(In nD methods for VIEs, only the second term in the $[X^{\dagger}, Y]_+$ anticommutator is retained, and, therefore, higher-order density matrices must be recruited for the evaluation of matrix elements.) The metrics in Eqs. (28)–(31) are defined in terms of the HF determinant, $|HF\rangle$, and the first-order double and second order single replacement operators in the CHF basis,

$$T_2^{(1)} = \frac{1}{4}\sum_{ij}^{occ}\sum_{ab}^{vir}\frac{\langle ij\|ab\rangle}{\varepsilon_i + \varepsilon_j - \varepsilon_a - \varepsilon_b}\,a_a^{\dagger}a_b^{\dagger}a_j a_i, \tag{32}$$

$$T_1^{(2)} = \sum_{i}^{occ}\sum_{a}^{vir}\frac{1}{2(\varepsilon_i - \varepsilon_a)}\left(\sum_{jk}^{occ}\sum_{b}^{vir}\frac{\langle jk\|ab\rangle\langle bi\|jk\rangle}{\varepsilon_j + \varepsilon_k - \varepsilon_a - \varepsilon_b} + \sum_{j}^{occ}\sum_{bc}^{vir}\frac{\langle ij\|bc\rangle\langle bc\|aj\rangle}{\varepsilon_i + \varepsilon_j - \varepsilon_b - \varepsilon_c}\right)a_a^{\dagger}a_i, \tag{33}$$

where $\langle pq\|rs\rangle$ represents an anti-symmetrized electron repulsion integral (ERI) in Dirac's notation. The order of contributions to $\boldsymbol{\Sigma}(E)$ in Eq. (18) is, therefore, determined in terms of the presence of the fluctuation potential operator, V, and the operators $T_2^{(1)}$ and $T_1^{(2)}$. (Notice, again, that the inverted matrix $[\boldsymbol{f}|(E\hat{I}\text{-}\hat{H})\boldsymbol{f}]^{-1}$ generates terms through infinite order.) The $T_2^{(1)}$ and $T_1^{(2)}$ operators enter non-linearly in the higher-order super-operator matrix elements resulting from the $[X|Y]_S$ metric, whereas for the other metric choices, these operators always make linear contributions to matrix elements.

Rowe's Hermitization for equation of motion theory[74] differs from Eq. (31) because different metrics are used for the super-operator Hamiltonian and identity matrices. It follows rigorously from the equation of motion only when the reference state is exact. Equations (29) and (30) can lead to non-Hermitian eigenvalue problems; Hermitized matrices are diagonalized in practice.[52,59–61] Equation (28) and improvements that may involve additional reference-state substitutions produce Hermitian matrices of order $n + 1$, provided that the resulting reference-state density matrices are correct through order n.[19,75] These formal complications and inconsistencies are avoided in Eq. (31).

Published under an exclusive license by AIP Publishing

Non-diagonal extensions of new-generation self-energies

The new non-diagonal, renormalized self-energy approximations introduced presently (NRP3, NRQ3, and NRL3) may be defined in terms of super-operator Hamiltonian couplings that suffice to recover all self-energy terms in their diagonal, explicitly renormalized antecedents (RP3, RQ3, and RL3). Table IV summarizes the order of terms through which each block of $\hat{\boldsymbol{H}}$ is evaluated. NRP3, NRQ3, and NRL3 are based on the Hermitized, intermediately normalized metric of Eq. (31). Older methods, such as ND2, 2ph-TDA, or 3+, evaluate all terms through a given order in the fluctuation potential and may be based on Eq. (28). In the latter methods, terms that are quadratic in ground-state correlation amplitudes appear in the third order couplings between simple (h and p) operators. For real orbitals, there is only a difference of a factor of two between the older (e.g., 3+) methods' second order couplings between simple and triple operators and those of the new methods. The same distinction exists between the old and new methods with respect to couplings between simple operators that involve second order single replacement (i.e., $T_1^{(2)}$) amplitudes. The previously derived NR2 methods based on Eqs. (29) and (30) bear a close resemblance to NRP3; the older method's first order treatment of the p-2hp block eliminates the need for ERIs with four virtual indices. There are no discrepancies between the old and new approaches in zeroth order and first order terms.

Of the self-energy alternatives examined in this work, only the BD-T1 method employs Brueckner orbitals. The same set of h, p, 2hp, and 2ph operators is represented in the super-operator Hamiltonian matrix. Couplings between 2ph and 2hp operators are set to zero, but 2ph–2ph and 2hp–2hp matrix elements are linear in the double substitution amplitudes, as are the couplings between simple and triple operators. Pseudo-canonical Brueckner orbital energies appear as diagonal elements in the h–h and p–p blocks of the generalized Fock, or $[\mathbf{a}^\dagger|\hat{H}\mathbf{a}^\dagger]$, matrix. Couplings between h and p operators do not vanish, for the Brillouin condition is not satisfied in general.

Algorithm for diagonal, explicitly renormalized self-energies

Energy-dependent self-energy matrices of the following form,

$$\boldsymbol{\Sigma}(E) = \hat{\boldsymbol{H}}_{13}(E\hat{\boldsymbol{I}} - \hat{\boldsymbol{H}})^{-1}_{33}\hat{\boldsymbol{H}}_{31}, \tag{34}$$

occur in the RP3, RQ3, RL3, and DR approximations. (The subscripts refer to the simple and triple field operators that are coupled in the super-operator Hamiltonian blocks present in renormalized self-energy matrices.)

To solve

$$(E\hat{\boldsymbol{I}} - \hat{\boldsymbol{H}})^{-1}\mathbf{b} = \mathbf{B} \tag{35}$$

or

$$\mathbf{0} = (E\hat{\boldsymbol{I}} - \hat{\boldsymbol{H}}_0 - \hat{\boldsymbol{V}})\mathbf{B} - \mathbf{b}, \tag{36}$$

TABLE IV. Orders retained in super-operator Hamiltonian matrices ($\hat{\boldsymbol{H}}$) of NRP3, NRQ3, and NRL3 self-energies for hole (h), particle (p), two-hole-one-particle (2hp), and two-particle-one-hole (2ph) operators.[a–f]

$\hat{\boldsymbol{H}}$	h	p	2hp	2ph
h	**NRP3** 0[e] **NRQ3** 3 **NRL3** 3 ND2 0[e] 3 + 3[c]	**NRP3** 0[e] **NRQ3** 3 **NRL3** 3 ND2 0[e] 3 + 3[c]	**NRP3** 2 **NRQ3** 2 **NRL3** 2 ND2 1 3 + 2	**NRP3** 1 **NRQ3** 1 **NRL3** 2 ND2 1 3 + 2
p		**NRP3** 0[e] **NRQ3** 3 **NRL3** 3 ND2 0[e] 3 + 3[c]	**NRP3** 2[b] **NRQ3** 2 **NRL3** 2 ND2 1 3 + 2	**NRP3** 1 **NRQ3** 1 **NRL3** 2 ND2 1 3 + 2
2hp			**NRP3** 1 **NRQ3** 1 **NRL3** 1 ND2 0[d,e] 3 + 1	**NRP3** 0[e,f] **NRQ3** 0[e,f] **NRL3** 0[e,f] ND2 0[e,f] 3 + 0[f]
2ph				**NRP3** 0[e] **NRQ3** 0[e] **NRL3** 1 ND2 0[d,e] 3 + 1

[a]Evaluation of $\hat{\boldsymbol{H}}$ with a Hermitized, intermediately normalized metric in **bold type**.
[b]NR2 is the same as NRP3, except that p-2hp couplings are evaluated in the first instead of the second order.
[c]3+ is identical to strict ADC(3); other versions of ADC(3) differ in their treatment of h–h, h–p, and p–p couplings.
[d]2ph-TDA differs from ND2 by introducing first order terms in the 2hp–2hp and 2ph–2ph blocks.
[e]First order terms and off-diagonal zeroth order terms vanish. CHF orbital energies of zeroth order occur in diagonal matrix elements. In the h–h, p–p, and h–p blocks, second order terms also vanish.
[f]The first non-vanishing 2hp–2ph couplings appear in the second order and contribute to the fourth- and higher-order self-energies.

let

$$\mathbf{R} = (E\hat{\boldsymbol{I}} - \hat{\boldsymbol{H}}_0)^{-1} = \mathbf{R}^\dagger, \tag{37}$$

$$\mathbf{B}_1 = \mathbf{R}\mathbf{b}, \tag{38}$$

$$\mathbf{B}_{n+1} = \mathbf{R}\hat{\mathbf{V}}\mathbf{B}_n, \tag{39}$$

implying that

$$\mathbf{B}_n = (\mathbf{R}\hat{\mathbf{V}})^{n-1}\mathbf{B}_1. \tag{40}$$

The target may be expanded in terms of a basis,

$$\mathbf{B} = \sum_{k=1}^{n} \alpha_k \mathbf{B}_k. \tag{41}$$

Published under an exclusive license by AIP Publishing

After inserting the expansion into Eq. (36) and projecting against $\boldsymbol{B}_m{}^\dagger$,

$$\sum_{k=1}^{n} \alpha_k \mathbf{B}_m^\dagger (E\mathbf{1} - \hat{\boldsymbol{H}}_0 - \hat{\mathbf{V}})\mathbf{B}_k - \mathbf{B}_m^\dagger \mathbf{b} = \mathbf{0}, \tag{42}$$

or

$$\sum_{k=1}^{n} \alpha_k [\mathbf{b}^\dagger (\mathbf{R}\hat{\mathbf{V}})^{m+k-2}\mathbf{R}\mathbf{b} - \mathbf{b}^\dagger (\mathbf{R}\hat{\mathbf{V}})^{m+k-1}\mathbf{R}\mathbf{b}] - \mathbf{b}^\dagger \mathbf{R}(\hat{\mathbf{V}}\mathbf{R})^{m-1}\mathbf{b} = \mathbf{0}. \tag{43}$$

Let

$$\boldsymbol{\sigma}^{(m+k)} = \mathbf{b}^\dagger (\mathbf{R}\hat{\mathbf{V}})^{m+k-2}\mathbf{R}\mathbf{b}, \tag{44}$$

where the superscript labels the order of the contribution to the self-energy matrix. [$\boldsymbol{R}$ of Eq. (37) is defined to be of zeroth order, and $\boldsymbol{b}$ of Eqs. (34) and (35) enters in first order.]

Therefore,

$$\sum_{k=1}^{n} \alpha_k (\boldsymbol{\sigma}^{(m+k)} - \boldsymbol{\sigma}^{(m+k+1)}) - \boldsymbol{\sigma}^{(m+1)} = \mathbf{0}. \tag{45}$$

One may solve for the expansion coefficients with

$$\boldsymbol{\alpha} = (\boldsymbol{\sigma}^{(m+k)} - \boldsymbol{\sigma}^{(m+k+1)})^{-1}\boldsymbol{\sigma}^{(m+1)}. \tag{46}$$

For methods where only one diagonal element (with orbital index p) of the self-energy matrix is needed,

$$\boldsymbol{\alpha} = \mathbf{X}^{-1}\mathbf{S}, \tag{47}$$

where

$$X_{ij} = \sigma_{pp}^{(i+j)} - \sigma_{pp}^{(i+j+1)} \tag{48}$$

and

$$S_i = \sigma_{pp}^{(i+1)}. \tag{49}$$

The bottleneck step with quintic arithmetic scaling is the following matrix multiplication in Eq. (39):

$$\tilde{\boldsymbol{B}}_{n+1} = \hat{\boldsymbol{V}}\mathbf{B}_n. \tag{50}$$

Generation of $\boldsymbol{B}_n$ is necessary to produce $\boldsymbol{\sigma}^{(2n-1)}$ and $\boldsymbol{\sigma}^{(2n)}$ (*vide infra*).

An efficient algorithm may be constructed after defining

$$\mathbf{b} \equiv \mathbf{b}_1 = \hat{\boldsymbol{H}}_{31}, \tag{51}$$

$$\mathbf{b}_n \equiv \hat{\boldsymbol{V}}\mathbf{B}_{n-1}. \tag{52}$$

In this notation,

$$\sigma_{pp}^{(2n)} = \mathbf{b}_n^\dagger \mathbf{B}_n, \tag{53}$$

$$\sigma_{pp}^{(2n+1)} = \mathbf{b}_{n+1}^\dagger \mathbf{B}_n, \tag{54}$$

$$\Sigma_{pp}^{(n)} = \hat{\boldsymbol{H}}_{13}\mathbf{B}_{n-1} = \mathbf{c}^\dagger \mathbf{B}_{n-1}, \tag{55}$$

$$\Sigma_{pp}(E) = \mathbf{c}^\dagger \mathbf{B} = \sum_{k}^{n} \alpha_k \mathbf{c}^\dagger \mathbf{B}_k = \sum_{k}^{n} \alpha_k \Sigma^{(k+1)}. \tag{56}$$

Step 1: For iteration n,

$$\mathbf{B}_n = \mathbf{R}\mathbf{b}_n. \tag{57}$$

Step 2: Calculate $\sigma^{(2n)}$ and $\Sigma^{(n+1)}$ with Eqs. (53) and (55).
Step 3: Evaluate $\boldsymbol{b}_{n+1}$ with Eq. (52).
Step 4: Calculate $\sigma^{(2n+1)}$ with Eq. (54).
Step 5: Solve for α_k where $k = 1, \ldots, n$ with Eqs. (47)–(49).
Step 6: Evaluate the self-energy matrix element with Eq. (56) and compare it to the value obtained with the result of iteration $n-1$. If it is not converged, update n in step 1 and continue.

Note that for diagonal self-energy methods, the result of the first iteration,

$$\Sigma_{pp} = \frac{\sigma_{pp}^{(2)}}{\sigma_{pp}^{(2)} - \sigma_{pp}^{(3)}}\Sigma_{pp}^{(2)}, \tag{58}$$

resembles the approximate 2hp and 2ph renormalizations used in P3+, Q3+, L3+B, and OVGF-B. For each value of n, only one quintic contraction [Eq. (52)] is needed. This method requires no more quintic steps than the simple summation of terms in each order according to

$$\Sigma_{pp} = \sum_{k} \Sigma_{pp}^{(k)}. \tag{59}$$

Generalizations to off-diagonal self-energy matrix elements require only the substitution of pq subscripts for pp subscripts in Eqs. (53)–(56). The algorithm may be applied to any partitioning of the Hamiltonian, including cases where $\hat{\boldsymbol{H}}_0$ is not diagonal.

COMPUTATIONAL METHODS

All calculations were performed with the development version of Gaussian[76] with new links for electron propagator methods. After self-consistent-field calculations, the set of ERIs required for the calculation of self-energy matrix elements is transformed to the CHF basis and stored on disk. The largest subsets of ERIs needed for each self-energy approximation are displayed in Table III, where V is assumed to be larger than O. Core orbitals are not considered in self-energy summations. To evaluate the performance of the new methods, standard values of VIEs obtained with higher level IP-EOM-CC (ionization potential, equation-of-motion, and coupled-cluster) methods are invoked.

First, the performance of the new methods is tested against a set of 34 VIEs obtained at the IP-EOM-CCSDTQ/cc-pVTZ (ionization potential, equation of motion, coupled cluster reference state with single, double, triple, and quadruple substitution operators;[12] correlation consistent polarized valence triple ζ atomic basis set[77]) level and drawn from 11 closed-shell molecules.[67] Second, the methods are tested on an IP-EOM-CCSDT/cc-pVTZ benchmark set of

Published under an exclusive license by AIP Publishing

170 VIEs from 33 closed-shell molecules[67] contained in the original study.[38] Both sets of standard VIEs pertain to small and medium-sized molecules with H, C, N, O, and F nuclei. The MAE, mean signed error (MSE), standard deviation, and maximum error of the IP-EOM-CCSDT data with respect to the IP-EOM-CCSDTQ results are 0.03, 0.00, 0.02, and 0.10 eV, respectively. The negligible statistical differences strongly indicate that the data obtained at both levels of theory are excellent approximations to FCI results with a cc-pVTZ basis.

Some data in both benchmark sets correspond to relatively high-energy valence final states with significant 2s atomic contributions to their Dyson orbitals and probability factors (pole strengths) that fall below 0.85 for diagonal self-energy methods. These states have relatively low single orbital (simple field operator) characters in their IP-EOM-CCSD[78] eigenvectors and require higher-level IP-EOM-CC approximations for reliable results. It is unusual for final states above 25 eV to conform even qualitatively to the strictures of Koopmans's identity. The onset of the inner-valence region, where the breakdown of the Koopmans picture has been amply documented,[79] demands a more flexible treatment of relaxation and correlation effects. Inner-valence final states present serious challenges for all methods presently considered, including those where non-diagonal self-energy matrices are evaluated.

Consequently, the following ten problematic states (6σ of HCCCN; $3\sigma_g$, $3\sigma_u$ of HC_4H; $5a_1$ of $C_2H_2F_2$; $4a_1$, $4b_2$ of *cis*-$C_2H_2F_2$; $5a_1$ of CH_3CN; $5a_1$ of CH_3NC; $1b_1$ of O_3; and $2a_g$ of C_2H_4) can be dropped from the IP-EOM-CCSDT/cc-pVTZ set to obtain a subset of 160 VIEs. The exclusion of these ten states is justified not only by their convergence failure but also by the large statistical errors obtained from several self-energy approximations and IP-EOM-CCSD. Balanced treatments of these states require terms arising from at least the five-fold operator manifold (i.e., products of three annihilators and two creators) in the self-energy matrices. None of the self-energies considered in this work involve five-fold operators. The set of 160 VIEs still contains many lower lying valence states with large 2s atomic contributions to Dyson orbitals and a relatively low single orbital character. The standard subset of 96 VIEs comprises only those states for which all methods obtain probability factors of 0.85 or above. Thus, the three sets of VIE standards present a realistic and challenging test of the predictive capabilities of the new methods under consideration. The complete set of calculated results and accompanying statistics are provided in the supplementary material.

For diagonal methods, energy iterations are performed with Eq. (25) until self-consistency to within 0.001 eV is achieved. For explicitly renormalized diagonal methods, the new algorithm that involves solutions to linear equations [see Eq. (47)] is employed. Non-diagonal, renormalized self-energies require solutions of the eigenvalue problem of Eq. (22); standard diagonalization techniques for electron propagator methods have been employed.[80,81]

NUMERICAL RESULTS

The first test considers the 34 VIEs calculated with IP-EOM-CCSDTQ as a standard of comparison. (See Table V and Figs. 1–3.) MAEs near 0.1 eV are achieved by the diagonal RL3 method and its non-Dyson variant, nD-RL3. (Non-Dyson variants eliminate the *E*-dependence of 2ph terms in calculations of VIEs and, therefore, require fewer arithmetic operations.) These results imply that energy dependence in the 2ph part of the self-energy is not a crucial factor in the success of RL3. This high accuracy is retained when the diagonal approximation is abandoned in the NRL3 self-energy. A comparison of the RL3 and NRL3 histograms in Figs. 2 and 3 indicates the data are almost identical. Only the more computationally intensive BD-T1 method, with its iterative sixth-power scaling in the reference-state calculation (see Table III), yields data of similar quality. The approximately renormalized L3+B method and its non-Dyson counterpart (nD-L3+B) produce MAEs near 0.15 eV. A slight loss of accuracy accompanies the use of approximate renormalization. Q3+, RQ3, and RP3 also have MAEs close to 0.15, but their arithmetic O^2V^3 bottlenecks and transformed ERI requirements are less demanding. The explicitly renormalized, non-diagonal variants NRQ3 and NRP3 display similar quality. The NR2 method, which is closely related to NRP3, also has an MAE near 0.15 eV. The best OVGF version (A) and P3+ with MAEs near 0.25 eV are less accurate. OVGF is also more costly than Q3+. Several well-known methods produce MAEs of about 0.3 eV (chiefly with overestimates), including the strict (3+) and Schirmer–Angonoa versions of ADC(3), the DR method, and the os-nD-D2 and os-D2 self-energies, but with markedly different arithmetic scaling factors. [In a recent test of nD-ADC(3) for VIEs of closed-shell molecules, an average MAE of 0.35 eV was reported.[82]] When this level of accuracy is acceptable, os-D2 and os-nD-D2 are preferable because of their arithmetic efficiency. IP-EOM-CCSD expends similar effort in its reference state phase as BD-T1, but with lower accuracy.[67] Diagonal low-order (D2 and D3) self-energies and their non-Dyson variants (nD-D2 and nD-D3), non-diagonal second order (ND2), and 2ph-TDA are not competitive. The overestimates of the third order methods are worse than the underestimates of the second order methods.

The larger and somewhat less rigorous standard of 160 VIEs calculated with IP-EOM-CCSDT provides a second test. (See Table VI and Figs. 4–6.) Many of the trends seen in the previous test reappear presently. There is little deterioration in the quality of the RL3 and nD-RL3 results. The sharply peaked and balanced histograms of RL3 in Fig. 5 and of NRL3 in Fig. 6 are almost identical; removal of the diagonal approximation has almost no effect. In fact, the latter method now achieves an MAE below 0.1 eV, and the non-diagonal, sixth-power BD-T1 and NR2 methods are slightly worse. The profile of IP-EOM-CCSD has an even greater tendency to overestimate. L3+B and its non-Dyson variant again produce MAEs near 0.15 eV, but with the computational advantage of an approximate instead of an explicit renormalization procedure. As in the previous test, Q3+, RQ3, and RP3 succeed in matching the latter MAE target, but with less computational effort. Their non-diagonal counterparts, NRQ3 and NRP3, are slightly more accurate. The widely used OVGF-A and P3+ methods, with MAEs above 0.2 eV, are less successful; the latter alternative is more accurate and efficient. The DR method and the two opposite-spin, second order approximations with cubic scaling yield MAEs near 0.35 eV. The two ADC(3) variants' MAEs exceed 0.4 eV. IP-EOM-CCSD is less accurate than the arithmetically comparable BD-T1 method. The failures of D2, D3, and their non-Dyson variants recur for the same reasons as found in the previous test. The ND2 and 2ph-TDA methods are not useful in either test.

Published under an exclusive license by AIP Publishing

TABLE V. Error distributions (eV) vs IP-EOM-CCSDTQ/cc-pVTZ for 34 VIEs.

Method class	Method[a]	MAE[b,c]	MSE[d]	σ[e]	Max. AE[f]
Uncorrelated	KT	1.512	1.432	1.093	4.374
Diagonal second order	D2	0.616	−0.515	0.511	1.470
	os-D2	0.307	0.201	0.372	1.498
	nD-D2	0.640	−0.545	0.520	1.515
	os-nD-D2	**0.298**	0.188	0.369	1.474
Diagonal post second order	DR	0.321	0.269	0.307	1.089
	D3	0.696	0.661	0.540	2.070
	nD-D3	0.684	0.649	0.535	2.066
	OVGF-A	0.256	0.110	0.336	1.123
	OVGF-B	0.300	0.234	0.330	1.084
	OVGF-C	0.341	0.315	0.315	1.178
	nD-OVGF-A	0.250	0.088	0.338	1.058
	nD-OVGF-B	0.286	0.215	0.320	1.028
	nD-OVGF-C	0.322	0.297	0.304	1.110
	P3	0.287	0.259	0.286	0.966
	P3+	0.235	0.110	0.272	0.948
	Q3	0.226	0.189	0.262	0.789
	Q3+	**0.177**	0.040	0.229	0.773
	L3	0.224	0.196	0.258	0.860
	nD-L3	0.211	0.178	0.251	0.824
	L3+A	0.226	−0.057	0.272	0.862
	L3+B	0.176	0.050	0.235	0.851
	L3+C	0.202	0.079	0.260	0.860
	nD-L3+A	0.222	−0.054	0.267	0.826
	nD-L3+B	**0.172**	0.045	0.231	0.815
	nD-L3+C	0.194	0.070	0.251	0.825
	RP3	0.167	−0.023	0.196	0.509
	RQ3	0.151	−0.081	0.165	0.524
	RL3	0.109	−0.058	0.139	0.502
	nD-RL3	**0.118**	−0.079	0.140	0.537
Non-diagonal	ND2	0.598	−0.484	0.530	1.381
	2ph-TDA	0.654	−0.653	0.316	1.685
	3+	0.288	0.248	0.257	0.891
	ADC(3)	0.300	0.288	0.223	0.880
	NR2	**0.167**	−0.042	0.193	0.531
	BD-T1	0.123	0.064	0.166	0.684
	NRP3	0.167	−0.043	0.194	0.540
	NRQ3	**0.162**	−0.107	0.158	0.549
	NRL3	**0.113**	−0.070	0.135	0.517
	IP-EOM-CCSD	0.180	0.140	0.202	0.834
	IP-EOM-CCSDT	0.030	0.002	0.038	0.103

[a]New methods in **bold type**.
[b]Optimal methods in **bold type.**
[c]MAE = mean absolute error.
[d]MSE = mean signed error.
[e]σ = standard deviation.
[f]Max. AE = maximum absolute error.

Published under an exclusive license by AIP Publishing

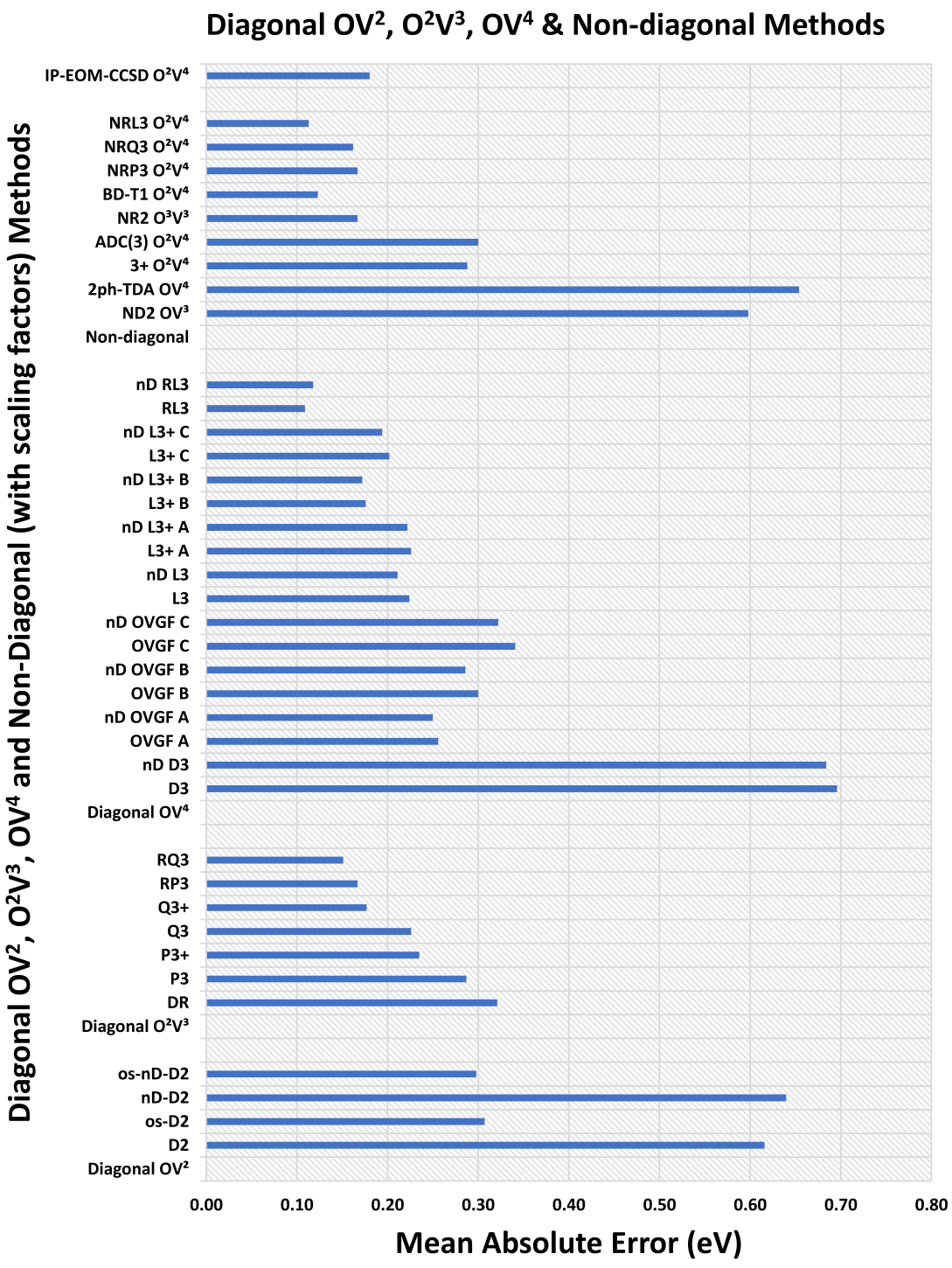


FIG. 1. Mean absolute errors (eV) vs IP-EOM-CCSDTQ/cc-pVTZ standards for 34 VIEs and arithmetic scaling factors.

Published under an exclusive license by AIP Publishing

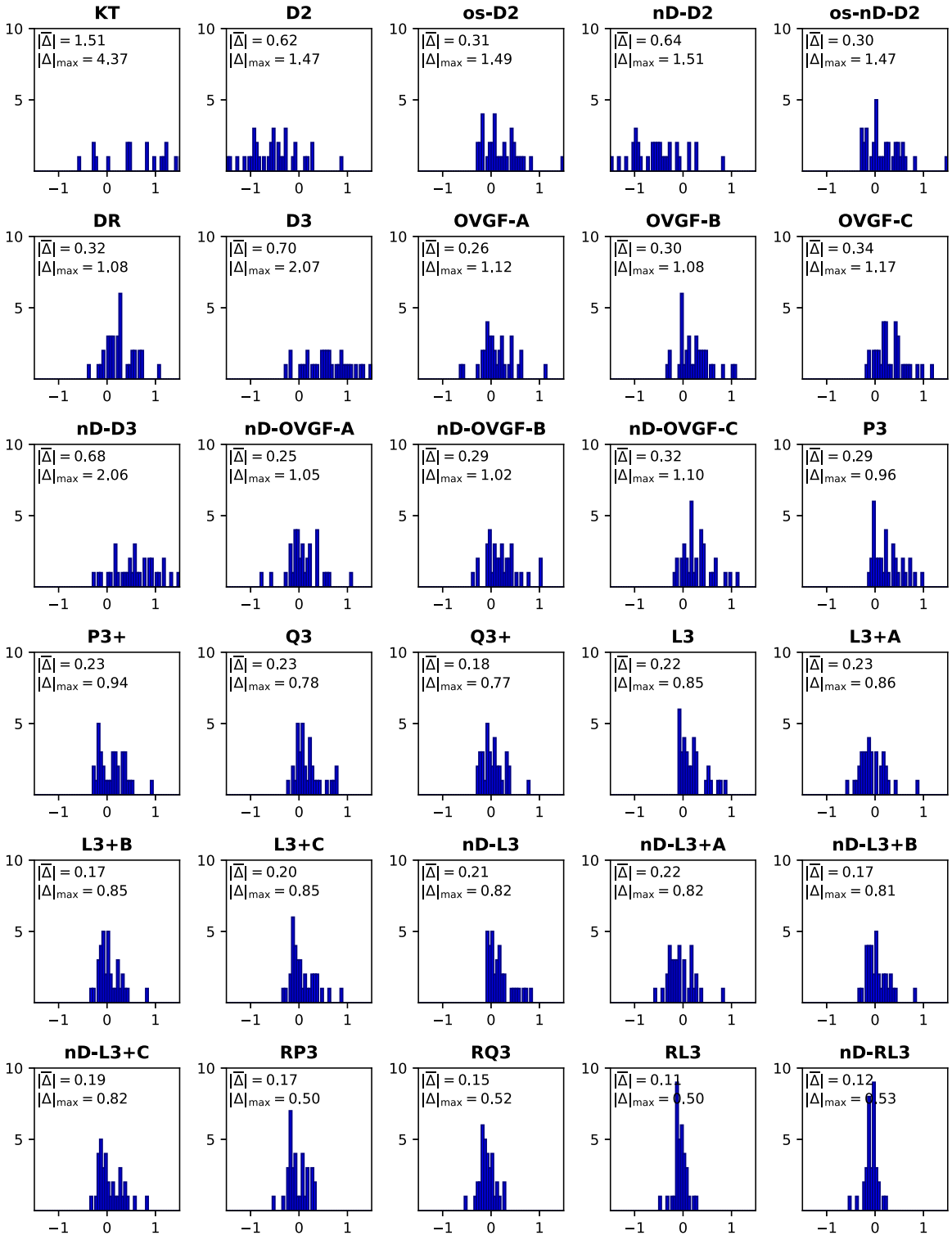


FIG. 2. Histograms of Error Distributions (eV) vs IP-EOM-CCSDTQ/cc-pVTZ standards for 34 VIEs: diagonal self-energy methods.

Published under an exclusive license by AIP Publishing

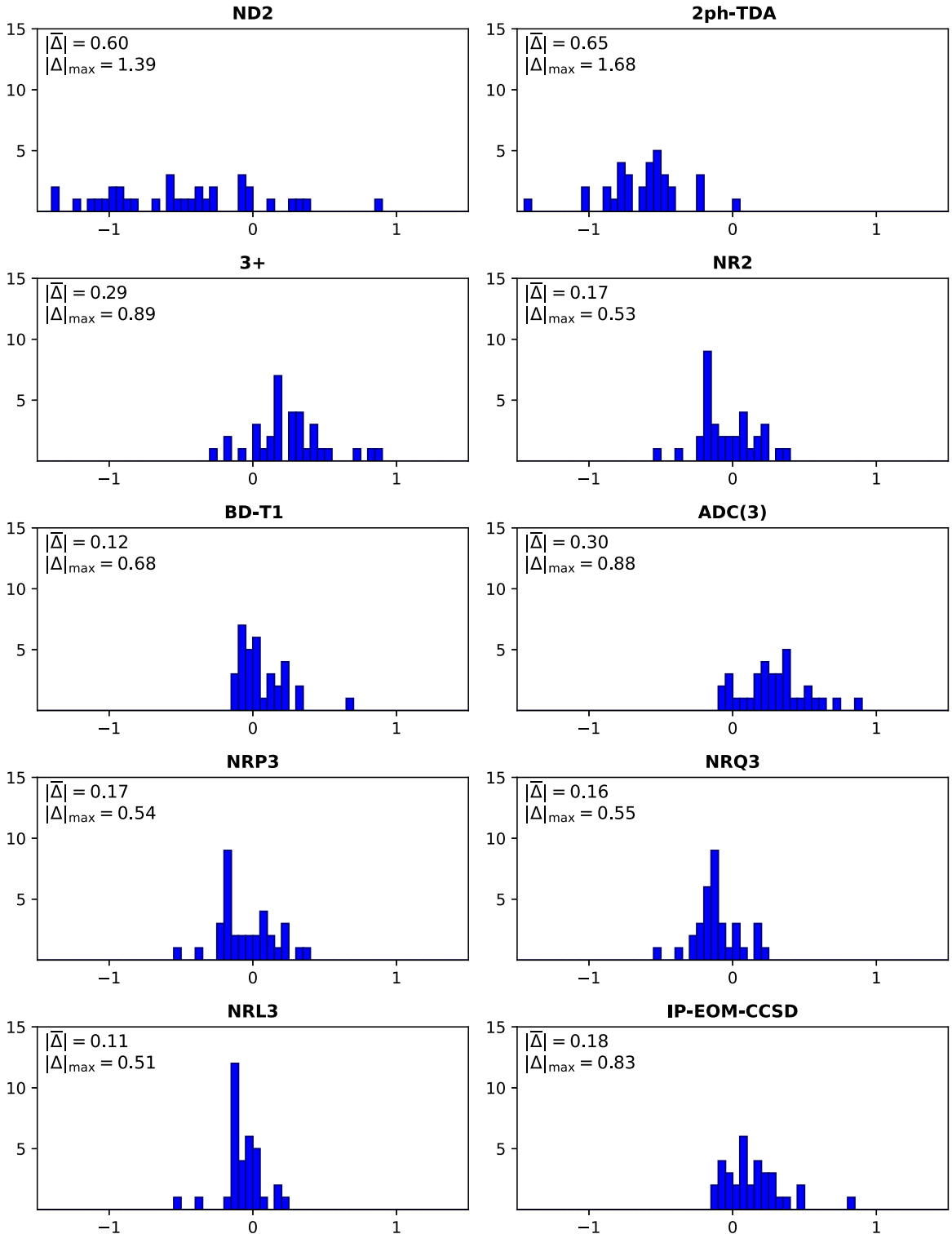


FIG. 3. Histograms of Error Distributions (eV) vs IP-EOM-CCSDTQ/cc-pVTZ standards for 34 VIEs: non-diagonal self-energy methods.

Published under an exclusive license by AIP Publishing

TABLE VI. Error distributions (eV) vs IP-EOM-CCSDT/cc-pVTZ for 160 VIEs.

Method class	Method[a]	MAE[b,c]	MSE[d]	σ[e]	Max. AE[f]
Uncorrelated	KT	1.815	1.786	1.004	4.459
Diagonal second order	D2	0.586	−0.548	0.414	1.491
	os-D2	0.356	0.330	0.285	1.470
	nD-D2	0.620	−0.584	0.425	1.573
	os-nD-D2	**0.340**	0.314	0.281	1.446
Diagonal post second order	DR	0.340	0.320	0.260	1.082
	D3	0.829	0.806	0.572	2.738
	nD-D3	0.813	0.790	0.569	2.738
	OVGF-A	0.289	0.226	0.283	1.044
	OVGF-B	0.389	0.322	0.339	1.331
	OVGF-C	0.434	0.410	0.308	1.341
	nD-OVGF-A	0.274	0.203	0.281	1.015
	nD-OVGF-B	0.370	0.298	0.335	1.301
	nD-OVGF-C	0.412	0.388	0.302	1.310
	P3	0.353	0.341	0.287	1.303
	P3+	0.216	0.169	0.225	0.983
	Q3	0.299	0.273	0.271	1.213
	Q3+	**0.166**	0.102	0.196	0.752
	L3	0.285	0.269	0.251	1.145
	nD-L3	0.264	0.246	0.244	1.109
	L3+A	0.143	0.012	0.200	0.834
	L3+B	0.152	0.100	0.186	0.822
	L3+C	0.163	0.116	0.193	0.842
	nD-L3+A	0.142	0.015	0.200	0.797
	nD-L3+B	**0.148**	0.094	0.186	0.785
	nD-L3+C	0.158	0.108	0.192	0.805
	RP3	0.162	0.043	0.267	2.075
	RQ3	0.141	−0.016	0.213	1.514
	RL3	0.117	−0.016	0.212	1.832
	nD-RL3	**0.112**	−0.037	0.168	0.783
Non-diagonal	ND2	0.609	−0.544	0.547	3.081
	2ph-TDA	0.662	−0.662	0.227	1.689
	3+	0.409	0.365	0.334	1.380
	ADC(3)	0.424	0.387	0.340	1.743
	NR2	**0.130**	0.017	0.193	0.888
	BD-T1	0.143	0.113	0.150	0.701
	NRP3	0.130	−0.015	0.191	0.791
	NRQ3	**0.128**	−0.066	0.166	0.789
	NRL3	**0.088**	−0.043	0.123	0.525
	IP-EOM-CCSD	0.211	0.197	0.173	0.887

[a]New methods in **bold type**.
[b]Optimal methods in **bold type**.
[c]MAE = mean absolute error.
[d]MSE = mean signed error.
[e]σ = standard deviation.
[f]Max. AE = maximum absolute error.

Published under an exclusive license by AIP Publishing

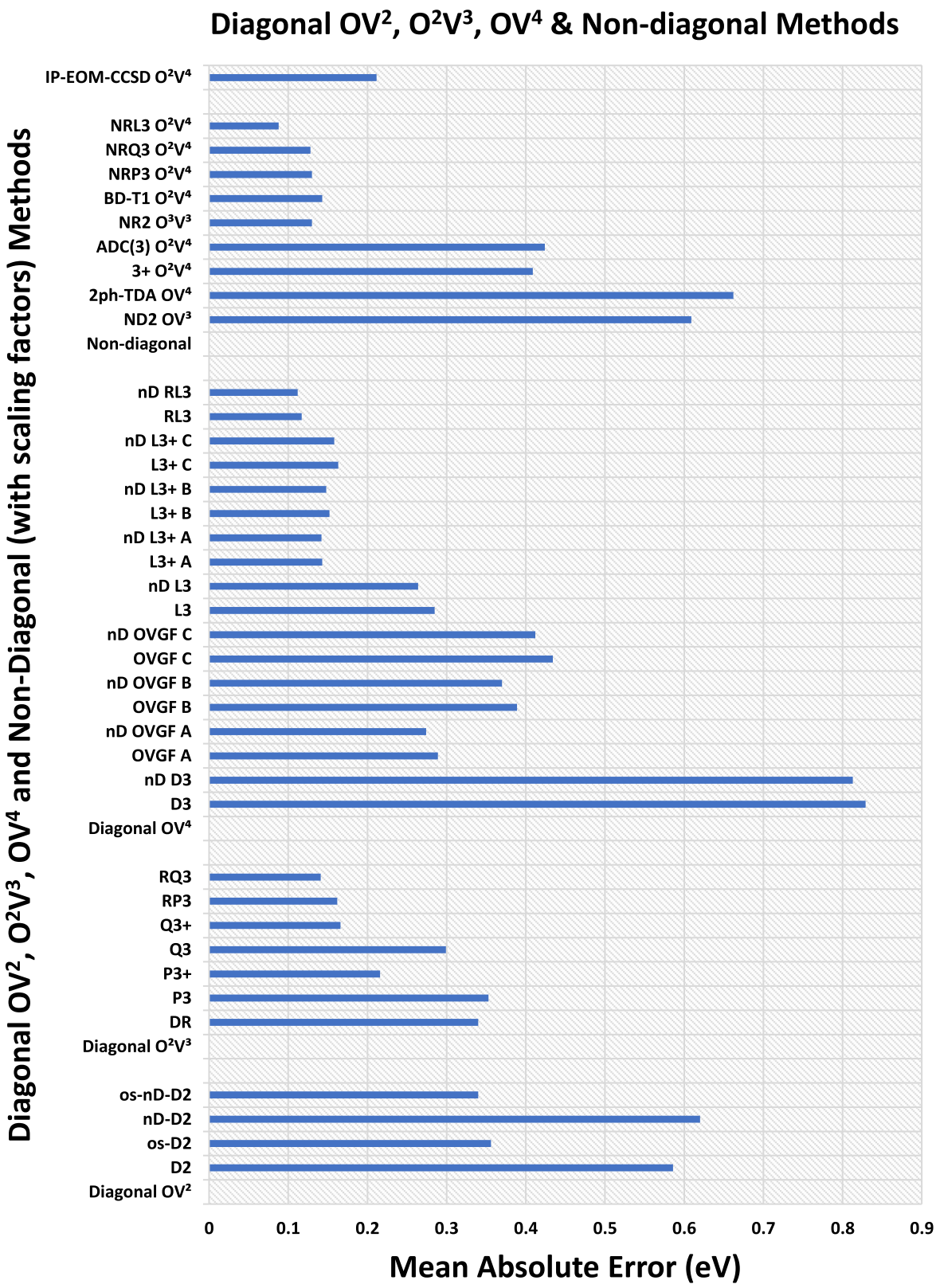


FIG. 4. Mean absolute errors (eV) vs IP-EOM-CCSDT/cc-pVTZ standards for 160 VIEs and arithmetic scaling factors.

Published under an exclusive license by AIP Publishing

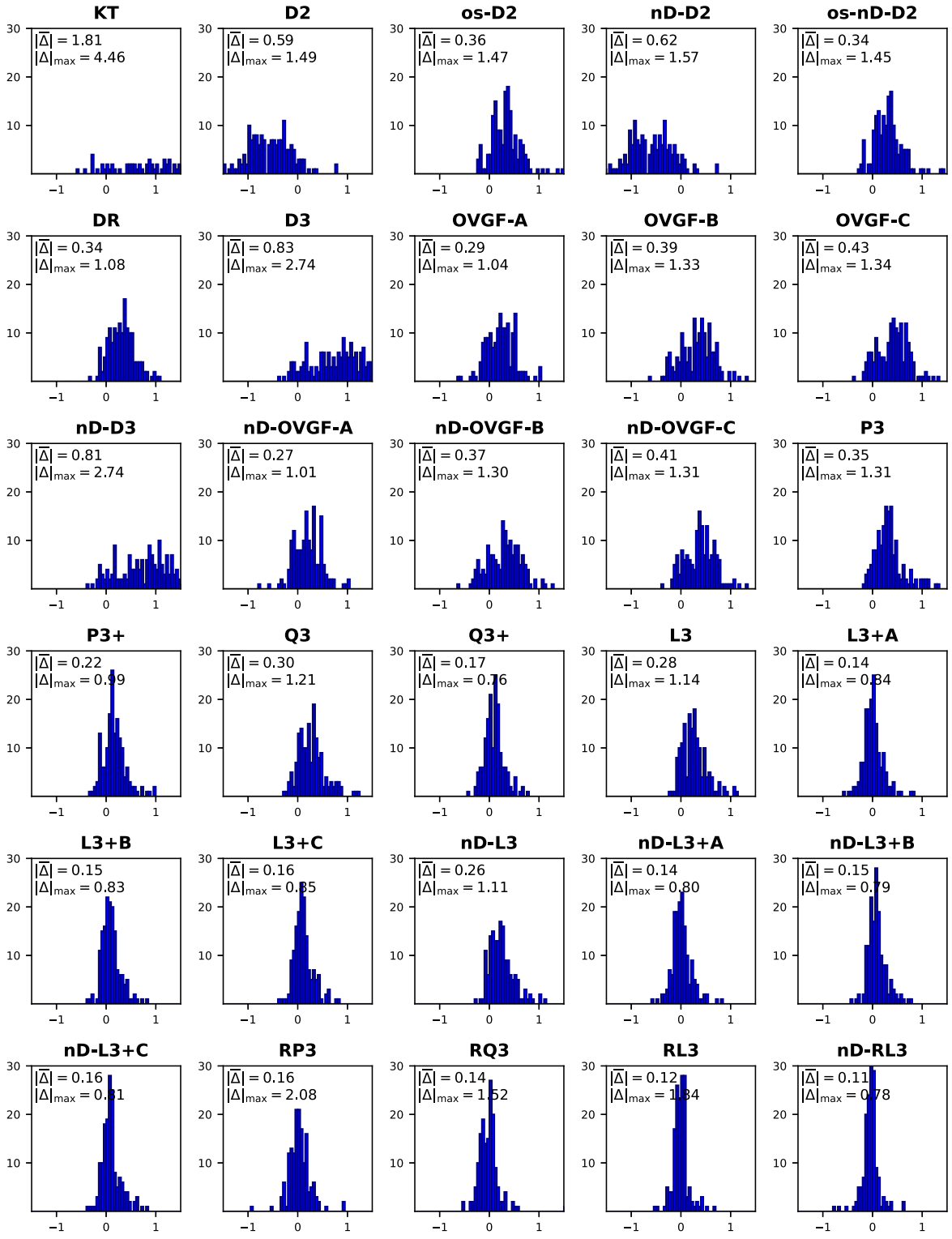


FIG. 5. Histograms of Error Distributions (eV) vs IP-EOM-CCSDT/cc-pVTZ standards for 160 VIEs: diagonal self-energy methods.

Published under an exclusive license by AIP Publishing

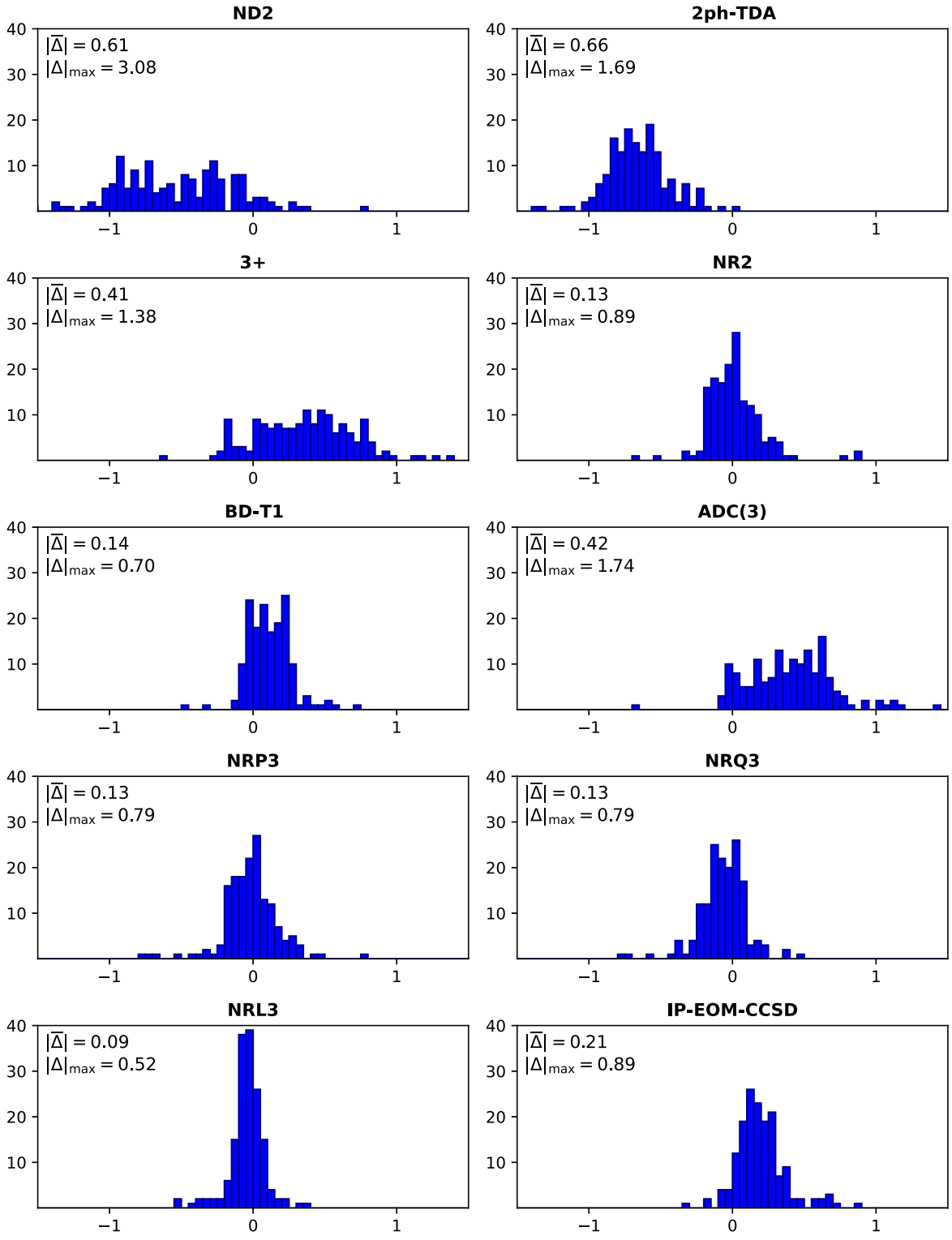


FIG. 6. Histograms of Error Distributions (eV) vs IP-EOM-CCSDT/cc-pVTZ standards for 160 VIEs: non-diagonal self-energy methods.

Published under an exclusive license by AIP Publishing

TABLE VII. Error distributions (eV) vs IP-EOM-CCSDT/cc-pVTZ for 96 VIEs where probability factors ≥0.85.

Method class	Method[a]	MAE[b,c]	MSE[d]	σ[e]	Max. AE[f]
Uncorrelated	KT	1.497	1.471	0.907	2.839
Diagonal second order	D2	0.627	−0.624	0.357	1.389
	os-D2	0.254	0.220	0.195	0.643
	nD-D2	0.660	−0.657	0.371	1.442
	os-nD-D2	**0.242**	0.206	0.193	0.634
Diagonal post second order	DR	0.246	0.213	0.209	0.706
	D3	0.690	0.666	0.488	1.592
	nD-D3	0.677	0.652	0.483	1.577
	OVGF-A	0.211	0.145	0.220	0.574
	OVGF-B	0.338	0.262	0.312	0.818
	OVGF-C	0.346	0.321	0.265	0.845
	nD-OVGF-A	0.198	0.125	0.216	0.591
	nD-OVGF-B	0.323	0.241	0.307	0.794
	nD-OVGF-C	0.328	0.301	0.259	0.821
	P3	0.236	0.220	0.175	0.762
	P3+	0.141	0.077	0.149	0.425
	Q3	0.220	0.186	0.199	0.710
	Q3+	**0.126**	0.042	0.145	0.386
	L3	0.195	0.177	0.168	0.630
	nD-L3	0.178	0.157	0.161	0.602
	L3+A	0.105	−0.058	0.122	0.404
	L3+B	0.098	0.036	0.117	0.362
	L3+C	0.097	0.041	0.115	0.356
	nD-L3+A	0.104	−0.058	0.120	0.399
	nD-L3+B	**0.094**	0.027	0.116	0.360
	nD-L3+C	0.094	0.032	0.114	0.355
	RP3	0.115	0.008	0.145	0.369
	RQ3	0.103	−0.027	0.126	0.307
	RL3	0.076	−0.011	0.098	0.324
	nD-RL3	**0.075**	−0.035	0.095	0.362
Non-diagonal	ND2	0.679	−0.676	0.486	3.081
	2ph-TDA	0.629	−0.629	0.204	1.384
	3+	0.382	0.338	0.309	0.906
	ADC(3)	0.345	0.337	0.230	0.775
	NR2	**0.097**	−0.016	0.120	0.335
	BD-T1	0.102	0.075	0.099	0.261
	NRP3	0.102	−0.023	0.137	0.712
	NRQ3	**0.100**	−0.052	0.128	0.710
	NRL3	**0.060**	−0.026	0.074	0.370
	IP-EOM-CCSD	0.135	0.119	0.099	0.352

[a]New methods in **bold type**.
[b]Optimal methods in **bold type**.
[c]MAE = mean absolute error.
[d]MSE = mean signed error.
[e]σ = standard deviation.
[f]Max. AE = maximum absolute error.

Published under an exclusive license by AIP Publishing

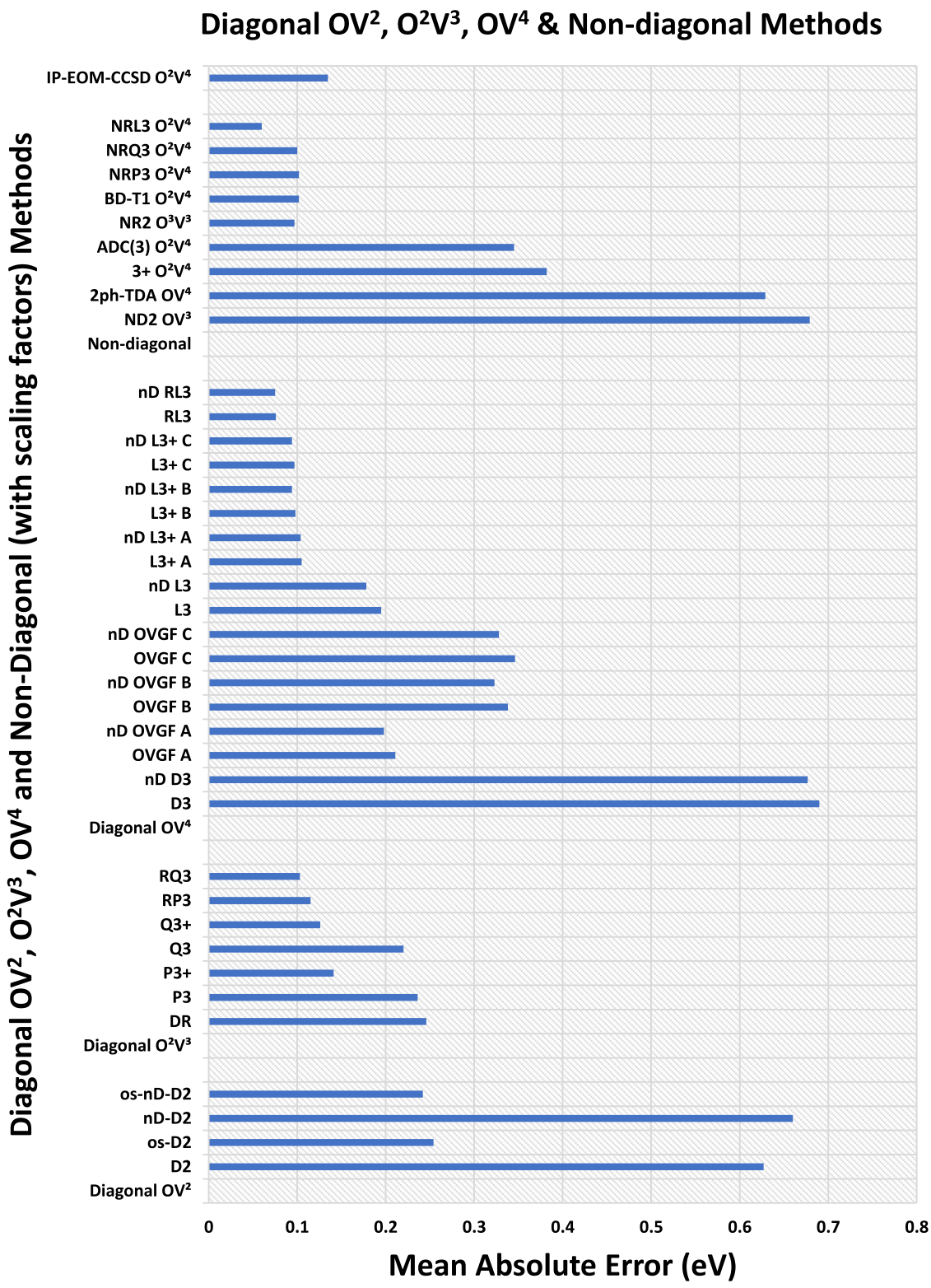


FIG. 7. Mean absolute errors (eV) vs IP-EOM-CCSDT/cc-pVTZ standards for 96 VIEs and arithmetic scaling factors.

Published under an exclusive license by AIP Publishing

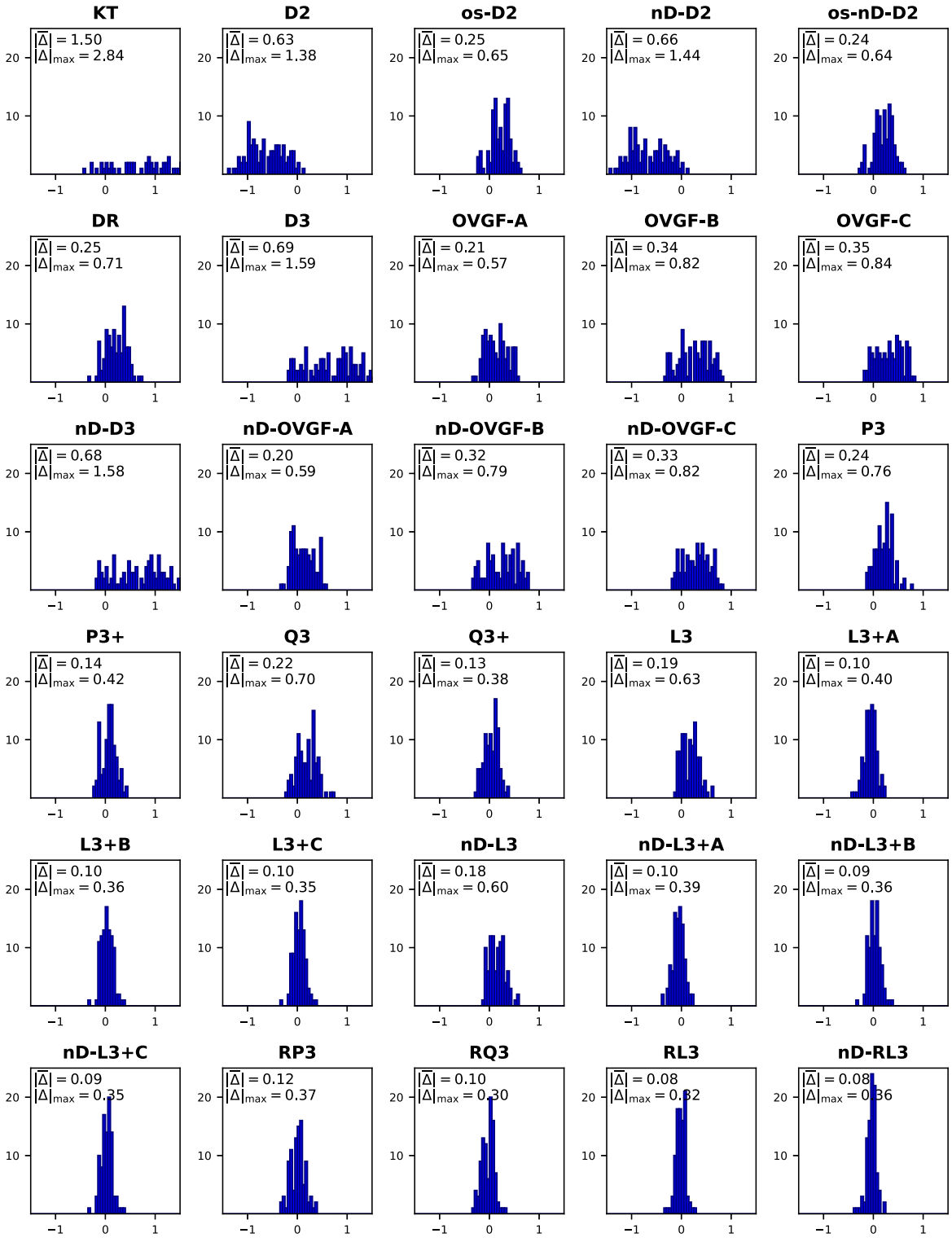


FIG. 8. Histograms of Error Distributions (eV) vs IP-EOM-CCSDT/cc-pVTZ standards for 96 VIEs: diagonal self-energy methods.

Published under an exclusive license by AIP Publishing

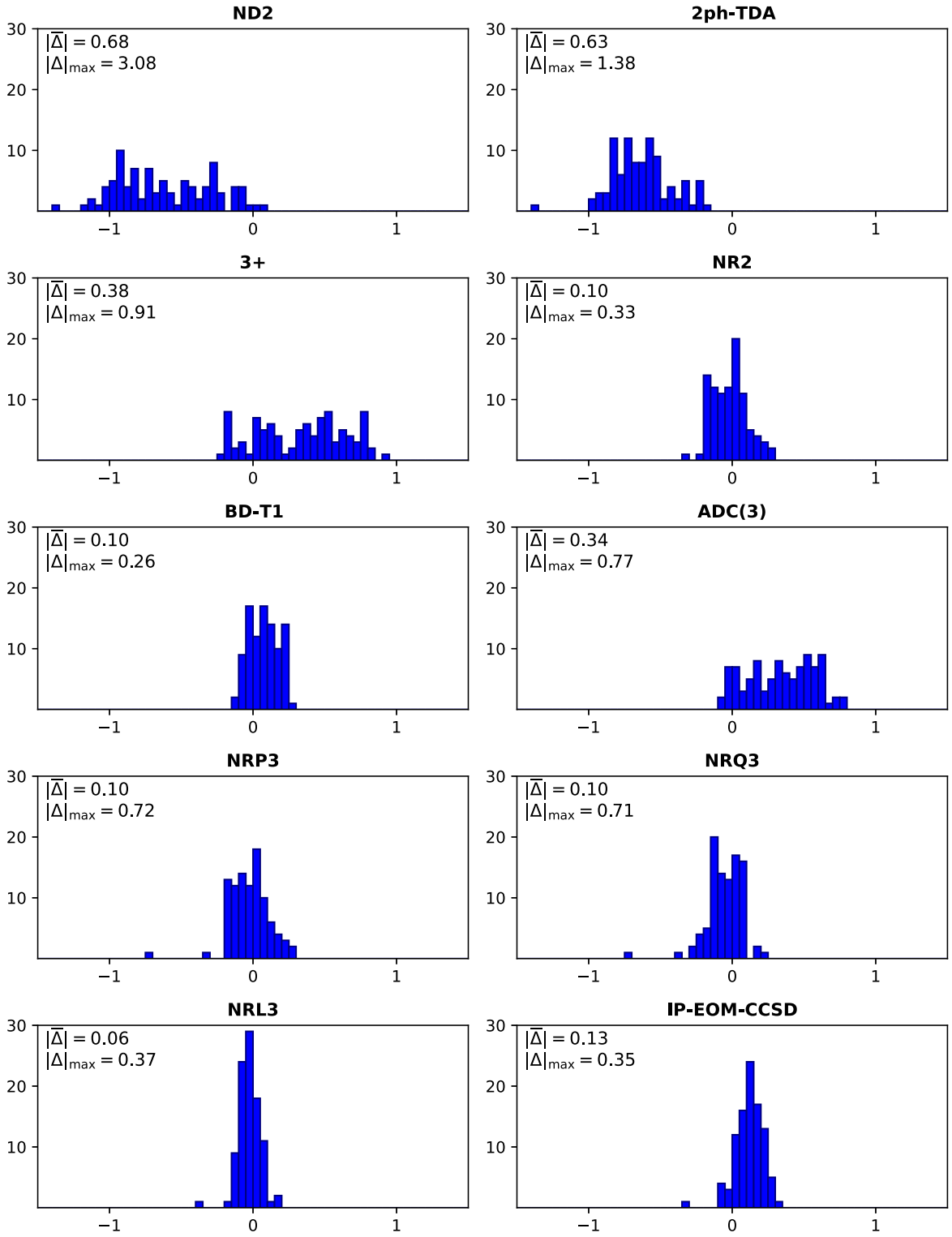


FIG. 9. Histograms of Error Distributions (eV) vs IP-EOM-CCSDT/cc-pVTZ standards for 96 VIEs: non-diagonal self-energy methods.

Published under an exclusive license by AIP Publishing

In general, the results of the first and second tests lead to the same conclusions on non-diagonal methods, the diagonal self-energy approximation, and approximate treatments of renormalization. The histograms in Figs. 3 and 6 display the balance of underestimates and overestimates obtained for NRP3, NRQ3, and NRL3 and the clear improvement in the narrowness of the profile associated with the latter method. Despite the lack of renormalized ground-state substitution amplitudes employed in BD-T1 and IP-EOM-CCSD, the new non-diagonal methods produce smaller error measures and are less likely to be biased in favor of overestimates. The NR2 method, which closely resembles NRP3, also performs reasonably well. Overestimates dominate underestimates in the two histograms of 3+ and ADC(3). Comparisons between the three new non-diagonal methods (NRP3, NRQ3, and NRL3) and their diagonal, renormalized antecedents (RP3, RQ3, and RL3) indicate that little loss of accuracy in VIE prediction is associated with the diagonal approximation. The replacement of explicit renormalizations with nearly effortless approximations in P3+, Q3+, and L3+ introduces errors of only a few hundredths of an eV. Ordered according to decreasing error measures and increasing computational effort, the following diagonal methods offer the best compromises between accuracy and arithmetic efficiency: os-nD-D2, Q3+, nD-L3+B, and nD-RL3. For the non-diagonal methods, the same sequence is NR2, NRQ3, and NRL3.

The present methods are most likely to produce accurate VIEs when probability factors approach unity. A separate assessment of the 96 cases where probability factors from all methods exceed 0.85 may therefore provide a clearer understanding of predictive capabilities when only the lowest VIEs (i.e., those most likely to have large probability factors) are sought. Table VII and Figs. 7–9 display data on these cases. The hierarchy of accuracy seen in Table VII and Fig. 7 closely resembles the precedent set in Table VI and Fig. 4, but MAEs for the most accurate methods decline even further. For this easier test set, several methods attain MAEs of 0.10 eV or less, including the three new non-diagonal self-energies (NRL3, NRQ3, and NRP3), the explicitly renormalized diagonal self-energies RL3 and nD-RL3, and even the approximately renormalized L3+B and nD-L3+B methods. The explicitly renormalized, diagonal methods RQ3 and RP3 have MAEs that only slightly exceed 0.10 eV, as does the approximately renormalized, diagonal Q3+ method. The MAEs for RP3, RQ3, and RL3 (0.12, 0.10, and 0.08 eV, respectively) are in almost perfect agreement with their counterparts from the previously published study of 80 VIEs in which many cases were discarded for want of convergence in the order-by-order algorithm for explicitly renormalized self-energies.[38] The DR and the two opposite-spin, second order methods produce MAEs near 0.25 eV. These three methods have a greater tendency to overestimate VIEs. IP-EOM-CCSD is competitive (MAE = 0.13 eV), but at a much higher cost.[67] Two non-diagonal methods of lower or equal arithmetic scaling, NR2 and BD-T1, produce lower errors. The MAEs of OVGF-A and its non-Dyson variant with OV^4 scaling are larger than those of P3+, Q3+, RP3, and RQ3, all of which have only O^2V^3 arithmetic bottlenecks and no need for ERIs with four virtual indices.

A comparison of the histograms in Fig. 8 discloses that improvements in accuracy may be procured at the cost of greater arithmetic operations. The cubically scaling os-D2 and os-nD-D2 approximations correspond to MAEs near 0.25 eV. Two fifth-power methods, P3+ and Q3+, that do not require a full transformation of the ERIs and that have O^2V^3 arithmetic scaling produce MAEs below 0.15 eV. Their explicitly renormalized counterparts, RP3 and RQ3, are somewhat better, with the latter method attaining an MAE of 0.10 eV. The last option, where the highest accuracy is sought, is provided by the approximately renormalized L3+B method and its non-Dyson variant and by the explicitly renormalized RL3 and nD-RL3 self-energies. These choices correspond to MAEs of 0.10 eV or less. The same hierarchy of methods inferred from the previous two sets of data remains valid for the 96 VIE set.

For the non-diagonal methods examined in Fig. 9, the progression of narrowing profiles with greater cost recommends NRQ3 and NRL3 as the best options. Their respective MAEs of 0.10 and 0.06 eV are achieved with a single sixth-power contraction that requires no iterations. A less demanding alternative is provided by NR2. Whereas ND2 and 2ph-TDA tend to underestimate VIEs, the opposite trend dominates in 3+, ADC(3), and IP-EOM-CCSD calculations. Because MAEs for non-diagonal methods with fifth-power arithmetic scaling are larger than those of several fifth-power diagonal methods, their chief advantage lies in the production of Dyson orbitals that are linear combinations of CHF orbitals.

The set of 160 VIEs has 96 relatively easy cases (where probability factors exceed 0.85 for all methods) and 64 relatively hard cases with appreciable correlation-state (i.e., shake-up) characters. Methods identified as optimal in Tables VI and VII (for the 160 VIE sets and the 96 relatively easy cases, respectively) undergo declines in MAEs that range from 0.1 (for cubically scaling os-nD-D2) to 0.028 eV (for the non-diagonal NRQ3 and NRL3 methods). The remaining optimal diagonal methods (Q3+, nD-L3+B, and nD-RL3) have MAEs that decrease only by 0.04–0.05 eV. These small effects indicate that the four optimal diagonal methods remain useful for the entire set of 160 VIEs. For the NRQ3 and NRL3 methods, MAEs change very little when relatively hard cases are included in the test set.

In diagonal, explicitly renormalized calculations (i.e., for DR, RP3, RQ3, and RL3 self-energies), iterations that pertain to the evaluation of a self-energy matrix element are followed by iterations on the energy parameter, *E*. Table VIII displays the count of successfully converged cases (out of 170 VIEs) for each of these four self-energies and for both algorithms (order-by-order summation and solution of linear equations). In the first column of numerical

TABLE VIII. Number of converged states in old and new algorithms for evaluating diagonal, explicitly renormalized self-energy matrix elements: all 170 VIEs included.

	Number of converged final states	
Methods	Order-by-order algorithm	Linear equation algorithm
DR	122	170
RP3	119	163
RQ3	119	162
RL3	119	161

Published under an exclusive license by AIP Publishing

data, either the summation or the energy iterations fail. (The latter case typically pertains to states with low probability factors and relatively high VIEs.) In the second column, failures pertain to energy iterations only. The new algorithm based on linear equations succeeds in all cases (i.e., at all energies), even when the energy iterations fail.

CONCLUSIONS

A new generation of renormalized, diagonal self-energies has been extended to include non-diagonal alternatives. Improvements of a few hundredths of an eV in the accuracy of predictions on vertical ionization energies have been achieved, and Dyson orbitals expressed as linear combinations of canonical Hartree–Fock orbitals have been obtained with the new non-diagonal self-energies. In exchange for these benefits, non-iterative sixth power summations that constitute bottleneck contractions have been introduced. The superior accuracy and efficiency of these methods and their diagonal counterparts with respect to widely used, older methods have been established. In addition, the efficacy of approximate renormalizations in achieving only slightly lower accuracy with reduced cost has been demonstrated.

The best compromises in accuracy and efficiency among the non-diagonal methods are the NRQ3 and NRL3 self-energies. These closely related extensions of the diagonal explicitly renormalized RQ3 and RL3 methods have average errors of 0.10 or 0.06 eV, respectively, when they are applied to 96 final states with probability factors (norms of Dyson orbitals, or pole strengths) that exceed 0.85. These sixth-power methods are more accurate than alternatives with the same arithmetic scaling factor (e.g., BD-T1 and IP-EOM-CCSD) and require far fewer bottleneck contractions. The slightly less accurate NRQ3 alternative requires fewer OV^4 iterations than NRL3. Future implementations may avoid the sixth-power steps entirely by increasing the number of fifth-power steps in matrix-vector multiplications that occur during super-operator Hamiltonian diagonalizations.

Not much accuracy is lost when the diagonal approximation is made. The RQ3, RL3, and nD-RL3 methods have average errors of 0.10 eV or less for the outer-valence set of 96 vertical ionization energies with probability factors that exceed the recommended threshold of 0.85. By converging in all presently considered cases, the new algorithm based on the solution of linear equations for explicitly renormalized diagonal methods enables more thorough comparisons of methods. When the explicit renormalizations present in each of these methods are replaced by approximate renormalizations in the Q3+, L3+B, and nD-L3+B self-energies, the average errors increase only by a few hundredths of an eV. When MAEs of 0.25 eV are acceptable, the most efficient alternative is os-nD-D2.

An illustrative example of compromises between accuracy and efficiency is summarized in Fig. 10 for a case where V/O = 26 (e.g., carbon clusters with a cc-pVQZ basis). The OV^2, O^2V^3, O^3V^3, OV^4, and O^2V^4 scaling factors may be expressed solely in terms of V^α as $V^{2.175}$, $V^{3.351}$, $V^{3.526}$, $V^{4.175}$, and $V^{4.351}$, respectively. A plot of α-2 vs MAE for the five most accurate (i.e., smallest MAE) representatives of each scaling factor (os-nD-D2, Q3+, NR2, L3+B, and NRL3, respectively) indicates that new-generation self-energies have supplanted their predecessors with the same arithmetic scaling factors in the present tests. (NR2 has no new-generation competitor with O^3V^3 scaling.) For example, os-nD-D2 has the same arithmetic scaling factor as D2 but is clearly more accurate for the set of 96 VIEs.

The predictive and computational advantages of the new generation of self-energies follow from:

- adoption of a single super-operator metric that imposes Hermiticity on the super-operator Hamiltonian matrix and size-extensivity on reference state total energies and
- subsequent identification and retention of consequent second and third order terms.

Derivations of older methods employ variable metrics to obtain all terms of a given order and, therefore, produce operator couplings

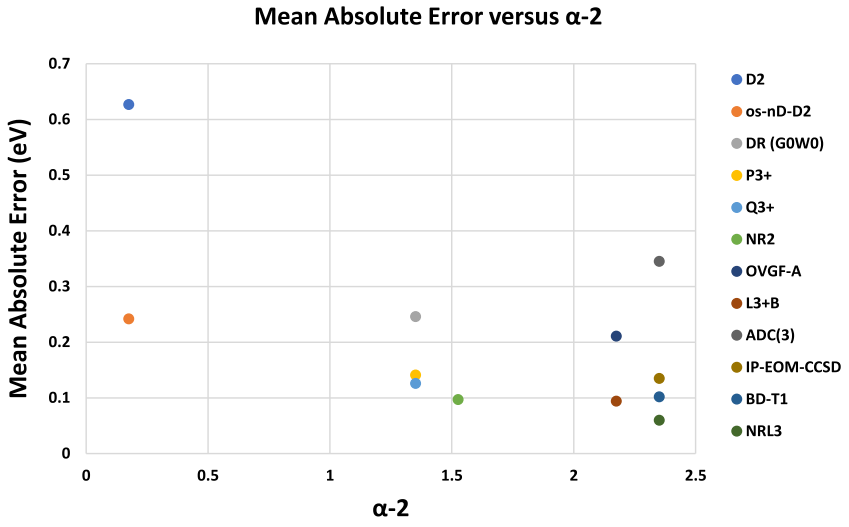


FIG. 10. Mean absolute errors (eV) of various self-energies vs arithmetic scaling factor V^α exponent for V/O = 26.

Published under an exclusive license by AIP Publishing

that may be linear or quadratic in ground-state correlation amplitudes. Differences between the two approaches arise in the blocks of the super-operator Hamiltonian matrices that are diagonalized to obtain electron binding energies. In the new generation of methods, there are no constant self-energy terms that are quadratic in ground-state correlation amplitudes. In addition, couplings between simple and triple field operators appear with an extra factor of one-half.

Computational strategies for calculating electron binding energies of larger molecules, including composite procedures for the estimation of basis-set and correlation effects,[83] are now under study. Programs have already been written for unrestricted Hartree–Fock spin-orbitals; studies of open-shell reference states where spin contamination is acceptably low are also in progress.

SUPPLEMENTARY MATERIAL

See the supplementary material for the results of calculations on VIEs.

ACKNOWLEDGMENTS

The authors thank Manuel Díaz Tinoco and Héctor Hernández Corzo for their valuable discussions and technical support.

AUTHOR DECLARATIONS

Conflict of Interest

The authors have no conflicts to disclose.

Author Contributions

Ernest Opoku: Conceptualization (supporting); Data curation (lead); Formal analysis (supporting); Investigation (lead); Methodology (supporting); Software (supporting); Validation (lead); Visualization (lead); Writing – original draft (supporting); Writing – review & editing (supporting). **Filip Pawłowski**: Conceptualization (supporting); Data curation (supporting); Formal analysis (equal); Investigation (supporting); Methodology (supporting); Resources (supporting); Software (supporting); Supervision (supporting); Validation (supporting); Writing – original draft (supporting); Writing – review & editing (supporting). **J. V. Ortiz**: Conceptualization (lead); Data curation (supporting); Formal analysis (equal); Funding acquisition (lead); Investigation (supporting); Methodology (equal); Project administration (equal); Resources (lead); Software (lead); Supervision (lead); Validation (supporting); Visualization (supporting); Writing – original draft (lead); Writing – review & editing (equal).

DATA AVAILABILITY

The data that support the findings of this study are available within the article and its supplementary material.

REFERENCES

[1] T. Koopmans, Physica **1**(1–6), 104–113 (1934).
[2] J. V. Ortiz and R. A. Zalik, J. Chem. Phys. **153**(11), 114122 (2020).
[3] J. V. Ortiz, *Advances in Quantum Chemistry* (Academic Press, 2022), Vol. 85, pp. 109–155.
[4] J. V. Ortiz, J. Chem. Phys. **153**(7), 070902 (2020).
[5] J. V. Ortiz, in *Chemical Reactivity*, edited by L. v. S. Savas Kaya, G. Serdaroglu, and L. Guo (Elsevier, Amsterdam, 2023), Vol. 1, pp. 606.
[6] E. R. Davidson, J. V. Ortiz, and V. N. Staroverov, J. Chem. Phys. **155**(5), 051102 (2021).
[7] M. A. Díaz-Tinoco and J. V. Ortiz, J. Chem. Phys. **145**(14), 147101 (2016).
[8] M. Díaz-Tinoco and J. V. Ortiz, Phys. Chem. Chem. Phys. **18**, 15456–15457 (2016).
[9] M. Díaz-Tinoco and J. V. Ortiz, ChemPhysChem **17**(18), 2945–2946 (2016).
[10] V. V. Zakjevskii, S. J. King, O. Dolgounitcheva, V. G. Zakrzewski, and J. V. Ortiz, J. Am. Chem. Soc. **128**(41), 13350–13351 (2006).
[11] E. Opoku, F. Pawłowski, and J. V. Ortiz, J. Phys. Chem. A **127**(4), 1085–1101 (2023).
[12] R. J. Bartlett, Wiley Interdiscip. Rev.: Comput. Mol. Sci. **2**(1), 126–138 (2012).
[13] J. Schirmer, A. B. Trofimov, and G. Stelter, J. Chem. Phys. **109**(12), 4734–4744 (1998).
[14] L. Reining, Wiley Interdiscip. Rev.: Comput. Mol. Sci. **8**(3), e1344 (2018).
[15] J. Linderberg and Y. Öhrn, *Propagators in Quantum Chemistry*, 2nd ed. (Wiley-Interscience, Hoboken, NJ, 2004).
[16] P. Jørgensen and J. Simons, *Second Quantization-Based Methods in Quantum Chemistry* (Academic Press, New York, 1981).
[17] J. Schirmer, *Many-Body Methods for Atoms, Molecules and Clusters* (Springer International Publishing AG, 2018).
[18] H. H. Corzo and J. V. Ortiz, in *Advances in Quantum Chemistry*, edited by J. R. Sabin and E. J. Brändas (Academic Press, 2017), Vol. 74, pp. 267–298.
[19] J. V. Ortiz, in *Annual Reports in Computational Chemistry*, edited by D. A. Dixon (Elsevier, 2017), Vol. 13, pp. 139–182.
[20] J. V. Ortiz, Wiley Interdiscip. Rev.: Comput. Mol. Sci. **3**(2), 123–142 (2013).
[21] A. Banerjee, R. Shepard, and J. Simons, Int. J. Quantum Chem. **14**, 389–404 (1978).
[22] D. L. Yeager, Adv. Quantum Chem. **50**, 289–313 (2005).
[23] I. M. Mazin and A. Y. Sokolov, J. Chem. Theory Comput. **17**(10), 6152–6165 (2021).
[24] D. J. Thouless, *The Quantum Mechanics of Many-Body Systems* (Academic Press, New York, 1961).
[25] C.-H. Hu, D. P. Chong, and M. E. Casida, J. Electron Spectrosc. Relat. Phenom. **85**(1–2), 39–46 (1997).
[26] J. Romero, J. A. Charry, H. Nakai, and A. Reyes, Chem. Phys. Lett. **591**, 82–87 (2014).
[27] F.-H. Lim, M. Nishida, Y. Hori, T. Ida, and M. Mizuno, Chem. Phys. Lett. **678**, 159–166 (2017).
[28] S. Śmiga and I. Grabowski, J. Chem. Theory Comput. **14**(9), 4780–4790 (2018).
[29] L. S. Cederbaum, Theor. Chim. Acta **31**(3), 239–260 (1973).
[30] H. H. Corzo, A. Galano, O. Dolgounitcheva, V. G. Zakrzewski, and J. V. Ortiz, J. Phys. Chem. A **119**(33), 8813–8821 (2015).
[31] D. P. Chong, F. G. Herring, and D. McWilliams, J. Chem. Phys. **61**(1), 78–84 (1974).
[32] D. P. Chong, F. G. Herring, and D. McWilliams, J. Chem. Phys. **61**(3), 958–962 (1974).
[33] D. P. Chong, F. G. Herring, and D. McWilliams, J. Chem. Phys. **61**(9), 3567–3570 (1974).
[34] S. Hirata, M. R. Hermes, J. Simons, and J. V. Ortiz, J. Chem. Theory Comput. **11**(4), 1595–1606 (2015).
[35] S. Hirata, A. E. Doran, P. J. Knowles, and J. V. Ortiz, J. Chem. Phys. **147**(4), 044108 (2017).
[36] W. von Niessen, J. Schirmer, and L. S. Cederbaum, Comput. Phys. Rep. **1**, 57–125 (1984).
[37] J. V. Ortiz, in *Computational Chemistry: Reviews of Current Trends*, edited by J. Leszczynski (World Scientific, Singapore, 1997), Vol. 2, pp. 1–61.
[38] E. Opoku, F. Pawłowski, and J. V. Ortiz, J. Chem. Phys. **155**(20), 204107 (2021).
[39] E. Opoku, F. Pawłowski, and J. V. Ortiz, J. Chem. Theory Comput. **18**(8), 4927–4944 (2022).

Published under an exclusive license by AIP Publishing

[40]J. V. Ortiz, J. Chem. Phys. **104**(19), 7599–7605 (1996).
[41] A. M. Ferreira, G. Seabra, O. Dolgounitcheva, V. G. Zakrzewski, and J. V. Ortiz, in *Quantum-Mechanical Prediction of Thermochemical Data*, edited by J. Cioslowski (Springer, Dordrecht, Netherlands, 2001), pp. 131–160.
[42]J. V. Ortiz, Int. J. Quantum Chem. **105**(6), 803–808 (2005).
[43]R. M. Richard, M. S. Marshall, O. Dolgounitcheva, J. V. Ortiz, J.-L. Brédas, N. Marom, and C. D. Sherrill, J. Chem. Theory Comput. **12**(2), 595–604 (2016).
[44]L. Gallandi, N. Marom, P. Rinke, and T. Körzdörfer, J. Chem. Theory Comput. **12**(2), 605–614 (2016).
[45]J. W. Knight, X. Wang, L. Gallandi, O. Dolgounitcheva, X. Ren, J. V. Ortiz, P. Rinke, T. Körzdörfer, and N. Marom, J. Chem. Theory Comput. **12**(2), 615–626 (2016).
[46]O. Dolgounitcheva, M. Díaz-Tinoco, V. G. Zakrzewski, R. M. Richard, N. Marom, C. D. Sherrill, and J. V. Ortiz, J. Chem. Theory Comput. **12**(2), 627–637 (2016).
[47]I. Tamm, J. Phys. USSR **9**, 449 (1945).
[48]S. M. Dancoff, Phys. Rev. **78**(4), 382–385 (1950).
[49]S. J. Bintrim and T. C. Berkelbach, J. Chem. Phys. **154**(4), 041101 (2021).
[50]J. Schirmer and L. S. Cederbaum, J. Phys. B: At. Mol. Phys. **11**, 1889–1900 (1978).
[51] J. Schirmer, L. S. Cederbaum, and O. Walter, Phys. Rev. A **28**(3), 1237–1259 (1983).
[52]J. V. Ortiz, J. Chem. Phys. **108**, 1008–1014 (1998).
[53]K. A. Brueckner, Phys. Rev. **96**(2), 508–516 (1954).
[54]R. K. Nesbet, Phys. Rev. **109**(5), 1632–1638 (1958).
[55]J. Čížek and J. Paldus, Phys. Scr. **21**, 251–254 (1980).
[56]R. J. Bartlett and G. D. Purvis, Phys. Scr. **21**, 255–265 (1980).
[57]R. A. Chiles and C. E. Dykstra, J. Chem. Phys. **74**(8), 4544–4556 (1981).
[58]N. C. Handy, J. A. Pople, M. Head-Gordon, K. Raghavachari, and G. W. Trucks, Chem. Phys. Lett. **164**(2–3), 185–192 (1989).
[59]J. V. Ortiz, J. Chem. Phys. **109**, 5741–5746 (1998).
[60]J. V. Ortiz, Chem. Phys. Lett. **296**(5–6), 494–498 (1998).
[61] J. V. Ortiz, Chem. Phys. Lett. **297**(3–4), 193–199 (1998).
[62]J. V. Ortiz, Adv. Quantum Chem. **35**, 33–52 (1999).
[63]J. Schirmer and G. Angonoa, J. Chem. Phys. **91**, 1754–1761 (1989).
[64]A. B. Trofimov and J. Schirmer, J. Chem. Phys. **123**(14), 144115 (2005).
[65]L. Storchi, G. Vitillaro, and F. Tarantelli, J. Comput. Chem. **30**(5), 818–825 (2009).
[66]G. Angonoa, O. Walter, and J. Schirmer, J. Chem. Phys. **87**(12), 6789–6801 (1987).
[67]D. S. Ranasinghe, J. T. Margraf, A. Perera, and R. J. Bartlett, J. Chem. Phys. **150**(7), 074108 (2019).
[68]S. Kanchanakungwankul and D. G. Truhlar, J. Chem. Theory Comput. **17**(8), 4823–4830 (2021).
[69]O. Goscinski and B. Lukman, Chem. Phys. Lett. **7**, 573–576 (1970).
[70]B. T. Pickup and O. Goscinski, Mol. Phys. **26**, 1013–1035 (1973).
[71] P. O. Löwdin, Phys. Rev. **139**(2A), 357–372 (1965).
[72]R. Manne, Chem. Phys. Lett. **45**(3), 470–472 (1977).
[73]C. Møller and M. S. Plesset, Phys. Rev. **46**(7), 618–622 (1934).
[74]D. J. Rowe, Rev. Mod. Phys. **40**(1), 153–166 (1968).
[75]C. Nehrkorn, G. D. Purvis, and Y. Öhrn, J. Chem. Phys. **64**(4), 1752–1756 (1976).
[76]M. J. Frisch, G. W. Trucks, H. B. Schlegel, G. E. Scuseria, M. A. Robb, J. R. Cheeseman, G. Scalmani, V. Barone, G. A. Petersson, H. Nakatsuji, X. Li, M. Caricato, A. V. Marenich, J. Bloino, B. G. Janesko, R. Gomperts, B. Mennucci, H. P. Hratchian, J. V. Ortiz, A. F. Izmaylov, J. L. Sonnenberg, D. Williams-Young, F. Ding, F. Lipparini, F. Egidi, J. Goings, B. Peng, A. Petrone, T. Henderson, D. Ranasinghe, V. G. Zakrzewski, J. Gao, N. Rega, G. Zheng, W. Liang, M. Hada, M. Ehara, K. Toyota, R. Fukuda, J. Hasegawa, M. Ishida, T. Nakajima, Y. Honda, O. Kitao, H. Nakai, T. Vreven, K. Throssell, J. A. Montgomery, J. E. Peralta, F. Ogliaro, M. J. Bearpark, J. J. Heyd, E. N. Brothers, K. N. Kudin, V. N. Staroverov, T. A. Keith, R. Kobayashi, J. Normand, K. Raghavachari, A. P. Rendell, J. C. Burant, S. S. Iyengar, J. Tomasi, M. Cossi, J. M. Millam, M. Klene, C. Adamo, R. Cammi, J. W. Ochterski, R. L. Martin, K. Morokuma, O. Farkas, J. B. Foresman, and D. J. Fox, Gaussian Development Version, Revision I.14, Gaussian, Inc., Wallingford, CT, 2018.
[77]T. H. Dunning, Jr., J. Chem. Phys. **90**(2), 1007–1023 (1989).
[78]J. F. Stanton and J. Gauss, J. Chem. Phys. **101**(10), 8938–8944 (1994).
[79]L. S. Cederbaum, W. Domcke, J. Schirmer, and W. Von Niessen, Adv. Chem. Phys. **65**, 115–159 (1986).
[80]J. Baker and B. T. Pickup, Chem. Phys. Lett. **76**, 537–541 (1980).
[81] V. G. Zakrzewski, O. Dolgounitcheva, and J. V. Ortiz, Int. J. Quantum Chem. **75**(4–5), 607–614 (1999).
[82]S. Banerjee and A. Y. Sokolov, J. Chem. Theory Comput. **19**(11), 3037–3053 (2023).
[83]M. Díaz-Tinoco, O. Dolgounitcheva, V. G. Zakrzewski, and J. V. Ortiz, J. Chem. Phys. **144**(22), 224110 (2016).

Published under an exclusive license by AIP Publishing

Appendix D

E. Opoku, F. Pawłowski and J. V. Ortiz, "Electron–Propagator Self–Energies Versus Improved GW100 Vertical Ionization Energies", *J. Chem. Theory Comp.*, 18, 4927–44 (2022)

JCTC Journal of Chemical Theory and Computation

pubs.acs.org/JCTC Article

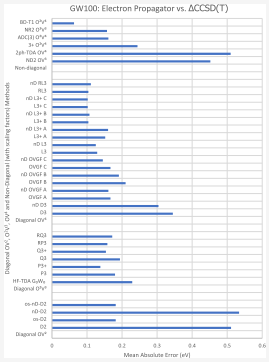
Electron Propagator Self-Energies versus Improved GW100 Vertical Ionization Energies

Ernest Opoku, Filip Pawłowski, and J. V. Ortiz*

Cite This: J. Chem. Theory Comput. 2022, 18, 4927−4944 Read Online

ACCESS | Metrics & More | Article Recommendations | Supporting Information

ABSTRACT: *Ab initio* electron propagator (EP) methods that are free of adjustable parameters in their self-energy formulae and in the generation of their orbital bases have been applied to the calculation of the lowest vertical ionization energies (VIEs) of the GW100 set. An improved set of standard results accompanied by irreducible representation assignments has been produced indirectly with coupled-cluster singles and doubles plus perturbative triples, i.e., CCSD(T), total energy differences at initial-state geometries reoptimized (in 28 cases) with the largest applicable point groups. The best compromises of accuracy and efficiency belong to a new generation of EP self-energies, several members of which may be derived from an intermediately normalized, Hermitized super-operator metric. The following diagonal self-energy methods are optimal: opposite-spin non-Dyson second order (os-nD-D2), approximately renormalized partial third order (P3+), approximately renormalized quasiparticle third order (Q3+), and non-Dyson approximately renormalized linear third order version B (nD-L3+B). Their mean absolute errors (MAEs) in electron volts and arithmetic scaling factors expressed in terms of occupied (O) and virtual (V) orbital dimensions are, respectively, (0.18, OV^2), (0.14, O^2V^3), (0.15, O^2V^3), and (0.11, OV^4). The 0.06 eV MAE for the non-diagonal, sixth-power (O^2V^4) Brueckner doubles, triple-field operator (BD-T1) EP method is exceeded by the 0.1 eV MAE with respect to experiments in seventh-power, ΔCCSD(T) calculations and indicates that BD-T1 may serve as a direct, spin-symmetry-conserving alternative in the generation of standard results for VIEs of larger, closed-shell molecules.

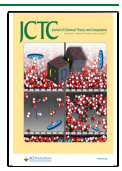


1. INTRODUCTION

Ab initio electron propagator theory (EPT)[1−3] has been applied by quantum chemists to the calculation of molecular and atomic ionization energies (IEs) for over 50 years.[4−7] In most applications, perturbative corrections to the results of Koopmans's identity,[8] i.e., the negatives of canonical Hartree−Fock (HF) orbital energies, have been expressed in the self-energy operator of the Dyson equation. The latter terms describe the diminishing effects on the predicted IEs of orbital relaxation in final, cationic states and differential electron correlation, which usually, but not always, has the opposite sign. This approximate cancellation of errors often produces fortuitous agreement with experiments for the first few IEs of closed-shell molecules and atoms. Of equal import to the understanding of ionization experiments is the close resemblance that usually exists between the highest occupied canonical HF orbitals and Dyson orbitals[9] of electron removal obtained using methods that account for relaxation and correlation.[10] The satisfactory approximation of Dyson orbitals by canonical HF orbitals typically has two dimensions: minimal interference from other orbitals and probability (i.e., intensity) factors that are close to unity.

The self-energies in the widest use for the lowest IEs of closed-shell species therefore typically make the diagonal, or quasiparticle, approximation in the self-energy matrix. By neglecting off-diagonal elements in the canonical HF basis, an order of magnitude greater arithmetic *efficiency* may be procured with little loss of *accuracy*. The effect of this simplification on a Dyson orbital is to make it equal to the product of a canonical HF orbital times the square root of the probability factor, which arises from the energy dependence of the self-energy operator. Several of these diagonal methods require only terms of second (e.g., D2) or second and third order (e.g., D3) in the Møller−Plesset fluctuation potential.[11] Renormalized alternatives include select classes of terms (e.g., ring diagrams in the G_0W_0 family of methods[12]) in all perturbation orders. Approximately renormalized approximations (e.g., the three outer-valence Green's function, or OVGF, methods[13,14] and the P3+[15] method) perform estimates of the latter summations with information extracted from second-order and third-order calculations. A new generation of self-energy approximations of all three types (i.e., finite-order, renormalized, and approximately renormalized) that is based on an alternative approach to performing reference-state averages has recently been introduced and compared to its antecedents with respect to accuracy and computational

Received: May 12, 2022
Published: July 13, 2022



ACS Publications © 2022 American Chemical Society

https://doi.org/10.1021/acs.jctc.2c00502
J. Chem. Theory Comput. 2022, 18, 4927−4944

efficiency.[16] The dual advantages of these relatively new methods have been demonstrated versus a data set of high-level calculations that approach the full configuration interaction (FCI) limit in polarized triple ζ basis sets.[17]

Non-diagonal renormalized (NR) self-energies have advantages in calculations on higher IEs of the inner-valence and core regions of ionization spectra. In the former cases, wherein zeroth-order Koopmans-like final states are submerged in a sea of shake-up (two-hole one-particle or more complex) configurations, Dyson orbitals usually have low probability factors and may have major contributions from several canonical HF constituents. (Intense vibronic mixing is also likely to complicate interpretations of inner-valence spectra that typically exhibit broad, poorly resolved features.) The frozen-orbital, uncorrelated approximations of Koopmans's theorem (KT) therefore lose their qualitative validity for inner-valence IEs.[18] Strong final-state orbital relaxation dominates differential correlation effects in core IEs. In a frozen orbital basis, strong relaxation must be described by NR self-energies which give an ample scope for improvements on canonical HF orbitals and their energies.

The applicability of NR methods is limited by increased requirements of arithmetic operations or other computational resources. Numerical comparisons between the two types of self-energy approximations revealed that diagonal, low-order methods can surpass NR ones with respect to accuracy and efficiency for outer-valence IEs.[16,19−21] A reward of greater accuracy in exchange for additional computational effort accompanied the use of some, but not all, NR methods. The advantageous methods of the latter set included the NR second-order[22] (NR2) and the Brueckner doubles (BD), triple-field operator[16,23−28] (BD-T1) approximations.

Testing the utility of *ab initio*, electron propagator (EP) methods for calculating vertical IEs (VIEs) of a variety of closed-shell atoms and molecules drawn from many sectors of the periodic table is the chief object of the present study. (Electron attachment energies and open-shell initial states are not considered in this work.) The GW100 set of atoms and molecules[29,30] has often been used for this purpose by developers of related methods, usually of the G_0W_0 family,[12] wherein the diagonal approximation is also made, but in a Kohn−Sham orbital basis. VIEs obtained with ΔCCSD(T) calculations and a def2-TZVPP basis set[31] have been promulgated as standards of comparison.[32,33] A recent update resolved some, but not all, of the difficulties of interpretation that accompany the partial or complete abandonment of spatial or spin symmetry.[33] The present study therefore begins with a re-examination of the GW100 ΔCCSD(T) VIEs and the production of a revised set of data that will remain useful in subsequent assessments of emerging methods. An alternative standard based on BD-T1 VIEs is also examined.

In this work, methods and procedures that introduce adjustable parameters in self-energy formulae, in the construction of an orbital basis, or in the selection of a preferred approximation are not considered. Approximate self-energies are classified according to their arithmetic and storage demands. Statistical measures of error are extracted from VIE data compiled in the Supporting Information. These data enable identification of the best compromises of accuracy and computational efficiency. Acronyms pertaining to diagonal self-energy approximations are listed in Appendix 1.

2. ELECTRON PROPAGATOR THEORY

2.1. General Concepts. With the adoption of an orthonormal spin−orbital basis, u, with indices p and q, elements of the EP matrix,

$$\langle\langle a_p(t);\ a_q^\dagger(t')\rangle\rangle = -i\Theta(t-t')\langle\Psi_0^N|a_p(t)a_q^\dagger(t')|\Psi_0^N\rangle + i\Theta(t'-t)\langle\Psi_0^N|a_q^\dagger(t')a_p(t)|\Psi_0^N\rangle \quad (1)$$

may be defined in terms of the Heaviside step function (θ) and an N-electron, reference (initial) eigenstate, Ψ_0^N. In its spectral form, this element's Fourier transform,

$$\langle\langle a_p;\ a_q^\dagger\rangle\rangle_E = \lim_{\eta\to 0^+}\left[\sum_R \frac{\langle\Psi_0^N|a_p|R\rangle\langle R|a_q^\dagger|\Psi_0^N\rangle}{E + E_0(N) - E_R(N+1) + i\eta} + \sum_S \frac{\langle\Psi_0^N|a_q^\dagger|S\rangle\langle S|a_p|\Psi_0^N\rangle}{E - E_0(N) + E_S(N-1) - i\eta}\right] \quad (2)$$

contains summations over final eigenstates with $N+1$ or $N-1$ electrons. Poles originating in the R and S summations correspond, respectively, to energies of electron attachment (i.e., electron affinities) and detachment (e.g., IEs of molecules). Residues (numerators associated with poles) are expressed in terms of products of Feynman−Dyson amplitudes,

$$f_p^R = \langle\Psi_0^N|a_p|R\rangle \quad (3)$$

$$g_p^S = \langle S|a_p|\Psi_0^N\rangle \quad (4)$$

that may be used to obtain Dyson spin-orbitals of attachment and detachment according to the following,

$$\varphi_R^{\text{Dyson}}(x_1) = \sqrt{N+1}\int \Psi_0^{N*}(x_2,\ x_3,\ x_4,\ ...,\ x_{N+1})\,\Psi_R(x_1,\ x_2,\ x_3,\ ...,\ x_{N+1})\,dx_2dx_3dx_4...dx_{N+1} = \sum_R f_p^R u_p(x_1) \quad (5)$$

$$\varphi_S^{\text{Dyson}}(x_1) = \sqrt{N}\int \Psi_S^{*}(x_2,\ x_3,\ x_4,\ ...,\ x_N)\,\Psi_0^N(x_1,\ x_2,\ x_3,\ ...,\ x_N)\,dx_2dx_3dx_4...dx_N = \sum_S g_p^S u_p(x_1) \quad (6)$$

In eq 2, the plus sign between the attachment and detachment summations requires the presence of an anticommutator in the definition of a super-operator metric,

$$[X|Y] = \langle\Psi_0^N|X^\dagger Y + YX^\dagger|\Psi_0^N\rangle \quad (7)$$

wherein X and Y are members of a set of second-quantized-operator products (w) with creators exceeding annihilators by one, for example, $a_p^\dagger$ (hole and particle, or h and p), $a_p^\dagger a_q^\dagger a_r$ ($2hp$ and $2ph$), and $a_p^\dagger a_q^\dagger a_r^\dagger a_s a_t$ ($3h2p$ and $3p2h$).[34] Identity and Hamiltonian super-operators defined by

$$\hat{I}X = X \quad (8)$$

$$\hat{H}X = HX - XH \quad (9)$$

enable expression of EP matrix elements as

https://doi.org/10.1021/acs.jctc.2c00502
J. Chem. Theory Comput. 2022, 18, 4927−4944

$$\langle\langle a_p;\, a_q^\dagger\rangle\rangle_E = G_{pq}(E) = [a_p^\dagger|(E\hat{I} - \hat{H})^{-1}a_q^\dagger] \tag{10}$$

In the EP matrix, the resolvent super-operator,

$$\mathbf{G}(E) = [\mathbf{a}^\dagger|(E\hat{I} - \hat{H})^{-1}\mathbf{a}^\dagger] \tag{11}$$

may be expressed by an inverse matrix after introducing an inner projection[35] with **w** operators according to

$$\mathbf{G}(E) = [\mathbf{a}^\dagger|\mathbf{w}][\mathbf{w}|(E\hat{I} - \hat{H})\mathbf{w}]^{-1}[\mathbf{w}|\mathbf{a}^\dagger] \tag{12}$$

The **w** operator manifold may be partitioned into a set of simple, normalized field operators and an orthogonalized complement, **f**, such that $[\mathbf{a}^\dagger|\mathbf{f}] = \mathbf{0}$. The inverse form of the Dyson equation therefore reads

$$\mathbf{G}^{-1}(E) = [\mathbf{a}^\dagger|(E\hat{I} - \hat{H})\mathbf{a}^\dagger] - [\mathbf{a}^\dagger|\hat{H}\mathbf{f}][\mathbf{f}|(E\hat{I} - \hat{H})\mathbf{f}]^{-1}[\mathbf{f}|\hat{H}\mathbf{a}^\dagger] \tag{13}$$

Another form of the inverse Dyson equation may be rederived by recognizing that

$$[a_p^\dagger|\hat{H}a_q^\dagger] = h_{pq}^{(1)} + \sum_{rs}\langle pr||qs\rangle\rho_{rs} = F_{pq} \tag{14}$$

where ρ is the one-electron reduced-density matrix (1-RDM) of the reference state and $\boldsymbol{F}$ is a generalized Fock matrix with the usual one-electron ($h^{(1)}$) and anti-symmetrized, two-electron (Dirac notation) matrix elements. In the spin−orbital basis that diagonalizes $h^{(1)} + v$ with eigenvalues e^v, one may define a reference, inverse EP matrix,

$$\mathbf{G}_0^{-1}(E) = E1 - \mathbf{e}^v \tag{15}$$

with vanishing off-diagonal elements. The inverse Dyson equation acquires its familiar form,

$$\mathbf{G}^{-1}(E) = \mathbf{G}_0^{-1}(E) - \boldsymbol{\Sigma}(E) \tag{16}$$

where the self-energy matrix, $\Sigma(E)$, includes constant (i.e., energy-independent) and energy-dependent terms according to

$$\boldsymbol{\Sigma}(E) = \mathbf{F} - \mathbf{h}^{(1)} - \mathbf{v} + [\mathbf{a}^\dagger|\hat{H}\mathbf{f}][\mathbf{f}|(E\hat{I} - \hat{H})\mathbf{f}]^{-1}[\mathbf{f}|\hat{H}\mathbf{a}^\dagger] \tag{17}$$

If v is chosen to be the Coulomb-exchange potential of the HF, self-consistent field, then

$$\boldsymbol{\Sigma}(E) = \boldsymbol{\Sigma}(\infty) + [\mathbf{a}^\dagger|\hat{H}\mathbf{f}][\mathbf{f}|(E\hat{I} - \hat{H})\mathbf{f}]^{-1}[\mathbf{f}|\hat{H}\mathbf{a}^\dagger] \tag{18}$$

where elements of the constant term in the self-energy matrix,

$$\Sigma_{pq}(\infty) = \sum_{rs}\langle pr||qs\rangle(\rho_{rs} - \rho_{rs}^{HF}) \tag{19}$$

arise only from correlation contributions to the 1-RDM. When v is the Coulomb-exchange operator of HF theory, final-state orbital relaxation and differential correlation terms in the self-energy matrix are easily identified.[36,37] For this choice, the sum of the first three terms in eq 17 vanishes through second order in the fluctuation potential and corresponds to the energy-independent terms of eq 19 in higher orders. Eigenfunctions obtained with alternative local or nonlocal potentials usually produce non-diagonal, energy-independent, first-order terms that involve the nonlocal, HF exchange operator in eq 18.

Regardless of the orbitals' provenance, poles of $\boldsymbol{G}(E)$, or zeroes of $\boldsymbol{G}^{-1}(E)$, occur at energies (E_X) where the quasiparticle eigenvalue equation is satisfied:

$$[\mathbf{F} + \boldsymbol{\Sigma}(E_X)]\mathbf{C}(E_X) = E_X\mathbf{C}(E_X) \tag{20}$$

The corresponding probability factors (Π_X) equal the norms of the Dyson spin-orbitals[9] and may be determined using

$$\Pi_X = \int|\varphi^{\mathrm{Dyson}}(x)|^2\,\mathrm{d}x = \left(1 - \mathbf{C}^\dagger(E_X)\left[\frac{\mathrm{d}\boldsymbol{\Sigma}(E)}{\mathrm{d}E}\right]_{E=E_X}\mathbf{C}(E_X)\right)^{-1} \tag{21}$$

Elements of $\boldsymbol{C}(E_X)$ are related to Feynman−Dyson amplitudes and Dyson spin-orbitals according to

$$\varphi_X^{\mathrm{Dyson}}(x) = \Pi_X^{0.5}\sum_p C_p(E_X)u_p(x) \tag{22}$$

Many of the methods examined presently employ canonical, HF spin-orbitals and ignore off-diagonal elements of the self-energy matrix. In such cases, each canonical spin-orbital generates its own, independent set of electron binding energies obtained by iterating the diagonal quasiparticle equation

$$\mathrm{e}_p^{HF} + \Sigma_{pp}(E_{Xp}) = E_{Xp} \tag{23}$$

with respect to E. At convergence, Koopmans results (e_p^{HF}) are corrected by diagonal elements of the self-energy matrix. Probability factors involve derivatives of the diagonal elements with respect to E, where

$$\Pi_{Xp} = \left[1 - \frac{\mathrm{d}\Sigma_{pp}(E)}{\mathrm{d}E}|_{E=E_{Xp}}\right]^{-1} \tag{24}$$

Dyson spin-orbitals become proportional to canonical, HF spin-orbitals

$$\varphi_{Xp}^{\mathrm{Dyson}}(x) = \Pi_{Xp}^{0.5}u_p^{HF}(x) \tag{25}$$

For a given p, many values of E_{Xp} may be found in principle, but usually only those poles whose probability factors exceed 0.85 are likely to be reliable within the diagonal approximation. The remaining electron binding energies with their relatively small probability factors may have some qualitative meaning despite the clear need for improvements from NR self-energy approximations that are appropriate for correlation states.

2.2. Self-Energy Approximations. The simplest (and usually the largest) relaxation and correlation corrections to canonical, HF orbital energies occur in second order in the Møller−Plesset fluctuation potential.[11] When $|\Psi_{\mathrm{o}}^{\mathrm{N}}\rangle$ is approximated by a HF wavefunction, **f** is restricted to triple-field ($2hp$ and $2ph$) operator products, and first-order couplings between the latter operators are neglected, the non-diagonal, second-order (ND2) self-energy emerges as

$$\boldsymbol{\Sigma}^{(2)}(E) = [\mathbf{a}^\dagger|\hat{H}\mathbf{f}_3]_1[\mathbf{f}_3|(E\hat{I} - \hat{H})\mathbf{f}_3]_0^{-1}[\mathbf{f}_3|\hat{H}\mathbf{a}^\dagger]_1 \tag{26}$$

Subscripts outside square brackets stand for the highest order of the fluctuation potential that is retained in the corresponding matrix's elements. (Zeroth-order matrix elements of $\hat{H}$ between $\mathbf{f}_3$ and $\mathbf{a}^\dagger$ vanish.) The p-th diagonal second-order (D2) self-energy matrix element in terms of HF canonical spin-orbitals reads

$$\Sigma_{pp}^{D2}(E) = \frac{1}{2}\Sigma_a^{\mathrm{vir}}\Sigma_{ij}^{\mathrm{occ}}\frac{|\langle pa||ij\rangle|^2}{E + \mathrm{e}_a - \mathrm{e}_i - \mathrm{e}_j} + \frac{1}{2}\Sigma_i^{\mathrm{occ}}\Sigma_{ab}^{\mathrm{vir}}\frac{|\langle pi||ab\rangle|^2}{E + \mathrm{e}_i - \mathrm{e}_a - \mathrm{e}_b} \tag{27}$$

https://doi.org/10.1021/acs.jctc.2c00502
J. Chem. Theory Comput. 2022, 18, 4927−4944

At $E = \varepsilon_p$, the second-order, Rayleigh−Schrödinger perturbation theory (RSPT2) result is obtained.[38−40] Same-spin and opposite-spin terms in the two summations have been assigned empirically adjusted coefficients in several modified self-energies that conserve the efficient cubic arithmetic scaling of the D2 method.[41−44] A simpler, interpretable alternative that avoids the introduction of parameters adjusted with respect to a set of data is considered presently: neglect of the same-spin terms. This opposite-spin, second-order method has recently been denoted by os-D2.[16] Another simplification arises from the non-Dyson (nD) approach, which neglects the electron affinity (EA) term in the EP matrix (see eq 2), has only one term in its super-operator metric therefore (compare with eq 7), and yields a diagonal second-order self-energy that is identical to that of D2 of eq 27 except that the second (2*ph*) term is energy-independent, with E set equal to ε_p for electron detachments.[45] (In EA calculations, the roles with respect to energy dependence of the 2*hp* and 2*ph* terms are reversed.) The nD-D2 and os-nD-D2 methods procure a minor advantage, for the usual OV^2 bottleneck (where O and V are dimensions of the occupied and virtual orbital spaces) is no longer energy-dependent and therefore requires no iterations (see Appendix 2 for explicit formulae.). The fundamental bottleneck is the fourth-power transformation of the electron repulsion integrals (ERIs) to the HF basis for a given p in D2 calculations. In fact, the ERI transformation may be avoided entirely with semidirect EP algorithms.[46,47]

Keeping first-order couplings between triple-field operators in the central inverted matrix yields the 2*ph*-TDA[48] self-energy,

$$\mathbf{\Sigma}^{\text{2ph-TDA}}(E) = [\mathbf{a}^\dagger|\hat{H}\mathbf{f}_3]_1[\mathbf{f}_3|(E\hat{I} - \hat{H})\mathbf{f}_3]_1^{-1}[\mathbf{f}_3|\hat{H}\mathbf{a}^\dagger]_1 \tag{28}$$

No correlation corrections to the HF reference state are included. The inverted matrix generates ring, ladder, and mixed ring−ladder terms of all orders with anti-symmetrized vertices. This method offers a qualitatively correct description of primary and correlation states but has not been combined in practice with the diagonal self-energy approximation.

A recently examined member of the G_0W_0 family of methods[49] that lies within the nonempirical scope of the present study may be defined by neglecting the following: (a) off-diagonal elements in eq 28 of the self-energy matrix, (b) ladder and ring exchange terms arising from the $[\mathbf{f}_3|(E\hat{I}-\hat{H})\mathbf{f}_3]_1$ matrix, and (c) exchange terms in the $[\mathbf{a}^\dagger|\hat{H}\mathbf{f}_3]_1$ and $[\mathbf{f}_3|\hat{H}\mathbf{a}^\dagger]_1$ matrices. Only ERIs of the single bar (i.e., not anti-symmetrized) $\langle ab|ij\rangle$ type are needed in the $\hat{H}$ couplings between $\mathbf{f}_3$ operators. Instead of the usual random-phase approximation excitation energies and transition amplitudes that typify G_0W_0 calculations, their Tamm−Dancoff approximation (TDA) counterparts appear in this level of theory. The resulting HF-TDA G_0W_0 self-energy therefore contains a subset of terms (i.e., exchange-less ring diagrams in all orders) that occur in the 2*ph*-TDA self-energy.

All third-order contributions to the self-energy are present in the 3+ self-energy, where

$$\mathbf{\Sigma}^{3+}(E) = \mathbf{\Sigma}_3(\infty) + [\mathbf{a}^\dagger|\hat{H}\mathbf{f}_3]_2[\mathbf{f}_3|(E\hat{I} - \hat{H})\mathbf{f}_3]_1^{-1}[\mathbf{f}_3|\hat{H}\mathbf{a}^\dagger]_2 \tag{29}$$

Higher orders denoted by the brackets' subscripts and the subscript in the energy-independent term involve first-order double and second-order single replacements with respect to $|HF\rangle$ and $\langle HF|$ in eq 7. Terms beyond the third order are generated by the inverted matrix as they are in the 2*ph*-TDA self-energy. This approximation is a member of the family of ADC(3) (third-order algebraic diagrammatic construction) methods and is sometimes known as strict ADC(3).[50] Other members of this family replace $\Sigma_3(\infty)$ with its fourth-order counterpart or with renormalized procedures[51] in which the trace of ρ used to evaluate the energy-independent term (see eq 19) is not necessarily equal to the number of electrons. [An efficient, non-Dyson variant of ADC(3)[52] has recently been implemented.[53−55]] As with 2*ph*-TDA, the non-diagonal 3+ self-energy has always been evaluated in practice; diagonal ADC(3) calculations have not appeared in print.

Neglect of terms beyond the third order produces the following, finite-order expression,

$$\begin{aligned}\mathbf{\Sigma}^{(3)}(E) &= \mathbf{\Sigma}^{(2)}(E) + \mathbf{\Sigma}_3(\infty)\\ &+ [\mathbf{a}^\dagger|\hat{H}\mathbf{f}_3]_1[\mathbf{f}_3|(E\hat{I} - \hat{H})\mathbf{f}_3]_0^{-1}[\mathbf{f}_3|\hat{V}\mathbf{f}_3]_1[\mathbf{f}_3|(E\hat{I} - \hat{H})\mathbf{f}_3]_0^{-1}[\mathbf{f}_3|\hat{H}\mathbf{a}^\dagger]_1\\ &+ [\mathbf{a}^\dagger|\hat{H}\mathbf{f}_3]_2[\mathbf{f}_3|(E\hat{I} - \hat{H})\mathbf{f}_3]_0^{-1}[\mathbf{f}_3|\hat{H}\mathbf{a}^\dagger]_1\\ &+ [\mathbf{a}^\dagger|\hat{H}\mathbf{f}_3]_1[\mathbf{f}_3|(E\hat{I} - \hat{H})\mathbf{f}_3]_0^{-1}[\mathbf{f}_3|\hat{H}\mathbf{a}^\dagger]_2\end{aligned} \tag{30}$$

where $\hat{V}$ is the fluctuation potential super-operator. By neglecting off-diagonal terms in eq 30, the diagonal, third-order self-energy (D3) is obtained. When evaluated at $E = e_p$, D3 equals the third-order, Rayleigh−Schrödinger perturbation theory (RSPT3) result.[38−40] Convergence of eq 23 for the D3 self-energy precedes estimates obtained with the three OVGFs known as the A, B, and C versions.[13] Diagonal elements of the D3 self-energy matrix may be represented by eight terms:

$$\Sigma^{(3)} = S_{2hp} + S_{2ph} + C_D + C_S + R_{2hp} + R_{2ph} + P_{2hp} + P_{2ph} \tag{31}$$

(Energy dependence has been suppressed for the S, R, and P terms in this notation.) The two *second-order* contributions of eq 27 are represented by the first two terms. *Constant* (i.e., energy-independent) terms arising from first-order double and second-order single replacements in the reference state are denoted by the third and fourth terms. *Ring and ladder* terms occur in the fifth and sixth positions. Energy-dependent terms that involve *perturbative* first-order double replacements are in the seventh and eighth positions. R_{2hp} and R_{2ph} correspond to the term with two energy-dependent denominators (i.e., the third term of eq 30) in $\Sigma^{(3)}(E)$. The P_{2hp} and P_{2ph} terms have contributions from the last two matrix products in $\Sigma^{(3)}(E)$ which are Hermitian conjugates of each other. Formulae for each of these third-order summations are available in several reviews.[13,14] In this notation, the OVGF self-energies may be expressed as follows

$$\Sigma^{\text{OVGF-A}} = \Sigma^{(3)} + \frac{S_{2hp} + S_{2ph}}{S_{2hp} + S_{2ph} - P_{2hp} - P_{2ph}}(C_D + C_S + R_{2hp} + R_{2ph} + P_{2hp} + P_{2ph}) \tag{32}$$

$$\Sigma^{\text{OVGF-B}} = \Sigma^{(2)} + C_D + C_S + \frac{S_{2hp}}{S_{2hp} - P_{2hp}}(R_{2hp} + P_{2hp}) + \frac{S_{2ph}}{S_{2ph} - P_{2ph}}(R_{2ph} + P_{2ph}) \tag{33}$$

https://doi.org/10.1021/acs.jctc.2c00502
J. Chem. Theory Comput. 2022, 18, 4927−4944

$$\Sigma^{\text{OVGF-C}} = \Sigma^{(2)} + (C_D + C_S + R_{2hp} + R_{2ph} + P_{2hp} + P_{2ph})\times \frac{R_{2hp} + R_{2ph} + P_{2hp} + P_{2ph}}{\frac{S_{2hp} - P_{2hp}}{S_{2hp}}(R_{2hp} + P_{2hp}) + \frac{S_{2ph} - P_{2ph}}{S_{2ph}}(R_{2ph} + P_{2ph})} \tag{34}$$

Despite the simplicity of these formulae for estimating higher-order self-energy terms, the accuracy of the computationally less demanding OVGF methods is competitive with that of the family of ADC(3) methods for the lowest IEs of closed-shell molecules and anions in comparisons with experiments[21,56] and with VIE data of nearly FCI quality in a triple ζ plus polarization basis.[16] The OVGF methods require only trivial computational work after the D3 calculation concludes.

In IE calculations, terms with $2ph$ subscripts are less sensitive to E than the $2hp$ terms. In the nD methods (e.g., nD-D2 and os-nD-D2), $2ph$ terms in $\Sigma_{pp}(E)$ reappear with energy-independent denominators that equal their energy-dependent counterparts evaluated at $E = \epsilon_p^{HF}$. This simplification eliminates energy iterations for the costliest terms with OV^4 arithmetic scaling and defines the nD variants of D3 and the three OVGF versions.

Whereas the ADC and OVGF methods may be improved by adding complicated, computationally demanding replacements of higher orders to $|\Psi_0\rangle$ and $\langle\Psi_0^N|$ in eq 7 and by increasing operator manifolds beyond $\mathbf{f}_3$, an alternative approach has examined the consequences of adopting intermediate normalization, which is responsible for size-extensive total energies in many-body theories, in the choice of the super-operator metric.[16] An antecedent to this strategy occurred in the P3 self-energy's derivation,[57] where such a choice recovered MP2 total energies evaluated with the EP at the cost of producing non-Hermitian super-operator matrices that were subsequently Hermitized in calculations. Separate derivations were required for IE and EA calculations.[58] To improve on this antecedent, intermediate normalization has been combined with Hermitization and retention of all resulting third-order terms.[16]

A new class of approximate self-energies has thus been based on an intermediately normalized, Hermitized super-operator metric,

$$[X|Y] = \frac{1}{2}(\langle HF|(X^\dagger Y + YX^\dagger)(1 + T_2^{(1)} + T_1^{(2)})|HF\rangle + \langle HF|(1 + T_2^{(1)} + T_1^{(2)})^\dagger(X^\dagger Y + YX^\dagger)|HF\rangle) \tag{35}$$

X and Y may be h, p, $2hp$, or $2ph$ operators. First-order, double and second-order, single replacements appearing in

$$T_2^{(1)} = \frac{1}{4}\sum_{ij}^{\text{occ}}\sum_{ab}^{\text{vir}}\frac{\langle ij||ab\rangle}{\mathrm{e}_i + \mathrm{e}_j - \mathrm{e}_a - \mathrm{e}_b}a_i^\dagger a_j^\dagger a_a a_b \tag{36}$$

$$T_1^{(2)} = \sum_{i}^{\text{occ}}\sum_{a}^{\text{vir}}\frac{1}{2(\mathrm{e}_i - \mathrm{e}_a)}\left(\sum_{jk}^{\text{occ}}\sum_{b}^{\text{vir}}\frac{\langle jk||ab\rangle\langle bi||jk\rangle}{\mathrm{e}_j + \mathrm{e}_k - \mathrm{e}_a - \mathrm{e}_b} + \sum_{j}^{\text{occ}}\sum_{bc}^{\text{vir}}\frac{\langle ij||bc\rangle\langle bc||aj\rangle}{\mathrm{e}_i + \mathrm{e}_j - \mathrm{e}_b - \mathrm{e}_c}\right)a_i^\dagger a_a \tag{37}$$

occur only *linearly* in the consequent elements of the Hermitian super-operator matrix. (The P3 and non-diagonal, renormalized, second-order or NR2[22,58,59] self-energies were derived from a nonsymmetric metric without single replacement operators; separate derivations for IE and EA cases were required.[58]) The self-energy generated by the metric of eq 35 displays an equivalent treatment of $2hp$ and $2ph$ terms (vide infra) that is characteristic of theories that conserve time-reversal symmetry. All *third-order* terms that emerge from this *linear* choice of metric and *ring-ladder renormalizations* are kept in the RL3 self-energy, whose elements employed presently read

$$\begin{aligned}\mathbf{\Sigma}^{\text{RL3}}(E) = \frac{1}{2}(&\mathbf{C}_S + [\mathbf{a}^\dagger|\hat{H}\mathbf{f}_{2ph}]_2[\mathbf{f}_{2ph}|(E\hat{I} - \hat{H})\mathbf{f}_{2ph}]_1^{-1}[\mathbf{f}_{2ph}|\hat{H}a^\dagger]_1 \\ &+ [\mathbf{a}^\dagger|\hat{H}\mathbf{f}_{2ph}]_1[\mathbf{f}_{2ph}|(E\hat{I} - \hat{H})\mathbf{f}_{2ph}]_1^{-1}[\mathbf{f}_{2ph}|\hat{H}\mathbf{a}^\dagger]_2 \\ &+ [\mathbf{a}^\dagger|\hat{H}\mathbf{f}_{2hp}]_1[\mathbf{f}_{2hp}|(E\hat{I} - \hat{H})\mathbf{f}_{2hp}]_1^{-1}[\mathbf{f}_{2hp}|\hat{H}\mathbf{a}^\dagger]_2 \\ &+ [\mathbf{a}^\dagger|\hat{H}\mathbf{f}_{2hp}]_2[\mathbf{f}_{2hp}|(E\hat{I} - \hat{H})\mathbf{f}_{2hp}]_1^{-1}[\mathbf{f}_{2hp}|\hat{H}\mathbf{a}^\dagger]_1)\end{aligned} \tag{38}$$

where $\mathbf{C}_S$ is the non-diagonal matrix generalization of C_S. The $T_1^{(2)}$ operators in eq 35 are needed to recover the third-order C_S term in eq 38. The C_D term, which is often a source of instability with respect to basis sets in practice, is eliminated for it has a quadratic dependence on reference-state substitution amplitudes that is absent in eq 35 thanks to the linear parametrization of the reference wavefunction. It is possible that improved stability and accuracy could be procured by the inclusion of the fourth-order, energy-independent self-energy, which includes many computationally demanding quadratic terms, for example, those that depend on $T_3^{(2)}$ and $T_2^{(1)}$ amplitudes. (The $\Sigma(4+)$ self-energy in nD-ADC(3) calculations is such a proposal.[60]) The costs of lowered efficiency and interpretability are unlikely to be proportionate to the corresponding benefits of accuracy. Omission of quadratic terms therefore offers an attractive combination of efficiency, interpretability, and (vide infra) accuracy. Ring and ladder terms that are independent of reference-state substitution amplitudes are unchanged with respect to their counterparts in $2ph$-TDA, 3+, and ADC(3), but terms that are linear in those amplitudes are multiplied by a factor of one-half because of the Hermitization in the metric of eq 35. The latter terms (i.e., the seventh and eighth terms in eq 31) are usually the largest in the D3 self-energy, and their double weighting is chiefly responsible for the overestimated IEs that typify these calculations. Simplifications of IP-EOM-CCSD equations that employ $T_2^{(1)}$ amplitudes instead of their CCSD T_2 counterparts in the interest of greater arithmetic efficiency obtain the same coefficients for analogous terms[61,62] (see also the original derivation of the P3 method[57]) and produce no analogues of C_D. An equivalent expression for super-operator Hamiltonian matrix elements in terms of a single-determinant reference state (e.g., HF) and the similarity-transformed Hamiltonian that occurs in unitary coupled-cluster theory[63] provides another justification for the omission of quadratic terms. The Baker−Campbell−Hausdorff expansion of the latter operator in terms of commutators of the original Hamiltonian with the cluster (T) operator generates a series of Hermitian model Hamiltonians, which may be truncated after the term that is linear in T.

Fourth-order and many higher-order terms in the RL3 self-energy are easily identified after expansion of the inverted

https://doi.org/10.1021/acs.jctc.2c00502
J. Chem. Theory Comput. 2022, 18, 4927−4944

matrices. The costliest arithmetic operations involve couplings between 2*ph* operators that appear in third and higher orders. Considerable numerical evidence indicates that these terms have relatively little importance in IE calculations for closed-shell molecules.[57] Their neglect defines the renormalized, quasiparticle (RQ3) self-energy for the calculation of IEs, which retains RL3's 2*hp*, third-order terms:

$$\begin{aligned}\mathbf{\Sigma}^{\mathrm{RQ3}}(E) = {} & \frac{1}{2}\mathbf{C}_S + [\mathbf{a}^\dagger|\hat{H}\mathbf{f}_{2ph}]_1[\mathbf{f}_{2ph}|(E\hat{I}-\hat{H})\mathbf{f}_{2ph}]_0^{-1}[\mathbf{f}_{2ph}|\hat{H}\mathbf{a}^\dagger]_1 \\ & + \frac{1}{2}[\mathbf{a}^\dagger|\hat{H}\mathbf{f}_{2hp}]_2[\mathbf{f}_{2hp}|(E\hat{I}-\hat{H})\mathbf{f}_{2hp}]_1^{-1}[\mathbf{f}_{2hp}|\hat{H}\mathbf{a}^\dagger]_1 \\ & + \frac{1}{2}[\mathbf{a}^\dagger|\hat{H}\mathbf{f}_{2hp}]_1[\mathbf{f}_{2hp}|(E\hat{I}-\hat{H})\mathbf{f}_{2hp}]_1^{-1}[\mathbf{f}_{2hp}|\hat{H}\mathbf{a}^\dagger]_2\end{aligned} \tag{39}$$

The second term equals the second term in eq 27. Omission of the constant term arising from second-order, single replacements in the reference state yields the RP3 self-energy,

$$\begin{aligned}\mathbf{\Sigma}^{\mathrm{RP3}}(E) = {} & [\mathbf{a}^\dagger|\hat{H}\mathbf{f}_{2ph}]_1[\mathbf{f}_{2ph}|(E\hat{I}-\hat{H})\mathbf{f}_{2ph}]_0^{-1}[\mathbf{f}_{2ph}|\hat{H}\mathbf{a}^\dagger]_1 \\ & + \frac{1}{2}[\mathbf{a}^\dagger|\hat{H}\mathbf{f}_{2hp}]_2[\mathbf{f}_{2hp}|(E\hat{I}-\hat{H})\mathbf{f}_{2hp}]_1^{-1}[\mathbf{f}_{2hp}|\hat{H}\mathbf{a}^\dagger]_1 \\ & + \frac{1}{2}[\mathbf{a}^\dagger|\hat{H}\mathbf{f}_{2hp}]_1[\mathbf{f}_{2hp}|(E\hat{I}-\hat{H})\mathbf{f}_{2hp}]_1^{-1}[\mathbf{f}_{2hp}|\hat{H}\mathbf{a}^\dagger]_2\end{aligned} \tag{40}$$

The RP3 self-energy resembles that of the NR2 approximation for IEs; its diagonal third-order terms are the same as those of P3.

Neglect of fourth- and higher-order terms generated by the expansion of the inverted matrices in the RL3, RQ3, and RP3 self-energies, respectively, defines their L3, Q3, and P3 counterparts:

$$\Sigma^{\mathrm{L3}} = S_{2hp} + S_{2ph} + \frac{1}{2}(C_S + P_{2hp} + P_{2ph}) + R_{2hp} + R_{2ph} \tag{41}$$

$$\Sigma^{\mathrm{Q3}} = S_{2hp} + S_{2ph} + \frac{1}{2}(C_S + P_{2hp}) + R_{2hp} \tag{42}$$

$$\Sigma^{\mathrm{P3}} = S_{2hp} + S_{2ph} + \frac{1}{2}P_{2hp} + R_{2hp} \tag{43}$$

Factors of one-half appear because of the new choice of the super-operator metric in eq 35. Only P3 has been derived, implemented, and applied previously.[57] The original P3 derivation assumed a super-operator metric with $T_2^{(1)}$ but without $T_1^{(2)}$ replacements.

The approximately renormalized, partial third-order self-energy[64] (P3+) for IEs may be expressed in a manner similar to that of the OVGF-B formula,

$$\Sigma^{\mathrm{P3+}} = \Sigma^{(2)} + \frac{S_{2hp}}{S_{2hp} - \frac{1}{2}P_{2hp}}\left(R_{2hp} + \frac{1}{2}P_{2hp}\right) \tag{44}$$

(P3+ denotes the *approximately* renormalized partial third-order method, whereas it previously was simply called the renormalized partial third-order method.) The present convention of abbreviations assigns the + sign to approximately renormalized methods and reserves *R* for methods in which higher-order terms are *explicitly* evaluated. Using similar arguments, the Q3+ method may be defined

$$\Sigma^{\mathrm{Q3+}} = \Sigma^{(2)} + \frac{1}{2}C_S + \frac{S_{2hp}}{S_{2hp} - \frac{1}{2}P_{2hp}}\left(R_{2hp} + \frac{1}{2}P_{2hp}\right) \tag{45}$$

Because RL3, unlike P3+ and Q3+, treats 2*hp* and 2*ph* operators on an equal footing, A, B, and C versions of L3+ may be defined by analogy to the three OVGF versions

$$\Sigma^{\mathrm{L3+A}} = \Sigma^{(2)} + \frac{S_{2hp} + S_{2ph}}{S_{2hp} + S_{2ph} - \frac{1}{2}(P_{2hp} + P_{2ph})} \times \left[C_S + R_{2hp} + R_{2ph} + \frac{1}{2}(P_{2hp} + P_{2ph})\right] \tag{46}$$

$$\Sigma^{\mathrm{L3+B}} = \Sigma^{(2)} + C_S + \frac{S_{2hp}}{S_{2hp} - \frac{1}{2}P_{2hp}}\left(R_{2hp} + \frac{1}{2}P_{2hp}\right) + \frac{S_{2ph}}{S_{2ph} - \frac{1}{2}P_{2ph}}\left(R_{2ph} + \frac{1}{2}P_{2ph}\right) \tag{47}$$

$$\Sigma^{\mathrm{L3+C}} = \Sigma^{(2)} + \left[C_S + R_{2hp} + R_{2ph} + \frac{1}{2}(P_{2hp} + P_{2ph})\right]\times \frac{R_{2hp} + R_{2ph} + \frac{1}{2}(P_{2hp} + P_{2ph})}{\frac{S_{2hp} - \frac{1}{2}P_{2hp}}{S_{2hp}}\left(R_{2hp} + \frac{1}{2}P_{2hp}\right) + \frac{S_{2ph} - \frac{1}{2}P_{2ph}}{S_{2ph}}\left(R_{2ph} + \frac{1}{2}P_{2ph}\right)} \tag{48}$$

Pole searches typically start with HF orbital energies as initial guesses, evaluate derivatives of the diagonal self-energy matrix elements with respect to *E* (these data serve to determine probability factors), and use Newton's method for finding the roots of a function of a single variable (see eq 23). Three iterations usually supply convergence to within 0.01 eV. Pole searches with the approximately renormalized OVGF, P3+, Q3+, and L3+ self-energies are initiated, respectively, at the D3, P3, Q3, and L3 poles; agreement to within 0.01 eV usually requires but a single Newton iteration. Improvements based on the three + (i.e., approximately renormalized) methods require practically no additional work after P3, Q3, or L3 calculations are finished.

New methods that perform energy iterations on terms with 2*ph*−2*ph* couplings, (i.e., L3, RL3, and the three L3+ versions) involve many OV^4 steps. The nD versions of the L3+ and RL3 methods reduce the number of these summations to one.

The remaining NR EP methods examined presently, NR2 and BD-T1, may be rederived with metrics that differ from that of eq 35. In the former case, the super-operator couplings between h and 2*hp* operators are governed by a metric that omits single-replacement operators. All other $\hat{H}$ couplings are evaluated through first order, except for the zeroth order 2*ph*−2*ph* block. For BD-T1, the HF determinant and the double replacement amplitudes of eq 35 are replaced by their BD counterparts, and the single replacement amplitudes vanish.

3. METHODS

3.1. Direct versus Indirect Calculations. Lowest VIEs are calculated for each species in the GW100 set[29] using the coupled-cluster (CC) and EP approaches. CC calculations

https://doi.org/10.1021/acs.jctc.2c00502
J. Chem. Theory Comput. 2022, 18, 4927−4944

employ the cluster operator involving only single and double particle−hole replacements, that is, the CCSD model.[65] In addition, approximate, perturbative corrections to the CCSD ground-state energy arising from connected triple replacements are calculated in the CCSD(T) model.[66] The ΔCCSD(T) VIE reads

$$\mathrm{VIE}_{\mathrm{CCSD(T)}} = E^{\mathrm{cation}}_{\mathrm{CCSD(T)}} - E^{\mathrm{neutral}}_{\mathrm{CCSD(T)}} \quad (49)$$

Whereas the ΔCC methods require two separate ground-state energy calculations (for the neutral and for the cation), a VIE may alternatively be obtained from the CC theory in a single-step calculation by seeking eigenvalues of the ionization potential, equation-of-motion CC (IP-EOM-CC[67]) Hamiltonian matrix. Results obtained for IP-EOM-CCSD and IP-EOM-CCSDT models[17] (the latter involving all triple replacements in the cluster operator) are used here to establish the BD-T1 EP method[9,23−25,27,28,68] as a new benchmark for the GW100 set (vide infra).

In the EPT, VIEs are obtained in a single-step calculation as a negative of an EP pole calculated at the equilibrium geometry of the neutral's ground state. Both non-diagonal EP methods and diagonal, or quasiparticle, methods are employed in the present work. Among quasiparticle methods, those recently derived[16] from an intermediately normalized, Hermitized super-operator metric (as described in Section 2) are used along with their antecedents. All the EP methods employed in the present work and their arithmetic scaling factors are listed in Table 1.

3.2. Basis Sets and Frozen-Core Approximations. To ensure maximum compatibility with the previous GW100 benchmark studies,[29,32] the same def2-TZVPP basis sets[31] and frozen-core approximations (see Table 5 in the latter study[32]) have been adopted. In additional comparisons of ΔCCSD, ΔCCSD(T), and BD-T1 VIEs against IP-EOM-CCSDT results,[17] the cc-pVTZ basis set[69] was employed throughout.

Table 1. Arithmetic Scaling Factors of EP Methods[a]

method class	methods[b]	arithmetic bottleneck	bottleneck steps	largest ERI[c] subset
diagonal second order	D2, os-D2	OV^2	N_E	O^2V^2
	RSPT2, nD-D2, and os-nD-D2	OV^2	1	O^2V^2
diagonal post second order	RSPT3	OV^4	1	V^4
	D3 and OVGF	OV^4	N_E[d]	V^4
	P3, P3+, **Q3**, and **Q3+**	O^2V^3	1	OV^3
	L3 and **L3+**	OV^4	N_E[d]	V^4
	RP3 and **RQ3**	O^2V^3	1	OV^3
	RL3	OV^4	N_IN_E[d]	V^4
	HF-TDA G_0W_0	O^2V^3	N_IN_E	O^2V^2
non-diagonal	ND2	OV^3	N_I	OV^3
	2*ph*-TDA	OV^4	N_I	V^4
	3+	O^2V^4	1	V^4
	ADC(3)	O^2V^4	N_I	V^4
	NR2	O^3V^3	1	OV^3
	BD-T1	O^2V^4	BD[e]	V^4

[a]O = # occupied orbitals, V = # virtual orbitals, N_E = energy iterations, and N_I = inverse-expansion iterations. [b]New methods in the **bold type**. [c]ERI = electron repulsion integral. [d]Reduction by a factor of N_E occurs in non-Dyson (nD) versions. [e]The O^2V^4 arithmetic bottleneck occurs in the BD, coupled-cluster, reference-state calculation; the subsequent EP bottleneck is OV^4.

3.3. Equilibrium Structures. Both ΔCC and EP calculations of the first VIEs for the GW100 set have been carried out at the ground-state geometries of the neutral species taken from the original definition of the GW100 set.[29] These geometries were assumed in the two previous ΔCCSD(T) GW100 benchmark studies.[32,33] (Bruneval et al.[33] note, after Maggio et al.,[70] that there are problems with the phenol and vinyl bromide structures in the original GW100 set[29] and therefore report VIEs for both the original and corrected geometries for these two molecules.) To enable final-state assignments to irreducible representations of the full point groups of neutral structures and to avoid lower-symmetry geometries with only trivial energetic differences from global minima, 28 of the original structures have been modified (vide infra). These corrections had a negligible effect (a few thousands of an electron volt) on the final VIEs in most cases. In five cases (C_3H_6, C_8H_8, CH_4O, C_2H_4O, and Si_5H_{12}), however, the geometry corrections were nontrivial, and structural reoptimizations were needed. The model of the original GW100 article[29] was used: the PBE density functional approximation[71,72] and the def2-QZVP basis set.[73] (For the five aforementioned cases, full geometry optimizations and harmonic vibrational frequency calculations were executed to verify that each structure is a true minimum on its potential energy surface, has no imaginary frequency, and has converged to its appropriate point-group symmetry.)

3.4. Reference Determinants. HF reference determinants are assumed in all correlated methods but BD-T1, where the BD[74,75] reference determinant was employed. As observed by Krause et al.,[32] for 25 neutrals in the GW100 set, the restricted HF (RHF) wavefunction exhibits an instability. We confirmed this result and in addition found internal instabilities in unrestricted HF (UHF) wavefunctions for 34 cations. Instability in *both* the neutral and cationic HF wavefunctions occurs in nine species, which leads in total to 50 species with an HF instability in the neutral, the cation, or both (see Table 2 for details). The single replacement amplitudes in the CCSD wavefunction, should, however, remedy the instabilities in the underlying HF reference to a large extent.[76−78] (A recent example of this effect was demonstrated numerically in a study of the electron detachment energies of a closed-shell pentagonal diphosphatriazolate anion,[56] where the CCSD wavefunction optimization starting from a UHF solution for the first $^2B_2$ state of the neutral still led to the experimentally meaningful *second* $^2B_2$ state). For the 50 species with HF instabilities, ΔCCSD(T) VIEs based on the unstable HF solutions have been compared against those based on the HF wavefunction which was corrected for the instability. (HF constraints were systematically relaxed until a stable HF wavefunction was found[79] in Gaussian 16.[80]) The comparison led to the mean absolute error (MAE) being less than 0.06 eV. For 11 species (BH_3, C_2H_3Br, C_2H_3I, C_4H_{10}, CH_4, CH_4N_2O, GeH_4, Li_2, MgF_2, N_2, and SiH_4), the absolute discrepancy did not exceed 0.005 eV; for seven of these systems (BH_3, C_4H_{10}, CH_4, CH_4N_2O, GeH_4, MgF_2, and SiH_4), the ΔCCSD(T) VIE is identical whether the reference HF wavefunction is corrected for the instability or not. For 19 species, the discrepancy was not larger than 0.05 eV. A discrepancy greater than 0.1 eV was found only for six systems (AlF_3, BN, C_2H_6, MgO, O_3, and SO_2). Within the latter subset, only C_2H_6 and MgO showed discrepancies significantly above 0.1 eV (0.33 and 0.42 eV,

https://doi.org/10.1021/acs.jctc.2c00502
J. Chem. Theory Comput. 2022, 18, 4927−4944

Table 2. GW100 Benchmarks: ΔCCSD(T) and BD-T1 VIEs[a] (eV), Point Groups, and Dyson Orbital Irreducible Representations

formula[b]	name	frozen core[c]	point group	hole	ΔCCSD(T)	BD-T1	notes[d]
Ag_2	silver dimer	2	$D_{\infty h}$	σ_g	7.495	7.527	
AlF_3	aluminum fluoride	8	D_{3h}	a_2'	15.457	15.436	C
AlI_3	aluminum iodide	17	D_{3h}	a_2'	9.815	9.788	C
Ar	argon	5	K_h	p	15.544	15.589	
As_2	arsenic dimer	18	$D_{\infty h}$	π_u	9.876	9.923	N, C
AsH_3	arsine	9	C_{3v}	a_1	10.398	10.400	
B_2H_6	diborane	2	D_{2h}	b_{1g}	12.263	12.233	C
BeO	beryllium monoxide	2	$C_{\infty v}$	π	9.943	10.161	
BF	fluoroborane	2	$C_{\infty v}$	σ	11.087	11.155	
BH_3	borane	1	D_{3h}	e′	13.276	13.284	C
BN	boron nitride	2	$C_{\infty v}$	π	12.215	12.008	N, C
Br_2	bromine	28	$D_{\infty h}$	π_g	10.536	10.568	C
C_2H_2	acetylene	2	$D_{\infty h}$	π_u	11.424	11.473	
C_2H_3Br	vinyl bromide	16	C_s	a″	9.271	9.246	N
C_2H_3Cl	vinyl chloride	7	C_s	a″	10.093	10.068	
C_2H_3F	vinyl fluoride	3	C_s	a″	10.554	10.540	
C_2H_3I	vinyl iodide	6	C_s	a″	9.328	9.320	N, C
C_2H_4	ethylene	2	D_{2h}	b_{3u}	10.667	10.632	
C_2H_4O	acetaldehyde	3	C_s	a	10.190	10.183	
C_2H_6	ethane	2	D_{3d}	e_g	13.041	12.649	C
C_2H_6O	ethanol	3	C_S	a″	10.685	10.636	
C_3H_6	cyclopropane	3	D_{3h}	e′	10.849	10.759	
C_3H_8	propane	3	C_{2v}	b_2	12.048	12.062	C, K
C_4	tetracarbon	4	D_{2h}	a_g	11.281	11.236	N, C
C_4H_{10}	butane	4	C_{2h}	a_g	11.567	11.466	C
$C_4H_{10}O$	ethoxy ethane	5	C_{2v}	b_1	9.816	9.782	
$C_4H_4N_2O_2$	uracil	8	C_s	a″	9.483	9.458	
$C_4H_5N_3O$	cytosine	8	C_1	a	8.771	8.751	
C_5H_5N	pyridine	6	C_{2v}	a_1	9.730	9.630	N, K
$C_5H_5N_5$	adenine	10	C_1	a	8.330	8.289	
$C_5H_5N_5O$	guanine	11	C_1	a	8.034	7.986	
C_5H_6	cyclopentadiene	5	C_{2v}	a_2	8.712	8.650	N
$C_5H_6N_2O_2$	thymine	9	C_s	a″	9.081	9.042	
C_6F_6	hexafluorobenzene	12	D_{6h}	e_{1g}	10.026	10.048	N
C_6H_6	benzene	6	D_{6h}	e_{1g}	9.360	9.264	N
C_6H_6O	phenol	7	C_s	a″	8.747	8.656	N
C_6H_7N	aniline	7	C_s	a′	8.044	7.929	N
C_7H_8	toluene	7	C_s	a′	8.968	8.855	N
C_8H_{10}	ethylbenzene	8	C_s	a′	8.919	8.812	N
C_8H_8	cyclooctatetraene	8	D_{2d}	a_1	8.359	8.305	N, C
CBr_4	carbon tetrabromide	57	T_d	t_1	10.463	10.446	C
CCl_4	carbon tetrachloride	21	T_d	t_1	11.558	11.548	C
CF_4	carbon tetrafluoride	5	T_d	t_1	16.301	16.274	C
CH_2O	formaldehyde	2	C_{2v}	b_2	10.840	10.796	
CH_2O_2	formic acid	3	C_s	a′	11.421	11.459	
CH_4	methane	1	T_d	t_2	14.373	14.317	C
CH_4N_2O	urea	4	C_2	b	10.053	10.115	C
CH_4O	methanol	2	C_s	a″	11.069	11.005	
CI_4	tetraiodomethane	17	T_d	t_1	9.266	9.230	C
Cl_2	chlorine	10	$D_{\infty h}$	π_g	11.413	11.408	C
CO	carbon monoxide	2	$C_{\infty v}$	σ	14.209	14.055	
CO_2	carbon dioxide	3	$D_{\infty h}$	π_g	13.711	13.709	
CS_2	carbon disulfide	11	$D_{\infty h}$	π_g	9.981	9.949	
Cu_2	copper dimer	18	$D_{\infty h}$	σ_g	7.566	7.603	
CuCN	copper cyanide	11	$C_{\infty v}$	σ	10.854	10.852	K
F_2	fluorine	2	$D_{\infty h}$	π_g	15.747	15.542	N, C
GaCl	gallium monochloride	14	$C_{\infty v}$	σ	9.771	9.820	
GeH_4	germane	9	T_d	t_2	12.497	12.518	C
H_2	hydrogen	0	$D_{\infty h}$	σ_g	16.403	16.399	
H_2NNH_2	hydrazine	2	C_2	b	9.720	9.582	C

https://doi.org/10.1021/acs.jctc.2c00502
J. Chem. Theory Comput. 2022, 18, 4927−4944

Table 2. continued

formula[b]	name	frozen core[c]	point group	hole	ΔCCSD(T)	BD-T1	notes[d]
H_2O	water	1	C_{2v}	b_1	12.565	12.492	
H_2S	hydrogen sulfide	5	C_{2v}	b_1	10.310	10.311	
HCl	hydrogen chloride	5	$C_{\infty v}$	π	12.593	12.612	
HCN	hydrogen cyanide	2	$C_{\infty v}$	π	13.723	13.770	
He	helium	0	K_h	s	24.512	24.515	
HF	hydrogen fluoride	1	$C_{\infty v}$	π	16.026	16.006	
HN_3	hydrogen azide	3	C_s	a″	10.676	10.642	
HOOH	hydrogen peroxide	2	C_2	b	11.587	11.402	C
I_2	iodine	8	$D_{\infty h}$	π_g	9.509	9.493	C
K_2	dipotassium	10	$D_{\infty h}$	σ_g	4.075	4.107	N
KBr	potassium bromide	19	$C_{\infty v}$	π	8.127	8.202	
KH	potassium hydride	5	$C_{\infty v}$	σ	6.128	6.161	
Kr	krypton	14	K_h	p	13.940	14.015	
Li_2	lithium dimer	0	$D_{\infty h}$	σ_g	5.266	5.312	N
LiF	lithium fluoride	1	$C_{\infty v}$	π	11.321	11.440	
LiH	lithium hydride	0	$C_{\infty v}$	σ	7.962	7.963	
$MgCl_2$	magnesium chloride	12	$D_{\infty h}$	π_g	11.665	11.736	C
MgF_2	magnesium fluoride	4	$D_{\infty h}$	π_g	13.709	13.883	C
MgO	magnesium monoxide	3	$C_{\infty v}$	π	7.909	8.493	N
N_2	nitrogen	2	$D_{\infty h}$	σ_g	15.569	15.379	C, K
Na_2	sodium dimer	2	$D_{\infty h}$	σ_g	4.955	4.975	N
Na_4	sodium tetramer	4	D_{2h}	b_{1u}	4.243	4.278	N
Na_6	sodium hexamer	6	C_{5v}	e_1	4.396	4.375	N, C
NaCl	sodium chloride	6	$C_{\infty v}$	π	9.027	9.096	
Ne	neon	1	K_h	p	21.321	21.345	
NH_3	ammonia	1	C_{3v}	a′	10.807	10.720	
O_3	ozone	3	C_{2v}	a_1	12.819	12.590	N, C, K
OCS	carbon oxysulfide	7	$C_{\infty v}$	π	11.173	11.167	
OCSe	carbon oxyselenide	7	$C_{\infty v}$	π	10.460	10.476	
P_2	phosphorus dimer	10	$D_{\infty h}$	π_u	10.530	10.571	N, C
PH_3	phosphine	5	C_{3v}	a_1	10.523	10.526	
PN	phosphorus mononitride	6	$C_{\infty v}$	σ	11.813	11.631	N, K
Rb_2	dirubidium	0	$D_{\infty h}$	σ_g	3.941	3.957	N
SF_4	sulfur tetrafluoride	9	C_{2v}	a_1	12.589	12.663	
Si_2H_6	disilane	10	D_{3d}	a_{1g}	10.645	10.653	
Si_5H_{12}	pentasilane	25	C_{2v}	b_2	9.286	9.304	
SiH_4	silane	5	T_d	t_2	12.796	12.815	C
SO_2	sulfur dioxide	7	C_{2v}	a_1	12.416	12.286	C
TiF_4	titanium fluoride	9	T_d	t_1	15.476	15.756	C
Xe	xenon	4	K_h	p	12.260	12.285	

[a]In the def2-TZVPP basis. [b]Species are ordered alphabetically according to the formula. [c]Number of frozen-core orbitals as defined by Krause et al.[32] and employed also by Bruneval et al.[33] and in this work. [d]N denotes an instability in the HF reference wavefunction of the neutral. C denotes an instability in the HF reference wavefunction of the cation. K denotes a Koopmans defect.

respectively). Spin contamination of the cationic UHF wavefunction was usually smaller when the internal instability was not redressed. We have therefore chosen to employ ΔCC results based on the unstable HF solutions in comparisons with EP calculations, and the latter are consequently also based on unstable, closed-shell HF solutions. (In other words, closed-shell HF was used for all neutral species and UHF not corrected for instabilities was employed for cations.) ΔCCSD(T) results obtained in this way are directly comparable to those recently reported by Bruneval et al.,[33] who did not correct for HF instabilities, as well. Krause et al.,[32] on the other hand, who carried out ΔCCSD(T) calculations for the GW100 set for the first time, chose to correct the HF instabilities before executing CC calculations.

3.5. Assignment of the Lowest VIEs. Orderings of final states that differ from those predicted at the KT level were considered. For each species in the GW100 set and for each EPT method, five VIEs (pertaining to the highest occupied molecular orbital, or HOMO, and four occupied orbitals preceding the HOMO in ascending energetic order) were calculated, and the lowest value was selected. Koopmans defects occurred in the def2-TZVPP basis for six systems: C_3H_8, C_5H_5N, CuCN, N_2, O_3, and PN (see Table 2). The incorrect energetic order at the KT level pertained to the HOMO and HOMO − 1 (an occupied orbital with the highest energy below the HOMO energy) for all these systems but pyridine (C_5H_5N), where it involved the HOMO and HOMO − 2.

The irreducible representation of the hole pertaining to the final, cationic state was assigned to each species (see the fifth column of Table 2) based on the lowest VIE obtained in the BD-T1 calculation. [In addition, the agreement between the irreducible representation determined by BD-T1 and that obtained for the CCSD(T) cationic state was confirmed.]

https://doi.org/10.1021/acs.jctc.2c00502
J. Chem. Theory Comput. 2022, 18, 4927−4944

Table 3. Sources of 46 Discrepancies between the ΔCCSD(T)/def2-TZVPP VIEs Obtained for the GW100 Set by Bruneval et al.[33] and Krause et al.[32]

source of discrepancy	affected species[a]
Bruneval et al.[33] use the RHF reference state for neutrals and the UHF reference state not corrected for instabilities for the cations, whereas Krause et al.[32] always correct for HF instabilities of both neutrals and cations	AlF_3, AlI_3, As_2, B_2H_6, BH_3, BN, Br_2, C_2H_6, C_3H_8, C_4, pyridine, C_5H_6, C_6H_6, aniline, C_7H_8, C_8H_{10}, C_8H_8, CBr_4, CCl_4, CF_4, CI_4, Cl_2, F_2, H_2NNH_2, HOOH, I_2, K_2, $MgCl_2$, MgO, N_2, Na_2, Na_4, Na_6, O_3, P_2, PN, Rb_2, SO_2, and TiF_4
Krause et al.[32] report a VIE that corresponds to an excited cationic state	uracil, cytosine, HCN, SO_2, and BN
Krause et al.[32] use S instead of Se	OCSe
neutral CCSD(T) energy of Krause et al.[32] disagrees with that of Bruneval et al.[33]	BN
omission by Krause et al.[32] from the original definition[29] of the GW100 set	Xe
marginal discrepancy (0.001−0.002 eV), likely originating from thresholds used in the calculations or from rounding errors	BeO and Si_5H_{12}

[a]SO_2 and BN have >1 sources of disagreement and therefore appear twice and thrice, respectively.

Choosing the lowest of five VIEs for each EPT method in an unbiased manner (i.e., uninformed by results of high-level methods or experiments) incurs a risk that in the case of lower-level methods, such as D2, the apparently lowest VIE might not always correspond to the irreducible representation of the true lowest VIE. The advantage of such an agnostic approach, however, is that it gives a fair comparison of the *predictive power* of the methods.

3.6. Software. All calculations were performed using Gaussian 16, Revision A 03,[80] and using a development version of Gaussian,[81] where a variety of EP approximations, including BD-T1,[23−25,27,68] and a set of recently introduced methods,[16] have been implemented. In the case of F_2, for which the ΔCCSD(T) VIE obtained in this work and that reported by Bruneval et al.[33] differ significantly (vide infra), the neutral's CCSD(T) ground-state energy has been calculated using Dalton,[82] and the ΔCCSD(T) VIE has been calculated using CFOUR.[83]

3.7. Error Measures. For each method, an error of the lowest VIE of a given species (denoted by subscript i) with respect to the benchmark value has been calculated as

$$\delta_i = \mathrm{VIE}_i - \mathrm{VIE}_i^{\mathrm{benchmark}} \tag{50}$$

Subsequently, for a given method, the average error ($\overline{\delta}$), the standard deviation of the population (σ_δ; the 100 species with the diverse electronic structure patterns of the GW100 set may be considered to be a population for the purposes of the statistical analysis performed here), the MAE ($|\overline{\delta}|$), and the maximum absolute error ($|\delta|_{\mathrm{max}}$) have been determined according to the following formulae:

$$\overline{\delta} = \frac{1}{100}\sum_{i=1}^{100}\delta_i \tag{51}$$

$$\sigma_\delta = \sqrt{\frac{\sum_{i=1}^{100}(\delta_i - \overline{\delta})^2}{100}} \tag{52}$$

$$|\overline{\delta}| = \frac{\sum_{i=1}^{100}|\delta_i|}{100} \tag{53}$$

$$|\delta|_{\mathrm{max}} = \max_{i=1,100}|\delta_i| \tag{54}$$

4. IMPROVED GW100 ΔCCSD(T) BENCHMARKS

The first ΔCCSD(T) benchmark values of VIEs for the GW100 set were reported by Krause et al. in 2015.[32] Bruneval et al.[33] repeated ΔCCSD(T) VIE calculations for the GW100 set and found 46 discrepancies with respect to results reported by Krause et al. but provided only a limited discussion of reasons underpinning them. In Sections 4.1 and 4.2, sources of discrepancies between these two, previous benchmark sets are analyzed. In the current work, ΔCCSD(T) calculations have been executed using the same software as that used by Bruneval et al.[33] (see Section 3 for computational details). Agreement with the latter authors was not achieved for four systems (see Section 4.3.).

4.1. Discrepancies between Previous Benchmarks. Independent execution of ΔCCSD(T) VIE calculations for the entire GW100 set has enabled identification of the sources of the 46 discrepancies between Bruneval et al. and Krause et al., which are summarized in the first column of Table 3. Bruneval et al. ignore HF instabilities, but Krause et al. prefer reference determinants with lower total energies and broken symmetry; 39 VIEs are affected. The alternative ΔCCSD(T) VIEs differ significantly for only two systems; these discrepancies are 0.33 eV for C_2H_6 and 0.42 eV for MgO. In five cases (uracil, cytosine, HCN, SO_2, and BN), Krause et al. converged to a cationic CCSD(T) energy that does not correspond to the lowest VIE but to an excited cationic state. The present results for uracil and cytosine therefore agree with those of Bruneval et al., wherein the final state is $^2A''$ instead of $^2A'$. (The separation of the two states is approximately 0.6 eV.) A similar agreement is obtained for the $^2\Pi$ final state of HCN^+, whereas the result of Krause et al. pertains to $^2\Sigma$. The VIE of SO_2 calculated by the latter authors pertains to the second excited state ($^2A_2$) of the cation, whereas the value reported by Bruneval et al. for the correct, $^2A_1$ final state agrees with recent high-accuracy calculations[84−87] and photoelectron experiments.[88] BD-T1 calculations agree with Bruneval et al. that the lowest state of BN^+ is $^2\Pi$, not $^2\Sigma$. The present results also do not reproduce the initial-state total energy of BN reported by Krause et al. The latter authors performed calculations on OCSe with the Se atom mistakenly replaced by S and omitted Xe, a member of the GW100 set. (The calculations of Krause et al. were published before the final version of the article that defined the GW100 set.[29]). For BeO and Si_5H_{12}, the small discrepancies (0.001 and 0.002 eV, respectively) between the ΔCCSD(T) results by Bruneval et al. and by Krause et al. may originate from using two different codes (Gaussian 16[80] and CFOUR,[83] respectively), numerical thresholds, or rounding errors. Bruneval et al. name uracil, cytosine, MgO, and SO_2 as the species for which the most noticeable differences (larger than 0.4 eV) occur.

4.2. Point Groups and Assignments. Incorrect assignments of final states may be avoided by exploitation of the full

https://doi.org/10.1021/acs.jctc.2c00502
J. Chem. Theory Comput. 2022, 18, 4927−4944

point-group symmetry of a molecule. In 28 cases of the original GW100 set,[29] this advantage is declined, to the detriment of all subsequent studies that have employed this standard. In most cases, geometries of higher symmetry change VIEs by only thousandths of an electron volt. For C_3H_6, C_8H_8, CH_4O, C_2H_4O, and Si_5H_{12}, the changes indicated a need for geometry reoptimization and confirming frequency calculations (see Section 3.3.). The recommended symmetry-corrected geometries are provided (see Supporting Information) in the form of Z-matrices to ensure that the point groups stay intact when switching between quantum chemistry packages.

Bruneval et al. ascribe the discrepancy between their SO_2 VIE and that of Krause et al. to differences in their reference determinants, but our results indicate a difference of only 0.12 eV. Symmetry criteria proved indispensable in establishing the relevance of final-state total energies to a given VIE.

4.3. Discrepancies with Previous Benchmarks. The lowest ΔCCSD(T) VIEs presented in Table 2 were obtained using the same computational approach as that employed by Bruneval et al. (see Section 3 for computational details). In addition, geometries of 28 species now conform to their full point groups, as described in the previous subsection. Before correcting the structures, however, results obtained with the old geometries were compared to those reported by Bruneval et al. Four nontrivial discrepancies (see Table 4) occurred:

Table 4. Sources of Discrepancies with ΔCCSD(T)/def2-TZVPP VIEs of Bruneval et al.[33]

source of discrepancy	affected species
Bruneval et al.[33] use the HF reference state for the neutral corrected for instabilities	C_6F_6 and C_6H_6O
discrepancy with the present results remains unexplained; for F_2, Dalton[82] and CFOUR[83] agree with the present results	F_2 and OCSe

C_6F_6 (0.09 eV), C_6H_6O (0.04 eV), F_2 (0.12 eV), and OCSe (0.01 eV). The results of Bruneval et al. for C_6F_6 and C_6H_6O were reproduced by replacing an HF-unstable reference with a stabilized one for the neutral species. (Had Bruneval et al. remained consistent by ignoring HF instabilities in all their calculations, the number of discrepancies with Krause et al. would have grown from 46 to 48.). The source of the discrepancies between the present results and those by Bruneval et al. for F_2 and OCSe could not be identified. The larger discrepancy (0.12 eV) occurred for F_2. A variety of convergence options for the CC part of the calculations, various frozen-core choices (including all electrons being correlated) and several different revisions of Gaussian 16, compiled for various architectures, were examined. The F_2 CCSD(T) ground-state energy obtained in this work using Gaussian 16[80] was reproduced using Dalton,[82] and the ΔCCSD(T) VIE was confirmed using CFOUR.[83] Differences with van Setten's ΔCCSD(T) VIE values for F_2 and OCSe remain unexplained.

5. BD-T1 BENCHMARKS

Potential disadvantages of the indirect, ΔCCSD(T) method for calculating benchmark VIEs of closed-shell molecules include the following: (1) spin-symmetry-broken final states, (2) seventh-power arithmetic scaling, (3) need for final-state calculations with reference determinants of different irreducible representations when assignments are in doubt, (4) inability to distinguish or obtain more than one final state of the same irreducible representation due to choices of reference determinants or uncertain results from correlation amplitude optimization, and (5) dependence of results on the stability of the reference determinants for highly correlated states. Direct alternatives based on a closed-shell reference determinant, such as IP-EOM-CC[89] and various EP methods, offer advantages with respect to items 1, 3, and 4. Optimization of reference determinants or inclusion of higher (e.g., triple or quadruple replacement) operator manifolds may ameliorate item 5, perhaps at the cost of greater computational challenges than those of item 2.

Data from a recent study of EP methods that employed IP-EOM-CCSD, IP-EOM-CCSDT, and IP-EOM-CCSDTQ benchmarks are displayed in Table 5.[16] Agreement between

Table 5. Error Measures (eV) vs EOM-CC Benchmarks[17] of the Lowest cc-pVTZ VIEs of 33 Molecules[a]

method	average error	standard deviation	MAE	maximum absolute error
Errors versus IP-EOM-CCSDTQ[b]				
ΔCCSD	−0.018	0.130	0.106	0.290
IP-EOM-CCSD	0.037	0.125	0.110	0.263
BD-T1	−0.042	0.071	0.072	0.138
ΔCCSD(T)	0.016	0.025	0.021	0.070
IP-EOM-CCSDT	−0.012	0.025	0.024	0.053
Errors versus IP-EOM-CCSDT				
ΔCCSD	0.009	0.168	0.120	0.489
IP-EOM-CCSD	0.096	0.085	0.110	0.243
BD-T1	0.009	0.064	0.054	0.138
ΔCCSD(T)	0.026	0.037	0.034	0.111
Errors versus ΔCCSD(T)				
ΔCCSD	−0.017	0.141	0.114	0.378
BD-T1	−0.016	0.074	0.059	0.208

[a]All VIEs were obtained using the cc-pVTZ basis and are available in the Supporting Information. EOM-CC benchmarks[17] pertain to molecules with first and second period nuclei. [b]A smaller subset of 11 VIEs is considered for the IP-EOM-CCSDTQ benchmark.

the two latter methods in calculations with the cc-pVTZ basis was very close; one may regard these results as a convenient alternative to FCI. (Only the lowest VIEs of molecules with first and second period nuclei are included.) To these data, ΔCCSD(T) results have been added presently; they agree with IP-EOM-CCSDTQ about as well as with IP-EOM-CCSDT. Some reduction in quality occurs for ΔCCSD and IP-EOM-CCSD. Errors obtained with BD-T1[9,23−25,27,28,68] lie between those of IP-EOM-CCSDT and IP-EOM-CCSD. Ground-state and IE steps, respectively, have sixth- and fifth-power arithmetic scaling in IP-EOM-CCSD and BD-T1 calculations. The latter method's accuracy and efficiency make it a reasonable alternative to ΔCCSD(T), IP-EOM-CCSD, and IP-EOM-CCSDT for the creation of benchmark data. When the set of VIEs was expanded to include excited cationic states, BD-T1 produced an MAE of 0.09 eV with respect to IP-EOM-CCSDT standards; the corresponding error measures for IP-EOM-CCSD and ADC(3) were 0.12 and 0.32 eV, respectively.[16] These results bode well for BD-T1 benchmarks that include several VIEs per molecule. The BD-T1 method's employment of an approximate Brueckner reference determinant endows it with greater predictive capabilities for highly correlated initial states. This capability was amply demonstrated in recent applications to diradicaloid ozone, iso-

https://doi.org/10.1021/acs.jctc.2c00502
J. Chem. Theory Comput. 2022, 18, 4927−4944

electronic SO_2 and S_3 molecules, and double Rydberg anions.[9,23−25,27,28,68,87,90]

6. EP RESULTS

Measures of error with respect to the improved ΔCCSD(T) VIEs of the GW100 set obtained with EP methods are listed in Table 6. MAEs are represented graphically in Figure 1.

Table 6. Errors (eV) with Respect to ΔCCSD(T)/def2-TZVPP Standards for GW100 IEs Listed in Table 2

method class	method[a]	MAE[b]	standard deviation	maximum absolute error
uncorrelated	KT	0.646	0.722	2.508
diagonal second order	D2	0.511	0.581	3.248
	os-D2	0.182	0.287	1.626
	nD-D2	0.534	0.604	3.388
	os-nD-D2	**0.182**	0.290	1.692
diagonal post second order	HF-TDA G_0W_0	0.229[d]	0.243	0.796
	D3	0.345[c]	0.597	3.714
	nD-D3	0.304[c]	0.492	2.279
	OVGF-A	0.167[c]	0.247	1.268
	OVGF-B	0.210[c]	0.348	2.164
	OVGF-C	0.167[c]	0.279	1.716
	nD-OVGF-A	0.161[c]	0.211	0.853
	nD-OVGF-B	0.191[c]	0.279	1.250
	nD-OVGF-C	0.145[c]	0.224	1.127
	P3	0.180	0.262	1.496
	P3+	**0.138**	0.181	0.968
	Q3	0.194	0.329	2.258
	Q3+	**0.154**	0.234	1.669
	L3	0.129	0.257	1.849
	nD-L3	0.125	0.259	1.915
	L3+A	0.152	0.186	1.027
	L3+B	0.104	0.188	1.381
	L3+C	0.102	0.183	1.256
	nD-L3+A	0.160	0.190	1.039
	nD-L3+B	**0.107**	0.191	1.416
	nD-L3+C	0.102	0.178	1.285
	RP3	0.158[d]	0.174	0.660
	RQ3	0.172[d]	0.155	0.545
	RL3	0.104[d]	0.111	0.450
	nD-RL3	0.111[d]	0.110	0.488
non-diagonal	ND2	0.452	0.486	2.527
	2*ph*-TDA	0.510	0.278	1.543
	3+	0.244	0.396	2.334
	ADC(3)	0.161	0.227	0.832
	NR2	0.157	0.134	0.500
	BD-T1	0.063	0.100	0.584

[a]New methods in **bold type**. [b]Optimal methods in **bold type**. [c]Based on 99 converged cases for D3 and OVGF methods and their nD variants. [d]Based on 93, 95, 95, 94, and 94 converged cases for HF-TDA-G_0W_0, RP3, RQ3, RL3, and nD-RL3, respectively.

Histograms with more detailed information on the distribution of errors are shown in Figure 2. [In the Supporting Information, histograms that instead employ BD-T1 standards demonstrate that MAEs do not differ from their ΔCCSD(T) counterparts by more than 0.03 eV.] For the D3 and OVGF methods and their nD variants, iterations with respect to *E* do not converge for MgO, a molecule with strong multiconfigurational character. For the HF-TDA-G_0W_0, RP3, RQ3, RL3, and nD-RL3 methods, order-by-order expansion of the *E*-dependent inverse matrix is achieved only in 93, 95, 95, 94, and 94 cases, respectively, and statistics therefore are based only on the converged cases. Measures of error calculated only for the 88 cases in which no methods encounter convergence difficulties are lower than those of the main text (see histograms in the Supporting Information).

The uncorrelated, frozen-orbital KT approximation tends to overestimate VIEs, but there are many underestimates as well. KT values have the highest MAE and standard deviation with respect to the present ΔCCSD(T) standards, both being approximately equal to 0.7 eV. Despite these shortcomings, correlated calculations (vide infra) confirm the qualitative validity of the KT picture with probability factors that exceed 0.85 in the vast majority of the 100 cases. The lowest VIEs of closed-shell molecules provide the best opportunities for perturbative corrections to KT results.

Not much improvement in the MAE (to 0.5 eV) occurs in cubically scaling D2 calculations, which require only a partial integral transformation with fourth-power arithmetic scaling that constitutes the practical bottleneck (see Table 1.). The non-Dyson version (nD-D2) also has an MAE of 0.5 eV. The D2 method tends to underestimate VIEs with very few exceptions, even when basis set effects are exhausted[21,56,66] (see Figure 2.) nD-D2's histogram strongly resembles that of D2. Considerable improvement in the MAE with respect to ΔCCSD(T) standards (to 0.2 eV) occurs for the modifications of D2 that include only opposite-spin terms: os-D2 and os-nD-D2. A similar degree of improvement was seen in previous tests for valence IEs in the cc-pVTZ basis.[16] Elimination of the energy dependence of the 2*ph* self-energy terms in the nD methods has little effect on the VIE predictions. Whereas the D2 and nD-D2 errors are among the largest in Figure 1, their os-D2 and os-nD-D2 counterparts are comparable to those of several more costly methods. The numerical success of the os-D2 and os-nD-D2 methods for the GW100 set rests on the predictable underestimates of D2. The present results suggest that useful data may be generated on large molecules with opposite-spin second-order methods that are free of empirical or adjusted parameters, are easily interpretable in terms of relaxation and correlation contributions to the self-energy,[36] and impose minimal computational costs beyond the preceding HF calculation.

The next level of computational effort depicted in Figure 1 corresponds to O^2V^3 arithmetic scaling, comprises the HF-TDA-G_0W_0, P3, P3+, Q3, Q3+, RP3, and RQ3 diagonal self-energies, and still does not exceed that of the preceding, partial ERI transformation whose OV^4 arithmetic scaling factor follows from the absence of integrals with four virtual indices in the diagonal self-energy formulae for VIEs. The parameter-free HF-TDA-G_0W_0 method has the additional advantage of not requiring ERIs with one occupied and three virtual indices. (The latter ERIs reappear when EAs are calculated, as do the four-particle ERIs in the other six methods.) This highly competitive, but parameter-free, version of G_0W_0 theory produces an MAE of 0.23 eV that nevertheless slightly exceeds the values obtained with os-D2 or os-nD-D2. (A recent numerical test of HF-TDA-G_0W_0 reached similar numerical conclusions and was accompanied by a proposal for a highly efficient, fourth-power algorithm.[91]) P3 and Q3 errors indicate marginal or no improvement over the two latter results, but their approximately renormalized (P3+ and Q3+) counterparts are clearly better, with MAEs of 0.14 and 0.15 eV, respectively.

https://doi.org/10.1021/acs.jctc.2c00502
J. Chem. Theory Comput. 2022, 18, 4927−4944

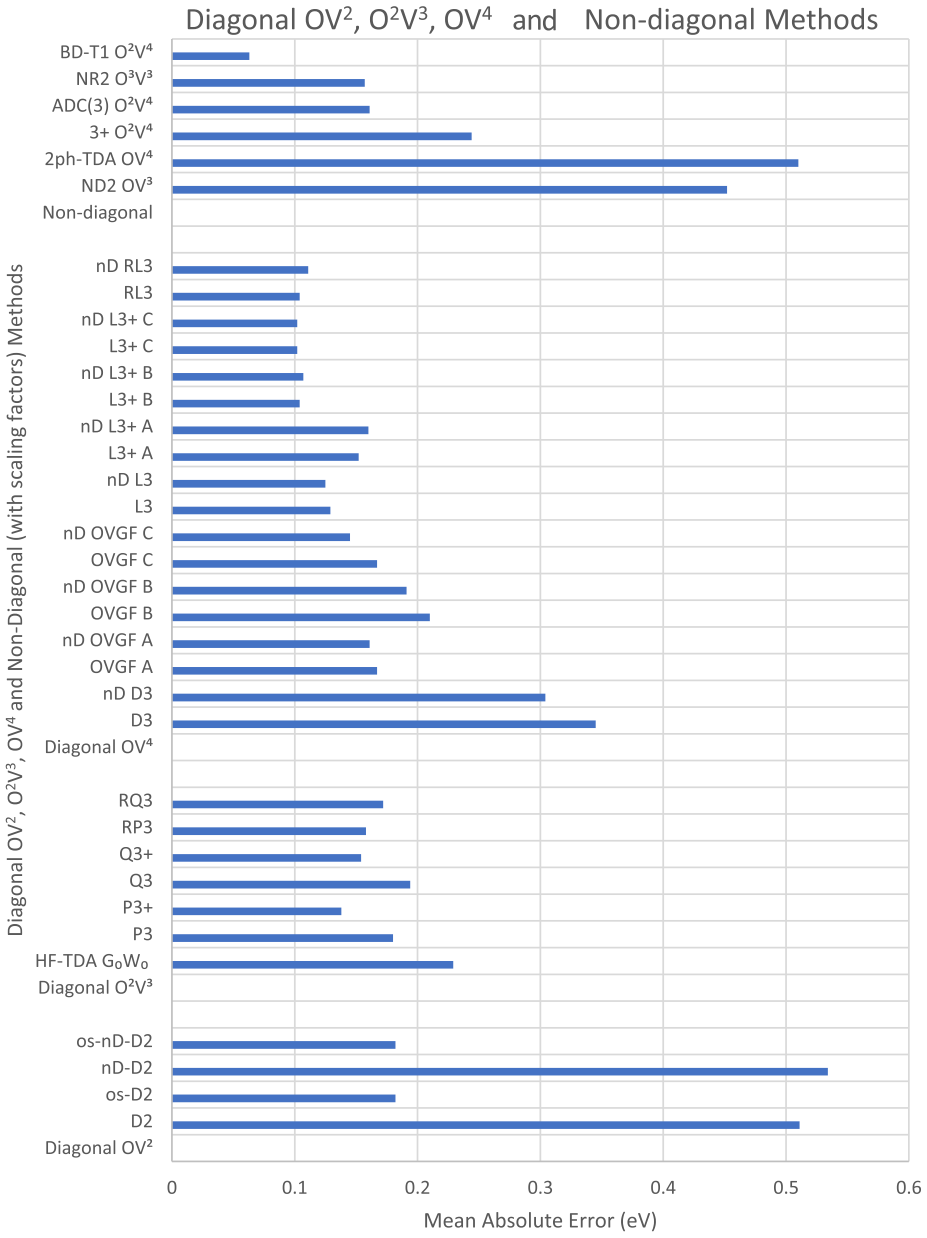


Figure 1. MAEs (eV) vs ΔCCSD(T) GW100 VIEs and arithmetic scaling factors.

Explicitly renormalized versions that extend P3 and Q3 (i.e., RP3 and RQ3) yield MAEs that are slightly larger (0.16 and 0.17 eV). In both approaches to renormalization, the tendency of the P3 and Q3 methods to overestimate VIEs is diminished. Because the P3+ and Q3+ self-energies involve only a trivial calculation at the conclusion of a P3 or Q3 calculation and do not require iterative evaluations of higher-order terms, these approximately renormalized methods offer the best compromise of accuracy and efficiency in the second group of methods in Figure 1. HF-TDA-G_0W_0 retains an advantage with respect to storage of ERIs, but it may be overcome by P3+ and Q3+ with semidirect algorithms for the noniterative summations that involve ERIs with one occupied and three virtual indices.[46,47]

In the next category of diagonal self-energy methods aggregated in Figure 1 are those with OV^4 arithmetic bottlenecks. All methods in this class have self-energy formulae that involve ERIs with four virtual indices. Ladder diagrams having this requirement may be evaluated with ERIs in the HF basis or using semidirect algorithms.[46,47] The D3 MAE shown in Figure 1, 0.34 eV, is lower than that of D2. The three OVGF versions and their non-Dyson equivalents, where diagrams with 2*ph* denominators are evaluated once for *E* set equal to the KT value, produce MAEs of 0.14−0.21 eV. All six of these approximations involve only trivial efforts after the D3 calculation is completed. The non-Dyson methods have the additional advantage of eliminating iterations in OV^4 contractions. The similarity of pairs of histograms pertaining to the A, B, or C Dyson and non-Dyson versions of OVGF indicate that the 2*ph* terms depend only weakly on their *E* arguments. An even better MAE (0.13 eV) occurs for L3. Whereas the A modifications of L3 do not improve on L3's MAE, the B and C approximate renormalizations certainty do so, with MAEs of 0.10−0.11 eV. The latter level of accuracy also characterizes the explicitly renormalized RL3 method, which requires iterative OV^4 contractions. Whereas RL3 tends

https://doi.org/10.1021/acs.jctc.2c00502
J. Chem. Theory Comput. 2022, 18, 4927−4944

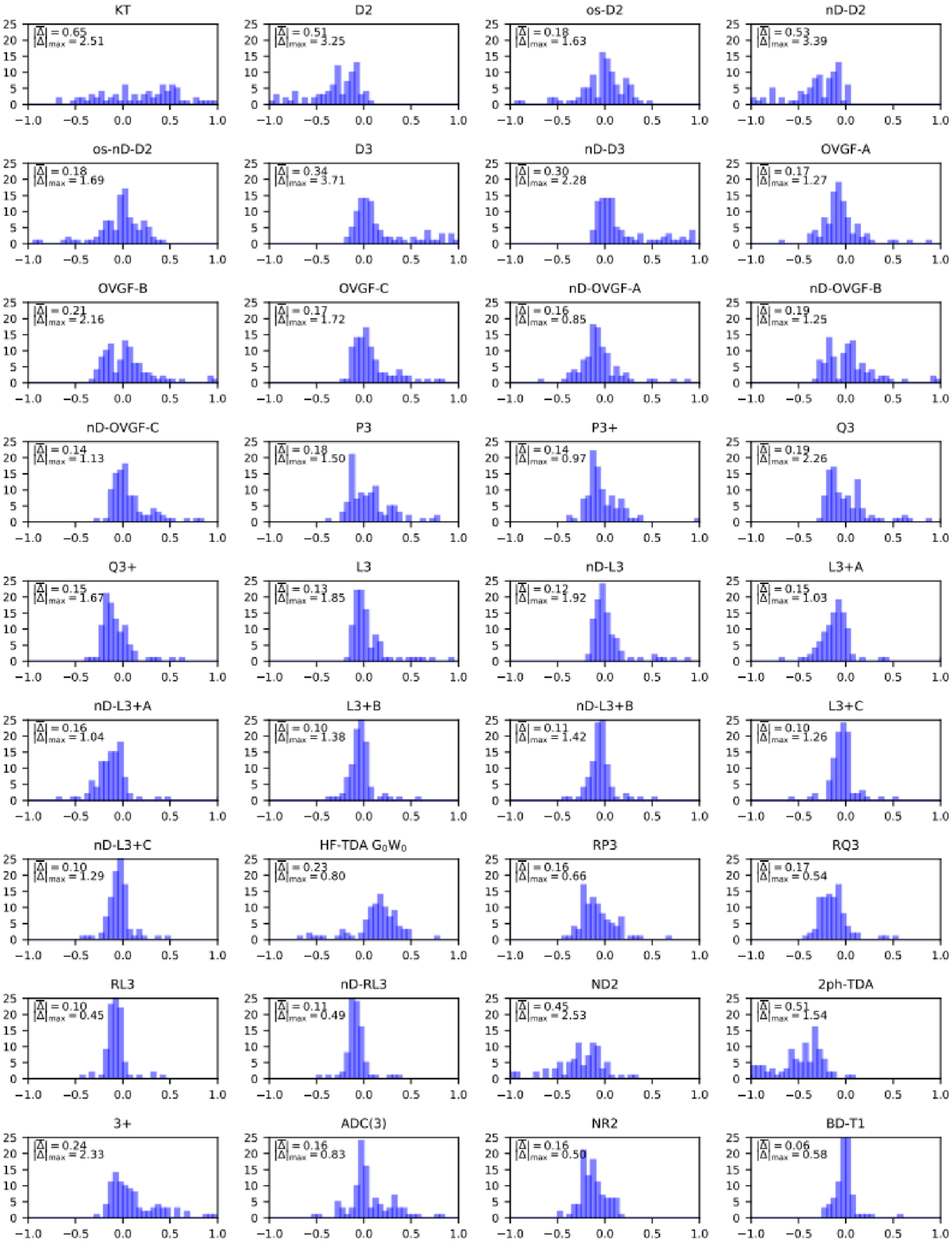


Figure 2. Histograms of error criteria (eV) vs ΔCCSD(T)/def2-TZVPP standards for GW100 VIEs.

https://doi.org/10.1021/acs.jctc.2c00502
J. Chem. Theory Comput. 2022, 18, 4927−4944

to underestimate VIEs, four of its approximately renormalized counterparts (L3+B, nD-L3+B, L3+C, and nD-L3+C) display the same trend in the histograms of Figure 2. The nD-L3+B and nD-L3+C methods present the best compromise of accuracy and efficiency in the OV^4 class for the GW100 set; there appears to be no penalty for fixing E to the KT value in the evaluation of 2*ph* terms. Because nD-L3+B employs the same renormalization scheme as those present in P3+ and Q3+, it is the preferred option.

Another reason to prefer the B version is the failure of the A and C versions to produce physically meaningful probability factors between 0 and 1 for Li_2, Na_2, or H_2 (see the Supporting Information, where negative probability factors or probability factors listed as unity denote problematic cases). D3 can produce positive instead of negative derivatives of the self-energy matrix element with respect to E; these pathologies can also spread to the OVGF methods.

Results from the non-diagonal category of EPT self-energies are shown at the top of Figure 1. The non-diagonal second-order and 2*ph*-TDA methods produce lower accuracy with higher computational effort than most of the diagonal self-energies whose results appear in the same figure. Both methods tend to underestimate VIEs (see Figure 2.). For VIEs of closed-shell molecules, other options are clearly preferable. The 3+ self-energy, also known as the strict version of ADC(3), has an MAE of 0.24 eV but no apparent advantages over the methods in the O^2V^3 and OV^4 classes except for D3. The ND2, 2*ph*-TDA and 3+ methods produce notable outliers, that is, absolute errors greater than 1.5 eV. The ADC(3) version represented presently employs a renormalized scheme for constant diagrams[51] and has a competitive MAE of 0.16 eV. Efficient implementations that could lower the formal arithmetic scaling from iterative N^6 to N^5 could suffice to make this option competitive for the GW100 set. The advantages of 2*ph*-TDA, 3+, and ADC(3) include their first-order description of correlation states. The NR2 method delivers practically the same MAE as that of ADC(3), but with a reduced, noniterative, O^3V^3 bottleneck. The best performance is obtained for BD-T1, whose MAE of 0.06 eV makes it almost indistinguishable in quality from the ΔCCSD(T) standard, which is likely to suffer from errors of approximately 0.1 eV with respect to FCI. Support for the latter estimate is provided by the present data on the five atoms in the GW100 set (He, Ne, Ar, Kr, and Xe). ΔCCSD(T) and BD-T1 produce MAEs of 0.14 and 0.13 eV, respectively, with respect to highly precise, experimental VIEs. Similar estimates of the intrinsic accuracy of the ΔCCSD(T) benchmark have appeared recently.[92]

The observations of this section are based on the lowest VIEs only but strongly resemble those made in a recent study where the set of VIEs was expanded to include excited cationic states.[16]

7. CONCLUSIONS

The results of Table 6 and Figures 1 and 2 on the GW100 set of the lowest VIEs provide ample justification for the use of diagonal self-energy approximations in each of the three classes (OV^2, O^2V^3, and OV^4) of arithmetic scaling. When a quick estimate is needed for a large database in which individual cases are not as important as the aggregate error or when an ERI transformation with quintic arithmetic scaling is infeasible, the easily interpretable os-nD-D2 method is advantageous. The P3+ and Q3+ methods, with their lower MAEs and standard deviations, are the best options when a partial atomic-to-molecular orbital transformation that excludes ERIs with four virtual indices is feasible, for the subsequent VIE calculation in both cases has a lower arithmetic scaling factor (noniterative O^2V^3) than that of the preceding transformation. These two methods have MAEs near 0.15 eV. The next level of accuracy, 0.1 eV, which approaches that of the ΔCCSD(T) standard with respect to experiments, is attained with noniterative OV^4 scaling in the nD-L3+B method. The proximity of BD-T1 results to those of ΔCCSD(T) and the advantages of standards based on direct instead of indirect calculation of vertical electron binding energies suggest that subsequent tests of EP, G_0W_0, and related methods may employ a BD-T1 standard for higher VIEs and perhaps for other kinds of electron binding energies as well.

APPENDIX 1

The following table provides acronyms for diagonal self-energy approximations.

acronym	full name
D2	diagonal second order
os-D2	opposite-spin D2
nD-D2	non-Dyson D2
os-nD-D2	opposite-spin non-Dyson D2
D3	diagonal third order
OVGF	outer valence Green's function (versions A, B, and C)
P3	partial third order
P3+	approximately renormalized partial third order
Q3	quasiparticle third order
Q3+	approximately renormalized quasiparticle third order
L3	linear third order
L3+	approximately renormalized linear third order (versions A, B, and C)
RP3	explicitly renormalized partial third order
RQ3	explicitly renormalized quasiparticle third order
RL3	explicitly renormalized linear third order
HF-TDA G_0W_0	Hartree-Fock Tamm-Dancoff G_0W_0

APPENDIX 2

Formulae of diagonal self-energy matrix elements in approximations that involve only opposite-spin second-order terms are given below in terms of canonical closed-shell HF orbitals.

$$\Sigma_{kk}^{\text{os-D2}}(E) = \Sigma_a^{\text{vir}}\Sigma_{ij}^{\text{occ}}\frac{|\langle ka|ij\rangle|^2}{E + \varepsilon_a - \varepsilon_i - \varepsilon_j} + \Sigma_i^{\text{occ}}\Sigma_{ab}^{\text{vir}}\frac{|\langle ki|ab\rangle|^2}{E + \varepsilon_i - \varepsilon_a - \varepsilon_b}$$

For the os-nD-D2 self-energy, $E = \varepsilon_k$ in the second term (i.e., no iterations with respect to E are performed).

ASSOCIATED CONTENT

Supporting Information

The Supporting Information is available free of charge at https://pubs.acs.org/doi/10.1021/acs.jctc.2c00502.

Individual VIEs underlying the statistics in Table 5 (XLSX)

Individual VIEs underlying the statistics in Table 6 (XLSX)

https://doi.org/10.1021/acs.jctc.2c00502
J. Chem. Theory Comput. 2022, 18, 4927−4944

Histograms of error criteria (eV) versus BD-T1 standards for GW100 VIEs (PDF)
Histograms of error criteria (eV) versus ΔCCSD(T)/def2-TZVPP standards for GW88 VIEs (PDF)
Histograms of error criteria (eV) versus BD-T1 standards for GW88 VIEs (PDF)
Z-matrices for all the studied species ensuring the correct point group symmetry (ZIP)

AUTHOR INFORMATION

Corresponding Author

J. V. Ortiz − *Department of Chemistry and Biochemistry, Auburn University, Auburn, Alabama 36849-5312, United States;* orcid.org/0000-0002-9277-0226; Email: ortiz@auburn.edu

Authors

Ernest Opoku − *Department of Chemistry and Biochemistry, Auburn University, Auburn, Alabama 36849-5312, United States;* orcid.org/0000-0002-4271-6838

Filip Pawłowski − *Department of Chemistry and Biochemistry, Auburn University, Auburn, Alabama 36849-5312, United States*

Complete contact information is available at: https://pubs.acs.org/10.1021/acs.jctc.2c00502

Notes

The authors declare no competing financial interest.

ACKNOWLEDGMENTS

This work was supported through the NSF grant CHE-1565760 to Auburn University. The authors thank Dr. Manuel Díaz Tinoco and Dr. Héctor Hernández Corzo for valuable discussions and the Alabama Supercomputer Center for computing resources.

REFERENCES

(1) Linderberg, J.; Öhrn, Y. *Propagators in Quantum Chemistry*, 2nd ed.; Wiley-Interscience: Hoboken NJ, 2004.
(2) Jørgensen, P.; Simons, J. *Second Quantization-Based Methods in Quantum Chemistry*; Academic Press: New York, 1981.
(3) Schirmer, J. *Many-Body Methods for Atoms, Molecules and Clusters*; Springer International Publishing AG, 2018.
(4) Cederbaum, L. S.; Hohlneicher, G.; Peyerimhoff, S. Calculation of the vertical ionization potentials of formaldehyde by means of perturbation theory. *Chem. Phys. Lett.* **1971**, *11*, 421−424.
(5) Doll, J. D.; Reinhardt, W. P. Many-body Green's functions for finite, nonuniform systems. Applications to closed-shell atoms. *J. Chem. Phys.* **1972**, *57*, 1169−1184.
(6) Purvis, G. D.; Öhrn, Y. Atomic and molecular electronic spectra and properties from the electron propagator. *J. Chem. Phys.* **1974**, *60*, 4063−4069.
(7) Smith, W. D.; Chen, T. T.; Simons, J. Theoretical studies of molecular ions. Vertical ionization potentials of hydrogen fluoride. *J. Chem. Phys.* **1974**, *61*, 2670−2674.
(8) Koopmans, T. Über die Zuordnung von Wellenfunktionen und Eigenwerten zu den Einzelnen Elektronen Eines Atoms. *Physica* **1934**, *1*, 104−113.
(9) Ortiz, J. V. Dyson-orbital concepts for description of electrons in molecules. *J. Chem. Phys.* **2020**, *153*, 070902.
(10) Díaz-Tinoco, M.; Corzo, H. H.; Pawłowski, F.; Ortiz, J. V. Do Dyson Orbitals resemble canonical Hartree−Fock orbitals? *Mol. Phys.* **2019**, *117*, 2275−2283.
(11) Møller, C.; Plesset, M. S. Note on an Approximation Treatment for Many-Electron Systems. *Phys. Rev.* **1934**, *46*, 618−622.
(12) Reining, L. The GW approximation: content, successes and limitations. *Wiley Interdiscip. Rev.: Comput. Mol. Sci.* **2018**, *8*, No. e1344.
(13) von Niessen, W.; Schirmer, J.; Cederbaum, L. S. Computational methods for the one-particle Green's function. *Comput. Phys. Rep.* **1984**, *1*, 57−125.
(14) Ortiz, J. V. The Electron Propagator Picture of Molecular Electronic Structure. In *Computational Chemistry: Reviews of Current Trends*; Leszczynski, J., Ed.; Vol. *2*; World Scientific, Singapore, 1997; pp 1−61.
(15) Ortiz, J. V. An efficient, renormalized self-energy for calculating the electron binding energies of closed-shell molecules and anions. *Int. J. Quantum Chem.* **2005**, *105*, 803−808.
(16) Opoku, E.; Pawłowski, F.; Ortiz, J. V. A new generation of diagonal self-energies for the calculation of electron removal energies. *J. Chem. Phys.* **2021**, *155*, 204107.
(17) Ranasinghe, D. S.; Margraf, J. T.; Perera, A.; Bartlett, R. J. Vertical valence ionization potential benchmarks from equation-of-motion coupled cluster theory and QTP functionals. *J. Chem. Phys.* **2019**, *150*, 074108.
(18) Cederbaum, L. S.; Domcke, W.; Schirmer, J.; Von Niessen, W. Correlation effects in the ionization of molecules: breakdown of the molecular orbital picture. *Adv. Chem. Phys.* **1986**, *65*, 115−159.
(19) Dolgounitcheva, O.; Díaz-Tinoco, M.; Zakrzewski, V. G.; Richard, R. M.; Marom, N.; Sherrill, C. D.; Ortiz, J. V. Accurate Ionization Potentials and Electron Affinities of Acceptor Molecules IV: Electron-Propagator Methods. *J. Chem. Theory Comput.* **2016**, *12*, 627−637.
(20) Dolgounitcheva, O.; Díaz-Tinoco, M.; Zakrzewski, V. G.; Richard, R. M.; Marom, N.; Sherrill, C. D.; Ortiz, J. V. Correction to Accurate Ionization Potentials and Electron Affinities of Acceptor Molecules IV: Electron-Propagator Methods. *J. Chem. Theory Comput.* **2017**, *13*, 389−391.
(21) Corzo, H. H.; Galano, A.; Dolgounitcheva, O.; Zakrzewski, V. G.; Ortiz, J. V. NR2 and P3+: Accurate, Efficient Electron-Propagator Methods for Calculating Valence, Vertical Ionization Energies of Closed-Shell Molecules. *J. Phys. Chem. A* **2015**, *119*, 8813−8821.
(22) Ortiz, J. V. A nondiagonal, renormalized extension of partial third-order quasiparticle theory: comparisons for closed-shell ionization energies. *J. Chem. Phys.* **1998**, *108*, 1008−1014.
(23) Ortiz, J. V. Electron detachment energies of closed-shell anions calculated with a renormalized electron propagator. *Chem. Phys. Lett.* **1998**, *296*, 494−498.
(24) Ortiz, J. V. Single-reference electron propagator calculations on vertical ionization energies of ozone. *Chem. Phys. Lett.* **1998**, *297*, 193−199.
(25) Ortiz, J. V. Orbital and shakeup operator renormalizations in electron propagator theory. *J. Chem. Phys.* **1998**, *109*, 5741−5746.
(26) Ortiz, J. V. Second-order shakeup terms in electron propagator calculations on F_2 and H_2O_2. *Int. J. Quantum Chem.* **1998**, *69*, 175−182.
(27) Ortiz, J. V. Approximate Brueckner orbitals in electron propagator calculations. *Int. J. Quantum Chem.* **1999**, *75*, 615−621.
(28) Ortiz, J. V. Electron propagator theory: an approach to prediction and interpretation in quantum chemistry. *Wiley Interdiscip. Rev.: Comput. Mol. Sci.* **2013**, *3*, 123−142.
(29) van Setten, M. J.; Caruso, F.; Sharifzadeh, S.; Ren, X.; Scheffler, M.; Liu, F.; Lischner, J.; Lin, L.; Deslippe, J. R.; Louie, S. G.; et al. GW100: Benchmarking G0W0 for Molecular Systems. *J. Chem. Theory Comput.* **2015**, *11*, 5665−5687.
(30) Caruso, F.; Dauth, M.; van Setten, M. J.; Rinke, P. Benchmark of GW Approaches for the GW100 Test Set. *J. Chem. Theory Comput.* **2016**, *12*, 5076−5087.
(31) Weigend, F.; Ahlrichs, R. Balanced basis sets of split valence, triple zeta valence and quadruple zeta valence quality for H to Rn: Design and assessment of accuracy. *Phys. Chem. Chem. Phys.* **2005**, *7*, 3297−3305.

(32) Krause, K.; Harding, M. E.; Klopper, W. Coupled-cluster reference values for the GW27 and GW100 test sets for the assessment of GW methods. *Mol. Phys.* **2015**, *113*, 1952−1960.
(33) Bruneval, F.; Dattani, N.; van Setten, M. J. The GW Miracle in Many-Body Perturbation Theory for the Ionization Potential of Molecules. *Front. Chem.* **2021**, *9*, 749779.
(34) Manne, R. A completeness theorem for operator spaces. *Chem. Phys. Lett.* **1977**, *45*, 470−472.
(35) Löwdin, P.-O. Studies in perturbation theory. X. Lower bounds to energy eigenvalues in perturbation-theory ground state. *Phys. Rev.* **1965**, *139*, A357−A372.
(36) Pickup, B. T.; Goscinski, O. Direct calculation of ionization energies. I. Closed shells. *Mol. Phys.* **1973**, *26*, 1013−1035.
(37) Born, G.; Kurtz, H. A.; Öhrn, Y. Elementary finite order perturbation theory for vertical ionization energies. *J. Chem. Phys.* **1978**, *68*, 74−85.
(38) Hirata, S.; Hermes, M. R.; Simons, J.; Ortiz, J. V. General-Order Many-Body Green's Function Method. *J. Chem. Theory Comput.* **2015**, *11*, 1595−1606.
(39) Hirata, S.; Doran, A. E.; Knowles, P. J.; Ortiz, J. V. One-particle many-body Green's function theory: Algebraic recursive definitions, linked-diagram theorem, irreducible-diagram theorem, and general-order algorithms. *J. Chem. Phys.* **2017**, *147*, 044108.
(40) Chong, D. P.; Herring, F. G.; McWilliams, D. Perturbation corrections to Koopmans' theorem. I. Double-zeta Slater-type-orbital basis. *J. Chem. Phys.* **1974**, *61*, 78−84.
(41) Hu, C.-H.; Chong, D. P.; Casida, M. E. The parametrized second-order Green function times screened interaction (pGW2) approximation for calculation of outer valence ionization potentials. *J. Electron Spectrosc. Relat. Phenom.* **1997**, *85*, 39−46.
(42) Lim, F.-H.; Nishida, M.; Hori, Y.; Ida, T.; Mizuno, M. Optimization of the spin-component-scaled factor for electron propagator method. *Chem. Phys. Lett.* **2017**, *678*, 159−166.
(43) Romero, J.; Charry, J. A.; Nakai, H.; Reyes, A. Improving quasiparticle second order electron propagator calculations with the spin-component-scaled technique. *Chem. Phys. Lett.* **2014**, *591*, 82−87.
(44) Śmiga, S.; Grabowski, I. Spin-Component-Scaled ΔMP2 Parametrization: Toward a Simple and Reliable Method for Ionization Energies. *J. Chem. Theory Comput.* **2018**, *14*, 4780−4790.
(45) Schirmer, J.; Trofimov, A. B.; Stelter, G. A non-Dyson third-order approximation scheme for the electron propagator. *J. Chem. Phys.* **1998**, *109*, 4734−4744.
(46) Zakrzewski, V. G.; Ortiz, J. V. Semidirect algorithms in electron propagator calculations. *J. Electron. Spectrosc. Relat. Phenom.* **1994**, *52*, 23−27.
(47) Zakrzewski, V. G.; Ortiz, J. V. Semidirect algorithms for third-order electron propagator calculations. *Int. J. Quantum Chem.* **1995**, *53*, 583−590.
(48) Schirmer, J.; Cederbaum, L. S. The two-particle-hole Tamm-Dancoff approximation (2ph-TDA) equations for closed-shell atoms and molecules. *J. Phys. B* **1978**, *11*, 1889−1900.
(49) Bintrim, S. J.; Berkelbach, T. C. Full-frequency GW without frequency. *J. Chem. Phys.* **2021**, *154*, 041101.
(50) Schirmer, J.; Cederbaum, L. S.; Walter, O. New approach to the one-particle Green's function for finite Fermi systems. *Phys. Rev. A* **1983**, *28*, 1237−1259.
(51) Schirmer, J.; Angonoa, G. On Green-function calculations of the static self-energy part, the ground state energy, and expectation values. *J. Chem. Phys.* **1989**, *91*, 1754−1761.
(52) Trofimov, A. B.; Schirmer, J. Molecular ionization energies and ground- and ionic-state properties using a non-Dyson electron propagator approach. *J. Chem. Phys.* **2005**, *123*, 144115.
(53) Dempwolff, A. L.; Schneider, M.; Hodecker, M.; Dreuw, A. Efficient implementation of the non-Dyson third-order algebraic diagrammatic construction approximation for the electron propagator for closed- and open-shell molecules. *J. Chem. Phys.* **2019**, *150*, 064108.
(54) Banerjee, S.; Sokolov, A. Y. Third-order algebraic diagrammatic construction theory for electron attachment and ionization energies: Conventional and Green's function implementation. *J. Chem. Phys.* **2019**, *151*, 224112.
(55) Banerjee, S.; Sokolov, A. Y. Efficient implementation of the single-reference algebraic diagrammatic construction theory for charged excitations: Applications to the TEMPO radical and DNA base pairs. *J. Chem. Phys.* **2021**, *154*, 074105.
(56) Díaz-Tinoco, M.; Corzo, H. H.; Ortiz, J. V. Electron Propagator Methods for Vertical Electron Detachment Energies of Anions: Benchmarks and Case Studies. *J. Chem. Theory Comput.* **2018**, *14*, 5881−5895.
(57) Ortiz, J. V. Partial third-order quasiparticle theory: comparisons for closed-shell ionization energies and an application to the Borazine photoelectron spectrum. *J. Chem. Phys.* **1996**, *104*, 7599−7605.
(58) Corzo, H. H.; Ortiz, J. V. Electron Propagator Theory. In *Advances in Quantum Chemistry*; Sabin, J. R., Brändas, E. J., Eds.; Academic Press, 2017; Vol. *74*, pp 267−298.
(59) Ortiz, J. V. Interpreting Bonding and Spectra With Correlated, One-Electron Concepts From Electron Propagator Theory. In *Annual Reports in Computational Chemistry*; Dixon, D. A., Ed.; Elsevier, 2017; Vol. *13*, pp 139−182.
(60) Storchi, L.; Vitillaro, G.; Tarantelli, F. Implementation and use of a direct, partially integral-driven non-Dyson propagator method for molecular ionization. *J. Comput. Chem.* **2009**, *30*, 818−825.
(61) Nooijen, M.; Snijders, J. G. Second order many-body perturbation approximations to the coupled cluster Green's function. *J. Chem. Phys.* **1995**, *102*, 1681−1688.
(62) Stanton, J. F.; Gauss, J. Perturbative treatment of the similarity transformed Hamiltonian in equation-of-motion coupled-cluster approximations. *J. Chem. Phys.* **1995**, *103*, 1064−1076.
(63) Prasad, M. D.; Pal, S.; Mukherjee, D. Some aspects of self-consistent propagator theories. *Phys. Rev. A* **1985**, *31*, 1287−1298.
(64) Ortiz, J. V. An efficient, renormalized self-energy for calculating the electron binding energies of closed-shell molecules and anions. *Int. J. Quantum Chem.* **2005**, *105*, 803−808.
(65) Purvis, G. D.; Bartlett, R. J. A full coupled-cluster singles and doubles model: The inclusion of disconnected triples. *J. Chem. Phys.* **1982**, *76*, 1910−1918.
(66) Raghavachari, K.; Trucks, G. W.; Pople, J. A.; Head-Gordon, M. A fifth-order perturbation comparison of electron correlation theories. *Chem. Phys. Lett.* **1989**, *157*, 479−483.
(67) Stanton, J. F.; Gauss, J. Analytic energy derivatives for ionized states described by the equation-of-motion coupled cluster method. *J. Chem. Phys.* **1994**, *101*, 8938−8944.
(68) Ortiz, J. V. Approximate Brueckner orbitals and shakeup operators in electron propagator calculations: applications to F^- and OH^-. *Int. J. Quantum Chem.* **1998**, *70*, 651−658.
(69) Dunning, T. H. Gaussian basis sets for use in correlated molecular calculations. I. The atoms boron through neon and hydrogen. *J. Chem. Phys.* **1989**, *90*, 1007−1023.
(70) Maggio, E.; Liu, P.; van Setten, M. J.; Kresse, G. GW100: A Plane Wave Perspective for Small Molecules. *J. Chem. Theory Comput.* **2017**, *13*, 635−648.
(71) Perdew, J. P.; Burke, K.; Ernzerhof, M. Generalized gradient approximation made simple. *Phys. Rev. Lett.* **1996**, *77*, 3865−3868.
(72) Perdew, J. P.; Burke, K.; Ernzerhof, M. Generalized gradient approximation made simple. *Phys. Rev. Lett.* **1997**, *78*, 1396.
(73) Weigend, F.; Furche, F.; Ahlrichs, R. Gaussian basis sets of quadruple zeta valence quality for atoms H−Kr. *J. Chem. Phys.* **2003**, *119*, 12753−12762.
(74) Chiles, R. A.; Dykstra, C. E. An electron pair operator approach to coupled cluster wave functions. Application to diatomic hydrogen, diatomic beryllium, and diatomic magnesium and comparison with CEPA methods. *J. Chem. Phys.* **1981**, *74*, 4544−4556.
(75) Handy, N. C.; Pople, J. A.; Head-Gordon, M.; Raghavachari, K.; Trucks, G. W. Size-consistent Brueckner theory limited to double substitutions. *Chem. Phys. Lett.* **1989**, *164*, 185−192.

https://doi.org/10.1021/acs.jctc.2c00502
J. Chem. Theory Comput. 2022, 18, 4927−4944

(76) Laidig, W. D.; Purvis, G. D., III; Bartlett, R. J. Localized orbitals in the coupled cluster singles and doubles model. *J. Electron. Spectrosc. Relat. Phenom.* **1982**, *22*, 561−573.
(77) Sekino, H.; Bartlett, R. J. Nuclear spin-spin coupling constants evaluated using many body methods. *J. Chem. Phys.* **1986**, *85*, 3945−3949.
(78) Salter, E. A.; Sekino, H.; Bartlett, R. J. Property evaluation and orbital relaxation in coupled cluster methods. *J. Chem. Phys.* **1987**, *87*, 502−509.
(79) Seeger, R.; Pople, J. A. Self-consistent molecular orbital methods. XVII. Constraints and stability in Hartree-Fock theory. *J. Chem. Phys.* **1977**, *66*, 3045−3050.
(80) Frisch, M. J.; Trucks, G. W.; Schlegel, H. B.; Scuseria, G. E.; Robb, M. A.; Cheeseman, J. R.; Scalmani, G.; Barone, V.; Petersson, G. A.; Nakatsuji, H.; et al. *Gaussian 16*; Gaussian, Inc.: Wallingford CT, 2016.
(81) Frisch, M. J.; Trucks, G. W.; Schlegel, H. B.; Scuseria, G. E.; Robb, M. A.; Cheeseman, J. R.; Scalmani, G.; Barone, V.; Petersson, G. A.; Nakatsuji, H.; et al. *Gaussian Development Version*, Revision I.14; Gaussian Inc.: Wallingford CT, 2018.
(82) Aidas, K.; Angeli, C.; Bak, K. L.; Bakken, V.; Bast, R.; Boman, L.; Christiansen, O.; Cimiraglia, R.; Coriani, S.; Dahle, P.; et al. The Dalton quantum chemistry program system. *Wiley Interdiscip. Rev.: Comput. Mol. Sci.* **2014**, *4*, 269−284.
(83) Matthews, D. A.; Cheng, L.; Harding, M. E.; Lipparini, F.; Stopkowicz, S.; Jagau, T.-C.; Szalay, P. G.; Gauss, J.; Stanton, J. F. Coupled-cluster techniques for computational chemistry: The CFOUR program package. *J. Chem. Phys.* **2020**, *152*, 214108.
(84) Li, W.-Z.; Huang, M.-B.; Chen, B.-Z. The 1^2A_1, 1^2B_2, and 1^2A_2 states of the SO_2^+ ion studied using multiconfiguration second-order perturbation theory. *J. Chem. Phys.* **2004**, *120*, 4677−4682.
(85) Palme, M. H.; Shaw, D. A.; Guest, M. F. The electronically excited and ionic states of sulphur dioxide: An *ab initio* molecular orbital CI study and comparison with spectral data. *Mol. Phys.* **2005**, *103*, 1183−1200.
(86) Chang, J.-L.; Huang, S.-T.; Chen, C.-C.; Yang, T.-T.; Hsiao, C.-C.; Lu, H.-Y.; Lee, C.-L. Theoretical calculations of C_{2v} excited states of SO_2^+. *Chem. Phys. Lett.* **2010**, *486*, 12−15.
(87) Pawłowski, F.; Ortiz, J. V. Ionization Energies and Dyson Orbitals of the Iso-electronic SO_2, O_3, and S_3 Molecules from Electron Propagator Calculations. *J. Phys. Chem. A* **2021**, *125*, 3664−3680.
(88) Yencha, A. J.; Truong, S. Y.; King, G. C. Threshold photoelectron spectrocopy of SO_2 over the photon energy range 12-50 eV. *J. Electron Spectrosc. Relat. Phenom.* **2019**, *233*, 38−50.
(89) Bartlett, R. J. Coupled-cluster theory and its equation-of-motion extensions. *Wiley Interdiscip. Rev. Comput. Mol. Sci.* **2012**, *2*, 126−138.
(90) Opoku, E.; Pawłowski, F.; Ortiz, J. V. Electron binding energies and Dyson orbitals of $O_nH_{2n+1}^{+,0,-}$ clusters: Double Rydberg anions, Rydberg radicals, and micro-solvated hydronium cations. *J. Chem. Phys.* **2021**, *154*, 234304.
(91) Bintrim, S. J.; Berkelbach, T. C. Full-frequency GW without frequency. *J. Chem. Phys.* **2021**, *154*, 041101.
(92) Kanchanakungwankul, S.; Truhlar, D. G. Examination of How Well Long-Range-Corrected Density Functionals Satisfy the Ionization Energy Theorem. *J. Chem. Theory Comput.* **2021**, *17*, 4823−4830.

https://doi.org/10.1021/acs.jctc.2c00502
J. Chem. Theory Comput. 2022, 18, 4927−4944

Appendix E

E. Opoku, F. Pawłowski and J. V. Ortiz, "Electron−Propagator Methods Versus Experimental Ionization Energies", *J. Chem. Phys.*, 162, 064102 (2025)

The Journal of Chemical Physics ARTICLE pubs.aip.org/aip/jcp

Electron-propagator methods versus experimental ionization energies

Cite as: J. Chem. Phys. 162, 064102 (2025); doi: 10.1063/5.0250732
Submitted: 26 November 2024 • Accepted: 20 January 2025 •
Published Online: 10 February 2025

View Online Export Citation CrossMark

Ernest Opoku, Filip Pawłowski, and J. V. Ortiz[a]

AFFILIATIONS

Department of Chemistry and Biochemistry, Auburn University, Auburn, Alabama 36849-5312, USA

[a]Author to whom correspondence should be addressed: ortiz@auburn.edu

ABSTRACT

Select electron-propagator (EP) methods agree as closely with experimental standards for molecular vertical ionization energies as they do with computational data of nearly full-configuration-interaction quality. Several EP methods consistently attain higher accuracy than alternatives with equal arithmetic bottlenecks expressed in terms of occupied (O) and virtual (V) orbital dimensions. The cubically scaling methods realize a mean absolute error (MAE) below 0.2 eV and are feasible whenever conventional self-consistent-field calculations are performed. O^2V^3-scaling EP self-energies achieve an MAE slightly above 0.1 eV and are as feasible as conventional second-order perturbative calculations of total energies. OV^4 methods are more accurate (MAEs ~0.075 eV) than ΔCCSD(T) and are more efficient than third-order total-energy calculations. An equally accurate generalization with full self-energy matrices and non-iterative O^2V^4 contractions produces Dyson orbitals in their most general form. Composite EP models that accurately estimate the effects of basis-set saturation drastically improve efficiency without sacrificing accuracy. No adjustable parameters are employed in the self-energy formulas or in the generation of reference-state orbitals. When Dyson-orbital probability factors indicate that Koopmans's theorem is qualitatively valid, simple perturbative corrections suffice to approach chemical accuracy.

Published under an exclusive license by AIP Publishing. https://doi.org/10.1063/5.0250732

INTRODUCTION

Choosing the right molecule for a given purpose is often a matter of fulfilling a set of structural, spectroscopic, thermodynamic, or reactivity criteria. Purely inductive approaches to molecular optimization rely on the existence of copious data and empirical correlations. Their deductive counterparts exploit unifying physical principles that constitute the common origins of diverse properties. To realize their predictive aims, both approaches frequently require electron binding energies. Among these properties, vertical ionization energies (VIEs) of molecules are in especially high demand. Interpretations of photoelectron spectra and scattering experiments are often facilitated by predictions of VIEs. This paper, therefore, aims to identify unbiased, transparent, efficient, and accurate means of calculating this widely sought information.

Recent tests of a new generation of *ab initio* electron-propagator (EP) methodology have been based exclusively on comparisons to computational data.[1–6] In these tests, EP approximations have achieved unprecedented accuracy and efficiency in the prediction of VIEs. Methods with cubic arithmetic scaling have produced mean absolute errors (MAEs) of 0.2 eV for closed-shell molecules. Fifth-power extensions have approached chemical accuracy (average errors of 0.04 eV or 1 kcal/mol). The new methods contain no adjustable parameters. Correlation and relaxation corrections to the results of Koopmans's Theorem[7] (KT) are easily identified in computational formulas. In this work, numerical tests employ standards of accuracy based on *experimental* data for the first time.

EP calculations also yield Dyson orbitals as eigenfunctions of an effective operator whose eigenvalues equal electron binding energies.[8,9] Dyson orbitals that correspond to VIEs may be conceived as overlaps between wavefunctions with N and N − 1 electrons.[10] A variety of experimental techniques provide verification of the absolute amplitudes and phases of Dyson orbitals. Unlike other kinds of orbitals that are introduced as computational or interpretive conveniences, Dyson orbitals can be measured. They also are related to total energies, one-electron reduced density matrices and properties, and several varieties of transition probabilities and spectroscopic intensities.[10] In general, Dyson orbitals are not normalized to unity. Their norms are proportional to transition probabilities in

the sudden approximation. Because they pertain to all final states with N − 1 electrons, the Dyson orbitals constitute an over-complete, non-orthogonal set of one-electron functions.

Solutions of the Dyson equation produce electron binding energies and corresponding Dyson orbitals directly. Therefore, optimization of many-electron total energies and wavefunctions may be avoided in EP calculations. Differences between the one-electron properties of an initial, N-electron state and a final, cationic state with N − 1 electrons may also be inferred.[11–13]

Numerical tests of predictive capabilities may refer to experimental or computational standards. The purely computational option is exemplified by comparisons between approximate methods and full configuration interaction in a fixed orbital basis. Data of the latter type are available for small, simple molecules only. Such restricted samples do not capture the variety of molecular structures and properties that are likely to be relevant in practice. Approximate methods may provide reasonable alternatives to full configuration interaction when they demonstrate a converged approach to

TABLE I. Approximate, electron-propagator methods: Acronyms and classifications.

Acronym[a]	Full name
Diagonal second-order self-energies (category 1)	
D2	Diagonal second order
os-D2	Opposite-spin D2
nD-D2	Non-Dyson D2
os-nD-D2	Opposite-spin non-Dyson D2
Diagonal post second-order self-energies (categories 2, 3 and 4)	
D3—Category 2	Diagonal third order
nD-D3—Category 2	Non-Dyson D3
OVGF—Category 3	Outer-valence Green's function (versions A, B and C)
nD-OVGF—Category 3	Non-Dyson OVGF (versions A, B and C)
P3—Category 2	Partial third order
P3+—Category 3	Approximately renormalized partial third order
Q3—Category 2	Quasiparticle third order
Q3+—Category 3	Approximately renormalized quasiparticle third order
L3—Category 2	Linear third order
nD-L3—Category 2	Non-Dyson L3
L3+—Category 3	Approximately renormalized linear third order (versions A, B, and C)
nD-L3+—Category 3	Non-Dyson L3+ (versions A, B, and C)
RP3—Category 4	Explicitly renormalized partial third order
RQ3—Category 4	Explicitly renormalized quasiparticle third order
RL3—Category 4	Explicitly renormalized linear third order
nD-RL3—Category 4	Non-Dyson RL3
DR—Category 4	Diagonal (renormalized) ring approximation (HF-TDA-G_0W_0)
Non-diagonal self-energies (category 5)	
ND2	Non-diagonal, second order
2ph-TDA	Two-particle-one-hole Tamm–Dancoff approximation
3+	Non-diagonal third order
ADC(3)	Third order algebraic diagrammatic construction
NR2	Non-diagonal, renormalized, second order
BD-T1	Brueckner doubles with triple field operators
NRP3	Non-diagonal extension of RP3
NRQ3	Non-diagonal extension of RQ3
NRL3	Non-diagonal extension of RL3
Composite models	
CMX, X = 1-8	Composite model X

[a]For new-generation methods in bold type: N = non-diagonal; nD = non-Dyson; R = explicitly renormalized; and + = approximately renormalized.

Published under an exclusive license by AIP Publishing

TABLE II. Requirements for arithmetic scaling and transformed electron-repulsion integrals (ERIs) in electron-propagator methods.[a]

Method class	Methods[b]	Arithmetic bottleneck	Bottleneck steps	Largest ERI[c] subset
Diagonal 2nd order	D2, **os-D2**	OV^2	N_E	O^2V^2[d]
	RSPT2, nD-D2, **os-nD-D2**	OV^2	Non-iterative	O^2V^2[d]
Diagonal post 2nd order and approximately renormalized (+)	RSPT3	OV^4	Non-iterative	V^4
	D3, OVGF	OV^4	N_E[e]	V^4
	IE: P3, P3+, **Q3, Q3+**	O^2V^3	Non-iterative	OV^3
	EA: P3, P3+, **Q3, Q3+**	OV^4	N_E	V^4
	L3, L3+	OV^4	N_E[e]	V^4
Diagonal post 2nd order and explicitly renormalized (R)	**IE: RP3, RQ3**	O^2V^3	Non-iterative	OV^3
	EA: RP3, RQ3	OV^4	N_IN_E	V^4
	RL3	OV^4	N_IN_E[e]	V^4
	IE: DR	O^2V^3	N_IN_E	O^2V^2
	EA: DR	O^2V^3	N_IN_E	OV^3
Non-diagonal and renormalized (NR) or non-diagonal only (ND2)	ND2 (not renormalized)	OV^3	N_I	OV^3
	2ph-TDA	OV^4	N_I	V^4
	3+	O^2V^4	Non-iterative	V^4
	ADC(3)	O^2V^4	N_I	V^4
	IE: NR2	O^3V^3	Non-iterative[f]	OV^3
	EA: NR2	O^2V^4	Non-iterative[f]	V^4
	BD-T1	O^2V^4	BD[g]	V^4
	NRP3	O^2V^4	Non-iterative[f]	V^4
	NRQ3	O^2V^4	Non-iterative[f]	V^4
	NRL3	O^2V^4	Non-iterative[f]	V^4

[a]O = # occupied orbital, V = # virtual orbitals, N_E = energy iterations, and N_I = inverse-expansion or linear-equation iterations for diagonal methods and Hamiltonian-vector multiplications for non-diagonal methods.
[b]New methods in **bold type**. IE = ionization energy (electron detachment). EA = electron affinity (electron attachment).
[c]ERI = electron repulsion integral.
[d]See Eqs. (10) and (11). The size of the largest block of ERIs *per state* is proportional to OV^2.
[e]Reduction by a factor of N_E occurs in non-Dyson (nD) versions for electron detachments.
[f]N_I OV^4 iterative steps for 3+, ADC(3), and NRL3; N_I O^3V^2 iterative steps for NR2, NRP3, and NRQ3 IEs; N_I OV^4 iterative steps for NR2, NRP3, and NRQ3 EAs.
[g]The O^2V^4 arithmetic bottleneck occurs in the Brueckner doubles, coupled-cluster, reference-state calculation; the subsequent electron-propagator bottleneck is OV^4.

electron correlation. Close agreement between two levels of ionization-potential, equation-of-motion, coupled-cluster (IP-EOM-CC) theory may suffice to demonstrate convergence. A representative set of VIEs of closed-shell molecules was created to optimize parameters in the Quantum Theory Project (QTP) density functionals.[14] A mean absolute discrepancy below 0.05 eV resulted for the consecutive SDT and SDTQ approximations. (S, D, T, and Q stand for single, double, triple, and quadruple substitutions in the reference state's cluster operator.) The QTP set includes molecules with nuclei from the first three periods and considers ground and excited final (cationic) states. In the present study, *all* molecules in the QTP set are included for the first time. The correlation-consistent, triple-ζ basis is employed.

Tests of the latter kind reveal the ability of an approximate method to describe the electron correlation that characterizes a given basis. Unfortunately, small basis sets may produce exaggerated or diminished correlation effects, especially when localized, negative charges accumulate. Experimental data confirmed by computational verification can provide a foundation for complementary tests that are less dependent on basis choices. Such a set of experimental VIEs of closed-shell molecules has been developed at Cambridge University (CU) for tests of density-functional and EP methods.[15] A critical comparison of experimental and computational data enabled these authors to eliminate large discrepancies and thereby produce a more reliable set of standards. Their ΔCCSD(T) calculations produced a MAE between experiment and theory of only 0.08 eV (see Table S1 in the supplementary material). The bonding patterns that typify basic organic and inorganic molecules are well represented in the CU data.

Numerical tests discussed below examine five categories of EP methodology. These categories differ in their self-energy operators that describe the effects of electron correlation and final-state orbital relaxation. Table I displays acronyms and classifications for each approximate self-energy. Arithmetic scaling factors and required electron repulsion integrals (ERIs) pertaining to each method are shown in Table II. The most flexible and computationally

Published under an exclusive license by AIP Publishing

demanding category includes all elements of the self-energy operator's matrix and certain classes of perturbative corrections in all orders. These non-diagonal, renormalized, fifth-category methods produce Dyson orbitals as a linear combination of basis orbitals. To focus on valence electron binding energies, the fourth category of methods neglects off-diagonal elements of the self-energy matrix in the canonical Hartree–Fock (HF) basis. Explicitly calculated renormalizations remain in the diagonal elements, but the Dyson orbitals become proportional to canonical HF orbitals. In the third category, approximate renormalizations replace their explicit counterparts in the diagonal elements of the self-energy matrix. Ratios of easily evaluated second-order and third-order diagrams occur in the approximately renormalized self-energy formulas. Abandonment of all terms beyond the third order defines the second category. Because third-category, approximate renormalizations involve only trivial additional calculations, the second category is useful chiefly for analysis of correlation and relaxation effects. Finally, one arrives at the first category, which demands no self-energy terms beyond second order. These methods involve only trivial computational effort; their *de facto* computational bottlenecks occur prior to their execution. Despite their simplicity and efficiency, they generate usefully accurate data. Numerical comparisons between recently developed members of each category and their older antecedents enable the identification of the best compromises of accuracy and efficiency.

Composite models constitute a final step toward the widespread application of the most efficient and accurate methods.[16] First-category methods provide a convenient means toward the exhaustion of basis-set effects. Higher-category methods with more steeply scaling arithmetic bottlenecks typically reveal their differential contributions to results of high accuracy with smaller basis sets. Various combinations of methods and basis sets may be judged vs the CU data. Practical suggestions for the employment of composite models conclude this paper. The theory and the information that suffice to reproduce the data underlying the conclusions are also included below. Methods that appeal to adjustable parameters in self-energy formulas or in the generation of reference orbitals are excluded from consideration in this study.

THEORY

For every VIE that pertains to an initial, molecular state with N electrons and the pth final, cationic state, there is a Dyson orbital defined by

$$\phi_p^{Dyson}(x) = \sqrt{N}\int \Psi^*_{cation,p}(x_2, x_3, x_4, \ldots, x_N) \times \Psi_{molecule}(x_1, x_2, x_3, \ldots, x_n) dx_2 dx_3 dx_4 \ldots dx_N, \quad (1)$$

where x_v is the space-spin coordinate of electron v.[10] The corresponding VIE is the negative of the electron binding energy, E_p, where

$$E_p = E_{molecule} - E_{cation,p} = -(VIE)_p. \quad (2)$$

Electron binding energies and *normalized* Dyson orbitals emerge as eigenvalues and eigenfunctions of the Dyson quasiparticle equation,[17]

$$[\hat{F} + \hat{\Sigma}(E_p)]\varphi_p^{Dyson}(x) = E_p \varphi_p^{Dyson}(x). \quad (3)$$

The operator in this pseudo-eigenvalue equation has Fock and self-energy components with circumflex accents. The generalized Fock operator's Coulomb and exchange contributions depend on the one-electron reduced density matrix (1RDM) of the initial state. At self-consistency, one of the eigenvalues of the operator must equal the argument of the self-energy operator. In general, Dyson orbitals are not normalized to unity. Their norms, denoted by Π_p, are known as probability factors, intensity factors, or pole strengths. (The latter term arises from the equivalence of the poles of the electron propagator, or many-body Green's function, with electron binding energies.[18,19]) These factors may be inferred from the derivatives of the normalized Dyson orbital's self-energy matrix element with respect to the energy parameter.[9] Evaluation of this matrix element occurs at the self-consistent value of the energy, where

$$\Pi_p = \int |\phi_p^{Dyson}(x)|^2 dx = \left[1 - \frac{\int \varphi_p^{Dyson*} \hat{\Sigma}(E) \varphi_p^{Dyson} dx}{dE}\Big|_{E=E_p}\right]^{-1}. \quad (4)$$

Dyson orbitals, therefore, are related to their normalized counterparts by

$$\phi_p^{Dyson}(x) = \Pi_p^{\frac{1}{2}} \varphi_p^{Dyson}(x). \quad (5)$$

For calculations on outer valence electron binding energies of closed-shell molecules, off-diagonal elements of the self-energy operator in the canonical HF basis are usually negligible. (Neglect of all self-energy matrix elements and correlation in the reference state's 1RDM recovers the HF equations and Koopmans's identity.) Their annulment constitutes the diagonal approximation, which reduces arithmetic bottlenecks by a factor proportional to molecular size. In the diagonal approximation, Dyson orbitals are proportional to normalized, canonical HF orbitals, where

$$\phi_{p,i}^{Dyson}(x) = \Pi_p^{\frac{1}{2}} \psi_i^{HF}(x). \quad (6)$$

For VIEs, many values of p may pertain to an occupied, canonical HF orbital with index i. In most cases, just one value of p has a dominant probability factor. (The sum of these probability factors equals unity in the diagonal self-energy approximation.) Probability factors that exceed 0.85 confirm the qualitative validity of the diagonal approximation and of the assumptions of Koopmans's identity. Retention of off-diagonal elements of the self-energy operator yields Dyson orbitals as linear combinations of canonical HF orbitals.

Formulas for the matrix elements of the Fock and self-energy operators define the approximate methods of Table I. In many cases, contributions to the Fock matrix elements arise from correlation improvements to the initial state's 1RDM. These terms are often called energy-independent or constant self-energy matrix elements. The matrix form of the Dyson quasiparticle equation in the canonical HF basis, therefore, reads

$$[\boldsymbol{\varepsilon} + \boldsymbol{\Sigma}^{constant} + \boldsymbol{\Sigma}(E)]\mathbf{C}^{Dyson} = E\mathbf{C}^{Dyson}, \quad (7)$$

Published under an exclusive license by AIP Publishing

where $\boldsymbol{\varepsilon}$ is a diagonal matrix containing canonical HF orbital energies. When the energy argument is self-consistent on the left and right sides of Eq. (7), the corresponding eigenvector yields the normalized Dyson orbital. In the diagonal self-energy approximation, each occupied canonical HF orbital has its set of correlated VIEs that are determined by

$$\varepsilon_i + \Sigma_{ii}^{constant} + \Sigma_{ii}(E) = E. \tag{8}$$

For the methods of Table I, it is possible to separate terms that arise from two-hole-one-particle (2hp) and two-particle-one-hole (2ph) second-quantized operators. For VIEs, the former terms describe orbital relaxation and electron correlation in final states. The 2ph terms represent initial-state correlation. For several self-energy approximations, there is an arithmetic advantage in using their non-Dyson versions, where the simplified quasiparticle equation reads

$$\varepsilon_i + \Sigma_{ii}^{constant} + \Sigma_{ii}^{2ph}(\varepsilon_i) + \Sigma_{ii}^{2hp}(E) = E. \tag{9}$$

Setting the E argument in the 2ph term to the Koopmans energy eliminates iterations in bottleneck contractions for the methods denoted by nD in Table I.

The most familiar self-energy, diagonal second-order or D2, has vanishing constant terms, a 2hp term and a 2ph term,

$$\Sigma_{ii}(E) = \frac{1}{2}\frac{|\langle ia\|jk\rangle|^2}{E+\varepsilon_a-\varepsilon_j-\varepsilon_k} + \frac{1}{2}\frac{|\langle ij\|ab\rangle|^2}{E+\varepsilon_j-\varepsilon_a-\varepsilon_b}. \tag{10}$$

(Einstein summation and Dirac, anti-symmetrized ERI notations are used; occupied and virtual spin-orbitals are denoted, respectively, by i, j, k, . . . and a, b, c, . . .) The modification that considers only opposite-spin electron correlation (os-D2) involves direct (single-bar) ERIs according to

$$\Sigma_{ii}(E) = \frac{|\langle iA|jK\rangle|^2}{E+\varepsilon_A-\varepsilon_j-\varepsilon_K} + \frac{|\langle iJ|aB\rangle|^2}{E+\varepsilon_J-\varepsilon_a-\varepsilon_B} \tag{11}$$

(capital letters denote spin-orbitals with spin opposite to that of i). The os-nD-D2 alternative fixes E at ε_i in the second term. These category-1 methods have cubic arithmetic scaling and, for each VIE, require only a quartically scaling ERI transformation with one fixed orbital index. The self-energy of Eq. (11) differs from the second-order terms included in the exchange-less G_0W_0 approximation[20] for closed-shell reference states because it has no factor of two.

To the 2hp part of the self-energy, the P3 method[21] adds third-order ring and ladder[22,23] terms. It also adds 2hp corrections that involve reference-state double replacements in first order. The latter improvement introduces a non-iterative O^2V^3 bottleneck, but energy iterations in Eq. (8) have only O^3V^2 scaling. The more recently introduced Q3 method[1] improves on P3 with constant self-energy terms that arise from reference-state single replacements in second order. These non-iterative terms distinguish Q methods from their P antecedents and require only O^2V^3 summations. Approximate higher order corrections in the P3+ and Q3+ category-3 methods involve only trivial arithmetic operations. Explicit evaluation of ring and ladder 2hp corrections in all orders occurs in the category-4 RP3 and RQ3 methods. Their consequent iterative procedures still conform to O^3V^2 scaling. The P and Q methods for VIEs include only second-order 2ph terms in the self-energy. P3+, RP3, Q3+, and RQ3 do not require ERIs with four virtual indices, and therefore, their *de facto* bottlenecks occur in the ERI transformation.[1,6] The demands for operations and storage of these category-2, category-3, and category-4 methods resemble those of second-order (MP2) total energy calculations.

For VIEs, the 2ph diagrammatic equivalents of the 2hp improvements discussed above are needed to achieve higher accuracy. Evaluation of these terms in the L3, L3+, and RL3 methods requires ERIs with four virtual indices and OV^4 arithmetic scaling.[1,6] Energy iterations with this scaling do not occur in the nD versions of L3, L3+, and RL3. Three alternative approximation formulas (denoted by A, B, and C) have been tested for L3+. The B version generates superior numerical results and retains the pair-correlation concepts of second-order theories. D3 and its approximately renormalized Outer Valence Green Function,[22,24] or OVGF, extensions (also labeled A, B, and C) perform OV^4 contractions. They also require ERIs with four virtual indices and have more efficient nD versions. Operations with OV^4 scaling are less numerous than those of the partial ERI transformation that precedes a conventional MP2 calculation.

Non-diagonal, renormalized (category-5) generalizations of the RP3, RQ3, and RL3 (category-4) self-energies involve non-iterative contractions with O^2V^4 arithmetic scaling.[3] The resulting NRP3, NRQ3, and NRL3 methods are less demanding than previously developed methods with iterative O^2V^4 bottlenecks. The latter set includes BD-T1[17] and the standard Schirmer–Angonoa version of ADC(3).[25,26] A similar requirement accompanies the ground-state optimization of IP-EOM-CCSD[27] calculations. In the 3+ method,[28] also known as the strict third-order version of ADC(3), the O^2V^4 bottleneck is non-iterative. A non-iterative O^3V^3 bottleneck pertains to the NR2 method[29] for VIEs. In 2ph-TDA calculations,[19] OV^4 scaling prevails.

The parameter-free diagonal ring (DR) self-energy (i.e., G_0W_0 with HF orbitals and Tamm–Dancoff excitations[30]) for VIEs has O^2V^3 scaling. It requires no ERIs with three or four virtual indices. Because it invokes the diagonal approximation and contains ring terms in all orders, it is classified here as a category-4 method.

The new generation of post-second-order methods is founded on an alternative approach to the derivation of corrections to KT results in Eq. (7). Matrix elements of the superoperator Hamiltonian ($\hat{H}$) between second-quantized operators (e.g., h, p, 2hp, and 2ph types) are the building blocks of $\Sigma^{constant}$ and $\Sigma(E)$. In older approaches, correlation corrections to reference-state density matrices were added as needed to generate self-energy terms of a given order. (The slow convergence of the usual finite-order series of self-energies has been demonstrated numerically.[31–33]) Newer variants instead employ a constant treatment of reference-state correlation that imposes two conditions.[1,6] The first is the Hermiticity of the $\hat{\boldsymbol{H}}$ matrix. The second is intermediate normalization and the consequent size-extensive total energies of the reference state. (This approach differs from the Hermitization suggested in the founding works of equation-of-motion theory,[34] for spurious terms are not retained and Hermitized.) All resulting terms through third order in the fluctuation potential remain in the L3 self-energy. Renormalized (L3+ and RL3) and non-diagonal (NRL3) extensions

Published under an exclusive license by AIP Publishing

procure increased accuracy. P and Q variants offer optimal accuracy while requiring higher efficiency.

COMPUTATIONAL METHODS

All results on VIEs are based on HF self-consistent-field wavefunctions except those of BD-T1 EP calculations, which use Brueckner-doubles[35] (BD) coupled-cluster pseudo-canonical orbitals. ERIs transformed to the HF or BD pseudo-canonical basis are stored on disk. The largest subsets of ERIs required for each EP approximation are listed in Table II. Electron correlation treatments exclude core orbitals in ΔCCSD(T) and EP calculations, i.e., the standard frozen-core approximation is in effect. All new methods have been implemented as new links in the development version of Gaussian software.[36] The diagonal electron propagator methods in Table II have also been implemented with Abelian-symmetry-adapted, semidirect algorithms.

IP-EOM-CCSDTQ benchmarks

Geometries for 14 small molecules were obtained from the QTP study. This test set considers several transitions per molecule and includes 42 VIEs. To facilitate a robust test of all methods, any state where at least one method obtains probability factors below the 0.85 recommended threshold is excluded from further consideration. The subset of transitions with high probability factors comprises 27 VIEs. Statistical error measures involving all 42 VIEs are available in the supplementary material.

IP-EOM-CCSDT VIE benchmarks

This dataset applies to 201 VIEs from 41 molecules. After eliminating 85 VIEs in which at least one method obtains a probability factor below the 0.85 threshold, 116 VIEs are left. Therefore, the statistics presented in Table IV and Fig. 2 are based on this subset of VIEs. Exhaustive statistics that consider all 201 data are provided in the supplementary material. Previously published tests of the new methods did not consider molecules containing third row nuclei.

Cambridge experimental standards

The geometries and experimental VIEs of 136 closed-shell molecules have been taken from the CU study.[15] To validate the reliability of the experimental standards, CCSD(T) total energy differences have been computed. [CCSD(T) stands for coupled-cluster theory with single and double replacements and approximate triple replacements.[37]] The aug-cc-pVDZ and aug-cc-pVTZ basis sets[38] were used for the ΔCCSD(T) calculations. Our ΔCCSD(T)/aug-cc-pVTZ results agree with those in the published CU data. Unrestricted HF reference orbitals were used in cationic final-state calculations. Inverse quartically extrapolated [i.e., $(l + 1/2)^{-4}$] total energies obtained with augmented triple and double ζ basis sets define the complete-basis-set (CBS) VIE standards. The experimental VIE standards and their ΔCCSD(T) counterparts have been assembled in the supplementary material. All probability factors exceed the 0.85 recommended threshold for diagonal EP methods and confirm the qualitative validity of perturbative improvements to KT predictions. All EP results pertain to the lowest VIE of each molecule. The same double-triple-ζ extrapolation technique was employed. Because the CU study did not report molecular point groups and irreducible representations of the hole states, these classifications are next to the standard VIEs. This information facilitates spectral assignments, especially when the order of final states predicted by KT is incorrect. Undetected Koopmans defects in 12 molecules (assembled in the supplementary material) led to incorrect conclusions on P3 statistical errors in the CU report.[15] In each of these cases, the correct HF orbital energy was not selected for improvement with EP methods.

The following equations define EP composite models denoted by CMX (where X = 1–8). The CU VIEs are used as standards for evaluating the performance of CMX models,

$$E^{CM1} = E^{Q3+}_{aug-cc-pVDZ} + E^{os-nD-D2}_{CBS(DT)} - E^{os-nD-D2}_{aug-cc-pVDZ}, \quad (12)$$

$$E^{CM2} = E^{nD-L3+B}_{aug-cc-pVDZ} + E^{os-nD-D2}_{CBS(DT)} - E^{os-nD-D2}_{aug-cc-pVDZ}, \quad (13)$$

$$E^{CM3} = E^{nD-RL3}_{aug-cc-pVDZ} + E^{os-nD-D2}_{CBS(DT)} - E^{os-nD-D2}_{aug-cc-pVDZ}, \quad (14)$$

$$E^{CM4} = E^{Q3+}_{aug-cc-pVTZ} + E^{os-nD-D2}_{CBS(TQ)} - E^{os-nD-D2}_{aug-cc-pVTZ}, \quad (15)$$

$$E^{CM5} = E^{nD-L3+B}_{aug-cc-pVTZ} + E^{os-nD-D2}_{CBS(TQ)} - E^{os-nD-D2}_{aug-cc-pVTZ}, \quad (16)$$

$$E^{CM6} = E^{nD-RL3}_{aug-cc-pVTZ} + E^{os-nD-D2}_{CBS(TQ)} - E^{os-nD-D2}_{aug-cc-pVTZ}, \quad (17)$$

$$E^{CM7} = E^{CM4} + E^{nD-L3+B}_{aug-cc-pVDZ} - E^{Q3+}_{aug-cc-pVDZ}, \quad (18)$$

$$E^{CM8} = E^{NRL3}_{aug-cc-pVDZ} + E^{os-nD-D2}_{CBS(DT)} - E^{os-nD-D2}_{aug-cc-pVDZ}. \quad (19)$$

The first three models combine double-triple-ζ extrapolations with the os-nD-D2 self-energy and three increasingly difficult post-second-order methods (Q3+, nD-L3+B, and nD-RL3) with the smaller basis. In models CM4 through CM6, the same sequence of calculations occurs with quadruple and triple ζ basis sets. CM7 improves on CM4 with the difference between Q3+ and nD-L3+B results at the double ζ level. CM8 resembles CM1, CM2, and CM3 but employs NRL3 instead for post-second-order effects.

RESULTS AND DISCUSSION

IP-EOM-CC/cc-pVTZ standards

Table III and Fig. 1 display error measures vs IP-EOM-CCSDTQ standards obtained with the cc-pVTZ basis. The two category-1 methods that retain same-spin contributions (D2 and nD-D2) produce MAEs that are half as large as those of KT. Useful predictive quality emerges from the category-1 methods that neglect same-spin electron correlation, os-D2 and os-nD-D2 (see the bottom four bars of Fig. 1 and the top two sections of Table III). Histograms (see the top rows in Figs. S1 and S2 of the supplementary material) demonstrate the tendency of the D2 and nD-D2 methods to underestimate VIEs. The two opposite-spin-only methods

Published under an exclusive license by AIP Publishing

TABLE III. Error distributions (eV) with respect to IP-EOM-CCSDTQ/cc-pVTZ standards.

Method class	Method[a]	Mean absolute error[b]	Mean signed error	Standard deviation	Maximum absolute error
Uncorrelated	KT	1.001	0.899	0.831	2.551
Diagonal 2nd order	D2	0.515	−0.477	0.442	1.410
	os-D2	0.204	0.073	0.268	0.659
	nD-D2	0.539	−0.491	0.466	1.463
	os-nD-D2	**0.198**	0.055	0.267	0.644
Diagonal post 2nd order	DR	0.238	0.173	0.250	0.810
	D3	0.429	0.379	0.400	1.468
	nD-D3	0.418	0.371	0.396	1.455
	OVGF-A	0.118	0.008	0.159	0.421
	OVGF-B	0.162	0.075	0.207	0.569
	OVGF-C	0.188	0.143	0.191	0.681
	nD-OVGF-A	0.123	−0.003	0.166	0.395
	nD-OVGF-B	0.158	0.061	0.202	0.542
	nD-OVGF-C	0.173	0.131	0.183	0.655
	P3	0.166	0.120	0.210	0.727
	P3+	0.160	0.015	0.191	0.395
	Q3	0.123	0.052	0.178	0.675
	Q3+	**0.124**	−0.054	0.137	0.335
	L3	0.107	0.067	0.146	0.595
	nD-L3	0.100	0.054	0.140	0.567
	L3+A	0.174	−0.123	0.158	0.425
	L3+B	0.103	−0.035	0.128	0.331
	L3+C	0.111	−0.023	0.145	0.351
	nD-L3+A	0.169	−0.123	0.151	0.420
	nD-L3+B	**0.100**	−0.041	0.125	0.336
	nD-L3+C	0.106	−0.030	0.137	0.331
	RP3	0.152	−0.036	0.168	0.322
	RQ3	0.139	−0.103	0.121	0.323
	RL3	0.091	−0.061	0.101	0.345
	nD-RL3	**0.096**	−0.077	0.101	0.383
Non-diagonal	ND2	0.515	−0.478	0.449	1.381
	2ph-TDA	0.567	−0.567	0.273	1.405
	3+	0.205	0.146	0.221	0.710
	ADC(3)	0.211	0.175	0.202	0.726
	NR2	0.150	−0.064	0.157	0.356
	BD-T1	**0.071**	−0.006	0.082	0.163
	NRP3	0.150	−0.064	0.156	0.358
	NRQ3	0.154	−0.128	0.115	0.379
	NRL3	**0.100**	−0.085	0.094	0.391
	IP-EOM-CCSD	0.102	0.052	0.111	0.263
	IP-EOM-CCSDT	0.022	−0.016	0.022	0.054

[a]New methods in bold type.
[b]Optimal methods in bold type.

have much more balanced histograms and MAEs of only 0.2 eV. Category-1 calculations of a single VIE demand only cubically scaling sets of ERIs and arithmetic operations with OV^2 arithmetic bottlenecks. With efficient algorithms, they are practically free once the preceding self-consistent field is converged.

The remaining methods that employ the diagonal self-energy approximation (i.e., categories two, three, and four) have fifth-power arithmetic scaling. Some of these methods do not require a full transformation of ERIs, for matrix elements with four virtual indices are absent from their self-energy formulae. Because their arithmetic scaling factors equal only O^2V^3 (see legend of Table II), their *de facto* bottlenecks still occur in the ERI transformation. Data from Table III and the second lowest set of bars in Fig. 1 indicate that Q3+ is a better category-3 choice than P3+. Similar conclusions apply to their category-2 counterparts Q3 and P3 and their category-4 counterparts RP3 and RQ3. The advantage of the Q methods vs the P methods arises from the inclusion of energy-independent terms in the self-energy. These terms are determined by single-

Published under an exclusive license by AIP Publishing

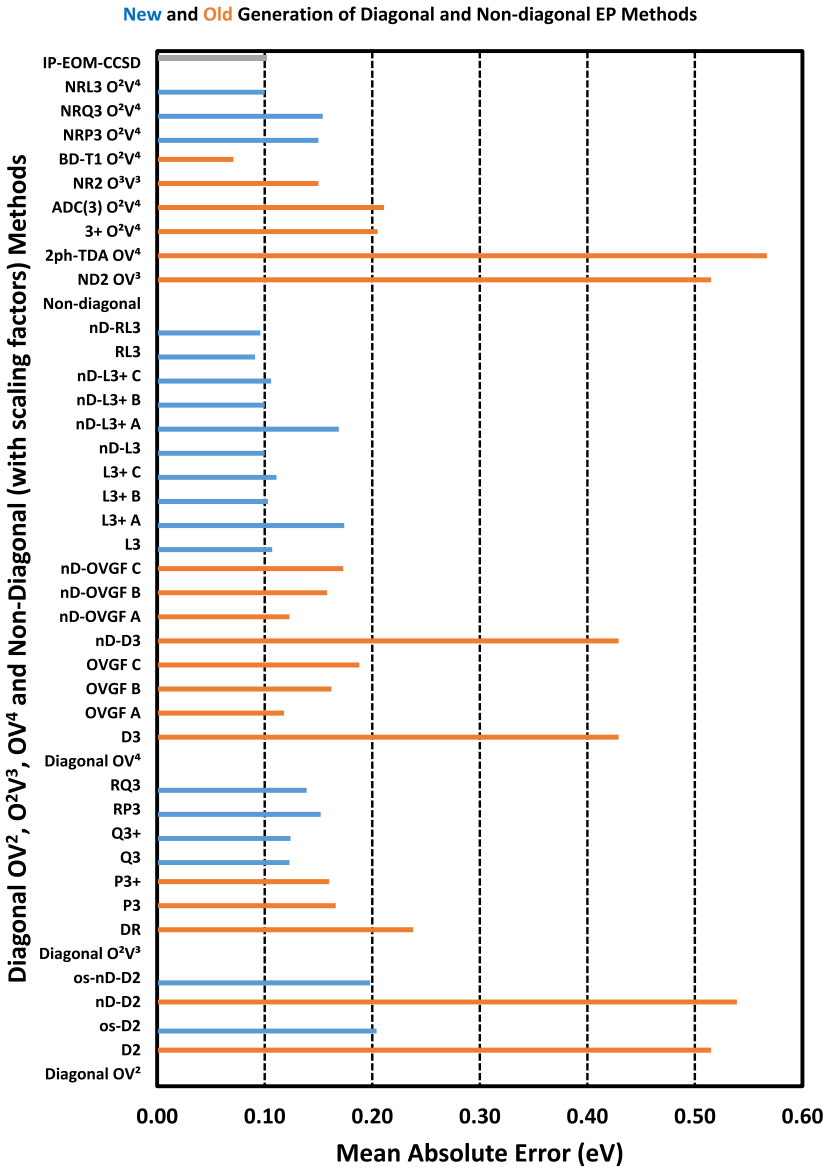


FIG. 1. Mean absolute errors (eV) of electron-propagator methods vs IP-EOM-CCSDTQ/cc-pVTZ VIE standards.

replacement amplitudes in the reference state. Histograms for the P and Q methods indicate that approximate (+) and explicit (R) renormalizations repress outliers. Q3+ and RQ3 are useful improvements over the best category-1 methods for two reasons. First, their MAEs are below 0.15 eV, and second, their *de facto* bottlenecks still occur in the preceding ERI transformation. Q3+ demands fewer arithmetic operations than RQ3 and, therefore, is recommended in Table III.

A parameter-free version of G_0W_0 theory possesses an O^2V^3 bottleneck and does not require ERIs with three or four virtual indices. Because it makes the *diagonal* self-energy operator approximation and sums exchange-less *ring* terms in all orders, it is denoted by DR. Its MAE exceeds 0.2 eV. The category-1 os-D2 and os-nD-D2 methods are more accurate and efficient. The DR histogram also has a large width combined with a tendency to overestimate VIEs. It therefore may generate fortuitously good agreement with experiment in combination with small basis sets.

The next set of category-2, category-3, and category-4 methods in Fig. 1 has a common arithmetic scaling factor, OV^4, and requires ERIs with four virtual indices. Of the older methods denoted by orange bars, only OVGF-A and its non-Dyson version are as accurate as the more efficient Q3+ self-energy. The MAEs of all three methods equal 0.12 eV. Among the methods with OV^4 scaling, the L3+B and RL3 self-energies and their nD counterparts yield MAEs near 0.10 eV. The histograms of the explicitly renormalized RL3 and nD-RL3 alternatives are especially narrow. Only small differences appear between the histograms of the Dyson and nD versions of a self-energy. This agreement implies that the

Published under an exclusive license by AIP Publishing

TABLE IV. Error distributions (eV) with respect to IP-EOM-CCSDT/cc-pVTZ standards.

Method class	Method[a]	Mean absolute error[b]	Mean signed error	Standard deviation	Maximum absolute error
Uncorrelated	KT	1.445	1.407	0.926	2.839
Diagonal 2nd order	D2	0.594	−0.583	0.373	1.389
	os-D2	0.247	0.215	0.197	0.756
	nD-D2	0.626	−0.613	0.391	1.442
	os-nD-D2	**0.235**	0.200	0.195	0.740
Diagonal post 2nd order	DR	0.247	0.218	0.210	0.767
	D3	0.674	0.648	0.497	1.592
	nD-D3	0.662	0.635	0.492	1.577
	OVGF-A	0.214	0.148	0.223	0.574
	OVGF-B	0.333	0.258	0.316	0.818
	OVGF-C	0.345	0.318	0.271	0.845
	nD-OVGF-A	0.203	0.129	0.219	0.591
	nD-OVGF-B	0.319	0.238	0.311	0.794
	nD-OVGF-C	0.327	0.300	0.265	0.821
	P3	0.250	0.230	0.192	0.762
	P3+	0.153	0.093	0.163	0.595
	Q3	0.232	0.191	0.211	0.710
	Q3+	**0.138**	0.053	0.158	0.392
	L3	0.206	0.188	0.180	0.630
	nD-L3	0.189	0.168	0.172	0.602
	L3+A	0.124	−0.022	0.216	1.796
	L3+B	0.109	0.052	0.132	0.448
	L3+C	0.109	0.058	0.130	0.473
	nD-L3+A	0.115	−0.031	0.164	1.037
	nD-L3+B	**0.103**	0.043	0.128	0.418
	nD-L3+C	0.104	0.048	0.127	0.444
	RP3	0.122	0.020	0.154	0.440
	RQ3	0.112	−0.019	0.135	0.307
	RL3	0.082	0.002	0.107	0.324
	nD-RL3	**0.081**	−0.020	0.105	0.362
Non-diagonal	ND2	0.646	−0.643	0.472	3.081
	2ph-TDA	0.610	−0.610	0.201	1.384
	3+	0.372	0.327	0.312	0.906
	ADC(3)	0.343	0.319	0.258	0.775
	NR2	0.097	−0.010	0.120	0.335
	BD-T1	0.104	0.080	0.102	0.319
	NRP3	0.096	−0.011	0.119	0.337
	NRQ3	0.100	−0.042	0.115	0.358
	NRL3	**0.065**	−0.020	0.081	0.370
	IP-EOM-CCSD	0.137	0.124	0.102	0.529

[a]New methods in bold type.
[b]Optimal methods in bold type.

2ph terms corresponding to the increased arithmetic bottleneck are insensitive to energy iterations. MAEs slightly below 0.10 eV correspond to the nD-L3+B and nD-RL3 self-energies, and they are also recommended.

Non-diagonal self-energies are listed in the top sector of Fig. 1 and at the bottom of Table III. Corresponding histograms are also in the supplementary material. The non-diagonal and 2ph-TDA self-energies are not competitive and have a pronounced tendency to underestimate VIEs. ADC(3) has an iterative O^2V^4 bottleneck and an MAE above 0.2 eV. Its simplified counterpart, 3+, has a non-iterative O^2V^4 bottleneck and a similar MAE. These two methods tend to overestimate VIEs. The best of the older methods are NR2 and BD-T1. Their histograms, especially in the BD-T1 case, are sharply peaked. The latter method has an iterative O^2V^4 bottleneck associated with its preliminary BD coupled-cluster step. It achieves the highest accuracy of all EP methods. NR2 has no need for ERIs with four virtual indices, but it is less accurate than the best category-3 and category-4 methods. Three non-diagonal generalizations (NRP3, NRQ3, and NRL3) are also considered. All three have MAEs that are close to those of their diagonal counterparts (RP3, RQ3, and

Published under an exclusive license by AIP Publishing

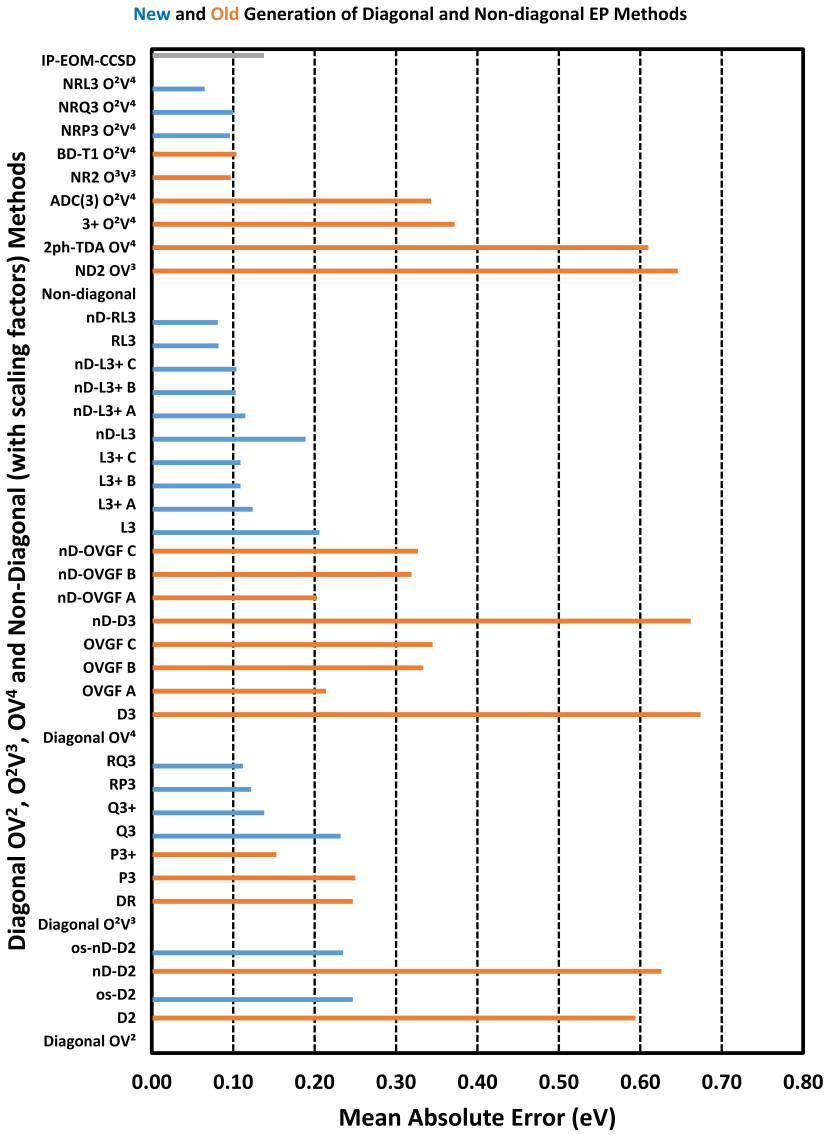


FIG. 2. Mean absolute errors (eV) of electron-propagator methods vs IP-EOM-CCSDT/cc-pVTZ VIE standards.

RL3). NRL3 is the most accurate choice. Its MAE of 0.10 eV is almost identical to that of IP-EOM-CCSD, but its O^2V^4 bottleneck is not iterative. In Table III, only BD-T1 and IP-EOM-CCSDT have clearly lower MAEs.

Table IV and Fig. 2 correspond to the larger set of IP-EOM-CCSDT standards. A comparison of Figs. 1 and 2 confirms the qualitative conclusions reached above with the IP-EOM-CCSDTQ VIEs. Some quantitative differences are noteworthy. For the category-1 methods, the advantages of the opposite-spin self-energies remain, but the MAEs have risen to ~0.25 eV. Among the methods with O^2V^3 arithmetic scaling, the MAEs of Q3+ (0.14 eV) and RQ3 (0.11 eV) have, respectively, increased and decreased slightly. These two choices are more efficient and accurate than the older methods with OV^4 bottlenecks. The DR self-energy is comparable in quality to the best category-1 methods. New methods with OV^4 scaling recommended in Table I (nD-L3+B and nD-RL3) are still attractive options. RL3 and nD-RL3, respectively, achieve MAEs of 0.08 eV. Their histograms (see Figs. S3 and S4 in the supplementary material) are even sharper than those of Q3+ and RQ3. Among the older non-diagonal methods represented by orange bars in Fig. 2, BD-T1 and NR2 still have the lowest MAEs. For this set of data, the NRL3 method has the lowest MAE, 0.07 eV. This accuracy is purchased at the price of a non-iterative O^2V^4 step. The MAE for the iterative O^2V^4 IP-EOM-CCSD method is approximately twice as large. The histograms display a steady sharpening that accompanies the progression from NRP3 to NRQ3 to NRL3.

Published under an exclusive license by AIP Publishing

TABLE V. Error distributions (eV) of many-body methods in CBS with respect to Cambridge experimental VIE standards.

Method class	Method[a]	Mean absolute error[b]	Mean signed error	Standard deviation	Maximum absolute error
Uncorrelated	KT	0.756	0.692	0.742	2.700
Diagonal 2nd order	D2	0.380	−0.366	0.359	1.459
	os-D2	0.188	0.162	0.162	0.659
	nD-D2	0.401	−0.388	0.377	1.515
	os-nD-D2	**0.182**	0.155	0.161	0.646
Diagonal post 2nd order	DR	0.396	0.386	0.219	1.705
	D3	0.388	0.365	0.418	1.681
	nD-D3	0.381	0.359	0.414	1.671
	OVGF-A	0.122	−0.007	0.152	0.413
	OVGF-B	0.190	0.074	0.234	0.690
	OVGF-C	0.197	0.166	0.199	0.673
	nD-OVGF-A	0.121	−0.019	0.149	0.392
	nD-OVGF-B	0.184	0.060	0.230	0.671
	nD-OVGF-C	0.186	0.156	0.192	0.654
	P3	0.233	0.206	0.193	0.926
	P3+	0.156	0.113	0.157	0.487
	Q3	0.170	0.103	0.189	0.695
	Q3+	**0.116**	0.011	0.140	0.339
	L3	0.139	0.117	0.136	0.540
	nD-L3	0.133	0.108	0.134	0.507
	L3+A	0.100	−0.070	0.106	0.382
	L3+B	0.083	0.028	0.098	0.288
	L3+C	0.086	0.042	0.098	0.263
	nD-L3+A	0.110	−0.082	0.112	0.414
	nD-L3+B	**0.079**	0.015	0.098	0.330
	nD-L3+C	0.080	0.029	0.098	0.302
	RP3	0.130	0.049	0.156	0.404
	RQ3	0.117	−0.051	0.133	0.314
	RL3	0.073	−0.004	0.094	0.321
	nD-RL3	**0.075**	−0.019	0.097	0.367
Non-diagonal	ND2	0.422	−0.404	0.393	1.429
	2ph-TDA	0.527	−0.519	0.291	1.663
	3+	0.252	0.190	0.302	1.141
	ADC(3)	0.211	0.194	0.198	0.682
	NR2	0.123	0.008	0.156	0.438
	BD-T1	**0.091**	0.060	0.097	0.355
	NRP3	0.124	0.007	0.156	0.439
	NRQ3	0.123	−0.082	0.129	0.402
	NRL3	**0.078**	−0.035	0.095	0.367
	ΔCCSD(T)	0.094	0.073	0.091	0.257

[a]New methods in bold type.
[b]Optimal methods in bold type.

Cambridge experimental standards

Table V and Fig. 3 exhibit error measures obtained with a double-triple CBS extrapolation and various EP methods. Experimentally derived VIEs and confirming computational data obtained with ΔCCSD(T)/CBS total energies are in Table S1 of the supplementary material.

Patterns seen in Figs. 1 and 2 appear again in Fig. 3. The best category-1 (diagonal, OV^2 scaling) methods at the bottom neglect same-spin electron correlation. Whereas the D2 and nD-D2 self-energies produce MAEs near 0.4 eV, their opposite-spin competitors yield errors that are approximately half as large. These two methods have only a slight tendency to overestimate VIEs. (See the first line of histograms in Fig. S5 of the supplementary material.) The os-nD-D2 method, therefore, is recommended for its efficiency and MAE below 0.2 eV in Table V.

Results for categories 2 through 4 are present in the next highest sector (diagonal, O^2V^3 scaling) of Fig. 3. All P and Q methods

Published under an exclusive license by AIP Publishing

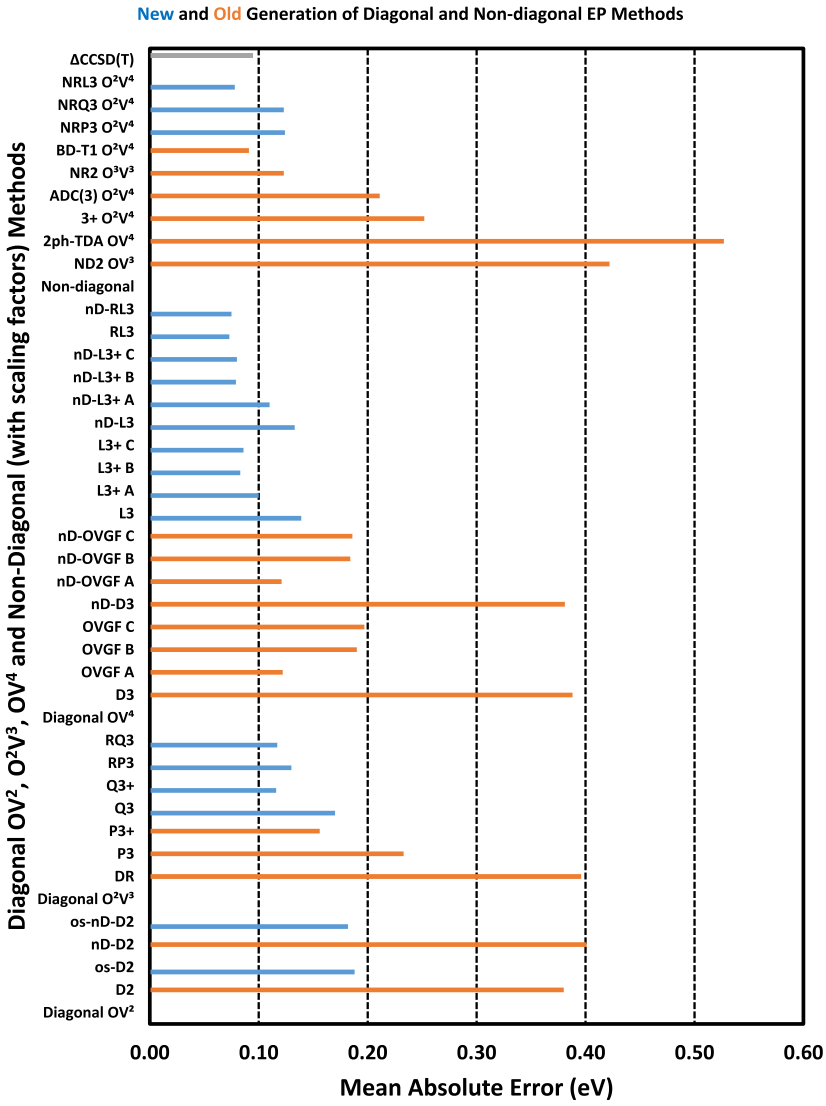


FIG. 3. Mean absolute errors (eV) of electron-propagator methods in CBS vs Cambridge experimental VIE standards.

achieve lower MAEs than the opposite-spin methods of category 1. The Q3+ and RQ3 self-energies offer an excellent compromise of accuracy and efficiency. Their histograms are more sharply peaked and display fewer outliers than their competitors in category 1. Q3+, with its partial transformation of ERIs, non-iterative O^2V^3 bottleneck, and MAE of only 0.12 eV, is recommended in Table V.

The DR method's MAE is approximately equal to those of D2 and nD-D2. Better accuracy can be procured at a lower cost with the opposite-spin, second-order options.

Elevation of the bottleneck step to OV^4 scaling is assumed in the penultimate sector of Fig. 3. Among the older methods, only OVGF-A and its non-Dyson counterpart are competitive. Greater accuracy can be achieved with L3+B, nD-L3+B, RL3, and nD-RL3, whose MAEs vary between 0.07 and 0.08 eV. Inspection of the corresponding histograms indicates little variation in results when the simplifying nD versions are used. This outcome leads to the recommendations of Table V.

In the topmost sector of Fig. 3, results for non-diagonal methods are shown. Among the orange bars (for older methods), the ND2, 2ph-TDA, 3+, and ADC(3) methods are not competitive with BD-T1 and NR2. Of the recently introduced NRP3, NRQ3, and NRL3 alternatives, the latter is the best choice. Its MAE at 0.08 eV is the lowest of the three. Histograms in Fig. S6 of the supplementary material show the balanced and narrow distribution of NRL3 errors. Whereas BD-T1 requires O^2V^4 iterations, NRL3's bottleneck of the same magnitude is non-iterative. This combination of accuracy and efficiency provides convincing support for the recommendation of NRL3 in Table V. The mean signed error and the MAE for NRL3 (−0.035 and 0.078 eV) are slightly better than their ΔCCSD(T) counterparts (0.073 and 0.094 eV).

Published under an exclusive license by AIP Publishing

TABLE VI. Error distributions (eV) of composite electron-propagator methods with respect to Cambridge experimental VIE standards.

Composite methods	Mean absolute error	Mean signed error	Standard deviation	Maximum absolute error
CM1	0.129	0.056	0.157	0.911
CM2	0.103	0.070	0.105	0.306
CM3	0.087	0.038	0.104	0.339
CM4	0.136	0.093	0.142	0.430
CM5	0.117	0.100	0.101	0.350
CM6	0.096	0.066	0.098	0.281
CM7	0.135	0.108	0.133	0.870
CM8	0.083	0.032	0.105	0.380

An accuracy of 0.1 eV as measured by MAEs may be achieved more efficiently with composite models. (An alternative approach based on explicitly correlated treatments of operator spaces also has shown considerable promise for deterministic[39–41] and stochastic algorithms.[42,43]) Eight alternatives discussed above generate the data of Table VI and the bar graphs of Fig. 4. CM1, CM2, CM3, and CM8 employ D-T data for Q3+, nD-L3+B, nD-RL3, and NRL3, respectively. The two latter options generate slightly lower MAEs near 0.085 eV. CM4, CM5, and CM6 are the T-Q counterparts of CM1, CM2, and CM3, respectively. Only slight increases in the MAEs of 0.01 eV occur with the T-Q data. A somewhat more complicated scheme, CM7, employs three basis sets and the os-nD-D2, Q3+, and nD-L3+B self-energies. Its MAE is approximately the same as those of the simpler CM1 and CM4 formulae. CM8 involves the non-diagonal NRL3 self-energy and achieves the lowest MAE, 0.083 eV. Histograms in Fig. S7 acquire narrower profiles with improvements in the quality of the post-second-order methods. This test indicates that predictive quality associated with CBS ΔCCSD(T) calculations may be obtained with much more efficient models. For example, the CM6 model requires only nD-RL3/aug-cc-pVDZ and os-nD-D2/aug-cc-pVTZ data, but its MAE is 0.087 eV. Even the most efficient model, CM1, achieves an MAE of 0.13 eV with only the modest demands of Q3+/aug-cc-pVDZ and os-nD-D2/aug-cc-pVTZ calculations. The insensitivity of the results to the details of the models is an encouraging indication of stability with respect to self-energy and basis-set improvements.

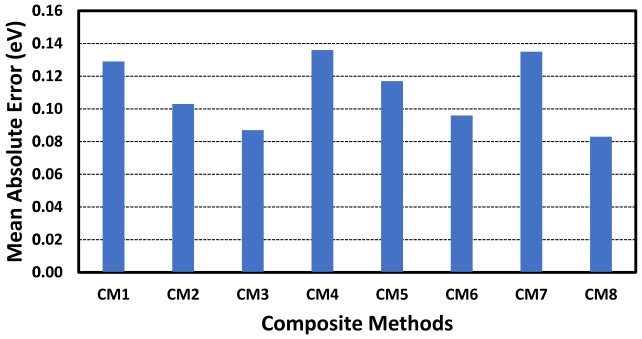


FIG. 4. Mean absolute errors (eV) of composite electron-propagator methods vs Cambridge experimental VIE standards.

CONCLUSIONS

A consistent account of errors with respect to experimental and high-level computational standards emerges from Tables III–V and Figs. 1–3. Errors of a self-energy approximation obtained vs two exhaustive IP-EOM-CC standards in a polarized triple-ζ basis are in close agreement with those obtained vs experiment. The methods that merit recommendation are identical in all three tests.

The computational demands made by the opposite-spin, second-order methods (os-D2 and os-nD-D2) do not exceed those of a conventional self-consistent-field calculation. For each VIE, only a cubically scaling set of ERIs is needed, and therefore, the requisite partial integral transformation has quartic scaling. Only a trivial number of arithmetic operations is required, for cubic scaling prevails. For these minor investments, the returns are substantial. MAEs are below 0.2 eV for the Cambridge set of experimental VIEs. A simplified model of opposite-spin correlation is paired with same-spin correlation treated at the HF level.

The Q3+ method has a better balance of underestimates and overestimates and an MAE vs experiment that is slightly above 0.1 eV. It does not invoke ERIs with four virtual indices. Furthermore, its O^2V^3 arithmetic bottleneck is below that of the partial integral transformation that precedes an ordinary MP2 calculation. Whenever the latter type of calculation is feasible, Q3+ is also feasible.

The parameter-free DR method (G_0W_0 with canonical HF orbitals and Tamm–Dancoff excitations) delivers an MAE of 0.4 eV and systematically overestimates . Its arithmetic bottleneck scales as O^2V^3. The DR method's chief advantage for VIEs is the absence of ERIs with three or four virtual indices in its formulas.

MAEs of 0.07–0.08 eV obtain for the L3+B and RL3 self-energies. Their nD counterparts yield almost identical errors and mitigate the effort associated with their common OV^4 bottlenecks. These approximations require a full active-orbital ERI transformation with fifth-power arithmetic scaling. Their computational demands are less than those of electron correlation methods with couplings between doubly substituted Slater determinants, such as MP3 and CCSD. OVGF-A remains a useful albeit somewhat less efficient and accurate method of this class.

Category-1 through category-4 methods employ the diagonal self-energy approximation in the canonical HF basis. Each of the corresponding Dyson orbitals for VIEs, therefore, equals a product of an occupied orbital and a square root of a probability factor. Each of the self-energy terms is interpretable in terms of differential contributions to electron-pair correlation energies or final-state orbital relaxation.

The non-diagonal NRL3 method delivers Dyson orbitals in their general form, a linear combination of basis orbitals. Its MAE of 0.08 eV is approximately the same as that of RL3 for the VIEs of the experimental Cambridge set. It introduces non-iterative O^2V^4 operations and outperforms its similarly demanding competitors such as ADC(3) and BD-T1. The error measures of NRL3 are lower than those of ΔCCSD(T), a method with a seventh-power bottleneck.

Published under an exclusive license by AIP Publishing

Composite models efficiently capture basis set effects with opposite-spin, second-order methods and higher correlation effects with the Q3+, L3+B, or RL3 self-energies. These models require only polarized triple-ζ, second-order and polarized double-ζ, higher-order calculations. Their MAEs lie between 0.13 and 0.08 eV for the experimental Cambridge set of molecular VIEs. For general calculations on the lowest VIEs of closed-shell molecules, the CM3 model is the best option. When Dyson orbitals in their general form are needed for calculating transition intensities or correlation final states, CM8 is preferable.

The self-energy approximations recommended in this study also have shown considerable promise in the evaluation of molecular vertical electron affinities.[4–6,44] These precedents have relied chiefly on comparisons with high-level calculations. Standard data based on experiments are needed to execute a counterpart study for electron affinities.

Explicitly renormalized methods may be more advantageous than their approximately renormalized antecedents in tests on larger molecules. This hypothesis remains to be tested.

The need for experimentally based data is not confined to vertical electron affinities. Definitive numerical tests pertaining to excited cationic final states with valence and core vacancies require this information.

SUPPLEMENTARY MATERIAL

See the supplementary material for standards, histograms, and calculated data on VIEs.

ACKNOWLEDGMENTS

The authors thank Dr. Manuel Díaz-Tinoco, Dr. Reza Hemmati, and Dr. Abdulrahman Zamani for valuable discussions and the Alabama Supercomputer Authority for computing resources.

AUTHOR DECLARATIONS

Conflict of Interest

The authors have no conflicts to disclose.

Author Contributions

Ernest Opoku: Conceptualization (equal); Data curation (lead); Formal analysis (equal); Investigation (lead); Validation (lead); Visualization (lead); Writing – original draft (equal); Writing – review & editing (equal). **Filip Pawłowski**: Formal analysis (equal); Resources (equal); Supervision (equal); Writing – review & editing (equal). **J. V. Ortiz**: Conceptualization (lead); Formal analysis (equal); Methodology (equal); Project administration (equal); Resources (equal); Software (lead); Supervision (equal); Validation (equal); Writing – original draft (equal); Writing – review & editing (equal).

DATA AVAILABILITY

The data that support the findings of this study are available within the article and its supplementary material.

REFERENCES

[1] E. Opoku, F. Pawłowski, and J. V. Ortiz, J. Chem. Phys. **155**(20), 204107 (2021).
[2] E. Opoku, F. Pawłowski, and J. V. Ortiz, J. Chem. Theory Comput. **18**(8), 4927–4944 (2022).
[3] E. Opoku, F. Pawłowski, and J. V. Ortiz, J. Chem. Phys. **159**(12), 124109 (2023).
[4] E. Opoku, F. Pawłowski, and J. V. Ortiz, J. Phys. Chem. A **128**(34), 7311–7330 (2024).
[5] E. Opoku, F. Pawłowski, and J. V. Ortiz, J. Chem. Theory Comput. **20**(1), 290–306 (2024).
[6] E. Opoku, F. Pawłowski, and J. V. Ortiz, J. Phys. Chem. A **128**(8), 1399–1416 (2024).
[7] T. Koopmans, Physica **1**(1–6), 104–113 (1934).
[8] H. H. Corzo and J. V. Ortiz, in *Advances in Quantum Chemistry*, edited by J. R. Sabin and E. J. Brändas (Academic Press, 2017), Vol. 74, pp. 267–298.
[9] J. V. Ortiz, in *Annual Reports in Computational Chemistry*, edited by D. A. Dixon (Elsevier, 2017), Vol. 13, pp. 139–182.
[10] J. V. Ortiz, J. Chem. Phys. **153**(7), 070902 (2020).
[11] J. Cioslowski and J. V. Ortiz, J. Chem. Phys. **96**(11), 8379–8389 (1992).
[12] J. V. Ortiz, Int. J. Quantum Chem. **44**(26), 1–11 (1992).
[13] J. V. Ortiz, J. Chem. Phys. **112**(1), 56–68 (2000).
[14] D. S. Ranasinghe, J. T. Margraf, A. Perera, and R. J. Bartlett, J. Chem. Phys. **150**(7), 074108 (2019).
[15] S. McKechnie, G. H. Booth, A. J. Cohen, and J. M. Cole, J. Chem. Phys. **142**(19), 194114 (2015).
[16] M. Díaz-Tinoco, O. Dolgounitcheva, V. G. Zakrzewski, and J. V. Ortiz, J. Chem. Phys. **144**(22), 224110 (2016).
[17] J. V. Ortiz, Wiley Interdiscip. Rev.: Comput. Mol. Sci. **3**(2), 123–142 (2013).
[18] J. Linderberg and Y. Öhrn, *Propagators in Quantum Chemistry*, 2nd ed. (Wiley-Interscience, Hoboken, NJ, 2004).
[19] J. Schirmer, *Many-Body Methods for Atoms, Molecules and Clusters* (Springer International Publishing AG, 2018).
[20] L. Reining, Wiley Interdiscip. Rev.: Comput. Mol. Sci. **8**(3), e1344 (2018).
[21] J. V. Ortiz, J. Chem. Phys. **104**(19), 7599–7605 (1996).
[22] W. von Niessen, J. Schirmer, and L. S. Cederbaum, Comput. Phys. Rep. **1**, 57–125 (1984).
[23] P. Jørgensen and J. Simons, *Second Quantization-Based Methods in Quantum Chemistry* (Academic Press, New York, 1981).
[24] J. V. Ortiz, in *Computational Chemistry: Reviews of Current Trends*, edited by J. Leszczynski (World Scientific, Singapore, 1997), Vol. 2, pp. 1–61.
[25] J. Schirmer, L. S. Cederbaum, and O. Walter, Phys. Rev. A **28**(3), 1237–1259 (1983).
[26] J. Schirmer and G. Angonoa, J. Chem. Phys. **91**, 1754–1761 (1989).
[27] J. F. Stanton and J. Gauss, J. Chem. Phys. **101**(10), 8938–8944 (1994).
[28] J. V. Ortiz, J. Chem. Phys. **99**, 6716–6726 (1993).
[29] J. V. Ortiz, J. Chem. Phys. **108**, 1008–1014 (1998).
[30] S. J. Bintrim and T. C. Berkelbach, J. Chem. Phys. **154**(4), 041101 (2021).
[31] S. Hirata, M. R. Hermes, J. Simons, and J. V. Ortiz, J. Chem. Theory Comput. **11**(4), 1595–1606 (2015).
[32] S. Hirata, A. E. Doran, P. J. Knowles, and J. V. Ortiz, J. Chem. Phys. **147**(4), 044108 (2017).
[33] S. Hirata, I. Grabowski, J. V. Ortiz, and R. J. Bartlett, Phys. Rev. A **109**(5), 052220 (2024).
[34] D. J. Rowe, Rev. Mod. Phys. **40**(1), 153–166 (1968).

Published under an exclusive license by AIP Publishing

[35]N. C. Handy, J. A. Pople, M. Head-Gordon, K. Raghavachari, and G. W. Trucks, Chem. Phys. Lett. **164**(2-3), 185–192 (1989).
[36]M. J. Frisch, G. W. Trucks, H. B. Schlegel, G. E. Scuseria, M. A. Robb, J. R. Cheeseman, G. Scalmani, V. Barone, G. A. Petersson, H. Nakatsuji, X. Li, M. Caricato, A. V. Marenich, J. Bloino, B. G. Janesko, R. Gomperts, B. Mennucci, H. P. Hratchian, J. V. Ortiz, A. F. Izmaylov, J. L. Sonnenberg, D. Williams-Young, F. Ding, F. Lipparini, F. Egidi, J. Goings, B. Peng, A. Petrone, T. Henderson, D. Ranasinghe, V. G. Zakrzewski, J. Gao, N. Rega, G. Zheng, W. Liang, M. Hada, M. Ehara, K. Toyota, R. Fukuda, J. Hasegawa, M. Ishida, T. Nakajima, Y. Honda, O. Kitao, H. Nakai, T. Vreven, K. Throssell, J. A. Montgomery, J. E. Peralta, F. Ogliaro, M. J. Bearpark, J. J. Heyd, E. N. Brothers, K. N. Kudin, V. N. Staroverov, T. A. Keith, R. Kobayashi, J. Normand, K. Raghavachari, A. P. Rendell, J. C. Burant, S. S. Iyengar, J. Tomasi, M. Cossi, J. M. Millam, M. Klene, C. Adamo, R. Cammi, J. W. Ochterski, R. L. Martin, K. Morokuma, O. Farkas, J. B. Foresman, and D. J. Fox, *Gaussian development version, Revision I.14*, Gaussian, Inc., Wallingford CT, 2018.
[37]K. Raghavachari, G. W. Trucks, J. A. Pople, and M. Head-Gordon, Chem. Phys. Lett. **157**(6), 479–483 (1989).
[38]R. A. Kendall, T. H. Dunning, and R. J. Harrison, J. Chem. Phys. **96**(9), 6796–6806 (1992).
[39]Y.-y. Ohnishi and S. Ten-no, J. Comput. Chem. **37**, 2447–2453 (2016).
[40]F. Pavošević, C. Peng, J. V. Ortiz, and E. F. Valeev, J. Chem. Phys. **147**(12), 121101 (2017).
[41]N. K. Teke, F. Pavošević, C. Peng, and E. F. Valeev, J. Chem. Phys. **150**(21), 214103 (2019).
[42]C. M. Johnson, A. E. Doran, S. L. Ten-no, and S. Hirata, J. Chem. Phys. **149**(17), 174112 (2018).
[43]A. E. Doran and S. Hirata, J. Chem. Theory Comput. **15**(11), 6097–6110 (2019).
[44]E. Opoku, F. Pawłowski, and J. V. Ortiz, J. Phys. Chem. A **128**(23), 4730–4749 (2024).

Published under an exclusive license by AIP Publishing

Appendix F

E. Opoku, F. Pawłowski and J. V. Ortiz, "Simplified Ring and Ladder Renormalizations in Electron−Propagator Calculations of Molecular Ionization Energies", *J. Phys. Chem. A*, 129, 3597–3612 (2025)

THE JOURNAL OF PHYSICAL CHEMISTRY A
A JOURNAL OF THE AMERICAN CHEMICAL SOCIETY

pubs.acs.org/JPCA Article

Simplified Ring and Ladder Renormalizations in Electron-Propagator Calculations of Molecular Ionization Energies

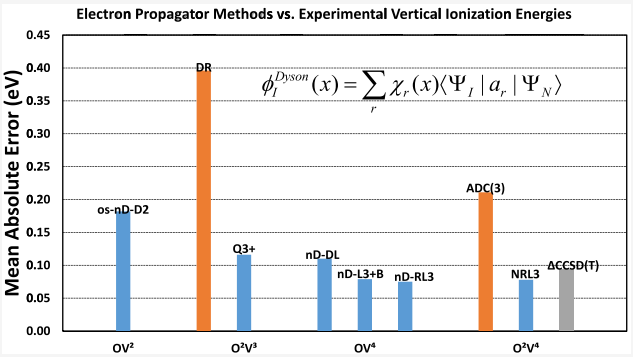
Published as part of The Journal of Physical Chemistry A special issue "Forty Years of Response Function Theory".

Ernest Opoku, Filip Pawłowski, and J. V. Ortiz*

Cite This: *J. Phys. Chem. A* 2025, 129, 3597−3612 Read Online

ACCESS | Metrics & More | Article Recommendations | Supporting Information

ABSTRACT: The self-energy operator of the *ab initio* Dyson quasiparticle equation generates orbital-relaxation and differential-correlation corrections to Koopmans predictions of electron binding energies. Among the most important corrections are terms that may be expressed as ring and ladder diagrams. Inclusions of such terms in all orders of the fluctuation potential constitute renormalizations. The ability of several renormalized self-energies to predict molecular ionization energies has been tested versus reliable computational and experimental standards. These results reveal the superior accuracy and efficiency of several new-generation electron-propagator methods. They also demonstrate the strengths and weaknesses of self-energies that include ring or ladder renormalizations only and of methods that allow interactions between these terms. Whereas a simplified ladder method produces useful results, its simplified ring counterpart is more computationally efficient, but less accurate. New-generation alternatives to both methods are more accurate and efficient. No adjustable parameters are included in the generation of reference orbitals or in the formulation of the self-energy approximations examined in this work.



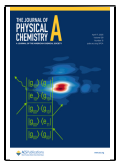
INTRODUCTION

The Dyson quasiparticle equation is a convenient vehicle for the determination of molecular electron binding energies and their associated Dyson orbitals.[1−5] It encompasses the Hartree−Fock (HF) equations and therefore recovers the uncorrelated, frozen-orbital picture of Koopmans's identity[6] as a special case. The self-energy operator of the Dyson quasiparticle equation can be improved systematically up to the full-configuration-interaction limit.[7−9] It therefore can capture orbital relaxation and differential correlation contributions to exact electron binding energies. *Ab initio*, approximate self-energy operators have typically reposed on HF orbitals in molecular calculations, but alternative reference orbitals and states are also feasible. Many varieties of Kohn−Sham orbitals have been adopted in the GW family of self-energy approximations.[10,11] For reference states with relatively strong electron correlation, approximate Brueckner orbitals may be an advantageous alternative.[12,13] Multiconfigurational, self-consistent-field wave functions have provided practical reference states for small molecules with qualitatively unpaired electrons.[14,15] Perturbative corrections to the Koopmans picture continue to evolve toward greater accuracy, increased computational efficiency and deeper understanding.[16,17] These improvements follow from amplifications of ionization operator manifolds beyond the simple creators and annihilators of second quantization and from corrections to reference states. One may also employ correlated model Hamiltonians to derive the same reference-state benefits.[18]

The importance of self-energy terms that arise from reference-state correlation amplitudes has been demonstrated repeatedly in molecular calculations.[16] The new generation of perturbative self-energies[19,20] achieves highly advantageous combinations of accuracy and efficiency with a balanced introduction of reference-state corrections. These advances build on previously implemented methods that also appealed to perturbative improvements to reference states.[3,4]

An alternative strategy completely avoids corrections of the latter type and concentrates solely on amplifications of the operator manifold in the derivation of approximate self-energies. Approaches of this kind also can reach exactitude in the

Received: February 17, 2025
Revised: March 25, 2025
Accepted: March 28, 2025
Published: April 7, 2025



ACS Publications © 2025 American Chemical Society

https://doi.org/10.1021/acs.jpca.5c01079
J. Phys. Chem. A 2025, 129, 3597−3612

Table 1. Acronyms and Full Names of Approximate, Electron-Propagator Methods

acronym[a]	full name
	Diagonal Second-Order Self-Energies
D2	Diagonal second order
os-D2	Opposite-spin D2
nD-D2	Non-Dyson D2
os-nD-D2	Opposite-spin non-Dyson D2
	Diagonal Post Second-Order Self-Energies
D3	Diagonal (not renormalized) third order
nD-D3	Non-Dyson D3
OVGF-	Outer-Valence Green's Function (Versions A, B and C)
nD-OVGF	Non-Dyson OVGF (Versions A, B and C)
P3	Partial third order
P3+	Approximately renormalized partial third order
Q3	Quasiparticle third order
Q3+	Approximately renormalized quasiparticle third order
L3	Linear third order
nD-L3	Non-Dyson L3
L3+	Approximately renormalized linear third order (Versions A, B and C)
nD-L3+	Non-Dyson L3+ (Versions A, B and C)
RP3	Explicitly renormalized partial third order
RQ3	Explicitly renormalized quasiparticle third order
RL3	Explicitly renormalized linear third order
nD-RL3	Non-Dyson RL3
DR	Diagonal ring (without exchange) approximation (HF-TDA-G_0W_0)
DL	Diagonal ladder (with exchange) approximation
nD-DL	Non-Dyson DL
D-2ph-TDA	Diagonal two-particle-one-hole Tamm−Dancoff approximation
nD-D-2ph-TDA	Non-Dyson D-2ph-TDA
D3+	Diagonal (renormalized) third order
nD-D3+	Non-Dyson D3+
	Nondiagonal Self-Energies
ND2	Nondiagonal, second order
2ph-TDA	Nondiagonal two-particle-one-hole Tamm−Dancoff approximation
3+	Nondiagonal (renormalized) third order, i.e., strict version of ADC(3)
ADC(3)	Third order algebraic diagrammatic construction
NR2	Nondiagonal, renormalized, second order
BD-T1	Brueckner doubles with triple field operators
NRP3	Nondiagonal extension of RP3
NRQ3	Nondiagonal extension of RQ3
NRL3	Nondiagonal extension of RL3

[a]For new-generation methods in **bold type:** *N* = nondiagonal; nD = non-Dyson; R = explicitly renormalized; + = approximately renormalized.

calculation of electron binding energies of reference states with N electrons.[21] (Unfortunately, exact Dyson orbitals and reference-state properties are not equally accessible to this approach.) Manne's union of nh($n-1$)p [i.e., h, 2hp, 3h2p, ⋯, Nh($N-1$)p] and np($n-1$)h [i.e., p, 2ph, 3p2h, ⋯, ($N+1$)pNh] operators[22] casts complementary roles in the calculation of electron removal and addition energies. The former set of operators describes orbital relaxation and differential correlation effects in final states when an electron is removed. Differential correlation in the initial state becomes the province of the np($n-1$)h operators. These roles switch when an electron is added instead.

Several self-energy approximations in wide use abstain from the introduction of perturbative, reference-state-correlation amplitudes. First-order, single-replacement amplitudes vanish in the second-order self-energy that builds on HF reference states. (They may reappear when reference determinants do not fulfill the usual Brillouin condition[23,24] for spin−orbital substitutions.) The second-order approximation employs 2h1p and 2p1h operators and retains only zeroth-order couplings between them. (Occupied and virtual spin−orbitals defined by a reference determinant are labeled respectively as holes, or h, and particles, or p.) With the same manifold of h, p, 2h1p and 2p1h operators, the 2ph-TDA (two-particle-one-hole Tamm−Dancoff approximation) self-energy restores these couplings through first order.[25] Expansion of this renormalized self-energy past second order produces ring and ladder terms, in addition to mixed ring-ladder summations starting in fourth order. All vertices are antisymmetrized, i.e., Coulomb and exchange terms retain an equal status in all formulas.

The 2ph-TDA is easy to define. It assumes HF reference states and includes only single and triple field operators in its ionization manifold. Unfortunately, in practice, the 2ph-TDA self-energy has no advantage of accuracy or efficiency over the second-order approximation for calculating electron affinities or outer-valence ionization energies.[16,20] Its chief advantage is the ability to give a qualitative account of correlation final states. (For example, inner-valence ionization energies have operators

https://doi.org/10.1021/acs.jpca.5c01079
J. Phys. Chem. A 2025, 129, 3597−3612

that are dominated by 2h1p contributions.) There are no guarantees: simple, appealing methods can be impractical.

Increased complexity, whether from reference-state corrections or amplified operator manifolds, accompanies the derivation of more accurate and computationally demanding approximations. For example, the third-order, algebraic-diagrammatic-construction self-energies, collectively known as ADC(3),[26] introduce at least two kinds of reference-state correlation amplitudes. These include first-order-double and second-order-single replacements; some versions of ADC(3) also incorporate higher-order replacements.[27]

An alternative strategy seeks greater accuracy or efficiency with physically motivated simplifications.[28] For example, ring diagrams, encountered in the random-phase approximation (RPA) of the polarization propagator,[1] are often associated with treatments of long-range correlation. Ladder diagrams, with similar associations to the RPA two-electron propagator, are held to represent short-range correlation. Effective interactions that replace bare Coulomb repulsions may be constructed from either RPA antecedent. In this work, inquiry into whether less complexity might redound to greater accuracy is constrained by another requirement: *no adjustable parameters may be invoked*. All calculations employ the canonical HF basis or the semicanonical Brueckner-doubles[29] basis. No adjustable weights are applied to terms in approximate self-energy formulas.

By neglecting terms in the 2ph-TDA couplings between triple field operators, self-energies that include only ring or ladder terms may be constructed. The usual numerical techniques employed in 2ph-TDA calculations seek only a few eigenvalues of a symmetric matrix.[30] A generalized eigenvalue problem that involves the familiar A and B blocks of RPA need not be solved. No contractions with greater than fifth-power arithmetic scaling occur.

The ring simplification of 2ph-TDA has been examined numerically. This member of the GW family employs HF orbitals and TDA (instead of RPA) excitation energies and operators. Initial results demonstrated the superiority of the TDA alternative in calculations on small molecules.[31] Neglect of the off-diagonal elements of the self-energy matrix in the canonical HF basis defines the G_0W_0@(HF-TDA) method. (Zero subscripts denote the GW versions that annul off-diagonal self-energy terms, regardless of the orbital basis employed.) In this work, it will be called by a shorter name: the diagonal ring (DR) approximation.

Its counterpart that evaluates only the ladder terms in 2ph-TDA will be denoted by DL (for diagonal ladder). This approximate self-energy has not been examined numerically. Whereas the DR method does not include exchange terms in couplings between 2h1p or 2p1h operators, the DL method does include such terms.

A review of concepts that underlie the Dyson quasiparticle equation and the related diagonalization of the superoperator Hamiltonian matrix follows this section. Relationships between DR, DL, 2ph-TDA and other self-energy approximations provide a theoretical context for numerical comparisons. The latter data on molecular ionization energies comprise new and old methods and enable identification of the best compromises of accuracy and efficiency. (Table 1 presents a list of self-energy approximations and their acronyms.) Two numerical comparisons refer to *ab initio* standards of nearly full-configuration-interaction quality for a large set of representative closed-shell molecules in a constant basis set.[32] A third test on the smaller, GW20 set compares recently published results that employ RPA transition energies[33] with their TDA counterparts. The final standard of comparison comprises a set of molecular ionization energies derived from experiments and confirmed by calculations of high quality.[34] A summary of recommendations for routine calculations and an assessment of the utility of the presently considered methods with no reference-state corrections conclude this work.

THEORY

Vertical ionization energies (VIEs) and Dyson orbitals are embedded in the denominators and numerators of the electron propagator (EP) matrix in its energy-dependent, spectral form.[1−5] The *r*-*s* element of the EP matrix, $G_{rs}(E)$, involves an *N*-electron initial state, Ψ_N, with energy E_N, and summations over final states with $N \pm 1$ electrons. Creation and annihilation operators for the *r* and *s* members of an orthonormal set of spin−orbitals connect the initial and final states in the numerators. Corresponding denominators vanish when the energy parameter, *E*, equals an ionization energy or an electron affinity in the respective *I* or *A* summations. $G_{rs}(E)$ depends on two space-spin coordinates and the energy variable according to

$$G_{rs}(E) = \lim_{\eta \to 0}\left[\sum_{A}^{e^-\text{attachments}} \frac{\langle \Psi_N | a_r | \Psi_A \rangle \langle \Psi_A | a_s^\dagger | \Psi_N \rangle}{E + E_N - E_A + i\eta} + \sum_{I}^{e^-\text{detachments}} \frac{\langle \Psi_N | a_s^\dagger | \Psi_I \rangle \langle \Psi_I | a_r | \Psi_N \rangle}{E - E_N + E_I - i\eta}\right] \quad (1)$$

Dyson orbitals for ionization energies and electron affinities are defined by two integrations over all electronic coordinates save one[35]

$$\phi_A^{\text{Dyson}}(x_1) = \sqrt{N+1} \int \Psi_N^*(x_2, x_3, x_4, \cdots, x_N, x_{N+1}) \Psi_A (x_1, x_2, x_3, \cdots, x_N, x_{N+1}) dx_2 dx_3 dx_4 \cdots dx_N dx_{N+1} \quad (2)$$

$$\phi_I^{\text{Dyson}}(x_1) = \sqrt{N} \int \Psi_I^*(x_2, x_3, x_4, \cdots, x_N) \Psi_N (x_1, x_2, x_3, \cdots, x_N) dx_2 dx_3 dx_4 \cdots dx_N \quad (3)$$

Amplitudes in the numerators of eq 1 equal the expansion coefficients in an orthonormal spin−orbital basis (χ), where

$$\phi_A^{\text{Dyson}}(x) = \sum_r \chi_r(x) \langle \Psi_N | a_r | \Psi_A \rangle \quad (4)$$

$$\phi_I^{\text{Dyson}}(x) = \sum_r \chi_r(x) \langle \Psi_I | a_r | \Psi_N \rangle \quad (5)$$

Electron binding energies in eq 1 equal the eigenvalues of the superoperator Hamiltonian matrix, $\hat{\boldsymbol{H}}$. For Manne's set of ionization operators,[22] the superoperator metric matrix, designated by square brackets, invokes an anticommutator[36] such that

$$[\tau_\mu | \tau_\nu] = \langle \Psi_N | \tau_\mu^\dagger \tau_\nu + \tau_\nu \tau_\mu^\dagger | \Psi_N \rangle \quad (6)$$

The anticommutator's presence is a consequence of including both summations in eq 1. Non-Dyson (nD) variants of the EP that include only one summation require just one of the two terms in the anticommutator.[37] As this alternative approach decouples calculations of ionization energies and electron affinities, it requires reduced density matrices of higher order.

https://doi.org/10.1021/acs.jpca.5c01079
J. Phys. Chem. A 2025, 129, 3597−3612

The superoperator Hamiltonian matrix, in turn, introduces a commutator with the second-quantized Hamiltonian, H, according to

$$\hat{H}_{\mu\nu} = [\tau_\mu|\hat{H}\tau_\nu] = [\tau_\mu|H\tau_\nu - \tau_\nu H] \tag{7}$$

For a set of orthonormal (according to eq 6) operators, electron binding energies (e) equal eigenvalues of $\hat{\boldsymbol{H}}$. Approximations to the reference state in eqs 6 and 7 do not necessarily preserve the Hermiticity of the superoperator Hamiltonian matrix.[4] Elements of the eigenvectors ($\boldsymbol{C}$) that pertain to simple field operators (i.e., h and p) in the eigenvalue equations

$$\sum_{\nu}^{\text{operators}} \hat{H}_{\mu\nu} C_{\nu I} = C_{\mu I} e_I \tag{8}$$

equal the coefficients in eqs 4 and 5. Because the norm of the eigenvector is typically set to unity, the sum of the squares of these coefficients is bounded by zero and unity

$$0 \le \sum_{\nu}^{\text{h}} |C_{\nu I}|^2 + \sum_{\nu}^{\text{p}} |C_{\nu I}|^2 \le 1 \tag{9}$$

Couplings between the two sets of operators in Manne's set imply that p (or h) operators also participate in electron detachments (or attachments). Equation 9 also implies that in general Dyson orbitals are not normalized to unity. Norms of the Dyson orbitals, Π_I, are known as probability factors, intensity factors, or pole strengths. They are determined entirely by the h and p sectors of the eigenvectors of eq 8

$$\Pi_I = \sum_{\nu}^{\text{h}} |C_{\nu I}|^2 + \sum_{\nu}^{\text{p}} |C_{\nu I}|^2 \tag{10}$$

Partitioning of the operator space focuses attention on final states with probability factors near unity. After choosing the primary space (P) to comprise h and p operators and orthonormalizing the secondary operators (Q) of higher rank, one obtains

$$[\hat{\mathbf{H}}_{PP} + \hat{\mathbf{H}}_{PQ}(E\hat{\mathbf{I}}_{QQ} - \hat{\mathbf{H}}_{QQ})^{-1}\hat{\mathbf{H}}_{QP}]\mathbf{c}_{PI} = \mathbf{c}_{PI} e_I \tag{11}$$

The first term within the square brackets of eq 11 is a generalized Fock matrix, $\boldsymbol{F}$, with elements

$$F_{rs} = h_{rs}^{(1)} + \sum_{tu} \langle rt||su\rangle \langle \Psi_N|a_t^\dagger a_u|\Psi_N\rangle \tag{12}$$

The second term is the energy-dependent self-energy matrix, $\sum(E)$, of the Dyson quasiparticle equation,

$$[\mathbf{F} + \mathbf{\Sigma}(E)]\mathbf{c} = \mathbf{c}e \tag{13}$$

At self-consistency, E equals one of eigenvalues of eq 13. Corresponding probability factors may be determined with

$$\Pi_I = \left[1 - \frac{\mathrm{d}\mathbf{c}_I^\dagger \mathbf{\Sigma}(E)\mathbf{c}_I}{\mathrm{d}E}\Big|_{E=e_I}\right]^{-1} \tag{14}$$

Eqs 8−11, 13 and 14 also apply when the final state index is A instead of I, i.e., for electron attachments instead of detachments.

The operator manifold for the second-order and 2ph-TDA self-energies comprises h, p, 2h1p and 2p1h sectors. The P space of eq 11 spans the h and p operators; 2h1p and 2p1h operators populate the Q space. Because there are no correlation amplitudes in the reduced density matrices used to evaluate $\hat{\boldsymbol{H}}$, all matrix elements have terms of order zero or one only. In the canonical HF basis, $\boldsymbol{F}$ is diagonal, with

$$F_{rs} = \epsilon_r \delta_{rs} \tag{15}$$

P-Q matrix elements equal antisymmetrized electron repulsion integrals (ERIs)

$$\hat{H}_{r,aij} = \langle ra||ij\rangle \tag{16}$$

$$\hat{H}_{r,iab} = \langle ri||ab\rangle \tag{17}$$

(Occupied, or h, and virtual, or p, spin−orbital indices are denoted respectively by $i,j,k,\cdots$ and $a,b,c,\cdots$ The three-index subscripts assume $i < j$ and $a < b$.) For the second-order self-energy, the zeroth-order Q−Q matrix is diagonal in the 2h1p−2h1p and 2p1h−2p1h blocks

$$\hat{H}^{(0)}_{aij,bkl} = \delta_{ab}\delta_{ik}\delta_{jl}(\epsilon_i + \epsilon_j - \epsilon_a) \tag{18}$$

$$\hat{H}^{(0)}_{iab,jcd} = \delta_{ij}\delta_{ac}\delta_{bd}(\epsilon_a + \epsilon_b - \epsilon_i) \tag{19}$$

First-order couplings in the Q−Q block are retained in 2ph-TDA calculations

$$\hat{H}^{(1)}_{aij,bkl} = \hat{H}^{(0)}_{aij,bkl} - \delta_{ab}\langle ij||kl\rangle - (1 - P_{ij})(1 - P_{kl})\delta_{ik}\langle bj||la\rangle \tag{20}$$

$$\hat{H}^{(1)}_{iab,jcd} = \hat{H}^{(0)}_{iab,jcd} + \delta_{ij}\langle ab||cd\rangle + (1 - P_{ab})(1 - P_{cd})\,\delta_{ac}\langle jb||di\rangle \tag{21}$$

Couplings between 2h1p and 2p1h operators vanish through first order.

Electron binding energies may be extracted from eqs 8 or 13. In the former case, seeking eigenvalues of a large, Hermitian matrix in the former case involves repeated matrix-vector multiplications. Evaluation of the self-energy matrix dominates in the latter case. Here, the most difficult task is usually solving linear equations for the product of the inverse matrix in eq 11 with its $\hat{\boldsymbol{H}}_{QP}$ neighbor. In second-order calculations, where $\hat{\boldsymbol{H}}_{QQ}$ is diagonal, both approaches have the same quartic arithmetic scaling factor. For the 2ph-TDA method, these scaling factors increase to fifth-power and sixth-power, respectively, with the algorithms of eqs 8 and 13.

The diagonal self-energy approximation may be introduced for additional computational efficiency and interpretive simplicity. A highly simplified version of the Dyson quasiparticle equation in the canonical HF basis requires only iterations of the energy variable

$$\epsilon_p^{HF} + \Sigma_{pp}(E) = E \tag{22}$$

By ignoring off-diagonal elements of second-order $\sum(E)$ in the canonical HF basis, the bottleneck acquires cubic scaling. An equivalent approximation in eq 8 is neglect of all P operators but one per final state. For the 2ph-TDA self-energy, the evaluation of a single diagonal element of $\sum(E)$ scales quintically. (The fifth-power scaling in eq 8 is unaffected by reduction of the P space's rank.) The diagonal self-energy approximation also forces Dyson orbitals to be proportional to canonical HF orbitals, albeit with probability factors that may deviate from unity. This approximation is usually excellent for outer-valence ionization energies of closed-shell molecules. When probability

https://doi.org/10.1021/acs.jpca.5c01079
J. Phys. Chem. A 2025, 129, 3597−3612

Table 2. Requirements for Arithmetic Scaling and Transformed Electron-Repulsion Integrals (ERIs) in Electron-Propagator Methods[a]

method class	methods[b]	arithmetic bottleneck	bottleneck steps	largest ERI[c] subset
diagonal 2nd order	D2, **os-D2**	OV^2	N_E	O^2V^2
	RSPT2, nD-D2, **os-nD-D2**	OV^2	Noniterative	O^2V^2
diagonal Post 2nd	RSPT3	OV^4	Noniterative	V^4
order & Approximately	D3, OVGF	OV^4	N_E[d]	V^4
renormalized (+)	IE: P3, P3+, **Q3**, **Q3+**	O^2V^3	Noniterative	OV^3
	L3, **L3+**	OV^4	N_E[d]	V^4
diagonal Post 2nd	**IE: RP3**, **RQ3**	O^2V^3	Noniterative	OV^3
order & explicitly	**RL3**	OV^4	N_IN_E[d]	V^4
renormalized (R)	IE: DR	O^2V^3	N_IN_E	O^2V^2
	DL	OV^4	N_IN_E[d]	V^4
	D-2ph-TDA	OV^4	N_I[d]	V^4
	D3+	OV^4	N_E[d]	V^4
nondiagonal &	ND2 (not renormalized)	OV^3	N_I	OV^3
renormalized (NR)	2ph-TDA	OV^4	N_I	V^4
or nondiagonal only	3+	O^2V^4	Noniterative	V^4
(ND2)	ADC(3)	O^2V^4	N_I	V^4
	IE: NR2	O^3V^3	Noniterative[f]	OV^3
	BD-T1	O^2V^4	BD[e]	V^4
	NRP3	O^2V^4	Noniterative[f]	V^4
	NRQ3	O^2V^4	Noniterative[f]	V^4
	NRL3	O^2V^4	Noniterative[f]	V^4

[a]O = # occupied orbital, V = # virtual orbitals, N_E = energy iterations, N_I = inverse-expansion or linear-equation iterations for diagonal methods and Hamiltonian-vector multiplications for nondiagonal methods. [b]New methods in **bold type**. IE = ionization energy (electron detachment). EA = electron affinity (electron attachment). [c]ERI = electron repulsion integral. [d]Reduction by a factor of N_E occurs in non-Dyson (nD) versions for electron detachments. [e]The O^2V^4 arithmetic bottleneck occurs in the Brueckner Doubles, coupled-cluster, reference-state calculation; the subsequent electron-propagator bottleneck is OV^4. [f]N_I OV^4 iterative steps for 3+, ADC(3) and NRL3; N_I O^3V^2 iterative steps for NR2, NRP3 and NRQ3 IEs; N_I OV^4 iterative steps for NR2, NRP3 and NRQ3 EAs.

factors decline below 0.85, secondary operators are too important to trust diagonal self-energies.

The ERIs in eqs 20 and 21 are responsible for the generation of ring, ladder, and mixed-ring ladder terms in the 2ph-TDA self-energy. Third-order ladder terms arise from the ERIs with four occupied or four virtual indices. Ring terms in third order are associated with the ERIs having two occupied and two virtual indices. In both cases, the electron interactions pertain to antisymmetrized ERIs. Expansion of the inverse matrix in eq 11 generates terms in all orders of the Møller−Plesset fluctuation potential.[38]

A member of the GW family of self-energy approximations may be defined by neglecting exchange terms in eqs 16 and 17 and ladder and ring-exchange terms in eqs 20 and 21. Whereas $\langle jb|la\rangle$ and $\langle jb|di\rangle$ ERIs represent repulsions between occupied-virtual electron densities, their exchanged counterparts, $\langle bj|al\rangle$ and $\langle jb|id\rangle$, do not. This simplification of 2ph-TDA has been denoted by GW@(HF-TDA), for it is based on HF orbitals and TDA excitation energies and operators.[31] The remaining terms from eqs 20 and 21 equal exchange-less TDA Hamiltonian matrix elements shifted by an orbital energy. Equation 8 offers a fifth-power alternative to fully diagonalizing the TDA Hamiltonian matrix (a sixth-power task) as a preliminary step. When the diagonal approximation is invoked, the bottleneck steps of eqs 8 and 13 have fifth-power scaling. The resulting G_0W_0@(HF-TDA) method accounts for exchange-less ring terms in all orders of the fluctuation potential. It therefore is called presently the diagonal ring (DR) method. The computational demands of DR include an O^2V^3 arithmetic bottleneck, where O and V are the dimensions of the occupied and virtual orbital sets. (Table 2 lists the arithmetic bottlenecks and ERI requirements of various self-energy approximations.) For ionization energies, DR does not require ERIs with three or four virtual indices in the HF basis.

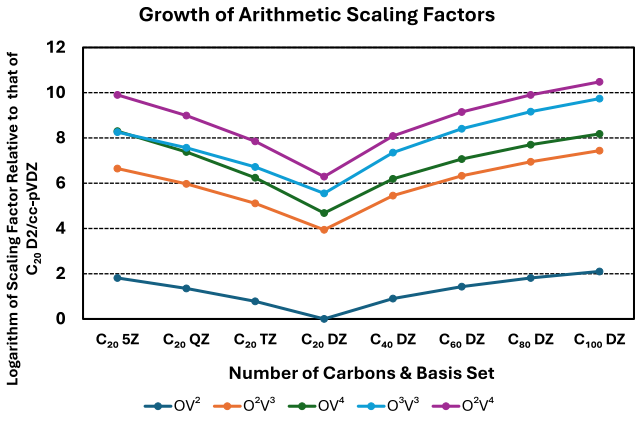


Figure 1. Logarithms of arithmetic scaling factors relative to a diagonal, second-order (D2) cc-pVDZ calculation on C_{20}.

An alternative simplification of the 2ph-TDA self-energy neglects only the last terms in eqs 20 and 21. No terms are discarded in eqs 16 and 17. Retention of the exchange-including second terms produces ladder summations in all orders of the fluctuation potential. Matrix elements in eqs 20 and 21 equal TDA Hamiltonian matrix elements in a basis of $(N \pm 2)$-electron determinants that are shifted by an orbital energy. Full diagonalizations of matrices with V^2 dimensions are clearly less feasible than fifth-power algorithms based on eq 8. With the introduction of the diagonal self-energy approximation, eq 13

https://doi.org/10.1021/acs.jpca.5c01079
J. Phys. Chem. A 2025, 129, 3597−3612

Table 3. Error Distributions (eV) versus IP-EOM-CCSDTQ/cc-pVTZ Standards

method class	method[a,b]	mean absolute error[c]	mean signed error	standard deviation	maximum unsigned error
uncorrelated	KT	1.001	0.899	0.831	2.551
diagonal 2nd order	D2	0.515	−0.477	0.442	1.410
	os-D2	0.204	0.073	0.268	0.659
	os-nD-D2	**0.198**	0.055	0.267	0.644
diagonal post 2nd order	D3	0.429	0.379	0.400	1.468
	OVGF-A	0.118	0.075	0.207	0.569
	P3+	0.160	0.015	0.191	0.395
	Q3+	**0.124**	−0.054	0.137	0.335
	L3+B	0.103	−0.035	0.128	0.331
	nD-L3+B	**0.100**	−0.041	0.125	0.336
	RL3	0.091	−0.061	0.101	0.345
	nD-RL3	**0.096**	−0.077	0.101	0.383
	DR	0.238	0.173	0.250	0.810
	DL	0.188	0.065	0.286	1.113
	nD-DL	0.189	0.055	0.286	1.103
	D-2ph-TDA	0.565	−0.565	0.266	1.432
	nD-D-2ph-TDA	0.590	−0.590	0.277	1.485
	D3+	0.199	0.136	0.220	0.696
	nD-D3+	0.190	0.122	0.215	0.670
nondiagonal	2ph-TDA	0.567	−0.567	0.273	1.405
	3+	0.205	0.146	0.221	0.710
	ADC(3)	0.211	0.175	0.202	0.726
	NR2	0.150	−0.064	0.157	0.356
	BD-T1	**0.071**	−0.006	0.082	0.163
	NRL3	**0.100**	−0.085	0.094	0.391
	IP-EOM-CCSD	0.102	0.052	0.111	0.263

[a]Numerical results from ref 17 except for methods in italics. [b]New methods in **bold type**. [c]Optimal methods in **bold type**.

also acquires fifth-power arithmetic scaling. Consequently, the resulting diagonal self-energy that includes ladder terms with exchange in all orders is denoted by DL, or the diagonal ladder method. DL has an OV^4 arithmetic bottleneck whose iterations may be minimized by a non-Dyson version for ionization energies. In this alternative, self-energy terms arising from 2ph operators are evaluated at $E = \varepsilon_p$ in eq 22. These operations require ERIs with four virtual indices.

Numerical tests discussed below reveal the quality of several diagonal self-energy methods, such as DR, DL, D-2ph-TDA and D3+. (The two latter methods are diagonal versions of 2ph-TDA and the strict version of ADC(3), also known as 3+). Table 2 divides self-energy approximations into four categories. The three least computationally demanding sets employ the diagonal approximation in the canonical HF basis. Diagonal self-energies that require evaluation of no terms beyond second order in the fluctuation potential have cubic arithmetic scaling. The second category comprises methods that compute only second-order and third-order terms. Approximately renormalized members of this group include the new-generation Q3+ and L3+ methods[16,19] and the three older outer valence Green function (OVGF)[39,40] self-energies. Explicit evaluation of higher order terms distinguishes the third category from the second. In addition to the DR and DL self-energies, D-2ph-TDA and D3+ are present in the third group. The new-generation RP3, RQ3 and RL3 approximations[16,19] are also members of the third group. All methods in the second and third groups have fifth-power arithmetic bottlenecks. Nondiagonal self-energies, which generate Dyson orbitals as linear combinations of HF orbitals, belong to the fourth category. The 2ph-TDA method belongs to this group, as well as its ADC(3) and 3+ extensions. The NR2[41] and BD-T1[12,13] methods are present here, as are the new-generation NRP3, NRQ3 and NRL3 alternatives.[20] Except for 2ph-TDA, these self-energies have sixth-power bottlenecks.

Figure 1 illustrates the importance of arithmetic scaling factors by plotting the growth of operations versus system or basis size. These data pertain to calculations on carbon clusters (C_{20}, C_{40}, C_{60}, ⋯) that employ correlation-consistent basis sets.[42] The D2 (i.e., OV^2) result for C_{20} with the valence double-ζ (cc-pVDZ or DZ) basis is set to zero on the logarithmically scaled vertical axis. (See the C_{20} DZ label in the fourth abscissa position.) All other data for larger clusters (fifth through eighth abscissa positions) or basis sets (first through third abscissa positions) are relative to this standard. Curves for the OV^2, O^2V^3, OV^4, O^3V^3, and O^2V^4 cases demonstrate the advantages of low arithmetic scaling factors as basis sets and system size increase. Ten orders of magnitude are spanned in this illustration.

COMPUTATIONAL METHODS

All EP calculations of VIEs employ restricted HF self-consistent-field wave functions, except for the BD-T1 case, which assumes Brueckner-doubles (BD) coupled-cluster pseudocanonical orbitals.[29] All molecules considered have closed-shell singlet ground states. ERIs transformed into the HF or BD pseudocanonical basis are stored on disk. Table 2 lists the largest subsets of ERIs required for each EP approximation. Electron correlation treatments in EP calculations exclude core orbitals, employing the standard frozen-core approximation. The newly developed methods have been integrated as additional links in the development version of Gaussian software.[43] Furthermore, the diagonal EP methods in Tables 1 and 2 have been implemented using Abelian-group-adapted, semidirect algorithms.

https://doi.org/10.1021/acs.jpca.5c01079
J. Phys. Chem. A 2025, 129, 3597−3612

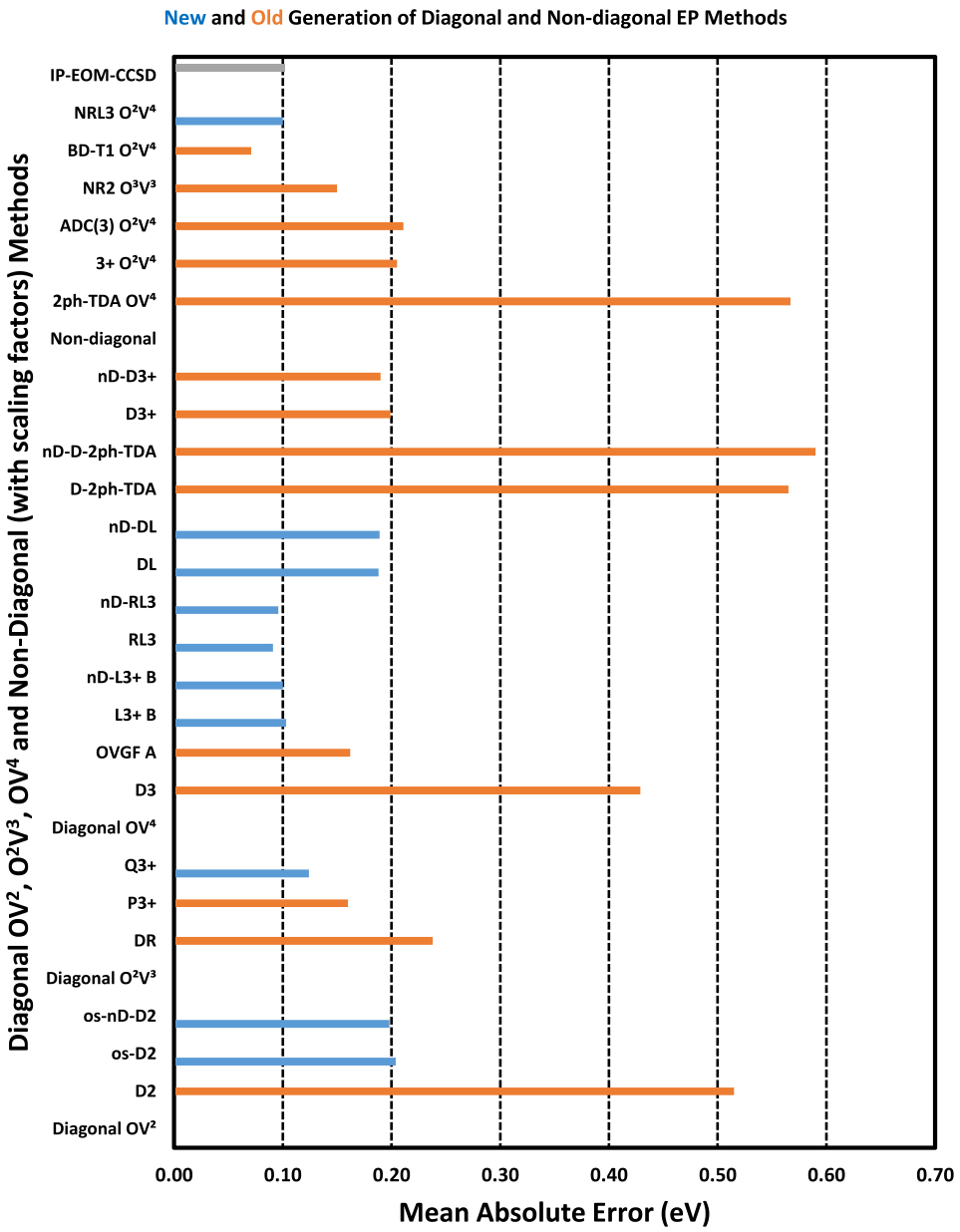


Figure 2. Mean absolute errors (eV) of electron-propagator methods versus IP-EOM-CCSDTQ/cc-pVTZ VIE standards.

IP-EOM-CCSDTQ Standards. To generate standard data for judging the quality of Kohn−Sham orbital energies, several levels of ionization-potential, equation-of-motion, coupled-cluster calculations were executed in the cc-pVTZ basis.[32] Close agreement between results generated at the SDT and SDTQ (single, double, triple and quadruple operators, respectively) levels established the high accuracy of the data. (Mean absolute discrepancies between SDT and SDTQ results were approximately 0.03 eV). This study provided geometries for 14 small molecules, with the test set covering multiple transitions per molecule and incorporating 42 VIEs. To maintain a stringent assessment, transitions were excluded when any method produced probability factors below the recommended threshold of 0.85. This filtering process reduced the data set to 27 VIEs with high probability factors. Comprehensive statistical analyses for the full set of 42 VIEs are detailed in the Supporting Information. All EP calculations on the IP-EOM-CCSDTQ set use the same cc-pVTZ basis.

IP-EOM-CCSDT Standards. This data set includes 201 VIEs derived from 41 molecules. Following the exclusion of 85 VIEs where at least one method produced a probability factor below the 0.85 threshold, 116 VIEs remained for analysis. Consequently, the statistics presented in the Tables and Figures are based on this refined subset. Comprehensive statistical analyses encompassing all 201 VIEs are available in the Supporting Material. All calculations on the IP-EOM-CCSDT set were executed with the cc-pVTZ basis.

GW20 Standards. The geometries of all 20 molecules in the GW20 data set were sourced from a prior study.[33] All calculations for the GW20 data set were performed using the def2-TZVPP basis. Standard ΔCCSD(T)[44] data were determined for only the lowest VIE of each molecule. The performance of the G_0T_0 and G_0W_0 methods discussed below was based on these standards. Like G_0T_0 and G_0W_0, the DL and DR methods assume the diagonal approximation in the canonical HF basis. The two latter methods differ from G_0T_0

https://doi.org/10.1021/acs.jpca.5c01079
J. Phys. Chem. A 2025, 129, 3597−3612

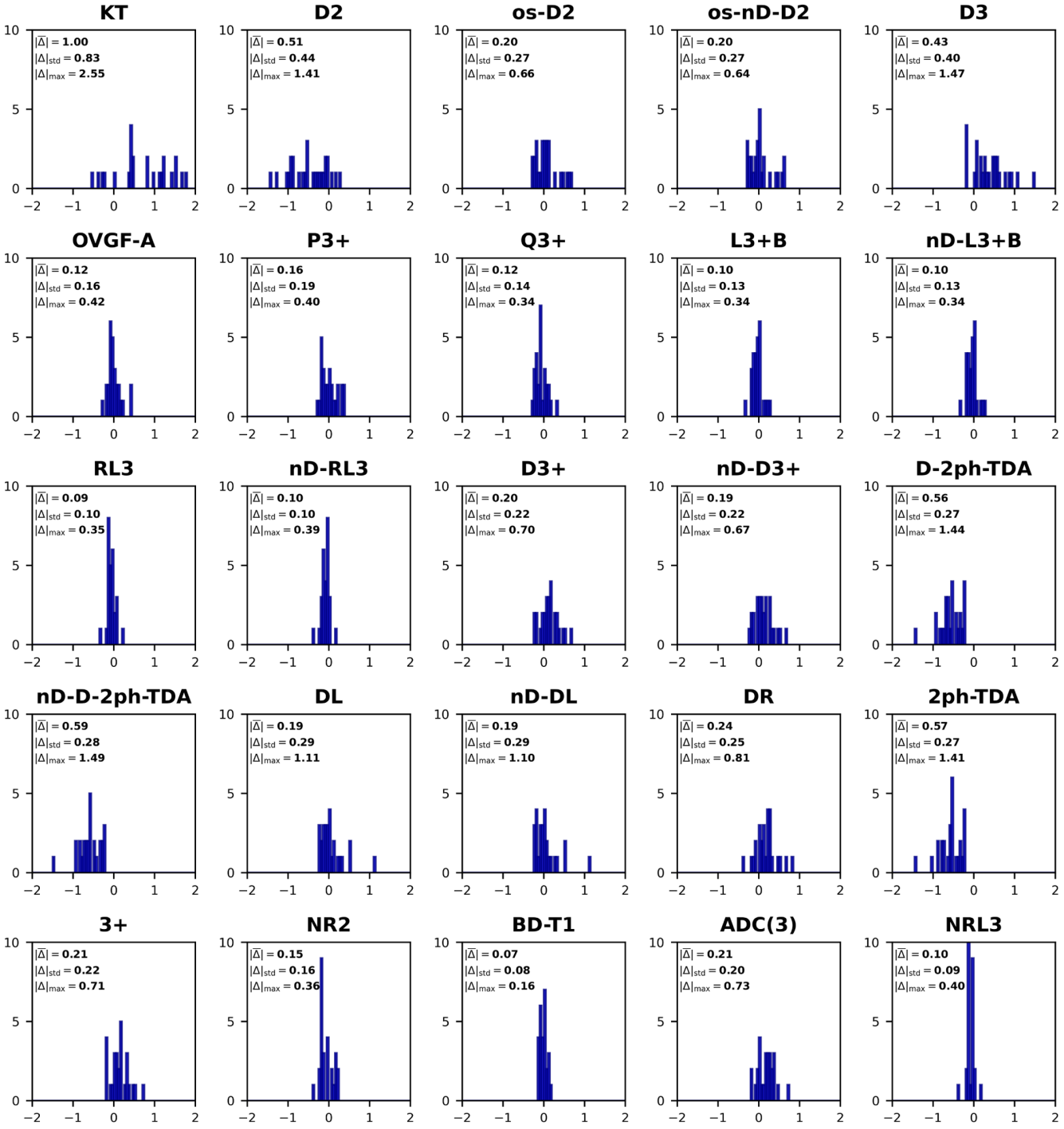


Figure 3. Histograms of error distributions (eV) versus IP-EOM-CCSDTQ/cc-pVTZ VIE standards.

and G_0W_0 by their use of TDA instead of RPA transition energies and operators. For DR and G_0W_0, the transitions refer to excitations that conserve the number of electrons, N. In DL and G_0T_0 calculations, the relevant transitions have final states with $N \pm 2$ electrons.

Experimental Standards. Molecular geometries and experimental VIEs for a set of 136 closed-shell molecules were obtained from a previous study.[17] To assess the reliability of these experimental reference values, total energy differences were computed using coupled-cluster theory with single, double, and perturbative triple excitations [CCSD(T)]. The ΔCCSD(T) calculations were performed with the augmented correlation-consistent polarized valence double-ζ (aug-cc-pVDZ) and triple-ζ (aug-cc-pVTZ) basis sets. To establish complete-basis-set (CBS) VIE reference values, total energies were extrapolated using an inverse quartic dependence on basis set cardinal numbers [i.e., $(1 + 1/2)^{-4}$], incorporating augmented double-ζ and triple-ζ basis sets. The experimental VIE standards, along with their ΔCCSD(T) counterparts, are provided in the Supporting Information. Only the lowest VIEs of each molecule are considered here.

The close agreement between the ΔCCSD(T)/CBS VIEs and experimental values confirms the reliability of the latter data and supports their use as benchmark references for assessing the

https://doi.org/10.1021/acs.jpca.5c01079
J. Phys. Chem. A 2025, 129, 3597−3612

Table 4. Error Distributions (eV) versus IP-EOM-CCSDT/cc-pVTZ Standards

method class	method[a,b]	mean absolute error[c]	mean signed error	standard deviation	maximum unsigned error
uncorrelated	KT	1.445	1.407	0.926	2.839
diagonal 2nd order	D2	0.594	−0.583	0.373	1.389
	os-D2	0.247	0.215	0.197	0.756
	os-nD-D2	**0.235**	0.200	0.195	0.740
diagonal post 2nd order	D3	0.674	0.648	0.497	1.592
	OVGF-A	0.214	0.258	0.316	0.818
	P3+	0.153	0.093	0.163	0.595
	Q3+	**0.138**	0.053	0.158	0.392
	L3+B	0.109	0.052	0.132	0.448
	nD-L3+B	**0.103**	0.043	0.128	0.418
	RL3	0.082	0.002	0.107	0.324
	nD-RL3	**0.081**	−0.020	0.105	0.362
	DR	0.247	0.218	0.210	0.767
	DL	0.161	0.120	0.166	0.766
	nD-DL	0.151	0.106	0.163	0.752
	D-2ph-TDA	0.603	−0.603	0.245	1.411
	nD-D-2ph-TDA	0.636	−0.636	0.256	1.464
	D3+	0.362	0.314	0.309	0.870
	nD-D3+	0.346	0.295	0.304	0.846
nondiagonal	2ph-TDA	0.610	−0.610	0.201	1.384
	3+	0.372	0.327	0.312	0.906
	ADC(3)	0.343	0.319	0.258	0.775
	NR2	0.097	−0.010	0.120	0.335
	BD-T1	0.104	0.080	0.102	0.319
	NRL3	**0.065**	−0.020	0.081	0.370
	IP-EOM-CCSD	0.137	0.124	0.102	0.529

[a]Numerical results from ref 17 except for methods in italics. [b]New methods in **bold type**. [c]Optimal methods in **bold type**.

accuracy of the EP methods. Consequently, experimental VIEs serve as the standard against which the performance of EP methods is evaluated.

All computed probability factors exceeded the recommended threshold of 0.85 for diagonal EP methods and upheld the qualitative validity of perturbative corrections to Koopmans-based predictions. The EP calculations were also obtained with the aug-cc-pVDZ and aug-cc-pVTZ basis sets. VIEs were extrapolated to the CBS limit using the inverse quartic formula mentioned above.

Convergence of Renormalized Calculations. Many of the self-energies examined below involve explicit renormalization, i.e., terms in all orders of the fluctuation potential are calculated, not estimated. An algorithm based on solutions of linear equations converges consistently for RL3, DL, D-2ph-TDA, D3+ and their non-Dyson variants. Similar success occurs in DR calculations. When exchange terms are added to the DR self-energy, this algorithm fails to converge for approximately half of the VIEs. DR with exchange therefore has been excluded from the statistical analysis of numerical data.

RESULTS AND DISCUSSION

Table 3 and Figures 2 and 3 summarize measures of error with respect to the IP-EOM-CCSDTQ standards. In Figure 2, blue and orange horizontal bars respectively represent mean absolute errors (MAEs) for new-generation and older self-energy approximations. DR and diagonal versions of old methods, such as D-2ph-TDA, D3+ and their non-Dyson variants, have been assigned orange bars. DL and its non-Dyson variant have blue bars.

The lowest sector in Figure 2 with three bars pertains to diagonal self-energies with cubic arithmetic scaling. The MAEs near 0.2 eV of the opposite-spin, second-order methods are lower than those of most of the orange-bar methods with higher arithmetic scaling. Figure 3's histograms demonstrate that the D2 self-energy usually overestimates the exact correction to Koopmans results. A usefully balanced description combines same-spin interaction at the HF level with second-order opposite-spin correlation. Similar trends emerge from inspection of Table 4 and Figures 4 and 5, which pertain to the IP-EOM-CCSDT standards. MAEs are somewhat larger for the latter calculations. This trend may result from lower accuracy with respect to full configuration interaction caused by neglect of Q cluster operators.

The next sector of horizontal bars in Figures 2 and 4 considers methods with O^2V^3 scaling. The approximately renormalized Q3+ method is more accurate than its P3+ antecedent. Both methods have lower MAEs, standard deviations and maximum errors than DR. (See Tables 3 and 4). Complete omission of ERIs with more than two virtual indices is the lone computational advantage of DR over Q3+ and P3+. Several prominent overestimates may be discerned in the DR histograms of Figures 3 and 5.

The third, OV^4-scaling category of diagonal self-energies includes approximately and explicitly renormalized alternatives. OVGF methods are based on the set of second-order and third-order diagrams that respectively define D2 and D3. (The need for renormalizations is clear, for D3 results are worse than those of D2 in Table 4 and Figure 4). Better results with an approximate renormalization flow from the L3+B method and its non-Dyson variant. These methods produce MAEs near 0.1 eV. Their explicitly renormalized counterparts, RL3 and nD-RL3, exhibit slightly smaller error measures in Tables 3 and 4. Corresponding histograms are sharply peaked and become even

https://doi.org/10.1021/acs.jpca.5c01079
J. Phys. Chem. A 2025, 129, 3597−3612

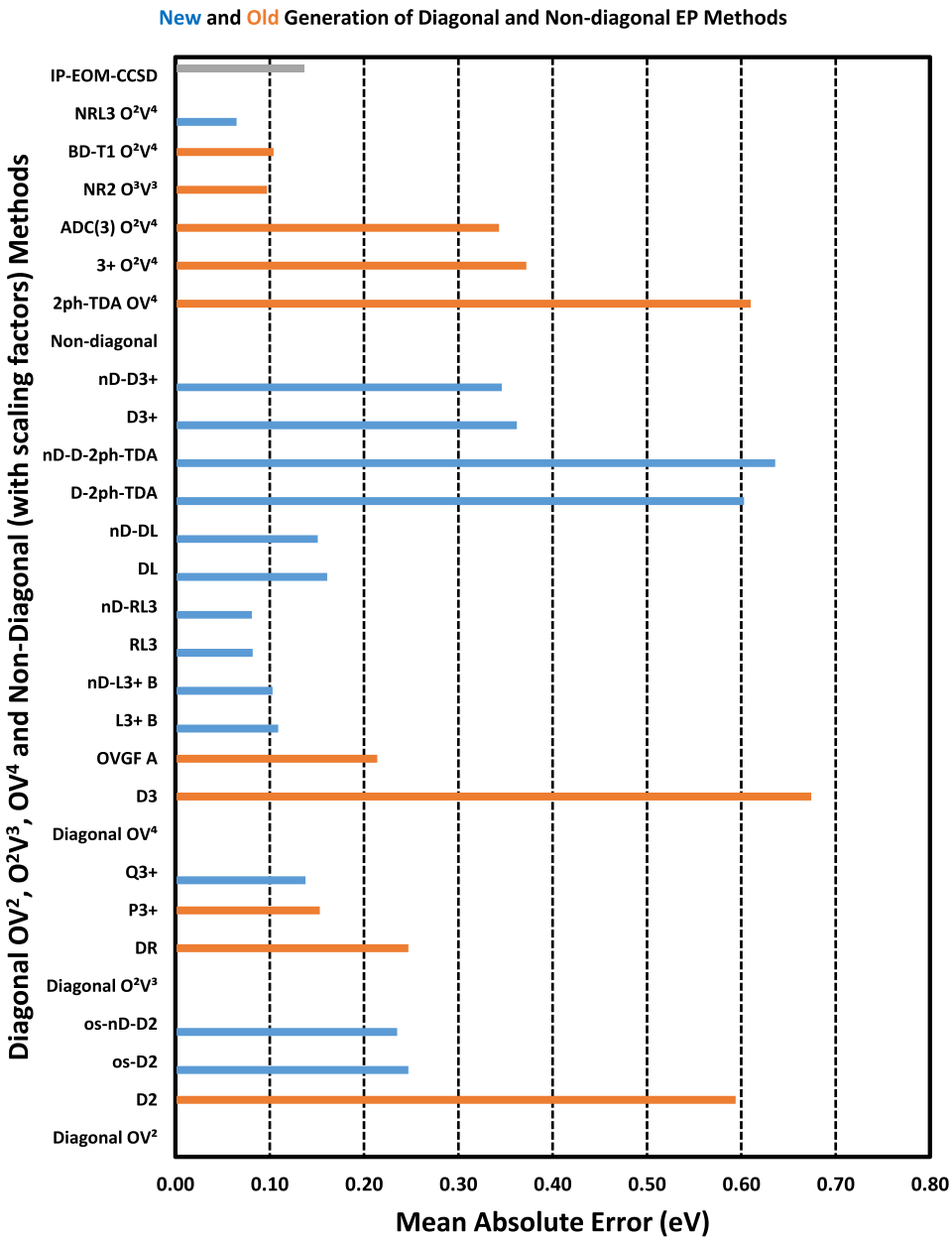


Figure 4. Mean absolute errors (eV) of electron-propagator methods versus IP-EOM-CCSDT/cc-pVTZ VIE standards.

more so when the nondiagonal generalization, NRL3, is employed. The latter method's MAE is only 0.065 eV in Table 4, but it is achieved at the price of a noniterative O^2V^4 step.

The DL method and its non-Dyson variant, which also pertain to the OV^4 category, produce larger MAEs than RL3 and nD-RL3. These results are better than those of DR, which has a greater tendency to overestimate VIEs than DL and nD-DL. The two latter methods' histograms in Figure 5 are taller and narrower than that of DR. A comparison of histograms in Figures 3 and 5 indicates that overestimates predominate for DL and DR. The widely used nondiagonal 3+ and ADC(3) methods have larger MAEs than DL for both data sets. DR performs better than 3+ and ADC(3) only in the IP-EOM-CCSDT test. DL produces slightly smaller errors than the best cubically scaling alternatives, but it is not more accurate than the O^2V^3-scaling Q3+ method. DR's error measures are slightly larger than those of os-D2 and os-nD-D2.

Diagonal versions of 2ph-TDA and 3+ in their regular and non-Dyson forms (D-2ph-TDA, nD-D-2ph-TDA, D3+ and nD-D3+) generate relatively large errors that resemble those of their original, nondiagonal counterparts (2ph-TDA and 3+). (Compare data in the top two sectors of Figures 2 and 4 for nondiagonal and diagonal self-energies.) The latter results indicate that the diagonal approximation works well for the present data sets. Underestimates are more numerous than overestimates for 2ph-TDA and its diagonal versions. Additional terms arising from reference-state correlation corrections distinguish 3+ and ADC(3) from 2ph-TDA and, as in DR and DL calculations, yield overestimates again.

Despite the presence of the DR and DL self-energy terms in their 2ph-TDA generalization, they do not suffice to explain the latter method's numerical trends. The numerous overestimates of DR and DL displayed in the histograms contrast with the underestimates that dominate in the 2ph-TDA case. The

https://doi.org/10.1021/acs.jpca.5c01079
J. Phys. Chem. A 2025, 129, 3597−3612

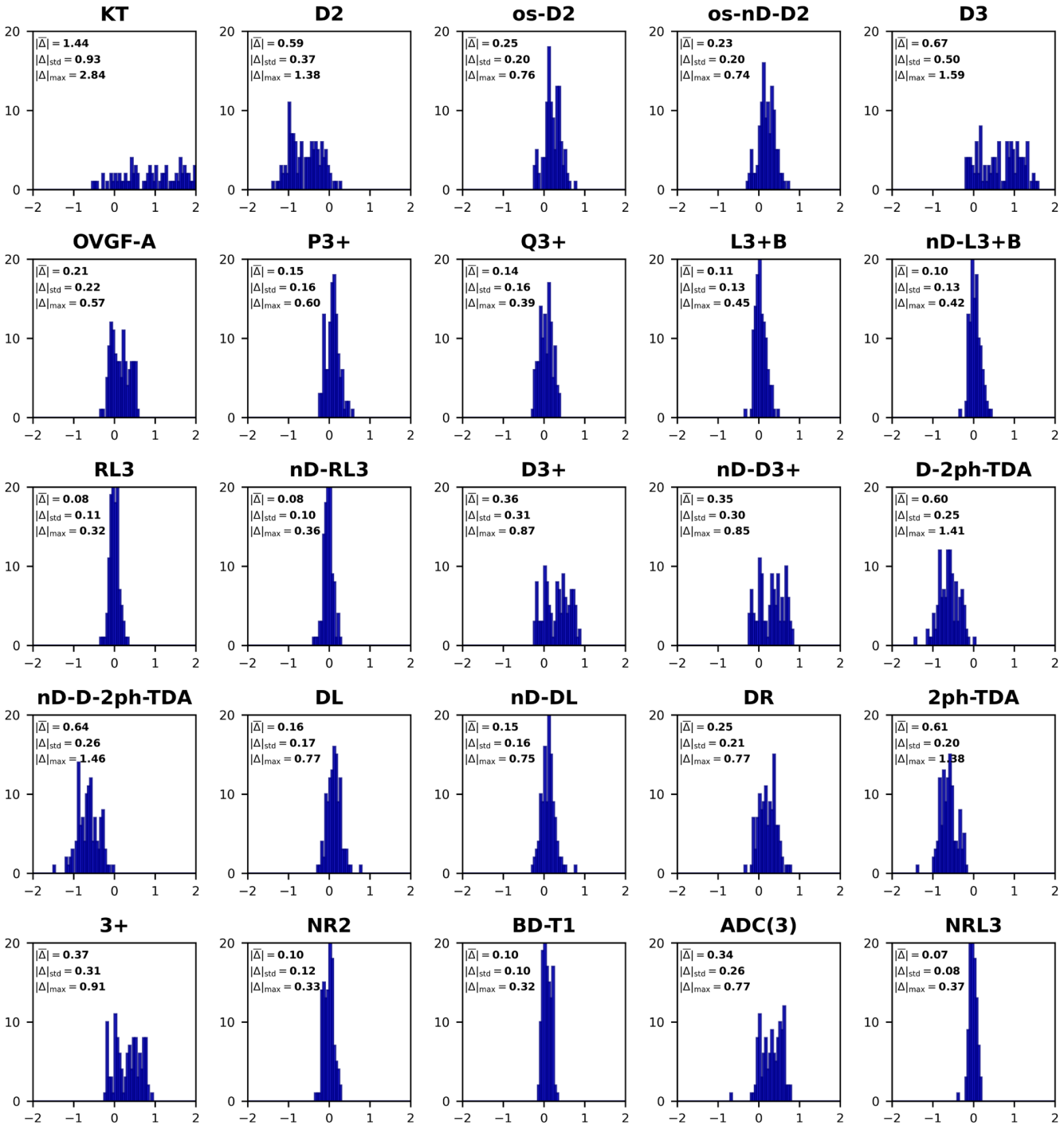


Figure 5. Histograms of error distributions (eV) versus IP-EOM-CCSDT/cc-pVTZ VIE standards.

presence of ring-exchange terms in 2ph-TDA and this method's inclusion of mixed ring-ladder diagrams lead to qualitatively different patterns of error. Copious numerical instabilities associated with small denominators occur in the 2hp renormalizations when ring-exchange terms are added to the exchange-less DR self-energy. Ladder terms with exchange in the 2h1p-2h1p superoperator couplings are needed for convergence when ring-exchange terms are included. These results indicate that there are no numerically negligible terms in eqs 20 and 21 for the present data sets.

Considerable improvements over 2ph-TDA results accompany inclusion of the terms in 3+ and ADC(3) that arise from ground-state correlation amplitudes. Corresponding MAEs decline from 0.6 to 0.3−0.4 eV. For the outer-valence VIEs under study here, the diagonal approximation works well, for MAEs of diagonal and nondiagonal variants are almost identical. Discrepancies between 3+ and ADC(3) are minor. The non-Dyson and regular versions of the diagonal 2ph-TDA self-energies also agree closely.

Among the diagonal methods with OV^4 arithmetic scaling, the RL3 and nD-RL3 methods still outperform D3+, DL and their non-Dyson variants. In fact, the approximately renormalized L3+B and nD-L3+B alternatives also produce lower MAEs than the diagonal and original versions of 2ph-TDA and 3+. Among

https://doi.org/10.1021/acs.jpca.5c01079
J. Phys. Chem. A 2025, 129, 3597−3612

the older methods in this category, OVGF-A is best; it also has a lower MAE than D3+ and the nondiagonal 3+ and ADC(3) self-energies.

Nondiagonal self-energies have the advantage of producing Dyson orbitals in their most general form, a linear combination of basis orbitals. They also can describe correlation final states, which are not considered in this study. The top sectors of Figures 2 and 4 indicate that 2ph-TDA is not competitive in predicting outer valence VIEs. 3+ and ADC(3) are markedly better, but two older methods, NR2 and BD-T1, have lower MAEs. NR2 has the additional advantage of a lower sixth-power arithmetic scaling factor, O^3V^3. The noniterative character of NRL3's O^2V^4 scaling gives it an advantage of efficiency over IP-EOM-CCSD. The latter method's scaling factor is iterative because of its optimization of reference-state cluster amplitudes. BD-T1 has the lowest MAE in Figure 2, but NRL3 has this distinction in Figure 4.

Results that refer to the ΔCCSD(T)/def2-TZVPP standards for the GW20 set appear in Table 5. Whereas the G_0W_0 and G_0T_0 data of a previous study[33] and the present DR results produce MAEs near 0.25 eV, the DL value is 0.19 eV. The latter error measure is practically unchanged in its non-Dyson version, which eliminates all but one of the bottleneck (OV^4) summations. Mean signed errors are only slightly negative for DR, DL and nD-DL. This result is qualitatively opposite from the overestimates seen in Tables 3 and 4 and in the histograms of Figures 3 and 5. In calculations with the similar cc-pVTZ basis, ΔCCSD(T) VIEs tend to be higher than their IP-EOM-CCSDT and IP-EOM-CCSDTQ counterparts for the GW20 set. (See Supporting Information). Adoption of IP-EOM-CC/def2-TZVPP standards would probably lead to a sign change in the third column of Table 5 for DR, DL and nD-DL. An increase in mean signed errors for G_0W_0 and DR may also occur. These preliminary data indicate that better accuracy accompanies the ladder renormalization and TDA excitation energies and operators. DL and nD-DL give the best VIEs, but DR requires fewer arithmetic operations and a smaller set of ERIs.

The final test employs the Cambridge experimental standards.[34] Table 6 and Figures 6 and 7 present data whose qualitative trends strongly resemble those of the previous tests. The opposite-spin modifications of D2 are distinguished by their MAEs below 0.2 eV and their cubic arithmetic scaling. As in the previous tests, the os-D2 and nD-os-D2 methods have a greater tendency to overestimate than to underestimate VIEs. The MAE of DR approaches 0.4 eV, but Q3+, with an identical O^2V^3 scaling factor, has an MAE near 0.1 eV. The DR method produces very few underestimates; most of its errors are overestimates. Q3+ produces a much more symmetrical profile in Figure 7. Among the self-energy approximations with OV^4 scaling in the middle of Figure 6, the new-generation methods

Table 5. Error Distributions (eV) versus ΔCCSD(T)/def2-TZVPP Standards of the GW20

method	mean absolute error	mean signed error	standard deviation	maximum unsigned error
G_0W_0[33]	0.259	0.220	0.257	0.790
G_0T_0[33]	0.250	−0.171	0.274	0.780
DR[a]	0.269	−0.019	0.331	0.662
DL[a]	0.194	−0.024	0.235	0.500
nD-DL[a]	0.197	−0.032	0.239	0.520

[a]This work.

Table 6. Error Distributions (eV) of Electron-Propagator Methods in CBS versus Cambridge Experimental VIEs Standards

method class	method[a,b]	mean absolute error[c]	mean signed error	standard deviation	maximum unsigned error
uncorrelated	KT	0.756	0.692	0.742	2.700
diagonal 2nd order	D2	0.380	−0.366	0.359	1.459
	os-D2	0.188	0.162	0.162	0.659
	os-nD-D2	**0.182**	0.155	0.161	0.646
diagonal post 2nd order	D3	0.388	0.365	0.418	1.681
	OVGF-A	0.122	0.074	0.234	0.690
	P3+	0.156	0.113	0.157	0.487
	Q3+	**0.116**	0.011	0.140	0.339
	L3+B	0.083	0.028	0.098	0.288
	nD-L3+B	**0.079**	0.015	0.098	0.330
	RL3	0.073	−0.004	0.094	0.321
	nD-RL3	**0.075**	−0.019	0.097	0.367
	DR	0.396	0.386	0.219	1.705
	DL	0.116	0.036	0.144	0.585
	nD-DL	0.110	0.027	0.140	0.574
	D-2ph-TDA	0.493	−0.485	0.271	1.432
	nD-D-2ph-TDA	0.520	−0.512	0.283	1.484
	D3+	0.205	0.145	0.243	0.745
	nD-D3+	0.198	0.133	0.237	0.716
nondiagonal	2ph-TDA	0.527	−0.519	0.291	1.663
	3+	0.252	0.190	0.302	1.141
	ADC(3)	0.211	0.194	0.198	0.682
	NR2	0.123	0.008	0.156	0.438
	BD-T1	0.091	0.060	0.097	0.355
	NRL3	**0.078**	−0.035	0.095	0.367
	ΔCCSD(T)	0.094	0.073	0.091	0.257

[a]Numerical results from ref 17 except for methods in *italics*. [b]New methods in **bold type**. [c]Optimal methods in **bold type**.

https://doi.org/10.1021/acs.jpca.5c01079
J. Phys. Chem. A 2025, 129, 3597−3612

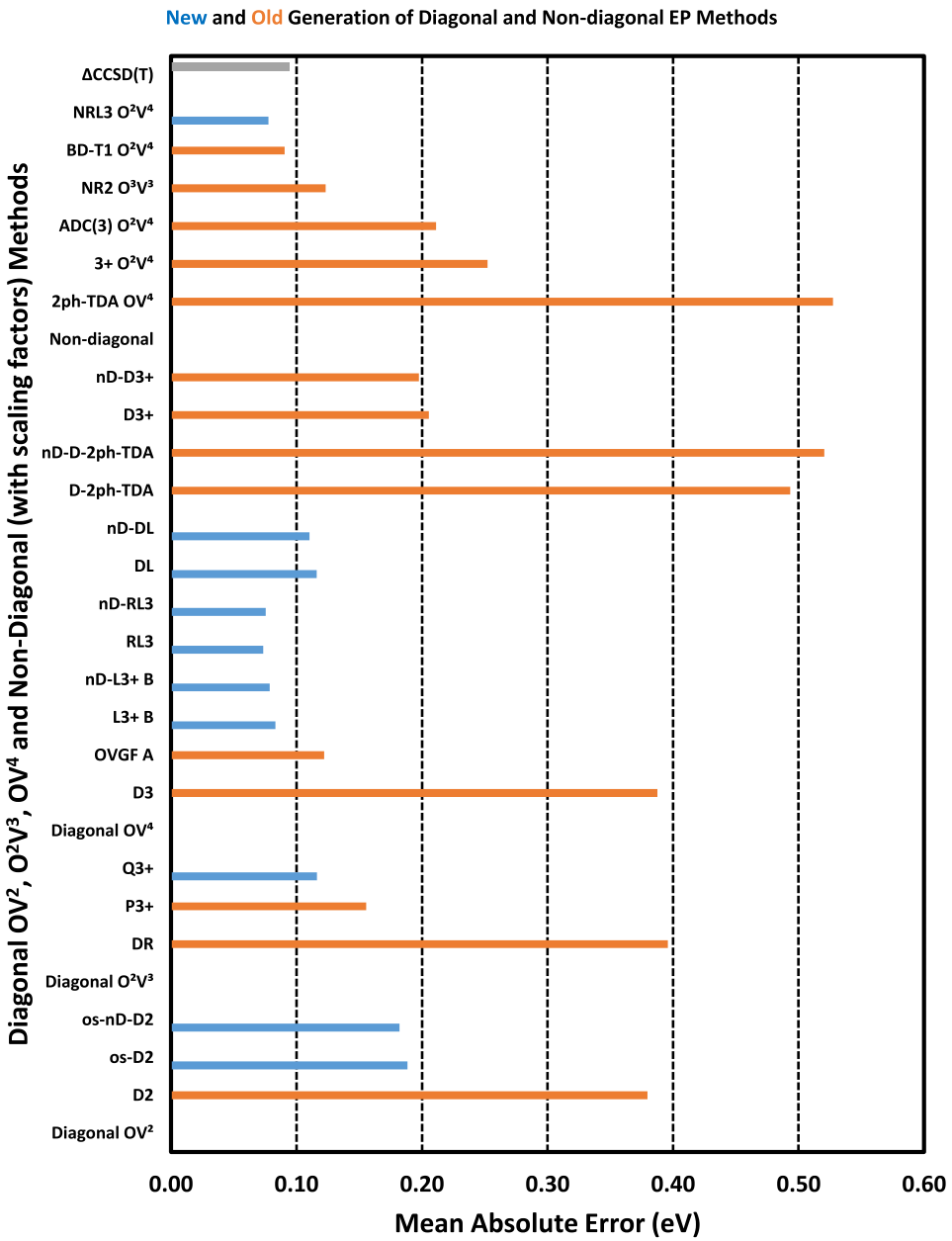


Figure 6. Mean absolute errors (eV) of CBS electron-propagator methods versus Cambridge experimental VIE standards.

are clearly superior to the older alternatives. The latter group includes D3, OVGF and the diagonal versions of 2ph-TDA and 3+. The DL self-energy and its non-Dyson version produce MAEs slightly above 0.1 eV. Even lower error measures of 0.07−0.08 eV emerge from L3+B, RL3 and their non-Dyson variants. Histograms for these four methods are taller and sharper than that of DL. In this category, the nD-L3+B alternative is the most efficient, for it relies only on approximate renormalization procedures. Within the nondiagonal category, the new-generation alternative, NRL3, generates the lowest MAE, 0.08 eV. Slightly higher error measures belong to the older, sixth-power NR2 and BD-T1 approximations. All these methods are competitive with the seventh-power ΔCCSD(T) method.

CONCLUSIONS

Numerical tests of self-energy approximations have employed two kinds of VIE standards. The first kind consists of computational data of almost exact quality in a fixed basis set. The second standard comprises experimental data that have been verified by approximate agreement with ΔCCSD(T) calculations. Analysis of the errors produced by various self-energy approximations leads to the following conclusions on the DR and DL simplifications of 2ph-TDA and competing methods.

- TDA excitation energies and operators are superior to their RPA counterparts for the construction of self-energies with ring or ladder renormalizations.
- For VIEs with probability factors above 0.85, the diagonal self-energy approximation in the canonical HF basis leads to no deterioration in predictive quality.
- DL's inclusion of ladder self-energy terms with exchange generates lower errors than DR's inclusion of exchange-less ring terms.

https://doi.org/10.1021/acs.jpca.5c01079
J. Phys. Chem. A 2025, 129, 3597−3612

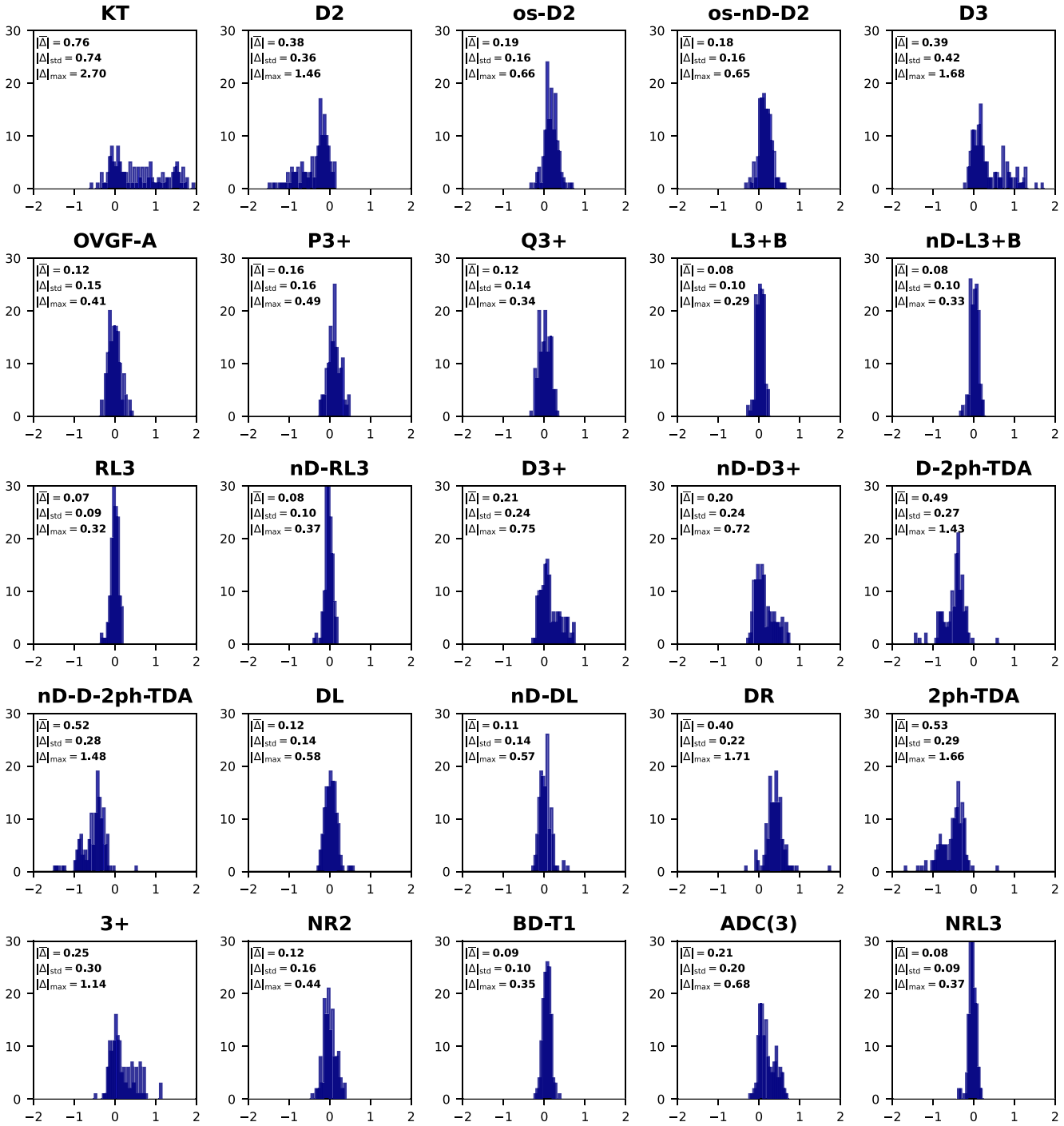


Figure 7. Histograms of error distributions (eV) of CBS electron-propagator methods versus Cambridge experimental VIE standards.

- Addition of exchange terms to ring-renormalized self-energies often leads to numerical instabilities.
- All terms in the superoperator couplings between 2h1p and 2p1h operators in eqs 20 and 21 are important in reliable calculations of molecular VIEs.
- Correlation improvements to reference states are necessary for producing the lowest MAEs obtained in this study, but do not necessarily require sixth-power arithmetic scaling factors.
- The new-generation RL3 method, its non-Dyson variant, and its nondiagonal generalization produce MAEs below 0.1 eV with fifth-power or noniterative sixth power arithmetic scaling.
- L3+B and nD-L3+B are more efficient, approximately renormalized alternatives to RL3 and nD-RL3 with similar error measures.
- DL produces useful data but competing methods with the same OV^4 arithmetic scaling factor (e.g., RL3, L3+B) are more accurate.
- Somewhat lower accuracy (0.1 < MAE < 0.2 eV) with OV^2 or O^2V^3 arithmetic scaling is available with opposite-spin, second order and Q3+ self-energies.

https://doi.org/10.1021/acs.jpca.5c01079
J. Phys. Chem. A 2025, 129, 3597−3612

- The opposite-spin, second order and Q3+ methods are more accurate and efficient alternatives to DR.

■ ASSOCIATED CONTENT

Supporting Information

The Supporting Information is available free of charge at https://pubs.acs.org/doi/10.1021/acs.jpca.5c01079.

Molecular electron detachment energies, QTP_IEs (XLSX)

Molecular electron detachment energies, GW20_IEs (XLSX)

Molecular electron detachment energies, Cambridge_IEs (XLSX)

■ AUTHOR INFORMATION

Corresponding Author

J. V. Ortiz − *Department of Chemistry and Biochemistry, Auburn University, Auburn, Alabama 36849-5312, United States;* orcid.org/0000-0002-9277-0226; Email: ortiz@auburn.edu

Authors

Ernest Opoku − *Department of Chemistry and Biochemistry, Auburn University, Auburn, Alabama 36849-5312, United States;* orcid.org/0000-0002-4271-6838

Filip Pawłowski − *Department of Chemistry and Biochemistry, Auburn University, Auburn, Alabama 36849-5312, United States;* orcid.org/0000-0002-5928-2140

Complete contact information is available at: https://pubs.acs.org/10.1021/acs.jpca.5c01079

Notes

The authors declare no competing financial interest.

■ ACKNOWLEDGMENTS

The authors thank Dr. Reza Hemmati and Dr. Abdulrahman Zamani for valuable discussions and the Alabama Supercomputer Center for computing resources. EO is grateful to Auburn University for financial support through the Harry Merriwether Fellowship.

■ REFERENCES

(1) Linderberg, J.; Öhrn, Y. *Propagators in Quantum Chemistry*, 2nd ed.; Wiley-Interscience: Hoboken NJ, 2004.

(2) Schirmer, J. *Many-Body Methods for Atoms, Molecules and Clusters*; Springer International Publishing AG, 2018.

(3) Ortiz, J. V. Electron propagator theory: an approach to prediction and interpretation in quantum chemistry. *WIREs Comput. Mol. Sci.* **2013**, *3*, 123−142.

(4) Ortiz, J. V. Interpreting Bonding and Spectra With Correlated, One-Electron Concepts From Electron Propagator Theory. In *Annual Reports in Computational Chemistry*; Dixon, D. A., Ed.; Elsevier, 2017 Chapter Four, Vol. *13*, pp 139−182.

(5) Jørgensen, P.; Simons, J. *Second Quantization-Based Methods in Quantum Chemistry*; Academic Press, New York, 1981.

(6) Koopmans, T. Über die Zuordnung von Wellenfunktionen und Eigenwerten zu den Einzelnen Elektronen Eines Atoms. *Physica* **1934**, *1*, 104−113.

(7) Hirata, S.; Hermes, M. R.; Simons, J.; Ortiz, J. V. General-Order Many-Body Green's Function Method. *J. Chem. Theory Comput.* **2015**, *11*, 1595−1606.

(8) Hirata, S.; Doran, A. E.; Knowles, P. J.; Ortiz, J. V. One-particle many-body Green's function theory: Algebraic recursive definitions, linked-diagram theorem, irreducible-diagram theorem, and general-order algorithms. *J. Chem. Phys.* **2017**, *147*, No. 044108.

(9) Öhrn, Y.; Born, G.Molecular Electron Propagator Theory and Calculations. In *Advances in Quantum Chemistry*; Elsevier, 1981; Vol. *13*, pp 1−88.

(10) Reining, L. The GW approximation: content, successes and limitations. *WIREs Comput. Mol. Sci.* **2018**, *8*, No. e1344.

(11) Knight, J. W.; Wang, X.; Gallandi, L.; Dolgounitcheva, O.; Ren, X.; Ortiz, J. V.; Rinke, P.; Körzdörfer, T.; Marom, N. Accurate Ionization Potentials and Electron Affinities of Acceptor Molecules III: A Benchmark of GW Methods. *J. Chem. Theory Comput.* **2016**, *12*, 615−626.

(12) Ortiz, J. V. Approximate Brueckner orbitals and shakeup operators in electron propagator calculations: applications to F- and OH. *Int. J. Quantum Chem.* **1998**, *70*, 651−658.

(13) Ortiz, J. V. Approximate Brueckner orbitals in electron propagator calculations. *Int. J. Quantum Chem.* **1999**, *75*, 615−621.

(14) Yeager, D. L. The multiconfigurational spin-tensor electron propagator method (MCSTEP). *Adv. Quantum Chem.* **2005**, *50*, 289−313.

(15) Banerjee, S.; Sokolov, A. Y. Algebraic Diagrammatic Construction Theory for Simulating Charged Excited States and Photoelectron Spectra. *J. Chem. Theory Comput.* **2023**, *19*, 3037−3053.

(16) Opoku, E.; Pawłowski, F.; Ortiz, J. V. New-Generation Electron-Propagator Methods for Molecular Electron-Binding Energies. *J. Phys. Chem. A* **2024**, *128*, 1399−1416.

(17) Opoku, E.; Pawłowski, F.; Ortiz, J. V. Electron-propagator methods versus experimental ionization energies. *J. Chem. Phys.* **2025**, *162*, No. 064102.

(18) Prasad, M. D.; Pal, S.; Mukherjee, D. Some aspects of self-consistent propagator theories. *Phys. Rev. A* **1985**, *31*, 1287−1298.

(19) Opoku, E.; Pawłowski, F.; Ortiz, J. V. A new generation of diagonal self-energies for the calculation of electron removal energies. *J. Chem. Phys.* **2021**, *155*, No. 204107.

(20) Opoku, E.; Pawłowski, F.; Ortiz, J. V. A new generation of non-diagonal, renormalized self-energies for calculation of electron removal energies. *J. Chem. Phys.* **2023**, *159*, No. 124109.

(21) Simons, J. The electron propagator and superoperator resolvent. *J. Chem. Phys.* **1976**, *64*, 4541−4543.

(22) Manne, R. A completeness theorem for operator spaces. *Chem. Phys. Lett.* **1977**, *45*, 470−472.

(23) Brillouin, L. Les problèmes de perturbations et les champs self-consistents. *J. Phys. Radium* **1932**, *3*, 373−389.

(24) Brillouin, L. Le champ self-consistent de Fock pour les électrons des métaux. *J. Phys. Radium* **1934**, *5*, 413−418.

(25) Schirmer, J.; Cederbaum, L. S. The two-particle-hole Tamm-Dancoff approximation (2ph-TDA) equations for closed-shell atoms and molecules. *J. Phys. B: At. Mol. Phys.* **1978**, *11*, 1889−1900.

(26) Schirmer, J.; Cederbaum, L. S.; Walter, O. New approach to the one-particle Green's function for finite Fermi systems. *Phys. Rev. A* **1983**, *28*, 1237−1259.

(27) Schirmer, J.; Angonoa, G. On Green-function calculations of the static self-energy part, the ground state energy, and expectation values. *J. Chem. Phys.* **1989**, *91*, 1754−1761.

(28) Mattuck, R. D. *A Guide to Feynman Diagrams in the Many-body Problem*; McGraw-Hill, New York, 1976.

(29) Handy, N. C.; Pople, J. A.; Head-Gordon, M.; Raghavachari, K.; Trucks, G. W. Size-consistent Brueckner theory limited to double substitutions. *Chem. Phys. Lett.* **1989**, *164*, 185−192.

(30) Baker, J.; Pickup, B. T. A method for molecular ionization potentials. *Chem. Phys. Lett.* **1980**, *76*, 537−541.

(31) Bintrim, S. J.; Berkelbach, T. C. Full-frequency GW without frequency. *J. Chem. Phys.* **2021**, *154*, No. 041101.

(32) Ranasinghe, D. S.; Margraf, J. T.; Perera, A.; Bartlett, R. J. Vertical valence ionization potential benchmarks from equation-of-motion coupled cluster theory and QTP functionals. *J. Chem. Phys.* **2019**, *150*, No. 074108.

(33) Orlando, R.; Romaniello, P.; Loos, P.-F. The three channels of many-body perturbation theory: GW, particle−particle, and electron−hole T-matrix self-energies. *J. Chem. Phys.* **2023**, *159*, No. 184113.
(34) McKechnie, S.; Booth, G. H.; Cohen, A. J.; Cole, J. M. On the accuracy of density functional theory and wave function methods for calculating vertical ionization energies. *J. Chem. Phys.* **2015**, *142*, No. 194114.
(35) Ortiz, J. V. Dyson-orbital concepts for description of electrons in molecules. *J. Chem. Phys.* **2020**, *153*, No. 070902.
(36) Pickup, B. T.; Goscinski, O. Direct calculation of ionization energies. I. Closed shells. *Mol. Phys.* **1973**, *26*, 1013−1035.
(37) Schirmer, J.; Trofimov, A. B.; Stelter, G. A non-Dyson third-order approximation scheme for the electron propagator. *J. Chem. Phys.* **1998**, *109*, 4734−4744.
(38) Møller, C.; Plesset, M. S. Note on an Approximation Treatment for Many-Electron Systems. *Phys. Rev.* **1934**, *46*, 618−622.
(39) von Niessen, W.; Schirmer, J.; Cederbaum, L. S. Computational methods for the one-particle Green's function. *Comput. Phys. Rep.* **1984**, *1*, 57−125.
(40) Ortiz, J. V. The Electron Propagator Picture of Molecular Electronic Structure. In *Computational Chemistry: Reviews of Current Trends*; Leszczynski, J., Ed.; World Scientific: Singapore, 1997; Vol. *2*, pp 1−61.
(41) Ortiz, J. V. A nondiagonal, renormalized extension of partial third-order quasiparticle theory: comparisons for closed-shell ionization energies. *J. Chem. Phys.* **1998**, *108*, 1008−1014.
(42) Dunning, T. H. Gaussian basis sets for use in correlated molecular calculations. I. The atoms boron through neon and hydrogen. *J. Chem. Phys.* **1989**, *90*, 1007−1023.
(43) Frisch, M. J.; Trucks, G. W.; Schlegel, H. B.; Scuseria, G. E.; Robb, M. A.; Cheeseman, J. R.; Scalmani, G.; Barone, V.; Petersson, G. A.; Nakatsuji, H.et al. *Gaussian Development Version, Revision I.14*; Gaussian Inc.: Wallingford CT, 2018.
(44) Raghavachari, K.; Trucks, G. W.; Pople, J. A.; Head-Gordon, M. A fifth-order perturbation comparison of electron correlation theories. *Chem. Phys. Lett.* **1989**, *157*, 479−483.

https://doi.org/10.1021/acs.jpca.5c01079
J. Phys. Chem. A 2025, 129, 3597−3612

Appendix G

E. Opoku, F. Pawłowski and J. V. Ortiz, "New−Generation Electron−Propagator Methods for Calculations of Electron Affinities and Ionization Energies: Tests on Organic Photovoltaic Molecules", *J. Chem. Theory Comp.*, 20, 290–306 (2024)

JCTC Journal of Chemical Theory and Computation

pubs.acs.org/JCTC Article

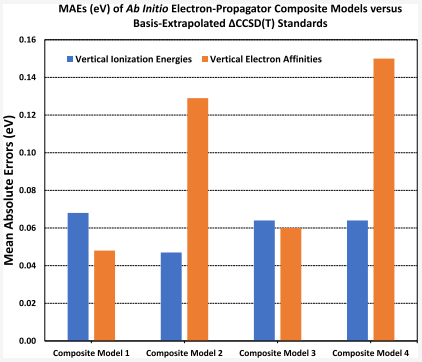
New-Generation Electron-Propagator Methods for Calculations of Electron Affinities and Ionization Energies: Tests on Organic Photovoltaic Molecules

Ernest Opoku, Filip Pawłowski, and J. V. Ortiz*

Cite This: *J. Chem. Theory Comput.* 2024, 20, 290−306 Read Online

ACCESS | Metrics & More | Article Recommendations | Supporting Information

ABSTRACT: A new generation of *ab initio* electron-propagator self-energies recently superseded its antecedents' accuracy and computational efficiency in calculating vertical ionization energies (VIEs) of closed-shell molecules. (See *J. Chem. Phys.* **2021,** *155,* 204107, *J. Chem. Theory Comput.* **2022,** *18,* 4927, *J. Chem. Phys.* **2023,** *159,* 124109.) No adjustable parameters were introduced in the generation of reference orbitals or in the construction of self-energies. The same approach has been extended in this work to vertical electron affinities (VEAs). Calculations were performed on 24 conjugated, organic photovoltaic molecules with diverse functional groups. These molecules are considerably larger than those studied in previous tests on VIEs. Several new-generation self-energies produce mean absolute errors (MAEs) below 0.1 eV versus ΔCCSD(T) (i.e., total energy differences from the coupled-cluster singles, doubles, and perturbative triples method) VIEs and VEAs obtained with identical basis sets. A composite model employs cubically and quintically scaling algorithms and power-law basis-set extrapolations based on augmented double−triple or triple-quadruple ζ data. Its MAEs are near 0.05 eV versus benchmark values, with 0.03 eV error bars for the lowest VIE and the highest VEA of each molecule. A more efficient and equally accurate composite model for calculating VIEs avoids full transformations of electron repulsion integrals to the molecular orbital basis. High probability factors support the diagonal self-energy approximation, wherein Dyson orbitals are proportional to canonical, Hartree−Fock orbitals.

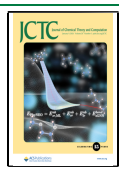


INTRODUCTION

Advocates of reductive and inductive approaches to understanding chemistry agree on the importance of electron-binding energies. Reductionists attempt to deduce molecular properties from fundamental physical principles; inductionists rely on the recognition of patterns in copious data. Experiments that measure electron binding energies test the predictive power of the reductionist methodology. Electron binding energies are perennial inputs for pattern recognition in chemistry. To enable pattern recognition by students, basic chemistry textbooks discuss periodic trends in atomic ionization energies and electron affinities. Qualitative chemical bonding theories typically connect electron binding energies to molecular reactivity and structure. In these theories, electron binding energies often emerge as eigenvalues of an effective operator, whose associated eigenfunctions are delocalized molecular orbitals.

Electron binding energies also may be determined *ab initio* as eigenvalues of an effective operator in the Dyson quasiparticle equation of electron propagator theory (EPT).[1−4] This energy-dependent, nonlocal, and systematically improvable operator has generalized Fock and energy-dependent self-energy components. The generalized Fock component comprises Coulomb and exchange operators that depend on the one-electron-reduced density matrix (1RDM) of the N-electron initial state. This energy-independent operator may be separated into uncorrelated and correlated terms. Whereas the former term is the Fock operator of Hartree−Fock (HF) theory, the latter term is often called the energy-independent (or infinite-energy limit) self-energy, $\sum(\infty)$. Remaining self-energy term describes orbital relaxation in the final states with $N \pm 1$ electrons and the differential effects of electron correlation. This energy-dependent component of the effective operator constitutes the remainder of the self-energy operator, $\sum'(E)$. The effective operator also may be expressed as the sum of the uncorrelated Fock operator and the energy-independent and energy-dependent parts of the self-energy. Electron binding energies equal self-consistent eigenvalues of the effective operator, i.e., where an eigenvalue equals E.

Received: August 30, 2023
Revised: November 16, 2023
Accepted: December 4, 2023
Published: December 27, 2023



ACS Publications © 2023 American Chemical Society

https://doi.org/10.1021/acs.jctc.3c00954
J. Chem. Theory Comput. 2024, 20, 290−306

Associated eigenfunctions are proportional to Dyson orbitals[5,6] whose norms are easily inferred from derivatives of the eigenvalues with respect to the energy. (Norms are also known as probability factors, intensity factors, or pole strengths.) Dyson orbitals associated with electron binding energies are scaled overlaps between initial and final states.[5] They may be used to calculate transition probabilities in the sudden approximation for a variety of spectroscopic and scattering experiments. Summing the squared moduli of the Dyson orbitals associated with energies of electron removal yields the electron density function of the initial state. The same set of Dyson orbitals can be used to construct the initial state's 1RDM. In combination with electron binding energies, the Dyson orbitals also are related to the initial state's total energy. In general, the Dyson orbitals constitute an overcomplete set of one-electron functions that describe initial-state properties and transitions between initial and final states. A complete, one-electron picture of electronic structure that rigorously generalizes uncorrelated molecular orbital concepts emerges from solutions of the Dyson quasiparticle equation.

EPT[7−10] therefore provides an ideal framework for calculating a molecule's lowest ionization energy (IE), largest electron affinity (EA), and associated Dyson orbitals *ab initio*. Dyson orbitals are generated in every calculation of an electron binding energy, and one-electron interpretations are thereby facilitated. Since the advent of EPT methods in the 1970s, many approximations of the effective operator of the Dyson quasiparticle equation have been introduced. (See acronyms and definitions in Table 1.) The utility of competing approximations may be judged according to three criteria: predictive accuracy, computational efficiency, and interpretive transparency. This review aims to compare accuracy and efficiency and to conserve transparency. Therefore, methods that introduce adjustable parameters in the generation of reference orbitals or in the construction of self-energies are excluded henceforth.

In perturbative, *ab initio* EPT, the most frequently chosen zeroth order approximation employs the canonical HF (CHF) orbitals and energies of Koopmans's identity.[11] The mean absolute error (MAE) at this level lay between 1 and 2 eV in recent tests on outer-valence, vertical IEs (VIEs) of closed-shell molecules.[12] [VIE data based on equation-of-motion, coupled-cluster (EOM-CC) calculations of near full configuration interaction accuracy in a fixed basis constitute the standards of comparison.[13] CHF orbital energies for several classes of molecules (e.g., *N*-heterocyclic molecules and nucleic-acid bases) frequently produce incorrect sequences of final states known as Koopmans defects.[14−16] The nondiagonal, second-order self-energy[17] (ND2) often suffices to restore the correct order of final states, but it usually overestimates the needed corrections. The resulting underestimates of VIEs typically persist even when large, flexible basis sets are used.[18] For the first few VIEs of a closed-shell molecule, the second-order self-energy matrix tends to be diagonally dominant in the CHF basis. Neglect of off-diagonal elements produces only minor changes in the numerical results. This outcome suggests that CHF orbitals are usually good zeroth-order approximations to Dyson orbitals for these final states.[19] Assumption of a diagonal second-order (D2) self-energy matrix leads to algorithms whose arithmetic bottlenecks scale cubically. These algorithms therefore are practically effortless once the transformation of the electron repulsion integrals (ERIs) to the CHF basis is complete. Unfortunately, the MAE of this method (see Figure 1) remained high at approximately 0.6−0.7 eV for outer-valence VIEs whose probability factors are above 0.85.[12] The diagonal third-order[20] (D3) self-energy's MAE was larger than that of D2 despite the fifth-power arithmetic scaling of the additional calculations.[12] A major advance was based on the observation that D3 results tend to overestimate VIEs, whereas those of D2 underestimate them. A remedy appeared in the form of approximations to infinite-order summations (i.e., renormalizations) of certain classes of self-energy terms. These approximations require only trivial calculations that involve ratios of certain second-order and third-order contributions.[21] The A, B, and C versions of the outer-valence Green function (OVGF)[10] succeeded in lowering MAEs to 0.2−0.3 eV. Part of this success was based on a selection procedure containing several parameters.[22] Better results were achieved with the partial third-order (P3) self-energy[23] and its approximately renormalized extension, P3+.[24] The latter methods also feature an arithmetic bottleneck (O^2V^3, where O and V respectively are the dimensions of the occupied and virtual orbital sets) that

Table 1. Acronyms for Approximate, Electron-Propagator Self-Energies

acronym[a]	full name
	Diagonal Self-Energies
D2	diagonal second order
os-D2	opposite-spin D2
nD-D2	non-Dyson D2
os-nD-D2	opposite-spin non-Dyson D2
D3	diagonal third order
nD-D3	non-Dyson D3
OVGF	outer-valence Green's function (versions A, B, and C)
nD-OVGF	non-Dyson OVGF (versions A, B, and C)
P3	partial third order
P3+	approximately renormalized partial third order
Q3	quasiparticle third order
Q3+	approximately renormalized quasiparticle third order
L3	linear third order
nD-L3	non-Dyson L3
L3+	approximately renormalized linear third order (versions A, B, and C)
nD-L3+	non-Dyson L3+ (versions A, B, and C)
RP3	explicitly renormalized partial third order
RQ3	explicitly renormalized quasiparticle third order
RL3	explicitly renormalized linear third order
nD-RL3	non-Dyson RL3
DR	diagonal (renormalized) ring approximation (HF-TDA-G_0W_0)
	Nondiagonal Self-Energies
ND2	nondiagonal, second order
2ph-TDA	two-particle-one-hole Tamm−Dancoff approximation
3+	nondiagonal third order
ADC(3)	third-order algebraic diagrammatic construction
NR2	nondiagonal, renormalized, second order
BD-T1	Brueckner doubles with triple-field operators
NRP3	nondiagonal extension of RP3
NRQ3	nondiagonal extension of RQ3
NRL3	nondiagonal extension of RL3
CMX, $X = 1-4$	composite model X

[a]For new-generation methods in bold type: *N* = nondiagonal; nD = non-Dyson; R = explicitly renormalized; + = approximately renormalized.

https://doi.org/10.1021/acs.jctc.3c00954
J. Chem. Theory Comput. 2024, 20, 290−306

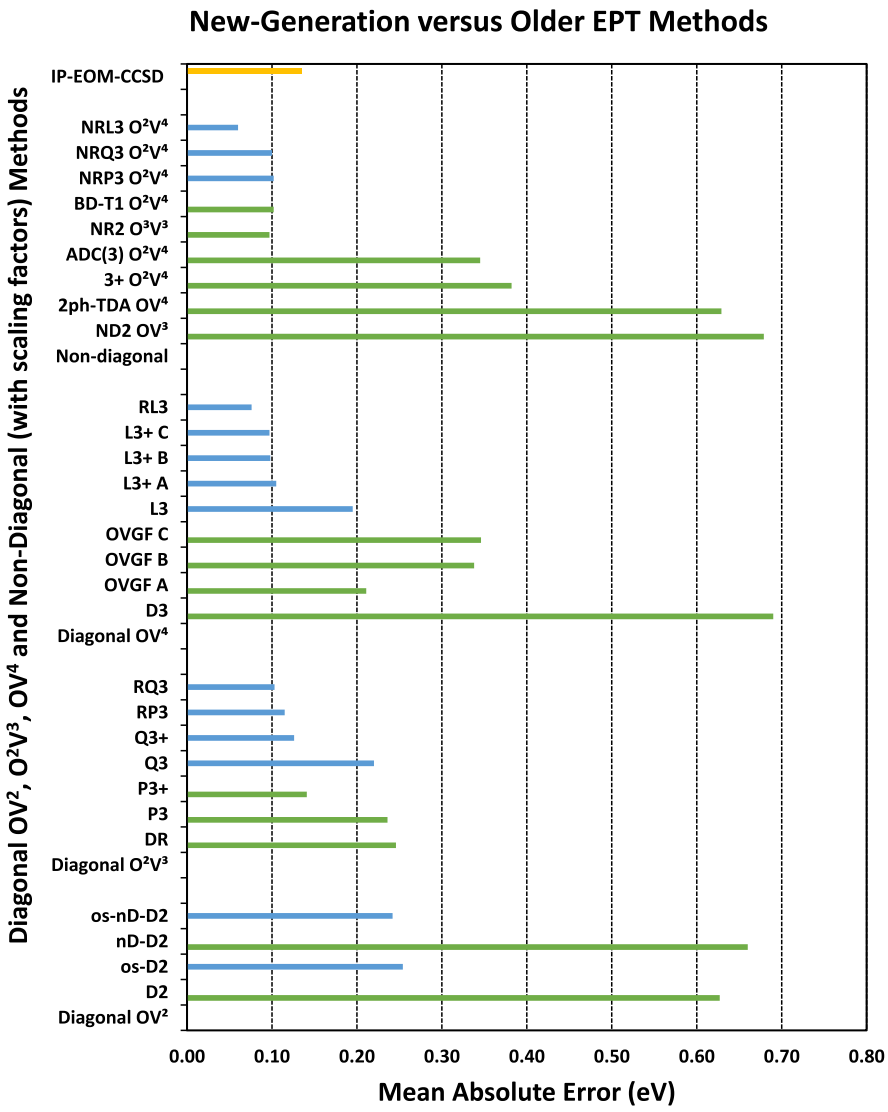
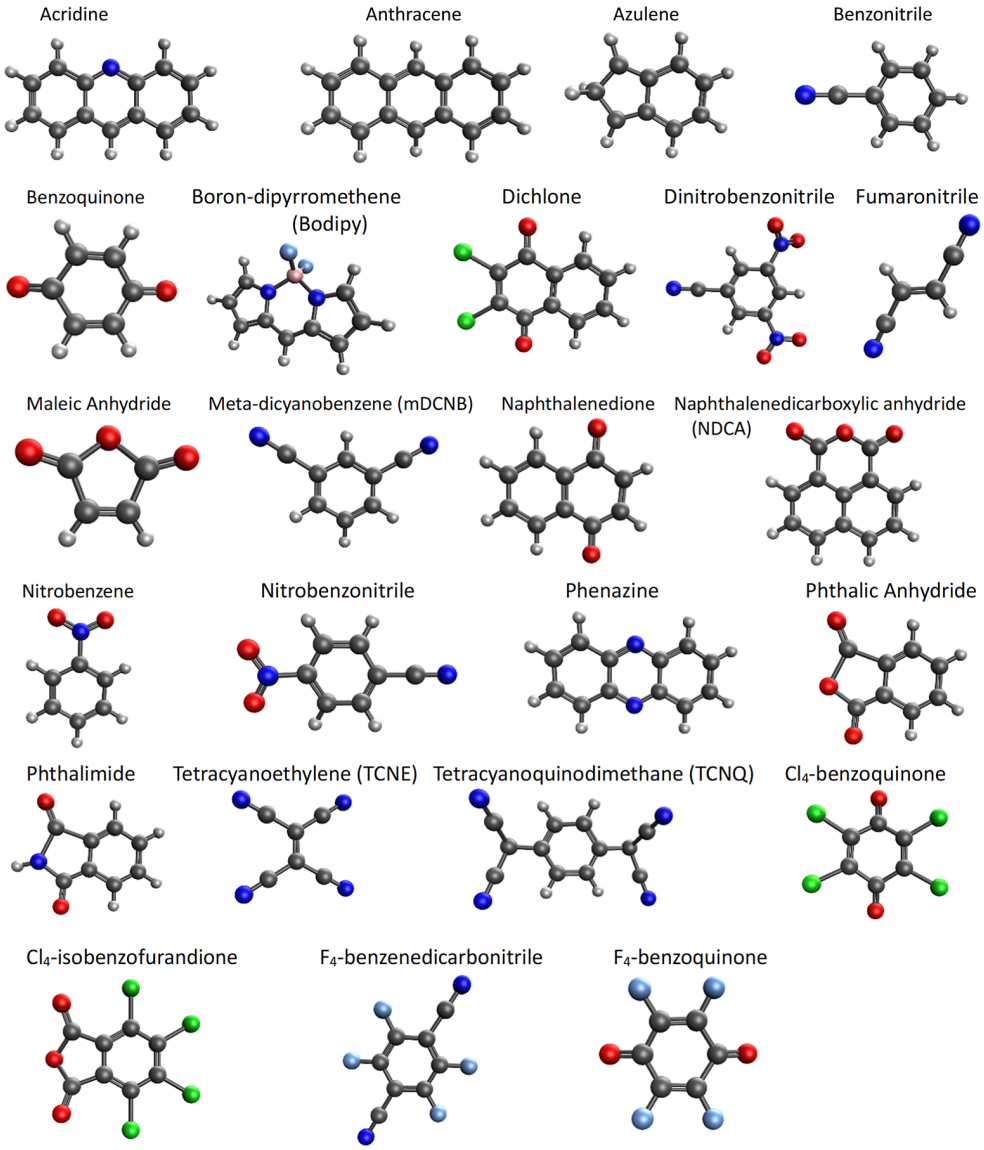


Figure 1. Mean absolute errors[a] (eV) versus IP-EOM-CCSDT/cc-pVTZ standards for 96 outer-valence VIEs and arithmetic scaling factors.[12] [a]New-generation EPT, older EPT, and IP-EOM-CCSD MAEs are represented by blue, green and yellow bars, respectively.

is lower than that (OV^4) of D3 and OVGF. (In P3+ calculations, an approximate renormalization that resembles that of the B version of OVGF is employed; no selection procedure is introduced.) All diagonal methods such as OVGF and P3+ produce Dyson orbitals that equal a CHF orbital multiplied by the square root of the probability factor, Π. Diagonal methods are applicable only to outer-valence VIEs in which Koopmans' results are qualitatively valid (i.e., where Π > 0.85). They cannot be applied to correlation (i.e., shakeup) final states.

The latter restriction may be overcome by abandoning the diagonal self-energy approximation and introducing explicitly evaluated (i.e., not approximated) renormalizations. In the two-particle-one-hole Tamm−Dancoff approximation (2ph-TDA) self-energy,[25] there are ring, ladder, and mixed ring-ladder diagrams in all orders of the Møller−Plesset fluctuation potential.[26] These diagrams are expressed in terms of antisymmetric, two-electron vertices that include direct and exchange terms. This level of theory suffices to produce a first-order description of correlation of final states. Unfortunately, its relatively high MAEs for outer-valence VIEs do not justify its quintic (OV^4) arithmetic scaling.[12] Inclusion of additional terms that occur in the third-order self-energy results in the 3+ method.[27] This approximation also is known as the strict version of the third-order algebraic diagrammatic construction, or ADC(3).[28] The latter method may be implemented with noniterative sixth power (O^2V^4) contractions or with an increased number of quintic steps. Improved treatments of the energy-independent self-energy that are complete through the fourth order are present in the standard ADC(3) version, which involves iterative sixth power summations.[29] Non-Dyson (nD) versions of ADC(3) restricted to VIEs reduce the number of bottleneck steps.[30] MAEs for valence VIEs exceeded 0.3 eV in several tests of ADC(3) versions.[12,31,32] A fourth-order extension, ADC(4),[28] also has been implemented;[33] ADC(2) is identical to ND2. The nondiagonal, renormalized, second-order (NR2) method[34] recovers all terms in P3 and explicitly evaluates the renormalizations estimated in P3+. NR2 introduces only a noniterative bottleneck with O^3V^3 arithmetic scaling and obtains MAEs near 0.2 eV.[12] For difficult cases where correlation in the initial state is relatively strong, the Brueckner doubles (BD),[35−40] triple-field operator (BD-

https://doi.org/10.1021/acs.jctc.3c00954
J. Chem. Theory Comput. 2024, 20, 290−306



[a] Color Code: H=light gray; B=pink; C=gray; N=blue; O=red; F=light blue; and Cl=green.

Figure 2. 24 organic photovoltaic molecules. Color code: H = light gray; B = pink; C = gray; N = blue; O = red; F = light blue; and Cl = green.

T1)[41−44] method may be employed. It requires O^2V^4 contractions in its coupled-cluster amplitude optimizations and yields MAEs of approximately 0.1 eV.[12] Several methods based on multiconfigurational, self-consistent-field Ansätze for initial states also have been introduced.[45−47] All nondiagonal methods (including 2ph-TDA, 3+, ADC(3), NR2, and BD-T1) produce Dyson orbitals as a linear combination of CHF or BD orbitals. This advantage does not necessarily imply that predictions of electron binding energies will be superior to those of the best diagonal self-energies.

Recently, a new generation of diagonal self-energy approximations (see blue MAE bars in Figure 1) for VIEs of closed-shell molecules has surpassed its antecedents' predictive accuracy and computational efficiency.[12,48,49] (Corrections to formulas published in the latter works have been published recently.[50,51]) The opposite-spin, second-order (os-D2) self-energy and its non-Dyson counterpart (os-nD-D2) have cubic scaling and a much lower MAE (near 0.2 eV) than D2 or nD-D2. The approximately renormalized, third-order quasiparticle (Q3+) method improves slightly on P3+ (MAE ≈ 0.15 eV) without changing the arithmetic scaling of the bottleneck contractions. The approximately renormalized, linear, third-order, version B (L3+B) self-energy has the same arithmetic scaling as OVGF, but a lower MAE near 0.1 eV. Explicitly renormalized versions of these diagonal methods, RQ3 and RL3, respectively, produce slight improvements over Q3+ and L3+B. They also surpass another explicitly renormalized, diagonal method that belongs to the G_0W_0 family of methods and that employs CHF orbitals and Tamm−Dancoff excitations.[52] Like other G_0W_0 methods, this completely *ab initio* self-energy sums ring diagrams (without exchange) in all orders of the fluctuation potential. It simultaneously constitutes a diagonal simplification of 2ph-TDA in which ring-exchange and ladder terms are neglected. In previous studies, it has been denominated by the relatively long acronym HF-TDA-G_0W_0, but here it is called simply the

https://doi.org/10.1021/acs.jctc.3c00954
J. Chem. Theory Comput. 2024, 20, 290−306

diagonal ring (DR) approximation. The latest extension of the new generation includes nondiagonal methods that contain all terms found in their diagonal antecedents.[53] Slight improvements in MAEs are realized by the nondiagonal NRQ3 and NRL3 methods over their explicitly renormalized, diagonal counterparts, RQ3 and RL3. These results indicate that fortuitous error cancellations pertaining to the diagonal approximation are not responsible for its success. MAEs for NRQ3 and NRL3 lie between 0.05 and 0.1 eV for outer-valence VIEs.

Considerably less is known about the performance of *ab initio* electron-propagator methods for the calculation of vertical EAs (VEAs) of closed-shell molecules. Various ADC methods have been applied chiefly to uncharged initial states without vertically bound anions in small basis-set calculations or to cationic initial states.[54] Electron correlation is likely to be weak in both cases. Unbound anions of six closed-shell atoms, five nucleobases, and five small molecules and bound anions of six other small molecules were considered in another study.[55] A set of 16 VEAs of eight small molecules, 15 of which are negative in reference calculations, also has been calculated.[56] MAEs of approximately 0.1 eV have been reported for a small number of cases that pertain to positive VEAs of closed-shell molecules.

Practical calculations that involve bound anionic final states require basis sets with many diffuse and polarization functions. Therefore, standard data that incorporate basis-set extrapolations on uncharged, closed-shell initial states and anionic doublet final states are needed. Such a data set was generated recently to examine the performance of density functional models, the G_0W_0 family of approximations, and electron propagator methods.[57−61] The 24 organic acceptors of Figure 2 were selected; these molecules are relevant to the optimization of photovoltaic materials. VIEs and VEAs were determined by extrapolated ΔCCSD(T) and ΔMP2 (second-order many-body perturbation theory) calculations. The authors assumed the additivity of basis-set and postsecond-order correlation effects and estimated uncertainties of 0.03 eV in these standard data.[57]

In the present work, the new generation of diagonal self-energies is tested on the 23 VEAs and 24 VIEs of the same closed-shell molecules. One anion is discarded because it is not vertically bound. Such numerical results are artifacts of basis sets that provide weak tests of a method's ability to describe relaxation and correlation effects. Each molecule is considerably larger than those included in the data set of nearly full-configuration-interaction quality produced with the cc-pVTZ basis set for VIEs.[13]

Before performing these numerical tests, distinct formulas are required to define the VEA counterparts of the P3+, Q3+, RP3, and RQ3 self-energies for VIEs. In nD variants for VEAs (as opposed to VIEs), terms with 2hp denominators (instead of 2ph-denominator terms) are evaluated noniteratively with respect to energy. Because V is much larger than O in most practical applications, almost no arithmetic advantage is realized. In all other cases, only the orbital index of the diagonal self-energy matrix elements needs to be changed from occupied to virtual. The corresponding arithmetic bottlenecks are unaffected.

THEORY

Dyson Quasiparticle Equation. The $p-q$ element of the double-time, electron-propagator matrix

$$\langle\langle a_p(t);\ a_q^\dagger(t')\rangle\rangle = -i\Theta(t-t')\langle\Psi_0^N|a_p(t)a_q^\dagger(t')|\Psi_0^N\rangle + i\Theta(t'-t)\langle\Psi_0^N|a_q^\dagger(t')a_p(t)|\Psi_0^N\rangle \quad (1)$$

is defined in terms of the N-electron reference eigenstate, Ψ_0^N, the Heaviside step function (Θ), and an orthonormal spin−orbital basis, u, with general indices p, q, r, ...[7] After a Fourier transform between the time (t) and energy (E) regimes, the resulting spectral form

$$\langle\langle a_p;\ a_q^\dagger\rangle\rangle_E = \lim_{\eta\to 0^+}\left[\sum_R \frac{\langle\Psi_0^N|a_p|R\rangle\langle R|a_q^\dagger|\Psi_0^N\rangle}{E + E_0(N) - E_R(N+1) + i\eta} + \sum_S \frac{\langle\Psi_0^N|a_q^\dagger|S\rangle\langle S|a_p|\Psi_0^N\rangle}{E - E_0(N) + E_S(N-1) - i\eta}\right] = G_{pq}(E) \quad (2)$$

requires summations over final-state eigenfunctions with $N \pm 1$ electrons. Poles of this energy-dependent function occur when one of the denominators in the R or S summations vanishes. These values of E correspond respectively to energies of electron attachment and detachment. Residues of the electron propagator (i.e., numerators corresponding to vanishing denominators) equal products of Feynman−Dyson amplitudes

$$f_p^R = \langle\Psi_0^N|a_p|R\rangle \quad (3)$$

$$g_p^S = \langle S|a_p|\Psi_0^N\rangle \quad (4)$$

In the u basis, these amplitudes are coefficients in the expansion of Dyson spin−orbitals[5] of electron attachment and detachment so that

$$\varphi_R^{\text{Dyson}}(x_1) = \sqrt{N+1}\int \Psi_0^{N*}(x_2, x_3, x_4, \cdots, x_{N+1})\Psi_R(x_1, x_2, x_3, \cdots, x_{N+1})\mathrm{d}x_2\ \mathrm{d}x_3\ \mathrm{d}x_4\cdots\mathrm{d}x_{N+1} = \sum_R f_p^R u_p(x_1) \quad (5)$$

$$\varphi_S^{\text{Dyson}}(x_1) = \sqrt{N}\int \Psi_S^{*}(x_2, x_3, x_4, \cdots, x_N)\Psi_0^N(x_1, x_2, x_3, \cdots, x_N)\mathrm{d}x_2\ \mathrm{d}x_3\ \mathrm{d}x_4\cdots\mathrm{d}x_N = \sum_S g_p^S u_p(x_1) \quad (6)$$

In the electron-propagator methods examined in this work, poles of $\mathbf{G}(E)$, the electron-propagator matrix, occur at energies (E_X) that satisfy the Dyson quasiparticle equation

$$[\mathbf{F} + \mathbf{\Sigma}(E_X)]\mathbf{C}(E_X) = E_X\mathbf{C}(E_X) \quad (7)$$

The poles are eigenvalues of an energy-dependent operator with two terms. The first term (F) is the usual Fock operator of the Hartree−Fock theory. Second is the self-energy operator, $\sum(E)$, which describes electron correlation and orbital relaxation. Energy-independent (i.e., constant) self-energy terms are included in $\sum(E)$. The probability factor (or norm of the Dyson spin−orbital[5]), Π, may be calculated with

https://doi.org/10.1021/acs.jctc.3c00954
J. Chem. Theory Comput. 2024, 20, 290−306

$$\Pi_X = \int |\varphi_X^{\text{Dyson}}(x)|^2 \mathrm{d}x = \left(1 - \mathbf{C}^{\dagger}(E_X)\left[\frac{\mathrm{d}\mathbf{\Sigma}(E)}{\mathrm{d}E}\right]_{E=E_X}\mathbf{C}(E_X)\right)^{-1} \quad (8)$$

Feynman−Dyson amplitudes and Dyson spin−orbitals may be inferred from the eigenvectors with

$$\varphi_X^{\text{Dyson}}(x) = \Pi_X^{0.5}\sum_p C_p(E_X)u_p(x) \quad (9)$$

Methods that employ CHF spin−orbitals and ignore off-diagonal elements of the self-energy matrix are the chief concerns of this work. Each CHF spin−orbital corresponds to a set of electron binding energies obtained after iterating with respect to E in the diagonal quasiparticle equation

$$e_p^{\text{HF}} + \Sigma_{pp}(E_{Xp}) = E_{Xp} \quad (10)$$

In eq 10, Koopmans' results (e_p^{HF}) are improved only by diagonal elements of the self-energy matrix. Probability factors are obtained from

$$\Pi_{Xp} = \left[1 - \left.\frac{\mathrm{d}\Sigma_{pp}(E)}{\mathrm{d}E}\right|_{E=E_{Xp}}\right]^{-1} \quad (11)$$

and Dyson spin−orbitals become proportional to CHF spin−orbitals

$$\varphi_{Xp}^{\text{Dyson}}(x) = \Pi_{Xp}^{0.5}u_p^{\text{HF}}(x) \quad (12)$$

For a given spin−orbital p, many values of E_{Xp} exist, but usually only those poles with $\Pi > 0.85$ are sought. In the diagonal self-energy approximation, the sum of the probability factors for a given p equals unity. The remaining electron binding energies with low values of Π provide only a rough description of the correlation states. Such states are better described by renormalized, nondiagonal self-energy approximations.

Self-Energy Approximations. Self-energy approximations of the new generation and some of their most widely used antecedents have been examined in several recent numerical studies.[12,48,49,53] A list of acronyms is shown in Table 1. For each approximation, arithmetic bottlenecks are given in terms of the dimensions of the occupied (O) and virtual (V) orbital spaces in Table 2. Most of the self-energy formulas are identical for calculations of VIEs and VEAs. For these cases, self-energy formulas remain the same for all values of p in eq 10. Different formulas for VIEs and VEAs apply to the P3, P3+, Q3, Q3+, RP3, and RQ3 self-energies. In addition, the non-Dyson (nD) versions of D2, os-D2, OVGF, L3, L3+, and RL3 self-energies deactivate energy dependence in 2ph denominators for VIE calculations and in 2hp denominators for VEA calculations. This deactivation is achieved by setting the $E = \varepsilon_p$ in the self-energy terms with these denominators.

D2 self-energy matrix elements have two (2hp and 2ph) summations over CHF spin−orbitals

Table 2. Arithmetic Scaling and Transformed Integral Requirements of Electron-Propagator Methods[a]

method class	methods[b]	arithmetic bottleneck	bottleneck steps	largest ERI[c] subset
diagonal 2nd order	D2, **os-D2**	OV^2	N_E	O^2V^2
	RSPT2, nD-D2, **os-nD-D2**	OV^2	1	O^2V^2
diagonal post 2nd order	RSPT3	OV^4	1	V^4
	D3, OVGF	OV^4	N_E[d]	V^4
	P3, P3+, **Q3, Q3+** (IEs)	O^2V^3	1	OV^3
	P3, P3+, **Q3, Q3+** (EAs)	OV^4	1	V^4
	L3, L3+	OV^4	N_E[d]	V^4
	RP3, RQ3 (IEs)	O^2V^3	1	OV^3
	RP3, RQ3 (EAs)	OV^4	1	V^4
	RL3	OV^4	N_IN_E[d]	V^4
	DR (IEs)	O^2V^3	N_IN_E	O^2V^2
	DR (EAs)	O^2V^3	N_IN_E	OV^3
nondiagonal	ND2	OV^3	N_I	OV^3
	2ph-TDA	OV^4	N_I	V^4
	3+	O^2V^4	1	V^4
	ADC(3)	O^2V^4	N_I	V^4
	NR2 (IEs)	O^2V^3	1	OV^3
	NR2 (EAs)	OV^4	1	V^4
	BD-T1	O^2V^4	BD[e]	V^4

[a] O = number of occupied orbitals, V = number of virtual orbitals, N_E = energy iterations, N_I = inverse-expansion iterations. [b] New methods in bold type. [c] ERI = electron repulsion integral. [d] Reduction by a factor of N_E occurs in non-Dyson (nD) versions. [e] The O^2V^4 arithmetic bottleneck occurs in the Brueckner Doubles, coupled-cluster, reference-state calculation; the subsequent electron-propagator bottleneck is OV^4.

$$\Sigma_{pp}^{D2}(E) = \frac{1}{2}\sum_a^{\text{vir}}\sum_{ij}^{\text{occ}}\frac{|\langle pa||ij\rangle|^2}{E + \varepsilon_a - \varepsilon_i - \varepsilon_j} + \frac{1}{2}\sum_i^{\text{occ}}\sum_{ab}^{\text{vir}}\frac{|\langle pi||ab\rangle|^2}{E + \varepsilon_i - \varepsilon_a - \varepsilon_b} = S_{2\text{hp}} + S_{2\text{ph}} \quad (13)$$

(Energy dependence is suppressed in the $S_{2\text{hp}}$ and $S_{2\text{ph}}$ notations for the 2hp and 2ph summations.) At $E = \varepsilon_p$, the second-order, Rayleigh−Schrödinger perturbation theory (RSPT2) expression is recovered.[62−64] Same-spin and opposite-spin terms in the two summations have been assigned empirically optimized weights with respect to small data sets in several modified self-energies.[65−68] To avoid the introduction of adjustable parameters, a more easily interpretable alternative simply neglects the same-spin terms. This option depends on the antisymmetric reference determinant and the opposite-spin self-energy to deliver a balanced account of exchange and correlation. This resulting opposite-spin, second-order self-energy is denoted by os-D2.[12,48] In VIE calculations, the nD approach yields a diagonal second-order self-energy identical to D2 except that the second (2ph) term is energy-independent, with $E = \varepsilon_p$ for electron detachments.[69] The roles of the 2hp and 2ph terms are reversed in the EA calculations. The nD-D2 and os-nD-D2 alternatives are based on these modifications. The nD methods procure a minor

https://doi.org/10.1021/acs.jctc.3c00954
J. Chem. Theory Comput. 2024, 20, 290−306

advantage for VIEs, for the usual OV^2 bottleneck is no longer energy-dependent. It therefore requires no iterations. For VEA calculations, the O^2V (2hp) term no longer requires iterations, but this computational advantage is negligible. In practice, the bottleneck occurs during the ERI transformation to the CHF basis, which may be reduced from fifth to fourth power dependence for a given p.

First-order couplings between f_3 operators in the 2ph-TDA[25] self-energy

$$\sum^{\text{2ph-TDA}}(E) = [\mathbf{a}^\dagger|\hat{H}\mathbf{f}_3]_1[\mathbf{f}_3|(E\hat{I} - \hat{H})\mathbf{f}_3]_1^{-1}[\mathbf{f}_3|\hat{H}\mathbf{a}^\dagger]_1 \quad (14)$$

generate ring and ladder terms of all orders with antisymmetrized vertices [i.e., ERIs where $\langle pq||rs\rangle = \langle pq|rs\rangle - \langle pq|sr\rangle = (pr||qs) = (pr|qs) - (ps|qr)$]. (See previous studies on the new generation of self-energies for a derivation that employs the super operator notation of eq 14.[12,48,53]) A member of the G_0W_0 family of methods that lies within the scope of the present study may be defined with three simplifications. After neglecting off-diagonal elements of $\sum(E)$, ladder and ring-exchange terms in the $[\boldsymbol{f}_3|(E\hat{I} - \hat{H})\boldsymbol{f}_3]_1$ matrix and exchange terms in the $[\boldsymbol{a}^\dagger|\hat{H}\mathbf{f}_3]_1$ and $[\mathbf{f}_3|\hat{H}\boldsymbol{a}^\dagger]_1$ matrices are omitted. Instead of the customary random-phase-approximation excitation energies and transition amplitudes of the G_0W_0 methodology, their Tamm−Dancoff approximation (TDA) counterparts are embedded in this approximate self-energy. The resulting HF-TDA-G_0W_0 or DR (vide supra) self-energy contains a subset of terms that occur in eq 14. (Details are presented in Appendix A.) Another alternative, the T-matrix method, retains ladders and neglects ring- and ring-exchange terms.

All terms through third order only are represented by

$$\begin{aligned}\sum^{(3)}(E) = \sum^{(2)}(E) + \sum\nolimits_3(\infty) + [\mathbf{a}^\dagger|\hat{H}\mathbf{f}_3]_1 \\ [\mathbf{f}_3|(E\hat{I} - \hat{H})\mathbf{f}_3]_0^{-1}[\mathbf{f}_3|\hat{V}\mathbf{f}_3]_1[\mathbf{f}_3|(E\hat{I} - \hat{H})\mathbf{f}_3]_0^{-1} \\ [\mathbf{f}_3|\hat{H}\mathbf{a}^\dagger]_1 + [\mathbf{a}^\dagger|\hat{H}\mathbf{f}_3]_2[\mathbf{f}_3|(E\hat{I} - \hat{H})\mathbf{f}_3]_0^{-1}[\mathbf{f}_3|\hat{H}\mathbf{a}^\dagger]_1 \\ + [\mathbf{a}^\dagger|\hat{H}\mathbf{f}_3]_1[\mathbf{f}_3|(E\hat{I} - \hat{H})\mathbf{f}_3]_0^{-1}[\mathbf{f}_3|\hat{H}\mathbf{a}^\dagger]_2 \quad (15)\end{aligned}$$

where $\hat{V}$ is the fluctuation-potential superoperator. D3 retains only the diagonal elements in eq 15. At $E = e_p$ D3 equals the third-order, Rayleigh−Schrödinger perturbation theory (RSPT3) result.[62−64] Elements of the D3 self-energy matrix may be collected in eight terms as

$$\begin{aligned}\sum^{(3)} = S_{2hp} + S_{2ph} + C_D + C_S + R_{2hp} + R_{2ph} + P_{2hp} \\ + P_{2ph} \quad (16)\end{aligned}$$

Constant terms arising from first-order double and second-order single replacements in the reference state are denoted by the third and fourth terms of eq 16 and the second term of eq 15. Ring and ladder terms occur in the fifth and sixth positions of eq 16 and the third term of eq 15. Energy-dependent terms that involve perturbative first-order double replacements (i.e., vertex corrections) are in the seventh and eighth positions of eq 16 and the fourth and fifth terms of eq 15. Summations in R_{2hp} and R_{2ph} have two energy-dependent denominators. The P_{2hp} and P_{2ph} terms have contributions from the last two matrix products in $\sum^{(3)}(E)$ that are Hermitian conjugates of each other. Explicit formulas for the six third-order summations appear in Appendix B.[10,27]

A new generation of approximate self-energies recently has been based on an intermediately normalized, Hermitized superoperator metric[12,48,50,51]

$$\begin{aligned}[X|Y] = \frac{1}{2}(\langle \text{HF}|(X^\dagger Y + YX^\dagger)(1 + T_2^{(1)} + T_1^{(2)})| \\ \text{HF}\rangle + \langle \text{HF}|(1 + T_2^{(1)} + T_1^{(2)})^\dagger(X^\dagger Y + YX^\dagger)| \\ \text{HF}\rangle) \quad (17)\end{aligned}$$

where X and Y may be h, p, 2hp, or 2ph operators. First-order, double, and second-order, single replacements appearing in

$$\begin{aligned}T_2^{(1)} &= \frac{1}{4}\sum_{ij}^{\text{occ}}\sum_{ab}^{\text{vir}}\frac{\langle ij||ab\rangle}{e_i + e_j - e_a - e_b}a_a^\dagger a_b^\dagger a_i a_j \\ &= \frac{1}{4}\sum_{ij}^{\text{occ}}\sum_{ab}^{\text{vir}} t_{ij}^{ab(1)}a_a^\dagger a_b^\dagger a_i a_j \quad (18)\end{aligned}$$

$$\begin{aligned}T_1^{(2)} &= \sum_{i}^{\text{occ}}\sum_{a}^{\text{vir}}\frac{1}{2(e_i - e_a)}\Big(\sum_{jk}^{\text{occ}}\sum_{b}^{\text{vir}} t_{jk}^{ab(1)}\langle bi| \\ &\quad |jk\rangle + \sum_{j}^{\text{occ}}\sum_{bc}^{\text{vir}} t_{ij}^{bc(1)}\langle bc||aj\rangle\Big)a_a^\dagger a_i \\ &= \sum_{i}^{\text{occ}}\sum_{a}^{\text{vir}} t_i^{a(2)}a_a^\dagger a_i \quad (19)\end{aligned}$$

occur linearly in the resulting elements of the Hermitian superoperator matrix. All third-order terms that can be generated with this linear choice of metric and ring-ladder renormalizations are retained in the RL3 self-energy

$$\begin{aligned}\boldsymbol{\Sigma}^{\text{RL3}}(E) = \frac{1}{2}(\mathbf{C}_S + [\mathbf{a}^\dagger|\hat{H}\mathbf{f}_{2ph}]_2[\mathbf{f}_{2ph}|(E\hat{I} - \hat{H})\mathbf{f}_{2ph}]_1^{-1} \\ [\mathbf{f}_{2ph}|\hat{H}\mathbf{a}^\dagger]_1 + [\mathbf{a}^\dagger|\hat{H}\mathbf{f}_{2ph}]_1[\mathbf{f}_{2ph}|(E\hat{I} - \hat{H})\mathbf{f}_{2ph}]_1^{-1} \\ [\mathbf{f}_{2ph}|\hat{H}\mathbf{a}^\dagger]_2 + [\mathbf{a}^\dagger|\hat{H}\mathbf{f}_{2hp}]_1[\mathbf{f}_{2hp}|(E\hat{I} - \hat{H})\mathbf{f}_{2hp}]_1^{-1} \\ [\mathbf{f}_{2hp}|\hat{H}\mathbf{a}^\dagger]_2 + [\mathbf{a}^\dagger|\hat{H}\mathbf{f}_{2hp}]_2[\mathbf{f}_{2hp}|(E\hat{I} - \hat{H})\mathbf{f}_{2hp}]_1^{-1} \\ [\mathbf{f}_{2hp}|\hat{H}\mathbf{a}^\dagger]_1) \quad (20)\end{aligned}$$

where $\mathbf{C}_S$ is the nondiagonal matrix generalization of C_S. The ring and ladder terms are identical to those encountered in 2ph-TDA, 3+, and ADC(3), but the terms that are linear in reference-state correlation amplitudes are now multiplied by a factor of one-half because of eq 17. These terms are usually the largest in the D3 self-energy, and they are chiefly responsible for the typical overestimates of third-order VIE results.

The lengthiest arithmetic operations in RL3 involve couplings between 2ph operators occurring in third and higher orders, for they require ERIs with four virtual indices. These terms usually have relatively little importance in calculations of VIEs.[23] Their neglect defines a renormalized, quasi-particle self-energy for the calculation of VIEs (denoted by RQ3) that retains RL3's 2hp, third-order terms. RQ3 calculations for VEAs may be defined by instead neglecting 2hp terms in third order so that

https://doi.org/10.1021/acs.jctc.3c00954
J. Chem. Theory Comput. 2024, 20, 290−306

$$\boldsymbol{\Sigma}^{\mathrm{RQ3}}(E) = \frac{1}{2}\mathbf{C}_{\mathrm{S}} + [\mathbf{a}^{\dagger}|\hat{H}\mathbf{f}_{2\mathrm{hp}}]_1[\mathbf{f}_{2\mathrm{hp}}|(E\hat{I} - \hat{H})\mathbf{f}_{2\mathrm{hp}}]_0^{-1} [\mathbf{f}_{2\mathrm{hp}}|\hat{H}\mathbf{a}^{\dagger}]_1 + \frac{1}{2}[\mathbf{a}^{\dagger}|\hat{H}\mathbf{f}_{2\mathrm{ph}}]_2[\mathbf{f}_{2\mathrm{ph}}|(E\hat{I} - \hat{H})\mathbf{f}_{2\mathrm{ph}}]_1^{-1} [\mathbf{f}_{2\mathrm{ph}}|\hat{H}\mathbf{a}^{\dagger}]_1 + \frac{1}{2}[\mathbf{a}^{\dagger}|\hat{H}\mathbf{f}_{2\mathrm{ph}}]_1[\mathbf{f}_{2\mathrm{ph}}|(E\hat{I} - \hat{H})\mathbf{f}_{2\mathrm{ph}}]_1^{-1} [\mathbf{f}_{2\mathrm{ph}}|\hat{H}\mathbf{a}^{\dagger}]_2 \quad (21)$$

The second term is the 2hp summation in the usual, second-order self-energy (i.e., the first term in eq 13). Dropping the constant term arising from second-order, single replacements in the reference state yields the RP3 self-energy for VEAs

$$\boldsymbol{\Sigma}^{\mathrm{RP3}}(E) = [\mathbf{a}^{\dagger}|\hat{H}\mathbf{f}_{2\mathrm{hp}}]_1[\mathbf{f}_{2\mathrm{hp}}|(E\hat{I} - \hat{H})\mathbf{f}_{2\mathrm{hp}}]_0^{-1}[\mathbf{f}_{2\mathrm{hp}}|\hat{H}\mathbf{a}^{\dagger}]_1 + \frac{1}{2}[\mathbf{a}^{\dagger}|\hat{H}\mathbf{f}_{2\mathrm{ph}}]_2[\mathbf{f}_{2\mathrm{ph}}|(E\hat{I} - \hat{H})\mathbf{f}_{2\mathrm{ph}}]_1^{-1}[\mathbf{f}_{2\mathrm{ph}}|\hat{H}\mathbf{a}^{\dagger}]_1 + \frac{1}{2}[\mathbf{a}^{\dagger}|\hat{H}\mathbf{f}_{2\mathrm{ph}}]_1[\mathbf{f}_{2\mathrm{ph}}|(E\hat{I} - \hat{H})\mathbf{f}_{2\mathrm{ph}}]_1^{-1}[\mathbf{f}_{2\mathrm{ph}}|\hat{H}\mathbf{a}^{\dagger}]_2 \quad (22)$$

The RP3 self-energies are closely related to their NR2 counterparts for VIEs and VEAs; their diagonal third-order terms are identical to those of P3.

Neglect of fourth- and higher-order terms generated by the inverted matrices in eqs 20−22 defines the L3, Q3, and P3 self-energy matrices for VEAs

$$\Sigma^{\mathrm{L3}} = S_{2\mathrm{hp}} + S_{2\mathrm{ph}} + \frac{1}{2}(C_{\mathrm{S}} + P_{2\mathrm{hp}} + P_{2\mathrm{ph}}) + R_{2\mathrm{hp}} + R_{2\mathrm{ph}} \quad (23)$$

$$\Sigma^{\mathrm{Q3}} = S_{2\mathrm{hp}} + S_{2\mathrm{ph}} + \frac{1}{2}(C_{\mathrm{S}} + P_{2\mathrm{ph}}) + R_{2\mathrm{ph}} \quad (24)$$

$$\Sigma^{\mathrm{P3}} = S_{2\mathrm{hp}} + S_{2\mathrm{ph}} + \frac{1}{2}P_{2\mathrm{ph}} + R_{2\mathrm{ph}} \quad (25)$$

Factors of half appear because of the new choice of superoperator metric.

The approximately renormalized, partial third-order self-energy[24] (P3+) for VEAs may be recovered in an expression analogous to that used in OVGF-B so that

$$\Sigma^{\mathrm{P3+}} = \Sigma^{(2)} + \frac{S_{2\mathrm{ph}}}{S_{2\mathrm{ph}} - \frac{1}{2}P_{2\mathrm{ph}}}\left(R_{2\mathrm{ph}} + \frac{1}{2}P_{2\mathrm{ph}}\right) \quad (26)$$

The present convention assigns the + sign to approximately renormalized methods and reserves R for methods in which higher-order terms are explicitly evaluated. With similar arguments, the Q3+ method for VEAs may be obtained

$$\Sigma^{\mathrm{Q3+}} = \Sigma^{(2)} + \frac{1}{2}C_{\mathrm{S}} + \frac{S_{2\mathrm{ph}}}{S_{2\mathrm{ph}} - \frac{1}{2}P_{2\mathrm{ph}}}\left(R_{2\mathrm{ph}} + \frac{1}{2}P_{2\mathrm{ph}}\right) \quad (27)$$

RL3 treats 2hp and 2ph operators on an equal footing. Therefore, A, B, and C versions of L3+ that are valid for VIEs and VEAs may be defined by analogy to the three OVGF alternatives

$$\Sigma^{\mathrm{L3+A}} = \Sigma^{(2)} + \frac{S_{2\mathrm{hp}} + S_{2\mathrm{ph}}}{S_{2\mathrm{hp}} + S_{2\mathrm{ph}} - \frac{1}{2}(P_{2\mathrm{hp}} + P_{2\mathrm{ph}})}\left[\frac{1}{2}C_{\mathrm{S}} + R_{2\mathrm{hp}} + R_{2\mathrm{ph}} + \frac{1}{2}(P_{2\mathrm{hp}} + P_{2\mathrm{ph}})\right] \quad (28)$$

$$\Sigma^{\mathrm{L3+B}} = \Sigma^{(2)} + \frac{1}{2}C_{\mathrm{S}} + \frac{S_{2\mathrm{hp}}}{S_{2\mathrm{hp}} - \frac{1}{2}P_{2\mathrm{hp}}}\left(R_{2\mathrm{hp}} + \frac{1}{2}P_{2\mathrm{hp}}\right) + \frac{S_{2\mathrm{ph}}}{S_{2\mathrm{ph}} - \frac{1}{2}P_{2\mathrm{ph}}}\left(R_{2\mathrm{ph}} + \frac{1}{2}P_{2\mathrm{ph}}\right) \quad (29)$$

$$\Sigma^{\mathrm{L3+C}} = \Sigma^{(2)} + \left[\frac{1}{2}C_{\mathrm{S}} + R_{2\mathrm{hp}} + R_{2\mathrm{ph}} + \frac{1}{2}(P_{2\mathrm{hp}} + P_{2\mathrm{ph}})\right]\times \frac{R_{2\mathrm{hp}} + R_{2\mathrm{ph}} + \frac{1}{2}(P_{2\mathrm{hp}} + P_{2\mathrm{ph}})}{\frac{S_{2\mathrm{hp}} - \frac{1}{2}P_{2\mathrm{hp}}}{S_{2\mathrm{hp}}}\left(R_{2\mathrm{hp}} + \frac{1}{2}P_{2\mathrm{hp}}\right) + \frac{S_{2\mathrm{ph}} - \frac{1}{2}P_{2\mathrm{ph}}}{S_{2\mathrm{ph}}}\left(R_{2\mathrm{ph}} + \frac{1}{2}P_{2\mathrm{ph}}\right)} \quad (30)$$

For VIEs, RQ3 and Q3+ procure an arithmetic advantage over RL3 and L3+, respectively, by eliminating OV^4 contractions and ERIs with four virtual indices. Their equivalents for VEAs do not reduce any bottlenecks when V is larger than O.

Pole search algorithms use CHF orbital energies as initial guesses and evaluate derivatives of the diagonal self-energy matrix elements with respect to E. (These data are also needed to determine probability factors.) Newton's method is employed for finding the roots of a function of a single variable (see eq 10). When probability factors exceed 0.85, three iterations almost always suffice for convergence to within 0.01 eV. Pole searches with the OVGF, P3+, Q3+, and L3+ self-energies are initiated, respectively, at the D3, P3, Q3, and L3 poles. Agreement to within 0.01 eV is usually obtained after a single Newton iteration. Practically no additional work is needed for the three + (i.e., approximately renormalized) methods once P3, Q3, or L3 calculations are complete.

Arithmetic scaling factors that pertain to bottleneck steps for various approximate self-energies are summarized in Table 2. For P3, P3+, Q3, Q3+, RP3, RQ3, DR, and NR2, scaling factors or ERI requirements are larger for VEAs than for VIEs when V > O.

A summary of the characteristics of several diagonal, new-generation self-energies accompanied by comparisons with the older P3 and P3+ self-energies is presented in Table 3.

Table 3. Characteristics of New-Generation, Diagonal, Self-Energy Approximations

	no neglect of terms generated by eq 17	neglect of postsecond-order 2ph (for VIEs) or 2hp (for VEAs) terms	neglect of constant terms and of postsecond-order 2ph (for VIEs) or 2hp (for VEAs) terms
explicitly renormalized	RL3	RQ3	RP3
approximately renormalized	L3+ (versions A, B & C)	Q3+	P3+
second- and third-order terms only	L3	Q3	P3

COMPUTATIONAL METHODS

All computations were executed with the development version of Gaussian[70] wherein all electron propagator methods have been implemented. Following self-consistent-field calculations, the required ERIs needed for evaluating the self-energy matrix elements are transformed to the CHF basis and saved on disk. Table 2 exhibits the largest subsets of ERIs required for each

https://doi.org/10.1021/acs.jctc.3c00954
J. Chem. Theory Comput. 2024, 20, 290−306

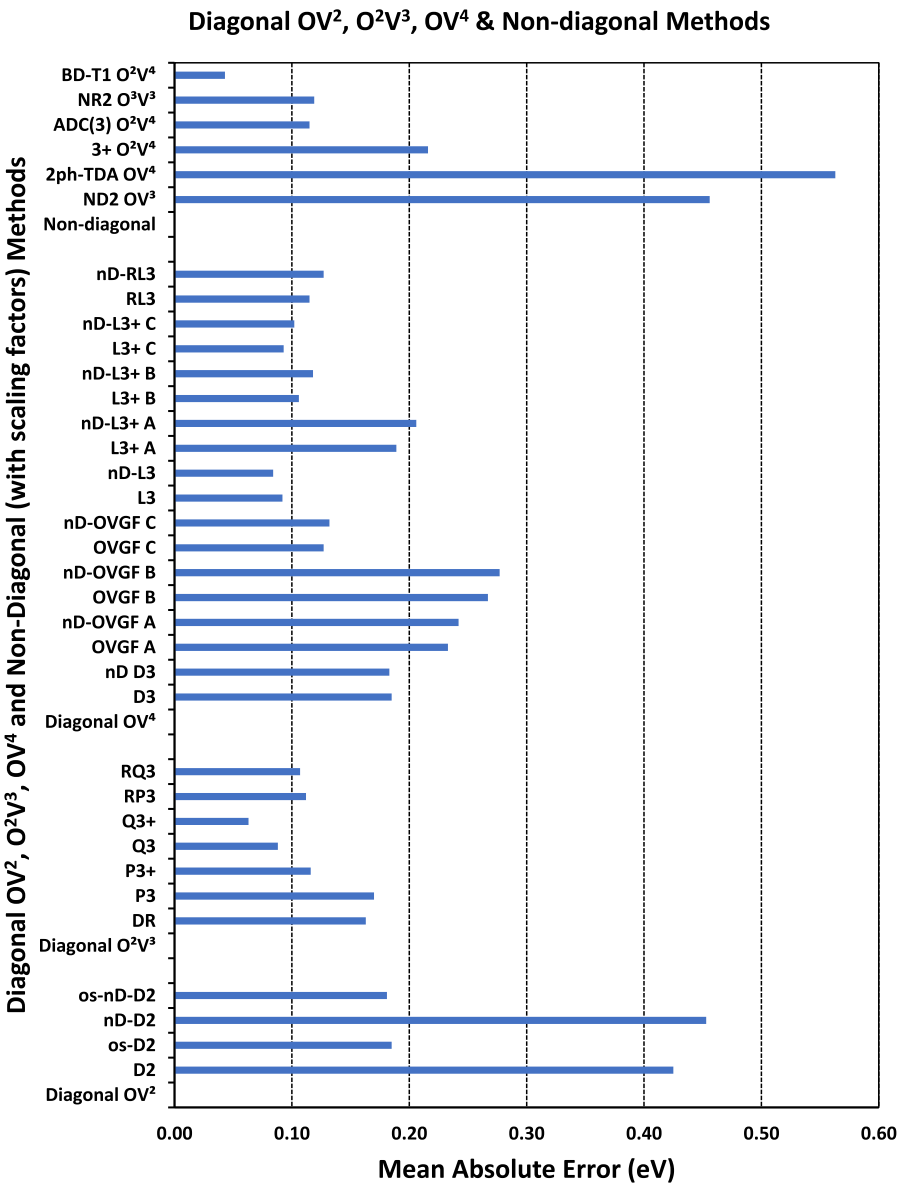


Figure 3. Mean absolute errors (eV) versus 24 ΔCCSD(T)/aug-cc-pVDZ VIE standards and arithmetic scaling factors.

self-energy approximation with the assumption that V exceeds O. (For the 24 molecules under consideration, the average value of V/O equals 9.36 when aug-cc-pVTZ basis sets are used.) Self-energy summations do not take core orbitals into account.

Table S4 displays standard VIEs and VEAs of organic photovoltaic molecules calculated at the ΔCCSD(T) level with the aug-cc-pVDZ and aug-cc-pVTZ basis sets. Four composite methods denoted by CMX (where X = 1−4) have been developed for VIEs and VEAs in accordance with eqs 31−34

$$E^{\mathrm{CM1}} = E^{\mathrm{nD\text{-}L3+B}}_{\mathrm{aug\text{-}cc\text{-}pVDZ}} + E^{\mathrm{os\text{-}nD\text{-}D2}}_{\mathrm{CBS(DT)}} - E^{\mathrm{os\text{-}nD\text{-}D2}}_{\mathrm{aug\text{-}cc\text{-}pVDZ}} \quad (31)$$

$$E^{\mathrm{CM2}} = E^{\mathrm{Q3+}}_{\mathrm{aug\text{-}cc\text{-}pVDZ}} + E^{\mathrm{os\text{-}nD\text{-}D2}}_{\mathrm{CBS(DT)}} - E^{\mathrm{os\text{-}nD\text{-}D2}}_{\mathrm{aug\text{-}cc\text{-}pVDZ}} \quad (32)$$

$$E^{\mathrm{CM3}} = E^{\mathrm{nD\text{-}L3+B}}_{\mathrm{aug\text{-}cc\text{-}pVTZ}} + E^{\mathrm{os\text{-}nD\text{-}D2}}_{\mathrm{CBS(TQ)}} - E^{\mathrm{os\text{-}nD\text{-}D2}}_{\mathrm{aug\text{-}cc\text{-}pVTZ}} \quad (33)$$

$$E^{\mathrm{CM4}} = E^{\mathrm{Q3+}}_{\mathrm{aug\text{-}cc\text{-}pVTZ}} + E^{\mathrm{os\text{-}nD\text{-}D2}}_{\mathrm{CBS(TQ)}} - E^{\mathrm{os\text{-}nD\text{-}D2}}_{\mathrm{aug\text{-}cc\text{-}pVTZ}} \quad (34)$$

Complete basis set (CBS) results in the composite methods are based on a two-point (double−triple or triple-quadruple) inverse quartic extrapolation, i.e., $(l + 1/2)^{-4}$, scheme. Data in the Supporting Information have been used to confirm that quartically extrapolated data are very close to their cubically (i.e., l^{-3}), extrapolated counterparts. The last two terms in each CMX equation provide a basis-set correction estimated with os-nD-D2 to Q3+ or nD-L3+B and aug-cc-pVDZ and aug-cc-pVTZ basis sets. The complete set of calculated results and accompanying statistics is provided in the Supporting Information.

NUMERICAL RESULTS AND DISCUSSION

VIEs and VEAs of 24 organic photovoltaic molecules were calculated at the ΔCCSD(T) level with the aug-cc-pVDZ basis set. These calculations were repeated with the aug-cc-pVTZ basis set, but the four molecules with the largest basis sets were omitted (see Table S4). MAEs, mean signed errors (MSEs), standard deviations (σ), and maximum absolute errors (max.

https://doi.org/10.1021/acs.jctc.3c00954
J. Chem. Theory Comput. 2024, 20, 290−306

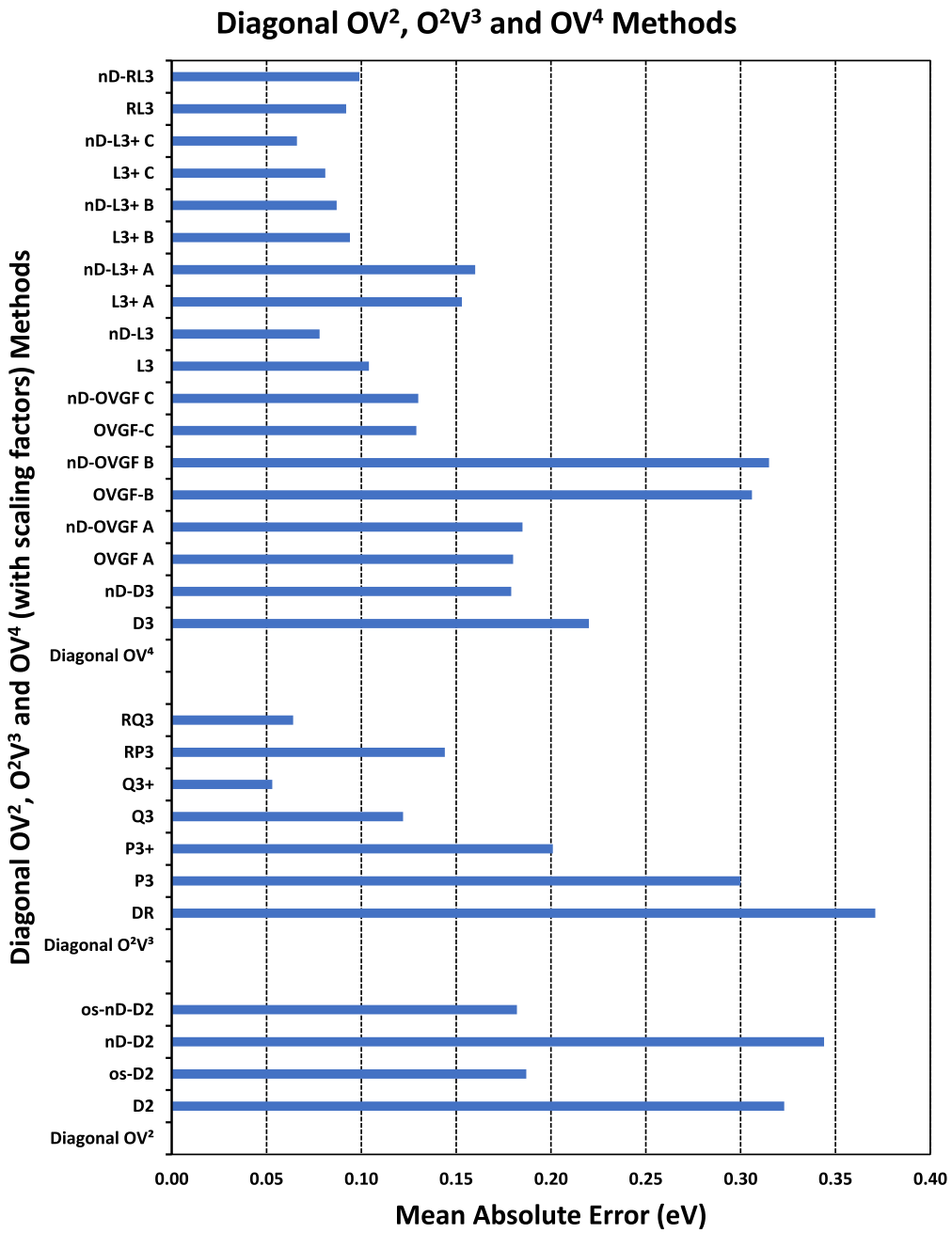


Figure 4. Mean absolute errors (eV) versus 20 ΔCCSD(T)/aug-cc-pVTZ VIE standards and arithmetic scaling factors.

AEs) produced with the same basis sets are shown in Tables S5 (24 VIEs, aug-cc-pVDZ), S6 (20 VIEs, aug-cc-pVTZ), S7 (23 VEAs, aug-cc-pVDZ) and S8 (19 VEAs, aug-cc-pVTZ). Corresponding bar graphs of MAEs are shown in Figures 3−6. Histograms that display the full sets of errors are listed in Figures S7−S10.

Constant Basis Comparisons: Vertical Ionization Energies. The errors obtained with Koopmans's theorem (KT) are considerably lower than those obtained in previous tests on smaller molecules.[12] MAEs near 0.5 eV occur for both basis sets; overestimates are more numerous than underestimates. D2 and nD-D2 are better, with MAEs between 0.3 and 0.5 eV that arise chiefly from underestimates. This tendency can be ameliorated by including only opposite-spin correlation and relaxation effects in the os-D2 and os-nD-D2 self-energies; MAEs below 0.2 eV result. The histograms display the tendency of D2 and nD-D2 to underestimate VIEs. A good balance of underestimates and overestimates occurs for os-D2 and os-nD-D2. Whereas the maximum errors are near 1 eV for D2 and nD-D2, these data are near 0.4 eV for os-D2 and os-nD-D2. Numerically similar errors occurred in previous tests on the two opposite-spin methods.[12,48] These options emerge as economical, cubic scaling alternatives when only low accuracy is required or when a fifth-power ERI transformation is infeasible. In a second-order calculation of a single VIE or VEA, all ERIs in eq 13 have a p index in common and therefore the transformation requires only fourth-power arithmetic scaling.

The next category of arithmetic effort (O^2V^3 scaling) includes the approximately renormalized P3+ and Q3+

https://doi.org/10.1021/acs.jctc.3c00954
J. Chem. Theory Comput. 2024, 20, 290−306

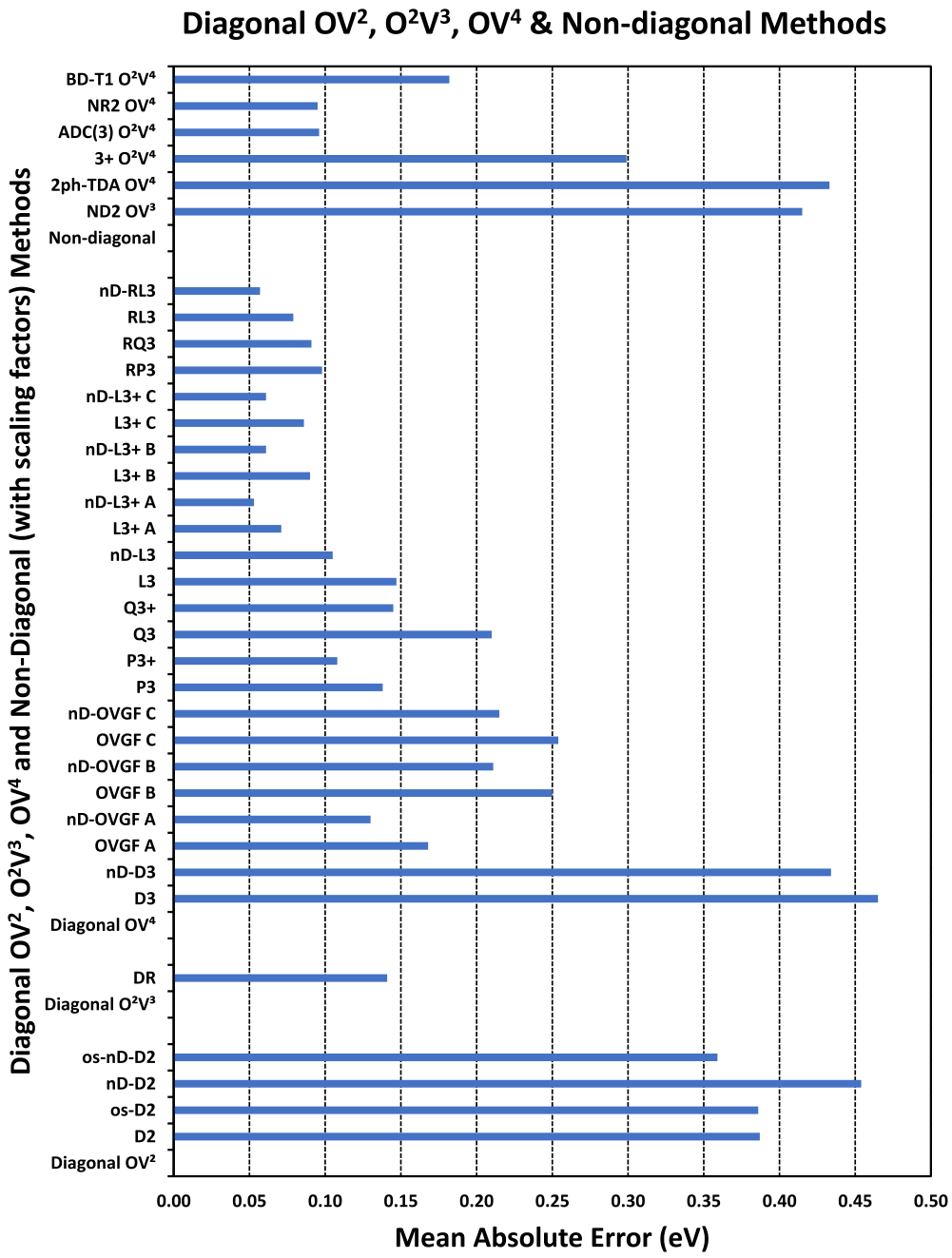


Figure 5. Mean absolute errors (eV) versus 23 ΔCCSD(T)/aug-cc-pVDZ VEA standards and arithmetic scaling factors.

methods, their explicitly renormalized extensions (RP3 and RQ3), and the DR self-energy. All methods produce MAEs below 0.2 eV for aug-cc-pVDZ, but the aug-cc-pVTZ results are markedly worse for DR. (The latter results illustrate the need for tests that involve more than one basis.) For both basis sets, the MAE for Q3+ is near 0.05 eV. RQ3 results are only slightly worse. The Q3+ and RQ3 histograms are well balanced between overestimates and underestimates. When only a partial transformation that excludes ERIs with four virtual indices (as in MP2 calculations) is feasible, these two options are advantageous. Q3+ and RQ3 respectively provide better error measures than P3+ and RP3 and require only additional steps with O^2V^3 scaling. Q3+ is an especially attractive option because it requires no iterations that pertain to renormalizations, has a single O^2V^3 step, and obtains results that are slightly more accurate than RQ3.

The third class of diagonal self-energy methods requires a full set of ERIs and OV^4 contractions. All new-generation methods except L3+A and its nD variant (i.e., RL3, L3+B, L3+C, and L3 and their nD variants) have MAEs near 0.1 eV for both basis sets. As L3+B is an extension of Q3+ and P3+, it may be considered the preferred option among the approximately renormalized self-energies. There is little decline in accuracy with the more efficient nD-L3+B method, nor is there significant improvement with the explicitly renormalized RL3 or nD-RL3 self-energies. Lower accuracy is achieved with D3, OVGF, and their nD variants; OVGF version C is the best in this set of older methods. Note that Q3+ produces slightly higher accuracy than L3+B, RL3, and their nD variants in these

https://doi.org/10.1021/acs.jctc.3c00954
J. Chem. Theory Comput. 2024, 20, 290−306

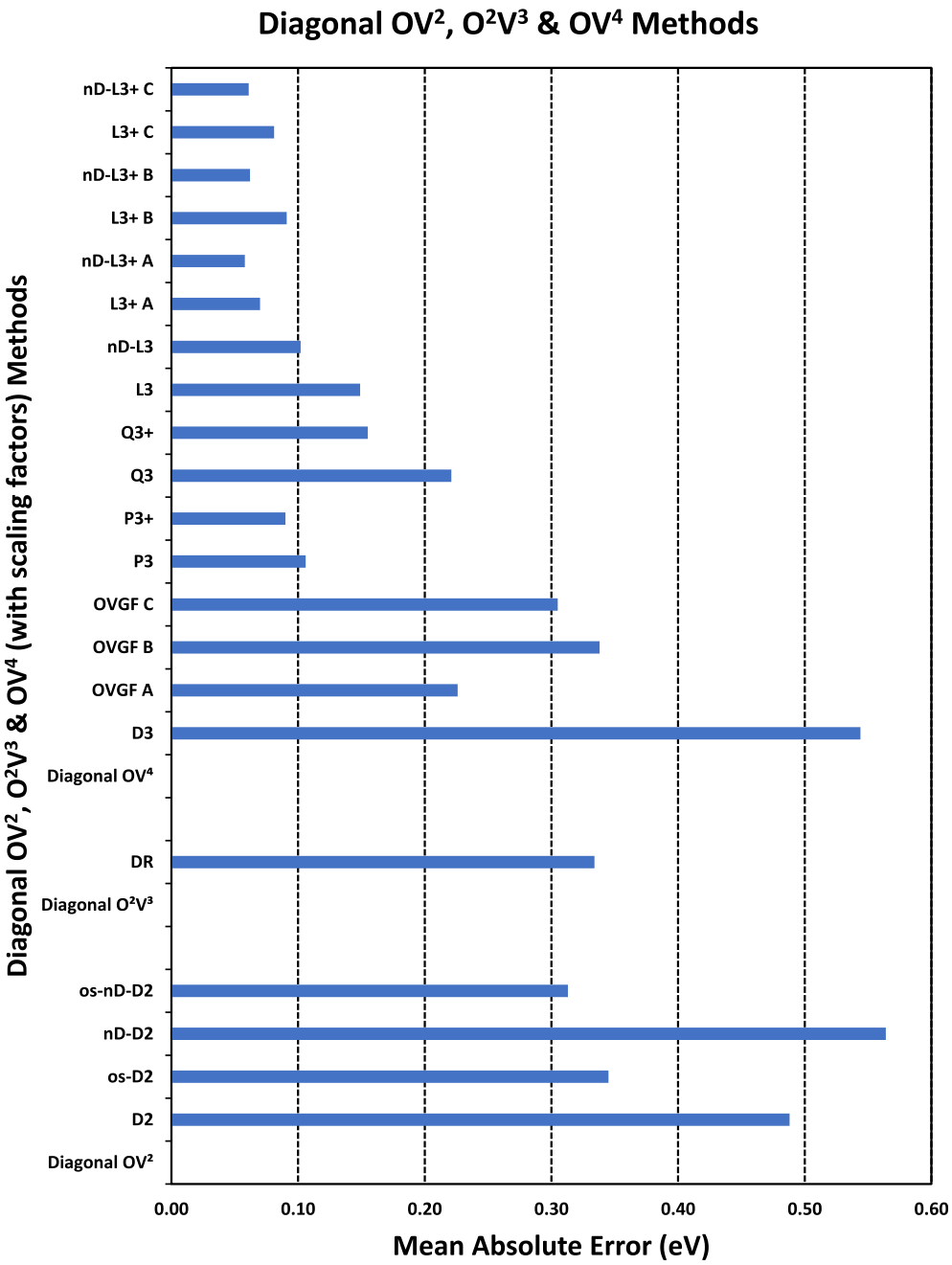


Figure 6. Mean absolute errors (eV) versus 19 ΔCCSD(T)/aug-cc-pVTZ VEA standards and arithmetic scaling factors.

tests despite its lower arithmetic scaling factor. The approximate renormalizations of L3+B and L3+C are of relatively little consequence, but the L3+A version is inferior to L3. Explicit renormalizations in RL3 deliver little or no improvement over L3. This relative stability contrasts with changes seen in the three OVGF versions versus D3 results. OVGF-B is worse than D3 for both basis sets, as is OVGF-A for the smaller basis. Whereas the L3+B and L3+C methods show a close accumulation of columns in the histograms, the OVGF methods have separated columns and higher maximum errors. The latter methods' failures originate in their dependence on D3 results, which are more dispersed than those of L3. Efficiencies in VIE calculations realized with nD versions are not accompanied by significant losses of accuracy.

Of the nondiagonal methods examined with the aug-cc-pVDZ basis, only the ADC(3), NR2 and BD-T1 self-energies are competitive with respect to accuracy. NR2 and ADC(3) have similar MAEs, but NR2 is faster. BD-T1 is the most accurate alternative with an MAE below 0.05 eV for the aug-cc-pVDZ set. Only BD-T1 surpasses the best O^2V^3 and OV^4 methods in this respect.

Constant Basis Comparisons: Vertical Electron Affinities. Whereas orbital relaxation in final states and differential electron correlation usually have opposite signs in VIE calculations, such cancellations rarely occur for VEAs. MAEs of 1.3−1.4 eV are obtained at the KT level; underestimates occur in every case. Ordinary second-order calculations (ND2, D2, and nD-D2) overestimate the needed correction. The aug-cc-pVDZ MAEs of ∼0.4 eV increase to ∼0.5 with aug-cc-

https://doi.org/10.1021/acs.jctc.3c00954
J. Chem. Theory Comput. 2024, 20, 290−306

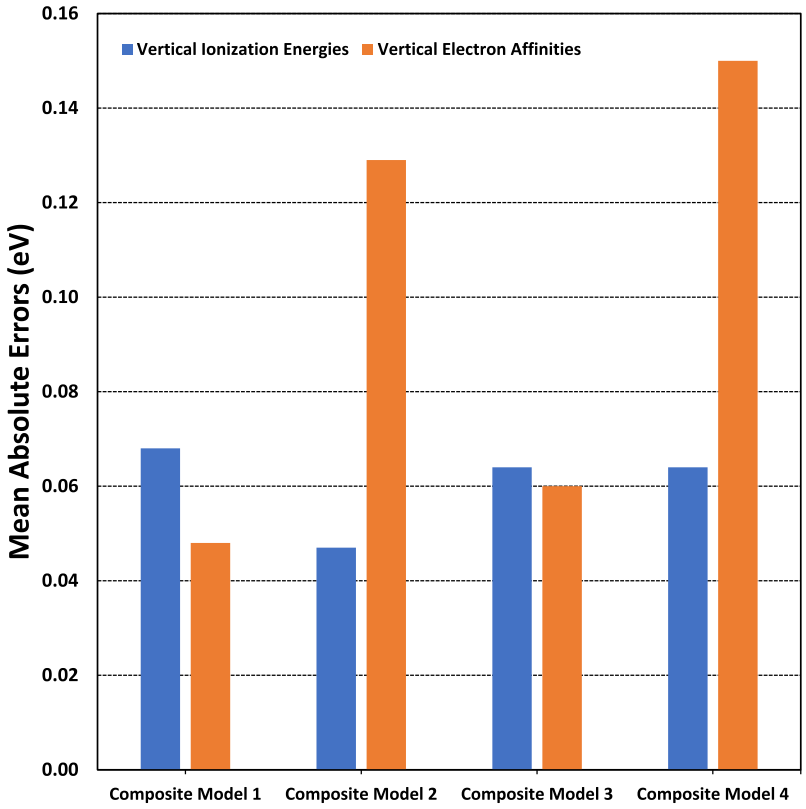


Figure 7. Mean absolute errors (eV) of EPT composite models versus ΔCCSD(T)/CBS VIE and VEA standards.

pVTZ. These trends explain why the opposite-spin alternatives, os-D2 and os-nD-D2, produce smaller MAEs and underestimated VEAs. These cubically scaling, clearly interpretable methods surpass CHF orbital energies in accuracy at a minimal extra cost. Their MAEs are between 20 and 30% of those of their KT counterparts.

In VEA calculations, the DR method retains the O^2V^3 arithmetic scaling and requires ERIs with only three virtual indices. Its MAE of 0.14 eV in aug-cc-pVDZ calculations contrasts with the 0.33 eV result obtained with aug-cc-pVTZ. The latter result is no better than its os-nD-D2 counterpart. Histograms indicate that DR tends to overestimate VEAs in both basis sets. As in the VIE tests, the quality of DR VEA results deteriorates markedly for the larger basis. This outcome underlines the importance of examining more than one basis in constant-basis tests.

The next level of computational effort requires ERIs with four virtual indices and OV^4 arithmetic scaling. MAEs of all three approximately renormalized L3+ extensions and their nD variants lie below 0.1 eV for both basis sets; all three realize improvements over those of L3 and nD-L3. The L3+B version is preferred for the sake of uniformity with the VIE results. This method has a greater tendency to underestimate than overestimate VEAs. For the aug-cc-pVDZ test, the histograms of the renormalized RL3 and nD-RL3 methods closely resemble those of L3+B and nD-L3+B. The Q3+, P3+, RQ3, and RP3 methods neglect terms found in L3+B, but there are no advantages of accuracy or reduced arithmetic bottlenecks. These results indicate that neglect of easily calculated, postsecond-order 2hp terms leads to lower accuracy for VEA calculations. Larger errors occur for D3, its approximately renormalized OVGF extensions, and their nD variants. All of these methods underestimate VEAs.

In aug-cc-pVDZ calculations, the best nondiagonal results (MAEs below 0.1 eV) correspond to the NR2 and ADC(3) methods. NR2 is the more efficient alternative. Whereas BD-T1 sets the standards for accuracy in VIE calculations, its MAE for aug-cc-pVDZ VEAs is 0.18 eV. The corresponding histogram indicates that errors occur in a highly restricted range with a standard deviation of only 0.02 eV. This result suggests that there may be an improvement over BD-T1 that could yield highly accurate results. The remaining nondiagonal methods are not competitive.

COMPOSITE MODELS

VIEs and VEAs employed as standards in previous tests (see CBS values in Table S4) were calculated with MP2 and CCSD(T) total energy differences.[57] Relatively large (through quadruple or quintuple ζ) and small (through triple ζ) augmented, correlation-consistent basis sets[71] were used, respectively, in the two types of calculations. Final errors were estimated to be 0.03 eV or less.

The CMX composite models are being assessed presently. All four employ relatively large basis sets in calculations with small arithmetic scaling factors and relatively small basis sets in calculations with large arithmetic scaling factors. (Related models for VIEs of molecules and vertical electron detachment energies of anions have been employed previously.[49,72]) The os-D2 and os-nD-D2 methods are the most accurate methods with cubic arithmetic scaling in the aug-cc-pVTZ tests (see Figures 4 and 6 and Tables S6 and S8). The latter option is chosen for composite models because it has a minor computational advantage for VIEs. Among the VIE methods with O^2V^3 scaling, Q3+ offers the best combination of accuracy and efficiency. For VIE and VEA methods with OV^4 scaling,

https://doi.org/10.1021/acs.jctc.3c00954
J. Chem. Theory Comput. 2024, 20, 290−306

the nD-L3+B and nD-L3+C options produce high accuracy with the greatest economy of arithmetic operations. The nD-L3+B alternative is preferred for tests on composite models because of its resemblance to Q3+. Error measures are summarized in Table S9 and Figure 7; corresponding histograms for VIEs and VEAs appear in Figures 8 and 9.

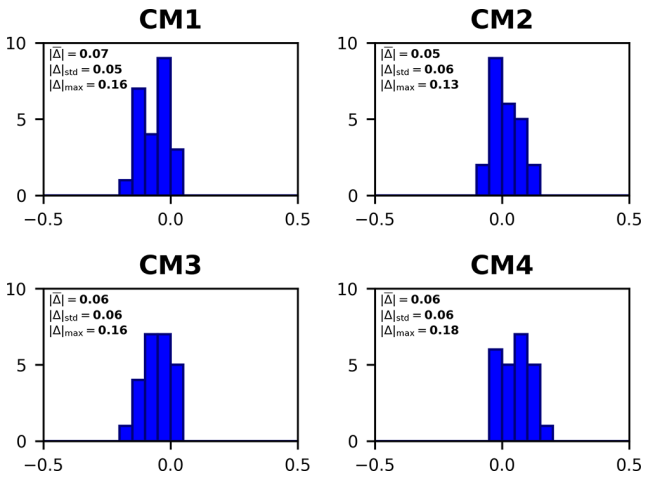


Figure 8. Histograms of VIE error distributions (eV): ΔCCSD(T)/CBS versus EPT composite models.

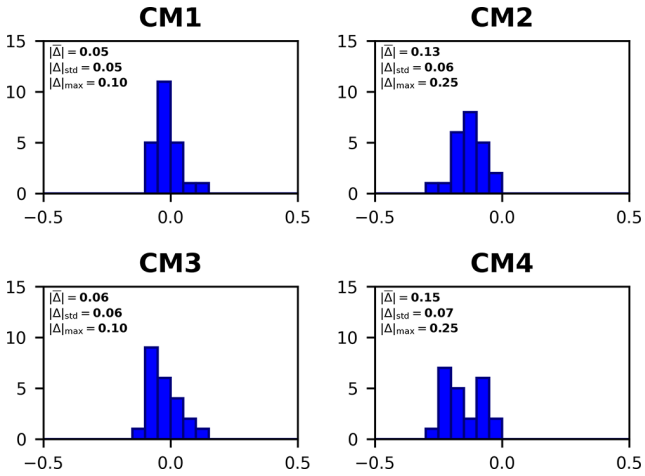


Figure 9. Histograms of VEA error distributions (eV): ΔCCSD(T)/CBS versus EPT composite models.

All models perform well for VIEs, with MAEs approximately equal to 0.05 eV. With respect to the first option (CM1), a small improvement is made by replacing nD-L3+B with Q3+ in the second option (CM2). Underestimates and overestimates dominate, respectively, in CM1 and CM2. Using larger basis sets leads to almost no improvement in the MAE for CM3. There is little difference between the CM2 and CM4 profiles. In general, the improvement realized with CM2 (i.e., replacing nD-L3+B with the more efficient and accurate Q3+) is more important than extrapolations inferred from larger basis sets.

The chief difference between VIE and VEA results is the lack of an advantage for Q3+ over nD-L3+B in the latter case. The CM1 and CM3 MAEs and MSEs are superior to those of CM2 and CM4. As with the VIE results, larger basis sets are practically inconsequential for VEA calculations.

Probability factors exceed 0.85 in all os-nD-D2, Q3+, and nD-L3+B calculations. The average probability factors are 0.87 for VIEs and 0.92 for VEAs. These data validate the diagonal approximation and the proportionality of Dyson orbitals to CHF orbitals for closed-shell organic molecules of similar size and complexity.

CONCLUSIONS

The new generation of diagonal self-energy approximations has been extended to vertical electron affinities. Six methods (P3, P3+, RP3, Q3, Q3+, and RQ3, see Tables 1 and 3) for vertical ionization energies and their vertical electron affinity counterparts differ in their neglect of certain postsecond-order two-particle-one-hole and two-hole-one-particle terms, respectively. Non-Dyson variants for vertical ionization energies and electron affinities have two-particle-one-hole and two-hole-one-particle terms that respectively become energy-independent. The remaining new-generation methods have identical formulas for both kinds of vertical electron binding energies. Methods adapted for vertical ionization energies realize lower arithmetic bottlenecks when the number of virtual orbitals exceeds the number of occupied orbitals. No such advantage accrues to their vertical electron affinity counterparts.

The accuracy obtained in previous tests on vertical ionization energies of smaller species is conserved in applications on 24 larger, conjugated organic-photovoltaic molecules. Mean absolute errors of vertical electron binding energies versus ΔCCSD(T) standards in identical basis sets are below 0.1 eV for new-generation methods with fifth-power scaling.

Composite models of vertical ionization energies and electron affinities have been compared to basis-set-extrapolated standards that are estimated to have errors below 0.03 eV. The first composite model (CM1, see eq 31) is based on the nD-L3+B and os-nD-D2 self-energies. CM1 produces vertical ionization energies and electron affinities with MAEs close to 0.05 eV. Its lengthiest calculations employ aug-cc-pVTZ basis sets with the cubically scaling os-nD-D2 self-energy and aug-cc-pVDZ basis sets with the nD-L3+B self-energy. The latter calculation's arithmetic bottleneck has a linear dependence on the number of occupied orbitals and a quartic dependence on the number of virtual orbitals. The second model (CM2, see eq 32), which replaces nD-L3+B with Q3+, is a more efficient and slightly more accurate alternative for vertical ionization energies. It does not require a full transformation of the electron repulsion integrals to the canonical Hartree−Fock basis. CM2's arithmetic bottleneck scales quadratically with the number of occupied orbitals and cubically with the number of virtual orbitals. This model is an attractive option for the assignment of photoelectron spectra. CM3 and CM4 (eqs 33 and 34) data demonstrate that basis set improvements are of little consequence.

Numerical confirmation of the utility of the diagonal approximation is provided by the high probability factors obtained in the composite-model calculations. These results imply that scaled canonical Hartree−Fock orbitals are useful approximations of Dyson orbitals for the lowest ionization energy and the highest electron affinity. (The scaling factor equals the square root of the probability factor, which equals unity in the absence of electron correlation.) This conclusion is likely to be valid for organic molecules of similar size and complexity. Numerical evidence is stronger for electron affinities than for ionization energies.

https://doi.org/10.1021/acs.jctc.3c00954
J. Chem. Theory Comput. 2024, 20, 290−306

Generalizations to unrestricted Hartree−Fock spin−orbitals have already been programmed. Studies of open-shell reference states with low spin contamination are in progress. Gradient formulas derived for the NR2 method[73] are directly applicable to the calculation of adiabatic electron binding energies with the new generation of methods. Density fitting[74,75] and Cholesky decomposition[76] approaches to integral approximation have been used to improve the efficiency of related electron propagator methods and are applicable to the new-generation methods.

APPENDIX A

Diagonal Ring Superoperator Matrix Elements

Superoperator matrix elements needed for the 2ph-TDA self-energy (see eq 28) include

$$[a_p^\dagger|\hat{H}a_a a_i^\dagger a_j^\dagger]_1 = \langle \mathbf{pa}|\mathbf{ij}\rangle - \langle pa|ji\rangle \tag{A1}$$

$$[a_p^\dagger|\hat{H}a_i a_a^\dagger a_b^\dagger]_1 = \langle \mathbf{pi}|\mathbf{ab}\rangle - \langle pi|ba\rangle \tag{A2}$$

$$[a_a a_i^\dagger a_j^\dagger|\hat{V}a_b a_k^\dagger a_l^\dagger]_1 = (1 - P_{ij})(1 - P_{kl})\delta_{ik}[\langle bj|al\rangle - \langle \mathbf{bj}|\mathbf{la}\rangle] - \delta_{ab}\langle ij||kl\rangle \tag{A3}$$

$$[a_i a_a^\dagger a_b^\dagger|\hat{V}a_j a_c^\dagger a_d^\dagger]_1 = -(1 - P_{ab})(1 - P_{cd})\delta_{ac}[\langle jb|id\rangle - \langle \mathbf{jb}|\mathbf{di}\rangle] + \delta_{ij}\langle ab||cd\rangle \tag{A4}$$

In the diagonal ring (DR, i.e., HF-TDA-G_0W_0) self-energy, only the terms with bold orbital indices are retained. Exchange terms in eqs A1 and A2 are omitted. The same change is made in the Hermitian conjugate matrices. Ring-exchange and ladder terms in eqs A3 and A4 are ignored. Only the ring vertices survive. The latter terms correspond to repulsions between electron densities that equal products of occupied and virtual orbitals. Long-range, dispersion forces are described in terms of such interactions.

APPENDIX B

Third-Order Self-Energy Summations

The six third-order terms with real spin−orbitals that contribute to $\sum_{pp}(E)$ in eq 16 are shown below. The $t_{ij}^{ab(1)}$ and $t_i^{a(2)}$ amplitudes are given in eqs 18 and 19. Occupied and virtual spin−orbitals are designated, respectively, as i, j, k, l and a, b, c, d.

$$C_D = \frac{1}{2}\sum_{ab}\langle ap||bp\rangle \sum_{ijc} t_{ij}^{ac(1)} t_{ij}^{bc(1)} - \frac{1}{2}\sum_{ij}\langle ip||jp\rangle \sum_{abk} t_{ik}^{ab(1)} t_{jk}^{ab(1)} \tag{A5}$$

$$C_S = 2\sum_{ia}\langle ip||ap\rangle t_i^{a(2)} \tag{A6}$$

$$R_{2hp} = \sum_{ai<j} \frac{U_{paij}(E)\langle ij||pa\rangle}{E + \epsilon_a - \epsilon_i - \epsilon_j} \tag{A7}$$

where

$$U_{paij}(E) = -\sum_{k<l}\frac{\langle pa||kl\rangle\langle kl||ij\rangle}{E + \epsilon_a - \epsilon_k - \epsilon_l} - (1 - P_{ij})\sum_{kb}\frac{\langle pb||jk\rangle\langle ak||bi\rangle}{E + \epsilon_b - \epsilon_j - \epsilon_k} \tag{A8}$$

$$R_{2ph} = \sum_{ia<b}\frac{U_{piab}(E)\langle ab||pi\rangle}{E + \epsilon_i - \epsilon_a - \epsilon_b} \tag{A9}$$

where

$$U_{piab}(E) = \sum_{c<d}\frac{\langle pi||cd\rangle\langle cd||ab\rangle}{E + \epsilon_i - \epsilon_c - \epsilon_d} + (1 - P_{ab})\sum_{jc}\frac{\langle pj||bc\rangle\langle ic||ja\rangle}{E + \epsilon_j - \epsilon_b - \epsilon_c} \tag{A10}$$

$$P_{2hp} = 2\sum_{ai<j}\frac{\langle pa||ij\rangle W_{paij}}{E + \epsilon_a - \epsilon_i - \epsilon_j} \tag{A11}$$

where

$$W_{paij} = \sum_{b<c} t_{ij}^{bc(1)}\langle bc||pa\rangle + (1 - P_{ij})\sum_{kb} t_{jk}^{ba(1)}\langle bi||pk\rangle \tag{A12}$$

$$P_{2ph} = 2\sum_{ia<b}\frac{\langle pi||ab\rangle W_{piab}}{E + \epsilon_i - \epsilon_a - \epsilon_b} \tag{A13}$$

where

$$W_{piab} = -\sum_{j<k} t_{jk}^{ab(1)}\langle jk||pi\rangle - (1 - P_{ab})\sum_{jc} t_{ji}^{bc(1)}\langle ja||pc\rangle \tag{A14}$$

ASSOCIATED CONTENT

Supporting Information

The Supporting Information is available free of charge at https://pubs.acs.org/doi/10.1021/acs.jctc.3c00954.

(ZIP)
(XLSX)
(XLSX)
(XLSX)
(PDF)

AUTHOR INFORMATION

Corresponding Author

J. V. Ortiz − *Department of Chemistry and Biochemistry, Auburn University, Auburn, Alabama 36849-5312, United States;* orcid.org/0000-0002-9277-0226; Email: ortiz@auburn.edu

Authors

Ernest Opoku − *Department of Chemistry and Biochemistry, Auburn University, Auburn, Alabama 36849-5312, United States;* orcid.org/0000-0002-4271-6838

Filip Pawłowski − *Department of Chemistry and Biochemistry, Auburn University, Auburn, Alabama 36849-5312, United States*

Complete contact information is available at: https://pubs.acs.org/10.1021/acs.jctc.3c00954

https://doi.org/10.1021/acs.jctc.3c00954
J. Chem. Theory Comput. 2024, 20, 290−306

Notes

The authors declare no competing financial interest.

■ ACKNOWLEDGMENTS

The authors thank Dr. Manuel Díaz Tinoco for valuable discussions and the Alabama Supercomputer Center for computing resources.

■ REFERENCES

(1) Ortiz, J. V. Electron propagator theory: an approach to prediction and interpretation in quantum chemistry. *Wiley Interdiscip. Rev.: Comput. Mol. Sci.* **2013**, *3*, 123−142.
(2) Ortiz, J. V. Chapter Four—Interpreting Bonding and Spectra With Correlated, One-Electron Concepts From Electron Propagator Theory. In *Annual Reports in Computational Chemistry*; Dixon, D. A., Ed.; Elsevier, 2017; Vol. *13*, pp 139−182.
(3) Corzo, H. H.; Ortiz, J. V. Chapter Thirteen—Electron Propagator Theory: Foundations and Predictions. In *Advances in Quantum Chemistry*; Sabin, J. R., Brändas, E. J., Eds.; Academic Press, 2017; Vol. *74*, pp 267−298.
(4) Ortiz, J. V. Recent progress in electron-propagator, extended-Koopmans-theorem and self-consistent-field approaches to the interpretation and prediction of electron binding energies. In *Advances in Quantum Chemistry*; Academic Press, 2022; Vol. *85*, pp 109−155.
(5) Ortiz, J. V. Dyson-orbital concepts for description of electrons in molecules. *J. Chem. Phys.* **2020**, *153*, 070902.
(6) Ortiz, J. V. Dyson orbitals and chemical bonding. In *Chemical Reactivity*; Savas Kaya, L. v. S., Goncagul, S., Lei, G., Eds.; Elsevier: Amsterdam, 2023; Vol. *1*, p 606.
(7) Linderberg, J.; Öhrn, Y. *Propagators in Quantum Chemistry*, 2nd ed.; Wiley-Interscience: Hoboken NJ, 2004.
(8) Jørgensen, P.; Simons, J. *Second Quantization-Based Methods in Quantum Chemistry*; Academic Press: New York, 1981.
(9) Schirmer, J. *Many-Body Methods for Atoms, Molecules and Clusters*; Springer International Publishing AG, 2018.
(10) von Niessen, W.; Schirmer, J.; Cederbaum, L. S. Computational methods for the one-particle Green's function. *Comput. Phys. Rep.* **1984**, *1*, 57−125.
(11) Koopmans, T. Über die Zuordnung von Wellenfunktionen und Eigenwerten zu den Einzelnen Elektronen Eines Atoms. *Physica* **1934**, *1*, 104−113.
(12) Opoku, E.; Pawłowski, F.; Ortiz, J. V. A new generation of diagonal self-energies for the calculation of electron removal energies. *J. Chem. Phys.* **2021**, *155*, 204107.
(13) Ranasinghe, D. S.; Margraf, J. T.; Perera, A.; Bartlett, R. J. Vertical valence ionization potential benchmarks from equation-of-motion coupled cluster theory and QTP functionals. *J. Chem. Phys.* **2019**, *150*, 074108.
(14) Dolgounitcheva, O. G.; Zakrzewski, V.; Ortiz, J. Electron Propagator Calculations on the Ionization Energies of Nucleic Acid Bases, Base-Water Complexes and Base Dimers. *Fundamental World of Quantum Chemistry: A Tribute to the Memory of Per-Olov Löwdin*; Kluwer: Dordrecht, 2003; Vol. *2*, pp 525−555.
(15) Zakrzewski, V. G.; Dolgounitcheva, O.; Zakjevskii, A. V.; Ortiz, J. V. Ab initio electron propagator methods: applications to fullerenes and nucleic acid fragments. *Annu. Rep. Comput. Chem.* **2010**, *6*, 79−94.
(16) Zakrzewski, V. G.; Dolgounitcheva, O.; Zakjevskii, A. V.; Ortiz, J. V. Ab initio electron propagator calculations on electron detachment energies of fullerenes, macrocyclic molecules, and nucleotide fragments. *Adv. Quantum Chem.* **2011**, *62*, 105−136.
(17) Thouless, D. J. *The Quantum Mechanics of Many-Body Systems*; Academic Press: New York, 1961.
(18) Corzo, H. H.; Galano, A.; Dolgounitcheva, O.; Zakrzewski, V. G.; Ortiz, J. V. NR2 and P3+: Accurate, Efficient Electron-Propagator Methods for Calculating Valence, Vertical Ionization Energies of Closed-Shell Molecules. *J. Phys. Chem. A* **2015**, *119*, 8813−8821.
(19) Díaz−Tinoco, M.; Corzo, H. H.; Pawłowski, F.; Ortiz, J. V. Do Dyson Orbitals resemble canonical Hartree−Fock orbitals? *Mol. Phys.* **2019**, *117*, 2275−2283.
(20) Cederbaum, L. S. Direct calculation of ionization potentials of closed-shell atoms and molecules. *Theor. Chim. Acta* **1973**, *31*, 239−260.
(21) Cederbaum, L. S. One-body Green's function for atoms and molecules. Theory and application. *J. Phys. B: At. Mol. Phys.* **1975**, *8*, 290−303.
(22) Ortiz, J. V. The electron propagator picture of molecular electronic structure. *Comput. Chem.* **1997**, *2*, 1−61.
(23) Ortiz, J. V. Partial third-order quasiparticle theory: comparisons for closed-shell ionization energies and an application to the Borazine photoelectron spectrum. *J. Chem. Phys.* **1996**, *104*, 7599−7605.
(24) Ortiz, J. V. An efficient, renormalized self-energy for calculating the electron binding energies of closed-shell molecules and anions. *Int. J. Quantum Chem.* **2005**, *105*, 803−808.
(25) Schirmer, J.; Cederbaum, L. S. The two-particle-hole Tamm-Dancoff approximation (2ph-TDA) equations for closed-shell atoms and molecules. *J. Phys. B: At. Mol. Phys.* **1978**, *11*, 1889−1900.
(26) Møller, C.; Plesset, M. S. Note on an Approximation Treatment for Many-Electron Systems. *Phys. Rev.* **1934**, *46*, 618−622.
(27) Ortiz, J. V. The Electron Propagator Picture of Molecular Electronic Structure. In *Computational Chemistry: Reviews of Current Trends*; Leszczynski, J., Ed.; World Scientific: Singapore, 1997; Vol. *2*, pp 1−61.
(28) Schirmer, J.; Cederbaum, L. S.; Walter, O. New approach to the one-particle Green's function for finite Fermi systems. *Phys. Rev. A* **1983**, *28*, 1237−1259.
(29) Schirmer, J.; Angonoa, G. On Green's function calculations of the static self-energy part, the ground state energy and expectation values. *J. Chem. Phys.* **1989**, *91*, 1754−1761.
(30) Trofimov, A. B.; Schirmer, J. Molecular ionization energies and ground- and ionic-state properties using a non-Dyson electron propagator approach. *J. Chem. Phys.* **2005**, *123*, 144115.
(31) Banerjee, S.; Sokolov, A. Y. Algebraic Diagrammatic Construction Theory for Simulating Charged Excited States and Photoelectron Spectra. *J. Chem. Theory Comput.* **2023**, *19*, 3037−3053.
(32) Dreuw, A.; Papapostolou, A.; Dempwolff, A. L. Algebraic Diagrammatic Construction Schemes Employing the Intermediate State Formalism: Theory, Capabilities, and Interpretation. *J. Phys. Chem. A* **2023**, *127*, 6635−6646.
(33) Angonoa, G.; Walter, O.; Schirmer, J. Theoretical K-shell ionization spectra of N2 and CO by a fourth-order Green's function method. *J. Chem. Phys.* **1987**, *87*, 6789−6801.
(34) Ortiz, J. V. A nondiagonal, renormalized extension of partial third-order quasiparticle theory: comparisons for closed-shell ionization energies. *J. Chem. Phys.* **1998**, *108*, 1008−1014.
(35) Brueckner, K. A. Nuclear Saturation and Two-Body Forces. II. Tensor Forces. *Phys. Rev.* **1954**, *96*, 508−516.
(36) Nesbet, R. K. Brueckner's Theory and the Method of Superposition of Configurations. *Phys. Rev.* **1958**, *109*, 1632−1638.
(37) Cizek, J.; Paldus, J. Coupled Cluster Approach. *Phys. Scr.* **1980**, *21*, 251−254.
(38) Bartlett, R. J.; Purvis, G. D. Molecular Applications of Coupled Cluster and Many-Body Perturbation Methods. *Phys. Scr.* **1980**, *21*, 255−265.
(39) Chiles, R. A.; Dykstra, C. E. An electron pair operator approach to coupled cluster wave functions. Application to He_2, Be_2, and Mg_2 and comparison with CEPA methods. *J. Chem. Phys.* **1981**, *74*, 4544−4556.
(40) Handy, N. C.; Pople, J. A.; Head-Gordon, M.; Raghavachari, K.; Trucks, G. W. Size-consistent Brueckner theory limited to double substitutions. *Chem. Phys. Lett.* **1989**, *164*, 185−192.
(41) Ortiz, J. V. Orbital and shakeup operator renormalizations in electron propagator theory. *J. Chem. Phys.* **1998**, *109*, 5741−5746.

https://doi.org/10.1021/acs.jctc.3c00954
J. Chem. Theory Comput. 2024, 20, 290−306

(42) Ortiz, J. V. Electron detachment energies of closed-shell anions calculated with a renormalized electron propagator. *Chem. Phys. Lett.* **1998**, *296*, 494−498.
(43) Ortiz, J. V. Single-reference electron propagator calculations on vertical ionization energies of ozone. *Chem. Phys. Lett.* **1998**, *297*, 193−199.
(44) Ortiz, J. V. Toward an exact one-electron picture of chemical bonding. *Adv. Quantum Chem.* **1999**, *35*, 33−52.
(45) Banerjee, A.; Shepard, R.; Simons, J. One-particle Green's function with multiconfiguration reference states. *Int. J. Quantum Chem., Quantum Chem. Symp.* **1978**, *14* (S12), 389−404.
(46) Yeager, D. L. The multiconfigurational spin-tensor electron propagator method (MCSTEP). *Adv. Quantum Chem.* **2005**, *50*, 289−313.
(47) Mazin, I. M.; Sokolov, A. Y. Multireference Algebraic Diagrammatic Construction Theory for Excited States: Extended Second-Order Implementation and Benchmark. *J. Chem. Theory Comput.* **2021**, *17*, 6152−6165.
(48) Opoku, E.; Pawłowski, F.; Ortiz, J. V. Electron Propagator Self-Energies versus Improved GW100 Vertical Ionization Energies. *J. Chem. Theory Comput.* **2022**, *18*, 4927−4944.
(49) Opoku, E.; Pawłowski, F.; Ortiz, J. V. Electron Propagator Theory of Vertical Electron Detachment Energies of Anions: Benchmarks and Applications to Nucleotides. *J. Phys. Chem. A* **2023**, *127*, 1085−1101.
(50) Opoku, E.; Pawłowski, F.; Ortiz, J. V. Erratum: "A new generation of diagonal self-energies for the calculation of electron removal energies" [J. Chem. Phys 155, 204107 (2021)]. *J. Chem. Phys.* **2023**, *159*, 069901.
(51) Opoku, E.; Pawłowski, F.; Ortiz, J. V. Correction to "Electron-Propagator Self-Energies versus Improved GW100 Vertical Ionization Energies. *J. Chem. Theory Comput.* **2023**, *19*, 5648.
(52) Bintrim, S. J.; Berkelbach, T. C. Full-frequency GW without frequency. *J. Chem. Phys.* **2021**, *154*, 041101.
(53) Opoku, E.; Pawłowski, F.; Ortiz, J. V. A new generation of non-diagonal, renormalized self-energies for calculation of electron removal energies. *J. Chem. Phys.* **2023**, *159*, 124109.
(54) Dempwolff, A. L.; Belogolova, A. M.; Trofimov, A. B.; Dreuw, A. Intermediate state representation approach to physical properties of molecular electron-attached states: Theory, implementation, and benchmarking. *J. Chem. Phys.* **2021**, *154*, 104117.
(55) Banerjee, S.; Sokolov, A. Y. Third-order algebraic diagrammatic construction theory for electron attachment and ionization energies: Conventional and Green's function implementation. *J. Chem. Phys.* **2019**, *151*, 224112.
(56) Chatterjee, K.; Sokolov, A. Y. Extended Second-Order Multireference Algebraic Diagrammatic Construction Theory for Charged Excitations. *J. Chem. Theory Comput.* **2020**, *16*, 6343−6357.
(57) Richard, R. M.; Marshall, M. S.; Dolgounitcheva, O.; Ortiz, J. V.; Brédas, J. L.; Marom, N.; Sherrill, C. D. Accurate Ionization Potentials and Electron Affinities of Acceptor Molecules I. Reference Data at the CCSD(T) Complete Basis Set Limit. *J. Chem. Theory Comput.* **2016**, *12*, 595−604.
(58) Gallandi, L.; Marom, N.; Rinke, P.; Körzdörfer, T. Accurate Ionization Potentials and Electron Affinities of Acceptor Molecules II: Non-Empirically Tuned Long-Range Corrected Hybrid Functionals. *J. Chem. Theory Comput.* **2016**, *12*, 605−614.
(59) Knight, J. W.; Wang, X.; Gallandi, L.; Dolgounitcheva, O.; Ren, X.; Ortiz, J. V.; Rinke, P.; Körzdörfer, T.; Marom, N. Accurate Ionization Potentials and Electron Affinities of Acceptor Molecules III: A Benchmark of GW Methods. *J. Chem. Theory Comput.* **2016**, *12*, 615−626.
(60) Dolgounitcheva, O.; Díaz-Tinoco, M.; Zakrzewski, V. G.; Richard, R. M.; Marom, N.; Sherrill, C. D.; Ortiz, J. V. Accurate Ionization Potentials and Electron Affinities of Acceptor Molecules IV: Electron-Propagator Methods. *J. Chem. Theory Comput.* **2016**, *12*, 627−637.
(61) Dolgounitcheva, O.; Díaz-Tinoco, M.; Zakrzewski, V. G.; Richard, R. M.; Marom, N.; Sherrill, C. D.; Ortiz, J. V. Correction to Accurate Ionization Potentials and Electron Affinities of Acceptor Molecules IV: Electron-Propagator Methods. *J. Chem. Theory Comput.* **2017**, *13*, 389−391.
(62) Hirata, S.; Hermes, M. R.; Simons, J.; Ortiz, J. V. General-Order Many-Body Green's Function Method. *J. Chem. Theory Comput.* **2015**, *11*, 1595−1606.
(63) Hirata, S.; Doran, A. E.; Knowles, P. J.; Ortiz, J. V. One-particle many-body Green's function theory: Algebraic recursive definitions, linked-diagram theorem, irreducible-diagram theorem, and general-order algorithms. *J. Chem. Phys.* **2017**, *147*, 044108.
(64) Chong, D. P.; Herring, F. G.; McWilliams, D. Perturbation corrections to Koopmans' theorem. I. Double-zeta Slater-type-orbital basis. *J. Chem. Phys.* **1974**, *61*, 78−84.
(65) Hu, C.-H.; Chong, D. P.; Casida, M. E. The parametrized second-order Green function times screened interaction (pGW2) approximation for calculation of outer valence ionization potentials. *J. Electron Spectrosc. Relat. Phenom.* **1997**, *85*, 39−46.
(66) Lim, F.-H.; Nishida, M.; Hori, Y.; Ida, T.; Mizuno, M. Optimization of the spin-component-scaled factor for electron propagator method. *Chem. Phys. Lett.* **2017**, *678*, 159−166.
(67) Romero, J.; Charry, J. A.; Nakai, H.; Reyes, A. Improving quasiparticle second order electron propagator calculations with the spin-component-scaled technique. *Chem. Phys. Lett.* **2014**, *591*, 82−87.
(68) Śmiga, S.; Grabowski, I. Spin-Component-Scaled ΔMP2 Parametrization: Toward a Simple and Reliable Method for Ionization Energies. *J. Chem. Theory Comput.* **2018**, *14*, 4780−4790.
(69) Schirmer, J.; Trofimov, A. B.; Stelter, G. A non-Dyson third-order approximation scheme for the electron propagator. *J. Chem. Phys.* **1998**, *109*, 4734−4744.
(70) Frisch, M. J.; Trucks, G. W.; Schlegel, H. B.; Scuseria, G. E.; Robb, M. A.; Cheeseman, J. R.; Scalmani, G.; Barone, V.; Petersson, G. A.; Nakatsuji, H.; et al. *Gaussian Development Version*. Revision I.14; Gaussian Inc.: Wallingford, CT, 2018.
(71) Kendall, R. A.; Dunning, T. H.; Harrison, R. J. Electron affinities of the first-row atoms revisited. Systematic basis sets and wave functions. *J. Chem. Phys.* **1992**, *96*, 6796−6806.
(72) Díaz-Tinoco, M.; Dolgounitcheva, O.; Zakrzewski, V. G.; Ortiz, J. V. Composite electron propagator methods for calculating ionization energies. *J. Chem. Phys.* **2016**, *144*, 224110.
(73) Ortiz, J. V. Energy gradients and effective density differences in electron propagator theory. *J. Chem. Phys.* **2000**, *112*, 56−68.
(74) Flores-Moreno, R.; Ortiz, J. V. Integral approximations in ab initio, electron propagator calculations. *J. Chem. Phys.* **2009**, *131*, 124110.
(75) Flores-Moreno, R.; Ortiz, J. V. Efficient and Accurate Electron Propagator Methods and Algorithms. In *Practical Aspects of Computational Chemistry: Methods, Concepts and Applications*; Leszczynski, J., Shukla, M. K., Eds.; Springer Netherlands: Dordrecht, 2010; pp 1−17.
(76) Vysotskiy, V. P.; Cederbaum, L. S. On the Cholesky decomposition for electron propagator methods: General aspects and application on C60. *J. Chem. Phys.* **2010**, *132*, 044110.

https://doi.org/10.1021/acs.jctc.3c00954
J. Chem. Theory Comput. 2024, 20, 290−306

Appendix H

E. Opoku, F. Pawłowski and J. V. Ortiz, "Electron Propagator Theory of Vertical Electron Detachment Energies of Anions: Benchmarks and Applications to Nucleotides", *J. Phys. Chem. A*, 127, 1085–101 (2023)

THE JOURNAL OF PHYSICAL CHEMISTRY A
A JOURNAL OF THE AMERICAN CHEMICAL SOCIETY

pubs.acs.org/JPCA Article

Electron Propagator Theory of Vertical Electron Detachment Energies of Anions: Benchmarks and Applications to Nucleotides

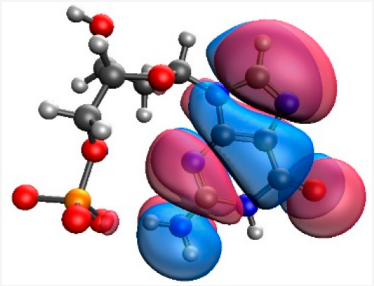
Published as part of The Journal of Physical Chemistry virtual special issue "MQM 2022: The 10th Triennial Conference on Molecular Quantum Mechanics".

Ernest Opoku, Filip Pawłowski, and J. V. Ortiz*

Cite This: *J. Phys. Chem. A* 2023, 127, 1085−1101 Read Online

ACCESS | Metrics & More | Article Recommendations | Supporting Information

ABSTRACT: A new generation of *ab initio* electron-propagator self-energy approximations that are free of adjustable parameters is tested on a benchmark set of 55 vertical electron detachment energies of closed-shell anions. Comparisons with older self-energy approximations indicate that several new methods that make the diagonal self-energy approximation in the canonical Hartree−Fock orbital basis provide superior accuracy and computational efficiency. These methods and their acronyms, mean absolute errors (in eV), and arithmetic bottlenecks expressed in terms of occupied (O) and virtual (V) orbitals are the opposite-spin, non-Dyson, diagonal second-order method (os-nD-D2, 0.2, OV^2), the approximately renormalized quasiparticle third-order method (Q3+, 0.15, O^2V^3) and the approximately renormalized, non-Dyson, linear, third-order method (nD-L3+, 0.1, OV^4). The Brueckner doubles with triple field operators (BD-T1) nondiagonal electron-propagator method provides such close agreement with coupled-cluster single, double, and perturbative triple replacement total energy differences that it may be used as an alternative means of obtaining standard data. The new methods with diagonal self-energy matrices are the foundation of a composite procedure for estimating basis-set effects. This model produces accurate predictions and clear interpretations based on Dyson orbitals for the photoelectron spectra of the nucleotides found in DNA.



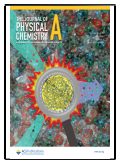
INTRODUCTION

To enable discovery of unprecedented molecular anions and to understand their structure, spectra, and chemical bonding, computational chemists have repeatedly turned to the methods of *ab initio* electron propagator theory.[1−6] Among the advantages of this approach are direct calculation of electron binding energies and their corresponding Dyson orbitals,[7] a high degree of accuracy relative to computational effort, and ease of qualitative interpretation in terms of familiar concepts. Direct calculation of the energy difference between two states that differ in their electron counts by one avoids the evaluation of total energies whose absolute values are typically many orders of magnitude greater than molecular electron affinities or electron detachment energies of anions. Direct determination of Dyson orbitals bypasses the generation of complicated many-electron state functions that are usually defined in terms of a multitude of wavefunction amplitudes. By focusing computational resources in this way, a desired level of accuracy may be procured with fewer arithmetic operations than those required by indirect procedures. Kinetic, nuclear attraction, Coulomb repulsion, exchange, relaxation, and correlation contributions to an electron binding energy are easily identified.[5,6] The probability factor defined by the norm of the Dyson orbital is an index of validity for qualitative interpretations based on molecular orbital concepts.[7] The largest absolute amplitudes and the nodes of Dyson orbitals provide insights into bonding relationships that connect structure and reactivity to spectra.

Early developers of electron propagator methods turned their attention to molecular anions almost as soon as new capabilities were introduced. Perturbative corrections to canonical Hartree−Fock orbital energies (i.e., the results of Koopmans's identity[8]) derived with the closely related equation-of-motion formalism were demonstrated in applications to small anions.[9−14] Orbital relaxation and perturbative correlation corrections were incorporated in other early approaches.[15−17] A series of tests on low-order approximations established their utility in the interpretation of anion photoelectron spectra.[18−28] Subsequent improvements that incorporate strong correlation or relativistic corrections in reference states also have been tested.[29−33]

A profusion of applications to anions with novel structures and bonding patterns ensued that frequently featured

Received: November 29, 2022
Revised: December 31, 2022
Published: January 19, 2023



ACS Publications © 2023 American Chemical Society

https://doi.org/10.1021/acs.jpca.2c08372
J. Phys. Chem. A 2023, 127, 1085−1101

collaboration with experimental researchers. Photoelectron spectra of small boron clusters with negative charges were interpreted.[34−37] Clusters with planar tetracoordinate carbon nuclei were shown to exist.[38] The occurrence of all-metal aromaticity in small clusters was advocated.[39,40] All-metal antiaromatic clusters were reported.[41] Wheel-like clusters with boron or carbon nuclei in hypercoordinate positions were discovered.[42,43] Anionic boron clusters with structures reminiscent of organic aromatics such as naphthalene were studied.[44,45] Novel structures with larger numbers of boron atoms,[46,47] aluminum-doped boron clusters,[48,49] and stoichiometrically induced structural changes in carbon−boron clusters[50] were convincingly established. Isoelectronic analogies between C and Al^- were exploited in searches for metallic clusters that resemble alkanes or alkynes.[51,52]

Electron propagator methods have been prominent in the discovery of multiply charged anions that are stable in the gas phase. Early applications to $Ni(CN)_4^{2-}$ with perturbative methods[53] were followed by examinations of complexes composed of transition metals with halide ligands.[54,55] The stability of doubly charged carbon cluster anions with acetylenic features was demonstrated.[56,57] Subsequent calculations disclosed the feasibility of extending this structural motif to quadruply charged carbon anions.[58] A substituted Ni phthalocyanine with a metastable −4 charge was examined as well.[59] The introduction of fully relativistic generalizations of electron propagator methods facilitated studies of platinum complexes with halide or cyanide ligands.[60−65] Electron binding energies of SiF_6^{2-} also have been calculated.[66] Electron detachment energies of doubly charged anions defined as twice-deprotonated organic acids such as oxalate were studied,[67,68] as were aromatic dicarboxylates.[69]

Since the introduction of the concept of a superhalogen (i.e., a species whose electron affinity exceeds those of the halogen atoms),[70] electron propagator methods have proven to be especially efficient and reliable tools in their identification and optimization.[71] The importance of electron correlation in determining reliable electron detachment energies of superhalide anions was emphasized at an early stage.[72] Metal (M with m valence electrons) halide (X) anions with the general formula $M_iX_{mi+1}^-$ that exhibit delocalization of Dyson orbitals over many halogen centers have been especially frequent objects of study.[73−90] Extensions to alternative electronegative ligands have been shown to be feasible.[91−102] Even organic ligands such as carboxylates and amino acids or fluoroborate tripods were discovered to be suitable for constructing superhalogens.[103−105] Connections between the search for more powerful superhalogens with record-setting electron detachment energies and the optimization of superacids with superlative Brønsted acidity have been identified after analysis of electron propagator calculations on icosahedral carboranes.[106,107] OF_3^- turns out to be a superhalogen,[108] as do large $H_nF_{n+1}^-$ clusters with extraordinarily large electron detachment energies,[109] alkali-metal complexes with borane,[110] $HF−MF_n^-$ clusters,[83] boron−nitrogen fluoride oligomers,[111] NaCl clusters,[112] noble-gas fluorides,[113] BO_2^-,[114] and (by a narrow margin) BS_2^-.[115] Direct calculation of improvements to canonical Hartree−Fock energies has proven to be a crucial advantage in superhalide clusters where the qualifying electron detachment energy does not correspond to the highest occupied molecular orbital.[116−119] For example, in clusters with CN ligands, the order of σ and π orbitals may be reversed by electron correlation.

Anionic fragments of nucleic acids and other molecules of biochemical importance have been frequent targets of electron propagator methodology. Photoelectron spectra of anions of the purine and pyrimidine bases that occur in the multiply charged anions known as DNA and RNA have been interpreted with electron propagator methods.[120−124] Predictions of the electron detachment energies of deprotonated bases have been made.[125] Photoelectron spectra of an anion of a uracil−water complex with a hydrogen bond between the molecules have been assigned.[126] The transition between valence-bound and diffuse-bound anions that occurs as a coordinating water molecule is replaced by a noble-gas atom has been interpreted, with the uracil−Xe complex exhibiting both possibilities in the same spectrum.[127] Several studies of nucleotide and dinucleotide electron detachment energies have produced thorough assignments of photoelectron spectra and have demonstrated the variable order of phosphate-centered and base-centered holes in final states.[128−132] Photoelectron spectra of a class of enzymatically important anions, metal sulfide clusters, have been assigned with the aid of electron propagator methods.[133]

Metal oxide cluster anions whose reactivity has implications for catalysis and related technologies have been studied with a view to assignment of photoelectron spectra. Aluminum oxide cluster anions, especially those with formal metal oxidation states below +3, may have spectra that correspond to more than one isomer.[134−140] Spectra of the products of reactions between these clusters and various molecules have been interpreted.[141,142] Silicon and transition-metal oxide clusters also have been considered.[143,144]

Calculations of the electron detachment energies of double Rydberg anions have provided definitive assignments of photoelectron spectra and have offered testable predictions for further experimentation. Tetrahedral NH_4^- and its complexes with ammonia molecules and the C_{3v} isomer of OH_3^- and its complexes with water molecules have been examined in detail.[145−151] Double Rydberg anions with ammonium cores coordinated to water molecules were predicted recently.[152] Tetrahedral and sawhorse structures of PH_4^- were discovered.[153] Replacement of hydrogen atoms by monovalent substituents has yielded several stable structures with double Rydberg characteristics.[154] Methylated, annulated, and paramagnetic double Rydberg anions also have been predicted to be stable.[155]

Several kinds of anionic metal coordination complexes have been studied with electron propagator methods. The double Rydberg concept of a diffuse electron pair that surrounds a molecular cationic core has been extended to $M(NH_3)_n$ solvated electron precursors, which also have anions with positive electron detachment energies.[156,157] Calculations on the electron detachment energies of $ZnC_5H_5^-$,[158] $ZnCH_3^-$,[159] $ScC_6H_6^-$,[160] and $BeC_5H_5^-$[161] have been performed.

Establishment of the structure of gas-phase clusters by reconciling calculations with photoelectron spectra has been a frequent goal of electron propagator studies. Carbon cluster anions with three to 13 nuclei as well as the anion of C_{60} have been tackled.[162−168] Electron detachment energies of anionic clusters of Li, Al, and Si have been determined.[169−171] Electron detachment energies of ionically bound anionic clusters, such as those of sodium chloride, have been interpreted successfully.[172] Mixed alkali−semiconductor anions,[173] aluminum hydrides,[174] quadrupole-bound anions,[175] organic electron acceptors,[176,177] and azolide anions[178] are among the

https://doi.org/10.1021/acs.jpca.2c08372
J. Phys. Chem. A 2023, 127, 1085−1101

diverse species that have been characterized with electron propagator methods.

The effects of solvation on halide electron detachment energies have been studied with a combination of strategies, including microsolvation, continuum models, and Monte Carlo sampling of solvent configurations.[179−183]

Electron detachment energies of singlet anions of free radicals have provided information on ground and excited doublet states of organic radical scavengers and superalkali clusters.[184−186]

Most of these calculations have been performed with a canonical Hartree−Fock basis of spin-orbitals and the diagonal self-energy approximation, which neglects off-diagonal self-energy matrix elements. The most employed diagonal self-energies are the outer valence Green's function (OVGF),[4,187] the partial third order approximation (P3),[188] and its approximately renormalized extension (P3+).[138] For vertical electron detachment energies (i.e., where the reference state is anionic and the final state is uncharged), these three methods have arithmetic scaling factors of OV^4, O^2V^3, and O^2V^3, respectively, where O and V denote the numbers of occupied and virtual orbitals, respectively, produced by the Hartree−Fock calculation. The OVGF encompasses three formulas, known as the A, B and C versions, for estimating self-energy terms beyond third order. A procedure (originally developed for calculations of molecular ionization energies) that attempts to identify the best alternative invokes several numerical parameters.[187]

Recent tests on vertical ionization energies of closed-shell molecules demonstrated that a new generation of self-energy approximations produces better accuracy than its older counterparts with equal or reduced arithmetic scaling factors.[189,190] For example, the linear, third-order, version B (L3+B) approximation produces lower mean absolute errors for two data sets than the OVGF-B procedure while retaining the latter method's OV^4 arithmetic scaling.

In this work, a previously published data set of 55 vertical electron detachment energies[33] serves as a standard of comparison for judging the performance of diagonal self-energy approximations in calculating vertical electron detachment energies of closed-shell anions. After a review of the theory that underlies the diagonal self-energy approximations that will be compared, numerical calculations are presented and statistically analyzed. These data lead to specific recommendations for users of computational chemistry software. To facilitate the exhaustion of basis-set effects and self-energy corrections, an efficient composite model has been developed. Applications to the nucleotide anions of DNA illustrate the interpretive capabilities of some of the new methods under present scrutiny.

THEORY

Let an orthonormal spin-orbital basis u with indices p and q define the field operators that occur in the pq element of the electron propagator matrix,

$$\langle\langle a_p(t);\, a_q^\dagger(t')\rangle\rangle = -\mathrm{i}\Theta(t-t')\langle\Psi_0^N|a_p(t)a_q^\dagger(t')|\Psi_0^N\rangle + \mathrm{i}\Theta(t'-t)\langle\Psi_0^N|a_q^\dagger(t')a_p(t)|\Psi_0^N\rangle \quad (1)$$

which is defined in terms of the Heaviside step function (Θ) and an N-electron reference (initial) eigenstate, Ψ_0^N. This element's Fourier transform in its spectral form,

$$\langle\langle a_p;\, a_q^\dagger\rangle\rangle_E = \lim_{\eta\to 0^+}\left[\sum_R \frac{\langle\Psi_0^N|a_p|R\rangle\langle R|a_q^\dagger|\Psi_0^N\rangle}{E + E_0(N) - E_R(N+1) + \mathrm{i}\eta} + \sum_S \frac{\langle\Psi_0^N|a_q^\dagger|S\rangle\langle S|a_p|\Psi_0^N\rangle}{E - E_0(N) + E_S(N-1) - \mathrm{i}\eta}\right] \quad (2)$$

has summations over final eigenstates with $N+1$ or $N-1$ electrons. Poles originating in the two summations over R and S occur respectively at energies of electron attachment (i.e., electron affinities) and detachment (e.g., ionization energies of molecules or electron detachment energies of molecular anions). The numerators associated with the poles (i.e., the residues) are products of Feynman−Dyson amplitudes,

$$f_p^R = \langle\Psi_0^N|a_p|R\rangle \quad (3)$$

$$g_p^S = \langle S|a_p|\Psi_0^N\rangle \quad (4)$$

Dyson spin-orbitals of attachment and detachment may be expressed as

$$\varphi_R^{\mathrm{Dyson}}(x_1) = \sqrt{N+1}\int \Psi_0^{N*}(x_2, x_3, x_4, \cdots, x_{N+1})\,\Psi_R(x_1, x_2, x_3, \cdots, x_{N+1})\,\mathrm{d}x_2\,\mathrm{d}x_3\,\mathrm{d}x_4\cdots\mathrm{d}x_{N+1} = \sum_R f_p^R u_p(x_1) \quad (5)$$

$$\varphi_S^{\mathrm{Dyson}}(x_1) = \sqrt{N}\int \Psi_S^{*}(x_2, x_3, x_4, \cdots, x_N)\,\Psi_0^N(x_1, x_2, x_3, \cdots, x_N)\,\mathrm{d}x_2\,\mathrm{d}x_3\,\mathrm{d}x_4\cdots\mathrm{d}x_N = \sum_S g_p^S u_p(x_1) \quad (6)$$

The plus sign between the R and S summations in eq 2 requires that an anticommutator be present in the definition of a superoperator metric

$$[X|Y] = \langle\Psi_0^N|X^\dagger Y + YX^\dagger|\Psi_0^N\rangle \quad (7)$$

such that X and Y are members of a set of second-quantized-operator products (w) with creators exceeding annihilators by one, e.g., $a_p^\dagger$ (hole and particle, or h and p), $a_p^\dagger a_q^\dagger a_r$ (2hp and 2ph), $a_p^\dagger a_q^\dagger a_r^\dagger a_s a_t$ (3h2p and 3p2h).[191] Identity and Hamiltonian superoperators that act in this space are defined by

$$\hat{I}X = X \quad (8)$$

$$\hat{H}X = HX - XH \quad (9)$$

In this notation, the electron propagator matrix elements read as

$$\langle\langle a_p;\, a_q^\dagger\rangle\rangle_E = G_{pq}(E) = [a_p^\dagger|(E\hat{I} - \hat{H})^{-1}a_q^\dagger] \quad (10)$$

The resolvent superoperator $\mathbf{G}(E)$, given by

$$\mathbf{G}(E) = [\mathbf{a}^\dagger|(E\hat{I} - \hat{H})^{-1}\mathbf{a}^\dagger] \quad (11)$$

may be related to an inverse matrix after introduction of an inner projection[192] with w operators according to

$$\mathbf{G}(E) = [\mathbf{a}^\dagger|\mathbf{w}][\mathbf{w}|(E\hat{I} - \hat{H})\mathbf{w}]^{-1}[\mathbf{w}|\mathbf{a}^\dagger] \quad (12)$$

The w operator space may be partitioned into a set of simple normalized field operators $\mathbf{a}$ and an orthogonalized comple-

https://doi.org/10.1021/acs.jpca.2c08372
J. Phys. Chem. A 2023, 127, 1085−1101

ment $\mathbf{f}$ with the requirement that $[\mathbf{a}^\dagger|\mathbf{f}] = \mathbf{0}$. The *inverse form of the Dyson equation* arises from this partitioning as follows:

$$\mathbf{G}^{-1}(E) = [\mathbf{a}^\dagger|(E\hat{I} - \hat{H})\mathbf{a}^\dagger] - [\mathbf{a}^\dagger|\hat{H}\mathbf{f}][\mathbf{f}|(E\hat{I} - \hat{H})\mathbf{f}]^{-1}[\mathbf{f}|\hat{H}\mathbf{a}^\dagger] \tag{13}$$

An alternative way of writing the inverse Dyson equation may be obtained by using

$$[a_p^\dagger|\hat{H}a_q^\dagger] = h_{pq}^{(1)} + \sum_{rs} \langle pr||qs\rangle \rho_{rs} = F_{pq} \tag{14}$$

where $\boldsymbol{\rho}$ is the one-electron reduced density matrix (1-RDM) of the reference state and $\mathbf{F}$ is a generalized Fock matrix with the usual one-electron ($h^{(1)}$) and antisymmetrized two-electron (Dirac notation) matrix elements. In the spin-orbital basis of eigenfunctions of $h^{(1)} + v$ with eigenvalues e^v, a reference inverse electron propagator matrix may be defined by

$$\mathbf{G}_0^{-1}(E) = E\mathbf{1} - \mathbf{e}^v \tag{15}$$

with vanishing off-diagonal elements. The inverse Dyson equation now appears in its most familiar form,

$$\mathbf{G}^{-1}(E) = \mathbf{G}_0^{-1}(E) - \boldsymbol{\Sigma}(E) \tag{16}$$

where the self-energy matrix $\boldsymbol{\Sigma}(E)$ comprises constant (i.e., energy-independent) and energy-dependent terms according to

$$\boldsymbol{\Sigma}(E) = \mathbf{F} - \mathbf{h}^{(1)} - \mathbf{v} + [\mathbf{a}^\dagger|\hat{H}\mathbf{f}][\mathbf{f}|(E\hat{I} - \hat{H})\mathbf{f}]^{-1}[\mathbf{f}|\hat{H}\mathbf{a}^\dagger] \tag{17}$$

If v is chosen to be the Coulomb−exchange operator of a Hartree−Fock self-consistent field, then

$$\boldsymbol{\Sigma}(E) = \boldsymbol{\Sigma}(\infty) + [\mathbf{a}^\dagger|\hat{H}\mathbf{f}][\mathbf{f}|(E\hat{I} - \hat{H})\mathbf{f}]^{-1}[\mathbf{f}|\hat{H}\mathbf{a}^\dagger] \tag{18}$$

where elements of the energy-independent term in the self-energy matrix,

$$\Sigma_{pq}(\infty) = \sum_{rs} \langle pr||qs\rangle(\rho_{rs} - \rho_{rs}^{\mathrm{HF}}) \tag{19}$$

are generated by correlation contributions to the 1-RDM. When v is the Hartree−Fock Coulomb−exchange operator, final-state-orbital relaxation and differential correlation terms in the self-energy matrix may be distinguished from each other.[193,194] With this assumption, the sum of the first three terms in eq 17 equals zero through second order in the fluctuation potential and makes contributions to the energy-independent terms of eq 19 in higher orders. Eigenfunctions obtained with alternative local or nonlocal choices for v generally produce nondiagonal energy-independent first-order terms that involve the nonlocal HF exchange operator anyway in eq 18.

For any choice of orbitals, poles of $\mathbf{G}(E)$ (or zeroes of $\mathbf{G}^{-1}(E)$) are equal to energies (E_X) where the quasiparticle eigenvalue equation is satisfied:

$$[\mathbf{F} + \boldsymbol{\Sigma}(E_X)]\mathbf{C}(E_X) = E_X\mathbf{C}(E_X) \tag{20}$$

The associated probability factors Π_X are equal to the norms of the Dyson spin-orbitals[7] and are determined by

$$\Pi_X = \int |\varphi^{\mathrm{Dyson}}(x)|^2 \, dx = \left(1 - \mathbf{C}^\dagger(E_X)\left[\frac{d\boldsymbol{\Sigma}(E)}{dE}\right]_{E=E_X}\mathbf{C}(E_X)\right)^{-1} \tag{21}$$

The elements of the $\mathbf{C}(E_X)$ eigenvectors have the following relationship to the Feynman−Dyson amplitudes and Dyson spin-orbitals:

$$\varphi_X^{\mathrm{Dyson}}(x) = \Pi_X{}^{0.5} \sum_p C_p(E_X)u_p(x) \tag{22}$$

Many of the methods under examination in this work employ the physically reasonable canonical spin-orbitals of HF theory and set off-diagonal elements of the self-energy matrix to zero. This choice implies that each canonical spin-orbital generates its own independent set of electron binding energies that are obtained by iterating (with respect to E) the *diagonal quasiparticle equation*:

$$e_p^{\mathrm{HF}} + \Sigma_{pp}(E_{Xp}) = E_{Xp} \tag{23}$$

Therefore, at convergence, Koopmans results (e_p^{HF}) are corrected by the diagonal elements of the self-energy matrix. The probability factors are related to derivatives of the diagonal elements with respect to E:

$$\Pi_{Xp} = \left[1 - \left.\frac{d\Sigma_{pp}(E)}{dE}\right|_{E=E_{Xp}}\right]^{-1} \tag{24}$$

In this diagonal approximation, the Dyson spin-orbitals are required to be proportional to the canonical Hartree−Fock spin−orbitals:

$$\varphi_{Xp}^{\mathrm{Dyson}}(x) = \Pi_{Xp}{}^{0.5}u_p^{\mathrm{HF}}(x) \tag{25}$$

Whereas in principle many values of E_{Xp} may be found for a given p, only those poles whose probability factors exceed 0.85 are likely to be reliable when the diagonal approximation is made. The remaining electron binding energies with their relatively small probability factors may provide qualitative clues about correlation states, but there is a clear need in such cases for more complicated and flexible self-energy approximations that include at least all couplings between simple ($\mathbf{a}$) and triple ionization operators in $\mathbf{f}$.

Perturbative expressions for the self-energy matrix elements needed in eqs 20 and 23 have been thoroughly analyzed, and systematic approaches for generating all terms through any order in the Møller−Plesset fluctuation potential have been established.[195,196] Second-order methods with nondiagonal (ND2) or diagonal (D2) self-energy matrices provide the simplest and usually the largest relaxation and correlation corrections to canonical Hartree−Fock orbital energies.[193] These methods typically underestimate the vertical ionization energies of closed-shell molecules even when the basis sets are saturated.[189,190] This defect persists when the 2ph term, which accounts for ground-state correlation,[193] becomes energy-independent in the non-Dyson (nD) version of D2 (nD-D2).[189,190] To mitigate this systematic error, the opposite-spin-only (os) versions of D2 and nD-D2 have been introduced.[189,190] Although the resulting os-D2 and os-nD-D2 methods have no adjustable parameters, they produce average absolute errors for vertical ionization energies that are less than half those of the D2 and nD-D2 methods (i.e., approximately 0.2 vs 0.5 eV). After completion of a partial integral transformation that requires only N^4 arithmetic operations for each electron binding energy, all four diagonal second-order methods are practically free because they have only OV^2 bottlenecks.

https://doi.org/10.1021/acs.jpca.2c08372
J. Phys. Chem. A 2023, 127, 1085−1101

Diagonal third-order (D3) calculations typically make the opposite error: their overestimates of vertical ionization energies are exacerbated by enlargement of basis sets.[189,190] To remedy this deficiency and to estimate the effects of higher-order terms, the three OVGF versions were introduced.[4] Whereas the diagonal self-energy matrix elements of D3 require OV^4 arithmetic operations, the OVGF extensions involve only trivial evaluations of scaling factors. The parametrized selection procedure[187] usually chooses the A version in calculations of ionization energies, but the B and C versions are favored for the relatively low magnitudes that typify electron detachment energies of anions. The P3 and P3+ methods have no selection parameters and require O^2V^3 arithmetic operations. P3+ mean absolute errors were lower than those of the OVGF approach in recent tests.[33,189,190,197]

Members of the fecund *GW* family of methods[198] may be based on Kohn−Sham orbitals produced with a multitude of density functional approximations or with orbitals defined by self-consistency in the *G* or *W* ingredients of the self-energy. Most *GW* calculations employ a diagonal self-energy approximation in a fixed orbital basis (i.e., they involve the G_0W_0 branch of the family) and a so-called one-shot (single Newton iteration) approximation to energy self-consistency in eq 23. Here we avoid orbitals, self-energies, and selection procedures that are based on adjustable parameters and therefore employ a G_0W_0 version based on canonical Hartree−Fock orbitals and exchangeless Tamm−Dancoff excitations instead of the commonly encountered combination of Kohn−Sham orbitals with exchangeless random-phase-approximation excitations. The resulting HF-TDA-G_0W_0 self-energy sums exchangeless ring diagrams in all orders of the fluctuation potential and is a simplified version of the two-particle−one-hole Tamm−Dancoff approximation[199] (2ph-TDA), which includes exchange as well as ladder and mixed ring−ladder terms in all orders.[189,190,200]

A new generation of self-energy approximations features ring−ladder renormalizations with exchange and retains terms that contain ground-state correlation amplitudes (e.g., first-order double replacements or $T_2^{(1)}$) in the D3, OVGF, P3, and P3+ self-energies.[189,190] To derive the renormalized linear third order (RL3) self-energy, a Hermitized, intermediately normalized superoperator metric, defined by

$$[X|Y] = \frac{1}{2}(\langle \mathrm{HF}|(X^\dagger Y + YX^\dagger)(1 + T_2^{(1)} + T_1^{(2)})|\mathrm{HF}\rangle + \langle \mathrm{HF}|(1 + T_2^{(1)} + T_1^{(2)})^\dagger(X^\dagger Y + YX^\dagger)|\mathrm{HF}\rangle) \quad (26)$$

has been adopted. This choice suffices to recover the third-order terms that are linear in ground-state correlation amplitudes, but some of them now have different coefficients than in D3. The RL3 self-energy requires OV^4 arithmetic operations. Tests on ionization energies yield mean absolute errors of 0.1 eV. Because the bottleneck contractions pertain to four-particle-ladder self-energy terms that do not have a large effect on ionization energies, a simplified version that neglects higher-order couplings between 2ph operators has been examined. The resulting renormalized quasiparticle third-order approximation (RQ3) has O^2V^3 arithmetic scaling and only slightly worse errors (∼0.15 eV) for ionization energies. Further neglect of terms descended from second-order single-replacement (i.e., $T_1^{(2)}$) amplitudes defines the renormalized partial third-order (RP3) method.

Finite-order truncations at third order of the three latter methods constitute the L3, Q3, and P3 methods, respectively. Approximate renormalizations that resemble those of the OVGF methods generate the L3+, Q3+, and P3+ self-energies. Only one version is necessary for Q3+ and P3+. The B approximate renormalization of L3+ employs the same approach and has been adopted as the standard version. Whereas the OV^4 bottleneck of RL3 is iterative because of its infinite-order summations, there is only a single OV^4 step for each energy iteration in L3+. The P3+ and Q3+ self-energies have noniterative O^2V^3 bottlenecks. To improve the efficiency of the L3+ method, a non-Dyson version has been introduced that eliminates energy dependence in the OV^4 summations, has only one bottleneck contraction for each final state, and retains practically the same degree of accuracy. Tests on ionization energies of closed-shell molecules and atoms indicate that the approximately renormalized methods (i.e., P3+, Q3+, and L3+) deliver results that are superior to their strictly third-order counterparts (P3, Q3, and L3) and are just as accurate in comparison to their explicitly renormalized antecedents (RP3, RQ3, and RL3).

Comparisons with predicted vertical electron detachment energies generated with nondiagonal self-energies also will be made below. ND2, 2ph-TDA, the third-order algebraic diagrammatic construction (ADC(3)) in its strict version[201] (also known as the 3+ method[202]) and Schirmer−Angonoa version,[203] the nondiagonal second-order renormalized approximation (NR2),[204] and the Brueckner-doubles, triple-field-operator (BD-T1) method[29,31,205−208] will be considered. The three latter methods have sixth-power arithmetic bottlenecks. The O^2V^4 contractions that occur in ADC(3) and BD-T1 are more costly than the O^3V^3 bottleneck in NR2 calculations of ionization energies and electron detachment energies.

Self-energy acronyms and arithmetic scaling factors are summarized in Table 1. For several methods that require electron repulsion integrals with four virtual indices and that involve OV^4 bottlenecks, there is an arithmetic advantage in using their non-Dyson modifications, wherein energy-dependent self-energy terms that exhibit 2ph denominators become energy-independent by setting E to ε_p in $\Sigma_{pp}(E)$. These modified self-energies may be derived from the second term in eq 2 and by retaining only the second term in the anticommutator in eq 7. The resulting Hilbert space methods (i.e., there is no longer explicit coupling between electron attachment and detachment operators as in the Dyson equation) constitute a bridge between electron propagator and equation-of-motion coupled-cluster methods.[209]

RESULTS AND DISCUSSION

Standards and Tests. A set of 55 vertical electron detachment energies of 36 closed-shell anions have been calculated with ΔCCSD(T) (i.e., total energy differences based on coupled-cluster theory with single and double replacements[210] and approximate triple replacements[211]) cubically extrapolated total energies obtained with augmented quadruple- and triple-ζ basis sets.[212] Members of the test set include anions of atoms, diatomics (XY), HXY triatomics, and XH_n polyatomics with X and Y nuclei taken from the first three periods.[33] As assignment problems often require the identification of Koopmans defects (where the latter approximation predicts the order of final states incorrectly), there are many anions in the data set with σ-hole and π-hole final states that correspond to low vertical electron detachment

https://doi.org/10.1021/acs.jpca.2c08372
J. Phys. Chem. A 2023, 127, 1085−1101

Table 1. Arithmetic Scaling Factors of Electron Propagator Methods[a]

method class	method(s)[b]	arithmetic bottleneck	bottleneck steps	largest ERI[c] subset
diagonal second-order	D2, os-D2	OV^2	N_E	O^2V^2
	RSPT2, nD-D2, **os-nD-D2**	OV^2	1	O^2V^2
diagonal post-second-order	RSPT3	OV^4	1	V^4
	D3, OVGF	OV^4	N_E[d]	V^4
	P3, P3+, **Q3**, **Q3+**	O^2V^3	1	OV^3
	L3, **L3+**	OV^4	N_E[d]	V^4
	RP3, **RQ3**	O^2V^3	1	OV^3
	RL3	OV^4	$N_I N_E$[d]	V^4
	HF-TDA G_0W_0	O^2V^3	$N_I N_E$	O^2V^2
nondiagonal	ND2	OV^3	N_I	OV^3
	2ph-TDA	OV^4	N_I	V^4
	3+	O^2V^4	1	V^4
	ADC(3)	O^2V^4	N_I	V^4
	NR2	O^3V^3	1	OV^3
	BD-T1	O^2V^4	BD[e]	V^4

[a]O = no. of occupied orbitals; V = no. of virtual orbitals; N_E = no. of energy iterations; N_I = no. of inverse-expansion iterations. [b]New methods are shown in **bold** type. [c]ERI = electron repulsion integral. [d]A reduction by a factor of N_E occurs in non-Dyson versions. [e]The O^2V^4 arithmetic bottleneck occurs in the Brueckner doubles (BD) coupled-cluster reference-state calculation; the subsequent electron propagator bottleneck is OV^4.

energies. An alternative standard based on BD-T1 results also has been generated (see Table 2). Mean errors, mean absolute errors, standard deviations, and maximum errors with respect to these standards have been generated for each self-energy approximation (see Table 3 and Figure 1). A comprehensive listing of all numerical data is given in the Supporting Information. Error distributions are represented in the histograms of Figure 2. Almost all of the probability factors listed in the Supporting Information exceed 0.85 and provide additional validation for employment of the present methods. Whereas remarks made below on the accuracy of the results pertain to the basis-set-extrapolated data represented in the tables and figures, they are equally applicable to data listed in the Supporting Information that were obtained with augmented double-, triple-, and quadruple-ζ basis sets. Recommendations made in the Conclusions therefore are based on four sets of comparisons, only one of which is discussed in the text below. All of the calculations were performed with the development version of Gaussian.[213] Core orbitals were eliminated from the self-energy summations.

Table 3 and Figure 2 clearly display the deficiencies of Koopmans results for vertical electron detachment energies of closed-shell anions. In most cases, overestimates occur chiefly because of neglect of orbital relaxation in final-state uncharged doublets. The incidence of errors is spread evenly over the abscissa from −0.5 to 1.0 eV. The mean unsigned (absolute) error (MUE) is 0.6 eV.

Some improvement in the spread of errors occurs for the D2 and nD-D2 methods, but the MUE is reduced only to 0.5 eV. Underestimates are much more common than overestimates because of a tendency to exaggerate the importance of final-state orbital relaxation and differential electron correlation. It is possible to take advantage of this systematic bias by neglecting same-spin terms in the self-energy summations. The os-D2 and os-nD-D2 results have lower MUEs near 0.2 eV, and their

Table 2. Test Anions, Point Groups, Hole States, and ΔCCSD(T)/CBS and BD-T1/CBS Standards (in eV)

test anion	point group	hole state	ΔCCSD(T)	BD-T1
AlH_4^-	T_d	$2-4\ ^2t_2$	4.910	4.952
AlO^-	$C_{\infty v}$	$3-4\ ^2\pi$	3.450	3.796
		$5\ ^2\sigma$	2.700	2.712
AlS^-	$C_{\infty v}$	$3-4\ ^2\pi$	3.450	3.533
		$5\ ^2\sigma$	2.770	2.804
BH_4^-	T_d	$2-4\ ^2t_2$	4.680	4.674
BO^-	$C_{\infty v}$	$3-4\ ^2\pi$	5.770	6.026
		$5^2\ \sigma$	2.560	2.595
BS^-	$C_{\infty v}$	$3-4\ ^2\pi$	4.470	4.604
		$5\ ^2\sigma$	2.450	2.457
CH_3^-	C_{3v}	$4\ ^2a_1$	0.410	0.407
Cl^-	K_h	$2-4\ ^2P$	3.690	3.735
CN^-	$C_{\infty v}$	$3\ ^2\sigma$	3.950	3.875
		$4-5\ ^2\pi$	5.120	5.285
CP^-	$C_{\infty v}$	$3\ ^2\sigma$	2.950	2.843
		$4-5\ ^2\pi$	3.740	3.847
F^-	K_h	$2-4\ ^2P$	3.440	3.703
$HAlCl^-$	C_s	$6\ ^2a'$	2.000	2.041
$HAlP^-$	$C_{\infty v}$	$3\ ^2\sigma$	3.900	3.926
		$4-5\ ^2\pi$	2.260	2.266
HBF^-	C_s	$6\ ^2a'$	0.620	0.671
HBN^-	$C_{\infty v}$	$3\ ^2\sigma$	3.900	3.905
		$4-5\ ^2\pi$	3.080	3.130
HCC^-	$C_{\infty v}$	$3\ ^2\sigma$	3.110	3.057
		$4-5\ ^2\pi$	3.470	3.556
HCO^-	C_s	$6\ ^2a'$	0.640	0.660
HNB^-	$C_{\infty v}$	$3-4\ ^2\pi$	4.190	4.324
		$5\ ^2\sigma$	1.880	1.923
HNF^-	C_s	$6\ ^2a'$	4.270	4.320
		$7\ ^2a''$	1.270	1.290
HOO^-	C_s	$6\ ^2a'$	2.150	2.200
		$7\ ^2a''$	1.580	1.580
$HPAl^-$	C_s	$4\ ^2a''$	2.440	2.484
		$5\ ^2a'$	2.220	2.238
$HPCl^-$	C_s	$6\ ^2a'$	4.690	4.718
		$7\ ^2a''$	1.700	1.703
$HSiS^-$	C_s	$5\ ^2a''$	4.060	4.121
		$6\ ^2a'$	2.420	2.399
$HSiSi^-$	C_s	$4\ ^2a''$	2.440	2.379
		$5\ ^2a'$	2.400	2.405
HSS^-	C_{2v}	$6\ ^2a'$	2.880	2.907
		$7\ ^2a''$	2.140	2.129
NH_2^-	C_{2v}	$4\ ^2b_1$	0.750	0.786
OCl^-	$C_{\infty v}$	$6-7\ ^2\pi$	2.550	2.537
OF^-	$C_{\infty v}$	$6-7\ ^2\pi$	2.700	2.716
OH^-	$C_{\infty v}$	$3-4\ ^2\pi$	1.840	1.996
PH_2^-	C_{2v}	$4\ ^2b_1$	1.260	1.268
SCl^-	$C_{\infty v}$	$6-7\ ^2\pi$	2.800	2.803
SF^-	$C_{\infty v}$	$6-7\ ^2\pi$	2.570	2.628
SH^-	$C_{\infty v}$	$3-4\ ^2\pi$	2.360	2.400
SiH_3^-	C_{3v}	$4\ ^2a'$	1.870	1.872
SiN^-	$C_{\infty v}$	$3\ ^2\sigma$	3.060	3.075
		$4-5\ ^2\pi$	3.260	3.002
SiP^-	$C_{\infty v}$	$3\ ^2\sigma$	3.150	3.191
		$4-5\ ^2\pi$	3.100	2.985

https://doi.org/10.1021/acs.jpca.2c08372
J. Phys. Chem. A 2023, 127, 1085−1101

Table 3. Error Distributions (in eV) with Respect to ΔCCSD(T)/CBS Standards

method class	method[a]	mean unsigned error[b]	mean signed error	standard deviation	maximum unsigned error
uncorrelated	KT	0.603	0.526	0.626	1.987
diagonal second-order	D2	0.482	−0.477	0.466	2.047
	os-D2	0.174	−0.060	0.251	0.858
	nD-D2	0.507	−0.501	0.487	2.107
	os-nD-D2	**0.179**	−0.071	0.256	0.887
diagonal post-second-order	HF-TDA G_0W_0	0.265	0.208	0.220	0.701
	D3	0.637	0.618	0.911	4.020
	nD-D3	0.576	0.559	0.809	3.627
	OVGF-A	0.137	−0.015	0.193	0.802
	OVGF-B	0.228	0.181	0.345	1.640
	OVGF-C	0.243	0.225	0.290	1.353
	nD-OVGF-A	0.137	−0.036	0.190	0.791
	nD-OVGF-B	0.206	0.150	0.309	1.641
	nD-OVGF-C	0.218	0.202	0.269	1.348
	P3	0.293	0.233	0.401	1.586
	P3+	**0.166**	0.092	0.229	0.887
	Q3	0.281	0.198	0.433	1.704
	Q3+	**0.160**	0.049	0.243	0.972
	L3	0.226	0.209	0.348	1.457
	nD-L3	0.219	0.202	0.341	1.463
	L3+A	0.129	−0.075	0.149	0.475
	L3+B	0.097	0.067	0.170	0.752
	L3+C	0.100	0.072	0.159	0.676
	nD-L3+A	0.127	−0.090	0.135	0.486
	nD-L3+B	**0.086**	0.056	0.159	0.740
	nD-L3+C	0.089	0.062	0.145	0.660
	RP3	0.133	−0.001	0.187	0.867
	RQ3	0.163	−0.084	0.160	0.424
	RL3	0.079	−0.036	0.088	0.259
	nD-RL3	**0.084**	−0.049	0.084	0.232
nondiagonal	ND2	0.517	−0.417	0.453	2.366
	2ph-TDA	0.525	−0.525	0.244	1.126
	3+	0.224	0.200	0.320	1.392
	ADC(3)	0.200	0.148	0.241	0.813
	NR2	**0.125**	−0.056	0.140	0.551
	BD-T1	**0.062**	0.035	0.089	0.346

[a]New methods are shown in **bold** type. [b]Optimal methods are shown in **bold** type.

mean signed errors are −0.06 and −0.07 eV, respectively. These methods provide a satisfactory degree of accuracy with only minor post-SCF computational effort. When the emphasis is on average performance for a large data set, os-D2 and os-nD-D2, the best options in the bottom (cubically scaling) set of graphs in Figure 1, are potentially useful. Another reason to thoroughly examine approximations with only second-order terms stems from their frequently observed parallelism with respect to higher-order methods when basis-set improvements are made.[214,215] These cubically scaling methods therefore can provide reliable refinements in composite procedures (see below) that employ low-order approximations to estimate the effects of basis-set saturation.

The next higher set of graphs in Figure 1 pertains to methods with O^2V^3 scaling. The P3 and Q3 self-energies, which contain no renormalizations that require repeated bottleneck steps, and the HF-TDA-G_0W_0 method, which does, yield MUEs between 0.25 and 0.3 eV. The latter method has the advantage of not requiring electron repulsion integrals with one occupied and three virtual indices. (Transformed integrals with four virtual indices are not required by any of the methods in this set.) By employing simple, noniterative renormalization estimates, the P3+ and Q3+ methods achieve MUEs of 0.17 and 0.16 eV, respectively. (These error indices are better than those for many of the methods in the next category; *vide infra*.) Mean signed errors are below 0.1 eV in both cases; the Q3+ results are very well balanced in this respect. The tendency of P3, Q3, and HF-TDA-G_0W_0 to overestimate is not as pronounced with P3+ and Q3+.

In the next grouping of bar graphs in Figure 1, the methods with OV^4 scaling are represented. The worst results belong to the D3 and nD-D3 methods, which are inferior to their second-order counterparts. Overestimates dominate the corresponding histograms in Figure 2. OVGF-A succeeds in reducing the MUE to 0.14 eV. (The OVGF selection procedure[187] never chooses this version for the present data set.) The results for the more efficient non-Dyson version are practically identical. The B and C versions are less successful, with MUEs between 0.2 and 0.3 eV. L3 also produces a noteworthy improvement, with a MUE of 0.23 eV. The approximately renormalized B extension and the non-Dyson version are even better: 0.10 for L3+B and 0.09 eV for nD-L3+B. (Improvement also is present in the mean signed error and the standard deviation.) With the explicitly renormalized

https://doi.org/10.1021/acs.jpca.2c08372
J. Phys. Chem. A 2023, 127, 1085−1101

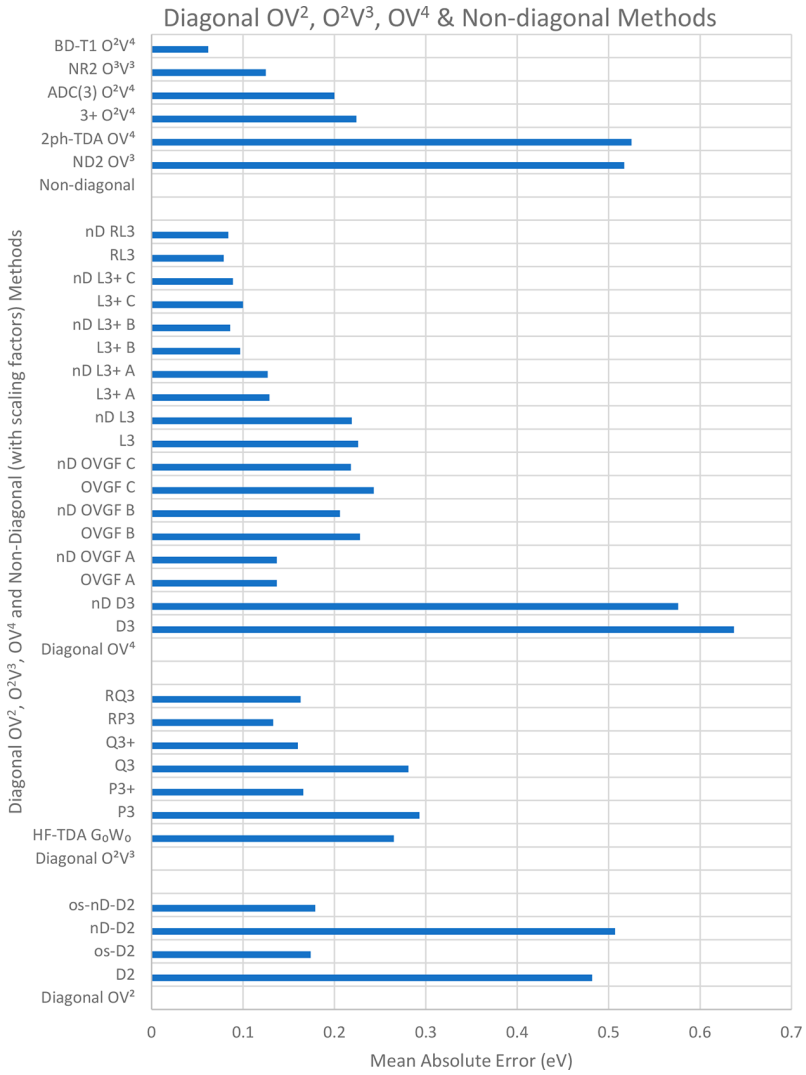


Figure 1. Mean absolute errors (in eV) vs ΔCCSD(T) standards and arithmetic scaling factors.

RL3 method and its non-Dyson version, MUEs of 0.08 eV are realized. Whereas the mean signed errors for L3+B and nD-L3+B are positive (0.06−0.07 eV), these data are slightly negative (between −0.04 and −0.05 eV) for RL3 and nD-RL3.

Examination of the data for nondiagonal self-energy methods indicates that only the most advanced members of this category are suitable for routine calculations of vertical electron detachment energies. The ND2 results are worse than those of D2. Whereas 2ph-TDA is useful for obtaining a first-order account of correlation final states where 2hp (shakeup) operators dominate, it is not capable of competitively delivering data on the lowest electron binding energies of anions. The 3+ method and the Schirmer−Angonoa version of ADC(3) include all self-energy terms in 2ph-TDA and generate Dyson orbitals that incorporate interference between Hartree−Fock orbitals. Their MUEs near 0.2 eV can be achieved by less computationally intensive means (see above). In contrast to the tendency to underestimate seen for ND2 and 2ph-TDA, 3+ and ADC(3) produce more overestimates than underestimates. NR2, with its relatively low O^3V^3 scaling, also can produce more general Dyson orbitals according to eq 22. Its MUE near 0.1 eV may make it a useful compromise in cases where final states have enhanced shakeup character. NR2 has a greater tendency to underestimate electron detachment energies, with a mean signed error of −0.06 eV.

The results for the BD-T1 method underlie the sharpest peak, centered near 0.0 eV, in the histograms of Figure 2. Given the average errors (inferred from experimental atomic data on ionization energies) over 0.1 eV for ΔCCSD(T) calculations[216] and the symmetry breaking in final doublet states that necessarily accompanies them, BD-T1 constitutes an attractive alternative standard that retains symmetry via direct calculation of electron binding energies and is an order of magnitude less computationally demanding.

Application of Composite Methods to Nucleotides. The multiply charged anion known as DNA consists of two helical polymers attached to each other by hydrogen bonds between purine−pyrimidine base pairs. The monomers of the polymers are nucleotides that have a phosphate anion covalently bound to a nucleoside consisting of a sugar covalently bound to a base. The localization of holes produced by photoionization or other insults to genetic material on the base, sugar, or phosphate constituents of nucleotides exerts considerable influence over subsequent reactivity and the chemical consequences of radiation damage.[217,218]

https://doi.org/10.1021/acs.jpca.2c08372
J. Phys. Chem. A 2023, 127, 1085−1101

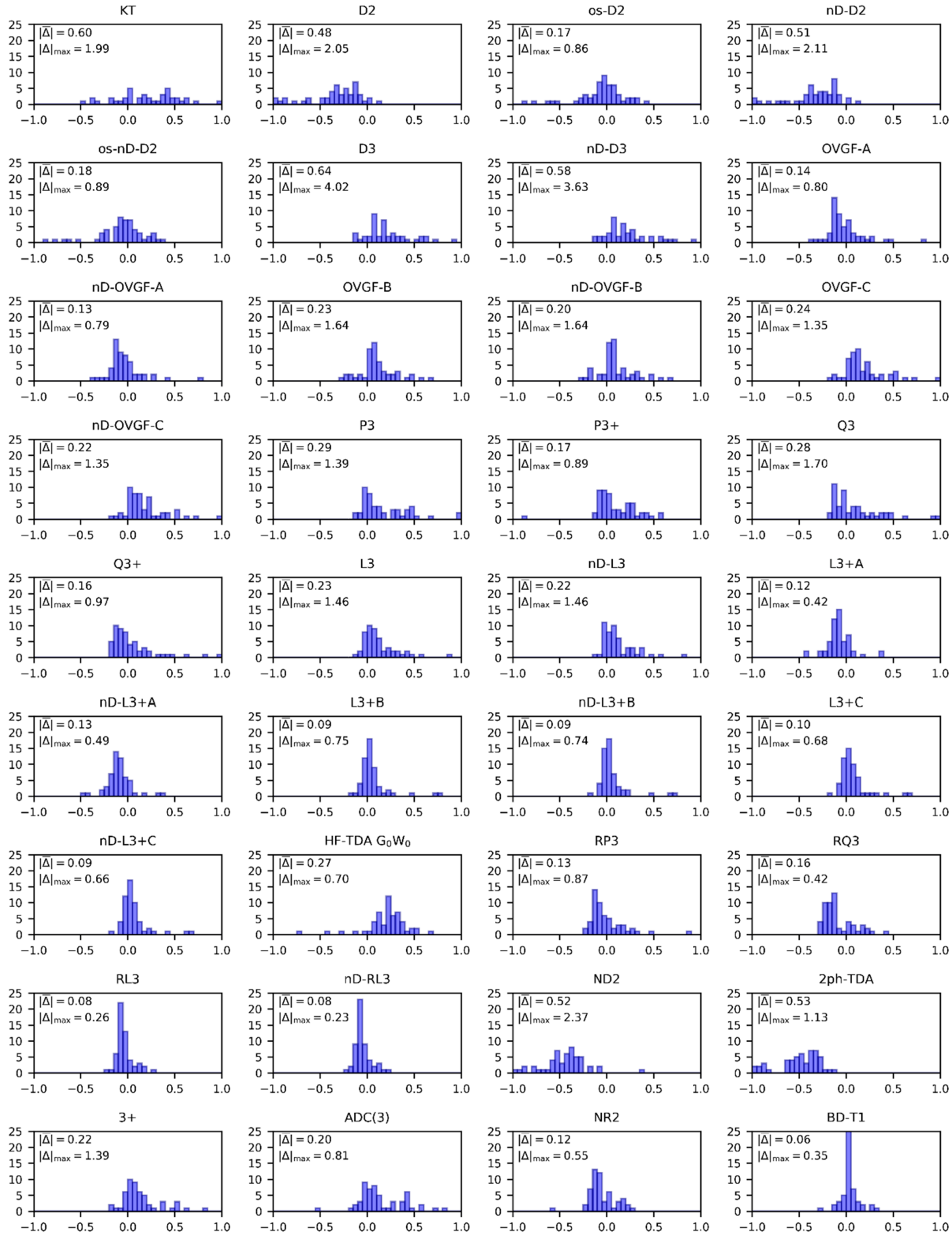


Figure 2. Histograms of error distributions (in eV) vs ΔCCSD(T)/CBS standards.

Gas-phase anion photoelectron spectra have been interpreted previously with P3/6-311++G(d,p) calculations[129,130] on the lowest-energy conformations of the nucleotide anions, which in all four cases exhibit the C_1 point group. (Cartesian coordinates of the optimized geometries, including a corrected set for adenosine, are given in the Supporting Information.) *As assignments of electron binding energies with respect to spatial symmetry are nugatory, it is necessary to inspect the localization of the Dyson orbitals to determine whether electron density has been removed chiefly from the phosphate anion, the sugar bridge, or the base.* In the last case, holes may be delocalized π orbitals or relatively localized σ lone-pair functions.

https://doi.org/10.1021/acs.jpca.2c08372
J. Phys. Chem. A 2023, 127, 1085−1101

Table 4. Vertical Electron Detachment Energies (in eV) of Deoxyribonucleotide Anions

	Dyson orbital	P3[129,130]	KT/aug-cc-pVQZ	*E*(composite)	expt[220]
$dAMP^-$	A π_1	6.155	6.092	6.138	6.05 ± 0.50
	PO_4^-	6.076	7.797	6.204	6.05 ± 0.50
	PO_4^-, S	6.391	8.128	6.502	~6.4
	PO_4^-, S	6.622	8.301	6.727	~6.7
	PO_4^-, S	6.765	7.696	6.728	~6.7
	A π_2	6.888	8.352	6.958	~6.9
	n_1 A	7.246	8.860	7.202	~7.1
	n_2 A	7.299	8.971	7.296	~7.1
$dGMP^-$	G π_1	5.012	5.202	5.008	5.05 ± 0.10
	PO_4^-	6.189	7.908	6.393	~6.1
	PO_4^-	6.535	8.248	6.709	~6.4
	n, G, S, PO_4^-	6.842	8.091	6.782	~6.8
	G, S, PO_4^-	6.747	8.481	6.823	~6.9
	π_2, G, S	6.962	8.597	6.939	~7.0
$dTMP^-$	T π_1	6.155	6.667	6.137	5.85 ± 0.50
	PO_4^-	6.236	8.035	6.338	~6.2
	PO_4^-, S	6.596	8.333	6.677	~6.6
	PO_4^-, S	6.838	8.544	6.902	~6.8
	PO_4^-, S	6.827	8.490	6.904	~6.8
	PO_4^-, S	7.372	9.114	7.435	~7.4
	T, S, PO_4^-	7.661	9.300	7.800	~7.5
	n T, PO_4^-	7.658	9.350	7.815	~7.5
$dCMP^-$	PO_4^-	5.995	7.674	6.170	5.80 ± 0.50
	C π_1	6.473	7.061	6.464	~6.4−6.5
	PO_4^-	6.412	8.026	6.580	~6.4−6.5
	C, S. PO_4^-	6.981	8.356	6.847	~6.7
	C, S. PO_4^-	6.861	8.472	7.044	~6.9
	C, S. PO_4^-	7.182	8.991	7.368	~7.1
	PO_4^-, S	7.376	8.613	7.477	~7.3

After confirming previous results, os-D2, os-nD-D2, HF-TDA-G_0W_0, P3+, and Q3+ calculations were executed with the aug-cc-pvdz and aug-cc-pvtz basis sets. In addition, nD-L3+B calculations were performed with the former basis set. This combination of results enables an estimate of nD-L3+B/aug-cc-pvtz values by assuming the additivity of basis-set and self-energy (Q3+ vs nD-L3+B) effects. Basis-set effects beyond aug-cc-pvtz may be estimated with a cubic extrapolation[219] of os-nD-D2 results obtained with aug-cc-pvtz and aug-cc-pvqz functions, i.e., a complete basis set (cbs) approximation. The resulting composite model of vertical electron detachment energies consists of five terms:

$$E_{\text{composite}} = E_{\text{atz}}^{\text{Q3+}} + E_{\text{adz}}^{\text{nD-L3+B}} - E_{\text{adz}}^{\text{Q3+}} + E_{\text{cbs}}^{\text{os-nD-D2}} - E_{\text{atz}}^{\text{os-nD-D2}} \quad (27)$$

(See complete data in the Supporting Information.) The largest basis sets occur for guanosine and encompass 650, 1361, and 2442 contracted Gaussians, respectively, for the nD-L3+B/aug-cc-pvdz, Q3+/aug-cc-pvtz, and os-nD-D2/aug-cc-pvqz calculations.

Comparison of the Koopmans's theorem (KT) column (see Table 4) with that of the present composite electron propagator model indicates that the former assignment has several qualitative defects. For all four nucleotides, the sequence of final states obtained with KT differs from the predictions made by correlated electron propagator methods. Plots of orbitals that correspond to the first two vertical electron detachment energies of each nucleotide are displayed in Figure 3. (Additional plots are available in the Supporting

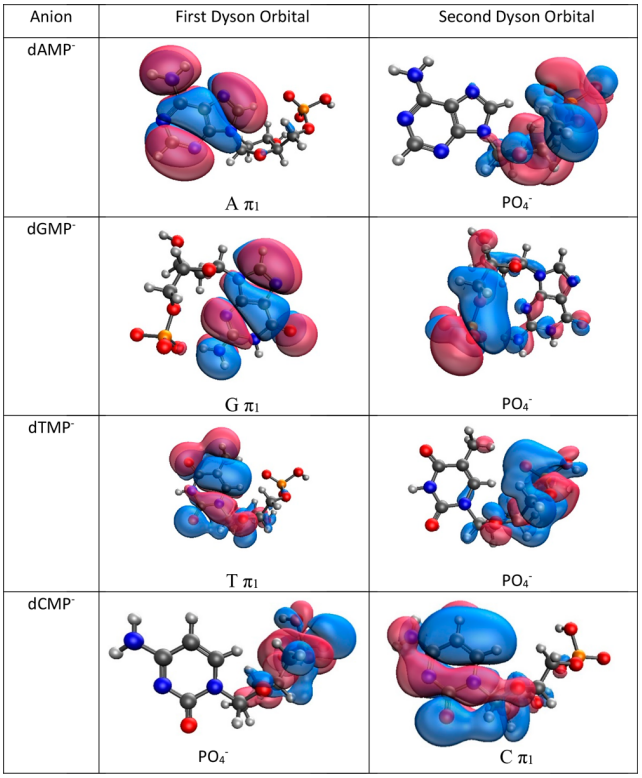


Figure 3. Dyson orbitals of vertical electron detachment of deoxyribonucleotide anions.

https://doi.org/10.1021/acs.jpca.2c08372
J. Phys. Chem. A 2023, 127, 1085−1101

Information.) In general, reductions in the predicted electron detachment energies from the self-energy terms are larger for phosphate-centered orbitals (~1.4−1.7 eV) than for base-centered π orbitals (<0.6 eV). Base-centered σ orbitals for adenosine also have large self-energy corrections.

For guanidine ($dGMP^-$), there is clear agreement between KT and the composite electron propagator method that the lowest vertical electron detachment energy pertains to the base and that this value, 5.01 eV, is the lowest for the four nucleotides. This conclusion is confirmed by the anion photoelectron experiment,[220] where only guanidine has a well-separated peak at a relatively low energy (5.05 ± 0.10 eV). The next two predicted vertical electron detachment energies of guanidine correspond to phosphate orbitals and are well-separated from the previous peak energy. Two orbitals that are more delocalized follow, and the sixth (and last) calculated state pertains to a more strongly bound base π orbital. A defect in the KT ordering occurs (at 8.09 eV) for the fourth vertical electron detachment energy. The predicted values for the second through sixth states lie within the bounds of the broad feature seen in the experiment, whose maximum near 7.0 eV coincides well with the composite model's result for the second base π-hole final state. Discrepancies with the previous P3/6-311++G(d,p) calculations[129,130] are ~0.2 eV or less, but the order of the fourth and fifth states is different.

For adenosine ($dAMP^-$), the composite model predicts that a phosphate orbital and a base π orbital practically coincide. Both results (6.20 and 6.14 eV, respectively) concur with the experimentally based estimate of 6.05 ± 0.50 eV for the lowest vertical electron detachment energy. KT results erroneously predict a gap of 1.7 eV between the two states, with the base π-vacancy state being lower. Three phosphate orbitals (with a KT defect of final-state ordering), another base π orbital, and two base σ orbitals align well with a broad feature seen in the experiment.[220] The two base σ-hole final states are in close agreement with the spectral peak maximum seen near 7.1 eV. A fortuitous agreement with the older calculations[129,130] also appears in this case, but the order of the first two states differs.

Whereas KT predicts that the lowest vertical electron detachment energy of thymidine ($dTMP^-$) pertains to a base π orbital that is separated by 1.4 eV from the lowest phosphate hole state, the composite electron propagator model favors the former state with a separation from the latter state of only 0.2 eV. The estimate for the lowest vertical electron detachment energy in the experimental report is 5.85 ± 0.50 eV;[220] the composite electron propagator prediction lies within the latter bounds at 6.14 eV. Four additional phosphate orbitals and two delocalized orbitals follow at higher energies that lie within the broad peak of the experiment. Cancellations of basis and self-energy errors in previous calculations[129] again result in good agreement with the present results.

For cytidine ($dCMP^-$), KT predicts that the lowest vertical detachment energy pertains to a base π orbital, but the present results find that final state to be the second-lowest. The composite electron propagator model favors a phosphate orbital; the predicted value for the lowest transition is 6.17 eV, in reasonable agreement with the experimentally based value of 5.80 ± 0.50 eV.[220] Higher transition energies lie under the broad features seen in the anion photoelectron spectrum. Discrepancies with the previous calculations[129] amount to less than 0.2 eV.

For three out of the four nucleotides, the lowest vertical electron detachment energy is predicted by the composite model to pertain to a base π Dyson orbital. Only in the cytidine case is a phosphate orbital associated with the lowest transition. In guanidine, the lowest vertical electron detachment energy is clearly separated from other transitions and may be assigned without hesitation to a base π Dyson orbital. In the remaining nucleotides, phosphate and base π Dyson orbitals have energies within a few tenths of an electronvolt of each other. Close agreement with the previous calculations[129] frequently occurs in the latter work because of a systematic cancellation of errors wherein a relatively small basis set that leads to underestimates is combined with the P3 method's tendency to overestimate (see Figure 2).

CONCLUSIONS

Numerical results on the closed-shell anions in the vertical electron detachment energy data set indicate that the following methods provide the best accuracy for a given level of arithmetic effort:

- The os-nD-D2 method involves only trivial arithmetic effort (with cubic scaling) after a partial transformation of the electron repulsion integrals from the contracted Gaussian to the canonical Hartree−Fock orbital basis. For a single final state, the latter step may be accomplished with a fourth-power scaling algorithm. Both opposite-spin second-order methods provide efficient, unbiased means of generating data on vertical electron detachment energies with a mean unsigned error of approximately 0.2 eV.
- When a partial electron repulsion integral transformation that scales as ON^4 is feasible (as in, for example, conventional MP2 calculations), the P3+ and Q3+ methods, with their lower, noniterative O^2V^3 bottlenecks provide a convenient way to generate data with a mean unsigned error of approximately 0.15 eV. Useful data also may be generated with the HF-TDA-G_0W_0 method, which has a reduced requirement for transformed integrals and an iterative O^2V^3 bottleneck.
- Arithmetic effort comparable to that of an ON^4 integral transformation (but less than that of a full N^5-scaling transformation) characterizes the methods with OV^4 scaling. The nD-L3+B method realizes a mean unsigned error of approximately 0.1 eV. Similar quality may be achieved with the nD-RL3 method, which requires more bottleneck steps.
- To improve the quality of Dyson orbitals by allowing them to become linear combinations of canonical Hartree−Fock orbitals, nondiagonal self-energies must be employed. The NR2 method produces a mean unsigned error of approximately 0.1 eV with O^3V^3 scaling. Somewhat larger mean unsigned errors (~0.2 eV) are obtained with the Schirmer−Angonoa version of ADC(3).
- The BD-T1 method has a sixth-power scaling factor, O^2V^4, that originates in the Brueckner doubles coupled-cluster step preceding the electron propagator calculation of electron detachment energies. Unlike ΔCCSD-(T), BD-T1's direct calculation of vertical electron detachment energies introduces no loss of spin symmetry in final doublet states. Its mean unsigned error below 0.1 eV establishes it as an alternative generator of standard data.

https://doi.org/10.1021/acs.jpca.2c08372
J. Phys. Chem. A 2023, 127, 1085−1101

Calculations on the four nucleotide anions of DNA demonstrate the importance of self-energy corrections in procuring the correct order of final states, especially when the point group is C_1 and the crucial interpretive task pertains to the localization of Dyson orbitals. The present calculations provide a convincing account of the energetic ordering of base-centered versus phosphate-centered vacancies. The latter cases exhibit markedly larger corrections to uncorrelated orbital energies. Final estimates of nD-L3+B/aug-cc-pvqz results may be based on relatively easily obtained Q3+/aug-cc-pvdz, Q3+/aug-cc-pvtz, nD-L3+B/aug-cc-pvdz, and os-nD-D2/aug-cc-pvqz data and the reasonable assumption of the separability of basis-set and relaxation−correlation effects. The availability of several approximate self-energies with differing levels of accuracy and computational efficiency is a promising portent for future calculations on increasingly complicated systems with composite models.

■ ASSOCIATED CONTENT

Supporting Information

The Supporting Information is available free of charge at https://pubs.acs.org/doi/10.1021/acs.jpca.2c08372.

Benchmark data (XLSX)
Electron binding energies (Tables S1−S4) and Dyson orbitals (Figures S1−S4) (PDF)
Test anion geometries (ZIP)
Nucleotide geometries (ZIP)

■ AUTHOR INFORMATION

Corresponding Author

J. V. Ortiz − *Department of Chemistry and Biochemistry, Auburn University, Auburn, Alabama 36849-5312, United States;* orcid.org/0000-0002-9277-0226; Email: ortiz@auburn.edu

Authors

Ernest Opoku − *Department of Chemistry and Biochemistry, Auburn University, Auburn, Alabama 36849-5312, United States;* orcid.org/0000-0002-4271-6838

Filip Pawłowski − *Department of Chemistry and Biochemistry, Auburn University, Auburn, Alabama 36849-5312, United States*

Complete contact information is available at: https://pubs.acs.org/10.1021/acs.jpca.2c08372

Notes

The authors declare no competing financial interest.

■ ACKNOWLEDGMENTS

Part of this research was accomplished with support from National Science Foundation Grant CHE-1565760 to Auburn University.

■ REFERENCES

(1) Linderberg, J.; Öhrn, Y. *Propagators in Quantum Chemistry*, 2nd ed.; Wiley-Interscience: Hoboken, NJ, 2004.
(2) Jørgensen, P.; Simons, J. *Second Quantization-Based Methods in Quantum Chemistry*; Academic Press: New York, 1981.
(3) Schirmer, J. *Many-Body Methods for Atoms, Molecules and Clusters*; Springer International Publishing AG, 2018.
(4) von Niessen, W.; Schirmer, J.; Cederbaum, L. S. Computational methods for the one-particle Green's function. *Comput. Phys. Rep.* **1984**, *1*, 57−125.
(5) Corzo, H. H.; Ortiz, J. V. Electron Propagator Theory: Foundations and Predictions. *Adv. Quantum Chem.* **2017**, *74*, 267−298.
(6) Ortiz, J. V. Interpreting Bonding and Spectra with Correlated, One-Electron Concepts from Electron Propagator Theory. *Annu. Rep. Comput. Chem.* **2017**, *13*, 139−182.
(7) Ortiz, J. V. Dyson-orbital concepts for description of electrons in molecules. *J. Chem. Phys.* **2020**, *153*, 070902.
(8) Koopmans, T. Über die Zuordnung von Wellenfunktionen und Eigenwerten zu den Einzelnen Elektronen Eines Atoms. *Physica* **1934**, *1*, 104−113.
(9) Simons, J.; Smith, W. D. Theory of electron affinities of small molecules. *J. Chem. Phys.* **1973**, *58*, 4899−4907.
(10) Simons, J. Theoretical studies of negative molecular ions. *Annu. Rev. Phys. Chem.* **1977**, *28*, 15−45.
(11) Simons, J. Theoretical studies of negative molecular ions. *Theor. Chem.* **1978**, *3*, 1−13.
(12) Simons, J. Electron propagator studies of molecular anions. *Int. J. Quantum Chem., Quantum Chem. Symp.* **1982**, *22*, 575−581.
(13) Simons, J. Molecular Anions. *J. Phys. Chem. A* **2008**, *112*, 6401−6511.
(14) Simons, J. Theoretical study of negative molecular ions. *Annu. Rev. Phys. Chem.* **2011**, *62*, 107−128.
(15) Ortiz B., J. V.; Öhrn, Y. Electron propagator theory of molecular anions. *J. Chem. Phys.* **1980**, *72*, 5744−5751.
(16) Ortiz B., J. V.; Öhrn, Y. Electron propagator calculations of molecular electron affinities. *Chem. Phys. Lett.* **1981**, *77*, 548−554.
(17) Ortiz, J. V.; Basu, R.; Öhrn, Y. Electron-propagator calculations with a transition-operator reference. *Chem. Phys. Lett.* **1983**, *103*, 29−34.
(18) Ortiz, J. V. Many-body theory of the ionization energies of CH_3^-, SiH_3^-, and GeH_3^-. *J. Am. Chem. Soc.* **1987**, *109*, 5072−5076.
(19) Ortiz, J. V. Applying electron propagator theory to electron affinities. *Int. J. Quantum Chem.* **1987**, *32*, 469−473.
(20) Ortiz, J. V. Direct versus indirect many-body methods for calculating vertical electron affinities: applications to F^-, OH^-, NH_2^-, CN^-, Cl^-, SH^- and PH_2^-. *Chem. Phys. Lett.* **1987**, *136*, 387−391.
(21) Ortiz, J. V. Electron affinity calculations on NH_2^-, PH_2^-, CN^-, SH^-, OH^-, Cl^-, and F^-: basis sets and direct vs indirect methods. *J. Chem. Phys.* **1987**, *86*, 308−312.
(22) Ortiz, J. V. Applications of electron propagator theory to the electron affinities of AsH_2, SeH, Br, SbH_2, TeH, and I. *J. Chem. Phys.* **1987**, *87*, 1701−1704.
(23) Ortiz, J. V. Electron binding energies of anionic alkali metal atoms from partial fourth-order electron propagator theory calculations. *J. Chem. Phys.* **1988**, *89*, 6348−6352.
(24) Ortiz, J. V. Electron binding energies of anionic alkali metal triatomics from partial fourth-order electron propagator theory calculations. *J. Chem. Phys.* **1988**, *89*, 6353−6356.
(25) Ortiz, J. V. Partial fourth order electron propagator theory. *Int. J. Quantum Chem., Quantum Chem. Symp.* **1988**, *34*, 431−436.
(26) Ortiz, J. V. Electron propagator calculations with nondiagonal partial fourth-order self-energies and unrestricted hartree-fock reference states. *Int. J. Quantum Chem., Quant. Chem. Symp.* **1989**, *36*, 321−332.
(27) Zakrzewski, V. G.; Boldyrev, A. I. The upper ionization potentials of F^-, LiF_2^-, BeF_3^-, BO_2^-, AlO_2^-, and NO_3^-) ions calculated by Green function method. *J. Chem. Phys.* **1990**, *93*, 657−660.
(28) Dolgounitcheva, O.; Zakrzewski, V. G.; Ortiz, J. V. Comparison of electron propagator methods for calculating electron detachment energies of anions. *Int. J. Quantum Chem.* **1997**, *65*, 463−469.
(29) Ortiz, J. V. Electron detachment energies of closed-shell anions calculated with a renormalized electron propagator. *Chem. Phys. Lett.* **1998**, *296*, 494−498.
(30) Ortiz, J. V. Approximate Brueckner orbitals and shakeup operators in electron propagator calculations: applications to F^- and OH^-. *Int. J. Quantum Chem.* **1998**, *70*, 651−658.

(31) Ortiz, J. V. Approximate Brueckner orbitals in electron propagator calculations. *Int. J. Quantum Chem.* **1999**, *75*, 615−621.
(32) Pawłowski, F.; Ortiz, J. V. Relativistic electron detachment energies and spin-orbit splittings from quasiparticle electron propagator calculations. *Mol. Phys.* **2020**, *118*, No. e1700314.
(33) Díaz-Tinoco, M.; Corzo, H. H.; Ortiz, J. V. Electron Propagator Methods for Vertical Electron Detachment Energies of Anions: Benchmarks and Case Studies. *J. Chem. Theory Comput.* **2018**, *14*, 5881−5895.
(34) Zhai, H.-J.; Wang, L.-S.; Alexandrova, A. N.; Boldyrev, A. I.; Zakrzewski, V. G. Photoelectron Spectroscopy and ab Initio Study of B_3^- and B_4^- Anions and Their Neutrals. *J. Phys. Chem. A* **2003**, *107*, 9319−9328.
(35) Zhai, H.-J.; Wang, L.-S.; Alexandrova, A. N.; Boldyrev, A. I. Electronic structure and chemical bonding of B_5^- and B_5 by photoelectron spectroscopy and ab initio calculations. *J. Chem. Phys.* **2002**, *117*, 7917−7924.
(36) Alexandrova, A. N.; Boldyrev, A. I.; Zhai, H.-J.; Wang, L.-S. Photoelectron spectroscopy and ab initio study of the doubly antiaromatic B_6^{2-} dianion in the LiB_6^- cluster. *J. Chem. Phys.* **2005**, *122*, 054313.
(37) Alexandrova, A. N.; Zhai, H.-J.; Wang, L.-S.; Boldyrev, A. I. Molecular Wheel B_8^{2-} as a New Inorganic Ligand. Photoelectron Spectroscopy and ab Initio Characterization of LiB_8^-. *Inorg. Chem.* **2004**, *43*, 3552−3554.
(38) Wang, L.-S.; Boldyrev, A. I.; Li, X.; Simons, J. Experimental Observation of Pentaatomic Tetracoordinate Planar Carbon-Containing Molecules. *J. Am. Chem. Soc.* **2000**, *122*, 7681−7687.
(39) Li, X.; Kuznetsov, A. E.; Zhang, H.-F.; Boldyrev, A. I.; Wang, L.-S. Observation of all-metal aromatic molecules. *Science* **2001**, *291*, 859−861.
(40) Boldyrev, A. I.; Wang, L.-S. All-Metal Aromaticity and Antiaromaticity. *Chem. Rev.* **2005**, *105*, 3716−3757.
(41) Kuznetsov, A. E.; Birch, K. A.; Boldyrev, A. I.; Li, X.; Zhai, H.-J.; Wang, L.-S. All-Metal Antiaromatic Molecule: Rectangular Al_4^{4-} in the $Li_3Al_4^-$ Anion. *Science* **2003**, *300*, 622−625.
(42) Zhai, H.-J.; Alexandrova, A. N.; Birch, K. A.; Boldyrev, A. I.; Wang, L.-S. Hepta- and Octacoordinate Boron in Molecular Wheels of Eight- and Nine-Atom Boron Clusters: Observation and Confirmation. *Angew. Chem., Int. Ed.* **2003**, *42*, 6004−6008.
(43) Averkiev, B. B.; Wang, L.-M.; Huang, W.; Wang, L.-S.; Boldyrev, A. I. Experimental and theoretical investigations of CB_8^-: towards rational design of hypercoordinated planar chemical species. *Phys. Chem. Chem. Phys.* **2009**, *11*, 9840−9849.
(44) Alexandrova, A. N.; Boldyrev, A. I.; Zhai, H.-J.; Wang, L.-S. All-boron aromatic clusters as potential new inorganic ligands and building blocks in chemistry. *Coord. Chem. Rev.* **2006**, *250*, 2811−2866.
(45) Sergeeva, A. P.; Zubarev, D. Y.; Zhai, H.-J.; Boldyrev, A. I.; Wang, L.-S. A Photoelectron Spectroscopic and Theoretical Study of B_{16}^- and B_{16}^{2-}: An All-Boron Naphthalene. *J. Am. Chem. Soc.* **2008**, *130*, 7244−7246.
(46) Sergeeva, A. P.; Averkiev, B. B.; Zhai, H.-J.; Boldyrev, A. I.; Wang, L.-S. All-boron analogues of aromatic hydrocarbons: B_{17}^- and B_{18}. *J. Chem. Phys.* **2011**, *134*, 224304.
(47) Piazza, Z. A.; Li, W.-L.; Romanescu, C.; Sergeeva, A. P.; Wang, L.-S.; Boldyrev, A. I. A photoelectron spectroscopy and ab initio study of B_{21}^-: Negatively charged boron clusters continue to be planar at 21. *J. Chem. Phys.* **2012**, *136*, 104310.
(48) Galeev, T. R.; Romanescu, C.; Li, W.-L.; Wang, L.-S.; Boldyrev, A. I. Valence isoelectronic substitution in the B_8^- and B_9^- molecular wheels by an Al dopant atom: Umbrella-like structures of AlB_7^- and AlB_8. *J. Chem. Phys.* **2011**, *135*, 104301.
(49) Li, W.-L.; Romanescu, C.; Galeev, T. R.; Wang, L.-S.; Boldyrev, A. I. Aluminum Avoids the Central Position in AlB_9^- and AlB_{10}^-: Photoelectron Spectroscopy and ab Initio Study. *J. Phys. Chem. A* **2011**, *115*, 10391−10397.
(50) Wang, L.-M.; Averkiev, B. B.; Ramilowski, J. A.; Huang, W.; Wang, L.-S.; Boldyrev, A. I. Planar to Linear Structural Transition in Small Boron-Carbon Mixed Clusters: $C_xB_{5-x}^-$ (x = 1−5). *J. Am. Chem. Soc.* **2010**, *132*, 14104−14112.
(51) Popov, I. A.; Zhang, X.; Eichhorn, B. W.; Boldyrev, A. I.; Bowen, K. H. Aluminum chain in $Li_2Al_3H_8^-$ as suggested by photoelectron spectroscopy and ab initio calculations. *Phys. Chem. Chem. Phys.* **2015**, *17*, 26079−26083.
(52) Zhang, X.; Popov, I. A.; Lundell, K. A.; Wang, H.; Mu, C.; Wang, W.; Schnoeckel, H.; Boldyrev, A. I.; Bowen, K. H. Realization of an Al≡Al Triple Bond in the Gas-Phase $Na_3Al_2^-$ Cluster via Double Electronic Transmutation. *Angew. Chem., Int. Ed.* **2018**, *57*, 14060−14064.
(53) Taylor, D. A.; Hillier, I. H.; Vincent, M.; Guest, M. F.; MacDowell, A. A.; Von Niessen, W.; Urch, D. S. The valence ionization energies of tetracyanonickelate anion ($Ni(CN)_4^{2-}$) studied by X-ray emission spectroscopy and by an ab initio Green's function calculation. *Chem. Phys. Lett.* **1985**, *121*, 482−484.
(54) Gutowski, M.; Boldyrev, A. I.; Simons, J.; Rak, J.; Blazejowski, J. Properties of Closed-Shell, Octahedral, Multiply-Charged Hexafluorometallates MF_6^{3-}, M = Sc, Y, La, ZrF_6^{2-}, and TaF_6^-. *J. Am. Chem. Soc.* **1996**, *118*, 1173−1180.
(55) Gutowski, M.; Boldyrev, A. I.; Ortiz, J. V.; Simons, J. Vertical Electron Detachment Energies for Octahedral Closed-Shell Multiply-Charged Anions. *J. Am. Chem. Soc.* **1994**, *116*, 9262−9268.
(56) Zakrzewski, V. G.; Ortiz, J. V. Semidirect algorithms in electron propagator calculations. *Int. J. Quantum Chem., Quantum Chem. Symp.* **1994**, *52*, 23−27.
(57) Dolgounitcheva, O.; Zakrzewski, V. G.; Ortiz, J. V. Structure, bonding, and energetics of C_7^{2-} isomers. *J. Chem. Phys.* **1998**, *109*, 87−93.
(58) Enlow, M.; Ortiz, J. V.; Lüthi, H. P. Tetrahedral quadranionic carbon clusters. *Mol. Phys.* **1997**, *92*, 441−444.
(59) Dolgounitcheva, O.; Zakrzewski, V. G.; Ortiz, J. V. Ab initio electron propagator calculations on electron detachment energies of nickel phthalocyanine tetrasulfonate tetraanions. *Int. J. Quantum Chem.* **2012**, *112*, 184−194.
(60) Sommerfeld, T.; Feuerbacher, S.; Pernpointner, M.; Cederbaum, L. S. Electronic structure of isolated PtX_6^{2-}(X = F, Cl, Br) dianions. *J. Chem. Phys.* **2003**, *118*, 1747−1755.
(61) Pernpointner, M.; Breidbach, J.; Cederbaum, L. S. Remarkable interplay of electron correlation and relativity in the photodetachment spectrum of $PtCl_6^{2-}$. *J. Chem. Phys.* **2005**, *122*, 064311.
(62) Pernpointner, M.; Cederbaum, L. S. PtF_6^{2-} dianion and its detachment spectrum: A fully relativistic study. *J. Chem. Phys.* **2007**, *126*, 144310.
(63) Pernpointner, M.; Rapps, T.; Cederbaum, L. S. Jahn-Teller distortions in the photodetachment spectrum of $PtCl_6^{2-}$: A four-component relativistic study. *J. Chem. Phys.* **2009**, *131*, 044322.
(64) Pernpointner, M. A fully relativistic study of the and photodetachment spectra. *Chem. Phys.* **2007**, *338*, 44−52.
(65) Pernpointner, M.; Rapps, T.; Cederbaum, L. S. Photodetachment spectra of the PtX_4^{2-} (X = F, Cl, Br) dianions and their Jahn−Teller distortions: A fully relativistic study. *J. Chem. Phys.* **2008**, *129*, 174302.
(66) Gnaser, H.; Golser, R.; Pernpointner, M.; Forstner, O.; Kutschera, W.; Priller, A.; Steier, P.; Wallner, A. Identification of the SiF_6^{2-} dianion by accelerator mass spectrometry and a fully relativistic computation of its photodetachment spectrum. *Phys. Rev. A* **2008**, *77*, 053203.
(67) Herbert, J. M.; Ortiz, J. V. Ab Initio Investigation of Electron Detachment in Dicarboxylate Dianions. *J. Phys. Chem. A* **2000**, *104*, 11786−11795.
(68) Kambalapalli, S.; Ortiz, J. V. Solvated Succinate Dianion: Structures, Electron Binding Energies, and Dyson Orbitals. *J. Phys. Chem. A* **2003**, *107*, 10360−10369.
(69) Enlow, M.; Ortiz, J. V. Aromatic Carboxylate Superhalogens and Multiply Charged Anions. *J. Phys. Chem. A* **2002**, *106*, 5373−5379.

https://doi.org/10.1021/acs.jpca.2c08372
J. Phys. Chem. A 2023, 127, 1085−1101

(70) Gutsev, G. L.; Boldyrev, A. I. The theoretical investigation of the electron affinity of chemical compounds. *Adv. Chem. Phys.* **2007**, *61*, 169−221.
(71) Sikorska, C.; Ignatowska, D.; Freza, S.; Skurski, P. The performance of selected ab initio methods in estimating electron binding energies of superhalogen anions. *J. Theor. Comput. Chem.* **2011**, *10*, 93−109.
(72) Zakzhevskii, V. G.; Boldyrev, A. I. Role of electron correlation in the calculation of the electron affinity of superhalogens. *Zh. Neorg. Khim.* **1989**, *34*, 1368−1371.
(73) Anusiewicz, I.; Skurski, P. An ab initio study on BeX_3^- superhalogen anions (X = F, Cl, Br). *Chem. Phys. Lett.* **2002**, *358*, 426−434.
(74) Anusiewicz, I.; Sobczyk, M.; Dąbkowska, I.; Skurski, P. An ab initio study on MgX_3^- and CaX_3^- superhalogen anions (X = F, Cl, Br). *Chem. Phys.* **2003**, *291*, 171−180.
(75) Sobczyk, M.; Sawicka, A.; Skurski, P. Theoretical search for anions possessing large electron binding energies. *Eur. J. Inorg. Chem.* **2003**, *2003*, 3790−3797.
(76) Smuczynska, S.; Skurski, P. Introducing various ligands into superhalogen anions reduces their electronic stabilities. *Chem. Phys. Lett.* **2008**, *452*, 44−48.
(77) Sikorska, C.; Smuczynska, S.; Skurski, P.; Anusiewicz, I. BX_4^- and AlX_4^- Superhalogen Anions (X = F, Cl, Br): An ab Initio Study. *Inorg. Chem.* **2008**, *47*, 7348−7354.
(78) Marchaj, M.; Freza, S.; Skurski, P. Why Are SiX_5^- and GeX_5^- (X = F, Cl) Stable but Not CF_5^- and CCl_5^-? *J. Phys. Chem. A* **2012**, *116*, 1966−1973.
(79) Sikorska, C.; Skurski, P. The saturation of the excess electron binding energy in $Al_nF_{3n+1}^-$ (n = 1−5) anions. *Chem. Phys. Lett.* **2012**, *536*, 34−38.
(80) Marchaj, M.; Freza, S.; Skurski, P. The existence and stability of the anions matching the MF_{k+2}^- formula (M = Li, Na, K, Be, Mg, Ca, B, Al, Ga). *Chem. Phys. Lett.* **2013**, *560*, 15−21.
(81) Wilenska, D.; Skurski, P.; Anusiewicz, I. High-symmetry compact structures are preferred equilibrium configurations of $Li_nF_{n+1}^-$ (n = 2−5) superhalogen anions. *J. Fluorine Chem.* **2014**, *168*, 99−104.
(82) Czapla, M.; Skurski, P. Strength of the Lewis-Bronsted Superacids Containing In, Sn, and Sb and the Electron Binding Energies of Their Corresponding Superhalogen Anions. *J. Phys. Chem. A* **2015**, *119*, 12868−12875.
(83) Czapla, M.; Ciepła, O.; Brzeski, J.; Skurski, P. Formation of Enormously Strongly Bound Anionic Clusters Predicted in Binary Superacids. *J. Phys. Chem. A* **2018**, *122*, 8539−8548.
(84) Anusiewicz, I.; Freza, S.; Skurski, P. Stability of the $Ti_nF_{4n+1}^-$ and $Ge_nF_{4n+1}^-$ superhalogen anions and the acidity of the HTi_nF_{4n+1} and HGe_nF_{4n+1} (n = 1−3) superacids. *Polyhedron* **2018**, *144*, 125−130.
(85) Cyraniak, A.; Skurski, P.; Czapla, M. The presence of two different central atoms increases the strength of Lewis-Brønsted superacids. *Chem. Phys. Lett.* **2019**, *717*, 77−81.
(86) Anusiewicz, I.; Skurski, P. Unusual structures of $Mg_2F_5^-$ superhalogen anion. *Chem. Phys. Lett.* **2007**, *440*, 41−44.
(87) Anusiewicz, I. $Mg_2Cl_5^-$ and $Mg_3Cl_7^-$ Superhalogen Anions. *Aust. J. Chem.* **2008**, *61*, 712−717.
(88) Yang, H.; Li, Y.; He, H.-M.; Tong, J.; Wu, D.; Li, Z.-R. Superhalogen properties of hetero-binuclear anions $MM'F_4^-$ and $MM''F_5^-$ (M = Li, Na; M′ = Be, Mg, Ca; M″ = B, Al, Ga). *Chem. Phys. Lett.* **2017**, *684*, 273−278.
(89) Czapla, M. Dinuclear superhalogen anions containing two different central atoms. *J. Fluorine Chem.* **2017**, *199*, 97−102.
(90) Sikorska, C. Mg_3F_7: A superhalogen with potential for new. *Int . J. Quantum Chem.* **2018**, *118*, e25728.
(91) Smuczynska, S.; Skurski, P. Halogenoids as Ligands in Superhalogen Anions. *Inorg. Chem.* **2009**, *48*, 10231−10238.
(92) Sikorska, C.; Freza, S.; Skurski, P.; Anusiewicz, I. Theoretical Search for Alternative Nine-Electron Ligands Suitable for Superhalogen Anions. *J. Phys. Chem. A* **2011**, *115*, 2077−2085.
(93) Sikorska, C.; Skurski, P. Towards an understanding of the nature of superhalogen anions: an ab initio study of the system. *Mol. Phys.* **2012**, *110*, 1447−1452.
(94) Anusiewicz, I. Electrophilic Substituents as Ligands in Superhalogen Anions. *J. Phys. Chem. A* **2009**, *113*, 6511−6516.
(95) Swierszcz, I.; Anusiewicz, I. Neutral and anionic superhalogen hydroxides. *Chem. Phys.* **2011**, *383*, 93−100.
(96) Swierszcz, I.; Anusiewicz, I. The possibility of forming superhalogen anions with hydroperoxide groups as ligands. *Mol. Phys.* **2013**, *111*, 377−385.
(97) Sieradzan, I.; Anusiewicz, I. The electronic stability decrease in the $BF_{4-n}(R)_n^-$ anions (R = CH_3, C_2H_5; n = 0−4). *Chem. Phys.* **2013**, *425*, 55−61.
(98) Sieradzan, I.; Skurski, P.; Anusiewicz, I. The $PF_{6-n}(R)_n^-$ anions (R = CH_3, C_2H_5; n = 0−6): the dependence of the electronic stability on the number of non-electronegative alkyl ligands. *Mol. Phys.* **2014**, *112*, 2811−2819.
(99) Sikorska, C. Utilizing fluoroxyl groups as ligands in superhalogen anions: An ab initio study of the $M(OF)_{k+1}^-$ systems (M = Li, Na, K, Be, Mg, Ca, B, Al). *Chem. Phys. Lett.* **2015**, *638*, 179−186.
(100) Zhao, R.-F.; Yu, L.; Zhou, F.-Q.; Li, J.-F.; Yin, B. Could the increased structural versatility imposed by non-halogen ligands bring something new for polynuclear superhalogens? A case study on binuclear $[Mg_2L_5]^-$ (L = $^-$OH, $^-$OOH and $^-$OF) anions. *Phys. Chem. Chem. Phys.* **2017**, *19*, 26986−26995.
(101) Yang, H.; Li, Y.; He, H.-M.; Yu, D.; Wu, D.; Li, Z.-R. Heterobinuclear superhalogen anions with cyanide and/or isocyanide as ligands. *Chem. Phys. Lett.* **2018**, *713*, 203−209.
(102) Li, J.-F.; Yin, B. Exploring the Superhalogen Properties of Polynuclear Structures without Halogen Ligands: A Combined Ab Initio and DFT Study on Triple-Bridged $[Mg_2L_5]^{-1}$ (L = $^-$OCN, $^-$SCN) Anions. *J. Phys. Chem. A* **2021**, *125*, 3378−3386.
(103) Anusiewicz, I. Superhalogen Anions Utilizing Acidic Functional Groups As Ligands. *J. Phys. Chem. A* **2009**, *113*, 11429−11434.
(104) Sieradzan, I.; Anusiewicz, I. Amino acids form strongly bound anions when substituted with superhalogen ligands. *J. Chem. Phys.* **2013**, *138*, 134310−134316.
(105) Cyraniak, A.; Czapla, M. Tripodal podand ligand with a superhalogen nature as an effective molecular trap. *Symmetry* **2020**, *12*, 1441.
(106) Díaz-Tinoco, M.; Ortiz, J. V. Carborane superhalide bases and their conjugate Brønsted-Lowry Superacids: Electron binding energies and Dyson orbitals. *Chem. Phys.* **2019**, *521*, 77−84.
(107) Brzeski, J.; Czapla, M.; Skurski, P. Icosahedral Carborane Superacids and their Conjugate Bases Comprising H, F, Cl, and CN Substituents: A Theoretical Investigation of Monomeric and Dimeric Cages. *ChemPlusChem* **2020**, *85*, 312−318.
(108) Anusiewicz, I.; Freza, S.; Sikorska, C.; Skurski, P. A strongly bound OF_3^- anion and its unstable parent neutral OF_3 species. *Chem. Phys. Lett.* **2010**, *493*, 234−237.
(109) Freza, S.; Skurski, P. Enormously large (approaching 14 eV!) electron binding energies of $[H_nF_{n+1}]^-$ (n = 1−5, 7, 9, 12) anions. *Chem. Phys. Lett.* **2010**, *487*, 19−23.
(110) Anusiewicz, I.; Skurski, P. Attaching Be or Mg to BH3 results in the formation of $BeBH_3$ and $MgBH_3$ molecules capable of forming stable anions. *Chem. Phys. Lett.* **2018**, *698*, 19−23.
(111) Cyraniak, A.; Faron, D.; Freza, S.; Anusiewicz, I.; Skurski, P. Superhalogen anions supported by the systems comprising alternately aligned boron and nitrogen central atoms. *Front. Chem.* **2022**, *10*, 863408.
(112) Sommerfeld, T.; Bhattarai, B.; Vysotskiy, V. P.; Cederbaum, L. S. Correlation-bound anions of NaCl clusters. *J. Chem. Phys.* **2010**, *133*, 114301.
(113) Sikorska, C. Are noble gas molecules able to exhibit a superhalogen nature? *RSC Adv.* **2016**, *6*, 103418−103427.
(114) Ortiz, J. V. Electron propagator theory of boron oxide and borate (BO_2 and BO_2^-) electronic structure. *J. Chem. Phys.* **1993**, *99*, 6727−6731.

https://doi.org/10.1021/acs.jpca.2c08372
J. Phys. Chem. A 2023, 127, 1085−1101

(115) Ortiz, J. V. Electron propagator theory of boron sulfide (BS_2) and BS_2^- electronic structure. *Chem. Phys. Lett.* **1993**, *214*, 467−472.
(116) Díaz-Tinoco, M.; Ortiz, J. V. Comment on: "Probing the Properties of Polynuclear Superhalogens without Halogen Ligand via ab Initio Calculations: A Case Study on Double-Bridged $[Mg_2(CN)_5]^{-1}$ Anions" by Li et al. *ChemPhysChem* **2016**, *17*, 2945−2946.
(117) Diaz-Tinoco, M. A.; Ortiz, J. V. Comment on "Is the regulation of the electronic properties of organic molecules by polynuclear superhalogens more effective than that by mononuclear superhalogens? A high-level ab initio case study" by M.-M. Li, J.-F. Li, H. Bai, Y.-Y. Sun, J.-L. Li and B. Yin, Phys. Chem. Chem. Phys., 2015, 17, 20338. *Phys. Chem. Chem. Phys.* **2016**, *18*, 15456−15457.
(118) Diaz-Tinoco, M.; Ortiz, J. V. Comment on "Are polynuclear superhalogens without halogen atoms probable? A high-level ab initio case study on triple-bridged binuclear anions with cyanide ligands" [J. Chem. Phys. 140, 094301 (2014)]. *J. Chem. Phys.* **2016**, *145*, 147101.
(119) Li, J.-F.; Li, M.-M.; Bai, H.; Sun, Y.-Y.; Li, J.-L.; Yin, B. Reply to: "Comment on Probing the Properties of Polynuclear Superhalogens without Halogen Ligand via ab Initio Calculations: A Case Study on Double-Bridged $[Mg_2(CN)_5]^{-1}$ Anions by Li et al.". *ChemPhysChem* **2016**, *17*, 2947.
(120) Dolgounitcheva, O.; Zakrzewski, V. G.; Ortiz, J. V. Structures and electron detachment energies of uracil anions. *Chem. Phys. Lett.* **1999**, *307*, 220−226.
(121) Dolgounitcheva, O.; Zakrzewski, V. G.; Ortiz, J. V. Diffuse-Bound and Valence-Bound Anions of Cytosine. *J. Phys. Chem. A* **2001**, *105*, 8782−8786.
(122) Dolgounitcheva, O.; Zakrzewski, V. G.; Ortiz, J. V. Electron propagator and coupled-cluster calculations on the photoelectron spectra of thiouracil and dithiouracil anions. *J. Chem. Phys.* **2011**, *134*, 074305.
(123) Chen, J.; Buonaugurio, A.; Dolgounitcheva, O.; Zakrzewski, V. G.; Bowen, K. H.; Ortiz, J. V. Photoelectron Spectroscopy of the 6-Azauracil Anion. *J. Phys. Chem. A* **2013**, *117*, 1079−1082.
(124) Corzo, H. H.; Dolgounitcheva, O.; Zakrzewski, V. G.; Ortiz, J. V. Valence-Bound and Diffuse-Bound Anions of 5-Azauracil. *J. Phys. Chem. A* **2014**, *118*, 6908−6913.
(125) Vazquez, M.-V.; Martinez, A.; Dolgounitcheva, O.; Ortiz, J. V. Deprotonated Cytosine Anions: A Theoretical Prediction of Photoelectron Spectra. *J. Phys. Chem. A* **2006**, *110*, 11174−11177.
(126) Dolgounitcheva, O.; Zakrzewski, V. G.; Ortiz, J. V. Anionic and Neutral Complexes of Uracil and Water. *J. Phys. Chem. A* **1999**, *103*, 7912−7917.
(127) Streit, L.; Dolgounitcheva, O.; Zakrzewski, V. G.; Ortiz, J. V. Valence and diffuse-bound anions of noble-gas complexes with uracil. *J. Chem. Phys.* **2012**, *137*, 194310.
(128) Dolgounitcheva, O.; Zakrzewski, V. G.; Ortiz, J. V. Electron binding energies of nucleobases and nucleotides. *Int. J. Quantum Chem.* **2002**, *90*, 1547−1554.
(129) Zakjevskii, V. V.; King, S. J.; Dolgounitcheva, O.; Zakrzewski, V. G.; Ortiz, J. V. Base and Phosphate Electron Detachment Energies of Deoxyribonucleotide Anions. *J. Am. Chem. Soc.* **2006**, *128*, 13350−13351.
(130) Zakjevskii, V. V.; Dolgounitcheva, O.; Zakrzewski, V. G.; Ortiz, J. V. Electron propagator studies of vertical electron detachment energies and isomerism in purinic deoxyribonucleotides. *Int. J. Quantum Chem.* **2007**, *107*, 2266−2273.
(131) Zakrzewski, V. G.; Dolgounitcheva, O.; Zakjevskii, A. V.; Ortiz, J. V. Ab initio electron propagator methods: applications to nucleic acids fragments and metallophthalocyanines. *Int. J. Quantum Chem.* **2010**, *110*, 2918−2930.
(132) Zakrzewski, V. G.; Dolgounitcheva, O.; Zakjevskii, A. V.; Ortiz, J. V. Ab initio electron propagator calculations on electron detachment energies of fullerenes, macrocyclic molecules, and nucleotide fragments. *Adv. Quantum Chem.* **2011**, *62*, 105−136.
(133) Yin, S.; Bernstein, E. R. Fe−V sulfur clusters studied through photoelectron spectroscopy and density functional theory. *Phys. Chem. Chem. Phys.* **2018**, *20*, 22610−22622.
(134) Martinez, A.; Tenorio, F. J.; Ortiz, J. V. Electronic Structure of AlO_2, AlO_2^-, Al_3O_5, and $Al_3O_5^-$ Clusters. *J. Phys. Chem. A* **2001**, *105*, 11291−11294.
(135) Martinez, A.; Tenorio, F. J.; Ortiz, J. V. Electronic Structure of Al_3O_n and $Al_3O_n^-$ (n = 1−3) Clusters. *J. Phys. Chem. A* **2001**, *105*, 8787−8793.
(136) Martinez, A.; Sansores, L. E.; Salcedo, R.; Tenorio, F. J.; Ortiz, J. V. Al_3O_n and $Al_3O_n^-$ (n = 1−3) Clusters: Structures, Photoelectron Spectra, Harmonic Vibrational Frequencies, and Atomic Charges. *J. Phys. Chem. A* **2002**, *106*, 10630−10635.
(137) Martinez, A.; Tenorio, F. J.; Ortiz, J. V. Al_3O_4 and $Al_3O_4^-$ Clusters: Structure, Bonding, and Electron Binding Energies. *J. Phys. Chem. A* **2003**, *107*, 2589−2595.
(138) Ortiz, J. V. An efficient, renormalized self-energy for calculating the electron binding energies of closed-shell molecules and anions. *Int. J. Quantum Chem.* **2005**, *105*, 803−808.
(139) Guevara-Garcia, A.; Martinez, A.; Ortiz, J. V. Electron binding energies and Dyson orbitals of $Al_5O_m^-$ (m = 3, 4, 5) and $Al_5O_5H_2$. *J. Chem. Phys.* **2007**, *127*, 234302.
(140) Ortiz, J. V. Brueckner orbitals, Dyson orbitals, and correlation potentials. *Int. J. Quantum Chem.* **2004**, *100*, 1131−1135.
(141) Tenorio, F. J.; Murray, I.; Martinez, A.; Klabunde, K. J.; Ortiz, J. V. Products of the addition of water molecules to $Al_3O_3^-$ clusters: Structure, bonding, and electron binding energies in $Al_3O_4H_2^-$, $Al_3O_5H_4^-$, $Al_3O_4H_2$, and $Al_3O_5H_4$. *J. Chem. Phys.* **2004**, *120*, 7955−7962.
(142) Guevara-Garcia, A.; Martinez, A.; Ortiz, J. V. Are structures with Al−H bonds represented in the photoelectron spectrum of $Al_3O_4H_2^-$? *J. Chem. Phys.* **2006**, *124*, 214304.
(143) Tiznado, W.; Oña, O. B.; Caputo, M. C.; Ferraro, M. B.; Fuentealba, P. Theoretical Study of the Structure and Electronic Properties of $Si_3O_n^-$ and $Si_6O_n^-$ (n = 1−6) Clusters. Fragmentation and Formation Patterns. *J. Chem. Theory Comput.* **2009**, *5*, 2265−2273.
(144) Rezaei, M.; Öğüt, S. Photoelectron spectra of early 3d-transition metal dioxide molecular anions from GW calculations. *J. Chem. Phys.* **2021**, *154*, 094307.
(145) Ortiz, J. V. Vertical and adiabatic ionization energies of NH_4^- isomers via electron propagator theory and many body perturbation theory calculations with large basis sets. *J. Chem. Phys.* **1987**, *87*, 3557−3562.
(146) Ortiz, J. V. Ionization energies of OH_3^- isomers. *J. Chem. Phys.* **1989**, *91*, 7024−7029.
(147) Ortiz, J. V. A double Rydberg anion with a hydrogen bond and a solvated double Rydberg anion: Interpretation of the photoelectron spectrum of $N_2H_7^-$. *J. Chem. Phys.* **2002**, *117*, 5748−5756.
(148) Melin, J.; Ortiz, J. V. OH_3^- and $O_2H_5^-$ double Rydberg anions: Predictions and comparisons with NH_4^- and $N_2H_7^-$. *J. Chem. Phys.* **2007**, *127*, 014307.
(149) Melin, J.; Seabra, G.; Ortiz, J. V. Electronic structure and reactivity in double Rydberg anions: characterization of a novel kind of electron pair. *Theor. Comput. Chem.* **2007**, *19*, 87−100.
(150) Díaz-Tinoco, M.; Ortiz, J. V. Double Rydberg anions with solvated ammonium kernels: Electron binding energies and Dyson orbitals. *J. Chem. Phys.* **2019**, *151*, 054301.
(151) Opoku, E.; Pawłowski, F.; Ortiz, J. V. Electron binding energies and Dyson orbitals of $O_nH_{2n+1}^{+,0,-}$ clusters: Double Rydberg anions, Rydberg radicals, and micro-solvated hydronium cations. *J. Chem. Phys.* **2021**, *154*, 234304.
(152) Opoku, E.; Pawłowski, F.; Ortiz, J. V. Double Rydberg anions, Rydberg radicals and micro-solvated cations with ammonium-water kernels. *Phys. Chem. Chem. Phys.* **2022**, *24*, 18347−18360.
(153) Ortiz, J. V. Structures and properties of double-Rydberg anions. *J. Phys. Chem.* **1990**, *94*, 4762−4763.
(154) Hopper, H.; Lococo, M.; Dolgounitcheva, O.; Zakrzewski, V. G.; Ortiz, J. V. Double-Rydberg Anions: Predictions on $NH_3AH_n^-$ and $OH_2AH_n^-$ Structures. *J. Am. Chem. Soc.* **2000**, *122*, 12813−12818.

https://doi.org/10.1021/acs.jpca.2c08372
J. Phys. Chem. A 2023, 127, 1085−1101

(155) Díaz-Tinoco, M. A.; Ortiz, J. V. Dyson Orbitals and Double Rydberg Anions: Methylated, Annulated and Paramagnetic. *J. Phys. Chem. A* **2019**, *123*, 10961−10967.
(156) Ariyarathna, I. R.; Khan, S. N.; Pawłowski, F.; Ortiz, J. V.; Miliordos, E. Aufbau Rules for Solvated Electron Precursors: $Be(NH_3)_4^{0,\pm}$ Complexes and Beyond. *J. Phys. Chem. Lett.* **2018**, *9*, 84−88.
(157) Almeida, N. M. S.; Pawłowski, F.; Ortiz, J. V.; Miliordos, E. Transition-metal solvated-electron precursors: diffuse and 3d electrons in $V(NH_3)_6^{0,\pm}$. *Phys. Chem. Chem. Phys.* **2019**, *21*, 7090−7097.
(158) Zakrzewski, V. G.; Ortiz, J. V. Electron Propagator Theory of ZnC_5H_5, $Zn(C_5H_5)_2$, and Related Ions. *J. Phys. Chem.* **1994**, *98*, 13198−13202.
(159) Zakrzewski, V. G.; Ortiz, J. V. Electron propagator theory of $ZnCH_3$, $Zn(CH_3)_2$, and related ions. *J. Chem. Phys.* **1994**, *100*, 6508−6513.
(160) Kambalapalli, S.; Ortiz, J. V. Electronic Structure of $ScC_6H_6^-$ and ScC_6H_6: Geometries, Electron Binding Energies, and Dyson Orbitals. *J. Phys. Chem. A* **2004**, *108*, 2988−2992.
(161) Dolgounitcheva, O.; Zakrzewski, V. G.; Ortiz, J. V. Electronic structure of a beryllium half-sandwich complex, $Be(\eta^5\text{-}C_5H_5)$. *Int. J. Quantum Chem.* **2012**, *112*, 2981−2985.
(162) Ortiz, J. V. Electron-propagator calculations on the adiabatic electron binding energies of the carbon trimer. *J. Chem. Phys.* **1992**, *97*, 7531−7536.
(163) Ortiz, J. V. Electron propagator calculations on the electron affinity of C_5. *Chem. Phys. Lett.* **1993**, *216*, 319−323.
(164) Ortiz, J. V. Improved electron propagator methods: an investigation of the carbon tetraatomic neutral molecule, mononegative ion, and monopositive ion (C_4, C_4^-, and C_4^+). *J. Chem. Phys.* **1993**, *99*, 6716−6726.
(165) Ortiz, J. V.; Zakrzewski, V. G. Electron binding energies of linear C_3, C_5, C_7, and C_9 clusters. *J. Chem. Phys.* **1994**, *100*, 6614−6619.
(166) Zakrzewski, V. G.; Ortiz, J. V. Electron propagator calculations on linear and branched carbon cluster dianions. *J. Chem. Phys.* **1995**, *102*, 294−300.
(167) Ohno, M.; Zakrzewski, V. G.; Ortiz, J. V.; von Niessen, W. Theoretical study of the valence ionization energies and electron affinities of linear C_{2n+1} (n = 1−6) clusters. *J. Chem. Phys.* **1997**, *106*, 3258−3269.
(168) Zakrzewski, V. G.; Dolgounitcheva, O.; Ortiz, J. V. Electron Propagator Calculations on the Ground and Excited States of C_{60}^-. *J. Phys. Chem. A* **2014**, *118*, 7424−7429.
(169) Alexandrova, A. N.; Boldyrev, A. I.; Li, X.; Sarkas, H. W.; Hendricks, J. H.; Arnold, S. T.; Bowen, K. H. Lithium cluster anions: Photoelectron spectroscopy and ab initio calculations. *J. Chem. Phys.* **2011**, *134*, 044322.
(170) Dolgounitcheva, O.; Zakrzewski, V. G.; Ortiz, J. V. Ground state and vertical electron detachment energies of icosahedral and D_{5h} Al_{13}. *J. Chem. Phys.* **1999**, *111*, 10762−10765.
(171) Tiznado, W. A.; Fuentealba, P.; Ortiz, J. V. Pseudopotential and electron propagator methods for the calculation of the photoelectron spectra of anionic silicon clusters: Predictions on Si_{10}. *J. Chem. Phys.* **2005**, *123*, 144314.
(172) Alexandrova, A. N.; Boldyrev, A. I.; Fu, Y.-J.; Yang, X.; Wang, X.-B.; Wang, L.-S. Structure of the $Na_xCl_{x+1}^-$ (x = 1−4) clusters via ab initio genetic algorithm and photoelectron spectroscopy. *J. Chem. Phys.* **2004**, *121*, 5709−5719.
(173) Li, S.-D.; Ren, G.-M.; Jin, Z.-H. An ab initio investigation on the vertical electron detachment energies of semiconductor-alkali binary anions E_nA^- (A = K, Na, Li; E = Ge, Si; n = 1−10). *J. Chem. Phys.* **2003**, *119*, 10063−10068.
(174) Tian, S. X. Ab initio study of structures and energies of Al_2H_4 and $Al_2H_4^-$. *Theor. Chem. Acc.* **2006**, *115*, 291−297.
(175) Sommerfeld, T. Multipole-bound states of succinonitrile and other dicarbonitriles. *J. Chem. Phys.* **2004**, *121*, 4097−4104.
(176) Dolgounitcheva, O.; Díaz-Tinoco, M.; Zakrzewski, V. G.; Richard, R. M.; Marom, N.; Sherrill, C. D.; Ortiz, J. V. Accurate Ionization Potentials and Electron Affinities of Acceptor Molecules IV: Electron-Propagator Methods. *J. Chem. Theory Comput.* **2016**, *12*, 627−637.
(177) Dolgounitcheva, O.; Díaz-Tinoco, M.; Zakrzewski, V. G.; Richard, R. M.; Marom, N.; Sherrill, C. D.; Ortiz, J. V. Correction to Accurate Ionization Potentials and Electron Affinities of Acceptor Molecules IV: Electron-Propagator Methods. *J. Chem. Theory Comput.* **2017**, *13*, 389−391.
(178) Melin, J.; Singh, R. K.; Mishra, M. K.; Ortiz, J. V. Tautomeric forms of azolide anions: vertical electron detachment energies and Dyson orbitals. *J. Phys. Chem. A* **2007**, *111*, 13069−13074.
(179) Canuto, S.; Coutinho, K.; Cabral, B. J. C.; Zakrzewski, V. G.; Ortiz, J. V. Delocalized water and fluoride contributions to Dyson orbitals for electron detachment from the hydrated fluoride anion. *J. Chem. Phys.* **2010**, *132*, 214507.
(180) Dolgounitcheva, O.; Zakrzewski, V. G.; Ortiz, J. V. Delocalization of Dyson orbitals in F-(H_2O) and Cl-(H_2O). *Int. J. Quantum Chem.* **2011**, *111*, 1701−1708.
(181) Dolgounitcheva, O.; Zakrzewski, V. G.; Ortiz, J. V. Electron detachment energies of aqueous and cluster halide anions from electron propagator calculations with the polarizable continuum model. *Int. J. Quantum Chem.* **2012**, *112*, 3840−3848.
(182) Dolgounitcheva, O.; Zakrzewski, V. G.; Ortiz, J. V. Assignment of photoelectron spectra of halide-water clusters: Contrasting patterns of delocalization in Dyson orbitals. *J. Chem. Phys.* **2013**, *138*, 164317.
(183) Dolgounitcheva, O.; Zakrzewski, V. G.; Streit, L.; Ortiz, J. V. Microsolvation effects on the electron binding energies of halide anions. *Mol. Phys.* **2014**, *112*, 332−339.
(184) Zein, S.; Ortiz, J. V. Interpretation of the photoelectron spectra of superalkali species: Li_3O and Li_3O^-. *J. Chem. Phys.* **2011**, *135*, 164307.
(185) Zein, S.; Ortiz, J. V. Interpretation of the photoelectron spectra of superalkali species: Na_3O and Na_3O^-. *J. Chem. Phys.* **2012**, *136*, 224305.
(186) Pérez-González, A.; Galano, A.; Ortiz, J. V. Vertical Ionization Energies of Free Radicals and Electron Detachment Energies of Their Anions: A Comparison of Direct and Indirect Methods Versus Experiment. *J. Phys. Chem. A* **2014**, *118*, 6125−6131.
(187) Zakrzewski, V. G.; Ortiz, J. V.; Nichols, J. A.; Heryadi, D.; Yeager, D. L.; Golab, J. T. Comparison of perturbative and multiconfigurational electron propagator methods. *Int. J. Quantum Chem.* **1996**, *60*, 29−36.
(188) Ortiz, J. V. Partial third-order quasiparticle theory: comparisons for closed-shell ionization energies and an application to the Borazine photoelectron spectrum. *J. Chem. Phys.* **1996**, *104*, 7599−7605.
(189) Opoku, E.; Pawłowski, F.; Ortiz, J. V. A new generation of diagonal self-energies for the calculation of electron removal energies. *J. Chem. Phys.* **2021**, *155*, 204107.
(190) Opoku, E.; Pawłowski, F.; Ortiz, J. V. Electron Propagator Self-Energies versus Improved GW100 Vertical Ionization Energies. *J. Chem. Theory Comput.* **2022**, *18*, 4927−4944.
(191) Manne, R. A completeness theorem for operator spaces. *Chem. Phys. Lett.* **1977**, *45*, 470−472.
(192) Löwdin, P. O. Studies in perturbation theory. X. Lower bounds to energy eigenvalues in perturbation-theory ground state. *Phys. Rev.* **1965**, *139*, A357−A372.
(193) Pickup, B. T.; Goscinski, O. Direct calculation of ionization energies. I. Closed shells. *Mol. Phys.* **1973**, *26*, 1013−1035.
(194) Born, G.; Kurtz, H. A.; Öhrn, Y. Elementary finite order perturbation theory for vertical ionization energies. *J. Chem. Phys.* **1978**, *68*, 74−85.
(195) Hirata, S.; Hermes, M. R.; Simons, J.; Ortiz, J. V. General-Order Many-Body Green's Function Method. *J. Chem. Theory Comput.* **2015**, *11*, 1595−1606.

https://doi.org/10.1021/acs.jpca.2c08372
J. Phys. Chem. A 2023, 127, 1085−1101

(196) Hirata, S.; Doran, A. E.; Knowles, P. J.; Ortiz, J. V. One-particle many-body Green's function theory: Algebraic recursive definitions, linked-diagram theorem, irreducible-diagram theorem, and general-order algorithms. *J. Chem. Phys.* **2017**, *147*, 044108.
(197) Corzo, H. H.; Galano, A.; Dolgounitcheva, O.; Zakrzewski, V. G.; Ortiz, J. V. NR2 and P3+: Accurate, Efficient Electron-Propagator Methods for Calculating Valence, Vertical Ionization Energies of Closed-Shell Molecules. *J. Phys. Chem. A* **2015**, *119*, 8813−8821.
(198) Reining, L. The GW approximation: content, successes and limitations. *Wiley Interdiscip. Rev.: Comput. Mol. Sci.* **2018**, *8*, No. e1344.
(199) Schirmer, J.; Cederbaum, L. S. The two-particle-hole Tamm-Dancoff approximation (2ph-TDA) equations for closed-shell atoms and molecules. *J. Phys. B* **1978**, *11*, 1889−1900.
(200) Bintrim, S. J.; Berkelbach, T. C. Full-frequency GW without frequency. *J. Chem. Phys.* **2021**, *154*, 041101.
(201) Schirmer, J.; Cederbaum, L. S.; Walter, O. New approach to the one-particle Green's function for finite Fermi systems. *Phys. Rev. A* **1983**, *28*, 1237−1259.
(202) Ortiz, J. V. The electron propagator picture of molecular electronic structure. *Comput. Chem. (Singapore)* **1997**, *2*, 1−61.
(203) Schirmer, J.; Angonoa, G. On Green-function calculations of the static self-energy part, the ground state energy, and expectation values. *J. Chem. Phys.* **1989**, *91*, 1754−1761.
(204) Ortiz, J. V. A nondiagonal, renormalized extension of partial third-order quasiparticle theory: comparisons for closed-shell ionization energies. *J. Chem. Phys.* **1998**, *108*, 1008−1014.
(205) Ortiz, J. V. Single-reference electron propagator calculations on vertical ionization energies of ozone. *Chem. Phys. Lett.* **1998**, *297*, 193−199.
(206) Ortiz, J. V. Orbital and shakeup operator renormalizations in electron propagator theory. *J. Chem. Phys.* **1998**, *109*, 5741−5746.
(207) Ortiz, J. V. Second-order shakeup terms in electron propagator calculations on F2 and H_2O2. *Int. J. Quantum Chem.* **1998**, *69*, 175−182.
(208) Ortiz, J. V. Electron propagator theory: an approach to prediction and interpretation in quantum chemistry. *Wiley Interdiscip. Rev.: Comput. Mol. Sci.* **2013**, *3*, 123−142.
(209) Bartlett, R. J. Coupled-cluster theory and its equation-of-motion extensions. *Wiley Interdiscip. Rev.: Comput. Mol. Sci.* **2012**, *2*, 126−138.
(210) Purvis, G. D.; Bartlett, R. J. A full coupled-cluster singles and doubles model: The inclusion of disconnected triples. *J. Chem. Phys.* **1982**, *76*, 1910−1918.
(211) Raghavachari, K.; Trucks, G. W.; Pople, J. A.; Head-Gordon, M. A fifth-order perturbation comparison of electron correlation theories. *Chem. Phys. Lett.* **1989**, *157*, 479−483.
(212) Kendall, R. A.; Dunning, T. H.; Harrison, R. J. Electron affinities of the first-row atoms revisited. Systematic basis sets and wave functions. *J. Chem. Phys.* **1992**, *96*, 6796−6806.
(213) Frisch, M. J.; Trucks, G. W.; Schlegel, H. B.; Scuseria, G. E.; Robb, M. A.; Cheeseman, J. R.; Scalmani, G.; Barone, V.; Petersson, G. A.; Nakatsuji, H.; et al. *Gaussian Development Version*, rev. I.14; Gaussian, Inc.: Wallingford, CT, 2018.
(214) Díaz-Tinoco, M.; Dolgounitcheva, O.; Zakrzewski, V. G.; Ortiz, J. V. Composite electron propagator methods for calculating ionization energies. *J. Chem. Phys.* **2016**, *144*, 224110.
(215) Bruneval, F. Optimized virtual orbital subspace for faster GW calculations in localized basis. *J. Chem. Phys.* **2016**, *145*, 234110.
(216) Kanchanakungwankul, S.; Truhlar, D. G. Examination of How Well Long-Range-Corrected Density Functionals Satisfy the Ionization Energy Theorem. *J. Chem. Theory Comput.* **2021**, *17*, 4823−4830.
(217) Boudaiffa, B.; Cloutier, P.; Hunting, D.; Huels, M. A.; Sanche, L. Resonant formation of DNA strand breaks by low-energy (3 to 20 eV) electrons. *Science* **2000**, *287*, 1658−1660.
(218) Alizadeh, E.; Orlando, T. M.; Sanche, L. Biomolecular damage induced by ionizing radiation: the direct and indirect effects of low-energy electrons on DNA. *Annu. Rev. Phys. Chem.* **2015**, *66*, 379−398.
(219) Halkier, A.; Helgaker, T.; Jørgensen, P.; Klopper, W.; Koch, H.; Olsen, J.; Wilson, A. K. Basis-set convergence in correlated calculations on Ne, N_2, and H_2O. *Chem. Phys. Lett.* **1998**, *286*, 243−252.
(220) Yang, X.; Wang, X.-B.; Vorpagel, E. R.; Wang, L.-S. Direct experimental observation of the low ionization potentials of guanine in free oligonucleotides by using photoelectron spectroscopy. *Proc. Natl. Acad. Sci. U. S. A.* **2004**, *101*, 17588−17592.

https://doi.org/10.1021/acs.jpca.2c08372
J. Phys. Chem. A 2023, 127, 1085−1101

Appendix I

E. Opoku, F. Pawłowski and J. V. Ortiz, "New−Generation Electron−Propagator Methods for Vertical Electron Detachment Energies of Molecular Anions: Benchmarks and Applications to Model Green−Fluorescent−Protein Chromophores", *Phys. Chem. Chem. Phys.* 26, 9915–9930 (2024)

PCCP

ROYAL SOCIETY OF CHEMISTRY

PAPER

View Article Online
View Journal | View Issue

Check for updates

Cite this: *Phys. Chem. Chem. Phys.*, 2024, **26**, 9915

New-generation electron-propagator methods for vertical electron detachment energies of molecular anions: benchmarks and applications to model green-fluorescent-protein chromophores†

Ernest Opoku, Filip Pawłowski and J. V. Ortiz *

Ab initio electron-propagator calculations continue to be useful companions to experimental investigations of electronic structure in molecular anions. A new generation of electron-propagator methods recently has surpassed its antecedents' predictive accuracy and computational efficiency. Interpretive clarity has been conserved, for no adjustable parameters have been introduced in the preparation of molecular orbitals or in the formulation of approximate self-energies. These methods have employed the diagonal self-energy approximation wherein each Dyson orbital equals a canonical Hartree–Fock orbital times the square root of a probability factor. Numerical tests indicate that explicitly renormalized, diagonal self-energies are needed when Dyson orbitals have large valence nitrogen, oxygen or fluorine components. They also demonstrate that even greater accuracy can be realized with generalizations that do not employ the diagonal self-energy approximation in the canonical Hartree–Fock basis. Whereas the diagonal methods have fifth-power arithmetic scaling factors, the non-diagonal generalizations introduce only non-iterative sixth-power contractions. Composite models conserve the accuracy of the most demanding combinations of self-energy approximations and flexible basis sets with drastically reduced computational effort. Composite-model results on anions that resemble the chromophore of the green fluorescent protein illustrate the interpretive capabilities of explicitly renormalized self-energies. Accurate predictions on the lowest vertical electron detachment energy of each anion confirm experimental data and the utility of the diagonal self-energy approximation.

Received 30th January 2024,
Accepted 8th March 2024

DOI: 10.1039/d4cp00441h

rsc.li/pccp

1. Introduction

Electron-propagator calculations have been a frequent and persistent accompaniment to reports of anion photoelectron spectra.[1–7] The theory that underlies these calculations may be expressed in terms of an eigenvalue equation with an effective one-electron operator.[8–11] In addition to the kinetic, nuclear-attraction, Coulomb and exchange components found in the Hartree–Fock equations, the self-energy operator also appears. The latter term describes orbital relaxation and differential correlation effects on electron detachment energies. The form of the exact self-energy operator is known and *ab initio* approximations to it have been widely applied. When electron-propagator calculations are performed on an anionic reference state, electron detachment energies emerge as eigenvalues of a non-local, energy-dependent operator. In addition, the one-electron eigenfunctions are proportional to Dyson orbitals. The proportionality factor, known as a probability factor or pole strength, may be determined from the energy derivative of the self-energy contribution to the eigenvalue. Spectral intensities in the sudden approximation may be calculated with transition integrals between continuum functions and Dyson orbitals.[11] The eigenvalue equation offers a convenient generalization of Koopmans's identity for the lowest electron detachment energies of closed-shell molecules and ions. Electron-propagator methodology conserves a one-electron picture of chemical bonding to the greatest extent possible in an exact, *ab initio* theory. It also provides diagnostics based on probability factors when that picture becomes invalid and well-defined procedures for describing qualitatively important correlation effects.

Whereas older self-energy approximations have aided interpretations of spectra since the 1970s,[12–15] a new generation of electron-propagator methods has surpassed their accuracy and computational efficiency. These advantages have entailed no sacrifice of interpretability, for no adjustable parameters have been introduced in the preparation of orbitals or in the self-energy formulae. For a given level of computational effort,

Department of Chemistry and Biochemistry, Auburn University, Auburn, AL 36849-5312, USA. E-mail: ezo0009@auburn.edu, flp0008@auburn.edu, ortiz@auburn.edu

† Electronic supplementary information (ESI) available. See DOI: https://doi.org/10.1039/d4cp00441h

This journal is © the Owner Societies 2024

Table 1 Acronyms for electron propagator self-energies

Acronym[a]	Full name
Diagonal self-energies	
D2	Diagonal second order
os-D2	Opposite-spin D2
nD-D2	non-Dyson D2
os-nD-D2	Opposite-spin non-Dyson D2
D3	Diagonal third order
nD-D3	non-Dyson D3
OVGF	Outer-Valence Green's Function (Versions A, B and C)
nD-OVGF	non-Dyson OVGF (Versions A, B and C)
P3	Partial third order
P3+	Approximately renormalized partial third order
Q3	Quasiparticle third order
Q3+	Approximately renormalized quasiparticle third order
L3	Linear third order
nD-L3	non-Dyson L3
L3+	Approximately renormalized linear third order (Versions A, B and C)
nD-L3+	non-Dyson L3+ (Versions A, B and C)
RP3	Explicitly renormalized partial third order
RQ3	Explicitly renormalized quasiparticle third order
RL3	Explicitly renormalized linear third order
nD-RL3	non-Dyson RL3
DR	Diagonal (renormalized) ring approximation (HF-TDA-G_0W_0)
Non-diagonal self-energies	
ND2	Non-diagonal, second order
2ph-TDA	Two-particle-one-hole Tamm–Dancoff approximation
3+	Non-diagonal third order
ADC(3)	Third order algebraic diagrammatic construction
NR2	Non-diagonal, renormalized, second order
BD-T1	Brueckner doubles with triple field operators
NRP3	Non-diagonal extension of RP3
NRQ3	Non-diagonal extension of RQ3
NRL3	Non-diagonal extension of RL3

[a] New-generation methods are in bold type. N = non-diagonal; nD = non-Dyson; R = explicitly renormalized; + = approximately renormalized.

determined by the arithmetic scaling of bottleneck operations, a higher level of accuracy has been realized.[5,16–19] For example, the three older, outer valence Green's function (OVGF, versions A, B and C) self-energies[15,20,21] and a recently developed method have identical fifth-power bottlenecks. (See Table 1 for a complete set of self-energy acronyms; Table 2 lists the scaling of arithmetic bottlenecks for each method.) The latter alternative, the approximately renormalized linear third order (L3+B) self-energy, has produced lower mean absolute errors in several recent tests *versus* standard data.[5,16–19] Even higher levels of accuracy have been achieved with methods that introduce more steps with the same scaling factor. In addition, new-generation self-energies with only cubically scaling computational demands have closely approached the accuracy of the best OVGF options. Several other widely applied methods have now been surpassed in a similar manner. Examples of older diagonal approximations include the diagonal second order (D2) and approximately renormalized partial third order[22–24] (P3+) self-energies. Among the older non-diagonal, renormalized examples are the strict[20] (3+) and standard[25] Dyson versions of the third order algebraic diagrammatic construction[26] [ADC(3)]. Comparisons have also been made to a fully *ab initio* member of the G_0W_0 family methods[27] that employs canonical Hartree–Fock orbitals and Tamm–Dancoff excitations.[28] This G_0W_0@HF-TDA method has a diagonal self-energy that comprises ring terms in all orders and therefore is denoted by DR below. These conclusions are based on numerical tests *versus* the QTP,[16,18] GW100,[17] OPV24[19] and VEDE55[5] data bases of electron binding energies.

Underlying the efficient fifth-power and third-power scaling factors of these methods is the diagonal self-energy approximation. By neglecting off-diagonal elements of the self-energy operator in the canonical Hartree–Fock orbital basis, sixth-power algorithms may be avoided. (For example, coupled-cluster and configuration interaction methods that include double orbital substitutions are in the sixth-power category.)

Table 2 Arithmetic scaling requirements of electron-propagator methods[a]

Method class	Methods[b]	Arithmetic bottleneck	Bottleneck steps	Largest ERI[c] subset
Diagonal 2nd order	D2, os-D2	OV^2	N_E	O^2V^2
	RSPT2, nD-D2, **os-nD-D2**	OV^2	Non-iterative	O^2V^2
Diagonal post 2nd order	RSPT3	OV^4	Non-iterative	V^4
	D3, OVGF	OV^4	N_E[d]	V^4
	P3, P3+, **Q3**, **Q3+**	O^2V^3	Non-iterative	OV^3
	L3, **L3+**	OV^4	N_E[d]	V^4
	RP3, **RQ3**	O^2V^3	Non-iterative	OV^3
	RL3	OV^4	N_IN_E[d]	V^4
	DR	O^2V^3	N_IN_E	O^2V^2
Non-diagonal	ND2	OV^3	N_I	OV^3
	2ph-TDA	OV^4	N_I	V^4
	3+	O^2V^4	Non-iterative[f]	V^4
	ADC(3)	O^2V^4	N_I[f]	V^4
	NR2	O^3V^3	Non-iterative[f]	OV^3
	BD-T1	O^2V^4	BD[e]	V^4
	NRP3, **NRQ3**, **NRL3**	O^2V^4	Non-iterative[f]	V^4

[a] O = # occupied orbital, V = # virtual orbitals, N_E = energy iterations, N_I = inverse-expansion or linear-equation iterations for diagonal methods and Hamiltonian-vector multiplications for non-diagonal methods. [b] New methods in bold type. [c] ERI = electron repulsion integral. [d] Reduction by a factor of N_E occurs in non-Dyson (nD) versions. [e] The O^2V^4 arithmetic bottleneck occurs in the Brueckner doubles, coupled-cluster, reference-state calculation; the subsequent electron-propagator bottleneck is OV^4. [f] N_I OV^4 iterative steps for 3+, ADC(3) and NRL3; N_I O^3V^2 iterative steps for NR2, NRP3 and NRQ3.

This journal is © the Owner Societies 2024

This advantage has enabled widespread application of electron-propagator methodology to the interpretation of spectra. The price that is paid for this expedient is a constraint on the resulting Dyson orbitals, for they become proportional to canonical Hartree–Fock orbitals.

The latest methodological developments restore non-diagonal elements of the self-energy matrix while retaining all terms that appeared in their diagonal antecedents.[18] This restoration allows the Dyson orbitals to be expressed in their most general form, a linear combination of basis functions, *e.g.*, the canonical Hartree–Fock orbitals. The validity of the diagonal approximation may be tested *via* comparisons of electron binding energies and Dyson orbitals. Numerical data of this kind for anionic reference states is presented in this work for the first time.

These tests are performed on a previously devised set of 55 vertical electron detachment energies (VEDEs) pertaining to 36 closed-shell anions.[5] Nuclei from the first three periods (elements X and Z) are represented in the X^-, XZ^-, XH_n^- and HXZ^- anions of the VEDE55 set. Basis-set extrapolated data on VEDEs computed with a high level of theory constitute the standard of comparison. Calculations performed with each of the self-energy approximations are used to obtain basis-set-extrapolated results. Error measures and arithmetic scaling factors are the criteria that determine the best combinations of accuracy and computational efficiency.

To rapidly approximate results obtained with the best self-energy approximations and the most flexible basis sets, several composite methods has been devised and tested.[5,19] These techniques assume the additivity of basis-set and correlation corrections to lower-level calculations.[29] In this work, new composite models with explicitly renormalized diagonal or non-diagonal renormalized self-energy components are introduced. The success of these models indicates that calculations of high accuracy are feasible for considerably larger molecules and ions.

The 2008 Nobel Prize in Chemistry recognized the discovery of the green fluorescent protein (GFP), the foundation of myriad optical characterizations of biological structures.[30] Electron propagator techniques developed in this work may be applied to the chromophoric center that is responsible for the intense fluorescence of GFP. This fragment of the protein is a closed-shell anion that contains a phenolate moiety covalently bound to an imidazolinone ring. Recent anion photoelectron spectroscopy experiments have measured the VEDEs of the *p*-hydroxybenzylidene-2,3-dimethylimidazoline anion (*p*-HBDI$^-$) and two substituted analogues.[31–39] The latter anions display two substitutions on the phenolate ring with fluorine (DF-HBDI$^-$) or methoxy (*syn*-DM-HBDI$^-$) groups. Experiments have also been performed on the three phenolate anions (PhO$^-$, DF-PhO$^-$, *syn*-DM-PhO$^-$) that are formed when a hydrogen atom resides in the *ipso* position.[40–44] Applications to these anions of the new, composite electron-propagator models demonstrate their interpretive capabilities, confirm precise spectral data, and provide information to stimulate further experimentation.

2. Theory and computational methods

2.1 Electron propagator theory

Many kinds of electron-propagator calculations are executed by software organized around the Dyson quasiparticle equation. (Commercially available software with electron-propagator capabilities has been in use for thirty years.[45]) This pseudo-eigenvalue equation involves a one-electron operator that is energy-dependent and non-local. With the introduction of an orthonormal orbital basis, it can be cast in terms of matrices (in bold type) as follows:

$$[\boldsymbol{F} + \boldsymbol{\Sigma}'(E_X)]\mathbf{C}(E_X) = E_X\mathbf{C}(E_X) \quad (1)$$

where X is a final-state label. Elements of the generalized Fock matrix, $\boldsymbol{F}$, depend on the one-electron reduced density matrix, $\boldsymbol{\rho}$, according to

$$\boldsymbol{F}_{pq} = \mathrm{h}_{pq}^{(1)} + \langle pr||qs\rangle\boldsymbol{\rho}_{rs}, \quad (2)$$

where p, q, r and s are general spin-orbital indices, $h^{(1)}$ is the one-electron operator and anti-symmetrized electron repulsion integrals (ERIs) are written in Dirac's format. Einstein's notation for summations is assumed for indices that occur more than once in a product. In general, $\boldsymbol{\rho}$ is not idempotent; it need not correspond to a single Slater determinant. In fact, correlation contributions to $\boldsymbol{\rho}$ are often included in widely used electron-propagator methods. The one-electron operator includes only kinetic-energy and nuclear-attraction components in most calculations, but it may also contain external fields. This option has been employed in solvation modelling[46,47] and is suitable for investigations of anionic resonances.[48–51] The second part of the operator matrix in eqn (1) corresponds to the energy-dependent part of the self-energy, $\Sigma'(E)$. Not all values of E satisfy eqn (1). Those that do satisfy it equal electron binding energies (*i.e.*, poles of the electron propagator) and may be called self-consistent. An eigenvector corresponding to a self-consistent eigenvalue defines a linear combination of basis functions that is proportional to a Dyson orbital. The norm of the Dyson orbital is known as a probability factor, an intensity factor or a pole strength. It may be determined with

$$\begin{aligned}\Pi_X &= \int\left|\phi_X^{\mathrm{Dyson}}(x)\right|^2\mathrm{d}x \\ &= \left[1 - \left.\frac{\mathrm{d}\mathbf{C}^\dagger(E)\Sigma'(E)C(E)}{\mathrm{d}E}\right|_{E=E_X}\right]^{-1}.\end{aligned} \quad (3)$$

Probability factors vary between zero and unity. Intensities in the sudden approximation[52] are proportional to probability factors and squared moduli of transition matrix elements between normalized Dyson orbitals and continuum functions. In the exact electron propagator, the sum of the probability factors equals the number of electrons. A convenient criterion of one-electron (*e.g.*, Koopmans-like) character for an electron binding energy is a probability factor greater than or equal to 0.85. Correlation final states[53] (*e.g.*, simple shake-ups) have lower probability factors.

When a basis of canonical Hartree–Fock orbitals is assumed, the uncorrelated and correlated parts of $\boldsymbol{F}$ are represented respectively as $\boldsymbol{F}^{\mathrm{HF}}$ and $\Sigma(\infty)$. In this case,

$$F_{pq} = F_{pq}^{\mathrm{HF}} + \Sigma_{pq}(\infty) = \delta_{pq}\varepsilon_{pq} + \Sigma_{pq}(\infty), \tag{4}$$

where ε_{p} is the p-th canonical Hartree–Fock orbital energy. Correlation contributions to $\boldsymbol{\rho}$ are responsible for the last term. The total self-energy matrix, $\Sigma(E)$, therefore has energy-dependent and energy-independent parts, where

$$\Sigma_{pq}(E) = \Sigma'_{pq}(E) + \Sigma_{pq}(\infty). \tag{5}$$

When the absolute value of E increases without bound, the limit of the total self-energy equals its energy-independent part. A diagonal matrix of canonical Hartree–Fock orbital energies ($\boldsymbol{\varepsilon}$) and the self-energy matrix consequently appear in the Dyson quasiparticle equation:

$$[\boldsymbol{\varepsilon} + \Sigma(E_{\mathrm{X}})]\mathbf{C}(E_{\mathrm{X}}) = E_{\mathrm{X}}\mathbf{C}(E_{\mathrm{X}}). \tag{6}$$

When other orbital basis sets (*e.g.*, Kohn–Sham) are chosen, the Hartree–Fock exchange operator may be incorporated in the self-energy term. In the canonical Hartree–Fock basis, constant self-energy terms vanish in first and second order in the Møller–Plesset fluctuation potential.[54] Neglect of the self-energy operator in eqn (6) recovers the Koopmans-identity approximation[55] for electron binding energies and Dyson orbitals that equal canonical Hartree–Fock orbitals.

For the smallest electron detachment energies and the largest electron attachment energies of closed-shell species, off-diagonal elements of $\Sigma(E)$ in eqn (6) are often neglected. The diagonal self-energy approximation reduces arithmetic operations and forces Dyson orbitals to be proportional to canonical Hartree–Fock orbitals. Unit eigenvectors from eqn (6) simplify the probability factor of eqn (3), for the energy derivative of only a single self-energy matrix element is needed.

Several levels of diagonal self-energy approximations have been implemented and examined in numerical tests. All involve perturbative self-energy corrections to Koopmans results that may be classified according to orders of the Møller–Plesset fluctuation potential. The simplest class involves only second-order terms and requires arithmetic operations that scale cubically with the size of the system. Next in computational difficulty are the third-order methods, which have fifth-power arithmetic scaling. A third level comprises approximately renormalized methods that require almost no additional computational effort. This class employs only second-order and third-order terms to estimate certain classes of corrections in all higher orders. At the fourth and highest level are diagonal methods that explicitly evaluate the higher-order terms.

A new generation of diagonal self-energies spans all four levels and includes members that surpass their respective predecessors' accuracy.[5,16–19] Opposite-spin (os) second-order methods achieve higher accuracy by avoiding the tendency of full second-order calculations to exaggerate orbital relaxation and final-state differential correlation. Whereas full third-order and second-order results have similar absolute errors but with opposite signs, the recently introduced third-order methods are clearly more accurate. They provide a better reference for approximately renormalized self-energies that achieve smaller error measures than those of their predecessors. Their explicitly renormalized counterparts compete successfully against an *ab initio* version of G_0W_0 (DR), wherein ring self-energy terms are included in all orders. Mean absolute errors decline from 0.2 eV at the second-order level to below 0.1 eV at the explicitly renormalized level. These advances are achieved without the introduction of adjustable parameters in the generation of an orbital basis or in the self-energy formulae.

New-generation third-order methods and their renormalized extensions are founded on a different approach to deriving self-energy approximations. Elements of the generalized Fock and energy-dependent self-energy matrices may be expressed in terms of a super-operator Hamiltonian matrix, $\hat{\boldsymbol{H}}$. Sub-blocks of this matrix appear in general expressions of $\boldsymbol{F}$ and $\boldsymbol{\Sigma}'(E)$:

$$F_{\mathrm{pq}} = \left[a_{\mathrm{p}}^{\dagger}|\hat{H}a_{\mathrm{q}}^{\dagger}\right] \tag{7}$$

$$\Sigma'_{pq}(E) = \left[a_p^{\dagger}|\hat{H}\boldsymbol{f}\right]\left[\boldsymbol{f}|(E\hat{I} - \hat{H})\boldsymbol{f}\right]^{-1}\left[\boldsymbol{f}|\hat{H}a_q^{\dagger}\right]. \tag{8}$$

When $\hat{H}$ acts on an ionization operator, z, it forms a commutator with the Hamiltonian, *i.e.*, $\hat{H}z = Hz - zH$.[56] In derivations of previous approximations, the secondary ionization operator manifold, $\boldsymbol{f}$, and perturbative improvements to reference-state density matrices were introduced. Operators and density matrices that sufficed to produce all self-energy terms up to a desired order were chosen. For example, to generate all third-order terms in $\boldsymbol{F}$, $\boldsymbol{\rho}$ in second order must be invoked. To recover some of the third-order terms in $\Sigma'(E)$, first-order corrections to the two-electron reduced density matrices are used to evaluate $[\boldsymbol{f}|\hat{H}a^{\dagger}]$ and its adjoint. Non-vanishing first-order couplings between $\boldsymbol{f}$ and $a^{\dagger}$ occur only for triple field-operator products ($\boldsymbol{f}_3$) with two creators ($a^{\dagger}$ operators) and one annihilator (a). Products of two occupied (h for hole) creators and one unoccupied (p for particle) annihilator occur in the 2hp sector of $\boldsymbol{f}_3$. The 2ph sector comprises products of two unoccupied creators and one occupied annihilator. Only the Hartree–Fock three-electron reduced density matrix is needed for the inverted matrix in eqn (8). These choices suffice for the 3+ self-energy, which is also known as the strict version of the third-order algebraic diagrammatic construction or ADC(3). By discarding all fourth-order and higher-order terms, the third-order self-energy is recovered. Many higher order terms are also included in the 3+ self-energy; they are discarded in calculations that employ the third-order self-energy.

To obtain new-generation third-order methods, a fixed super-operator metric is introduced where the overlap between the z_1 and z_2 ionization operators reads

$$\begin{aligned}[z_1|z_2] = &\frac{1}{2}\left\langle HF\middle|\left(z_1^{\dagger}z_2 + z_2z_1^{\dagger}\right)(1+W)\middle|HF\right\rangle \\ &+\frac{1}{2}\left\langle HF\middle|(1+W)^{\dagger}\left(z_1^{\dagger}z_2 + z_2z_1^{\dagger}\right)\middle|HF\right\rangle.\end{aligned} \tag{9}$$

This journal is © the Owner Societies 2024

This choice forces the super-operator Hamiltonian matrix to be Hermitian. Its intermediate normalization enables total energy expressions based on contour integrations to be size-extensive.[57] The latter property differs from the Hermitization procedure of equation-of-motion theory.[58] Whereas the latter strategy can Hermitize spurious terms, the new metric may be used to recover many-body energy expressions. To obtain third-order contributions to $\Sigma(E)$, the following approximation is made:

$$W \approx T_2^{(1)} + T_1^{(2)}. \quad (10)$$

First-order double substitutions and second-order single substitutions occur linearly in all super-operator matrix elements. No elements that are bi-linear (*i.e.*, quadratic when real) in reference-state substitution amplitudes are present. In accord with eqn (9), matrix elements that are linear in these amplitudes are multiplied by one half. Self-energy terms that are free of reference-state correlation amplitudes (*e.g.*, ring and ladder summations) remain the same.

Omission of self-energy terms of fourth and higher orders results in the linear, third-order (L3) self-energy. The most promising of its approximately renormalized extensions (L3+B) performs separate renormalization estimates for the 2hp and 2ph members of $\boldsymbol{f}_3$. The explicitly renormalized version (RL3) contains all terms present in L3 as well as ring, ladder and mixed ring-ladder terms in all orders.

For electron detachment energies, self-energy terms beyond second order that involve 2ph operators define computational bottlenecks but often have relatively little numerical importance.[22,23,59,60] Omission of these terms at the three levels discussed in the previous paragraph defines the quasiparticle third order (Q3) method and its approximately (Q3+) and explicitly (RQ3) renormalized extensions. OV^4 bottlenecks characterize L3, L3+B, and RL3 calculations of all electron binding energies. Q3, Q3+ and RQ3 calculations of electron detachment energies have O^2V^3 bottlenecks and no need for ERIs with four virtual indices. In several numerical tests, only minor increases in mean absolute errors with respect to the L methods have occurred for their three Q counterparts.

The OV^4 bottleneck for electron detachment energies can be minimized by ignoring the energy dependence of self-energy terms generated by 2ph operators. By substituting the Koopmans guess for E in these terms, the non-Dyson (nD) versions of L3, L3+B and RL3 may be defined.

Each of the summations (or diagrams) in the diagonal self-energy formulae may be interpreted in terms of electron-pair correlation and orbital relaxation concepts.[61,62] For electron detachment energies, second-order and third-order terms generated by 2ph operators in the $\boldsymbol{f}_3$ set are associated with initial-state differential correlation. Pair correlation energies present in the initial state that are absent in the final state are responsible for these self-energy terms. Terms in $\Sigma_{ii}(E)$ that descend only from final-state orbital relaxation are easily identified when $E = \varepsilon_i$, where i is an occupied spin-orbital index. Ring, ladder and certain other summations that include T_2 (*i.e.*, double substitution) correlation amplitudes have terms where one or more occupied orbital indices equal i. Whereas these terms correspond solely to orbital relaxation, the remaining ones in these 2hp diagrams originate from final-state differential correlation. Additional electron-pair correlation that arises from the newly vacant i spin-orbital is responsible for the latter terms. Energy-independent, third-order self-energy terms arise from orbital relaxation in final-state electron-pair correlation energies.

Instead of solving for electron binding energies and Dyson orbitals with the Dyson quasiparticle equation, one may diagonalize the super-operator Hamiltonian matrix, $\hat{\boldsymbol{H}}$. Eigenvalues of $\hat{\boldsymbol{H}}$ equal electron binding energies. Eigenvector elements corresponding to simple creation operators ($a^\dagger$) equal orbital basis coefficients in the Dyson orbitals. A variety of techniques for the diagonalization of Hermitian matrices of high rank has been employed.[63–65] The Dyson quasiparticle equation may be regarded as a partitioned version[66] (with $a^\dagger$ and $\boldsymbol{f}$ sectors) of the diagonalization of $\hat{\boldsymbol{H}}$.

This approach is advantageous for self-energies that are non-diagonal and renormalized. The former property is realized by including all simple creators in the space of ionization operators. Renormalization is achieved by including off-diagonal matrix elements of $(\boldsymbol{f}|(E\hat{I} - \hat{H})\boldsymbol{f})$. Expansion of the inverse of the latter matrix about its diagonal, zeroth order component generates terms in all orders of the fluctuation potential. (See eqn (8).)

Non-diagonal, renormalized (NR) generalizations of the L3, RL3, Q3 and RQ3 self-energies have been introduced recently.[18] In numerical tests on ionization energies of closed-shell molecules, they have produced lower errors than their diagonal predecessors. These methods also require non-iterative, sixth-power matrix multiplications for the evaluation of second-order terms in the $(\boldsymbol{f}|\hat{H}a^\dagger)$ matrices and their adjoints. In the NRL3 method, the super-operator metric of eqn (9) is assumed. The $(a^\dagger|\hat{H}a^\dagger)$, $(\boldsymbol{f}|\hat{H}a^\dagger)$ and $(\boldsymbol{f}|\hat{H}\boldsymbol{f})$ matrices are evaluated respectively in third, second and first orders in the fluctuation potential. All terms present in the L3 and RL3 self-energies are also present in the NRL3 self-energy. Neglect of second-order $(\boldsymbol{f}_{2ph}|\hat{H}a^\dagger)$ and first-order $(\boldsymbol{f}_{2ph}/(E\hat{I} - \hat{H})\boldsymbol{f}_{2ph})$ terms yields the NRQ3 version of $\hat{\boldsymbol{H}}$ for electron detachment energies. The orders of the NRL3 blocks of $\hat{\boldsymbol{H}}$ are the same as in the 3+ method[20] [*i.e.*, the strict version of ADC(3)],[15,26] but there are no terms that are bi-linear in the reference-state correlation amplitudes of eqn (10). No constant self-energy terms that depend on T_2 amplitudes are included. [Constant terms that are quadratic in these amplitudes appear in 3+ and ADC(3).] In the NR versions of $\hat{\boldsymbol{H}}$, terms that are linear in reference-state correlation amplitudes are multiplied by one half. Programs that currently execute any version of ADC(3) therefore may be easily modified to perform NRL3, NRQ3 or NRP3 calculations.

2.2 Comparison to equation-of-motion, coupled-cluster theory

Electron-propagator and equation-of-motion, coupled-cluster[67] (EOM-CC) methods have several common features that are

This journal is © the Owner Societies 2024

characteristic of many-body theories.[68] Both approaches to the calculation of spectra generate algebraically connected formulae that preserve correct separation limits. In many-body theories, separation of a molecule into two remote fragments ($\alpha\beta \rightarrow \alpha + \beta$) produces transitions that equal those of the individual fragments.

Whereas EOM-CC theory leads to separate equations for energies of electron detachment and attachment, $\boldsymbol{f}$ operators of both types interact in the Dyson quasiparticle equation. For example, the second-order self-energy has energy-dependent 2hp and 2ph terms that correspond respectively to final-state and initial-state correlation effects for electron detachment energies. The roles of the two terms are reversed for electron attachments. A single energy-dependent, non-local potential encompasses both cases. An intermediate approach occurs in nD versions of self-energies, wherein energy-dependence is eliminated for initial-state terms, as in EOM-CC theory.

In Dyson and nD versions of electron-propagator theory, the superoperator Hamiltonian matrix is Hermitian. Eigenvalues of these matrices (*i.e.*, electron binding energies) therefore are real. Left and right eigenvectors are adjoints of each other. Dyson orbitals therefore are unambiguously defined. The effective Hamiltonian matrix of EOM-CC theory is non-Hermitian. Its eigenvalues are not necessarily real, but this formal deficiency is seldom encountered in calculations on closed-shell molecules. Left and right eigenvectors that include the amplitudes of the Dyson orbitals are not adjoints of each other. Well-defined transition probabilities must involve both eigenvectors.

EOM-CC calculations of transition energies are typically preceded by determination of the reference state's coupled-cluster wavefunction. In EOM-CCSD calculations,[69] this preliminary result requires iterations with an O^2V^4 arithmetic scaling factor. This sixth-power stage is followed by fifth-power iterations that pertain to electron binding energies. An approximation to the EOM-CCSD method avoids the reference-state optimization by substitution of first-order cluster amplitudes to realize fifth-power scaling.[70] Optimizations of reference-state wavefunctions respectively acquire eighth-power and tenth-power scaling factors when triple and quadruple substitutions are included. In tests *versus* EOM-CCSDT/cc-pVTZ vertical ionization energy standards, EOM-CCSD produced larger error measures than NR2, BD-T1 and several, less costly, new-generation electron-propagator methods.[16,18]

2.3 Computational methods

Geometries of all 36 closed-shell molecular anions in the test set corresponding to 55 VEDEs were taken from previous studies.[5,71] The test set consists of molecular anions whose nuclei are drawn from the first three periods. Simple hydrides (XH_n^-), atoms (X^-), di-atomics (XZ^-), and tri-atomic hydrides (HXZ^-) are included in an unbiased manner. ERIs are transformed to the canonical Hartree–Fock basis and stored on disk. Table 2 presents the most extensive subsets of ERIs needed for each self-energy approximation. Core orbitals are excluded from self-energy summations. All computations were executed with the development version of Gaussian wherein all electron propagator methods have been implemented.[72] Electron propagator calculations have been performed on all the test anions using the aug-cc-pVDZ, aug-cc-pVTZ, and aug-cc-pVQZ basis sets. The standard test set of VEDEs was inferred from ΔCCSD(T) (*i.e.*, total energy differences based on coupled-cluster theory with single and double replacements and approximate triple replacements[73]) inverse quartically extrapolated [*i.e.*, $(l+\frac{1}{2})^{-4}$] total energies obtained with augmented quadruple and triple ζ basis sets.[74] Contour plots of Dyson orbitals have been generated with GaussView.[75]

Table 4 and Fig. 4 and 5 display statistics obtained from composite electron propagator methods. Eight composite methods denoted by CMX (where $X = 1$–8) have been developed for VEDEs:

$$E^{\mathrm{CM1}} = E^{\mathrm{nD\text{-}L3+B}}_{\mathrm{aug\text{-}cc\text{-}pVDZ}} + E^{\mathrm{os\text{-}nD\text{-}D2}}_{\mathrm{CBS(DT)}} - E^{\mathrm{os\text{-}nD\text{-}D2}}_{\mathrm{aug\text{-}cc\text{-}pVDZ}} \quad (11)$$

$$E^{\mathrm{CM2}} = E^{\mathrm{Q3+}}_{\mathrm{aug\text{-}cc\text{-}pVDZ}} + E^{\mathrm{os\text{-}nD\text{-}D2}}_{\mathrm{CBS(DT)}} - E^{\mathrm{os\text{-}nD\text{-}D2}}_{\mathrm{aug\text{-}cc\text{-}pVDZ}} \quad (12)$$

$$E^{\mathrm{CM3}} = E^{\mathrm{nD\text{-}L3+B}}_{\mathrm{aug\text{-}cc\text{-}pVTZ}} + E^{\mathrm{os\text{-}nD\text{-}D2}}_{\mathrm{CBS(TQ)}} - E^{\mathrm{os\text{-}nD\text{-}D2}}_{\mathrm{aug\text{-}cc\text{-}pVTZ}} \quad (13)$$

$$E^{\mathrm{CM4}} = E^{\mathrm{Q3}}_{\mathrm{aug\text{-}cc\text{-}pVTZ}} + E^{\mathrm{os\text{-}nD\text{-}D2}}_{\mathrm{CBS(TQ)}} - E^{\mathrm{os\text{-}nD\text{-}D2}}_{\mathrm{aug\text{-}cc\text{-}pVTZ}} \quad (14)$$

$$E^{\mathrm{CM5}} = E^{\mathrm{nD\text{-}RL3}}_{\mathrm{aug\text{-}cc\text{-}pVDZ}} + E^{\mathrm{os\text{-}nD\text{-}D2}}_{\mathrm{CBS(DT)}} - E^{\mathrm{os\text{-}nD\text{-}D2}}_{\mathrm{aug\text{-}cc\text{-}pVDZ}} \quad (15)$$

$$E^{\mathrm{CM6}} = E^{\mathrm{nD\text{-}RL3}}_{\mathrm{aug\text{-}cc\text{-}pVTZ}} + E^{\mathrm{os\text{-}nD\text{-}D2}}_{\mathrm{CBS(TQ)}} - E^{\mathrm{os\text{-}nD\text{-}D2}}_{\mathrm{aug\text{-}cc\text{-}pVTZ}} \quad (16)$$

$$E^{\mathrm{CM7}} = E^{\mathrm{Q3+}}_{\mathrm{aug\text{-}cc\text{-}pVTZ}} + E^{\mathrm{nD\text{-}L3+B}}_{\mathrm{aug\text{-}cc\text{-}pVDZ}} - E^{\mathrm{Q3+}}_{\mathrm{aug\text{-}cc\text{-}pVDZ}} + E^{\mathrm{os\text{-}nD\text{-}D2}}_{\mathrm{CBS(TQ)}} - E^{\mathrm{os\text{-}nD\text{-}D2}}_{\mathrm{aug\text{-}cc\text{-}pVTZ}} \quad (17)$$

$$E^{\mathrm{CM8}} = E^{\mathrm{NRL3}}_{\mathrm{aug\text{-}cc\text{-}pVDZ}} + E^{\mathrm{os\text{-}nD\text{-}D2}}_{\mathrm{CBS(DT)}} - E^{\mathrm{os\text{-}nD\text{-}D2}}_{\mathrm{aug\text{-}cc\text{-}pVDZ}} \quad (18)$$

Complete basis set (CBS) results in the composite methods are based on a two-point (double–triple or triple–quadruple) inverse quartic extrapolation, *i.e.*, $(l+\frac{1}{2})^{-4}$, scheme. Data in the ESI† confirm that quartically extrapolated data are very close to their cubically (*i.e.*, l^{-3}) extrapolated counterparts.[5]

Geometries of the three small GFP anions (phenolate and substituted analogues)[40] were optimized with MP2 in conjunction with the aug-cc-pVTZ basis set. The geometries of the large GFP anions (*p*-hydroxybenzylidene-2,3-dimethyl-4-imidazolinone and substituted analogues)[31,32] were optimized with the B3LYP/6-311++G(2d,p) model.[76]

3. Results and discussion

3.1 Tests on vertical electron detachment energies of small anions

Error statistics that compare self-energy approximations to ΔCCSD(T) standards obtained with the same basis set have been compiled for three cases: aug-cc-pVDZ, aug-cc-pVTZ and aug-cc-pVQZ. These data do not differ significantly from comparisons that are based on inverse quartically extrapolated results. Table 3 and Fig. 1–3 display this information. In a previous work on the same set of 55 VEDEs, inverse cubic extrapolations were employed and data for the NR methods were absent.[5]

Whereas MAEs in Table 3 for D2 and nD-D2 are near 0.5 eV, much lower values emerge from os-D2 and os-nD-D2 calculations.

This journal is © the Owner Societies 2024

Table 3 Error distributions (eV) with respect to ΔCCSD(T)/CBS standards

Method class	Method[a]	Mean unsigned error[b]	Mean signed error	Standard deviation	Maximum unsigned error
Uncorrelated	KT	0.613	0.537	0.628	2.017
Diagonal 2nd order	D2	0.482	−0.477	0.466	2.043
	os-D2	0.176	−0.059	0.251	0.853
	nD-D2	0.506	−0.501	0.487	2.104
	os-nD-D2	**0.180**	−0.070	0.256	0.882
Diagonal post 2nd order	DR	0.258	0.199	0.221	0.711
	D3	0.642	0.624	0.910	4.018
	nD-D3	0.581	0.564	0.808	3.622
	OVGF-A	0.136	−0.009	0.196	0.822
	OVGF-B	0.235	0.189	0.347	1.654
	OVGF-C	0.249	0.230	0.291	1.363
	nD-OVGF-A	0.135	−0.029	0.192	0.810
	nD-OVGF-B	0.212	0.158	0.311	1.655
	nD-OVGF-C	0.224	0.207	0.270	1.358
	P3	0.288	0.235	0.387	1.577
	P3+	0.159	0.094	0.212	0.781
	Q3	0.280	0.200	0.431	1.696
	Q3+	**0.158**	0.051	0.242	0.965
	L3	0.228	0.213	0.347	1.450
	nD-L3	0.220	0.206	0.340	1.457
	L3+A	0.125	−0.070	0.149	0.464
	L3+B	0.098	0.071	0.169	0.748
	L3+C	0.101	0.076	0.158	0.669
	nD-L3+A	0.124	−0.085	0.135	0.466
	nD-L3+B	**0.086**	0.060	0.158	0.735
	nD-L3+C	0.089	0.065	0.144	0.653
	RP3	0.129	−0.006	0.176	0.764
	RQ3	0.160	−0.082	0.159	0.417
	RL3	**0.076**	−0.031	0.087	0.253
	nD-RL3	**0.081**	−0.045	0.083	0.227
Non-diagonal	ND2	0.508	−0.423	0.418	2.077
	2ph-TDA	0.521	−0.521	0.244	1.128
	3+	0.230	0.207	0.323	1.407
	ADC(3)	0.201	0.153	0.239	0.823
	NR2	**0.123**	−0.056	0.136	0.514
	BD-T1	**0.066**	0.043	0.089	0.345
	NRP3	0.126	−0.055	0.142	0.519
	NRQ3	0.161	−0.104	0.146	0.382
	NRL3	**0.079**	−0.046	0.090	0.305

[a] New methods in bold type. [b] Optimal methods in bold type.

The two latter cubically scaling methods produce MAEs below 0.2 eV and are practically free after the ERI transformation. They contain no adjustable parameters and may be analyzed in terms of simple electron-pair correlations and orbital relaxation concepts. Fig. 2 reveals that the two os methods' errors are more evenly distributed between underestimates and overestimates of VEDEs. Both methods produce absolute errors above 0.3 eV for the same eight anions. (This set comprises VEDEs of AlO^-, CP^-, F^-, HBN^-, HCC^-, NH_2^-, OH^-, and SiN^-). In most of these cases, the Dyson orbital is localized near an electronegative center, *i.e.* N, O or F.

Some additional computational effort is necessary for the three Q approximations. Without any estimates of terms beyond third-order, Q3 attains a MAE below 0.3 eV. Its approximately renormalized extension, Q3+, achieves a MAE that is slightly smaller than those of the two os, second-order diagonal methods. Q3 and Q3+ have non-iterative O^2V^3 arithmetic scaling and therefore the $O(N_{basis})^4$ computational bottleneck still occurs in the partial transformation of ERIs. With an iterative O^2V^3 bottleneck, the renormalized DR method produces a larger MAE of 0.26 eV. The latter alternative has the advantage (*versus* Q3, Q3+ and RQ3) of not needing ERIs with three virtual indices. DR's histogram displays a greater tendency to overestimate than to underestimate VEDEs. RQ3 is a more accurate alternative with the same iterative bottleneck. Its MAE of 0.16 eV is almost identical to that of Q3+, but its standard deviation and maximum unsigned error are significantly lower. Among the methods with bottlenecks below that of MP2's partial integral transformation, RQ3 is least likely to produce absolute errors over 0.3 eV. Whereas Q3+ fails according to the latter criterion for six VEDEs, RQ3 fails for only those of two anions, AlO^- and F^-.

The next level of arithmetic scaling, OV^4, pertains to D3 and its approximately renormalized OVGF extensions. D3's MAE is worse than that of D2. Whereas D2 underestimates VEDEs, D3 overestimates them. OVGF-A and its nD variant reduce the MAE to 0.14 eV. The other two OVGF alternatives and their nD variants are less successful. With the same computational effort, L3 produces a MAE that is about a third as large as the MAE of D3. The approximately renormalized L3+B extension and its nD variant generate MAEs of 0.10 and 0.09 eV respectively. Whereas L3+B produces absolute errors above 0.3 eV in four cases, its explicitly renormalized counterpart, RL3,

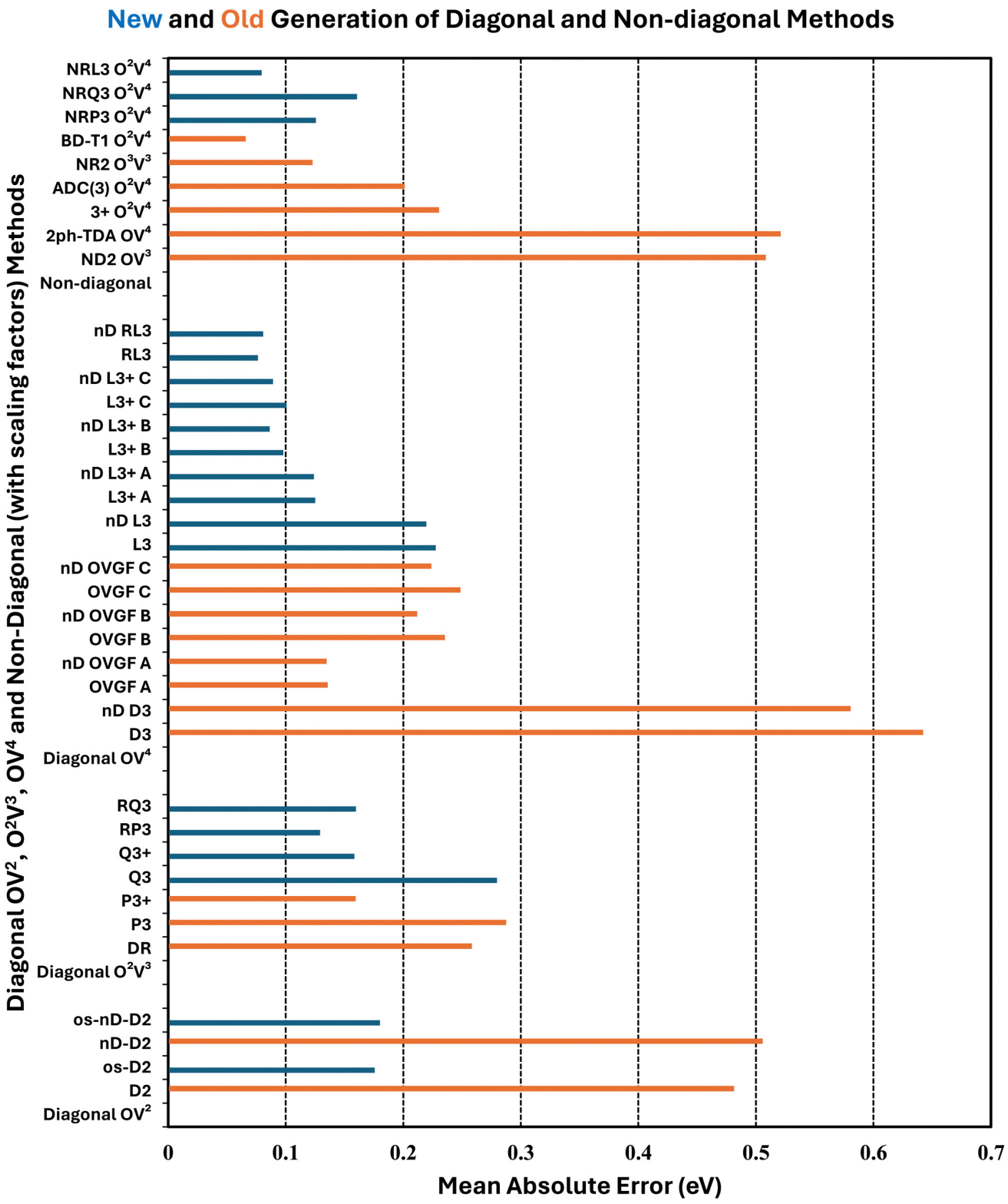


Fig. 1 Mean absolute errors (eV) *versus* ΔCCSD(T)/CBS standards and arithmetic scaling factors.

produces none^{-}. RL3 and its nD variant have MAEs of 0.08 eV and markedly lower standard deviations and maximum errors the L3+B. The histograms of the diagonal self-energies with OV^4 bottlenecks clearly indicate the superior reliability of RL3 and nD-RL3.

Comparisons between diagonal methods with OV^4 arithmetic scaling and non-diagonal methods pertain to the two top sectors of Fig. 1. ND2 and 2ph-TDA are decidedly disadvantageous. The strict (3+) and standard (Schirmer-Angonoa[25]) Dyson versions of ADC(3) produce MAEs near 0.2 eV. The latter method has iterative O^2V^4

This journal is © the Owner Societies 2024

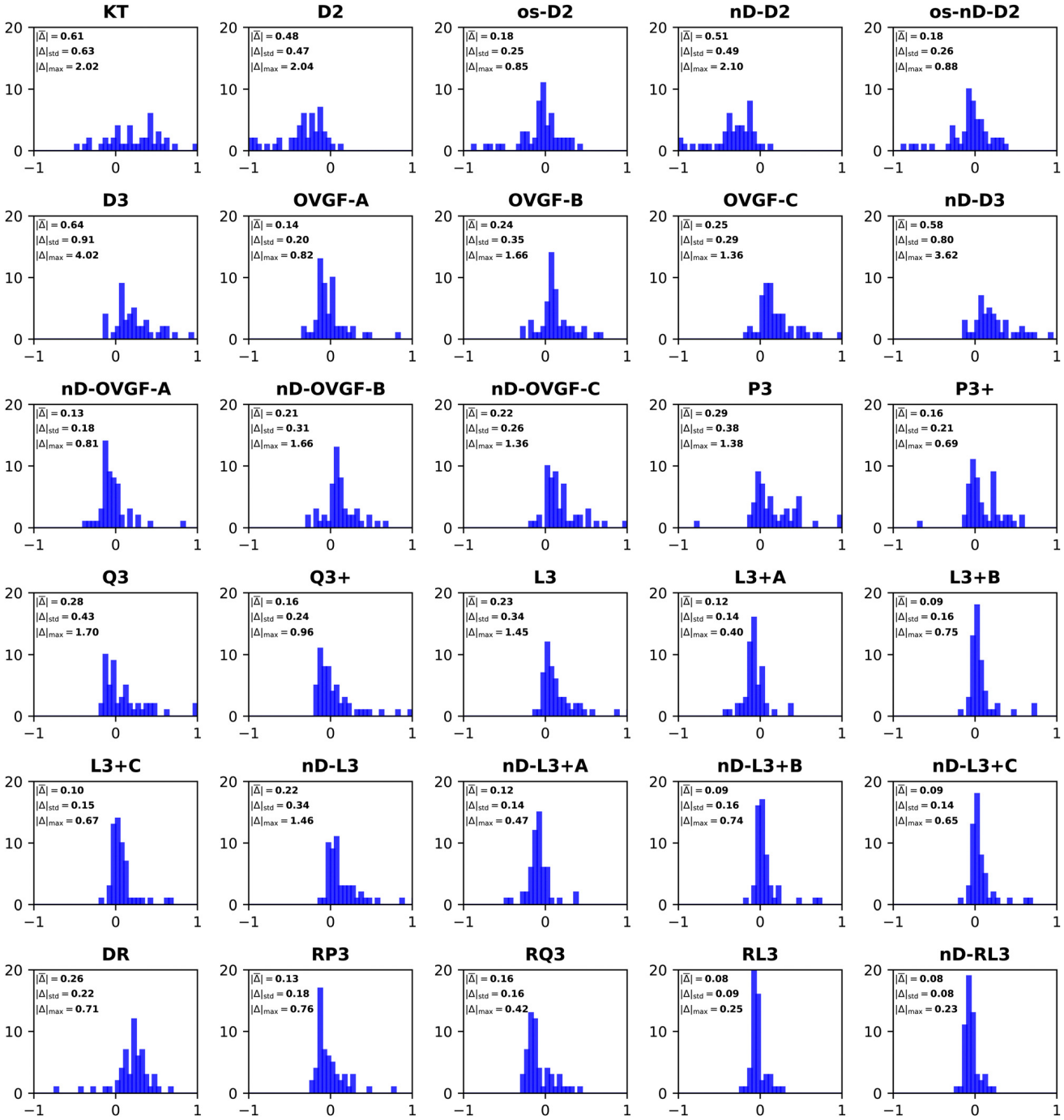


Fig. 2 Histograms of error distributions (eV) *versus* ΔCCSD(T)/CBS standards: diagonal EP methods.

scaling that occurs in its evaluation of ρ. Only the NR2 and BD-T1 methods with non-iterative O^3V^3 and iterative O^2V^4 scaling, respectively, remain competitive with the best diagonal alternatives.

RQ3 and its non-diagonal extension NRQ3 produce almost identical error measures. Their maximum errors are only ~0.4 eV; both produce absolute errors above 0.3 eV in only two cases. The histograms of RQ3 and NRQ3 also closely resemble each other. NRQ3 requires a non-iterative O^2V^4 step not found in RQ3, but, like all non-diagonal methods, it yields a more general expression of the Dyson orbitals.

RL3 and NRL3 behave in a similar manner, but they attain higher accuracy than RQ3 and NRQ3. MAEs do not rise from NRL3 to RL3, *i.e.*, when the diagonal approximation is made. NRL3 produces only one absolute error above 0.3 eV. (NRL3's error for $HPCl^-$ is only 0.305 eV.) With MAEs near 0.08 eV, RL3 and NRL3 approach the limits of the accuracy of the ΔCCSD(T) standard.

A closer inspection of the results confirms that errors greater than or equal to 0.3 eV become less numerous with increased arithmetic effort. The cases of F^- and OH^- are notorious in the

This journal is © the Owner Societies 2024

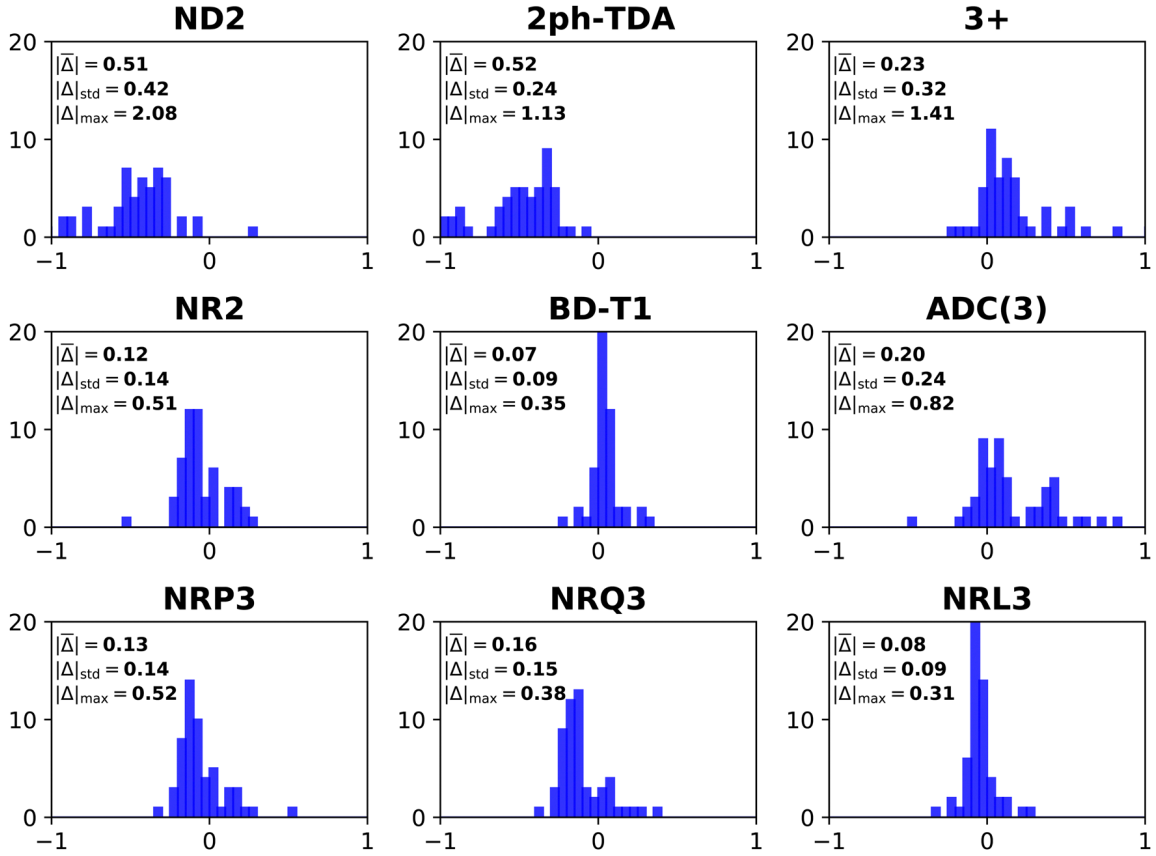


Fig. 3 Histograms of error distributions (eV) *versus* ΔCCSD(T)/CBS standards: non-diagonal EP methods.

history of electron propagator calculations on anions. Absolute errors of D2 and OVGF range from 0.8 to 2.0 eV for F^- and from 0.4 to 1.7 eV for OH^-. Improvements of approximately 0.1 eV occur between Q3+, RQ3 and NRQ3 and L3+B, RL3 and NRL3, respectively. Third-order and higher-order terms that describe initial-state differential correlation are therefore significant; exaggerations at the second-order level are thereby redressed. From L3+B to RL3 or NRL3, absolute errors for F^- and OH^- decline respectively from 0.7 to 0.2 and from 0.5 to 0.1 eV. These results imply that the crucial improvement over L3+B is replacing approximate with explicit renormalization and that the diagonal approximation introduces only minor errors. Explicit renormalization, as realized in RL3 and NRL3 calculations, is indicated for VEDEs whose Dyson orbitals are localized near N, O or F nuclei.

3.2 Composite models

Basis-set effects on electron-propagator poles are often approximately constant with respect to changes in self-energy approximations.[29] Composite models (CM) assume the validity of this assumption while attempting to achieve high accuracy with reduced computational effort. Eqn (11)–(18) define the components of eight composite models. Table 4 and Fig. 4 display error measures. Histograms are shown in Fig. 5. All composite models employ os-nD-D2 calculations to estimate complete-basis-set extrapolations based on double–triple or triple–quadruple ζ data. In CM1-CM6 and in CM8, the higher-order method may be Q3+, nD-L3+B, or nD-RL3; two basis sets are used in each model. CM7 employs nD-L3+B, Q3+ and os-nD-D2 data and involves three basis sets. CM1 and CM2 differ in their use of L3+B and Q3+, respectively. Both models employ double and triple ζ basis sets. The MAE of the slower CM1 model is about 0.1 eV, whereas CM2's MAE is closer to 0.2 eV. Upgrading basis sets to triple and quadruple ζ (see CM3 and CM4 results.) has little effect on the MAEs. When the better self-energy is nD-RL3, an explicitly renormalized diagonal method, MAEs decline below 0.1 eV with double-triple ζ and with triple-quadruple ζ data. (See CM5 and CM6 results.) The previously introduced CM7 model makes small improvements over CM1 and CM3. In CM8, the non-diagonal renormalized NRL3 is introduced at the double ζ level. This model yields the lowest MAE.

Table 4 Error distributions (eV) with respect to ΔCCSD(T)/CBS standards

Composite model (CM)	Mean unsigned error	Mean signed error	Standard deviation	Maximum unsigned error
CM1	0.101	0.072	0.163	0.851
CM2	0.185	0.054	0.301	1.400
CM3	0.107	0.098	0.159	0.820
CM4	0.162	0.065	0.244	1.030
CM5	0.079	−0.024	0.101	0.346
CM6	0.065	−0.010	0.085	0.309
CM7	0.080	0.034	0.094	0.321
CM8	0.059	−0.005	0.086	0.377

This journal is © the Owner Societies 2024

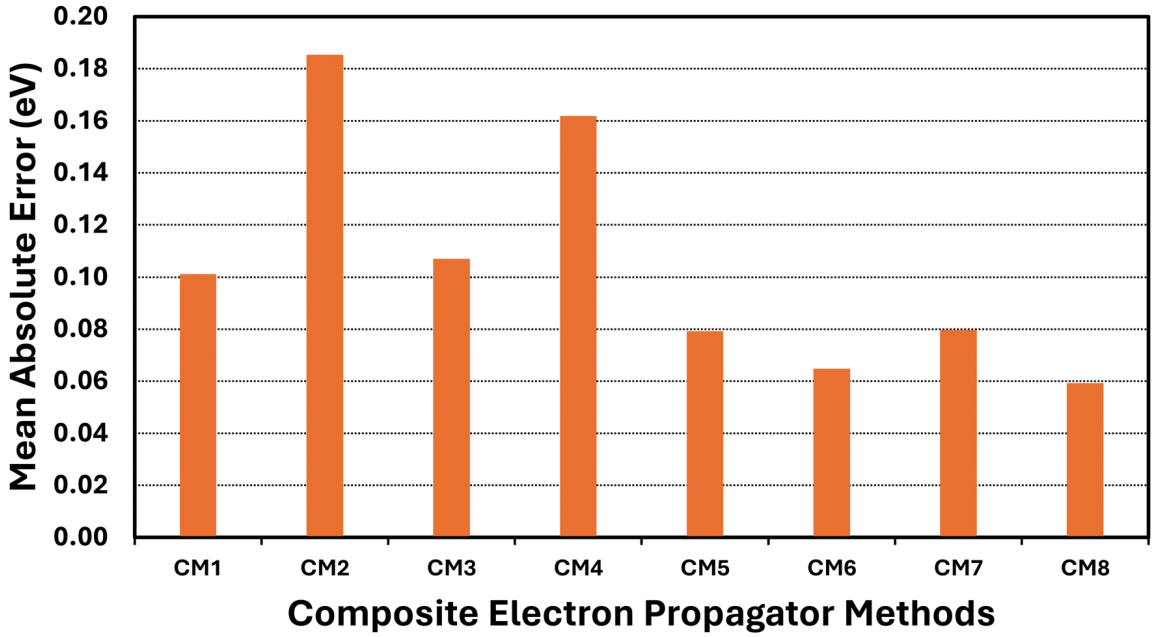


Fig. 4 Mean absolute errors (eV) of composite EP methods *versus* ΔCCSD(T)/CBS standards and arithmetic scaling factors.

A comparison of the CM1–CM4 histograms leads to two conclusions. First, errors grow when Q3+ replaces L3+B as the more advanced self-energy. Second, only minor improvements occur when the triple–quadruple ζ combination replaces the double–triple ζ combination. The CM5 and CM6 histograms demonstrate that large errors are almost eliminated when the nD-RL3 self-energy is used instead of Q3+ or L3+B. Both models produce an absolute error above 0.3 eV only for AlO^-. Basis-set improvements (compare CM5 and CM6) make only small changes to the profile of errors. The extra calculations required by CM7 produce improvements over CM1 and CM3. Only one large error occurs: the VEDE of SiN^-. The sharpest profile pertains to CM8, which fails only for the difficult AlO^- case.

3.3 GFP model anions

The lowest VEDEs of six GFP model anions are displayed in Table 5. Composite models with explicitly renormalized diagonal (CM5) or non-diagonal renormalized (CM8) self-energy components are in excellent agreement with experiment in all cases. For PhO^- and *p*-$HBDI^-$, the CM8 predictions lie within the experimental error bars. Similar success obtains for CM5 in the PhO^- case. Discrepancies between the two models are somewhat larger (∼0.05 eV) for the three phenolate anions than for the three anions which closely resemble GFP's chromophore. Both models account for basis-set effects beyond the aug-cc-pVTZ level. Agreement between CM5 and CM6 results obtained for the VEDE55 data set strongly suggests that further basis-set improvements are unlikely to produce significant changes.

Previous calculations (see Table 5) indicate that results obtained with the aug-cc-pVDZ basis are approximately 0.2 eV lower than those obtained with the aug-cc-pVTZ basis. Augmented basis sets of quadruple ζ and higher quality are likely to increase extrapolated VEDEs by at least 0.1 eV. (Data at the os-D2/aug-cc-pVQZ level confirm this estimate.) None of the previous calculations includes an estimate of the effects of larger basis sets. Iterative procedures with O^2V^4 arithmetic scaling accompany EOM-CCSD[69] and ΔCCSD(T) calculations; the latter method also has a non-iterative, seventh power step. The bottlenecks steps of the renormalized terms in CM5 and CM8 have lower arithmetic scaling and need be performed only at the aug-cc-pVDZ level.

Delocalized π Dyson orbitals with b_1 or a'' irreducible representation labels correspond to the lowest VEDEs of the six anions. (See Fig. 6 for NRL3/aug-cc-pVDZ Dyson orbitals.) Antibonding phase relationships between oxygen and nearby carbon ring functions are present in each case. Basis functions centered on the fluoride and methoxy oxygen nuclei have appreciable amplitudes in the substituted anions. These contributions to Dyson orbitals indicate that explicitly renormalized self-energies are likely to produce better results than approximately renormalized self-energies. This hypothesis is confirmed by the ∼0.05 eV reduction of VEDEs that is realized by nD-RL3 *versus* nD-L3+B. A reduction of similar magnitude *versus* nD-RL3 accompanies the use of NRL3 for the three phenolates, but not for the three larger anions. These corrections are essential for the high accuracy attained by the CM5 and CM8 calculations.

Probability factors provide deeper insight into the strength of relaxation and correlation effects. For the three phenolates, nD-L3+B, nD-RL3 and NRL3 probability factors with the aug-cc-pVDZ basis are 0.92, 0.90 and 0.86, respectively. In the NRL3 calculations, the reference canonical Hartree–Fock orbital has a coefficient of 0.99 in the normalized Dyson orbitals. These data confirm the qualitative validity of the diagonal self-energy approximation. Relaxation and correlation effects are somewhat

This journal is © the Owner Societies 2024

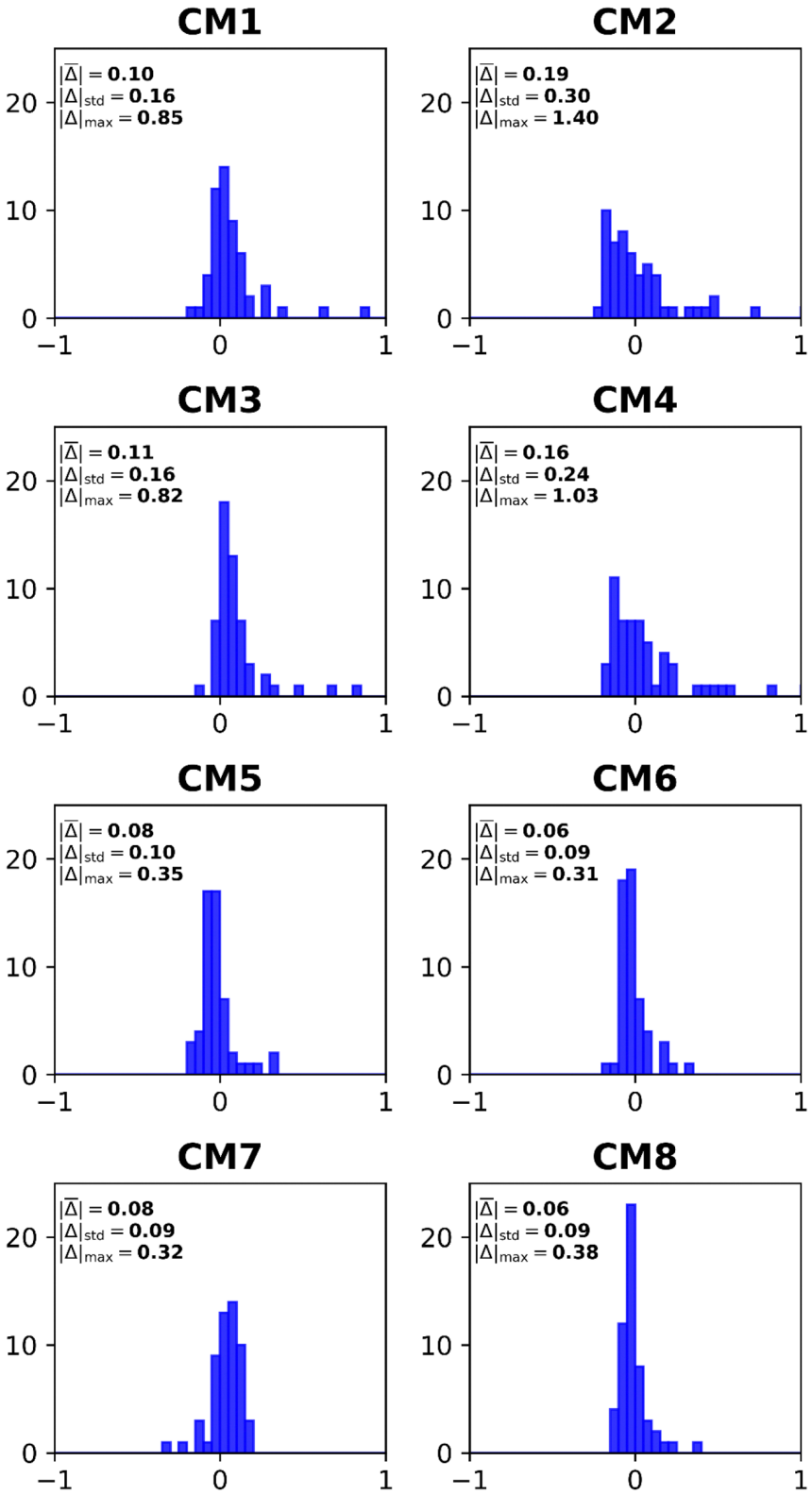


Fig. 5 Histograms of error distributions (eV) *versus* ΔCCSD(T)/CBS standards: composite EP methods.

stronger for the three HBDI$^-$ anions, where the same three self-energies produce probability factors of 0.90, 0.87 and 0.83. The latter figure is below the conventional 0.85 threshold for the validity of the diagonal approximation. Despite this marginal result, the reference orbital's coefficient in the Dyson orbital exceeds 0.99. The diagonal self-energy approximation is qualitatively valid, but off-diagonal couplings allow greater flexibility in the description of relaxation and correlation.

This journal is © the Owner Societies 2024

Table 5 Lowest vertical electron detachment energies (eV) of GFP model anions

Anion	Final state	Experiment	CM5	CM8	Previous calculations
PhO^-	$^2B_1$	2.26 ± 0.03[a]	***2.28***	***2.23***	2.06[a] 2.08[f] 2.25[g] 2.27[h]
DF-PhO^-	$^2B_1$	2.61 ± 0.03[a]	2.71	2.66	2.50[a]
Syn-DM-PhO^-	$^2B_1$	~ 2.35[a]	2.42	2.37	2.20[a]
p-$HBDI^-$	$^2A''$	2.74 ± 0.04[b]	2.80	***2.78***	2.66[c] 2.78[d] 2.74[e] 2.65[i]
DF-$HBDI^-$	$^2A''$	2.98 ± 0.04[b]	3.05	3.04	2.93[c] 3.02[d] 2.99[e]
Syn-DM-$HBDI^-$	$^2A''$	2.7 ± 0.04[b]	2.82	2.81	2.61[c] 2.77[d] 2.69[e]

[a] Anion photoelectron spectroscopy and EOM-CCSD/aug-cc-pVDZ calculations.[40] [b] Anion photoelectron spectroscopy.[31] [c] EOM-CCSD with aug-cc-pVDZ for *p*-$HBDI^-$ and DF-$HBDI^-$ and with 6-311++G(d,p) for *syn*-DM-$HBDI^-$.[31] [d] OVGF/6-311++G(3df,3pd).[32] [e] XMCQDPT2/aug-cc-pVTZ.[32] [f] EOM-CCSD/aug-cc-pVDZ.[78] [g] EOM-CCSD/aug-cc-pVTZ.[78] [h] ΔCCSD(T)/aug-cc-pVTZ.[78] [i] ΔωB97X-D/aug-cc-pVDZ.[78]

4. Conclusions

For VEDEs of closed-shell anions, the os-D2 and os-nD-D2 methods offer an excellent compromise of trivial post-Hartree–Fock computational effort and mean absolute errors below 0.2 eV. These methods are likely to be useful in interpreting and predicting anion photoelectron spectra and other experiments that measure vertical electron detachment energies. For large systems wherein full transformations of electron repulsion integrals are infeasible, they provide a unique opportunity for prediction and detailed analysis. Surveys of large data sets assembled for the optimization of properties also may be undertaken efficiently. Large errors (*i.e.*, above 0.3 eV) are relatively frequent at this level of theory. This disadvantage

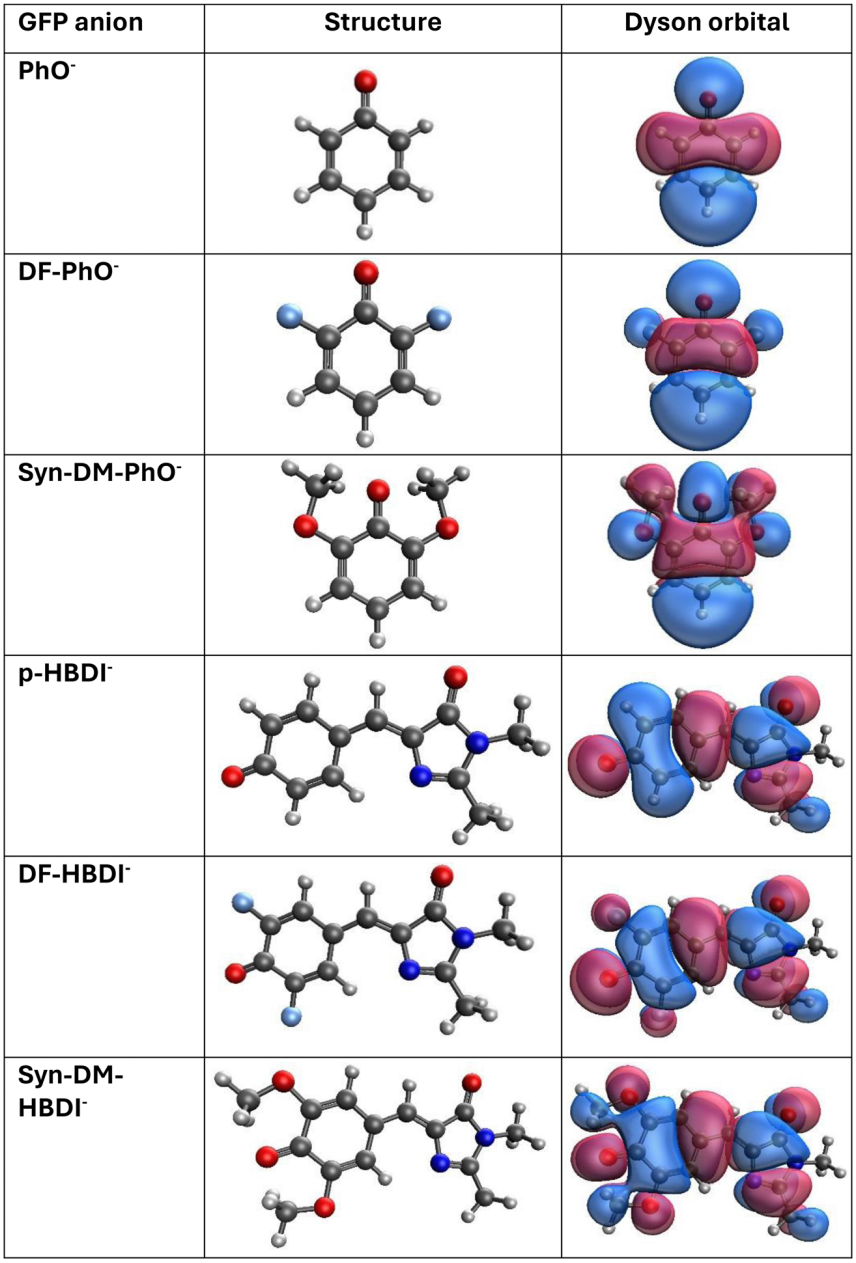


Fig. 6 Structures and Dyson orbitals for vertical electron detachment energies of model GFP anions.

This journal is © the Owner Societies 2024

may become more tolerable when partial transformations with fourth-power scaling are implemented for the highly constrained set of required integrals.

The RQ3 method still has a lower arithmetic bottleneck for electron detachment energies than the preceding partial electron repulsion integral transformation. It requires transformed integrals with three virtual indices in only one matrix multiplication step. In comparison with os-D2, os-nD-D2 and Q3+, RQ3 has a diminished tendency to produce large errors.

The best options at the next level of computational effort are the approximately renormalized L3+B and nD-L3+B self-energies. Their mean absolute errors for the present data set are below 0.1 eV. At the cost of more OV^4 iterations, the RL3 method and its nD variant attained practically the same mean absolute error with no absolute errors above 0.25 eV.

Diagonal, explicitly renormalized self-energies and their non-diagonal, renormalized generalizations produce vertical electron detachment energies and corresponding mean absolute errors that are in close agreement. This result provides a foundation for employment of the diagonal methods in calculations on closed-shell anions. Dyson orbitals and probability factors also agree very well. Non-diagonal self-energies yield Dyson orbitals with a single dominant contribution from a high-lying canonical Hartree–Fock orbital. The success of RL3 and its approximately renormalized simplification, L3+B, is not founded on a fortuitous cancellation of errors connected to the diagonal approximation.

When Dyson orbitals are localized near N, O or F nuclei, large errors are less likely with explicitly renormalized instead of approximately renormalized methods. Such cases may be anticipated by the presence of lone pairs in Lewis structures of the anions. For this class of anions, the RQ3, RL3 or nD-RL3 methods are preferable to os-D2, os-nD-D2, Q3+ and L3+B.

Results of difficult calculations that require large basis sets and self-energies with high arithmetic scaling factors can be accurately approximated with composite models. These methods assume the additivity of basis-set effects and self-energy improvements and therefore require only a set of less demanding calculations. Explicitly renormalized diagonal and non-diagonal renormalized methods produce lower average measures of error in composite models and reduce the number of large errors.

Composite-model calculations have been applied successfully to a set of six anions that resemble the GFP chromophore. Models with explicitly renormalized self-energies produce fast, accurate predictions of vertical electron detachment energies that include basis-set extrapolations. These predictions are directly comparable to experimental data and lie within 0.1 eV of experimental error bounds for the lowest final state.

This study demonstrates the capabilities of composite models and their new-generation self-energy components for prediction and interpretation of electron-detachment experiments on closed-shell anions. Closely related methods for electron attachment energies of closed-shell molecules have been applied successfully to organic photovoltaic molecules.[19] Definitive tests that include diagonal and non-diagonal self-energies and consider closed-shell molecules with positive electron affinities are in progress.

The dominance of a single Slater determinant in the reference state is assumed in most many-body theories, including the electron-propagator methods examined in this work. Despite this assumption, excellent results for the ionization energies of ozone, a molecule with high multiconfigurational character, have been obtained with the BD-T1 approximation.[77] Methylene is another small molecule with qualitatively important configuration interaction in its ground, singlet state. Its vertical ionization energy (10.396 ± 0.003 eV, see NIST tables) is accurately predicted by L3+B (10.423) and RL3 (10.398) with the aug-cc-pVQZ basis. The limitations of single-reference electron-propagator methods have yet to be established in numerical tests.

Data availability

Data on calculated vertical electron detachment energies that support the findings of this study are available within the manuscript and the ESI.†

Conflicts of interest

There are no conflicts to declare.

Acknowledgements

The authors thank Dr Manuel Díaz-Tinoco for valuable discussions and the Alabama Supercomputer Center for computing resources.

References

1 J. Simons and W. D. Smith, *J. Chem. Phys.*, 1973, **58**, 4899–4907.
2 J. Simons, *Annu. Rev. Phys. Chem.*, 1977, **28**, 15–45.
3 J. Simons, *Theor. Chem.*, 1978, **3**, 1–3.
4 J. Simons, *Int. J. Quantum Chem., Quantum Chem. Symp.*, 1982, **16**, 575–581.
5 E. Opoku, F. Pawłowski and J. V. Ortiz, *J. Phys. Chem. A*, 2023, **127**, 1085–1101.
6 M. Díaz-Tinoco, H. H. Corzo and J. V. Ortiz, *J. Chem. Theory Comput.*, 2018, **14**, 5881–5895.
7 A. Pérez-González, A. Galano and J. V. Ortiz, *J. Phys. Chem. A*, 2014, **118**, 6125–6131.
8 J. V. Ortiz, *Wiley Interdiscip. Rev.: Comput. Mol. Sci.*, 2013, **3**, 123–142.
9 J. V. Ortiz, in *Annual Reports in Computational Chemistry*, ed. D. A. Dixon, Elsevier, 2017, vol. 13, pp.139–182.
10 H. H. Corzo and J. V. Ortiz, in *Adv. Quantum Chem.*, ed. J. R. Sabin and E. J. Brändas, Academic Press, 2017, vol. 74, pp. 267–298.
11 J. V. Ortiz, *J. Chem. Phys.*, 2020, **153**, 070902.

 This journal is © the Owner Societies 2024

12 J. Linderberg and Y. Öhrn, *Propagators in Quantum Chemistry, Second Edition*, Wiley-Interscience, Hoboken NJ, 2004.
13 P. Jørgensen and J. Simons, *Second Quantization-Based Methods in Quantum Chemistry*, Academic Press, New York, 1981.
14 J. Schirmer, *Many-Body Methods for Atoms, Molecules and Clusters*, Springer International Publishing AG, 2018.
15 W. von Niessen, J. Schirmer and L. S. Cederbaum, *Comput. Phys. Rep.*, 1984, **1**, 57–125.
16 E. Opoku, F. Pawłowski and J. V. Ortiz, *J. Chem. Phys.*, 2021, **155**, 204107.
17 E. Opoku, F. Pawłowski and J. V. Ortiz, *J. Chem. Theory Comput.*, 2022, **18**, 4927–4944.
18 E. Opoku, F. Pawłowski and J. V. Ortiz, *J. Chem. Phys.*, 2023, **159**, 124109.
19 E. Opoku, F. Pawłowski and J. V. Ortiz, *J. Chem. Theory Comput.*, 2024, **20**, 290–306.
20 J. V. Ortiz, in *Computational Chemistry: Reviews of Current Trends*, ed. J. Leszczynski, World Scientific, Singapore, 1997, vol. 2, pp.1–61.
21 V. G. Zakrzewski, J. V. Ortiz, J. A. Nichols, D. Heryadi, D. L. Yeager and J. T. Golab, *Int. J. Quantum Chem.*, 1996, **60**, 29–36.
22 J. V. Ortiz, *J. Chem. Phys.*, 1996, **104**, 7599–7605.
23 J. V. Ortiz, *Int. J. Quantum Chem.*, 2005, **105**, 803–808.
24 A. M. Ferreira, G. Seabra, O. Dolgounitcheva, V. G. Zakrzewski and J. V. Ortiz, in *Quantum-Mechanical Prediction of Thermochemical Data*, ed. J. Cioslowski, Springer, Netherlands, Dordrecht, 2001, pp.131–160.
25 J. Schirmer and G. Angonoa, *J. Chem. Phys.*, 1989, **91**, 1754–1761.
26 J. Schirmer, L. S. Cederbaum and O. Walter, *Phys. Rev. A: At., Mol., Opt. Phys.*, 1983, **28**, 1237–1259.
27 L. Reining, *Wiley Interdiscip. Rev.: Comput. Mol. Sci.*, 2018, **8**, e1344.
28 S. J. Bintrim and T. C. Berkelbach, *J. Chem. Phys.*, 2021, **154**, 041101.
29 M. Díaz-Tinoco, O. Dolgounitcheva, V. G. Zakrzewski and J. V. Ortiz, *J. Chem. Phys.*, 2016, **144**, 224110.
30 R. Y. Tsien, *Annu. Rev. Biochem.*, 1998, **67**, 509–544.
31 J. L. Woodhouse, A. Henley, R. Lewin, J. M. Ward, H. C. Hailes, A. V. Bochenkova and H. H. Fielding, *Phys. Chem. Chem. Phys.*, 2021, **23**, 19911–19922.
32 A. V. Bochenkova, C. R. S. Mooney, M. A. Parkes, J. L. Woodhouse, L. Zhang, R. Lewin, J. M. Ward, H. C. Hailes, L. H. Andersen and H. H. Fielding, *Chem. Sci.*, 2017, **8**, 3154–3163.
33 Y. Toker, D. B. Rahbek, B. Klærke, A. V. Bochenkova and L. H. Andersen, *Phys. Rev. Lett.*, 2012, **109**, 128101.
34 D. A. Horke and J. R. R. Verlet, *Phys. Chem. Chem. Phys.*, 2012, **14**, 8511–8515.
35 C. R. S. Mooney, M. E. Sanz, A. R. McKay, R. J. Fitzmaurice, A. E. Aliev, S. Caddick and H. H. Fielding, *J. Phys. Chem. A*, 2012, **116**, 7943–7949.
36 S. H. M. Deng, X.-Y. Kong, G. Zhang, Y. Yang, W.-J. Zheng, Z.-R. Sun, D.-Q. Zhang and X.-B. Wang, *J. Phys. Chem. Lett.*, 2014, **5**, 2155–2159.
37 C. R. S. Mooney, M. A. Parkes, L. Zhang, H. C. Hailes, A. Simperler, M. J. Bearpark and H. H. Fielding, *J. Chem. Phys.*, 2014, **140**, 205103.
38 C. W. West, J. N. Bull, A. S. Hudson, S. L. Cobb and J. R. R. Verlet, *J. Phys. Chem. B*, 2015, **119**, 3982–3987.
39 C. McLaughlin, M. Assmann, M. A. Parkes, J. L. Woodhouse, R. Lewin, H. C. Hailes, G. A. Worth and H. H. Fielding, *Chem. Sci.*, 2017, **8**, 1621–1630.
40 J. L. Woodhouse, A. Henley, M. A. Parkes and H. H. Fielding, *J. Phys. Chem. A*, 2019, **123**, 2709–2718.
41 C. S. Anstöter, C. R. Dean and J. R. R. Verlet, *Phys. Chem. Chem. Phys.*, 2017, **19**, 29772–29779.
42 R. F. Gunion, M. K. Gilles, M. L. Polak and W. C. Lineberger, *Int. J. Mass Spectrom. Ion Processes*, 1992, **117**, 601–620.
43 J. B. Kim, T. I. Yacovitch, C. Hock and D. M. Neumark, *Phys. Chem. Chem. Phys.*, 2011, **13**, 17378–17383.
44 H.-T. Liu, C.-G. Ning, D.-L. Huang, P. D. Dau and L.-S. Wang, *Angew. Chem., Int. Ed.*, 2013, **52**, 8976–8979.
45 M. J. Frisch, G. W. Trucks, H. B. Schlegel, P. M. W. Gill, B. G. Johnson, M. A. Robb, J. R. Cheeseman, T. A. Keith, G. A. Petersson, J. A. Montgomery Jr., K. Raghavachari, M. A. Al-Laham, V. G. Zakrzewski, J. V. Ortiz, J. B. Foresman, J. Cioslowski, B. B. Stefanov, A. Nanayakkara, M. Challacombe, C. Y. Peng, P. Y. Ayala, W. Chen, M. W. Wong, J. L. Andres, E. S. Replogle, R. Gomperts, R. L. Martin, D. J. Fox, J. S. Binkley, D. J. Defrees, J. Baker, J. P. Stewart, M. Head-Gordon, C. Gonzalez and J. A. Pople, *Gaussian 94*, Gaussian, Inc., Pittsburgh PA, 1995.
46 S. Canuto, K. Coutinho, B. J. C. Cabral, V. G. Zakrzewski and J. V. Ortiz, *J. Chem. Phys.*, 2010, **132**, 214507.
47 O. Dolgounitcheva, V. G. Zakrzewski, L. Streit and J. V. Ortiz, *Mol. Phys.*, 2014, **112**, 332–339.
48 K. D. Jordan, V. K. Voora and J. Simons, *Theor. Chem. Acc.*, 2014, **133**, 1–15.
49 R. A. Donnelly and J. Simons, *J. Chem. Phys.*, 1980, **73**, 2858–2866.
50 M. Mishra, P. Froelich and Y. Öhrn, *Chem. Phys. Lett.*, 1981, **81**, 339–346.
51 M. K. Mishra and A. Venkatnathan, *Int. J. Quantum Chem.*, 2002, **90**, 1334–1347.
52 T. Åberg, *Phys. Rev.*, 1967, **156**, 35–41.
53 S. J. Desjardins, A. D. O. Bawagan, Z. F. Liu, K. H. Tan, Y. Wang and E. R. Davidson, *J. Chem. Phys.*, 1995, **102**, 6385–6399.
54 C. Møller and M. S. Plesset, *Phys. Rev.*, 1934, **46**, 618–622.
55 T. Koopmans, *Physica*, 1934, **1**, 104–113.
56 O. Goscinski and B. Lukman, *Chem. Phys. Lett.*, 1970, **7**, 573–576.
57 J. V. Ortiz, *Int. J. Quantum Chem., Quantum Chem. Symp.*, 1995, **29**, 331–337.
58 D. J. Rowe, *Rev. Mod. Phys.*, 1968, **40**, 153–166.
59 A. M. Ferreira, G. Seabra, O. Dolgounitcheva, V. G. Zakrzewski and J. V. Ortiz, *Understanding Chem. React.*, 2001, **22**, 131–160.
60 J. V. Ortiz, *J. Chem. Phys.*, 1998, **108**, 1008–1014.
61 B. T. Pickup and O. Goscinski, *Mol. Phys.*, 1973, **26**, 1013–1035.

This journal is © the Owner Societies 2024

62 G. Born, H. A. Kurtz and Y. Öhrn, *J. Chem. Phys.*, 1978, **68**, 74–85.
63 J. Baker and B. T. Pickup, *Chem. Phys. Lett.*, 1980, **76**, 537–541.
64 J. Baker and B. T. Pickup, *Mol. Phys.*, 1983, **49**, 651–662.
65 H. G. Weikert, H. D. Meyer, L. S. Cederbaum and F. Tarantelli, *J. Chem. Phys.*, 1996, **104**, 7122–7138.
66 P. O. Löwdin, *Phys. Rev.*, 1965, **139**, 357–372.
67 R. J. Bartlett, *Wiley Interdiscip. Rev.: Comput. Mol. Sci.*, 2012, **2**, 126–138.
68 I. Shavitt and R. J. Bartlett, *Many-Body Methods in Chemistry and Physics: MBPT and Coupled-Cluster Theory*, Cambridge University Press, New York, 2009.
69 J. F. Stanton and J. Gauss, *J. Chem. Phys.*, 1994, **101**, 8938–8944.
70 M. Nooijen and J. G. Snijders, *J. Chem. Phys.*, 1995, **102**, 1681–1688.
71 M. Diaz-Tinoco, H. H. Corzo and J. V. Ortiz, *J. Chem. Theory Comput.*, 2018, **14**, 5881–5895.
72 M. J. Frisch, G. W. Trucks, H. B. Schlegel, G. E. Scuseria, M. A. Robb, J. R. Cheeseman, G. Scalmani, V. Barone, G. A. Petersson, H. Nakatsuji, X. Li, M. Caricato, A. V. Marenich, J. Bloino, B. G. Janesko, R. Gomperts, B. Mennucci, H. P. Hratchian, J. V. Ortiz, A. F. Izmaylov, J. L. Sonnenberg, D. Williams-Young, F. Ding, F. Lipparini, F. Egidi, J. Goings, B. Peng, A. Petrone, T. Henderson, D. Ranasinghe, V. G. Zakrzewski, J. Gao, N. Rega, G. Zheng, W. Liang, M. Hada, M. Ehara, K. Toyota, R. Fukuda, J. Hasegawa, M. Ishida, T. Nakajima, Y. Honda, O. Kitao, H. Nakai, T. Vreven, K. Throssell, J. A. Montgomery, J. E. Peralta, F. Ogliaro, M. J. Bearpark, J. J. Heyd, E. N. Brothers, K. N. Kudin, V. N. Staroverov, T. A. Keith, R. Kobayashi, J. Normand, K. Raghavachari, A. P. Rendell, J. C. Burant, S. S. Iyengar, J. Tomasi, M. Cossi, J. M. Millam, M. Klene, C. Adamo, R. Cammi, J. W. Ochterski, R. L. Martin, K. Morokuma, O. Farkas, J. B. Foresman and D. J. Fox, *Gaussian development version, Revision I.14*, Gaussian Inc., Wallingford CT, 2018.
73 K. Raghavachari, G. W. Trucks, J. A. Pople and M. Head-Gordon, *Chem. Phys. Lett.*, 1989, **157**, 479–483.
74 R. A. Kendall, T. H. Dunning and R. J. Harrison, *J. Chem. Phys.*, 1992, **96**, 6796–6806.
75 R. Dennington, T. A. Keith and J. M. Millam, *GaussView, Version 6*, Semichem Inc., Shawnee Mission, KS, 2016.
76 M. J. Frisch, G. W. Trucks, H. B. Schlegel, G. E. Scuseria, M. A. Robb, J. R. Cheeseman, G. Scalmani, V. Barone, G. A. Petersson, H. Nakatsuji, X. Li, M. Caricato, A. V. Marenich, J. Bloino, B. G. Janesko, R. Gomperts, B. Mennucci, H. P. Hratchian, J. V. Ortiz, A. F. Izmaylov, J. L. Sonnenberg, D. Williams-Young, F. Ding, F. Lipparini, F. Egidi, J. Goings, B. Peng, A. Petrone, T. Henderson, D. Ranasinghe, V. G. Zakrzewski, J. Gao, N. Rega, G. Zheng, W. Liang, M. Hada, M. Ehara, K. Toyota, R. Fukuda, J. Hasegawa, M. Ishida, T. Nakajima, Y. Honda, O. Kitao, H. Nakai, T. Vreven, K. Throssell, J. A. Montgomery, J. E. Peralta, F. Ogliaro, M. J. Bearpark, J. J. Heyd, E. N. Brothers, K. N. Kudin, V. N. Staroverov, T. A. Keith, R. Kobayashi, J. Normand, K. Raghavachari, A. P. Rendell, J. C. Burant, S. S. Iyengar, J. Tomasi, M. Cossi, J. M. Millam, M. Klene, C. Adamo, R. Cammi, J. W. Ochterski, R. L. Martin, K. Morokuma, O. Farkas, J. B. Foresman and D. J. Fox, *Gaussian 16*, Gaussian, Inc., Wallingford CT, 2016.
77 F. Pawłowski and J. V. Ortiz, *J. Phys. Chem. A*, 2021, **125**, 3664–3680.
78 K. B. Bravaya and A. I. Krylov, *J. Phys. Chem. A*, 2013, **117**, 11815–11822.

This journal is © the Owner Societies 2024

Appendix J

E. Opoku, F. Pawłowski and J. V. Ortiz, "*Ab Initio* Electron Propagators with an Hermitian, Intermediately Normalized Superoperator Metric Applied to Vertical Electron Affinities", *J. Phys. Chem. A*, 128, 4730–4749 (2024)

THE JOURNAL OF PHYSICAL CHEMISTRY A
A JOURNAL OF THE AMERICAN CHEMICAL SOCIETY

pubs.acs.org/JPCA Article

Ab Initio Electron Propagators with an Hermitian, Intermediately Normalized Superoperator Metric Applied to Vertical Electron Affinities

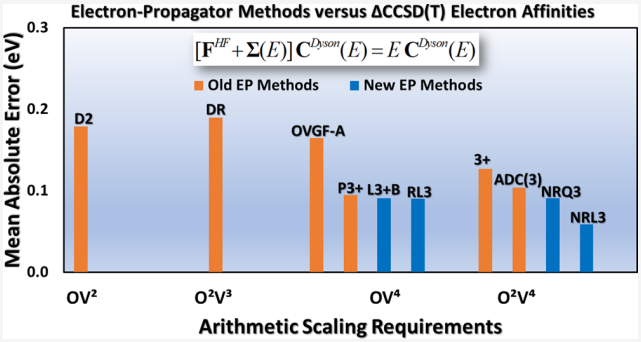
Published as part of The Journal of Physical Chemistry A virtual special issue "Gustavo Scuseria Festschrift".

Ernest Opoku, Filip Pawłowski, and J. V. Ortiz*

Cite This: *J. Phys. Chem. A* 2024, 128, 4730–4749 Read Online

ACCESS | Metrics & More | Article Recommendations | Supporting Information

ABSTRACT: New-generation *ab initio* electron propagator methods for calculating electron detachment energies of closed-shell molecules and anions have surpassed their predecessors' accuracy and computational efficiency. Derived from an Hermitian, intermediately normalized superoperator metric, these methods contain no adjustable parameters. To assess their versatility, a standard set (NIST-50-EA) of 50 vertical electron affinities of small closed-shell molecules based on NIST reference data has been created. Errors with respect to reference data on 23 large, conjugated organic photovoltaic (OPV23) molecules have also been analyzed. All final states are valence anions that correspond to electron affinities between 0.2 and 4.2 eV. For a given scaling of the arithmetic bottleneck, the new-generation methods obtain the lowest mean absolute errors (MAEs). The best methods with fifth-power arithmetic scaling realize MAEs below 0.1 eV. Composite models comprising cubically and quintically scaling calculations executed with large and small basis sets, respectively, produce OPV23 MAEs near 0.05 eV. The accuracy of quintically scaling methods executed with large basis sets is thereby procured with reduced computational effort. New-generation results obtained with and without the diagonal self-energy approximation in the canonical Hartree−Fock basis have been compared. These results indicate that Dyson orbitals closely resemble canonical Hartree−Fock orbitals multiplied by the square root of a probability factor above 0.85.

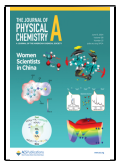


INTRODUCTION

Electron propagator methodology[1,2] has been the servant of research into chemical bonding in anions since the 1970s.[3−5] This approach to molecular electronic structure[6−8] features propitious combinations of accuracy and efficiency in the prediction of energies of electron detachment and attachment.[9−11] The electron propagator is a function of only three variables: an energy parameter and two space-spin coordinates. Its singularities, or poles, equal electron binding energies. Dyson orbitals, overlaps between N-electron initial states and final states with $N \pm 1$ electrons, are related to the electron propagator's residues, numerators associated with vanishing denominators.[12] Electron binding energies and their Dyson orbitals are eigenvalues and eigenfunctions of a one-electron operator with kinetic, nuclear attraction, Coulomb, exchange, relaxation, and differential correlation components. They may also be determined by solving an Hermitian eigenvalue problem in a space of operators instead of the Slater determinants of configuration interaction. In *ab initio* electron propagator theory, correlated Dyson orbital energies provide the best one-electron picture of electronic structure that is compatible with experiments. The formalism also enables diagnosis of the inevitable cases where one-electron pictures become invalid.

Several perturbative approaches to the one-electron Dyson quasiparticle equation have exploited the advantages of the Hartree−Fock orbital basis.[13,14] With this choice, zeroth order electron binding energies equal the predictions of Koopmans's theorem,[15] and corresponding Dyson orbitals equal canonical Hartree−Fock orbitals. The full operator in the Dyson quasiparticle eigenvalue equation has a Fock part with one-electron and Coulomb-exchange constituents. The other part is the energy-dependent self-energy operator wherein orbital relaxation and correlation effects reside. Several algorithms suffice for the evaluation of the self-energy matrix in any order[16,17] of the Møller−Plesset fluctuation potential.[18] To

Received: March 28, 2024
Revised: May 15, 2024
Accepted: May 16, 2024
Published: May 30, 2024



ACS Publications © 2024 American Chemical Society

https://doi.org/10.1021/acs.jpca.4c02050
J. Phys. Chem. A 2024, 128, 4730−4749

Table 1. Acronyms for Approximate, Electron Propagator Self-Energies

acronym[a]	full name
diagonal self-energies	
D2	diagonal second order
os-D2	opposite-spin D2
nD-D2	non-Dyson D2
os-nD-D2	opposite-spin non-Dyson D2
D3	diagonal third order
nD-D3	non-Dyson D3
OVGF	outer-valence Green's function (versions A, B, and C)
nD-OVGF	non-Dyson OVGF (versions A, B, and C)
P3	partial third order
P3+	approximately renormalized partial third order
Q3	quasiparticle third order
Q3+	approximately renormalized quasiparticle third order
L3	linear third order
nD-L3	non-Dyson L3
L3+	approximately renormalized linear third order (versions A, B, and C)
nD-L3+	non-Dyson L3+ (versions A, B, and C)
RP3	explicitly renormalized partial third order
RQ3	explicitly renormalized quasiparticle third order
RL3	explicitly renormalized linear third order
nD-RL3	non-Dyson RL3
DR	diagonal (renormalized) ring approximation (HF-TDA-G_0W_0)
nondiagonal self-energies	
ND2	nondiagonal, second order
2ph-TDA	two-particle-one-hole Tamm−Dancoff approximation
3+	nondiagonal third order
ADC(3)	third-order algebraic diagrammatic construction
NR2	nondiagonal, renormalized, second order
BD-T1	Brueckner doubles with triple-field operators
NRP3	nondiagonal extension of RP3
NRQ3	nondiagonal extension of RQ3
NRL3	nondiagonal extension of RL3
CMX, X = 1−**12**	composite model X

[a]For new-generation methods in **bold type**: N = nondiagonal; nD = non-Dyson; R = explicitly renormalized; + = approximately renormalized.

accelerate the exhaustion of basis set effects, explicitly correlated evaluations of the second-order self-energy matrix have been implemented.[19−21] Monte Carlo algorithms for the second-order and third-order self-energy approximations show considerable promise for calculations on large molecules.[22,23]

Terms of second and third order have provided estimates of higher-order corrections in approximately renormalized methods. Ignoring off-diagonal self-energy couplings between orbitals creates useful compromises of accuracy and efficiency for electron binding energies of closed-shell molecules. This approximation constrains Dyson orbitals to be proportional to canonical Hartree−Fock orbitals. The three outer-valence Green functions (OVGFs)[13,14] and the approximately renormalized partial third-order (P3+) self-energy[24−27] belong to this category of methods. (Table 1 has a full set of acronyms.)

Subsequent perturbative developments have retained off-diagonal self-energy couplings and performed summations of certain classes of terms in all orders. Practical algorithms for this class of methods have been based on large-matrix diagonalization instead of the one-electron operator of the Dyson quasiparticle equation.[28,29] In nondiagonal methods, Dyson orbitals assume their most general form, a linear combination of basis orbitals. Electron binding energies corresponding to correlation final states[30] or even to the complete failure of one-electron pictures[31] have been readily identified. This set of methods includes the two-particle-one-hole Tamm−Dancoff approximation (2ph-TDA),[32] the third-order algebraic diagrammatic construction [ADC(3)],[33] and its strict variant also known as 3+.[34] Improved accuracy and arithmetic efficiency have been obtained with the nondiagonal renormalized second-order (NR2) methods.[27,35] A related extension (BD-T1) uses approximate Brueckner orbitals obtained in a coupled cluster doubles calculation.[36]

A third trend in perturbative methods is based on the GW family of self-energy approximations.[37] All these methods perform a summation of ring self-energy diagrams in all orders of the fluctuation potential. They employ Kohn−Sham orbitals more often than Hartree−Fock orbitals and usually neglect exchange terms in the ring diagrams. Kohn−Sham reference orbitals require incorporation of differences between nonlocal, Hartree−Fock exchange and exchange-correlation operators into the self-energy operator. In self-consistent variants, an optimization of the orbitals occurs. Most often performed are calculations, denoted by G_0W_0, that ignore off-diagonal self-energy couplings in a fixed orbital basis.[38]

Multiconfigurational spin-tensor electron propagator calculations have been performed with a variety of complete active space reference states.[39] Recent perturbative extensions of a multiconfigurational reference, algebraic diagrammatic construction have adopted the Dyall partitioning of the Hamil-

https://doi.org/10.1021/acs.jpca.4c02050
J. Phys. Chem. A 2024, 128, 4730−4749

tonian.[40] The efficacy of these approaches has been demonstrated for small open-shell and biradical species.

A new generation of perturbative, *ab initio* electron propagator methods appeared in 2021.[41] These methods introduce no adjustable parameters in the preparation of reference orbitals or in self-energy formulas. A series of tests versus standard ionization energies of molecules and electron detachment energies of anions has been performed[4,5,42−44] and reviewed.[45] In these tests, the new methods exhibit combinations of accuracy and efficiency that are superior to those of their predecessors. New methods with lesser computational demands repeatedly surpass the accuracy of older methods that are more difficult to execute. A recent study extended and tested new-generation methods with diagonal self-energies for calculating electron affinities (EAs), that is, negatives of electron attachment energy differences.[44] (EAs of molecules and electron detachment energies of molecular anions are identical; ionization energies equal the work necessary for removal of an electron from a molecule.) Another recent publication introduced nondiagonal generalizations of new-generation methods but reported no tests on EAs.[43]

Electron binding energies are easier to define, understand, and measure than other indices of a molecule's tendency to attract electrons.[46] When bases of chemical data are assembled for practical purposes, equilibrium nuclear positions and electron binding energies are among the most valued molecular properties. Despite this conceptual and experimental clarity, in comparison with data on ionization energies, information on EAs is sparse. The so-called molecular space is replete with cases where EAs are not even positive, real numbers. Spectroscopic measurements of ionization energies with a stable molecular target may not involve specialized techniques of sample preparation. This relative simplicity contrasts with more challenging anion electron detachment experiments that feature specialized apparatus for ion synthesis and isolation. Measured adiabatic EAs and vertical electron detachment energies of anions may differ markedly from vertical EAs (VEAs) of molecules. The latter, experimentally elusive quantities are the simplest, most lucid indices of a stable molecule's tendency to acquire additional electronic charge. Because the definition of VEAs specifies identical nuclear positions for a molecule and its anion, these data provide insights into sudden or subtle perturbations. Sudden processes include collisions with fast projectiles such as high-energy photons or electrons. Subtle perturbations may accompany the approach of a nucleophile, that is, a molecule or ion with a tendency to donate electrons.

When molecular VEAs have real, positive values, the corresponding final states may be classified as diffuse-bound or valence-bound anions.[47] The former category encompasses species wherein an electron is weakly bound by the molecule's electrostatic field; these complexes are often called dipole-bound anions.[48] Dispersion, an effect of electron correlation, between a molecule and a diffuse electron may also be responsible for the stability of diffuse-bound anions. Electron attachment in these cases does not substantially alter nuclear positions. Therefore, peak positions seen in anion photodetachment spectra are excellent approximations to VEAs. Electron binding energies of diffuse-bound anions typically have values near or below 0.1 eV. Dyson orbitals of electron attachment consist chiefly of diffuse functions that bear little resemblance to valence atomic orbitals centered on the molecule's nuclei.

Larger VEAs and corresponding Dyson orbitals built chiefly of valence atomic orbitals characterize the other category, the more robust valence-bound anions. Attachment of an electron to a molecule in these cases may lead to a pattern of strengthened and weakened chemical bonds. Such patterns are often related to phase relationships between valence atomic constituents of the Dyson orbitals. (Another, intermediate category wherein low-lying Rydberg functions are major contributors to Dyson orbitals will be considered elsewhere.[49−54]) VEAs of closed-shell molecules with valence-bound anions are the chief concern of the present study.

The following section on Theory reviews the foundations of the Dyson quasiparticle equation, alternative algorithmic strategies based on large-matrix diagonalization, and self-energy approximations. It precedes a guide to computational details and the development of a small-molecule, standard data set (NIST-50-EA). (NIST stands for the National Institute of Standards and Technology.) No negative EAs appear in this set, for their Dyson orbitals are likely to resemble continuum functions expelled by orthogonalization to remote locations. Such cases entail weak relaxation and correlation effects that are unrepresentative of valence-bound anions and provide poor tests of the new methodology. Numerical results pertain to the NIST-50-EA data set and to a standard set of 23 organic photovoltaic (OPV23) molecules.[55] Recently developed, non-diagonal, renormalized self-energies produce EAs for the first time. Numerical tests on composite models that involve a combination of methods and basis sets demonstrate their ability to make accurate predictions at a reduced cost. Recommendations for potential appliers of new techniques follow from an examination of error statistics and the computational demands of each method.

THEORY

Electron Propagator Concepts. The Fourier transform of the $p-q$ element of the electron propagator matrix has the following spectral representation:[6]

$$\langle\langle a_p; a_q^\dagger\rangle\rangle_E = \lim_{\eta\to 0}\Big[\sum_R \frac{\langle 0|a_p|R\rangle\langle R|a_q^\dagger|0\rangle}{E + E_0(N) - E_R(N+1) + i\eta} + \sum_S \frac{\langle 0|a_q^\dagger|S\rangle\langle S|a_p|0\rangle}{E - E_0(N) + E_S(N-1) - i\eta}\Big] \quad (1)$$

The creation ($a^\dagger$) and annihilation (a) operators refer to an orthonormal basis of spin−orbitals $u_p(x)$, $u_q(x)$, $u_r(x)$,.... Poles occur at values of E that equal electron attachment energies in the R summation or electron detachment energies in the S summation. Residues depend on Feynman−Dyson amplitudes that connect the N-electron reference state, |0>, to final states with $N + 1$ electrons (|R>) or $N - 1$ electrons (|S>). Dyson orbitals are related to these amplitudes as follows:[12]

$$\phi_R^{\text{Dyson}}(x_1) = \sqrt{N+1}\int \Psi_0^*(x_2, x_3, x_4, ..., x_{N+1})\,\Psi_R(x_1, x_2, x_3, ..., x_{N+1})\,dx_2dx_3dx_4 ... dx_{N+1} = \sum_p u_p(x_1)\langle 0|a_p|R\rangle \quad (2)$$

https://doi.org/10.1021/acs.jpca.4c02050
J. Phys. Chem. A 2024, 128, 4730−4749

$$\phi_S^{\text{Dyson}}(x_1) = \sqrt{N}\int \Psi_S^*(x_2, x_3, x_4, ..., x_N)\Psi_0(x_1, x_2, x_3, ..., x_N)\mathrm{d}x_2\mathrm{d}x_3\mathrm{d}x_4 ... \mathrm{d}x_N = \sum_p u_p(x_1)\langle S|a_p|0\rangle \quad (3)$$

Matrices of the electron propagator, also known as the one-electron Green's function, have the following form,

$$\langle\langle \mathbf{a}; \mathbf{a}^\dagger\rangle\rangle_E = \mathbf{G}(E) = [\mathbf{a}^\dagger|(E\hat{I} - \hat{H})^{-1}\mathbf{a}^\dagger] \quad (4)$$

where matrices are denoted by bold type.[56] Identity and Hamiltonian superoperators act on ionization operators according to

$$\hat{I}X = X \quad (5)$$

$$\hat{H}X = [H, X]_- \quad (6)$$

where H is the second-quantized Hamiltonian.[57] A complete set of ionization operators, X, comprises products of n creators and $n-1$ annihilators, where $n = 1, 2, 3, ..., N+1$.[58] For example, the two-hole-one-particle (2hp) operators, $a_i^\dagger a_j^\dagger a_a$, with $i < j$ have two occupied (i, j, k,...) and one virtual (a, b, c,...) indices. In the same set, there are also 2ph operators with two virtual and one occupied indices, for example, $a_a^\dagger a_b^\dagger a_i$. The anticommutator of X and Y occurs in the definition of the superoperator metric:

$$[X|Y] = \langle 0|X^\dagger Y + YX^\dagger|0\rangle \quad (7)$$

The resolvent superoperator may be converted to a matrix inversion with an inner projection manifold[59] of ionization operators, $\boldsymbol{h}$, resulting in

$$\mathbf{G}(E) = [\mathbf{a}^\dagger|\mathbf{h}][\mathbf{h}|(E\hat{I} - \hat{H})\mathbf{h}]^{-1}[\mathbf{h}|\mathbf{a}^\dagger] \quad (8)$$

One may partition $\boldsymbol{h}$ into a primary space of simple annihilation operators ($\boldsymbol{a}^\dagger$, i.e., where $n = 1$) and an orthonormal secondary space, $\boldsymbol{f}$, where $[\boldsymbol{a}^\dagger|\boldsymbol{f}] = \mathbf{0}$ and $[\boldsymbol{f}|\boldsymbol{f}] = \mathbf{1}$. Poles are equal to the eigenvalues of $\hat{\boldsymbol{H}}$ in this partitioned basis of operators. The Feynman−Dyson amplitudes equal elements of the eigenvectors that are in the primary space of operators. Pole-search algorithms often appeal to techniques for finding a small number of eigenvalues and eigenvectors of large, symmetric matrices.[28,29,60] Despite the absence of variational principles for electron binding energies, these algorithms usually converge on eigenvalues in the middle of the spectrum of $\hat{\boldsymbol{H}}$.

An alternative strategy exploits the partitioned blocks of $\hat{\boldsymbol{H}}$ and focuses on the inverse of the electron propagator matrix:

$$\mathbf{G}^{-1}(E) = [\mathbf{a}^\dagger|(E\hat{I} - \hat{H})\mathbf{a}^\dagger] - [\mathbf{a}^\dagger|\hat{H}\mathbf{f}][\mathbf{f}|(E\hat{I} - \hat{H})\mathbf{f}]^{-1}[\mathbf{f}|\hat{H}\mathbf{a}^\dagger] \quad (9)$$

Poles occur when the determinant of $\boldsymbol{G}^{-1}(E)$ vanishes, that is, when a zero eigenvalue is present. This condition requires that E satisfy the Dyson quasiparticle equation:

$$\{[\mathbf{a}^\dagger|\hat{H}\mathbf{a}^\dagger] + [\mathbf{a}^\dagger|\hat{H}\mathbf{f}][\mathbf{f}|(E\hat{I} - \hat{H})\mathbf{f}]^{-1}[\mathbf{f}|\hat{H}\mathbf{a}^\dagger]\}\mathbf{C}(E) = E\mathbf{C}(E) \quad (10)$$

Superoperator couplings within the primary space correspond to a generalized Fock matrix, where

$$[a_p^\dagger|\hat{H}a_q^\dagger] = F_{pq} = h_{pq}^{(1)} + \langle pr||qs\rangle\rho_{rs} \quad (11)$$

In eq 11, $\boldsymbol{\rho}$ is the one-electron reduced density matrix, Dirac's notation for antisymmetrized electron repulsion integrals is adopted, and $h^{(1)}$ is the one-electron operator. Einstein notation for summation over common indices appears in the Coulomb-exchange term. In the canonical Hartree−Fock basis, contributions from the idempotent and correlation contributions to $\boldsymbol{\rho}$ produce two terms:

$$F_{pq} = \epsilon_p\delta_{pq} + \Sigma_{pq}(\infty) \quad (12)$$

The first term recovers reference electron binding energies at the level of Koopmans's theorem.[15] The second term belongs to the energy-independent part of the self-energy. The other term in eq 10 is the energy-dependent part of the self-energy:

$$\Sigma'_{pq}(E) = [a_p^\dagger|\hat{H}\mathbf{f}][\mathbf{f}|(E\hat{I} - \hat{H})\mathbf{f}]^{-1}[\mathbf{f}|\hat{H}a_q^\dagger] \quad (13)$$

Combining the energy-dependent and energy-independent parts of the self-energy leads to a compact expression of the Dyson quasiparticle equation in the canonical Hartree−Fock basis:

$$[\boldsymbol{\epsilon} + \boldsymbol{\Sigma}(\infty) + \boldsymbol{\Sigma}'(E)]\mathbf{C}(E) = [\boldsymbol{\epsilon} + \boldsymbol{\Sigma}(E)]\mathbf{C}(E) = E\mathbf{C}(E) \quad (14)$$

All relaxation and correlation corrections to the diagonal $\boldsymbol{\epsilon}$ matrix occur in the complete self-energy matrix, $\boldsymbol{\Sigma}(E)$. These contributions can be identified explicitly, improved systematically, and interpreted lucidly with familiar qualitative concepts. Elements of $\mathbf{C}(E)$ are proportional to Feynman−Dyson amplitudes. The proportionality constant is the square root of the probability factor, which is also known as the pole strength or intensity factor. The probability factor is also equal to the norm of the Dyson orbital. For final state τ, a calculation of the probability factor invokes derivatives of self-energy matrix elements with respect to energy according to

$$\Pi_\tau = \int \mathrm{d}x \left|\phi_\tau^{\text{Dyson}}\left(x\right)\right|^2 = \left[1 - \mathbf{C}^\dagger\left(E_\tau\right)\frac{\mathrm{d}\boldsymbol{\Sigma}(E)}{\mathrm{d}E}\bigg|_{E=E_\tau}\mathbf{C}\left(E_\tau\right)\right]^{-1} \quad (15)$$

Bound-continuum transition intensities are proportional to probability factors in the sudden approximation.[61] The Feynman−Dyson amplitudes read

$$\langle R|a_p|0\rangle = \sqrt{\Pi_R}\,C_p(E_R) \quad (16)$$

$$\langle 0|a_p|S\rangle = \sqrt{\Pi_S}\,C_p(E_S) \quad (17)$$

Koopmans's identity is qualitatively relevant but quantitatively deficient for the lowest electron detachment energies and highest electron attachment energies of typical closed-shell molecules. For these cases, neglect of the off-diagonal elements of the self-energy matrix reduces arithmetic bottlenecks by an order of magnitude in N_{basis}. In the diagonal approximation, there is a separate Dyson quasiparticle equation for each canonical Hartree−Fock orbital:

$$\epsilon_p + \Sigma_{pp}(E) = E \quad (18)$$

Probability factors above 0.85 generally suffice to validate the diagonal approximation. Below this threshold, f operators acquire qualitative importance in the description of correlation (e.g., shakeup)[30] final states. Probability factors in the diagonal approximation depend only on the energy derivative of a single self-energy matrix element:

https://doi.org/10.1021/acs.jpca.4c02050
J. Phys. Chem. A 2024, 128, 4730−4749

Table 2. Arithmetic Scaling and Transformed Integral Requirements of Electron Propagator Methods[a]

level and method class	methods[b]	arithmetic bottleneck	bottleneck steps	largest ERI[c] subset
1, diagonal 2nd order	D2, **os-D2**	OV^2	N_E	O^2V^2
	RSPT2, nD-D2, **os-nD-D2**	OV^2	noniterative	O^2V^2
2 and 3, diagonal post 2nd order and approximately renormalized (+)	RSPT3	OV^4	noniterative	V^4
	D3, OVGF	OV^4	N_E[d]	V^4
	IE: P3, P3+, **Q3, Q3+**	O^2V^3	noniterative	OV^3
	EA: P3, P3+, **Q3, Q3+**	OV^4	N_E	V^4
	L3, L3+	OV^4	N_E[d]	V^4
4, diagonal post 2nd order and explicitly renormalized (R)	**IE: RP3, RQ3**	O^2V^3	noniterative	OV^3
	EA: RP3, RQ3	OV^4	N_IN_E	V^4
	RL3	OV^4	N_IN_E[d]	V^4
	IE: DR	O^2V^3	N_IN_E	O^2V^2
	EA: DR	O^2V^3	N_IN_E	OV^3
nondiagonal	ND2	OV^3	N_I	OV^3
5, nondiagonal and renormalized (NR)	2ph-TDA	OV^4	N_I	V^4
	3+	O^2V^4	noniterative	V^4
	ADC(3)	O^2V^4	N_I	V^4
	IE: NR2	O^3V^3	noniterative[f]	OV^3
	EA: NR2	O^2V^4	noniterative[f]	V^4
	BD-T1	O^2V^4	BD[e]	V^4
	NRP3	O^2V^4	noniterative[f]	V^4
	NRQ3	O^2V^4	noniterative[f]	V^4
	NRL3	O^2V^4	noniterative[f]	V^4

[a]O = # occupied orbital, V = # virtual orbitals, N_E = energy iterations, N_I = inverse-expansion or linear-equation iterations for diagonal methods and Hamiltonian-vector multiplications for nondiagonal methods. [b]New methods in **bold type**. IE = ionization energy (electron detachment). EA = electron affinity (electron attachment). [c]ERI = electron repulsion integral. [d]Reduction by a factor of N_E occurs in non-Dyson (nD) versions for electron detachments. [e]The O^2V^4 arithmetic bottleneck occurs in the Brueckner doubles, coupled cluster, reference-state calculation; the subsequent electron propagator bottleneck is OV^4. [f]N_I OV^4 iterative steps for 3+, ADC(3) and NRL3; N_I O^3V^2 iterative steps for NR2, NRP3, and NRQ3 IEs; N_I OV^4 iterative steps for NR2, NRP3, and NRQ3 EAs.

$$\Pi_{\tau,p} = \left[1 - \left.\frac{d\Sigma_{pp}(E)}{dE}\right|_{E=E_\tau}\right]^{-1} \quad (19)$$

Eq 18 may have many solutions, $E_{\tau p}$, for a given p. Only solutions with probability factors above 0.85 are likely to have predictive value. Because the sum of probability factors equals unity, there are usually many solutions that provide primitive descriptions of correlation states. Dyson orbitals in the diagonal approximation equal the product of a canonical Hartree−Fock orbital and the square root of the probability factor. The diagonal approximation is equivalent to solving for the eigenvalues of $\hat{\boldsymbol{H}}$ such that there is only one operator in the primary space, $\boldsymbol{a}^\dagger$.

Self-Energy Approximations and Arithmetic Bottlenecks. There are five levels of computational effort that lead to progressively more accurate predictions of EAs.[4,41−44] The criteria of effort and accuracy, respectively, are arithmetic scaling factors of bottleneck operations (see Table 2) and mean absolute errors (MAEs) versus standard values. Optimum choices depend on the computational resources at one's disposal. Formulas for self-energy and $\hat{\boldsymbol{H}}$ matrices are available in previous publications.[4,41−44]

In the lowest level of effort are methods that have cubic scaling factors and a limited need for electron repulsion integrals in the canonical Hartree−Fock basis. These methods involve the evaluation of diagonal, second-order self-energy terms only. All electron repulsion integrals in these terms for a given final state share a single spin−orbital index. Therefore, the atomic to molecular integral transformation demands only a quartically scaling algorithm. Once this transformation is complete, evaluation of the second-order self-energy terms is practically free of cost. The arithmetic bottleneck is OV^2, where O and V, respectively, are the dimensions of the occupied and virtual orbital spaces. (V is larger than O in practice.) The same formulas apply to energies of electron attachment and detachment in the D2 (diagonal second order) and os-D2 (opposite spin D2) self-energies. Minor arithmetic economies accompany the non-Dyson (nD) versions of these two methods.

Diagonal methods that evaluate the second-order and third-order self-energy terms constitute the next level. Whereas methods in this class for electron detachments may have O^2V^3 or OV^4 arithmetic bottlenecks, only the latter scaling factor applies to electron attachments. The partial third-order (P3) and quasiparticle third-order (Q3) methods for detachments eschew transformed integrals with four virtual indices, but their electron attachment versions do not. Whereas there are two versions of P3 and Q3 for detachments and attachments, the diagonal (D3) and linear (L3) third-order methods have only one. Arithmetic bottlenecks occur in fewer matrix multiplications in nD variants of D3 and L3 for electron detachments. For electron attachments, the nD modifications have no effect on the number of bottleneck contractions, for they affect only easier steps.

A third set of methods involves only trivial calculations beyond the previous level. In these approximately renormalized self-energies, estimates of higher-order terms need only second-order and third-order terms as input. The three OVGF[13,14] options are in this third category, for they are approximately renormalized extensions of D3. Several methods denoted by a plus sign (e.g., P3+, Q3+, L3+) also estimate higher-order terms with second-order and third-order results. As in the second level,

https://doi.org/10.1021/acs.jpca.4c02050
J. Phys. Chem. A 2024, 128, 4730−4749

Table 3. NIST Test Molecules (NIST-50-EA), Point Groups, Dyson Orbital Labels, and ΔCCSD(T) Standards (eV) in aug-cc-pVXZ (X = D,T,Q) and Complete Basis Set Limit (CBS)

molecules	names	point group	orbital	aug-cc-pVDZ	aug-cc-pVTZ	aug-cc-pVQZ	CBS	NIST value
BeO	beryllium oxide	$C_{\infty v}$	σ	2.142	2.153	2.165	2.172	2.337
BeS	beryllium sulfide	$C_{\infty v}$	σ	2.209	2.241	2.264	2.277	
BN	boron nitride	$C_{\infty v}$	σ	2.954	3.121	3.161	3.184	3.160
BP	boron monophosphide	$C_{\infty v}$	σ	2.906	3.065	3.103	3.125	
C_2	carbon diatomic	$D_{\infty h}$	σ_g	2.989	3.155	3.191	3.212	3.273
HCCN	cyanomethylene	C_s	a″	2.351	2.472	2.506	2.525	2.560
C_3	carbon trimer	$D_{\infty h}$	π_g	1.799	1.944	1.976	1.995	1.995
C_3O	tricarbon monoxide	$C_{\infty v}$	π	0.422	0.599	0.630	0.649	1.237
C_4	carbon tetramer	$D_{\infty h}$	σ_u	4.032	4.157	4.191	4.211	3.882
CCl_2	dichloromethylene	$C_{2\,V}$	b_1	0.998	1.141	1.212	1.253	1.603
Cl_2	chlorine diatomic	$D_{\infty h}$	σ_u	0.637	0.690	0.774	0.823	2.5 ± 0.20
ClF	chlorine monofluoride	$C_{\infty v}$	σ	0.277	0.389	0.472	0.520	2.86 ± 0.20
HNS	sulfur imide	C_s	a″	0.971	1.128	1.189	1.225	1.270
Li_2	lithium diatomic	$D_{\infty h}$	σ_u	0.363	0.369	0.369	0.369	0.540
$LiBH_4$	lithium borohydride	C_3	a	0.416	0.411	0.411	0.411	
LiCl	lithium chloride	$C_{\infty v}$	σ	0.562	0.560	0.561	0.562	0.593
LiCN	lithium cyanide	C_s	a′	0.522	0.519	0.519	0.520	
LiF	lithium fluoride	$C_{\infty v}$	σ	0.358	0.350	0.352	0.352	0.500
LiH	lithium hydride	$C_{\infty v}$	σ	0.302	0.295	0.297	0.298	0.340
$LiNH_2$	lithium amide	C_{2V}	a_1	0.242	0.249	0.251	0.252	
LiOH	lithium hydroxide	$C_{\infty v}$	σ	0.192	0.196	0.199	0.201	
$MgCl_2$	magnesium dichloride	$D_{\infty h}$	σ_g	0.422	0.454	0.473	0.485	
MgF_2	magnesium fluoride	$D_{\infty h}$	σ_g	0.262	0.290	0.306	0.315	
MgO	magnesium oxide	$C_{\infty v}$	σ	1.697	1.568	1.590	1.568	1.62
Na_2	sodium diatomic	$D_{\infty h}$	σ_u	0.380	0.391	0.392	0.391	0.540
$NaBH_4$	sodium borohydride	C_{3V}	a_1	0.599	0.590	0.587	0.590	
NaCl	sodium chloride	$C_{\infty v}$	σ	0.678	0.678	0.677	0.678	0.730
NaCN	sodium cyanide	C_s	a′	0.632	0.633	0.631	0.633	
NaF	sodium fluoride	$C_{\infty v}$	σ	0.494	0.478	0.473	0.478	0.520
NaH	sodium hydride	$C_{\infty v}$	σ	0.326	0.332	0.333	0.333	0.366
NaLi	lithium sodium	$C_{\infty v}$	σ	0.352	0.362	0.361	0.362	0.452
$NaNH_2$	sodium amide	C_{2V}	a_1	0.407	0.411	0.409	0.411	
NaOH	sodium hydroxide	$C_{\infty v}$	σ	0.379	0.376	0.372	0.376	
O_3	ozone	C_{2V}	b_1	1.730	1.868	1.933	1.970	2.100
P_2	phosphorus diatomic	$D_{\infty h}$	π_g	0.268	0.481	0.534	0.565	0.590
S_3	sulfur trimer	C_{2V}	b_1	2.088	2.245	2.317	2.358	2.093
SiF_2	Silicon difluoride	C_{2V}	b_1	0.062	0.147	0.177	0.195	0.100 ± 0.100
SiH_2	silicon dihydride	C_{2V}	b_1	0.945	1.028	1.046	1.057	1.123 ± 0.022
SiO_2	silicon dioxide	$D_{\infty h}$	σ_g	1.248	1.446	1.515	1.555	2.1 ± 0.100
SO_2	sulfur dioxide	C_{2V}	b_1	0.798	0.965	1.027	1.062	1.110
CCH_2	vinylidene	C_{2V}	b_2	0.257	0.344	0.360	0.369	0.490
Cl_2O	dichlorine monoxide	C_{2V}	a_1	0.888	0.988	1.076	1.126	1.300
ClF_3	chlorine trifluoride	C_{2V}	a_1	0.998	1.074	1.144	1.184	2.40 ± 0.10
H_2CS	thioformaldehyde	C_{2V}	b_1	0.052	0.193	0.244	0.274	0.465
OS_2	disulfur monoxide	C_s	a″	1.313	1.466	1.526	1.561	1.877
S_4	sulfur tetramer	C_{2V}	a_2	1.929	2.116	2.195	2.241	2.220
SiC_2	silicon dicarbide	C_{2V}	b_2	1.019	1.110	1.133	1.147	1.370
$SiCl_2$	dichlorosilylene	C_{2V}	b_1	0.791	0.892	0.936	0.962	0.770
SO_2Cl_2	sulfuryl chloride	C_{2V}	a_1	1.180	1.238	1.302	1.339	2.424
SO_3	sulfur trioxide	D_{3h}	a_1'	0.125	0.437	0.536	0.594	1.900

nD versions of OVGF and L3+ procure only negligible advantages for calculations of electron attachment energies.

The highest level of diagonal methods replaces approximate renormalization with explicit renormalization. R denotes these options in the RP3, RQ3, and RL3 self-energies. There are separate electron detachment and attachment versions for RP3 and RQ3. Their bottlenecks have O^2V^3 and OV^4 arithmetic scaling for detachments and attachments, respectively. Only one self-energy formula exists for RL3, which has OV^4 arithmetic scaling in its regular and nD variants. Another diagonal, explicitly renormalized method based on canonical Hartree−Fock orbitals and Tamm−Dancoff excitations belongs to the G_0W_0 family of self-energies.[62] Because the self-energy formula includes ring terms in all orders, it is denominated as the diagonal ring (DR) method. This alternative's arithmetic bottleneck has O^2V^3

https://doi.org/10.1021/acs.jpca.4c02050
J. Phys. Chem. A 2024, 128, 4730−4749

arithmetic scaling and demands fewer electron repulsion integrals.

The highest level of self-energies abandons the diagonal approximation and evaluates renormalizations explicitly. Three nondiagonal, renormalized (NR) methods have noniterative O^2V^4 arithmetic bottlenecks that apply to electron detachment and electron attachment energies. Competing methods include the third-order algebraic diagrammatic construction, or ADC(3),[33] and its strict variant, also known as 3+.[14] Iterative and noniterative O^2V^4 arithmetic bottlenecks, respectively, characterize ADC(3) and 3+. The detachment version of the nondiagonal, renormalized, second-order[35] (NR2) method has O^3V^3 scaling, but this factor grows to O^2V^4 for attachments. Brueckner doubles, triple-field-operator[36] (BD-T1) self-energies depend on iterative O^2V^4 steps in their preceding coupled cluster calculations. An older nondiagonal, renormalized self-energy, the two-particle-one-hole Tamm−Dancoff approximation (2ph-TDA) has OV^4 scaling.[32] Nondiagonal, second-order calculations have a fourth-order (OV^3) bottleneck.

Derivations of terms in the self-energy matrix of a given order in the fluctuation potential may employ diagrammatic or algebraic techniques. Two choices define the latter approach. The first identifies a subset of $\boldsymbol{h}$, the ionization operator space. The second invokes perturbative corrections to the Hartree−Fock description of |0> that suffice to produce the requisite terms in eq 7. For example, the triple-field operator manifold, or $\boldsymbol{f}_3$, and the Hartree−Fock reference state suffice to derive the second-order self-energy. The constant third-order self-energy requires first-order-double $[T_2^{(1)}]$ and second-order-single replacements $[T_1^{(2)}]$ in the reference state. Only the former replacements arise for certain energy-dependent self-energy terms in the third order. The same choices suffice for blocks of $\boldsymbol{H}$ in nondiagonal, renormalized methods. For example, the 3+ version of $\hat{\boldsymbol{H}}$ introduces $T_2^{(1)}$ and $T_2^{(1)}$ to evaluate $(\mathbf{a}^\dagger|\hat{H}\mathbf{a}^\dagger)$, $T_2^{(1)}$ to evaluate $(\mathbf{a}^\dagger|\hat{H}\mathbf{f}_3)$ and its adjoint, and no correlation amplitudes to evaluate $(\mathbf{f}_3|\hat{H}\mathbf{f}_3)$. Diagonalization of the resulting $\hat{\boldsymbol{H}}$ matrix is equivalent to using a self-energy with all third-order terms and certain classes of higher-order terms in all orders.

Instead of variable choices that suffice for terms of a certain order, new-generation methods make fixed choices for $\boldsymbol{h}$ and reference-state improvements. The superoperator metric

$$[X|Y] = \frac{1}{2}\langle HF|(X^\dagger Y + YX^\dagger)(1 + T)|HF\rangle + \frac{1}{2}\langle HF|(1 + T^\dagger)(X^\dagger Y + YX^\dagger)|HF\rangle \quad (20)$$

imposes Hermiticity in $\hat{\boldsymbol{H}}$ and size-extensivity (via intermediate normalization) in ground-state energies. Choices that pertain to the level-two through level-five methods discussed above include an operator manifold with $\boldsymbol{a}^\dagger$ and $\boldsymbol{f}_3$ and an approximate T:

$$T \approx T_2^{(1)} + T_1^{(2)} \quad (21)$$

Whereas Hermitization in equation-of-motion theory allows inclusion of spurious terms,[63] finite-order and renormalized self-energies derived with this superoperator metric contain only connected terms. All elements of $\hat{\boldsymbol{H}}$ are at most linear in T amplitudes.

COMPUTATIONAL METHODS

Experimental EAs in the NIST chemistry webbook[64] provided candidates for a test set of 50 molecules. Small closed-shell molecules with bound anionic final states containing atomic nuclei from the first three periods are eligible. VEAs computed with CCSD(T) total energy differences constituted inclusion criteria. [CCSD(T) stands for coupled cluster theory with single and double replacements and approximate triple replacements.[65]] The aug-cc-pVDZ, aug-cc-pVTZ, and aug-cc-pVQZ basis sets were used.[66] Molecules without vertically bound anionic states at this level of theory were excluded. This survey considered only one anionic state per molecule. To facilitate rapid testing of new methodologies at the complete-basis-set limit (CBS) without prohibitive cost, each molecule in the set may have no more than six nuclei.

This unbiased selection procedure led to the identification of 38 closed-shell molecules with bound valence anionic states (Table 3). Twelve additional molecules increased the sample size to a more statistically significant level. Two magnesium halides are known to possess bound anionic final states; their EAs are not yet reported in the NIST database.[67] BeS and BP were added because they are isoelectronic, respectively, to BeO and BN. The remaining eight molecules explore ligand substitution in alkali metal complexes.[68] Whereas these eight molecules are present in the NIST database, their experimental EAs are not yet documented. The resulting 50 (NIST-50-EA) molecules are chemically diverse, main-group compounds that contain every element in the first three periods except He, Ne, and Al. This set represents an improvement over prior attempts[67,69,70] to create EA standards for small, closed-shell molecules. It also contains all small, closed-shell molecules present in a compendium[71] of experimental and theoretical EAs. Because NIST values in Table 3 have large uncertainties and correspond to adiabatic EAs, they are unsuitable for characterizing new methods. For numerical tests on vertical transitions, CBS ΔCCSD(T) data provide an unambiguous standard.

CCSD/aug-cc-pVTZ optimizations constrained to the highest possible point group produced the molecular structures in the NIST-50-EA set. Because all harmonic frequencies have positive, real values, the optimized structures are minima in their potential energy surfaces.

The NIST-50-EA standard of VEAs rests on ΔCCSD(T) calculations with the aug-cc-pVDZ, aug-cc-pVTZ, and aug-cc-pVQZ basis sets. Data for anionic final states are practically identical with unrestricted Hartree−Fock (UHF) and restricted open-shell Hartree−Fock (ROHF) reference determinants. (See Supporting Information.) Data presented throughout the text, tables, and figures are based on ROHF reference orbitals. Inverse quartically extrapolated [i.e., $(l + 1/2)^{-4}$] total energies obtained with augmented quadruple and triple ζ basis sets define the CBS extrapolated VEA standards. In cases where the triple-ζ result exceeds its quadruple-ζ counterpart, the latter result replaces the CBS value. Electron correlation treatments exclude core orbitals, that is, the standard frozen-core approximation is in effect. To test the effects of tight d functions on results obtained for molecules with third-period nuclei,[72] ΔCCSD(T) VEAs were determined with the aug-cc-pV(T+d)Z basis. The MAE with respect to aug-cc-pVTZ data is 0.00 eV. The mean signed error also equals 0.00 eV. The standard deviation is 0.02 eV, and the maximum error is 0.08 eV. (See Supporting Information.) These data indicate that tight d functions are unlikely to have an important effect on the conclusions of the present study.

Electron propagator calculations are based on Hartree−Fock self-consistent-field wavefunctions for all methods except BD-T1, where Brueckner doubles (BD) reference orbitals are assumed instead. Electron repulsion integrals (ERIs) sub-

https://doi.org/10.1021/acs.jpca.4c02050
J. Phys. Chem. A 2024, 128, 4730−4749

sequently are transformed to the Hartree−Fock or Brueckner doubles basis and are stored on disk. Table 2 lists the largest subsets of ERIs required for each self-energy approximation. In accordance with the ΔCCSD(T) calculations, self-energy summations excluded core orbitals. All electron propagator calculations for the NIST-50-EA set employed the aug-cc-pVDZ, aug-cc-pVTZ, and aug-cc-pVQZ basis sets.

Almost all probability factors exceed the 0.85 threshold for diagonal self-energy methods and confirm the qualitative validity of perturbative improvements to Koopmans results. Several methods obtain probability factors near 0.8 for BN, BP, C_2, MgO, O_3, and S_4; these molecules have high multiconfigurational character. Detailed results for the NIST-50-EA set of small closed-shell molecules are given in the Supporting Information.

Geometries of the OPV23 set, consisting of 23 large organic conjugated molecules, were taken from previous studies.[44] (One member of the original set of 24 molecules does not have a bound, anionic state.) Electron propagator calculations for the OPV23 set assume the same aug-cc-pVXZ basis sets. Inputs for inverse quartic extrapolations included augmented double-triple ζ or augmented triple-quadruple ζ VEA data.

The development version of Gaussian generated Hartree−Fock wavefunctions and transformed electron repulsion integrals used in the electron propagator calculations.[73]

Eqs 22−33 define the composite electron propagator models denoted by CMX (where X = 1−12). CBS VEAs of the OPV23 set[55] provide standards for assessing the performance of CMX models.

$$E^{\mathrm{CM1}} = E^{\mathrm{nD-L3+B}}_{\mathrm{aug-cc-pVDZ}} + E^{\mathrm{os-nD-D2}}_{\mathrm{CBS(DT)}} - E^{\mathrm{os-nD-D2}}_{\mathrm{aug-cc-pVDZ}} \quad (22)$$

$$E^{\mathrm{CM2}} = E^{\mathrm{Q3+}}_{\mathrm{aug-cc-pVDZ}} + E^{\mathrm{os-nD-D2}}_{\mathrm{CBS(DT)}} - E^{\mathrm{os-nD-D2}}_{\mathrm{aug-cc-pVDZ}} \quad (23)$$

$$E^{\mathrm{CM3}} = E^{\mathrm{nD-L3+B}}_{\mathrm{aug-cc-pVTZ}} + E^{\mathrm{os-nD-D2}}_{\mathrm{CBS(TQ)}} - E^{\mathrm{os-nD-D2}}_{\mathrm{aug-cc-pVTZ}} \quad (24)$$

$$E^{\mathrm{CM4}} = E^{\mathrm{Q3+}}_{\mathrm{aug-cc-pVTZ}} + E^{\mathrm{os-nD-D2}}_{\mathrm{CBS(TQ)}} - E^{\mathrm{os-nD-D2}}_{\mathrm{aug-cc-pVTZ}} \quad (25)$$

$$E^{\mathrm{CM5}} = E^{\mathrm{nD-RL3}}_{\mathrm{aug-cc-pVDZ}} + E^{\mathrm{os-nD-D2}}_{\mathrm{CBS(DT)}} - E^{\mathrm{os-nD-D2}}_{\mathrm{aug-cc-pVDZ}} \quad (26)$$

$$E^{\mathrm{CM6}} = E^{\mathrm{NRL3}}_{\mathrm{aug-cc-pVDZ}} + E^{\mathrm{os-nD-D2}}_{\mathrm{CBS(DT)}} - E^{\mathrm{os-nD-D2}}_{\mathrm{aug-cc-pVDZ}} \quad (27)$$

$$E^{\mathrm{CM7}} = E^{\mathrm{nD-L3+B}}_{\mathrm{aug-cc-pVDZ}} + E^{\mathrm{D2}}_{\mathrm{CBS(DT)}} - E^{\mathrm{D2}}_{\mathrm{aug-cc-pVDZ}} \quad (28)$$

$$E^{\mathrm{CM8}} = E^{\mathrm{Q3+}}_{\mathrm{aug-cc-pVDZ}} + E^{\mathrm{D2}}_{\mathrm{CBS(DT)}} - E^{\mathrm{D2}}_{\mathrm{aug-cc-pVDZ}} \quad (29)$$

$$E^{\mathrm{CM9}} = E^{\mathrm{nD-L3+B}}_{\mathrm{aug-cc-pVTZ}} + E^{\mathrm{D2}}_{\mathrm{CBS(TQ)}} - E^{\mathrm{D2}}_{\mathrm{aug-cc-pVTZ}} \quad (30)$$

$$E^{\mathrm{CM10}} = E^{\mathrm{Q3+}}_{\mathrm{aug-cc-pVTZ}} + E^{\mathrm{D2}}_{\mathrm{CBS(TQ)}} - E^{\mathrm{D2}}_{\mathrm{aug-cc-pVTZ}} \quad (31)$$

$$E^{\mathrm{CM11}} = E^{\mathrm{nD-RL3}}_{\mathrm{aug-cc-pVDZ}} + E^{\mathrm{D2}}_{\mathrm{CBS(DT)}} - E^{\mathrm{D2}}_{\mathrm{aug-cc-pVDZ}} \quad (32)$$

$$E^{\mathrm{CM12}} = E^{\mathrm{NRL3}}_{\mathrm{aug-cc-pVDZ}} + E^{\mathrm{D2}}_{\mathrm{CBS(DT)}} - E^{\mathrm{D2}}_{\mathrm{aug-cc-pVDZ}} \quad (33)$$

RESULTS AND DISCUSSION

NIST Closed-Shell Electron Affinities. For the NIST-50-EA set of closed-shell molecules, standard EAs calculated at the ΔCCSD(T) level with complete basis set (CBS) extrapolations are tabulated in Table 3. These data, which vary between 0.2 and 4.2 eV, imply that all anionic final states in this set are valence-bound.

Table 4. Error Distributions (eV) with Respect to ΔCCSD(T)/CBS NIST-EA-50 Standards

method class	method[a]	mean absolute error[b]	mean signed error	standard deviation	maximum unsigned error
uncorrelated	KT	0.730	−0.730	0.608	1.967
diagonal 2nd order	D2	**0.179**	0.122	0.244	0.891
	os-D2	0.280	−0.258	0.254	0.880
	nD-D2	0.197	0.143	0.264	0.954
	os-nD-D2	0.265	−0.159	0.324	1.185
diagonal post 2nd order	DR	0.190	0.101	0.267	1.065
	D3	0.232	−0.192	0.260	0.822
	nD-D3	0.227	−0.198	0.248	0.798
	OVGF-A	0.165	−0.103	0.213	0.738
	OVGF-B	0.194	−0.137	0.227	0.697
	OVGF-C	0.183	−0.128	0.220	0.679
	nD-OVGF-A	0.151	−0.113	0.179	0.626
	nD-OVGF-B	0.183	−0.144	0.205	0.687
	nD-OVGF-C	0.170	−0.136	0.193	0.668
	P3	0.099	−0.037	0.151	0.588
	P3+	0.095	−0.020	0.153	0.618
	Q3	0.133	−0.112	0.168	0.816
	Q3+	0.111	−0.085	0.132	0.440
	L3	0.121	−0.088	0.151	0.514
	nD-L3	0.096	−0.073	0.149	0.507
	L3+A	0.107	−0.056	0.144	0.535
	L3+B	0.111	−0.073	0.145	0.502
	L3+C	0.109	−0.060	0.161	0.528
	nD-L3+A	0.091	−0.041	0.146	0.569
	nD-L3+B	**0.097**	−0.058	0.145	0.525
	nD-L3+C	0.108	−0.044	0.174	0.619
	RP3	0.118	0.058	0.191	0.901
	RQ3	0.104	−0.022	0.186	0.815
	RL3	0.090	−0.025	0.158	0.614
	nD-RL3	**0.093**	−0.006	0.163	0.669
nondiagonal	ND2	0.234	0.216	0.255	0.868
	2ph-TDA	0.271	0.270	0.236	0.964
	3+	0.127	−0.066	0.181	0.510
	ADC(3)	0.104	0.045	0.206	1.180
	NR2	0.153	0.145	0.173	0.883
	BD-T1	0.167	−0.166	0.145	0.655
	NRP3	0.153	0.146	0.174	0.895
	NRQ3	**0.091**	0.071	0.123	0.603
	NRL3	**0.059**	0.046	0.110	0.575

[a]New methods in **bold type.** [b]Optimal methods in **bold type.**

Table 4 and Figure 1 display error statistics for various approximate methods. The predictions of Koopmans's theorem (KT) are invariably underestimates of the EAs. (See histograms in Figure 2.) Partial cancellations between orbital relaxation and differential correlation effects with opposite signs usually occur for electron detachment energies. Unfortunately, the two effects generally have the same sign for electron attachments.

D2 reduces the MAE of KT by a factor of four. The nD variant is slightly less successful. Opposite-spin (os) versions, which neglect the same-spin terms in the self-energy, are somewhat worse. Whereas os methods improved on D2 and nD-D2 for

https://doi.org/10.1021/acs.jpca.4c02050
J. Phys. Chem. A 2024, 128, 4730−4749

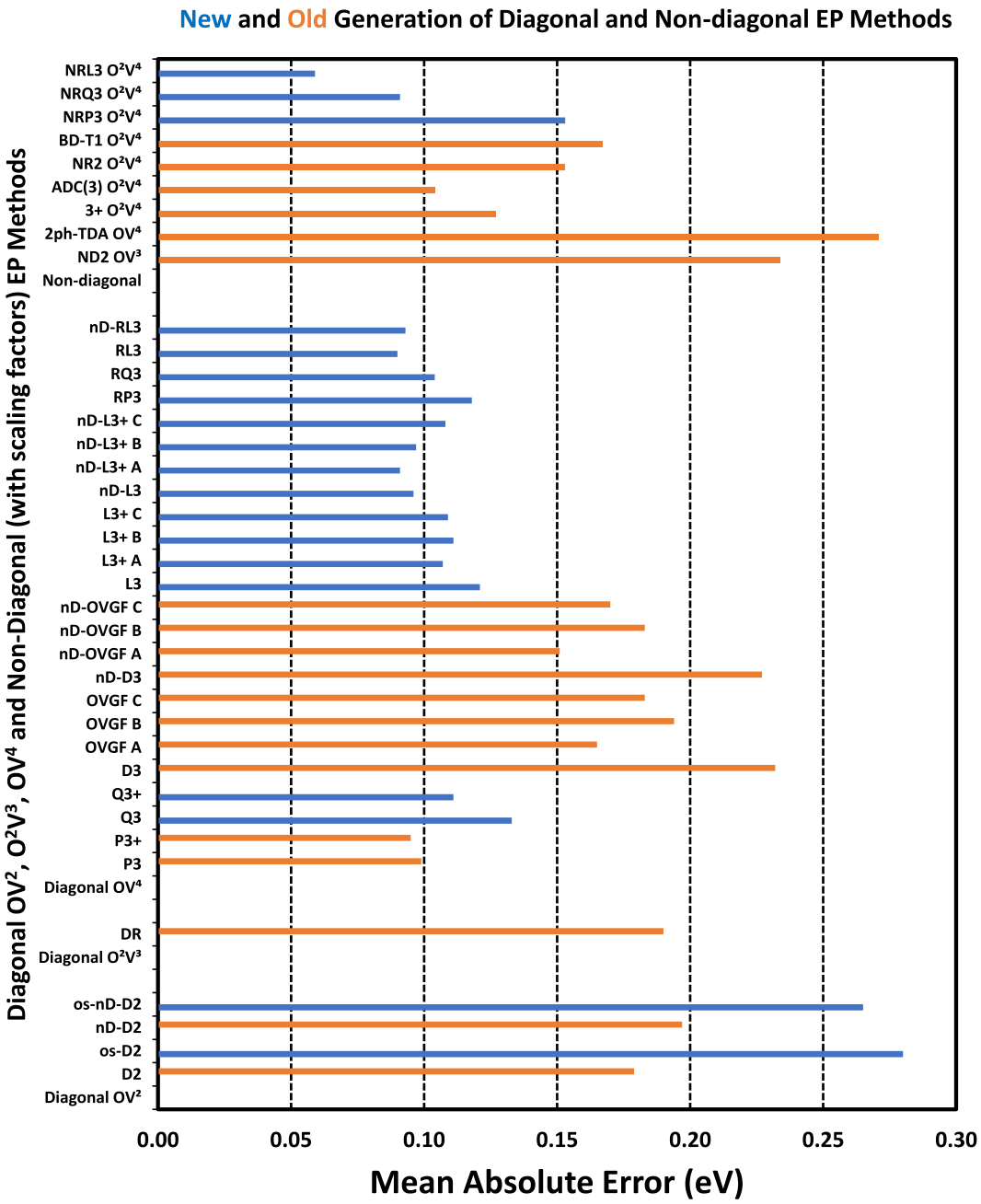


Figure 1. Mean absolute errors (eV) of electron propagator methods versus ΔCCSD(T)/CBS NIST-EA-50 standards.

electron detachment energies, they produce no advantage for electron attachments to small molecules. Second-order relaxation and final-state differential correlation effects are too large in D2 electron detachment energies. Neglect of the same-spin terms in the self-energy mitigates this systematic, reproducible trend. The resulting balanced models, os-D2 and os-nD-D2, describe the same-spin interactions with the exchange potential and os interactions at the second-order level. For EAs, D2 again overestimates the needed corrections to KT, but neglect of the same-spin terms leads to underestimates. (See histograms in Figure 2.) With an MAE slightly below 0.2 eV, D2 is a useful, highly efficient improvement over KT.

Among the second-level methods, which require only evaluation of third-order terms, the performance of the recently introduced Q3 and L3 methods is noteworthy. Their P3 predecessor joins them in producing MAEs near 0.1 eV. The close resemblance of their histograms indicates that third-order terms of orbital relaxation and final-state differential correlation overcome the exaggerations of D2. This agreement also indicates that the constant terms of Q3 and L3 and the third-order initial-state correlation terms of L3 have only minor importance. The lack of energy dependence in the 2hp terms of the nD variant of L3 also makes little difference in the results. A closer examination of individual cases (and the corresponding histograms) shows that two persistent outliers remain for L3: C_2 and BN. Both molecules have a strong multiconfigurational character. The D3 self-energy and its nD variant have somewhat higher MAEs than their second-order counterparts. Their histograms are approximate mirror images of those of D2 and

https://doi.org/10.1021/acs.jpca.4c02050
J. Phys. Chem. A 2024, 128, 4730−4749

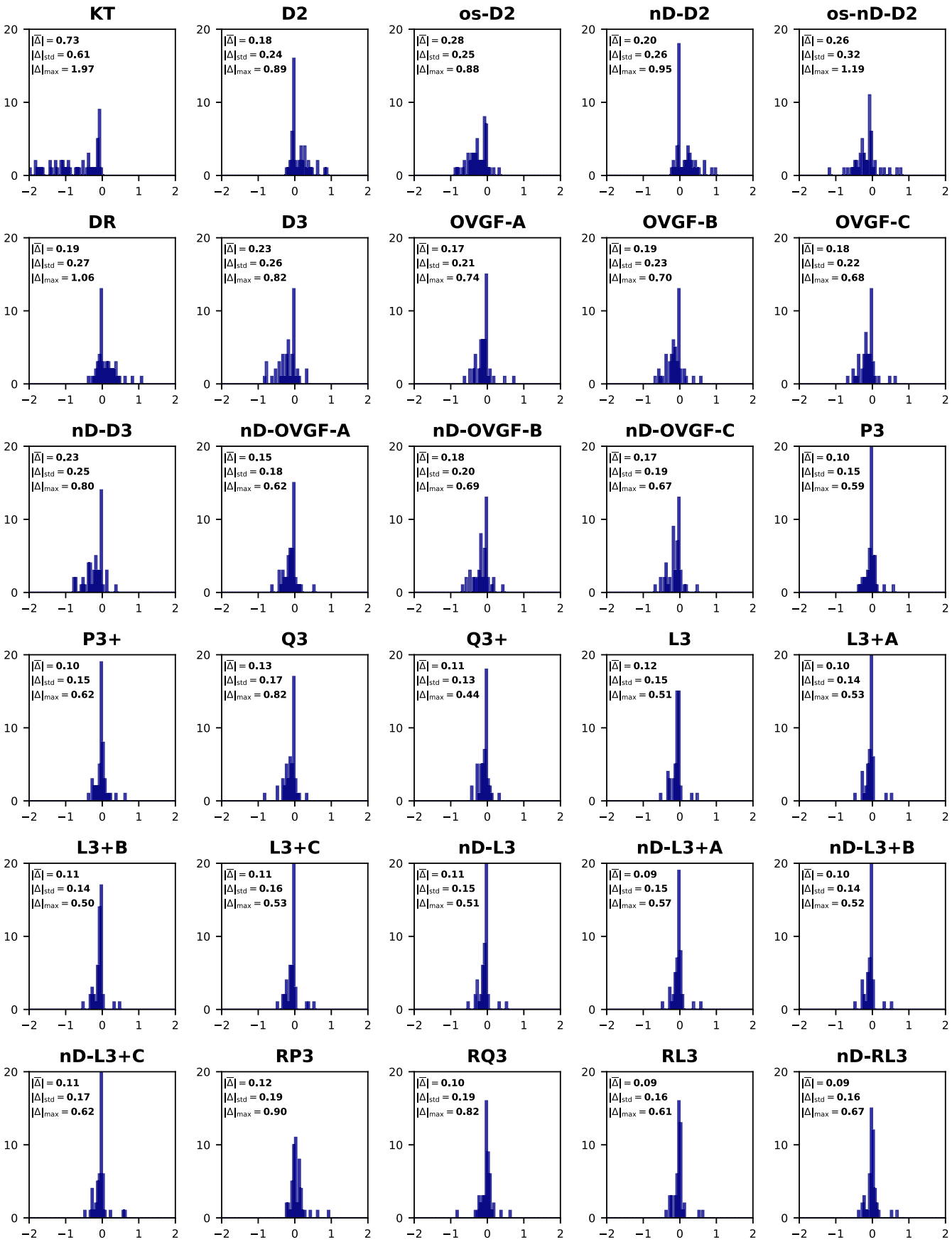


Figure 2. Histograms of error distributions (eV) versus ΔCCSD(T)/CBS NIST-EA-50 standards: diagonal EP methods.

https://doi.org/10.1021/acs.jpca.4c02050
J. Phys. Chem. A 2024, 128, 4730−4749

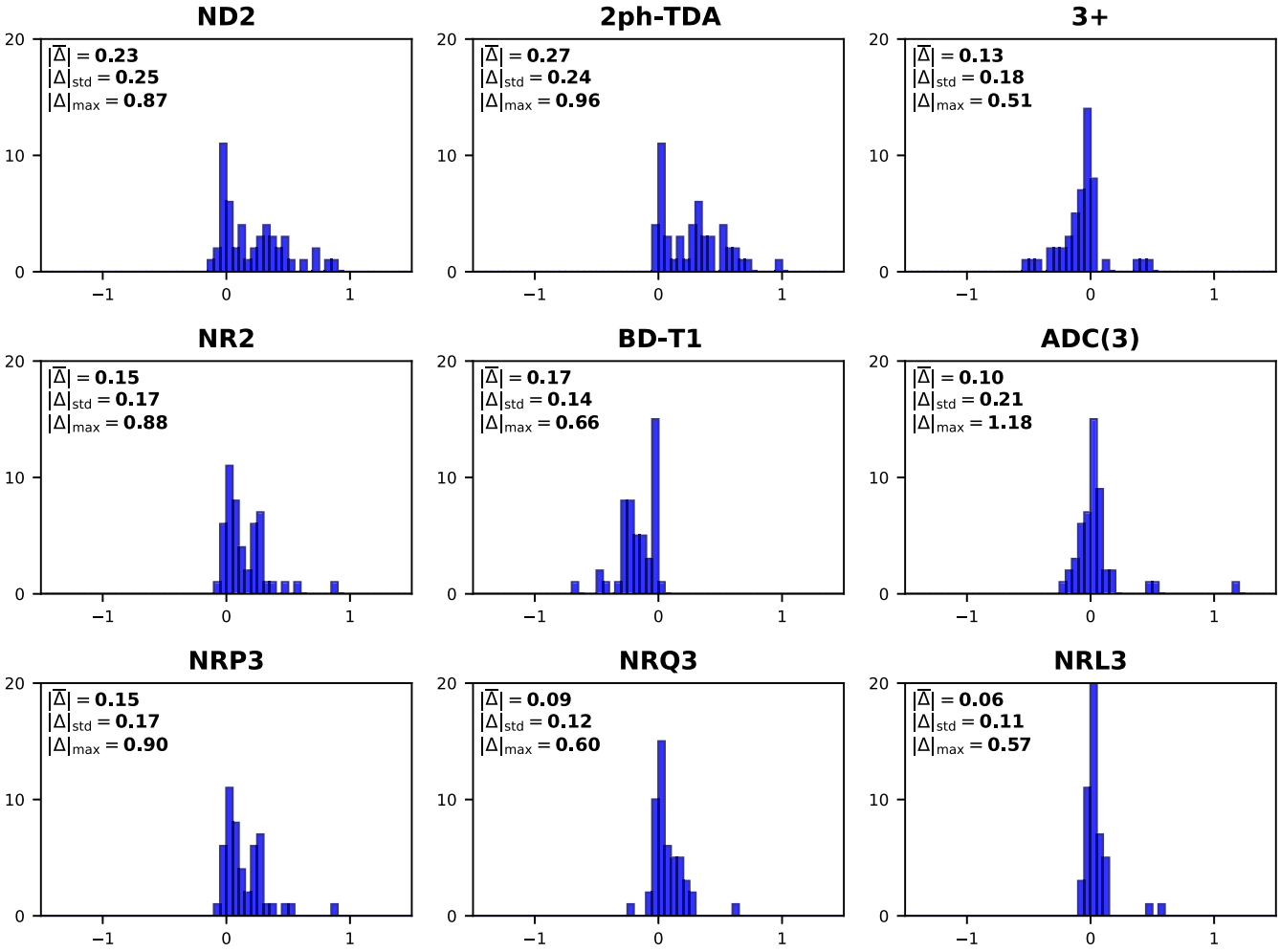


Figure 3. Histograms of error distributions (eV) versus ΔCCSD(T)/CBS NIST-EA-50 standards: nondiagonal EP methods.

nD-D2, for they feature more underestimates than overestimates of EAs.

Approximate renormalizations produce minor improvements. Q3+ and three L3+ versions are better than Q3 and L3 by only 0.01−0.02 eV, as shown in the MAE column of Table 4. MAEs near 0.1 eV accompany methods whose arithmetic scaling factor is only OV^4. Because of its easily interpretable separation of relaxation and correlation terms, L3+B is the best approximately renormalized option. The OVGF extensions of D3 produce MAEs that exceed 0.15 eV.

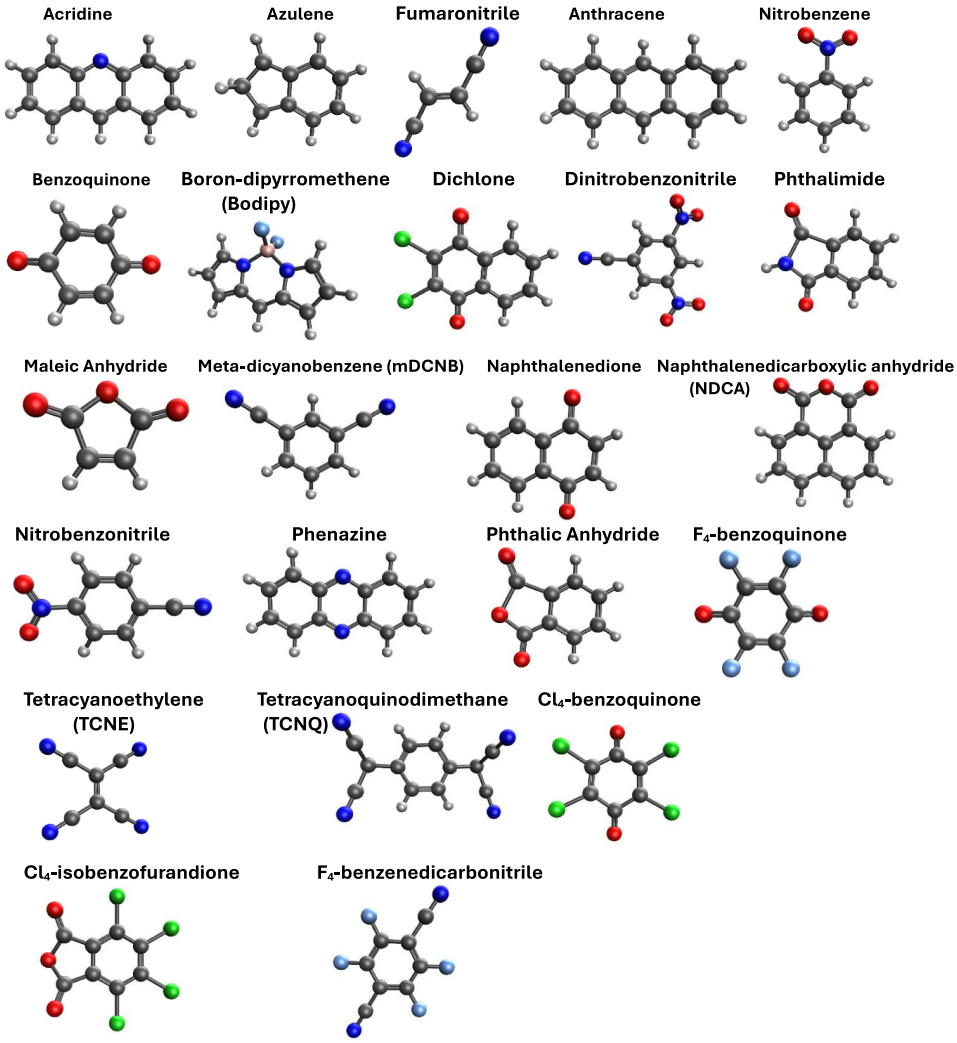
The fourth level, with diagonal, explicitly renormalized self-energies, also produces minor improvements. RL3 and its nD variant achieve MAEs of 0.09 eV. Histograms of RP3, RQ3, RL3, and nD-RL3 closely resemble their second-level and third-level counterparts. Two multiconfigurational molecules, C_2 and BN, prevent the error statistics from being even lower. The DR method also pertains to the diagonal, explicitly renormalized class. Its errors closely resemble those of the more efficient D2 method.

The lowest MAE generated by the nondiagonal, renormalized methods is 0.06 eV. NRL3′s performance surpasses those of RP3 and RQ3. Only the unusually large errors of C_2 and BN prevent the MAE from becoming even lower. (See histograms in Figure 3.) The quality of data produced by BD-T1 and ADC(3), two methods with iterative O^2V^4 bottlenecks, is inferior. The EA version of NR2 remains competitive by virtue of its noniterative O^2V^4 scaling. A fifth power method, 3+, also produces a relatively small MAE near 0.1 eV. The ND2 method produces data that closely resemble those of D2. The least advantageous balance of accuracy and efficiency occurs for 2ph-TDA. The most sharply peaked histogram of Figure 3 belongs to NRL3, the best compromise of accuracy and efficiency in the nondiagonal, renormalized class.

In almost all cases, probability factors that exceed 0.85 confirm the validity of the diagonal approximation. Exceptions occur in RL3 calculations on the multiconfigurational BN, BP, C_2, MgO, O_3, and S_4 molecules. With the aug-cc-pVQZ basis, these pole strengths vary between 0.787 for C_2 and 0.835 for BP. NRL3 produces probability factors for these molecules that differ by less than 0.01. All five NRL3 Dyson orbitals of electron attachment have a dominant canonical Hartree−Fock component with an expansion coefficient above 0.99. The corresponding electron detachment energies differ from their RL3 counterparts by less than 0.04 eV. These data indicate that the diagonal approximation remains valid for electron binding energies and Dyson orbitals even for the multiconfigurational molecules in the NIST-50-EA set.

The percentage difference between ΔCCSD and ΔCCSD(T) total atomization energies, %TAE[(T)], has been used as a diagnostic of multiconfigurational character.[74] When the same criterion is applied to the EAs of the NIST-50-EA set of molecules, subsets with %EA[(T)] less than 10 or 5%,

https://doi.org/10.1021/acs.jpca.4c02050
J. Phys. Chem. A 2024, 128, 4730−4749



Color Code: H=light gray; B=pink; C=gray; N=blue; O=red; F=light blue; and Cl=green.

Figure 4. 23 Organic photovoltaic molecules in the OPV23 set. Color code: H = light gray; B = pink; C = gray; N = blue; O = red; F = light blue; and Cl = green.

respectively, have 38 or 29 members. MAEs of the recommended L3+B, nD-L3+B, RL3, nD-RL3, and NRL3 methods differ by only 0.02 eV when the 10% criterion is employed. With the 5% set, MAEs decline with respect to the full set's results by 0.01−0.03 eV. (See data in Supporting Information.)

Organic Photovoltaic Molecules. VEAs of 23 organic acceptor molecules have been determined with ΔCCSD(T)/aug-cc-pVDZ total energy differences. The OPV23 set (Figure 4) comprises molecules that are considerably larger than those of the NIST-50-EA test set. It is now possible to assess VEAs produced by recently developed nondiagonal renormalized methods versus reference data for the OPV23 set.

Consequences of the size difference are evident in the error data for the KT and second-order results. (See Table 5 and Figure 5.) The signs of the errors are the same as those obtained for the NIST-50-EA set, but the MAEs are almost twice as large. For this set of data, the os-D2 and D2 MAEs are almost identical. Whereas the os variant underestimates, D2 overestimates. There is a noteworthy difference between the regular and nD variants that reveals a relatively strong energy dependence in the 2hp term of D2. Contributions to initial-state, electron-pair correlation energies from the virtual orbital of KT are associated with this term. With the second-order, diagonal methods, the MAE of KT declines approximately by a factor of 0.3. Unfortunately, these cubically scaling self-energy approximations now obtain MAEs near 0.4 eV for EAs.

Considerable improvements occur at the next level, which necessitates the evaluation of third-order terms. The MAEs of L3 and nD-L3 are 0.15 and 0.10 eV, respectively. The histograms of these two methods (see Figure 6) are more sharply peaked than those of D3 or P3. Whereas P3 produces an even smaller MAE, Q3's value is worse. The MAE of D3, 0.46 eV, is decidedly worse than that of D2 (0.39 eV), with underestimates replacing overestimates of EAs. The new-generation, diagonal, third-order methods provide a better reference point for subsequent renormalizations than D3.

Whereas approximate renormalizations had little importance for the NIST-50-EA set, they produce significant improvements for the OPV23 molecules. All three L3+ self-energies and their nD variants yield MAEs between 0.05 and 0.09 eV. Q3+ does not exhibit the same degree of success. This discrepancy indicates the importance of the Koopmans orbital (i.e., the canonical Hartree−Fock LUMO) in third-order, initial-state

https://doi.org/10.1021/acs.jpca.4c02050
J. Phys. Chem. A 2024, 128, 4730−4749

Table 5. Error Distributions (eV) with Respect to ΔCCSD(T)/aug-cc-pVDZ OPV23 Standards

method class	method[a]	mean absolute error[b]	mean signed error	standard deviation	maximum unsigned error
uncorrelated	KT	1.308	−1.308	0.166	1.493
diagonal 2nd order	D2	0.387	0.387	0.143	0.698
	os-D2	0.386	−0.386	0.122	0.567
	nD-D2	0.454	0.454	0.148	0.776
	os-nD-D2	**0.359**	−0.359	0.123	0.543
diagonal post 2nd order	DR	0.141	0.136	0.122	0.378
	D3	0.465	−0.465	0.122	0.788
	nD-D3	0.434	−0.434	0.126	0.765
	OVGF-A	0.168	−0.168	0.056	0.298
	OVGF-B	0.250	−0.250	0.083	0.463
	OVGF-C	0.254	−0.254	0.063	0.406
	nD-OVGF-A	0.130	−0.130	0.056	0.262
	nD-OVGF-B	0.211	−0.211	0.087	0.429
	nD-OVGF-C	0.215	−0.215	0.064	0.370
	P3	0.138	−0.124	0.109	0.314
	P3+	0.108	−0.058	0.108	0.244
	Q3	0.210	−0.210	0.072	0.336
	Q3+	0.145	−0.145	0.064	0.242
	L3	0.147	−0.147	0.063	0.244
	nD-L3	0.105	−0.103	0.059	0.195
	L3+A	0.071	−0.035	0.070	0.125
	L3+B	0.090	−0.084	0.059	0.155
	L3+C	0.086	−0.072	0.065	0.156
	nD-L3+A	0.053	0.011	0.068	0.177
	nD-L3+B	**0.061**	−0.037	0.056	0.100
	nD-L3+C	0.061	−0.025	0.062	0.119
	RP3	0.098	0.009	0.115	0.228
	RQ3	0.091	−0.077	0.072	0.179
	RL3	0.079	−0.072	0.062	0.167
	nD-RL3	**0.057**	−0.024	0.060	0.102
nondiagonal	ND2	0.415	0.415	0.134	0.749
	2ph-TDA	0.433	0.433	0.108	0.665
	3+	0.299	−0.299	0.100	0.572
	ADC(3)	0.096	−0.095	0.069	0.207
	NR2	0.095	0.045	0.112	0.278
	BD-T1	0.182	−0.182	0.018	0.214
	NRP3	0.095	0.045	0.113	0.279
	NRQ3	**0.069**	−0.041	0.068	0.132
	NRL3	**0.063**	−0.044	0.056	0.126

[a]New methods in **bold type**. [b]Optimal methods in **bold type**.

Table 6. Error Distributions (eV) with Respect to ΔCCSD(T)/CBS OPV23 Standards

composite methods	mean absolute error	mean signed error	standard deviation	maximum unsigned error
CM1	0.048	−0.022	0.051	0.100
CM2	0.129	−0.129	0.061	0.254
CM3	0.060	−0.028	0.060	0.105
CM4	0.150	−0.150	0.068	0.252
CM5	0.046	−0.008	0.055	0.115
CM6	0.051	−0.029	0.052	0.122
CM7	0.053	0.051	0.052	0.169
CM8	0.071	−0.057	0.061	0.166
CM9	0.060	−0.018	0.065	0.119
CM10	0.140	−0.140	0.072	0.237
CM11	0.066	0.064	0.055	0.194
CM12	0.052	0.044	0.051	0.152

correlation for larger molecules. L3+ errors are even better than their counterparts for the NIST-50-EA set. The MAEs of the OVGF methods increase for the larger molecules; only the A version remains competitive.

For the OPV23 set, MAEs obtained with the new, explicitly renormalized diagonal self-energies are nearly identical to those of the NIST-50-EA set. RL3 and nD-RL3 MAEs of 0.08 and 0.06 in Table 5 are almost identical to those of Table 4. These results also closely resemble those (see L3+ results in Table 5) obtained with approximate renormalizations.

Nondiagonal, renormalized extensions maintain the same record of accuracy. NRL3's MAE of 0.06 eV is the best in the fifth level of self-energies. Its histogram (see Figure 7) is sharply peaked and centered around zero. ADC(3) also performs well, but with a need for iterative O^2V^4 matrix multiplications. The less costly NR2 method succeeds to about the same extent. The third-order treatment of constant self-energy terms results in the less accurate predictions of 3+. Despite its improved reference state, BD-T1 is not competitive for EAs. The sharpness of its

https://doi.org/10.1021/acs.jpca.4c02050
J. Phys. Chem. A 2024, 128, 4730−4749

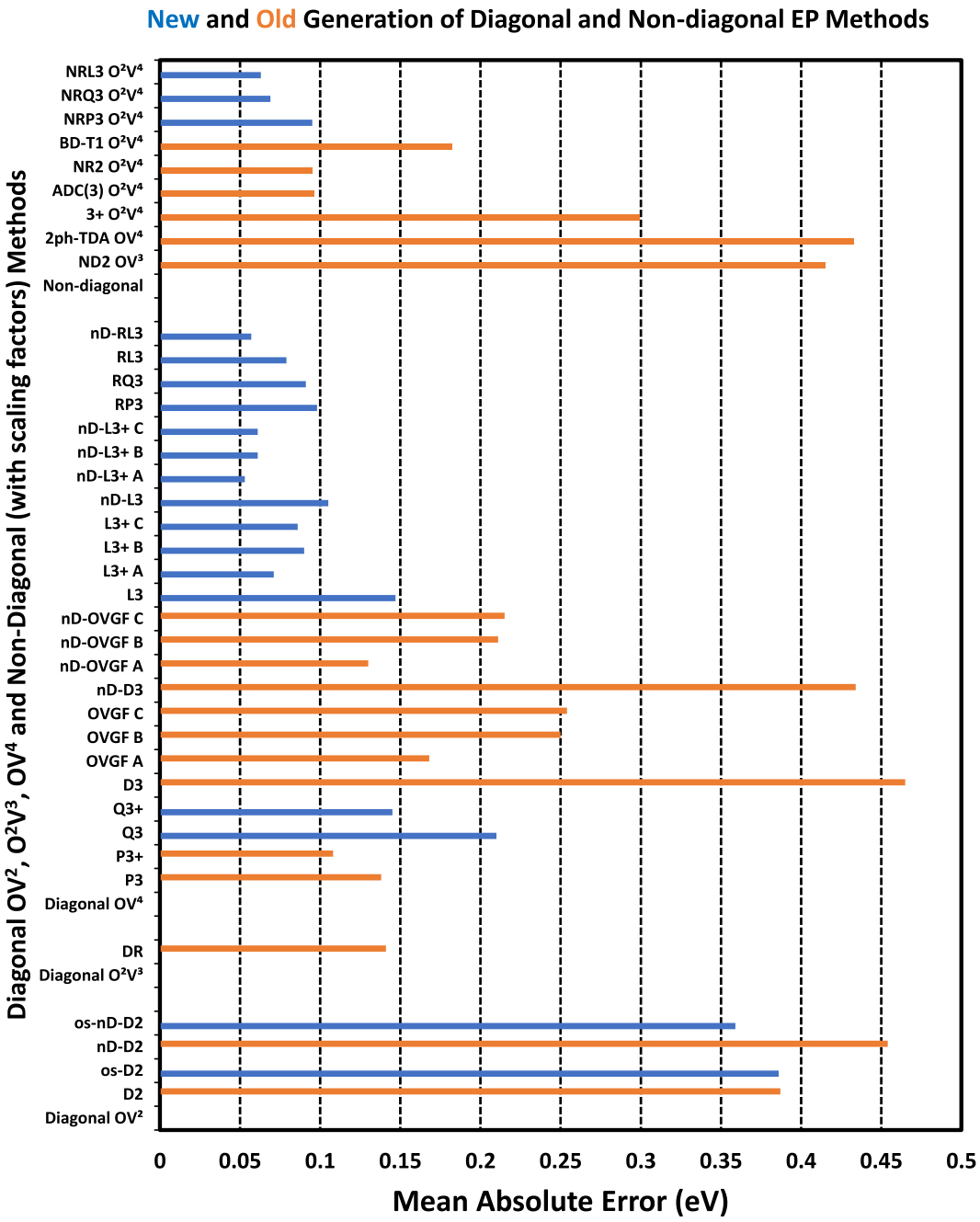


Figure 5. Mean absolute errors (eV) of electron propagator methods versus ΔCCSD(T)/aug-cc-pVDZ OPV23 standards.

histogram indicates that its somewhat lower accuracy is accompanied by relatively high precision, that is, its underestimates are very consistent.

These results indicate the need for renormalizations in calculations on larger molecules. The errors of second-order methods grow with increased molecular dimensions. The third-order terms of L3 and subsequent approximate or explicit renormalizations correct D2's exaggeration of orbital relaxation and final-state differential correlation.

Three kinds of data confirm the validity of the diagonal approximation. Probability factors exceed 0.85 in all cases; discrepancies between RL3 and NRL3 probability factors are less than 0.03. Absolute discrepancies between RL3 and NRL3 EAs never exceed 0.03 eV. All NRL3 Dyson orbitals have a dominant canonical Hartree−Fock component whose coefficient is at least 0.99.

VEAs based on extrapolated ΔCCSD(T) and ΔMP2 results obtained with basis sets up to the aug-cc-pVQZ or aug-cc-pV5Z levels provide a standard for composite models.[55] In eqs 22−33, the lower-level method is D2 or os-nD-D2. The upper-level method may be nD-L3+B, Q3+, nD-RL3, or NRL3. The alternative models include double-triple ζ or triple-quadruple ζ combinations of basis sets. Table 6 and Figure 8 display MAEs. Figure 9 presents an array of histograms.

Comparisons of CM1 versus CM2, CM3 versus CM4, CM7 versus CM8, and CM9 versus CM10 establish the superiority of nD-L3+B to Q3+. The minor differences between CM1 and CM7 and between CM3 and CM9 indicate that os-nD-D2 and D2 are equally suitable lower-level methods. Negligible

https://doi.org/10.1021/acs.jpca.4c02050
J. Phys. Chem. A 2024, 128, 4730−4749

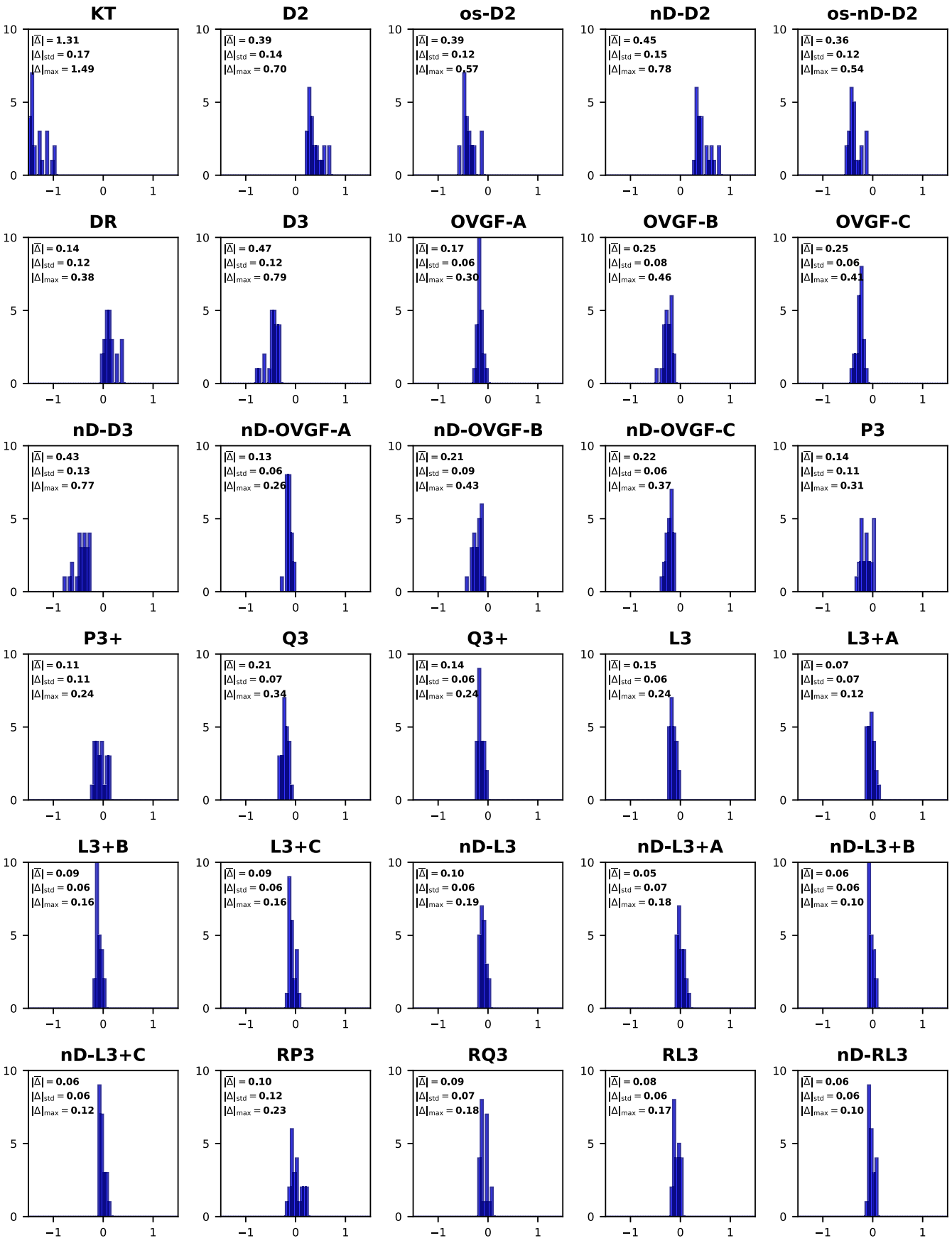


Figure 6. Histograms of error distributions (eV) versus ΔCCSD(T)/aug-cc-pVDZ OPV23 standards: diagonal EP methods.

https://doi.org/10.1021/acs.jpca.4c02050
J. Phys. Chem. A 2024, 128, 4730−4749

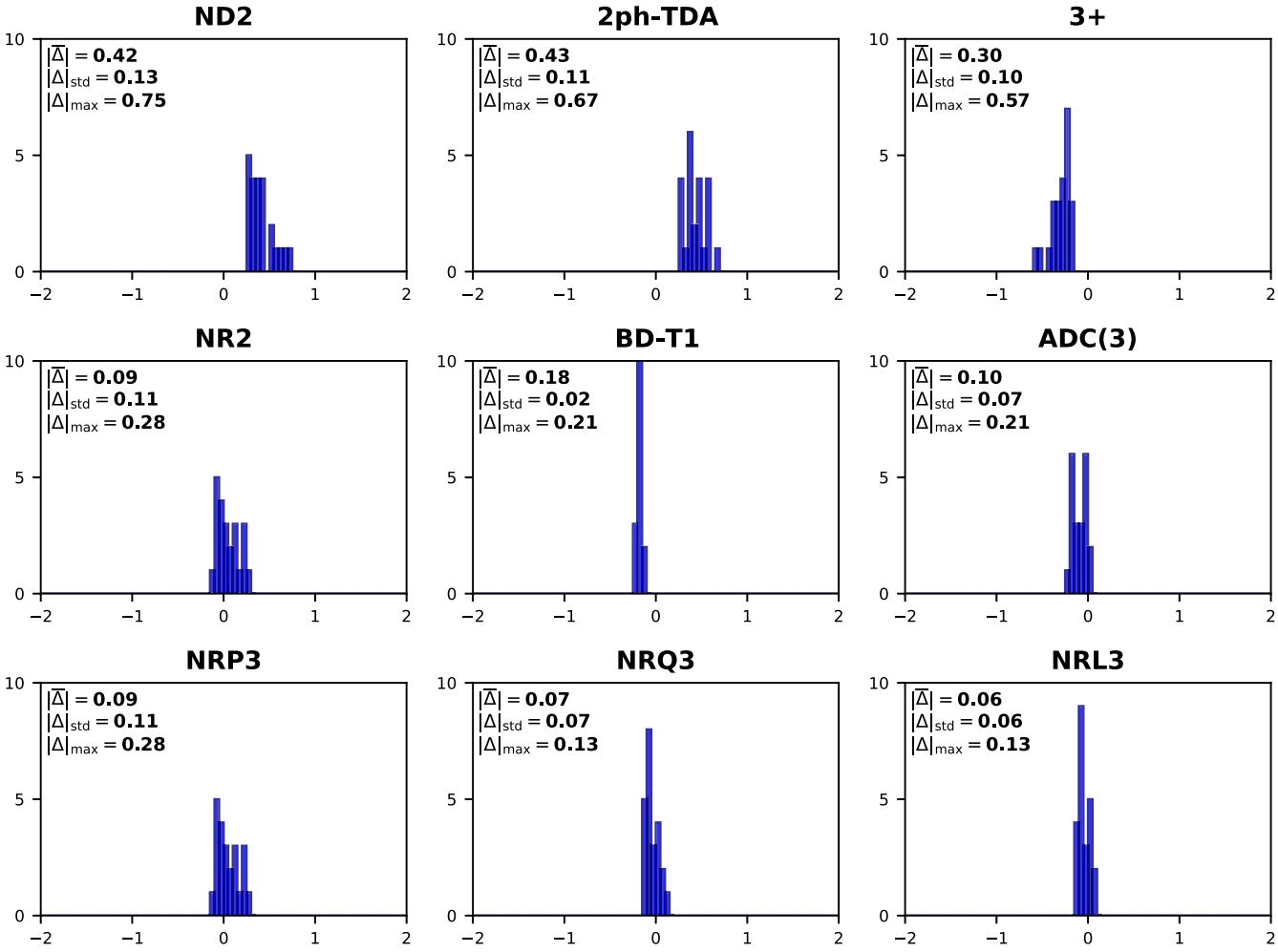


Figure 7. Histograms of error distributions (eV) versus ΔCCSD(T)/aug-cc-pVDZ OPV23 standards: nondiagonal EP methods.

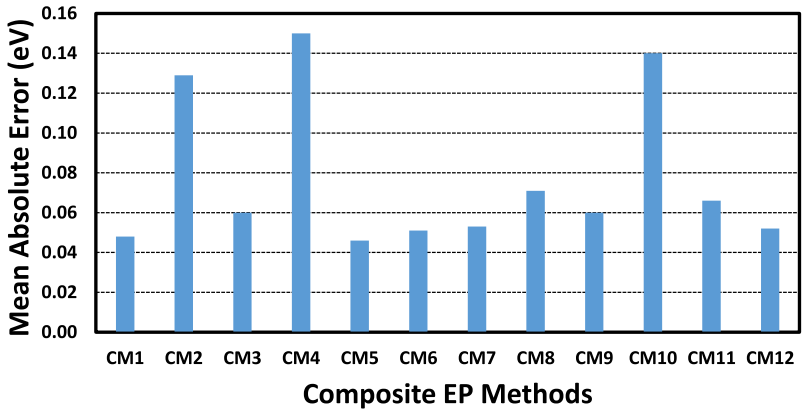


Figure 8. Mean absolute errors (eV) of composite electron propagator methods versus ΔCCSD(T)/CBS OPV23 electron affinity standards.

differences in quality between CM1 and CM3 and between CM7 and CM9 imply that the results are stable with respect to basis improvements. Substitution of diagonal renormalized or nondiagonal renormalized methods for approximately renormalized methods (see CM5 and CM6 versus CM1 or CM11 and CM12 versus CM7) makes little difference in the quality of the results. CM1 provides excellent agreement with standard data. L3+ methods with augmented double ζ basis sets and second-order methods with augmented triple ζ basis sets are efficient components for reliable composite models.

CONCLUSIONS

Electron propagator methodology for calculating VEAs of closed-shell molecules offers several levels of accuracy and efficiency.

The diagonal, second-order method and its opposite-spin variant reduce the MAE of a set of Koopmans's theorem

https://doi.org/10.1021/acs.jpca.4c02050
J. Phys. Chem. A 2024, 128, 4730−4749

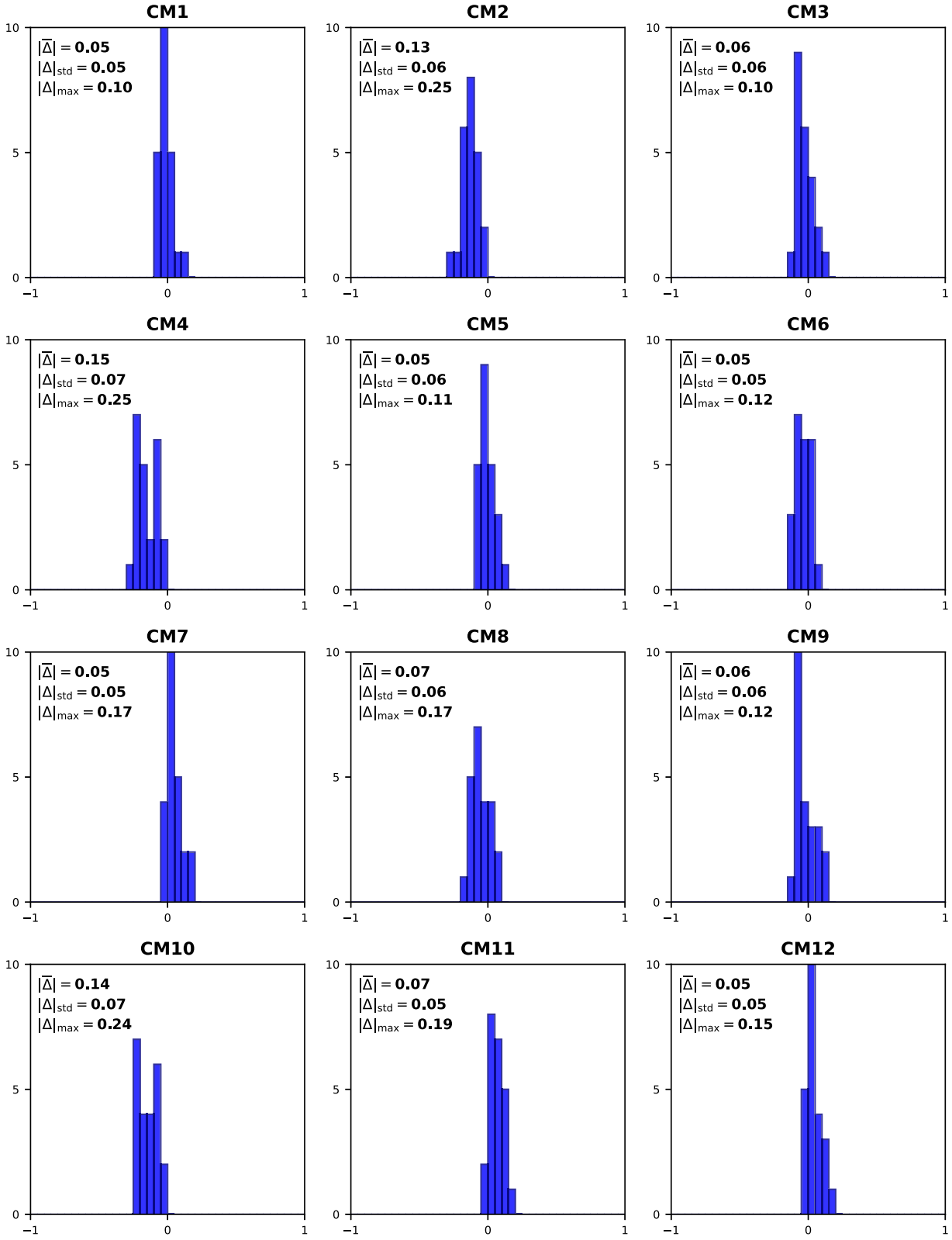


Figure 9. Histograms of error distributions (eV) versus ΔCCSD(T)/CBS OPV23 standards: composite EP methods.

calculations by a factor of 0.2−0.4. These methods demand only a cubically scaling set of transformed electron repulsion integrals. For a single electron binding energy, efficient transformation algorithms with quartic scaling require fewer operations than an MP2 calculation. Interpretations of these post-Hartree−Fock results may be stated in terms of orbital relaxation and differential correlation contributions arising from the simple self-energy expression.

The L3+B method, which employs an approximately renormalized, diagonal self-energy, obtains average errors

https://doi.org/10.1021/acs.jpca.4c02050
J. Phys. Chem. A 2024, 128, 4730−4749

below 0.1 eV. Its explicitly renormalized extension, RL3, performs more bottleneck operations and achieves slightly greater accuracy. These two diagonal self-energy methods have OV^4 arithmetic scaling factors. Additional small improvements in accuracy accompany upgrading to the NRL3 method, which generates Dyson orbitals in their general form, a linear combination of Hartree−Fock orbitals. This extra information necessitates a noniterative O^2V^4 arithmetic bottleneck.

Previously introduced self-energy approximations such as P3+, NR2, and the *ab initio* G_0W_0 variant DR can also be competitive alternatives. Trivial modifications to programs that perform older kinds of diagonal or nondiagonal renormalized calculations suffice to execute new-generation methods. The success of the latter methods is a consequence of eqs 20 and 21, which impose Hermiticity in $\hat{\boldsymbol{H}}$ and size-extensive total energies.

Reliable composite models enable accurate predictions on larger molecules. These models combine renormalized methods executed with augmented double ζ basis sets and second-order methods executed with augmented triple ζ basis sets. MAEs near 0.05 eV occurred for the set of 23 organic acceptors that are of interest in the design of photovoltaic devices.

For the NIST-50-EA and OPV23 data sets, the diagonal approximation has a negligible effect on the predicted VEAs. Dyson orbitals expressed by the NRL3 method as a linear combination of canonical Hartree−Fock orbitals closely resemble their counterparts generated with the diagonal RL3 self-energy. The chief deficiency of Dyson orbitals produced at the Hartree−Fock level is not the absence of interference from other orbitals. To improve this uncorrelated level of theory, it is necessary only to consider the energy-dependent, diagonal elements of the self-energy matrix. This correction to Koopmans's identity provides a probability factor that is less than unity and accurate predictions of the EA. Data obtained for the NIST-50-EA set indicate that qualitative failures of the Koopmans picture of electron attachment do not necessarily appear for multiconfigurational molecules. Conditions that suffice to produce such failures are now under investigation.

■ ASSOCIATED CONTENT

Supporting Information

The Supporting Information is available free of charge at https://pubs.acs.org/doi/10.1021/acs.jpca.4c02050.

Composite vertical electron affinities versus OPV23 standard (XLSX)

NIST-EA-50 nuclear coordinates (ZIP)

Vertical electron affinities versus OPV23 standard (XLSX)

OPV23 nuclear coordinates (ZIP)

NIST-50-EA electron affinities (XLSX)

■ AUTHOR INFORMATION

Corresponding Author

J. V. Ortiz − *Department of Chemistry and Biochemistry, Auburn University, Auburn, Alabama 36849-5312, United States;* orcid.org/0000-0002-9277-0226; Email: ortiz@auburn.edu

Authors

Ernest Opoku − *Department of Chemistry and Biochemistry, Auburn University, Auburn, Alabama 36849-5312, United States;* orcid.org/0000-0002-4271-6838

Filip Pawłowski − *Department of Chemistry and Biochemistry, Auburn University, Auburn, Alabama 36849-5312, United States*

Complete contact information is available at: https://pubs.acs.org/10.1021/acs.jpca.4c02050

Notes

The authors declare no competing financial interest.

■ ACKNOWLEDGMENTS

The authors thank Dr. Manuel Díaz-Tinoco for valuable discussions and the Alabama Supercomputer Center for computing resources.

■ REFERENCES

(1) Linderberg, J.; Öhrn, Y. *Theoretical Chemistry: a Series of Monographs No. 3: Propagators in Quantum Chemistry*; Academic, 1973.

(2) Cederbaum, L. S.; Domcke, W. Theoretical aspects of ionization potentials and photoelectron spectroscopy: a Green's function approach. *Adv. Chem. Phys.* **1977**, *36*, 205−344.

(3) Simons, J.; Smith, W. D. Theory of electron affinities of small molecules. *J. Chem. Phys.* **1973**, *58*, 4899−4907.

(4) Opoku, E.; Pawłowski, F.; Ortiz, J. V. Electron Propagator Theory of Vertical Electron Detachment Energies of Anions: Benchmarks and Applications to Nucleotides. *J. Phys. Chem. A* **2023**, *127* (4), 1085−1101.

(5) Opoku, E.; Pawłowski, F.; Ortiz, J. V. New-generation electron-propagator methods for vertical electron detachment energies of molecular anions: benchmarks and applications to model green-fluorescent-protein chromophores. *Phys. Chem. Chem. Phys.* **2024**, *26* (13), 9915−9930.

(6) Linderberg, J.; Öhrn, Y. *Propagators in Quantum Chemistry*, 2nd ed.; Wiley-Interscience, 2004.

(7) Schirmer, J. *Many-Body Methods for Atoms, Molecules and Clusters*; Springer International Publishing AG, 2018.

(8) Jørgensen, P.; Simons, J. *Second Quantization-Based Methods in Quantum Chemistry*; Academic Press, 1981.

(9) Ortiz, J. V. Electron propagator theory: an approach to prediction and interpretation in quantum chemistry. *Wiley Interdisciplinary Reviews: Computational Molecular Science* **2013**, *3* (2), 123−142.

(10) Corzo, H. H.; Ortiz, J. V. Chapter Thirteen - Electron Propagator Theory: Foundations and Predictions. In *Advances in Quantum Chemistry*; Sabin, J. R.; Brändas, E. J., Eds.; Academic Press, 2017; Vol. *74*, pp 267−298.

(11) Ortiz, J. V. Chapter Four - Interpreting Bonding and Spectra With Correlated, One-Electron Concepts From Electron Propagator Theory. In *Annual Reports in Computational Chemistry*; Dixon, D. A., Ed.; Elsevier, 2017; Vol. *13*, pp 139−182.

(12) Ortiz, J. V. Dyson-orbital concepts for description of electrons in molecules. *J. Chem. Phys.* **2020**, *153* (7), No. 070902.

(13) von Niessen, W.; Schirmer, J.; Cederbaum, L. S. Computational methods for the one-particle Green's function. *Comput. Phys. Rep.* **1984**, *1*, 57−125.

(14) Ortiz, J. V. The Electron Propagator Picture of Molecular Electronic Structure. In *Computational Chemistry: Reviews of Current Trends*; Leszczynski, J., Ed.; World Scientific, 1997; Vol. *2*, pp 1−61.

(15) Koopmans, T. Über die Zuordnung von Wellenfunktionen und Eigenwerten zu den Einzelnen Elektronen Eines Atoms. *Physica* **1934**, *1* (1−6), 104−113.

(16) Hirata, S.; Hermes, M. R.; Simons, J.; Ortiz, J. V. General-Order Many-Body Green's Function Method. *J. Chem. Theory Comput.* **2015**, *11* (4), 1595−1606.

(17) Hirata, S.; Doran, A. E.; Knowles, P. J.; Ortiz, J. V. One-particle many-body Green's function theory: Algebraic recursive definitions, linked-diagram theorem, irreducible-diagram theorem, and general-order algorithms. *J. Chem. Phys.* **2017**, *147* (4), No. 044108.

(18) Møller, C.; Plesset, M. S. Note on an Approximation Treatment for Many-Electron Systems. *Phys. Rev.* **1934**, *46* (7), 618−622.
(19) Ohnishi, Y.-Y.; Ten-no, S. Explicitly correlated frequency-independent second-order green's function for accurate ionization energies. *J. Comput. Chem.* **2016**, *37*, 2447−2453.
(20) Pavošević, F.; Peng, C.; Ortiz, J. V.; Valeev, E. F. Communication: Explicitly correlated formalism for second-order single-particle Green's function. *J. Chem. Phys.* **2017**, *147* (12), No. 121101.
(21) Teke, N. K.; Pavošević, F.; Peng, C.; Valeev, E. F. Explicitly correlated renormalized second-order Green's function for accurate ionization potentials of closed-shell molecules. *J. Chem. Phys.* **2019**, *150* (21), No. 214103.
(22) Johnson, C. M.; Doran, A. E.; Ten-no, S. L.; Hirata, S. Monte Carlo explicitly correlated many-body Green's function theory. *J. Chem. Phys.* **2018**, *149* (17), No. 174112.
(23) Doran, A. E.; Hirata, S. Monte Carlo Second- and Third-Order Many-Body Green's Function Methods with Frequency-Dependent, Nondiagonal Self-Energy. *J. Chem. Theory Comput.* **2019**, *15* (11), 6097−6110.
(24) Ortiz, J. V. Partial third-order quasiparticle theory: Comparisons for closed-shell ionization energies and an application to the Borazine photoelectron spectrum. *J. Chem. Phys.* **1996**, *104* (19), 7599−7605.
(25) Ferreira, A. M.; Seabra, G.; Dolgounitcheva, O.; Zakrzewski, V. G.; Ortiz, J. V. Application and testing of diagonal, partial third-order electron propagator approximations. In *Quantum-Mechanical Prediction of Thermochemical Data*; Springer Dordrecht, 2001; Vol. *22*, pp 131−160.
(26) Ortiz, J. V. An efficient, renormalized self-energy for calculating the electron binding energies of closed-shell molecules and anions. *Int. J. Quantum Chem.* **2005**, *105*, 803−808.
(27) Corzo, H. H.; Galano, A.; Dolgounitcheva, O.; Zakrzewski, V. G.; Ortiz, J. V. NR2 and P3+: Accurate, Efficient Electron-Propagator Methods for Calculating Valence, Vertical Ionization Energies of Closed-Shell Molecules. *J. Phys. Chem. A* **2015**, *119* (33), 8813−8821.
(28) Baker, J.; Pickup, B. T. A method for molecular ionization potentials. *Chem. Phys. Lett.* **1980**, *76*, 537−541.
(29) Weikert, H. G.; Meyer, H. D.; Cederbaum, L. S.; Tarantelli, F. Block Lanczos and many-body theory: application to the one-particle Green function. *J. Chem. Phys.* **1996**, *104*, 7122−7138.
(30) Desjardins, S. J.; Bawagan, A. D. O.; Liu, Z. F.; Tan, K. H.; Wang, Y.; Davidson, E. R. Correlation states of ethylene. *J. Chem. Phys.* **1995**, *102*, 6385−6399.
(31) Cederbaum, L. S.; Domcke, W.; Schirmer, J.; Von Niessen, W. Correlation effects in the ionization of molecules: breakdown of the molecular orbital picture. *Adv. Chem. Phys.* **1986**, *65*, 115−159.
(32) Schirmer, J.; Cederbaum, L. S. The two-particle-hole Tamm-Dancoff approximation (2ph-TDA) equations for closed-shell atoms and molecules. *J. Phys. B* **1978**, *11*, 1889−1900.
(33) Schirmer, J.; Cederbaum, L. S.; Walter, O. New approach to the one-particle Green's function for finite Fermi systems. *Phys. Rev. A* **1983**, *28* (3), 1237−1259.
(34) Ortiz, J. V. The electron propagator picture of molecular electronic structure. *Comput. Chem. (Singapore)* **1997**, *2*, 1−61.
(35) Ortiz, J. V. A nondiagonal, renormalized extension of partial third-order quasiparticle theory: comparisons for closed-shell ionization energies. *J. Chem. Phys.* **1998**, *108*, 1008−1014.
(36) Ortiz, J. V. Toward an exact one-electron picture of chemical bonding. *Adv. Quantum Chem.* **1999**, *35*, 33−52.
(37) Reining, L. The GW approximation: content, successes and limitations. *Wiley Interdiscip. Rev.: Comput. Mol. Sci.* **2018**, *8* (3), No. e1344.
(38) Knight, J. W.; Wang, X.; Gallandi, L.; Dolgounitcheva, O.; Ren, X.; Ortiz, J. V.; Rinke, P.; Körzdörfer, T.; Marom, N. Accurate Ionization Potentials and Electron Affinities of Acceptor Molecules III: A Benchmark of GW Methods. *J. Chem. Theory Comput.* **2016**, *12* (2), 615−626.
(39) Yeager, D. L. The multiconfigurational spin-tensor electron propagator method (MCSTEP). *Adv. Quantum Chem.* **2005**, *50*, 289−313.
(40) Chatterjee, K.; Sokolov, A. Y. Second-Order Multireference Algebraic Diagrammatic Construction Theory for Photoelectron Spectra of Strongly Correlated Systems. *J. Chem. Theory Comput.* **2019**, *15* (11), 5908−5924.
(41) Opoku, E.; Pawłowski, F.; Ortiz, J. V. A new generation of diagonal self-energies for the calculation of electron removal energies. *J. Chem. Phys.* **2021**, *155* (20), No. 204107.
(42) Opoku, E.; Pawłowski, F.; Ortiz, J. V. Electron Propagator Self-Energies versus Improved GW100 Vertical Ionization Energies. *J. Chem. Theory Comput.* **2022**, *18* (8), 4927−4944.
(43) Opoku, E.; Pawłowski, F.; Ortiz, J. V. A new generation of non-diagonal, renormalized self-energies for calculation of electron removal energies. *J. Chem. Phys.* **2023**, *159* (12), No. 124109.
(44) Opoku, E.; Pawłowski, F.; Ortiz, J. V. New-Generation Electron-Propagator Methods for Calculations of Electron Affinities and Ionization Energies: Tests on Organic Photovoltaic Molecules. *J. Chem. Theory Comput.* **2024**, *20* (1), 290−306.
(45) Opoku, E.; Pawłowski, F.; Ortiz, J. V. New-Generation Electron-Propagator Methods for Molecular Electron-Binding Energies. *J. Phys. Chem. A* **2024**, *128* (8), 1399−1416.
(46) Mulliken, R. S. New electroaffinity scale; together with data on valence states and on valence ionization potentials and electron affinities. *J. Chem. Phys.* **1934**, *2*, 782−793.
(47) Simons, J. Molecular Anions Perspective. *J. Phys. Chem. A* **2023**, *127* (18), 3940−3957.
(48) Jordan, K. D.; Wang, F. Theory of dipole-bound anions. *Annu. Rev. Phys. Chem.* **2003**, *54*, 367−396.
(49) Ortiz, J. V. Vertical and adiabatic ionization energies of NH_4^- isomers via electron propagator theory and many body perturbation theory calculations with large basis sets. *J. Chem. Phys.* **1987**, *87* (6), 3557−3562.
(50) Gutowski, M.; Simons, J.; Hernandez, R.; Taylor, H. L. "Double-Rydberg" molecular anions. *J. Phys. Chem.* **1988**, *92* (22), 6179−6182.
(51) Díaz-Tinoco, M.; Ortiz, J. V. Double Rydberg anions with solvated ammonium kernels: Electron binding energies and Dyson orbitals. *J. Chem. Phys.* **2019**, *151* (5), No. 054301.
(52) Díaz-Tinoco, M. A.; Ortiz, J. V. Dyson Orbitals and Double Rydberg Anions: Methylated, Annulated and Paramagnetic. *J. Phys. Chem. A* **2019**, *123*, 10961−10967.
(53) Opoku, E.; Pawłowski, F.; Ortiz, J. V. Electron binding energies and Dyson orbitals of $O_nH2_{n+1}^{+,0,-}$ clusters: Double Rydberg anions, Rydberg radicals, and micro-solvated hydronium cations. *J. Chem. Phys.* **2021**, *154* (23), No. 234304.
(54) Opoku, E.; Pawłowski, F.; Ortiz, J. V. Double Rydberg anions, Rydberg radicals and micro-solvated cations with ammonium−water kernels. *Phys. Chem. Chem. Phys.* **2022**, *24* (30), 18347−18360.
(55) Richard, R. M.; Marshall, M. S.; Dolgounitcheva, O.; Ortiz, J. V.; Brédas, J.-L.; Marom, N.; Sherrill, C. D. Accurate Ionization Potentials and Electron Affinities of Acceptor Molecules I. Reference Data at the CCSD(T) Complete Basis Set Limit. *J. Chem. Theory Comput.* **2016**, *12* (2), 595−604.
(56) Pickup, B. T.; Goscinski, O. Direct calculation of ionization energies. *I. Closed shells. Mol. Phys.* **1973**, *26*, 1013−1035.
(57) Goscinski, O.; Lukman, B. Moment-conserving decoupling of Green functions via Pade approximants. *Chem. Phys. Lett.* **1970**, *7*, 573−576.
(58) Manne, R. A completeness theorem for operator spaces. *Chem. Phys. Lett.* **1977**, *45* (3), 470−472.
(59) Löwdin, P. O. Studies in perturbation theory. X. Lower bounds to energy eigenvalues in perturbation-theory ground state. *Phys. Rev.* **1965**, *139* (2), A357−A372.
(60) Ortiz, J. V. Improved electron propagator methods: an investigation of the carbon tetraatomic neutral molecule, mononegative ion, and monopositive ion (C_4, C_4^-, and C_4^+). *J. Chem. Phys.* **1993**, *99* (9), 6716−6726.

https://doi.org/10.1021/acs.jpca.4c02050
J. Phys. Chem. A 2024, 128, 4730−4749

(61) Åberg, T. Theory of x-ray satellites. *Phys. Rev.* **1967**, *156* (1), 35−41.
(62) Bintrim, S. J.; Berkelbach, T. C. Full-frequency GW without frequency. *J. Chem. Phys.* **2021**, *154* (4), No. 041101.
(63) Rowe, D. J. Equations-of-Motion Method and the Extended Shell Model. *Rev. Mod. Phys.* **1968**, *40* (1), 153−166.
(64) WebBook, N. C. *NIST Standard Reference Database Number 69*. https://doi.org/10.18434/T4D303.
(65) Raghavachari, K.; Trucks, G. W.; Pople, J. A.; Head-Gordon, M. A fifth-order perturbation comparison of electron correlation theories. *Chem. Phys. Lett.* **1989**, *157* (6), 479−483.
(66) Kendall, R. A.; Dunning, T. H.; Harrison, R. J. Electron affinities of the first-row atoms revisited. Systematic basis sets and wavefunctions. *J. Chem. Phys.* **1992**, *96* (9), 6796−6806.
(67) Ma, F.; Wang, Z.; Guo, M.; Wang, F. Approximate equation-of-motion coupled-cluster methods for electron affinities of closed-shell molecules. *J. Chem. Phys.* **2020**, *152* (12), No. 124111.
(68) Jagau, T. C. Non-iterative triple excitations in equation-of-motion coupled-cluster theory for electron attachment with applications to bound and temporary anions. *J. Chem. Phys.* **2018**, *148* (2), No. 024104.
(69) Ermis, B.; Ekinci, E.; Bozkaya, U. State-Of-The-Art Computations of Vertical Electron Affinities with the Extended Koopmans' Theorem Integrated with the CCSD(T) Method. *J. Chem. Theory Comput* **2021**, *17* (12), 7648−7656.
(70) Curtiss, L. A.; Redfern, P. C.; Raghavachari, K.; Pople, J. A. Assessment of Gaussian-2 and density functional theories for the computation of ionization potentials and electron affinities. *J. Chem. Phys.* **1998**, *109* (1), 42−55.
(71) Rienstra-Kiracofe, J. C.; Tschumper, G. S.; Schaefer, H. F., 3rd; Nandi, S.; Ellison, G. B. Atomic and molecular electron affinities: photoelectron experiments and theoretical computations. *Chem. Rev.* **2002**, *102* (1), 231−282.
(72) Karton, A. Tightening the Screws: The Importance of Tight d Functions in Coupled-Cluster Calculations up to the CCSDT(Q) Level. *J. Phys. Chem. A* **2022**, *126* (45), 8544−8555.
(73) Frisch, M. J.; Trucks, G. W.; Schlegel, H. B.; Scuseria, G. E.; Robb, M. A.; Cheeseman, J. R.; Scalmani, G.; Barone, V.; Petersson, G. A.; Nakatsuji, H. et al. *Gaussian development version, Revision I.14*; Gaussian Inc., 2018.
(74) Karton, A. A computational chemist's guide to accurate thermochemistry for organic molecules. *WIREs Computational Molecular Science* **2016**, *6* (3), 292−310.

https://doi.org/10.1021/acs.jpca.4c02050
J. Phys. Chem. A 2024, 128, 4730−4749

Appendix K

E. Opoku, F. Pawłowski and J. V. Ortiz, "Electron Binding Energies of Open−Shell Species from Diagonal Electron−Propagator Self−Energies with Unrestricted Hartree−Fock Spin−Orbitals", *J. Phys. Chem. A*, 128, 7311–7330 (2024)

THE JOURNAL OF PHYSICAL CHEMISTRY A
A JOURNAL OF THE AMERICAN CHEMICAL SOCIETY

pubs.acs.org/JPCA Article

Electron Binding Energies of Open-Shell Species from Diagonal Electron-Propagator Self-Energies with Unrestricted Hartree−Fock Spin−Orbitals

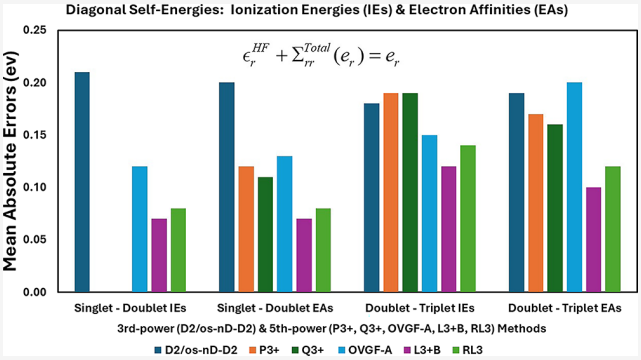
Published as part of The Journal of Physical Chemistry A virtual special issue "Rodney J. Bartlett Festschrift".

Ernest Opoku, Filip Pawłowski, and J. V. Ortiz*

Cite This: *J. Phys. Chem. A* 2024, 128, 7311−7330 Read Online

ACCESS | Metrics & More | Article Recommendations | Supporting Information

ABSTRACT: For closed-shell molecules, valence electron binding energies may be calculated accurately and efficiently with *ab initio* electron-propagator methods that have surpassed their predecessors. Advantageous combinations of accuracy and efficiency range from cubically scaling methods with mean errors of 0.2 eV to quintically scaling methods with mean errors of 0.1 eV or less. The diagonal self-energy approximation in the canonical Hartree−Fock basis is responsible for the enhanced efficiency of several methods. This work examines the predictive capabilities of diagonal self-energy approximations when they are generalized to the canonical spin−orbital basis of unrestricted Hartree−Fock (UHF) theory. Experimental data on atomic electron binding energies and high-level, correlated calculations in a fixed basis for a set of open-shell molecules constitute standards of comparison. A review of the underlying theory and analysis of numerical errors lead to several recommendations for the calculation of electron binding energies: (1) In calculations that employ the diagonal self-energy approximation, Koopmans's identity for UHF must be qualitatively correct. (2) Closed-shell reference states are preferable to open-shell reference states in calculations of molecular ionization energies and electron affinities. (3) For molecular electron binding energies between doublets and triplets, calculations of electron detachment energies are more accurate and efficient than calculations of electron attachment energies. When these recommendations are followed, mean absolute errors increase by approximately 0.05 eV with respect to their counterparts obtained with closed-shell reference orbitals.



INTRODUCTION

Building on foundations laid over several decades,[1−3] *ab initio* electron-propagator theory and computational practice continue to advance on several fronts. For valence electron-binding energies of closed-shell molecules and anions, several methods have attained mean absolute errors (MAEs) that approach chemical accuracy, or 0.05 eV.[4−11] These innovations have reduced computational bottlenecks to quintic arithmetic scaling. When mean average errors of 0.2 eV suffice to interpret experiments, cubically scaling methods may be employed. Deeper understanding of the convergence of perturbative approaches to exact propagators has provided a roadmap to convergent, infinite-order strategies.[12−14] Monte Carlo algorithms for the evaluation of low-order self-energies have offered a promising alternative route to applications on large systems.[15,16] Explicitly correlated approaches have accelerated the exhaustion of basis-set effects.[17−19] Interest in methods employing multiconfigurational reference states[20] has been revived and extended with intricate perturbative improvements.[21−25] More efficient implementations of non-Dyson (see below) variants of single-reference, algebraic-diagrammatic-construction self-energies[26] have become available to general users.[25,27,28]

Ab initio electron-propagator methods conserve the chief features of the molecular orbital picture of electronic structure.[29−33] Electron-binding energies emerge as eigenvalues of a one-electron operator whose systematically improvable terms are easily related to qualitative concepts. From the same calculations, eigenfunctions provide Dyson orbitals, transition probabilities and their contributions to reference state total energies and density matrices. Transparent interpretations follow from a complete absence of adjustable parameters in

Received: June 28, 2024
Revised: July 29, 2024
Accepted: July 31, 2024
Published: August 14, 2024



ACS Publications © 2024 American Chemical Society

https://doi.org/10.1021/acs.jpca.4c04318
J. Phys. Chem. A 2024, 128, 7311−7330

the optimization of reference orbitals and in the construction of correlated one-electron operators.[8]

Energies of electron detachment or attachment that connect closed-shell initial states to doublet final states have been the principal target of electron-propagator methods. Five levels of approximations that perturbatively refine the predictions of Koopmans's identity[34] are integrated into widely applied software.

Level 1: Nondiagonal Renormalized Self-Energy Matrices. Diagonalization of a large Hermitian matrix is necessary in the most accurate and computationally intensive methods. The number of second-quantized operator products consisting of n simple creators and n-1 simple annihilators determines the rank of this matrix. Its elements derive from superoperator expressions that involve a commutator with the second-quantized Hamiltonian. A superoperator metric that suffices to recover the Dyson equation also involves an anticommutator.[35] In this approach, electron detachment and attachment energies emerge from the same equations. Operators with n hole and n-1 particle indices are coupled to their counterparts with n particle and n-1 hole indices. The former operators describe final-state relaxation and correlation effects in calculations of electron detachment energies (EDEs). The latter operators capture the components of initial-state correlation that vanish with the loss of an electron. For electron attachments, the roles of the two types of operators switch. In non-Dyson approaches, the anticommutator is absent from the metric and a separation between electron detachment and electron attachment operators is in effect. Non-Dyson (nD) methods are a bridge between the Dyson equation and many-body methods in Hilbert space, such as equation-of-motion, coupled-cluster theory.[36] Dyson and nD methods in this level-1-category generate self-energy operators with nondiagonal matrices and renormalizations that include terms in all orders of the Møller-Plesset fluctuation potential.[37] To obtain useful predictions for the assignment of spectra, these methods demand algorithms with at least sixth-power arithmetic scaling. Examples include the third and fourth order algebraic diagrammatic constructions,[38] the nondiagonal, renormalized second order method,[39] and the Brueckner-Doubles-Triple-Field-Operator method.[40] The most recently developed non-diagonal, renormalized (NR) methods have noniterative, sixth-power arithmetic scaling.[7] One member of the latter set, NRL3, approaches chemical accuracy, with mean errors near 0.05 eV for valence electron-binding energies of closed-shell molecules.

Copious trials have revealed that the Dyson orbitals produced by NR methods for valence electron binding energies closely resemble canonical Hartree−Fock (CHF) orbitals.[7,41] Despite the interference between CHF orbitals allowed by these calculations of Dyson orbitals, little mixing typically occurs. In such cases, the Dyson orbital equals a single CHF orbital times a constant plus minor terms involving other CHF orbitals. This trend is more pronounced for electron attachments than for electron detachments in tests on organic photovoltaic molecules.[10]

Level 2: Diagonal Explicitly Renormalized Self-Energy Matrices. The above observations provide the foundation for the next class of methods wherein off-diagonal elements of the self-energy operator are set to zero.[4−11] These diagonal, renormalized (R) methods' electron binding energies seldom differ from their NR counterparts by more than a few hundredths of an eV. Their advantages include iterative, fifth-power arithmetic scaling factors. In several trials, the RL3 member of this set has attained mean errors of 0.1 eV or less. R methods do not allow interference between CHF orbitals in Dyson orbitals, but their probability factors agree closely with those obtained by NR methods. Some versions of slightly lower accuracy do not require full transformations of the electron repulsion integrals (ERIs) to the CHF basis for electron detachments. Repeated fifth-power contractions that pertain to renormalizations impose practical limits on calculations with large basis sets. In the family of GW methods,[42] the G_0W_0 members also neglect off-diagonal self-energy matrix elements, incorporate ring-diagram renormalizations without exchange and ignore ladder diagrams completely.

Level 3: Diagonal Approximately Renormalized Self-Energy Matrices. Approximately renormalized methods require fewer rate-limiting, fifth-power operations. This third class involves evaluation of only second-order and third-order self-energy terms. Ratios of these terms occur in equations that estimate higher-order corrections pertaining to renormalization. The latest versions of these approximately renormalized (denoted by +) self-energies typically achieve agreement with their R counterparts to within a few hundredths of an eV. This class includes the widely used outer valence Green's function[43,44] (OVGF) and renormalized partial third order[45,46] (P3+) methods, which now compete with more efficient and accurate alternatives. Its newest members include the Q3+ and L3+B methods.[4]

Level 4: Diagonal Third-Order Self-Energy Matrices. A seldom used, but conceptually instructive, fourth class of methods omits the renormalized estimates of the third class. Here, only second-order and third-order terms occur in the diagonal self-energy matrix. Because the approximate renormalizations demand only trivial calculations, the fourth-class methods have no computational advantages over third-class methods. Full third-order diagonal (D3) calculations generally produce poor predictions of electron binding energies. More recent derivations identify terms that lead to more accurate predictions and more efficient calculations. (Examples include the Q3 and L3 self-energies.) They also point the way to advantageous members of the level-3, approximately renormalized class.[4−11]

Level 5: Diagonal Second-Order Self-Energy Matrices. Some of the best compromises of accuracy and efficiency occur in the fifth class wherein only diagonal, second-order self-energy expressions appear. Full second-order (D2) results dependably overestimate corrections to occupied CHF orbital energies by 0.5 eV or more. With the neglect of same-spin terms, mean errors decline to 0.2 eV. Cubic arithmetic scaling factors pertain to the members of this class of methods. For a given CHF orbital, all necessary ERIs have one index in common. Therefore, only a fourth-power transformation to the CHF basis is necessary. The effective operator embodied by the opposite-spin, second-order method (os-D2) is especially easy to interpret in terms of orbital relaxation and pair-correlation effects. (The nD counterpart of os-D2, os-nD-D2, yields similar results.) Such calculations usually capture the essence of corrections to Koopmans's identity by relying on a balance between exchange and second-order opposite-spin correlation. For electron attachments, the cancellations that occur for electron detachments are generally absent, necessitating the use of higher levels of theory.

Classes two through five have hitherto employed the diagonal self-energy approximation in the closed-shell CHF orbital basis. In all cases considered so far, the initial states have been singlets

https://doi.org/10.1021/acs.jpca.4c04318
J. Phys. Chem. A 2024, 128, 7311−7330

and the final states have been doublets. Probability factors have provided diagnostics of the validity of these methods, for values below 0.85 indicate significant correlation-state (for example, two-hole-one-particle shakeup) character. No spin contamination is present. Prudent employment of these classes of methods requires that Koopmans's identity be qualitatively valid.

The most obvious path to generalizing diagonal self-energies to initial states with higher spin multiplicities employs the spin−orbital formulation of previously published work. Calculations based on unrestricted Hartree−Fock (UHF) spin−orbitals are almost as feasible as their closed-shell counterparts. (Early realizations of this approach began with calculations on the oxygen molecule in the 1970s.[47]) Koopmans's identity assumes that final states have a dominant Slater determinant in the initial state's orbital basis. Spin contamination produced by noninteger overlaps between occupied α and β spin−orbitals may occur in initial states. The frozen-orbital final-state determinants assumed in Koopmans's identity may exhibit even greater contamination, especially for electron attachments. Numerical tests of diagonal self-energies based on UHF spin−orbitals therefore should consider at best only those cases where Koopmans's identity is qualitatively valid. Most transitions from an open-shell initial state to low-spin final states do not fulfill this requirement. Consider, for example, electron detachment from the $^2B_1$ ground state of NH_2 to the $^1B_1$ final state of NH_2^+. Here, semioccupied $1b_1$ and $3a_1$ molecular orbitals generate two important determinants for the singlet.

The Theory section summarizes the theoretical and algorithmic characteristics shared by all methods that employ the diagonal self-energy approximation in the UHF spin−orbital basis. Techniques that lead to standard data and comparisons to results of electron-propagator calculations are presented in the Computational Methods section. Atomic spectra provide excellent standards for tests with large, flexible basis sets that reveal the intrinsic capabilities of self-energy approximations. High-level, correlated calculations obtained with a fixed basis set for a recently developed set of vertical electron-binding energies of open-shell molecules[48] constitute another standard. Comparisons of error measures generated by electron-propagator methods appear in the section on Results and Discussion. Recommendations for users of diagonal-self-energy methods identify the best compromises of accuracy and efficiency in the Conclusions section.

THEORY

Algorithms that execute *ab initio* electron propagator calculations may be based on the Dyson quasiparticle equation:

$$[\hat{F} + \hat{\Sigma}(E_p)]\varphi_p^{\text{Dyson}} = E_p\varphi_p^{\text{Dyson}} \tag{1}$$

The Fock and self-energy operators (with circumflex accents) act on the Dyson spin−orbital, φ_p^{Dyson}, corresponding to electron binding energy E_p. (Because the operator is energy-dependent, one is solving a pseudoeigenvalue equation.) Dyson spin−orbitals[49] are related to N-electron initial states and final states with $N \pm 1$ electrons through the following integrations over common spin−orbital (x) indices:

$$\varphi_p^{\text{Dyson}}(x_1) = \sqrt{N}\int dx_2dx_3dx_4\cdots dx_N \Psi_N(x_1, x_2, x_3, \cdots, x_N)\Psi^*_{N-1,p}(x_2, x_3, x_4, \cdots, x_N) \tag{2}$$

$$\varphi_p^{\text{Dyson}}(x_1) = \sqrt{N+1}\int dx_2dx_3dx_4\cdots dx_{N+1} \Psi^*_N(x_2, x_3, x_4, \cdots, x_{N+1})\Psi_{N+1,p}(x_1, x_2, x_3, \cdots, x_{N+1}) \tag{3}$$

In the first case, the p index refers to a transition to a final state with N-1 electrons. Equation 3 pertains to final states with N+1 electrons. Self-consistent solutions of the Dyson quasiparticle equation require the self-energy operator's energy argument to equal one of the pseudoeigenvalues. For electron detachments and attachments, the electron-binding energies are related respectively to differences of total energies by

$$E_p = E_N - E_{N-1} \tag{4}$$

$$E_p = E_{N+1} - E_N \tag{5}$$

The Fock operator has one-electron, Coulomb and exchange components, but the underlying one-electron reduced density matrix (1RDM) is not necessarily that of a Slater determinant. Most of the effects of orbital relaxation in final states and differential electron correlation reside in the self-energy operator of eq 1.

The Dyson quasiparticle equation is a formally exact generalization of the Hartree−Fock equations that produces improved electron binding energies and Dyson orbitals. It resembles the Kohn−Sham equations, but its operators may be *systematically* improved. The energy dependence of its self-energy operator permits the Dyson orbitals to have noninteger normalization integrals that are proportional to transition intensities.

Practical calculations employ an orthonormal basis of spin−orbitals, leading to the matrix equation

$$[\boldsymbol{F} + \Sigma(E_p)]\mathbf{C}_p = E_p\mathbf{C}_p \tag{6}$$

The $\mathbf{C}_p$ vector provides a linear combination of basis spin−orbitals that is proportional to φ_p^{Dyson}. In the CHF basis, the Fock matrix is separable into components produced by the uncorrelated and correlated contributions to the 1RDM. The former contribution is a diagonal matrix of orbital energies ($\boldsymbol{\epsilon}^{\text{HF}}$) and the latter is known as the energy-independent, or constant, self-energy, where

$$\boldsymbol{F} = \boldsymbol{\epsilon}^{\text{HF}} + \boldsymbol{\Sigma}(\infty) \tag{7}$$

The total self-energy matrix, $\boldsymbol{\Sigma}^{\text{Total}}(\text{E})$, is the sum of the constant and energy-dependent self-energy terms and therefore the matrix form of the Dyson quasiparticle equation reads

$$[\boldsymbol{\epsilon}^{\text{HF}} + \boldsymbol{\Sigma}^{\text{Total}}(E_p)]\mathbf{C}_p = E_p\mathbf{C}_p \tag{8}$$

When the absolute value of the energy increases without bound, the total self-energy matrix approaches its constant component, or

$$\lim_{|E|\to\infty} \boldsymbol{\Sigma}^{\text{Total}}(E) = \boldsymbol{\Sigma}(\infty) \tag{9}$$

The norms of the Dyson orbitals are known as probability factors, intensity factors or pole strengths. Probability factors (Π_p) are proportional to transition intensities in the sudden approximation. Numerical expressions involve derivatives of the self-energy matrix elements with respect to energy, where

$$\Pi_p \equiv \int |\varphi_p^{\text{Dyson}}(x)|^2 dx = \left[1 - \mathbf{C}_p^\dagger \frac{d\Sigma(E)}{dE}\bigg|_{E=E_p}\mathbf{C}_p\right]^{-1} \tag{10}$$

https://doi.org/10.1021/acs.jpca.4c04318
J. Phys. Chem. A 2024, 128, 7311−7330

Equation 8 has been solved for the outer-valence electron binding energies and Dyson orbitals of many closed-shell molecules and ions. For almost all transitions, the Dyson orbital approximately equals a CHF orbital times the square root of a probability factor. Neglect of off-diagonal elements in the total self-energy matrix is a good approximation that reduces arithmetic scaling bottlenecks by an order of magnitude. (See Tables 1 and 2.) The resulting diagonal self-energy methods

Table 1. Acronyms and Full Names of Electron-Propagator Methods with Diagonal Self-Energy Matrices

Acronym[a]	Full name
D2	Diagonal second order
os-D2	Opposite-spin D2
nD-D2	non-Dyson D2
os-nD-D2	Opposite-spin non-Dyson D2
D3	Diagonal third order
nD-D3	non-Dyson D3
OVGF	Outer-Valence Green's Function (Versions A, B and C)
nD-OVGF	non-Dyson OVGF (Versions A, B and C)
P3	Partial third order
P3+	Approximately renormalized partial third order
Q3	Quasiparticle third order
Q3+	Approximately renormalized quasiparticle third order
L3	Linear third order
nD-L3	non-Dyson L3
L3+	Approximately renormalized linear third order (Versions A, B and C)
nD-L3+	non-Dyson L3+ (Versions A, B and C)
RP3	Explicitly renormalized partial third order
RQ3	Explicitly renormalized quasiparticle third order
RL3	Explicitly renormalized linear third order
nD-RL3	non-Dyson RL3

[a]For new-generation methods in **bold type:** nD = non-Dyson; R = explicitly renormalized; + = approximately renormalized.

produce electron binding energies that seldom differ from their nondiagonal counterparts by more than 0.05 eV. In this simplified approach, one solves for the self-consistent electron binding energy e_r with

$$\epsilon_r^{\mathrm{HF}} + \Sigma_{rr}^{\mathrm{Total}}(e_r) = e_r \tag{11}$$

The consequent Dyson orbital also has a simplified form:

$$\varphi^{\mathrm{Dyson}} = \left[1 - \left.\frac{d\Sigma_{rr}(E)}{dE}\right|_{E=e_r}\right]^{-0.5} \varphi_r^{\mathrm{CHF}} = \Pi_{e_r}^{-0.5}\varphi_r^{\mathrm{CHF}} \tag{12}$$

Whereas there are many solutions of eq 11, only one produces a probability factor that exceeds 0.8 in a typical calculation. (In calculations that assume a diagonal total self-energy matrix, the sum of the probability factors for a given r equals unity.) Diagonal self-energy corrections shift CHF orbital energies and produce probability factors that are less than unity.

Calculations performed with self-energy matrices chosen to be diagonal in the CHF basis assume that Koopmans's identity is qualitatively correct for the final state. Probability factors that exceed 0.85 provide confirmation of this assumption. The diagonal class of self-energy approximations is not suitable for correlation states where, for example, Slater determinants with two-hole-one-particle configurations dominate. Because qualitatively correct low-spin final states with two or more open shells require more than one Slater determinant, they also are excluded from consideration below.

Table 2. Arithmetic Scaling and Transformed Electron-Repulsion-Integral Requirements of Electron-Propagator Methods[a]

Method Class	Methods[b]	Arithmetic bottleneck	Bottleneck Steps	Largest ERI[c] subset
Diagonal 2nd order	D2, **os-D2**	OV^2	N_E	O^2V^2
	RSPT2, nD-D2, **os-nD-D2**	OV^2	Noniterative	O^2V^2
Diagonal Post 2nd	RSPT3	OV^4	Noniterative	V^4
Order& Approximately	D3, OVGF	OV^4	N_E[d]	V^4
Renormalized (+)	IE: P3, P3+, **Q3, Q3+**	O^2V^3	Noniterative	OV^3
	EA: P3, P3+, **Q3, Q3+**	OV^4	N_E	V^4
	L3, L3+	OV^4	N_E[d]	V^4
Diagonal Post 2nd	**IE: RP3, RQ3**	O^2V^3	Noniterative	OV^3
Order& Explicitly	**EA: RP3, RQ3**	OV^4	N_IN_E	V^4
Renormalized (R)	**RL3**	OV^4	N_IN_E[d]	V^4

[a]O = # occupied orbitals, V = # virtual orbitals, N_E = energy iterations, N_I = inverse-expansion or linear-equation iterations for diagonal methods and Hamiltonian-vector multiplications for non-diagonal methods. [b]New methods in **bold type**. IE = ionization energy (electron detachment). EA = electron affinity (electron attachment). [c]ERI = electron repulsion integral. [d]Reduction by a factor of N_E occurs in non-Dyson (nD) versions for electron detachments.

COMPUTATIONAL METHODS

The new-generation diagonal self-energies, as outlined in Table 1, are available in the development version of Gaussian[50] using UHF-reference spin−orbitals. At the end of the self-consistent-field calculations, transformation to the UHF basis and storage on disk of ERIs take place. (Refer to Table 2 for the largest subsets of ERIs needed for each diagonal self-energy approximation.) There are internal options in the implementation that allow the user to invoke a method of choice from Table 1 and a spin−orbital window. Calculations of the self-energy matrix elements for orbitals of interest employ transformed ERIs and spin−orbital energies. Methods in Table 1 have been implemented with Abelian-symmetry-adapted, semidirect algorithms.

To benchmark the performance of the new methods, we have used a data set of vertical electron binding energies of open-shell atoms and molecules.[48] Table 3 exhibits experimental data on 19 EDEs of open-shell atoms and atomic anions. (Ionization energy data are available at physics.nist.gov; see the Wikipedia article for electron affinities and references therein.) CCSD(T) [coupled-cluster theory with full single and double substitutions and approximate triple substitutions[51]] total energy differences obtained with various basis sets agree closely with experiments. The CCSD(T) calculations employ UHF spin−orbitals for all open-shell states; calculations on closed-shell final states use restricted Hartree−Fock orbitals. Spin contamination in reference determinants is minor in all cases. The difference between the expectation value of S^2 in the reference determinant

https://doi.org/10.1021/acs.jpca.4c04318
J. Phys. Chem. A 2024, 128, 7311−7330

Table 3. Electron Detachment Energies (eV) of 19 Open-Shell Atomic Species, Ground and Final States, Basis Sets, Spin Contamination, Experimental Standards and Many-Body Calculations (eV)[a]

Ground States	Final States	Basis Sets	$\langle \Delta S^2 \rangle_G$	$\langle \Delta S^2 \rangle_F$	Experiment	ΔCCSD(T)	KT	D2	os-nD-D2	OVGF-A	P3+	Q3+	L3+B	nD-L3+B	RL3	nD-RL3
^{2}Li	^{1}Li$^+$	cc-pV5Z	0.00	0.00	5.39	5.34	5.34	5.37	5.36	5.38	5.37	5.37	5.38	5.38	5.38	5.38
^{2}B	^{1}B$^+$	cc-pV6Z	0.01	0.01	8.30	8.24	8.68	8.50	8.59	8.45	8.34	8.28	8.41	8.41	8.25	8.24
^{3}B$^-$	^{2}B	aug-cc-pV5Z	0.01	0.01	0.28	0.25	0.78	0.33	0.79	0.34	0.25	0.21	0.35	0.33	0.20	0.18
^{3}C	^{2}C$^+$	cc-pV6Z	0.01	0.01	11.26	11.22	11.95	11.41	11.78	11.37	11.26	11.20	11.33	11.32	11.18	11.17
^{4}C$^-$	^{3}C	aug-cc-pV5Z	0.01	0.01	1.26	1.24	2.13	1.07	1.98	1.34	1.21	1.20	1.31	1.29	1.17	1.15
^{4}N	^{3}N$^+$	cc-pV6Z	0.01	0.01	14.53	14.51	15.53	14.55	15.27	14.61	14.49	14.44	14.55	14.54	14.43	14.42
^{3}O	^{4}O$^+$	cc-pV6Z	0.01	0.01	13.62	13.56	14.20	13.19	13.31	13.50	13.41	13.40	13.52	13.51	13.50	13.49
^{2}O$^-$	^{3}O	aug-cc-pV5Z	0.01	0.01	1.46	1.42	2.17	0.19	0.90	1.71	1.54	1.76	1.74	1.73	1.45	1.44
^{2}F	^{3}F$^+$	cc-pV6Z	0.00	0.00	17.42	17.39	18.50	16.60	17.15	17.42	17.27	17.30	17.35	17.34	17.31	17.30
^{2}Na	^{1}Na$^+$	cc-pV5Z	0.00	0.00	5.14	5.08	4.96	5.03	4.99	5.07	5.03	5.04	5.05	5.05	5.05	5.05
^{2}Al	^{1}Al$^+$	cc-pV5Z	0.00	0.02	5.99	5.97	5.95	5.99	6.04	5.99	5.91	5.86	5.98	5.98	5.91	5.91
^{3}Al$^-$	^{2}Al	aug-cc-pV5Z	0.02	0.02	0.43	0.44	0.61	0.54	0.73	0.53	0.45	0.40	0.50	0.50	0.41	0.40
^{3}Si	^{2}Si$^+$	cc-pV5Z	0.02	0.02	8.15	8.14	8.20	8.19	8.29	8.19	8.09	8.05	8.17	8.17	8.08	8.08
^{4}Si$^-$	^{3}Si	aug-cc-pV5Z	0.00	0.00	1.39	1.41	1.69	1.49	1.78	1.48	1.42	1.37	1.47	1.46	1.38	1.37
^{4}P	^{3}P$^+$	cc-pV5Z	0.00	0.00	10.49	10.51	10.67	10.59	10.74	10.58	10.49	10.44	10.55	10.55	10.46	10.45
^{3}P$^-$	^{4}P	aug-cc-pV5Z	0.03	0.01	0.75	0.71	0.67	0.59	0.62	0.61	0.62	0.56	0.71	0.71	0.66	0.66
^{3}S	^{4}S$^+$	cc-pV5Z	0.01	0.01	10.36	10.28	10.33	10.23	10.28	10.23	10.20	10.11	10.29	10.29	10.25	10.25
^{2}S$^-$	^{3}S	aug-cc-pV5Z	0.01	0.01	2.08	2.06	2.33	1.80	2.00	1.97	2.03	1.97	2.08	2.07	2.03	2.02
^{2}Cl	^{3}Cl$^+$	cc-pV5Z	0.01	0.01	12.97	12.91	13.08	12.81	12.94	12.85	12.86	12.77	12.92	12.91	12.89	12.89
MSE						−0.03	0.34	−0.15	0.12	0.02	−0.06	−0.08	0.02	0.01	−0.07	−0.07
σ						0.03	0.37	0.35	0.35	0.11	0.07	0.11	0.09	0.08	0.03	0.04
MAE						0.04	0.38	0.23	0.29	0.09	0.07	0.11	0.07	0.06	0.07	0.07
Max. Error						0.08	1.08	1.27	0.73	0.25	0.21	0.30	0.28	0.27	0.12	0.13

[a]Error measures refer to experimental standards.

https://doi.org/10.1021/acs.jpca.4c04318
J. Phys. Chem. A 2024, 128, 7311−7330

Table 4. Electron Attachment Energies (eV) of 12 Open-Shell Atomic Cations, Ground and Final States, Basis Sets, Spin Contamination, Experimental Standards and Many-Body Calculations (eV)[a]

Ground States	Final States	Basis Sets	$<\Delta S^2>_G$	$<\Delta S^2>_F$	Experiment	ΔCCSD(T)	KT	D2	os-nD-D2	OVGF-A	P3+	Q3+	L3+B	nD-L3+B	RL3	nD-RL3
$^2Be^+$	^1Be	cc-pV5Z	0.00	0.05	9.323	9.297	7.78	8.99	8.97	9.07	9.08	9.08	9.08	9.08	9.27	9.27
$^2C^+$	^3C	cc-pV6Z	0.01	0.01	11.260	11.220	9.86	11.23	10.51	11.19	11.38	11.35	11.22	11.23	11.33	11.35
$^3N^+$	^4N	cc-pV6Z	0.01	0.01	14.534	14.513	12.53	14.47	13.22	14.40	14.63	14.59	14.44	14.46	14.58	14.60
$^4O^+$	^3O	cc-pV6Z	0.01	0.11	13.618	13.563	10.40	13.08	12.70	13.05	13.27	13.24	13.18	13.19	13.41	13.42
$^3F^+$	^2F	cc-pV6Z	0.01	0.07	17.422	17.388	13.43	17.02	16.08	16.83	17.09	17.08	17.01	17.02	17.23	17.24
$^2Ne^+$	^1Ne	cc-pV6Z	0.00	0.05	21.565	21.567	16.85	21.40	19.81	20.97	21.27	21.29	21.21	21.23	21.40	21.42
$^2Mg^+$	^1Mg	cc-pV5Z	0.00	0.05	7.646	7.531	6.40	7.47	7.40	7.47	7.48	7.48	7.48	7.48	7.61	7.61
$^2Si^+$	^3Si	cc-pV5Z	0.02	0.02	8.152	8.141	7.15	8.13	7.66	8.08	8.18	8.16	8.10	8.11	8.16	8.17
$^3P^+$	^4P	cc-pV5Z	0.01	0.01	10.487	10.507	9.23	10.56	9.80	10.44	10.58	10.56	10.47	10.49	10.54	10.56
$^4S^+$	^3S	cc-pV5Z	0.00	0.06	10.360	10.277	8.35	10.20	9.94	10.07	10.28	10.24	10.17	10.18	10.29	10.31
$^3Cl^+$	^2Cl	cc-pV5Z	0.01	0.05	12.968	12.915	10.65	12.92	12.36	12.70	12.94	12.90	12.82	12.84	12.94	12.96
$^2Ar^+$	^1Ar	cc-pV5Z	0.01	0.04	15.759	15.759	13.23	15.89	15.02	15.55	15.83	15.79	15.69	15.72	15.79	15.81
MSE						−0.03	−2.27	−0.15	−0.80	−0.27	−0.09	−0.11	−0.19	−0.17	−0.05	−0.03
σ						0.04	1.12	0.19	0.44	0.20	0.17	0.16	0.14	0.14	0.09	0.10
MAE						0.04	2.27	0.18	0.80	0.27	0.16	0.16	0.19	0.17	0.08	0.08
Max. Error						0.12	4.71	0.54	1.75	0.60	0.35	0.38	0.44	0.43	0.21	0.20

[a]Error measures refer to the experimental standards.

https://doi.org/10.1021/acs.jpca.4c04318
J. Phys. Chem. A 2024, 128, 7311−7330

Table 5. Electron Attachment Energies (eV) of 11 Open-Shell Atoms, Ground and Final States, Basis Sets, Spin Contamination, Experimental Standards and Many-Body Calculations (eV)[a]

Ground States	Final States	$\langle \Delta S^2 \rangle_G$	$\langle \Delta S^2 \rangle_F$	Experiment	ΔCCSD(T)	KT	D2	os-nD-D2	OVGF-A	P3+	Q3+	L3+B	nD-L3+B	RL3	nD-RL3
aug-cc-pV5Z basis set															
^{2}Li	^{1}Li$^-$	0.00	0.64	0.618	0.62	−0.12	0.16	0.16	0.19	0.19	0.19	0.19	0.19	0.32	0.32
^{2}B	^{3}B$^-$	0.01	0.01	0.280	0.25	−0.59	−0.17	−0.40	−0.16	−0.11	−0.12	−0.15	−0.15	−0.03	−0.03
^{3}C	^{4}C$^-$	0.01	0.01	1.262	1.24	−0.44	0.69	−0.05	0.68	0.81	0.79	0.72	0.73	0.94	0.95
^{3}O	^{2}O$^-$	0.01	0.55	1.461	1.42	−1.57	−0.10	−0.53	−0.16	−0.05	−0.05	−0.07	−0.07	0.17	0.18
^{2}F	^{1}F$^-$	0.00	0.31	3.401	3.40	−0.92	2.11	1.00	1.83	2.01	2.06	2.01	2.01	2.32	2.33
^{2}Na	^{1}Na$^-$	0.00	0.66	0.548	0.54	−0.10	0.15	0.15	0.17	0.17	0.17	0.17	0.17	0.28	0.28
^{2}Al	^{3}Al$^-$	0.02	0.02	0.433	0.44	−0.25	0.21	−0.04	0.20	0.26	0.24	0.22	0.22	0.31	0.32
^{3}Si	^{4}Si$^-$	0.02	0.02	1.390	1.41	0.28	1.25	0.66	1.18	1.30	1.28	1.22	1.23	1.35	1.36
^{4}P	^{3}P$^-$	0.00	0.43	0.747	0.71	−0.75	0.22	0.07	0.15	0.27	0.25	0.22	0.22	0.35	0.36
^{3}S	^{2}S$^-$	0.01	0.23	2.077	2.06	−0.03	1.68	1.25	1.53	1.72	1.69	1.63	1.65	1.81	1.82
^{2}Cl	^{1}Cl$^-$	0.01	0.12	3.613	3.50	1.11	3.46	2.69	3.17	3.42	3.39	3.31	3.33	3.48	3.50
MSE					−0.02	−1.75	−0.56	−0.99	−0.64	−0.53	−0.54	−0.58	−0.57	−0.41	−0.40
σ					0.03	1.11	0.43	0.62	0.47	0.45	0.43	0.43	0.43	0.38	0.38
MAE					0.03	1.75	0.56	0.99	0.64	0.53	0.54	0.58	0.57	0.41	0.40
Max. Error					0.12	4.32	1.56	2.40	1.62	1.51	1.51	1.53	1.53	1.29	1.29
cc-pV5Z basis set															
^{2}Li	^{1}Li$^-$	0.00	0.27	0.618	0.58	−0.35	0.22	0.22	0.27	0.27	0.27	0.27	0.27	0.47	0.47
^{2}B	^{3}B$^-$	0.01	0.01	0.280	0.11	−0.98	−0.12	−0.59	−0.12	0.00	−0.02	−0.09	−0.08	0.07	0.08
^{3}C	^{4}C$^-$	0.01	0.01	1.262	1.11	−0.68	0.79	−0.17	0.76	0.93	0.91	0.81	0.83	1.01	1.03
^{3}O	^{2}O$^-$	0.01	0.21	1.461	1.15	−2.36	0.34	−0.42	0.19	0.39	0.40	0.35	0.36	0.61	0.62
^{2}F	^{1}F$^-$	0.00	0.14	3.401	3.15	−1.33	2.51	1.13	2.12	2.36	2.41	2.35	2.36	2.60	2.61
^{2}Na	^{1}Na$^-$	0.00	0.31	0.548	0.52	−0.27	0.23	0.21	0.26	0.26	0.26	0.26	0.26	0.43	0.43
^{2}Al	^{3}Al$^-$	0.02	0.02	0.433	0.33	−0.47	0.23	−0.13	0.21	0.30	0.28	0.23	0.24	0.33	0.33
^{3}Si	^{4}Si$^-$	0.02	0.02	1.390	1.32	0.18	1.26	0.61	1.17	1.31	1.29	1.22	1.23	1.32	1.33
^{4}P	^{3}P$^-$	0.00	0.13	0.747	0.53	−1.19	0.31	0.10	0.20	0.39	0.35	0.30	0.32	0.45	0.46
^{3}S	^{2}S$^-$	0.01	0.11	2.077	1.93	−0.20	1.76	1.27	1.57	1.80	1.75	1.69	1.71	1.84	1.86
^{2}Cl	^{1}Cl$^-$	0.01	0.08	3.613	3.52	1.04	3.48	2.68	3.16	3.44	3.39	3.31	3.33	3.45	3.47
MSE					−0.14	−2.04	−0.44	−0.99	−0.55	−0.40	−0.41	−0.47	−0.46	−0.30	−0.28
σ					0.09	1.20	0.29	0.59	0.36	0.32	0.30	0.30	0.30	0.26	0.26
MAE					0.14	2.04	0.44	0.99	0.55	0.40	0.41	0.47	0.46	0.30	0.28
Max. Error					0.31	4.73	1.13	2.27	1.28	1.07	1.06	1.11	1.11	0.85	0.84

[a]Error measures refer to the experimental standards.

https://doi.org/10.1021/acs.jpca.4c04318
J. Phys. Chem. A 2024, 128, 7311−7330

and the exact eigenvalue of S^2 defines the degree of spin contamination. ($\Delta S^2 = < S^2>_{exact} - < S^2>_{UHF}$). Whereas spin-contamination in ground (reference) state determinants is denoted by $< \Delta S^2>_G$, its counterpart for frozen-orbital, final-state determinants assumed in Koopmans's identity is denoted by $< \Delta S^2>_F$ in the Tables. Electron propagator calculations of EDEs employ the same basis sets; error measures with respect to experimental data also appear in Table 3. Tables 4 and 5 show experimental and ΔCCSD(T) data for 23 electron attachment energies (EAEs) of open-shell atoms and atomic cations. Electron propagator and ΔCCSD(T) results with the same basis sets appear in Tables 4, 5 and 6 with their corresponding error measures. All electrons are included in correlation treatments in the open-shell atomic species for ΔCCSD(T) and electron-propagator calculations.

A previous study of many-body methods provides geometries of the 40 open-shell molecules in the OM-40 set.[48] Tables 7-17 present reference data and error measures for the molecular set. Whereas the original OM-40 study presented separate data for cases with low and high spin contamination in reference states, no separations are considered here. The ΔCCSD(T) vertical ionization energies (IEs) and electron affinities (EAs) have been calculated with ROHF (restricted open-shell Hartree−Fock) and UHF reference states. Our ROHF- based ΔCCSD(T) IEs and EAs are in good agreement with the previously published ones.[48] Because the focus of the current manuscript concerns UHF spin−orbitals, we have created UHF-based ΔCCSD(T) IE and EA standards for the OM-40 data set. All calculations on the OM-40 set employed the aug-cc-pVDZ basis set[52] that was used previously in creating the ROHF-based ΔCCSD(T) IE and EA standards.[48] There are only negligible differences between ROHF and UHF-based ΔCCSD(T) IE and EA results. Twenty-two of the 40 open-shell molecules have high spin contamination in their ground states ($\Delta S^2 \geq 0.1$) whereas the remaining 18 have negligible spin contamination. We omit core orbitals in all ΔCCSD(T) and electron-propagator calculations on the open-shell molecules.

Electron propagator calculations employed the same basis sets that were used in generating ΔCCSD(T) values. For EAs of the 40 open-shell molecules (OM-40), four cases (CH_3, NO, NS and O_2) were excluded from the original test set because they do not have vertically bound, anionic, final states at the ΔCCSD-(T)/aug-cc-pVDZ level.

RESULTS AND DISCUSSION

Atomic Electron Binding Energies. *Electron Detachment Energies of Atoms and Anions.* Experimental data on EDEs of 7 atomic anions and 12 atoms constitute the standard for many-body calculations. (See Table 3.) All electron-propagator reference states have nonsinglet multiplicities. Differences between UHF expectation values of S^2 and exact values are small. The Supporting Information contains a full set of data that includes all four second-order options and all three OVGF methods. D2 and os-nD-D2 represent the former set. The A variant of OVGF produces lower error measures than the B and C options in most cases.

With the use of basis sets of at least quintuple-ζ quality, ΔCCSD(T) yields an MAE (0.04 eV) that achieves chemical accuracy (1 kcal/mol). Basis sets include diffuse augmentations when the reference state is anionic. With the same basis sets, Koopmans's theorem (KT) results generate an MAE close to 0.4 eV. D2's MAE is closer to 0.2 eV. The os-nD-D2 method has no advantage over D2 for open-shell initial states, for its MAE is 0.3

Table 6. Electron Detachment Energies (eV) of 11 Open-Shell Atomic Anions, Ground and Final States, Basis Sets, Spin Contamination, Experimental Standards and Many-Body Calculations (eV)[a]

Final States	Ground States	Basis Sets	$<\Delta S^2>_F$	$<\Delta S^2>_G$	Experiment	ΔCCSD(T)	KT	D2	os-nD-D2	OVGF-A	P3+	Q3+	L3+B	nD-L3+B	RL3	nD-RL3
^{2}Li	^{1}Li$^-$	aug-cc-pV5Z	-	-	0.618	0.62	0.39	0.51	0.51	0.52	0.46	0.43	0.54	0.54	0.44	0.44
^{2}B	^{3}B$^-$	aug-cc-pV5Z	0.01	0.01	0.280	0.25	0.78	0.33	0.79	0.34	0.25	0.21	0.35	0.33	0.20	0.18
^{3}C	^{4}C$^-$	aug-cc-pV5Z	0.01	0.01	1.262	1.24	2.13	1.07	1.98	1.34	1.21	1.20	1.31	1.29	1.17	1.15
^{3}O	^{2}O$^-$	aug-cc-pV5Z	0.01	0.02	1.461	1.42	2.17	0.17	0.87	1.69	1.47	1.70	1.69	1.68	1.44	1.42
^{2}F	^{1}F$^-$	aug-cc-pV5Z	-	-	3.401	3.40	4.92	1.40	2.54	4.22	3.84	4.27	4.13	4.12	3.62	3.59
^{2}Na	^{1}Na$^-$	aug-cc-pV5Z	-	-	0.548	0.54	0.36	0.50	0.49	0.51	0.46	0.43	0.51	0.52	0.43	0.43
^{2}Al	^{3}Al$^-$	aug-cc-pV5Z	0.02	0.02	0.433	0.44	0.61	0.54	0.73	0.53	0.45	0.40	0.50	0.50	0.41	0.40
^{3}Si	^{4}Si$^-$	aug-cc-pV5Z	0.00	0.00	1.390	1.41	1.69	1.49	1.78	1.48	1.42	1.37	1.47	1.46	1.38	1.37
^{4}P	^{3}P$^-$	aug-cc-pV5Z	0.01	0.03	0.747	0.71	0.67	0.59	0.62	0.61	0.62	0.56	0.71	0.71	0.66	0.66
^{3}S	^{2}S$^-$	aug-cc-pV5Z	0.01	0.01	2.077	2.06	2.33	1.80	2.00	1.97	2.03	1.97	2.08	2.07	2.03	2.02
^{2}Cl	^{1}Cl$^-$	aug-cc-pV5Z	-	-	3.613	3.50	4.09	3.26	3.57	3.59	3.67	3.62	3.68	3.67	3.62	3.61
MSE						−0.02	0.39	−0.38	0.00	0.09	0.01	0.03	0.10	0.10	−0.04	−0.05
σ						0.03	0.49	0.63	0.44	0.25	0.15	0.29	0.21	0.21	0.10	0.09
MAE						0.03	0.48	0.43	0.34	0.16	0.10	0.17	0.13	0.12	0.08	0.08
Max. Error						0.12	1.52	2.01	0.86	0.81	0.44	0.87	0.73	0.71	0.22	0.19

[a]Error measures refer to the experimental standards.

https://doi.org/10.1021/acs.jpca.4c04318
J. Phys. Chem. A 2024, 128, 7311−7330

Table 7. Vertical Ionization Energies (eV) of 17 Open-Shell Molecules for Doublet-to-Singlet Transitions[b]

Molecules	$<\Delta S^2>_G$	$<\Delta S^2>_F$	ΔCCSD(T)	KT	D2	os-nD-D2	OVGF-A	P3+	Q3+	L3+B	nD-L3+B	RL3	nD-RL3	EOM-CCSD[a]	ADC(3)[a]
AlO	0.06	0.65	9.82	9.80	9.64	9.71	9.70	9.58	9.61	9.81	9.81	9.61	9.60	9.26	9.05
BeH	0.00	0.01	8.30	8.48	8.34	8.42	8.33	8.28	8.27	8.33	8.33	8.27	8.27	8.32	8.28
BO	0.06	1.03	12.94	13.73	12.81	13.24	13.62	13.50	13.77	13.68	13.66	13.57	13.54	13.22	13.17
C_2H_3	0.25	0.35	9.59	11.10	9.69	10.33	9.91	9.77	9.71	9.83	9.81	9.70	9.68	9.72	9.84
C_3H_3	0.00	0.29	8.51	9.78	8.56	8.98	8.73	8.73	8.61	8.70	8.67	8.60	8.58	8.66	8.67
C_3H_5	0.22	0.22	7.96	9.16	7.96	8.36	8.13	8.07	7.97	8.09	8.06	7.97	7.95	8.05	8.09
CH	0.01	0.01	10.43	11.54	10.48	10.84	10.52	10.34	10.32	10.48	10.46	10.32	10.30	10.46	10.37
CH_2CHO	0.19	0.24	10.15	11.42	10.09	10.49	10.33	10.13	10.17	10.22	10.19	10.15	10.09	10.22	10.25
CH_2CN	0.24	0.24	10.07	11.59	10.07	10.54	10.29	10.30	10.17	10.25	10.22	10.13	10.10	10.23	10.20
CH_3	0.01	0.01	9.63	10.44	9.41	9.78	9.58	9.45	9.41	9.54	9.53	9.52	9.50	9.60	9.64
CN	0.49	2.25	13.53	15.36	12.81	13.66	13.76	13.56	13.56	13.62	13.59	13.60	13.57	13.84	13.93
CNC	0.14	0.14	9.54	10.64	9.74	10.10	9.81	9.82	9.69	9.83	9.81	9.72	9.69	9.78	9.66
NO	0.10	0.14	9.52	11.81	9.00	9.93	9.75	9.67	9.58	9.58	9.55	9.54	9.50	9.56	9.71
NO_2	0.02	0.06	11.07	13.93	10.31	11.39	11.40	11.51	11.31	11.23	11.18	11.14	11.09	11.23	11.22
NS	0.05	0.82	8.70	10.25	8.64	9.13	9.06	9.02	8.94	9.00	8.97	8.94	8.91	8.79	8.91
PH_2	0.02	0.02	9.65	10.24	9.67	9.82	9.69	9.57	9.54	9.68	9.67	9.58	9.57	9.67	9.62
SiF	0.02	0.02	7.47	7.94	7.51	7.68	7.52	7.46	7.41	7.55	7.54	7.45	7.44	7.52	7.43
MSE				1.19	−0.13	0.32	0.19	0.11	0.07	0.15	0.13	0.05	0.03	0.07	0.07
σ				0.71	0.27	0.19	0.18	0.21	0.23	0.18	0.18	0.18	0.18	0.18	0.24
MAE				1.20	0.19	0.34	0.21	0.19	0.15	0.16	0.14	0.12	0.11	0.14	0.18
Max. Error				2.86	0.76	0.73	0.68	0.55	0.83	0.74	0.72	0.63	0.60	0.56	0.77

[a]Data taken from ref 48. [b]All many-body calculations were performed with the aug-cc-pVDZ basis set. Error measures refer to the ΔCCSD(T) standards. Electron-propagator and EOM-CCSD results are based on molecular (uncharged) reference states.

https://doi.org/10.1021/acs.jpca.4c04318
J. Phys. Chem. A 2024, 128, 7311−7330

Table 8. Vertical Electron Affinities (eV) of 17 Open-Shell Molecules for Singlet-to-Doublet Transitions[c]

Molecules	ΔCCSD(T)	KT	D2	os-nD-D2	OVGF-A	P3+	Q3+	L3+B	nD-L3+B	RL3	nD-RL3	EOM-CCSD[b]	ADC(3)[b]
AlO	9.82	9.42	9.93	9.60	9.94	9.67	9.82	9.85	9.87	9.79	9.81	9.26	9.05
BeH	8.30	7.89	8.26	8.11	8.28	8.32	8.32	8.29	8.29	8.33	8.33	8.32	8.28
BO	12.94	12.49	13.65	13.20	12.68	13.35	13.00	13.07	13.08	13.18	13.19	13.22	13.17
C_2H_3	9.59	7.59	9.85	8.94	9.38	9.61	9.61	9.53	9.55	9.61	9.64	9.72	9.84
C_3H_3	8.51	6.88	8.72	7.94	8.35	8.47	8.46	8.43	8.47	8.48	8.52	8.66	8.67
C_3H_5	7.96	6.14	8.06	7.27	7.74	7.88	7.87	7.81	7.85	7.85	7.90	8.05	8.09
CH	10.43	9.04	10.39	9.78	10.40	10.59	10.59	10.44	10.45	10.55	10.57	10.46	10.37
CH_2CHO	10.15	8.46	10.32	9.49	9.97	10.10	10.09	10.05	10.09	10.08	10.13	10.22	10.25
CH_2CN	10.07	8.47	10.35	9.55	9.91	10.04	10.02	10.01	10.05	10.07	10.11	10.23	10.20
CH_3	9.63	7.74	9.57	8.75	9.40	9.59	9.59	9.51	9.52	9.58	9.59	9.60	9.64
CN	13.53	14.28	14.87	14.41	14.42	14.46	14.12	14.45	14.46	14.60	14.62	13.84	13.93
CNC	9.54	8.09	9.85	9.08	9.52	9.69	9.68	9.60	9.64	9.66	9.70	9.78	9.66
NO	9.52	9.07	9.67	9.29	9.56	9.53	9.31	9.58	9.59	9.67	9.69	9.56	9.71
NO_2	11.07	11.04	11.43	11.02	11.26	10.93	10.69	11.17	11.17	11.21	11.21	11.23	11.22
NS	8.70	8.29	9.08	8.67	8.74	8.66	8.50	8.70	8.72	8.78	8.80	8.79	8.91
PH_2	9.65	8.53	9.76	9.18	9.65	9.83	9.82	9.70	9.71	9.75	9.77	9.67	9.62
SiF	7.47	6.90	7.53	7.25	7.46	7.62	7.56	7.52	7.52	7.55	7.56	7.52	7.43
MSE		−0.98	0.26	−0.32	−0.02	0.08	0.01	0.05	0.07	0.11	0.13	0.07	0.07
σ		0.76	0.33	0.41	0.26	0.25	0.20	0.23	0.23	0.26	0.25	0.18	0.24
MAE		1.06	0.28	0.45	0.16	0.15	0.14	0.12	0.11	0.14	0.15	0.14	0.18
Max. Error		2.01	1.35	0.88	0.89	0.93	0.59	0.92	0.93	1.07	1.09	0.56	0.77
MSE[a]		−1.08	0.19	−0.39	−0.07	0.03	−0.03	−0.01	0.01	0.05	0.07	0.06	0.05
σ[a]		0.65	0.19	0.29	0.13	0.14	0.14	0.08	0.07	0.09	0.08	0.18	0.23
MAE[a]		1.08	0.21	0.42	0.12	0.10	0.11	0.07	0.06	0.08	0.09	0.13	0.16
Max. Error[a]		2.01	0.71	0.88	0.26	0.41	0.38	0.15	0.13	0.24	0.25	0.56	0.77

[a]CN is excluded from the statistics. [b]Data taken from ref 48. [c]All many-body calculations were performed with the aug-cc-pVDZ basis set. Error measures refer to the ΔCCSD(T) standards. Electron-propagator results except those of ADC(3) are based on cationic, closed-shell reference states. EOM-CCSD and ADC(3) data are identical to those of Table 6.

eV. Approximately renormalized methods fare better. Q3+ achieves an MAE of only 0.11 eV with O^2V^3 arithmetic scaling. The more demanding OVGF-A, L3+B and nD-L3+B alternatives with OV^4 scaling factors produce MAEs of 0.11, 0.07, and 0.06 eV, respectively. The two explicitly renormalized methods, RL3 and nD-RL3, have MAEs of 0.07 eV. Electron-propagator methods for EDEs with fifth-power scaling and low spin-contamination in reference determinants make excellent predictions for open-shell atoms and atomic anions.

Electron Attachment Energies of Atoms and Cations. Table 4 displays EAEs of 12 atomic cations with nonsinglet initial states. UHF wave functions for the initial states supply the reference spin−orbitals; spin contamination is small in all cases. Large errors obtained with KT decline by an order of magnitude in D2 calculations. The os-nD-D2 alternative is markedly worse, with an MAE of 0.8 eV. Among the approximately renormalized methods, the MAEs vary from 0.27 eV (OVGF-A) to 0.16 eV (P3+ and Q3+). Only the explicitly renormalized self-energies, RL3 and nD-RL3, produce a definite improvement over D2 with MAEs of 0.08 eV. The quality of these EAE results is approximately the same as for EDEs of atoms and atomic anions. The largest errors in the last six columns pertain to O and F, which exhibit the largest values of $< \Delta S^2 >_F$.

Much lower accuracy is reported in Table 5 for EAEs of 11 atoms examined with the aug-cc-pV5Z basis set. KT results have the correct sign in only two cases, Si and Cl. These qualitative failures indicate that the CHF orbitals considered in eq 11 are not good approximations to Dyson orbitals. Diffuse functions succeed in lowering CHF orbital energies, but electron-propagator results become worse in many cases. (Note the deterioration of $< \Delta S^2 >_F$ when diffuse functions are added to the cc-pV5Z basis.) All electron-propagator methods improve on KT results, but their MAEs for D2 and the fifth-power methods vary between 0.4 and 0.6 eV. Table 6 repeats data from Table 3 for EDEs of anions and presents error measures that pertain only to the 11 cases of Table 5. EDEs of atomic anions are considerably more accurate than EAEs of atoms. The largest errors in Table 6 pertain to the EDE of F^-, where all methods save RL3 and nD-RL3 generate unsatisfactory results. But for this exceptional case of strong correlation, all the renormalized methods would have MAEs of 0.1 eV or less. For electron affinities, there is a clear advantage in calculating EDEs of anions instead of EAEs of atoms.

Molecular Ionization Energies. *Doublet Molecule to Singlet Cation Transitions.* Ionization energies of 17 doublets where final states have closed-shell configurations occupy Table 7. ΔCCSD(T)/aug-cc-pVDZ calculations supply standards of comparison and enable comparisons with previously published IP-EOM-CCSD and ADC(3) results obtained with same basis set.[48] Spin contamination in UHF reference determinants (as a percentage of the exact value) has values as high as 66% for CN. KT results have an MAE of 1.2 eV. D2 realizes a considerable improvement (MAE = 0.19 eV) with only cubic arithmetic scaling. The larger errors reported by os-nD-D2 indicate that this modification of D2 has no practical advantage for this set of EAEs. The OVGF methods also fail to improve on D2 despite their OV^4 scaling factors. (The best OVGF results belong to the A variant.) The Q3+ self-energy realizes a somewhat smaller MAE (0.15 eV) with O^2V^3 scaling. The approximately renormalized methods with OV^4 scaling, L3+B and its nD variant, lead to MAEs of 0.16 and 0.14 eV, respectively. Explicitly renormalized self-energies (RL3 and nD-RL3) respectively obtain the lowest MAEs: 0.12 and 0.11 eV. These values are lower than their IP-EOM-CCSD and ADC(3) counterparts at

https://doi.org/10.1021/acs.jpca.4c04318
J. Phys. Chem. A 2024, 128, 7311−7330

0.14 and 0.18 eV. There is little correlation between reference-state spin contamination and the accuracy of the electron-propagator predictions. The largest errors pertain to BO, whose spin contamination is only 8%. (Note the large value of $<\Delta S^2>_F$ for BO^+.) Omission of this case for Q3+, L3+B, nD-L3+B, RL3, and nD-RL3 produces MAEs of 0.12, 0.13, 0.11, 0.09, and 0.08 eV, respectively. Large spin contamination plagues the determinants of CN and CN^+, but P3+, Q3+, L3+B, RL3 and nD-RL3 results are nonetheless satisfactory. For this set of EDEs, the quality of electron-propagator calculations is only slightly inferior to that obtained for closed-shell reference states.

The same ionization energies may be computed as EAEs of cationic initial states with closed-shell configurations. Table 8 contains the corresponding data for electron-propagator calculations and repeats the ΔCCSD(T), IP-EOM-CCSD and ADC(3) columns from Table 7. The case of the EAE of CN^+ is noteworthy for its large errors, which probably stem from its multiconfigurational character. (CN^+ is iso-electronic with the notorious biradicaloid C_2.) When this case is omitted from the statistics, MAEs decline from 1.1 to 0.2 eV when D2 corrects KT. (Table 8 also discloses the higher error measures obtained when the CN/CN^+ data remain in the statistical analysis.) There is no advantage in using os-nD-D2 for electron attachments, for its errors are larger than those of D2. OVGF results are better than those of D2, but L3+B and nD-L3+B MAEs are clearly smaller at 0.07 and 0.06 eV, respectively. (For EAEs, there is no arithmetic advantage in using Q3+ instead of L3+B; see Table 2.) RL3 and nD-RL3 errors are only slightly worse at 0.08 and 0.09 eV. All quintically scaling electron-propagator methods achieve lower MAEs than IP-EOM-CCSD and ADC(3) for this set of electron binding energies. The latter methods are likely to perform better when they also employ closed-shell reference states for the calculation of EAEs. Electron-propagator results are slightly better in Table 8 than in Table 7, except in the case of D2. There is a noticeable advantage in accuracy that accompanies closed-shell reference states, but arithmetic scaling factors are more favorable when calculating EDEs of open-shell species.

Doublet Molecule to Triplet Cation Transitions. Removal of an electron from an uncharged doublet to produce a cationic triplet is the subject of Table 9. The *r* index of eq 11 employed in diagonal self-energies belongs to an occupied, β spin−orbital. MAEs decline from 0.75 to 0.48 to 0.18 as KT is corrected by D2 and os-nD-D2. This pattern recapitulates the pattern in the reduction of errors seen repeatedly for ionization energies of closed-shell molecules. The success of os-nD-D2 is not surpassed by the OVGF methods or even by the approximately renormalized P3+ and Q3+ methods. The latter methods, with their O^2V^3 scaling factors and without the need for ERIs with four virtual indices, obtain MAEs of 0.19 eV. Only with the advent of OV^4 scaling in L3+B and nD-L3+B does the MAE decline to the lower values of 0.12 and 0.13 eV, respectively. Explicitly renormalized methods are somewhat worse, with MAEs of 0.14 and 0.16 for RL3 and nD-RL3. ADC(3) produces larger errors at greater cost. IP-EOM-CCSD has an MAE that is only slightly lower than that of L3+B. The largest errors in the renormalized self-energy methods pertain to two cases, CHN_2 and CP, that also have the spin contamination above 47%. In the other nine cases, the MAE of RL3 is only 0.1 eV.

Triplet Molecule to Quartet Cation Transitions. There are only four cases in this category. (See Table 10.) New-generation diagonal self-energy methods produce MAEs between 0.17 and 0.26 eV. Data from IP-EOM-CCSD calculations are much

Table 9. Vertical Ionization Energies (eV) of 11 Open-Shell Molecules for Doublet-to-Triplet Transitions[b]

Molecules	$<\Delta S^2>_G$	$<\Delta S^2>_F$	ΔCCSD(T)	KT	D2	os-nD-D2	OVGF-A	P3+	Q3+	L3+B	nD-L3+B	RL3	nD-RL3	EOM-CCSD[a]	ADC(3)[a]
CHN_2	0.36	0.19	9.73	10.30	9.18	9.46	9.44	9.38	9.35	9.45	9.42	9.39	9.36	9.76	9.44
CP	0.97	0.50	10.69	10.70	10.47	10.54	10.47	10.41	10.36	10.50	10.49	10.43	10.41	10.78	10.39
FO	0.04	0.04	12.81	14.94	11.97	12.90	12.88	12.60	12.62	12.67	12.64	12.61	12.57	13.49	12.96
HO_2	0.01	0.01	11.40	13.38	10.76	11.72	11.64	11.37	11.41	11.46	11.43	11.41	11.37	11.43	11.74
N_3	0.18	0.17	10.77	10.73	10.43	10.65	10.49	10.70	10.65	10.62	10.62	10.60	10.59	10.78	10.36
NCO	0.11	0.10	11.70	12.19	11.26	11.75	11.53	11.63	11.60	11.62	11.60	11.59	11.57	11.70	11.57
NH_2	0.01	0.01	11.85	12.61	11.19	11.57	11.75	11.52	11.57	11.72	11.70	11.71	11.69	11.78	11.95
OH	0.01	0.01	12.75	13.92	11.81	12.34	12.79	12.37	12.53	12.61	12.59	12.59	12.57	12.64	13.03
SCN	0.24	0.21	10.42	10.61	10.13	10.44	10.24	10.25	10.23	10.31	10.30	10.28	10.27	10.45	10.24
SF	0.01	0.01	10.11	10.77	9.97	10.26	10.11	10.06	10.01	10.16	10.15	10.11	10.10	10.19	10.09
SH	0.01	0.01	10.00	10.30	9.81	9.93	9.93	9.81	9.81	9.98	9.97	9.95	9.95	10.03	9.99
MSE				0.75	−0.48	−0.06	−0.09	−0.19	−0.19	−0.10	−0.12	−0.14	−0.16	0.07	−0.04
σ				0.70	0.25	0.20	0.16	0.12	0.11	0.10	0.10	0.10	0.10	0.20	0.23
MAE				0.75	0.48	0.18	0.15	0.19	0.19	0.12	0.13	0.14	0.16	0.11	0.20
Max. Error				2.13	0.93	0.41	0.29	0.38	0.38	0.28	0.31	0.33	0.36	0.68	0.41

[a]Data taken from ref 48. [b]All many-body calculations were performed with the aug-cc-pVDZ basis set. Error measures refer to the ΔCCSD(T) standards. Electron-propagator and EOM-CCSD results are based on molecular (uncharged) reference states.

https://doi.org/10.1021/acs.jpca.4c04318
J. Phys. Chem. A 2024, 128, 7311−7330

Table 10. Vertical Ionization Energies (eV) of 4 Open-Shell Molecules for Triplet-to-Quartet Transitions[a]

Molecules	$<\Delta S^2>_G$	$<\Delta S^2>_F$	ΔCCSD(T)	KT	D2	os-nD-D2	OVGF-A	P3+	Q3+	L3+B	nD-L3+B	RL3	nD-RL3	EOM-CCSD[b]	ADC(3)[b]
BN	0.06	0.06	11.26	11.85	10.53	10.76	11.07	10.91	10.98	11.08	11.05	10.99	10.97	11.25	11.25
BP	0.25	0.01	9.14	9.31	8.93	8.99	8.98	8.88	8.86	9.02	9.01	8.90	8.89	9.18	8.94
Si_2	0.02	0.02	7.66	7.99	7.54	7.68	7.60	7.52	7.45	7.67	7.66	7.61	7.59	7.74	7.59
SiC	0.58	0.02	8.69	8.35	8.29	8.32	8.29	8.20	8.16	8.34	8.34	8.28	8.27	8.68	8.23
MSE				0.19	−0.37	−0.25	−0.20	−0.31	−0.33	−0.16	−0.17	−0.24	−0.26	0.03	−0.18
σ				0.34	0.24	0.20	0.12	0.13	0.12	0.13	0.13	0.13	0.13	0.04	0.17
MAE				0.36	0.37	0.26	0.20	0.31	0.33	0.17	0.18	0.24	0.26	0.04	0.18
Max. Error				0.59	0.74	0.50	0.39	0.49	0.53	0.35	0.35	0.41	0.41	0.08	0.46

[a]All many-body calculations were performed with the aug-cc-pVDZ basis set. Error measures refer to the ΔCCSD(T) standards. Electron-propagator and EOM-CCSD results are based on molecular (uncharged) reference states. [b]Data taken from ref 48.

better. These preliminary results indicate that orbital relaxation effects are important and that nondiagonal self-energy methods are needed.

Triplet Molecule to Doublet Cation Transitions. Data on the eight cases of this set are shown in Table 11. Addition of D2 corrections to KT reduces the MAE from 1.6 to 0.3 eV. Whereas D2 tends to underestimate ionization energies, os-nD-D2 overestimates by approximately that same amount. MAEs decline steadily from OVGF-A (0.17 eV) to Q3+ (0.16 eV) and L3+B (0.16 eV). Explicitly renormalized methods (RL3 and nD-RL3) attain lower MAEs (0.14 eV). IP-EOM-CCSD and ADC(3) produce slightly more accurate MAEs (0.10 eV) while requiring arithmetic operations with sixth-power scaling.

Molecular Electron Affinities. *Doublet Molecule to Singlet Anion Transitions.* For the 22 molecules in this set, the MAE of KT is relatively large: 2.35 eV. (See Table 12.) D2 reduces this error index to 0.6 eV. For EAEs, os-nD-D2 fails again to improve on D2. Only the RL3 and nD-RL3 self-energies realize improvement, with MAEs close to 0.5 eV. The superior performance of IP-EOM-CCSD and ADC(3) (MAEs = 0.17 and 0.29 eV, respectively) confirm the need for nondiagonal self-energies that describe strong relaxation effects. The deficiencies of the diagonal self-energies arise from the poor qualitative description of these transitions given by Koopmans's identity. In several cases, the KT result has the wrong sign. Even with low spin contamination in the reference determinant, the virtual orbital need not be a good approximation to the Dyson orbital. In UHF calculations, virtual β orbitals are not required to be orthogonal to occupied α orbitals. These overlaps may exacerbate spin contamination ($<\Delta S^2>_F$) in the frozen-orbital determinant of the final state that is assumed in Koopmans's identity.

A better approach that employs diagonal self-energies is calculation of EDEs of closed-shell anions. Table 13 starts with an MAE for KT that is only 0.73 eV. The os-nD-D2 method reduces this error index to 0.20 eV. OVGF results are better, but the faster Q3+ method reports an MAE of only 0.11 eV. L3+B and its nD variant have MAEs of 0.07 eV with the same scaling factor as OVGF. RL3 and nD-RL3 have slightly larger errors (MAE = 0.08 and 0.09, respectively). All renormalized self-energy methods surpass the predictive performance of UHF-based IP-EOM-CCSD and ADC(3). The latter methods are likely to improve with the use of closed-shell reference states. The advantages of this approach over its alternative that computes EAEs with an open-shell reference determinant are apparent from comparisons of Tables 12 and 13.

Doublet Molecule to Triplet Anion Transitions. Only four molecules pertain to this category, but the results confirm some previously observed trends. The r index in eq 11 pertains to an unoccupied α spin−orbital. In Table 14, D2 corrections to KT reduce the MAE from 1.3 to 0.2 eV. The KT results are poor and obtain the wrong sign in two cases. As before, there is no advantage in the os-nD-D2 method for EAEs. OVGF methods realize no improvement over D2. Q3+ and L3+B produce MAEs near 0.2 eV. Only the RL3 and nD-RL3 report acceptable (below 0.2 eV) errors and MAEs of 0.10 eV. The latter datum is competitive with its ADC(3) counterpart, 0.16 eV. IP-EOM-CCSD yields excellent results and an MAE that approaches chemical accuracy. In calculations of EAEs, better descriptions of the Dyson orbital are needed. Despite the challenge posed by the poor zeroth order result, explicitly renormalized self-energies still generate data that disagree with ΔCCSD(T) by 0.2 eV or less.

https://doi.org/10.1021/acs.jpca.4c04318
J. Phys. Chem. A 2024, 128, 7311−7330

Table 11. Vertical Ionization Energies (eV) of 8 Open-Shell Molecules for Triplet-to-Doublet Transitions[a]

Molecules	$\langle\Delta S^2\rangle_G$	$\langle\Delta S^2\rangle_F$	ΔCCSD(T)	KT	D2	os-nD-D2	OVGF-A	P3+	Q3+	L3+B	nD-L3+B	RL3	nD-RL3	EOM-CCSD[b]	ADC(3)[b]
C_4O	0.21	0.21	9.59	10.83	9.60	9.87	9.75	9.91	9.71	9.77	9.74	9.65	9.61	9.78	9.56
CH_2	0.02	0.02	10.27	11.13	10.12	10.62	10.26	10.08	10.07	10.20	10.19	10.15	10.13	10.24	10.27
CNN	0.26	0.39	11.19	12.30	11.42	11.73	11.57	11.57	11.51	11.59	11.57	11.47	11.44	11.40	11.36
HCCN	0.40	0.40	10.46	12.12	10.53	11.06	10.76	10.69	10.59	10.69	10.66	10.54	10.50	10.63	10.65
NH	0.02	0.02	13.33	14.86	13.05	13.87	13.43	13.13	13.16	13.28	13.26	13.15	13.13	13.29	13.41
O_2	0.05	0.05	12.24	15.32	11.32	12.24	12.38	12.21	12.09	12.07	12.02	11.97	11.93	12.09	12.39
S_2	0.05	0.05	9.27	10.56	9.00	9.35	9.34	9.24	9.18	9.27	9.24	9.16	9.13	9.28	9.33
SO	0.06	0.09	10.27	11.91	10.10	10.53	10.52	10.48	10.39	10.45	10.42	10.29	10.26	10.28	10.39
MSE				1.55	−0.18	0.33	0.17	0.09	0.01	0.08	0.06	−0.03	−0.06	0.05	0.09
σ				0.63	0.32	0.21	0.12	0.21	0.17	0.18	0.18	0.16	0.16	0.12	0.07
MAE				1.55	0.26	0.33	0.17	0.20	0.16	0.16	0.16	0.14	0.14	0.10	0.10
Max. Error				3.08	0.92	0.59	0.37	0.38	0.31	0.40	0.38	0.27	0.32	0.21	0.19

[a]All many-body calculations were performed with the aug-cc-pVDZ basis set. Error measures refer to the ΔCCSD(T) standards. Electron-propagator and EOM-CCSD results are based on molecular (uncharged) reference states. [b]Data taken from ref 48.

The alternative approach that employs an anionic reference state gives superior results. (See Table 15.) KT's MAE of 0.94 eV is reduced to 0.13 eV with D2 corrections. In this set, os-nD-D2 provides no advantage in accuracy and confirms trends seen for other classes of EAEs. OVGF methods likewise fail to improve on D2. The faster Q3+ method realizes a slight improvement, but L3+B does not. (Slightly better results are produced by L3+A for this set of data.) With the use of explicitly renormalized self-energies, the MAE finally declines to 0.09 eV. The latter result is better than that of ADC(3) at 0.16 eV. IP-EOM-CCSD attains chemical accuracy at 0.05 eV. These preliminary results await confirmation or refutation with larger sets of data.

Triplet Molecule to Doublet Anion Transitions. The last set of transitions comprises 11 cases. Treating this transition as an electron affinity associated with an unoccupied β spin−orbital yields the electron-propagator data of Table 16. KT results produce an MAE of 1.85 eV; most cases have incorrect signs. D2 corrections reduce this error index to 0.5 eV. Once again, there is no reason to use the os-nD-D2 method for EAEs. No improvements to D2 results are made by any of the quintically scaling self-energies with approximate renormalizations. Only the explicitly renormalized methods attain MAEs near 0.45 eV. ADC(3) and IP-EOM-CCSD have lower MAEs of 0.20 and 0.13 eV, respectively. Nondiagonal self-energies are needed in calculations of EAEs of these open-shell molecules.

Reversing the roles of neutral and anionic states proves again to be advantageous. (See Table 17.) The MAE of KT is only 0.4 eV. D2's MAE is somewhat worse, but its counterpart for the os-nD-D2 method is only 0.19 eV. For anion EDEs, os-nD-D2 again improves on D2. Q3+ succeeds in efficiently producing an improvement that is somewhat smaller than those of the slower OVGF methods. (The B variant is better than the A variant for this set.) L3+B, RL3 and their nD variants yield MAEs between 0.10 and 0.13 eV. The MAE of ADC(3) is larger (0.20 eV), but IP-EOM-CCSD's MAE is competitive at 0.13 eV. The advantages of computing EDEs instead of EAEs reappear for this set of data.

Aggregate Error Measures for Molecules. Figure 1 displays aggregate error measures for the best methods discovered in numerical tests and their OVGF and P3+ antecedents. Results for second-order (D2 or os-nD-D2), P3+, Q3+, OVGF (A or B), L3+B and RL3 self-energies appear in four sectors. MAEs for ionization energies of doublet molecules calculated as electron affinities of closed-shell cations populate the Singlet-Doublet IEs sector. (Q3+ and P3+ are absent, for these methods have the same arithmetic scaling as L3+B for electron attachments and omit some of L3+B's self-energy terms.) The next sector treats electron affinities of doublets as EDEs of closed-shell anions. Ionization energies that involve a doublet or triplet molecule and a cationic triplet or doublet are the concern of the third sector. (See Table 9.) MAEs that pertain to electron affinities of doublet or triplet molecules with triplet or doublet anions lie in the fourth sector. (See Table 17.) In all four sectors, there is a cubically scaling option that yields average errors of 0.2 eV. D2 is preferable in sector 1 and for the triplet molecules in sectors 3 and 4. In all other cases, os-nD-D2 is preferable. In sectors 2, 3 and 4, Q3+ has a lower arithmetic scaling factor, O^2V^3, than the methods to its right. It also has no need for ERIs with four virtual indices and therefore requires less memory and fewer input/output operations. From sector 2 to sector 4, Q3+'s MAE increases by 0.05 eV. OVGF methods have OV^4 scaling factors and require full transformations of ERIs. The best results obtained with the same scaling factor belong to

https://doi.org/10.1021/acs.jpca.4c04318
J. Phys. Chem. A 2024, 128, 7311−7330

Table 12. Vertical Ionization Energies (eV) of 22 Open-Shell Molecules for Doublet-to-Singlet Transitions[a]

Molecules	$\langle\Delta S^2\rangle_G$	$\langle\Delta S^2\rangle_F$	ΔCCSD(T)	KT	D2	os-nD-D2	OVGF-A	P3+	Q3+	L3+B	nD-L3+B	RL3	nD-RL3	EOM-CCSD[b]	ADC(3)[b]
AlO	0.06	0.39	2.58	−0.16	1.71	0.97	1.69	1.57	1.78	1.74	1.76	1.92	1.95	2.84	2.63
BeH	0.00	0.63	0.47	−0.55	−0.18	−0.22	−0.10	−0.08	−0.08	−0.09	−0.09	0.09	0.09	0.42	0.47
BO	0.06	0.34	2.37	0.64	1.91	1.69	1.69	1.96	1.87	1.87	1.88	2.08	2.08	2.29	2.10
C_2H_3	0.25	1.23	0.09	−1.06	−0.86	−0.95	−0.87	−0.85	−0.85	−0.85	−0.85	−0.84	−0.84	−0.14	−0.28
C_3H_3	0.00	0.55	0.54	−1.74	−0.10	−0.68	−0.28	−0.20	−0.15	−0.19	−0.18	−0.10	−0.08	0.32	0.16
C_3H_5	0.22	0.55	0.22	−2.11	−0.55	−1.10	−0.69	−0.63	−0.57	−0.84	−0.60	−0.52	−0.51	−0.04	−0.18
CH_2CHO	0.19	0.43	1.50	−1.16	0.76	0.08	0.62	0.63	0.73	0.70	0.72	0.81	0.83	1.24	1.16
CH_2CN	0.24	0.49	1.34	−1.03	0.77	0.13	0.54	0.63	0.68	0.65	0.67	0.75	0.77	1.16	0.98
CHN_2	0.36	0.58	1.51	−1.23	1.09	0.32	0.65	0.78	0.84	0.80	0.82	0.92	0.94	1.30	1.08
CN	0.49	0.71	3.74	1.03	3.13	2.68	2.92	3.05	3.09	3.07	3.09	3.32	3.33	3.52	3.49
CP	0.97	1.31	2.79	−0.27	1.67	1.11	1.42	1.59	1.61	1.57	1.58	1.81	1.82	2.39	2.08
FO	0.04	0.27	1.83	−1.38	1.26	0.33	0.84	0.98	1.03	1.03	1.05	1.24	1.26	1.66	1.47
HO_2	0.01	0.26	0.47	−2.55	−0.23	−1.09	−0.41	−0.44	−0.32	−0.31	−0.29	−0.13	−0.11	0.24	0.31
N_3	0.18	0.28	2.52	−0.62	2.47	1.37	1.69	1.84	1.93	1.90	1.93	2.02	2.05	2.34	2.01
NCO	0.11	0.21	3.28	0.61	3.10	2.18	2.68	2.73	2.82	2.81	2.85	2.91	2.95	3.14	2.95
NH_2	0.01	0.42	0.54	−1.94	−0.35	−0.94	−0.51	0.41	−0.37	−0.40	−0.40	−0.23	−0.22	0.41	0.16
NO_2	0.02	0.21	1.33	−0.23	1.16	0.64	0.89	0.89	0.83	0.98	1.01	1.12	1.15	1.21	1.22
OH	0.01	0.33	1.63	−1.76	0.54	−0.34	0.36	0.42	0.53	0.49	0.49	0.74	0.75	1.50	1.22
PH_2	0.02	0.25	1.04	−0.56	0.70	0.29	0.64	0.75	0.76	0.71	0.72	0.85	0.86	0.97	0.95
SCN	0.24	0.30	3.37	1.18	3.19	2.45	2.92	3.04	3.10	3.02	3.05	3.12	3.15	3.24	3.13
SF	0.01	0.14	2.08	0.36	1.85	1.34	1.73	1.88	1.87	1.85	1.86	2.00	2.02	2.02	2.00
SH	0.01	0.16	2.12	0.17	1.82	1.23	1.71	1.85	1.87	1.81	1.82	1.97	1.98	2.05	2.01
MSE				−2.35	−0.57	−1.18	−0.78	−0.66	−0.65	−0.68	−0.66	−0.52	−0.51	−0.15	−0.28
σ				0.65	0.30	0.35	0.27	0.30	0.26	0.27	0.26	0.25	0.26	0.12	0.18
MAE				2.35	0.57	1.18	0.78	0.66	0.65	0.68	0.66	0.52	0.51	0.17	0.29
Max. Error				3.39	1.12	1.97	1.37	1.21	1.18	1.22	1.21	0.98	0.97	0.40	0.71

[a]All many-body calculations were performed with the aug-cc-pVDZ basis set. Error measures refer to the ΔCCSD(T) standards. Electron-propagator and EOM-CCSD results are based on molecular (uncharged) reference states. [b]Data taken from ref 48.

https://doi.org/10.1021/acs.jpca.4c04318
J. Phys. Chem. A 2024, 128, 7311−7330

Table 13. Vertical Electron Affinities (eV) of 22 Open-Shell Molecules for Singlet-to-Doublet Transitions[a]

Molecules	ΔCCSD(T)	KT	D2	os-nD-D2	OVGF-A	P3+	Q3+	L3+B	nD-L3+B	RL3	nD-RL3	EOM-CCSD[b]	ADC(3)[b]
AlO	2.58	2.79	2.19	2.45	2.61	2.59	2.65	2.78	2.78	2.63	2.62	2.84	2.63
BeH	0.47	0.49	0.34	0.35	0.35	0.20	0.18	0.43	0.43	0.29	0.28	0.42	0.47
BO	2.37	2.91	2.30	2.44	2.37	2.35	2.27	2.45	2.44	2.33	2.32	2.29	2.10
C_2H_3	0.09	0.90	−0.42	−0.03	0.07	0.03	0.01	0.09	0.07	0.03	0.00	−0.14	−0.28
C_3H_3	0.54	0.84	0.19	0.43	0.40	0.51	0.46	0.49	0.48	0.45	0.44	0.32	0.16
C_3H_5	0.22	0.38	−0.15	0.04	0.05	0.12	0.10	0.15	0.14	0.09	0.08	−0.04	−0.18
CH_2CHO	1.50	1.81	1.00	1.28	1.36	1.42	1.43	1.45	1.44	1.39	1.38	1.24	1.16
CH_2CN	1.34	1.80	0.97	1.26	1.22	1.35	1.28	1.29	1.28	1.26	1.24	1.16	0.98
CHN_2	1.51	1.75	1.15	1.45	1.31	1.68	1.56	1.45	1.43	1.45	1.44	1.30	1.08
CN	3.74	5.26	3.30	3.93	3.78	3.84	3.70	3.76	3.73	3.69	3.66	3.52	3.49
CP	2.79	4.37	2.35	3.07	2.86	3.07	2.81	2.85	2.81	2.85	2.81	2.39	2.08
FO	1.83	3.71	0.45	1.52	2.12	1.66	1.87	1.86	1.83	1.72	1.68	1.66	1.47
HO_2	0.47	2.06	−1.13	−0.08	0.79	0.18	0.51	0.48	0.45	0.36	0.33	0.24	0.31
N_3	2.52	2.90	2.16	2.50	2.32	2.85	2.73	2.44	2.42	2.44	2.42	2.34	2.01
NCO	3.28	3.97	2.78	3.23	3.22	3.44	3.42	3.30	3.28	3.26	3.23	3.14	2.95
NH_2	0.54	1.32	−0.51	−0.05	0.64	0.45	0.62	0.60	0.58	0.53	0.51	0.41	0.16
NO_2	1.33	2.76	0.29	1.17	1.32	1.25	1.27	1.23	1.20	1.20	1.17	1.21	1.22
OH	1.63	2.96	−0.18	0.74	2.26	1.64	2.10	2.01	1.99	1.77	1.75	1.50	1.22
PH_2	1.04	1.22	0.81	0.89	0.95	0.88	0.89	1.03	1.02	1.00	0.99	0.97	0.95
SCN	3.37	3.85	3.08	3.40	3.29	3.37	3.33	3.35	3.34	3.32	3.30	3.24	3.13
SF	2.08	2.73	1.68	2.04	2.08	1.96	1.98	2.10	2.09	2.06	2.05	2.02	2.00
SH	2.12	2.58	1.70	1.96	2.09	1.97	2.02	2.12	2.11	2.10	2.09	2.05	2.01
MSE		0.73	−0.59	−0.15	0.00	−0.03	−0.01	0.02	0.00	−0.05	−0.07	−0.15	−0.28
σ		0.55	0.46	0.25	0.19	0.15	0.15	0.10	0.10	0.07	0.07	0.12	0.18
MAE		0.73	0.59	0.20	0.13	0.12	0.11	0.07	0.07	0.08	0.09	0.17	0.29
Max. Error		1.88	1.81	0.88	0.63	0.33	0.47	0.39	0.37	0.18	0.20	0.40	0.71

[a]All many-body calculations were performed with the aug-cc-pVDZ basis set. Error measures refer to the ΔCCSD(T) standards. Electron-propagator results are based on anionic, closed-shell reference states. EOM-CCSD and ADC(3) data are identical to those of Table 12. [b]Data taken from ref 48.

L3+B and RL3. In the first two sectors, these methods approach chemical accuracy. In the third and fourth sectors, their MAEs lie between 0.10 and 0.15 eV. The latter results are approximately 0.05 eV larger than their counterparts obtained with closed-shell reference states.

CONCLUSIONS

The following recommendations pertain to the use of *ab initio* electron-propagator methods with diagonal self-energies in the UHF spin−orbital basis.

- The qualitative correctness of Koopmans's identity for UHF is a necessary condition for the application of these methods. Strong multideterminantal character in initial-state or final-state wave functions cannot be captured with diagonal self-energies. The frozen-orbital Slater determinant of the final state must dominate its wave function. Probability factors that exceed 0.85 confirm that this condition is satisfied.
- Strong spin contamination in the reference determinant may lead to poor results. Spin contamination may be exacerbated in frozen-orbital, final-state determinants by virtual orbitals. In UHF theory, these orbitals are not constrained to be orthogonal to their occupied counterparts with opposite spin.
- For calculating electron affinities of molecules and molecular cations, adding an electron to a virtual, UHF, β spin−orbital is an inferior approach. Better results may be obtained by removing an electron from an occupied β spin−orbital associated with UHF or closed-shell Hartree−Fock wave functions.
- Electron detachment energies of open-shell atoms calculated with Q3+, L3+B and RL3 have MAEs below 0.1 eV, but their counterparts for electron attachments have larger errors. Spin contamination is negligible in UHF wave functions of light atoms and atomic anions. Therefore, it is also negligible in the frozen-orbital final state of Koopmans's identity for electron detachments. Spin contamination may become worse for electron attachments if the corresponding virtual orbital has large overlaps with occupied orbitals of the opposite spin.
- The present results confirm that closed-shell reference states are preferable to open-shell reference states in calculations of molecular ionization energies and electron affinities.
  - For ionization energies of doublets, one may calculate electron attachment energies of closed-shell cations or electron detachment energies of molecules. MAEs for the former option are smaller. For cubically scaling D2 calculations, the MAE is 0.2 eV. This error criterion falls to 0.1 eV for the quintically scaling L3+B and RL3 methods. The number of bottleneck steps may be reduced for the two latter options by using their non-Dyson variants. Less accurate calculations that employ UHF spin−orbitals for electron detachments from doublet molecules still yield useful data. The larger MAEs of Q3+, L3+B and RL3 are near 0.15 eV.
  - For electron affinities of doublets, MAEs for electron detachment energies of closed-shell anions are smaller than those for electron attachment

https://doi.org/10.1021/acs.jpca.4c04318
J. Phys. Chem. A 2024, 128, 7311−7330

Table 14. Vertical Electron Affinities (eV) of 4 Open-Shell Molecules for Doublet-to-Triplet Transitions[a]

Molecules	$\langle\Delta S^2\rangle_G$	$\langle\Delta S^2\rangle_F$	ΔCCSD(T)	KT	D2	os-nD-D2	OVGF-A	P3+	Q3+	L3+B	nD-L3+B	RL3	nD-RL3	EOM-CCSD[b]	ADC(3)[b]
CH	0.01	0.01	1.08	−0.53	0.70	−0.01	0.67	0.81	0.82	0.72	0.73	0.92	0.94	0.97	1.04
CNC	0.14	0.14	1.85	0.22	1.95	1.02	1.70	1.85	1.86	1.77	1.80	1.87	1.91	1.84	1.90
NS	0.05	0.10	0.94	−0.29	0.64	0.23	0.47	0.52	0.48	0.46	0.49	0.72	0.75	0.94	1.44
SiF	0.02	0.02	0.78	0.01	0.65	0.27	0.65	0.74	0.73	0.68	0.69	0.78	0.79	0.71	0.84
MSE				−1.31	−0.18	−0.78	−0.29	−0.18	−0.19	−0.25	−0.23	−0.09	−0.07	−0.05	0.14
σ				0.35	0.19	0.21	0.15	0.17	0.19	0.17	0.17	0.10	0.11	0.05	0.21
MAE				1.31	0.23	0.78	0.29	0.18	0.20	0.25	0.23	0.10	0.10	0.05	0.16
Max. Error				1.62	0.38	1.09	0.47	0.42	0.46	0.48	0.45	0.22	0.19	0.11	0.50

[a]All many-body calculations were performed with the aug-cc-pVDZ basis set. Error measures refer to the ΔCCSD(T) standards. Electron-propagator and EOM-CCSD results are based on molecular (uncharged) reference states. [b]Data taken from ref 48.

Table 15. Vertical Electron Affinities (eV) of 4 Open-Shell Molecules for Triplet-to-Doublet Transitions[a]

Molecules	$\langle\Delta S^2\rangle_G$	$\langle\Delta S^2\rangle_F$	ΔCCSD(T)	KT	D2	os-nD-D2	OVGF-A	P3+	Q3+	L3+B	nD-L3+B	RL3	nD-RL3	EOM-CCSD[b]	ADC(3)[b]
CH	0.01	0.01	1.08	2.11	0.76	1.43	1.18	0.93	0.98	1.10	1.08	0.99	0.97	0.97	1.04
CNC	0.14	0.14	1.85	2.86	1.91	2.36	2.05	2.04	1.96	2.06	2.04	1.95	1.93	1.84	1.90
NS	0.05	0.10	0.94	2.21	0.80	1.27	1.25	1.06	1.09	1.17	1.14	1.10	1.07	0.94	1.44
SiF	0.02	0.02	0.78	1.24	0.78	1.07	0.84	0.73	0.72	0.84	0.83	0.75	0.74	0.71	0.84
MSE				0.94	−0.10	0.37	0.17	0.03	0.02	0.13	0.11	0.04	0.02	−0.05	0.14
σ				0.30	0.15	0.09	0.10	0.14	0.11	0.09	0.09	0.10	0.10	0.05	0.21
MAE				0.94	0.13	0.37	0.17	0.13	0.11	0.13	0.11	0.09	0.09	0.05	0.16
Max. Error				1.27	0.32	0.51	0.31	0.19	0.15	0.23	0.20	0.16	0.13	0.11	0.50

[a]All many-body calculations were performed with the aug-cc-pVDZ basis set. Error measures refer to the ΔCCSD(T) standards. Electron-propagator results except those of ADC(3) are based on anionic reference states. EOM-CCSD and ADC(3) data are identical to those of Table 14. [b]Data taken from ref 48.

https://doi.org/10.1021/acs.jpca.4c04318
J. Phys. Chem. A 2024, 128, 7311−7330

Table 16. Vertical Electron Affinities (eV) of 11 Open-Shell Molecules for Triplet-to-Doublet Transitions[a]

Molecules	$\langle\Delta S^2\rangle_G$	$\langle\Delta S^2\rangle_F$	ΔCCSD(T)	KT	D2	os-nD-D2	OVGF-A	P3+	Q3+	L3+B	nD-L3+B	RL3	nD-RL3	EOM-CCSD[b]	ADC(3)[b]
BN	0.06	0.37	2.83	−0.03	2.08	1.47	1.74	1.92	1.95	1.91	1.92	2.12	2.12	2.71	2.46
BP	0.25	0.33	2.48	0.51	2.36	1.82	2.10	2.29	2.30	2.23	2.24	2.38	2.39	2.42	2.37
C_4O	0.21	0.27	2.65	0.67	2.80	2.20	2.32	2.46	2.45	2.45	2.50	2.53	2.58	2.60	2.47
CH_2	0.02	1.02	0.01	−1.11	−1.00	−1.03	−0.98	−0.98	−0.98	−0.98	−0.98	−0.95	−0.95	−0.11	−0.19
CNN	0.26	0.45	1.52	−1.22	1.02	0.35	0.74	0.84	0.92	0.86	0.88	1.00	1.03	1.31	1.17
HCCN	0.40	0.79	1.47	−1.09	0.44	−0.03	0.35	0.39	0.45	0.42	0.43	0.55	0.56	1.24	1.10
NH	0.02	1.02	0.06	−1.06	−0.95	−0.99	−0.94	−0.93	−0.93	−0.93	−0.93	−0.91	−0.91	−0.06	−0.18
S_2	0.05	0.12	1.34	0.12	1.25	0.91	1.16	1.21	1.24	1.17	1.20	1.27	1.30	1.27	1.33
Si_2	0.02	0.15	1.94	0.31	1.85	1.50	1.64	1.82	1.81	1.75	1.76	1.87	1.88	1.85	1.85
SiC	0.58	1.12	2.23	0.51	1.83	1.30	1.67	1.85	1.84	1.76	1.77	1.89	1.90	2.03	1.97
SO	0.06	0.20	0.83	-0.58	0.50	0.21	0.50	0.42	0.48	0.52	0.54	0.63	0.65	0.69	0.84
MSE				−1.85	-0.47	-0.88	−0.64	−0.55	−0.53	−0.56	−0.55	−0.45	−0.44	−0.13	−0.20
σ				0.61	0.40	0.36	0.34	0.37	0.36	0.35	0.36	0.36	0.37	0.06	0.13
MAE				1.85	0.50	0.88	0.64	0.55	0.53	0.56	0.55	0.45	0.44	0.13	0.20
Max. Error				2.86	1.03	1.50	1.12	1.08	1.02	1.05	1.04	0.97	0.97	0.23	0.37

[a]All many-body calculations were performed with the aug-cc-pVDZ basis set. Error measures refer to the ΔCCSD(T) standards. Electron-propagator and EOM-CCSD results are based on molecular (uncharged) reference states. [b]Data taken from ref 48.

Table 17. Vertical Electron Affinities (eV) of 11 Open-Shell Molecules for Doublet-to-Triplet Transitions[a]

Molecules	$\langle\Delta S^2\rangle_G$	$\langle\Delta S^2\rangle_F$	ΔCCSD(T)	KT	D2	os-nD-D2	OVGF-A	P3+	Q3+	L3+B	nD-L3+B	RL3	nD-RL3	EOM-CCSD[b]	ADC(3)[b]
BN	0.06	0.37	2.83	2.45	2.65	2.82	2.68	2.77	2.74	2.76	2.77	2.73	2.74	2.71	2.46
BP	0.25	0.33	2.48	2.60	2.36	2.50	2.51	2.44	2.40	2.51	2.50	2.45	2.44	2.42	2.37
C_4O	0.21	0.27	2.65	3.13	2.11	2.65	2.33	2.55	2.39	2.42	2.39	2.40	2.37	2.60	2.47
CH_2	0.02	1.02	0.01	−0.44	−0.51	−0.48	−0.08	−0.40	−0.32	−0.18	−0.18	−0.17	−0.16	−0.11	−0.19
CNN	0.26	0.45	1.52	1.83	0.86	1.17	1.39	1.32	1.33	1.32	1.30	1.31	1.29	1.31	1.17
HCCN	0.40	0.79	1.47	1.66	0.97	1.25	1.37	1.26	1.26	1.32	1.30	1.29	1.28	1.24	1.10
NH	0.02	1.02	0.06	0.18	−0.75	−0.53	0.26	−0.28	−0.10	−0.02	−0.03	−0.05	−0.05	−0.06	−0.18
S_2	0.05	0.12	1.34	1.87	0.90	1.34	1.41	1.15	1.16	1.27	1.25	1.26	1.24	1.27	1.33
Si_2	0.02	0.15	1.94	1.59	1.78	1.79	1.89	1.82	1.79	1.92	1.94	1.91	1.93	1.85	1.85
SiC	0.58	1.12	2.23	2.57	1.81	1.99	2.00	2.34	2.18	2.16	2.14	2.12	2.10	2.03	1.97
SO	0.06	0.20	0.83	1.59	0.30	0.81	1.03	0.73	0.77	0.84	0.82	0.82	0.80	0.69	0.84
MSE				0.15	−0.44	−0.19	−0.05	−0.15	−0.16	−0.10	−0.10	−0.12	−0.13	−0.13	−0.20
σ				0.38	0.21	0.20	0.16	0.14	0.08	0.08	0.09	0.08	0.08	0.06	0.13
MAE				0.37	0.44	0.19	0.14	0.17	0.16	0.10	0.11	0.12	0.13	0.13	0.20
Max. Error				0.75	0.81	0.59	0.32	0.41	0.33	0.24	0.26	0.25	0.28	0.23	0.37

[a]All many-body calculations were performed with the aug-cc-pVDZ basis set. Error measures refer to the ΔCCSD(T) standards. Electron-propagator results except those of ADC(3) are based on anionic reference states. EOM-CCSD and ADC(3) data are identical to those of Table 16. [b]Data taken from ref 48.

https://doi.org/10.1021/acs.jpca.4c04318
J. Phys. Chem. A 2024, 128, 7311−7330

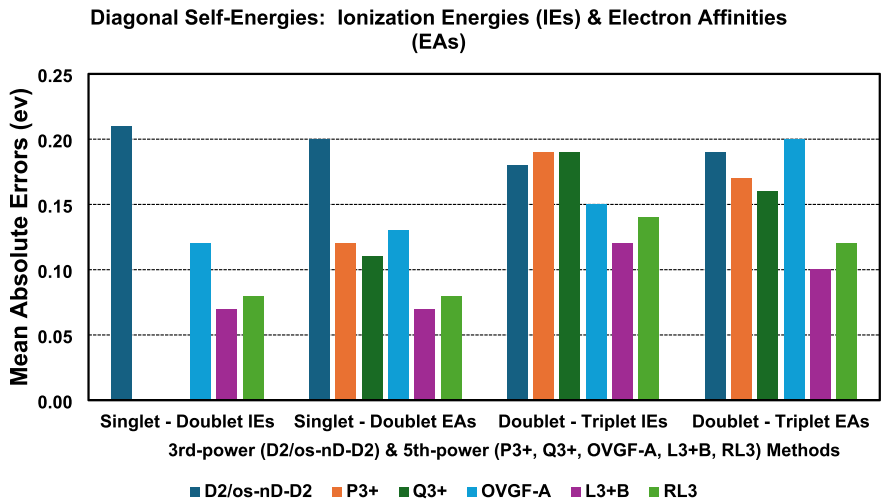


Figure 1. Errors of diagonal self-energies for open-shell molecules.

energies of doublet molecules. With the former choice, the cubically scaling os-nD-D2 method's MAE is 0.2 eV. Another efficient option, Q3+, produces an MAE of 0.11 eV. MAEs below 0.1 eV emerge from tests on L3+B, RL3 and their non-Dyson variants. The alternative of calculating electron attachment energies of doublets should be avoided because of the qualitative failures of Koopmans's theorem results.

- For doublet-to-triplet and triplet-to-doublet molecular ionization energies, the MAEs produced by L3+B and RL3 are 0.12 and 0.14 eV, respectively. These results are only about 0.05 eV larger than their counterparts produced with closed-shell reference states.
- For the four triplet-to-quartet molecular ionization energies, greater errors occurred. This preliminary result awaits confirmation with a larger set of data.
- For doublet-to-triplet and triplet-to-doublet molecular electron affinities, one may calculate electron attachment energies of molecules or electron detachment energies of anions. The latter option is preferable because it produces smaller mean absolute errors. The MAEs of L3+B and RL3 are approximately 0.1 eV. These results are up to 0.04 eV larger than those pertaining to electron detachment energies of closed-shell anions.

The recommended second-order, Q3+, L3+B and RL3 methods whose results are represented in Figure 1 have advantageous computational requirements. The D2 and os-nD-D2 methods involve algorithms with cubic arithmetic scaling. Q3+ for electron detachment energies is executed with a fifth-power algorithm with only a cubic dependence on the number of virtual orbitals. In practice, the *de facto* bottlenecks in these calculations occur in the partial transformation of electron repulsion integrals. The more accurate and computationally demanding L3+B and RL3 methods also have fifth-power arithmetic scaling. Their scaling factors have a fourth-power dependence on the number of virtual orbitals. Electron repulsion integrals with four virtual indices appear in their self-energy formulas. To reduce the number of bottleneck contractions for electron detachment energies, non-Dyson variants may be employed. The latter advantage is practically irrelevant for electron attachment energies, for non-Dyson variants do not affect the bottleneck steps. For similar reasons, there is no advantage in employing Q3+ instead of L3+B for electron attachment energies.

Recommended electron-propagator methods with diagonal self-energies in the canonical spin−orbital basis of unrestricted Hartree−Fock wave functions are only slightly less accurate than their closed-shell-reference counterparts. These methods, like their closed-shell antecedents, have no adjustable parameters. Improvements in accuracy may be realized by generalizing to nondiagonal self-energies. Alternative spin−orbital basis sets are also worth investigation.

■ ASSOCIATED CONTENT

Supporting Information

The Supporting Information is available free of charge at https://pubs.acs.org/doi/10.1021/acs.jpca.4c04318.

Molecular electron detachment energies, Molecules_Detachments.xlsx (XLSX)

Molecular electron attachment energies, Molecules_Attachments.xlsx (XLSX)

Atomic electron detachment energies, Atoms_Detachments.xlsx (XLSX)

Atomic electron attachment energies, Atoms_Attachments.xlsx (XLSX)

■ AUTHOR INFORMATION

Corresponding Author

J. V. Ortiz − *Department of Chemistry and Biochemistry, Auburn University, Auburn, Alabama 36849-5312, United States;* orcid.org/0000-0002-9277-0226; Email: ortiz@auburn.edu

Authors

Ernest Opoku − *Department of Chemistry and Biochemistry, Auburn University, Auburn, Alabama 36849-5312, United States;* orcid.org/0000-0002-4271-6838

Filip Pawłowski − *Department of Chemistry and Biochemistry, Auburn University, Auburn, Alabama 36849-5312, United States*

Complete contact information is available at: https://pubs.acs.org/10.1021/acs.jpca.4c04318

https://doi.org/10.1021/acs.jpca.4c04318
J. Phys. Chem. A 2024, 128, 7311−7330

Notes

The authors declare no competing financial interest.

■ ACKNOWLEDGMENTS

The authors thank Dr. Manuel Díaz-Tinoco for valuable discussions and the Alabama Supercomputer Center for computing resources.

■ REFERENCES

(1) Linderberg, J.; Öhrn, Y. *Propagators in Quantum Chemistry*, Second Edition; Wiley-Interscience, 2004.
(2) Schirmer, J. *Many-Body Methods for Atoms, Molecules and Clusters*, Springer International Publishing: Switzerland AG, 2018.
(3) Jørgensen, P.; Simons, J. *Second Quantization-Based Methods in Quantum Chemistry*; Academic Press, 1981.
(4) Opoku, E.; Pawłowski, F.; Ortiz, J. V. A new generation of diagonal self-energies for the calculation of electron removal energies. *J. Chem. Phys.* **2021**, *155* (20), 204107.
(5) Opoku, E.; Pawłowski, F.; Ortiz, J. V. Electron Propagator Self-Energies versus Improved GW100 Vertical Ionization Energies. *J. Chem. Theory Comput.* **2022**, *18* (8), 4927−4944.
(6) Opoku, E.; Pawłowski, F.; Ortiz, J. V. Electron Propagator Theory of Vertical Electron Detachment Energies of Anions: Benchmarks and Applications to Nucleotides. *J. Phys. Chem. A* **2023**, *127* (4), 1085−1101.
(7) Opoku, E.; Pawłowski, F.; Ortiz, J. V. A new generation of non-diagonal, renormalized self-energies for calculation of electron removal energies. *J. Chem. Phys.* **2023**, *159* (12), 124109.
(8) Opoku, E.; Pawłowski, F.; Ortiz, J. V. New-Generation Electron-Propagator Methods for Molecular Electron-Binding Energies. *J. Phys. Chem. A* **2024**, *128* (8), 1399−1416.
(9) Opoku, E.; Pawłowski, F.; Ortiz, J. V. New-generation electron-propagator methods for vertical electron detachment energies of molecular anions: benchmarks and applications to model green-fluorescent-protein chromophores. *Phys. Chem. Chem. Phys.* **2024**, *26* (13), 9915−9930.
(10) Opoku, E.; Pawłowski, F.; Ortiz, J. V. New-Generation Electron-Propagator Methods for Calculations of Electron Affinities and Ionization Energies: Tests on Organic Photovoltaic Molecules. *J. Chem. Theory Comput.* **2024**, *20* (1), 290−306.
(11) Opoku, E.; Pawłowski, F.; Ortiz, J. V. Ab Initio Electron Propagators with an Hermitian, Intermediately Normalized Super-operator Metric Applied to Vertical Electron Affinities. *J. Phys. Chem. A* **2024**, *128* (23), 4730−4749.
(12) Hirata, S.; Hermes, M. R.; Simons, J.; Ortiz, J. V. General-Order Many-Body Green's Function Method. *J. Chem. Theory Comput.* **2015**, *11* (4), 1595−1606.
(13) Hirata, S.; Doran, A. E.; Knowles, P. J.; Ortiz, J. V. One-particle many-body Green's function theory: Algebraic recursive definitions, linked-diagram theorem, irreducible-diagram theorem, and general-order algorithms. *J. Chem. Phys.* **2017**, *147* (4), 044108.
(14) Hirata, S.; Grabowski, I.; Ortiz, J. V.; Bartlett, R. J. Non-convergence of the Feynman-Dyson diagrammatic perturbation expansion of propagators. *Phys. Rev. A* **2024**, *109* (5), 052220.
(15) Johnson, C. M.; Doran, A. E.; Ten-no, S. L.; Hirata, S. Monte Carlo explicitly correlated many-body Green's function theory. *J. Chem. Phys.* **2018**, *149* (17), 174112.
(16) Doran, A. E.; Hirata, S. Monte Carlo Second- and Third-Order Many-Body Green's Function Methods with Frequency-Dependent. *Nondiagonal Self-Energy. J. Chem. Theory Comput.* **2019**, *15* (11), 6097−6110.
(17) Ohnishi, Y.-y.; Ten-no, S. Explicitly correlated frequency-independent second-order green's function for accurate ionization energies. *J. Comput. Chem.* **2016**, *37*, 2447−2453.
(18) Pavošević, F.; Peng, C.; Ortiz, J. V.; Valeev, E. F. Communication: Explicitly correlated formalism for second-order single-particle Green's function. *J. Chem. Phys.* **2017**, *147* (12), 121101.
(19) Teke, N. K.; Pavošević, F.; Peng, C.; Valeev, E. F. Explicitly correlated renormalized second-order Green's function for accurate ionization potentials of closed-shell molecules. *J. Chem. Phys.* **2019**, *150* (21), 214103.
(20) Yeager, D. L. The multiconfigurational spin-tensor electron propagator method (MCSTEP). *Adv. Quantum Chem.* **2005**, *50*, 289−313.
(21) Chatterjee, K.; Sokolov, A. Y. Second-Order Multireference Algebraic Diagrammatic Construction Theory for Photoelectron Spectra of Strongly Correlated Systems. *J. Chem. Theory Comput.* **2019**, *15* (11), 5908−5924.
(22) Chatterjee, K.; Sokolov, A. Y. Extended Second-Order Multireference Algebraic Diagrammatic Construction Theory for Charged Excitations. *J. Chem. Theory Comput.* **2020**, *16* (10), 6343−6357.
(23) de Moura, C. E. V.; Sokolov, A. Y. Simulating X-ray photoelectron spectra with strong electron correlation using multi-reference algebraic diagrammatic construction theory. *Phys. Chem. Chem. Phys.* **2022**, *24* (8), 4769−4784.
(24) Mazin, I. M.; Sokolov, A. Y. Core-Excited States and X-ray Absorption Spectra from Multireference Algebraic Diagrammatic Construction Theory. *J. Chem. Theory Comput.* **2023**, *19* (15), 4991−5006.
(25) Banerjee, S.; Sokolov, A. Y. Algebraic Diagrammatic Construction Theory for Simulating Charged Excited States and Photoelectron Spectra. *J. Chem. Theory Comput.* **2023**, *19* (11), 3037−3053.
(26) Schirmer, J.; Trofimov, A. B.; Stelter, G. A non-Dyson third-order approximation scheme for the electron propagator. *J. Chem. Phys.* **1998**, *109* (12), 4734−4744.
(27) Dempwolff, A. L.; Schneider, M.; Hodecker, M.; Dreuw, A. Efficient implementation of the non-Dyson third-order algebraic diagrammatic construction approximation for the electron propagator for closed- and open-shell molecules. *J. Chem. Phys.* **2019**, *150* (6), 064108.
(28) Dreuw, A.; Papapostolou, A.; Dempwolff, A. L. Algebraic Diagrammatic Construction Schemes Employing the Intermediate State Formalism: Theory, Capabilities, and Interpretation. *J. Phys. Chem. A* **2023**, *127* (32), 6635−6646.
(29) Ortiz, J. V. Electron propagator theory: an approach to prediction and interpretation in quantum chemistry. *Wiley Interdisciplinary Reviews: Computational Molecular Science* **2013**, *3* (2), 123−142.
(30) Corzo, H. H.; Ortiz, J. V. Chapter Thirteen - Electron Propagator Theory: Foundations and Predictions. In *Adv. Quantum Chem.*, Sabin, J. R.; Brändas, E. J., Eds.; Vol. *74*; Academic Press, 2017; pp 267−298.
(31) Ortiz, J. V. Chapter Four - Interpreting Bonding and Spectra With Correlated, One-Electron Concepts From Electron Propagator Theory. In *Annual Reports in Computational Chemistry*, Dixon, D. A., Ed.; Vol. *13*; Elsevier, 2017; pp 139−182.
(32) Díaz-Tinoco, M.; Pawłowski, F.; Ortiz, J. V. Dyson orbitals and chemical bonding. In *Chemical Reactivity*, Kaya, S., von Szentpaly, L.; Serdaroglu, G.; Guo, L.; Ed.; Vol. *1*; Elsevier, 2023; pp 27−64.
(33) Ortiz, J. V. Chapter Seven - Recent progress in electron-propagator, extended-Koopmans-theorem and self-consistent-field approaches to the interpretation and prediction of electron binding energies. In *Adv. Quantum Chem.*, Vol. *85* Academic Press, 2022; pp 109−155.
(34) Koopmans, T. Über die Zuordnung von Wellenfunktionen und Eigenwerten zu den Einzelnen Elektronen Eines Atoms. *Physica* **1934**, *1* (1−6), 104−113.
(35) Pickup, B. T.; Goscinski, O. Direct calculation of ionization energies. I. Closed shells. *Mol. Phys.* **1973**, *26*, 1013−1035.
(36) Bartlett, R. J. Coupled-cluster theory and its equation-of-motion extensions. *WIREs Computational Molecular Science* **2012**, *2* (1), 126−138.
(37) Møller, C.; Plesset, M. S. Note on an Approximation Treatment for Many-Electron Systems. *Phys. Rev.* **1934**, *46* (7), 618−622.
(38) Schirmer, J.; Cederbaum, L. S.; Walter, O. New approach to the one-particle Green's function for finite Fermi systems. *Phys. Rev. A* **1983**, *28* (3), 1237−1259.

https://doi.org/10.1021/acs.jpca.4c04318
J. Phys. Chem. A 2024, 128, 7311−7330

(39) Ortiz, J. V. A nondiagonal, renormalized extension of partial third-order quasiparticle theory: comparisons for closed-shell ionization energies. *J. Chem. Phys.* **1998**, *108*, 1008−1014.
(40) Ortiz, J. V. Toward an exact one-electron picture of chemical bonding. *Adv. Quantum Chem.* **1999**, *35*, 33−52.
(41) Díaz−Tinoco, M.; Corzo, H. H.; Pawłowski, F.; Ortiz, J. V. Do Dyson Orbitals resemble canonical Hartree−Fock orbitals? *Mol. Phys.* **2019**, *117* (17), 2275−2283.
(42) Reining, L. The GW approximation: content, successes and limitations. *Wiley Interdiscip. Rev.: Comput. Mol. Sci.* **2018**, *8* (3), e1344.
(43) von Niessen, W.; Schirmer, J.; Cederbaum, L. S. Computational methods for the one-particle Green's function. *Comput. Phys. Rep.* **1984**, *1*, 57−125.
(44) Ortiz, J. V. The Electron Propagator Picture of Molecular Electronic Structure. In *Computational Chemistry: Reviews of Current Trends*, Leszczynski, J., Ed.; Vol. 2; World Scientific Publishing Co Pte Ltd, 1997; pp 1−61.
(45) Ortiz, J. V. Partial third-order quasiparticle theory: Comparisons for closed-shell ionization energies and an application to the Borazine photoelectron spectrum. *J. Chem. Phys.* **1996**, *104* (19), 7599−7605.
(46) Ortiz, J. V. An efficient, renormalized self-energy for calculating the electron binding energies of closed-shell molecules and anions. *Int. J. Quantum Chem.* **2005**, *105*, 803−808.
(47) Purvis, G. D.; Öhrn, Y. Electron propagator calculations of the photoelectron spectrum for open shell molecules with applications to the oxygen molecule. *J. Chem. Phys.* **1975**, *62* (6), 2045−2049.
(48) Stahl, T. L.; Banerjee, S.; Sokolov, A. Y. Quantifying and reducing spin contamination in algebraic diagrammatic construction theory of charged excitations. *J. Chem. Phys.* **2022**, *157* (4), 044106.
(49) Ortiz, J. V. Dyson-orbital concepts for description of electrons in molecules. *J. Chem. Phys.* **2020**, *153* (7), 070902.
(50) Frisch, M. J.; Trucks, G. W.; Scalmani, G.; Cheeseman, J. R.; Li, X.; Bloino, J.; Janesko, B. G.; Marenich, A. V.; Zheng, J.; Lipparini, F.;et al.*Gaussian Development Version*, Revision J.28; Gaussian Inc., 2023.
(51) Raghavachari, K.; Trucks, G. W.; Pople, J. A.; Head-Gordon, M. A fifth-order perturbation comparison of electron correlation theories. *Chem. Phys. Lett.* **1989**, *157* (6), 479−483.
(52) Kendall, R. A.; Dunning, T. H.; Harrison, R. J. Electron affinities of the first-row atoms revisited. Systematic basis sets and wave functions. *J. Chem. Phys.* **1992**, *96* (9), 6796−6806.

https://doi.org/10.1021/acs.jpca.4c04318
J. Phys. Chem. A 2024, 128, 7311−7330

Appendix L

E. Opoku, F. Pawłowski and J. V. Ortiz, "Electron Binding Energies and Dyson Orbitals of $O_nH_{2n+1}^{+,0,-}$ Clusters: Double Rydberg Anions, Rydberg Radicals and Micro−Solvated Hydronium Cations", *J. Chem. Phys.*, 154, 234304 (2021)

The Journal of Chemical Physics ARTICLE scitation.org/journal/jcp

Electron binding energies and Dyson orbitals of $O_nH_{2n+1}^{+,0,-}$ clusters: Double Rydberg anions, Rydberg radicals, and micro-solvated hydronium cations

Cite as: J. Chem. Phys. **154**, 234304 (2021); doi: 10.1063/5.0053297
Submitted: 6 April 2021 • Accepted: 3 June 2021 •
Published Online: 17 June 2021

View Online Export Citation CrossMark

Ernest Opoku,[a] Filip Pawłowski,[b] and Joseph Vincent Ortiz[c]

AFFILIATIONS

Department of Chemistry and Biochemistry, Auburn University, Auburn, Alabama 36849-5312, USA

[a]ezo0009@auburn.edu
[b]filip@auburn.edu
[c]Author to whom correspondence should be addressed: ortiz@auburn.edu

ABSTRACT

Ab initio electron propagator methods are employed to predict the vertical electron attachment energies (VEAEs) of $OH_3^+(H_2O)_n$ clusters. The VEAEs decrease with increasing n, and the corresponding Dyson orbitals are diffused over exterior, non-hydrogen bonded protons. Clusters formed from OH_3^- double Rydberg anions (DRAs) and stabilized by hydrogen bonding or electrostatic interactions between ions and polar molecules are studied through calculations on $OH_3^-(H_2O)_n$ complexes and are compared with more stable $H^-(H_2O)_{n+1}$ isomers. Remarkable changes in the geometry of the anionic hydronium–water clusters with respect to their cationic counterparts occur. Rydberg electrons in the uncharged and anionic clusters are held near the exterior protons of the water network. For all values of n, the anion–water complex $H^-(H_2O)_{n+1}$ is always the most stable, with large vertical electron detachment energies (VEDEs). $OH_3^-(H_2O)_n$ DRA isomers have well separated VEDEs and may be visible in anion photoelectron spectra. Corresponding Dyson orbitals occupy regions beyond the peripheral O–H bonds and differ significantly from those obtained for the VEAEs of the cations.

Published under an exclusive license by AIP Publishing. https://doi.org/10.1063/5.0053297

I. INTRODUCTION

Transport, reactions, and structural characteristics of molecular ions in aqueous environments play important roles in many chemical and biological processes.[1–3] Seeking understanding of structural, electronic, and dynamic properties of protonated water clusters with cationic, neutral, or anionic charges ($O_nH_{2n+1}^{+,0,-}$) is also motivated by the involvement of such species in the formation of clouds and haze and in solvent effects in aqueous systems.[4] Concepts of acid–base chemistry are often defined in terms of proton transfer. Therefore, understanding the behavior of protons and other ions in water networks is a perennial concern in physical chemistry. However, hydrogen bond networks, such as protonated water clusters, present several structural and dynamical complexities which render them challenging to study.[5] Notwithstanding their ubiquitous presence in nature, protonated water clusters are elusive molecular entities that are extremely difficult to probe with direct experiments. Owing to the anomalously high mobility of protons in water, a detailed understanding of structures, transport mechanisms, and solvation in $H^+(H_2O)_n$ clusters remains a challenging goal. Considering the difficulty in direct experimental investigations, the chemistry of protonated water clusters and associated molecular ions stands to greatly benefit from quantum-chemical calculations.

Attachment of an electron to a protonated water cluster may give rise to a Rydberg molecule that departs from traditional concepts of chemical bonding. Rydberg molecules consist of a geometrically and electronically stable cationic core that binds a non-bonding electron held in a diffuse orbital.[6] In the case of double Rydberg anions (DRAs), a stable ground-state molecular cation binds a pair of diffuse electrons that are distributed over the periphery of the cationic core.[7] The electrons that bind to a cationic core in DRAs

and Rydberg neutrals may occupy orbitals with unusual amplitudes. The first DRA to be observed and characterized was tetrahedral NH_4^-.[7–9] Tetrahedral NH_4^- was anticipated in preceding computational studies.[10,11] Subsequent experimental[7,12] and theoretical[13–15] investigations have considered several isomers of $N_nH_{3n+1}^-$ DRAs that arise from hydrogen bonding or electrostatic interactions.

Theoretical studies have predicted and identified many DRAs without nitrogen atoms, such as OH_3^- and $O_2H_5^-$, that are authentic minima in potential energy surfaces (PESs) and that have positive vertical electron detachment energies (VEDEs).[6,15–20] Melton and Joy provided the first experimental and theoretical evidence for the existence of OH_3 radicals through the irradiation of water vapor with ionizing electrons.[21] Evidence from the kinetics of water radiolysis was provided for the existence of OH_3 as an intermediate.[22,23] Andersen *et al.*[24] reported that the mechanism of generating water molecules in interstellar clouds occurs through a dissociative recombination reaction of OH_3^+ with electrons. In this mechanism, Rydberg states of OH_3 appear as intermediates in agreement with later *ab initio* investigations.[25–29] Since their report,[24] the OH_3 radical and its solvated derivatives have attracted serious consideration in computational and experimental studies. Brozek-Pluska *et al.*[30] observed from femtosecond spectroscopy experiments that solvated oxonium radicals play a significant role in the domain of liquid phase reactivity.

Early computational and experimental studies on OH_3 radicals focused on analysis of electronic structure and ground-state stability. Some successive studies provided extensive details on Rydberg excited states and transition intensities of OH_3 and other radicals.[31–37] Recent studies[38,39] have combined *ab initio* electron propagator theory (EPT) and coupled-cluster (CC) methods with the molecular quantum defect orbital (MQDO) formalism to study the electronic absorption spectra of NH_4 and OH_3 Rydberg radicals. A few years later, cross sections for the ionization of NH_4 and OH_3 from their outermost shells were analyzed in terms of the photoelectron energy.[40] Chen and Davidson[41] studied the electronic structure of OH_3, NH_4, and FH_2 Rydberg molecules using second-order Møller–Plesset perturbation (MP2) theory.[42,43] They reported the relative stabilities of NH_4, OH_3, and FH_2 and their isotopic congeners and constructed PESs for these Rydberg neutrals.

In the case of hydrated proton clusters, past studies[44] have focused more on understanding the vibrational spectra of $H^+(H_2O)_n$, n = 2–28. There are two key structural proposals that pertain to the hydrated proton. Eigen[45] suggested a $O_4H_9^+$ complex in which an OH_3^+ core is strongly hydrogen-bonded to three H_2O molecules. Zundel[46] later proposed the formation of a $O_2H_5^+$ complex, in which the proton is shared between two H_2O molecules. Early *ab initio* and density functional theory (DFT) quantum-chemical investigations on $H^+(H_2O)_n$ clusters (n = 1–8),[47–52] vibrational spectroscopy experiments,[53] and molecular dynamics simulations[54–57] have led to the conclusion that the hydrated proton $H^+(H_2O)_n$ forms a fluxional defect in the hydrogen-bonded network, with both $H_9O_4^+$ and $H_5O_2^+$ occurring in the sense of limiting or ideal structures.[58] These works suggest that the rate-limiting step for proton transfer may not be an actual proton transfer through a hydrogen bond between OH_3^+ and a neighboring water molecule. Instead, it may involve rupture of a hydrogen bond between the first and second solvation shells of OH_3^+ induced by fluctuations that reduce the coordination number of a water molecule in the first solvation shell.[5,54]

Recently, Verma *et al.*[59] also reported that electron impact ionization of He droplets doped with clusters of water molecules yields water and $O_2H_5^+$ cations implanted in the droplets. They obtained infrared spectra by measuring the intensity of the cations released from the droplets upon laser excitation. The OH−stretch spectra of water (H_2O^+) and Zundel ($O_2H_5^+$) cations in helium droplets in the 3 μm region were reported. The authors[59] observed a significant difference in the intensity of the two components of the asymmetric vibrational bands in contrast with the results of a prior computational study that predicted very similar intensities under effective D_{2d} symmetry.[60]

Some recent theoretical studies on vibrational spectroscopy of hydrated proton clusters $H^+(H_2O)_n$ relied on vibrational second-order perturbation theory (VPT2),[61–66] with the electronic energies typically obtained from density functional theory (DFT) employing the B3LYP[67,68] functional. CC methods are less frequently used for the studies of larger solvated oxonium clusters due to their computational expense.[69] To address electron correlation, MP2 methods are generally used for geometry optimization as demonstrated by Xantheas[70] in the study of various isomers of $OH_3^+(H_2O)_{20}$. It has also been found that empirical or semiempirical potentials that adequately describe proton transfer processes can be used to probe the structure and dynamics of larger solvated oxonium systems.[71–73] Shi *et al.*[4] used a comprehensive genetic algorithm combined with density functional theory (CGA-DFT) to search the PES of $H^+(H_2O)_n$ clusters with n = 10–17 and simulated the IR spectra of the lowest energy structures with anharmonic corrections using the VPT2 method. Likewise, there have been theoretical studies on structure, vertical detachment energies, and electronic spectra of water cluster anions $(H_2O)_n^-$.[74–78]

Rydberg neutrals and DRAs arising from OH_3^+ have been studied since 1990.[6,15] Ortiz[20] presented structural and spectral predictions of the OH_3^- DRA. Electron propagator calculations combined with larger diffuse basis sets were used to obtain vertical electron binding energies for the OH_3^- DRA at the geometry of the anionic minimum. A later study[39] provided predictions of structures, vibrational frequencies, relative total energies, and electron binding energies on isomers of OH_3^- and $O_2H_5^-$ DRAs in comparison to NH_4^- and $N_2H_7^-$. No studies on $H^-(H_2O)_n$, $n \geq 3$ isomers have been performed. A careful search of the literature reveals no experimental evidence of the H_3O^- DRA or any of its higher clusters. However, the $H^-(H_2O)$ isomer of the OH_3^- DRA has been observed experimentally with a VEDE of 1.53 eV.[79] The $H^-(H_2O)$ isomer can be considered to be an H^- anion solvated by one water molecule. Considerable experimental efforts have been made to produce H_3O^- DRA with no success, perhaps because this species is much higher in energy than the $H^-(H_2O)$ isomer.[39] At the same time, the metastable Rydberg radicals, OH_3 and OD_3, have been identified with neutralized ion beam spectroscopy experiments by Porter and co-workers.[80–82] Sobolewski and Domcke[58] studied the structures and spectroscopy of cationic and neutral hydronium–water clusters arising from the Eigen-like model $H_3O^+(H_2O)_n$ and the Zundel-like geometries $O_2H_5^+(H_2O)_n$ at the MP2, complete-active-space self-consistent field, complete-active-space perturbation theory of second order, and DFT/B3LYP levels of theory. Okumura and co-workers[53] also reported combined experimental and computational

Published under an exclusive license by AIP Publishing

studies on vibrational spectroscopy of the hydrated hydronium cluster ions $OH_3^+(H_2O)_n$ (n = 1–3). These authors found that the Zundel cation $O_2H_5^+$ may have C_2 and C_S isomers, with the C_2 geometry being more stable. Similarly, the $O_3H_7^+$ structures were assigned to the C_S and C_{2v} point groups, with the C_S structure being the most stable. The Eigen cation $O_4H_9^+$ was assigned to the C_{3v} and D_{3h} point groups. The C_{3v} structure was reported as the most stable.

Despite all this progress, a thorough search of the chemical literature reveals no studies on the O_2H_5 Rydberg radical and corresponding higher $H(H_2O)_n$ clusters. In the case of DRAs, we found studies only on the OH_3^- and $O_2H_5^-$ species,[39] prompting the need for theoretical studies on larger clusters to offer correlative guidance for future experiments. Techniques of EPT provide reliable predictions for the discovery and identification of novel DRAs[9,39] and related solvated-electron precursors.[83–85] To extend the scope of double Rydberg concepts to oxygen-based systems, stabilization of the pyramidal H_3O^- DRA by hydrogen bonding or electrostatic interactions ought to be considered.

Herein, we have employed high-accuracy, *ab initio* EPT and CC methods with large, diffuse basis sets to study the hydronium O_nH_{2n+1} Rydberg molecules, $O_nH_{2n+1}^-$ DRAs, and related solvated species. In completing the first solvation shell, both the Eigen-like $H_3O^{\pm}(H_2O)_n$ structures and Zundel's $H_5O_2^{\pm}(H_2O)_{n-1}$ models are considered. Predictions of structures, vibrational frequencies, relative total energies, vertical electron binding energies, and Dyson orbitals associated with Rydberg neutrals and DRAs are investigated. Isomers that arise from electrostatic intermolecular interactions or hydrogen bonding to form hydride- and DRA-molecule complexes are all considered. Calculations on isomers of $O_nH_{2n+1}^{\pm}$ complexes with only their first solvation shells provide Aufbau rules for electrons that occupy the periphery of these complexes.

II. THEORY AND COMPUTATIONAL DETAILS

A. Summary of electron propagator theory

EPT[86–88] is a quantum-chemistry method that allows for calculating electron binding energies (e.g., electron attachment and detachment energies of molecular ions) directly, without any explicit reference to final state wave functions and their total energies. The electron attachment and detachment energies occur at poles of the electron propagator matrix, $\mathbf{G}(E)$,

$$G_{rs}(E) = \lim_{\eta\to+0}\left[\sum_{P}^{Attachment}\frac{\langle 0|a_r|P\rangle\langle P|a_s^\dagger|0\rangle}{E+E_0-E_P^+ + i\eta} + \sum_{P}^{Detachment}\frac{\langle 0|a_s^\dagger|P\rangle\langle P|a_r|0\rangle}{E-E_0+E_P^- - i\eta}\right], \quad (1)$$

where the N-electron state, $|0\rangle$, and the $(N \pm 1)$-electron states, $|P\rangle$, and their energies (E_0 and $E_P^{\pm}$, respectively) are the solutions to the Hamiltonian eigenvalue problem,

$$\begin{aligned} H|0\rangle_N &= E_0|0\rangle_N, \\ H|P\rangle_{N\pm1} &= E_P^{\pm}|P\rangle_{N\pm1}, \end{aligned} \quad (2)$$

a_r and $a_s^\dagger$ are the annihilation and creation operators, respectively, with the indices, r and s, referencing a basis (a finite, spin–orbital basis of a reference, Hartree–Fock state is assumed in the following, which implies that only discrete electron attachment, $E = E_P^+ - E_0$, and detachment, $E = E_0 - E_P^-$, energies are obtained), and the infinitesimal factor η ensures the correct Fourier transformation between the time-dependent definition of the electron propagator and its energy representation in the spectral form in Eq. (1).

While electron binding energies occur at the poles (i.e., vanishing denominators) of Eq. (1), the corresponding residues (i.e., numerators pertaining to the vanishing denominators) are products of Feynman–Dyson amplitudes,

$$C_{rP} = \begin{cases} \langle 0|a_r|P\rangle & \text{(electron attachment)} \\ \langle P|a_r|0\rangle & \text{(electron detachment)}, \end{cases} \quad (3)$$

and their complex conjugates. The Feynman–Dyson amplitudes are expansion coefficients of non-normalized Dyson spin–orbitals in the orthonormal, molecular spin–orbital basis $\{\chi_r\}_{r=1}^M$ (where M is the size of the basis),

$$\phi_P^{Dyson} = \sum_{r=1}^{M}\chi_r C_{rP}. \quad (4)$$

The probability, Γ_P, pertaining to the electron detachment/attachment process described by the non-normalized Dyson spin–orbital, ϕ_P^{Dyson}, therefore reads (recall that the basis $\{\chi_r\}_{r=1}^M$ is orthonormal)

$$\Gamma_P \equiv \int_{-\infty}^{\infty}\left(\phi_P^{Dyson}\right)^* \phi_P^{Dyson}\mathrm{d}x = \sum_{r=1}^{M}|C_{rP}|^2, \quad (5)$$

where x denotes the spatial and spin coordinates of the detached/attached electron (the x-dependence of ϕ_P^{Dyson} has been suppressed in the notation). The probability factor, Γ_P (referred to as a pole strength), may thus be used to normalize the Dyson spin–orbital ϕ_P^{Dyson} such that the unit-normalized Dyson spin–orbital reads

$$\varphi_P^{Dyson} = \Gamma_P^{-0.5}\phi_P^{Dyson}. \quad (6)$$

Dyson spin–orbitals describe the change in the electronic structure between the N-electron wave function, Ψ_N, representing the initial state $|0\rangle$, and the $(N \pm 1)$-electron wave function, $\Psi_{N\pm1,P}$, representing the final state $|P\rangle$, i.e., for electron detachment,

$$\phi_P^{Dyson} = N^{1/2}\int \mathrm{d}x_2\mathrm{d}x_3\cdots\mathrm{d}x_N \times \Psi_N(x_1,x_2,x_3,\cdots,x_N)\Psi_{N-1,P}^*(x_2,x_3,\cdots,x_N), \quad (7)$$

whereas for electron attachment,

$$\phi_P^{Dyson} = (N+1)^{1/2}\int \mathrm{d}x_2\mathrm{d}x_3\cdots\mathrm{d}x_{N+1} \times \Psi_{N+1,P}(x_1,x_2,x_3,\cdots,x_{N+1})\Psi_N^*(x_2,x_3,\cdots,x_{N+1}). \quad (8)$$

Published under an exclusive license by AIP Publishing

Dyson spin–orbitals thus convey information about correlated motion of electrons embedded in many-electron wave functions Ψ_N and $\Psi_{N\pm1,P}$ (which may, in principle, be made exact) and yet retain an easily interpretable, one-electron character [as the integration in Eqs. (7) and (8) is carried out over all spin–spatial, electronic coordinates, x_i, but one—x_1—on which the Dyson spin–orbital depends] analogous to that of the non-correlated, Hartree–Fock theory.

As electron binding energies occur at poles of $\mathbf{G}(E)$, they may conveniently be obtained by seeking zero eigenvalues of the inverse electron propagator matrix, $\mathbf{G}^{-1}(E)$, and the Dyson spin–orbitals are then determined by the eigenvectors corresponding to those zero eigenvalues. When the canonical Hartree–Fock reference state and the Møller–Plesset partitioning of the Hamiltonian are employed, the inverse electron propagator matrix takes the form

$$\mathbf{G}^{-1}(E) = E\mathbf{I} - \boldsymbol{\varepsilon} - \boldsymbol{\sigma}(E), \tag{9}$$

where $\boldsymbol{\varepsilon}$ is a diagonal matrix of Hartree–Fock orbital energies and $\boldsymbol{\sigma}(E)$ is a self-energy matrix which contains a part that does not depend on E and describes the correlation of the initial N-electron state $|0\rangle$ and a part that depends on E and describes differential (with respect to $|0\rangle$) correlation and orbital relaxation effects in the final, $(N \pm 1)$-electron state $|P\rangle$.

Retaining only the diagonal part in $\mathbf{G}^{-1}(E)$ is equivalent to the following choice of the Feynman–Dyson amplitudes:

$$C_{rP} = \delta_{rP} C \tag{10}$$

(where C is, in general, a complex number), and it leads to a particularly simple form of the electron binding energy pertaining to the final state $|P\rangle$ [cf. Eq. (9)],

$$E_P = \varepsilon_P + \sigma_{PP}(E). \tag{11}$$

The corresponding, non-normalized Dyson spin–orbital becomes just the normalized, canonical molecular spin–orbital (with the spin–orbital index equal to the index of the final state due to the diagonal approximation) rescaled by the pole strength [cf. Eqs. (4)–(6) and (10)],

$$\phi_P^{Dyson} = \Gamma_P^{0.5} \chi_P, \tag{12}$$

where the pole strength may be obtained from

$$\Gamma_P = \left(1 - \frac{\mathrm{d}\sigma_{PP}(E)}{\mathrm{d}E}\bigg|_{E=E_P}\right)^{-1}. \tag{13}$$

Systematic, perturbative approximations to E_P of Eq. (11) may be devised by collecting terms through a given order in the fluctuation potential. As zeroth- and first-order contributions to $\sigma_{PP}(E)$ vanish, the zeroth-order approximation to E_P is identical to the orbital energy, ε_P, and the corresponding Dyson orbital is identical to the canonical, Hartree–Fock orbital, χ_P [i.e., the zeroth-order approximation yields the Koopmans theorem (KT)[89] result], and the first-order approximation to E_P vanishes. Collecting all terms through second order in Eq. (11) leads to the diagonal, second-order method (D2),[87,90] and collecting all terms through third order gives the diagonal, third-order method (D3).[87,90,91] A scaled version of D3 has dubbed the outer-valence Green's function (OVGF)[92–94] method and comes in three variants—A, B, and C. Numerical criteria have been introduced to automatically choose among these variants in a given calculation.[92,94,95] A careful analysis of the physical importance, numerical stability, and computational cost of third-order contributions has allowed for proposing alternatives to D3, namely, the partial third-order (P3)[96] method and its renormalized counterpart (P3+).[87]

OVGF, P3 and, particularly, P3+ have been highly successful[97–99] in describing valence detachment energies and electron affinities of systems for which KT constitutes a valid zeroth-order approximation. This validity of KT, and hence the applicability limit of the diagonal, perturbative approximations may be quantified by the pole strength, Γ_P in Eq. (13), for if its value drops below 0.85,[100] the results of the diagonal, perturbative methods should be treated with caution. This usually happens for systems with strong correlation (many unpaired electrons) or for inner-shell ionization. In such cases, one needs to resort to non-diagonal methods, in which the eigenvalue problem of the super-operator Hamiltonian is solved in a truncated manifold of field operators. Among the non-diagonal methods, Brueckner doubles (BD)-T1[91,101–103] has proven particularly successful. In BD-T1, all blocks of the super-operator Hamiltonian that arise in the hole (h), particle (p), two-hole-one-particle (2hp), and two-particle-one-hole (2ph) operator manifold are considered except the second-order couplings between 2ph and 2hp operators. BD-T1 uses the Brueckner doubles (BD), rather than Hartree–Fock, reference state. BD-T1 not only improves upon the results of the diagonal methods, in particular in cases where the pole strength is less than 0.85, but, as any other non-diagonal method, also employs Eq. (4), rather than Eq. (12) (used in diagonal methods), to produce Dyson spin–orbitals, which will therefore have contributions from all canonical, Hartree–Fock spin–orbitals. Thus, in addition to providing high-accuracy, quantitative information on binding energies, BD-T1 is also capable of improving the description of corresponding orbitals that may sometimes alter the qualitative picture provided by the canonical molecular orbitals, as is, for example, the case for a copper chloride trimer, Cu_3Cl_3.[103]

B. Geometry optimizations, vibrational frequencies, vertical electron binding energies, and excitation energies

Optimizations of geometries of all the cationic and anionic isomers of the O_nH_{2n+1} (n = 1–6) species were performed, and their energies were determined. For cationic structures, initial guesses were obtained by constraining specific internal coordinates of the cations (bond lengths, bond angles, and dihedral angles) and optimizing the remaining internal coordinates. The resulting geometries were then used as an input for full geometry optimizations without any geometry or symmetry constraints. Previous literature[39,53,58,69,77] was consulted in arriving at initial guess input structures for the cations. The fully optimized cationic geometries were employed as initial structures for full anionic geometry optimizations. Initial guess structures for the remaining anionic geometries (hydride-molecule complexes and electrostatic structures with ionic and polar-molecule fragments) were obtained in analogy with nitrogen-based $N_nH^-_{3n+1}$ DRAs.[14] The work of Melin and Ortiz[39] also provided useful hints about the H^- molecule complexes and the electrostatic geometries. For n = 1–5, the global minima for

Published under an exclusive license by AIP Publishing

the cationic geometries strongly resemble the second most stable isomers of the anions. For n = 6, the Eigen-like geometry E2 is the second most stable isomer.

The full structural optimizations were initially executed at the Hartree–Fock, MP2, DFT/CAM-B3LYP,[104] and coupled-cluster singles-and-doubles (CCSD)[105] levels with a wide range of basis sets to identify an appropriate level of theory. The augmented, triple-ζ, correlation-consistent basis (aug-cc-pVTZ)[106,107] was found to be sufficient for cations and anions; similar conclusions for n = 1–2 were reached by Melin and Ortiz.[39] Generally, MP2 results obtained with the aug-cc-PVTZ basis set[106,107] were found to be in close agreement with those of the coupled-cluster single double perturbative triple [CCSD(T)]/aug-cc-pVTZ level (a similar observation was made in Ref. 69). We therefore used MP2/aug-cc-pVTZ to optimize geometries for all the hydronium–water clusters, except for n = 1 and n = 2, where we employed the CCSD(T)/aug-cc-pVTZ structures. Vibrational frequency calculations were carried out for all the geometries to ensure that all minima are characterized by all real vibrational frequencies. MP2 and CCSD(T) frequency calculations were carried out using analytical and numerical Hessians, respectively. Single-point calculations on the O_nH_{2n+1} radicals were performed at the equilibrium geometry of cationic/anionic $O_nH_{2n+1}^{+,-}$ complexes to determine vertical ionization energies.

Vertical electron affinities of ground-state cations ($H_nO_{2n+1}^{+}$) that correspond to various final states of O_nH_{2n+1} and VEDEs from the anions ($H_nO_{2n+1}^{-}$) were calculated with electron propagator methods described in Sec. III A using large basis sets augmented with Rydberg-type diffuse orbitals (described in Sec. III C). Vertical excitation energies were inferred from differences between the vertical electron affinities.

C. Basis sets

To determine an optimal basis set for EPT calculations (and hence for an appropriate description of the ground and excited states of all the radicals considered in this work), primitive, diffuse Gaussian functions were added to the standard aug-cc-pVTZ basis.[106,107] Exponents of these additional Gaussians were obtained by scaling the smallest exponents of the s, p, d, and f primitives of the original aug-cc-pVTZ basis set with the factor of 0.5. Convergence of electron binding energies with respect to the s, p, d, and f primitive Gaussian functions was obtained with an additional 4s4p4d diffuse set on all H atoms and a 4s4p4d4f set on all O atoms. At the geometry of cations and anions, several basis sets were tested for calculation of electron binding energies to ascertain a balance between accuracy and computational cost. For selected systems, we tested the aug-cc-pVXZ (X = T, Q, 5, 6), d-aug-cc-pVTZ, t-aug-cc-pVTZ, and q-aug-cc-pVTZ basis sets (the latter three basis sets contain, respectively, two, three, and four sets of diffuse, primitive functions with exponents obtained in the even-tempered manner starting from the exponents of the diffuse set of the original aug-cc-pVXZ basis).[108] The results were compared against those obtained using aug-cc-pVTZ plus the above-described, additional diffuse 4s4p4d/4s4p4d4f set. We found the d-aug-cc-pVTZ basis to be the optimal choice for both cations and anions. Therefore, except where stated otherwise, all the EPT calculations were executed with the d-aug-cc-pVTZ basis.

D. Software

All geometry optimizations and KT, D2, D3, OVGF, P3, and P3+ EPT calculations were performed with Gaussian 16.[109] The BD-T1 calculations were carried out with a development version of Gaussian. Dyson orbitals were plotted with GaussView[110] using a cube file with an enhanced edge size generated with Molden.[111] The Dyson orbitals were plotted with an iso-value of 0.08 a.u. for the cations and 0.004 a.u. for the anions. Red and green surfaces of Dyson orbitals displayed in Figs. 1–14 correspond to opposite phases of a real-valued wave function. The surfaces are semi-transparent (to display the underlying molecular framework), and therefore, the inner, nodal surfaces of the Dyson orbitals are also visible.

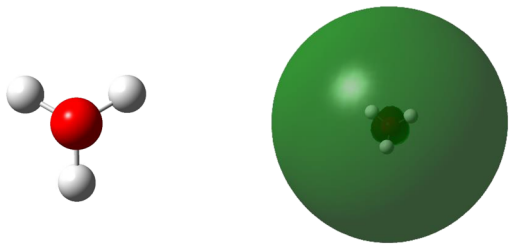


FIG. 1. n = 0: Optimized geometry and the Dyson orbital of electron attachment to the OH_3^+ cation.

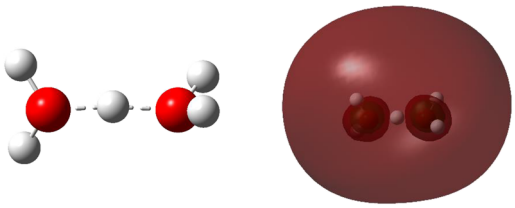


FIG. 2. Optimized geometry and the Dyson orbital of electron attachment to $O_2H_5^+$.

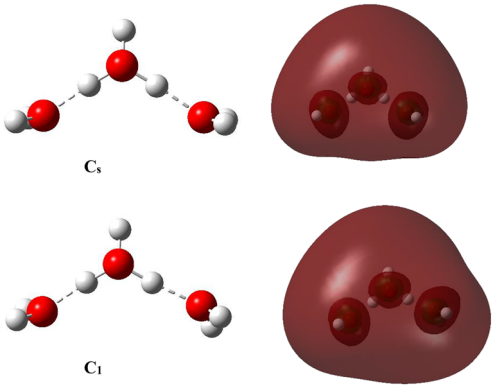


FIG. 3. n = 3: Optimized geometries and Dyson orbitals of electron attachment to $O_3H_7^+$ cations.

Published under an exclusive license by AIP Publishing

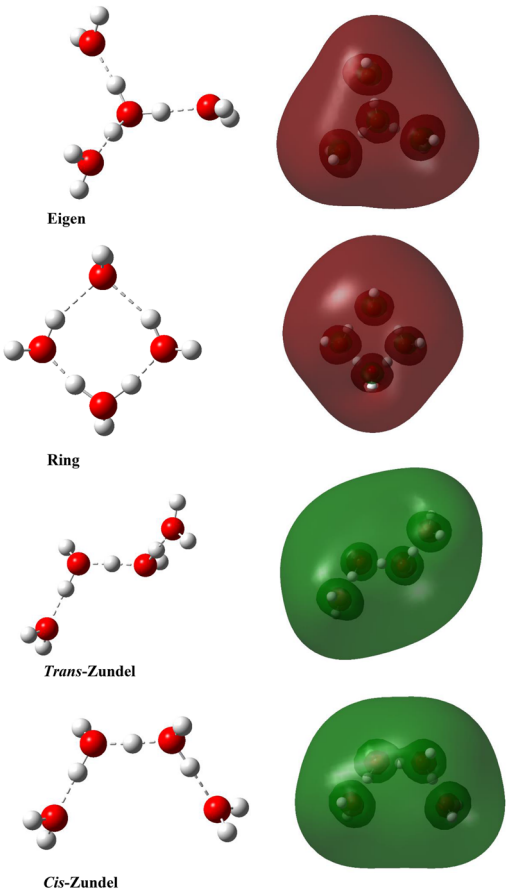


FIG. 4. $n = 3$: Optimized geometries and Dyson orbitals of electron attachment to $O_4H_9^+$ cations.

III. RESULTS AND DISCUSSION

A. O_nH_{2n+1} Rydberg molecules

This subsection presents the optimized ground-state geometries of closed-shell $O_nH_{2n+1}^+$ cations. For each cluster with a given n, relative energies are discussed along with geometric parameters. Vertical electron attachment energies (VEAEs) obtained with the KT, D2, D3, OVGF, P3, P3+, and BD-T1 methods are discussed. Subsection III B considers radical excitation energies of selected O_nH_{2n+1} clusters. Tables I–III and Figs. 1–6 present numerical and graphical data on the $O_nH_{2n+1}^{+,0}$ isomers.

Electron binding energies presented in Table I for all $O_nH_{2n+1}^+$ isomers do not vary much between the EPT methods. In all instances, pole strengths are above 0.85, indicating the adequacy of the diagonal, perturbative EPT methods. Therefore, unless stated otherwise, the discussion in the remainder of this subsection is focused on P3+ VEAEs.

1. OH_3^+

The optimized pyramidal ground-state structure of OH_3^+ belongs to the C_{3v} point group. OH_3^+ can be considered as the pyramidal C_{3v} analog of the sodium cation. All the O–H bond distances are equal (0.979 Å) at the CCSD(T)/aug-cc-pVTZ level (Fig. 1). OH_3^+ has a bound VEAE of 5.209 eV and a pole strength of 0.985, which suggests that electron correlation is not qualitatively important. The Dyson orbital for the lowest VEAE is a totally symmetric s-type function whose amplitude extends beyond the H nuclei. The two radial nodes in this Dyson orbital suggest resemblance to a 3s function in the united atom limit.

2. $O_2H_5^+$

Coordination of a water molecule to OH_3^+ through hydrogen bonding leads to the Zundel $O_2H_5^+$ cation, which is generally considered to have a symmetric hydrogen bridge with C_2 symmetry.[39,69]

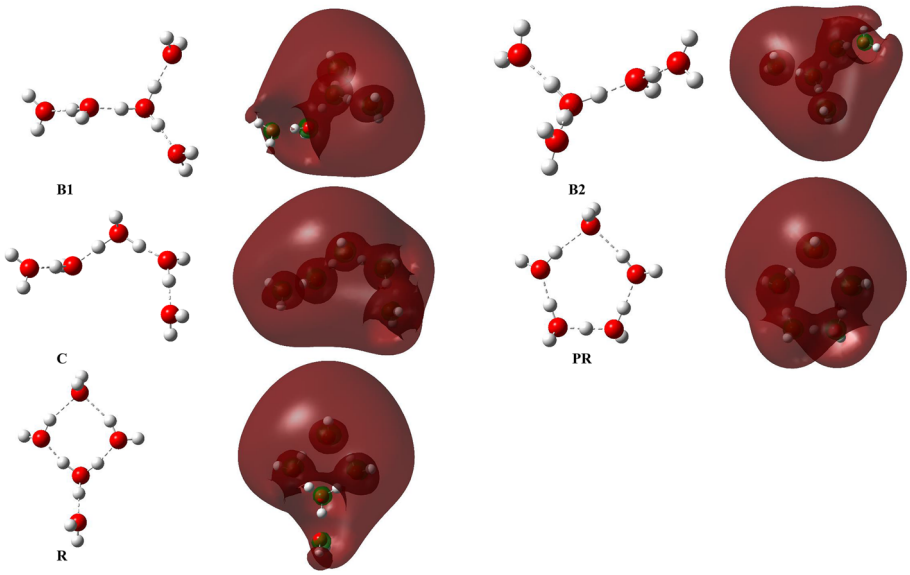


FIG. 5. $n = 4$: Optimized geometries and Dyson orbitals of electron attachment to $O_5H_{11}^+$ cations.

Published under an exclusive license by AIP Publishing

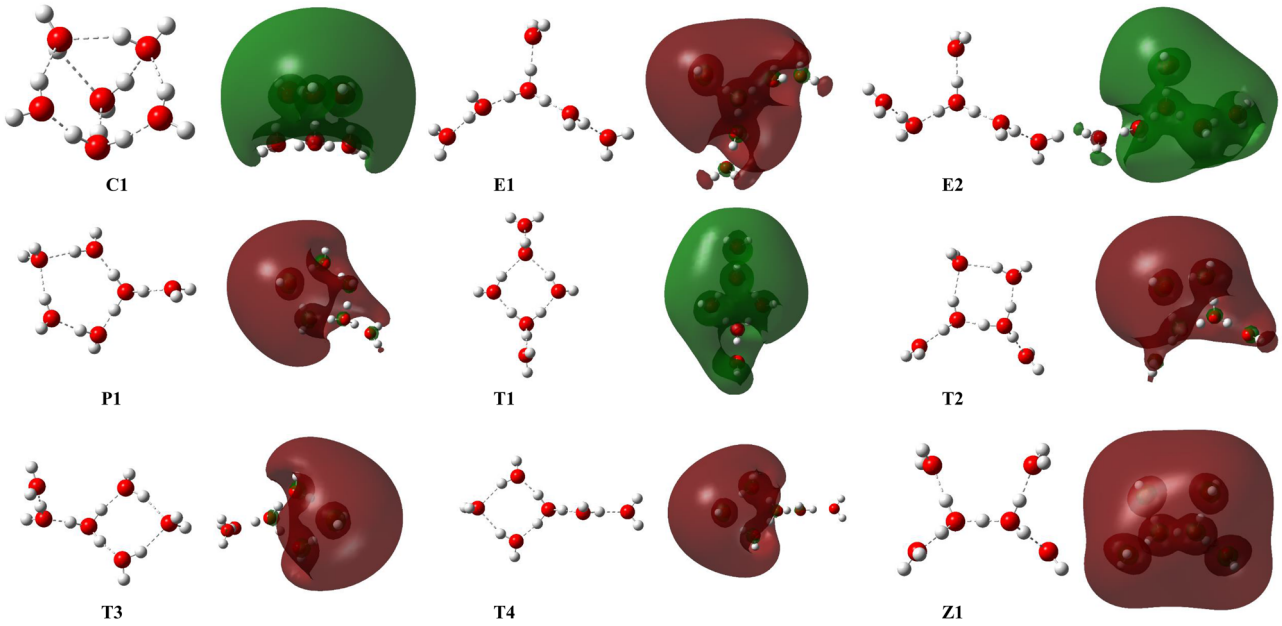


FIG. 6. $n = 5$: Optimized geometries and Dyson orbitals of electron attachment to $O_6H_{13}^+$ cations.

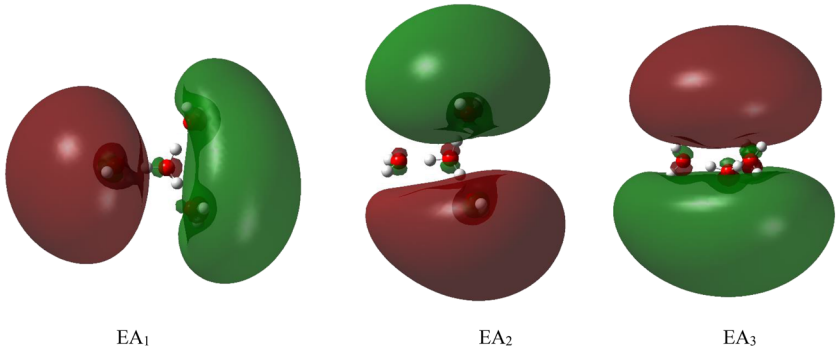


FIG. 7. Dyson orbitals of first three excited states of the Eigen O_4H_9 radical.

The bridging hydrogen atom is positioned at the distance of 1.20 Å from the oxygen nuclei of the two water molecules. Initial guesses corresponding to C_{2v}, D_{2h}, and D_{2d} symmetries converged to transition state geometries. Zundel $O_2H_5^+$ has a bound VEAE of 3.969 eV and a pole strength of 0.986. The near-unity pole strength confirms the adequacy of the one-electron picture of the VEAE. Therefore, the qualitative features of the Dyson orbital are identical to a Hartree–Fock virtual orbital. The totally symmetric diffuse Dyson

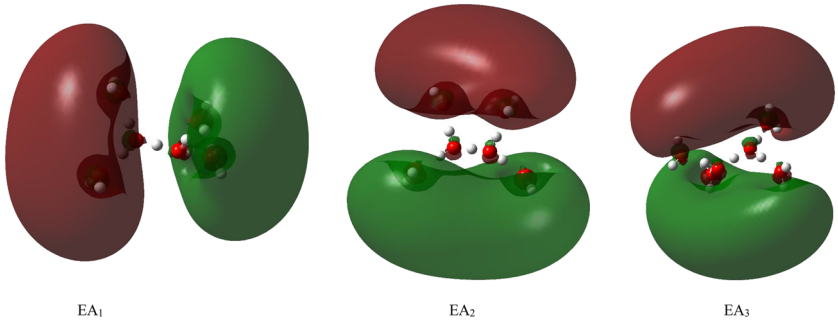


FIG. 8. Dyson orbitals of first three excited states of the Z1 O_6H_{13} radical.

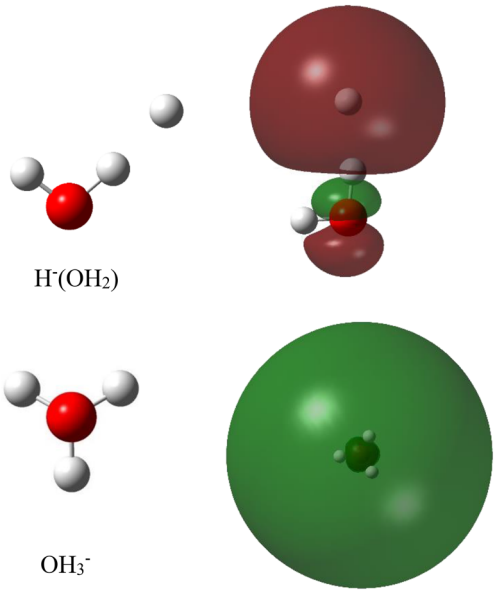


FIG. 9. n = 1: Optimized geometries and Dyson orbitals of electron detachment from anions.

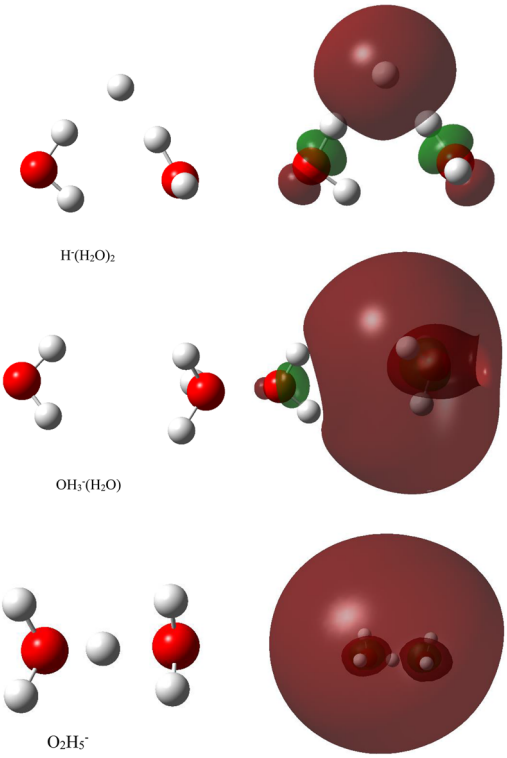


FIG. 10. n = 2: Optimized geometries and Dyson orbitals of electron detachment from anions.

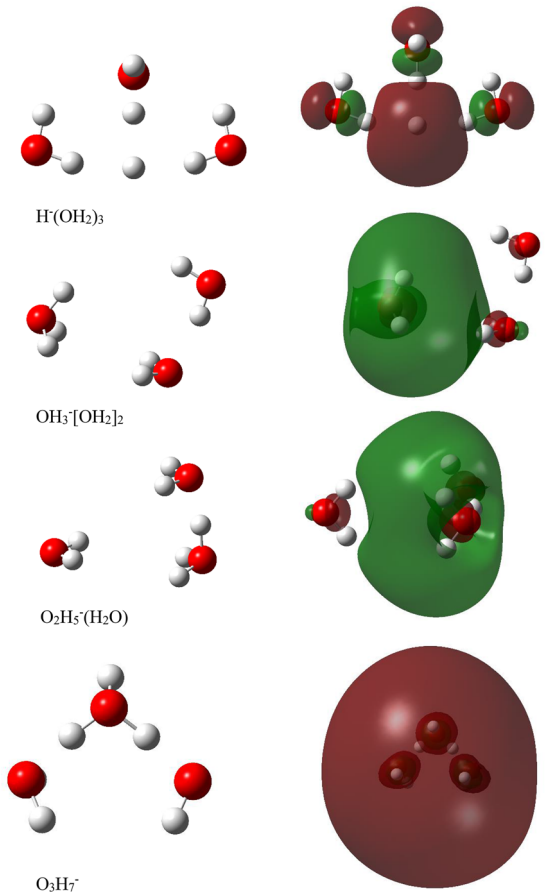


FIG. 11. n = 3: Optimized geometries and Dyson orbitals of electron detachment from anions.

orbital of the lowest electron attachment has its largest amplitudes beyond the periphery of the H nuclei.

3. $O_3H_7^+$

Two structures pertain to n = 3. The C_1 and C_s geometries are nearly identical and only differ in the relative orientation of the H nuclei as noted elsewhere.[69] The C_s geometry is only 0.004 eV more stable than the C_1 isomer (Fig. 3). Both isomers have a bound VEAE of 3.33 eV. Pole strengths of 0.987 imply that correlation effects are not significant, and the qualitative features of the Dyson orbitals are valid. The Dyson orbitals in both cases are diffuse *s*-like functions that spread over regions beyond the external non-bonding H nuclei. The Dyson orbital amplitudes are largest near non-bonding H in the OH_3^+ fragment.

4. $O_4H_9^+$

Addition of three water molecules to OH_3^+ through hydrogen bonding leads to four minima. Structures and Dyson orbitals for the lowest VEAE are displayed in Fig. 4. The Eigen isomer is the global minimum, whereas the *trans*-Zundel isomer is the least energetically stable. In the Eigen $O_4H_9^+$ isomer, three water molecules are engaged in hydrogen bonding with the H nuclei of

Published under an exclusive license by AIP Publishing

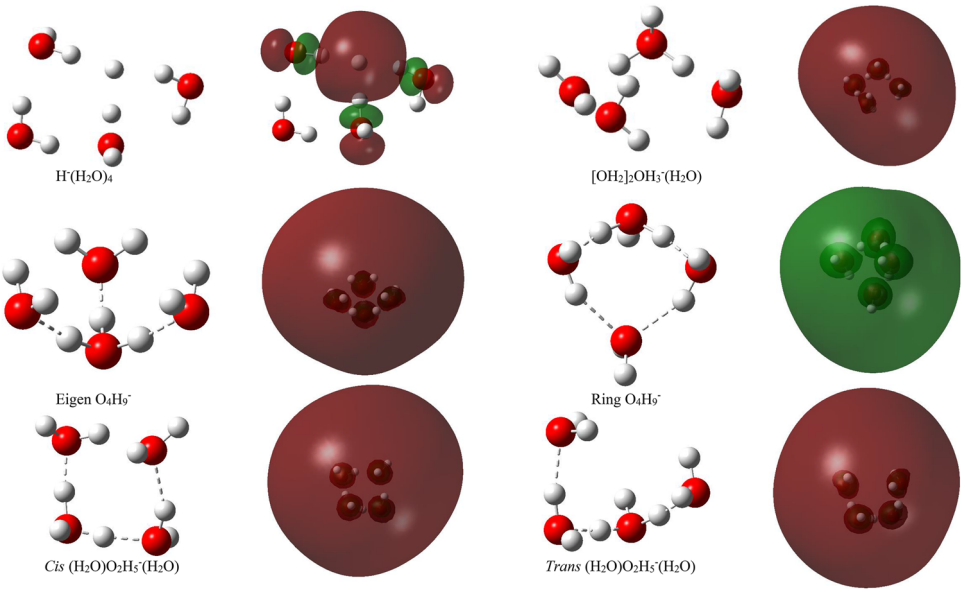


FIG. 12. $n = 4$: Optimized geometries and Dyson orbitals of electron detachment from $O_4H_9^-$ anions.

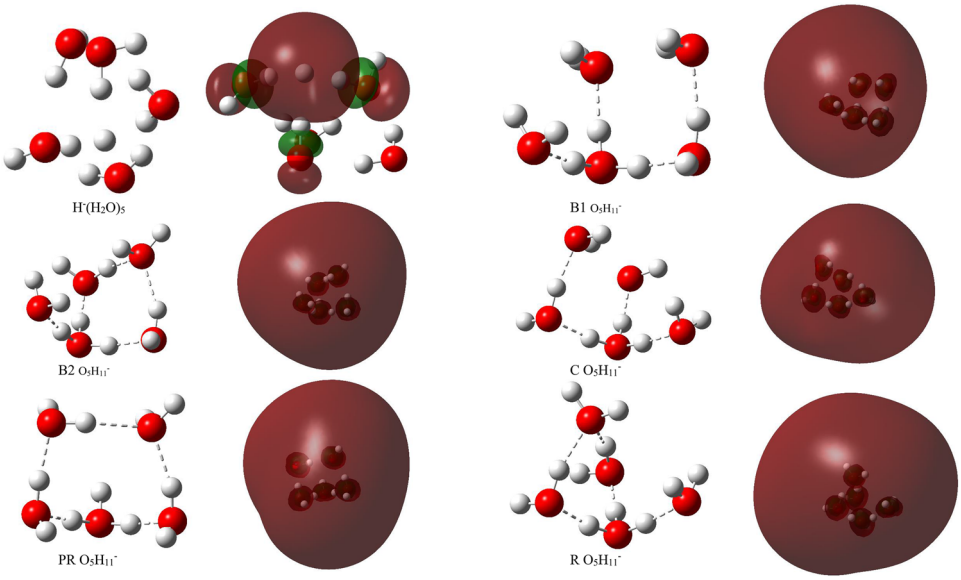


FIG. 13. $n = 5$: Optimized geometries and Dyson orbitals of electron detachment from $O_5H_{11}^-$ anions.

the OH_3^+ fragment in a C_3 arrangement. A proposed D_{3h} geometry[53] is found to be a transition state with an imaginary frequency of $-173.33i$ cm^{-1}. Sobolewski and Domcke[58] proposed a C_{3v} isomer that differs marginally by 1.0 kcal/mol from the C_3 isomer. A thorough search for the proposed C_{3v} isomer at B3LYP, MP2, and CCSD levels of theory in conjunction with several basis sets converged to transition state geometries in all instances. Note that the Eigen isomer has a completed solvation sphere for the central pyramidal OH_3^+ fragment, for there are three H–O–H bridges with surrounding water molecules through hydrogen bonding. The Eigen isomer has a bound VEAE of 2.917 eV, the least among isomers of the same composition. The VEAE corresponds to a diffuse Dyson orbital (see red contours) whose largest amplitudes occur beyond the protons at the periphery. Orthogonalization to valence *s* functions on the oxygen atoms contributes to the red contours.

In the ring isomer, there is a discernible $O_3H_7^+$ fragment with an acceptor H_2O molecule, which is shared by two of the water molecules from the $O_3H_7^+$ fragment. This isomer is ~0.10 eV less stable than the global minimum and possesses the largest VEAE among the $O_4H_9^+$ isomers. The nearly symmetric Dyson orbital is spread over the cationic $O_4H_9^+$ core with its largest lobes occurring on the acceptor water molecule.

Published under an exclusive license by AIP Publishing

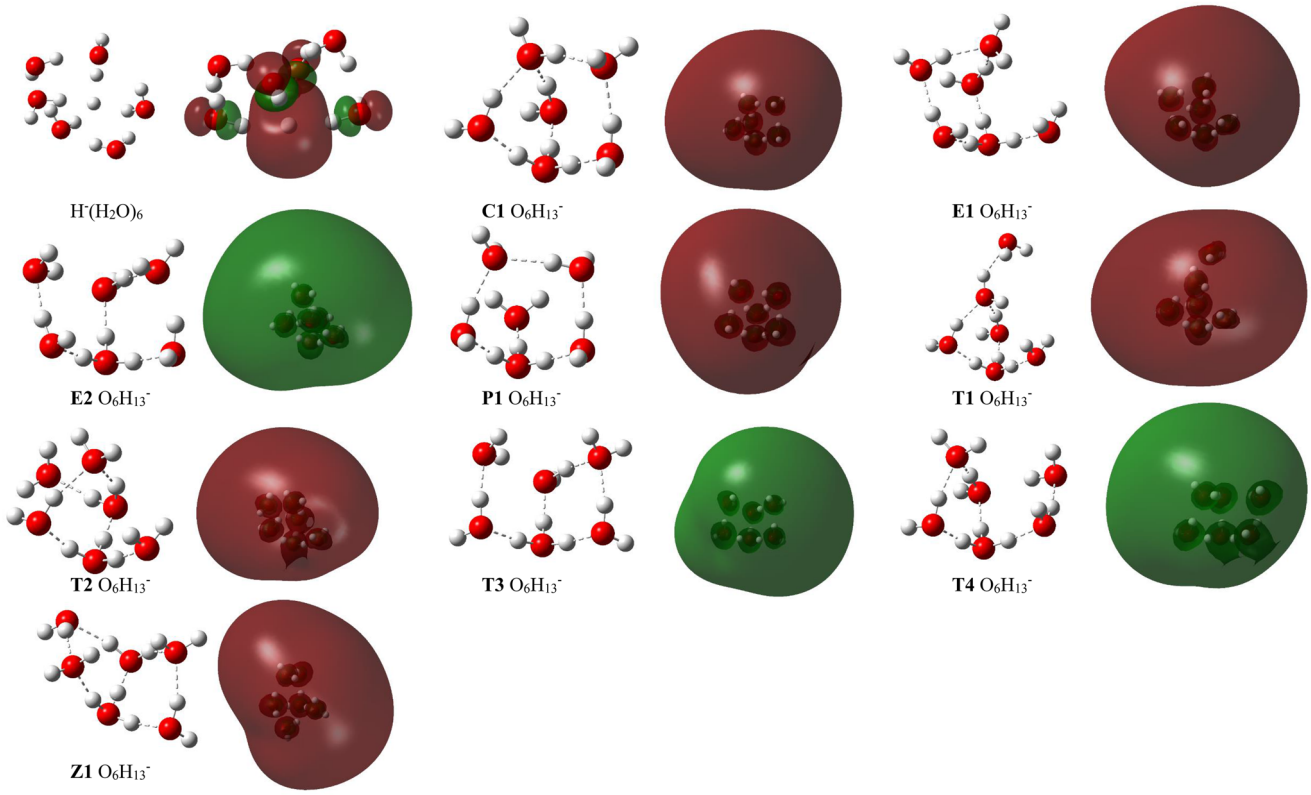


FIG. 14. $n = 6$: Optimized geometries and Dyson orbitals of electron detachment from $O_6H_{13}^-$ anions.

Coordination of two water molecules to a Zundel $O_2H_5^+$ ion leads to the *cis*- and *trans*-Zundel isomers with the C_2 point group. The structural features of the Zundel $O_2H_5^+$ ion fragment are retained in both isomers, for the symmetric hydrogen is positioned at 1.20 Å from the oxygen nuclei of the two neighboring water molecules. In both isomers, the Dyson orbital is diffused beyond the periphery of the external hydrogens. The green contours that arise from orthogonalization to the valence *s* function of O's present *cis*- and *trans*-like shapes, respectively. Both isomers have nearly the same VEAE of 2.94 eV, while the *cis*-isomer is ~0.12 eV energetically more stable than the *trans*. D2, D3, OVGA, P3, and P3+ results are in close agreement in all instances. Pole strengths of ~0.98 indicate that the diagonal self-energy approximations are reliable for qualitative predictions.

5. $O_5H_{11}^+$

For $n = 5$, there are five isomeric structures, which are displayed in Fig. 5 along with their Dyson orbitals. In the B1 and B2 isomers, a water molecule starts filling the second solvation shell of the Eigen $O_4H_9^+$ cation. In both instances, the Eigen $O_4H_9^+$ ion fragment is discernible, while an H_2O molecule enters the secondary solvation shell through hydrogen bonding. The two geometries are almost identical, and the positions of external H's constitute the chief difference. B1 is only 0.001 eV more stable than B2. The two isomers have nearly equal VEAEs of 2.65 eV. In both instances, the Dyson orbital is diffused over the Eigen $O_4H_9^+$ ion fragment. Minor delocalization onto the valence functions in the H_2O molecule within the secondary sphere can be seen.

In the C $O_5H_{11}^+$ isomer, an $O_3H_7^+$ ion fragment is discernible. Two water molecules form hydrogen bonds with the H_2O fragments in the $O_3H_7^+$ ion. In other words, the C $O_5H_{11}^+$ isomer can be considered to be a chain of water molecules with a non-symmetric hydrogen nucleus. A diffuse *s*-like function whose largest lobes occur on non-bonding H in the OH_3^+ ion fragment is the chief feature of the Dyson orbital. Orthogonalization to the valence *s* functions of the heavy atoms is also visible.

Interaction of a water molecule through hydrogen bonding to *cis*-Zundel $O_4H_9^+$ gives rise to the PR (pentagonal ring) $O_5H_{11}^+$ isomer, which is 0.005 eV less stable than B1. An H_2O molecule is shared by two water molecules from the *cis*-Zundel $O_4H_9^+$ ion fragment and forms a pentagonal ring geometry. This isomer has the largest VEAE, 2.899 eV, among the set. Only the PR isomer features the Zundel cation among the $O_5H_{11}^+$ isomers. The Dyson orbital spreads over the cation, and its largest amplitudes are visible on H's of the acceptor water molecule.

The remaining isomer (R isomer) can be regarded as an Eigen $O_4H_9^+$ cation coordinated to an acceptor water molecule to form a four-member ring framework. This isomer has a VEAE of

Published under an exclusive license by AIP Publishing

TABLE I. $O_nH_{2n+1}^+$ isomerization and vertical electron attachment energies (VEAEs). Pole strengths are in parentheses. All energies are in eV. Calculations were executed with the **d-aug-cc-pVTZ** basis set.

n	Isomer	Δ***E***	KT	D2	D3	OVGF	P3	P3+
1	OH_3^+	⋯	4.691	5.211 (0.986)	5.209 (0.984)	5.186 (0.985)	5.209 (0.985)	5.209 (0.985)
2	$O_2H_5^+$	⋯	3.527	3.969 (0.987)	3.969 (0.985)	3.960 (0.986)	3.969 (0.986)	3.969 (0.986)
3	C_s $O_3H_7^+$	0.000	2.941	3.329 (0.989)	3.333 (0.987)	3.330 (0.988)	3.333 (0.987)	3.333 (0.987)
	C_1 $O_3H_7^+$	0.004	2.937	3.331 (0.989)	3.335 (0.987)	3.333 (0.988)	3.335 (0.987)	3.334 (0.987)
4	Eigen $O_4H_9^+$	0.000	2.560	2.912 (0.990)	2.922 (0.988)	2.920 (0.989)	2.917 (0.988)	2.917 (0.988)
	Ring $O_4H_9^+$	0.101	2.727	3.141 (0.988)	3.144 (0.986)	3.141 (0.987)	3.144 (0.986)	3.144 (0.986)
	Cis-Zundel $O_4H_9^+$	0.083	2.572	2.932 (0.989)	2.937 (0.987)	2.940 (0.988)	2.937 (0.987)	2.937 (0.988)
	Trans-Zundel $O_4H_9^+$	0.202	2.584	2.930 (0.990)	2.935 (0.988)	2.935 (0.989)	2.935 (0.988)	2.935 (0.988)
5	B1 $O_5H_{11}^+$	0.000	2.315	2.638 (0.990)	2.645(0.989)	2.650 (0.989)	2.645 (0.989)	2.644 (0.989)
	B2 $O_5H_{11}^+$	0.001	2.317	2.643 (0.990)	2.649 (0.988)	2.655 (0.989)	2.649 (0.989)	2.649 (0.989)
	C $O_5H_{11}^+$	0.006	2.321	2.655 (0.990)	2.661 (0.988)	2.667 (0.989)	2.661 (0.988)	2.660 (0.988)
	PR $O_5H_{11}^+$	0.005	2.505	2.894 (0.988)	2.899 (0.986)	2.894 (0.987)	2.899 (0.986)	2.899 (0.986)
	R $O_5H_{11}^+$	0.002	2.421	2.786 (0.989)	2.792 (0.987)	2.790 (0.988)	2.792 (0.987)	2.791 (0.987)
6	C1 $O_6H_{13}^+$	0.135	2.439	2.836 (0.988)	2.840 (0.986)	2.834 (0.987)	2.840 (0.986)	2.840 (0.986)
	E1 $O_6H_{13}^+$	0.047	2.108	2.402 (0.991)	2.410 (0.989)	2.418 (0.990)	2.410 (0.989)	2.409 (0.989)
	E2 $O_6H_{13}^+$	0.051	2.112	2.410 (0.991)	2.417 (0.989)	2.425 (0.990)	2.417 (0.989)	2.417 (0.989)
	P1 $O_6H_{13}^+$	0.042	2.279	2.628 (0.989)	2.635 (0.987)	2.630 (0.988)	2.635 (0.987)	2.634 (0.988)
	T1 $O_6H_{13}^+$	0.050	2.188	2.519 (0.990)	2.526 (0.988)	2.528 (0.989)	2.526 (0.988)	2.525 (0.988)
	T2 $O_6H_{13}^+$	0.046	2.215	2.549 (0.990)	2.556 (0.988)	2.557 (0.989)	2.556 (0.988)	2.556 (0.988)
	T3 $O_6H_{13}^+$	0.059	2.248	2.588 (0.990)	2.595 (0.988)	2.593 (0.989)	2.595 (0.988)	2.594 (0.988)
	T4 $O_6H_{13}^+$	0.048	2.242	2.581 (0.990)	2.588 (0.988)	2.585 (0.989)	2.588 (0.988)	2.587 (0.988)
	Z1 $O_6H_{13}^+$	0.000	2.121	2.416 (0.991)	2.432 (0.989)	2.432 (0.990)	2.423 (0.989)	2.423 (0.989)

2.791 eV. In analogy to the PR $O_5H_{11}^+$ and ring $O_4H_9^+$ isomers, the Dyson orbital is a diffuse, symmetric function occurring over peripheral H's with its largest amplitudes on the acceptor water molecule.

6. $O_6H_{13}^+$

For n = 6, nine distinctive geometric isomers were located. Their structures and Dyson orbitals are displayed in Fig. 6. The C1

TABLE II. 20 lowest electron affinities (EAs) and radical excitation energies (EEs) for Eigen $O_4H_9^+$. All energies are in eV. Calculations were executed with the **d-aug-cc-pVTZ** basis set.

Final state	KT	D2	D3	OVGF	P3	P3+	P3+ EEs	OVGF EEs
1^2A_1	2.560	2.912	2.922	2.920	2.917	2.917	0.000	0.000
1^2E	2.026	2.259	2.267	2.266	2.266	2.266	0.651	0.654
2^2A_1	1.838	1.954	1.964	1.962	1.960	1.959	0.958	0.958
2^2E	1.372	1.458	1.463	1.462	1.463	1.462	1.455	1.458
3^2A_1	1.300	1.387	1.392	1.391	1.391	1.391	1.526	1.529
3^2E	1.288	1.353	1.359	1.359	1.358	1.358	1.559	1.561
4^2A_1	1.288	1.353	1.359	1.359	1.358	1.358	1.559	1.561
5^2A_1	1.079	1.215	1.219	1.219	1.217	1.217	1.700	1.701
4^2E	0.916	1.032	1.035	1.034	1.034	1.034	1.883	1.886
6^2A_1	0.854	0.930	0.936	0.935	0.932	0.932	1.985	1.985
7^2A_1	0.619	0.678	0.682	0.681	0.683	0.683	2.234	2.239
8^2A_1	0.537	0.601	0.608	0.607	0.607	0.607	2.310	2.313
5^2E	0.529	0.602	0.607	0.606	0.605	0.605	2.312	2.314
6^2E	0.518	0.565	0.569	0.569	0.568	0.568	2.349	2.351
9^2A_1	0.459	0.555	0.559	0.558	0.557	0.557	2.360	2.362
7^2E	0.437	0.507	0.513	0.512	0.513	0.512	2.405	2.405

Published under an exclusive license by AIP Publishing

TABLE III. 20 lowest electron affinities (EAs) and radical excitation energies (EEs) for Z1 $O_6H_{13}^+$. All energies are in eV. Calculations were executed with the **d-aug-cc-pVTZ** basis set.

Final state	KT	D2	D3	OVGF	P3	P3+	P3+ EEs	OVGF EEs
1^2A_1	2.121	2.416	2.432	2.432	2.423	2.423	0.000	0.000
2^2A_1	1.780	2.000	2.010	2.009	2.008	2.007	0.416	0.423
3^2A_1	1.727	1.909	1.920	1.918	1.917	1.916	0.507	0.514
4^2A_1	1.674	1.826	1.838	1.836	1.833	1.832	0.591	0.596
5^2A_1	1.357	1.481	1.487	1.486	1.487	1.487	0.936	0.946
6^2A_1	1.252	1.334	1.341	1.339	1.340	1.339	1.084	1.093
7^2A_1	1.206	1.278	1.286	1.284	1.283	1.283	1.140	1.148
1^2E	1.178	1.236	1.243	1.243	1.241	1.241	1.182	1.189
8^2A_1	1.029	1.145	1.151	1.150	1.147	1.147	1.276	1.282
9^2A_1	0.853	0.935	0.939	0.939	0.938	0.937	1.486	1.493
10^2A_1	0.830	0.886	0.891	0.890	0.890	0.889	1.534	1.542
11^2A_1	0.816	0.868	0.873	0.872	0.872	0.871	1.552	1.56
12^2A_1	0.742	0.851	0.855	0.855	0.854	0.854	1.569	1.577
13^2A_1	0.719	0.830	0.834	0.834	0.834	0.834	1.589	1.598
14^2A_1	0.666	0.758	0.763	0.762	0.763	0.763	1.660	1.67
15^2A_1	0.604	0.667	0.672	0.671	0.670	0.670	1.753	1.761
16^2A_1	0.532	0.637	0.643	0.642	0.641	0.641	1.782	1.79
17^2A_1	0.486	0.544	0.551	0.550	0.549	0.549	1.874	1.882
18^2A_1	0.439	0.521	0.529	0.528	0.525	0.525	1.898	1.904
19^2A_1	0.416	0.468	0.475	0.475	0.474	0.474	1.949	1.957

$O_6H_{13}^+$ isomer is a three-dimensional (3D) cage structure. In this isomer, there is a discernible Eigen $O_4H_9^+$ fragment whose external H's engage in hydrogen bonding with two H_2O molecules resulting in a 3D cage geometry. This structure has the largest VEAE of 2.840 eV among the isomers of the same composition, and it is the least energetically stable isomer. The Dyson orbital forms a cloud of diffuse symmetric *s* functions distributed over the 3D water network. Note that the Dyson orbital does not touch the OH_3^+ fragment core.

The E1 and E2 $O_6H_{13}^+$ isomers result from the Eigen $O_4H_9^+$ ion fragment with two water molecules that are engaged in hydrogen bonding. Note that two water molecules are in the secondary coordination sphere through hydrogen bonding with the peripheral hydrogens from the Eigen $O_4H_9^+$ ion fragment. In E1, the H_2O molecules in the secondary shell approach the $O_4H_9^+$ ion fragment in a *cis*-like fashion, whereas the *trans*-orientation is observed in E2. The E2 isomer is 0.003 eV more energetically stable than E1. Both isomers have VEAEs near 2.4 eV. The symmetric Dyson orbitals are diffused over exterior H's on the $O_4H_9^+$ ion fragments with minor delocalization onto the neighboring water molecules in the secondary sphere. The red and green contours are the key distinctive features in E1 and E2, respectively. Note that the Dyson orbital closely resembles that of the $O_4H_9^+$ ion.

Addition of a water molecule through hydrogen bonding with PR $O_5H_{11}^+$ results in the P1 $O_6H_{13}^+$ isomer. A diffuse Dyson orbital spread over H's in the PR $O_5H_{11}^+$ fragment is observed. Coordination of a water molecule to R $O_5H_{11}^+$ results in four isomers, T1–T4. In T1, the acceptor water molecule in the R $O_5H_{11}^+$ fragment engages in hydrogen bonding with an H_2O molecule. The diffuse Dyson orbital has its largest lobes around the regions of the acceptor water dimer. The isomer T2 of $O_6H_{13}^+$ contains a discernible Eigen $O_4H_9^+$ cation and forms a tetramer ring wherein a water molecule enters the second solvation sphere of the R $O_5H_{11}^+$ fragment. The Dyson orbital is distributed beyond the R $O_5H_{11}^+$ fragment with its largest amplitude on the acceptor water molecule in the tetramer ring. In the T3 and T4 $O_6H_{13}^+$ isomers, an H_2O forms a hydrogen bond with water in the R $O_5H_{11}^+$ fragment, which does not participate in any secondary hydrogen bonding. This results in the formation of a water dimer in the second shell in both isomers. The chief difference between the T3 and T4 isomers pertains to the relative orientations of the water dimer. In both cases, the Dyson orbital is diffused over the R $O_5H_{11}^+$ fragment ion.

The Z1 $O_6H_{13}^+$ isomer encompasses the Zundel $O_2H_5^+$ cation fragment. Each of the exterior protons in the Zundel $O_2H_5^+$ ion fragment engages in hydrogen bonding with an H_2O molecule to complete the first solvation shell in a C_2 symmetry arrangement. All structural features in the original Zundel $O_2H_5^+$ ion fragment are retained. The new hydrogen bonds occur at 1.67 Å. This isomer is the global minimum among the nine $O_6H_{13}^+$ isomers. It also has the smallest VEAE of 2.430 eV. Given the stability of this isomer, a peak near 2.4 eV is expected to dominate the photoelectron spectrum of O_6H_{13} isomers. Its Dyson orbital can be seen to spread over exterior H's to form a symmetric function. Orthogonalization to valence *s* functions of O's results in the red contours.

B. Radical excitation energies

Vertical electron affinities of cations and radical excitation energies for several electronic states of micro-solvated Eigen O_4H_9

Published under an exclusive license by AIP Publishing

and Z1 O_6H_{13} are shown in Tables II and III, respectively. Pole strengths for all the considered states are larger than 0.95, and hence, the diagonal approximation of the self-energy, wherein the Dyson orbitals are proportional to Hartree–Fock virtual orbitals (see Sec. II A), is qualitatively valid. Generally, there is good agreement between methods for electron affinities. Therefore, vertical excitation energies from the $^2A_1$ final states to higher electronic states may be inferred from P3+ and OVGF results shown in Tables II and III.

Orbital relaxation and correlation corrections to KT results become smaller for higher final electronic states of Eigen O_4H_9 and Z1 O_6H_{13}, which have unpaired electrons in increasingly diffuse Rydberg orbitals. For Eigen O_4H_9, the first 20 excitation energies fall within 0.7 and 2.4 eV. In Z1 O_6H_{13}, the excitation energies lie within 0.4 and 2.0 eV. Hence, the radical excitation energies are larger for Eigen O_4H_9 than for Z1 O_6H_{13}.

For both cations, excited states of the radicals correspond to diffuse Dyson orbitals (Figs. 7 and 8). The second and third electron affinities of Eigen O_4H_9 denoted as EA_1 and EA_2 correspond to a doubly degenerate (P_x and P_y) ^2E state with diffuse *p*-like orbitals (Fig. 7). Note the orthogonalization of the contours to the valence functions of O's. The higher P_z level corresponding to EA_3 is also diffused with orthogonalization to the O–H bonding functions. However, EA_1, EA_2, and EA_3 electron affinities of Z1 $O_6H_{13}^+$ correspond to non-degenerate final states with diffuse, *p*-like orbitals (Fig. 8). In all radical excited states considered presently, Dyson orbitals with diffuse *p*-like and *d*-like nodal patterns emerge.

C. $O_nH_{2n+1}^-$ double Rydberg anions

Geometry optimizations performed at the CCSD(T)/aug-cc-pVTZ (for n = 1, 2) and MP2/aug-cc-pVTZ (for n = 3–6) levels with default convergence criteria for all isomers converge to minima. A change in convergence criteria to 300 maximum cycles is necessary for *trans*-$(H_2O)O_2H_5^-(H_2O)$ and for Z1 $O_6H_{13}^-$. To judge the reliability of EPT methods for calculating VEDEs, a preliminary comparison with ΔCCSD(T) results was conducted for the OH_3^- DRA. The results in Table IV were obtained with various basis sets to evaluate the effectiveness of each method in describing electron correlation and orbital relaxation corrections to the KT results. Only the lowest VEDE was considered. Compared to ΔCCSD(T), KT results are too small, whereas D2, D3, P3+, and OVGF self-energy approximations are too large. D2 and OVGF have lower pole strengths. The BD-T1 result is the closest to ΔCCSD(T). A comparison of BD-T1 results obtained with various basis sets shows that BD-T1/d-aug-cc-pVTZ is the optimal level for computational accuracy and cost. Data from Table IV suggest that for DRAs, BD-T1 is the best EPT method. Of the remaining EPT methods, P3+ generally performs better than OVGF with respect to VEDEs and pole strengths. The data in Table IV show that improvements corresponding to the t-aug-cc-pVTZ, q-aug-cc-pVTZ, aug-cc-pVQZ, and aug-cc-pV5Z basis sets are not needed. Hence, unless stated otherwise, BD-T1/d-aug-cc-pVTZ results are discussed in the text.

1. OH_3^- isomers

Figure 9 displays the optimized geometries and Dyson orbitals for the lowest vertical electron detachment energies (VEDEs) for the hydride–water complex $H^-(OH_2)$ and the OH_3^- DRA. Numerical results for relative energies and electron binding energies are shown in Table V. The hydride–molecule complex is more stable than the OH_3^- DRA. In the former anion, the VEDE of the free hydride (0.75 eV) increases by 0.9 chiefly due to electrostatic interactions with the water molecule. The H_2O molecule approaches the free hydride with one of its protons in a C_s geometry. There is a minor increase in the length of the O–H bond that approaches H^-. A structure in which the hydride anion forms a symmetric bonding arrangement with the molecule's protons is a transition state.[20,39] The Dyson orbital is chiefly composed of diffuse *s* functions, which display no bonding relationship with valence functions on the closest O–H bonds. A totally symmetric Dyson orbital whose amplitudes are beyond the hydrogen nuclei is observed for the lowest VEDE of the OH_3^- DRA. This Dyson orbital smoothly correlates to the 3s orbital of Na^- in the united atom limit, for it has two radial nodes. The lowest VEDE of 0.537 eV nearly equals that of Na^- (0.55 eV). The Dyson orbital for the lowest VEDE closely resembles that of the first electron attachment energy of the cationic core OH_3^+, for both electron binding energies corresponding to the same final uncharged doublet OH_3 state. The O–H bond lengths are almost the same in the cation, neutral, and anion and imply the insignificance of the antibonding features in the Dyson orbital. The present results can be considered as an upper bound to previous calculations.[6,19,20,38,39]

TABLE IV. Comparison of VEDEs of the OH_3^- DRA calculated at different levels of theory. Pole strengths are in parentheses. All energies are in eV.

OH_3^-	VEDE
KT[a]	0.362
D2[a]	0.633 (0.830)
D3[a]	0.620 (0.874)
P3+[a]	0.622 (0.870)
OVGF[a]	0.481 (0.772)
BD-T1[a]	0.539 (0.862)
ΔCCSD(T)/d-aug-cc-pVTZ	0.536
BD-T1/aug-cc-pVTZ	0.431 (0.894)
BD-T1/d-aug-cc-pVTZ	0.537 (0.864)
BD-T1/t-aug-cc-pVTZ	0.539 (0.862)
BD-T1/q- aug-cc-pVTZ	0.539 (0.862)
BD-T1/aug-cc-pVQZ	0.458 (0.889)
BD-T1/aug-cc-pV5Z	0.486 (0.884)

[a]Calculation performed with the aug-cc-pVTZ basis augmented with an additional set of diffuse functions: 4s4p4d on all H atoms and 4s4p4d4f on all O atoms.

2. $O_2H_5^-$ isomers

There are three $O_2H_5^-$ isomers, and their optimized structures and Dyson orbitals are illustrated in Fig. 10. The most stable isomer is the hydride anion complex, which has two water molecules that weakly coordinate to the H^- via attractions to their protons. A peak around 2.5 eV is expected to dominate the photoelectron spectrum of $O_2H_5^-$ considering its high stability. The new water molecule increases the VEDE of the $H^-(OH_2)$ by 0.911 eV, and the Dyson orbital is localized on the hydride's nucleus.

The asymmetric hydrogen-bridged isomer has discernible OH_3^- and H_2O molecular fragments. The binding of the same two fragments by electrostatic interactions results in the least stable isomer. In the latter isomer, the Dyson orbital's amplitudes are largest outside the three H nuclei of the OH_3^- fragment. Minor

Published under an exclusive license by AIP Publishing

TABLE V. $O_nH_{2n+1}^-$ isomerization and vertical electron detachment energies (VEDEs). Pole strengths are in parentheses. All energies are in eV. Calculations were executed with the **d-aug-cc-pVTZ** basis set.

n	Isomer	Δ***E***	KT	D2	D3	OVGF	P3	P3+	BD-T1
1	$H^-(OH_2)$	0.000	2.009	1.522 (0.881)	1.695 (0.901)	1.732 (0.899)	1.505 (0.906)	1.506 (0.904)	1.659 (0.864)
	OH_3^-	1.540	0.338	0.658 (0.867)	0.494 (0.833)	0.409 (0.750)	0.585 (0.831)	0.591 (0.834)	0.537 (0.864)
2	$H^-(H_2O)_2$	0.000	8.159	5.446 (0.858)	7.501 (0.923)	6.925 (0.900)	6.656 (0.901)	2.401 (0.911)	2.570 (0.819)
	$OH_3^-(H_2O)$	2.238	0.500	0.873 (0.863)	0.726 (0.851)	0.700 (0.844)	0.837 (0.847)	0.840 (0.849)	0.803 (0.881)
	$O_2H_5^-$	1.323	0.244	0.603 (0.865)	0.435 (0.825)	0.336 (0.696)	0.529 (0.822)	0.536 (0.826)	0.519 (0.860)
3	$H^-(OH_2)_3$	0.000	3.715	3.131 (0.908)	3.392 (0.912)	3.394 (0.909)	3.159 (0.911)	3.156 (0.911)	3.352 (0.899)
	$OH_3^-[OH_2]_2$	2.454	0.685	1.105 (0.871)	0.974 (0.866)	0.961 (0.867)	1.089 (0.864)	1.090 (0.865)	1.066 (0.924)
	$O_2H_5^-(H_2O)$	2.607	0.371	0.781 (0.851)	0.607 (0.833)	0.572 (0.818)	0.736 (0.826)	0.740 (0.828)	0.731 (0.879)
	$O_3H_7^-$	2.491	0.209	0.609 (0.863)	0.432 (0.823)	0.341 (0.700)	0.540 (0.817)	0.547 (0.821)	0.537 (0.865)
4	$H^-(H_2O)_4$	0.000	4.303	3.669 (0.909)	3.947 (0.911)	3.936 (0.910)	3.711 (0.911)	3.707 (0.911)	3.899 (0.900)
	$[OH_2]_2OH_3–H_2O$	2.704	0.198	0.597 (0.844)	0.407 (0.809)	0.327 (0.706)	0.528 (0.798)	0.535 (0.803)	0.535 (0.867)
	Eigen $O_4H_9^-$	2.629	0.200	0.605 (0.857)	0.430 (0.820)	0.360 (0.736)	0.540 (0.812)	0.549 (0.817)	0.574 (0.874)
	Ring $O_4H_9^-$	2.780	0.157	0.610 (0.871)	0.437 (0.830)	0.342 (0.684)	0.551 (0.822)	0.557 (0.828)	0.521 (0.882)
	Cis-$(H_2O)O_2H_5^-(H_2O)$	2.789	0.151	0.541 (0.856)	0.364 (0.809)	0.244 (0.491)	0.465 (0.800)	0.472 (0.806)	0.450 (0.840)
	Trans-$(H_2O)O_2H_5^-(H_2O)$	2.638	0.151	0.541 (0.856)	0.364 (0.809)	0.244 (0.491)	0.465 (0.800)	0.599 (0.809)	0.596 (0.879)
5	$H^-(H_2O)_5$	0.000	4.655	3.984 (0.910)	4.270 (0.912)	4.250 (0.912)	4.042 (0.912)	4.036 (0.910)	4.218 (0.901)
	B1 $O_5H_{11}^-$	2.802	0.194	0.574 (0.833)	0.389 (0.801)	0.314 (0.708)	0.506 (0.788)	0.513 (0.793)	0.527 (0.905)
	B2 $O_5H_{11}^-$	2.745	0.179	0.544 (0.835)	0.358 (0.802)	0.281 (0.698)	0.475 (0.788)	0.482 (0.794)	0.484 (0.905)
	C $O_5H_{11}^-$	2.860	0.160	0.502 (0.823)	0.308 (0.788)	0.208 (0.599)	0.424 (0.773)	0.432 (0.779)	0.424 (0.848)
	PR $O_5H_{11}^-$	2.946	0.165	0.595 (0.838)	0.383 (0.793)	0.269 (0.521)	0.515 (0.777)	0.523 (0.785)	0.499 (0.845)
	R $O_5H_{11}^-$	2.884	0.146	0.576 (0.854)	0.397 (0.810)	0.296 (0.617)	0.508 (0.800)	0.515 (0.806)	0.506 (0.853)
6	$H^-(H_2O)_6$	0.000	5.233	4.514 (0.910)	4.774 (0.909)	4.755 (0.908)	4.558 (0.908)	4.553 (0.908)	
	C1 $O_6H_{13}^-$	3.025	0.101	0.522 (0.868)	0.379 (0.816)	0.275 (0.566)	0.379 (0.816)	0.469 (0.818)	
	E1 $O_6H_{13}^-$	2.878	0.154	0.490 (0.15)	0.292 (0.782)	0.208 (0.639)	0.414 (0.764)	0.422 (0.770)	
	E2 $O_6H_{13}^-$	2.868	0.160	0.548 (0.833)	0.361 (0.795)	0.267 (0.623)	0.477 (0.780)	0.484 (0.780)	
	P1 $O_6H_{13}^-$	2.906	0.154	0.549 (0.821)	0.339 (0.77)	0.225 (0.430)	0.464 (0.759)	0.472 (0.765)	
	T1 $O_6H_{13}^-$	3.174	0.161	0.567 (0.814)	0.337 (0.765)	0.224 (0.311)	0.473 (0.744)	0.482 (0.751)	
	T2 $O_6H_{13}^-$	3.026	0.165	0.620 (0.848)	0.445 (0.814)	0.376 (0.734)	0.565 (0.801)	0.570 (0.807)	
	T3 $O_6H_{13}^-$	2.997	0.118	0.490 (0.842)	0.322 (0.799)	0.210 (0.493)	0.421 (0.785)	0.428 (0.792)	
	T4 $O_6H_{13}^-$	2.898	0.159	0.573 (0.845)	0.397 (0.810)	0.313 (0.685)	0.512 (0.796)	0.518 (0.802)	
	Z1 $O_6H_{13}^-$	3.028	0.123	0.500 (0.826)	0.295 (0.776)	0.181 (0.284)	0.411 (0.759)	0.421 (0.767)	

delocalization onto the coordinated water molecule can be seen. The VEDE of the asymmetric hydrogen-bridged isomer of $O_2H_5^-$ differs by ~0.3 eV from $OH_3^-(H_2O)$. The Dyson orbital is a nearly symmetric *s* function with its largest lobes occurring on the protons. Plots of lower iso-values give credence to a Dyson orbital which predominantly accumulates on the OH_3^- fragment with minor delocalization to regions near the water molecule's H nuclei as observed in a preceding study[39] and in isomers of the $N_2H_7^-$ DRAs.[13,14]

3. $O_3H_7^-$ isomers

Interaction of a water molecule with the $O_2H_5^-$ isomers gives rise to four different anionic $O_3H_7^-$ clusters. The optimized structures and associated Dyson orbitals are displayed in Fig. 11. The hydride–molecule complex is the most energetically stable. This complex has a C_3 axis and a perpendicular plane through the hydride's nucleus. Two water molecules coordinate to $H^-(OH_2)$ with their protons. The coordination of an H_2O molecule increases the VEDE by 0.782 eV compared to $H^-(H_2O)_2$. The Dyson orbital is dominated by delocalized *s* functions on the hydride, whereas an antibonding relationship with the neighboring O–H bonds is seen. Given the high stability of this isomer, a peak near 3.4 eV is expected to dominate the photoelectron spectrum of $O_3H_7^-$. Other isomers containing the OH_3^- and $O_2H_5^-$ DRAs are energetically unstable and have VEDEs that are higher than the $O_3H_7^-$ DRA. The $OH_3^-[OH_2]_2$ isomer arises from addition of a water molecule to $OH_3^-(H_2O)$. The new water molecule forms a hydrogen-bonded water dimer, denoted as $[OH_2]_2$ with the H_2O fragment in $OH_3^-(H_2O)$. The newly coordinated water increases the VEDE by 0.263 eV compared with $OH_3^-(H_2O)$. The Dyson orbital is retained on the OH_3^- kernel with negligible red contours on the surrounding water dimer.

Addition of a water molecule to the $O_2H_5^-$ DRA through weak electrostatic interactions leads to the $O_2H_5^-(H_2O)$ isomer. The water molecule interacts with the hydrogen nuclei. The Dyson

Published under an exclusive license by AIP Publishing

orbital closely resembles that of $O_2H_5^-$, with its largest amplitudes at the peripherical hydrogens on the $O_2H_5^-$ fragment. Negligible antibonding relationships between the Dyson orbitals and valence functions on the water molecule are seen. This isomer is the least energetically stable among all the $O_3H_7^-$ isomers. The VEDE of $O_2H_5^-(H_2O)$ is 0.212 eV above that of $O_2H_5^-$. In the $O_3H_7^-$ DRA, two water molecules interact with two of the OH_3^- protons through hydrogen bonding. This structure can be considered as an $O_2H_5^-$ DRA in which one of the non-bonding hydrogens in OH_3^- forms a hydrogen bond with the water molecule. The VEDE of the $O_3H_7^-$ isomer is 0.018 eV larger than that of the $O_2H_5^-$ DRA. The Dyson orbital accumulates on the peripheral non-bonding hydrogens, with its largest amplitudes on non-bonding H's in the OH_3^- core and water fragments. The $O_3H_7^-$ DRA has almost the same VEDE as OH_3^-.

4. $O_4H_9^-$ isomers

For n = 4, six isomers were found on the PES. The graphical results are displayed in Fig. 12. The hydride–molecule complex is the global minimum. In this $H^-(H_2O)_4$ structure, each of the three coordinating water molecules interacts through one of its H nuclei with the hydride anion in $H^-(H_2O)_3$, increasing the VEDE of the latter anion complex by 0.547 eV. Delocalization of s functions on H^- is the most important feature of the Dyson orbital, with minor green and red contours on three of the neighboring water molecules. Addition of a water molecule to the $O_3H_7^-$ DRA leads to the $[OH_2]_2OH_3^-(H_2O)$ isomer. The new water molecule forms a hydrogen-bonded water dimer with one of the H_2O molecules in $O_3H_7^-$. This isomer is relatively unstable energetically and has a VEDE of 0.535 eV.

In the Eigen $O_4H_9^-$ isomer, three water molecules are hydrogen-bonded with the OH_3^- protons. It is the most energetically stable isomer after the hydride ion complex. The OH_3^- fragment imposes a rigid threefold geometry on this cluster. The relative stability of this isomer suggests that a micro-solvated OH_3^- cluster with a complete solvation shell is more stable than other isomers. The Dyson orbital is a localized function represented by red contours that spread over all the exterior non-bonding H nuclei in the water network. The next isomer is the ring form of $O_4H_9^-$, in which the $O_3H_7^-$ kernel is connected to a bridging water molecule that forms a four-member ring. The dominance of green contours on the acceptor water molecule is the characteristic feature of the Dyson orbital. Delocalization of the Dyson orbital over the remaining unshared H's can also be seen.

The last two structural isomers originate from the typical Zundel cationic structures where the proton is shared by two water molecules. For these isomers, each of the water molecules in the $O_2H_5^-$ fragment forms a hydrogen bond with one water molecule in the *cis*- and *trans*-orientations. In the *cis*-isomer, the new water molecule forms a water dimer. At the initial cationic geometry, the *trans*-anionic isomer converges to a structure that closely resembles the *cis*-isomer except for the orientation of H nuclei in the periphery. The structural distortion arises from the rotation of one $[H_2O]_2$ about the bridging H nuclei. The *trans*-isomer is more energetically stable than the *cis* by 0.151 eV. In addition, the VEDE of the *trans*-isomer is higher than that of the *cis*-isomer by 0.146 eV. The Dyson orbitals of both anions correspond to diffuse, red contours whose largest amplitudes occur on the exterior H nuclei. Minor antibonding relationships with the neighboring valence functions can also be seen.

5. $O_5H_{11}^-$ isomers

The coordination of a water molecule to the $O_4H_9^-$ isomers through hydrogen bonding or electrostatic interactions leads to six $O_5H_{11}^-$ isomers. Graphical results for the $O_5H_{11}^-$ isomers are displayed in Fig. 13. $H^-(H_2O)_5$ is at least 2.7 eV more energetically stable than the DRAs. The VEDE of $H^-(H_2O)_4$ increases by 0.329 eV upon the addition of an H_2O through electrostatic interactions. The Dyson orbital remains localized on the hydride's nucleus with slight delocalization onto water H's. Addition of a hydrogen-bonded water dimer denoted by $[H_2O]_2$ to the $O_3H_7^-$ DRA results in the B1 $O_5H_{11}^-$ isomer whose VEDE has decreased by 0.01 eV. In other words, the B1 $O_5H_{11}^-$ isomer is an Eigen $O_4H_9^-$ ion in which one of H's in the OH_3^- fragment engages in further hydrogen bonding. The Dyson orbital accumulates on the external hydrogens. The B2 $O_5H_{11}^-$ structure consists of an Eigen-like anionic fragment in which two of the H's in the OH_3^- fragment engage in further hydrogen bonding with a water molecule. The three water molecules that form hydrogen bonds with the H nuclei of OH_3^- DRA do so at 1.55 Å, suggesting typical hydrogen bonds. The water in the second solvation shell forms a hydrogen bond at 1.84 Å, suggesting a relatively weak hydrogen bond compared with those in the first solvation shell. There is a decrease in the VEDE by 0.09 eV compared to the Eigen $O_4H_9^-$ DRA.

The C $O_5H_{11}^-$ isomer has the smallest VEDE among the $O_5H_{11}^-$ structures. The parent cationic core forms a linear chain of water molecules with two H nuclei in the OH_3^+ unit. After optimization, the cationic chain $O_5H_{11}^+$ rearranges to form a book-like anionic isomer. Three water molecules form hydrogen bonds with the OH_3^- framework to complete the primary solvation shell, while the remaining water enters the secondary solvation shell. The Dyson orbital is diffused over the non-bonding H nuclei with its largest amplitudes on the exterior water H nuclei. The PR $O_5H_{11}^-$ isomer also undergoes structural rearrangement upon optimization at the cationic geometry to form another book-like isomer. In this isomer, an $O_3H_7^-$ DRA fragment can be seen. Each of the two water molecules forms hydrogen bonds with the H_2O molecules originally bonded to H nuclei in the OH_3^- fragment. This isomer has the lowest VEDE of 0.499 eV. The positive red contour of the Dyson orbital densely populates the regions between the non-bonded H nuclei in the OH_3^- fragment those from the two acceptor water molecules. Small, delocalized, and green contours are seen on the remaining non-bonding H nuclei. In the remaining ring $O_5H_{11}^-$ isomer, the parent cationic core forms a tetramer ring through hydrogen bonding with one acceptor H_2O. The optimized anionic geometry structurally looks like the parent cationic core. It has the lowest VEDE of 0.506 eV. The Dyson orbital spreads over the H nuclei of the acceptor water molecule with some negligible delocalization on neighboring non-bonding protons.

6. $O_6H_{13}^-$ isomers

There are ten geometric isomers of the anionic hydronium–water hexamer clusters. The optimized geometries and Dyson orbitals of the lowest VEDE are illustrated in Fig. 14. Only P3+ electron propagator calculations were carried out for these isomers, for data in Table V show that P3+ generally gives

Published under an exclusive license by AIP Publishing

good VEDEs compared to BD-T1, albeit with lower pole strengths. Hereafter, only P3+ results are discussed.

The hydride anion–molecule complex is the most energetically stable with the lowest VEDE of 4.553 eV. All the water molecules have their protons oriented toward the H^- anion. The Dyson orbital accumulates on the hydride anion and has antibonding relationships with valence functions on the neighboring O–H bonds. The remaining nine $O_6H_{13}^-$ isomers were obtained from their corresponding parent cationic cores. The cage C1 $O_6H_{13}^-$ isomer strongly retains its cationic geometry orientation with a VEDE of 0.469 eV. The diffuse Dyson orbital is spread chiefly over H's in the water network. Two structures pertain to the Eigen-like configurations E1 $O_6H_{13}^-$ and E2 $O_6H_{13}^-$, for their corresponding cationic cores contain the $O_4H_9^+$ Eigen fragment. The two new water molecules enter the second solvation shell through hydrogen bonding. The optimized anionic structures are distorted when compared with their cationic counterparts, for the two water molecules originally in the second solvation shell of the cationic core form a water dimer acceptor molecule in the molecular anion. The E1 $O_6H_{13}^-$ isomer has a smaller VEDE than the E2 $O_6H_{13}^-$. In both E1 $O_6H_{13}^-$ and E2 $O_6H_{13}^-$, the nearly symmetric diffuse Dyson orbitals are localized on H's of the water network.

The P1 $O_6H_{13}^-$ isomer arises from the parent cationic core in which the new water molecule enters the secondary solvation shell from the ring $O_5H_{11}^+$ isomer. A water dimer is formed in the second coordination shell of the anionic P1 $O_6H_{13}^-$ isomer. A near symmetric *s*-like Dyson orbital whose largest amplitudes occur over the peripheral water network can be seen. Four isomers arise from parent cationic cores that contain water tetramer rings. In the T1 $O_6H_{13}^-$ isomer, an Eigen-like $O_4H_9^-$ can been seen with a water molecule forming a bridging hydrogen bond with two of the water molecules in $O_4H_9^-$. The bridging water molecule forms an additional hydrogen bond with one of its protons to form a water dimer. A diffuse Dyson orbital spreads over the H nuclei of the water network. In the T2 $O_6H_{13}^-$ isomer, the bridging water molecule does not interact with the water in the second solvation shell as it forms a hydrogen bond with one of the water molecules directly bonded to the OH_3^- fragment. The Dyson orbital is diffused over the peripheral hydrogens with its largest amplitudes on the bridging water molecule and the one in the secondary shell. There are low amplitudes near the lone pairs on the oxygens.

The T3 and T4 $O_6H_{13}^-$ isomers have book-like structures. The Dyson orbital in both instances spreads over the regions of the water network with its highest amplitudes on the acceptor water molecules. The last isomer is the Z1 $O_6H_{13}^-$ isomer, which arises from the Zundel-like solvated cationic core. The anionic geometry contains the $O_2H_5^-$ fragment with a non-symmetric proton. Each of the exterior hydrogens in the $O_2H_5^-$ fragment was anticipated to form a hydrogen bond with a water molecule to complete the first solvation shell of the Zundel-like anionic isomer. However, the optimized geometry shows that one of the water molecules leaves the second solvation shell to form a water dimer with one of the exterior water molecules. This observation indicates that anionic hydronium–water clusters prefer the Eigen $O_4H_9^-$ geometry over the Zundel $O_6H_{13}^-$ structure. Sobolewski and Domcke[58] observed the same trend in $H_3O(H_2O)_n$ clusters composed of a hydronium radical and water molecules. The Dyson orbital of electron attachment is diffused over the $O_6H_{13}^+$ core.

IV. CONCLUSIONS

Micro-solvated H_3O^+ can exist in both Eigen-like $H_9O_4^+(H_2O)_n$ and Zundel-like $H_5O_2^+(H_2O)_n$ structures. The VEAEs of these cations decrease with increasing cluster size. The corresponding Dyson orbitals show that with increasing cluster size, the diffuse electron migrates from the closed-shell H_3O^+ core to form a cloud in the network of water molecules.

Solvation of the OH_3^- and $O_2H_5^-$ DRAs through electrostatic interactions or hydrogen bonding with their solvation shells results in remarkable changes in geometry with respect to cationic antecedents. Interaction of water molecules with the OH_3^- DRA leads to several cluster isomers in which the Dyson orbital is held at the periphery of the hydrogens in the water network. It is seen that the stable H_3O^- unit imposes a rigid structure on these complexes, especially for isomers with closed solvation shells, such as the Eigen $H_3O^-(H_2O)_3$ structure. The $O_2H_5^-$ fragment ion also imposes a rigid geometry on the Zundel $O_2H_5^-(H_2O)_4$ isomer. For all these clusters, the Rydberg electrons are held by the exterior protons from the water network.

Several isomers of oxygen-based OH_3^- DRAs may occur through hydrogen bonding, as $OH_3^-(H_2O)_n$ structures or as electrostatic $H^-(H_2O)_n$ complexes. For all values of *n*, the anion–water complex $H^-(H_2O)_n$ is always the most stable, with large VEDEs, which increase with cluster size. Generally, the $OH_3^-(H_2O)_n$ DRA isomers have well separated VEDEs and therefore should be visible in anion photoelectron spectra.

ACKNOWLEDGMENTS

This work was made possible, in part, by a grant of high-performance computing resources from the Alabama Supercomputing Center.

This work was supported by the National Science Foundation via Grant No. CHE-1565760 to Auburn University.

DATA AVAILABILITY

The data that support the findings of this study are available from the corresponding author upon reasonable request.

REFERENCES

[1] E. N. Baker and R. E. Hubbard, Prog. Biophys. Mol. Biol. **44**, 97 (1984).
[2] G. W. Robinson, P. J. Thistlethwaite, and J. Lee, J. Phys. Chem. **90**, 4224 (1986).
[3] R. Ludwig, Angew. Chem., Int. Ed. **40**, 1808 (2001).
[4] R. Shi, K. Li, Y. Su, L. Tang, X. Huang, L. Sai, and J. Zhao, J. Chem. Phys. **148**, 174305 (2018).
[5] M. Tuckerman, K. Laasonen, M. Sprik, and M. Parrinello, J. Chem. Phys. **103**, 150 (1995).
[6] M. Gutowski and J. Simons, J. Chem. Phys. **93**, 3874 (1990).
[7] J. T. Snodgrass, J. V. Coe, C. B. Freidhoff, K. M. McHugh, and K. H. Bowen, Faraday Discuss. Chem. Soc. **86**, 241 (1988).
[8] J. V. Coe, J. T. Snodgrass, C. B. Freidhoff, K. M. McHugh, and K. H. Bowen, J. Chem. Phys. **83**, 3169 (1985).
[9] J. V. Ortiz, J. Chem. Phys. **87**, 3557 (1987).
[10] H. Cardy, C. Larrieu, and A. Dargelos, Chem. Phys. Lett. **131**, 507 (1986).
[11] D. Cremer and E. Kraka, J. Phys. Chem. **90**, 33 (1986).
[12] S.-J. Xu, J. M. Nilles, J. H. Hendricks, S. A. Lyapustina, and K. H. Bowen, J. Chem. Phys. **117**, 5742 (2002).
[13] J. V. Ortiz, J. Chem. Phys. **117**, 5748 (2002).

Published under an exclusive license by AIP Publishing

[14]M. Díaz-Tinoco and J. V. Ortiz, J. Chem. Phys. **151**, 054301 (2019).
[15]J. V. Ortiz, J. Phys. Chem. **94**, 4762 (1990).
[16]J. Moc and K. Morokuma, Inorg. Chem. **33**, 551 (1994).
[17]N. Matsunaga and M. S. Gordon, J. Phys. Chem. **99**, 12773 (1995).
[18]M. Gutowski and J. Simons, J. Chem. Phys. **93**, 2546 (1990).
[19]M. Gutowski, J. Simons, R. Hernandez, and H. L. Taylor, J. Phys. Chem. **92**, 6179 (1988).
[20]J. V. Ortiz, J. Chem. Phys. **91**, 7024 (1989).
[21] C. E. Melton and H. W. Joy, J. Chem. Phys. **46**, 4275 (1967).
[22]M. S. Matheson, Radiat. Res., Suppl. **4**, 1 (1964).
[23]T. J. Sworski, J. Am. Chem. Soc. **86**, 5034 (1964).
[24]L. H. Andersen, O. Heber, D. Kella, H. B. Pedersen, L. Vejby-Christensen, and D. Zajfman, Phys. Rev. Lett. **77**, 4891 (1996).
[25]J. K. Park, Chem. Phys. Lett. **315**, 119 (1999).
[26]J. K. Park, B. G. Kim, and I. S. Koo, Chem. Phys. Lett. **356**, 63 (2002).
[27]A. E. Ketvirtis and J. Simons, J. Phys. Chem. A **103**, 6552 (1999).
[28]M. Kayanuma, T. Taketsugu, and K. Ishii, Chem. Phys. Lett. **418**, 511 (2006).
[29]M. Luo and M. Jungen, Chem. Phys. **241**, 297 (1999).
[30]B. Brozek-Pluska, D. Gliger, A. Hallou, V. Malka, and Y. A. Gauduel, Radiat. Phys. Chem. **72**, 149 (2005).
[31] R. P. A. Bettens, M. A. Collins, M. J. T. Jordan, and D. H. Zhang, J. Chem. Phys. **112**, 10162 (2000).
[32]S. Havriliak, T. R. Furlani, and H. F. King, Can. J. Phys. **62**, 1336 (1984).
[33]S. Havriliak and H. F. King, J. Am. Chem. Soc. **105**, 4 (1983).
[34]S. Raynor and D. R. Herschbach, J. Phys. Chem. **86**, 3592 (1982).
[35]B. N. McMaster, J. Mrozek, and V. H. Smith, Chem. Phys. **73**, 131 (1982).
[36]J. Kaspar and V. H. Smith, Chem. Phys. **90**, 47 (1984).
[37]E. Kassab and E. M. Evleth, J. Am. Chem. Soc. **109**, 1653 (1987).
[38]J. Melin, J. V. Ortiz, I. Martín, A. M. Velasco, and C. Lavín, J. Chem. Phys. **122**, 234317 (2005).
[39]J. Melin and J. V. Ortiz, J. Chem. Phys. **127**, 014307 (2007).
[40]A. M. Velasco, C. Lavín, I. Martín, J. Melin, and J. V. Ortiz, J. Chem. Phys. **131**, 024104 (2009).
[41] F. Chen and E. R. Davidson, J. Phys. Chem. A **105**, 10915 (2001).
[42]C. Møller and M. S. Plesset, Phys. Rev. **46**, 618 (1934).
[43]D. Cremer, Wiley Interdiscip. Rev.: Comput. Mol. Sci. **1**, 509 (2011).
[44]J. A. Fournier, C. T. Wolke, M. A. Johnson, T. T. Odbadrakh, K. D. Jordan, S. M. Kathmann, and S. S. Xantheas, J. Phys. Chem. A **119**, 9425 (2015).
[45]M. Eigen, Angew. Chem., Int. Ed. **3**, 1 (1964).
[46]G. Zundel, *The Hydrogen Bond: Recent Developments in Theory and Experiments. II. Structure and Spectroscopy*, 2nd ed. (North-Holland Publishing Co., North-Holland, Amsterdam, 1976).
[47]S. Tomoda and K. Kimura, Chem. Phys. **82**, 215 (1983).
[48]Y. Xie, R. B. Remington, and H. F. Schaefer, J. Chem. Phys. **101**, 4878 (1994).
[49]D. Wei and D. R. Salahub, J. Chem. Phys. **101**, 7633 (1994).
[50]F. F. Muguet, J. Mol. Struct.: THEOCHEM **368**, 173 (1996).
[51] C. V. Ciobanu, L. Ojamäe, I. Shavitt, and S. J. Singer, J. Chem. Phys. **113**, 5321 (2000).
[52]P. L. Geissler, T. Van Voorhis, and C. Dellago, Chem. Phys. Lett. **324**, 149 (2000).
[53]L. I. Yeh, M. Okumura, J. D. Myers, J. M. Price, and Y. T. Lee, J. Chem. Phys. **91**, 7319 (1989).
[54]D. Marx, M. E. Tuckerman, J. Hutter, and M. Parrinello, Nature **397**, 601 (1999).
[55]M. E. Tuckerman, D. Marx, M. L. Klein, and M. Parrinello, Science **275**, 817 (1997).
[56]C. Kobayashi, S. Saito, and I. Ohmine, J. Chem. Phys. **113**, 9090 (2000).
[57]S. Walbran and A. A. Kornyshev, J. Chem. Phys. **114**, 10039 (2001).
[58]A. L. Sobolewski and W. Domcke, J. Phys. Chem. A **106**, 4158 (2002).
[59]D. Verma, S. Erukala, and A. F. Vilesov, J. Phys. Chem. A **124**, 6207 (2020).
[60]O. Vendrell, F. Gatti, and H.-D. Meyer, J. Chem. Phys. **127**, 184303 (2007).
[61] Q. Yu, W. B. Carpenter, N. H. C. Lewis, A. Tokmakoff, and J. M. Bowman, J. Phys. Chem. B **123**, 7214 (2019).
[62]Q. Yu and J. M. Bowman, J. Am. Chem. Soc. **139**, 10984 (2017).
[63]T. K. Esser, H. Knorke, K. R. Asmis, W. Schöllkopf, Q. Yu, C. Qu, J. M. Bowman, and M. Kaledin, J. Phys. Chem. Lett. **9**, 798 (2018).
[64]Q. Yu and J. M. Bowman, J. Phys. Chem. A **123**, 1399 (2019).
[65]Q. Yu and J. M. Bowman, J. Chem. Phys. **146**, 121102 (2017).
[66]Q. Yu and J. M. Bowman, J. Phys. Chem. A **124**, 1167 (2020).
[67]A. D. Becke, J. Chem. Phys. **98**, 5648 (1993).
[68]P. J. Stephens, F. J. Devlin, C. F. Chabalowski, and M. J. Frisch, J. Phys. Chem. **98**, 11623 (1994).
[69]J. P. Heindel, Q. Yu, J. M. Bowman, and S. S. Xantheas, J. Chem. Theory Comput. **14**, 4553 (2018).
[70]S. S. Xantheas, Can. J. Chem. Eng. **90**, 843 (2012).
[71] U. W. Schmitt and G. A. Voth, J. Phys. Chem. B **102**(29), 5547 (1998).
[72]T. J. F. Day, A. V. Soudackov, M. Čuma, U. W. Schmitt, and G. A. Voth, J. Chem. Phys. **117**, 5839 (2002).
[73]Y. Wu, H. Chen, F. Wang, F. Paesani, and G. A. Voth, J. Phys. Chem. B **112**, 467 (2008).
[74]A. Ünal and U. Bozkaya, J. Chem. Phys. **148**, 124307 (2018).
[75]G. Meraj and A. Chaudhari, J. Mol. Liq. **190**, 1 (2014).
[76]C.-C. Zho, V. Vlček, D. Neuhauser, and B. J. Schwartz, J. Phys. Chem. Lett. **9**, 5173 (2018).
[77]A. L. Sobolewski and W. Domcke, Phys. Chem. Chem. Phys. **5**, 1130 (2003).
[78]R. Shi, Z. Zhao, X. Liang, Y. Su, L. Sai, and J. Zhao, Theor. Chem. Acc. **139**, 66 (2020).
[79]E. de Beer, E. H. Kim, D. M. Neumark, R. F. Gunion, and W. C. Lineberger, J. Phys. Chem. **99**, 13627 (1995).
[80]G. I. Gellene and R. F. Porter, J. Chem. Phys. **81**, 5570 (1984).
[81] B. W. Williams and R. F. Porter, J. Chem. Phys. **73**, 5598 (1980).
[82]D. M. Hudgins and R. F. Porter, Int. J. Mass Spectrom. Ion Processes **130**, 49 (1994).
[83]I. R. Ariyarathna, S. N. Khan, F. Pawłowski, J. V. Ortiz, and E. Miliordos, J. Phys. Chem. Lett. **9**, 84 (2018).
[84]I. R. Ariyarathna, F. Pawłowski, J. V. Ortiz, and E. Miliordos, Phys. Chem. Chem. Phys. **20**, 24186 (2018).
[85]I. R. Ariyarathna, F. Pawłowski, J. V. Ortiz, and E. Miliordos, J. Phys. Chem. A **124**, 505 (2020).
[86]J. Linderberg and Y. Öhrn, *Propagators in Quantum Chemistry* (John Wiley & Sons, Inc., Hoboken, NJ, 2004).
[87]H. H. Corzo and J. V. Ortiz, *Advances in Quantum Chemistry* (Academic Press, 2017), pp. 267–298.
[88]J. V. Ortiz, *Annual Reports in Computational Chemistry* (Elsevier, 2017), pp. 139–182.
[89]T. Koopmans, Physica **1**, 104 (1934).
[90]J. V. Ortiz, Int. J. Quantum Chem. **105**, 803 (2005).
[91] J. V. Ortiz, Wiley Interdiscip. Rev.: Comput. Mol. Sci. **3**, 123 (2013).
[92]W. von Niessen, J. Schirmer, and L. S. Cederbaum, Comput. Phys. Rep. **1**, 57 (1984).
[93]L. S. Cederbaum, "One-body Green's function for atoms and molecules: Theory and application," J. Phys. B: At. Mol. Phys. **8**, 290 (1975).
[94]V. G. Zakrzewski, J. V. Ortiz, J. A. Nichols, D. Heryadi, D. L. Yeager, and J. T. Golab, Int. J. Quantum Chem. **60**, 29 (1996).
[95]J. V. Ortiz, *Computational Chemistry: Reviews of Current* (World Scientific, 1997), pp. 1–61.
[96]J. V. Ortiz, J. Chem. Phys. **104**, 7599 (1996).
[97]V. G. Zakrzewski, O. Dolgounitcheva, A. V. Zakjevskii, and J. V. Ortiz, Int. J. Quantum Chem. **110**, 2918 (2010).
[98]V. G. Zakrzewski, O. Dolgounitcheva, A. V. Zakjevskii, and J. V. Ortiz, *Annual Reports in Computational Chemistry* (Elsevier, 2010), pp. 79–94.
[99]V. G. Zakrzewski, O. Dolgounitcheva, A. V. Zakjevskii, and J. V. Ortiz, *Advances in Quantum Chemistry* (Academic Press, 2011), pp. 105–136.
[100]M. Díaz–Tinoco, H. H. Corzo, F. Pawłowski, and J. V. Ortiz, Mol. Phys. **117**, 2275 (2019).
[101] J. V. Ortiz, J. Chem. Phys. **109**, 5741 (1998).

Published under an exclusive license by AIP Publishing

[102]J. V. Ortiz, Int. J. Quantum Chem. **75**, 615 (1999).
[103]J. V. Ortiz, J. Chem. Phys. **153**, 070902 (2020).
[104]T. Yanai, D. P. Tew, and N. C. Handy, Chem. Phys. Lett. **393**, 51 (2004).
[105]G. D. Purvis and R. J. Bartlett, J. Chem. Phys. **76**, 1910 (1982).
[106]T. H. Dunning, J. Chem. Phys. **90**, 1007 (1989).
[107]R. A. Kendall, T. H. Dunning, and R. J. Harrison, J. Chem. Phys. **96**, 6796 (1992).
[108]D. E. Woon and T. H. Dunning, J. Chem. Phys. **100**, 2975 (1994).
[109]Gaussian 16, Revision C.01, M. J. Frisch, G. W. Trucks, H. B. Schlegel, G. E. Scuseria, M. A. Robb, J. R. Cheeseman, G. Scalmani, V. Barone, G. A. Petersson, H. Nakatsuji, X. Li, M. Caricato, A. V. Marenich, J. Bloino, B. G. Janesko, R. Gomperts, B. Mennucci, H. P. Hratchian, J. V. Ortiz, A. F. Izmaylov, J. L. Sonnenberg, D. Williams-Young, F. Ding, F. Lipparini, F. Egidi, J. Goings, B. Peng, A. Petrone, T. Henderson, D. Ranasinghe, V. G. Zakrzewski, J. Gao, N. Rega, G. Zheng, W. Liang, M. Hada, M. Ehara, K. Toyota, R. Fukuda, J. Hasegawa, M. Ishida, T. Nakajima, Y. Honda, O. Kitao, H. Nakai, T. Vreven, K. Throssell, J. A. Montgomery, Jr., J. E. Peralta, F. Ogliaro, M. J. Bearpark, J. J. Heyd, E. N. Brothers, K. N. Kudin, V. N. Staroverov, T. A. Keith, R. Kobayashi, J. Normand, K. Raghavachari, A. P. Rendell, J. C. Burant, S. S. Iyengar, J. Tomasi, M. Cossi, J. M. Millam, M. Klene, C. Adamo, R. Cammi, J. W. Ochterski, R. L. Martin, K. Morokuma, O. Farkas, J. B. Foresman, and D. J. Fox, Gaussian, Inc., Wallingford, CT, 2016.
[110]GaussView, Version 6.1, R. Dennington, T. A. Keith, and J. M. Millam, Semichem, Inc., Shawnee Mission, KS, 2016.
[111]G. Schaftenaar and J. H. Noordik, J. Comput.-Aided Mol. Des. **14**, 123 (2000).

Published under an exclusive license by AIP Publishing

Appendix M

E. Opoku, F. Pawłowski and J. V. Ortiz, "Double Rydberg Anions, Rydberg Radicals and Micro−solvated Cations with Ammonium−Water Kernels", *Phys. Chem. Chem. Phys.*, 24, 18347-60 (2022).

PCCP

ROYAL SOCIETY OF CHEMISTRY

PAPER

View Article Online
View Journal | View Issue

Check for updates

Cite this: *Phys. Chem. Chem. Phys.*, 2022, **24**, 18347

Double Rydberg anions, Rydberg radicals and micro-solvated cations with ammonium–water kernels†

Ernest Opoku, Filip Pawłowski and Joseph Vincent Ortiz *

Highly accurate *ab initio* electron-propagator and coupled-cluster methods are employed to predict the vertical electron attachment energies (VEAEs) of $NH_4^+(H_2O)_n$ (n = 1–4) cationic clusters. The VEAEs decrease with increasing n and the corresponding Dyson orbitals are diffused over peripheral, non-hydrogen bonded protons. Clusters formed from NH_4^- double Rydberg anions (DRAs) and stabilized by hydrogen bonding or electrostatic interactions are studied through calculations on $NH_4^-(H_2O)_n$ complexes and are compared with more stable $H^-(NH_3)(H_2O)_n$ isomers. Structures that have cationic and anionic congeners have notable changes in geometry. For all values of n, the hydride–molecule complex $H^-(NH_3)(H_2O)_n$ is always the most stable, with large vertical electron detachment energies (VEDEs). $NH_4^-(H_2O)_n$ DRA isomers are predicted to have VEDEs that correspond to energetically well-separated peaks in an anion photoelectron spectrum. Less stable DRA isomers display proton donation from the tetrahedral NH_4^- fragment to water molecules and VEDEs close to those of previously discovered DRAs. The most stable DRA isomers feature tetrahedral NH_4^- fragments without H bridges to water molecules and VEDEs that increase with n. Dyson orbitals of $NH_4^-(H_2O)_n$ DRAs occupy regions beyond the exterior non-bridging O–H and N–H bonds. Thus, the Rydberg electrons in the uncharged Rydberg radicals and DRAs are held near the outer protons of the water and ammonia molecules. Several bound low-lying excited states of the doublet Rydberg radicals have single electrons occupying delocalized Dyson orbitals of s-like, p-like, d-like, or f-like nodal patterns with the following Aufbau principle: 1s, 1p, 1d, 2s, 2p, 1f.

Received 6th June 2022,
Accepted 18th July 2022

DOI: 10.1039/d2cp02570a

rsc.li/pccp

1. Introduction

In double Rydberg anions (DRAs), a closed-shell, cationic core binds a pair of electrons held in diffuse orbitals. For example, in the NH_4^- or OH_3^- DRAs, an ammonium or hydronium cation is surrounded by a pair of peripheral electrons. The first DRA, tetrahedral NH_4^-, was discovered by Bowen and co-workers[1,2] during a pioneering photoelectron spectroscopic study on an anion–molecule complex, $H^-(NH_3)$. As the NH_4^- DRA and $H^-(NH_3)$ have identical mass, their electron detachment energies appeared as separate peaks in the same spectrum. The persistence of the spectral peak at a low vertical electron detachment energy (VEDE) under a variety of ion-source conditions, the absence of an energetic shift after full deuterium substitution for the hydrogens and previous investigations on the NH_4 radical[3] led to the identification of tetrahedral NH_4^- as a DRA. The measured[1,2] VEDE of NH_4^- was 0.472 eV, an amount that resembled of the sodium atomic anion (0.548 eV).[4]

High-level theoretical calculations have provided strong complementary support for the identification of DRAs. Prior to the discovery[1] of the NH_4^- DRA, some theoretical studies[5,6] had considered the existence of a tetrahedral isomer of NH_4^-. Ortiz applied techniques of *ab initio* electron propagator theory (EPT) to study the geometric isomers and VEDEs of NH_4^- and proposed the tetrahedral structure to be a viable DRA.[7] The two stable isomers were assigned to a hydride–molecule complex $H^-(NH_3)$ and a tetrahedral counterpart, NH_4^-, with VEDEs of 1.20 eV and 0.42 eV, respectively, in precise agreement with the experimental[1,2] results. Evidence of the diffuse, Rydberg-state distribution of the two diffuse electrons which surround the NH_4^+ cationic core was provided.[7] Subsequent theoretical studies[8–12] on the NH_4^- DRA also reported the VEDE to be near 0.45 eV.

Photoelectron spectroscopy has enabled the identification of several DRA clusters among the $N_nH_{3n+1}^-$ (n = 1–5) isomers.[13,14] Isomers of DRAs belong to three categories: (1) hydrides coordinated to n solvent molecules, (2) electrostatically bound

Department of Chemistry and Biochemistry, Auburn University, Auburn, AL 36849-5312, USA. E-mail: ezo0009@auburn.edu, filip@auburn.edu, ortiz@auburn.edu

† Electronic supplementary information (ESI) available. See DOI: https://doi.org/10.1039/d2cp02570a

This journal is © the Owner Societies 2022

intermolecular complexes with solvent molecules and (3) hydrogen-bonded DRA–molecule complexes. *Ab initio* EPT studies[15,16] have revealed identical isomeric patterns and electron binding energies in close agreement with experimental data. More recent EPT investigations[17] have found three new classes of DRAs: methylated, annulated, and paramagnetic. Prior to this investigation, Hopper *et al.*[18] reported the existence of NH_3R^- and OH_2R^- (R = F, OH, NH_2, and CH_3) sets of DRAs that are stable minima in their potential energy surfaces and have positive VEDEs. A tetrahedral PH_4^- DRA has been identified in a study that also predicted a C_{2v} isomer with a lone-pair of electrons occupying an equatorial position in a trigonal bipyramidal arrangement.[12]

Ortiz[19] performed computational studies on OH_3^- isomers and identified a pyramidal, C_{3v} DRA with a VEDE of 0.43 eV. However, several experimental efforts to characterize the OH_3^- DRA have not been successful. Melin and Ortiz[20] therefore conducted *ab initio* EPT studies on the reaction barrier between the OH_3^- DRA and a hydride–water complex. The barrier between the NH_4^- DRA and a hydride–ammonia complex also was examined. The low reaction barrier between the OH_3^- DRA and the hydride–water complex indicates that the former species may be difficult to isolate. Evidence of the existence of $O_2H_5^-$ DRAs in analogy with $N_2H_7^-$ was also reported.[20] Several DRAs based on elements other than N are also known from computational studies.[21]

DRAs, Rydberg radicals, their electronic structure and reactivity have been reviewed elsewhere.[10,22] The lowest diffuse orbitals in DRAs and Rydberg radicals are spheroidal and mimic valence s orbitals of alkali atoms. In their excited states, orbitals with major contributions from diffuse s-, p-, d-, f-, or g functions may be occupied. Large molecular systems (such as clusters) may feature different types of Rydberg states and orbitals.[23,24] Previous[25] and recent[26] studies have established that these unique molecular systems also participate in Rydberg-type chemical bonding in analogy with alkali-metal diatomic molecules and larger clusters.[27] Rydberg patterns of chemical bonding also manifest in protein fragments.[28,29]

Discovery and identification of novel DRAs and solvated-electron precursors[30–32] (which include metal–ammonia complexes with diffuse electrons) have relied heavily on techniques of *ab initio* EPT.[7,20] In a recent publication[33] on this subject, we extended the scope of the DRA concept to oxygen-based systems with the general formula $O_nH_{2n+1}^-$. Isomers that feature hydride–water interactions were compared with species in which the pyramidal H_3O^- DRA is stabilized by ion–dipole or hydrogen-bonding interactions with water molecules. For all values of n studied, the anion–water complex $H^-(H_2O)_{n+1}$ is always the most stable and has relatively large VEDEs. DRA–molecule complexes (*i.e.*, $OH_3^-(H_2O)_n$ isomers) have much lower VEDEs and may be detectable in anion photoelectron spectra. For all $O_nH_{2n+1}^-$ DRAs, Dyson orbitals occupy regions beyond the peripheral O–H bonds. We also calculated the vertical electron attachment energies (VEAEs) of $OH_3^+(H_2O)_n$ clusters and excitation energies of the $OH_3(H_2O)_n$ Rydberg radicals. The VEAEs decrease with increasing n and the corresponding Dyson orbitals are diffused over exterior, non-hydrogen bonded protons.

Can the concepts of DRAs and their ion–molecule clusters be extended to systems in which the cationic kernel is not a protonated micro-solvent molecule? Are the same extensions applicable to Rydberg radicals and their micro-solvated clusters? These questions prompted a thorough search of the chemical literature and evidence of ammonium–water cationic clusters $NH_4^+(H_2O)_n$[34] was found. Structural and energetic properties of $NH_4^+(H_2O)_n$ clusters were probed[35] by free jet expansion experiments and *ab initio* calculations decades ago. Later computational studies also found several other low-lying isomers.[36–39] At the MP2 level of theory, in conjunction with correlation-consistent basis sets, Morrell and Shields[40] studied the $NH_4^+(H_2O)_n$ (n = 1–10) isomers with a view to their atmospheric abundance as a function of temperature. Pei *et al.*[34] also presented an extensive study on $NH_4^+(H_2O)_n$ (n = 1–10) isomers and the effects of temperature and humidity on cluster growth patterns.

$NH_4^+(H_2O)_n$ clusters are reportedly abundant in the biosphere and an understanding of them is essential for modeling atmospheric and interstellar processes.[41] Studies on electronic structure and properties of molecular ions in aqueous media provide theoretical guidance in many chemical and biological processes.[42–44] Concepts of acid–base chemistry, redox reactions, electrochemistry, and a multitude of organic and inorganic reactions are often defined in terms of proton and electron transfer. Understanding the behavior of protons and electrons in aqueous media is a perennial concern in physical chemistry.

Structure and bonding in micro-solvated $NH_4^{+,0,-}(H_2O)_n$ (n = 1–4) clusters therefore deserve further study. All cationic $NH_4^+(H_2O)_n$ isomers reported in the literature so far are reconsidered. Addition of an electron produces uncharged clusters in which an NH_4 Rydberg radical is coordinated to water molecules. Excitation energies of several low-lying states of $NH_4(H_2O)_n$ Rydberg radicals are also calculated. Three kinds of anionic structures emerge from geometry optimizations. Micro-solvated hydride anions are denoted henceforth by $H^-(NH_3)(H_2O)_n$. The NH_4^- DRA with coordinated water molecules is represented by $[NH_4^-](H_2O)_n$. The formula $NH_4^-(H_2O)_n$ stands for structures with two diffuse electrons and a cationic kernel in which ammonium forms hydrogen bonds with water molecules.

We have employed correlated *ab initio* electron-propagator and coupled-cluster methods with large, diffuse basis sets to study $NH_4^+(H_2O)_n$ clusters, $NH_4(H_2O)_n$ Rydberg molecules, $H^-(NH_3)(H_2O)_n$, $[NH_4^-](H_2O)_n$ and $NH_4^-(H_2O)_n$ DRAs and related micro-solvated species. The primary focus of this work is prediction of structures, relative total energies, vertical electron binding energies and Dyson orbitals of $NH_4^{+,0,-}(H_2O)_n$ (n = 1–4) clusters. Calculations on micro-solvated $NH_4^{+,0,-}(H_2O)_n$ (n = 1–4) clusters provide Aufbau rules for electrons that occupy the periphery of these complexes.

2. Theory and computational details

2.1 Summary of electron propagator theory

Ab initio methods of EPT[45–47] calculate electron binding energies directly, *i.e.*, without any explicit reference to final state wave

This journal is © the Owner Societies 2022

functions and their total energies. Electron attachment and detachment energies occur at poles of the electron propagator matrix, $G(E)$, whose elements read

$$G_{rs}(E) = \lim_{\eta\to+0}\left[\sum_{P}^{\text{Attachment}}\frac{\langle 0|a_r|P\rangle\langle P|a_s^\dagger|0\rangle}{E+E_0-E_P^+ + i\eta} + \sum_{P}^{\text{Detachment}}\frac{\langle 0|a_s^\dagger|P\rangle\langle P|a_r|0\rangle}{E-E_0+E_P^- - i\eta}\right], \quad (1)$$

where the N-electron reference state, $|0\rangle$, and the $(N\pm1)$-electron final states, $|P\rangle$, and their energies (E_0 and $E_P^\pm$, respectively) are the solutions to the Hamiltonian eigenvalue problem,

$$\begin{aligned} H|0\rangle_N &= E_0|0\rangle_N, \\ H|P\rangle_{N\pm1} &= E_P^\pm|P\rangle_{N\pm1}, \end{aligned} \quad (2)$$

a_r and $a_s^\dagger$ are annihilation and creation operators, respectively, with spin–orbital indices, r and s, and the infinitesimal factor η ensures the correct Fourier transformation between the time-dependent definition of the electron propagator and its energy representation. Electron binding energies occur at the poles (*i.e.*, vanishing denominators) of eqn (1). The residues (numerators) are products of Feynman–Dyson amplitudes,

$$C_{rP} = \begin{cases} \langle 0|a_r|P\rangle, & (\text{electron attachment}) \\ \langle P|a_r|0\rangle, & (\text{electron detachment}) \end{cases}, \quad (3)$$

and their complex conjugates, which suffice to construct Dyson spin–orbitals (ϕ^{Dyson}) of attachment and detachment. Thus, changes in electronic structure between the initial state, $|0\rangle$, and the $(N\pm1)$-electron final states, $|P\rangle$, are represented by Dyson orbitals of electron detachment,

$$\phi_P^{\text{Dyson}}(x_1) = N^{1/2}\int \mathrm{d}x_2\mathrm{d}x_3\ldots\mathrm{d}x_N\,\Psi_{N,0}(x_1,x_2,x_3,\ldots,x_N) \times \Psi^*_{N-1,P}(x_2,x_3,\ldots,x_N), \quad (4)$$

or those of electron attachment,

$$\phi_P^{\text{Dyson}}(x_1) = (N+1)^{1/2}\int \mathrm{d}x_2\mathrm{d}x_3\ldots\mathrm{d}x_{N+1} \times \Psi_{N+1,P}(x_1,x_2,x_3,\ldots,x_{N+1}) \times \Psi^*_{N,0}(x_2,x_3,\ldots,x_{N+1}). \quad (5)$$

The probability factor (also known as the intensity factor, pole strength, or the norm of the Dyson orbital), Γ_p, may be used to normalize the Dyson spin–orbitals of eqn (4) and (5) such that the unit-normalized Dyson spin–orbital, φ^{Dyson}, reads

$$\varphi_P^{\text{Dyson}} = {\Gamma_P}^{-0.5}\phi_P^{\text{Dyson}}. \quad (6)$$

When the canonical Hartree–Fock reference state and the Møller–Plesset partitioning of the Hamiltonian are employed, the inverse electron propagator matrix takes the form

$$\mathbf{G}^{-1}(E) = E\mathbf{I} - \boldsymbol{\varepsilon} - \boldsymbol{\sigma}(E), \quad (7)$$

where $\boldsymbol{\varepsilon}$ is a diagonal matrix of Hartree–Fock orbital energies and $\boldsymbol{\sigma}(E)$ is the self-energy matrix, which describes orbital relaxation in final states and differential electron correlation between initial and final states. Poles occur at values of E that yield vanishing eigenvalues of $\mathbf{G}^{-1}(E)$. Neglect of the self-energy matrix recovers the (zeroth-order) Koopmans's theorem (KT)[48] result. (The first-order correction vanishes.) In many low-order methods, off-diagonal elements of $\boldsymbol{\sigma}(E)$ in the canonical Hartree–Fock orbital basis are neglected. Subsequent retention of all terms through second or third order in the self-energy matrix leads to the diagonal, second-order (D2),[46,49] and diagonal third order (D3) methods.[46,49,50] Approximate treatments of higher order self-energy terms (*i.e.*, renormalizations that pertain to certain classes of self-energy terms in all orders of perturbation theory) that require almost no additional computational effort include the A, B and C variants of the outer-valence Green's function (OVGF).[51–53] Numerical criteria have been introduced to automatically choose among these variants in a given calculation.[51,53,54] An alternative, parameter-free approach to diagonal, low-order approximations which has achieved superior accuracy with lower cost has yielded the partial third-order (P3)[55] method and its approximately renormalized counterpart (P3+).[46,49] OVGF and P3+ have been highly successful[56–58] in describing valence detachment energies and electron affinities of systems for which KT constitutes a valid zeroth-order approximation. We have recently derived a new generation of diagonal electron propagator (EP) methods from an intermediately normalized, Hermitized metric that retain the computational advantages of their antecedents, but with higher accuracy.[59] When the probability factor obtained with one of the aforementioned approximations is below 0.85,[60] the results should be treated with caution. This typically happens for systems with strong correlation (such as DRAs, *vide infra*) in the initial state. Such cases require employment of non-diagonal, renormalized techniques[61] such as the BD-T1[50,61–63] method.

2.2 Geometry optimizations, vibrational frequencies, vertical electron binding energies and excitation energies

For cationic geometries, initial guess inputs were obtained by constraining specific internal coordinates of the cations (bond lengths, bond angles, dihedral angles) and optimizing the remaining internal coordinates. The resulting geometries were then used as an input for full geometry optimizations without any geometry or symmetry constraints. The geometries of optimized cationic isomers are identical to those in published works[34,36–39] on $NH_4^+(H_2O)_n$ clusters. The fully optimized cationic geometries were used as initial guess input structures for full anionic geometry optimizations. Initial input structures for the remaining anionic geometries (hydride–molecule complexes, DRA–molecule complexes) were obtained through informed guesses in analogy with nitrogen-based $N_nH_{3n+1}{}^-$[16] and oxygen-based $O_nH_{2n+1}{}^-$ DRAs.[33]

Structures of cations and anions were optimized at the MP2 level in conjunction with the augmented, correlation-consistent, triple-ζ (aug-cc-pVTZ)[64,65] basis. The same level of theory was found to be sufficient for cations and anions in previous studies

This journal is © the Owner Societies 2022

on $O_nH_{2n+1}^{+,0,-}$ clusters.[20,33] Vibrational frequencies of all the optimized geometries were real and positive.

Single-point energy calculations at the coupled-cluster singles-and-doubles (CCSD)[66] and coupled-cluster singles-and-doubles with perturbative triples (CCSD(T))[67] levels were carried out on the MP2/aug-cc-pVTZ optimized geometries to infer relative energies. To obtain vertical electron affinities or ionization energies based on the indirect coupled-cluster methods (ΔCCSD and ΔCCSD(T)), single-point calculations on the $NH_4(H_2O)_n$ radicals were performed at the equilibrium geometry of cationic or anionic $NH_4^{+,-}(H_2O)_n$ (n = 1–4) complexes. Unrestricted Hartree–Fock spin contaminations from the UCCSD and UCCSD(T) single-point calculations on the doublet Rydberg radicals were minor.

VEAEs of ground-state cations, $NH_4^+(H_2O)_n$, that correspond to various final states of $NH_4(H_2O)_n$ doublet Rydberg radicals and VEDEs from the anions, $NH_4^-(H_2O)_n$, were calculated with EPT methods at the optimized geometries of selected ions. Several bound low-lying vertical excitation energies of the doublet Rydberg radicals were inferred from differences between the vertical electron affinities.

2.3 Basis sets for EPT and coupled-cluster calculations

At the geometries of cations and anions, several basis sets were tested for calculation of electron binding energies to find a suitable balance between accuracy and computational cost. For selected systems, we tested the aug-cc-pVXZ (X = T, Q), d-aug-cc-pVTZ, t-aug-cc-pVTZ and q-aug-cc-pVTZ basis sets (the latter three basis sets contain respectively two, three and four sets of diffuse, primitive functions with exponents obtained in the even-tempered manner starting from the exponents of the diffuse set of the original aug-cc-pVTZ basis).[68] For both cations and anions, we found the d-aug-cc-pVTZ basis to be the optimal choice. The t-aug-cc-pVTZ, q-aug-cc-pVTZ, and aug-cc-pVQZ basis sets yield electron binding energies of similar quality as d-aug-cc-pVTZ. (See the performance of the tested basis sets in Tables S1–S3 of the ESI.†) In indirect coupled-cluster (ΔCCSD and ΔCCSD(T)) calculations for determining electron binding energies, the d-aug-cc-pVTZ basis set was found to be sufficient. Therefore, unless stated otherwise, all the EPT, ΔCCSD and ΔCCSD(T) results discussed in the text were executed with the d-aug-cc-pVTZ basis. Identical conclusions have been reached elsewhere for $O_nH_{2n+1}^-$ DRAs.[33]

2.4 Software

Full geometry optimizations, frequency analyses, coupled-cluster (CCSD and CCSD(T)), KT, D2, D3, OVGF(A, B, C), P3 and P3+ EPT calculations were carried out with Gaussian 16.[69] The BD-T1 EP method has been implemented in a development version of Gaussian.[70] Dyson orbitals were plotted with GaussView[71] using a cube file with an enhanced edge size generated with Molden.[72] The Dyson orbitals were plotted with an iso-value of 0.08 a.u. and 0.004 a.u. for the cations and anions, respectively. The red and green surfaces of Dyson orbitals displayed in all Figures correspond to opposite phases of a real-valued wavefunction. The surfaces of the Dyson orbitals are semi-transparent (to display the underlying molecular framework) and therefore the inner, nodal surfaces are also visible.

3. Results and discussion

3.1 Isomers, relative energies, electron affinities and Dyson orbitals of $NH_4^+(H_2O)_n$ cations

In this section, we present results for the optimized ground-state geometries of closed-shell $NH_4^+(H_2O)_n$ isomers. For each given n, the isomers, relative energies, and geometric parameters are discussed and compared with previously reported results (if any). The lowest VEAEs and associated Dyson orbitals obtained with the direct *ab initio* EPT methods—KT, D2, D3, OVGF, P3, and P3+—are discussed and compared with indirect coupled-cluster results, *i.e.*, ΔCCSD and ΔCCSD(T). Table 1 presents data on relative energies of all $NH_4^+(H_2O)_n$ isomers and VEAEs obtained with diagonal, perturbative *ab initio* EPT methods and indirect coupled-cluster methods. Fig. 1–4 also display the Dyson orbitals of electron attachment to the saturated $NH_4^+(H_2O)_n$ cations. Detailed results on relative energies and VEAEs of the $NH_4^+(H_2O)_n$ isomers are presented in Tables S4–S6 (ESI†).

The lowest VEAEs (Table 1) for all $NH_4^+(H_2O)_n$ isomers do not show much disparity between EPT methods. All EPT methods yield pole strengths above 0.85 and therefore lend

Table 1 $NH_4^+(H_2O)_n$ isomers[a] and vertical electron attachment energies (VEAEs). Pole strengths are in parentheses. All energies are in eV

n	Isomer	$\Delta E_{MP2-ZPE}^{CCSD(T)}$	KT	D2	D3	OVGF-A	OVGF-B	OVGF-C	P3	P3+	ΔCCSD(T)
1	**1a** $NH_4^+(H_2O)$	—	3.324	3.744 (0.988)	3.722 (0.987)	3.725 (0.987)	3.726 (0.986)	3.724 (0.986)	3.749 (0.986)	3.748 (0.986)	3.826
2	**2a** $NH_4^+(H_2O)_2$	0.000	2.836	3.220 (0.989)	3.217 (0.987)	3.218 (0.988)	3.221 (0.987)	3.217 (0.987)	3.226 (0.987)	3.226 (0.987)	3.332
	2b $NH_4^+(H_2O)_2$	0.130	2.969	3.361 (0.988)	3.348 (0.987)	3.350 (0.987)	3.352 (0.987)	3.349 (0.987)	3.368 (0.986)	3.367 (0.987)	3.456
3	**3a** $NH_4^+(H_2O)_3$	0.047	2.569	2.937 (0.989)	2.940 (0.988)	2.940 (0.988)	2.944 (0.987)	2.939 (0.987)	2.943 (0.987)	2.943 (0.987)	3.071
	3b $NH_4^+(H_2O)_3$	0.000	2.490	2.840 (0.990)	2.850 (0.988)	2.849 (0.988)	2.853 (0.988)	2.848 (0.988)	2.847 (0.988)	2.846 (0.988)	2.972
	3c $NH_4^+(H_2O)_3$	0.096	2.554	2.910 (0.989)	2.915 (0.988)	2.915 (0.988)	2.918 (0.988)	2.914 (0.988)	2.917 (0.987)	2.917 (0.987)	3.033
4	**4a** $NH_4^+(H_2O)_4$	0.088	2.362	2.698 (0.990)	2.706 (0.989)	2.705 (0.989)	2.709 (0.988)	2.705 (0.989)	2.706 (0.989)	2.705 (0.988)	2.834
	4b $NH_4^+(H_2O)_4$	0.014	2.301	2.638 (0.990)	2.649 (0.989)	2.647 (0.989)	2.652 (0.988)	2.647 (0.988)	2.645 (0.988)	2.645 (0.988)	2.785
	4c $NH_4^+(H_2O)_4$	0.133	2.385	2.734 (0.989)	2.742 (0.988)	2.740 (0.988)	2.745 (0.988)	2.741 (0.988)	2.742 (0.987)	2.741 (0.988)	2.878
	4d $NH_4^+(H_2O)_4$	0.067	2.269	2.591 (0.990)	2.607 (0.989)	2.604 (0.989)	2.609 (0.989)	2.605 (0.989)	2.599 (0.988)	2.599 (0.988)	2.730
	4e $NH_4^+(H_2O)_4$	0.000	2.256	2.574 (0.990)	2.591 (0.989)	2.587 (0.989)	2.593 (0.989)	2.589 (0.989)	2.582 (0.988)	2.581(0.989)	2.715

[a] Isomerization energies in third column are obtained at the CCSD(T) level with MP2 zero-point energy corrections.

This journal is © the Owner Societies 2022

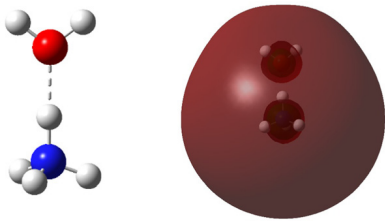


Fig. 1 Optimized geometry and Dyson orbital of electron attachment to $NH_4^+(H_2O)$.

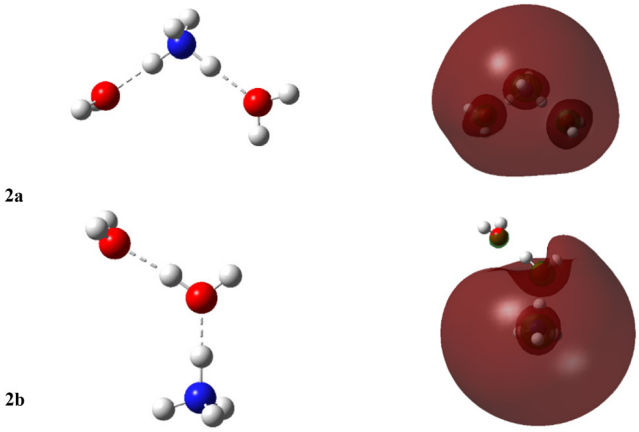


Fig. 2 Optimized geometries and Dyson orbitals of electron attachment to $NH_4^+(H_2O)_2$ cations.

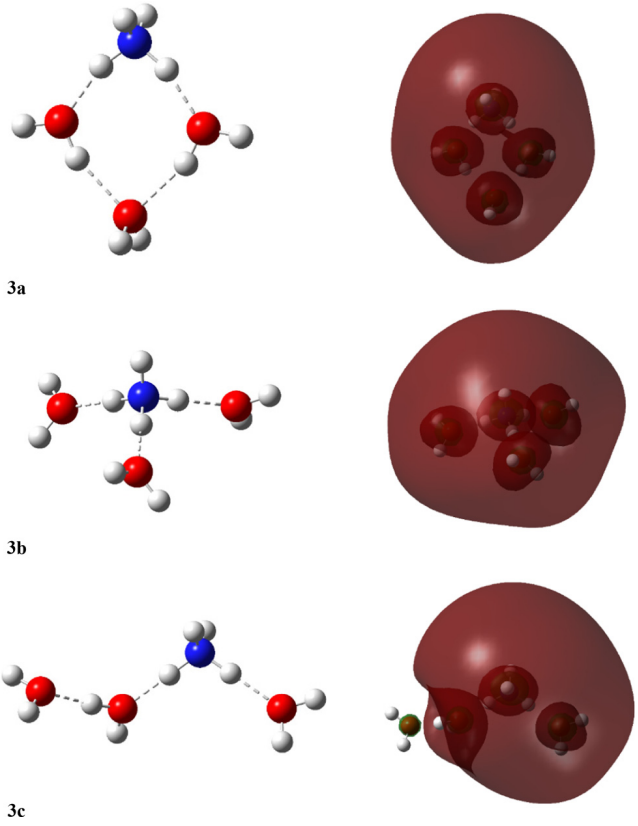


Fig. 3 Optimized geometries and Dyson orbitals of electron attachment to $NH_4^+(H_2O)_3$ cations.

credence to the adequacy of the diagonal, perturbative EPT methods. Hence, unless stated otherwise, discussion of the VEAEs and Dyson orbitals of the cations is based on the renormalized partial third order approximation (P3+) results.[49] VEAEs obtained with the indirect ΔCCSD(T) method and the d-aug-cc-pVTZ basis are in close agreement with those from EPT methods.

$NH_4^+(H_2O)$. Optimized $NH_4^+(H_2O)$ possesses a linear chain geometry and belongs to the C_2 point group as observed in the Zundel $O_2H_5^+$ cation.[33] The length of the hydrogen bond between the NH_4^+ fragment and the H_2O molecule is 1.64 Å. Thus, $NH_4^+(H_2O)$ forms an asymmetrically bridged NH_4^+–(H_2O) complex that is unlike the symmetric hydrogen bond found in the Zundel $O_2H_5^+$ cation.[33] The NH_4^+–(H_2O) complex resembles that of NH_4^+–(NH_3), which has been found as the central cationic kernel in $H^+(NH_3)_n$, n = 18, 20, 25, 30 clusters.[73] A search for an unusual isomer in which a binary-type hydrogen bond exists between two protons of the NH_4^+ fragment and the O nucleus of the H_2O molecule converged to the linear chain geometry as observed in previous studies.[34,74,75] As the NH_4^+–(H_2O) complex has a VEAE of 3.748 eV which is lower than the ionization potentials (IPs) of all alkaline atoms, it can be identified as a superalkali.[76] The Dyson orbital is quasi-spherical, with its maximum amplitudes near the NH_4^+ fragment (Fig. 1). The discernable orthogonalization to valence s functions on the oxygen and nitrogen nuclei contributes to the red contours. A similar Dyson orbital was identified in the Zundel $O_2H_5^+$ cation.[33]

$NH_4^+(H_2O)_2$ isomers. Two isomers, **2a** and **2b**, emerge from the addition of a water molecule to the $NH_4^+(H_2O)$ cation. In the triangular geometry **2a**, the lengths of the hydrogen bonds are 1.7172 and 1.7104 Å. In **2b**, the new H_2O molecule prefers to form a water dimer with the H_2O in the $NH_4^+(H_2O)$ cation. The hydrogen bond in the water dimer occurs at a length of 1.6921 Å. The proton lies at a typical covalent distance of 1.0753 Å from the nitrogen nucleus and exhibits an O–H separation of 1.5379 Å that is characteristic of a hydrogen bond. Relative energies in Table 1 show that **2a** is more stable than **2b**. Conclusions from previous studies[34,74,77] are in good agreement with our results and observations. The global minimum **2a** has a VEAE of 3.226 eV, which is 0.522 eV lower than the value for the $NH_4^+(H_2O)$ cation. Thus, superalkali[76] character increases with addition of a water molecule. An s-like Dyson orbital is obtained in both **2a** and **2b**. The Dyson orbitals (Fig. 2) have their largest amplitudes near the non-bonded proton positions of the NH_4^+ fragment in both isomers.

$NH_4^+(H_2O)_3$ isomers. Fig. 3 displays the optimized geometries and Dyson orbitals of three $NH_4^+(H_2O)_3$ isomers, **3a**, **3b**, and **3c**. **3a** has a rhombus C_{2v} geometry, whereas **3b** has a tapered geometry belonging to the C_3 point group. **3c** exhibits a linear chain structure. Relative energies (Table 1) favor the tapered C_3 geometry, **3b**, as the global minimum in agreement with some past studies based on density functional calculations.[34,74] The length of the H bonds between ammonium and water is 1.7702 Å in isomer **3b**. The geometry of **3a** is comparable to the lowest-energy geometry of the pure water cluster $(H_2O)_4$[78] and the lowest-energy geometry of $K^+(H_2O)_3$.[36] Thus, the hydrated

This journal is © the Owner Societies 2022

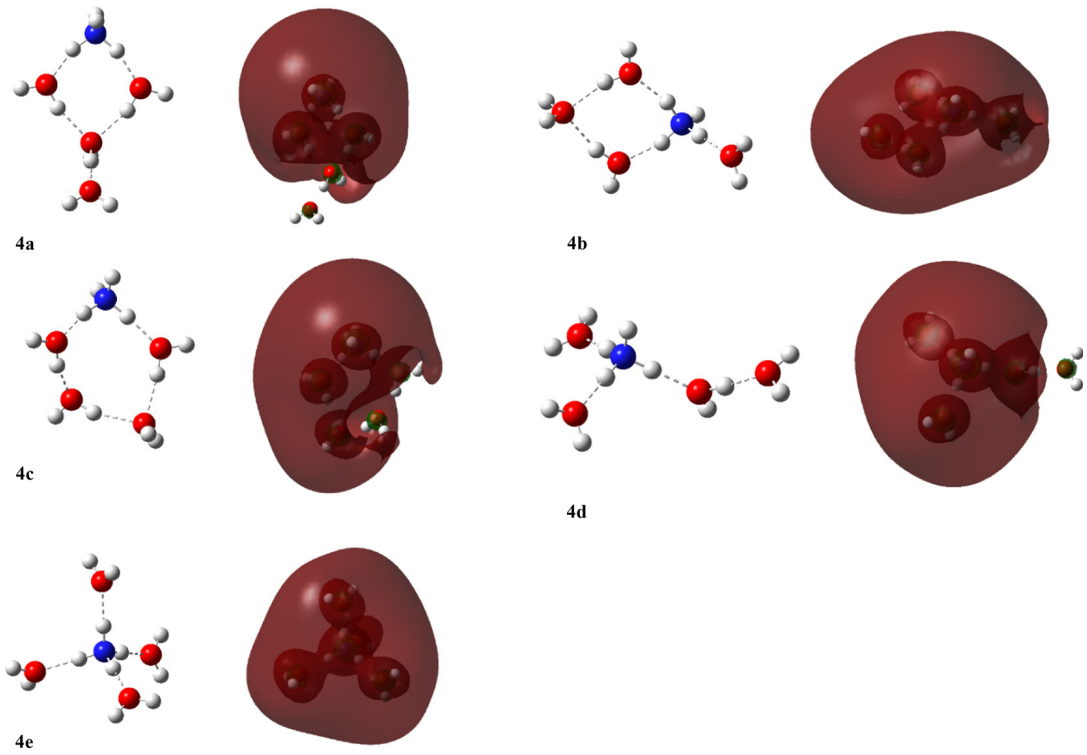


Fig. 4 Optimized geometries and Dyson orbitals of electron attachment to $NH_4^+(H_2O)_4$ cations.

ammonium cluster, $NH_4^+(H_2O)_3$, may have some attributes similar to those of pure water clusters and the monovalent $K^+(H_2O)_3$ cation. The least stable isomer, **3c**, has a geometry similar to the *cis* and *trans* Zundel isomers of $O_4H_9^+$ cations which were also found to be relatively unstable among their isomers.[33]

3a has a VEAE of 2.943 eV and its Dyson orbital is an *s*-like function which chiefly resides outside the positions of the non-bridging protons. The Dyson orbital of isomer **3b** (VEAE = 2.846 eV) is totally symmetric with its largest amplitudes beyond the non-bridging protons in the NH_4^+ fragment. For **3c**, whose VEAE is 2.917 eV, the s-like Dyson orbital covers the NH_4^+ fragment and the water molecules directly bonded to it. All three $NH_4^+(H_2O)_3$ isomers have VEAEs that are ~0.3–0.5 eV lower than those of the $NH_4^+(H_2O)_2$ isomers.

$NH_4^+(H_2O)_4$ isomers. Fig. 4 displays the five isomers (**4a–4e**) of $NH_4^+(H_2O)_4$ and their Dyson orbitals of electron attachment. In **4a**, the ammonium cation and three water molecules form two N–H···O and two O–H···O hydrogen bonds that constitute a ring whose structure is similar to an arrangement found in one of the isomers of $O_5H_{11}^+$.[33] Hydrogen bonds with O–H separations of 1.6753 Å and 1.831 Å pertain respectively to the upper (N–H···O) and lower (O–H···O) pairs of bridges that occur in the ring. The hydrogen bond outside the ring has a length of 1.7326 Å. **4a** has a VEAE of 2.705 eV with a quasi-spherical Dyson orbital that spreads over the non-bridging protons in the ring subunit with its maximum amplitude on the NH_4^+ fragment.

Adding a water molecule that bridges between two of the water molecules of **3b** leads to the formation of isomer **4b**. All hydrogen bonds with the NH_4^+ fragment have lengths of 1.7872 Å. This isomer has a VEAE of 2.581 eV and its Dyson orbital resides predominantly outside the positions of the non-bridging protons.

Isomer **4c** has a prism ring geometry similar to the prism ring isomer of $O_5H_{11}^+$.[33] This isomer has a VEAE of 2.741 eV with a diffuse s-like Dyson orbital that spreads over the non-bridging protons. In isomer **4d**, a **3b** fragment with an approximate C_3 axis has a water molecule that lies in the second solvation shell. The **4d** isomer has a VEAE of 2.599 eV and its Dyson orbital is distributed outside the exterior protons in the $NH_4^+(H_2O)_3$ fragment.

Some studies[36,39,74,75,77] have noted **4e** as the global minimum in perfect agreement with our data in Table 1, which favors **4e** as the lowest energy isomer, *i.e.*, the global minimum. In the **4e** geometry, the length of the H bond that links the water molecules to the NH_4^+ fragment is 1.8194 Å. This isomer has a tetracoordinated geometry, with the four water molecules individually bound to each hydrogen center on the ammonium core. This high-symmetry isomer resembles the tetracoordinated isomers of $Li^+(H_2O)_4$ and $Na^+(H_2O)_4$ reported in preceding studies.[36] This particularly interesting tetracoordinated isomer (**4e**) validates the data from free-jet expansion experiments[35] in which three $NH_4^+(H_2O)_n$ isomer classes were found, with a clear peak in the distribution and clusters of four, five and six water molecules being the most abundant. Thus, the dominant peak seen for $n = 4$[35] most likely corresponds to the S_4 point group. The S_4 point group was obtained as global minimum for $Li^+(H_2O)_4$, $Na^+(H_2O)_4$ and $NH_4^+(H_2O)_4$ in previous *ab initio* calculations on monovalent-cation water clusters.[36] Similar conclusions were

This journal is © the Owner Societies 2022

Table 2 First twenty radical excitation energies (EEs) of **3b** $NH_4^+(H_2O)_3$. All energies are in eV. The numbers in second column refer to Fig. 5

l	Dyson #	Final state	KT EEs	D2 EEs	D3 EEs	OVGF-B EEs	P3 EEs	P3+ EEs
s	1	1^2A	0.000	0.000	0.000	0.000	0.000	0.000
p	2, 3	1^2E	0.553	0.696	0.696	0.696	0.695	0.694
	4	2^2A	0.626	0.828	0.827	0.828	0.828	0.828
d	5, 6	2^2E	1.113	1.363	1.367	1.367	1.364	1.364
	7	3^2A	1.163	1.406	1.412	1.411	1.408	1.408
	8, 9	3^2E	1.244	1.533	1.536	1.535	1.535	1.534
s	10	4^2A	1.339	1.579	1.586	1.585	1.584	1.583
p	11, 12	4^2E	1.610	1.849	1.855	1.854	1.853	1.852
	13	5^2A	1.598	1.860	1.866	1.866	1.864	1.863
f	14, 15	5^2E	1.751	2.041	2.048	2.048	2.044	2.043
	16	6^2A	1.855	2.141	2.146	2.145	2.143	2.143
	17, 18	6^2E	1.912	2.190	2.194	2.194	2.192	2.192
	19	7^2A	1.998	2.241	2.248	2.247	2.244	2.244
	20	8^2A	1.962	2.245	2.249	2.250	2.248	2.248

reached in theoretical[16] and experimental[13] studies based on $NH_4^+(NH_3)_4$ clusters. Isomer **4e** has a VEAE of 2.581 eV. The totally symmetric, diffuse Dyson orbital (see red contour) that resides beyond the non-bridging protons is orthogonal to valence *s* functions of the oxygen and nitrogen nuclei. Overall, it is evident from Table 1 that with increasing n in $NH_4^+(H_2O)_n$, the VEAEs also decrease, thus enhancing super-alkali character.[76]

3.2 Radical excitation energies and Dyson orbitals of $NH_4(H_2O)_n$ Rydberg molecules

In anion photoelectron spectroscopy on DRAs, the final state of the doublet Rydberg radical may be an excited state instead of the ground-state. The excited states may be reached *via* simultaneous detachment of an electron from the Dyson orbital (of the lowest electron detachment energy) of the DRA and excitation from the same orbital to a more diffuse function, *i.e.*, through a shakeup process. Convincing examples have been reported in the spectra[14] of $N_nH_{3n+1}^-$ DRAs (for n = 4–6), where higher VEDEs were assigned to excited states of the doublet Rydberg radical and confirmed by EPT calculations.[16] Several shakeup states that correspond to excitation energies of the Rydberg neutrals can easily be accessed by calculating VEAEs of the closed shell cations. The vertical excitation energies of the doublet Rydberg radicals are inferred from differences between the VEAEs as shown in Tables S10 and S11 of ESI.†

To guide experimentation, we have calculated several radical excitation energies for the highly symmetric systems that may dominate anion photoelectron spectra. For **3b** $NH_4^+(H_2O)_3$ where the C_3 point group is obtained, several electron affinities of the cation corresponding to orbitals of higher angular momentum have been calculated. Vertical excitation energies thus inferred are displayed in Table 2. All VEAEs have pole strengths near unity. Excitation energies obtained with all the diagonal EPT methods are in close agreement. Dyson orbitals that correspond to several electron affinities are shown in Fig. 5. The excited states pertain to delocalized Dyson orbitals with s, p, d, and f nodal patterns that are orthogonalized to the N–H and O–H bond functions. Several excited states are doubly degenerate (^2E), and the remaining counterparts belong to the ^2A classification. All the bound excited states shown in the P3+ EEs column of Table 2 range from 0.694 to 2.248 eV. The approximate l quantum numbers are based on the angular nodes of the Dyson orbitals corresponding to electron affinities of the cations as displayed in Fig. 5.

For the tetracoordinated geometry of **4e** $NH_4^+(H_2O)_4$, several electron affinities of the cation corresponding to orbitals of higher angular momentum have been calculated. Their vertical excitation energies are listed in Table 3. Here also, the delocalized Dyson orbitals displayed in Fig. 6 typify p-, d-, and f-like nodal patterns with orthogonalizations to the N–H and O–H bond functions. The P3+ excitation energies lie between 0.578 and 1.983 eV. The contours of the Dyson orbitals in Fig. 6 (and their Aufbau principle) are similar to those observed in N_nH_{3n+1} and O_nH_{2n+1} Rydberg neutrals as well as solvated electron precursors.[16,30,32,33] Excited states of both radicals (**3b** $NH_4^+(H_2O)_3$ and **4e** $NH_4^+(H_2O)_4$) correspond to anion VEDEs below 2.5 eV and may be detectable in photoelectron experiments.

3.3 Isomers, relative energies, vertical electron detachment energies, and Dyson orbitals of $NH_4^-(H_2O)_n$ double Rydberg anions

Table 4 presents various isomers and their relative energies that pertain to $NH_4^-(H_2O)_n$ (n = 1–4) DRAs. It is evident that for all values of n, the hydride–molecule complex is the most stable isomer. Similar conclusions were reached for DRAs based on nitrogen[16] and oxygen.[33] Isomerization energies obtained with lower levels of theory (Table S7, ESI†) do not differ significantly from those obtained at the CCSD(T) level plus MP2 zero-point corrections shown in Table 4. Only results from the latter method are discussed in the text.

Results for the lowest VEDEs obtained at the uncorrelated (KT) level and with various diagonal self-energy approximations (D2, D3, OVGF, P3 and P3+) are reported in Table S8 (ESI†). In most cases, VEDEs calculated with EPT methods that retain only the diagonal self-energy matrix elements have pole strengths below 0.85. OVGF results are unencouraging and therefore not recommended for studies on DRAs as earlier noted in studies on $O_nH_{2n+1}^-$ DRAs.[33] When pole strengths are below 0.85, electron binding energies and associated Dyson orbitals of diagonal self-energy approximations should be treated with caution. Thus, approximations that retain the full self-energy matrix are convenient for such instances.

To facilitate reliable prediction of VEDEs, pole strengths and corresponding Dyson orbitals, we made use of the non-diagonal BD-T1[50,61–63] approximation, and the resulting data are included in Table 4. In BD-T1, all matrix blocks of the super-operator Hamiltonian that occur in the hole (h), particle (p), two-hole-one-particle (2hp) and two-particle-one-hole (2ph) operator manifolds are explicitly evaluated except the second-order couplings between 2ph and 2hp operators. The BD-T1 approximation employs the Brueckner doubles (BD) reference determinant[79–81] and its doubly excited amplitudes instead of the Hartree–Fock reference state. In addition to predicting high-accuracy VEDEs, Dyson orbitals from BD-T1 have better qualitative features than

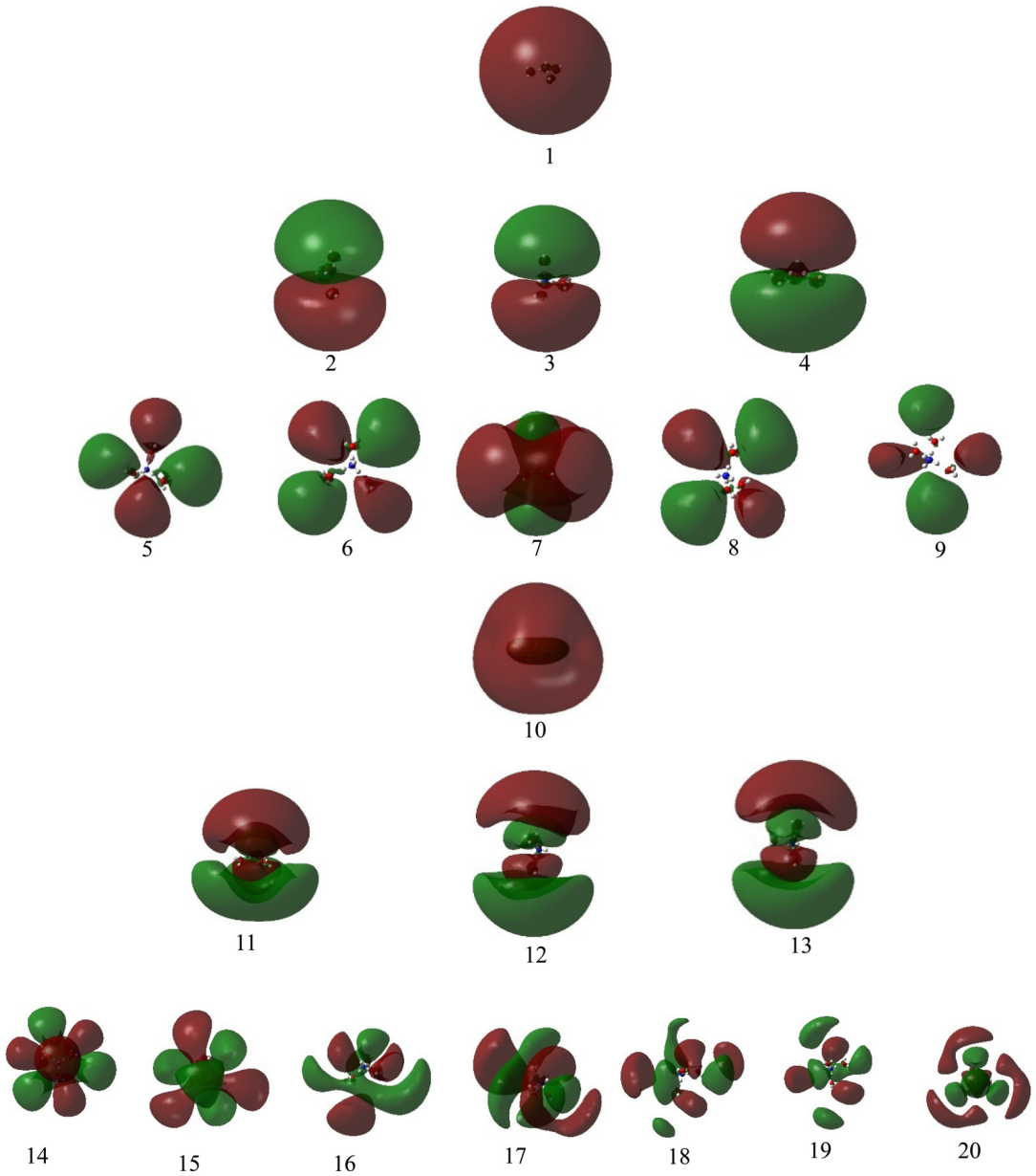


Fig. 5 Dyson orbitals of electron attachment to the cation for ground and excited states of the **3b** $NH_4(H_2O)_3$ Rydberg radical. The numerical labels correspond to those in the second column of Table 2 (Dyson #).

canonical molecular orbitals.[61] Hence, only VEDEs obtained with the BD-T1 method are discussed in the text.

To judge the reliability of the VEDEs predicted with EPT methods, we performed ΔCCSD(T) estimations of VEDEs with the d-aug-cc-pVTZ basis set and the results are also presented in Table 4. Optimized geometries and Dyson orbitals of the DRAs are displayed in Fig. 7–10. Note that all the reported Dyson orbitals are based on the highly accurate BD-T1 approximation. VEDEs obtained at the BD-T1 level agree closely with those from indirect ΔCCSD(T) calculations. (Detailed results for the indirect coupled-cluster methods are reported in Table S9, ESI.†) Note that throughout this section on anions, $H^-(NH_3)_n$ denotes hydride molecule complexes, $[NH_4^-](H_2O)_n$ designates NH_4^- DRA–water complexes without NH–O bridges, and $NH_4^-(H_2O)_n$ corresponds to micro-solvated DRAs that form H bridges with water molecules.

$NH_4^-(H_2O)$ isomers. For $n = 1$, three isomers are obtained as displayed in Fig. 7. In the $H^-(NH_3)H_2O$ complex, the hydride anion is weakly coordinated by the ammonia and water molecules, but this structure is the most stable. The predicted VEDE is near 2 eV. Given the high stability of this complex, a dominant peak near this range is anticipated in anion photoelectron spectra. The Dyson orbital of this complex is chiefly a totally symmetric *s*-function on the hydride's nucleus that displays anti-bonding relationships with N–H and O–H bond functions. The optimized geometry suggests that H^- has a stronger attraction towards the water molecule than the ammonia molecule. Thus, the VEDE of the free H^- (0.75 eV) has been

This journal is © the Owner Societies 2022

Table 3 First eighteen radical excitation energies (EEs) for 4e $NH_4^+(H_2O)_4$. All energies are in eV. The numbers in second column refer to Fig. 6

l	Dyson #	Final state	KT EEs	D2 EEs	D3 EEs	OVGF-B EEs	P3 EEs	P3+ EEs
s	1	1^2A_1	0.000	0.000	0.000	0.000	0.000	0.000
p	2	1^2B	0.449	0.579	0.583	0.583	0.578	0.578
	3, 4	1^2E	0.456	0.586	0.590	0.590	0.586	0.585
d	5	2^2B	0.945	1.168	1.178	1.177	1.170	1.170
	6, 7	2^2E	0.966	1.192	1.202	1.202	1.195	1.194
	8	2^2A	1.020	1.272	1.281	1.279	1.274	1.274
	9	3^2B	1.066	1.326	1.335	1.333	1.329	1.328
s	10	3^2A	1.147	1.341	1.354	1.352	1.348	1.347
p	11, 12	3^2E	1.403	1.633	1.645	1.644	1.638	1.638
	13	4^2B	1.444	1.646	1.657	1.656	1.651	1.650
	14	4^2A	1.550	1.801	1.814	1.813	1.804	1.804
	15	5^2A	1.568	1.825	1.838	1.837	1.829	1.828
d	16, 17	4^2E	1.668	1.934	1.944	1.943	1.936	1.936
	18	5^2B	1.761	1.979	1.989	1.988	1.984	1.983

increased by electrostatic and other interactions with the solvent molecules.

In the next most stable isomer, an NH_4^- DRA–molecule complex is formed and denoted by $[NH_4^-]H_2O$. This complex has C_{2v} symmetry with a VEDE of 0.684 eV. The diffuse Dyson orbital is held at the periphery of the NH_4^- DRA with minor delocalization. The two radial nodes anticipate the 3s united-atom limit for the Dyson orbital. Alternative DRA–molecule structures composed of OH_3^- and NH_3 fragments rearrange without a barrier under optimization to the $[NH_4^-]H_2O$ minimum.

In the least stable **1a** $NH_4^-(H_2O)$ isomer, a C_s cluster complex is obtained. The existing hydrogen bond between the N and O nuclei occurs at 1.8371 Å. The predicted VEDE of 0.495 eV is slightly above that of NH_4^- and $N_2H_7^-$ [16] as well as slightly below those of OH_3^- and $O_2H_5^-$ [33] DRAs. The Dyson

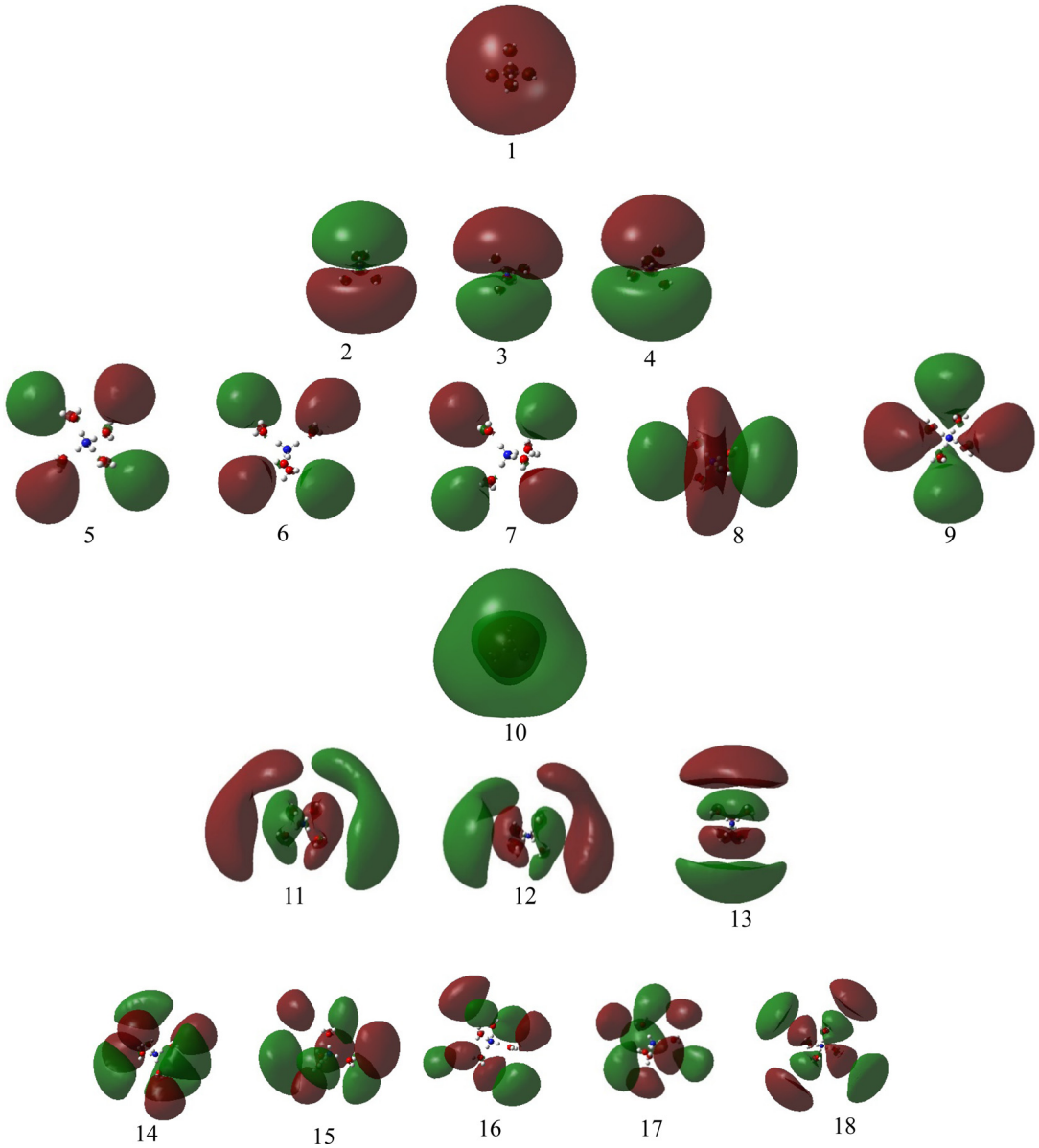


Fig. 6 Dyson orbitals of electron attachment to the cation for ground and excited states of the tetrahedral **4e** $NH_4(H_2O)_4$ Rydberg radical. The numerical labels correspond to those in the second column of Table 3 (Dyson #).

This journal is © the Owner Societies 2022

Table 4 $NH_4^-(H_2O)_n$ isomers and their vertical electron detachment energies (VEDEs). Pole strengths are in parentheses. All energies are in eV

n	Isomer	$\Delta E_{MP2\text{-}ZPE}^{CCSD(T)}$ [a]	KT	D2	P3+	BD-T1	ΔCCSD(T)
1	$H^-(NH_3)H_2O$	0.000	2.512	1.969 (0.893)	1.985 (0.908)	2.172 (0.882)	2.085
	$[NH_4^-]H_2O$	1.148	0.368	0.770 (0.877)	0.723 (0.854)	0.684 (0.881)	0.675
	1a $NH_4^-(H_2O)$	1.194	0.211	0.575 (0.872)	0.517 (0.835)	0.495 (0.862)	0.491
2	$H^-(NH_3)(H_2O)_2$	0.000	3.135	2.574 (0.903)	2.576 (0.908)	2.771 (0.831)	2.693
	$[NH_4^-](H_2O)_2$	1.667	0.490	0.954 (0.881)	0.920 (0.866)	0.886 (0.894)	0.886
	2a $NH_4^-(H_2O)_2$	1.641	0.186	0.607 (0.873)	0.558 (0.835)	0.539 (0.870)	0.553
	2b $NH_4^-(H_2O)_2$	1.557	0.238	0.621 (0.862)	0.568 (0.829)	0.552 (0.864)	0.556
3	$H^-(NH_3)(H_2O)_3$	0.000	3.980	3.352 (0.908)	3.364 (0.908)	3.567 (0.900)	3.470
	$[NH_4^-](H_2O)_3$	1.923	0.632	1.138 (0.886)	1.112 (0.874)	1.075 (0.899)	1.081
	3a $NH_4^-(H_2O)_3$	1.925	0.143	0.534 (0.860)	0.471 (0.812)	0.459 (0.856)	0.481
	3b $NH_4^-(H_2O)_3$	1.971	0.169	0.575 (0.857)	0.513 (0.809)	0.498 (0.856)	0.517
	3c $NH_4^-(H_2O)_3$	1.809	0.186	0.574 (0.863)	0.525 (0.827)	0.537 (0.868)	0.551
4	$H^-(NH_3)(H_2O)_4$	0.000	4.192	3.543 (0.908)	3.551 (0.903)	3.756 (0.896)	3.659
	$[NH_4^-](H_2O)_4$	2.061	0.730	1.240 (0.889)	1.213 (0.877)	1.177 (0.900)	1.183
	4a $NH_4^-(H_2O)_4$	2.126	0.141	0.523 (0.861)	0.470 (0.817)	0.473 (0.860)	0.481
	4b $NH_4^-(H_2O)_4$	2.195	0.148	0.522 (0.838)	0.452 (0.785)	0.432 (0.853)	0.439
	4c $NH_4^-(H_2O)_4$	2.178	0.162	0.521 (0.840)	0.457 (0.795)	0.455 (0.858)	0.474
	4d $NH_4^-(H_2O)_4$	2.264	0.173	0.586 (0.848)	0.529 (0.803)	0.515 (0.859)	0.530
	4e $NH_4^-(H_2O)_4$	2.318	0.183	0.566 (0.839)	0.509 (0.799)	0.534 (0.863)	0.564

[a] Isomerization energies in third column are obtained at the CCSD(T) level with MP2 zero-point energy corrections.

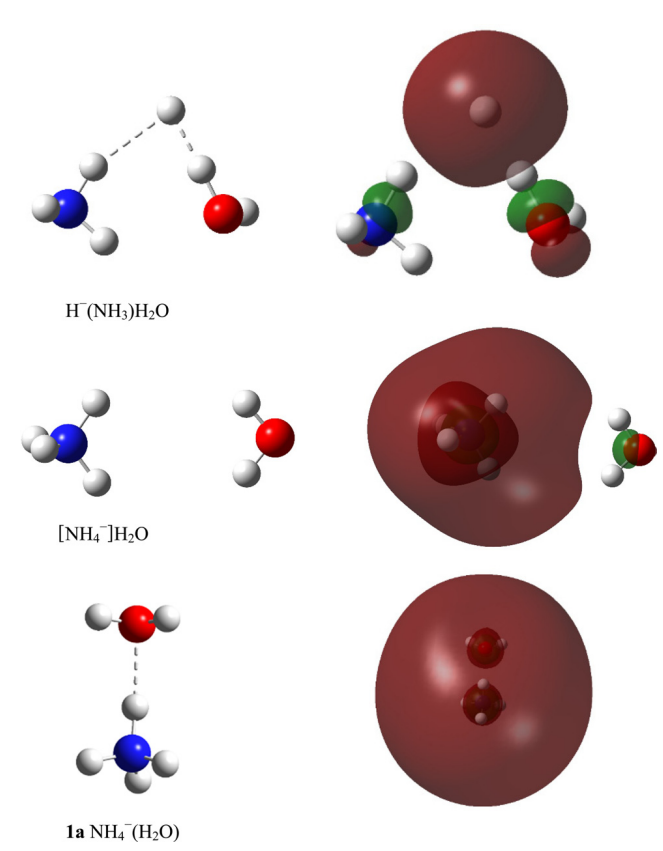


Fig. 7 n = 1 optimized geometries and Dyson orbitals of electron detachment from $NH_4^-(H_2O)$ isomers.

orbital is an approximately spherical function whose highest amplitudes occur beyond the non-bridging protons.

$NH_4^-(H_2O)_2$ isomers. The hydride–molecule complex retains its high stability upon addition of H_2O to form $H^-(NH_3)(H_2O)_2$. The VEDE increases by 0.599 eV from the $H^-(NH_3)H_2O$ complex. Thus, addition of a water molecule increases the VEDE. This may be attributed to the stronger attraction of the H^- towards

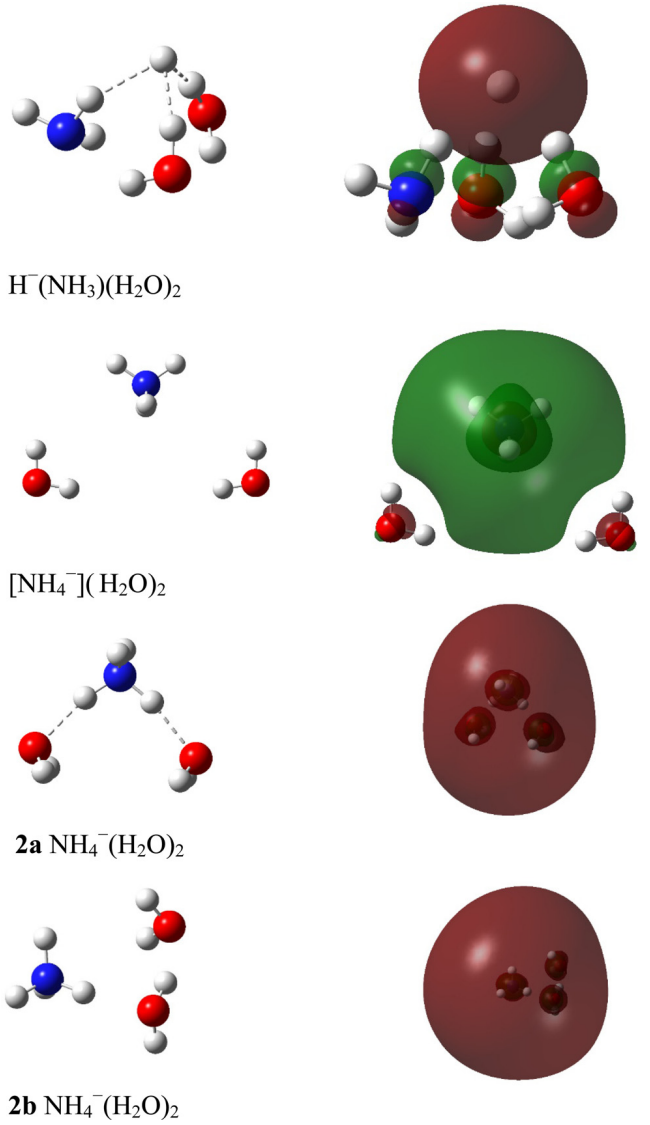


Fig. 8 n = 2 optimized geometries and Dyson orbitals of electron detachment from $NH_4^-(H_2O)_2$ isomers.

This journal is © the Owner Societies 2022

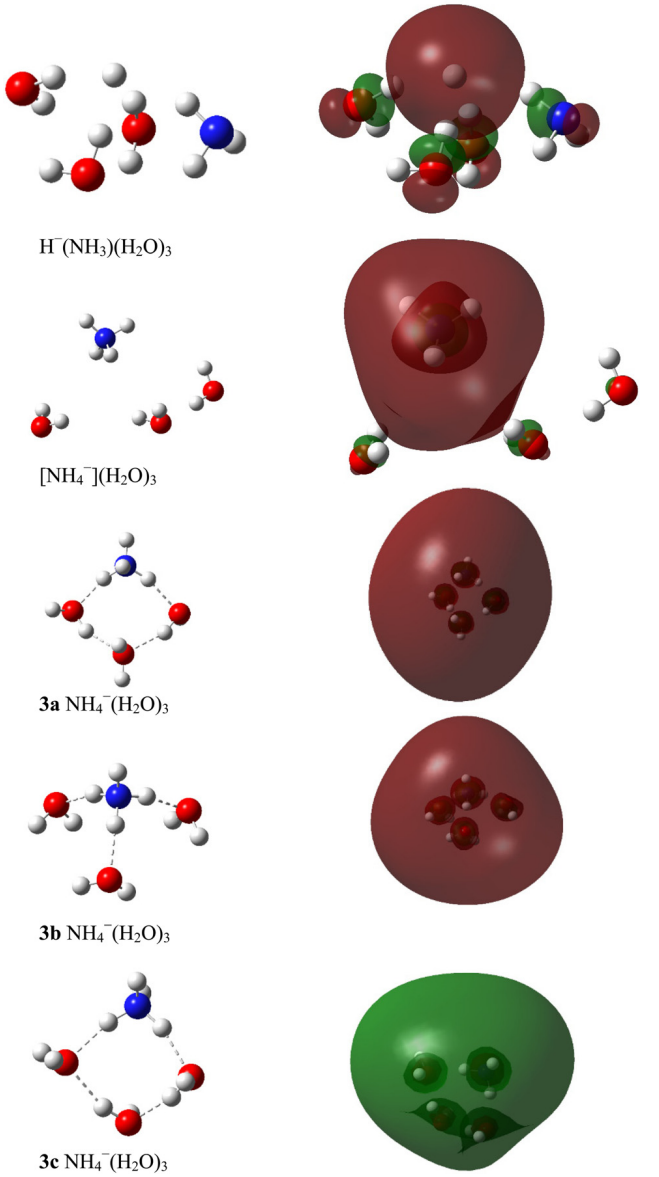


Fig. 9 n = 3 optimized geometries and Dyson orbitals of electron detachment from $NH_4^-(H_2O)_3$ isomers.

the water molecules than the ammonia. The totally symmetric diffuse Dyson orbital localizes near the H^- with slight anti-bonding relationships involving nearby solvent molecules.

In the $[NH_4^-](H_2O)_2$ DRA–molecule complex from Fig. 8, the NH_4^- DRA weakly interacts with the protons of the water molecules through electrostatic interactions in a C_{2v} arrangement. The VEDE is 0.886 eV. The Dyson orbital is a diffuse s-like function with two radial nodes and minor delocalization to neighboring solvent molecules.

The remaining two isomers, **2a** $NH_4^-(H_2O)_2$ and **2b** $NH_4^-(H_2O)_2$, are hydrogen-bonded DRA clusters. **2b** $NH_4^-(H_2O)_2$ is more stable than **2a** $NH_4^-(H_2O)_2$. In **2a** $NH_4^-(H_2O)_2$, two of the protons of NH_4^- engage in hydrogen bonding with water molecules in a C_{2v} arrangement. **2b** $NH_4^-(H_2O)_2$ has a discernable $NH_4^-(H_2O)$ fragment interacting with an additional water molecule engaging in hydrogen bonding to form a water dimer. VEDEs of 0.539 and 0.552 eV, respectively, are obtained for the **2a** and **2b** isomers. Both isomers have Dyson orbitals whose maximum amplitudes lie beyond the non-bridging protons on the periphery of the complex, especially those associated with the NH_4^- fragment.

$NH_4^-(H_2O)_3$ isomers. For n = 3, five isomers are obtained: a hydride–molecule complex, a DRA–molecule complex, and three hydrogen-bonded DRA clusters as displayed in Fig. 9. The hydride–molecule complex $H^-(NH_3)(H_2O)_3$, emerges as the most stable isomer with a VEDE of 3.567 eV. Again, the new water molecule contributes to an increase in the VEDE. The Dyson orbital is a totally symmetric function centered chiefly on the hydride's nucleus that forms anti-bonding relationships with neighboring N–H and O–H bond functions.

In the next isomer, the NH_4^- DRA weakly interacts with the protons of the three water molecules to form the DRA–molecule $[NH_4^-](H_2O)_3$ complex in which two H_2O molecules form a dimer. The VEDE is 1.075 eV, which is 0.189 eV higher than that of the $[NH_4^-](H_2O)_2$ DRA–molecule complex. The Dyson orbital is a symmetric s-like function spread over the NH_4^- kernel with minimal delocalization.

The remaining three isomers are micro-solvated DRA clusters: **3a** $NH_4^-(H_2O)_3$, **3b** $NH_4^-(H_2O)_3$, and **3c** $NH_4^-(H_2O)_3$. Of this set, **3c** is the most stable. **3a** and **3c** are ring structures that differ in relative orientations of their protons. **3b** retains its C_3 symmetry upon addition of two electrons to the **3b** $NH_4^+(H_2O)_3$ cation. VEDEs near 0.5 eV are obtained for the three micro-solvated DRAs. The Dyson orbitals of **3a** and **3c** are diffused over the non-bridging protons. For **3b**, the pyramidal C_3 symmetry of its cation and anion yields a symmetric diffuse Dyson orbital that extends beyond the outer protons.

$NH_4^-(H_2O)_4$ isomers. Coordination of a water molecule through hydrogen bonding or electrostatic interactions to the five latter structures accounts for all seven isomers in Fig. 10 when n = 4. The hydride cluster, $H^-(NH_3)(H_2O)_4$, is the most stable with a large VEDE of 3.756 eV. The spherical Dyson orbital occupying the H^- ion also has some antibonding relationships with nearby N–H and O–H bond functions. The H^- ion is closer to the water molecules than to the ammonia molecule.

In the DRA–molecule complex, $[NH_4^-](H_2O)_4$, the NH_4^- DRA is stabilized by a linear chain of four water molecules. With a VEDE of 1.177 eV, its Dyson orbital spreads over the NH_4^- fragment. Minor delocalization from the nearest H_2O is discernable, and the green contours arise from orthogonalization to the valence nitrogen functions with three radial nodes. The data of Table 4 indicate that the DRA–molecule complex, $[NH_4^-](H_2O)_4$, is the second most stable isomer.

The five remaining isomers, **4a–4e** $NH_4^-(H_2O)_4$, are micro-solvated DRAs arising from the reduction of their respective cationic congeners. **4a** has a three-dimensional cage structure with C_s symmetry. **4e** has a tetracoordinate NH_4^- fragment joined to a water molecule that forms hydrogen bonds with another water molecule and the anionic center. Note that a tetracoordinate NH_4^- was identified in $N_nH_{3n+1}^-$ DRAs with similar geometric features.[16] All the micro-solvated DRAs have VEDEs near 0.5 eV. The diffuse s-like Dyson orbitals spread over

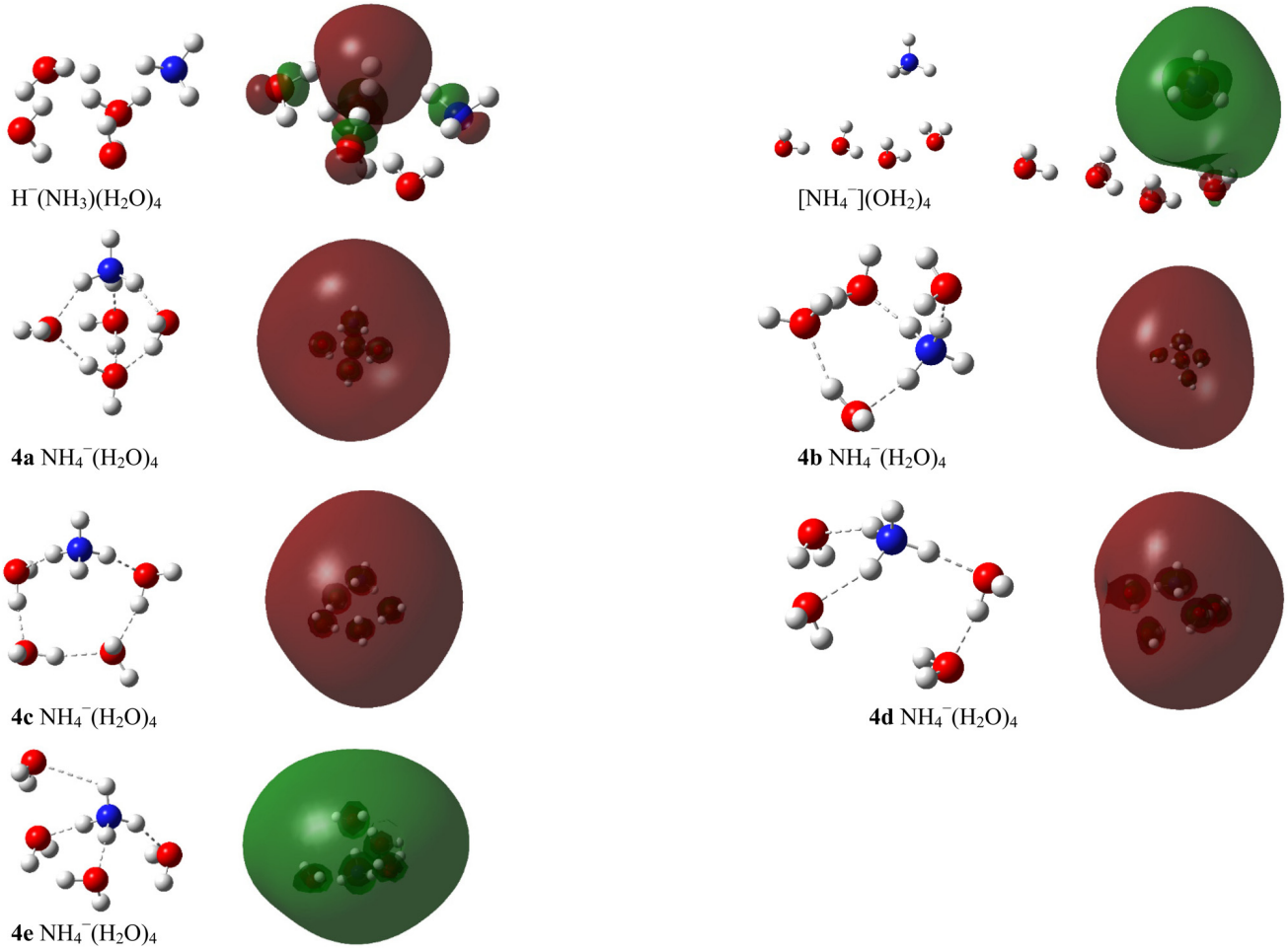


Fig. 10 n = 4 optimized geometries and Dyson orbitals of electron detachment from $NH_4^-(H_2O)_4$ isomers.

the exterior nonbonding protons with orthogonalizations to the valence functions on the nitrogen and the oxygen nuclei. For **4e**, a symmetric Dyson orbital whose amplitudes in green surround the peripheral protons displays nodes that result in red s-like contours on the N and O centers.[16]

4. Conclusions

A new family of DRAs that is based on micro-solvation of tetrahedral NH_4^- by one to four water molecules has been identified and its VEDEs and corresponding Dyson orbitals have been predicted. *Ab initio* electron-propagator (*i.e.*, direct) and coupled-cluster (*i.e.*, indirect) methods have been employed to predict electron binding energies of cationic, radical and anionic species. Several approximate electron propagator methods predict VEDEs that are in close agreement with those obtained with ΔCCSD(T). The BD-T1 method predicts the most reliable VEDEs. Vertical electron attachment energies (VEAEs) of $NH_4^+(H_2O)_n$ (n = 1–4) cationic clusters were calculated with the direct and indirect methods. The VEAEs decrease with increasing n and the corresponding Dyson orbitals are diffused over peripheral, non-hydrogen bonded protons.

Clusters formed from NH_4^- DRAs and stabilized by hydrogen bonding or electrostatic interactions are less stable than $H^-(NH_3)(H_2O)_n$ isomers. For all values of n, the hydride–molecule complex $H^-(NH_3)(H_2O)_n$ is always the most stable and has the largest VEDEs. DRAs formed from electrostatic interactions between NH_4^- and water molecules, denoted by $[NH_4^-](H_2O)_n$, are more stable than the $NH_4^-(H_2O)_n$ DRAs that exhibit NH–O hydrogen bridges. The latter species have VEDEs near 0.5 eV and therefore resemble the original DRAs. Variations in these VEDEs are consequences of distinct coordination environments that include proton donations by the tetrahedral anion to water molecules. Whereas total energies of $N_nH_{3n+1}^-$ [16] and $O_nH_{2n+1}^-$ [33] DRAs favor formation of H bonds, the opposite trend emerges for the present systems. An increasing sequence of larger, well-separated VEDEs for the $[NH_4^-](H_2O)_n$ DRAs, wherein the tetrahedral NH_4^- fragment interacts with water molecules without formation of H bridges, has been established. Dyson orbitals of electron attachment to $NH_4^+(H_2O)_n$ cations and of detachment from $NH_4^-(H_2O)_n$ DRAs occupy regions beyond the exterior non-bridging O–H and N–H bonds. Thus, the Rydberg electrons in the uncharged Rydberg radicals and DRAs are held near the outer protons of the water and ammonia molecules. The low-lying excited states of the doublet Rydberg radicals have a single

This journal is © the Owner Societies 2022

electron occupying extended s-like, p-like, d-like, or f-like Dyson orbitals with the following Aufbau principle: 1s, 1p, 1d, 2s, 2p, 1f. As $NH_4^-(H_2O)_n$ DRAs isomers have well separated VEDEs and experimentally accessible total energies, they are expected to appear in mass-selected, anion photoelectron spectra that typically detect low-lying isomers.

Data availability

The data that support the findings of this study are available within the manuscript and the ESI.† The ESI† contains the Cartesian coordinates of all optimized cationic and anionic geometries. Appropriate tables that support the findings in this study are also included. Sample input files for electron propagator theory calculations are provided in the ESI† as well.

Funding

This work was supported by the National Science Foundation *via* grant CHE-1565760 to Auburn University.

Conflicts of interest

There are no conflicts to declare.

Acknowledgements

The authors thank the Alabama Supercomputer Center for computing resources.

References

1 J. T. Snodgrass, J. V. Coe, C. B. Freidhoff, K. M. McHugh and K. H. Bowen, *Faraday Discuss., Chem. Soc.*, 1988, **86**, 241–256.
2 J. V. Coe, J. T. Snodgrass, C. B. Freidhoff, K. M. McHugh and K. H. Bowen, *J. Chem. Phys.*, 1985, **83**, 3169–3170.
3 G. Herzberg and J. T. Hougen, *J. Mol. Spectrosc.*, 1983, **97**, 430–440.
4 J. V. Ortiz, *J. Chem. Phys.*, 1988, **89**, 6348–6352.
5 D. Cremer and E. Kraka, *J. Phys. Chem.*, 1986, **90**, 33–40.
6 H. Cardy, C. Larrieu and A. Dargelos, *Chem. Phys. Lett.*, 1986, **131**, 507–512.
7 J. V. Ortiz, *J. Chem. Phys.*, 1987, **87**, 3557–3562.
8 M. Gutowski, J. Simons, R. Hernandez and H. L. Taylor, *J. Phys. Chem.*, 1988, **92**, 6179–6182.
9 M. Gutowski and J. Simons, *J. Chem. Phys.*, 1990, **93**, 3874–3880.
10 J. Simons and M. Gutowski, *Chem. Rev.*, 1991, **91**, 669–677.
11 J. Wang and R. J. Boyd, *Can. J. Phys.*, 1994, **72**, 851–855.
12 N. Matsunaga and M. S. Gordon, *J. Phys. Chem.*, 1995, **99**, 12773–12780.
13 S. J. Xu, J. M. Nilles, J. H. Hendricks, S. A. Lyapustina and K. H. Bowen, *J. Chem. Phys.*, 2002, **117**, 5742–5747.
14 D. Radisic, S. T. Stokes and K. H. Bowen, *J. Chem. Phys.*, 2005, **123**, 011101.
15 J. V. Ortiz, *J. Chem. Phys.*, 2002, **117**, 5748–5756.
16 M. Díaz-Tinoco and J. V. Ortiz, *J. Chem. Phys.*, 2019, **151**, 054301.
17 M. Diáz-Tinoco and J. V. Ortiz, *J. Phys. Chem. A*, 2019, **123**, 10961–10967.
18 H. Hopper, M. Lococo, O. Dolgounitcheva, V. G. Zakrzewski and J. V. Ortiz, *J. Am. Chem. Soc.*, 2000, **122**, 12813–12818.
19 J. V. Ortiz, *J. Chem. Phys.*, 1989, **91**, 7024–7029.
20 J. Melin and J. V. Ortiz, *J. Chem. Phys.*, 2007, **127**, 014307.
21 J. V. Ortiz, *J. Phys. Chem.*, 1990, **94**, 4762–4763.
22 J. Melin, G. Seabra and J. V. Ortiz, *Theor. Comput. Chem.*, 2007, **19**, 87–100.
23 A. I. Boldyrev and J. Simons, *J. Chem. Phys.*, 1998, **97**, 6621.
24 I. Anusiewicz, S. Freza, M. Bobrowski and P. Skurski, *J. Chem. Phys.*, 2021, **154**, 104302.
25 R. Barrios, P. Skurski and J. Simons, *J. Phys. Chem. A*, 2000, **104**, 10855–10858.
26 M. V. Ivanov, A. I. Krylov and S. Zilberg, *J. Phys. Chem. Lett.*, 2020, **11**, 2284–2290.
27 R. Riedel, A. G. Seel, D. Malko, D. P. Miller, B. T. Sperling, H. Choi, T. F. Headen, E. Zurek, A. Porch, A. Kucernak, N. C. Pyper, P. P. Edwards and A. G. M. Barrett, *J. Am. Chem. Soc.*, 2021, **143**, 3934–3943.
28 I. Anusiewicz, P. Skurski and J. Simons, *J. Phys. Chem. B*, 2014, **118**, 7892–7901.
29 J. P. Simons, *J. Chem. Phys.*, 2022, **156**, 100901.
30 I. R. Ariyarathna, S. N. Khan, F. Pawłowski, J. V. Ortiz and E. Miliordos, *J. Phys. Chem. Lett.*, 2018, **9**, 84–88.
31 I. R. Ariyarathna, F. Pawłowski, J. V. Ortiz and E. Miliordos, *Phys. Chem. Chem. Phys.*, 2018, **20**, 24186–24191.
32 I. R. Ariyarathna, F. Pawłowski, J. V. Ortiz and E. Miliordos, *J. Phys. Chem. A*, 2020, **124**, 505–512.
33 E. Opoku, F. Pawłowski and J. V. Ortiz, *J. Chem. Phys.*, 2021, **154**, 234304.
34 S. T. Pei, S. Jiang, Y. R. Liu, T. Huang, K. M. Xu, H. Wen, Y. P. Zhu and W. Huang, *J. Phys. Chem. A*, 2015, **119**, 3035–3047.
35 Y. S. Wang, H. C. Chang, J. C. Jiang, S. H. Lin, Y. T. Lee and H. C. Chang, *J. Am. Chem. Soc.*, 1998, **120**, 8777–8788.
36 H. M. Lee, P. Tarakeshwar, J. Park, M. R. Kołaski, Y. Jin Yoon, H. B. Yi, W. Y. Kim and K. S. Kim, *J. Phys. Chem. A*, 2004, **108**, 2949–2958.
37 S. Karthikeyan, J. N. Singh, M. Park, R. Kumar and K. S. Kim, *J. Chem. Phys.*, 2008, **128**, 5648.
38 J. Douady, F. Calvo and F. Spiegelman, *J. Chem. Phys.*, 2008, **129**, 154305.
39 Y. L. Zhao, M. Meot-Ner and C. Gonzalez, *J. Phys. Chem. A*, 2009, **113**, 2967–2974.
40 T. E. Morreis and G. C. Shields, *J. Phys. Chem. A*, 2010, **114**, 4266–4271.
41 R. P. Wayne, *Chemistry of atmospheres*, Oxford University Press, Oxford, UK, 1991.
42 E. N. Baker and R. E. Hubbard, *Prog. Biophys. Mol. Biol.*, 1984, **44**, 97–179.
43 G. W. Robinson, P. J. Thistlethwaite and J. Lee, *J. Phys. Chem.*, 1986, **90**, 4224–4233.

44 R. Ludwig, *Angew. Chem., Int. Ed.*, 2001, **40**, 1808–1827.
45 J. Linderberg and Y. Öhrn, *Propagators in Quantum Chemistry*, John Wiley & Sons, Inc., Hoboken, NJ, USA, 2004.
46 H. H. Corzo and J. V. Ortiz, *Advances in Quantum Chemistry*, Academic Press Inc., 2017, vol. 74, pp. 267–298.
47 J. V. Ortiz, *Annual Reports in Computational Chemistry*, Elsevier Ltd, 2017, vol. 13, pp. 139–182.
48 T. Koopmans, *Physica*, 1934, **1**, 104–113.
49 J. V. Ortiz, *Int. J. Quantum Chem.*, 2005, **105**, 803–808.
50 J. V. Ortiz, *Wiley Interdiscip. Rev.: Comput. Mol. Sci.*, 2013, **3**, 123–142.
51 W. von Niessen, J. Schirmer and L. S. Cederbaum, *Comput. Phys. Rep.*, 1984, **1**, 57–125.
52 L. S. Cederbaum, *J. Phys. B: At. Mol. Phys.*, 1975, **8**, 290–303.
53 V. G. Zakrzewski, J. V. Ortiz, J. A. Nichols, D. Heryadi, D. L. Yeager and J. T. Golab, *Int. J. Quantum Chem.*, 1996, **60**, 29–36.
54 J. V. Ortiz, *Computational Chemistry: Reviews of Current*, World Scientific, 1997, pp. 1–61.
55 J. V. Ortiz, *J. Chem. Phys.*, 1996, **104**, 7599–7605.
56 V. G. Zakrzewski, O. Dolgounitcheva, A. V. Zakjevskii and J. V. Ortiz, *Int. J. Quantum Chem.*, 2010, **110**, 2918–2930.
57 V. G. Zakrzewski, O. Dolgounitcheva, A. V. Zakjevskii and J. V. Ortiz, *Annual Reports in Computational Chemistry*, Elsevier BV, 2010, vol. 6, pp. 79–94.
58 V. G. Zakrzewski, O. Dolgounitcheva, A. V. Zakjevskii and J. V. Ortiz, *Advances in Quantum Chemistry*, Academic Press Inc., 2011, vol. 62, pp. 105–136.
59 E. Opoku, F. Pawłowski and J. V. Ortiz, *J. Chem. Phys.*, 2021, **155**, 204107.
60 M. Díaz–Tinoco, H. H. Corzo, F. Pawłowski and J. V. Ortiz, *Mol. Phys.*, 2019, **117**, 2275–2283.
61 J. V. Ortiz, *J. Chem. Phys.*, 2020, **153**, 070902.
62 J. V. Ortiz, *J. Chem. Phys.*, 1998, **109**, 5741–5746.
63 J. V. Ortiz, *Int. J. Quantum Chem.*, 1999, **75**, 615–621.
64 T. H. Dunning, *J. Chem. Phys.*, 1989, **90**, 1007–1023.
65 R. A. Kendall, T. H. Dunning and R. J. Harrison, *J. Chem. Phys.*, 1992, **96**, 6796–6806.
66 G. D. Purvis and R. J. Bartlett, *J. Chem. Phys.*, 1982, **76**, 1910–1918.
67 K. Raghavachari, G. W. Trucks, J. A. Pople and M. Head-Gordon, *Chem. Phys. Lett.*, 1989, **157**, 479–483.
68 D. E. Woon and T. H. Dunning, *J. Chem. Phys.*, 1994, **100**, 2975–2988.
69 M. J. Frisch, G. W. Trucks, H. B. Schlegel, G. E. Scuseria, M. A. Robb, J. R. Cheeseman, G. Scalmani, V. Barone, G. A. Petersson, H. Nakatsuji, X. Li, M. Caricato, A. V. Marenich, J. Bloino, B. G. Janesko, R. Gomperts, B. Mennucci, H. P. Hratchian, J. V. Ortiz, A. F. Izmaylov, J. L. Sonnenberg, D. Williams-Young, F. Ding, F. Lipparini, F. Egidi, J. Goings, B. Peng, A. Petrone, T. Henderson, D. Ranasinghe, V. G. Zakrzewski, J. Gao, N. Rega, G. Zheng, W. Liang, M. Hada, M. Ehara, K. Toyota, R. Fukuda, J. Hasegawa, M. Ishida, T. Nakajima, Y. Honda, O. Kitao, H. Nakai, T. Vreven, K. Throssell, J. A. Montgomery Jr., J. E. Peralta, F. Ogliaro, M. J. Bearpark, J. J. Heyd, E. N. Brothers, K. N. Kudin, V. N. Staroverov, T. A. Keith, R. Kobayashi, J. Normand, K. Raghavachari, A. P. Rendell, J. C. Burant, S. S. Iyengar, J. Tomasi, M. Cossi, J. M. Millam, M. Klene, C. Adamo, R. Cammi, J. W. Ochterski, R. L. Martin, K. Morokuma, O. Farkas, J. B. Foresman and D. J. Fox, *Gaussian 16, Revision A.01*, Gaussian, Inc., Wallingford, CT, 2016.
70 M. J. Frisch, G. W. Trucks, H. B. Schlegel, G. E. Scuseria, M. A. Robb, J. R. Cheeseman, G. Scalmani, V. Barone, G. A. Petersson, H. Nakatsuji, X. Li, M. Caricato, A. V. Marenich, J. Bloino, B. G. Janesko, R. Gomperts, B. Mennucci, H. P. Hratchian, J. V. Ortiz, A. F. Izmaylov, J. L. Sonnenberg, D. Williams-Young, F. Ding, F. Lipparini, F. Egidi, J. Goings, B. Peng, A. Petrone, T. Henderson, D. Ranasinghe, V. G. Zakrzewski, J. Gao, N. Rega, G. Zheng, W. Liang, M. Hada, M. Ehara, K. Toyota, R. Fukuda, J. Hasegawa, M. Ishida, T. Nakajima, Y. Honda, O. Kitao, H. Nakai, T. Vreven, K. Throssell, J. A. Montgomery Jr., J. E. Peralta, F. Ogliaro, M. J. Bearpark, J. J. Heyd, E. N. Brothers, K. N. Kudin, V. N. Staroverov, T. A. Keith, R. Kobayashi, J. Normand, K. Raghavachari, A. P. Rendell, J. C. Burant, S. S. Iyengar, J. Tomasi, M. Cossi, J. M. Millam, M. Klene, C. Adamo, R. Cammi, J. W. Ochterski, R. L. Martin, K. Morokuma, O. Farkas, J. B. Foresman and D. J. Fox, *Gaussian Development Version, Revision 1.14*, Gaussian, Inc., Wallingford, CT, 2018.
71 R. Dennington, T. A. Keith and J. M. Millam, *GaussView, Version 6.1*, Semichem Inc., Shawnee Mission, KS, 2019.
72 G. Schaftenaar and J. H. Noordik, *J. Comput. Aided Mol. Des.*, 2000, **14**, 123–134.
73 A. Malloum, J. J. Fifen and J. Conradie, *J. Chem. Phys.*, 2018, **149**, 244301.
74 F. C. Pickard IV, M. E. Dunn and G. C. Shields, *J. Phys. Chem. A*, 2005, **109**, 4905–4910.
75 J. C. Jiang, *J. Phys. Chem. A*, 1999, **103**, 3123–3135.
76 G. L. Gutsev and A. I. Boldyrev, *Chem. Phys. Lett.*, 1982, **92**, 262–266.
77 F. Zhao, C. Liu, L. Gong and Z. Yang, *Acta Chim. Sin.*, 2011, **69**, 1147–1150.
78 S. S. Xantheas, *Chem. Phys.*, 2000, **258**, 225–231.
79 K. A. Brueckner, *Phys. Rev.*, 1954, **96**, 508.
80 R. K. Nesbet, *Phys. Rev.*, 1958, **109**, 1632.
81 N. C. Handy, J. A. Pople, M. Head-Gordon, K. Raghavachari and G. W. Trucks, *Chem. Phys. Lett.*, 1989, **164**, 185–192.

This journal is © the Owner Societies 2022